NON-CODING RNAS IN HEAD AND NECK SQUAMOUS CELL CARCINOMA: FUNCTIONAL AND CLINICAL IMPLICATIONS.

EDITED BY: Wei Cao, Qiang Shen and Ming Yann Lim
PUBLISHED IN: Frontiers in Oncology

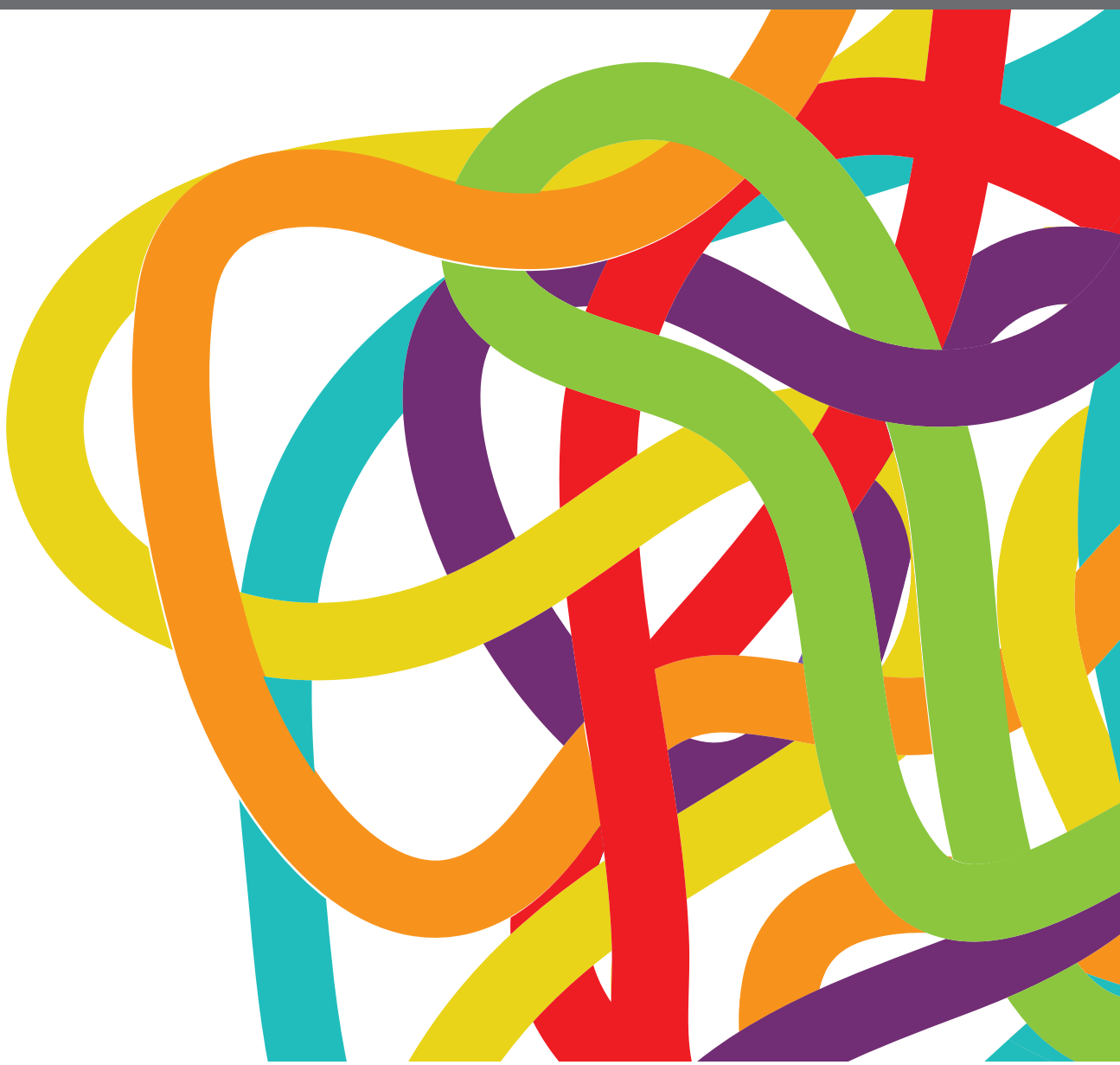

frontiers Research Topics

Frontiers eBook Copyright Statement

The copyright in the text of individual articles in this eBook is the property of their respective authors or their respective institutions or funders. The copyright in graphics and images within each article may be subject to copyright of other parties. In both cases this is subject to a license granted to Frontiers.

The compilation of articles constituting this eBook is the property of Frontiers.

Each article within this eBook, and the eBook itself, are published under the most recent version of the Creative Commons CC-BY licence. The version current at the date of publication of this eBook is CC-BY 4.0. If the CC-BY licence is updated, the licence granted by Frontiers is automatically updated to the new version.

When exercising any right under the CC-BY licence, Frontiers must be attributed as the original publisher of the article or eBook, as applicable.

Authors have the responsibility of ensuring that any graphics or other materials which are the property of others may be included in the CC-BY licence, but this should be checked before relying on the CC-BY licence to reproduce those materials. Any copyright notices relating to those materials must be complied with.

Copyright and source acknowledgement notices may not be removed and must be displayed in any copy, derivative work or partial copy which includes the elements in question.

All copyright, and all rights therein, are protected by national and international copyright laws. The above represents a summary only. For further information please read Frontiers' Conditions for Website Use and Copyright Statement, and the applicable CC-BY licence.

ISSN 1664-8714
ISBN 978-2-88974-317-9
DOI 10.3389/978-2-88974-317-9

About Frontiers

Frontiers is more than just an open-access publisher of scholarly articles: it is a pioneering approach to the world of academia, radically improving the way scholarly research is managed. The grand vision of Frontiers is a world where all people have an equal opportunity to seek, share and generate knowledge. Frontiers provides immediate and permanent online open access to all its publications, but this alone is not enough to realize our grand goals.

Frontiers Journal Series

The Frontiers Journal Series is a multi-tier and interdisciplinary set of open-access, online journals, promising a paradigm shift from the current review, selection and dissemination processes in academic publishing. All Frontiers journals are driven by researchers for researchers; therefore, they constitute a service to the scholarly community. At the same time, the Frontiers Journal Series operates on a revolutionary invention, the tiered publishing system, initially addressing specific communities of scholars, and gradually climbing up to broader public understanding, thus serving the interests of the lay society, too.

Dedication to Quality

Each Frontiers article is a landmark of the highest quality, thanks to genuinely collaborative interactions between authors and review editors, who include some of the world's best academicians. Research must be certified by peers before entering a stream of knowledge that may eventually reach the public - and shape society; therefore, Frontiers only applies the most rigorous and unbiased reviews.
Frontiers revolutionizes research publishing by freely delivering the most outstanding research, evaluated with no bias from both the academic and social point of view. By applying the most advanced information technologies, Frontiers is catapulting scholarly publishing into a new generation.

What are Frontiers Research Topics?

Frontiers Research Topics are very popular trademarks of the Frontiers Journals Series: they are collections of at least ten articles, all centered on a particular subject. With their unique mix of varied contributions from Original Research to Review Articles, Frontiers Research Topics unify the most influential researchers, the latest key findings and historical advances in a hot research area! Find out more on how to host your own Frontiers Research Topic or contribute to one as an author by contacting the Frontiers Editorial Office: frontiersin.org/about/contact

NON-CODING RNAS IN HEAD AND NECK SQUAMOUS CELL CARCINOMA: FUNCTIONAL AND CLINICAL IMPLICATIONS.

Topic Editors:
Wei Cao, Shanghai Jiao Tong University, China
Qiang Shen, Louisiana State University, United States
Ming Yann Lim, Tan Tock Seng Hospital, Singapore

Citation: Cao, W., Shen, Q., Lim, M. Y., eds. (2022). Non-Coding RNAs in Head and Neck Squamous Cell Carcinoma: Functional and Clinical Implications. Lausanne: Frontiers Media SA. doi: 10.3389/978-2-88974-317-9

Table of Contents

06 ***Editorial: "Non-Coding RNAs in Head and Neck Squamous Cell Carcinoma"***
Wei Cao, Qiang Shen and Ming Yann Lim

11 ***Long Non-Coding RNA* LINC02195 *as a Regulator of MHC I Molecules and Favorable Prognostic Marker for Head and Neck Squamous Cell Carcinoma***
Hao Li, Hong-Gang Xiong, Yao Xiao, Qi-Chao Yang, Shao-Chen Yang, Hong-Chao Tang, Wen-Feng Zhang and Zhi-Jun Sun

23 ***Analysis of Differentially Expressed Long Non-coding RNAs and the Associated TF-mRNA Network in Tongue Squamous Cell Carcinoma***
Mi Zhang, Zexi Chen, Sihui Zhang, Ling Wu, Yinghui Jie, Yunyang Liao, Yue Huang, Jiang Chen and Bin Shi

41 ***The Role of lncRNA Crosstalk in Leading Cancer Metastasis of Head and Neck Squamous Cell Carcinoma***
Yu Wang, Sinan Wang, Yu Ren and Xuan Zhou

48 ***Tumor Suppressor* LINC02487 *Inhibits Oral Squamous Cell Carcinoma Cell Migration and Invasion Through the USP17–SNAI1 Axis***
Lu Feng, Jianjun Zhang, Minglei Sun, Feng Qiu, Wantao Chen and Weiliu Qiu

61 ***miR-146a Overexpression in Oral Squamous Cell Carcinoma Potentiates Cancer Cell Migration and Invasion Possibly* via *Targeting HTT***
Liping Wang, Yunxin Chen, Yongyong Yan, Xueqi Guo, Ying Fang, Yucheng Su, Lijing Wang, Janak L. Pathak and Linhu Ge

74 ***Long Noncoding RNA AFAP1-AS1 Is a Critical Regulator of Nasopharyngeal Carcinoma Tumorigenicity***
Min Fang, Minjun Zhang, Yiqing Wang, Fangqiang Wei, Jianhui Wu, Xiaozhou Mou, Yigan Zhang, Xiaodong Liang and Jianming Tang

90 ***Expression Profile of Circular RNAs in Oral Squamous Cell Carcinoma***
Yanxiong Shao, Yuhan Song, Siming Xu, Siyi Li and Haiwen Zhou

102 ***Monocyte Chemoattractant Protein 1 Promotes VEGF-A Expression in OSCC by Activating ILK and MEK1/2 Signaling and Downregulating miR-29c***
Ming-Yu Lien, An-Chen Chang, Hsiao-Chi Tsai, Ming-Hsui Tsai, Chun-Hung Hua, Shih-Ping Cheng, Shih-Wei Wang and Chih-Hsin Tang

113 ***The Role of Exosomes in Thyroid Cancer and Their Potential Clinical Application***
Kaixiang Feng, Runsheng Ma, Lele Zhang, Hongqiang Li, Yifeng Tang, Gongbo Du, Dongpeng Niu and Detao Yin

125 ***CircRNA_ACAP2 Suppresses EMT in Head and Neck Squamous Cell Carcinoma by Targeting the miR-21-5p/STAT3 Signaling Axis***
Chuan Ma, Tingting Shi, Zhuli Qu, Aobo Zhang, Zuping Wu, Huaqiang Zhao, Haoming Zhao and Hongyu Chen

137 ***Down-Regulation of* MiR-181c-5p *Promotes Epithelial-to-Mesenchymal Transition in Laryngeal Squamous Cell Carcinoma* via *Targeting* SERPINE1**
Xin Li, Ping Wu, Yaoyun Tang, Yuhua Fan, Yalan Liu, Xing Fang, Wei Wang and Suping Zhao

151 ***Long Non-Coding RNA MAPK8IP1P2 Inhibits Lymphatic Metastasis of Thyroid Cancer by Activating Hippo Signaling* via *Sponging miR-146b-3p***
Xiaoli Liu, Qingfeng Fu, Xuehai Bian, Yantao Fu, Jingwei Xin, Nan Liang, Shijie Li, Yishen Zhao, Li Fang, Changlin Li, Jiao Zhang, Gianlorenzo Dionigi and Hui Sun

165 ***Downregulation of miR-146b-3p Inhibits Proliferation and Migration and Modulates the Expression and Location of Sodium/Iodide Symporter in Dedifferentiated Thyroid Cancer by Potentially Targeting MUC20***
Shasha Hou, Xiaorui Xie, Jing Zhao, Cailan Wu, Ning Li, Zhaowei Meng, Chunquan Cai and Jian Tan

177 ***Long Noncoding RNAs in the Metastasis of Oral Squamous Cell Carcinoma***
Yuming Xu, Erhui Jiang, Zhe Shao and Zhengjun Shang

192 ***Identification of Three Autophagy-Related Long Non-Coding RNAs as a Novel Head and Neck Squamous Cell Carcinoma Prognostic Signature***
Ya Guo, Peng Tao Yang, Zhong Wei Wang, Kun Xu, Wei Hua Kou and Heng Luo

205 ***Distinguishable Prognostic miRNA Signatures of Head and Neck Squamous Cell Cancer With or Without HPV Infection***
Xiao-jie Luo, Min Zheng, Ming-xin Cao, Wei-long Zhang, Mei-chang Huang, Li Dai, Ya-ling Tang and Xin-hua Liang

216 ***Down-Regulation of Long Non-Coding RNA TINCR Induces Cell Dedifferentiation and Predicts Progression in Oral Squamous Cell Carcinoma***
Zehang Zhuang, Jing Huang, Weiwang Wang, Cheng Wang, Pei Yu, Jing Hu, Haichao Liu, Hanqi Yin, Jinsong Hou and Xiqiang Liu

230 ***A Super-Enhancer Driven by FOSL1 Controls miR-21-5p Expression in Head and Neck Squamous Cell Carcinoma***
Yuehan Wan, Rosalie G. Hoyle, Nan Xie, Wenjin Wang, Hongshi Cai, Ming Zhang, Zhikun Ma, Gan Xiong, Xiuyun Xu, Zhengxian Huang, Xiqiang Liu, Jiong Li and Cheng Wang

240 ***Long Non-Coding RNA LINC01929 Accelerates Progression of Oral Squamous Cell Carcinoma by Targeting the miR-137-3p/FOXC1 Axis***
Hongze Che, Yanhai Che, Zhimin Zhang and Qing Lu

252 ***Research Progress of circRNAs in Head and Neck Cancers***
Panchun Li, Kunjie Zhu, Yongzhen Mo, Xiangying Deng, Xianjie Jiang, Lei Shi, Can Guo, Wenling Zhang, Zhaoyang Zeng, Guiyuan Li, Wei Xiong, Shanshan Zhang and Zhaojian Gong

267 ***A Novel Prognostic Signature Based on Metabolism-Related Genes to Predict Survival and Guide Personalized Treatment for Head and Neck Squamous Carcinoma***
Ying Li, Youliang Weng, Yuhui Pan, Zongwei Huang, Xiaochuan Chen, Wenquan Hong, Ting Lin, Lihua Wang, Wei Liu and Sufang Qiu

282 *LncRNA FENDRR in Carcinoma-Associated Fibroblasts Regulates the Angiogenesis of Oral Squamous Cell Carcinoma Through the PI3K/AKT Pathway*
Yuming Xu, Erhui Jiang, Zhe Shao and Zhengjun Shang

292 *Identification and Confirmation of the miR-30 Family as a Potential Central Player in Tobacco-Related Head and Neck Squamous Cell Carcinoma*
Tingting Zhang, Xueqin Zhu, Qiang Sun, Xing Qin, Zhen Zhang, Yuanyong Feng, Ming Yan and Wantao Chen

frontiers in Oncology

EDITORIAL
published: 23 December 2021
doi: 10.3389/fonc.2021.785001

Editorial: "Non-Coding RNAs in Head and Neck Squamous Cell Carcinoma"

Wei Cao[1,2*], *Qiang Shen*[3] *and Ming Yann Lim*[4]

[1] Department of Oral and Maxillofacial, Head and Neck Oncology, Shanghai Ninth People's Hospital, Shanghai Jiao Tong University School of Medicine, Shanghai, China, [2] Shanghai Key Laboratory of Stomatology, Shanghai Research Institute of Stomatology, National Clinical Research Center of Stomatology, Shanghai, China, [3] Department of Genetics, Stanley S. Scott Cancer Center, School of Medicine, Louisiana State University Health Sciences Center, New Orleans, LA, United States, [4] Department of Otorhinolaryngology, Tan Tock Seng Hospital, Singapore, Singapore

Keywords: non-coding RNAs, microRNAs, circular RNAs, long non-coding RNAs, head and neck squamous cell carcinoma

Editorial on the Research Topic

Non-Coding RNAs in Head and Neck Squamous Cell Carcinoma: Functional and Clinical Implications

Head and Neck Squamous Cell Carcinoma (HNSCC) is one of the most commonly reported malignant tumors in human beings, representing 5.3% of all cancers (1). In the past several years, there has been a lot of progress in revealing the mutational landscape of HNSCC. For example, a series of hotspot mutational genes such as *tumor protein p53* (TP53), *cyclin dependent kinase inhibitor 2A* (CDKN2A), *phosphatase and tensin homolog* (PTEN), *phosphatidylinositol-4,5-bisphosphate 3-kinase catalytic subunit alpha* (PIK3CA), and *notch receptor 1* (NOTCH1) were identified and tumors can be now classified based on genomic profiling (2, 3). In addition, epigenetic profiling revealed non-coding RNAs play a regulatory role in HNSCC (4, 5, Shao et al.). Non–coding RNAs including microRNAs (miRNAs), long non–coding RNAs (lncRNAs) and circular RNAs (circRNAs) have been found to be closely involved in the development and progression of HNSCC and partially associated with clinical significance of HNSCC patients.

PART I: MICRORNAS AND HNSCC

MicroRNAs are non–coding RNAs with about 22 nucleotides long that participate in the post–transcriptional regulation of gene expression involved in the proliferation, migration, metastasis and angiogenesis of cancer (6). For instant, microRNA–125a is responsible for the increased proliferation and migration of cancer cells by inhibiting the expression of the p53 protein (7). MicroRNA–363 promotes increased invasion and metastasis of HNSCC cells by targeting podoplanin protein (8). MicroRNA–300 influences epithelial to mesenchymal transition and metastasis by inhibiting the expression of the Twist (9). Paired box 4 (PAX4)–regulated microRNA–144/451 modulates invasion and metastasis by suppressing disintegrin and metalloproteinases (ADAMs) expression (10). MicroRNA–30e–5p inhibits angiogenesis and metastasis of cancer cells through directly targeting astrocyte elevated gene–1 (AEG–1) in

OPEN ACCESS

Edited and reviewed by:
Jan Baptist Vermorken, University of Antwerp, Belgium

***Correspondence:**
Wei Cao
caowei561521@hotmail.com

Specialty section:
This article was submitted to Head and Neck Cancer, a section of the journal Frontiers in Oncology

Received: *28 September 2021*
Accepted: *09 December 2021*
Published: *23 December 2021*

Citation:
Cao W, Shen Q and Lim MY (2021) Editorial: "Non-Coding RNAs in Head and Neck Squamous Cell Carcinoma". Front. Oncol. 11:785001. doi: 10.3389/fonc.2021.785001

HNSCC (11). In addition, a part of miRNAs derived from serum and salivary were found to be linked to the non–invasive diagnosis and prognosis of HNSCC patients. Serum exosomal microRNA–491–5p and microRNA–941 serve as the promising diagnostic biomarkers for HNSCC, respectively (12, 13). The three miRNA signature (microRNA–383, microRNA–615, and microRNA–877) or two–miRNA signature (miR–626 and miR–5100) act as the diagnostic and prognostic predictors for HNSCC patients, respectively (14, 15). Salivary miR–423–5p,miR–let–7a–5p,miR–3928 and a three–miRNA panel (miR–9, miR–134 and miR–191) could be used as novel non–invasive diagnostic biomarkers for HNSCC (16–18). More and more novel researches continue to strengthen the position of miRNAs as important regulator and useful biomarker in HNSCC as time goes on.

PART II: LONG NON–CODING RNAS AND HNSCC

LncRNAs also belong to a subgroup of non–coding RNAs that are at least 200 nucleotides long and the majority of them do not have proteincoding ability (19). lncRNAs can be detected both in the nucleus and cytoplasm, and their different locations mean different functions that were involved in regulation of gene expression, e.g., chromatin modification, interaction with transcriptional factors, mRNA processing, cell metabolism, proliferation, apoptosis, acting as "molecular sponge" and creating ribonucleoprotein complexes (19–22). For example, Metastasis–associated lung adenocarcinoma transcript 1 (MALAT1) has one of the most conserved primary and secondary structures of all lncRNAs (23). Knockdown of MALAT–1 led to impaired migration and proliferation ability *in vitro* and fewer metastases *in vivo* in HNSCC cells (24). MALAT–1 transcriptionally activated by signal transducer and activator of transcription 3 (STAT3) induces epithelial–to–mesenchymal transition (EMT) and accelerates HNSCC metastasis by interacting reciprocally with miR–30a (25). HOX transcript antisense RNA (HOTAIR) is expressed from locus *homeobox C cluster* (HOXC) and lncRNA HOTAIR transcriptionally activated by STAT3 interact with pEZH2–S21 resulting in proliferation and the growth of HNSCC xenograft tumors *in vivo* (26). Besides, some of lncRNAs functionally act as tumor suppressors, e.g., lincRNA–p21 (27) or LINC02487(Feng et al.), long non–coding RNA Fer–1–like protein 4 (FER1L4) (28), and growth arrest specific 5 (GAS5) (29), but others play an oncogenic role, e.g., ring finger and CCCH–type domains 2 (RC3H2) (30), FOXD2 adjacent opposite strand RNA 1 (FOXD2–AS1) (31), KTN1 antisense RNA 1(KTN1–AS1) (32), LINC00460 (33), H19 imprinted maternally expressed transcript (H19) (34), small nucleolar RNA host gene 6 (SNHG6) (35), urothelial cancer associated 1 (UCA1) (36), or ZNFX1 antisense RNA 1 (ZFAS1) (37), and can be used as therapeutic targets in the future. More and more evidences show that multiple lncRNAs–based signatures could be diagnostic and prognostic predictors of HNSCC patients by mathematical modeling. A nomogram based on an 8–lncRNA signature was identified as a novel diagnostic biomarker for HNSCC (38). A three–lncRNA signature was screened and identified to well predict the survival of HNSCC patients (39). Immune–related and autophagy–related lncRNA signatures were respectively developed into prognostic indicator for HNSCC (40, Guo et al).

PART III: CIRCULAR RNAS AND HNSCC

circRNAs are a novel subclass of non–coding RNAs, which are produced by reverse splicing and are characterized by a closed single–stranded structure and lack of 5′cap and 3′polyadenylation [poly(A)] tail (41). Currently, the most established function of circRNAs is that circRNAs can act as miRNA sponges resulting in the initiation and progression of cancer and play a regulatory role in the tumor microenvironment (TME) (42, 43). For example, circRNA Pvt1 oncogene (circPVT1) transcriptionally enhanced by the mut–p53/Yes1 associated transcriptional regulator (YAP)/TEAD complex promotes the proliferation of HNSCC cells by modulating the expression of miR–497–5p (44). CircRNA_036186 likely regulates 14–3–3ζ expression by functioning as a ceRNA in the development and progression of HNSCC (45). And the function as a ceRNA was also found to be in circRNA_100533 (46), circRNA myosin light chain kinase (circMYLK) (47), circRNA_0042666 (48), circRNA_100290 (49), circRNA_0000140 (50), circRNA Matrin 3(circMATR3) (51), circRNA_0000495 (52),circRNA coronin 1C (circCORO1C) (53), circRNA_0036722 (54), circRNA_0000218 (55), circRNA epithelial stromal interaction 1(circEPSTI1) (56), circRNA_103862 (57), circRNA_009755 (58), circRNA septin 9 (circSEPT9) (59), circRNA par–3 family cell polarity regulator (circPARD3) (60), circRNA BICD cargo adaptor 2 (circBICD2) (61), circKIAA0907 (62), circRNA_0023028 (63), circRNA_0000700 (64), circRNA ATP binding cassette subfamily B member 10 (circABCB10) (65), circRNA_0042823 (66), circBCL11B (67), circRNA fibronectin type III domain containing 3B (circFNDC3B) (68), and circRNA PTPRF interacting protein alpha 1(circPPFIA1) (69). In addition, a few circRNAs can directly interact with proteins and enzymes as protein scaffolds. For instance, circRNA G protein subunit gamma 7 (circGNG7) inhibits HNSCC cell proliferation by binding to serine residues 78 and 82 of Heat shock protein 27 (HSP27) (70). CircRNA FAT atypical cadherin 1(circFAT1) prevents STAT3 dephosphorylation by binding to STAT3, resulting in HNSCC stemness and immune evasion (71). Due to more stable than lncRNA and miRNA, circRNAs are regarded as an ideal diagnostic predictor tool in clinical practice. In HNSCC, circRNA_0003829 and circRNA_0036722 serve as diagnostic predictors with AUC=0.81 and AUC=0.83, respectively (54, 72). Plasma–derived the three circRNA panel well predicts the occurrence of HNSCC (73).

This Research Topic *"Non–coding RNAs in Head and Neck Squamous Cell Carcinoma: Functional and Clinical Implications"* includes 21 original articles and 3 review articles, which highlight the regulatory mechanism and clinical relevance of non–coding RNAs in HNSCC. For example, Wan et al. identifies a super–enhancer regulatory model of miR–21–5p by FOS like 1

(FOSL1), promoting malignant progression of HNSCC. The article by Li et al. discuss LINC02195 as a regulator of MHC I and the number of $CD8^+$ and $CD4^+$ T cells in the tumor microenvironment. Moreover, Wang et al. summarizes the crosstalk between lncRNAs and microRNAs as well as the detailed regulatory mechanism of the interaction. Additionally, Luo et al. identifies miRNAs signatures respectively for HPV+ and HPV− HNSCC, which are of great significance in evaluating patient survival. All of other articles mainly discuss the potential function of non–coding RNA as a ceRNA in HNSCC.

AUTHOR CONTRIBUTIONS

All authors listed have made a substantial, direct and intellectual contribution to the work, and approved it for publication.

FUNDING

WC was supported by grants from the National Natural Science Foundation of China (81972589).

REFERENCES

1. Aupérin A. Epidemiology of Head and Neck Cancers: An Update. *Curr Opin Oncol* (2020) 32(3):178–86. doi: 10.1097/CCO.0000000000000629
2. Stransky N, Egloff AM, Tward AD, Kostic AD, Cibulskis K, Sivachenko A, et al. The Mutational Landscape of Head and Neck Squamous Cell Carcinoma. *Science* (2011) 333:1157–60. doi: 10.1126/science.1208130
3. Agrawal N, Frederick MJ, Pickering CR, Bettegowda C, Chang K, Li RJ, et al. Exome Sequencing of Head and Neck Squamous Cell Carcinoma Reveals Inactivating Mutations in NOTCH1. *Science* (2011) 333:1154–7. doi: 10.1126/science.1206923
4. Karatas OF, Oner M, Abay A, Diyapoglu A. MicroRNAs in Human Tongue Squamous Cell Carcinoma: From Pathogenesis to Therapeutic Implications. *Oral Oncol* (2017) 67:124–30. doi: 10.1016/j.oraloncology.2017.02.015
5. Nohata N, Abba MC, Gutkind JS. Unraveling the Oral Cancer Lncrnaome: Identification of Novel lncRNAs Associated With Malignant Progression and HPV Infection. *Oral Oncol* (2016) 59:58–66. doi: 10.1016/j.oraloncology.2016.05.014
6. Nowicka Z, Stawiski K, Tomasik B, Fendler W. Extracellular miRNAs as Biomarkers of Head and Neck Cancer Progression and Metastasis. *Int J Mol Sci* (2019) 20:4799. doi: 10.3390/ijms20194799
7. Peng SY, Tu HF, Yang CC, Wu CH, Liu CJ, Chang KW, et al. miR–134 Targets PDCD7 to Reduce E–Cadherin Expression and Enhance Oral Cancer Progression. *Int J Cancer* (2018) 143(11):2892–904. doi: 10.1002/ijc.31638
8. Sun Q, Zhang J, Cao W, Wang X, Xu Q, Yan M, et al. Dysregulated miR–363 Affects Head and Neck Cancer Invasion and Metastasis by Targeting Podoplanin. *Int J Biochem Cell Biol* (2013) 45(3):513–20. doi: 10.1016/j.biocel.2012.12.004
9. Yu J, Xie F, Bao X, Chen W, Xu Q. miR–300 Inhibits Epithelial to Mesenchymal Transition and Metastasis by Targeting Twist in Human Epithelial Cancer. *Mol Cancer* (2014) 13:121. doi: 10.1186/1476–4598–13–121
10. Zhang J, Qin X, Sun Q, Guo H, Wu X, Xie F, et al. Transcriptional Control of PAX4–Regulated miR–144/451 Modulates Metastasis by Suppressing ADAMs Expression. *Oncogene* (2015) 34(25):3283–95. doi: 10.1038/onc.2014.259
11. Zhang S, Li G, Liu C, Lu S, Jing Q, Chen X, et al. miR–30e–5p Represses Angiogenesis and Metastasis by Directly Targeting AEG–1 in Squamous Cell Carcinoma of the Head and Neck. *Cancer Sci* (2020) 111(2):356–68. doi: 10.1111/cas.14259
12. Panvongsa W, Siripoon T, Worakitchanon W, Arsa L, Trachu N, Jinawath N, et al. Plasma Extracellular Vesicle microRNA–491–5p as Diagnostic and Prognostic Marker for Head and Neck Squamous Cell Carcinoma. *Cancer Sci* (2021) 112(10):4257–69. doi: 10.1111/cas.15067
13. Zhao Q, Zheng X, Guo H, Xue X, Zhang Y, Niu M, et al. Serum Exosomal miR–941 as a Promising Oncogenic Biomarker for Laryngeal Squamous Cell Carcinoma. *J Cancer* (2020) 11(18):5329–44. doi: 10.7150/jca.45394
14. Liu C, Yu Z, Huang S, Zhao Q, Sun Z, Fletcher C, et al. Combined Identification of Three miRNAs in Serum as Effective Diagnostic Biomarkers for HNSCC. *EBioMedicine* (2019) 50:135–43. doi: 10.1016/j.ebiom.2019.11.016
15. Shi J, Bao X, Liu Z, Zhang Z, Chen W, Xu Q. Serum miR–626 and miR–5100 are Promising Prognosis Predictors for Oral Squamous Cell Carcinoma. *Theranostics* (2019) 9(4):920–31. doi: 10.7150/thno.30339
16. Romani C, Salviato E, Paderno A, Zanotti L, Ravaggi A, Deganello A, et al. Genome–Wide Study of Salivary miRNAs Identifies miR–423–5p as Promising Diagnostic and Prognostic Biomarker in Oral Squamous Cell Carcinoma. *Theranostics* (2021) 11(6):2987–99. doi: 10.7150/thno.45157
17. Fadhil RS, Wei MQ, Nikolarakos D, Good D, Nair RG. Salivary microRNA miR–Let–7a–5p and miR–3928 Could Be Used as Potential Diagnostic Bio–Markers for Head and Neck Squamous Cell Carcinoma. *PloS One* (2020) 15(3):e0221779. doi: 10.1371/journal.pone.0221779
18. Salazar C, Nagadia R, Pandit P, Cooper–White J, Banerjee N, Dimitrova N, et al. A Novel Saliva–Based microRNA Biomarker Panel to Detect Head and Neck Cancers. *Cell Oncol (Dordr)* (2014) 37(5):331–8. doi: 10.1007/s13402–014–0188–2
19. Mercer TR, Dinger ME, Mattick JS. Long non–Coding RNAs: Insights Into Functions. *Nat Rev Genet* (2009) 10(3):155–9. doi: 10.1038/nrg2521
20. Prensner JR, Chinnaiyan AM. The Emergence of lncRNAs in Cancer Biology. *Cancer Discovery* (2011) 1(5):391–407. doi: 10.1158/2159–8290.CD–11–0209
21. Schmitt AM, Chang HY. Long Noncoding RNAs in Cancer Pathways. *Cancer Cell* (2016) 29(4):452–63. doi: 10.1016/j.ccell.2016.03.010
22. Jiang C, Li X, Zhao H, Liu H. Long Non–Coding RNAs: Potential New Biomarkers for Predicting Tumor Invasion and Metastasis. *Mol Cancer* (2016) 15(1):62. doi: 10.1186/s12943–016–0545–z
23. Tripathi V, Ellis JD, Shen Z, Song DY, Pan Q, Watt AT, et al. The Nuclear–Retained Noncoding RNA MALAT1 Regulates Alternative Splicing by Modulating SR Splicing Factor Phosphorylation. *Mol Cell* (2010) 39(6):925–38. doi: 10.1016/j.molcel.2010.08.011
24. Fang Z, Zhang S, Wang Y, Shen S, Wang F, Hao Y, et al. Long non–Coding RNA MALAT–1 Modulates Metastatic Potential of Tongue Squamous Cell Carcinomas Partially Through the Regulation of Small Proline Rich Proteins. *BMC Cancer* (2016) 16(1):706. doi: 10.1186/s12885–016–2735–x
25. Wang Y, Wu C, Zhang C, Li Z, Zhu T, Chen J, et al. TGF–β–Induced STAT3 Overexpression Promotes Human Head and Neck Squamous Cell Carcinoma Invasion and Metastasis Through Malat1/miR–30a Interactions. *Cancer Lett* (2018) 436:52–62. doi: 10.1016/j.canlet.2018.08.009
26. Sun S, Wu Y, Guo W, Yu F, Kong L, Ren Y, et al. STAT3/HOTAIR Signaling Axis Regulates HNSCC Growth in an EZH2–Dependent Manner. *Clin Cancer Res* (2018) 24(11):2665–77. doi: 10.1158/1078–0432.CCR–16–2248
27. Jin S, Yang X, Li J, Yang W, Ma H, Zhang Z. P53–Targeted lincRNA–P21 Acts as a Tumor Suppressor by Inhibiting JAK2/STAT3 Signaling Pathways in Head and Neck Squamous Cell Carcinoma. *Mol Cancer* (2019) 18(1):38. doi: 10.1186/s12943–019–0993–3
28. Jiao L, Liu S, Liu L, Hao P, Gong Z, Yan Z, et al. Long non–Coding RNA Fer–1–Like Family Member 4 Serves as a Tumor Suppressor in Laryngeal Squamous Cell Carcinoma Cells *via* Regulating the AKT/ERK Signaling Pathway. *Mol Med Rep* (2020) 22(6):5304–12. doi: 10.3892/mmr.2020.11598
29. Wang J, Zhu Y, Ni S, Liu S. LncRNA GAS5 Suppressed Proliferation and Promoted Apoptosis in Laryngeal Squamous Cell Carcinoma by Targeting MiR–26a–5p and Modifying Ulk2. *Cancer Manag Res* (2021) 13:871–87. doi: 10.2147/CMAR.S250778
30. Wu K, Jiang Y, Zhou W, Zhang B, Li Y, Xie F, et al. Long Noncoding RNA RC3H2 Facilitates Cell Proliferation and Invasion by Targeting MicroRNA–101–3p/EZH2 Axis in OSCC. *Mol Ther Nucleic Acids* (2020) 20:97–110. doi: 10.1016/j.omtn.2020.02.006

31. Liu Z, Zhou W, Lin C, Wang X, Zhang X, Zhang Y, et al. Dysregulation of FOXD2–AS1 Promotes Cell Proliferation and Migration and Predicts Poor Prognosis in Oral Squamous Cell Carcinoma: A Study Based on TCGA Data. *Aging (Albany NY)* (2020) 13(2):2379–96. doi: 10.18632/aging.202268
32. Jiang Y, Wu K, Cao W, Xu Q, Wang X, Qin X, et al. Long Noncoding RNA KTN1–AS1 Promotes Head and Neck Squamous Cell Carcinoma Cell Epithelial–Mesenchymal Transition by Targeting miR–153–3p. *Epigenomics* (2020) 12(6):487–505. doi: 10.2217/epi–2019–0173
33. Jiang Y, Cao W, Wu K, Qin X, Wang X, Li Y, et al. LncRNA LINC00460 Promotes EMT in Head and Neck Squamous Cell Carcinoma by Facilitating Peroxiredoxin–1 Into the Nucleus. *J Exp Clin Cancer Res* (2019) 38(1):365. doi: 10.1186/s13046–019–1364–z
34. Guan GF, Zhang DJ, Wen LJ, Xin D, Liu Y, Yu DJ, et al. Overexpression of lncRNA H19/miR–675 Promotes Tumorigenesis in Head and Neck Squamous Cell Carcinoma. *Int J Med Sci* (2016) 13(12):914–22. doi: 10.7150/ijms.16571
35. Guo T, Zambo KDA, Zamuner FT, Ou T, Hopkins C, Kelley DZ, et al. Chromatin Structure Regulates Cancer–Specific Alternative Splicing Events in Primary HPV–Related Oropharyngeal Squamous Cell Carcinoma. *Epigenetics* (2020) 15(9):959–71. doi: 10.1080/15592294.2020.1741757
36. Qian Y, Liu D, Cao S, Tao Y, Wei D, Li W, et al. Upregulation of the Long Noncoding RNA UCA1 Affects the Proliferation, Invasion, and Survival of Hypopharyngeal Carcinoma. *Mol Cancer* (2017) 16(1):68. doi: 10.1186/s12943–017–0635–6
37. Kolenda T, Guglas K, Kopczyńska M, Teresiak A, Bliźniak R, Mackiewicz A, et al. Oncogenic Role of ZFAS1 lncRNA in Head and Neck Squamous Cell Carcinomas. *Cells* (2019) 8(4):366. doi: 10.3390/cells8040366
38. Mao R, Chen Y, Xiong L, Liu Y, Zhang T. Identification of a Nomogram Based on an 8–lncRNA Signature as a Novel Diagnostic Biomarker for Head and Neck Squamous Cell Carcinoma. *Aging (Albany NY)* (2020) 12(20):20778–800. doi: 10.18632/aging.104014
39. Cao W, Liu JN, Liu Z, Wang X, Han ZG, Ji T, et al. A three–lncRNA Signature Derived From the Atlas of ncRNA in Cancer (TANRIC) Database Predicts the Survival of Patients With Head and Neck Squamous Cell Carcinoma. *Oral Oncol* (2017) 65:94–101. doi: 10.1016/j.oraloncology.2016.12.017
40. Chen Y, Luo TQ, Xu SS, Chen CY, Sun Y, Lin L, et al. An Immune–Related seven–lncRNA Signature for Head and Neck Squamous Cell Carcinoma. *Cancer Med* (2021) 10(7):2268–85. doi: 10.1002/cam4.3756
41. Meng S, Zhou H, Feng Z, Xu Z, Tang Y, Li P, et al. CircRNA: Functions and Properties of a Novel Potential Biomarker for Cancer. *Mol Cancer* (2017) 16 (1):94. doi: 10.1186/s12943–017–0663–2
42. He J, Xie Q, Xu H, Li J, Li Y. Circular RNAs and Cancer. *Cancer Lett* (2017) 396:138–44. doi: 10.1016/j.canlet.2017.03.027
43. Ma Z, Shuai Y, Gao X, Wen X, Ji J. Circular RNAs in the Tumour Microenvironment. *Mol Cancer* (2020) 19(1):8. doi: 10.1186/s12943–019–1113–0
44. Verduci L, Ferraiuolo M, Sacconi A, Ganci F, Vitale J, Colombo T, et al. The Oncogenic Role of Circpvt1 in Head and Neck Squamous Cell Carcinoma is Mediated Through the Mutant P53/YAP/TEAD Transcription–Competent Complex. *Genome Biol* (2017) 18(1):237. doi: 10.1186/s13059–017–1368–y
45. Wang WL, Yang Z, Zhang YJ, Lu P, Ni YK, Sun CF, et al. Competing Endogenous RNA Analysis Reveals the Regulatory Potency of circRNA_036186 in HNSCC. *Int J Oncol* (2018) 53(4):1529–43. doi: 10.3892/ijo.2018.4499
46. Zhu X, Shao P, Tang Y, Shu M, Hu WW, Zhang Y. Hsa_circRNA_100533 Regulates GNAS by Sponging Hsa_Mir_933 to Prevent Oral Squamous Cell Carcinoma. *J Cell Biochem* (2019) 120(11):19159–71. doi: 10.1002/jcb.29245
47. Duan X, Shen N, Chen J, Wang J, Zhu Q, Zhai Z. Circular RNA MYLK Serves as an Oncogene to Promote Cancer Progression *via* microRNA–195/Cyclin D1 Axis in Laryngeal Squamous Cell Carcinoma. *Biosci Rep* (2019) 39(9): BSR20190227. doi: 10.1042/BSR20190227
48. Wei Z, Chang K, Fan C. Hsa_circ_0042666 Inhibits Proliferation and Invasion *via* Regulating miR–223/TGFBR3 Axis in Laryngeal Squamous Cell Carcinoma. *BioMed Pharmacother* (2019) 119:109365. doi: 10.1016/j.biopha.2019.109365
49. Wang Z, Huang C, Zhang A, Lu C, Liu L. Overexpression of circRNA_100290 Promotes the Progression of Laryngeal Squamous Cell Carcinoma Through the miR–136–5p/RAP2C Axis. *BioMed Pharmacother* (2020) 125:109874. doi: 10.1016/j.biopha.2020.109874
50. Peng QS, Cheng YN, Zhang WB, Fan H, Mao QH, Xu P. circRNA_0000140 Suppresses Oral Squamous Cell Carcinoma Growth and Metastasis by Targeting miR–31 to Inhibit Hippo Signaling Pathway. *Cell Death Dis* (2020) 11(2):112. doi: 10.1038/s41419–020–2273–y
51. Wang Z, Wei P, Wei D, Cao S, Liu H, Chen L, et al. Effect of Up–Regulation of Circmatr3 on the Proliferation, Metastasis, Progression and Survival of Hypopharyngeal Carcinoma. *J Cell Mol Med* (2020) 24(8):4687–97. doi: 10.1111/jcmm.15134
52. Hao Y, Zhang D, Guo Y, Fu Z, Yu D, Guan G. miR–488–3p Sponged by Circ–0000495 and Mediated Upregulation of TROP2 in Head and Neck Squamous Cell Carcinoma Development. *J Cancer* (2020) 11(11):3375–86. doi: 10.7150/jca.40339
53. Wu Y, Zhang Y, Zheng X, Dai F, Lu Y, Dai L, et al. Circular RNA Circcoro1c Promotes Laryngeal Squamous Cell Carcinoma Progression by Modulating the Let–7c–5p/PBX3 Axis. *Mol Cancer* (2020) 19(1):99. doi: 10.1186/s12943–020–01215–4
54. Guo Y, Huang Q, Zheng J, Hsueh CY, Yuan X, Heng Y, et al. Diagnostic Role of Dysregulated Circular RNA Hsa_Circ_0036722 in Laryngeal Squamous Cell Carcinoma. *Onco Targets Ther* (2020) 13:5709–19. doi: 10.2147/OTT.S231076
55. Bai Y, Hou J, Wang X, Geng L, Jia X, Xiang L, et al. Circ_0000218 Plays a Carcinogenic Role in Laryngeal Cancer Through Regulating microRNA–139–3p/Smad3 Axis. *Pathol Res Pract* (2020) 216(9):153103. doi: 10.1016/j.prp.2020.153103
56. Wang J, Jiang C, Li N, Wang F, Xu Y, Shen Z, et al. The Circepsti1/Mir–942–5p/LTBP2 Axis Regulates the Progression of OSCC in the Background of OSF *via* EMT and the PI3K/Akt/mTOR Pathway. *Cell Death Dis* (2020) 11(8):682. doi: 10.1038/s41419–020–02851–w
57. Wang X, Wu T, Wang P, Yang L, Li Q, Wang J, et al. Circular RNA 103862 Promotes Proliferation and Invasion of Laryngeal Squamous Cell Carcinoma Cells Through the miR–493–5p/GOLM1 Axis. *Front Oncol* (2020) 10:1064. doi: 10.3389/fonc.2020.01064
58. Zhang B, Wang Z, Shen Y, Yang H. Silencing Circular RNA Hsa_Circ_009755 Promotes Growth and Metastasis of Oral Squamous Cell Carcinoma. *Genomics* (2020) 112(6):5275–81. doi: 10.1016/j.ygeno.2020.09.035
59. Ai Y, Tang Z, Zou C, Wei H, Wu S, Huang D. Circ_SEPT9, a Newly Identified Circular RNA, Promotes Oral Squamous Cell Carcinoma Progression Through miR–1225/PKN2 Axis. *J Cell Mol Med* (2020) 24(22):13266–77. doi: 10.1111/jcmm.15943
60. Gao W, Guo H, Niu M, Zheng X, Zhang Y, Xue X, et al. Circpard3 Drives Malignant Progression and Chemoresistance of Laryngeal Squamous Cell Carcinoma by Inhibiting Autophagy Through the PRKCI–Akt–mTOR Pathway. *Mol Cancer* (2020) 19(1):166. doi: 10.1186/s12943–020–01279–2
61. Qiu L, Zheng L, Gan C, Deng W, Sun Y, Wang T. Circbicd2 Targets miR–149–5p/IGF2BP1 Axis to Regulate Oral Squamous Cell Carcinoma Progression. *J Oral Pathol Med* (2021) 50(7):668–80. doi: 10.1111/jop.13156
62. Dong W, Zhao L, Zhang S, Zhang S, Si H. Circ–KIAA0907 Inhibits the Progression of Oral Squamous Cell Carcinoma by Regulating the miR–96–5p/UNC13C Axis. *World J Surg Oncol* (2021) 19(1):75. doi: 10.1186/s12957–021–02184–8
63. Zheng Y, Duan L, Yang Y, Luo D, Yan B. Circ_0023028 Contributes to the Progression of Laryngeal Squamous Cell Carcinoma by Upregulating LASP1 Through miR–486–3p. *Mol Cell Biochem* (2021) 476(8):2951–61. doi: 10.1007/s11010–021–04129–x
64. Fang J, Ji WH, Wang FZ, Xie TM, Wang L, Fu ZF, et al. Circular RNA Hsa_Circ_0000700 Promotes Cell Proliferation and Migration in Esophageal Squamous Cell Carcinoma by Sponging miR–1229. *J Cancer* (2021) 12 (9):2610–23. doi: 10.7150/jca.47112
65. Zhao J, Li XD, Wang M, Song LN, Zhao MJ. Circular RNA ABCB10 Contributes to Laryngeal Squamous Cell Carcinoma (LSCC) Progression by Modulating the miR–588/CXCR4 Axis. *Aging (Albany NY)* (2021) 13 (10):14078–87. doi: 10.18632/aging.203025
66. Wu T, Sun Y, Sun Z, Li S, Wang W, Yu B, et al. Hsa_circ_0042823 Accelerates Cancer Progression *via* miR–877–5p/FOXM1 Axis in Laryngeal Squamous Cell Carcinoma. *Ann Med* (2021) 53(1):960–70. doi: 10.1080/07853890.2021.1934725
67. Zeng W, Guo M, Yao L, Deng Z. Circular RNA Hsa_Circ_0033144 (CircBCL11B) Regulates Oral Squamous Cell Carcinoma Progression *via*

the miR–579/LASP1 Axis. *Bioengineered* (2021) 12(1):4111–22. doi: 10.1080/21655979.2021.1953214

68. Yang J, Cao XH, Luan KF, Huang YD. Circular RNA FNDC3B Protects Oral Squamous Cell Carcinoma Cells From Ferroptosis and Contributes to the Malignant Progression by Regulating miR–520d–5p/SLC7A11 Axis. *Front Oncol* (2021) 11:672724. doi: 10.3389/fonc.2021.672724
69. Shuang Y, Liu J, Niu J, Guo W, Li C. A Novel Circular RNA Circppfia1 Promotes Laryngeal Squamous Cell Carcinoma Progression Through Sponging miR–340–3p and Regulating ELK1 Expression. *Bioengineered* (2021) 12(1):5220–30. doi: 10.1080/21655979.2021.1959866
70. Ju H, Hu Z, Wei D, Huang J, Zhang X, Rui M, et al. A Novel Intronic Circular RNA, Circgng7, Inhibits Head and Neck Squamous Cell Carcinoma Progression by Blocking the Phosphorylation of Heat Shock Protein 27 at Ser78 and Ser82. *Cancer Commun (Lond)* (2021) 41(11):1152–72. doi: 10.1002/cac2.12213
71. Jia L, Wang Y, Wang CY. Circfat1 Promotes Cancer Stemness and Immune Evasion by Promoting STAT3 Activation. *Adv Sci (Weinh)* (2021) 8 (13):2003376. doi: 10.1002/advs.202003376
72. Zhang H, Shen Y, Zhang B, Qian M, Zhang Y, Yang H. Hsa_circ_0003829 Serves as a Potential Diagnostic Predictor for Oral Squamous Cell Carcinoma. *J Int Med Res* (2020) 48(9):300060520936880. doi: 10.1177/0300060520936880
73. Han J, Lin Q, Dong C. Plasma Cell–Free circRNAs Panel Act as Fingerprint Predicts the Occurrence of Laryngeal Squamous Cell Carcinoma. *Aging (Albany NY)* (2021) 13(13):17328–36. doi: 10.18632/aging.203215

Conflict of Interest: The authors declare that the research was conducted in the absence of any commercial or financial relationships that could be construed as a potential conflict of interest.

Publisher's Note: All claims expressed in this article are solely those of the authors and do not necessarily represent those of their affiliated organizations, or those of the publisher, the editors and the reviewers. Any product that may be evaluated in this article, or claim that may be made by its manufacturer, is not guaranteed or endorsed by the publisher.

Copyright © 2021 Cao, Shen and Lim. This is an open-access article distributed under the terms of the Creative Commons Attribution License (CC BY). The use, distribution or reproduction in other forums is permitted, provided the original author(s) and the copyright owner(s) are credited and that the original publication in this journal is cited, in accordance with accepted academic practice. No use, distribution or reproduction is permitted which does not comply with these terms.

frontiers in Oncology

ORIGINAL RESEARCH
published: 06 May 2020
doi: 10.3389/fonc.2020.00615

Long Non-coding RNA *LINC02195* as a Regulator of MHC I Molecules and Favorable Prognostic Marker for Head and Neck Squamous Cell Carcinoma

Hao Li[1†], *Hong-Gang Xiong*[1†], *Yao Xiao*[1], *Qi-Chao Yang*[1], *Shao-Chen Yang*[1], *Hong-Chao Tang*[1], *Wen-Feng Zhang*[1,2*] *and Zhi-Jun Sun*[1,2*]

[1] *The State Key Laboratory Breeding Base of Basic Science of Stomatology (Hubei-MOST) & Key Laboratory of Oral Biomedicine Ministry of Education, School & Hospital of Stomatology, Wuhan University, Wuhan, China,* [2] *Department of Oral and Maxillofacial Head Neck Surgery, School & Hospital of Stomatology, Wuhan University, Wuhan, China*

OPEN ACCESS

Edited by:
Wei Cao,
Shanghai Jiao Tong University, China

Reviewed by:
Cheng Wang,
Sun Yat-sen University, China
Xuan Zhou,
Tianjin Medical University Cancer Institute and Hospital, China

***Correspondence:**
Wen-Feng Zhang
zhangwf59@whu.edu.cn
Zhi-Jun Sun
sunzj@whu.edu.cn

[†] *These authors have contributed equally to this work*

Specialty section:
This article was submitted to Head and Neck Cancer, a section of the journal Frontiers in Oncology

Received: *05 March 2020*
Accepted: *03 April 2020*
Published: *06 May 2020*

Citation:
Li H, Xiong H-G, Xiao Y, Yang Q-C, Yang S-C, Tang H-C, Zhang W-F and Sun Z-J (2020) Long Non-coding RNA LINC02195 as a Regulator of MHC I Molecules and Favorable Prognostic Marker for Head and Neck Squamous Cell Carcinoma. Front. Oncol. 10:615. doi: 10.3389/fonc.2020.00615

The loss of major histocompatibility complex class I (MHC I) molecules is an important mechanism by which cancer cells escape immunosurveillance in head and neck squamous cell carcinoma (HNSCC). Several long non-coding RNAs (lncRNAs) have been implicated in immune response and regulation including antigen processing and presentation. However, few studies on lncRNAs regulating MHC I expression in HNSCC have been conducted. In this study, MHC I related lncRNAs were identified from the The Cancer Genome Atlas (TCGA) HNSCC database. One of the lncRNAs, *long intergenic non-protein coding RNA 2195* (*LINC02195*), was found to be associated with genes encoding MHC I molecules and patient prognosis in the TCGA database. KEGG and GO analyses suggested that *LINC02195* was closely related to antigen processing and presentation. qRT-PCR revealed high expression of *LINC02195* in human HNSCC tissues and HNSCC cell lines compared with normal mucosal tissues. *in situ* hybridization of the HNSCC tissue microarray revealed a correlation between high *LINC02195* expression and a favorable prognosis in our patient cohort. Silencing of *LINC02195* decreased MHC I protein expression, as evidenced by western blotting. Multiplex immunochemistry was performed to reveal the positive correlation between high *LINC02195* expression and an increased number of $CD8^+$ and $CD4^+$ T cells in the tumor microenvironment. Based on our study, *LINC02195* is a promising prognostic marker and a target for future therapeutic interventions.

Keywords: lncRNA, MHC, TCGA, tumor microenvironment, T cell

INTRODUCTION

Head and neck squamous cell carcinoma (HNSCC) accounts for 90% of all cases of head and neck cancers, which causes ∼430,000 deaths worldwide (1). HNSCC normally occurs in epithelial cells, including the mucosal lining of the upper airway and food passages (2). The general primary treatments for HNSCC include surgery, radiotherapy, chemotherapy and targeted therapy (3). In addition to these traditional treatments, immune checkpoint blockades such as anti-programmed cell death 1 (anti-PD-1) and anti-programmed

cell death 1 ligand 1 (anti-PD-L1) antibodies have displayed great efficacy in the treatment of HNSCC (3, 4). However, the response rate to immune checkpoint blockades remains poor (3, 5). To increase the response rate, we should reveal the immunosuppressive mechanisms of tumors.

One of the roles of the innate and adaptive immune systems is to eliminate tumors before they are detectable. One of the mechanisms by which malignant cells escape immunosurveillance and elimination is the loss or downregulation of major histocompatibility complex class I (MHC I) molecules, limiting the recognition of tumor antigens by cytotoxic $CD8^+$ T cells, which attack malignant cells (6). MHC I molecules are encoded by *human leukocyte antigen class I* (*HLA I*) genes mainly including *HLA-A*, *HLA-B,* and *HLA-C*, and are expressed by all somatic cells in humans (7). The deregulation of MHC I has been observed in various forms of cancer (8–10). Patients with lower levels of MHC I expression have poor survival for HNSCC (10). In addition, downregulation of MHC I in cancer cells was recently shown to be a mechanism underlying the immunotherapy resistance of cancer (11).

Long non-coding RNAs (lncRNAs) comprise various RNAs that are <200 nucleotides in length and have no protein-coding capacity. Several lncRNAs are abnormally expressed in various forms of cancer and are involved in the occurrence and development of tumors (12–14). With an increased understanding of lncRNAs, the important value of lncRNAs in treating tumors or predicting the prognosis of patients with tumors has been recognized (15). Notably, studies have recently been reported that some lncRNAs are identified as regulators of human immune system, particularly in anti-tumor immunity (16–18). A recent study discovered the association between lncRNAs and MHC I molecules. According to previous gene expression studies, the expression of the lncRNA *HCP5* is associated with *HLA-B* expression (19). The lncRNA *HOTAIR* was recently shown to promote *HLA-G* expression in gastric cancer (20). However, few studies on lncRNAs regulating MHC I expression in HNSCC have been performed.

Here, several differentially expressed lncRNAs were identified by analyzing of The Cancer Genome Atlas (TCGA) database. Furthermore, we investigated a highly expressed lncRNA, *long intergenic non-protein coding RNA 2195* (*LINC02195*, ENSG00000236481), which is closely associated with *HLA-A*, *-B, and -C* expression. Next, we investigated the biological function of *LINC02195* using bioinformatic analysis based on TCGA. A human tissue microarray (TMA) and *in situ* hybridization (ISH) were used to reveal the clinical role of *LINC02195*, and patients with high *LINC02195* expression achieved a good outcome in the HNSCC patient cohort. As shown in western blots, *LINC02195* silencing decreased the expression of MHC I molecules. By performing multiplex staining, a significant correlation between *LINC02195* and $CD8^+$ and $CD4^+$ T cell infiltration in the HNSCC microenvironment was revealed.

MATERIALS AND METHODS

Detailed information about the material and methods is provided in the **Supplementary Material**.

Study Population, RNA Expression Data, and Bioinformatic Analysis

The RNA expression data for HNSCC cases, which included 502 HNSCC tumor samples and 44 normal tissue samples were acquired from the TCGA database derived from the data portal (https://gdc.cancer.gov/). The dataset included the expression of RNA (mRNA and non-coding RNA) (level 3) and clinical data from 546 individuals. RNAs were identified using the Ensembl database. The differentially expressed lncRNAs (DElncRNAs) and mRNAs (DEmRNAs) were identified using the "edgeR" package. DEIncRNAs and DEmRNAs were analyzed by constructing a volcano plot with the "ggplot2" package in the R language.

Gene Enrichment and Functional Annotation Analysis

A subsequent functional enrichment analysis of the mRNAs (q values ≥ 0.4) was performed. The bubble map was drawn using the "ggplot2" R package. The mRNAs with significant Pearson's correlation coefficient values (|Pearson's correlation coefficient| ≥ 0.4) were included in further functional enrichment analyses. The Gene Ontology (GO) and Kyoto Encyclopedia of Genes and Genomes (KEGG) analyses were performed using the "clusterProfiler" package. The significant GO terms and KEGG pathways were identified as *LINC02195*-related biological functions and signaling pathways. Hierarchical clustering was performed using the "pheatmap" package in R language.

Human HNSCC Samples and Analysis

Ethical approval for this study was obtained from the Medical Ethics Committee of the School and Stomatology of Wuhan University (PI: Zhi-Jun Sun; 2014LUNSHENZI06). Human HNSCC samples were obtained from the Department of Oral and Maxillofacial Surgery, School and Hospital of Stomatology Wuhan University. The TNM classification at diagnosis was determined according to the 8th edition of TNM Classification of Malignant Tumors (UICC). The patient cohort included 5 patients with normal oral mucosae, 28 with oral epithelial dysplasia and 59 with HNSCC and 10 paired fresh HNSCC samples. The clinical characteristics, including TNM classification, histological grade and overall survival were available for all patients.

ISH was performed on a human HNSCC TMA with digoxigenin-labeled antisense oligonucleotide probes to examine the expression of *LINC02195*, as previously described (21). The probe sequence for *LINC02195* was 5′-DIG-TCCTTTGGAATCCTCCTACTTTGGCAGC-3′. IHC staining was performed as described (22). Signals were detected using biotinylated goat anti-rabbit or anti-mouse antibody followed by streptavidin HRP. Staining was visualized with DAB (Dako, USA), counterstained with hematoxylin (Dako), sealed with

neutral resins, and imaged. The scanning of the TMA and processing of histoscores were performed using previously described methods (22). A human leukocyte antigen (HLA) class I ABC antibody (1:300, Proteintech, USA) was used to detect MHC I molecules in human HNSCC samples.

Cell Lines, siRNAs, and Western Blotting

The cell lines SCC4, SCC9, and CAL27 were obtained from ATCC (American Type Culture Collection) and maintained as previously described (23). TCA8113 cells were acquired from the Ninth People's Hospital, Shanghai Jiao Tong University and maintained in DMEM containing 1% penicillin and streptomycin (Thermo Fisher, USA) and 10% fetal bovine serum (FBS, Gibco, USA). The human oral keratinocyte cell line (HOK) was obtained from ScienCell.

Small interfering RNAs (siRNAs) targeting *LINC02195* were purchased from GenePharma (China). SCC9 cells seeded in a 6-well plate were transfected with the siRNAs using Lipofectamine 3,000 (Invitrogen, USA) according to the manufacturer's instructions.

Western blotting with whole-cell protein extracts from SCC9 cells was performed as previously described (21). An HLA class I ABC antibody (15240-1-AP; Proteintech, USA) was used for western blotting. GAPDH served as an internal loading control. All western blots were performed three times.

Total RNA Extraction and Quantitative Reverse Transcription Polymerase Chain Reaction (qRT-PCR) Analysis

The total RNA extraction protocol and qRT-PCR analysis have been described previously (21). *LINC02195* expression was calculated with the comparative Ct method ($2^{-\Delta\Delta CT}$) and normalized to GAPDH expression. All qRT-PCR experiments were performed three times.

Multiplex IHC and Image Analysis

The Opal 7-Color Manual IHC Kit (NEL811001KT; PerkinElmer, Hopkinton, MA, USA) was used to stain the TMA as previously described (24). Briefly, for CD4, CD8, PD-1, and pan-keratin 4-plex staining, 4 types of tyramide system amplification (TSA) sensors (Opal520, Opal570, Opal620, and Opal690) were used. After all multiplex TSA staining protocols was completed, the slide was stained with DAPI and mounted. All slides were scanned using the PerkinElmer Vectra system (PerkinElmer). The tumor and stromal area were distinguished and calculated with inForm (inForm 2.1.1; PerkinElmer) software using pan-keratin as a tumor marker. From these data, the positive cell density was calculated using the following formula: positive cell density = the number of positive cells in the stroma ÷ the area of the stroma (calculating by image pixels).

Statistical Analysis

All data were statistically analyzed using Prism 8 software (GraphPad Software). One-way ANOVA (> 2 groups) or Student's *t*-tests (2 groups) (> 2 groups) were used to determine the significance of differences. Correlations were determined by calculating Pearson's correlation coefficient. Kaplan-Meier curves and Cox proportional hazards models were used to assess the prognostic value. Error bars are shown in the figures, and data are presented as the mean ± SEM. $P < 0.05$ was considered to be statistically significant, $^{*}P < 0.05$, $^{**}P < 0.01$, and $^{***}P < 0.001$.

RESULTS

LINC02195 Was Closely Correlated With *HLA I* Expression in the TCGA Database

The TCGA database was used to investigate and analyze the expression of lncRNAs and mRNAs with the "edgeR" package. Notably, 5,731 upregulated DEmRNAs and DElncRNAs and 3,397 downregulated DEmRNAs and DElncRNAs were identified in HNSCC tissues (**Figure 1A**). Then, we extracted DElncRNA from the TCGA database and explored the correlations with the genes encoding MHC I molecules in humans (*HLA-A*, *HLA-B,* and *HLA-C*). The Venn diagram revealed eight DElncRNAs that were simultaneously associated with *HLA-A*, *HLA-B,* and *HLA-C*, namely, *PSMB8-AS1*, *TTLL11-IT1*, *LINC02195*, *LINC00623*, *LINC07871*, *LINC00944*, *LINC02574,* and *MIR3945HG* (**Figure 1B** and **Supplementary Figure 1A**, |Pearson's correlation coefficient| ≥ 0.4). According to the subsequent survival analysis, only *LINC02195* and *LINC01871* were correlated with patient prognosis (**Figure 1C** and **Supplementary Figures 1B–H**). As shown in **Figure 1C**, the Kaplan-Meier analysis revealed a significant correlation between high *LINC02195* expression and good prognoses for patients with HNSCC in the TCGA database ($P = 0.0180$). The median histoscore was used as the cut-off. The Cox proportional hazards model also showed an association between *LINC02195* expression and a good outcome (**Table 1**). Considering the correlation with the expression of MHC I molecules and prognostic value, *LINC02195* was selected for further research in this study.

LINC02195 Was Expressed at High Levels in HNSCC and Correlated With a Good Prognosis

We next analyzed the expression and clinical features of *LINC02195* in patients with HNSCC. *LINC02195* was expressed at higher levels in tumor samples than in adjacent non-tumor tissues (**Figure 2A**, $P < 0.001$). Subsequently, 10 pairs of fresh HNSCC tissues matched with adjacent non-tumor tissues were used to verify the differential expression of *LINC02195*. Based on the qRT-PCR data, the expression in the HNSCC group was higher than that in the adjacent normal tissue group (**Figure 2B**, $P = 0.0012$). Then we explored the expression of *LINC02195* in human oral keratinocytes (HOKs) and the HNSCC cell lines SCC9, SCC4, TCA8113, and CAL27 using qRT-PCR. *LINC02195* was expressed at significantly higher levels in HNSCC cell lines than in HOKs (**Figure 2C**). Using ISH combined with a tissue microarray, *LINC02195* was expressed at higher levels in HNSCC tissues than in

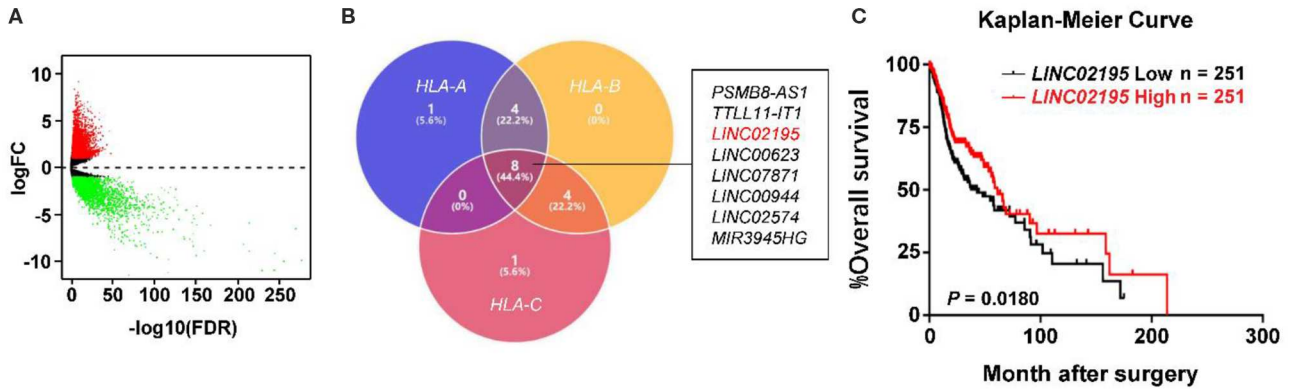

FIGURE 1 | *LINC02195* expression was closely correlated with MHC I molecules in the TCGA database. **(A)** Volcano plot of the differentially expressed lncRNAs between HNSCC tissues and adjacent tissues. The log2(fold change) on the X axis and−log10(*P*-value) on the Y axis are shown in the graph. Red dots represent high expression, and green dots represent low expression. Black shows lncRNA expression with both logFC < 1 and – log10 (*P*-value) < 0.05. Differentially expressed mRNAs and lncRNAs were calculated using edgeR, which identified upregulated overexpressed lncRNAs and 3,397 downregulated lncRNAs. **(B)** Venn diagram showing that eight DElncRNAs simultaneously associated with *HLA-A*, *HLA-B,* and *HLA-C*. **(C)** Kaplan-Meier survival curve of patients stratified according to low and high expression of *LINC02195* in the TCGA database (HNSCC). The median expression was used as the cut-off; $P = 0.0180$.

dysplastic tissue or the normal oral mucosa (**Figures 2D,E**, $P < 0.001$).

We analyzed the prognostic value of *LINC02195* and the relationship between clinicopathological data and *LINC02195* expression levels in the TCGA database and our patient cohort. The median histoscore was used as the cut-off. As shown in **Figure 2F**, the Kaplan-Meier analysis revealed a correlation between high *LINC02195* expression and a good prognosis for patients included in the TMA ($P = 0.0144$), consistent the result observed in TCGA. The Cox proportional hazards model also showed an association between *LINC02195* expression and a good outcome (**Table 2**).

As shown in **Table 3**, *LINC02195* expression was not correlated with other clinical data in the TCGA database including age, sex, pathological grade, pathological stage, T classification, and N classification. One-way ANOVA and post-Tukey test of the human HNSCC tissue microarray data did not reveal associations of the *LINC02195* expression level with the pathological grade, T classification, N classification, recurrence, radiotherapy, lymphatic metastasis, smoking, or alcohol consumption (**Supplementary Figure 2**).

LINC02195 Was an Immune-Related lncRNA

LINC02195-related mRNAs were selected for the gene annotation enrichment analysis to explore the biological functions of *LINC02195*. Sixty three enriched GO terms and 50 enriched KEGG pathways were associated with *LINC02195* (**Figure 3** and **Supplementary Table 1,2**, $P < 0.05$). As shown in **Figure 3A**, the most significantly enriched GO terms were carbohydrate binding, receptor ligand activity, cytokine receptor binding and activity and cytokine binding and activity. Similarly, the significantly enriched pathways were cytokine-cytokine receptor interaction, cell adhesion molecules, antigen processing and presentation, hematopoietic cell lineage and Th1 and Th2 cell differentiation (**Figures 3B,C**). Interestingly, in terms of cytokine-cytokine receptor interactions and cell adhesion molecules, the GO analysis indicated that *LINC02195* was closely correlated with immune factors such as chemokines, class I and II helical cytokines and the T cell receptor signaling pathway (**Supplementary Figure 3**). Based on these findings, *LINC02195* was an immune-related lncRNA.

LINC02195 Silencing Decreased the Expression of MHC I Molecules in HNSCC

The GO enrichment analysis also revealed a close association of *LINC02195* with MHC I protein binding (GO:0042288, $P = 1.67E{-}12$, **Supplementary Table 1**). Moreover, KEGG pathway analyses identified close associations of *LINC02195* with antigen processing and presentation (hsa04612, $P = 3.00E{-}30$, **Supplementary Table 2**). As shown in **Figure 4A**, *LINC02195* was closely correlated with the expression of *HLA-A*, *HLA-B,* and *HLA-C*, which encode classical MHC I molecules. Next, using an anti-HLA ABC antibody, the significant correlation between *LINC02195* and MHC I was confirmed in our patient cohort (**Figures 4B,C**, $P < 0.001$). *In vitro*, si*LINC02195* was used to silence the expression of *LINC02195*, and HLA-A, -B, and -C expression was downregulated when *LINC02195* was silenced (**Figures 4D,E**, $P < 0.001$).

LINC02195 Correlated With $CD8^+$ and $CD4^+$ T Cell Infiltration in the HNSCC Tumor Microenvironment (TME)

According to the KEGG pathway analysis, *LINC02195* was closely correlated with genes that are important for antigen processing and presentation (**Figure 5A**). T cells in the TME, which detect the antigens presented by MHC molecules, have been

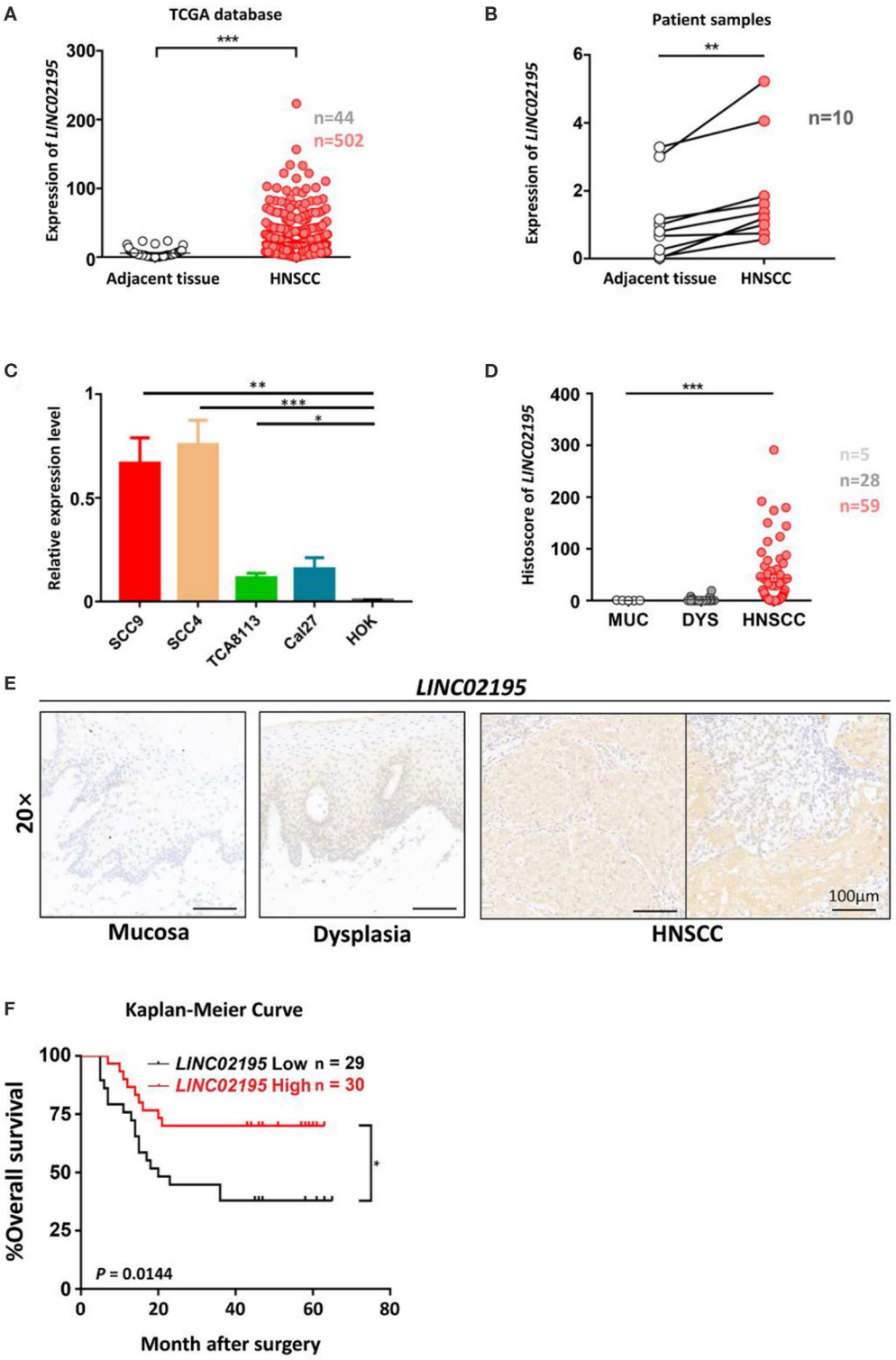

FIGURE 2 | *LINC02195* was expressed at high levels in HNSCC tissues. **(A)** Relative expression level of *LINC02195* in HNSCC and adjacent tissues from TCGA database. ***$P < 0.001$. **(B)** Relative expression level of *LINC02195* in HNSCC and adjacent tissue samples from patients with HNSCC. **$P < 0.01$. **(C)** Relative expression level of *LINC02195* in 5 HNSCC cell lines (SCC9, SCC4, TCA8113, CAL27) and HOKs. *$P < 0.05$, **$P < 0.01$, and ***$P < 0.001$. **(D–E)** Statistical analysis **(F)** and representative images **(E)** of ISH using the probe for *LINC02195* in normal mucosal, dysplastic and tumor tissues. Scale bar, 100 μm. **(F)** Kaplan-Meier curve of patients stratified according to low and high expression of *LINC02195* in the cohort of the TMA. The median expression was used as the cut-off; $P = 0.0144$.

TABLE 1 | Multivariate analysis of the overall survival of patients with HNSCC based on TCGA.

Parameters	HR (95%CI)	*P*-value
Sex	0.813 (0.594–1.113)	0.196
Age	1.021 (1.007–7.035)	0.003*
Pathological grade	1.047 (0.866–1.266)	0.637
Pathological stage	1.136 (0.964–1.338)	0.127
Tumor size	1.025 (0.901–1.164)	0.711
Node stage	1.125 (0.972–1.303)	0.115
LINC02195 expression	0.743 (.0557–0.991)	0.043*

Cox proportional hazards regression model.
HR hazard ratio, 95% CI 95% confidence interval.
**P < 0.05.*

TABLE 2 | Multivariate analysis of overall survival in patients with primary HNSCC.

Parameters	HR (95%CI)	*P*-value
Sex	0.866 (0.230–3.260)	0.832
Age	2.278 (0.905–5.731)	0.080
Pathological grade	1.333 (0.327–5.434)	0.688
Tumor size	1.363 (0.801–2.318)	0.254
Node stage	1.287 (0.767–2.162)	0.339
Smoking	0.850 (0.245–2.946)	0.798
Alcohol use	1.046 (0.349–3.134)	0.935
LINC02195 expression	0.366 (0.140–0.956)	0.040*

Cox proportional hazards regression model.
HR hazard ratio, 95% CI 95% confidence interval.
**P < 0.05.*

TABLE 3 | Relationship between *LINC02195* expression and clinical parameters of patients in TCGA.

Clinical parameter	*n*	*LINC02195* expression in TCGA database		
		Mean ± SED	*t*	*P*
Tumor vs. Normal				
Adjacent non-tumor tissue	44	5.68 ± 0.9405	4.123	<0.0001*
Tumor	502	21.66 ± 1.143		
Age (years)				
<60	245	21.73 ± 1.782	0.1238	0.9016
≥60	255	21.44 ± 1.458		
Sex				
Male	367	21.81 ± 1.354	0.2262	0.8211
Female	134	21.22 ± 2.149		
Pathological grade				
G1+G2	362	20.48 ± 1.3	1.402	0.1616
G3+G4	120	24.12 ± 2.234		
Pathological stage				
Stage I-II	95	22.93 ± 2.487	0.7006	0.4840
Stage III-IV	338	20.89±1.377		
T				
T1+T2	178	22.58 ± 1.823	0.9838	0.3258
T2+T3	267	20.22 ± 1.538		
N				
N0	170	21.13 ± 1.793	0.2114	0.8327
N1+N2+N3	238	21.66 ± 1.706		

reported to be associated with good clinical outcomes in patients with many types of cancer, including bladder, breast, ovarian, colorectal, and renal cancers (25, 26). The correlation between MHC I and *LINC02195* expression was previously proven. Additionally, the correlation between *LINC02195* and MHC II molecules was also highly significant (**Supplementary Figure 4**). Therefore, the correlation between *LINC02195* and T cells in TME was analyzed. By performing a bioinformatics analysis, we observed close correlations of *LINC02195* expression with *CD3D*, *CD3E*, *CD8A*, *CD8B,* and *CD4* expression in the TCGA database (**Figures 5B,C**). Pearson's correlation analysis revealed a strong association between *LINC02195* and T cells in the TME. Based on the hierarchical clustering analysis, *LINC02195* was more relevant to $CD8^+$ T cells than to $CD4^+$ T cells.

Multiplex IHC was performed to analyze the immune status in the TME and verify this finding. As shown in **Figure 6**, tumor tissues with high *LINC02195* expression exhibited more infiltrating $CD8^+$ and $CD4^+$ T cells than tumor tissues with low *LINC02195* expression (**Figure 6A**). Interestingly, Pearson's correlation analysis identified a positive correlation between the increase in *LINC02195* expression and the number of infiltrating $CD8^+$ and $CD4^+$ T cells (**Figures 6B,C**; CD8, $P < 0.0001$; CD4, $P = 0.0005$). The hierarchical clustering analysis further clarified the relationship among these molecules (**Figure 6D**).

DISCUSSION

In this study, the expression of the lncRNA *LINC02195* was closely associated with MHC molecules. Moreover, it was expressed at high levels in human HNSCC tissues, based on the analyses of TCGA database and patient samples. In addition, patients with high *LINC02195* expression exhibited better prognoses than patients with low *LINC02195* expression. We conducted GO and KEGG enrichment analyses to clarify the function and protein-protein interaction network of *LINC02195* by identifying *LINC02195*-related mRNAs in HNSCC tissues in the TCGA database and to determine the explanation for this outcome. *LINC02195* expression was closely correlated with the expression of MHC I molecules. Through further western blotting and immunostaining analysis, the correlation was further verified *in vitro*. Multiplex staining and Pearson's correlation analyses were used to verify the significant relationship between the lncRNA and infiltrating $CD8^+$ and $CD4^+$ T cells in TME.

LncRNAs have been widely investigated in recent years. An increasing number of lncRNAs have been shown to regulate the immune system (27). *LINC02195*, a newly annotated lncRNA, is located on chromosome 16p12.1. In normal tissues, it is expressed at high levels in the appendix, esophagus, lymph node, stomach, thyroid, some immune cell-rich places in our body, which suggest it may correlate with immune function (28). However, the relationship between *LINC02195* and HNSCC has

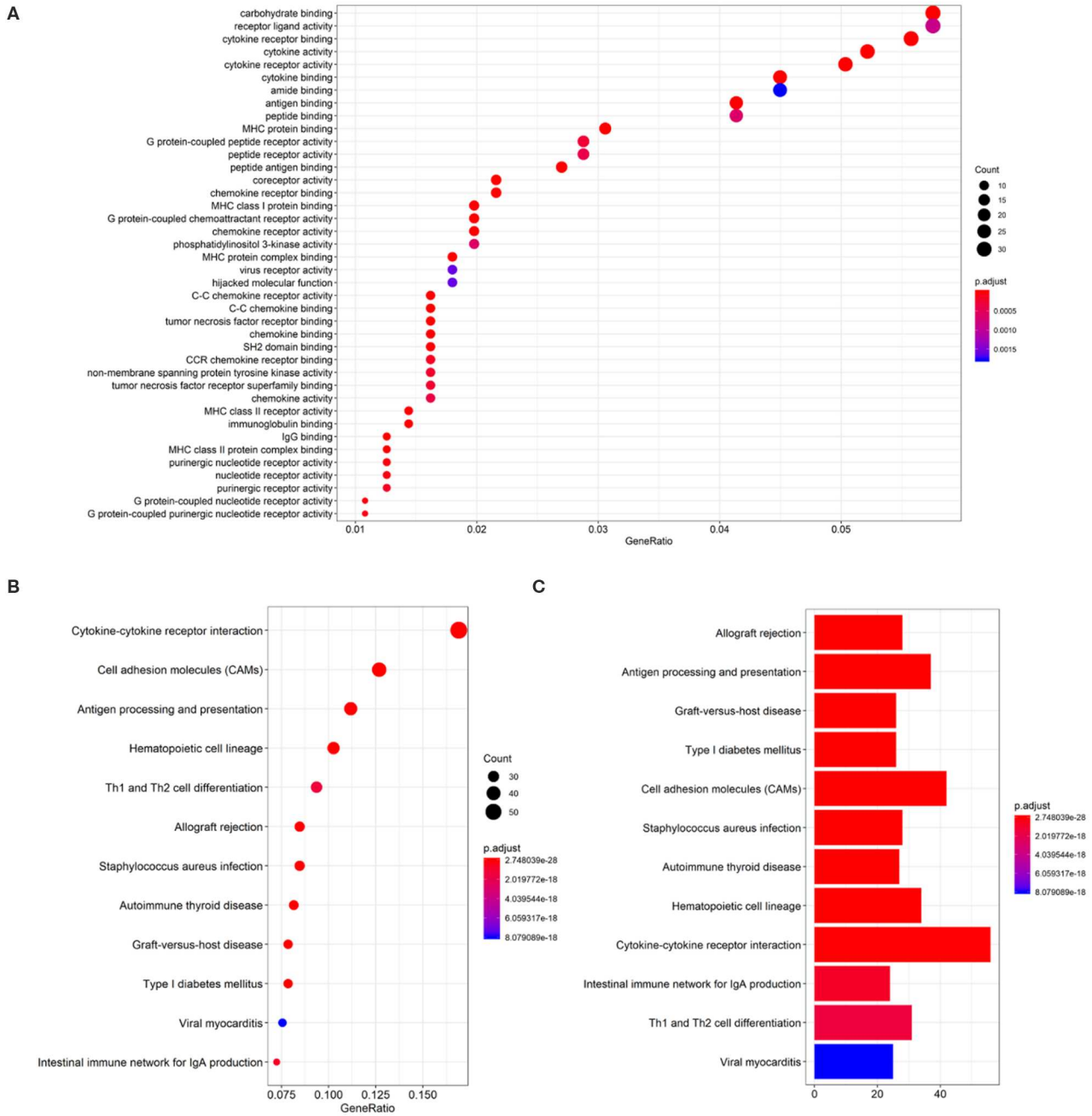

FIGURE 3 | GO and KEGG pathway enrichment analysis for *LINC02195*-related mRNAs based on TCGA database. **(A)** Plot of the enriched GO terms associated with *LINC02195*-related mRNAs. **(B,C)** Plot of the KEGG pathways associated with *LINC02195*-related mRNAs. $P < 0.05$ and Cor > 0.4 were used as the thresholds to select GO and KEGG terms.

not been revealed. In this study, *LINC02195* was confirmed to be associated with HNSCC by analyzing HNSCC and normal tissues. We found *LINC02195* is mostly found in the nucleus and cytoplasm by ISH. Moreover, high expression of this lncRNA was associated with a good prognosis for patients with HNSCC. GO and KEGG analyses revealed that *LINC02195* was an immune-related lncRNA. This lncRNA was correlated with antigen processing and presentation. MHC I molecules have a crucial role in this process, and previous studies have reported an association between the expression of the lncRNA *HCP5* expression was associated with *HLA-B* expression (19). In the present study, the Pearson's correlation analysis indicated a close correlation between genes encoding MHC I molecules with *LINC02195*. Moreover, western blotting revealed a decrease in MHC I levels

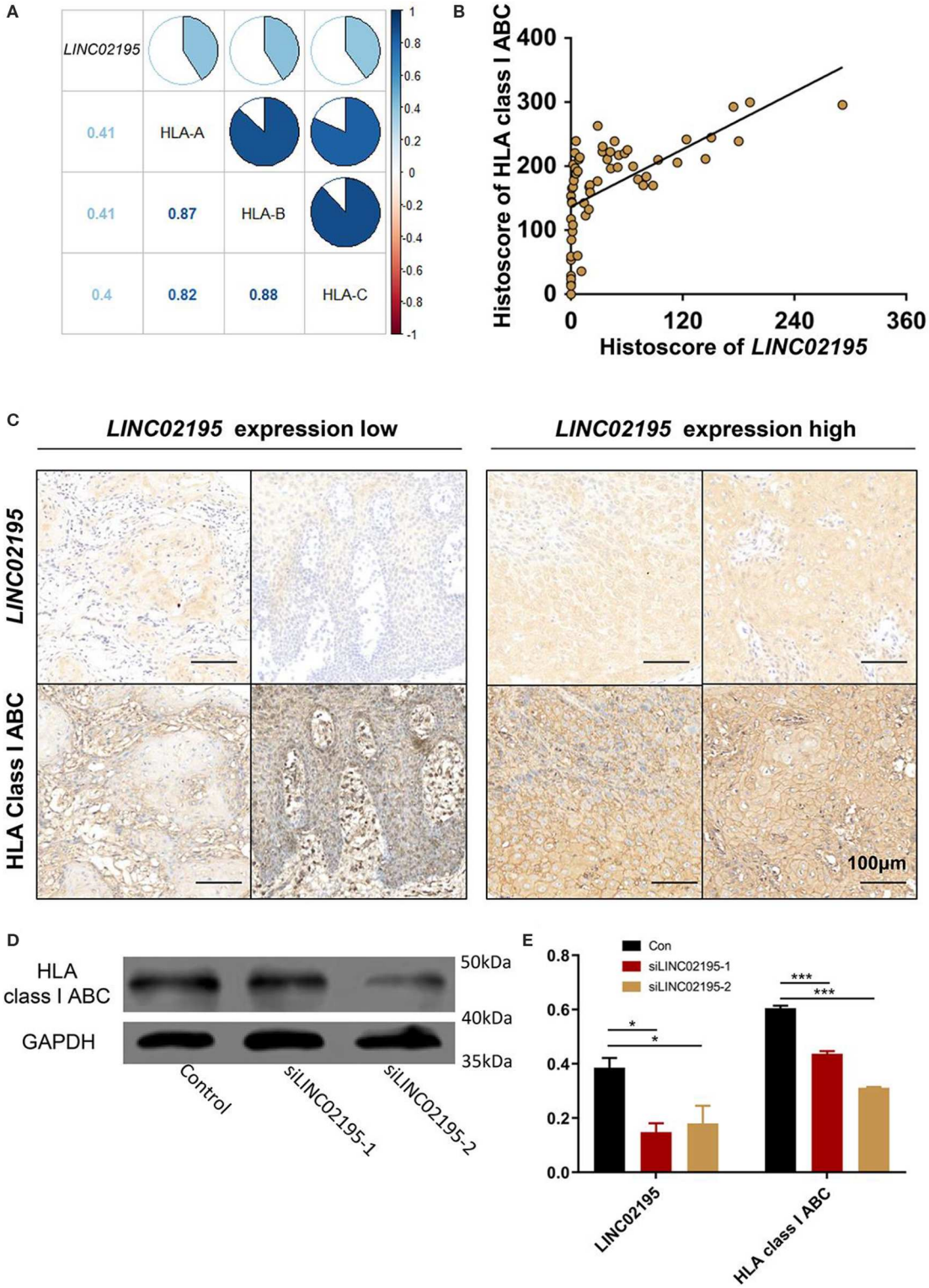

FIGURE 4 | *LINC02195* was closely correlated with the expression of MHC I molecule in tumor cells. **(A)** Pearson's correlation coefficients among *LINC02195*, *HLA-A*, *HLA-B,* and *HLA-C* expression in HNSCC samples from TCGA database. **(B)** Pearson's correlation coefficients between the histoscore of *LINC02195* and HLA class I ABC in the human HNSCC TMA; $P < 0.0001$, $r = 0.6103$. **(C)** Representative images of ISH and IHC for *LINC02195* and HLA class I ABC in human HNSCC specimens (low *LINC02195* expression vs. high *LIN02195* expression). Scale bar: 100 μm. **(D,E)** *in vitro*, *LINC02195* knockdown by using siLINC02195 downregulated the expression of HLA class I ABC in the SCC9 cell line. $^{*}P < 0.05$ and $^{***}P < 0.001$.

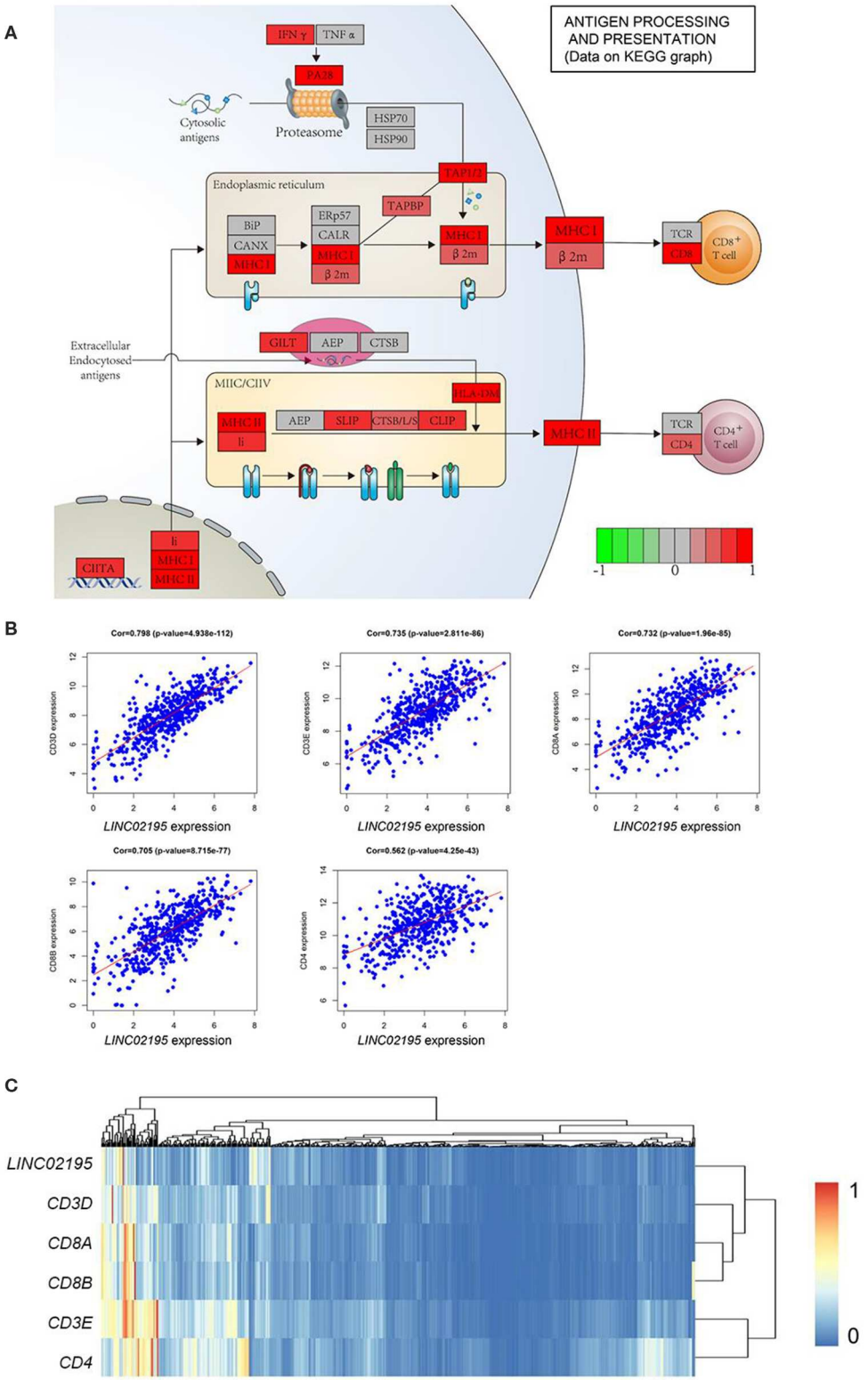

FIGURE 5 | *LINC02195* expression was positively correlated with genes involved in antigen processing and presentation. **(A)** KEGG pathway enrichment analyses showed a close correlation between *LINC02195* expression and antigen processing and presentation in both the MHC I and II pathways. **(B)** Pearson's correlation coefficients between *LINC02195* and *CD3D*, *CD3E*, *CD8A*, *CD8B,* or *CD4* gene expression based on TCGA data. **(C)** Hierarchical clustering analysis of *LINC02195*, *CD3D*, *CD3E*, *CD8A*, *CD8B,* and *CD4* in TCGA database.

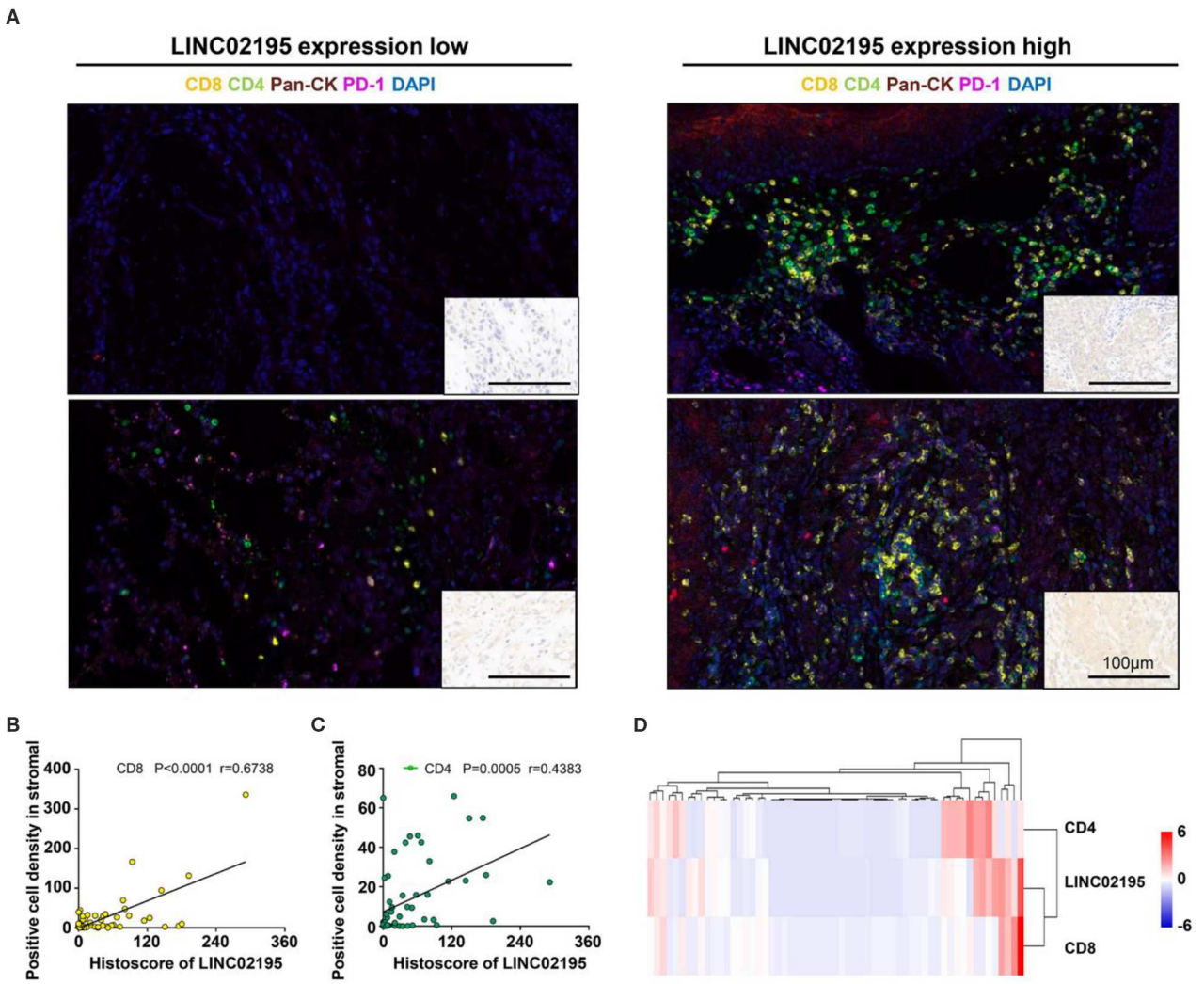

FIGURE 6 | LINC02195 expression was positively correlated with the infiltration of $CD8^+$ and $CD4^+$ T cells in the TME. **(A)** Representative image of multiplex staining (CD8, CD4, PD-1, pan-keratin, and DAPI) in human HNSCC specimens (low *LINC02195* expression vs. high *LINC02195* expression). Scale bar, 100 μm. **(B,C)** Pearson's correlation coefficient between the histoscore of *LINC02195* and the number of $CD8^+$ or $CD4^+$ cells in the human HNSCC TMA. **(D)** Hierarchical clustering analysis of *LINC02195*, CD4, and CD8 expression in human HNSCC samples ($n = 59$).

upon the silencing of *LINC02195*. The results suggested that *LINC02195* may interact with related enzymes or molecules encoding MHC I in the nucleus and further regulating the expression of MHC I molecules.

In recent years, the TME has attracted increasing attention from researchers because of its close correlation with prognosis and treatment. A number of various types of immune cells infiltrate the TME (25). Substantial T cell infiltration is associated with good clinical outcomes and positive responses to immunotherapy in many types of cancer (25, 29). However, the relationship between lncRNAs and T cells in the TME remains unclear. As shown in a previous study, *lnc-EGFR* stimulates Treg differentiation and subsequently promotes the immune evasion of hepatocellular cancer (18). According to another study, a lncRNA, *LINK-A*, downregulated cancer cell antigen presentation and was negatively correlated with T cells in the TME of triple-negative breast cancer (30). In the present study, gene enrichment and pathway analyses identified a strong correlation between *LINC02195* and T cells in the tumor context. Peptide–MHC I complexes are transported to the plasma membrane for cancer cell antigen presentation to $CD8^+$ T cells, which attack malignant cells. Next, through multiplex IHC of the human HNSCC TMA, we observed a positive correlation between *LINC02195* expression and the density of $CD8^+$ and $CD4^+$ T cells in the TME.

In summary, this study is the first to explore the role of *LINC02195* in HNSCC. High *LINC02195* expression were correlated with a good prognosis for patients with HNSCC. *LINC02195* may play a fundamental role in regulating the expression of MHC I molecules. In addition, *LINC02195* was

an immune-related lncRNA and positively correlated with an increased T cell density. This evidence, therefore, supports the hypothesis that *LINC02195* is a promising prognostic marker for HNSCC and a target for future therapeutic interventions.

DATA AVAILABILITY STATEMENT

The raw data supporting the conclusions of this article will be made available by the authors, without undue reservation, to any qualified researcher.

AUTHOR CONTRIBUTIONS

HL and H-GX contributed to conception, design, data acquisition, analysis, drafted, and critically revised the manuscript. YX, Q-CY, S-CY, and H-CT contributed to data acquisition, drafted and critically revised the manuscript. W-FZ and Z-JS contributed to conception, data analysis, and interpretation, drafted and critically revised the manuscript. All authors provided final approval and agreed to be accountable for all aspects of the study.

FUNDING

This study was supported by grants from the National Natural Science Foundation of China 81874131, 81672668, and 81672667. Z-JS was supported by the Fundamental Research Funds for the Central Universities of China 2042017kf0171 (Outstanding Young Scholars).

SUPPLEMENTARY MATERIAL

The Supplementary Material for this article can be found online at: https://www.frontiersin.org/articles/10.3389/fonc.2020.00615/full#supplementary-material

REFERENCES

1. Siegel RL, Miller KD, Jemal A. Cancer statistics, 2020. *CA Cancer J Clin*. (2020) 70:7–30. doi: 10.3322/caac.21590
2. Wyss A, Hashibe M, Chuang SC, Lee YC, Zhang ZF, Yu GP, et al. Cigarette, cigar, and pipe smoking and the risk of head and neck cancers: pooled analysis in the International Head and neck cancer epidemiology consortium. *Am J Epidemiol*. (2013) 178:679–90. doi: 10.1093/aje/kwt029
3. Cramer JD, Burtness B, Le QT, Ferris RL. The changing therapeutic landscape of head and neck cancer. *Nat Rev Clin Oncol*. (2019) 16:669–83. doi: 10.1038/s41571-019-0227-z
4. Ferris RL, Blumenschein G Jr, Fayette J, Guigay J, Colevas AD, Licitra L, et al. Nivolumab for recurrent squamous-cell carcinoma of the head and neck. *N Engl J Med*. (2016) 375:1856–67. doi: 10.1056/NEJMoa1602252
5. Ferris RL. Immunology and immunotherapy of head and neck cancer. *J Clin Oncol*. (2015) 33:3293–304. doi: 10.1200/JCO.2015.61.1509
6. Leone P, Shin EC, Perosa F, Vacca A, Dammacco F, Racanelli V. MHC class I antigen processing and presenting machinery: organization, function, and defects in tumor cells. *J Natl Cancer Inst*. (2013) 105:1172–87. doi: 10.1093/jnci/djt184
7. Neefjes J, Jongsma ML, Paul P, Bakke O. Towards a systems understanding of MHC class I and MHC class II antigen presentation. *Nat Rev Immunol*. (2011) 11:823–36. doi: 10.1038/nri3084
8. Garrido F, Ruiz-Cabello F, Aptsiauri N. Rejection versus escape: the tumor MHC dilemma. *Cancer Immunol Immunother*. (2017) 66:259–71. doi: 10.1007/s00262-016-1947-x
9. Aptsiauri N, Ruiz-Cabello F, Garrido F. The transition from HLA-I positive to HLA-I negative primary tumors: the road to escape from T-cell responses. *Curr Opin Immunol*. (2018) 51:123–32. doi: 10.1016/j.coi.2018.03.006
10. Yoo SH, Keam B, Ock CY, Kim S, Han B, Kim JW, et al. Prognostic value of the association between MHC class I downregulation and PD-L1 upregulation in head and neck squamous cell carcinoma patients. *Sci Rep*. (2019) 9:7680. doi: 10.1038/s41598-019-44206-2
11. Paulson KG, Voillet V, McAfee MS, Hunter DS, Wagener FD, Perdicchio M, et al. Acquired cancer resistance to combination immunotherapy from transcriptional loss of class I HLA. *Nat Commun*. (2018) 9:3868. doi: 10.1038/s41467-018-06300-3
12. Prensner JR, Chinnaiyan AM. The emergence of lncRNAs in cancer biology. *Cancer Discov*. (2011) 1:391–407. doi: 10.1158/2159-8290.CD-11-0209
13. Xiu DH, Liu GF, Yu SN, Li LY, Zhao GQ, Liu L, et al. Long non-coding RNA LINC00968 attenuates drug resistance of breast cancer cells through inhibiting the Wnt2/beta-catenin signaling pathway by regulating WNT2. *J Exp Clin Cancer Res*. (2019) 38:94. doi: 10.1186/s13046-019-1100-8
14. Liu H, Deng H, Zhao Y, Li C, Liang Y. LncRNA XIST/miR-34a axis modulates the cell proliferation and tumor growth of thyroid cancer through MET-PI3K-AKT signaling. *J Exp Clin Cancer Res*. (2018) 37:279. doi: 10.1186/s13046-018-0950-9
15. Wapinski O, Chang HY. Long noncoding RNAs and human disease. *Trends Cell Biol*. (2011) 21:354–61. doi: 10.1016/j.tcb.2011.04.001
16. Trimarchi T, Bilal E, Ntziachristos P, Fabbri G, Dalla-Favera R, Tsirigos A, et al. Genome-wide mapping and characterization of Notch-regulated long noncoding RNAs in acute leukemia. *Cell*. (2014) 158:593–606. doi: 10.1016/j.cell.2014.05.049
17. Wang P, Xue Y, Han Y, Lin L, Wu C, Xu S, et al. The STAT3-binding long noncoding RNA lnc-DC controls human dendritic cell differentiation. *Science*. (2014) 344:310–3. doi: 10.1126/science.1251456
18. Jiang R, Tang J, Chen Y, Deng L, Ji J, Xie Y, et al. The long noncoding RNA lnc-EGFR stimulates T-regulatory cells differentiation thus promoting hepatocellular carcinoma immune evasion. *Nat Commun*. (2017) 8:15129. doi: 10.1038/ncomms15129
19. Kulski JK. Long Noncoding RNA HCP5, a Hybrid HLA Class I endogenous retroviral gene: structure, expression, and disease associations. *Cells*. (2019) 8:480. doi: 10.3390/cells8050480
20. Song B, Guan Z, Liu F, Sun D, Wang K, Qu H. Long non-coding RNA HOTAIR promotes HLA-G expression via inhibiting miR-152 in gastric cancer cells. *Biochem Biophys Res Commun*. (2015) 464:807–13. doi: 10.1016/j.bbrc.2015.07.040
21. Xiong HG, Li H, Xiao Y, Yang QC, Yang LL, Chen L, et al. Long noncoding RNA MYOSLID promotes invasion and metastasis by modulating the partial epithelial-mesenchymal transition program in head and neck squamous cell carcinoma. *J Exp Clin Cancer Res*. (2019) 38:278. doi: 10.1186/s13046-019-1254-4
22. Li H, Yang LL, Xiao Y, Deng WW, Chen L, Wu L, et al. Overexpression of Golgi Phosphoprotein 2 is associated with poor prognosis in oral squamous cell carcinoma. *Am J Clin Pathol*. (2018) 150:74–83. doi: 10.1093/ajcp/aqy029
23. Chen L, Yang QC, Li YC, Yang LL, Liu JF, Li H, et al. Targeting CMTM6 suppresses stem cell-like properties and enhances antitumor immunity in head and neck squamous cell carcinoma. *Cancer Immunol Res*. (2020) 8:179–91. doi: 10.1158/2326-6066.CIR-19-0394
24. Xiao Y, Li H, Mao L, Yang QC, Fu LQ, Wu CC, et al. CD103(+) T and dendritic cells indicate a favorable prognosis in oral cancer. *J Dent Res*. (2019) 98:1480–7. doi: 10.1177/0022034519882618
25. Fridman WH, Zitvogel L, Sautes-Fridman C, Kroemer G. The immune contexture in cancer prognosis and treatment. *Nat Rev Clin Oncol*. (2017) 14:717–34. doi: 10.1038/nrclinonc.2017.101

26. Fridman WH, Pages F, Sautes-Fridman C, Galon J. The immune contexture in human tumours: impact on clinical outcome. *Nat Rev Cancer*. (2012) 12:298–306. doi: 10.1038/nrc3245
27. Li Y, Jiang T, Zhou W, Li J, Li X, Wang Q, et al. Pan-cancer characterization of immune-related lncRNAs identifies potential oncogenic biomarkers. *Nat Commun*. (2020) 11:1000. doi: 10.1038/s41467-020-14802-2
28. Fagerberg L, Hallstrom BM, Oksvold P, Kampf C, Djureinovic D, Odeberg J, et al. Analysis of the human tissue-specific expression by genome-wide integration of transcriptomics and antibody-based proteomics. *Mol Cell Proteomics*. (2014) 13:397–406. doi: 10.1074/mcp.M113.035600
29. Matsushita H, Vesely MD, Koboldt DC, Rickert CG, Uppaluri R, Magrini VJ, et al. Cancer exome analysis reveals a T-cell-dependent mechanism of cancer immunoediting. *Nature*. (2012) 482:400–4. doi: 10.1038/nature10755
30. Hu Q, Ye Y, Chan LC, Li Y, Liang K, Lin A, et al. Oncogenic lncRNA downregulates cancer cell antigen presentation and intrinsic tumor suppression. *Nat Immunol*. (2019) 20:835–51. doi: 10.1038/s41590-019-0400-7

Conflict of Interest: The authors declare that the research was conducted in the absence of any commercial or financial relationships that could be construed as a potential conflict of interest.

Copyright © 2020 Li, Xiong, Xiao, Yang, Yang, Tang, Zhang and Sun. This is an open-access article distributed under the terms of the Creative Commons Attribution License (CC BY). The use, distribution or reproduction in other forums is permitted, provided the original author(s) and the copyright owner(s) are credited and that the original publication in this journal is cited, in accordance with accepted academic practice. No use, distribution or reproduction is permitted which does not comply with these terms.

frontiers in Oncology

ORIGINAL RESEARCH
published: 14 August 2020
doi: 10.3389/fonc.2020.01421

Analysis of Differentially Expressed Long Non-coding RNAs and the Associated TF-mRNA Network in Tongue Squamous Cell Carcinoma

Mi Zhang[1,2], *Zexi Chen*[3], *Sihui Zhang*[3], *Ling Wu*[3], *Yinghui Jie*[3], *Yunyang Liao*[4], *Yue Huang*[4], *Jiang Chen*[1,2*] *and Bin Shi*[4*]

[1] School and Hospital of Stomatology, Fujian Medical University, Fuzhou, China, [2] Fujian Key Laboratory of Oral Diseases, School and Hospital of Stomatology, Fujian Medical University, Fuzhou, China, [3] Research Center of Dental and Craniofacial Implants, School and Hospital of Stomatology, Fujian Medical University, Fuzhou, China, [4] Department of Oral and Maxillofacial Surgery, The First Affiliated Hospital of Fujian Medical University, Fuzhou, China

Accumulating evidence indicates that long non-coding RNAs (lncRNAs) play crucial roles in tongue squamous cell carcinoma (TSCC) tumorigenesis. However, the comprehensive regulation of lncRNAs-transcription factors (TFs)-messenger RNAs (mRNAs) in TSCC remains largely unknown. The purpose of this study was to identify aberrantly expressed lncRNAs and the associated TF-mRNA network in TSCC. To explore lncRNA and mRNA expression profiles and their biological functions in TSCC, we surveyed the lncRNA and mRNA expression profiles of TSCC and adjacent tissues using next-generation RNA sequencing in six patients. Thousands of significantly differentially expressed lncRNAs (DELs) and mRNAs (DEGs) were identified. Gene Ontology (GO) and Kyoto Encyclopedia of Genes and Genomes (KEGG) pathway enrichment analyses were performed to demonstrate the principal functions of the significantly dysregulated lncRNAs and genes. A total of 40 DELs were screened between TSCC and adjacent non-cancerous tissues. Results obtained from GEPIA and StarBase confirmed the expression levels of nine pivotal DELs obtained in our study. Three of the nine deregulated DELs were identified to have a significant impact on the overall survival of TSCC patients, which were evaluated with GEPIA and StarBase. LncMAP was used to predict the lncRNA-TF-mRNA triplets in TSCC. Furthermore, based on these results, we established lncRNA-TF-mRNA coexpression networks for the up- and downregulated lncRNAs using Cytoscape. We also found that among the nine pivotal lncRNAs, there is limited research on the abnormally expressed lncRNAs, including RP11-54H7.4, CTD-2545M3.8, RP11-760H22.2, RP4-791M13.3, and LINC01405, in TSCC pathogenesis. This is the first study to show that RP11-54H7.4, LINC00152, and LINC01405 can be acted as a prognostic target for TSCC. Our findings provide a novel perspective and lay the foundation for future research on the potential roles of lncRNAs, TFs, and mRNAs in TSCC. Verification of the potential lncRNA-TF-mRNA regulatory networks will provide a more comprehensive understanding of the pathogenesis of TSCC.

Keywords: tongue squamous cell carcinomas, lncRNA, mRNA, transcription factor, network

OPEN ACCESS

Edited by:
Wei Cao,
Shanghai Jiao Tong University, China

Reviewed by:
Zheqi Liu,
Shanghai Jiao Tong University, China
Yanjie Zhang,
Shanghai Jiao Tong University, China

***Correspondence:**
Jiang Chen
jiangchen@fjmu.edu.cn
Bin Shi
shibin@fjmu.edu.cn

Specialty section:
This article was submitted to Head and Neck Cancer, a section of the journal Frontiers in Oncology

Received: *13 April 2020*
Accepted: *06 July 2020*
Published: *14 August 2020*

Citation:
Zhang M, Chen Z, Zhang S, Wu L, Jie Y, Liao Y, Huang Y, Chen J and Shi B (2020) Analysis of Differentially Expressed Long Non-coding RNAs and the Associated TF-mRNA Network in Tongue Squamous Cell Carcinoma. Front. Oncol. 10:1421. doi: 10.3389/fonc.2020.01421

INTRODUCTION

As the most lethal and commonly occurring oral malignancy, oral squamous cell carcinoma (OSCC) accounts for 95% of all oral cancer diagnoses and causes more than 500,000 deaths per year (1). Approximately 25–40% of OSCCs are diagnosed as tongue squamous cell carcinoma (TSCC) (2). TSCC is characterized by frequent lymphoid metastasis, a high rate of regional recurrence, and a poor prognosis. Moreover, despite great progress in surgical techniques, diagnostic procedures, chemotherapy, and radiotherapy, the 5-year overall survival rate of TSCC patients has not improved significantly over the past decades. Therefore, a better understanding of the molecular mechanisms behind the initiation and progression of TSCC may facilitate the diagnosis and treatment of this malignant tumor.

Long non-coding RNA (lncRNA) represents a class of RNA species that are transcribed predominantly by RNA polymerase II, with a length exceeding 200 nucleotides and no apparent protein-coding potential, as indicated by the lack of strongly translated open reading frames (ORFs) (3). lncRNA plays a crucial role in diverse biological systems through genomic imprinting, cell cycle regulation, and cell differentiation and has been linked to a number of human diseases, especially cancer (4, 5). Recently, growing evidence has demonstrated that lncRNAs may also have essential roles in TSCC. For example, overexpression of the lncRNA FALEC represses malignant behaviors in TSCC (6). Upregulation of the lncRNA HOTTIP in TSCC patients indicates a poor clinical prognosis (7). In TSCC cell lines, cell growth, invasion, and migration abilities are associated with the overexpression of MALAT-1 and AFAP1-AS1 via the Wnt signaling pathway, while the knockdown of MALAT-1 in TSCC cells leads to the upregulation of certain SPRR proteins (8–10). High expression of the lncRNA UCA1 has been linked to the migratory ability of epithelial cancer cells and regional lymph node metastasis in TSCC (11). Moreover, the lncRNAs KCNQ1OT1 and SNHG17 act as competing endogenous RNAs (ceRNAs) to regulate cell proliferation and cancer progression in TSCC (12, 13).

In our study, we analyzed the expression profiles of lncRNAs and mRNAs in TSCC tissue through high-throughput sequencing. In addition, we identified molecular function, cellular component, biological process, and pathway analyses enriched by mRNA-associated lncRNAs and differentially expressed mRNAs in TSCC. Furthermore, our work revealed several pivotal lncRNAs related to the overall survival of TSCC patients. Finally, to optimize the regulatory mechanism of lncRNAs, we further explored several reliable transcription factors (TFs) in the regulatory regions of lncRNAs and constructed a lncRNA-TF-mRNA coexpression network.

Abbreviations: DEL, differentially expressed lncRNA; DEG, differentially expressed mRNA; LncRNA, long non-coding RNA; TF, transcription factor; TSCC, tongue squamous cells carcinomas; HNSC, head and neck squamous cell carcinoma; GO, Gene Ontology; KEGG, Kyoto Encyclopedia of Genes and Genomes.

MATERIALS AND METHODS

Clinical Samples and Data Processing

Tumors and adjacent tongue tissues were obtained from patients with TSCC who underwent surgery at The First Affiliated Hospital of Fujian Medical University. Following surgical resection, six pairs of tissue samples were immediately immersed in liquid nitrogen and then stored at −80°C. Written informed consent was obtained from all participants in accordance with the Declaration of Helsinki, and the study protocol was approved by the Ethics Committee of The First Affiliated Hospital of Fujian Medical University (Fuzhou, China).

Next-generation RNA sequencing assays were performed to detect the mRNA and lncRNA expression profiles by KangChen Biotech (Shanghai, China) using an Illumina HiSeq 4,000 system (Illumina, San Diego, CA, USA). Solexa pipeline version 1.8 was used to align the reads to the genome, generate raw counts corresponding to each known gene (a total of 17,242 genes), and calculate the reads per kilobase per million (RPKM) values. The differentially expressed lncRNAs (DELs) and mRNAs (DEGs) were identified through fold change/*p*-value/FDR filtering [fold change $\geq$1.5, $p < 0.05$, and FDR (adjusted *p*-value) <0.05].

Then, the data associated with TSCC were also retrieved from The Cancer Genome Atlas (TCGA) database (https://portal.gdc.cancer.gov/) and were downloaded through GDC data transfer tool, including the RNA sequencing (RNA-Seq) of transcriptome profiling and clinical data. Then, in the predictive survival related model, we excluded 27 samples because they lacked complete clinical data. Finally, 146 TSCC samples and 15 normal control samples were collected in our study. EdgeR package in R (version 3.6.3) was used to identify the DELs. After that, we used the annotation file in GTF format (Homo_sapiens.GRCh38.100.chr.gtf) to identify and annotate DELs with the thresholds of |log2FC|>2.0 and FDR < 0.05.

Cell Lines

Three human TSCC cell lines, CAL-27, SCC-9, and SCC-25 were purchased from the American Type Culture Collection (ATCC; Manassas, VA, USA), and the human normal oral keratinocyte (hNOK) cell line was obtained from the Institute of Biochemistry and Cell Biology of the Chinese Academy of Sciences (Shanghai, China). CAL-27 cells and hNOK cells were grown in DMEM (Gibco) supplemented with 10% FBS (Invitrogen, Carlsbad, CA, USA). SCC-9 and SCC-25 cells were cultured in DMEM/F-12 (Gibco) supplemented with 10% FBS and 0.4 μg/ml hydrocortisone. All cells were maintained at 37°C in an incubator supplied with 5% CO_2.

RNA Extraction and Quantitative Real-Time PCR Analysis

Total RNA was extracted from tissues or cells using TRIzol reagent (Invitrogen, CA, USA) according to the manufacturer's instructions. Total RNA was reverse transcribed into cDNA using a PrimeScript RT reagent kit (TaKaRa). RT-qPCR analyses were performed using SYBR Green Master Mix (TaKaRa).

This process was performed using an Applied Biosystems 7,500 Real-Time PCR System. The results were normalized to the expression of glyceraldehyde-3-phosphate dehydrogenase (GAPDH). The relative expression level was calculated by the $2^{-\Delta\Delta}$ Ct method. The primers were provided by the SunYa Company.

Filtering DELs and DEGs

DELs and DEGs were selected using the following cut-off criteria: for DELs: the top 20 upregulated and downregulated lncRNAs, for DEGs: |log2-fold change| >2 and $p < 0.05$. Heatmap charts and volcano plots were established the gplots package in R software.

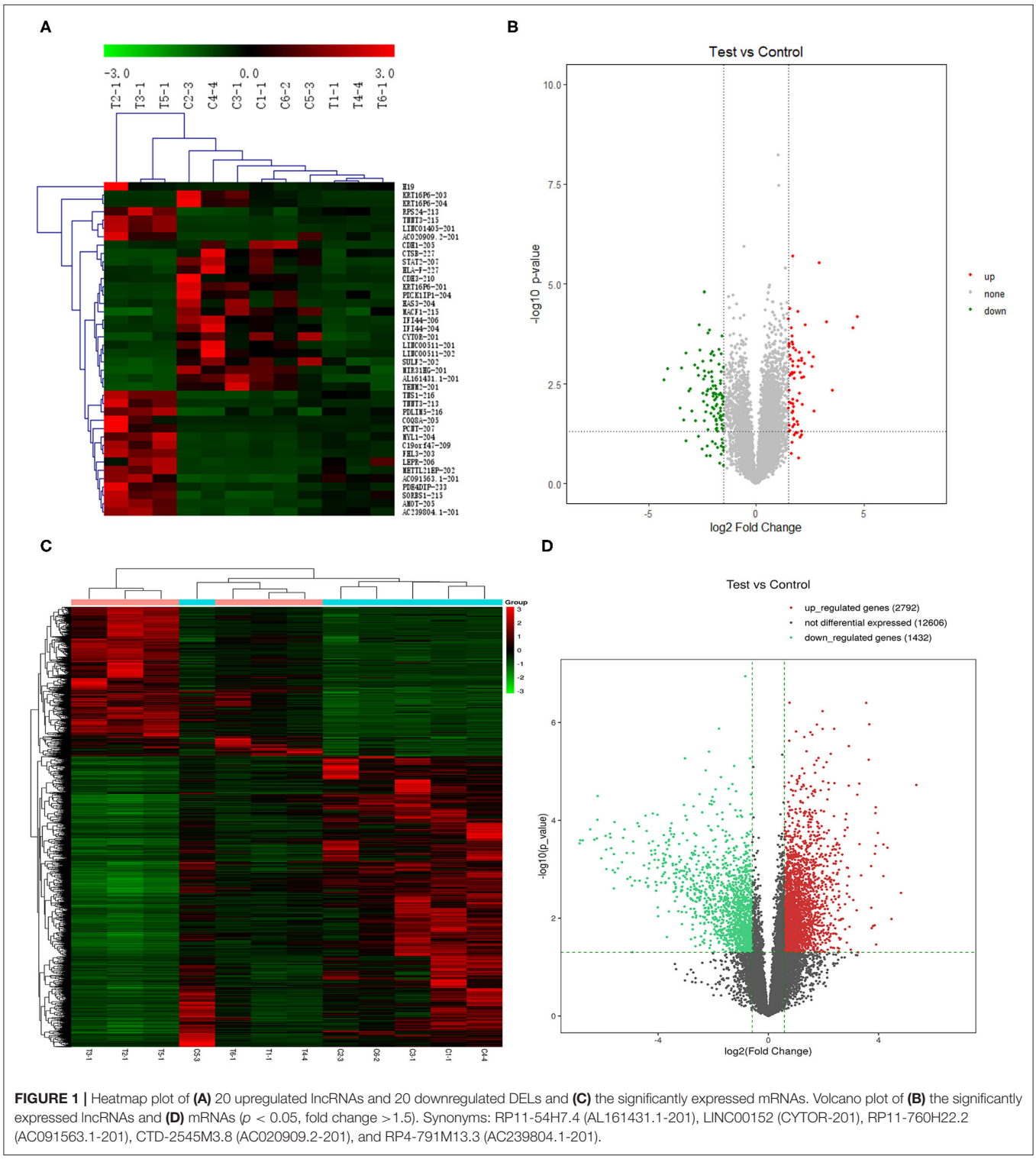

FIGURE 1 | Heatmap plot of **(A)** 20 upregulated lncRNAs and 20 downregulated DELs and **(C)** the significantly expressed mRNAs. Volcano plot of **(B)** the significantly expressed lncRNAs and **(D)** mRNAs ($p < 0.05$, fold change >1.5). Synonyms: RP11-54H7.4 (AL161431.1-201), LINC00152 (CYTOR-201), RP11-760H22.2 (AC091563.1-201), CTD-2545M3.8 (AC020909.2-201), and RP4-791M13.3 (AC239804.1-201).

Verification of DEL and DEG Expression in GEPIA and StarBase

To identify the DELs, we used GEPIA (http://gepia.cancer-pku.cn/detail.php) (14) and StarBase (http://starbase.sysu.edu.cn/) (15), publicly available online databases, to explore gene expression levels in tumors and normal tissues.

Gene Set Enrichment Analysis (GSEA)

GSEA is a calculation method used to determine whether a given gene set is significantly different between different groups. The genes in these gene sets have a certain degree of correlation (e.g., the same biological function, located close to each other on the chromosome or defined by themselves according to a certain standard). However, LncRNA can not be directly used for GSEA as mRNA, but the correlation between each DEL and all mRNAs can be calculated. Then, GSEA of DELs can be performed using GSEAPreranked in GSEA software.

The Gene Ontology (GO) project provides a controlled vocabulary to describe gene and gene products attributed in any organism (http://www.geneontology.org). GO covers three domains: biological process, cellular component, and molecular function. The lower the *p*-value is, the more significant the GO

TABLE 1 | Information on 40 DELs in TSCC.

Category	LncRNA symbol	Ensembl ID	Locus	log_2FC	*p*-value
Upregulated	KRT16P6-203	ENST00000583748	chr17:16722827-16725442	4.6923889	6.564E-05
	KRT16P6-204	ENST00000584481	chr17:16721306-16722677	4.494188	0.0001269
	CTSB-227	ENST00000533110	chr8:11705188-11707556	3.5230094	0.0047111
	KRT16P6-201	ENST00000417510	chr17:16721297-16725893	3.2691007	8.906E-05
	RP11-54H7.4	ENST00000618966	chr13:109921982-109926186	2.9241856	3.041E-06
	CDH1-205	ENST00000562836	chr16:68797197-68867441	2.672898	0.0157189
	MIR31HG-201	ENST00000304425	chr9:21455641-21559668	2.6329908	0.0006836
	IFI44-206	ENST00000472152	chr1:79115543-79129763	2.5667645	0.0011736
	STAT2-207	ENST00000556539	chr12:56735381-56743559	2.2608986	0.0001073
	LINC00152	ENST00000331944	chr2:87754948-87821037	2.2235254	0.0010058
	CDH3-210	ENST00000569117	chr16:68730047-68730826	2.219285	0.0021646
	PDZK1IP1-204	ENST00000491793	chr1:47649272-47651016	2.1330875	0.0106663
	LINC00511-201	ENST00000453722	chr17:70380443-70588943	2.0909352	0.0022785
	IFI44-204	ENST00000467790	chr1:79115527-79121196	2.0872088	0.0008379
	LINC00511-202	ENST00000457958	chr17:70399463-70588479	2.0860305	0.0007322
	HAS3-204	ENST00000568321	chr16:69140157-69140891	2.0859456	0.0488404
	MACF1-215	ENST00000473843	chr1:39900157-39901679	2.0165445	0.0016772
	HLA-F-227	ENST00000485513	chr6:29691717-29693076	1.9916707	0.0055367
	SULF2-202	ENST00000433632	chr20:46290178-46292298	1.9859734	0.0005177
	TENM2-201	ENST00000517586	chr5:167248073-167379660	1.949576	0.0008307
Downregulated	TNNT3-215	ENST00000639560	chr11:1949052-1959713	−4.262896	0.0025895
	LINC01405-201	ENST00000331096	chr12:111374406-111375255	−4.084115	0.0013337
	H19-212	ENST00000446406	chr11:2016446-2019057	−3.534739	0.0131478
	TNS1-216	ENST00000480665	chr2:218713195-218723356	−3.447791	0.0013045
	RPS24-213	ENST00000485708	chr10:79793602-79800428	−3.09478	0.0048687
	TNNT3-213	ENST00000492075	chr11:1946148-1955885	−2.969187	0.0151812
	CTD-2545M3.8	ENST00000595005	chr19:50990067-50990895	−2.809795	0.0268764
	MYL1-204	ENST00000496436	chr2:211155756-211168339	−2.693001	0.0012879
	C19orf47-209	ENST00000584868	chr19:40826987-40828246	−2.678462	0.0019579
	AMOT-205	ENST00000462114	chrX:112066365-112083911	−2.629755	0.0001059
	PCNT-207	ENST00000483844	chr21:47768153-47773240	−2.435337	0.0086552
	METTL21EP-202	ENST00000605100	chr13:103532449-103548383	−2.402461	0.0015185
	COQ8A-205	ENST00000478406	chr1:227127995-227175244	−2.383483	0.0264686
	PDLIM5-216	ENST00000511767	chr4:95376418-95471137	−2.286661	0.006016
	FHL3-203	ENST00000477194	chr1:38463017-38471278	−2.264287	0.0049033
	RP11-760H22.2	ENST00000520544	chr8:121064419-121068423	−2.21687	0.0001699
	PDE4DIP-233	ENST00000533845	chr1:144946702-144994925	−2.201192	0.0016894
	LEPR-206	ENST00000462765	chr1:65991372-66075951	−2.079886	0.0005774
	SORBS1-215	ENST00000474353	chr10:97101341-97321130	−2.077141	0.0008195
	RP4-791M13.3	ENST00000466343	chr1:144833168-144835867	−2.071663	0.0015749

term enrichment among the differentially expressed genes (a $p \leq 0.05$ is recommended). Pathway analysis is a functional analysis that maps genes to Kyoto Encyclopedia of Genes and Genomes (KEGG) pathways (http://www.genome.jp/kegg/). The *p*-value (EASE score, Fisher's *p*-value, or hypergeometric *p*-value) denotes the significance of the pathway correlated to the condition. The GO and KEGG pathway analyses were performed by KangChen Biotech (Shanghai, China).

Survival Analysis of the Candidate lncRNAs

The GEPIA and StarBase databases were used to evaluate the effects of DELs on the overall survival of patients with TSCC. The final lncRNA correlated with overall survival was thus regarded as the pivotal lncRNA. $p < 0.05$ was considered statistically significant using the log-rank test. The cut-off value between two groups was set as the "median."

Establishing the lncRNA-TF-mRNA Network

LncMAP (http://bio-bigdata.hrbmu.edu.cn/LncMAP/index.jsp) was used to analyze the lncRNA-TF-mRNA triplets in TSCC. A Venn diagram was drawn to determine the intersection between the mRNA in triplets and DEGs. The expression levels of these overlapping mRNAs were validated with GEPIA, and the correlation of the TF and mRNA was analyzed with StarBase. On the basis of these findings, we constructed a lncRNA-TF-mRNA regulatory network using Cytoscape (version 3.7.2) software to visualize their interactions. lncRNA-TF-mRNA triplets that showed no correlations with other triplets were excluded from the network.

Identification of the Prognostic Biomarkers

After analyzing the effects of pivotal DELs on the overall survival of patients with TSCC, we verified our findings in the TCGA difference analysis results, and it confirmed that LINC00152, LINC01405, RP11-54H7.4, and RP11-760H22.2 were simultaneously identified to be differentially expressed in TSCC. Thus, we also made the expression scatter and pairing plots of this four pivotal lncRNA by R software.

Statistical Analysis

Data are presented as the mean ± standard error (SE). Measured data were compared between groups using Student's paired *t*-tests or independent *t*-test. All statistical analyses were performed using SPSS and R software (version 22; IBM, Armonk, NY, USA) and presented graphically in GraphPad Prism 5.0 (GraphPad, La Jolla, CA, USA). Making the scatter diagram and paired plot by wilcoxon test in R software. All tests were two-tailed, and $p < 0.05$ was considered statistically significant.

RESULTS

Identification of the Candidate DELs and DEGs in TSCC

Tumor and adjacent tissue samples were collected from six patients with TSCC. The main clinical characteristics of the

TABLE 2 | Information on DEGs in TSCC.

Category	Gene symbol
Upregulated	MMP1, S100A7, PI3, MMP10, KRT17, LAMC2, COL1A1, KRTDAP, SERPINE1, S100A7A, CDH3, KLK5, KRT6B, CXCL10, KRT16, KRT14, ISG15, TYMP, MMP3, CXCL13, TNC, IFI30, MMP9, DEFB4A, TENM2, HAS3, MMP12, POSTN, IFI6, COL12A1, PLAU, GBP1, FSCN1, BNC1, ADAM12, COL3A1, CXCL9, PTHLH, LAMP3, KLK7, ADAMTS2, GBP5, KLK6, INHBA, TNS4, S100A12, SAMD9, MMP11, SERPINB4, OAS2, CTHRC1, S100A2, BST2, THBS2, CLCA2, DDX60, OAS3, KRT5, CXCL1, CPA4, COL5A1, CTSC, COL1A2, GJB6, OASL, MFAP2, EPSTI1, PYGL, TAP1, NELL2, IFI44, PTK7, COL7A1, SLC2A1, CPXM1, WFDC5, LAMB3, NME1-NME2, SCO2, COL5A2, RAB31, MYO1B, ACP5, MMP7, UBE2L6, RSAD2, RBP1, VMP1, IFIT3, PLEK2, GJA1, EPPK1, CASP14, FAT1, MX1, IGF2BP2, FAM83A, TGFBI, DNAH17, SPP1, CALML5, UBD, TTYH3, PARP14, MYBL2, FAM83B, THBS1, CLDN1, FBLIM1, UCN2, WARS, HELZ2, XAF1, TREM2, PDZK1IP1, STAT1, FABP5, ITGA3, CDC25B, TLR2, ADAMTS14, HIST1H2BO, ARNTL2, IFI27, CDC20, FAT2, WISP1, FCGR3A, LOXL2, MMP14, AIM2, IFI44L, GSDMC, GPR68, DDX58, IL12RB2, IFIH1, SULF2, GPRIN1, BASP1, MARCKSL1, RTP4, CRABP2, ENTPD7, HIST1H2AL, WNT7B, ACTN1, THY1, HIF1A, C6orf141, CTSV, HIST1H2AM, SOCS3, PLA2G7, COL4A1, STAT2, TPBG, SLC7A5, TPX2, APOBEC3A, IFFO2, PTGFRN, IFI16, ADAMTS12, SLC6A14
Downregulated	RORC, KLF15, LIFR, CAVIN2, PYGM, PAIP2B, VIT, CYP4B1, TLE2, CNTFR, SELENBP1, SLC25A4, PERM1, DEPTOR, HFE2, ATP2A1, CASQ1, FHL1, TNXB, LDB3, PPP1R3C, TNNC2, ENO3, PI16, PPARGC1A, FBXO40, CKMT2, AMOT, ANKRD2, NRAP, SLC2A4, SH3BGR, PLIN4, SCARA5, HSPB6, AC131097.2, MYOZ1, PGAM2, MB, PPP1R3A, MYH7, MYH2, CKM, MLIP, SPTB, RPL3L, EEF1A2, XIRP1, ATP1A2, ACTA1, ASB2, AMPD1, SRL, PRKAA2, MYBPC1, KLHL40, COX6A2, CA3, MYLK4, HIF3A, LDHD, CLEC3B, LMOD2, GDF10, MYOT, PEBP4, TCAP, PFKM, PADI2, MYOM1, GPT, MYH11, SYPL2, FXYD1, NFIX, CAND2, MYL2, SMTNL2, GAMT, SCN4A, SMYD1, COX7A1, LMOD1, TNNI2, FITM1, MYPN, SMTNL1, TRIM54, TMOD1, ANGPTL1, MYOZ2, AGBL1, CRYAB, TUBA8, SOD3, RRAGD, COQ8A, CMYA5, FABP3, MAOB, SORBS1, MYLK3, MLXIPL, ACACB, TPM2, DUSP13, NDRG2, MYLPF, RYR1, CHCHD10, MYL1, GPD1, LRRC2, ANKRD23, ART3, KLHL41, OBSCN, S100A1, PLN, NT5C1A, ADPRHL1, C10orf71, TTN, DUSP27, LRRC39, TMEM38A, SYNM, ABCA8, CACNA1S, AGL, SFRP1, RCAN2, CLIC5, SYNPO2, PHYH, HSPB7, MYBPC2, FNDC5, HRC, PLIN5, PLAC9, APOBEC2, MYOM2, CFD, NEB, ADSSL1, MYO18B, TCEA3, TNNT3, ACTN2, CAPN3, GPIHBP1, TNNT1, TMEM52, TRDN, PPP1R1A, MYL3, GOT1, STAC3, PDK4, SLC36A2, ADH1B, TXLNB, JPH1, FLNC, TNNC1, RTN2, FILIP1, SLN, GPC3, SPEG, MYH6, TMOD4, HSPB2, LMOD3, TMEM182, SMPX, DMD, CLCN4, DUSP26, AC083902.2, DES, ZBTB16, KLHL31, SNTA1, CHRDL1, ANO5, PHKG1, SGCA, AGT, RASD1, XIRP2, TRIM63, PKIA, MYF6, GRB14, CLCN1, SYNPO2L, MYH7B, NEURL1, USP13, CAMK2A, KLHL38, CAMK2B, JPH2, GMPR, UNC45B, LIMCH1, CALML6, MYOM3, HSPB8, KY, TRIM55, FHL3, ASB16, PDE4DIP, CACNG1, PLPP7, GADD45G, ACHE, ZNF106, JSRP1, ALDH1A1, PDLIM3, MYADML2, ASB5, AK1, BEST3, DYRK1B, PFKFB1, MYOZ3, ADH1C, NOS1, CSRP3, CFL2, TRIM72, SCN4B, SHISA4, DDIT4L, MYH14, PTGIS, MYLK2, CES1, ALPK3, TNNI1, TBX15, KLHL33, APOD, CAP2, PLA2G2A, CACNG6, PLIN1, TSPAN7, PGM1, SEMA6C, BIN1, MYH1, PRELP, RBM24, SH3BGRL2, CAV3, MFAP4, ANK1, STBD1, WNK2, PPP1R27, LPL, ADIPOQ, NEXN, NMRK2, CAVIN4, DPT, IP6K3, MGP, PRUNE2, CASQ2, HBA2, HBB, PODN, HSPB3, CILP, MYOG, MYH8, HBA1, KRT4

enrolled patients are summarized in **Supplementary Table 1**. After sequencing, a total of 51,349 transcripts were presented, of which 38,567 are involved in protein coding. Among these transcripts, 4,224 mRNAs and 1,470 lncRNAs were differentially expressed between TSCC tumor and adjacent tissues. Among the mRNAs, 2,792 were upregulated and 1,432 were downregulated. Among the lncRNAs identified, 947 were upregulated and in TSCC and 523 were downregulated in TSCC ($p < 0.05$).

We further screened the 40 DELs and 450 DEGs that were aberrantly expressed between all TSCC tumor and adjacent tissues. As shown in **Figure 1**, the heatmap plot of (A) the top 20 upregulated and downregulated DELs and (B) all significantly expressed mRNAs were shown. Moreover, the volcano plot of (C) the top 20 upregulated and downregulated DELs and (D) all significantly expressed mRNAs were constructed. The annotation of these DELs is summarized in **Table 1**. Information on the 450 DEGs is presented in **Table 2**.

Verification of the Expression of DELs and DEGs in Available Databases

After screening, the expression profiles of the candidate DELs and DEGs were further validated with GEPIA and StarBase. We confirmed that nine keyDELs were aberrantly expressed between TSCC tumor and normal tissues. In GEPIA, with RP11-54H7.4, MIR31HG, LINC00152, and LINC00511 being upregulated and H19, CTD-2545M3.8, RP11-760H22.2, and RP4-791M13.3 being consistently downregulated in head and neck squamous cell carcinoma (HNSC) (**Figure 2**). Moreover, the results acquired in StarBase verified that the expression of the candidate DELs, such

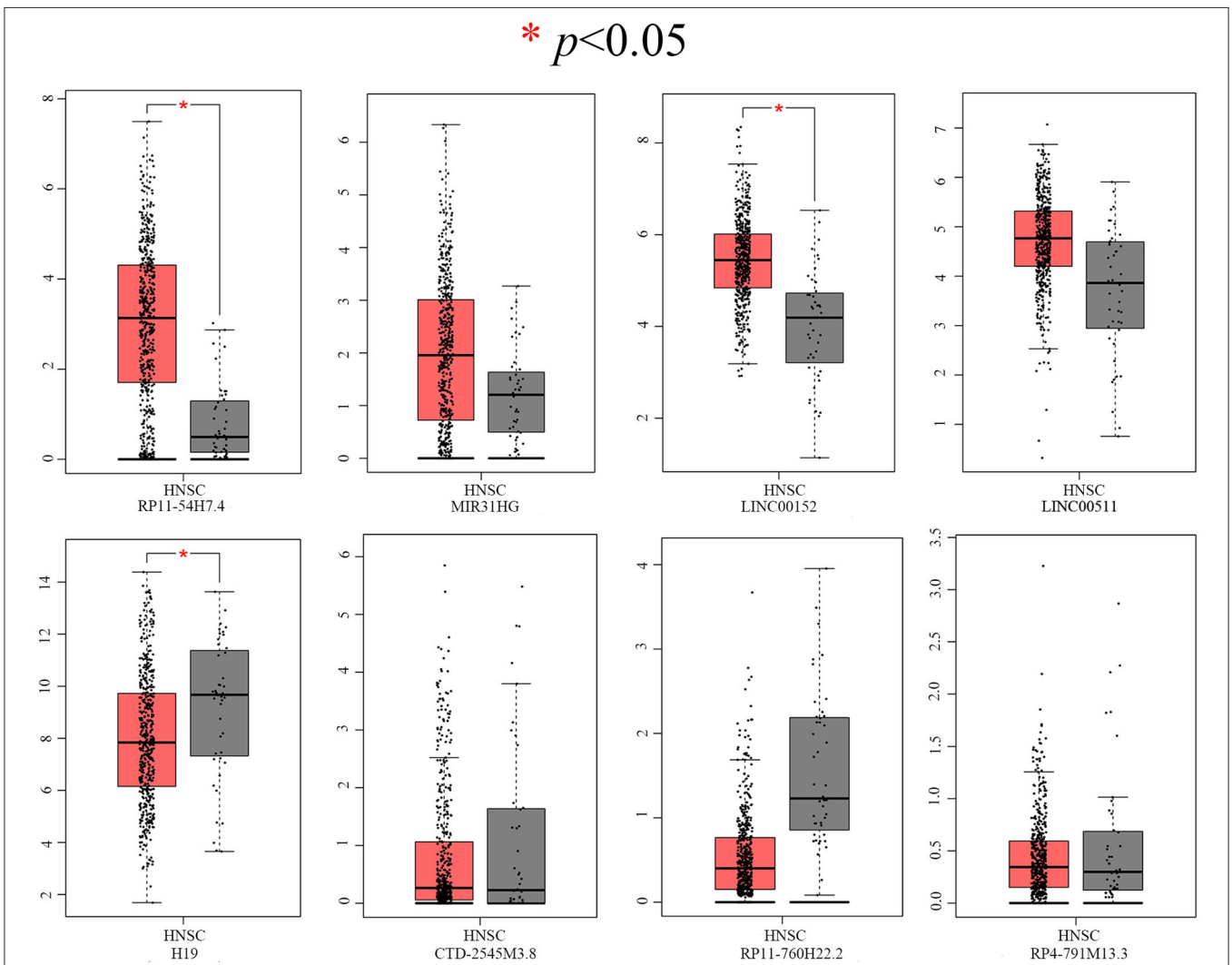

FIGURE 2 | Verification of RP11-54H7.4, MIR31HG, LINC00152, LINC00511, H19, CTD-2545M3.8, RP11-760H22.2, and RP4-791M13.3 expression in HNSC by GEPIA. The red box represents expression in tumor tissue, and the gray box represents expression in normal tissue. HNSC, head, and neck squamous cell carcinoma ($p < 0.05$).

as RP11-54H7.4, MIR31HG, LINC00152, and LINC00511, was upregulated while the expression of H19, RP11-760H22.2, and LINC01405 was downregulated in HNSC (**Figure 3**).

The GSEA Results of DELs

We also calculated the correlation between each DEL and all mRNAs so that GSEA could be performed using GSEAPreranked

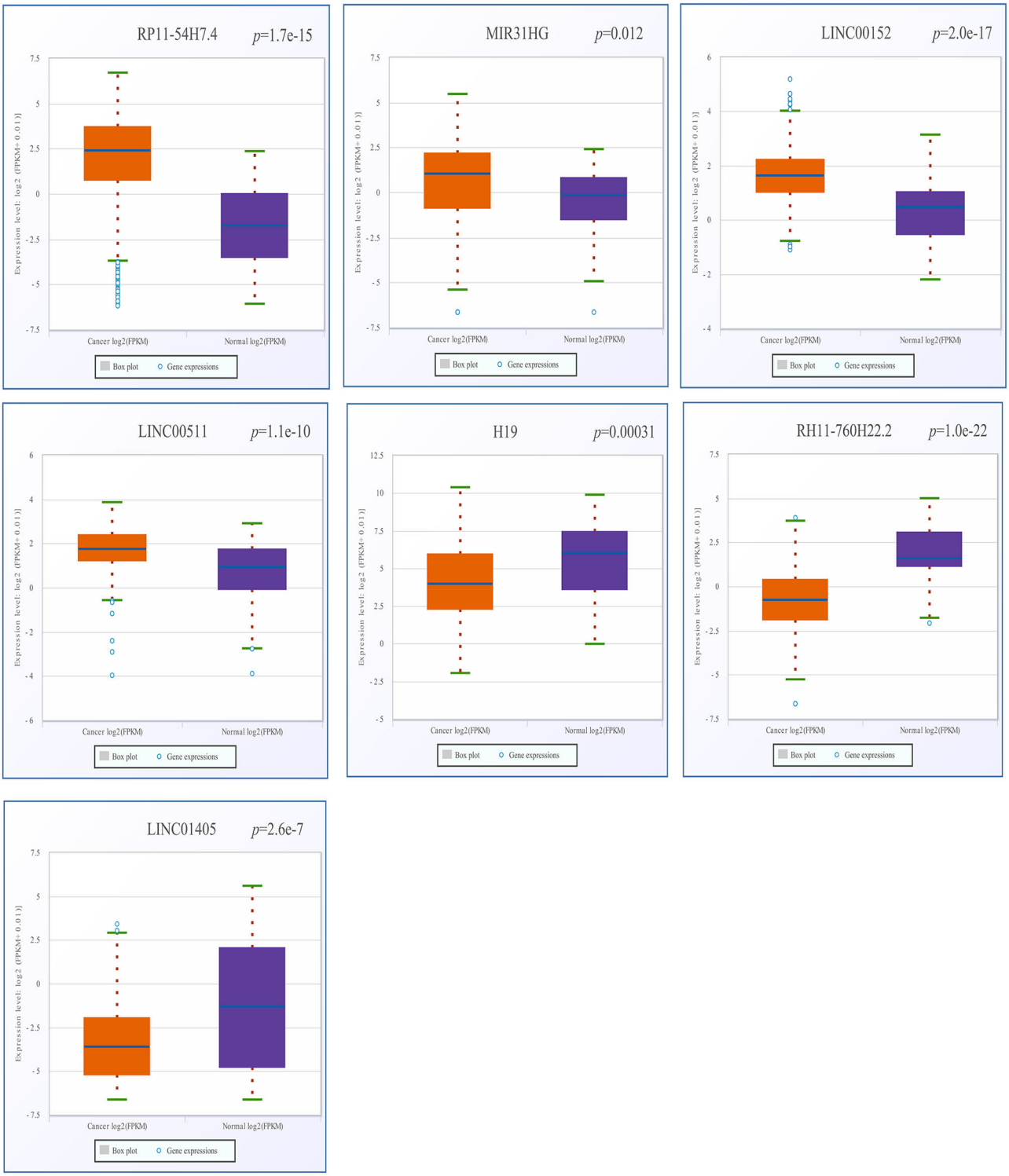

FIGURE 3 | Verification of RP11-54H7.4, MIR31HG, LINC00152, LINC00511, H19, RP11-760H22.2, and LINC01405 expression in HNSC by StarBase. The orange box represents expression in tumor tissue, and the purple box represents expression in normal tissue. HNSC, head, and neck squamous cell carcinoma.

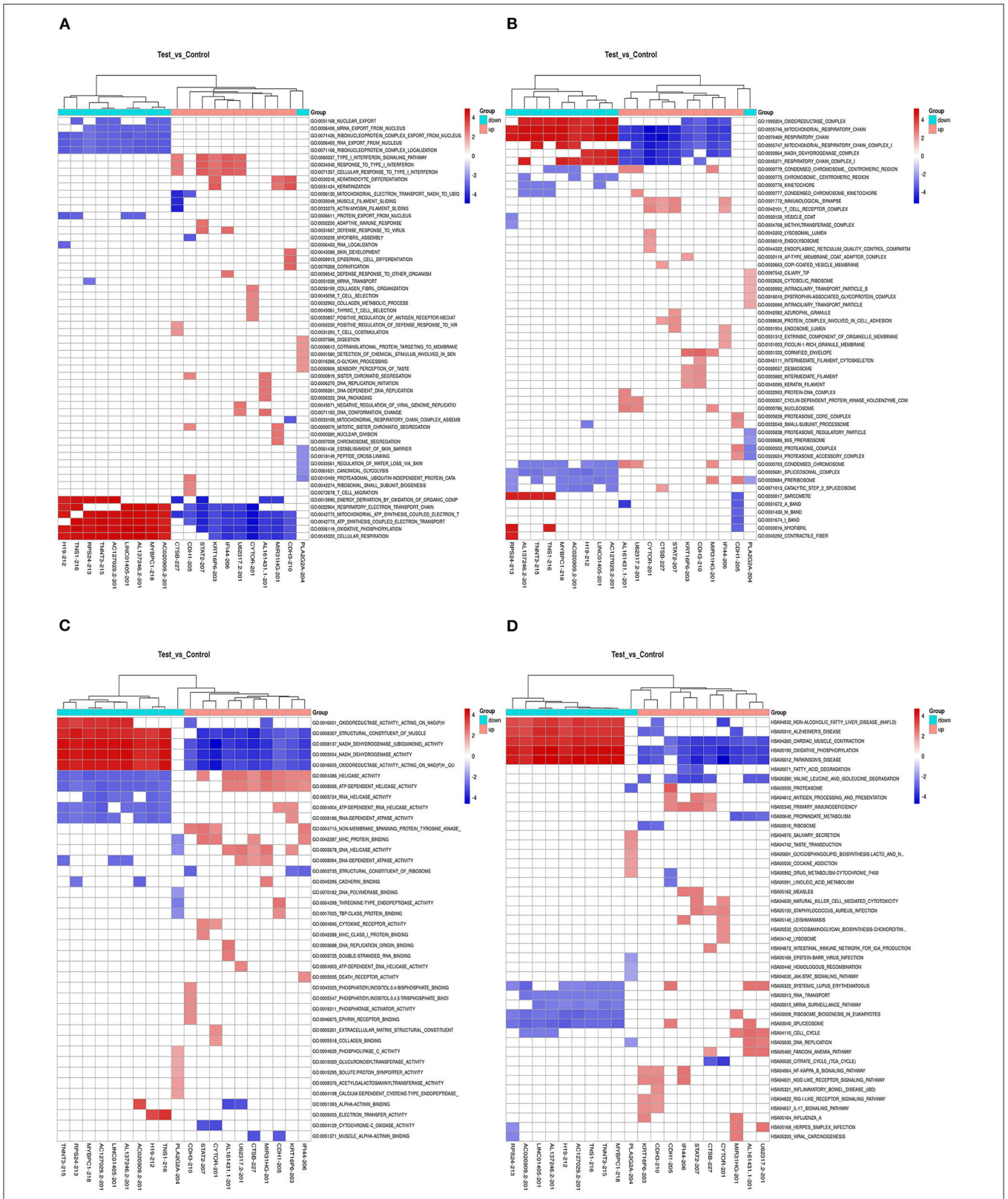

FIGURE 4 | The GSEA results the pivotal DELs. **(A)** Biological processes of the DELs. **(B)** Cellular component of the DELs. **(C)** Molecular functions of the DELs. **(D)** Pathway analysis of the DELs.

in GSEA software. The biological process (**Figure 4A**), cellular component (**Figure 4B**), molecular function (**Figure 4C**), and pathway (**Figure 4D**) analyses of the pivotal DELs, including KRT16P6-203, CTSB-227, RP11-54H7.4-201, CDH1-205, MIR31HG-201, IFI44-206, STAT2-207, LINC00152-201, CDH3-210, TNNT3-215, LINC01405-201, H19-212, TNS1-216, RPS24-213, and CTD-2545M3.8, were performed. Our data showed that the biological processes associated with the aberrantly regulated lncRNAs were cellular respiration, oxidative phosphorylation, and ATP synthesis coupled electron transport. The cellular components associated with the aberrantly regulated lncRNAs were the oxidoreductase complex mitochondrial respiratory chain and respiratory chain. The molecular functions associated with the aberrantly regulated lncRNAs were NADH

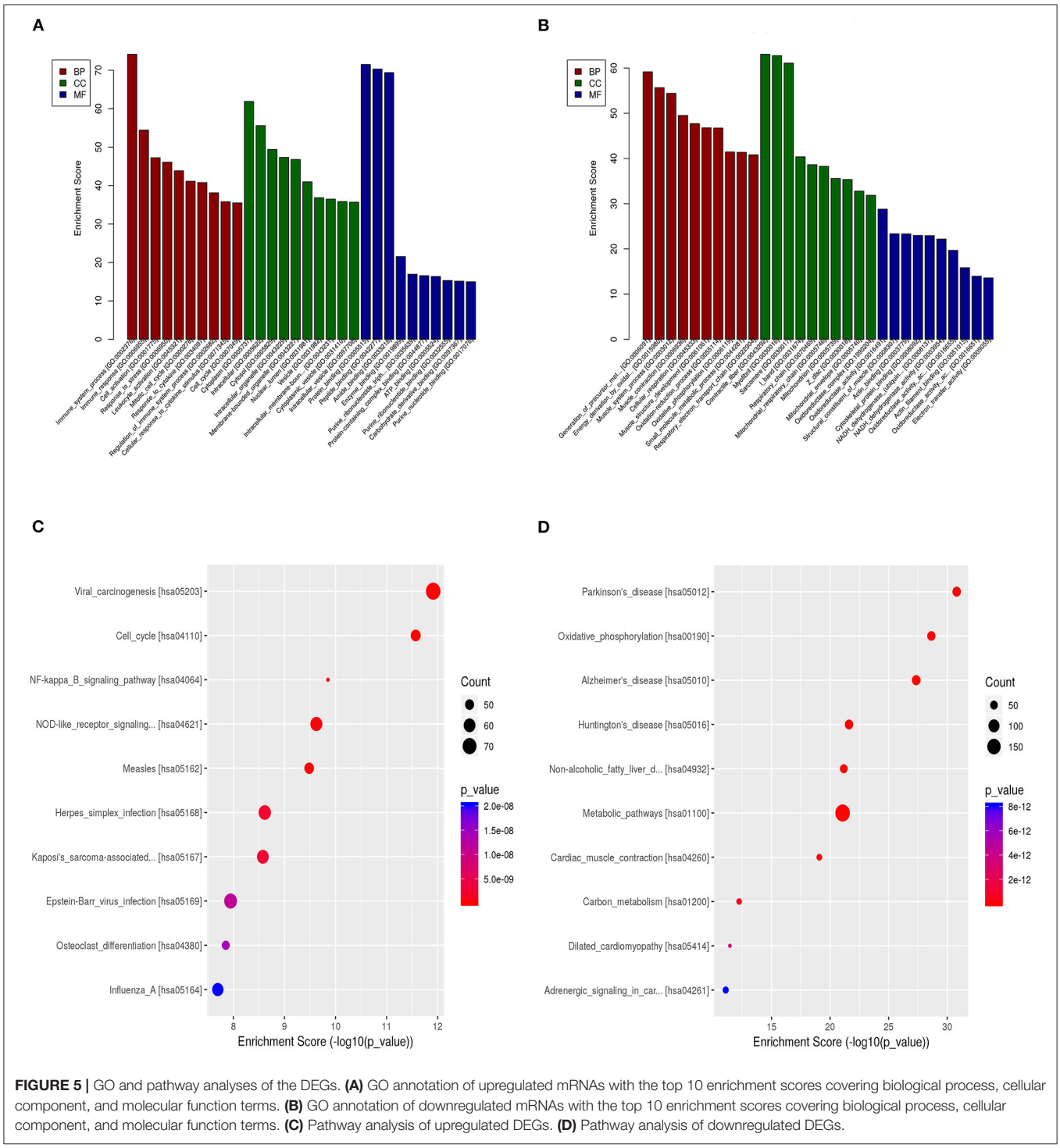

FIGURE 5 | GO and pathway analyses of the DEGs. **(A)** GO annotation of upregulated mRNAs with the top 10 enrichment scores covering biological process, cellular component, and molecular function terms. **(B)** GO annotation of downregulated mRNAs with the top 10 enrichment scores covering biological process, cellular component, and molecular function terms. **(C)** Pathway analysis of upregulated DEGs. **(D)** Pathway analysis of downregulated DEGs.

dehydrogenase activity and oxidoreductase activity. KEGG pathway enrichment analysis of the significant DELs was performed to understand gene-related pathways and molecular interactions. Our results showed that oxidative phosphorylation, RNA transport, and mRNA surveillance pathway were associated with the dysregulated lncRNAs. Meanwhile, the GSEA results of LINC00152, LINC01405, RP11-54H7.4, and RP11-760H22.2 were showed independently in **Supplementary Table 2**.

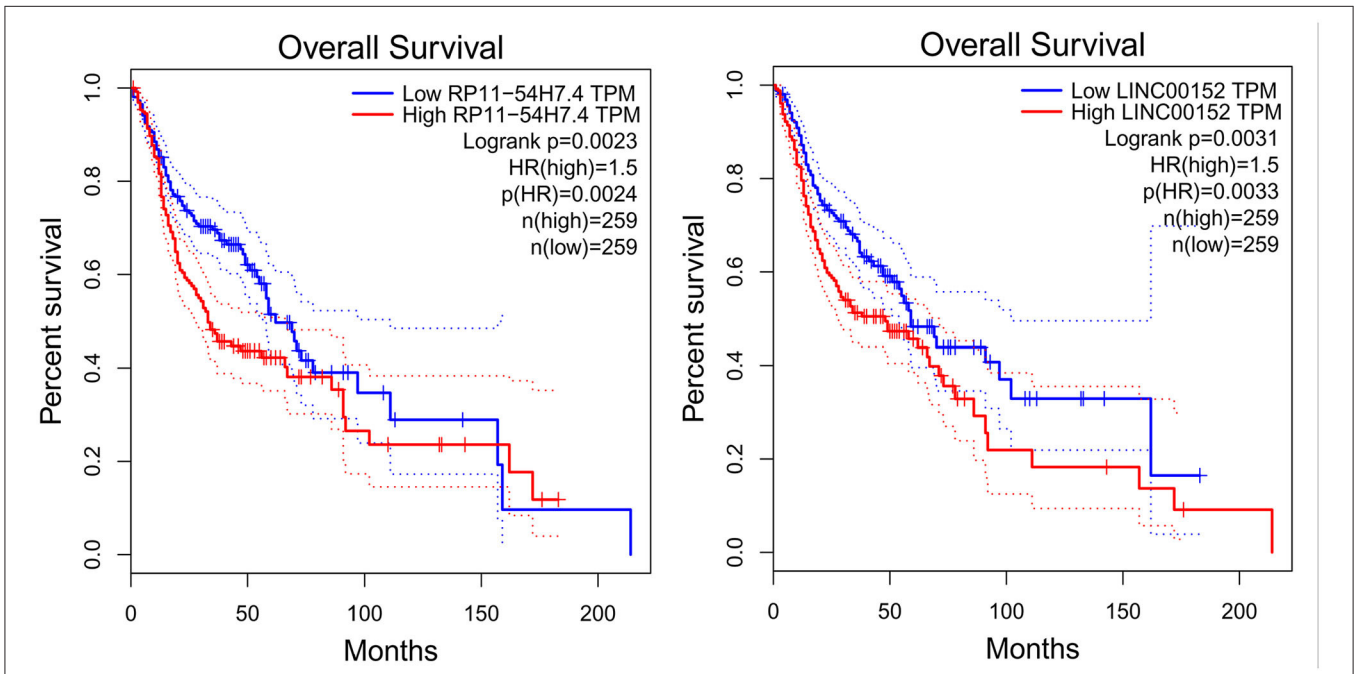

FIGURE 6 | Clinical prognostic significance of RP11-54H7.4 and LINC00152 in HNSC by GEPIA. HNSC, head, and neck squamous cell carcinoma.

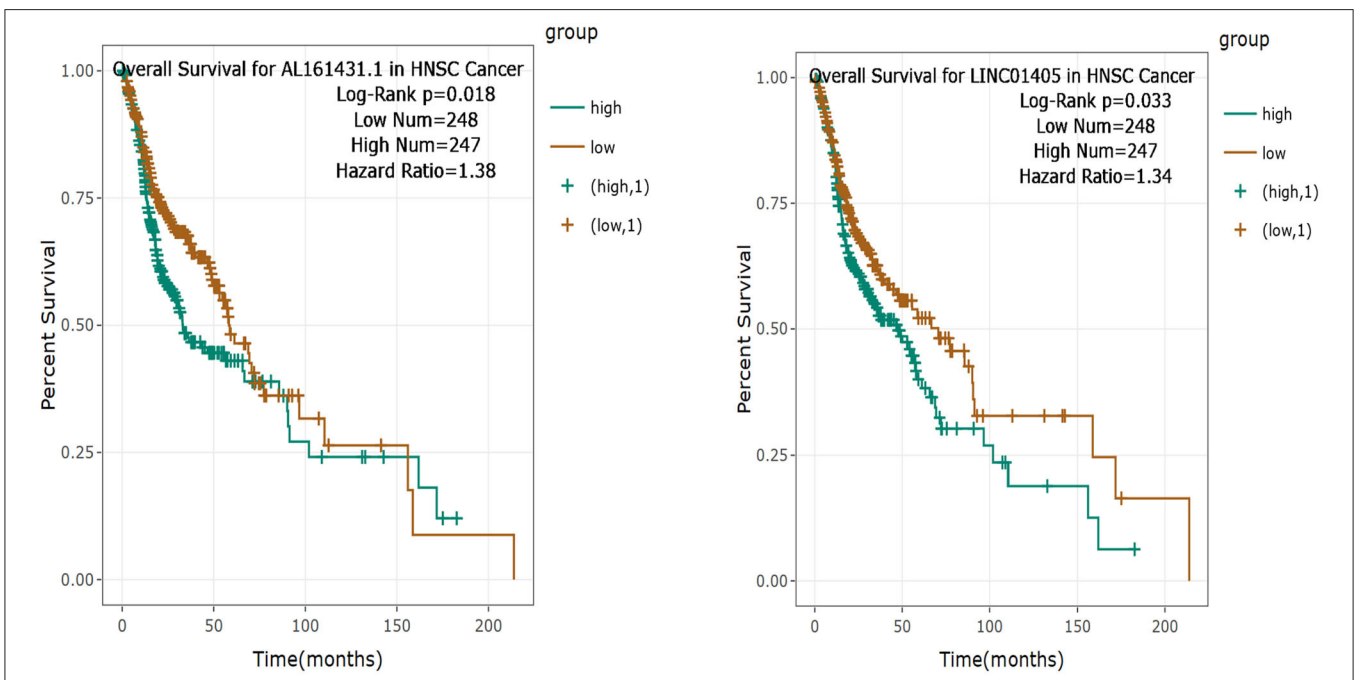

FIGURE 7 | Clinical prognostic significance of RP11-54H7.4 and LINC01405 in HNSC by StarBase. HNSC, head, and neck squamous cell carcinoma.

TABLE 3 | Intersecting mRNAs between mRNA in triplets and DEGs.

Ensembl ID	LncRNA symbol	TF symbol	Gene symbol
ENST00000304425	MIR31HG	SMAD2	FBLIM1, ACTN1, MYO1B
		E2F6	GPR68
		E2F4	FABP5
		NFKB1	DDX60, HELZ2, IFIH1
		SMARCC1	HSPB3
		SMAD4	MYO1B
		SMARCA4	ITGA3, PYGL
		EP300	GAMT
ENST00000331944	LINC00152	SMAD2	FBLIM1, ACTN1, MYO1B
		E2F6	GPR68
		E2F4	FABP5
		NFKB1	DDX60, HELZ2, IFIH1
		SMARCC1	HSPB3
		STAT1	ACP5
ENST00000453722	LINC00511	SMAD2	FBLIM1, ACTN1, MYO1B
ENST00000457958		E2F6	GPR68
		E2F4	FABP5
		SMARCA4	ITGA3, PYGL
		STAT1	ACP5
		REST	TNC
		CEBPA	S100A12
		MYC	SLC7A5
ENST00000446406	H19	ERG	SORBS1
		NFYB	AMOT, SLC2A4, DEPTOR, ADH1C, ACTN1
		RARA	TRIM55, LIMCH1
		E2F1	ACTN1
		PPARGC1A	ATP1A2
		TAF1	ZNF106
		STAT1	MLXIPL
ENST00000595005	CTD-2545M3.8	ERG	SORBS1
		NFYB	AMOT, SLC2A4, DEPTOR, ADH1C, ACTN1
		ZNF711	SLC25A4
		AR	XIRP1
ENST00000466343	RP4-791M13.3	ERG	SORBS1
		NFYB	AMOT, SLC2A4, DEPTOR, ADH1C, ACTN1
		RARA	TRIM55, LIMCH1
		SMAD2	CDH3, MYO1B, SLC7A5, ACTN1
		CEBPA	S100A12, PDZK1IP1
		TCF7L2	USP13
		E2F4	PYGL
		MED12	LIMCH1
ENST00000520544	RP11-760H22.2	ERG	SORBS1
		NFYB	AMOT, SLC2A4, DEPTOR, ADH1C, ACTN1
		RARA	TRIM55, LIMCH1
		E2F1	ACTN1
		SMAD2	CDH3, MYO1B, SLC7A5, ACTN1
		CEBPA	S100A12, PDZK1IP1
		TCF7L2	USP13
		E2F4	PYGL
		ESR2	ASB16
		MYC	PYGL
		E2F6	ACTN1
		TFAP2C	CPA4

Delineation of GO and KEGG Pathway Analyses of DEGs

GO enrichment analysis of the DEGs may reveal the roles of the significantly differentially regulated lncRNAs. Our data also showed that the biological processes associated with the upregulated mRNAs were immune system processes and the immune response (**Figure 5A**). The downregulated mRNAs were mostly enriched in the generation of precursor metabolites and energy, energy derivation by oxidation of organic compounds, and muscle system processes (**Figure 5B**). Regarding the cellular components, most of the upregulated mRNAs were related to the cytoplasm, intracellular and cytosol, and the downregulated mRNAs were mostly related to the contractile fiber, myofibril and sarcomere. Moreover, the molecular functions mainly associated with the upregulated mRNAs were protein binding, peptide binding, and amide binding, while those associated with the downregulated mRNAs were oxidoreductase activity, the structural constituent of muscle and actin binding. Importantly, KEGG pathway analysis of the DEGs revealed 20 pathways that could play pivotal roles in the mechanism of TSCC tumorigenesis, including the cell cycle, metabolic and NOD-like receptor signaling pathway (**Figures 5C,D**).

Clinical Prognostic Significance of the Pivotal DELs for TSCC Patients

Then, the significance of the nine key DELs on the overall survival of patients with TSCC was evaluated by GEPIA and StarBase independently. According to the results obtained from GEPIA (**Figure 6**), RP11-54H7.4, and LINC00152 are related to poor overall survival in patients with HNSC, while according to StarBase (**Figure 7**), RP11-54H7.4 and LINC01405 are associated with a poor prognosis for patients with HNSC. Clinical prognostic information on LINC01405 was unavailable in GEPIA, and details on CTD-2545M3.8 were not accessible in StarBase.

Construction and Analysis of the lncRNA-TF-mRNA Network

Next, LncMAP was applied to determine lncRNA-TF-mRNA triplets in TSCC. Seven of the nine pivotal DELs associated with TFs were traced. Venn diagrams were used to identify 33 overlapping mRNAs (i.e., overlapping mRNA in triplets and DEGs; **Table 3**). The expression of the intersecting mRNAs was further confirmed by GEPIA. The expression of S100A12, HSPB3, GAMT, FABP5, ASB16, CPA4, LIMCH1, MLXIPL, PDZK1IP1, TRIM55, USP13, XIRP1, and ZNF106 was not significantly different between HNSC and normal tissues (**Supplementary Figures 1, 2**). Moreover, the coexpression of TFs and overlapping mRNAs was analyzed with StarBase (**Supplementary Figures 3, 4**). Pairs of closely related TFs-mRNAs were used to build a regulatory network. Ultimately, we successfully constructed and visualized the lncRNA-TF-mRNA network, including the upregulated (**Figure 8A**) and downregulated (**Figure 8B**) DELs, with Cytoscape.

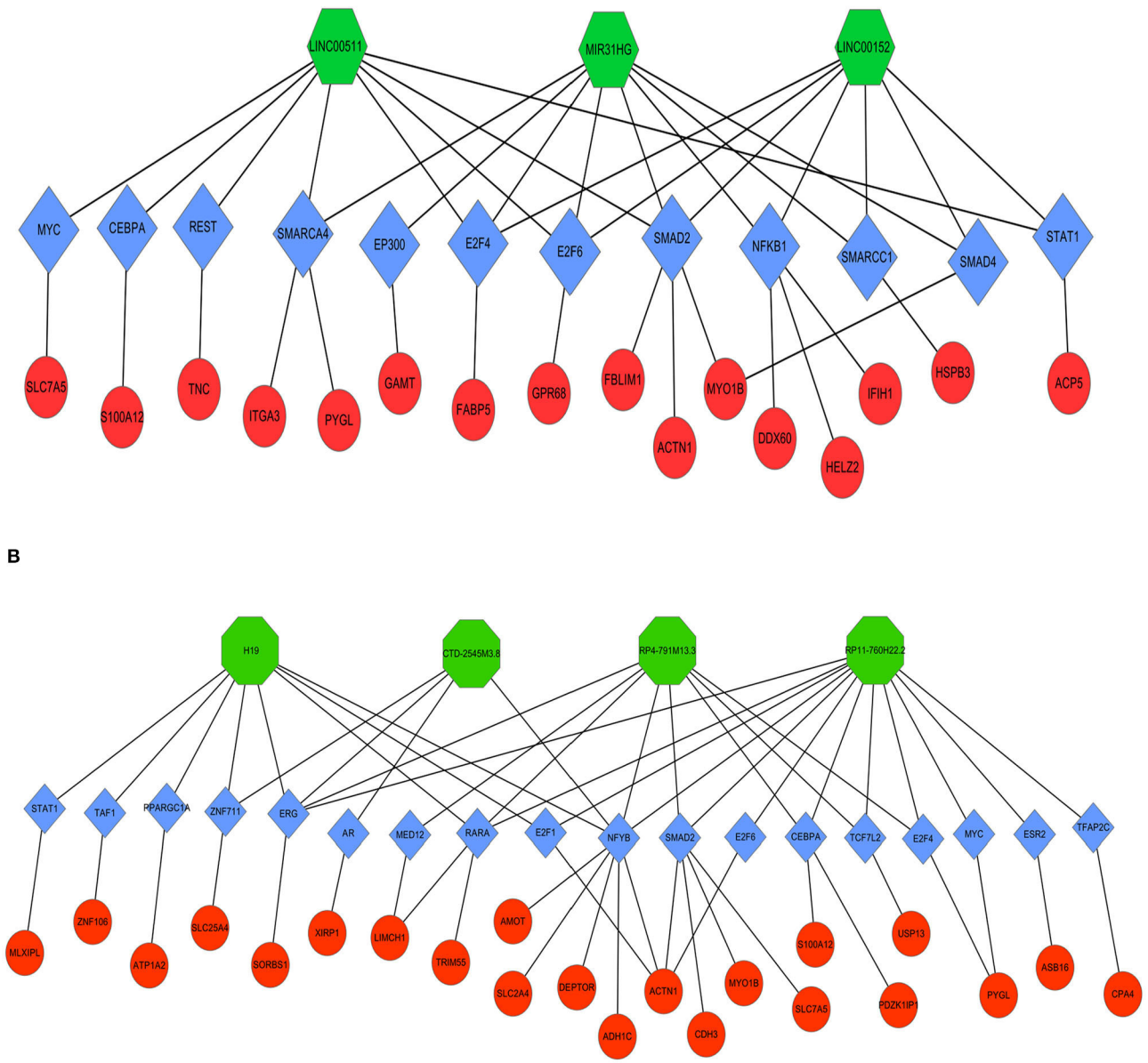

FIGURE 8 | Coexpression regulatory network of lncRNAs-TFs-mRNAs in TSCC. Octagons represent lncRNAs. Diamonds represent TFs. Ellipses represent mRNAs. **(A)** Upregulated DELs and **(B)** Downregulated DELs.

Screening Biomarkers

Furthermore, we also compared our findings with the DELs screened by TCGA database. As expected, several biomarker expression levels in our results were consistent with TCGA. A few DELs worth noting are RP11-54H7.4, LINC00152, LINC01405, and RP11-760H22.2. The expression of RP11-54H7.4, LINC00152, LINC01405, and RP11-760H22.2 were then analyzed in the TSCC and normal tissues, and their expression in the paired groups (**Figure 9**). Moreover, several pivotal GSEA results of them were performed by GSEA software independently (**Figure 10**).

Validation of the Candidate Biomarkers

qRT-PCR was performed to verify the expression levels of the candidate DELs in TSCC cell lines. The expression of CDH1-205, MIR31HG, IFI44-204, IFI44-206, RP11-54H7.4, CTSB-227, HAS3-204, CDH3-210, LEPR-206, AMOT-205, CTD-2545M3.8, LINC01405, RP11-760H22.2,

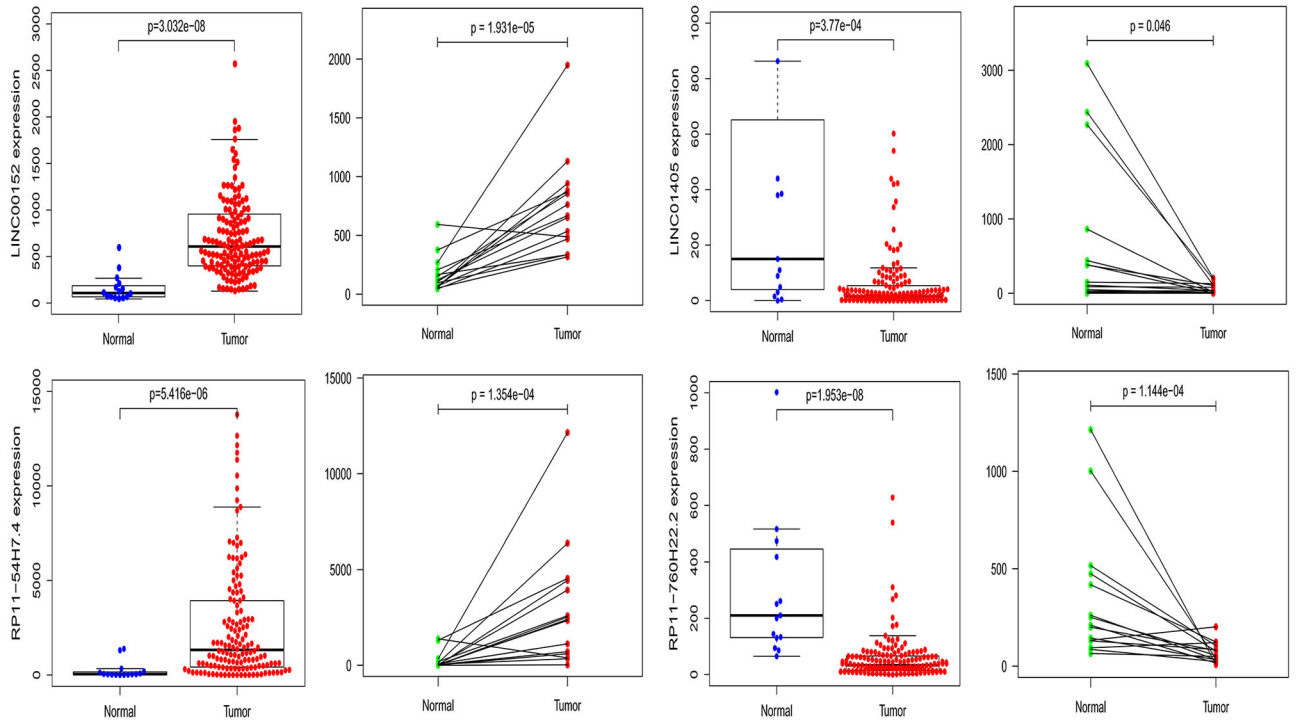

FIGURE 9 | The expression of RP11-54H7.4, LINC00152, LINC01405, and RP11-760H22.2 were then analyzed in the TSCC and normal tissues, and their expression in the paired groups.

LINC00152, and LINC00511 was consistent with the sequencing results (**Figure 11**). All primers information are listed in **Supplementary Table 3**.

DISCUSSION

Various studies have demonstrated that lncRNAs are abnormally expressed in diverse tumor types and have broad application prospects in cancer diagnosis, monitoring, prognosis, and treatment response prediction (7, 16, 17).

TSCC is the most common type of OSCC, and its pathogenesis involves the dysregulation of gene networks, including both protein-coding genes and non-coding RNAs (6–8). To date, multiple lncRNAs have been identified in TSCC, providing new perspectives for exploring the molecular mechanism of TSCC pathogenesis (18). In the current study, we sought to screen aberrantly expressed lncRNAs by performing RNA-seq analysis of TSCC tumor tissues. These data indicate that 51,349 transcripts, 38,567 of which are protein coding, 4,224 mRNAs and 1,470 lncRNAs are differentially expressed between TSCC tumor and adjacent tissues. Through data preprocessing and limma package analysis, we identified 40 candidate DELs in TSCC. Then, 15 dysregulated lncRNAs were further verified using qRT-PCR, the results may be related to the heterogeneity between different TSCC cell lines. We also selected nine pivotal lncRNAs through an online public database. Among them, in TSCC, RP11-54H7.4, MIR31HG, LINC00152, and LINC00511 were upregulated, while H19, CTD-2545M3.8, RP11-760H22.2, RP4-791M13.3, and LINC01405 were consistently downregulated. The most well-known lncRNA, MIR31HG, can act as a HIF-1α coactivator to modulate hypoxia signaling pathways in oral cancer (17). It has also been reported that the lncRNA MIR31HG facilitates HNSC cell proliferation and tumorigenesis via HIF1A and p21 by promoting cell cycle progression and inhibiting cell apoptosis (19). A previous study showed that LINC00152 might promote the growth and invasion of OSCC by regulating miR-139-5p (20). The same study proved that LINC00511 could modulate TSCC progression (21). Various findings have revealed that H19 plays a critical role in the regulation of TSCC migration and invasion (22, 23). Our results are consistent with those of previous studies, and we also found that there is limited research on RP11-54H7.4, CTD-2545M3.8, RP11-760H22.2, RP4-791M13.3, and LINC01405 in TSCC pathogenesis.

GO analysis of the DELs revealed that some biological processes and molecular functions, such as cellular respiration, and oxidative phosphorylation could be involved in the progression of TSCC. Annotation of the most significant KEGG pathways associated with the DELs manifested the important pathways that could play pivotal roles in the mechanism of TSCC tumorigenesis, including oxidative phosphorylation, RNA transport, and mRNA surveillance pathway, suggesting that dysregulated lncRNAs may have a great influence on these targets by regulating associated pathways in TSCC. However, the functions of most lncRNAs are not well-understood.

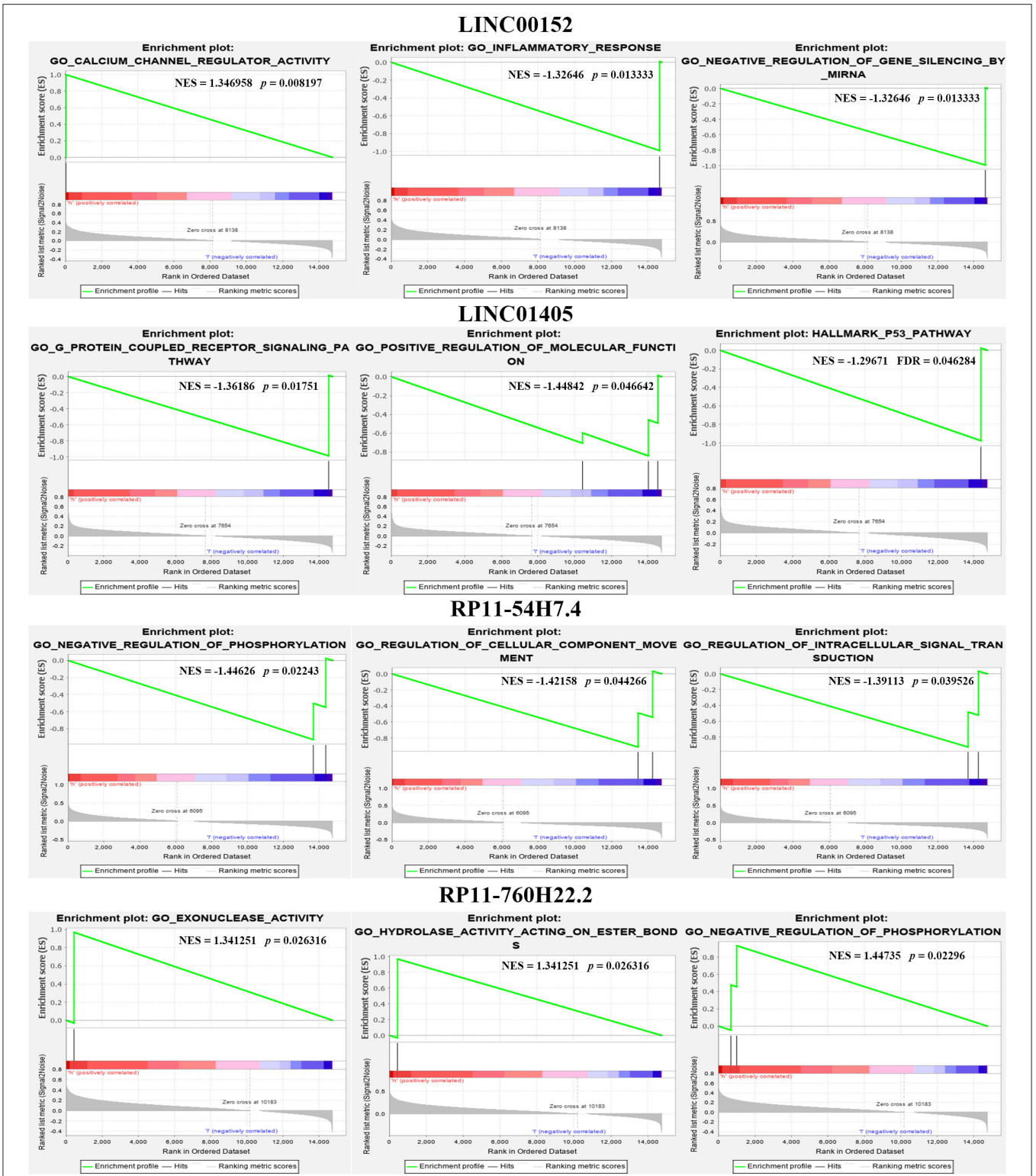

FIGURE 10 | Several pivotal GSEA results of RP11-54H7.4, LINC00152, LINC01405, and RP11-760H22.2 were performed by GSEA software independently.

The most significant GO terms of the DEGs were immune system processes, the immune response, and protein binding. KEGG pathway analysis of the DEGs revealed 20 pathways that could play pivotal roles in the mechanism of TSCC tumorigenesis, including the cell cycle, metabolic, and NOD-like receptor signaling pathway. The results suggest that these

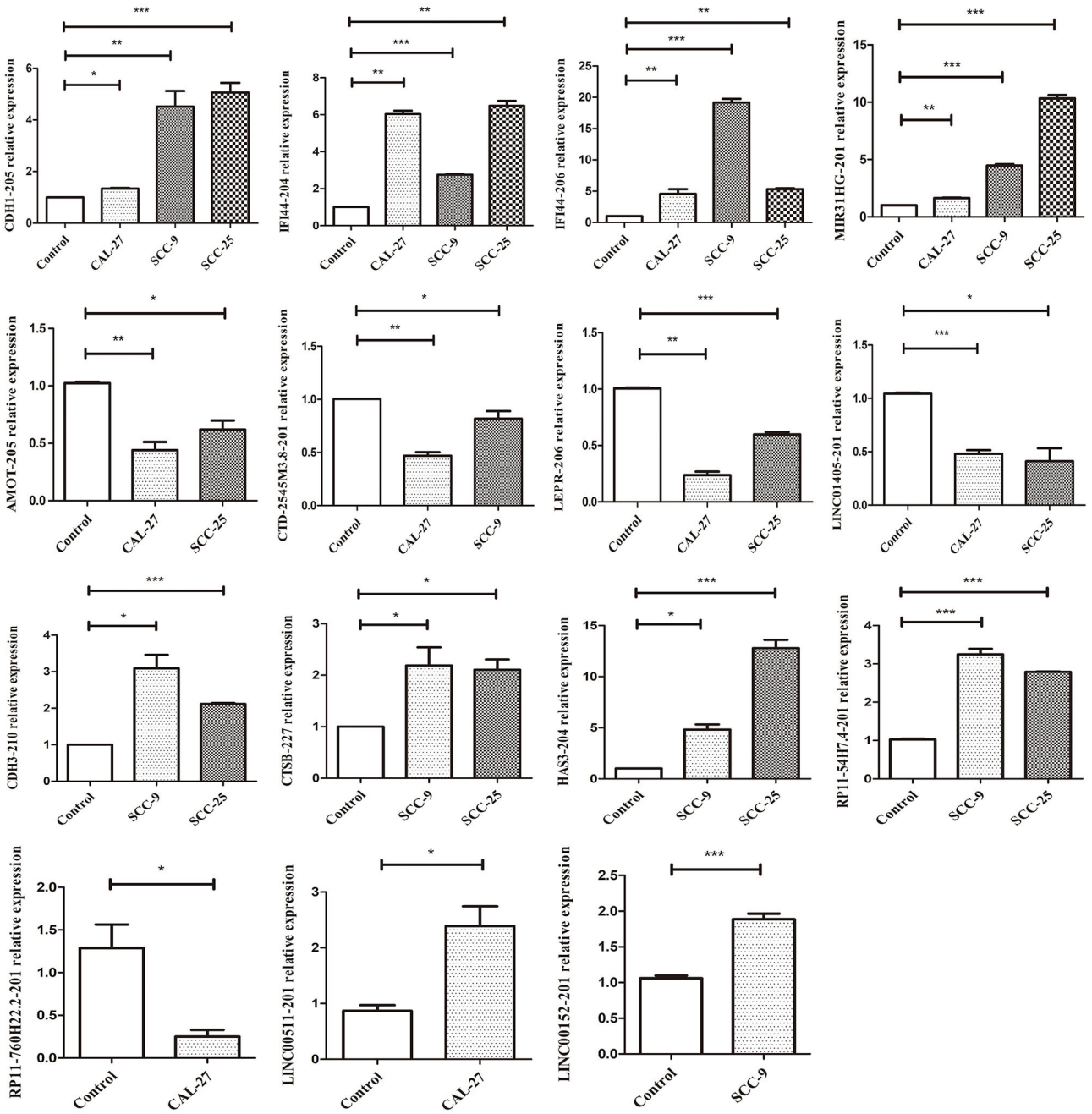

FIGURE 11 | qRT-PCR validation of significant DELs from sequencing (***$p < 0.001$, **$p < 0.01$, and *$p < 0.05$).

pathways might contribute significantly to the pathogenesis and progression of TSCC.

This study found that RP11-54H7.4, LINC00152, and LINC01405 are significantly aberrantly expressed based on the RNA-seq expression profile and associated with poor clinical outcomes in TSCC patients, the results are consistent with prior studies (24, 25). The expression of these lncRNAs was further confirmed in GEPIA and StarBase. Besides, the expression of RP11-54H7.4, LINC00152, LINC01405, and RP11-760H22.2 were also verified with TSCC samples in TCGA. Thus, RP11-54H7.4, LINC00152, and LINC01405 could represent prognostic biomarkers of TSCC.

Research shows that lncRNAs might play a role in trans-acting regulation via TFs, while the interactions between lncRNAs and TFs may ameliorate the expression levels of their target genes (26). The expression of target genes could also be regulated by TFs combining cis-elements at promoter locations (27). It is known that some TFs are involved in TSCC pathogenesis.

To further investigate the functions of DELs in TSCC, seven of nine pivotal DELs associated TFs, namely, SMAD2, E2F6, E2F4, CEBPA, STAT1, MYC, ERG, and NFYB, were further analyzed. Research has demonstrated that SMAD2 acts as a predictor of overall survival in OSCC patients (28). Additionally, SMAD2 directly binds to the lncRNA MACC1-AS1 promoter and thus increases MACC1-AS1 expression in nasopharyngeal carcinoma (29). Studies have also shown that silencing the lncRNA CEBPA-AS1 can regulate OSCC cell proliferation, cell apoptosis, migration, and invasion by targeting CEBPA and via a novel pathway, CEBPA/Bcl2 (30). Similarly, abundant studies demonstrated that E2F4, STAT1, MYC, ERG, and NFYB may play an important role in the pathogenesis and progression of various cancers, including OSCC, and the underlying mechanism may be related to dysregulated lncRNA (31–37). All of these studies confirm that the TFs screened in our research play a critical role in tumor pathogenesis. However, the underlying mechanisms remain unknown. Therefore, we hypothesized that these TFs play vital roles in the tumorigenesis of TSCC by regulating lncRNAs and mRNAs. In addition, the relationship between lncRNAs and TFs requires further investigation.

The overlapping genes were screened by comparing the mRNA in triplets and DEGs. Some vital mRNAs, including MYO1B, ACTN1, PYGL, S100A12, and SLC7A5, are associated with TSCC (38–40). We also found that many TF expression levels were significantly correlated with the expression of multiple protein-coding genes. We thus deduce that these TFs might be correlated with the carcinogenesis of TSCC by regulating coexpressing genes. Therefore, a coexpression network was built to further investigate the relationship of the dysregulated TFs and mRNAs. We were able to successfully build the lncRNA-TF-mRNA network by combining all the results. The lncRNA-TF-mRNA coexpression network was constructed to predict lncRNA function. More critically, the interaction network of the significantly dysregulated lncRNAs with their TFs and coding genes was delineated, which might provide new clues for elucidating the underlying mechanism of TSCC.

CONCLUSION

To conclude, we found a profile of dysregulated lncRNAs, TFs, and mRNAs that could serve as prospective clinical biomarkers because of their tissue specificity and association with the tumorigenesis and progression of TSCC. Our study might lay a foundation for further functional research on lncRNAs-TFs-mRNAs in TSCC. The composite analysis of lncRNAs, TFs, and differentially coexpressed genes may provide a more comprehensive understanding of the pathogenesis of TSCC. Our results also suggest that specific lncRNAs, TFs, and mRNAs could be valuable for the diagnosis and treatment of tongue cancer, contribute to the application of lncRNAs in cancer and provide deep insights into the biological mechanism of TSCC. Intriguingly, this is the first study to show that RP11-54H7.4, LINC00152, and LINC01405 can be acted as a prognostic target for TSCC.

Similar to other approaches, our study also had certain limitations. First, in the survival analysis, because of the lack of clinical data that matched our data, it was difficult to further validate some prognosis-related lncRNAs. Furthermore, the interaction between lncRNAs, TFs, and mRNAs still lacks experimental verification. These deficiencies will be improved by complementing these data in the future.

DATA AVAILABILITY STATEMENT

The datasets presented in this study can be found in online repositories. The names of the repository/repositories and accession number(s) can be found below: https://www.ncbi.nlm.nih.gov/geo/, GSE149008/b.

ETHICS STATEMENT

The studies involving human participants were reviewed and approved by Ethics Committee of the First Affiliated Hospital of Fujian Medical University. The patients/participants provided their written informed consent to participate in this study.

AUTHOR CONTRIBUTIONS

MZ: research design and implementation. ZC, YL, and YH: data analysis and interpretation. SZ, YJ, and LW: statistical analysis. MZ: writing of the manuscript. JC and BS: revision of the manuscript. All authors contributed to the article and approved the submitted version.

FUNDING

This work was supported by the National Natural Science Foundation of China (Grant No. 81771126) and Startup Fund for Scientific Research, Fujian Medical University (Grant No. 2016QH075).

ACKNOWLEDGMENTS

We would like to express our sincere thanks to all those who have helped us in the course of our writing this paper.

SUPPLEMENTARY MATERIAL

The Supplementary Material for this article can be found online at: https://www.frontiersin.org/articles/10.3389/fonc.2020.01421/full#supplementary-material

REFERENCES

1. Pannone G, Santoro A, Papagerakis S, Lo ML, De Rosa G, Bufo P. The role of human papillomavirus in the pathogenesis of head & neck squamous cell carcinoma: an overview. *Infect Agents Cancer*. (2011) 6:4. doi: 10.1186/1750-9378-6-4
2. Casiglia J, Woo SB. A comprehensive review of oral cancer. *Gen Dent*. (2001) 49:72–82.

3. Prensner JR, Chinnaiyan AM. The emergence of lncRNAs in cancer biology. *Cancer Discov*. (2011) 1:391–407. doi: 10.1158/2159-8290.CD-11-0209
4. Guo X, Gao L, Wang Y, Chiu DK, Wang T, Deng Y. Advances in long noncoding RNAs: identification, structure prediction and function annotation. *Brief Funct Genomics*. (2016) 15:38–46. doi: 10.1093/bfgp/elv022
5. Zhang Y, Liao G, Bai J, Zhang X, Xu L, Deng C, et al. Identifying cancer driver lncRNAs bridged by functional effectors through integrating multi-omics data in human cancers. *Mol Ther Nucleic Acids*. (2019) 17:362–73. doi: 10.1016/j.omtn.2019.05.030
6. Jia B, Xie T, Qiu X, Sun X, Chen J, Huang Z, et al. Long noncoding RNA FALEC inhibits proliferation and metastasis of tongue squamous cell carcinoma by epigenetically silencing ECM1 through EZH2. *Aging*. (2019) 11:4990–5007. doi: 10.18632/aging.102094
7. Zhang H, Zhao L, Wang YX, Xi M, Liu SL, Luo LL. Long non-coding RNA HOTTIP is correlated with progression and prognosis in tongue squamous cell carcinoma. *Tumour Biol*. (2015) 36:8805–9. doi: 10.1007/s13277-015-3645-2
8. Fang Z, Zhang S, Wang Y, Shen S, Wang F, Hao Y, et al. Long non-coding RNA MALAT-1 modulates metastatic potential of tongue squamous cell carcinomas partially through the regulation of small proline rich proteins. *BMC Cancer*. (2016) 16:706. doi: 10.1186/s12885-016-2735-x
9. Liang J, Liang L, Ouyang K, Li Z, Yi X. MALAT1 induces tongue cancer cells' EMT and inhibits apoptosis through Wnt/beta-catenin signaling pathway. *J Oral Pathol Med*. (2017) 46:98–105. doi: 10.1111/jop.12466
10. Wang ZY, Hu M, Dai M, Xiong J, Zhang S, Wu H, et al. Upregulation of the long non-coding RNA AFAP1-AS1 affects the proliferation, invasion and survival of tongue squamous cell carcinoma via the Wnt/β-catenin signaling pathway. *Mol Cancer*. (2018) 17:3. doi: 10.1186/s12943-017-0752-2
11. Fang Z, Wu L, Wang L, Yang Y, Meng Y, Yang H. Increased expression of the long non-coding RNA UCA1 in tongue squamous cell carcinomas: a possible correlation with cancer metastasis. *Oral Surg Oral Med Oral Pathol Oral Radiol*. (2014) 117:89–95. doi: 10.1016/j.oooo.2013.09.007
12. Zhang S, Ma H, Zhang D, Xie S, Wang W, Li Q, et al. LncRNA KCNQ1OT1 regulates proliferation and cisplatin resistance in tongue cancer via miR-211-5p mediated Ezrin/Fak/Src signaling. *Cell Death Dis*. (2018) 9:742. doi: 10.1038/s41419-018-0793-5
13. Liu X, Zhang B, Jia Y, Fu M. SNHG17 enhances the malignant characteristics of tongue squamous cell carcinoma by acting as a competing endogenous RNA on microRNA-876 and thereby increasing specificity protein 1 expression. *Cell Cycle*. (2020) 19:711–25. doi: 10.1080/15384101.2020.1727399
14. Tang Z, Li C, Kang B, Gao G, Li C, Zhang Z. GEPIA: a web server for cancer and normal gene expression profiling and interactive analyses. *Nucleic Acids Res*. (2017) 45:W98–102. doi: 10.1093/nar/gkx247
15. Li JH, Liu S, Zhou H, Qu LH, Yang JH. starBase v2.0: decoding miRNA-ceRNA, miRNA-ncRNA and protein-RNA interaction networks from large-scale CLIP-Seq data. *Nucleic Acids Res*. (2014) 42:D92–7. doi: 10.1093/nar/gkt1248
16. Arunkumar G, Murugan AK, Prasanna SRH, Subbiah S, Rajaraman R, Munirajan AK. Long non-coding RNA CCAT1 is overexpressed in oral squamous cell carcinomas and predicts poor prognosis. *Biomed Rep*. (2017) 6:455–62. doi: 10.3892/br.2017.876
17. Shih JW, Chiang WF, Wu A, Wu MH, Wang LY, Yu YL, et al. Long noncoding RNA LncHIFCAR/MIR31HG is a HIF-1alpha co-activator driving oral cancer progression. *Nat Commun*. (2017) 8:15874. doi: 10.1038/ncomms15874
18. Zhang L, Meng X, Zhu XW, Yang DC, Chen R, Jiang Y, et al. Long non-coding RNAs in Oral squamous cell carcinoma: biologic function, mechanisms and clinical implications. *Mol Cancer*. (2019) 18:102. doi: 10.1186/s12943-019-1021-3
19. Wang R, Ma Z, Feng L, Yang Y, Tan C, Shi Q, et al. LncRNA MIR31HG targets HIF1A and P21 to facilitate head and neck cancer cell proliferation and tumorigenesis by promoting cell-cycle progression. *Mol Cancer*. (2018) 17:162. doi: 10.1186/s12943-018-0916-8
20. Li M, Ning J, Li Z, Wang J, Zhao C, Wang L. LINC00152 promotes the growth and invasion of oral squamous cell carcinoma by regulating miR-139-5p. *Onco Targets Ther*. (2018) 11:6295–304. doi: 10.2147/OTT.S168807
21. Ding J, Yang C, Yang S. LINC00511 interacts with miR-765 and modulates tongue squamous cell carcinoma progression by targeting LAMC2. *J Oral Pathol Med*. (2018) 47:468–76. doi: 10.1111/jop.12677
22. Zhang DM, Lin ZY, Yang ZH, Wang YY, Wan D, Zhong JL, et al. lncRNA H19 promotes tongue squamous cell carcinoma progression through beta-catenin/GSK3beta/EMT signaling via association with EZH2. *Am J Transl Res*. (2017) 9:3474–86.
23. Kou N, Liu S, Li X, Li W, Zhong W, Gui L, et al. H19 facilitates tongue squamous cell carcinoma migration and invasion via sponging miR-let-7. *Oncol Res*. (2019) 27:173–82. doi: 10.3727/096504018X15202945197589
24. Yu J, Liu Y, Guo C, Zhang S, Gong Z, Tang Y, et al. Upregulated long non-coding RNA LINC00152 expression is associated with progression and poor prognosis of tongue squamous cell carcinoma. *J Cancer*. (2017) 8:523–30. doi: 10.7150/jca.17510
25. Pentenero M, Bowers LM, Jayasinghe R, Yap T, Cheong SC, Kerr AR, et al. World workshop on oral medicine VII: clinical evidence of differential expression of lncRNAs in oral squamous cell carcinoma: a scoping review. *Oral Dis*. (2019) 25 (Suppl. 1):88–101. doi: 10.1111/odi.13076
26. Vance KW, Sansom SN, Lee S, Chalei V, Kong L, Cooper SE, et al. The long non-coding RNA paupar regulates the expression of both local and distal genes. *EMBO J*. (2014) 33:296–311. doi: 10.1002/embj.201386225
27. Tian L, Cao J, Deng X, Zhang C, Qian T, Song X, et al. Unveiling transcription factor regulation and differential co-expression genes in duchenne muscular dystrophy. *Diagn Pathol*. (2014) 9:210. doi: 10.1186/s13000-014-0210-z
28. Mangone FR, Walder F, Maistro S, Pasini FS, Lehn CN, Carvalho MB, et al. Smad2 and Smad6 as predictors of overall survival in oral squamous cell carcinoma patients. *Mol Cancer*. (2010) 9:106. doi: 10.1186/1476-4598-9-106
29. Chen S, Luo X, Wu W, Li Y, Yu H, Wang Y, et al. The long non-coding RNA MACC1-AS1 promotes nasopharyngeal carcinoma cell stemness via suppressing miR-145-mediated inhibition on SMAD2/MACC1-AS1 axis. *Biomed Pharmacother*. (2020) 125:109986. doi: 10.1016/j.biopha.2020.109986
30. Guo Y, Ma Y, Hu X, Song R, Zhu L, Zhong M. Long non-coding RNA CEBPA-AS1 correlates with poor prognosis and promotes tumorigenesis via CEBPA/Bcl2 in oral squamous cell carcinoma. *Cancer Biol Ther*. (2018) 19:205–13. doi: 10.1080/15384047.2017.1416276
31. Russo G, Zamparelli A, Howard CM, Minimo C, Bellan C, Carillo G, et al. Expression of cell cycle-regulated proteins pRB2/p130, p107, E2F4, p27, and pCNA in salivary gland tumors: prognostic and diagnostic implications. *Clin Cancer Res*. (2005) 11:3265–73. doi: 10.1158/1078-0432.CCR-04-2508
32. Jung HM, Patel RS, Phillips BL, Wang H, Cohen DM, Reinhold WC, et al. Tumor suppressor miR-375 regulates MYC expression via repression of CIP2A coding sequence through multiple miRNA-mRNA interactions. *Mol Biol Cell*. (2013) 24:1638–48, S1–7. doi: 10.1091/mbc.e12-12-0891
33. Wu L, Zhao JC, Kim J, Jin HJ, Wang CY, Yu J. ERG is a critical regulator of Wnt/LEF1 signaling in prostate cancer. *Cancer Res*. (2013) 73:6068–79. doi: 10.1158/0008-5472.CAN-13-0882
34. Bing F, Zhao Y. Screening of biomarkers for prediction of response to and prognosis after chemotherapy for breast cancers. *Onco Targets Ther*. (2016) 9:2593–600. doi: 10.2147/OTT.S92350
35. Arunkumar G, Anand S, Raksha P, Dhamodharan S, Prasanna SRH, Subbiah S, et al. LncRNA OIP5-AS1 is overexpressed in undifferentiated oral tumors and integrated analysis identifies as a downstream effector of stemness-associated transcription factors. *Sci Rep*. (2018) 8:7018. doi: 10.1038/s41598-018-25451-3
36. Xu H, Jiang Y, Xu X, Su X, Liu Y, Ma Y, et al. Inducible degradation of lncRNA Sros1 promotes IFN-γ-mediated activation of innate immune responses by stabilizing Stat1 mRNA. *Nat Immunol*. (2019) 20:1621–30. doi: 10.1038/s41590-019-0542-7
37. Ryan N, Anderson K, Volpedo G, Hamza O, Varikuti S, Satoskar AR, et al. STAT1 inhibits T-cell exhaustion and myeloid derived suppressor cell accumulation to promote antitumor immune responses in head and neck squamous cell carcinoma. *Int J Cancer*. (2020) 146:1717–29. doi: 10.1002/ijc.32781

38. Ohmura G, Tsujikawa T, Yaguchi T, Kawamura N, Mikami S, Sugiyama J, et al. Aberrant myosin 1b expression promotes cell migration and lymph node metastasis of HNSCC. *Mol Cancer Res*. (2015) 13:721–31. doi: 10.1158/1541-7786.MCR-14-0410
39. Gao W, Li JZ, Chen SQ, Chu CY, Chan JY, Wong TS. Decreased brain-expressed X-linked 4 (BEX4) expression promotes growth of oral squamous cell carcinoma. *J Exp Clin Cancer Res*. (2016) 35:92. doi: 10.1186/s13046-016-0355-6
40. Wang R, Zhou X, Wang H, Zhou B, Dong S, Ding Q, et al. Integrative analysis of gene expression profiles reveals distinct molecular characteristics in oral tongue squamous cell carcinoma. *Oncol Lett*. (2019) 17:2377–87. doi: 10.3892/ol.2018.9866

Conflict of Interest: The authors declare that the research was conducted in the absence of any commercial or financial relationships that could be construed as a potential conflict of interest.

Copyright © 2020 Zhang, Chen, Zhang, Wu, Jie, Liao, Huang, Chen and Shi. This is an open-access article distributed under the terms of the Creative Commons Attribution License (CC BY). The use, distribution or reproduction in other forums is permitted, provided the original author(s) and the copyright owner(s) are credited and that the original publication in this journal is cited, in accordance with accepted academic practice. No use, distribution or reproduction is permitted which does not comply with these terms.

frontiers in Oncology

REVIEW
published: 02 October 2020
doi: 10.3389/fonc.2020.561833

The Role of lncRNA Crosstalk in Leading Cancer Metastasis of Head and Neck Squamous Cell Carcinoma

Yu Wang[1,2,3], *Sinan Wang*[4,5], *Yu Ren*[6] *and Xuan Zhou*[1,2,3]*

[1] Department of Maxillofacial and Otorhinolaryngological Oncology, Tianjin Medical University Cancer Institute and Hospital, Tianjin, China, [2] Key Laboratory of Cancer Prevention and Therapy, Tianjin Cancer Institute, Tianjin, China, [3] National Clinical Research Center of Cancer, Tianjin, China, [4] Department of Gastroenterology and Hepatology, Tianjin Medical University General Hospital, Tianjin, China, [5] Tianjin Gastroenterology and Hepatology Institute, Tianjin Medical University, Tianjin, China, [6] Tianjin Research Center of Basic Medical Science, Tianjin Medical University, Tianjin, China

Head and neck squamous cell carcinoma (HNSCC) is the sixth most common type of human malignancy. For decades, research into HNSCC invasion and metastasis has been dedicated to the study of protein-coding genes. Along with whole-genome and transcriptome sequencing development, long non-coding RNA (lncRNA) has attracted greater attention. Compelling evidence has proven the critical role of lncRNAs in the occurrence and development of HNSCC by means of epigenetic modifications, regulation of gene transcription, and post-transcription level. More importantly, crosstalk between lncRNAs and microRNAs was recently proven to regulate HNSCC metastasis through EMT modification. Based on these, this review summarizes the critical roles of lncRNAs in HNSCC metastasis and the crosstalk between lncRNAs and microRNAs as well as the detailed regulatory mechanism of the interaction. Thus, a deeper understanding of the lncRNA network in cancer metastasis is finally uncovered in order to provide a rationale and innovative concepts toward new therapeutic strategies for the highly metastatic HNSCC.

Keywords: head and neck squamous cell carcinoma, long non-coding RNA, metastasis, EMT, invasion

OPEN ACCESS

Edited by:
Wei Cao,
Shanghai Jiao Tong University, China

Reviewed by:
Cheng Wang,
Sun Yat-sen University, China
Yanjie Zhang,
Shanghai Jiao Tong University, China
Madhu Khullar,
Post Graduate Institute of Medical Education and Research (PGIMER), India

***Correspondence:**
Xuan Zhou
byron2000zhou@sina.com

Specialty section:
This article was submitted to Head and Neck Cancer, a section of the journal Frontiers in Oncology

Received: *13 May 2020*
Accepted: *27 August 2020*
Published: *02 October 2020*

Citation:
Wang Y, Wang S, Ren Y and Zhou X (2020) The Role of lncRNA Crosstalk in Leading Cancer Metastasis of Head and Neck Squamous Cell Carcinoma. Front. Oncol. 10:561833. doi: 10.3389/fonc.2020.561833

INTRODUCTION

Head and neck squamous cell carcinoma (HNSCC) is the sixth most common type of human malignancy and involves carcinoma of several anatomic sites, such as lip, oral cavity, pharynx (nasopharynx, oropharynx, hypopharynx), and larynx, with an annual incidence of ∼500,000 (1). Even through systemic therapeutic strategies have developed, the 5-years overall survival (OS) of HNSCC patients is hardly satisfying (2). Evidence has shown that the relatively poor prognosis and high recurrence of HNSCC are mainly due to the high rate of local invasion and distant metastasis (3). Consequently, it is essential to explore the detailed molecular mechanisms involved in cancer metastatic cascade so as to promote the development of target therapy and improve the overall survival of HNSCC.

Experimental and clinical studies have attempted to establish the biological basis of this metastasis cascade. Mountains of evidence highlight the irreplaceable role of long non-coding RNA (lncRNA) in cancer metastasis, including HNSCC (4, 5). Such transcripts are widely validated not to produce functional proteins, but regulate gene expression at multiple levels and participate in cancer evolution and development (6). More importantly, unique cross-regulation between

lncRNA and miRNA was recently mentioned, and emerging evidence shows that such crosstalk has a great effect on human cancer metastasis, partially through EMT regulation (7). In this review, we summarize the correlation between lncRNA and EMT mediation and highlight the leading role of lncRNA/miRNA crosstalk in the metastasis of HNSCC.

LncRNAs INVOLVED IN HNSCC INVASION AND METASTASIS

LncRNAs are a heterogenous group of RNAs containing more than 200 nucleotides and recently involved in many biological processes (8). Their number is significantly larger than that of protein-coding genes and can act in a cis and/or in trans manner during the development of human cancers (9). They have well-defined subcellular sites, mainly concentrated in the nucleus and involved in the regulation of chromatin and chromosomal conformation (10).

In the past few years, there has been a paradigm shift in the understanding of non-coding RNAs (ncRNAs) and their role in cancer biology (11, 12). Due to the discovery of alternative splicing in 1970s, a major focus in various pathological and physiological processes shifted to the role of proteins and protein-coding RNAs and mutations as prominent mechanisms in disease etiology and pathophysiology. However, in 1977, the discovery of introns and ribozymes suggested the role of ncRNA as a regulatory molecule (13). Since then, more and more research focuses on lncRNAs, which are identified as playing critical roles in cancer metastasis regulation. LncRNAs are not only responsible for tumor proliferation, cell death regulation, and angiogenesis (14–16), but also for the invasion and metastasis of HNSCC (17–19). These lncRNAs described as potential transfer regulators are shown in **Table 1**.

LncRNA HOTAIR

LncRNA HOX transcript antisense RNA (HOTAIR) is one of the most well-studied oncogenic lncRNAs, originally characterized as a regulator of the HOX gene family, helping to control cellular identity (48). The 5′ terminal of HOTAIR can be combined with chromatin modified complex, and the 3′ terminal can bind to histone demethylase I complex. Therefore, HOTAIR regulates methylation or demethylation of H3K4me2 at the H3K27 site, which is involved in proliferation (49), apoptosis (50), and metastasis (51) of tumor cells. It was found that the expression of HOTAIR is increased in many subtypes of HNSCC. Compared with the normal oral epithelial cell lines, HOTAIR in OSCC Cal-27 and UM-1 cell lines increased significantly (52). In addition, *in vitro* experiments demonstrate that, compared with low invasiveness, HOTAIR in the invasive oral squamous cell carcinoma cell lines is upregulated. Moreover, knocking down HOTAIR expression levels globally inhibits cell proliferation, migration, and invasion (53). Furthermore, HOTAIR is confirmed to promote HNSCC invasion and metastasis (23) and triggers the EMT process through EZH2/H3K27me3 recruitment, which is proven to be negatively associated with clinical outcomes in HNSCC patients (54).

LncRNA UCA1

In tongue squamous cell carcinoma (TSCC), the expression level of lncRNA urothelial carcinoma antigen 1 (UCA1) is significantly increased and correlated with lymph node metastasis. In addition, the expression of UCA1 in lymph node metastasis is higher than that in the primary tumor. In a cell culture of TSCC, the overexpression of UCA1 promotes cell migration but has little effect on cell proliferation (32). Furthermore, UCA1 is also revealed to attenuate cell growth and metastasis of OSCC cell lines *in vitro* and *in vivo*, through WNT/β-catenin activation (28). Consequently, it is suggested that UCA1 may promote the metastasis of cancer cells and may be a prognostic indicator of lymph node metastasis in HNSCC.

LncRNA MALAT1

Abnormal expression of lncRNA metastasis–associated lung adenocarcinoma transcript 1 (MALAT1) is reported in multiple human cancers, including prostate cancer (55), colorectal cancer (56), hepatocellular carcinoma (57), and HNSCC (33, 34). Fang et al. reported globally increased MALAT1 expression levels in TSCC (32), especially in those with lymph node metastasis (35). DNA microarray analysis shows that MALAT1 significantly increases TSCC cell motility through regulating LAYN, CCT4, CTHRC1, and FHL1 expression levels, which are small proline-rich protein (SPRR) members (35). In parallel, Zhou and colleagues reveal that MALAT1 is significantly associated with poor prognosis in patients with OSCC and could promote invasion and metastasis of OSCC by means of EMT activation (34). In addition, by means of ChIP-PCR and RIP-PCR analysis, we also reveal that STAT3 may accelerate EMT progression and cancer metastasis through interaction with the MALAT1/miR-30a axis (33).

LncRNA H19

LncRNA H19 is described as participating in the metastasis of various cancers. In TSCC, H19 is demonstrated to be upregulated in the tumor tissue compared with adjacent samples. Furthermore, the expression level of H19 in metastatic tumor is significantly higher than in non-metastatic tumor. Subsequently, H19 is demonstrated to function as ceRNA to sponge let-7a, resulting in HMGA2 enhancement, and finally, increasing the capacity of TSCC invasion and metastasis (37). H19 is also found to be overexpressed in nasopharyngeal carcinoma (NPC) and to promote NPC cell invasion capacity via E-cadherin silencing and miR-630/EZH2 regulation (58). Mechanistically, Wu T. and colleagues report that H19 is overexpressed in laryngeal squamous cell carcinoma (LSCC) and accelerates LSCC tumor progression through miR-148a-3p attenuation and DNMT1 enhancement (39).

LncRNAs REGULATE HNSCC CELL MOTILITY VIA EMT MEDIATION

The main regulating factors of EMT include the EMT effect factor, EMT core regulating factor, and EMT induction factor (59). EMT effect factors are usually proteins that define epithelial or mesenchymal properties, such as E-cadherin, α-Catenin, γ-Catenin, Vim, and Fibronectin, which promote cell

TABLE 1 | lncRNAs in HNSCC metastasis.

LncRNA	Genome	Expression	Biological function and mechanism	References
NEAT1	11q13.1	- Upregulated in OSCC; - Overexpressed in LSCC	- Promoted cell motility of OSCC by sponging miR-365; - Regulated CDK6 in LSCC, mediated by miR-107	(20–22)
HOTAIR	12q13.13	- Overexpressed in OSCC and LSCC and correlated tumor metastasis; - Increased level of HOTAIR and miR-21 in the blood of patients with LSCC were associated with T classification and lymph node metastasis	- Promoted tumor metastasis through EZH2 recruitment and E-cadherin silencing in OSCC; - Triggered metastasis in OSCC through modulation of EMT; - Promoted OSCC metastasis through miR-326-MTA2 axis	(17, 19, 23–25)
HOTTIP	7p15.2	- Overexpressed in TSCC samples and associated with clinical stage, distant metastasis, and OS rate	- HOTTIP silencing repressed tumor cell growth and resulted in a great rise of miR-124-3p and E-cadherin expression and a distinct fall of HMGA2, β-catenin, and c-Myc protein levels	(26, 27)
UCA1	19p13.12	- Overexpressed in TSCC samples; - Potentially prognostic indicator of lymph node metastasis	- Promoted cell migration and invasion by targeting miR-143-3p in OSCC; - Modulated TGF-β induced EMT and OSCC invasion through JAG1/Notch; - Contributed to OSCC progression by regulating the WNT/β-catenin signaling pathway	(28–32)
MALAT1	11q13.1	- Overexpressed in LSCC and OSCC samples, especially in metastatic TSCC with cervical lymph node metastasis	- Potentiated metastasis of TSCC via miR-140-5p/PAK1 axis modulation; - Modulated TSCC metastasis partially through the regulation of SPRR; - Mediated the pro-metastatic role of STAT3 in HNSCC via interaction with miR-30a; - Promoted OSCC metastasis by inducing EMT	(20, 33–36)
H19	11p15.5	- Overexpressed in patients with LSCC and positively correlated with cervical lymph node metastasis	- Promoted TSCC metastasis through β-catenin/GSK3β/EMT axis; - Facilitated TSCC invasion via sponging miR-let-7	(37–39)
NAG7	3p25.3	- Downregulated in NPC samples and positively correlated with cervical lymph node metastasis	- Promoted NPC invasion and metastasis via regulation of ERalpha and JNK2/AP-1/MMP1 signaling pathways	(40, 41)
NKILA	20q13.31	- Downregulated in TSCC tissues	- Attenuated migration and invasion of TSCC via EMT suppression	(42)
LINC00467	1q32.3	- Overexpressed in HNSCC and positively correlated cell motility and EMT process	- Raised USP48 expression through miR-299-5p regulation	(43)
KTN1-AS1	14q22.3	- Upregulated in HNSCC tissues	- Promoted cell proliferation, migration, invasion through miR-153-3p sponge in HNSCC; - Aberrant expression of SNAI1 and ZEB2 mediated the role of KTN1-AS1 due to miR-153-3p exhibition	(44)
RC3H2	9q33.2	- Overexpressed in OSCC tissues and the FISH assay verified the cytoplasm location	- Promoted OSCC proliferation, invasion, metastasis and increased level of EZH2 and H3K27Me3 expression; - Served as ceRNA sponging miR-101-3p and targeted EZH2	(45)
AC091729.7	Chromosome 7	- Upregulated and closely connected with the OS of the sinonasal squamous cell carcinoma (SNSCC) patients	- Served as a novel biomarker and latent curative target in SNSCC, through SRSF2 combination	(46)
ADAMTS9-AS2	3p14.1	- Significantly upregulated in TSCC tissues from patients with lymph node metastasis and is closely associated with poor prognosis	- ADAMTS9-AS2 knockdown led to the inhibition of cell migration and invasion and reversed TGF-β1 induced EMT; - Shared the miRNA response elements (MREs) of miR-600 with EZH2	(47)

migration and invasion during EMT. Among them, E-cadherin is considered to be the leading force (60). The core regulatory factors of EMT are composed of transcription factors, including Snail-1, Snail-2, ZEB1, ZEB2, Twist-1, and Twist-2 as well as the newly discovered pair-related homeobox transcription factor 1 (Prrx1), which regulates the EMT process through E-cadherin mediation (60). Moreover, EMT inducers consist of several signaling pathways, including TGF-β/Smad, Wnt/β-catenin, Notch, and GF receptor signaling cascade. Most importantly, the TGF-β/Smad signaling pathway appears to be the major activator of EMT. In addition, tumor inflammation, and the hypoxia microenvironment also serve basic roles in EMT promotion.

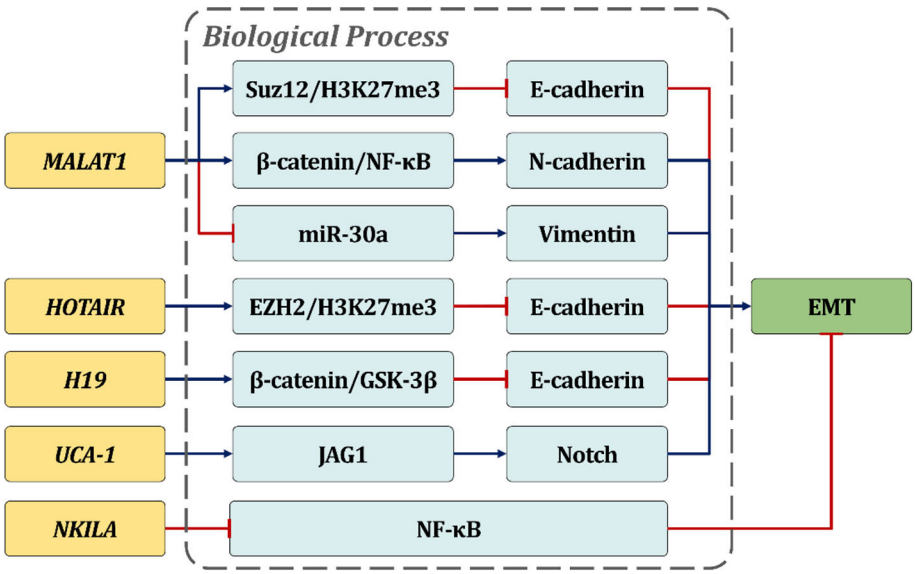

FIGURE 1 | LncRNAs regulate HNSCC cell motility via EMT mediation. The text in the boxes depicts the potential pro/anti-EMT mechanisms of lncRNAs in HNSCC.

Recently, it is confirmed that EMT is also regulated by post transcription factor lncRNA, which plays its role through regulatory effectors, transcription factors, and signal transduction pathways (61). Unlike microRNAs, which repress target gene expression levels post-transcriptionally, functional lncRNAs may influence the EMT process during cancer metastasis by regulating gene expression at different levels, including chromatin modification, transcription, and post-transcriptional processing (**Figure 1**). MALAT1 is widely confirmed as one of the most well-studied oncogenic lncRNAs that is confirmed to be involved in the EMT process. Fan Y. and colleagues illustrate that TGF-β overexpression in the tumor microenvironment could induce cancer metastasis through EMT regulation and validate MALAT1 as an important mediator of TGF-β related EMT (62). Mechanistically, MALAT1 is then proven to promote EMT through Suz12 recruitment, which acts as an H3K27 methyltransferase binding E-cadherin promoter and inhibiting its expression in a PRC2-dependent manner. Moreover, subsequent ChIP-PCR and luciferase reporter assays show that STAT3 might bind to the MALAT1 promoter region and transcriptionally activate its expression in order to induce EMT and accelerate HNSCC metastasis (33). In OSCC, MALAT1 is also reported to play oncogenic roles in EMT-related cancer metastasis. By means of siRNA, MALAT1 is validated to be required for maintaining EMT-mediated cell migration and invasion. MALAT1 knockdown significantly suppressed the expression levels of N-cadherin and Vimentin, but raised E-cadherin *in vitro*. Meanwhile, both cytoplasm and the nucleus NF-κB/β-catenin axis is significantly triggered after MALAT1 elevation. It is noteworthy that targeting MALAT1 globally inhibits the proliferation capacity of TSCCA-induced xenograft tumor, suggesting MALAT1 as an important prognostic factor of OSCC and a satisfactory target with therapeutic potential. Furthermore, MALAT1 also acts as a transcriptional regulator within the regulation of activating the Wnt/β-catenin signaling pathway (63). In addition to MALAT1, there are other lncRNAs proven to participate in EMT regulation, such as HOTAIR and H19. In OSCC, a significant negative correlation between HOTAIR and E-cadherin expression levels is found in both tumor tissues and cell lines. Meanwhile, HOTAIR is validated to trigger E-cadherin silencing through the recruitment of EZH2 and H3K27me3 in the promoter region of E-cadherin (23), indicating that HOTAIR might regulate OSCC metastasis in an epigenetic manner. On the other hand, compared with matched normal tissues, the expression of H19 is upregulated in TSCC specimens and significantly correlated with lymph node metastasis. Subsequently, H19 attenuation significantly suppresses cell motility *in vitro* through activation of β-Catenin/GSK3β/E-cadherin signaling. In addition, animal models show that H19 inhibition significantly impairs tumor progression and lung metastasis (38). Apart from those prometastatic lncRNAs, lncRNA NKILA is validated to inhibit the migration and invasion of OSCC (42). Mechanistic study shows that NKILA inhibits the phosphorylation of IκBα and NF-κB activation as well as the induction of the EMT process. An *in vivo* experimental metastasis model also demonstrates that NKILA inhibits lung metastasis of NOD/SCID mice with TSCC tumors, suggesting NKILA as a potential predictor for OS and distant metastasis in patients with TSCC.

LncRNA/MICRORNA INTERACTION IN HNSCC METASTASIS

During ncRNA crosstalk, on the one hand, the stability of lncRNA can be affected due to coaction with specific miRNA.

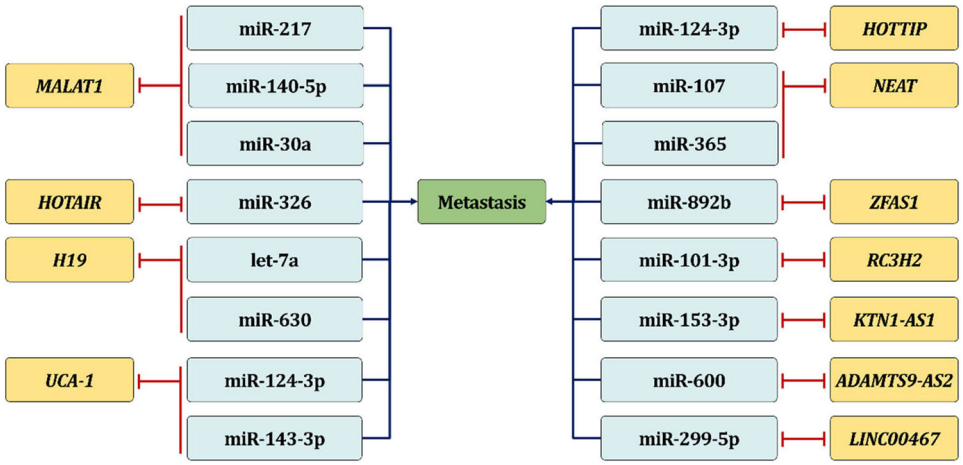

FIGURE 2 | LncRNA/microRNA interaction in HNSCC metastasis. LncRNA can serve as ceRNA in order to bind certain miRNA to isolate the miRNA from its target mRNA, thereby promoting HNSCC metastasis.

On the other hand, lncRNA, also known as competitive endogenous RNA, could bind certain miRNAs to isolate the miRNA from its target mRNA, thereby antagonizing miRNA's function (**Figure 2**). The tumor suppressor miR-217 is reported to inhibit MALAT1 through the Ago2-mediated pathway in order to inhibit EMT-related metastasis through upregulating E-cadherin and N-cadherin suppression (64). Similarly, the recruitment of miR-30a also reduces the stability of MALAT1 in HNSCC in order to inhibit the invasion capacity of tumor cells (33). Additionally, MALAT1 knockdown is also seen to completely suppress tumor progression through miR-140-5p elevation and PAK1 inhibition, both *in vitro* and in TSCC-induced xenograft tumors (36). Another lncRNA H19 is also widely mentioned in lncRNA/miRNA interaction. Kou N. and colleagues illustrate that H19 can act as ce-RNA to sponge let-7a, leading to the accumulation of metastasis regulator HMGA2, which is enriched in TSCC tissues and cell lines. Intriguingly, let-7a suppression significantly rescues the weakened tumor cell motility induced by sh-H19. These findings demonstrate that the H19/let-7a crosstalk plays a critical role in TSCC migration and invasion (37). Meanwhile, H19 is validated to regulate EZH2 by miR-630 silencing, which is a repressor of EZH2 and interacts with H19 in a sequence-specific manner, to inhibit the expression level of E-cadherin and eventually accelerate the invasion and metastasis of NPC (58). Other examples involving lncRNA ZFAS1 (65) and lncRNA UCA1 (29, 30) can also function as ceRNA during EMT-related cancer metastasis.

PERSPECTIVES

LncRNA is constitutively deregulated during the progression and development of human cancers and globally suggested as a critical regulator in tumor cell motility. At present, the understanding of lncRNA in HNSCC metastasis remains confused and ambiguous, and there is little information about the function of lncRNA in HNSCC, which needs further research. This review provides a comprehensive study of the expression profile of lncRNA in HNSCC and summarizes the control of ncRNA crosstalk on the EMT process, emphasizing the leading influence of lncRNA crosstalk in the metastasis of HNSCC. Even so, a great deal of work is still urgently required to characterize the complex ncRNA networks that contribute to HNSCC metastasis, and it is necessary to carry out further research to clarify the relationship between lncRNA and miRNA in order to seek better treatment strategies.

CONSENT FOR PUBLICATION

All authors agreed to the publication of this review.

AUTHOR CONTRIBUTIONS

YW and SW contributed to conception, drafting, interpretation, and manuscript revision. XZ and YR contributed to interpretation and manuscript revision. All authors provided final approval and agreed to be accountable for all aspects of the study.

FUNDING

This work was supported by the China National Natural Scientific Fund No. 81872206 (XZ); the Tianjin Municipal Education Commission Support Grant No. 2019KJ188 (YW); and the China National Natural Scientific Fund No. 81872495 (YR).

REFERENCES

1. Egger G, Liang G, Aparicio A, Jones PA. Epigenetics in human disease and prospects for epigenetic therapy. *Nature.* (2004) 429:457–63. doi: 10.1038/nature02625
2. Lam L, Logan RM, Luke C. Epidemiological analysis of tongue cancer in South Australia for the 24-year period, 1977-2001. *Austr Dental J.* (2006) 51:16–22. doi: 10.1111/j.1834-7819.2006.tb00395.x
3. Bhave SL, Teknos TN, Pan Q. Molecular parameters of head and neck cancer metastasis. *Crit Rev Eukaryot Gene Expr.* (2011) 21:143–53. doi: 10.1615/CritRevEukarGeneExpr.v21.i2.40
4. Guglas K, Bogaczynska M, Kolenda T, Rys M, Teresiak A, Blizniak R, et al. lncRNA in HNSCC: challenges and potential. *Contemp Oncol.* (2017) 21:259–66. doi: 10.5114/wo.2017.72382
5. Cao W, Liu JN, Liu Z, Wang X, Han ZG, Ji T, et al. A three-lncRNA signature derived from the Atlas of ncRNA in cancer (TANRIC) database predicts the survival of patients with head and neck squamous cell carcinoma. *Oral Oncol.* (2017) 65:94–101. doi: 10.1016/j.oraloncology.2016.12.017
6. Sanchez Calle A, Kawamura Y, Yamamoto Y, Takeshita F, Ochiya T. Emerging roles of long non-coding RNA in cancer. *Cancer Sci.* (2018) 109:2093–100. doi: 10.1111/cas.13642
7. Liz J, Esteller M. lncRNAs and microRNAs with a role in cancer development. *Biochim Biophys Acta.* (2016) 1859:169–76. doi: 10.1016/j.bbagrm.2015.06.015
8. Djebali S, Davis CA, Merkel A, Dobin A, Lassmann T, Mortazavi A, et al. Landscape of transcription in human cells. *Nature.* (2012) 489:101–8. doi: 10.1038/nature11233
9. Zhang R, Xia LQ, Lu WW, Zhang J, Zhu JS. LncRNAs and cancer. *Oncol Lett.* (2016) 12:1233–9. doi: 10.3892/ol.2016.4770
10. Khalil AM, Guttman M, Huarte M, Garber M, Raj A, Rivea Morales D, et al. Many human large intergenic non-coding RNAs associate with chromatin-modifying complexes and affect gene expression. *Proc Natl Acad Sci USA.* (2009) 106:11667–72. doi: 10.1073/pnas.0904715106
11. Salyakina D, Tsinoremas NF. Non-coding RNAs profiling in head and neck cancers. *NPJ Genomic Med.* (2016) 1:15004. doi: 10.1038/npjgenmed.2015.4
12. Manikandan M, Deva Magendhra Rao AK, Arunkumar G, Manickavasagam M, Rajkumar KS, Rajaraman R, et al. Oral squamous cell carcinoma: microRNA expression profiling and integrative analyses for elucidation of tumourigenesis mechanism. *Mol Cancer.* (2016) 15:28. doi: 10.1186/s12943-016-0512-8
13. Morris KV, Mattick JS. The rise of regulatory RNA. *Nat Rev Genet.* (2014) 15:423–37. doi: 10.1038/nrg3722
14. Ding L, Ren J, Zhang D, Li Y, Huang X, Hu Q, et al. A novel stromal lncRNA signature reprograms fibroblasts to promote the growth of oral squamous cell carcinoma via LncRNA-CAF/interleukin-33. *Carcinogenesis.* (2018) 39:397–406. doi: 10.1093/carcin/bgy006
15. Ma WQ, Chen J, Fang W, Yang XQ, Zhu A, Zhang D, et al. LncRNA INHBA-AS1 promotes cell growth, migration, and invasion of oral squamous cell carcinoma by sponging miR-143-3p. *Eur Rev Med Pharm Sci.* (2020) 24:1821–8. doi: 10.26355/eurrev_202002_20360
16. Zhang P, Liu Y, Li C, Zhang L, Liu Q, Jiang T. LncRNA PAPAS promotes oral squamous cell carcinoma by upregulating transforming growth factor-beta1. *J Cell Biochem.* (2019) 120:16120–7. doi: 10.1002/jcb.28893
17. Tao D, Zhang Z, Liu X, Zhang Z, Fu Y, Zhang P, et al. LncRNA HOTAIR promotes the invasion and metastasis of oral squamous cell carcinoma through metastasis-associated gene 2. *Mol Carcinogen.* (2020) 59:353–64. doi: 10.1002/mc.23159
18. Wang Y, Zhang X, Wang Z, Hu Q, Wu J, Li Y, et al. LncRNA-p23154 promotes the invasion-metastasis potential of oral squamous cell carcinoma by regulating Glut1-mediated glycolysis. *Cancer Lett.* (2018) 434:172–83. doi: 10.1016/j.canlet.2018.07.016
19. Lu MY, Liao YW, Chen PY, Hsieh PL, Fang CY, Wu CY, et al. Targeting LncRNA HOTAIR suppresses cancer stemness and metastasis in oral carcinomas stem cells through modulation of EMT. *Oncotarget.* (2017) 8:98542–52. doi: 10.18632/oncotarget.21614
20. Tang H, Wu Z, Zhang J, Su B. Salivary lncRNA as a potential marker for oral squamous cell carcinoma diagnosis. *Mol Med Rep.* (2013) 7:761–6. doi: 10.3892/mmr.2012.1254
21. Zou AE, Ku J, Honda TK, Yu V, Kuo SZ, Zheng H, et al. Transcriptome sequencing uncovers novel long non-coding and small nucleolar RNAs dysregulated in head and neck squamous cell carcinoma. *RNA.* (2015) 21:1122–34. doi: 10.1261/rna.049262.114
22. Wang P, Wu T, Zhou H, Jin Q, He G, Yu H, et al. Long non-coding RNA NEAT1 promotes laryngeal squamous cell cancer through regulating miR-107/CDK6 pathway. *J Exp Clin Cancer Res.* (2016) 35:22. doi: 10.1186/s13046-016-0297-z
23. Wu Y, Zhang L, Zhang L, Wang Y, Li H, Ren X, et al. Long non-coding RNA HOTAIR promotes tumor cell invasion and metastasis by recruiting EZH2 and repressing E-cadherin in oral squamous cell carcinoma. *Int J ogy.* (2015) 46:2586–94. doi: 10.3892/ijo.2015.2976
24. Wang J, Zhou Y, Lu J, Sun Y, Xiao H, Liu M, et al. Combined detection of serum exosomal miR-21 and HOTAIR as diagnostic and prognostic biomarkers for laryngeal squamous cell carcinoma. *Med Oncol.* (2014) 31:148. doi: 10.1007/s12032-014-0148-8
25. Nie Y, Liu X, Qu S, Song E, Zou H, Gong C. Long non-coding RNA HOTAIR is an independent prognostic marker for nasopharyngeal carcinoma progression and survival. *Cancer Sci.* (2013) 104:458–64. doi: 10.1111/cas.12092
26. Zhang H, Zhao L, Wang YX, Xi M, Liu SL, Luo LL. Long non-coding RNA HOTTIP is correlated with progression and prognosis in tongue squamous cell carcinoma. *Tumour Biol.* (2015) 36:8805–9. doi: 10.1007/s13277-015-3645-2
27. Xiong L, Tang Y, Tang J, Liu Z, Wang X. Downregulation of lncRNA HOTTIP suppresses the proliferation, migration, and invasion of oral tongue squamous cell carcinoma by regulation of HMGA2-mediated Wnt/beta-catenin pathway. *Cancer Biotherap Radiopharmac.* (2020). doi: 10.1089/cbr.2019.3017. [Epub ahead of print].
28. Yang YT, Wang YF, Lai JY, Shen SY, Wang F, Kong J, et al. Long non-coding RNA UCA1 contributes to the progression of oral squamous cell carcinoma by regulating the WNT/beta-catenin signaling pathway. *Cancer Sci.* (2016) 107:1581–9. doi: 10.1111/cas.13058
29. Zhang TH, Liang LZ, Liu XL, Wu JN, Su K, Chen JY, et al. LncRNA UCA1/miR-124 axis modulates TGFbeta1-induced epithelial-mesenchymal transition and invasion of tongue cancer cells through JAG1/Notch signaling. *J Cell Biochem.* (2019) 120:10495–504. doi: 10.1002/jcb.28334
30. Duan Q, Xu M, Wu M, Zhang X, Gan M, Jiang H. Long non-coding RNA UCA1 promotes cell growth, migration, and invasion by targeting miR-143-3p in oral squamous cell carcinoma. *Cancer Med.* (2020) 9:3115–29. doi: 10.1002/cam4.2808
31. Han R, Chen S, Wang J, Zhao Y, Li G. LncRNA UCA1 affects epithelial-mesenchymal transition, invasion, migration and apoptosis of nasopharyngeal carcinoma cells. *Cell Cycle.* (2019) 18:3044–53. doi: 10.1080/15384101.2019.1667707
32. Fang Z, Wu L, Wang L, Yang Y, Meng Y, Yang H. Increased expression of the long non-coding RNA UCA1 in tongue squamous cell carcinomas: a possible correlation with cancer metastasis. *Oral Surg Oral Med Oral Pathol Oral Radiol.* (2014) 117:89–95. doi: 10.1016/j.oooo.2013.09.007
33. Wang Y, Wu C, Zhang C, Li Z, Zhu T, Chen J, et al. TGF-beta-induced STAT3 overexpression promotes human head and neck squamous cell carcinoma invasion and metastasis through malat1/miR-30a interactions. *Cancer Lett.* (2018) 436:52–62. doi: 10.1016/j.canlet.2018.08.009
34. Zhou X, Liu S, Cai G, Kong L, Zhang T, Ren Y, et al. Long non coding RNA MALAT1 promotes tumor growth and metastasis by inducing epithelial-mesenchymal transition in oral squamous cell carcinoma. *Sci Rep.* (2015) 5:15972. doi: 10.1038/srep15972
35. Fang Z, Zhang S, Wang Y, Shen S, Wang F, Hao Y, et al. Long non-coding RNA MALAT-1 modulates metastatic potential of tongue squamous cell carcinomas partially through the regulation of small proline rich proteins. *BMC Cancer.* (2016) 16:706. doi: 10.1186/s12885-016-2735-x
36. Zhu M, Zhang C, Chen D, Chen S, Zheng H. lncRNA MALAT1 potentiates the progression of tongue squamous cell carcinoma through regulating miR-140-5p-PAK1 pathway. *OncoTargets Ther.* (2019) 12:1365–77. doi: 10.2147/OTT.S192069
37. Kou N, Liu S, Li X, Li W, Zhong W, Gui L, et al. H19 facilitates tongue squamous cell carcinoma migration and invasion via sponging miR-let-7. *Oncol Res.* (2019) 27:173–82. doi: 10.3727/096504018X15202945197589

38. Zhang DM, Lin ZY, Yang ZH, Wang YY, Wan D, Zhong JL, et al. lncRNA H19 promotes tongue squamous cell carcinoma progression through beta-catenin/GSK3beta/EMT signaling via association with EZH2. *Am J Transl Res.* (2017) 9:3474–86.
39. Wu T, Qu L, He G, Tian L, Li L, Zhou H, et al. Regulation of laryngeal squamous cell cancer progression by the lncRNA H19/miR-148a-3p/DNMT1 axis. *Oncotarget.* (2016) 7:11553–66. doi: 10.18632/oncotarget.7270
40. Zhang W, Huang C, Gong Z, Zhao Y, Tang K, Li X, et al. Expression of LINC00312, a long intergenic non-coding RNA, is negatively correlated with tumor size but positively correlated with lymph node metastasis in nasopharyngeal carcinoma. *J Mol Histol.* (2013) 44:545–54. doi: 10.1007/s10735-013-9503-x
41. Huang C, Wu M, Tang Y, Li X, Ouyang J, Xiao L, et al. NAG7 promotes human nasopharyngeal carcinoma invasion through inhibition of estrogen receptor alpha and up-regulation of JNK2/AP-1/MMP1 pathways. *J Cell Physiol.* (2009) 221:394–401. doi: 10.1002/jcp.21867
42. Huang W, Cui X, Chen J, Feng Y, Song E, Li J, et al. Long non-coding RNA NKILA inhibits migration and invasion of tongue squamous cell carcinoma cells via suppressing epithelial-mesenchymal transition. *Oncotarget.* (2016) 7:62520–32. doi: 10.18632/oncotarget.11528
43. Chen Y, Ding Y. LINC00467 enhances head and neck squamous cell carcinoma progression and the epithelial-mesenchymal transition process via miR-299-5p/ubiquitin specific protease-48 axis. *J Gene Med.* (2020) 22:e3184. doi: 10.1002/jgm.3184
44. Jiang Y, Wu K, Cao W, Xu Q, Wang X, Qin X, et al. Long non-coding RNA KTN1-AS1 promotes head and neck squamous cell carcinoma cell epithelial-mesenchymal transition by targeting miR-153-3p. *Epigenomics.* (2020) 12:487–505. doi: 10.2217/epi-2019-0173
45. Wu K, Jiang Y, Zhou W, Zhang B, Li Y, Xie F, et al. Long non-coding RNA RC3H2 facilitates cell proliferation and invasion by targeting MicroRNA-101-3p/EZH2 axis in OSCC. *Mol Therapy Nucleic Acids.* (2020) 20:97–110. doi: 10.1016/j.omtn.2020.02.006
46. Yu B, Qu L, Wu T, Yan B, Kan X, Zhao X, et al. A novel LncRNA, AC091729.7 promotes sinonasal squamous cell carcinomas proliferation and invasion through binding SRSF2. *Front Oncol.* (2019) 9:1575. doi: 10.3389/fonc.2019.01575
47. Li Y, Wan Q, Wang W, Mai L, Sha L, Mashrah M, et al. LncRNA ADAMTS9-AS2 promotes tongue squamous cell carcinoma proliferation, migration and EMT via the miR-600/EZH2 axis. *Biomed Pharmacotherapy.* (2019) 112:108719. doi: 10.1016/j.biopha.2019.108719
48. Rinn JL, Kertesz M, Wang JK, Squazzo SL, Xu X, Brugmann SA, et al. Functional demarcation of active and silent chromatin domains in human HOX loci by non-coding RNAs. *Cell.* (2007) 129:1311–23. doi: 10.1016/j.cell.2007.05.022
49. Bao X, Ren T, Huang Y, Sun K, Wang S, Liu K, et al. Knockdown of long non-coding RNA HOTAIR increases miR-454-3p by targeting Stat3 and Atg12 to inhibit chondrosarcoma growth. *Cell Death Dis.* (2017) 8:e2605. doi: 10.1038/cddis.2017.31
50. Li X, Wu Z, Mei Q, Li X, Guo M, Fu X, et al. Long non-coding RNA HOTAIR, a driver of malignancy, predicts negative prognosis and exhibits oncogenic activity in oesophageal squamous cell carcinoma. *Br J Cancer.* (2013) 109:2266–78. doi: 10.1038/bjc.2013.548
51. Gupta RA, Shah N, Wang KC, Kim J, Horlings HM, Wong DJ, et al. Long non-coding RNA HOTAIR reprograms chromatin state to promote cancer metastasis. *Nature.* (2010) 464:1071–6. doi: 10.1038/nature08975
52. Sun S, Wu Y, Guo W, Yu F, Kong L, Ren Y, et al. STAT3/HOTAIR signaling axis regulates HNSCC growth in an EZH2-dependent manner. *Clin Cancer Res.* (2018) 24:2665–77. doi: 10.1158/1078-0432.CCR-16-2248
53. Su SC, Hsieh MJ, Lin CW, Chuang CY, Liu YF, Yeh CM, et al. Impact of HOTAIR gene polymorphism and environmental risk on oral cancer. *J Dental Res.* (2018) 97:717–24. doi: 10.1177/0022034517749451
54. Cao W, Feng Z, Cui Z, Zhang C, Sun Z, Mao L, et al. Up-regulation of enhancer of zeste homolog 2 is associated positively with cyclin D1 overexpression and poor clinical outcome in head and neck squamous cell carcinoma. *Cancer.* (2012) 118:2858–71. doi: 10.1002/cncr.26575
55. Stone L. Prostate cancer: escaping enzalutamide: Malat1 contributes to resistance. *Nat Rev Urol.* (2017) 14:450. doi: 10.1038/nrurol.2017.91
56. Li P, Zhang X, Wang H, Wang L, Liu T, Du L, et al. MALAT1 Is associated with poor response to oxaliplatin-based chemotherapy in colorectal cancer patients and promotes chemoresistance through EZH2. *Mol Cancer Therap.* (2017) 16:739–51. doi: 10.1158/1535-7163.MCT-16-0591
57. Wang J, Wang H, Zhang Y, Zhen N, Zhang L, Qiao Y, et al. Mutual inhibition between YAP and SRSF1 maintains long non-coding RNA, Malat1-induced tumourigenesis in liver cancer. *Cell Signal.* (2014) 26:1048–59. doi: 10.1016/j.cellsig.2014.01.022
58. Li X, Lin Y, Yang X, Wu X, He X. Long non-coding RNA H19 regulates EZH2 expression by interacting with miR-630 and promotes cell invasion in nasopharyngeal carcinoma. *Biochem Biophys Res Commun.* (2016) 473:913–9. doi: 10.1016/j.bbrc.2016.03.150
59. Tsai JH, Yang J. Epithelial-mesenchymal plasticity in carcinoma metastasis. *Genes Dev.* (2013) 27:2192–206. doi: 10.1101/gad.225334.113
60. Nantajit D, Lin D, Li JJ. The network of epithelial-mesenchymal transition: potential new targets for tumor resistance. *J Cancer Res Clin Oncol.* (2015) 141:1697–713. doi: 10.1007/s00432-014-1840-y
61. Guo F, Parker Kerrigan BC, Yang D, Hu L, Shmulevich I, Sood AK, et al. Post-transcriptional regulatory network of epithelial-to-mesenchymal and mesenchymal-to-epithelial transitions. *J Hematol Oncol.* (2014) 7:19. doi: 10.1186/1756-8722-7-19
62. Fan Y, Shen B, Tan M, Mu X, Qin Y, Zhang F, et al. TGF-beta-induced upregulation of malat1 promotes bladder cancer metastasis by associating with suz12. *Clini Cancer Res.* (2014) 20:1531–41. doi: 10.1158/1078-0432.CCR-13-1455
63. Liang J, Liang L, Ouyang K, Li Z, Yi X. MALAT1 induces tongue cancer cells' EMT and inhibits apoptosis through Wnt/beta-catenin signaling pathway. *J Oral Pathol Med.* (2017) 46:98–105. doi: 10.1111/jop.12466
64. Lu L, Luo F, Liu Y, Liu X, Shi L, Lu X, et al. Posttranscriptional silencing of the lncRNA MALAT1 by miR-217 inhibits the epithelial-mesenchymal transition via enhancer of zeste homolog 2 in the malignant transformation of HBE cells induced by cigarette smoke extract. *Toxicol Appl Pharmacol.* (2015) 289:276–85. doi: 10.1016/j.taap.2015.09.016
65. Peng J, Liu F, Zheng H, Wu Q, Liu S. Long non-coding RNA ZFAS1 promotes tumorigenesis and metastasis in nasopharyngeal carcinoma by sponging miR-892b to up-regulate LPAR1 expression. *J Cell Mol Med.* (2020) 24:1437–50. doi: 10.1111/jcmm.14823

Conflict of Interest: The authors declare that the research was conducted in the absence of any commercial or financial relationships that could be construed as a potential conflict of interest.

Copyright © 2020 Wang, Wang, Ren and Zhou. This is an open-access article distributed under the terms of the Creative Commons Attribution License (CC BY). The use, distribution or reproduction in other forums is permitted, provided the original author(s) and the copyright owner(s) are credited and that the original publication in this journal is cited, in accordance with accepted academic practice. No use, distribution or reproduction is permitted which does not comply with these terms.

frontiers in Oncology

ORIGINAL RESEARCH
published: 29 October 2020
doi: 10.3389/fonc.2020.559808

Tumor Suppressor *LINC02487* Inhibits Oral Squamous Cell Carcinoma Cell Migration and Invasion Through the USP17–SNAI1 Axis

Lu Feng[1,2], *Jianjun Zhang*[2], *Minglei Sun*[1], *Feng Qiu*[1], *Wantao Chen*[1,2*] *and Weiliu Qiu*[1,2*]

[1] *Department of Oral and Maxillofacial Surgery, The First Affiliated Hospital of Zhengzhou University, Zhengzhou, China,*
[2] *Department of Oral and Maxillofacial-Head Neck Oncology, Ninth People's Hospital, Shanghai Jiao Tong University School of Medicine, Shanghai Key Laboratory of Stomatology, Shanghai, China*

OPEN ACCESS

Edited by:
Qiang Shen,
Louisiana State University, United States

Reviewed by:
Jinsong Hou,
Sun Yat-sen University, China
Guojun Li,
University of Texas MD Anderson Cancer Center, United States

****Correspondence:***
Weiliu Qiu
qiuwl@cae.cn
Wantao Chen
chenwantao2002@hotmail.com

Specialty section:
This article was submitted to Head and Neck Cancer, a section of the journal Frontiers in Oncology

Received: *07 May 2020*
Accepted: *23 September 2020*
Published: *29 October 2020*

Citation:
Feng L, Zhang J, Sun M, Qiu F, Chen W and Qiu W (2020) Tumor Suppressor LINC02487 Inhibits Oral Squamous Cell Carcinoma Cell Migration and Invasion Through the USP17–SNAI1 Axis. Front. Oncol. 10:559808. doi: 10.3389/fonc.2020.559808

Purpose: The aim of this study was to explore the functions and associated mechanisms of long noncoding RNA *LINC02487* in oral squamous cell carcinoma (OSCC).

Methods: The relative expression levels of *LINC02487* in OSCC cell lines and tissue samples were examined by RT-qPCR. Intracellular localization was determined using RNA fluorescence *in situ* hybridization. *LINC02487* was cloned into the pCMV-puro vector and then introduced into OSCC cells using lentiviral transfection. Cell processes, such as proliferation, apoptosis, migration, and invasion, were subsequently examined. *LINC02487*-binding proteins were identified by ChIRP–MS and confirmed by RNA immunoprecipitation. Protein expression was determined by western blotting assay.

Results: *LINC02487* has been reported to be downregulated in OSCC. Here, we confirmed that the expression of *LINC02487* was reduced in 6 OSCC cell lines compared with that in immortalized normal oral epithelial cells and in 50 OSCC samples compared with paired adjacent normal tissue in a Chinese population and that *LINC02487* expression levels were associated with cancer metastasis. We further identified that *LINC02487* was localized to the cytoplasm, aggregated around the nuclear membrane. Functional studies demonstrate that overexpression of *LINC02487* significantly suppresses cell migration and invasion and also inhibits cell proliferation. For the mechanism, we reveal that *LINC02487* directly binds to USP17, a deubiquitinating enzyme, and regulates cell migration and invasion through the USP17–SNAI1 axis in a process that involves epithelial–mesenchymal transition (EMT).

Conclusion: Our results confirm that long noncoding RNA *LINC02487* is downregulated in OSCC tissue samples and cell lines. We also find that *LINC02487* acts as a tumor suppressor through the USP17–SNAI1 axis.

Keywords: long noncoding RNA, oral squamous cell carcinoma, tumor suppressor, deubiquitinating enzyme, migration, invasion

INTRODUCTION

Oral squamous cell carcinoma (OSCC) is the most frequently diagnosed cancer of the oral cavity and oropharynx and ranks as the sixth most common malignancy in Asia. Nearly 274,300 new cases are diagnosed each year, accounting for approximately 3.8% of all cancer cases (1–3). According to recent data, China has an estimated 48,100 new OSCC cases and 22,100 OSCC-related deaths per year (4, 5). Tobacco smoking and alcohol consumption are the main risk factors for the disease, and together are responsible for approximately 75% of OSCCs. Betel quid chewing and viral infections, such as that with high-risk human papillomavirus (HPV), are also considered causative of OSCC (6). Few improvements have been made to the overall prognosis for advanced-stage OSCC in the past two to three decades, resulting in a heavy disease burden for patients and their families (7, 8). Identifying efficient biomarkers and therapeutic targets as well as better understanding the mechanisms underlying OSCC development and progression continue to be the focus of intensive research.

It is estimated that more than 70% of the human genome can be transcribed; however, most transcripts do not serve as blueprints for protein synthesis (9). Analysis of the most recent GENCODE release indicates that only 34% of the human genome comprises protein-coding genes, and the rest consists of noncoding genes, including loci for small noncoding RNAs (sncRNAs, <200 nt), long noncoding RNAs (lncRNAs, >200 nt), and pseudogenes (10). The human genome contains more than 15,000 lncRNA genes that give rise to more than 28,000 lncRNA transcripts, comprising nearly 14% of the total number of transcripts (GENCODE) (10). Small noncoding RNAs, such as microRNAs, are well characterized and have been shown to have important roles in cancer, including oral cancer (11–14). Meanwhile, lncRNAs have gained increasing interest in the last two decades and have potential as diagnostic and/or prognostic biomarkers for cancer, including OSCC (15–17).

Long noncoding RNA *LINC02487*, previously known as *LOC441178*, is 2557 bp long and located in chromosome 6. This lncRNA is reportedly downregulated in OSCCs in a study that used a microarray data set consisting of 167 cancers and 45 healthy oral mucosae, which was further validated in three independent data sets (18). Its low expression level in OSCC was also found to be associated with shorter postoperative survival time (19). Given that the differences in expression were stable and significant, *LINC02487* has the potential for use as a biomarker in oral cancer diagnosis and prognosis. However, the precise role and underlying functional mechanism of *LINC02487* in OSCC development remain unknown. In this study, we confirm that the expression of *LINC02487* was dysregulated in OSCC samples from patients from a Chinese population and explore the biological functions of *LINC02487* in OSCC as well as the underlying molecular mechanisms, using several oral cancer cell lines.

Patients with advanced OSCC often progress to have local cervical lymph node involvement or distant metastasis, which are responsible for most cancer-related deaths (8, 20). Epithelial–mesenchymal transition (EMT) plays a critical role during cancer progression and is positively correlated with poor prognosis in cancer patients. The main features of EMT are the loss of epithelial characteristics (loss of cell–cell contact, cytoskeletal remodeling, polarity changes) and the acquisition of a mesenchymal phenotype, which result in increased cell motility and invasion, enhanced migratory capacity, and elevated resistance to apoptosis, eventually leading to distant metastasis (21–23). Recent evidence indicates that lncRNAs may be involved in EMT and tumor invasion-metastasis cascade *via* epigenetic modifications (24, 25). For example, lncRNA *SATB2-AS1* suppresses cancer progression through the regulation of SNAI1 expression in colorectal cancer (26), and lncRNA *ELIT-1* promotes EMT through the TGFβ/SMAD signaling pathway by acting as a SMAD3 cofactor (27). In this study, we also explore the connection between *LINC02487* and EMT in OSCC metastasis.

MATERIALS AND METHODS

Patient Samples and Public Databases

This study was approved by the Ethics Committee of Zhengzhou University. Tissue samples (including cancerous and paired adjacent normal tissues) and the corresponding clinical/pathological data were obtained from OSCC patients of the Sharing Platform for the Tissue Sample and Bioinformatics Database of Oral Maxillofacial Tumor (http://mdl.shsmu.edu.cn/OMNDB/page/home/home_en.jsp; Shanghai, China). This platform contains samples from the Department of Oral and Maxillofacial-Head and Neck Oncology, Ninth People's Hospital, Shanghai Jiao Tong University School of Medicine, China. Written informed consent was obtained from all the participants. Fifty pairs of samples were included in this study, and their clinical characteristics are summarized in **Table 1**. Relative *LINC02487* expression data for head and neck squamous cell carcinoma (HNSCC) patients and healthy controls were obtained from TANRIC, an open-access resource for interactive exploration of lncRNAs in cancer (https://ibl.mdanderson.org/tanric/_design/basic/main.html; data collected in 2018.08.06) (28), following the website's instructions and using data sets from The Cancer Genome Atlas (TCGA) (29).

TABLE 1 | The relationship between relative expression of *LINC02487* and clinical characteristics.

Characteristics		Relative Expression	*P*
Gender	male(n=32)	0.079 ± 0.020	0.068
	female(n=18)	0.158 ± 0.043	
Age	≥60ys(n=34)	0.112 ± 0.027	0.365
	<60ys(n=16)	0.097 ± 0.030	
Local invasion	Yes(n=15)	0.081 ± 0.037	0.21
	No(n=35)	0.118 ± 0.025	
Metastasis	Yes(n=26)	0.157 ± 0.040	0.03*
	No(n=24)	0.070 ± 0.018	
Tumor size	≥4cm(n=13)	0.099 ± 0.044	0.761
	<4cm(n=35)	0.114 ± 0.025	

*$P < 0.05$

Cell Lines and Cell Culture

The HEK293T cell line was obtained from the American Type Culture Collection (ATCC; Gaithersburg, MD, USA) and cultured in Dulbecco's modified Eagle's medium (DMEM) (Gibco/Invitrogen, Grand Island, NY, USA) supplemented with 10% (v/v) fetal bovine serum (FBS) (Gibco). The OSCC cell lines HN6 and HN30 were obtained from Shanghai Key Laboratory of Stomatology (Shanghai, China) and cultured in DMEM supplemented with 10% FBS, penicillin (100 units/mL), and streptomycin (100 μg/mL) in a humidified incubator with 5% CO_2. The immortalized normal oral epithelial cell line hTERT-OME was purchased from abm™ (Vancouver, BC, Canada) and cultured in a 1:1 mixture of DMEM and Ham's F12 medium (Gibco/Invitrogen) supplemented with 10% FBS, penicillin (100 units/mL), and streptomycin (100 μg/mL). The remaining OSCC cell lines (HN4, SCC9, SCC25, and Cal27) were also obtained from the Shanghai Key Laboratory of Stomatology and maintained as previously described (30).

Quantitative RT-PCR

Total cellular RNA was isolated using RNAiso Plus reagent (Takara Biomedical Technology, Beijing, China), and cDNA was generated using the PrimeScript™ RT reagent Kit (Takara). Real-time qPCR was performed on the Applied Biosystems StepOnePlus Real-Time PCR System (Thermo Fisher Scientific, Waltham, MA, USA) using the TB Green™ Premix Ex Taq™ PCR kit (Takara) following the manufacturer's instructions. Each sample was assayed in triplicate in 10-μL reaction volumes, and all expression levels were normalized against that of *GAPDH* mRNA unless otherwise specified. The mean threshold cycle (Ct) values were calculated from the triplicate Ct values. Samples that had Ct values with SD >0.35 in their triplicate run were repeated. The sequences of the primers used were as follows: *LINC02487*, Forward GGGTATTTTGTGCTCCCCCA and Reverse CAGGC ACTGAAGGTTCGGAT; *USP17*, Forward CTATCATTGCG GTCTTTGTCTCC and Reverse AAGTGATGCTACAGGC AGTGA; *SNAI1*, Forward GCTGCAGGACTCTAATCCAGA and Reverse ATCTCCGGAGGTGGGATG.

RNA Fluorescence In Situ Hybridization (FISH)

The lncRNA *LINC02487* probe mix was designed and synthesized by RiboBio (Guangzhou, China). Hybridization was performed using the Ribo™ FISH Kit (RiboBio) following the manufacturer's instructions and then observed using confocal laser microscopy (Nikon, Tokyo, Japan). The 18S ribosomal RNA and *U6* probe mixes were used for quality control.

Lentivirus-Mediated Overexpression

The pCMV-MCS-PGK-Puro vector (PHY-008, HanYin Biotech, Shanghai, China) was used for the stable overexpression of *LINC02487*. This vector contains a puromycin resistance gene and is introduced into cells using lentiviral transfection. Full-length *LINC02487* was synthesized, amplified, and cloned into the pCMV-puro lentiviral vector (HanYin Biotech). pCMV-puro empty-vector transduction particles were used as controls. Cells were seeded in a 6-well plate at a density of 6×10^5 cells/well 24 h before infection. The medium was removed, and 10–20 multiplicity of infection (MOI) of MISSION pCMV-LINC02487-puro lentiviral particles and 2 mL of Opti-MEM medium (Gibco) supplemented with polybrene (8 μg/mL, Sigma, St. Louis, MO, USA) was added to the cells. Lentiviral infection was performed at 37°C for 6 h unless intensive cell toxicity was observed. The medium was then replaced with 2 mL of fresh medium. Infected cells were allowed to grow for 48–72 h and then selected with puromycin-containing medium (Sigma). The expression of *LINC02487* was confirmed by RT-qPCR.

SiRNA or Plasmid Transfection

For the knockdown of *LINC02487* and *USP17*, small interfering RNAs (siRNAs) were designed and synthesized by RiboBio. For transient overexpression of tagged *USP17*, the pCMV-HA-puro vector was used, which contains a C-terminal HA epitope tag. Transfection was performed using Lipofectamine 3000 (Thermo Fisher Scientific) following the manufacturer's instructions. The expression of *LINC02487* was confirmed by RT-qPCR. The expression of mRNA *USP17* was confirmed by RT-qPCR, and the expression of protein USP17 was confirmed by western blotting.

Cell Proliferation Assays

Cell proliferation was determined by CCK-8 assay and EdU (5-ethynyl-20-deoxyuridine) staining. For the CCK-8 assay, 1000 cells of different groups/well were seeded into 96-well plates. At each time point (24, 48, 72, and 96 h after seeding), 10 μL of CCK-8 reagent (Beyotime Biotech, Shanghai, China), and 100 μL of medium were added to each well followed by incubation at 37°C for 2 h. The optical density of the wells was measured at 450 nm using a microplate reader (SpectraMax i3, Molecular Devices, San Jose, CA, USA). Data were from three separate experiments, each with three replications. For the EdU staining assay, the Cell-Light™ EdU Cell Proliferation Detection Kit (RiboBio) was used. Cells from different groups were seeded into 96-well plates at the appropriate density. After incubation at 37°C and 5% CO_2 for 48 h, 50 mM EdU reagent was added to the cells, followed by incubation for another 2 h. The cells were then fixed in 4% paraformaldehyde and stained with Apollo Dye solution to label proliferating cells. Nuclei were counterstained with DAPI. The cell proliferation rate was calculated according to the manufacturer's instructions. Images were obtained using a fluorescence microscope (Zeiss, Jena, Germany).

Clone Formation Assay

From each group, 500 cells were plated per well of a 6-well culture plate, three wells per group. The cells were incubated at 37°C for 14 days with the growth medium being replaced every third day. After 14 days, the cells were washed twice with phosphate buffer saline (PBS) and fixed in 4% paraformaldehyde and then stained with 0.5% crystal violet. The number of colonies containing ≥50 cells was counted under a microscope. These experiments were performed in triplicate.

Cell Apoptosis Assays

Analysis of cell apoptosis was performed using both flow cytometry and caspase-3 detection. For flow cytometry, the

Annexin V/FITC Apoptosis Detection Kit (BD Pharmingen, Franklin Lakes, NJ, USA) was used as per the manufacturer's instructions. The stained cells were analyzed on a FACSCalibur flow cytometer using CellQuestPro software (BD Pharmingen) to determine the rate of cell apoptosis. For the caspase-3 assay, caspase-3 activity was measured according to the rate of cleavage of the chromogenic caspase substrate, Ac-DEVD-pNA (acetyl-Asp-Glu-Val-Asp p-nitroanilide), using the Caspase-3 Activity Assay Kit (Beyotime Biotech). Cells from each group were harvested, and approximately 50 pg of total protein was added to a reaction buffer containing Ac-DEVD-pNA (2 mM), followed by incubation for 2 h at 37°C; the absorbance of the yellow pNA cleavaged from its corresponding precursor was measured at 405 nm using a spectrometer (SpectraMax i3, Molecular Devices). The specific caspase activity, normalized for total protein content of the cell lysates, was then expressed as a fold change compared with the baseline.

Wound Healing Assay

Cells were cultured in 6-well plates until they had reached 70%–90% confluence. A scratch was made on the bottom of each well using a 10-μL tip to form wounds. The cells were then washed twice with PBS and cultured under the previous conditions. The wounds were imaged at different time points, and the distance migrated by cells from five different areas for each wound was measured. For each visual field, two straight lines were drawn in the front of both sides of the gap, and the average distance was calculated as the average of the distance of the two lines at the left, middle, and right points of the view.

Cell Migration and Invasion Assays

A total of 4×10^4 cells were suspended in 100 μL of DMEM without FBS and seeded into the top chamber of 24-well plate transwell inserts (BD Pharmingen) with an 8-μm membrane pore size. Medium containing 10% FBS was placed into the lower chamber as a chemoattractant. After incubating for 24 h, the cells that did not migrate through the pores were manually removed with a cotton swab. Cells at the bottom of the membrane were fixed and stained with a crystal violet solution (Beyotime Biotech) and then counted and imaged under a microscope. Cell numbers were calculated in eight random fields for each chamber, and the average value was calculated. Each experiment was conducted in triplicate. The cell count index was also used as the counting of migrated cells. Stained cells from the bottom of the chambers were eluted with 500 μL of 33% acetic acid; the absorbance of the eluant was read under a microplate reader at 570 nm (SpectraMax i3, Molecular Devices), and the optical density was recorded as the cell count index to reflect cell number. Cell invasion assays were performed using Matrigel (diluted 1:5 with medium without FBS; BD Pharmingen)-coated transwell inserts following the same procedure as described above.

Chromatin Isolation by RNA Purification (ChIRP)

An optimized ChIRP assay to identify lncRNA-associated proteins was performed following previously described protocols (31–33) with modifications. The EZ-Magna ChIRP™ RNA Interactome Kit (Merck Millipore, Darmstadt, Germany) was used on the immortalized normal oral epithelial cell line hTERT-OME. Twenty antisense DNA tiling probes targeting *LINC02487* were designed using the online probe designer at singlemoleculefish.com (http://www.singlemoleculefish.com/designer.html) and synthesized (Sangong Biotech) with Biotin-TEG at the 3′ end. Probes were separated into two pools (even and odd) to help eliminate nonspecific signals. A LacZ probe set was used as a negative control, and a blank control without probes was used to eliminate background interference. Approximately 1×10^8 cells were used per reaction. Cells of the four groups (even, odd, LacZ, and blank) were harvested and cross-linked with formaldehyde to preserve RNA interaction, following which the cell pellets were lysed and sonicated in a water bath at 4°C to shear the complex. The cell lysates were incubated with the biotinylated DNA probes and subjected to capture by streptavidin magnetic beads. The RNA was then extracted from the ChIRP samples and quantified by RT-qPCR as quality control. The proteins were subsequently precipitated, separated by bis–tris SDS–PAGE (Invitrogen) for mass spectrometry (ChIRP–MS) (Applied Protein Technology, Shanghai, China), and verified by western blotting (ChIRP–WB). The raw data from the mass spectrometry were analyzed and searched using Mascot in the UniProt database (34). Peptides with a false discovery rate (FDR) <1% were chosen for further data processing.

RNA Immunoprecipitation (RIP)

RIP was performed as previously described (35–37) with the following modifications. First, the RIP assay was conducted in 293T cells transiently expressing HA-tagged USP17 through plasmid transfection. A total of 2×10^7 cells were used per reaction. Second, immunoprecipitation was performed by incubating cell lysates containing RNA–protein complexes with anti-HA-coated magnetic beads. Third, biotin-coupled magnetic beads were used as control. Briefly, cells were cross-linked and lysed in the presence of an RNase inhibitor and a protease inhibitor cocktail, followed by sonication on ice. After immunoprecipitation, purified beads containing RNA–protein complexes were washed following standard procedures. The protein samples were retrieved and detected by western blotting as quality control. The RNA samples were extracted using the RNeasy MinElute Cleanup Kit (Qiagen, Düsseldorf, Germany) and detected by RT-qPCR. The results were presented as *LINC02487* fold enrichment compared with the control.

Antibodies and Western Blot Analysis

Cells from different groups were harvested, rinsed twice with PBS buffer, and then lysed with lysis buffer (150 mM NaCl, 50 mM Tris-HCl pH 7.4, 1 mM EDTA, 1 mM $MgCl_2$, 0.5% NP-40, 1 mM Na3VO4, 1 mM NaF, protease inhibitor cocktail). Protein samples were heated to 95°C for 10 min and then resolved by SDS–PAGE and transferred to an Immobilon-P membrane (Millipore). The membrane was incubated with primary antibody at 4°C overnight and with secondary antibody at room temperature for 1 h. An ECL reagent (Millipore) was added for chemiluminescent detection. The primary antibodies used for immunoblotting were as follows: rabbit anti-USP17

(1:1000), anti-GAPDH (1:5000), anti-HA (1:3000), anti-SNAI1 (1:500), anti-N-cadherin (1:1000), anti-E-cadherin (1:1000), and anti-vimentin (1:1000).

Statistical Analysis

Statistical analyses were performed with GraphPad 7 (GraphPad Software, San Diego, CA, USA). The $2^{-\Delta\Delta CT}$ method was used to analyze the relative expression level of RNAs. All data were expressed as means ± SD of three or more independent experiments. Sample sizes were selected based on previous publications or related articles. A two-tailed Student's *t*-test was used for comparison between two groups. Multiple comparisons were made using one-way ANOVA. Statistical significance was determined at $P < 0.05$.

RESULTS

LINC02487 Was Downregulated in OSCC Samples and Cell Lines, and LINC02487 Expression Levels Were Correlated With Cancer Metastasis

To determine the status of *LINC02487* in OSCCs, we used RT-qPCR to compare the relative expression levels of *LINC02487* in 50 paired OSCC cancer tissues and adjacent normal tissues. The characteristics of all the patients and the relative *LINC02487* expression levels in the different groups are summarized in **Table 1**. The results showed that *LINC02487* expression was significantly downregulated in OSCC samples compared with that in paired adjacent normal tissues ($P < 0.01$) (**Figure 1A**). The average fold change was 51.4. Moreover, the expression level of *LINC02487* differed significantly between patients with or without near and/or distant metastasis, indicating that the *LINC02487* level was potentially associated with cancer metastasis (**Table 1**). We also evaluated *LINC02487* expression in OSCC cell lines. The results demonstrated that *LINC02487* expression was also downregulated in the OSCC cell lines HN4, HN6, HN30, SCC9, SCC25, and Cal27 compared with that in immortalized normal oral epithelial cell line hTERT-OME (**Figure 1B**). To confirm these results, we also analyzed the relative expression level of *LINC02487* in TCGA data and found that it was markedly lower in HNSCC than in normal controls ($P < 0.0001$) (**Figure 1C**).

LINC02487 Was Localized to the Cytoplasm and Aggregated Around the Nuclear Membrane

We next performed FISH to explore the subcellular localization of *LINC02487*. Confocal microscopy analysis showed that the *LINC02487* signal was mainly localized to the cytoplasm and aggregated around the nuclear membrane (**Figure 2**).

Overexpression of *LINC02487* Inhibited Cell Proliferation

To investigate the function of *LINC02487* in OSCCs, we established *LINC02487*-overexpressing HN6 and HN30 OSCC cell lines through the lentiviral transfection of pCMV-puro plasmids. RT-qPCR results showed a more than 3000-fold stable overexpression of *LINC02487* after transfection in HN6 cells and a more than 2000-fold overexpression in HN30 cells (**Figure 3A**). Next, we compared the phenotypic changes occurring in *LINC02487*-overexpressing cells compared with control cells. CCK-8 and EdU staining assays both revealed that cell viability was decreased in *LINC02487*-overexpressing cells (**Figures 3B, C**). Cell apoptosis was also examined through analysis of both caspase-3 activity and Annexin V/FITC staining in the two cell lines. Overall, no significant differences in the rate of apoptosis were found between the two cell lines (**Supplementary Figure 1A, B**). A colony formation assay showed that fewer clones formed with *LINC02487* overexpression (**Figure 3D**). Moreover, flow cytometry analysis demonstrated that the ratio of cells in the G1 phase of the cell cycle was increased in

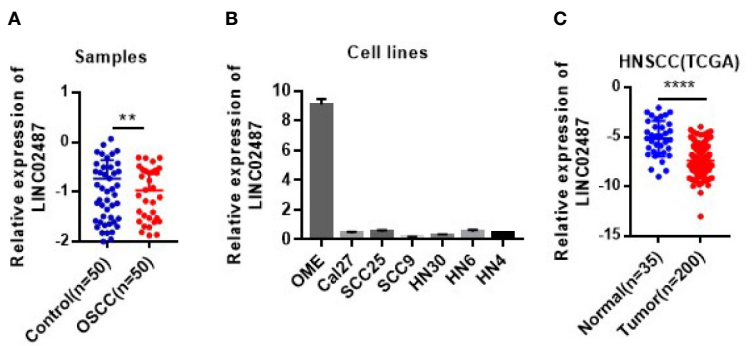

FIGURE 1 | The expression levels of *LINC02487* in tissue samples and cell lines. **(A)** The expression of *LINC02487* was downregulated in OSCC samples compared with paired adjacent normal tissues. **(B)** The relative expression levels of *LINC02487* were significantly lower in the OSCC cell lines Cal27, SCC25, SCC9, HN30, HN6, and HN4 than in the immortalized normal human oral mucosal epithelial cell line hTERT-OME. **(C)** The expression of *LINC02487* was downregulated in HNSCC samples compared with normal control samples in TCGA data sets. HNSCC, head and neck squamous cell carcinoma; ns, not significant; $^{**}P < 0.01$, $^{****}P < 0.0001$.

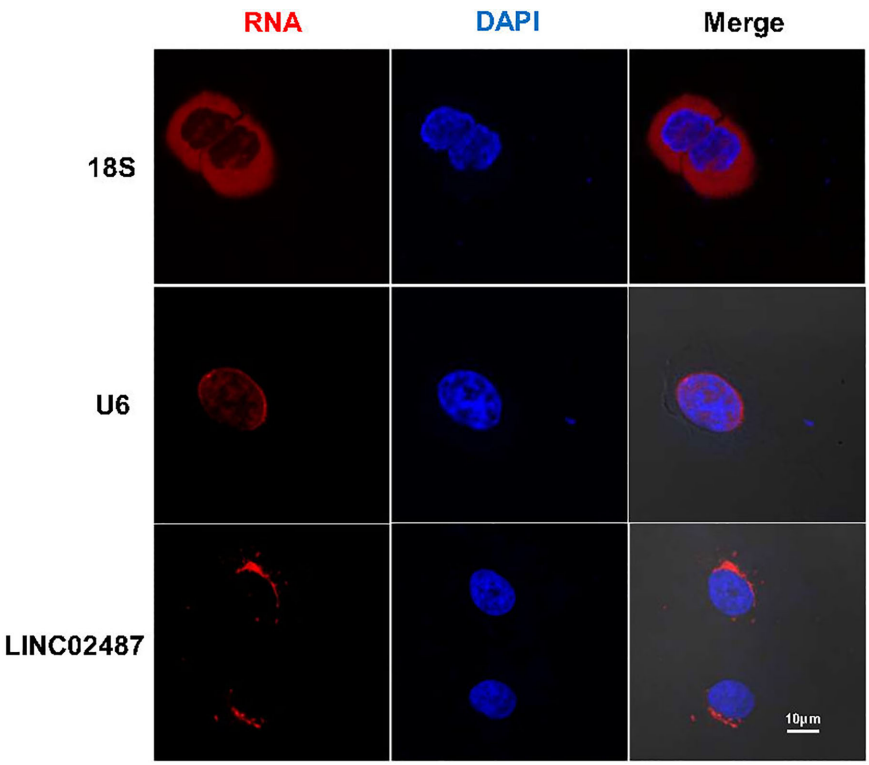

FIGURE 2 | Long noncoding RNA *LINC02487* was mainly localized to the cytoplasm and aggregated around the nuclear membrane. 18S ribosomal RNA and *U6* were used as controls. ns, not significant.

LINC02487-overexpressing cells (**Supplementary Figure 1C**). In summary, overexpression of *LINC02487* suppressed cell proliferation in OSCC cell lines.

Overexpression of *LINC02487* Significantly Inhibited Cell Migration and Invasion in OSCC Cells

To further explore the function of *LINC02487*, we investigated the effect of overexpressing *LINC02487* on the migratory and invasive capabilities of HN6 and HN30 cells. We first analyzed cell migration using a wound healing assay. A significant increase in the average migrated distance was observed in *LINC02487*-overexpressing cells compared with that in mock control cells (**Figures 4A, B**). Transwell assays with or without Matrigel-coated upper chambers showed that both migratory and invasive abilities were significantly suppressed in *LINC02487*-overexpressing cells (**Figures 4C, D**).

LINC02487 Directly Bound to USP17

To explore the mechanisms underlying *LINC02487* function, we purified its binding complexes and identified *LINC02487*-binding proteins by mass spectrometry (ChIRP–MS). As previously reported, peptides detected in both the even and odd groups but not in the LacZ and blank groups were considered to be *LINC02487*-binding proteins. Twenty-nine peptides representing two protein families were detected with most (26 out of 29) belonging to the ubiquitin carboxyl-terminal hydrolase 17 (USP17) family (**Figure 5A**). The mass spectrometry data is shown in the **Supplementary data**. Analysis of double-fluorescence staining by confocal microscopy showed that *LINC02487* and USP17 displayed a high ratio of overlap in the cytoplasm (**Figure 5B**). This result can also be confirmed by western blotting (ChIRP–WB) assay (**Figure 5C**). To verify this result, we then performed RNA immunoprecipitation using HA-tagged USP17; the complex was purified using HA magnetic beads, followed by detection of *LINC02487* by RT-qPCR. The result shows that *LINC02487* was more than three times higher in the USP17-HA group (**Figure 5D**). Together, these results demonstrate that *LINC02487* bound directly to USP17 and suggests that *LINC02487* may modulate cell functions through USP17.

LINC02487 Suppressed Tumor Migration and Invasion Through EMT-Related Processes

USP17 is reported to regulate cancer metastasis through modulation of EMT (38, 39). To determine whether *LINC02487* modulates OSCC cell function through this path, we examined EMT-related markers in *LINC02487*-overexpressing cell lines HN6 and HN30. The level of the epithelial marker E-cadherin was increased compared with that in

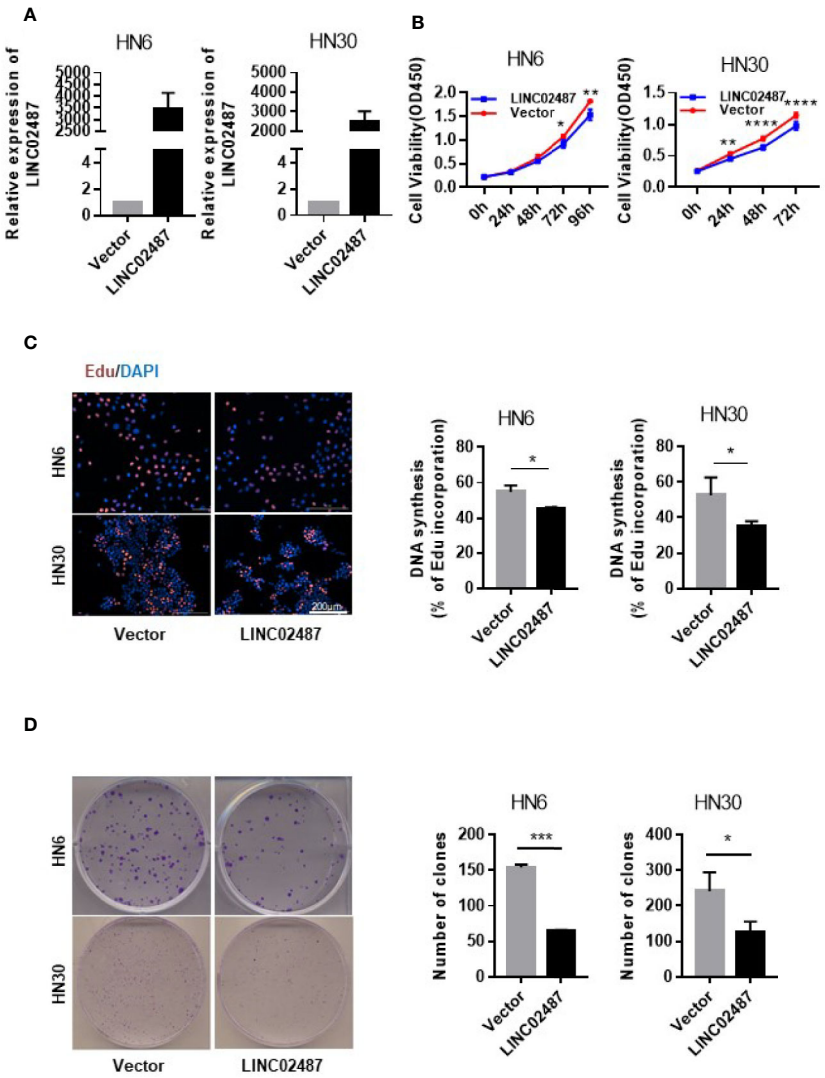

FIGURE 3 | Overexpression of *LINC02487* inhibited cell proliferation in the OSCC cell lines HN6 and HN30. **(A)** The relative expression level of *LINC02487* after lentiviral plasmid transfection. **(B, C)** CCK-8 and EdU staining assays showed that cell proliferation was inhibited after *LINC02487* overexpression. **(D)** Overexpression of *LINC02487* also diminished the colony-forming ability of OSCC cells. ns, not significant; $^{*}P < 0.05$, $^{**}P < 0.01$, $^{***}P < 0.001$, $^{****}P < 0.0001$.

control cells, and the levels of the mesenchymal markers N-cadherin and vimentin were decreased after *LINC02487* overexpression (**Figure 6A**). We also find that the expression of the key EMT regulator SNAI1 was increased at the mRNA level but decreased at the protein level; meanwhile, the expression of USP17 was decreased at both the mRNA and protein level (**Figures 6A, B**). This result could be explained by the posttranslational regulation resulting from the activity of the deubiquitinating enzyme USP17.

LINC02487 Inhibited EMT Through the USP17–SNAI1 Axis

We next determined whether the effect of *LINC02487* on cell mobility was mediated through the USP17–SNAI1 axis using the OSCC cell line HN6. First, we assessed the silencing efficiency of three siRNAs and selected siRNA-1 for subsequent experiments (**Figure 7A**). A transwell assay showed that knockdown of *LINC02487* increased the migratory ability of the HN6 cells (**Figure 7B**). We then performed a series of transwell and western blot assays to unravel the associated regulatory network. The results showed that knocking down USP17 decreased cell migration and invasion, and this effect could be rescued by simultaneously knocking down *LINC02487* and USP17 (**Figures 7C, D**). Western blotting assay further revealed that this rescue was mediated through the EMT process. When USP17 was knocked down, cells presented a more epithelial-like phenotype, and this effect could be rescued by silencing *LINC02487* (**Figure 7E**).

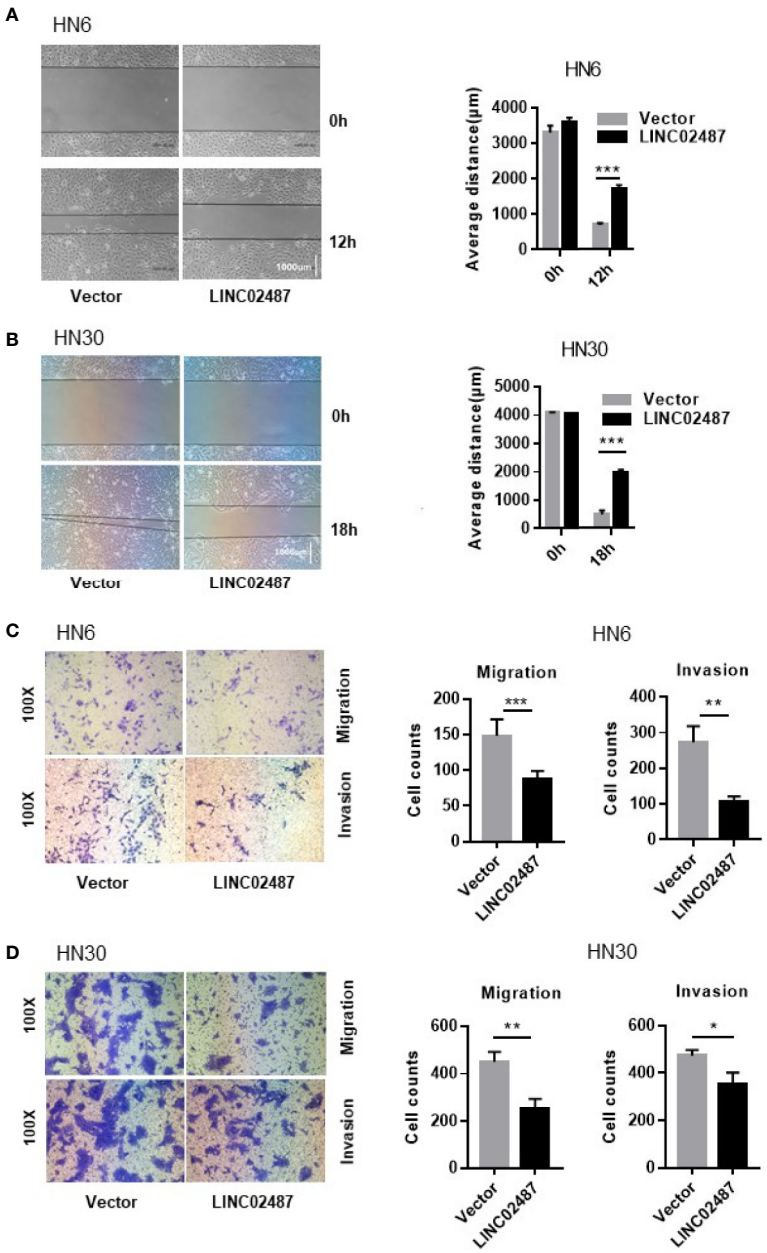

FIGURE 4 | Overexpression of *LINC02487* inhibited the migratory and invasive abilities of the OSCC cell lines HN6 and HN30. **(A, B)** A wound healing assay showed that overexpression of *LINC02487* affected cell migration. **(C, D)** A transwell assay showed that both cell migration (without Matrigel) and invasion (with Matrigel) were inhibited after *LINC02487* overexpression. ns, not significant; $^{*}P < 0.05$, $^{**}P < 0.01$, $^{***}P < 0.001$.

DISCUSSION

LncRNA expression contributes significantly to the whole transcriptome and is dysregulated in many cancer types, including OSCC (15, 40, 41). LncRNAs can be epigenetic, transcriptional, and posttranscriptional regulators in various cancer types (42–45). Studies have reported that *LINC02487* (previously known as *LOC441178*) is significantly downregulated in OSCC samples when compared with samples obtained from healthy controls (18, 19), and *LINC02487* expression levels were found to be associated with postoperative survival time, indicating that it has potential for use as a biomarker for OSCC diagnosis and prognosis. In this study, we find that *LINC02487* expression was significantly decreased in OSCC samples derived from a Chinese population; this is consistent with previous studies and confirms the similarity in *LINC02487* OSCC expression pattern between different continents and populations. As lncRNAs have been reported to display

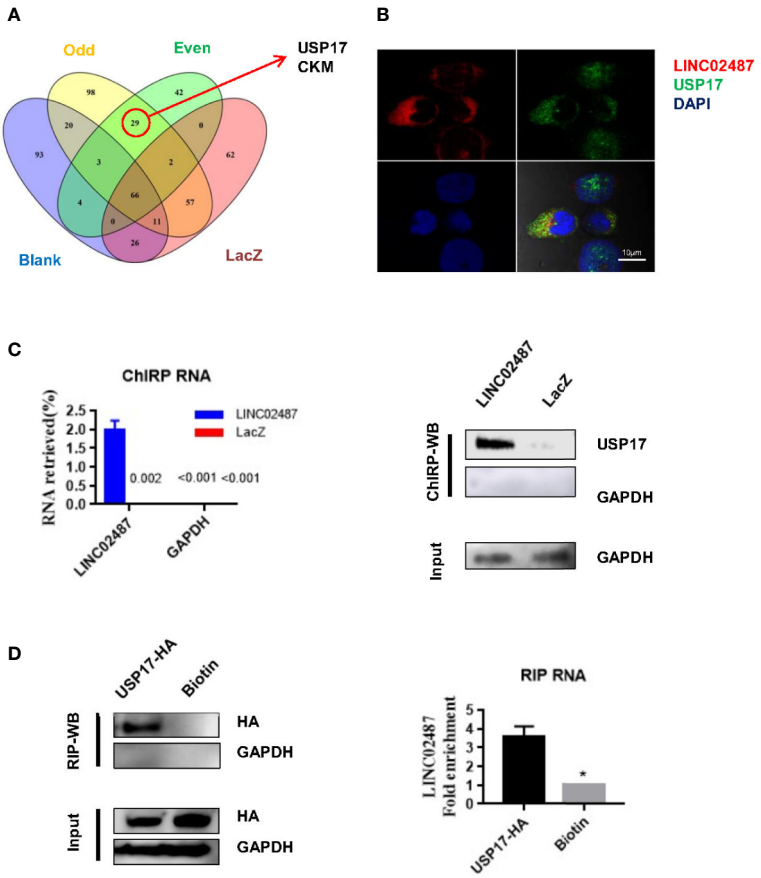

FIGURE 5 | *LINC02487* directly bound USP17. **(A)** Chromatin isolation by RNA purification–mass spectrometry (ChIRP–MS) results show that *LINC02487* binds primarily to two proteins: USP17 and CKM. **(B)** Colocalization of *LINC02487* and USP17 using confocal microscopy. **(C)** ChIRP-western blot demonstrated the direct binding of *LINC02487* and USP17; LacZ was used as control. **(D)** RNA immunoprecipitation confirmed the binding of *LINC02487* and USP17. Biotin beads were used as control. ns, not significant; $^{*}P < 0.05$.

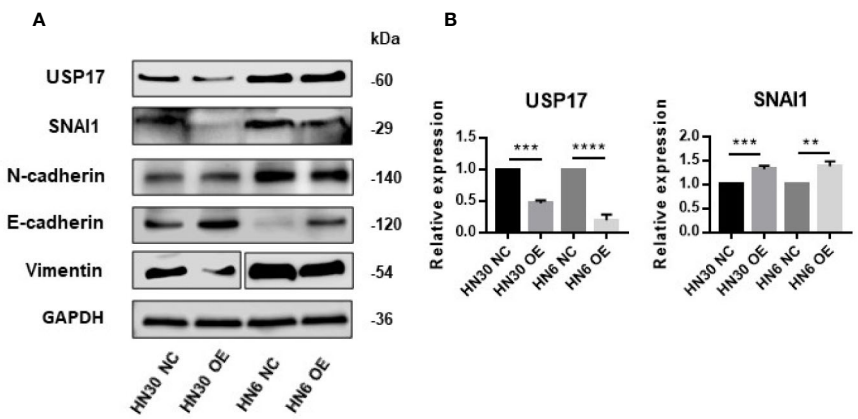

FIGURE 6 | Overexpression of *LINC02487* suppressed EMT through the USP17–SNAI1 axis. **(A)** The protein expression of USP17 and EMT-related markers in the OSCC cell lines HN30 and HN6. Blots for vimentin were spliced from two scans due to expression differences between the two cell lines. **(B)** The expression levels of *USP17* and *SNAI1* mRNA in the cell lines HN30 and HN6. ns, not significant; $^{**}P < 0.01$, $^{***}P < 0.001$, $^{****}P < 0.0001$.

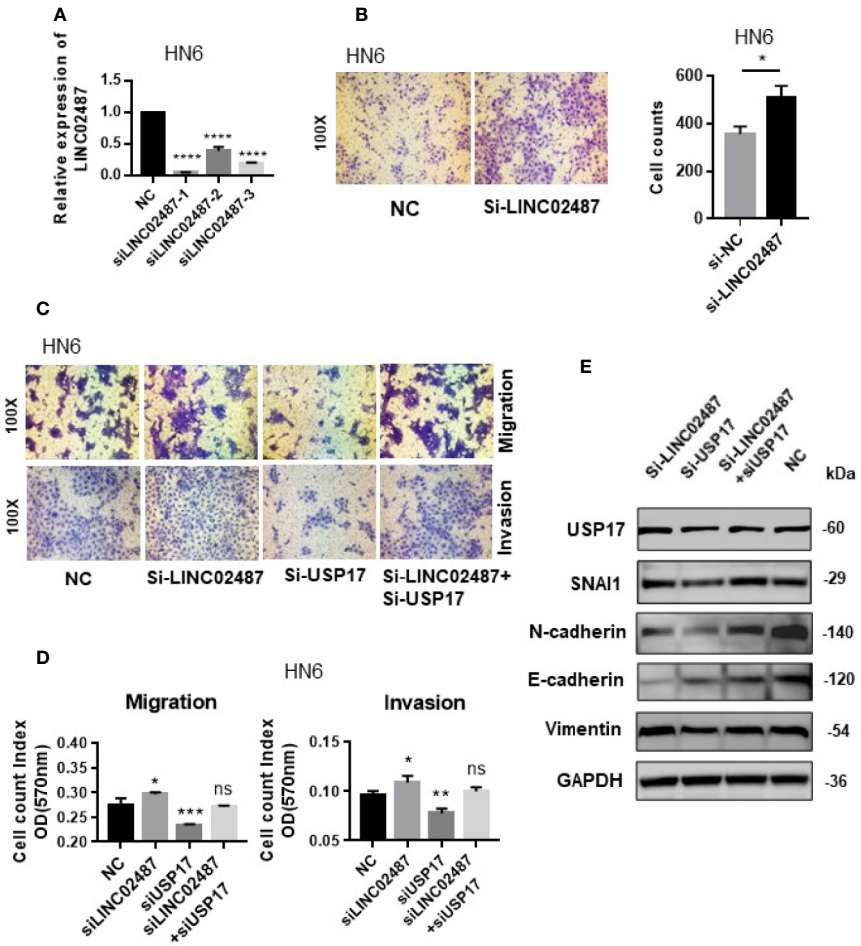

FIGURE 7 | **(A)** The efficiency of the three *LINC02487* siRNAs in the OSCC cell line HN6; Si-LINC02487-1 was chosen for subsequent experiments. **(B)** The knockdown of *LINC02487* increased cell migration. **(C, D)** The knockdown of *LINC02487* increased the migratory and invasive capacity of the OSCC cell line HN6 although knockdown of USP17 suppressed these processes. Simultaneous knockdown of *LINC02487* and USP17 restored cell functions. **(E)** Western blot assay showed that the changes in cell migratory ability were mediated through EMT. ns, not significant; $^{*}P < 0.05$, $^{**}P < 0.01$, $^{***}P < 0.001$, $^{****}P < 0.0001$.

additional tissue-specific expression patterns (10, 40), using TCGA data, we explored the *LINC02487* status in different cancer types through TANRIC, an open-access resource for interactive exploration of lncRNAs. The analysis indicates that *LINC02487* was also downregulated in HNSCC, but upregulated in breast cancer and kidney renal papillary cell carcinoma when compared with nontumor controls (data not shown). This result is also consistent with previous reports and is further confirmed in OSCC cell lines in a comparative analysis with immortalized normal oral epithelial cells. Additionally, the expression level of *LINC02487* is associated with cancer metastasis, indicating that this lncRNA may be involved in OSCC development.

Functionally, overexpression analysis shows that the increased expression of *LINC02487* influences several cell characteristics, including viability, mobility, and cell cycle progression. In particular, *LINC02487* gain-of-function inhibits cell proliferation, migration, and invasion, indicating that this lncRNA might play a role as a tumor suppressor in OSCC.

The functional mechanisms of lncRNAs are determined by their cellular localization, at least partially (24, 46). Most lncRNAs are predominantly localized to the chromatin and nucleus and have lower expression levels than coding mRNAs (10). In this study, we use FISH to show that *LINC02487* was mostly localized to the cytoplasm, and aggregated around the nuclear membrane. This suggests that *LINC02487* acts mainly at the posttranscriptional or posttranslational level.

We performed ChIRP–MS to explore the mechanisms underlying the cell functions of *LINC02487* and find that *LINC02487* bound directly to USP17. According to UniProt, USP17 is mainly found in the nucleus and endoplasmic reticulum (34, 47). In our study, we demonstrate that *LINC02487* was located in the cytoplasm, aggregated near the nuclear membrane, where USP17 is reported to also be localized (47). The binding of *LINC02487* and USP17 was further verified by ChIRP–WB and RIP. These results indicate that *LINC02487*-regulated cell functions may be mediated through USP17.

USP17 belongs to a subfamily of deubiquitinating enzymes (DUBs). These enzymes are key regulators of posttranslational protein modifications through ubiquitination in many cellular processes, including transcription, DNA repair, cell-cycle progression, and apoptosis (48, 49). Additionally, as a cytokine-inducible DUB, USP17 is also reported to inhibit proliferation, increase apoptosis, and regulate the G1/S phase transition of the cell cycle (50–52). Several studies also indicate that USP17 may be involved in cancer metastasis through EMT regulation (39, 49, 53). Tumor cells undergoing EMT acquire a mesenchymal phenotype and begin to express markers such as N-cadherin and lose the expression of epithelial markers such as E-cadherin, leading to tumor progression, invasion, and eventually distant metastasis. EMT is an essential step in cancer metastasis. Emerging evidence has shown that lncRNAs influence the EMT process mainly through cross-talk with master regulators, such as SNAI1 and ZEB (21, 25, 30, 54, 55). In this study, western blot analysis showed that overexpressing *LINC02487* led to the upregulation of the epithelial marker E-cadherin and downregulation of the mesenchymal markers N-cadherin and vimentin, indicating that *LINC02487* regulates cell invasion and migration through the EMT process. Mechanistically, we also tested the expression of USP17 and SNAI1 in the OSCC cell lines HN6 and HN30. Overexpression of *LINC02487* suppressed the expression of USP17 at both the mRNA and protein level. Interestingly, however, we found that overexpressing *LINC02487* led to a reduction in the protein level, but not the mRNA level, of SNAI1. The SNAI1 protein is highly unstable and can be posttranslationally degraded through the ubiquitin–proteasome pathway. USP17 is reported to exert its role in EMT through the posttranslational deubiquitination and stabilization of SNAI1. Inhibition of USP17 promotes SNAI1 degradation, thereby suppressing breast cancer invasion and metastasis (49, 53). Our findings are consistent with previous reports.

We further tested the cell function of *LINC02487* in the OSCC cell line HN6. As USP17 is known to have several cellular functions, we only tested its role in cell mobility. First, a transwell assay revealed that silencing *LINC02487* led to an increase in cell migration, whereas knocking down USP17 suppressed cell migration and invasion, and this effect could be rescued by the loss of *LINC02487*. We then examined the expression levels of EMT-related markers with the results demonstrating that the expression levels of these proteins were changed accordingly. When we silenced *LINC02487*, OSCC cells showed increased mesenchymal characteristics, and when USP17 was silenced, OSCC cells displayed a more epithelial phenotype. However, this effect could also be rescued by the loss of *LINC02487*. Together, these results indicate that *LINC02487* may be a negative regulator of USP17, and has a role in the EMT process through the USP17–SNAI1 axis. McFarlane et al. identify that USP17 is highly expressed in several tumor biopsies, and USP17 depletion significantly impairs G1-S phase transition and blocks cell proliferation (56). In our study, we observed that the overexpression of *LINC02487* exerted similar effects on cells (**Supplementary Figure 1C**). Whether it was also through the *LINC02487*-USP17 axis has yet to be proved. Altogether, we demonstrated that *LINC02487* binds directly to, and negatively regulates, USP17 in OSCC cells.

In conclusion, our study confirms that long noncoding RNA *LINC02487* is downregulated in OSCC samples and cell lines, and its expression level is correlated with cancer metastasis. We further show that *LINC02487* binds directly to USP17 and acts as a tumor suppressor through the USP17–SNAI1 axis.

DATA AVAILABILITY STATEMENT

The raw data supporting the conclusions of this article will be made available by the authors, without undue reservation.

ETHICS STATEMENT

The studies involving human participants were reviewed and approved by Ethics Committee of Zhengzhou University. The patients/participants provided their written informed consent to participate in this study.

AUTHOR CONTRIBUTIONS

Conception and design: LF, WC, and WQ. Development of methodology: LF and JZ. Data acquisition: LF, MS, and FQ. Data analysis and interpretation: LF, JZ, and WC. Writing, reviewing, and/or revision of the manuscript: LF, WC, and JZ. Study supervision: WQ and WC. All authors contributed to the article and approved the submitted version.

FUNDING

This paper was funded by grants from the Oral and Maxillofacial Surgery Academician Workstation of Zhengzhou (152PYSGZ040), the National Natural Science Foundation of China (81874126), and Shanghai Municipal Science and Technology Commission Funded Projects (18DZ2291500, 16140903300).

ACKNOWLEDGMENTS

Most of the research was carried out in the Shanghai Key Laboratory of Stomatology, Ninth People's Hospital, Shanghai Jiao Tong University School of Medicine, Shanghai, China. We would like to thank the staff of the Shanghai Key Laboratory of Stomatology (Qin Xu, Xu Wang, Ming Yan, Mingyu Li, Zhihui Li, and Jingsu Liu) for their kind and professional help.

SUPPLEMENTARY MATERIAL

The Supplementary Material for this article can be found online at: https://www.frontiersin.org/articles/10.3389/fonc.2020.559808/full#supplementary-material

REFERENCES

1. Ryerson AB, Eheman CR, Altekruse SF, Ward JW, Jemal A, Sherman RL, et al. Annual Report to the Nation on the Status of Cancer, 1975-2012, featuring the increasing incidence of liver cancer. *Cancer* (2016) 122(9):1312–37. doi: 10.1002/cncr.29936
2. Leemans CR, Braakhuis BJ, Brakenhoff RH. The molecular biology of head and neck cancer. *Nat Rev Cancer* (2011) 11(1):9–22. doi: 10.1038/nrc2982
3. Krishna Rao SV, Mejia G, Roberts-Thomson K, Logan R. Epidemiology of oral cancer in Asia in the past decade–an update (2000-2012). *Asian Pacific J Cancer Prev APJCP* (2013) 14(10):5567–77. doi: 10.7314/APJCP.2013.14.10.5567
4. Chen W, Zheng R, Baade PD, Zhang S, Zeng H, Bray F, et al. Cancer statistics in China, 2015. *CA: Cancer J Clin* (2016) 66(2):115–32. doi: 10.3322/caac.21338
5. Warnakulasuriya S. Global epidemiology of oral and oropharyngeal cancer. *Oral Oncol* (2009) 45(4-5):309–16. doi: 10.1016/j.oraloncology.2008.06.002
6. Shield K, Ferlay J, Jemal A, Sankaranarayanan R, Chaturvedi A, Bray F, et al. The global incidence of lip, oral cavity, and pharyngeal cancers by subsite in 2012. *CA: Cancer J Clin* (2017) 67(1):51–64. doi: 10.3322/caac.21384
7. Mendez E, Houck JR, Doody DR, Fan W, Lohavanichbutr P, Rue TC, et al. A genetic expression profile associated with oral cancer identifies a group of patients at high risk of poor survival. *Clin Cancer Res* (2009) 15(4):1353–61. doi: 10.1158/1078-0432.CCR-08-1816
8. Rivera C. Essentials of oral cancer. *Int J Clin Exp Pathol* (2015) 8(9):11884–94.
9. Gutschner T, Diederichs S. The hallmarks of cancer: a long non-coding RNA point of view. *RNA Biol* (2012) 9(6):703–19. doi: 10.4161/rna.20481
10. Derrien T, Johnson R, Bussotti G, Tanzer A, Djebali S, Tilgner H, et al. The GENCODE v7 catalog of human long noncoding RNAs: analysis of their gene structure, evolution, and expression. *Genome Res* (2012) 22(9):1775–89. doi: 10.1101/gr.132159.111
11. Gomes CC, de Sousa SF, Gomez RS. MicroRNAs: small molecules with a potentially role in oral squamous cell carcinoma. *Curr Pharm Design* (2013) 19(7):1285–91. doi: 10.2174/138161213804805694
12. Esteller M. Non-coding RNAs in human disease. *Nat Rev Genet* (2011) 12 (12):861–74. doi: 10.1038/nrg3074
13. Min A, Zhu C, Peng S, Rajthala S, Costea DE, Sapkota D. MicroRNAs as Important Players and Biomarkers in Oral Carcinogenesis. *BioMed Res Int* (2015) 2015:186904. doi: 10.1155/2015/186904
14. Taucher V, Mangge H, Haybaeck J. Non-coding RNAs in pancreatic cancer: challenges and opportunities for clinical application. *Cell Oncol* (2016) 39 (4):295–318. doi: 10.1007/s13402-016-0275-7
15. Feng L, Chen WT, Qiu WL. Long non-coding RNAs associated with oral squamous cell carcinoma. *Eur Rev Med Pharmacol Sci* (2019) 23(20):8888–96. doi: 10.26355/eurrev_201910_19284
16. Momen-Heravi F, Bala S. Emerging role of non-coding RNA in oral cancer. *Cell Signal* (2018) 42:134–43. doi: 10.1016/j.cellsig.2017.10.009
17. Yang B, Shen J, Xu L, Chen Y, Che X, Qu X, et al. Genome-Wide Identification of a Novel Eight-lncRNA Signature to Improve Prognostic Prediction in Head and Neck Squamous Cell Carcinoma. *Front Oncol* (2019) 9:898:898. doi: 10.3389/fonc.2019.00898
18. Feng L, Houck JR, Lohavanichbutr P, Chen C. Transcriptome analysis reveals differentially expressed lncRNAs between oral squamous cell carcinoma and healthy oral mucosa. *Oncotarget* (2017) 8(19):31521–31. doi: 10.18632/oncotarget.16358
19. Xu K, Tian H, Zhao S, Yuan D, Jiang L, Liu X, et al. Long Noncoding RNA LOC441178 Reduces the Invasion and Migration of Squamous Carcinoma Cells by Targeting ROCK1. *BioMed Res Int* (2018) 2018:4357647. doi: 10.1155/2018/4357647
20. Lee CC, Su YC, Hung SK, Chen PC, Huang CI, Huang WL, et al. Recommendation for incorporation of a different lymph node scoring system in future AJCC N category for oral cancer. *Sci Rep* (2017) 7 (1):14117. doi: 10.1038/s41598-017-06452-0
21. Grelet S, Link L, Howley B, Obellianne C, Palanisamy V, Gangaraju V, et al. A regulated PNUTS mRNA to lncRNA splice switch mediates EMT and tumour progression. *Nat Cell Biol* (2017) 19(9):1105–15. doi: 10.1038/ncb3595
22. Tam WL, Weinberg RA. The epigenetics of epithelial-mesenchymal plasticity in cancer. *Nat Med* (2013) 19(11):1438–49. doi: 10.1038/nm.3336
23. Lamouille S, Xu J, Derynck R. Molecular mechanisms of epithelial-mesenchymal transition. *Nat Rev Mol Cell Biol* (2014) 15(3):178–96. doi: 10.1038/nrm3758
24. Luo X, Qiu Y, Jiang Y, Chen F, Jiang L, Zhou Y, et al. Long non-coding RNA implicated in the invasion and metastasis of head and neck cancer: possible function and mechanisms. *Mol Cancer* (2018) 17: (1):14. doi: 10.1186/s12943-018-0763-7
25. Wang L, Yang F, Jia LT, Yang AG. Missing Links in Epithelial-Mesenchymal Transition: Long Non-Coding RNAs Enter the Arena. *Cell Physiol Biochem Int J Exp Cell Physiol Biochem Pharmacol* (2017) 44(4):1665–80. doi: 10.1159/000485766
26. Wang YQ, Jiang DM, Hu SS, Zhao L, Wang L, Yang MH, et al. SATB2-AS1 Suppresses Colorectal Carcinoma Aggressiveness by Inhibiting SATB2-Dependent Snail Transcription and Epithelial-Mesenchymal Transition. *Cancer Res* (2019) 79(14):3542–56. doi: 10.1158/0008-5472.Can-18-2900
27. Sakai S, Ohhata T, Kitagawa K, Uchida C, Aoshima T, Niida H, et al. Long Noncoding RNA ELIT-1 Acts as a Smad3 Cofactor to Facilitate TGFbeta/Smad Signaling and Promote Epithelial-Mesenchymal Transition. *Cancer Res* (2019) 79(11):2821–38. doi: 10.1158/0008-5472.Can-18-3210
28. Li J, Han L, Roebuck P, Diao L, Liu L, Yuan Y, et al. TANRIC: An Interactive Open Platform to Explore the Function of lncRNAs in Cancer. *Cancer Res* (2015) 75(18):3728–37. doi: 10.1158/0008-5472.CAN-15-0273
29. Leemans CR, Snijders PJF, Brakenhoff RH. The molecular landscape of head and neck cancer. *Nat Rev Cancer* (2018) 18(5):269–82. doi: 10.1038/nrc.2018.11
30. Jiang Y, Cao W, Wu K, Qin X, Wang X, Li Y, et al. LncRNA LINC00460 promotes EMT in head and neck squamous cell carcinoma by facilitating peroxiredoxin-1 into the nucleus. *J Exp Clin Cancer Res CR* (2019) 38(1):365. doi: 10.1186/s13046-019-1364-z
31. Chu C, Zhang QC, da Rocha ST, Flynn RA, Bharadwaj M, Calabrese JM, et al. Systematic discovery of Xist RNA binding proteins. *Cell* (2015) 161(2):404–16. doi: 10.1016/j.cell.2015.03.025
32. Chu C, Quinn J, Chang HY. Chromatin isolation by RNA purification (ChIRP). *J Visualized Experiments JoVE* (2012) 61):3912. doi: 10.3791/3912
33. Chu C, Chang HY. Understanding RNA-Chromatin Interactions Using Chromatin Isolation by RNA Purification (ChIRP). *Methods Mol Biol (Clifton NJ)* (2016) 1480:115–23. doi: 10.1007/978-1-4939-6380-5_10
34. Consortium TU. UniProt: a worldwide hub of protein knowledge. *Nucleic Acids Res* (2019) 47(D1):D506–d15. doi: 10.1093/nar/gky1049
35. Shih JW, Chiang WF, Wu ATH, Wu MH, Wang LY, Yu YL, et al. Long noncoding RNA LncHIFCAR/MIR31HG is a HIF-1alpha co-activator driving oral cancer progression. *Nat Commun* (2017) 8:15874. doi: 10.1038/ncomms15874
36. Tsai MC, Manor O, Wan Y, Mosammaparast N, Wang JK, Lan F, et al. Long noncoding RNA as modular scaffold of histone modification complexes. *Sci (N Y NY)* (2010) 329(5992):689–93. doi: 10.1126/science.1192002
37. Koster T, Staiger D. RNA-binding protein immunoprecipitation from whole-cell extracts. *Methods Mol Biol (Clifton NJ)* (2014) 1062:679–95. doi: 10.1007/978-1-62703-580-4_35
38. Song C, Liu W, Li J. USP17 is upregulated in osteosarcoma and promotes cell proliferation, metastasis, and epithelial-mesenchymal transition through stabilizing SMAD4. *Tumour Biol* (2017) 39(7):1010428317717138. doi: 10.1177/1010428317717138
39. Yildirim N, Kocal G, Isik Z, Saatli B, Saygili U, Uysal T, et al. Ubiquitin-Proteasome Axis, Especially Ubiquitin-Specific Protease-17 (USP17) Gene Family, is a Potential Target for Epithelial-Mesenchymal Transition in High-Grade Serous Ovarian Cancer. *Reprod Sci* (2018) 26(6):794–805. doi: 10.26226/morressier.59ba7299d462b80296ca20e4
40. Maruyama R, Suzuki H. Long noncoding RNA involvement in cancer. *BMB Rep* (2012) 45(11):604–11. doi: 10.5483/BMBRep.2012.45.11.227
41. Huarte M. The emerging role of lncRNAs in cancer. *Nat Med* (2015) 21 (11):1253–61. doi: 10.1038/nm.3981
42. Gibb EA, Enfield KS, Stewart GL, Lonergan KM, Chari R, Ng RT, et al. Long non-coding RNAs are expressed in oral mucosa and altered in oral premalignant lesions. *Oral Oncol* (2011) 47(11):1055–61. doi: 10.1016/j.oraloncology.2011.07.008
43. Gibb EA, Brown CJ, Lam WL. The functional role of long non-coding RNA in human carcinomas. *Mol Cancer* (2011) 10:38. doi: 10.1186/1476-4598-10-38
44. Anastasiadou E, Jacob LS, Slack FJ. Non-coding RNA networks in cancer. *Nat Rev Cancer* (2018) 18(1):5–18. doi: 10.1038/nrc.2017.99
45. Lee JT. Epigenetic regulation by long noncoding RNAs. *Sci (N Y NY)* (2012) 338(6113):1435–9. doi: 10.1126/science.1231776

46. Bartonicek N, Maag JL, Dinger ME. Long noncoding RNAs in cancer: mechanisms of action and technological advancements. *Mol Cancer* (2016) 15(1):43. doi: 10.1186/s12943-016-0530-6
47. Burrows JF, Kelvin AA, McFarlane C, Burden RE, McGrattan MJ, De la Vega M, et al. USP17 regulates Ras activation and cell proliferation by blocking RCE1 activity. *J Biol Chem* (2009) 284(14):9587–95. doi: 10.1074/jbc.M807216200
48. Burrows JF, Scott CJ, Johnston JA. The DUB/USP17 deubiquitinating enzymes: a gene family within a tandemly repeated sequence, is also embedded within the copy number variable beta-defensin cluster. *BMC Genomics* (2010) 11:250. doi: 10.1186/1471-2164-11-250
49. Wu Y, Wang Y, Lin Y. Dub3 inhibition suppresses breast cancer invasion and metastasis by promoting Snail1 degradation. *Nat Commun* (2017) 8:14228. doi: 10.1038/ncomms14228
50. de la Vega M, Kelvin AA, Dunican DJ, McFarlane C, Burrows JF, Jaworski J, et al. The deubiquitinating enzyme USP17 is essential for GTPase subcellular localization and cell motility. *Nat Commun* (2011) 2:259. doi: 10.1038/ncomms1243
51. Burrows JF, McGrattan MJ, Rascle A, Humbert M, Baek KH, Johnston JA. DUB-3, a cytokine-inducible deubiquitinating enzyme that blocks proliferation. *J Biol Chem* (2004) 279(14):13993–4000. doi: 10.1074/jbc.M311291200
52. Shin JM, Yoo KJ, Kim MS, Kim D, Baek KH. Hyaluronan- and RNA-binding deubiquitinating enzymes of USP17 family members associated with cell viability. *BMC Genomics* (2006) 7:292. doi: 10.1186/1471-2164-7-292
53. Liu T, Yu J, Deng M, Yin Y, Zhang H, Luo K, et al. CDK4/6-dependent activation of DUB3 regulates cancer metastasis through SNAIL1. *Nat Commun* (2017) 8:13923. doi: 10.1038/ncomms13923
54. Cao MX, Jiang YP, Tang YL, Liang XH. The crosstalk between lncRNA and microRNA in cancer metastasis: orchestrating the epithelial-mesenchymal plasticity. *Oncotarget* (2017) 8(7):12472–83. doi: 10.18632/oncotarget.13957
55. Zhou X, Liu S, Cai G, Kong L, Zhang T, Ren Y, et al. Long Non Coding RNA MALAT1 Promotes Tumor Growth and Metastasis by inducing Epithelial-Mesenchymal Transition in Oral Squamous Cell Carcinoma. *Sci Rep* (2015) 5:15972. doi: 10.1038/srep15972
56. McFarlane C, Kelvin AA, de la Vega M, Govender U, Scott CJ, Burrows JF, et al. The deubiquitinating enzyme USP17 is highly expressed in tumor biopsies, is cell cycle regulated, and is required for G1-S progression. *Cancer Res* (2010) 70(8):3329–39. doi: 10.1158/0008-5472.can-09-4152

Conflict of Interest: The authors declare that the research was conducted in the absence of any commercial or financial relationships that could be construed as a potential conflict of interest.

Copyright © 2020 Feng, Zhang, Sun, Qiu, Chen and Qiu. This is an open-access article distributed under the terms of the Creative Commons Attribution License (CC BY). The use, distribution or reproduction in other forums is permitted, provided the original author(s) and the copyright owner(s) are credited and that the original publication in this journal is cited, in accordance with accepted academic practice. No use, distribution or reproduction is permitted which does not comply with these terms.

frontiers in Oncology

ORIGINAL RESEARCH
published: 13 November 2020
doi: 10.3389/fonc.2020.585976

miR-146a Overexpression in Oral Squamous Cell Carcinoma Potentiates Cancer Cell Migration and Invasion Possibly *via* Targeting HTT

Liping Wang[1†], *Yunxin Chen*[1†], *Yongyong Yan*[1,2†], *Xueqi Guo*[1], *Ying Fang*[1], *Yucheng Su*[3], *Lijing Wang*[1,4], *Janak L. Pathak*[1,2*] *and Linhu Ge*[1,2*]

[1] *Affiliated Stomatology Hospital of Guangzhou Medical University, Guangzhou Key Laboratory of Basic and Applied Research of Oral Regenerative Medicine, Guangzhou, China,* [2] *Institute of Oral Disease, Guangzhou Medical University, Guangzhou, China,* [3] *Chinese Academy of Medical Sciences, Peking Union Medical College, Beijing, China,* [4] *School of Life Science and Biopharmaceutics, Vascular Biology Research Institute, Guangdong Pharmaceutical University, Guangzhou, China*

OPEN ACCESS

Edited by:
Wei Cao,
Shanghai Jiao Tong University, China

Reviewed by:
Yanjie Zhang,
Shanghai Jiao Tong University, China
Chengzhong Lin,
Shanghai Ninth People's Hospital, China

***Correspondence:**
Linhu Ge
gelinhu@yeah.net
Janak L. Pathak
j.pathak@gzhmu.edu.cn

†These authors have contributed equally to this work and share first authorship

Specialty section:
This article was submitted to Head and Neck Cancer, a section of the journal Frontiers in Oncology

Received: *22 July 2020*
Accepted: *14 October 2020*
Published: *13 November 2020*

Citation:
Wang L, Chen Y, Yan Y, Guo X, Fang Y, Su Y, Wang L, Pathak JL and Ge L (2020) miR-146a Overexpression in Oral Squamous Cell Carcinoma Potentiates Cancer Cell Migration and Invasion Possibly via Targeting HTT. Front. Oncol. 10:585976. doi: 10.3389/fonc.2020.585976

Huntingtin (HTT) is one of the target genes of miR-146-a and regulates various cancer cell activities. This study aims to explore the miR-146a expression pattern in oral squamous cell carcinoma (OSCC) and its role and mechanism in OSCC progression and metastasis *via* targeting the HTT gene. OSCC tissue and non-cancerous matched tissue (NCMT) were obtained from 14 patients. OSCC cell lines and normal HOK cells were used to analyze migration and invasion assay. OSCC-induced miR-146a knockout mice (B6.Cg-Mir146tm1.1Bal) model was developed. Transwell cell migration/invasion and scratch wound assays were used to investigate the OSCC cell migration and invasion *in vitro*. Kaplan-Meier survival analysis was used to investigate the association of HTT expression patterns in cancer tissue with patient survival percentage and duration. Pearson's correlation analysis tested the association between miR-146a and HTT expression in OSCC tissues. miR-146a mimic and inhibitor transfection were performed to overexpress and knockdown the miR-146a in OSCC cells, respectively. miR-146a expression was highly upregulated in OSCC tissues and OSCC cell lines. Cancer cell migration/invasion was enhanced in miR-146a overexpressed cells and reduced in mi-R146a knockdowned cells. HTT expression was reduced in OSCC tissues and cell lines compared to NCMT and HOK cells, respectively. HTT expression was downregulated in miR-146a overexpressed OSCC cells and upregulated in miR-146a knockdowned OSCC cells. The expression pattern of miR-146a in OSCC cell lines and tissues was inversely correlated with HTT expression. Prediction of miRNA target analysis showed that HTT possesses the binding sites for miR-146a. HTT overexpression in OSCC tissues was associated with patients' higher survival percentage and duration. HTT knockdown in OSCC cells enhanced miR-146a expression and cell migration/invasion. Inducing OSCC in miR-146a knockout mice increased the HTT expression in tongue tissue and alleviated the cancer aggressiveness and epithelial damage. Overexpressed miR-146a in OSCC

targets the HTT gene and enhances cancer cell migration/invasion unraveling the possible role of HTT in miR146a-mediated OSCC cell migration and invasion.

Keywords: oral squamous cell carcinoma, mir-146a, Huntington gene, migration, invasion, metastasis, tumorigenesis

INTRODUCTION

Oral cavity cancer is the most common head and neck cancer with poor prognosis and a high recurrence rate (1). Oral squamous cell carcinoma (OSCC) accounts for more than 90% of all head and neck cancer and is the sixth most common cancer worldwide (2, 3). The incidence rate of OSCC is increasing rapidly, especially among young and middle-aged individuals resulted from smoking and alcohol abuse. Despite the progress of surgery, radiotherapy, and chemotherapy treatments, the 5-year survival rate of OSCC patients was still less than 50% in the last 30 years (2, 4). OSCC has a high rate of metastasis in the head and neck region due to local invasion and due to lack of early diagnostic markers (5). The pathogenesis of OSCC is a complicated process, and the molecular mechanisms of OSCC tumorigenesis, progression, and metastasis are still unclear. Therefore, the molecular level understanding in OSCC progression and metastasis is necessary to unveil novel diagnostic and therapeutic targets.

MicroRNAs (miRNAs) are an evolutionarily conserved group of small single strand non-coding RNA molecules of 20 to 22 nucleotides that regulates mRNA expression at transcriptional and post-transcription level (6, 7). Emerging pieces of evidence had indicated that the mature miRNAs play critical roles in a broad range of physiologic and pathologic processes, such as development, cell proliferation, differentiation, apoptosis, signal transduction, and development of diseases, including inflammation and cancers (8–13). Literature had reported the involvement of various miRNAs, including miR-146a, miR-145, miR-433, miR-195-5p, and miR-375 in OSCC (14–17). Overexpression or underexpression of miRNAs regulates the OSCC development and progression. The role of miR-146a in various cancer etiology, including blood, breast, cervical, kidney, liver, and lung cancer, had been extensively studied (18). Only pieces of literature are available regarding the role of miR-146a in OSCC, and the results are controversial (17, 19, 20). Hung and colleagues reported the upregulation of miR-146a in OSCC tissues and blood circulation of OSCC patients, and the involvement in OSCC oncogenicity (17). Similarly, Min and colleagues reported a higher expression of miR-146a in OSCC (19). In contrast, Shi and colleagues reported the loss of miR-146a expression in high-grade oral cancer tumors and re-expression of miR-146a reduced oncogenic phenotypes and metastasis (20). Therefore, further studies are necessary to elucidate the exact expression pattern of miR-146a in OSCC as well as its role and mechanism in OSCC progression.

miR-146a targets specific genes, regulates signaling pathways, and involves in cancer biology (18). miR-146a targets IRAK1 and TRAF6 to promote NF-κB signaling in oral, cervical, breast, and prostate cancer (17, 18, 21). Similarly, miR-146a targets EGFR to promote growth and proliferative signaling of various cancer cells, including breast, liver, lung, prostate, and gastric cancer (18). However, other target genes of miR-146a and their role in OSCC etiology have not been fully understood. HTT gene mutation causes a neurodegenerative Huntington's disease (22). Most of the HTT-related studies are mainly focused on the role of HTT in the nervous system. The expression of the HTT gene and protein is ubiquitous. Some recent studies have reported the role of HTT in cancer development and progression. HTT expression is downregulated in breast cancer and regulates cancer cell differentiation *via* the maintenance of tight junctions (23). HTT gene expression is downregulated in oral cancer tissues and is one of the candidate genes involved in oral cancer biology (24). Moreover, miR-125b, miR-146a, miR-150, and miR-214 target both human and mice HTT and regulate diverse cellular processes (25, 26). However, whether the miR-146a targets the HTT gene in OSCC to regulate tumorigenesis and metastasis is still unknown.

In this study, we hypothesized that miR-146a targets the HTT gene to regulate OSCC cell migration and invasion. We found overexpressed miR-146a and underexpressed HTT in OSCC clinical tissues and cell lines. The overexpressed miR-146a downregulated HTT expression in OSCC cells, suggesting the HTT targeting potential of miR-146a. Overexpressed miR-146a or underexpressed HTT enhanced OSCC cell migration/invasion. Inducing OSCC in miR-146a knockout mice mitigated the cancer aggressiveness and tongue epithelial damage compared to in wild-type mice. For the first time, our study reported the overexpression of miR-146a in OSCC as an inducer of cancer cell migration and invasion possibly *via* targeting the HTT gene.

MATERIALS AND METHODS

OSCC Tissue Collection

A total of 14 patients with OSCC were included in this study. The independent diagnosis of each case was confirmed by both pathologists and physicians following the standard criteria (27). Surgical resection of primary tumors along with paired non-cancerous matched tissues (NCMT) from OSCC patients was collected with the written informed consent from the patients. NCMT sample was obtained from 2 cm distance of the tumor tissue. Tissue specimens were stained with H&E staining to distinguish cancerous tissue from NCMT. This study was approved by the Ethical Institutional Review Board of Affiliated Stomatology Hospital of Guangzhou Medical University (ethical approval number: KY2017018). All the procedures were per institutional ethical standards. All samples were obtained during tumor removal surgery and were frozen

immediately in liquid nitrogen and stored at −80°C until the detection of miR-146a and HTT. The tumors underwent TNM classification, according to the American Joint Committee on Cancer (AJCC) system (27). The patient's characteristics and demographics are presented in **Table 1**.

In Vitro Cell Culture Study

SCC9, SCC25, and CAL27 human oral squamous carcinoma cell lines were used in this study. SCC25 (CRL-1628) was purchased from ATCC. HOK cell line was obtained from ScienCell (Chemie Brunschwig, Basel, CH). SCC9 and CAL27 were obtained from the Key Laboratory of Oral Medicine, Affiliated Stomatology Hospital of Guangzhou Medical University. SCC25 cells were cultured in DMEM/F12 supplemented with 400 ng/ml hydrocortisone and 10% fetal bovine serum. SCC9 and CAL27 cells were cultured in DMEM/F12 supplemented with 10% FBS and 1% Penicillin-Streptomycin (Gibco, 15140122). All cells were incubated in an atmosphere of 5% CO_2 and saturated moisture at 37°C.

Cell Transfections

miR-146a mimic (cat. #4464066), miR-146a mimic negative control (designated miR-146a mimic NC, cat. #4464058), miR-146a inhibitor (cat. #4464084), and miR-146a inhibitor negative control (designated miR-146a inhibitor NC, cat. #4464076) were obtained from Thermo Fisher (life technology, Carlsbad, CA). Transfection was performed using GenMute @ (SignaGen) according to the manufacturer's protocol. Briefly, cells were seeded in 6-well plates at 30%–40% confluence for 24 h, transfected with miR-146a mimic, miR-146a mimic negative control, miR-146a inhibitor, and miR-146a inhibitor negative control at a final 50 nM concentration for 48 h.

TABLE 1 | Clinical parameters of OSCC patients.

Demographics	Patient number (n = 14)
Gender	
Male	7
Female	7
Age	
<50	6
>50	8
Lymph node metastasis	
Negative	3
Positive	11
TNM stage	
II	3
III	11

Knockdown of HTT Gene in OSCC Cells

HTT gene in OSCC cells was knock downed using si-RNA. HTT knockdown efficiency of three different si-RNAs (si-HTT1, si-HTT2, si-HTT3) in SCC9 and CAL27 cells was tested. Since, si-HTT1 (targeted sequence: GCACCTTCCTCCTGAGAAA, Guangzhou RIBOBIO) showed the highest inhibition of HTT expression, we used the si-HTT1 to downregulate the HTT in OSCC cells. HTT knockdown efficiency, miR-146 expression pattern, and OSCC cell migration and invasion were further analyzed.

The cells in the logarithmic growth phase were seeded in a 6-well plate. When the cell fusion degree was 80%, siRNA transfection was performed. The specific steps were performed according to the method provided in the instructions of the siRNA transfection kit. After the cells were transfected for 48 h. The morphological changes of cells were observed under an inverted light microscope, and total RNA was extracted, and the silencing effect was detected by quantitative real-time PCR (qRT-PCR).

Quantitative Real-Time PCR Assay

Total RNA was extracted from cultured cells, OSCC clinical tissues, and mice tongue tissues using TRIzol Reagent (Invitrogen, CA, USA). The miRNA was extracted from cultured cells using miRNAiso for small RNA reagent (TaKaRa, Dalian, China). The RNA samples were then reverse-transcribed into cDNA with the PrimeScript RT Master Mix (TaKaRa, Dalian, China) and the SYBR PrimeScript miRNA RT-PCR Kit (TaKaRa, Dalian, China). Real-time PCR was performed with the SYBR Premix Ex Taq II and the SYBR PrimeScript miRNA RT-PCR Kit (TaKaRa, Dalian, China), using an Applied Biosystems 7500 Sequence Detection System (Applied Biosystems, Foster City, CA, USA). The expression of HTT mRNA was quantified with GAPDH mRNA expression as an endogenous control. The levels of miR-146a were quantified with U6 control. Quantification of the relative levels was determined by the $^{\Delta\Delta}$Ct method (28). Primers used for qPCR are listed in **Table 2**.

Cell Invasion Assay

Cell invasion assay was performed using Transwell chambers (8.0 μm pore size; Corning, US). The chambers were prepared by thawing Matrigel (BD Bioscience, San Jose, CA) at 4°C, and then 100 μl of the thawed Matrigel was added to each insert. After incubating at room temperature for 1 h, the unsolidified liquid was gently removed by pipette. Transfected cells were starved overnight and then seeded in the upper chamber at a density of

TABLE 2 | Primers used in this study.

Gene	Forward Primer	Reverse Primer
GAPDH	GGAGCGAGATCCCTCCAAAAT	GGCTGTTGTCATACTTCTCATGG
Gapdh (M)	AGGTCGGTGTGAACGGATTTG	GGGGTCGTTGATGGCAACA
U6	GGAACGATACAGAGATTAGC	TGGAACGCTTCACGAATTTGCG
HTT (H)	GGGTGGGAAGAAGTCGTCTAG	GCTATGGAGCGGGTATCTGTT
miR-146a	UGAGAACUGAAUUCCAUGGGUU	ACACTCCAGCTGGGTGGTGCGGAGAGGGCCC
Htt (M)	CTGATGAAGGCTTTCGAGTCG	TGATTCACACGGTCTTTCTTGG

2.5×10^6 cells/ml in 200 µl of medium with no FBS. A medium with 10% FBS (600 µl) was added to the lower chamber. Following a 24 h-incubation at 37°C with 5% CO_2, non-invading cells in the upper chamber were removed with a cotton swab, and invading cells were fixed in 4% paraformaldehyde and stained with 0.5% crystal violet. Photographs were taken randomly from five fields of each membrane. The number of invading cells was expressed as the average number of cells per microscopic field over five fields.

Cell Migration Assay

For migration assays, a protocol similar to the invasion experiment. However, the upper chamber was not pre-coated with Matrigel, and cells in the upper chamber were seeded at a density of 1.0×10^6 cells/ml.

Scratch Wound Assay

The cell migration was measured by scratch wound assay. Transfected OSCC cells were cultured in 6-well plates to 100% confluence as monolayers and then scratched with a 200-µl sterile pipette tip (29). The medium and cell debris were aspirated away by PBS and replaced with 2 ml of fresh serum-free medium. The area between wound gaps was measured at different time points under an inverted phase-contrast microscope (Olympus, Germany) and then calculated by ImageJ software. Five randomly selected fields along each wound were marked, and each experiment was conducted in triplicate.

Mouse Model for Oral Cancer

Male C57BL/6 mice (wild-type) 6–7 weeks old, weighing 250–350 g, were obtained from Medical Laboratory Animal Center of Guangdong Province. miR-146a knockout mice (B6.Cg-Mir146$^{tm1.1Bal}$) were obtained from the Jackson Laboratory. All mice were housed at the Specific Pathogen Free (SPF) animal facility at Guangzhou Medical University according to animal protocol and regulation of the University Laboratory Animal Resources. All animal experiments were approved by Guangzhou Medical University Institutional Animal Care and Institutional Biosafety Committee (ethical approval number: 2020-002). Animal experiments were performed following the ARRIVE guidelines. OSCC was induced in wild-type (9 mice) and miR-146a (9 mice). The OSCC in mice was induced following the protocol established by our lab (30), as illustrated in **Supplementary Figure 1**. In brief, the mice were treated with freshly prepared 4-NQO (Cat# N8141; Sigma, St Louis, MO) for 10 weeks and then treated with normal drinking water for 10 weeks. 4-NQO (Sigma Chemical) was dissolved in propylene glycol (final concentration 5 mg/ml) and then added to the drinking water at 60 µg/ml, keeping at −20°C. Drinking water containing NQO was freshly prepared every week in deionized water and was stored in the dark at 4°C until used. Bottles containing 4-NQO-supplemented water were wrapped with foil to preclude photodegradation of the carcinogen and were changed at two- to three-day intervals throughout the study. The drinking water was changed every day, and mice were allowed access to the drinking water at all times while receiving treatment. The mice were anesthetized (xylazine, intraperitoneal injection, 0.13 mg/kg body weight) and euthanized by exsanguination prior to tissue collection. Mice were euthanized at 0, 16, and 20 weeks after treatment, respectively. The tongue tissues were collected and stored at −80°C for the histology and qPCR.

Hematoxylin and Eosin Staining

The tongue tissues were fixed in 4% paraformaldehyde for 16 hours, then dehydrated and embedded in paraffin. Sections (3 µm thick) were stained with hematoxylin and eosin (H&E). The sections of the tongue epithelium were photographed with an inverted optical microscope.

Immunochemistry

Immunohistochemistry was performed to observe the expression of HTT. The anti-HTT antibody (ab109115, Abcam) was incubated overnight at 4°C, followed by incubation with biotinylated anti-rabbit secondary antibodies for one hour and counterstained with hematoxylin to detect HTT expression on human OSCC tissue sections. The number of HTT-positive cells and nucleated cells in five random fields of view on each human OSCC tissue and NCMT tissue section were counted Using ImageJ software. Their ratio (HTT-positive cells/nucleated cells) was used for statistical analysis. **Table 1** summarizes the clinicopathological characteristics of patients with OSCC.

Kaplan-Meier Survival Analysis and Pearson's Correlation Analysis

Kaplan-Meier survival curve for 397 OSCC/HNSCC patients with high expression of HTT and 99 patients with low HTT expression was plotted to evaluate the survival percentage and duration as described previously (31). Primary data (survival duration and HTT expression) of the patients were taken from the Kaplan Meier plotter (http://www.oncolnc.org/). Pearson's correlation analysis was performed using GraphPad Prism 7.04 software to investigate the correlation between miR-146a and HTT expression in OSCC tissues.

Statistical Analysis

All statistical analyses were performed using GraphPad Prism 7.04 software and the SPSS 20.0 statistical package (SPSS, Inc., Chicago, IL, USA). Data were presented as the mean ± SD. A nonparametric unpaired Mann-Whitney test was used to compare the mean of two independent groups. Differences were examined using a one way ANOVA followed by Tukey-Kramer post-hoc test and independent samples t-test. Chi-Square was used to test differences between two or more group samples. $P < 0.05$ was considered statistically significant.

RESULTS

miR-146a Is Highly Expressed in OSCC

To explore the role of miR-146a in OSCC, we analyzed the expression of miR-146a in OSCC tissues and NCMT from 14 patients. Patient characteristics, demographics, and clinical data

are provided in **Table 1**. miR-146a was highly expressed in OSCC tissue compared to NCMT (**Figure 1A**). We also analyzed the miR-146a expression in OSCC cell lines and HOK cells. miR-146a expression was highly upregulated in all the OSCC cell lines tested (SCC9, SCC25, and CAL27) compared to HOK cells (**Figure 1B**). SCC9 showed the highest expression of miR-146 (135-fold higher) compared to HOK cells. The results of miR-146a expression from clinical samples directly correlated with the results from OSCC cell lines.

Overexpression of miR-146a Promotes OSCC Cell Migration and Invasion

miR-146a was transfected in OSCC cells to analyze the effect of miR146a on OSCC cell migration and invasion. Transfection of miR-146a successfully upregulated the expression of miR-146a in SCC9, SCC25, and CAL27 cells (**Figure 2A**). In vitro cell migration and invasion assay, showed a higher number of migrated and invaded cells in miR-146a transfected SCC9, SCC25, and CAL27 cells (**Figures 2B, C**). Quantitative analysis data showed that overexpression of miR-146a enhanced the cell migration and invasion by ~1.5-fold in SCC9, SCC25, and CAL27 cells (**Figures 2D, E**). This result indicates that the overexpressed miR-146a in OSCC cells promotes cancer cell migration and invasion.

Knockdown of miR-146a in OSCC Inhibits OSCC Cell Migration

We knockdowned miR-146a in OSCC cells to further confirm the role of miR-146a in OSCC migration and invasion. The transfection of miR-146a inhibitor dramatically reduced the expression of miR-146a expression in SCC9, SCC25, and CAL27 cells (**Figure 3A**). The scratch wound assay revealed that miR-146a knockdown reduces the migration of SCC9, SCC25, and CAL27 cells, as indicated by the higher wound area in the miR-146a inhibitor group (**Figures 3B–D**). The quantitative analysis of wound closure showed a higher wound area percentage in miR-146a inhibitor transfected SCC9, SCC25, and CAL27 cells (**Figures 3E–G**). Moreover, the knockdown of miR-146a inhibited the OSCC cell invasion (**Supplementary Figure 2**). Our results indicate that miR-146a overexpression and knockdown in OSCC have a stimulatory and inhibitory effect on cancer cell migration/invasion, respectively (**Figures 2** and **3**).

HTT Expression Is Downregulated in OSCC

Since miR-146a targets the HTT gene, we evaluated the expression pattern of the HTT gene in OSCC tissue and the role of the level of HTT expression on survival percentage and duration in oral cancer patients. We plotted the Kaplan-Meier survival curve from 397 OSCC/HNSCC patients with high HTT expression and 99 OSCC/HNSCC patients with low HTT expression. Cancer patients with higher HTT expression showed a better survival percentage with longer survival duration compared to the OSCC patients with HTT expression (**Figure 4A**). We also analyzed the HTT gene expression in OSCC tissues and NCMT of 14 patients as well as in OSCC cell lines. HTT expression was significantly downregulated in OSCC tissues compared to NCMT (**Figure 4B**). Similarly, the lower expression of the HTT gene was observed in OSCC cells (SCC9, SCC24, and CAL27) compared to HOK cells (**Figure 4C**). The immunohistochemistry study showed a lower expression of HTT protein in OSCC tissues compared to NCMT (**Figures 4D, E**). This result indicated that the downregulation of HTT in OSCC correlates with lower survival percentage and duration.

miR-146a Expression Inversely Correlates With HTT Expression in OSCC

Prediction of miRNA targets using TargetScanHuman online tool (http://www.targetscan.org/vert_72/) showed the binding site of miR146a in HTT gene (**Figure 5A**). We performed Pearson's correlation analysis to investigate the correlation between miR-146a and HTT expression in OSCC. As expected, the miR-146a expression in OSCC tissues was inversely correlated ($r = -0.7022$, $P = 0.01$) with the HTT expression (**Figure 5B**). The miR-146a transfected OSCC cells showed a lower expression of the HTT gene (**Figure 5C**). The knockdown of miR-146a in OSCC cells robustly enhanced the HTT gene expression (**Figure 5D**).

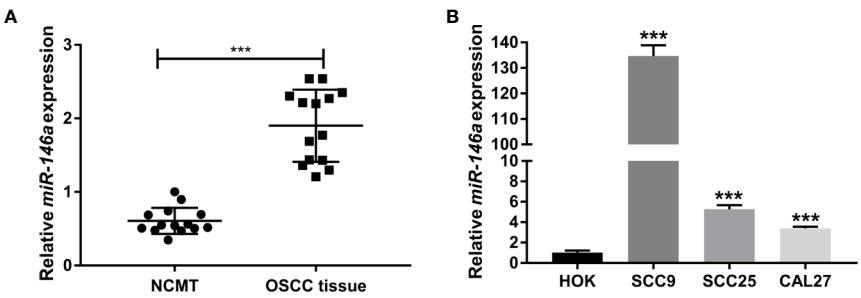

FIGURE 1 | MiR-146a expression was upregulated in OSCC tissues and OSCC cell lines. **(A)** MiR-146a expression pattern in OSCC tissues and non-cancerous matched tissues (n = 14). **(B)** MiR-146a expression pattern in HOK cells and OSCC cell lines (n = 3). Data are presented as mean ± SD. The significant difference, ***P < 0.001 [in **(B)** compared to HOK-group]. NCMT, non-cancerous matched tissue; OSCC, oral squamous cell carcinoma.

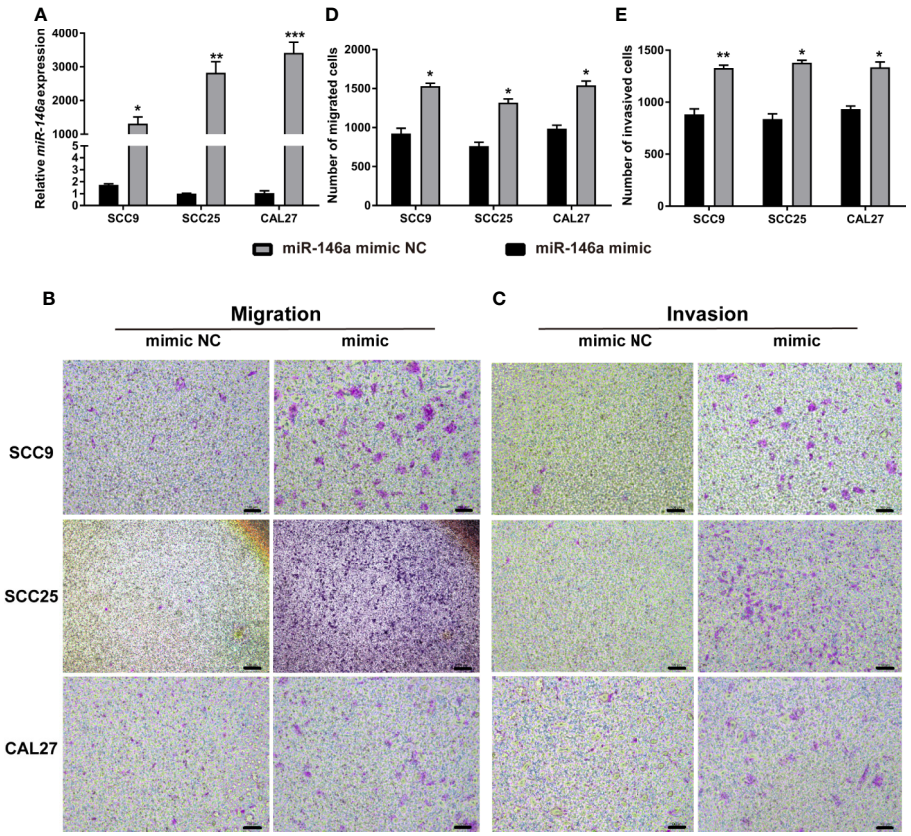

FIGURE 2 | Transfection of miR-146a in OSCC cells enhanced cell migration and invasion. **(A)** miR-146a expression pattern in OSCC cells transfected with miR-146a negative mimic control or miR-146a mimic. Representative microscopic images of **(B)** OSCC cell migration, and **(C)** OSCC cell invasion assays. Purple dots and patches indicate the migrated and invaded cells. Quantitative analysis of **(D)** migrated, and **(E)** invaded cells from figure B and C. Data are presented as mean ± SD form three independent experiments in triplicate. Significant effect of miR-146a transfection, *P < 0.05, **P < 0.01, and ***P < 0.001. NC, negative control. Scale bar, 100 μm.

Knockdown of HTT Enhances OSCC Cell Migration and Invasion

To analyze the role of HTT in OSCC cell migration and invasion, we knockdowned the HTT gene by using HTT specific si-RNA (**Figure 6A**). Interestingly, knockdown of HTT upregulated the miR-146a expression in OSCC cells (**Figure 6B**). This result further confirms the inverse correlation between miR-146a and HTT expression in OSCC cells, as observed in **Figure 5**.

Cell migration and invasion assay showed a higher number of migrated and invaded OSCC cells in HTT knockdown groups (**Figures 6C, D**). The quantitative analysis showed ≥ 1.5-fold higher number of migrated and invaded cells in HTT knockdowned OSCC cells (**Figures 6E, F**). This result indicates the inhibitory effect of HTT on OSCC cell migration and invasion.

Knockout of miR-146a Inhibits the OSCC Progression in Mice

We tested the role of miR-146a in OSCC progression in miR-146a knockout mice with OSCC. Inducing OSCC in wild-type mice showed the tongue epithelial damage at week 10. The higher degree of carcinoma aggressiveness and epithelium damage was observed at week 16 and 20 in wild-type mice (**Figure 7A**). In miR-146a knockout mice, OSCC progression was relatively slow, and the epithelial damage was mitigated compared to in wild-type mice at week 16 and 20, respectively (**Figure 7A**). Tongue epithelial damage was increased in OSCC wild-type mice at week 16 and 20. Interestingly, OSCC-induced epithelial damage was alleviated in miR-146a knockout mice (**Figure 7B**). We also analyzed the HTT mRNA expression in the tongue tissue of OSCC mice at week 20 (**Figure 7C**). HTT mRNA expression was highly upregulated in the OSCC tongue tissue of miR-146a knockout mice compared to wild-type mice. This result indicates the protective role of the HTT gene against OSCC by reducing the cancer aggressiveness and tongue epithelial damage.

DISCUSSION

Evidence from literature demonstrated that the over or under expression of miR-146a in specific cancer acts as either a cancer

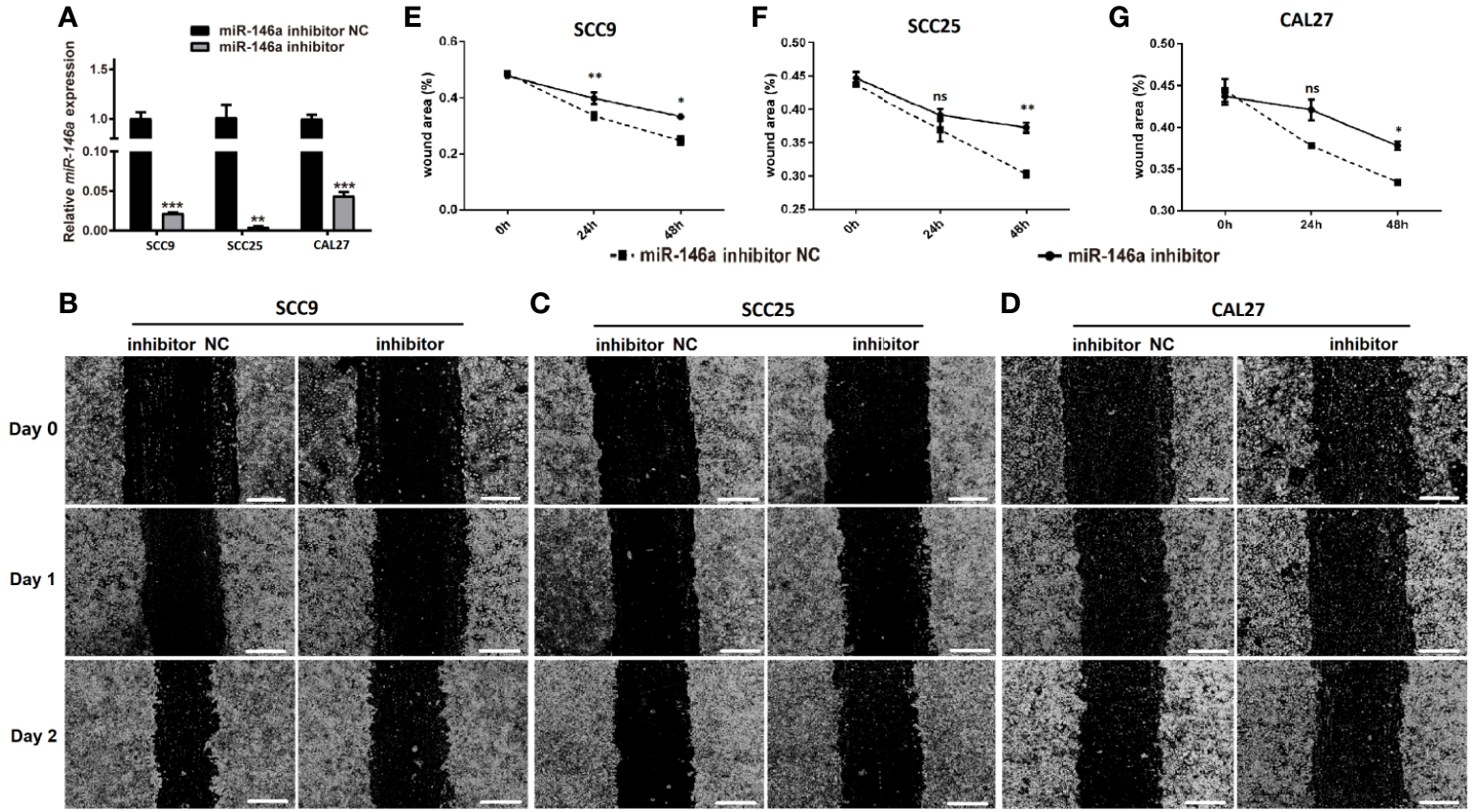

FIGURE 3 | The knockdown of miR-146a inhibited the OSCC cell migration in scratch wound assay. **(A)** Relative expression of miR-146a in OSCC cells transfected with miR-146a inhibitor or miR-146a negative control. Representative microscopic images scratch wound assay in **(B)** SCC9, **(C)** SCC25, and **(D)** CAL27 cells. In the scratch wound assay, quantitative analysis was performed on migrating cells at 0, 24, and 48, **(E)** SCC9, **(F)** SCC25, and **(G)** CAL27 cells. Data are presented as mean ± SD form three independent experiments in triplicate. Significant effect of the miR-146a inhibitor treatment, *P < 0.05, **P < 0.01, and ***P < 0.001. NC, negative control. Scale bar, 100 μm.

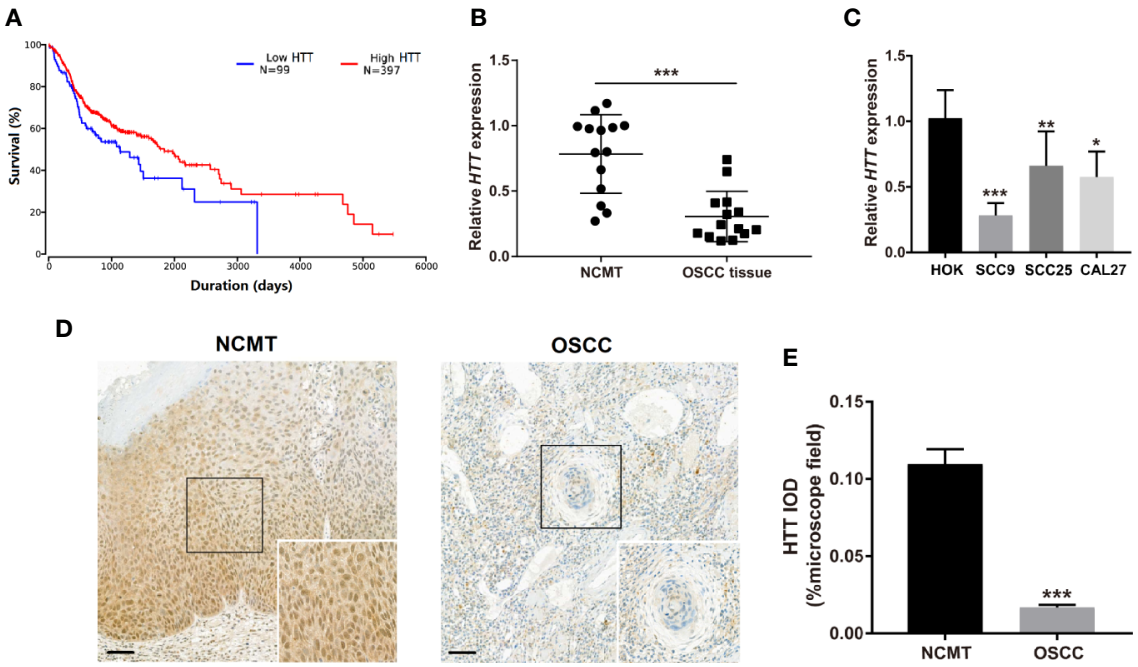

FIGURE 4 | HTT expression pattern in OSCC correlated with survival rate and duration. **(A)** Kaplan-Meier survival curves for 397 OSCC patients with high HTT expression and 99 OSCC patients with low HTT expression. **(B)** HTT mRNA expression pattern in OSCC tissue and non-cancerous matched tissue (n = 14). **(C)** HTT mRNA expression pattern in HOK cells and OSCC cell lines (n = 3). **(D)** Representative images of immunohistochemistry sections showing HTT protein expression in OSCC tissue and non-cancerous matched tissue. **(E)** Quantitative analysis of HTT protein expression in immunohistochemistry sections (n = 14). Data are presented as mean ± SD. Significant difference, *P < 0.05, **P < 0.01, and ***P < 0.001. Scale bar, 100 μm.

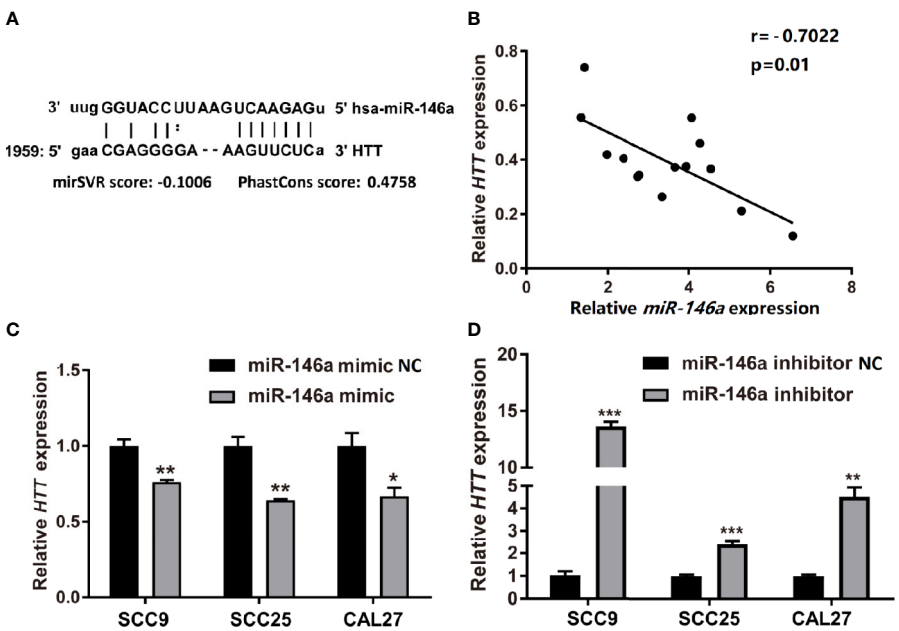

FIGURE 5 | HTT expression was inversely related to miR-146a expression in OSCC tissues. **(A)** The binding site of miR-146a in the HTT gene. **(B)** Pearson analysis showing the correlation between miR-146a and HTT mRNA expression level in OSCC tissues (n = 14; r = –0.7022, P < 0.01). HTT expression pattern in **(C)** miR-146a transfected, and **(D)** miR-146a knockdowned OSCC cells. Data are presented as mean ± SD form three independent experiments in triplicate. Significant effect of treatment, *P < 0.05, **P < 0.01, and ***P < 0.001. NC, negative control. Scale bar, 100 μm.

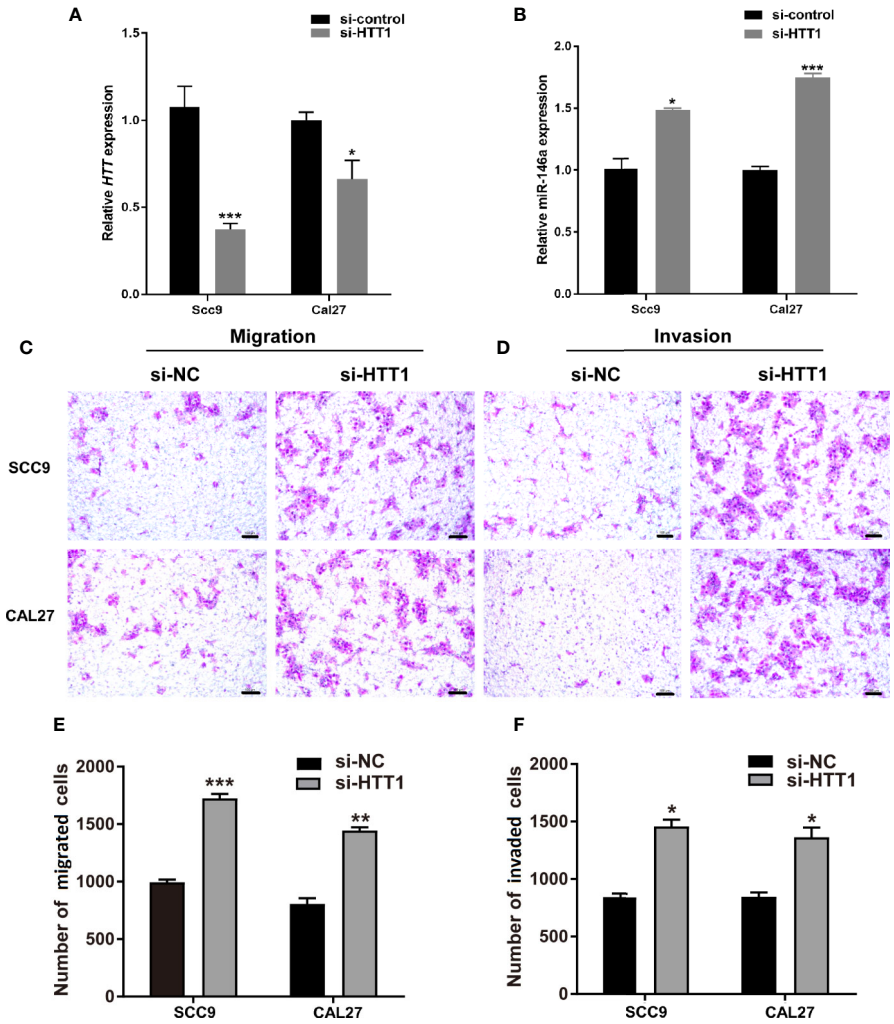

FIGURE 6 | HTT inhibits the migration and invasion of OSCC cell lines. **(A)** HTT expression pattern in OSCC cell lines transfected with HTT si-RNA. **(B)** miR-146a expression pattern in OSCC cells transfected with HTT si-RNA. Representative microscopic images of **(C)** OSCC cell migration, and **(D)** OSCC cell invasion assays. Quantitative analysis of **(E)** migrated, and **(F)** invaded cells (**F**). Data are presented as mean ± SD form three independent experiments in triplicate. Significant effect of treatment compared to a si-NC group, *P < 0.05, **P < 0.01, and ***P < 0.001. NC, negative control.

suppressor or inducer by targeting specific genes (18). However, the expression pattern and function of miR-146a in OSCC is still a controversy (17, 19, 20). This study investigated: (a) the expression pattern of miR-146a in OSCC tissues and cells, (b) unravel the possible target gene of miR-146a, and (c) the role of miR-146a in OSCC development and metastasis. miR-146a was overexpressed, and its possible target HTT gene and protein was underexpressed in OSCC tissues and cell lines. The expression of miR-146a and the HTT gene in OSCC was inversely correlated. The higher expression of HTT in cancer tissues correlated with higher survival percentage and duration. Overexpressed miR-146a enhanced OSCC cell migration and invasion possibly by targeting the HTT gene. Inducing OSCC in miR-146a knockout mice enhanced HTT expression in tongue OSCC tissue and alleviated cancer aggressiveness and tongue epithelial damage. **Figure 8** illustrated the main findings of this study. Our results showed that the overexpressed miR-146a in OSCC possibly targets the HTT gene to induce cancer cell migration and invasion, suggesting the role of miR-146a and HTT in OSCC progression, metastasis, and invasion.

Overexpression of miR-146a had been reported in various cancers, including breast (8, 32), gastric (33), cervical (21), and bladder cancer (34). The expression pattern of miR-146a in OSCC is still a controversy as two studies reported overexpression (17, 19), and one study reported underexpression (20). In this study, OSCC tissues from 14 patients and OSCC cell lines SCC9, SCC25, and CAL19 showed a higher expression of miR-146a. Overexpressed miR-146a in various cancers such as breast (8), bladder (34), gastric (35), and prostate cancer (36) had been reported to regulate cancer cell migration, invasion, and metastasis. Similar to other types of tumors, the metastasis of OSCC mostly involves local invasion restricted to the head and neck region that frequently remain

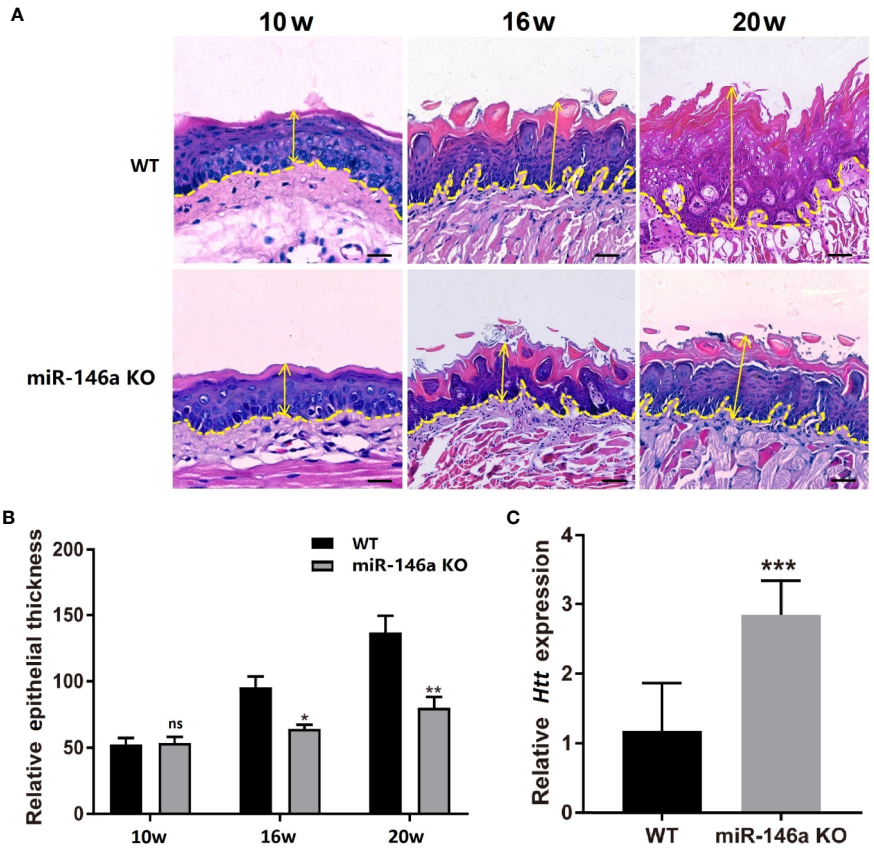

FIGURE 7 | Knocking out of miR-146a in mice mitigates OSCC progression and tongue epithelial layer damage. **(A)** Representative images of histological section (H&E staining) of tongue tissue of wild-type and miR-146a knockout mice with OSCC. **(B)** Quantitative analysis of tongue epithelium thickness. **(C)** HTT mRNA expression pattern in wild-type and miR-146 knockout mice. Data are presented as mean ± SD form three independent experiments in triplicate. Significant effect of treatment compared to WT, *P < 0.05, **P < 0.01, and ***P < 0.001. KO, knockout; WT, wild-type; ns, not significant. Scale bar, 100 μm.

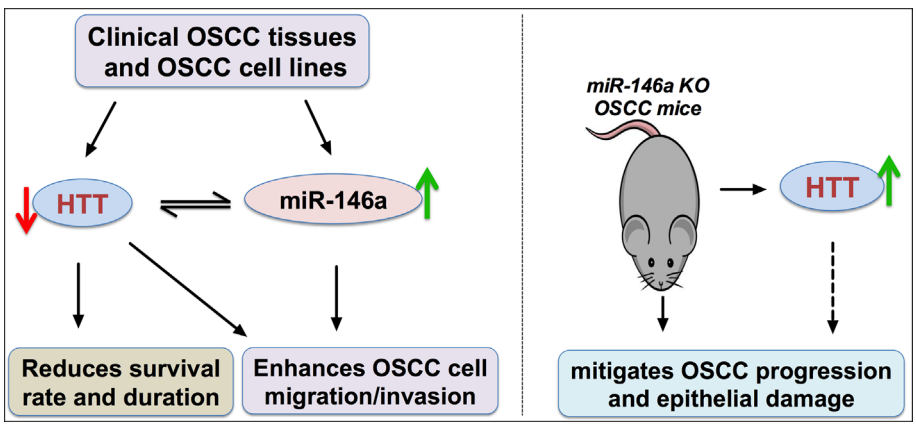

FIGURE 8 | Scheme of miR-146a/HTT axis-mediated possible mechanism of OSCC cell migration and invasion. Red arrow, downregulation; green arrow, upregulation.

undetected until the advanced stage. Irani S had summarized the distant metastasis of OSCC, including heart, lung, bone, and brain (37). Therefore, it is crucial to unravel the role of miR-146a on OSCC metastasis and its mechanism. We overexpressed and knockdowned the miR-146a in OSCC cell lines to investigate the role of miR-146a in OSCC migration and invasion. miR-146a overexpression promoted and knockdown inhibited the OSCC cell migration and invasion *in vitro* (**Figures 2** and **3**). Our data indicated the possible role of overexpressed miR-146a on OSCC metastasis.

Differentially expressed miR-146a targets specific genes, affects gene transcription and translation, and regulates tumor biology (18). TRAF6, IRAK1, and SOX2 had been reported as a target gene of miR-146a in OSCC (17, 19, 20). miR-146a has specificity to target the HTT gene, and HTT plays a vital role in oral and breast cancer biology and many other cellular activities (23–26). This study hypothesized that the miR-146a might target the HTT gene to regulate OSCC progression and metastasis. We extensively analyzed the expression pattern of HTT and its role in OSCC (**Figure 4**). HTT gene and protein expression were downregulated in OSCC tissues with higher pathological grade. A similar result in OSCC expression was observed in SCC9, SCC25, and CAL27 cells (**Figure 5**). Our results suggest HTT as a possible diagnostic or therapeutic target in OSCC. Thion and colleagues had reported the anti-metastatic role of the HTT gene in breast cancer (23, 38). We unraveled the strong association between the lower expression of HTT in OSCC/HNSCC with reduced survival rate/duration and vice versa, indicating a critical role of HTT in OSCC.

Since high throughput sequencing analysis revealed the HTT gene as a putative target of miR-146a, we further analyzed the regulatory role of miR-146a on HTT gene expression in OSCC. The expression patterns of miR-146a and HTT in OSCC tissues were inversely correlated. These findings inmiR-146a overexpression downregulated, and knockdown upregulated the HTT gene/protein expression in OSCC cells. Similarly, knockdown of the HTT gene upregulated miR-146a expression in OSCC cells. Our results indicate the HTT targeting potential of miR-146a in OSCC.

Results from literature and our current study showed that the lower expression of HTT in oral and breast cancer is related to cancer metastasis and lower patient survival (23, 24, 38). In this study, we found that knockdown of the HTT gene in OSCC cells robustly enhanced the cancer cell migration and invasion *in vitro*. HTT gene expression was upregulated in the OSCC tongue tissue of miR-146a knockout mice. Aggressive OSCC in tongue tissue with a disrupted tongue epithelial layer was observed in wild-type mice. In contrast, the reduced aggressiveness of OSCC in tongue tissue and intact tongue epithelial layer was observed in miR-14a knockout mice. Our results indicate the role of overexpressed miR-146a on OSCC aggressiveness *via* targeting the HTT gene.

In this study, we evaluated the expression pattern of miR-146a and HTT gene/protein, as well as HTT targeting potential of miR-146a in well-characterized OSCC clinical samples, mouse model, and cell lines. We also investigated the role of miR-146a in OSCC cell migration, invasion, and cancer aggressiveness. Use of OSCC mice model in miR-146a knockout mice to investigate the role of miR-146a in OSCC and HTT expression in another novelty of this study. This is the first study to illustrate the expression pattern of HTT in OSCC tissues and cell lines, as well as the role of miR-146a in OSCC development and HTT expression in knockout mice model. Using only 14 OSCC patients is a limitation of this study. Another limitation of this study is that we did not investigate the molecular mechanism of miR-146a/HTT-mediated OSCC cell migration/invasion and metastasis. Therefore, future research recruiting more OSCC patients and unraveling the molecular mechanism of miR-146a/HTT-mediated signaling pathways in OSCC metastasis are strongly recommended. Knockdown of HTT in OSCC cells enhanced the cancer cells migration and invasion, and miR-146a knockout OSCC mice showed higher expression of HTT and inhibited the cancer aggressiveness and epithelial damage (**Figures 7A–C**). Based on these results we predict that miR-146a overexpression in oral squamous cell carcinoma potentiates cancer cell migration and invasion possibly *via* targeting HTT. However, the future *in vitro* and *in vivo* studies, overexpressing HTT in miR-146a overexpressed OSCC cells or mice model, as well as inhibiting HTT in miR-146a knockdowned OSCC cells or miR-146a knockout OSCC mice model, are indispensable to further confirm the findings of this study.

CONCLUSION

miR-146a was overexpressed in OSCC tissues and cell lines. miR-146a overexpression and knockdown in OSCC cell lines enhanced and inhibited cell migration/invasion, respectively. HTT was underexpressed in OSCC, and the expression pattern was inversely correlated with the miR-146a. The knockdown of HTT in OSCC cells enhanced cell migration/invasion. Higher HTT expression in cancer tissues was associated with longer survival percentage and duration. miR-146a knockout OSCC mice model not only showed higher expression of HTT in tongue tissue but also mitigates the OSCC progression and tongue epithelial layer damage. Our results suggest the involvement of the miR-146a/HTT axis on OSCC cell migration and invasion.

DATA AVAILABILITY STATEMENT

The original contributions presented in the study are included in the article/**Supplementary Material**. Further inquiries can be directed to the corresponding authors.

ETHICS STATEMENT

The studies involving human participants were reviewed and approved by Ethical Institutional Review Board of Affiliated Stomatology Hospital of Guangzhou Medical University. The patients/participants provided their written informed consent to

participate in this study. The animal study was reviewed and approved by Guangzhou Medical University Institutional Animal Care and Institutional Biosafety Committee.

AUTHOR CONTRIBUTIONS

LPW, YY, YC, JP, and LG designed the study, interpreted the data, and finalized the manuscript. YC, XG, YF, LJW, and YS contributed to perform experiment, data collection, and interpretation. All authors contributed to the article and approved the submitted version.

FUNDING

This study was supported by the project of Guangzhou Science and Technology Bureau (2020020301), Department of Education of Guangdong Province (2018KTSCX186), Bureau of Technology Industry Business and Information of Liwan District, Guangzhou city (201804015), and The Project of Guangzhou Municipal Health Commission (20181A011103). High-level university construction funding of Guangzhou Medical University (02-412-B205002-1003018). The funding bodies played no role in the design of the study and collection, analysis, and interpretation of data and in writing the manuscript.

SUPPLEMENTARY MATERIAL

The Supplementary Material for this article can be found online at: https://www.frontiersin.org/articles/10.3389/fonc.2020.585976/full#supplementary-material

SUPPLEMENTARY FIGURE 1 | Scheme of OSCC development in miR-146a knockout mice.

SUPPLEMENTARY FIGURE 2 | The knockdown of miR-146a inhibited the OSCC cell invasion in transwell assay. **(A)** Representative microscopic images of OSCC cell invasion. **(B)** Quantitative analysis of invasive cells. Data are presented as mean ± SD form three independent experiments in triplicate. Significant effect of the miR-146a inhibitor treatment, *P < 0.05, NC, negative control. Scale bar: 100 μm.

REFERENCES

1. Warnakulasuriya S. Global epidemiology of oral and oropharyngeal cancer. *Oral Oncol* (2009) 45(4-5):309–16. doi: 10.1016/j.oraloncology.2008.06.002
2. Wang B, Zhang S, Yue K, Wang XD. The recurrence and survival of oral squamous cell carcinoma: a report of 275 cases. *Chin J Cancer* (2013) 32 (11):614–8. doi: 10.5732/cjc.012.10219
3. Cai Z, Liu Q. Understanding the Global Cancer Statistics 2018: implications for cancer control. *Sci China Life Sci* (2019) 62:1–4. doi: 10.1007/s11427-019-9816-1
4. Ho PS, Ko YC, Yang YH, Shieh TY, Tsai CC. The incidence of oropharyngeal cancer in Taiwan: an endemic betel quid chewing area. *J Oral Pathol Med* (2002) 31(4):213–9. doi: 10.1034/j.1600-0714.2002.310404.x
5. Perez-Sayans M, Suarez-Penaranda JM, Padin-Iruegas ME, Gayoso-Diz P, Reis-De Almeida M, Barros-Angueira F, et al. The Loss of p16 Expression Worsens the Prognosis of OSCC. *Appl Immunohistochem Mol Morphol AIMM* (2015) 23(10):724–32. doi: 10.1097/pai.0000000000000133
6. Kim J, Yao F, Xiao Z, Sun Y, Ma L. MicroRNAs and metastasis: small RNAs play big roles. *Cancer Metastasis Rev* (2018) 37(1):5–15. doi: 10.1007/s10555-017-9712-y
7. Catalanotto C, Cogoni C, Zardo G. MicroRNA in Control of Gene Expression: An Overview of Nuclear Functions. *Int J Mol Sci* (2016) 17(10): pii: E1712. doi: 10.3390/ijms17101712
8. Chen J, Jiang Q, Jiang XQ, Li DQ, Jiang XC, Wu XB, et al. miR-146a promoted breast cancer proliferation and invasion by regulating NM23-H1. *J Biochem* (2019) 167(1):41–8. doi: 10.1093/jb/mvz079
9. Chen Y, Yuan B, Chen G, Zhang L, Zhuang Y, Niu H, et al. Circular RNA RSF1 promotes inflammatory and fibrotic phenotypes of irradiated hepatic stellate cell by modulating miR-146a-5p. *J Cell Physiol* (2020) 235(11):8270–82. doi: 10.1002/jcp.29483
10. Zhang W, Xiao J, Lu X, Liu T, Jin X, Xiao Y, et al. PVT1 (rs13281615) and miR-146a (rs2910164) polymorphisms affect the prognosis of colon cancer by regulating COX2 expression and cell apoptosis. *J Cell Physiol* (2019) 234 (10):17538–48. doi: 10.1002/jcp.28377
11. Gharibi S, Moghimi B, Haghmorad D, Mahmoudi MB, Shahvazian E, Yadegari M, et al. Altered expression patterns of complement factor H and miR-146a genes in acute-chronic phases in experimental autoimmune encephalomyelitis mouse. *J Cell Physiol* (2019) 234(11):19842–51. doi: 10.1002/jcp.28583
12. Rupaimoole R, Slack FJ. MicroRNA therapeutics: towards a new era for the management of cancer and other diseases. *Nat Rev Drug Discov* (2017) 16 (3):203–22. doi: 10.1038/nrd.2016.246
13. He X, Zheng Y, Liu S, Shi S, Liu Y, He Y, et al. MiR-146a protects small intestine against ischemia/reperfusion injury by down-regulating TLR4/TRAF6/NF-kappaB pathway. *J Cell Physiol* (2018) 233(3):2476–88. doi: 10.1002/jcp.26124
14. Wang T, Ren Y, Liu R, Ma J, Shi Y, Zhang L, et al. miR-195-5p Suppresses the Proliferation, Migration, and Invasion of Oral Squamous Cell Carcinoma by Targeting TRIM14. *BioMed Res Int* (2017) 2017:7378148. doi: 10.1155/2017/7378148
15. Wang K, Jin J, Ma T, Zhai H. MiR-376c-3p regulates the proliferation, invasion, migration, cell cycle and apoptosis of human oral squamous cancer cells by suppressing HOXB7. *Biomed Pharmacother = Biomed Pharmacother* (2017) 91:517–25. doi: 10.1016/j.biopha.2017.04.050
16. Wang XC, Ma Y, Meng PS, Han JL, Yu HY, Bi LJ. miR-433 inhibits oral squamous cell carcinoma (OSCC) cell growth and metastasis by targeting HDAC6. *Oral Oncol* (2015) 51(7):674–82. doi: 10.1016/j.oraloncology.2015.04.010
17. Hung PS, Liu CJ, Chou CS, Kao SY, Yang CC, Chang KW, et al. miR-146a enhances the oncogenicity of oral carcinoma by concomitant targeting of the IRAK1, TRAF6 and NUMB genes. *PLoS One* (2013) 8(11):e79926. doi: 10.1371/journal.pone.0079926
18. Iacona JR, Lutz CS. miR-146a-5p: Expression, regulation, and functions in cancer. *Wiley Interdiscip Rev RNA* (2019) 10(4):e1533. doi: 10.1002/wrna.1533
19. Min SK, Jung SY, Kang HK, Park SA, Lee JH, Kim MJ, et al. Functional diversity of miR-146a-5p and TRAF6 in normal and oral cancer cells. *Int J Oncol* (2017) 51(5):1541–52. doi: 10.3892/ijo.2017.4124
20. Shi Z, Johnson JJ, Jiang R, Liu Y, Stack MS. Decrease of miR-146a is associated with the aggressiveness of human oral squamous cell carcinoma. *Arch Oral Biol* (2015) 60(9):1416–27. doi: 10.1016/j.archoralbio.2015.06.007
21. Hu Q, Song J, Ding B, Cui Y, Liang J, Han S. miR-146a promotes cervical cancer cell viability via targeting IRAK1 and TRAF6. *Oncol Rep* (2018) 39 (6):3015–24. doi: 10.3892/or.2018.6391
22. Wild EJ, Tabrizi SJ. Therapies targeting DNA and RNA in Huntington's disease. *Lancet Neurol* (2017) 16(10):837–47. doi: 10.1016/S1474-4422(17)30280-6
23. Thion MS, McGuire JR, Sousa CM, Fuhrmann L, Fitamant J, Leboucher S, et al. Unraveling the Role of Huntingtin in Breast Cancer Metastasis. *J Natl Cancer Institute* (2015) 107(10):pii: djv208. doi: 10.1093/jnci/djv208

24. Kumar R, Samal SK, Routray S, Dash R, Dixit A. Identification of oral cancer related candidate genes by integrating protein-protein interactions, gene ontology, pathway analysis and immunohistochemistry. *Sci Rep* (2017) 7 (1):2472. doi: 10.1038/s41598-017-02522-5
25. Das S, Bhattacharyya NP. Heat Shock Factor 1-Regulated miRNAs Can Target Huntingtin and Suppress Aggregates of Mutant Huntingtin. *Microrna* (2015) 4(3):185–93. doi: 10.2174/2211536605666151204111323
26. Sinha M, Ghose J, Bhattarcharyya NP. Micro RNA -214,-150,-146a and-125b target Huntingtin gene. *RNA Biol* (2011) 8(6):1005–21. doi: 10.4161/rna.8.6.16035
27. Lydiatt WM, Patel SG, O'Sullivan B, Brandwein MS, Ridge JA, Migliacci JC, et al. Head and Neck cancers-major changes in the American Joint Committee on cancer eighth edition cancer staging manual. *CA: Cancer J Clin* (2017) 67 (2):122–37. doi: 10.3322/caac.21389
28. Park YR, Kim SL, Lee MR, Seo SY, Lee JH, Kim SH, et al. MicroRNA-30a-5p (miR-30a) regulates cell motility and EMT by directly targeting oncogenic TM4SF1 in colorectal cancer. *J Cancer Res Clin Oncol* (2017) 143(10):1915–27. doi: 10.1007/s00432-017-2440-4
29. Sun X, Zhang L. MicroRNA-143 suppresses oral squamous cell carcinoma cell growth, invasion and glucose metabolism through targeting hexokinase 2. *Bioscience Rep* (2017) 37(3):pii: BSR20160404. doi: 10.1042/bsr20160404
30. Wu L, Jiang Y, Zheng Z, Li H, Cai M, Pathak JL, et al. mRNA and piRNA profile in chemical-induced oral squamous cell carcinoma mice model. *Exp Anim* (2020) 69(2):168–77. doi: 10.1538/expanim.19-0042
31. Anaya J. OncoLnc: linking TCGA survival data to mRNAs, miRNAs, and lncRNAs. *Peer J Comput Sci* (2016) 2:e67. doi: 10.7717/peerj-cs.67
32. Gao W, Hua J, Jia Z, Ding J, Han Z, Dong Y, et al. Expression of miR-146a-5p in breast cancer and its role in proliferation of breast cancer cells. *Oncol Lett* (2018) 15(6):9884–8. doi: 10.3892/ol.2018.8589
33. Adami B, Tabatabaeian H, Ghaedi K, Talebi A, Azadeh M, Dehdashtian E. miR-146a is deregulated in gastric cancer. *J Cancer Res Ther* (2019) 15(1):108–14. doi: 10.4103/jcrt.JCRT_855_17
34. Xiang W, Wu X, Huang C, Wang M, Zhao X, Luo G, et al. PTTG1 regulated by miR-146a-3p promotes bladder cancer migration, invasion, metastasis and growth. *Oncotarget* (2017) 8(1):664–78. doi: 10.18632/oncotarget.13507
35. Yao QY, Cao ZW, Tu CT, Zhao Y, Liu HC, Zhang SC. MicroRNA-146a acts as a metastasis suppressor in gastric cancer by targeting WASF2. *Cancer Lett* (2013) 335(1):219–24. doi: 10.1016/j.canlet.2013.02.031
36. Hou Z, Yin H, Chen C, Dai X, Li X, Liu B, et al. microRNA-146a targets the L1 cell adhesion molecule and suppresses the metastatic potential of gastric cancer. *Mol Med Rep* (2012) 6(3):501–6. doi: 10.3892/mmr.2012.946
37. Irani S. Distant metastasis from oral cancer: A review and molecular biologic aspects. *J Int Soc Prev Community Dent* (2016) 6(4):265–71. doi: 10.4103/2231-0762.186805
38. Thion MS, Humbert S. Cancer: From Wild-Type to Mutant Huntingtin. *J Huntingtons Dis* (2018) 7(3):201–8. doi: 10.3233/JHD-180290.9889077

Conflict of Interest: The authors declare that the research was conducted in the absence of any commercial or financial relationships that could be construed as a potential conflict of interest.

Copyright © 2020 Wang, Chen, Yan, Guo, Fang, Su, Wang, Pathak and Ge. This is an open-access article distributed under the terms of the Creative Commons Attribution License (CC BY). The use, distribution or reproduction in other forums is permitted, provided the original author(s) and the copyright owner(s) are credited and that the original publication in this journal is cited, in accordance with accepted academic practice. No use, distribution or reproduction is permitted which does not comply with these terms.

frontiers in Oncology

ORIGINAL RESEARCH
published: 23 November 2020
doi: 10.3389/fonc.2020.601055

Long Noncoding RNA AFAP1-AS1 Is a Critical Regulator of Nasopharyngeal Carcinoma Tumorigenicity

Min Fang[1†], Minjun Zhang[1,2†], Yiqing Wang[3], Fangqiang Wei[4], Jianhui Wu[5], Xiaozhou Mou[6,7], Yigan Zhang[8], Xiaodong Liang[1,2*] and Jianming Tang[1*]*

[1] Department of Radiation Oncology, Zhejiang Provincial People's Hospital, People's Hospital of Hangzhou Medical College, Hangzhou, China, [2] Graduate Department, Bengbu Medical College, Bengbu, China, [3] The Reproductive Medicine Special Hospital of the First Hospital of Lanzhou University, Key Laboratory for Reproductive Medicine and Embryo, Lanzhou, China, [4] Department of Hepatobiliary and Pancreatic Surgery, Zhejiang Provincial People's Hospital, People's Hospital of Hangzhou Medical College, Hangzhou, China, [5] Department of the Otolaryngology, Zhongshan City People's Hospital, Zhongshan Affiliated Hospital of Sun Yan-sen University, Zhongshan, China, [6] Key Laboratory of Tumor Molecular Diagnosis and Individualized Medicine of Zhejiang Province, Zhejiang Provincial People's Hospital, People's Hospital of Hangzhou Medical College, Hangzhou, China, [7] Clinical Research Institute, Zhejiang Provincial People's Hospital, People's Hospital of Hangzhou Medical College, Hangzhou, China, [8] The First School of Clinical Medicine, Lanzhou University, Lanzhou, China

Background: The long noncoding RNA actin filament associated protein 1 antisense RNA1 (AFAP1-AS1) is a critical player in various cancers. However, the clinical value and functional mechanisms of AFAP1-AS1 during the tumorigenicity of nasopharyngeal carcinoma (NPC) remain unclear. Here, we investigated the clinical application and potential molecular mechanisms of AFAP1-AS1 in NPC tumorigenesis and progression.

Methods: The expression level of AFAP1-AS1 was determined by qRT-PCR in 10 paired fresh human NPC tissues and adjacent normal tissues. RNAscope was performed on 100 paired paraffin-embedded NPC and adjacent nontumor specimens. The biological functions of AFAP1-AS1 were assessed by *in vitro* and *in vivo* functional experiments. RNA-protein pull-down assays were performed to detect and identify the AFAP1-AS1-interacting protein KAT2B. Protein-RNA immunoprecipitation (RIP) assays were conducted to examine the interaction of AFAP1-AS1 and KAT2B. Chromatin immunoprecipitation (ChIP) and luciferase analyses were utilized to identify the binding site of transcription intermediary factor 1 alpha (TIF1α) and H3K14ac on the RBM3 promoter.

Results: AFAP1-AS1 is upregulated in NPC and is a poor prognostic indicator for survival in NPC patients. AFAP1-AS1 was required for NPC proliferation *in vitro* and tumorigenicity *in vivo*. Mechanistic investigations suggested that AFAP1-AS1 binds to KAT2B and promotes acetyltransferase activation at two residues (E570/D610). KAT2B further promotes H3K14 acetylation and protein binding to the bromo domain of TIF1α. Consequently, TIF1α acts as a nuclear transcriptional coactivator of RBM3 transcription, leading to YAP mRNA stabilization and enhanced NPC tumorigenicity.

OPEN ACCESS

Edited by:
Wei Cao,
Shanghai Jiao Tong University, China

Reviewed by:
Xuan Zhou,
Tianjin Medical University Cancer Institute and Hospital, China
Yanjie Zhang,
Shanghai Jiao Tong University, China

***Correspondence:**
Jianming Tang
15900792812@163.com
Xiaodong Liang
lxdctopone@sina.com
Yigan Zhang
zhangyg16@lzu.edu.cn

[†]These authors have contributed equally to this work

Specialty section:
This article was submitted to Head and Neck Cancer, a section of the journal Frontiers in Oncology

Received: *31 August 2020*
Accepted: *19 October 2020*
Published: *23 November 2020*

Citation:
Fang M, Zhang M, Wang Y, Wei F, Wu J, Mou X, Zhang Y, Liang X and Tang J (2020) Long Noncoding RNA AFAP1-AS1 Is a Critical Regulator of Nasopharyngeal Carcinoma Tumorigenicity. Front. Oncol. 10:601055. doi: 10.3389/fonc.2020.601055

Conclusions: Our findings suggest that AFAP1-AS1 functions as an oncogenic biomarker and promotes NPC tumorigenicity through enhanced KAT2B acetyltransferase activation and YAP mRNA stabilization.

Keywords: lncRNA AFAP1-AS1, KAT2B, YAP, nasopharyngeal carcinoma, nasopharyngeal carcinoma tumorigenicity

INTRODUCTION

Nasopharyngeal carcinoma (NPC), a common head and neck malignancy, has a high incidence rate in Southern China (1–3). Although radiotherapy is one of the most effective treatments for NPC patients (4, 5), recurrence and local advancement often lead to treatment failure. Therefore, understanding the potential molecular mechanisms underlying NPC pathogenesis is urgent. The identification of novel therapeutic targets can help in the development of new therapeutic programs that will improve the overall survival rates of patients with NPC. Increasing evidence suggests that long noncoding RNAs (lncRNAs) play important roles in NPC tumorigenicity (6–8). However, the mechanisms through which NPC tumorigenicity is regulated remain poorly understood.

Actin filament associated protein 1 antisense RNA1 (AFAP1-AS1) is an oncogenic lncRNA associated with the pathogenesis of a variety of cancers. AFAP1-AS1 was first mapped to the antisense strand of AFAP1 DNA (9). Studies have shown that AFAP1-AS1 is upregulated in esophageal cancer (9), lung cancer (10), hepatocellular carcinoma (11), pancreatic cancer (12), colorectal cancer (13), and nasopharyngeal carcinoma (14). Recently, it was shown that higher AFAP1-AS1 expression levels are associated with a poor prognosis in NCP patients (15, 16). Recent evidence suggests that AFAP1-AS1 binds to and promotes EZH2 methyltransferase activity in colorectal cancer (13). AFAP1-AS1 has also been linked to regulation of the Rho/Rac pathway *via* competition with endogenous miR-423-5p (14). Interestingly, AFAP1-AS1 has been shown to influence both KRT1 and AFAP1 expression *via* both trans- and cis-regulatory mechanisms (17). Furthermore, AFAP1-AS1 was also shown to be a direct downstream gene target for c-Myc (18). However, the function of AFAP1-AS1 in NPC tumorigenicity remains largely unknown.

In this study, we used RNA-Seq and liquid chromatography–tandem mass spectrometry (LC-MS/MS) assays to evaluate NPC cell lines. Through our study, we identified a new molecular mechanism underlying the role of AFAP1-AS1 in NPC tumorigenicity. We found that AFAP1-AS1 enhances KAT2B acetyltransferase activation, which upregulates H3K14ac activity against TIF1α, resulting in enhanced RBM3 transcription and subsequent stabilization of YAP mRNA, inducing AFAP1-AS1-driven NPC tumorigenicity.

MATERIALS AND METHODS

Clinical Specimens

Ten pairs of freshly frozen NPC tumor and adjacent nontumor specimens were obtained from Zhongshan City People's Hospital. We also collected an additional 100 pairs of formalin-fixed paraffin-embedded NPC tumor and adjacent nontumor specimens from Zhengjiang Provincial People's Hospital. None of the samples were collected from patients undergoing chemo- or radiotherapy at the time of biopsy. Written ethics consent (No:2020QT254) was obtained from the Institutional Ethical Review Board of the Zhengjiang Provincial People's Hospital before the samples were analyzed.

Cell Culture

HNE-1, C666-1, SUNE-1, CNE-1, CNE-2, and NP69 cell lines were all procured from the Cell Bank of the Chinese Scientific Academy (Shanghai, China). NPC cell lines were maintained in Dulbecco's Modified Eagle's Medium (DMEM) supplemented with 10% fetal bovine serum. NP69 was cultured in DMEM/F12 supplemented with epidermal growth factor (20 ng/mL), cholera toxin (100 ng/mL), insulin (10 μg/mL), penicillin–streptomycin (100 μg/mL), hydrocortisone (0.5 μg/mL), and horse serum (5%). All cells were cultured in an incubator with CO_2 (5%) at 37°C. STR DNA fingerprinting was performed by the Shanghai Biowing Applied Biotechnology Co., Ltd. (Shanghai, China) to confirm identity before the start of the study.

Quantitative Reverse Transcriptase PCR Analysis

Quantitative reverse transcriptase PCR (qRT-PCR) was performed as previously described (6). Briefly, total RNA was isolated from NPC cell lines and the collected specimens using TRIzol reagent (Invitrogen), followed by reverse transcription using reverse transcriptase (Promega). Finally, the QuantiTect SYBR Green PCR Kit (Thermo Fisher) was used to perform qRT-PCR. mRNA quantification was normalized to β-actin. All the primers used in this study are listed in **Supplementary Table 1**.

Immunoprecipitation and Western Blotting Assays

Immunoprecipitation (IP) and Western blotting (WB) assays were conducted as previously described (19). The specific antibodies used were as follows: KAT2B (#3378, 1:1000, Cell Signaling Technology), H3K9ac (#9649, 1:1000, Cell Signaling Technology), H3K14ac (#26828, 1:1000, Cell Signaling Technology), H3K9ac (#9649, 1:1000, Cell Signaling Technology), Histone H3 (#4499, 1:1000, Cell Signaling Technology), TIF1α (ab38264, 1:1000, Abcam), TIF1β (#4124, 1:1000, Cell Signaling Technology), TIF1γ (#13387, 1:1000, Cell Signaling Technology), NCOA1 (#20301, 1:1000, Cell Signaling Technology), NCOA2 (#96687, 1:1000, Cell Signaling Technology), NCOA3 (#2126, 1:1000, Cell Signaling Technology), RBM3 (ab211356, 1:1000, Abcam), YAP (#14074, 1:1000, Cell Signaling Technology), Flag M2 antibody (#14793, 1:1000,

Cell Signaling Technology), HA antibody (#2367, 1:1000, Cell Signaling Technology), and β-actin (#4970, 1:1000, Cell Signaling Technology).

Colony Formation and Cell Proliferation Assays

To perform the colony formation assay, cells were seeded into six-well plates with DMEM supplemented with 10% fetal bovine serum and cultured (as described in the "Cell Culture" section) for approximately 10 days. The cell colonies were then fixed, stained, and counted. For the cell proliferation assays, cells were seeded into DMEM containing 10% fetal bovine serum, passaged, and finally detected using a WST-1 assay kit.

RNA Pull-Down and RNA Immunoprecipitation Assays

RNA pull-down and RNA immunoprecipitation (RIP) assays were performed as previously shown (20). The specific antibodies used were as follows: KAT2B (#3378, 1:1000, Cell Signaling Technology) and Flag M2 antibody (#14793, 1:1000, Cell Signaling Technology).

Chromatin Immunoprecipitation-qPCR

We first performed chromatin immunoprecipitation (ChIP) using the Chromatin Immunoprecipitation Kit (Millipore-17-408) in accordance with the manufacturer's instructions. Then, we purified the immunoprecipitated DNA using the phenol extraction method and quantified the relevant DNA using qPCR. All the primers used in this study are listed in **Supplementary Table 1**.

Promoter Reporter and Dual-Luciferase Assays

The RBM3 promoter was amplified from NP69 cells using PCR and then subcloned into an empty pGL3 vector. Renilla luciferase reporter plasmid was also transfected as a normalization control. Dual-luciferase assays were performed using a dual-luciferase assay kit (#E1910, Promega) according to the manufacturer's instructions. The details of the primers used to clone the RBM3 promoter are described in **Supplementary Table 1**.

In Situ Hybridization

In situ hybridization analysis of AFAP1-AS1 interactions was performed on paraffin-embedded sections using the RNAscope 2.5 HD Detection Reagent-BROWN kit (ACDBio). All analyses were carried out according to the manufacturer's instructions using an AFAP1-AS1–specific probe purchased from ACDBio.

Plasmids

AFAP1-AS1, KAT2B, TIF1α, and RBM3 transcripts from NP69 cells were amplified using RT-PCR, sequenced, and then subcloned into the pcDNA3.0 or pLVX-Puro vector (Clontech). AFAP1-AS1 or TIF1α-truncated constructs were generated using PCR with AFAP1-AS1 or TIF1α-pcDNA3.0 as templates and inserted into pcDNA3.0. $KAT2B^{E570A/D610A}$ and $TIF1\alpha^{F979A/N980A}$ point mutations were generated using a PCR-based site-directed mutagenesis kit from Invitrogen following the manufacturer's instructions.

shRNA Knockdown and Transfection

shRNA-knockdown and transfection assays were performed as previously described (21). shRNA sequences were purchased from Shanghai Biogene Co., Ltd. (Shanghai, China). These sequences and the packaging plasmids were transfected into HEK293 cells and used to generate viral particles. The supernatants were collected at 48 and 72 hours posttransfection and filtered through a 0.22 μm membrane (Millipore). The viruses were then concentrated. HNE-1 and CNE-2 cells were infected with these shRNA or shGFP control viruses in the presence of 8 μg/mL polybrene. Infected cells were enriched by selection with 5 μg/mL puromycin 48 hours after infection. Multiple monoclonal cultures were screened for shRNA integration and activity using WB and RT-PCR.

RNA-Seq and Differentially Expressed Gene Analysis

RNA-Seq and differentially expressed gene analysis were performed as previously described (6). RNA-Seq data generated in this study are available from the NCBI BioProject database (http://www.ncbi.nlm.nih.gov/bioproject) under Bioproject ID: PRJNA594347.

Mass Spectrometry of AFAP1-AS1-Associated Proteins

AFAP1-AS1 and its antisense plasmid were cut, transcribed, and biotin-labeled *in vitro* with Bio16-UTP (Life Technologies) using a MAXIscript T7 Transcription Kit (Life Technologies). Protein–RNA interactions in HNE-1 cell lysates were analyzed using a Pierce Magnetic RNA-Protein Pull-Down Kit (Life Technologies). The retrieved proteins were then subjected to WB analysis or resolved by gradient gel electrophoresis and subjected to LC-MS/MS sequencing and data analysis.

Immunohistochemical Staining

Immunohistochemistry (IHC) was performed using an anti-KAT2B antibody (#3378, 1:1000, Cell Signaling Technology). Each sample was assigned a score according to the intensity of the KAT2B staining (0 = no staining, 1 = weak staining, 2 = moderate staining, and 3 = strong staining) and the proportion of stained cells (0 = 0%, 1 = 1%–25%, 2 = 25%–50%, 3 = 50%–75%, 4 = 75%–100%). Negative control slides without primary antibodies were included as a reference. The core staining was scored as negative (0) when <10% tumor cells showed KAT2B expression. The stained tissues were scored by three individuals blinded to the clinical parameters.

Tumorigenesis Studies

To evaluate NPC tumorigenicity, four-week-old female BALB/c nude mice, maintained in a mouse-specific pathogen-free (SPF) facility, were injected subcutaneously with HNE-1 cells (2×10^6). All experimental procedures were performed in accordance with the Animal Care and Use Committee of Chinese Academy of Medical Science guidelines.

Statistics

All statistical analyses were performed using GraphPad Prism version 5.0 software. Survival rates were determined using the Kaplan-Meier method, and significance was determined using multiple comparison tests. A P value < 0.05 was considered statistically significant.

RESULTS

lncRNA AFAP1-AS1 Expression Is a Biomarker of Poor Prognosis in NPC Patients

To determine the roles of AFAP1-AS1 in NPC progression, we first evaluated changes in AFAP1-AS1 expression in HNE-1, C666-1, SUNE-1, CNE-1, CNE-2 NPC, and NP69 nasopharyngeal epithelial cells. As shown in **Figure 1A**, AFAP1-AS1 expression was higher in all five NPC cell lines than in the NP69 control, and its expression was the highest in HNE-1 and CNE-2 cells. To elaborate on these results, we examined AFAP1-AS1 expression in 10 pairs of freshly frozen NPC tumor and adjacent nontumor specimens using qRT-PCR. Interestingly, AFAP1-AS1 expression was significantly higher in NPC tumors than in their adjacent nontumor pair (**Figure 1B**). RNA *in situ* hybridization was then used to analyze AFAP1-AS1 expression in 100 pairs of paraffin-embedded NPC tumor and adjacent nontumor specimens, which revealed that AFAP1-AS1 expression was higher in NPC tumors (**Figures 1C, D**), confirming the aforementioned qRT-PCR result.

To reveal the clinical significance of AFAP1-AS1 expression in NPC, we analyzed the correlation between AFAP1-AS1 expression and NPC patient survival rates. Kaplan-Meier survival assays (**Figure 1E**) demonstrated that NPC patients with higher AFAP1-AS1 expression levels had lower overall survival rates than patients with lower AFAP1-AS1 expression levels. Additionally, AFAP1-AS1 was shown to be expressed in both the nucleus and cytoplasm of NPC (**Figures 1C, F, G**), suggesting that AFAP1-AS1 may have multiple functions in both the nucleus and cytoplasm of tumor cells. In conclusion, these data suggest that AFAP1-AS1 expression is a good biomarker for the prognosis of NPC patients.

AFAP1-AS1 Expression Is Important for NPC Growth and Tumorigenicity

To reveal whether AFAP1-AS1 is important for NPC tumorigenicity, we first depleted endogenous AFAP1-AS1 using two different shRNAs in both HNE-1 and CNE-2 cell lines (**Figure 2A**). We then performed RNA-Seq to compare mRNA expression profiles. Several differentially expressed genes (DEGs) were identified (P < 0.05 and a fold change > 1.5) in AFAP1-AS1 knockdown-inhibited HNE-1 cells (**Figure 2B**). These DEGs were then subjected to gene ontology (GO) analysis (**Figure 2C**), which revealed that the majority of enrichment occurred in the cellular proliferation pathways. These data suggest that AFAP1-AS1 may play a vital role in NPC proliferation.

To confirm the results of the RNA-Seq data, we evaluated the effects of AFAP1-AS1 depletion using cellular proliferation (**Figures 2D, E**) and colony formation (**Figures 2F, G**) assays in both HNE-1 and CNE-2 cells. AFAP1-AS1 knockdown markedly reduced HNE-1 tumorigenicity (**Figures 2H, I**). In contrast, AFAP1-AS1 overexpression promoted cellular proliferation and colony formation in NP69 cells (**Supplementary Figure 1**). Collectively, these data suggest that AFAP1-AS1 is important for NPC growth and tumorigenicity, and may be important in the transition of normal cells to tumor precursors.

AFAP1-AS1 Enhances NPC Cellular Proliferation *via* YAP

To understand the potential mechanisms by which AFAP1-AS1 enhances cellular proliferation, we first conducted Kyoto Encyclopedia of Genes and Genomes (KEGG) analysis. This analysis revealed that the Hippo signaling pathway was one of the top differentially changed AFAP1-AS1–induced pathways (**Figure 3A**). Furthermore, both mRNA and protein expression of YAP, a vital regulator of the Hippo pathway, were inhibited by AFAP1-AS1 depletion (**Figures 3B, C**), suggesting that YAP may be a critical component of the AFAP1-AS1-mediated network. Moreover, we found AFAP1-AS1 knockdown inhibited YAP expression *in vivo* (**Supplementary Figure 2**).

Interestingly, we found that YAP mRNA degraded faster upon AFAP1-AS1 knockdown in HNE-1 cells, which were treated with the RNA synthesis inhibitor actinomycin D, and analyzed at 0, 1, and 2 hours post-exposure (**Figures 3D, E**). These results indicate that AFAP1-AS1 may play a vital role in YAP mRNA stability.

To assess the role of YAP in AFAP1-AS1-regulated NPC proliferation, we overexpressed YAP in AFAP1-AS1–depleted HNE-1 and CNE-2 cells (**Figure 3F**). Exogenous YAP overexpression rescued AFAP1-AS1 depletion-inhibited cell proliferation (**Figure 3G**) and colony formation (**Figure 3H**). Taken together, these results reveal that YAP is a downstream effector of AFAP1-AS1–mediated NPC proliferation.

AFAP1-AS1 Physically Binds to KAT2B

Increasing evidence suggests that lncRNAs can exert their function through binding histone acetyltransferase proteins, including the KAT family proteins (6, 22). We hypothesized that AFAP1-AS1–mediated proliferation may rely on its association with certain KAT family proteins. As shown in **Figures 4A**, **B**, we used biotin-labeled RNA pull-down and mass spectrometry to establish that KAT2B was significantly associated with AFAP1-AS1. Thus, we selected KAT2B as the effector protein for all our downstream analyses. First, we validated the AFAP1-AS1/KAT2B association using an RNA pull-down and RNA Immunoprecipitation assay (**Figures 4B, C**), which also confirmed that AFAP1-AS1 did not bind to other KAT family proteins (KAT2A, KAT3A, KAT3B, KAT6A, KAT6B, KAT7, KAT8) (**Supplementary Figure 3A**). KAT2B is also a proven oncogene that activates gene transcription in medulloblastoma and glioblastoma (23). Second, we found that KAT2B was higher in NPC tumor tissues than in their adjacent

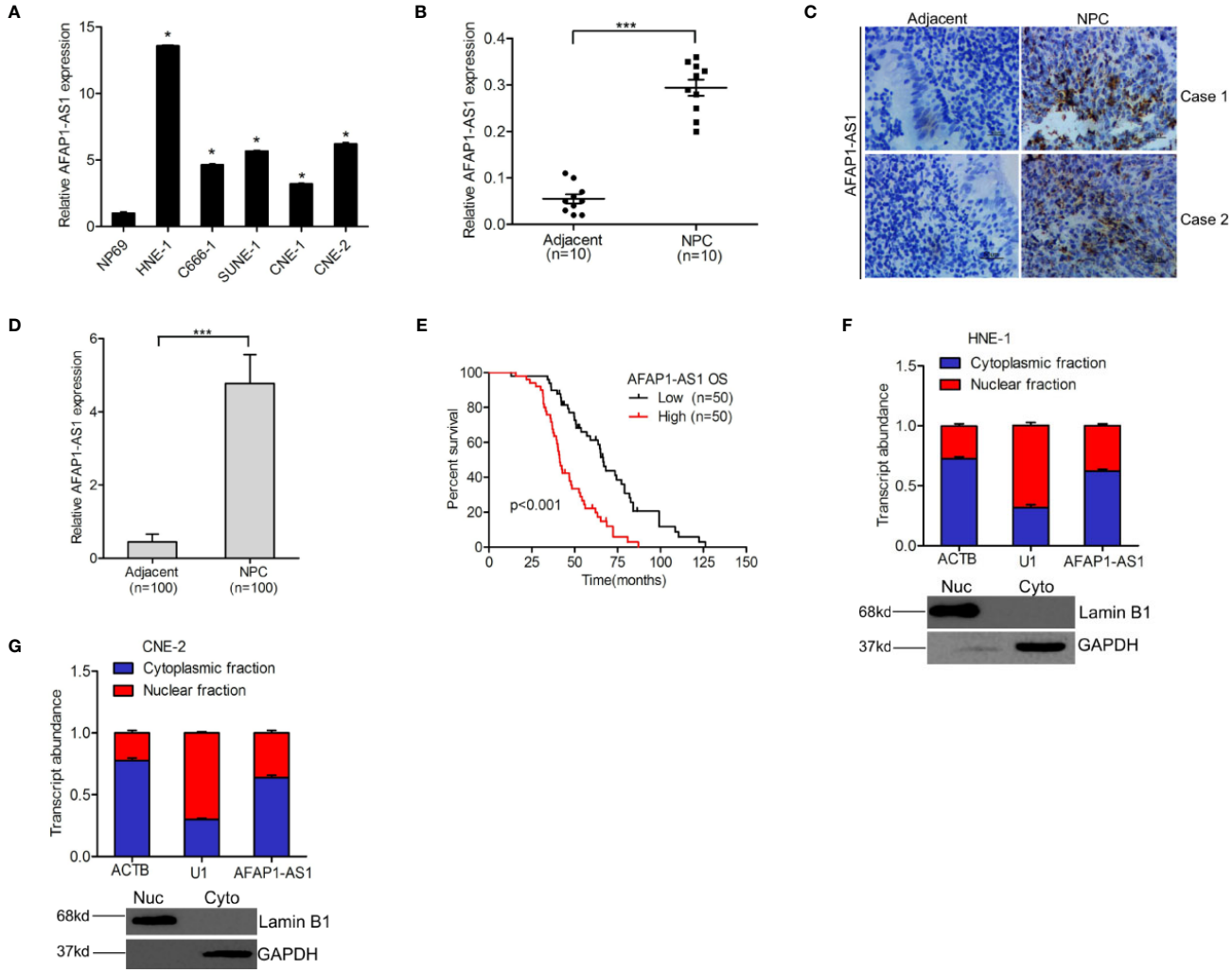

FIGURE 1 | lncRNA AFAP1-AS1 is a marker for poor prognostic outcomes in NPC patients. **(A)** AFAP1-AS1 expression in NPC cells and nasopharyngeal epithelial cells. **(B)** Compared with paired nontumor specimens, AFAP1-AS1 expression is upregulated in freshly frozen NPC tumor tissues. **(C)** Representative images of AFAP1-AS1 expression in paraffin-embedded NPC tumors and paired adjacent nontumor specimens detected using RNAscope. Scale bars: 50 μm. **(D)** Quantification of AFAP1-AS1 expression in **(C)**. **(E)** Kaplan-Meier analysis of overall survival (OS) in NPC patients with high vs. low AFAP1-AS1 expression. **(F, G)** AFAP1-AS1 is expressed in both the nucleus and cytoplasm of NPC cells as detected using qRT-PCR. Error bars represent the standard deviation for each value. $^{*}P < 0.05$. $^{***}P < 0.001$. The data represent three independent experiments. lncRNA, long noncoding RNA.

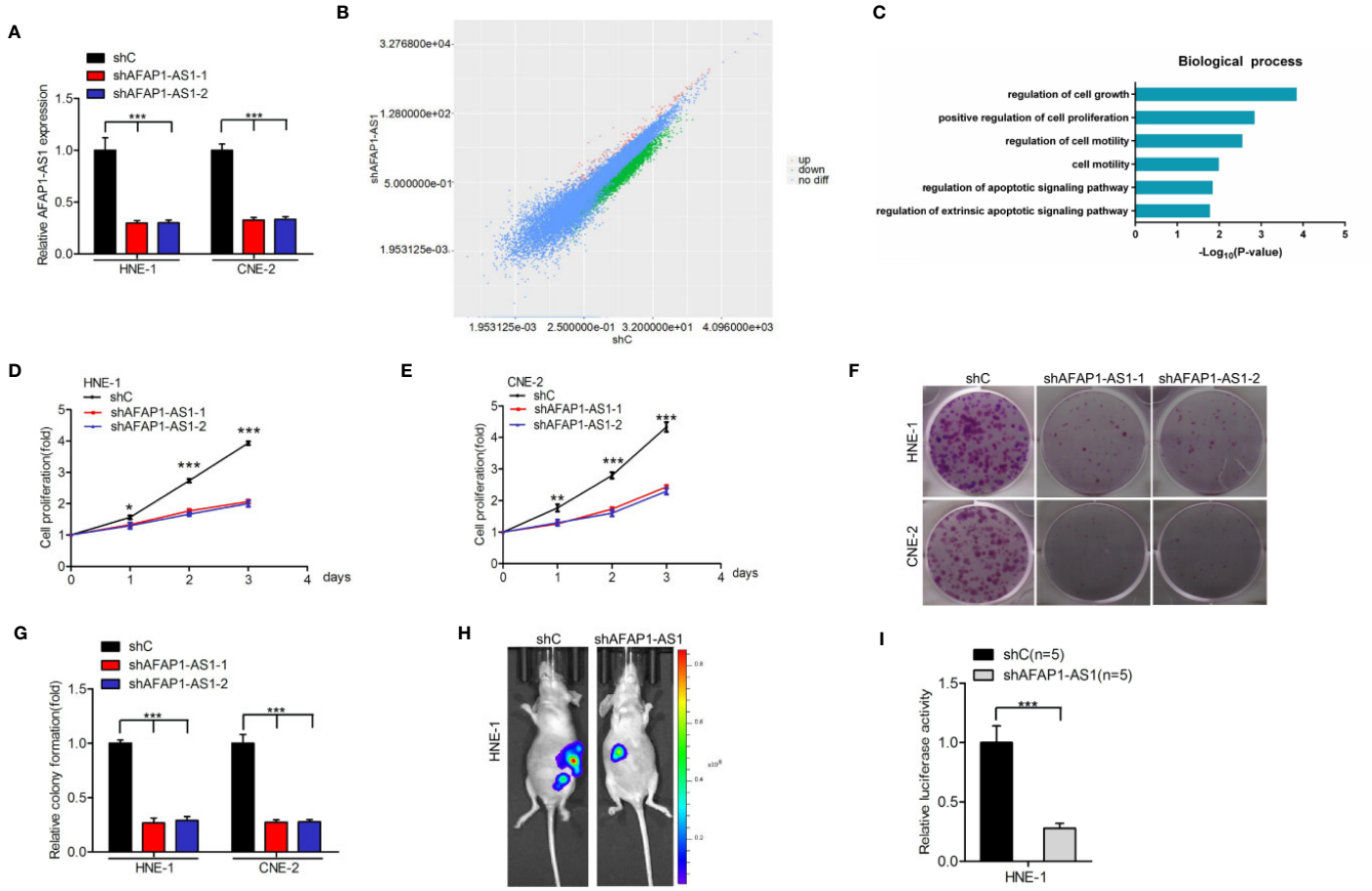

FIGURE 2 | AFAP1-AS1 is important for NPC growth and tumorigenicity. **(A)** qRT-PCR analysis of AFAP1-AS1 knockdown by two shRNAs (shAFAP1-AS1-1 and shAFAP1-AS1-2) vs. a control shRNA (shC). **(B)** Scatter plot of gene expression in HNE-1 cells transfected with AFAP1-AS1 shRNA (y-axis) compared with the control (x-axis). Green dots, genes that are significantly downregulated following AFAP1-AS1 knockdown. Red dots, genes that are significantly upregulated following AFAP1-AS1 knockdown. Black dots, genes with no change in expression following AFAP1-AS1 knockdown. **(C)** GO analyses of AFAP1-AS1 knockdown-associated biological process signaling pathways. **(D, E)** AFAP1-AS1 depletion-inhibited cellular proliferation in HNE-1 and CNE-2 cells. **(F)** Effects of AFAP1-AS1 depletion on cell colony formation. **(G)** Quantification of colony formation in **(F)**. **(H)** Representative bioluminescence images following AFAP1-AS1 depletion suppressing HNE-1 subcutaneous tumor growth. **(I)** Quantification of the bioluminescence activity in **(H)**. Error bars represent standard deviation. $^{*}P < 0.05$. $^{**}P < 0.01$. $^{***}P < 0.001$. The data represent three independent experiments. GO, gene ontology.

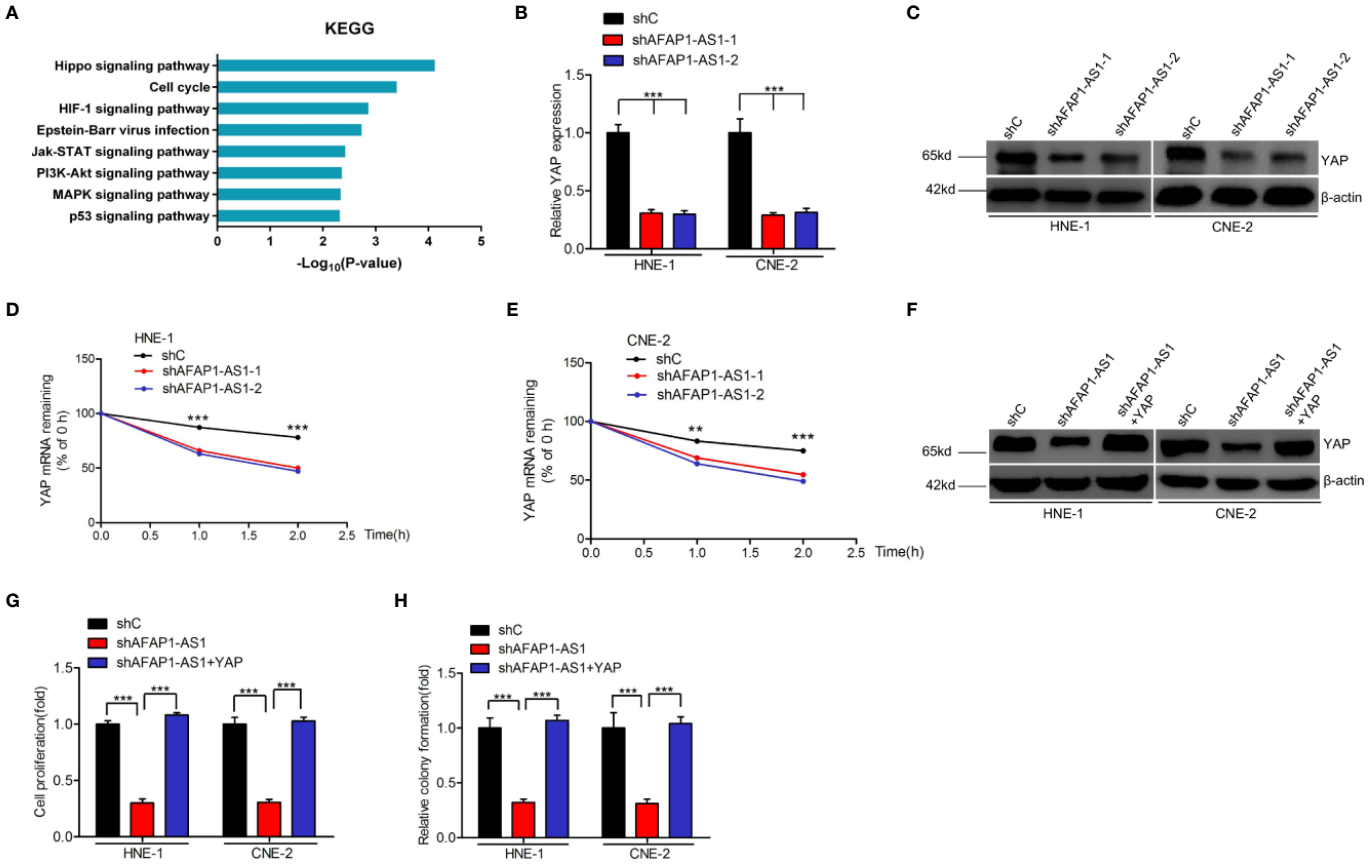

FIGURE 3 | AFAP1-AS1 enhances NPC cell proliferation *via* YAP stabilization. **(A)** KEGG analyses of AFAP1-AS1 knockdown-associated signaling pathways. **(B, C)** Effects of AFAP1-AS1 depletion on YAP mRNA **(B)** and protein **(C)** expression. **(D, E)** Effects of reduced YAP mRNA stability in AFAP1-AS1–depleted HNE-1 cells (compared to the control). Cells were treated with 1 μg/mL actinomycin D, and RNA was extracted at 0, 1, and 2 hours. **(F–H)** YAP rescued AFAP1-AS1 depletion-inhibited YAP expression **(F)**, cellular proliferation **(G)**, and colony formation **(H)**. Error bars represent standard deviation. $^{**}P < 0.01$. $^{***}P < 0.001$. The data represent three independent experiments.

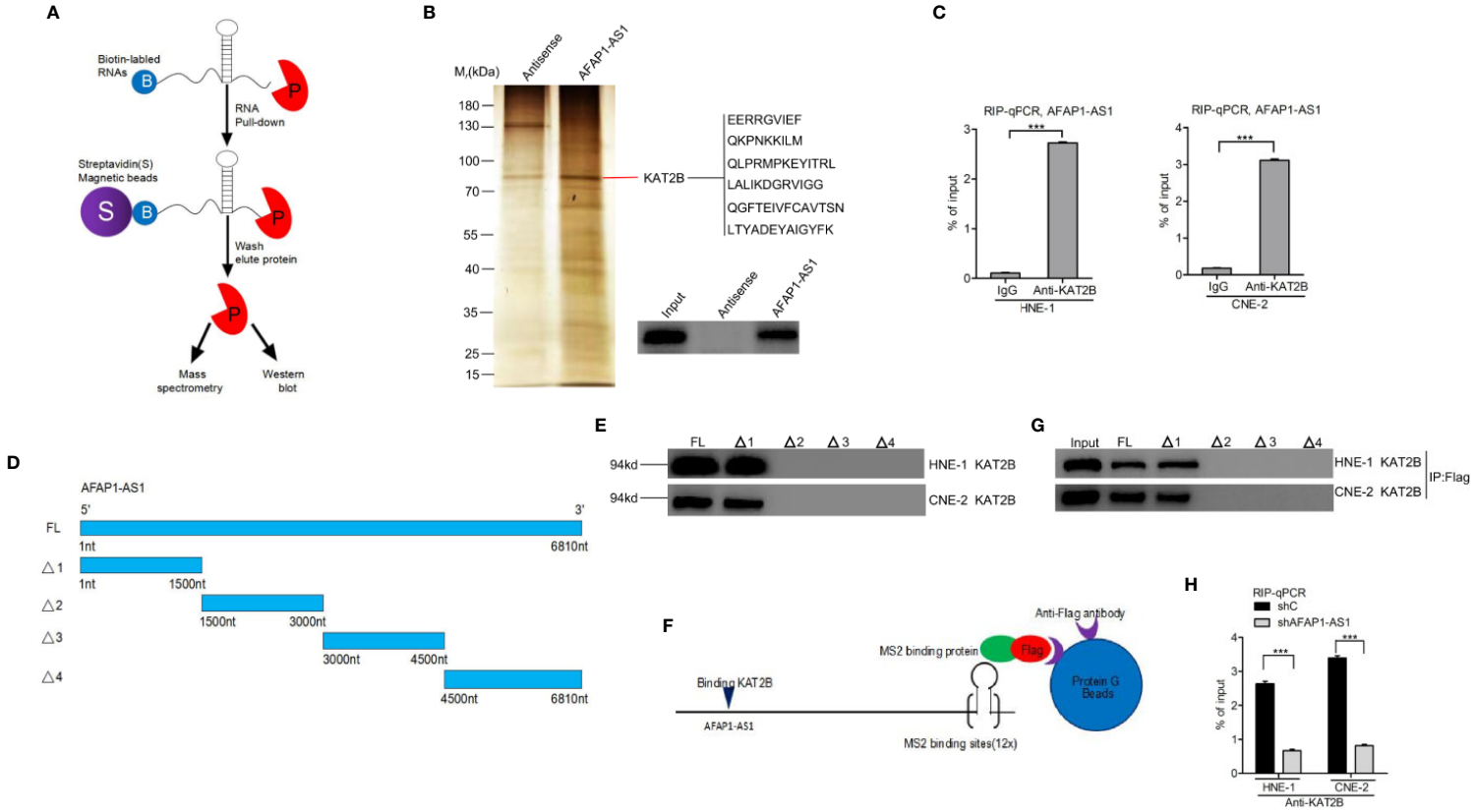

FIGURE 4 | AFAP1-AS1 physically binds to KAT2B. **(A)** Schematic description of the RNA pull-down assay for the identification of AFAP1-AS1–associated proteins. **(B)** Representative image of silver staining, revealing AFAP1-AS1–associated proteins in HNE-1 cells. **(C)** RIP assay showing that AFAP1-AS binds to KAT2B. **(D)** Schematics of full-length AFAP1-AS1 and various AFAP1-AS1 deletion mutants. **(E)** Effects of AFAP1-AS1 mutations on **(D)**. KAT2B binding evaluated by an RNA pull-down assay. **(F, G)** Western blot detection of KAT2B binding of AFAP1-AS1–truncated constructs using a Flag-MS2bp-MS2bs–based pull-down assay. **(H)** Effects of AFAP1-AS1 depletion on AFAP1-AS1 binding of KAT2B. Error bars represent standard deviation. ***$P < 0.001$. The data represent three independent experiments. RIP, RNA immunoprecipitation.

nontumor tissues (**Supplementary Figure 3B, C**). Taken together, these data indicate that AFAP1-AS1 directly binds to KAT2B, which then modulates histone modification.

To further validate these findings, we performed deletion mapping followed by a pull-down to reveal KAT2B associations with specific regions of AFAP1-AS1 (**Figures 4D, E**). As shown in **Figure 4E**, a region covering 0–1500 nucleotides at the 5′ end of AFAP1-AS1 is critical for KAT2B binding. A Flag-MS2bp-MS2bs system used in conjunction with immunoprecipitation assays demonstrated similar results (**Figures 4F, G**), suggesting that this was a valid observation and not the result of the assay design. Finally, AFAP1-AS1 depletion inhibited the KAT2B association in RIP qRT-PCR assays (**Figure 4H**).

AFAP1-AS1 Promotes YAP mRNA Stability *via* KAT2B

As YAP is an important downstream effector of AFAP1-AS1 and since AFAP1-AS1 is bound to KAT2B, we hypothesized that AFAP1-AS1 promotes YAP mRNA stability *via* KAT2B regulation in NPC cells. We first downregulated AFAP1-AS1 expression and found that both YAP mRNA and protein expression were also inhibited (**Figures 5A, B**). Moreover, KAT2B overexpression restored AFAP1-AS1 depletion-inhibited YAP protein (**Figure 5C**) and mRNA expression (**Figure 5D**) as well as improved its mRNA stability (**Figure 5G**) in NPC cells. Both cellular proliferation and colony formation were also rescued following KAT2B overexpression in AFAP1-AS1–depleted HNE-1 and CNE-2 cells (**Figures 5E, F**).

To evaluate the mechanisms underlying the AFAP1-AS1/KAT2B/YAP associations, we constructed full length AFAP1-AS1 WT, n-AFAP1-AS1 mutant, and c-AFAP1-AS1 mutant plasmids (**Figure 5H**) and designed specific qRT-PCR primers to detect their transcripts (**Figure 5I**). As shown in **Figure 5J–M**, n-AFAP1-AS1, which contains the AFAP1-AS1/KAT2B association domains, promoted YAP mRNA and protein expression, cell proliferation, and colony formation. The same was not true for the c-AFAP1-AS1 mutant, which lacked this functional domain. Taken together, our results suggest that AFAP1-AS1 promotes YAP mRNA stability by binding to KAT2B.

KAT2B Acetyltransferase Activity Promotes AFAP1-AS1–Induced Stabilization of YAP

As AFAP1-AS1 stabilized YAP mRNA by binding to KAT2B, we further explored the potential molecular mechanisms underlying this observation. To do this, we evaluated histone H3 acetylation levels in NPC cell lines. We found that the acetylated levels of H3K9 and H3K14, the proven targets of KAT2B (24), were upregulated in the presence of AFAP1-AS1. As shown in **Figure 6A**, AFAP1-AS1 knockdown decreased H3K9 and H3K14 acetylation, but did not impact KAT2B protein expression. When histone H3 acetylation marks were compared, H3K14 acetylation levels were particularly inhibited by AFAP1-AS1 depletion in both HNE-1 and CNE-2 cells (**Figure 6A**). These results indicate that AFAP1-AS1 may promote KAT2B acetyltransferase activity.

As the roles of H3K14 acetylation modulated by AFAP1-AS1 in NPC remain poorly understood, we sought to determine how H3K14ac modulation affects the function of AFAP1-AS1–regulated NPC cell proliferation. To assess whether KAT2B acetyltransferase activity promoted the function of AFAP1-AS1–stabilized YAP, we created a KAT2B acetyltransferase activity-deficient mutant, $KAT2A^{E570A/D601A}$ (25), and checked whether AFAP1-AS1 could bind to these KAT2B peptides (**Figure 4B**). Next, we hypothesized that the E570/D610 residues of KAT2B were critical for AFAP1-AS1–driven YAP stabilization. As shown in **Figure 6B**, n-AFAP1-AS1, but not c-AFAP1-AS1, mutants could rescue AFAP1-AS1 depletion-inhibited YAP expression. Exogenous $KAT2B^{WT}$, but not the $KAT2B^{E570A/D601A}$ mutant, restored KAT2B depletion-regulated changes in YAP expression (**Figure 6C**). Furthermore, YAP expression (**Figure 6D**), cell proliferation (**Figure 6E**), and colony formation (**Figure 6F**) abilities in AFAP1-AS1–depleted HNE-1 cells were suppressed by the overexpression of $KAT2B^{WT}$, but not the $KAT2B^{E570A/D601A}$ mutant. These data support our hypothesis that residues E570/D610 are required for AFAP1-AS1–modulated YAP stabilization.

Next, we evaluated whether the YAP inhibitor verteporfin mediates AFAP1-AS1–induced or KAT2B-induced NPC cellular proliferation. As shown in **Figure 6G**, verteporfin significantly decreased YAP expression in AFAP1-AS1-WT–overexpressed HNE-1 cells compared with that in c-AFAP1-AS1 or empty vector-overexpressing HNE-1 cells. We then observed that verteporfin markedly suppressed YAP expression (**Figure 6H**), cellular proliferation (**Figure 6I**), and colony formation (**Figure 6J**) in HNE-1 cells transfected with $KAT2B^{WT}$ compared with cells transfected with $KAT2B^{E570A/D601A}$ or empty vector controls. This led us to conclude that KAT2B acetyltransferase activity promotes AFAP1-AS1–mediated stabilization of YAP and cellular proliferation.

Binding of TIF1α to H3K14ac Is Required for AFAP1-AS1–Driven YAP Stabilization

Recent evidence has shown that H3 acetylation of the transcription intermediary factor (TIF) family of proteins is important for cell proliferation in a number of different cancers (26–29). We hypothesized that KAT2B enhanced H3K14 acetylation of TIF proteins, which then acted as transcriptional activators enhancing downstream gene expression, resulting in improved YAP stability and promoting NPC proliferation. To validate this hypothesis, we used immunoprecipitation to show that TIF1α, TIF1β, and TIF1γ, but not NCOA1, NCOA2, or NCOA3, bind to H3K14ac (**Supplementary Figure 4A**). Further investigations revealed that TIF1α, but not TIF1β or TIF1γ, rescued AFAP1-AS1 depletion-inhibited YAP mRNA stability (**Supplementary Figure 4B**). Thus, we focused on TIF1α for further investigation. To determine which region of TIF1α is critical

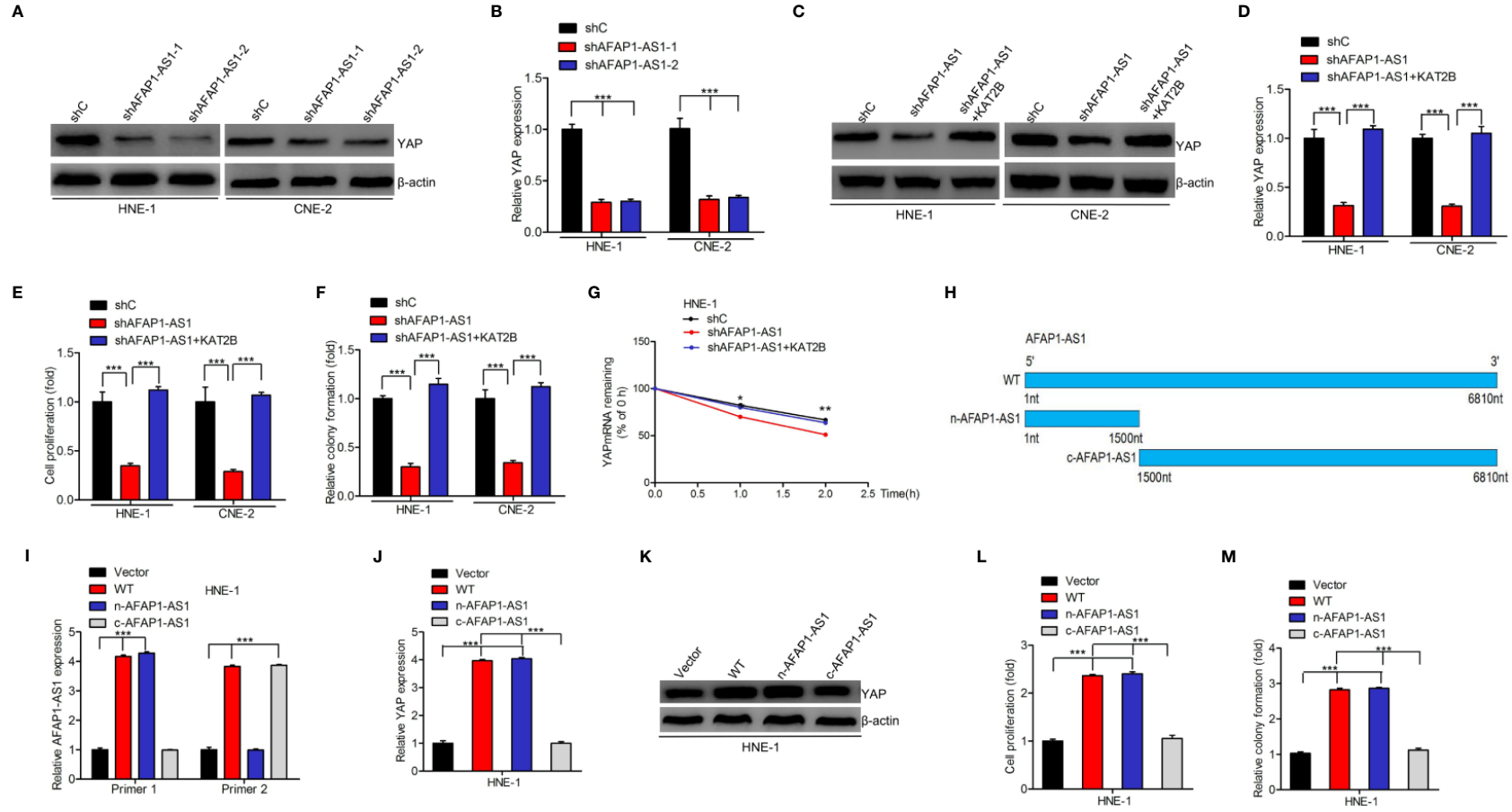

FIGURE 5 | AFAP1-AS1 promotes YAP mRNA stability *via* KAT2B. **(A, B)** AFAP1-AS1 depletion inhibited YAP protein **(A)** and mRNA **(B)** expression. **(C–G)** Effects of KAT2B overexpression on AFAP1-AS1 depletion: inhibited YAP protein expression **(C)**, YAP mRNA expression **(D)**, cellular proliferation **(E)**, colony formation **(F)**, and YAP mRNA stability **(G)**. **(H)** Schematics of full-length AFAP1-AS1 and AFAP1-AS1 deletion mutants at the nitrogen (N) or carbon **(C)** protein sites. **(I)** Effects of AFAP1-AS1 plasmids in **(H)** overexpressing HNE-1 cells. **(J–M)** Effects of AFAP1-AS1 plasmid in **(H)** overexpressing cells on YAP mRNA expression **(J)**, YAP protein expression **(K)**, cellular proliferation **(L)**, and colony formation (M). Error bars represent the standard deviation. $^{*}P < 0.05$. $^{**}P < 0.01$. $^{***}P < 0.001$. The data represent three independent experiments.

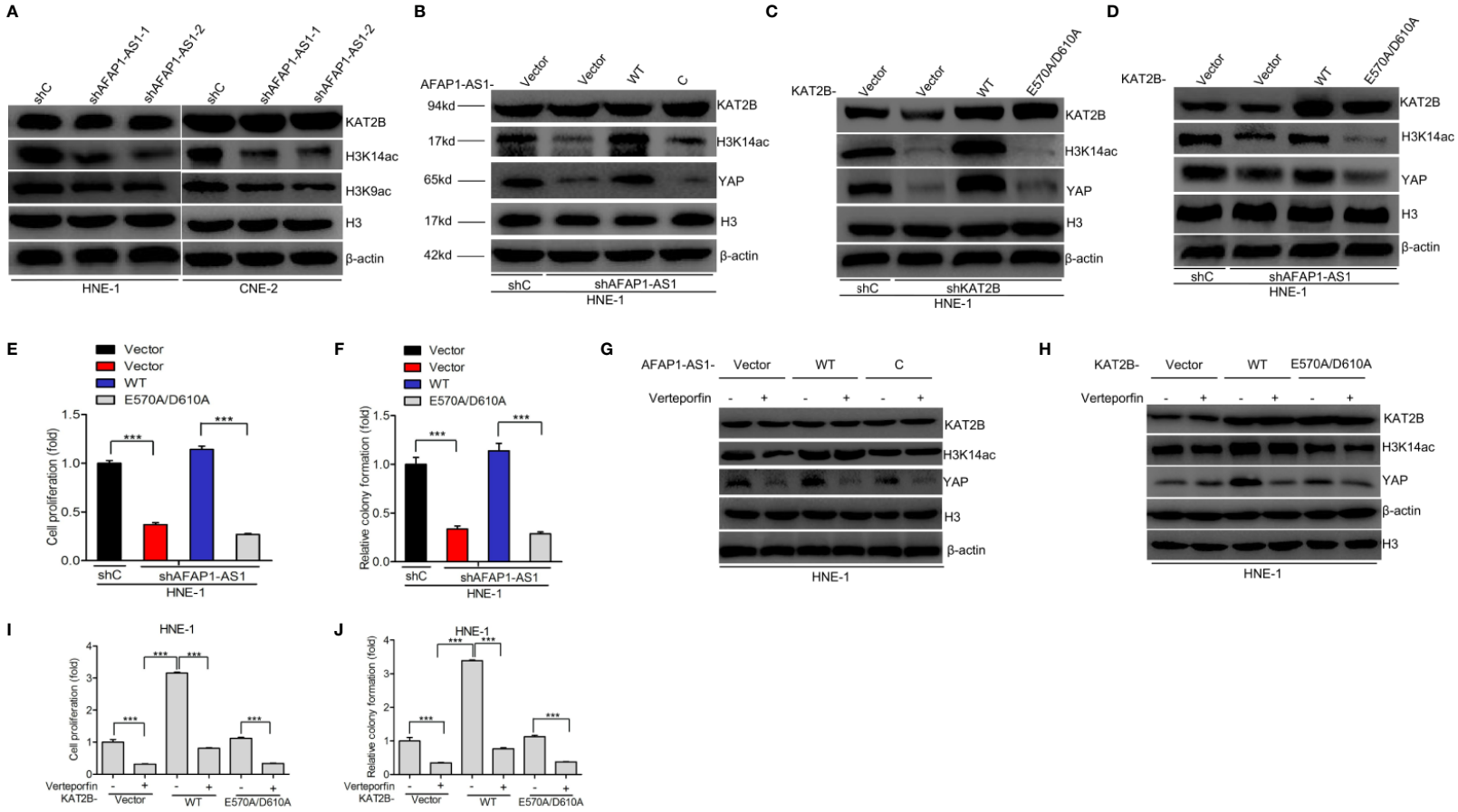

FIGURE 6 | KAT2B acetyltransferase activity promotes AFAP1-AS1 stabilization of YAP. **(A)** Effects of AFAP1-AS1 depletion on the acetylation of H3K9 and H3K14 and KAT2B expression. **(B)** Overexpression of AFAP1-AS1 wild-type, but not c-AFAP1-AS1 deletion mutants, rescues AFAP1-AS1 depletion-suppressed YAP expression. **(C)** Effects of overexpression of KAT2B wild-type and acetyltransferase activity-deficient mutant, E570A/D610A, on KAT2B depletion-suppressed YAP expression. **(D–F)** Overexpression of KAT2B wild-type, but not the acetyltransferase activity-deficient mutant E570A/D610A, restored AFAP1-AS1 depletion-suppressed YAP expression **(D)**, cellular proliferation **(E)**, and colony formation **(F)**. **(G)** Inhibition of YAP reduced AFAP1-AS1–enhanced YAP protein expression. **(H–J)** Effects of YAP inhibition on KAT2B-enhanced YAP protein expression **(H)**, cellular proliferation **(I)**, and colony formation **(J)**. Error bars represent standard deviation. ***$P < 0.001$. The data represent three independent experiments.

for the TIF1α association with H3K14ac, we created deletion mutants removing various functional regions of the protein (**Figure 7A**) and then transfected them into HNE-1 cells. As shown in **Figure 7B**, D2 and D3 mutants, but not the D1 mutant, without PHD and bromodomain domains could not associate with H3K14ac. This demonstrated that amino acids 824–1050 in TIF1α are critical for the interaction between TIF1α and H3K14ac. Next, we revealed that AFAP1-AS1 depletion suppressed the TIF1α association with H3K14ac, while exogenous KAT2B expression restored it (**Figures 7C, D**). We also found that $KAT2B^{WT}$ overexpression restored AFAP1-AS1–mediated interference between TIF1α and H3K14ac binding, but that $KAT2B^{E570A/D601A}$ overexpression could not (**Figure 7E**). A recent study reported that residues F979/N980 in TIF1α are required for its association with H3K9ac (23), and we hypothesized that TIF1α binds to H3K14ac *via* F979/N980. To test this hypothesis, we generated one $TIF1\alpha^{F979A/N980A}$ mutant in which the binding between H3K14ac and TIF1α was disrupted. As shown in **Figure 7F**, overexpression of $TIF1\alpha^{WT}$ rescued the AFAP1-AS1–mediated loss of TIF1α associated with H3K14ac, while overexpression of $TIF1\alpha^{F979A/N980A}$ did not. Moreover, $TIF1\alpha^{WT}$ overexpression, but not $TIF1\alpha^{F979A/N980A}$ overexpression, restored AFAP1-AS1 depletion-suppressed YAP mRNA stability (**Figure 7G**), cellular proliferation (**Figure 7H**), and colony formation (**Figure 7I**) in HNE-1 cells. Taken together, our results suggest that the interaction between TIF1α and H3K14ac is crucial for AFAP1-AS1–driven YAP stabilization.

TIF1α/H3K14ac Complex-Activated RBM3 Transcription Is Required for the AFAP1-AS1 Modulation of YAP Stability

Heatmaps of the RNA-Seq analysis revealed that RBM3 and its downstream genes (28) were significantly affected by KAT2B deletion (**Figure 8A**). RBM3 has been shown to stabilize YAP mRNA expression during cold stress (30). We hypothesized that activation of RBM3 transcription by the TIF1α/H3K14ac complex might be required for AFAP1-AS1 modulation of YAP stability. As shown in **Figures 8B**, **C**, KAT2B deletion markedly decreased RBM3 mRNA and protein expression. Overexpression of KAT2B restored AFAP1-AS1 knockdown-inhibited RBM3 expression (**Figure 8D**). We also determined that KAT2B bound to the RBM3 promoter at –879 to –634 bp (**Figure 8F**), and KAT2B overexpression restored the promoter activity of RBM3 suppressed by AFAP1-AS1 knockdown (**Figure 8E**). Knockdown of RBM3 suppressed YAP protein expression, mRNA expression, and mRNA stability (**Supplementary Figure 5**). Moreover, RBM3 overexpression restored AFAP1-AS1 knockdown or KAT2B knockout-suppressed YAP expression (**Figures 8G, H**). We further found that overexpression of $TIF1\alpha^{WT}$ restored the loss of YAP expression caused by AFAP1-AS1 depletion, but overexpression of $TIF1\alpha^{F979A/N980A}$ did not alter the YAP expression profile (**Figure 8I**). Consistent with these results, exogenous $TIF1\alpha^{WT}$ expression promoted TIF1α/H3K14ac binding to the RBM3 promoter, while exogenous expression of $TIF1\alpha^{F979A/N980A}$ did not (**Figures 8J, K**). These data support our conclusion that activation of RBM3 transcription by the TIF1α/H3K14ac complex is critical for AFAP1-AS1–mediated YAP stability.

DISCUSSION

Our results show that AFAP1-AS1 binds to KAT2B and induces KAT2B acetyltransferase activity in NPC cells. KAT2B-enhanced H3K14ac, in turn, binds to TIF1α, leading to the upregulation of RBM3 transcription, YAP mRNA stability, and increased NPC tumorigenicity (**Figure 8L**).

Our results also suggest that AFAP1-AS1 acts as an oncogene in NPC, which is in accordance with the results of previous studies (14–16). Additionally, AFAP1-AS1 expression was upregulated in NPC tissues, and the high level of expression was negatively associated with NPC survival prognosis. The results of the RNA-Seq data analysis show that AFAP1-AS1 is positively correlated with cellular proliferation-associated pathways. Moreover, AFAP1-AS1 is required for NPC cell proliferation and colony formation *in vitro* and tumorigenicity *in vivo*. These findings support our hypothesis that AFAP1-AS1 drives NPC tumorigenicity.

Our data also support the hypothesis that YAP stability is critical for AFAP1-AS1–driven cell proliferation in NPC. Previous studies have reported that AFAP1-AS1 promotes cell proliferation in non-small-cell lung cancer (31), colorectal cancer (32), triple-negative breast cancer (33), and esophageal squamous malignancies (34). However, the role and mechanism of AFAP1-AS1 in NPC pathogenesis remain poorly understood. AFAP1-AS1 has been reported to predict NPC survival prognosis and promote NPC metastasis through the inhibition of miR-423-5p (14). A study reported that AFAP1-AS1 depletion significantly suppresses NPC migration and invasion through the modification of the actin cytokeratin signaling pathway (15).

The Hippo-YAP signaling pathway is significantly altered after AFAP1-AS1 knockdown, as shown by the KEGG analysis performed using our RNA-Seq data. This links YAP signaling with NPC tumorigenesis, a finding consistent with those of previous reports (35). LncRNA THOR has also been reported to regulate YAP (36). This suggests that our AFAP1-AS1 model, which shows that lncRNA modulates YAP signaling, leading to enhanced NPC cell proliferation, may be feasible. Furthermore, YAP is reported to be a critical effector in the Hippo-YAP signaling pathway (37), and we observed that AFAP1-AS1 knockdown inhibited YAP expression. Additionally, lncRNA B4GALT1-AS1 enhanced YAP mRNA stability and promoted cell stemness and migration in osteosarcoma (38). We also found that AFAP1-AS1 stabilized YAP mRNA. In addition, RBM3, an RNA-binding protein, has been shown to function as an oncogene in many cancers (39, 40) and promote YAP mRNA

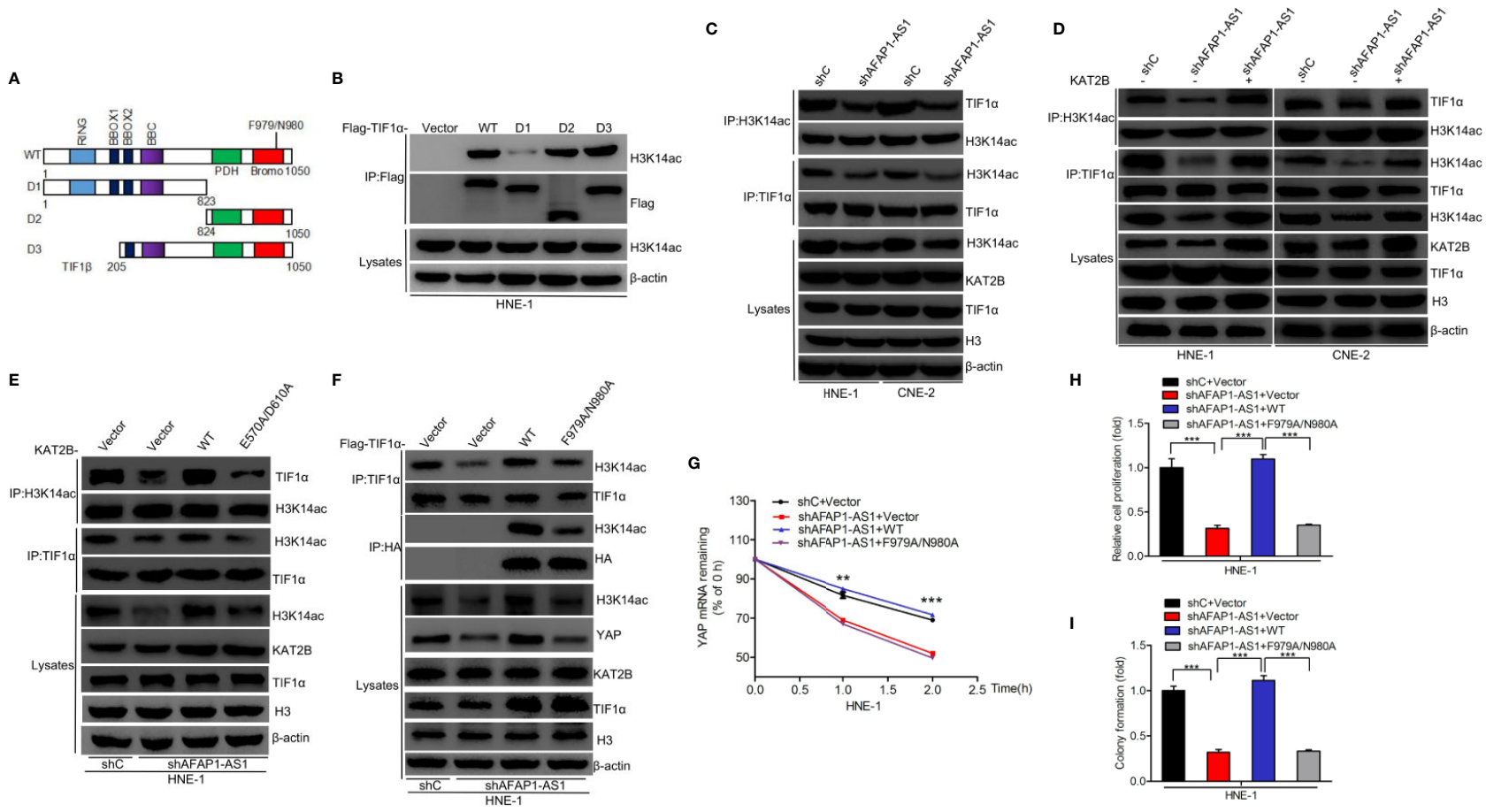

FIGURE 7 | Binding of H3K14ac to TIF1α is required for AFAP1-AS1–driven YAP stabilization. **(A)** Schematics of TIF1α^{WT} and various TIF1α deletion mutants. **(B)** H3K14ac interacts with TIF1α through amino acid residues 824–1050. **(C)** AFAP1-AS1 depletion inhibited TIF1α interaction with H3K14ac. **(D)** Effects of KAT2B overexpression on AFAP1-AS1 depletion-inhibited TIF1α interaction with H3K14ac. **(E)** Effects of KAT2B wild-type and E570A/D610A mutant overexpression on AFAP1-AS1 knockdown suppressed the binding of H3K14ac to TIF1α. **(F–I)** Overexpression of TIF1α wild-type and F979A/N980A mutant restored AFAP1-AS1 knockdown- suppressed binding of H3K14ac with TIF1α **(F)**, YAP mRNA stability **(G)**, cellular proliferation **(H)**, and colony formation **(I)**. Error bars represent standard deviation. $^{**}P < 0.01$. $^{***}P < 0.001$. The data represent three independent experiments.

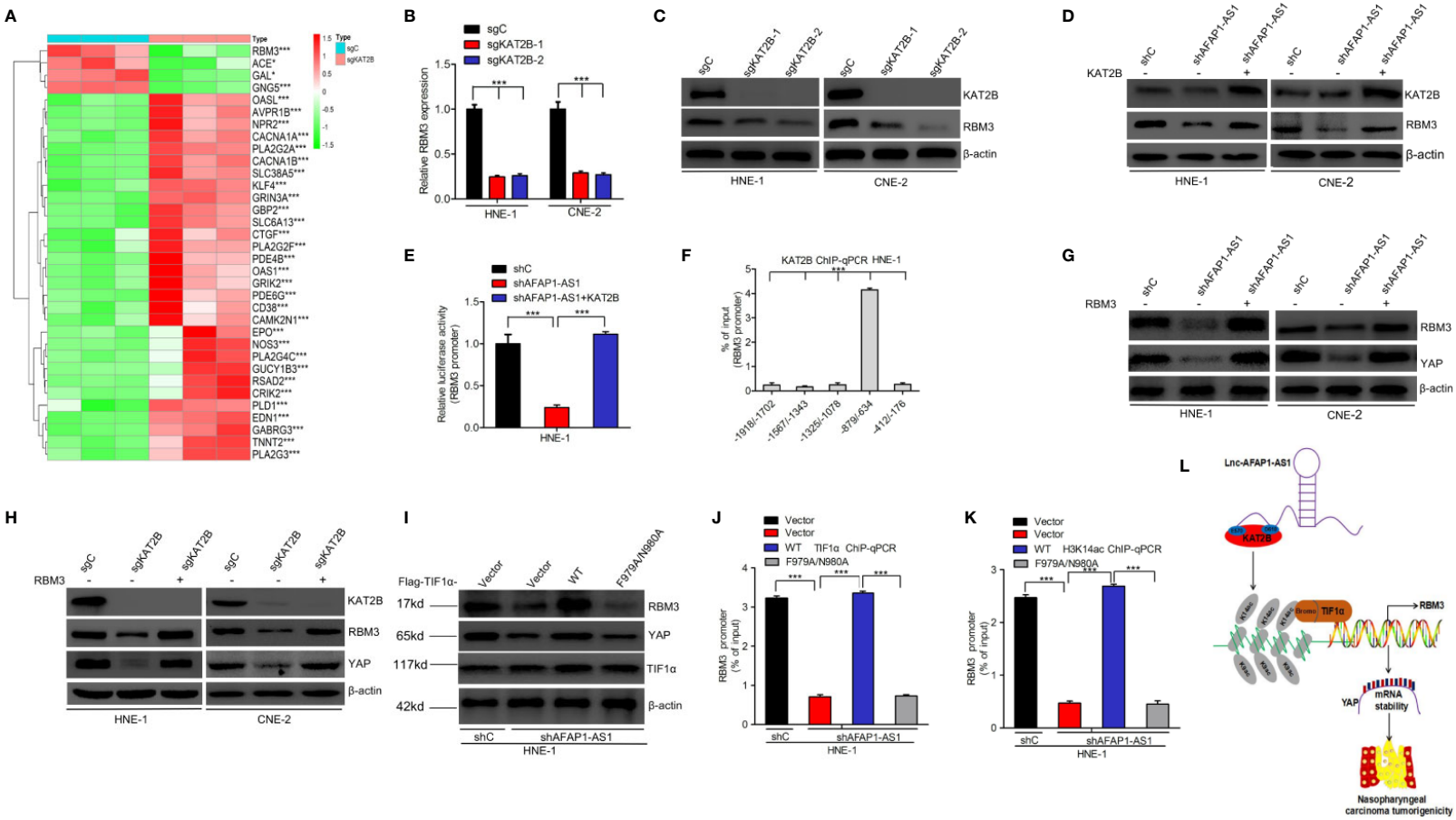

FIGURE 8 | TIF1α/H3K14ac complex activation of RBM3 transcription is required for AFAP1-AS1–modulation of YAP stability. **(A)** Heatmaps of RNA-Seq data for RBM3 and its target genes in HNE-1 cells with KAT2B sgRNA or a control sgRNA. **(B, C)**, KAT2B knockout inhibits RBM3 mRNA **(B)** and protein **(C)** expression. **(D, E)** Effects of KAT2B overexpression on AFAP1-AS1 knockdown-suppressed RBM3 protein expression **(D)** and RBM3 promoter activity **(E)**. **(F)** ChIP-qPCR assay of KAT2B binding at different loci within the RBM3 promoter. IgG is used as a control. **(G)** RBM3 overexpression rescues AFAP1-AS1 knockdown-mediated suppression of YAP. **(H)** Effects of RBM3 overexpression on KAT2B knockout-mediated YAP repression. **(I)** TIF1α wild-type, but not the F979A/N980A mutant, restores AFAP1-AS1 knockdown-suppressed YAP expression in HNE-1 cells. **(J, K)** Effect of TIF1α wild-type and F979A/N980A mutant overexpression on AFAP1-AS1 knockdown-suppressed TIF1α binding **(J)**, H3K14ac **(K)**, and the RBM3 promoter. **(L)** A working model for AFAP1-AS1–mediated NPC tumorigenicity. Error bars represent the standard deviation. *$P < 0.05$. ***$P < 0.001$.The data represent three independent experiment.

stability (30). Using RNA-Seq analysis, we showed that RBM3 expression was downregulated due to KAT2B deletion. We also noted that AFAP1-AS1 stabilized YAP mRNA, which could be rescued by RBM3 overexpression. In conclusion, our results support the hypothesis that AFAP1-AS1 regulates NPC cellular proliferation through the stabilization of YAP mRNA.

Our study demonstrates that AFAP1-AS1 binds to KAT2B and enhances its acetyltransferase activity, which, in turn, upregulates TIF1α/H3K14ac complex formation and RBM3 transcription, thus leading to increased YAP mRNA stability. Previous studies have revealed that the KAT family protein KAT2A can bind to the lncRNAs GClnc1 and PVT1 in gastric cancer and NPC, respectively (6, 22). However, the specific KAT family protein member that binds to AFAP1-AS1 was unknown. Herein, we provide data suggesting that AFAP1-AS1 binds to KAT2B and validated these interactions using a KAT2B E570A/D610A mutant that suppressed AFAP1-AS1–enhanced KAT2B acetyltransferase activity. In accordance with previous reports on KAT2B histone acetylation modifications (30), our results revealed that KAT2B increased H3K14ac levels in NPC cells, while an F979A/N980A mutant in the bromodomain domain of TIF1α impaired TIF1α binding to H3K14ac, and inhibited AFAP1-AS1–induced and KAT2B-induced NPC cell proliferation. Moreover, the binding of TIF1α to H3K14ac was important for AFAP1-AS1–mediated YAP mRNA stabilization. We also determined that RBM3 expression stabilized YAP, and its overexpression rescued YAP stability that was inhibited by AFAP1-AS1 knockdown or KAT2B knockout. TIF1α and H3K14ac can directly bind to downstream gene promoters and enhance their expression (6, 30). We showed that TIF1α and H3K14ac directly promoted RBM3 transcription by binding to its promoter. These data help identify the mechanism of AFAP1-AS1–driven YAP mRNA stabilization as being mediated by KAT2B acetyltransferase activity and TIF1α/H3K14ac complex-promotion of RBM3 transcription inducing NPC cell proliferation

In conclusion, our data demonstrate that AFAP1-AS1 is a potential target for the development of novel therapeutic interventions in NPC. We uncovered a novel molecular mechanism wherein the KAT2B/H3K14ac/TIF1α/RBM3/YAP signaling pathway is important for AFAP1-AS1–driven NPC tumorigenicity. This information may contribute to the creation of personalized treatments for NPC patients.

DATA AVAILABILITY STATEMENT

The datasets presented in this study can be found in online repositories. The names of the repository/repositories and accession number(s) can be found in the article/**Supplementary Material**.

ETHICS STATEMENT

The animal study was reviewed and approved by Institutional Ethical Review Board of the Zhengjiang Provincial People's Hospital.

AUTHOR CONTRIBUTIONS

All authors were involved in the experiments for this paper. MF, JT, and YZ participated in the writing of the manuscript. All authors contributed to the article and approved the submitted version.

FUNDING

This study was supported in part by grants from National Natural Science Foundation of China (Grant number: 81672430 to XM); National Natural Science Foundation of China (Grant number: 81960624 to YW); Zhejiang Provincial Nature Science Foundation of China (Grant number: LY18H160035 to XL); Zhejiang Provincial People's Hospital Scientific Research Returned Foundation for The Excellent Youth (Grant number: ZRY2018B002 to JT); Zhejiang Provincial Nature Science Foundation of China (Grant number: LQ20H160063 to JT); Science and Technology Program of Gansu Province (Grant number: 18JR3RA262 to YW). Zhejiang Provincial Nature Science Foundation of China (Grant number: LY21H160051 to MF).

SUPPLEMENTARY MATERIAL

The Supplementary Material for this article can be found online at: https://www.frontiersin.org/articles/10.3389/fonc.2020.601055/full#supplementary-material

REFERENCES

1. Xiong W, Zeng ZY, Xia JH, Xia K, Shen SR, Li XL, et al. A susceptibility locus at chromosome 3p21 linked to familial nasopharyngeal carcinoma. *Cancer Res* (2004) 64:1972–4. doi: 10.1158/0008-5472.can-03-3253
2. Zeng Z, Huang H, Zhang W, Xiang B, Zhou M, Zhou Y, et al. Nasopharyngeal carcinoma: advances in genomics and molecular genetics. *Sci China Life Sci* (2011) 54:966–75. doi: 10.1007/s11427-011-4223-5
3. Yi M, Cai J, Li J, Chen S, Zeng Z, Peng Q, et al. Rediscovery of NF-kappaB signaling in nasopharyngeal carcinoma: how genetic defects of NF-kappaB pathway interplay with EBV in driving oncogenesis? *J Cell Physiol* (2018) 233:5537–49. doi: 10.1002/jcp.26410
4. He Y, Jing Y, Wei F, Tang Y, Yang L, Luo J, et al. Long non-coding RNA PVT1 predicts poor prognosis and induces radioresistance by regulating DNA repair and cell apoptosis in nasopharyngeal carcinoma. *Cell Death Dis* (2018) 9:235. doi: 10.1038/s41419-018-0265-y
5. Tang L, Wei F, Wu Y, He Y, Shi L, Xiong F, et al. Role of metabolism in cancer cell radioresistance and radiosensitization methods. *J Exper Clin Cancer Res* (2018) 37:87. doi: 10.1186/s13046-018-0758-7
6. Wang Y, Chen W, Lian J, Zhang H, Yu B, Zhang M, et al. The lncRNA PVT1 regulates nasopharyngeal carcinoma cellular proliferation via activating the KAT2A acetyltransferase and stabilizing HIF-1α. *Cell Death Differ* (2020) 27:695–710. doi: 10.1038/s41418-019-0381-y
7. Chen G, Sun W, Hua X, Zeng W, Yang L. Long non-coding RNA FOXD2-AS1

aggravates nasopharyngeal carcinoma carcinogenesis by modulating miR-363-5p/S100A1 pathway. *Gene* (2018) 645:76–84. doi: 10.1016/j.gene.2017.12.026
8. Zhang W, Du M, Wang T, Chen W, Wu J, Li Q, et al. Long non-coding RNA LINC01133 mediates nasopharyngeal carcinoma tumorigenesis by binding to YBX1. *Am J Cancer Res* (2019) 9:779–90.
9. Wu W, Bhagat TD, Yang X, Song JH, Cheng Y, Agarwal R, et al. Hypomethylation of noncoding DNA regions and overexpression of the long noncoding RNA, AFAP1-AS1, in Barrett' s esophagus and esophageal adenocarcinoma. *Gastroenterology* (2013) 144:956–66. doi: 10.1053/j.gastro.2013.01.019
10. Deng J, Liang Y, Liu C, He S, Wang S. The up-regulation of long non-coding RNA AFAP1-AS1 is associated with the poor prognosis of NSCLC patients. *BioMed Pharmacot* (2015) 75:8–11. doi: 10.1016/j.biopha.2015.07.003
11. Lu X, Zhou C, Li R, Liang Z, Zhai W, Zhao L, et al. Critical role for the long non-coding RNA AFAP1-AS1 in the proliferation and metastasis of hepatocellular carcinoma. *Tumour Biol* (2016) 37:9699–707. doi: 10.1007/s13277-016-4858-8
12. Fu X, Liu D, Yan T, Yang J, Yang M, Li J, et al. Analysis of long non-coding RNA expression profiles in pancreatic ductal adenocarcinoma. *Sci Rep* (2016) 6:33535. doi: 10.1038/srep33535
13. Tang J, Zhong G, Wu J, Chen H, Jia Y. Long noncoding RNA AFAP1-AS1 facilitates tumor growth through enhancer of zeste homolog 2 in colorectal cancer. *Am J Cancer Res* (2018) 8:892–902.
14. Lian Y, Xiong F, Yang L, Bo H, Gong Z, Wang Y, et al. Long noncoding RNA AFAP1-AS1 acts as a competing endogenous RNA of miR-423-5p to facilitate nasopharyngeal carcinoma metastasis through regulating the Rho/Rac pathway. *J Exp Clin Cancer Res* (2018) 37:253. doi: 10.1186/s13046-018-0918-9
15. Bo H, Gong Z, Zhang W, Li X, Zeng Y, Liao Q, et al. Upregulated long non-coding RNA AFAP1-AS1 expression is associated with progression and poor prognosis of nasopharyngeal carcinoma. *Oncotarget* (2015) 6:20404–18. doi: 10.18632/oncotarget.4057
16. Tang Y, He Y, Shi L, Yang L, Wang J, Lian Y, et al. Co-expression of AFAP1-AS1 and PD-1 predicts poor prognosis in nasopharyngeal carcinoma. *Oncotarget* (2017) 8:39001–11. doi: 10.18632/oncotarget.16545
17. Peng B, Liu A, Yu X, Xu E, Dai J, Li M, et al. Silencing of lncRNA AFAP1-AS1 suppressed lung cancer development by regulatory mechanism in cis and trans. *Oncotarget* (2017) 8:93608–23. doi: 10.18632/oncotarget.20549
18. Wei F, Jing YZ, He Y, Tang YY, Yang LT, Wu YF, et al. Cloning and characterization of the putative AFAP1-AS1 promoter region. *J Cancer* (2019) 10:1145–53. doi: 10.7150/jca.29049
19. Lv D, Li Y, Zhang W, Alvarez A, Song L, Tang J, et al. TRIM24 Is an Oncogenic Transcriptional Co-Activator of STAT3 in Glioblastoma. *Nat Commun* (2017) 8:1454. doi: 10.1038/s41467-017-01731-w
20. Tang J, Zhong G, Zhang H, Yu B, Wei F, Luo L, et al. LncRNA DANCR upregulates PI3K/AKT signaling through activating serine phosphorylation of RXRA. *Cell Death Dis* (2018) 9:1167. doi: 10.1038/s41419-018-1220-7
21. Sang Y, Li Y, Song L, Alvarez AA, Zhang W, Lv D, et al. TRIM59 Promotes 723 Gliomagenesis by Inhibiting TC45 Dephosphorylation of STAT3. *Cancer Res* (2018) 78:1792–804. doi: 10.1158/0008-5472.CAN-17-2774
22. Sun TT, He J, Liang Q, Ren LL, Yan TT, Yu TC, et al. LncRNA GClnc1 promotes gastric carcinogenesis and may act as a modular scaffold of WDR5 and KAT2A complexes to specify the histone modification pattern. *Cancer Discov* (2016) 6:784–801. doi: 10.1158/2159-8290.CD-15-0921
23. Malatesta M, Steinhauer C, Mohammad F, Pandey D, Squatrito M, Helin K, et al. Histone acetyltransferase PCAF is required for Hedgehog-Gli-dependent transcription and cancer cellular proliferation. *Cancer Res* (2013) 73:6323–33. doi: 10.1158/0008-5472.CAN-12-4660
24. Jin Q, Yu LR, Wang L, Zhang Z, Kasper LH, Lee JE, et al. Distinct roles of GCN5/PCAF-mediated H3K9ac and CBP/p300-mediated H3K18/27ac in nuclear receptor transactivation. *EMBO J* (2011) 30:249–62. doi: 10.1038/emboj.2010.318
25. Fournier M, Orpinell M, Grauffel C, Scheer E, Garnier JM, Ye T, et al. KAT2A/KAT2B-targeted acetylome reveals a role for PLK4 acetylation in preventing centrosome amplification. *Nat Commun* (2016) 7:13227. doi: 10.1038/ncomms13227
26. Tsai WW, Wang Z, Yiu TT, Akdemir KC, Xia W, Winter S, et al. TRIM24 links a non-canonical histone signature to breast cancer. *Nature* (2010) 468:927–32. doi: 10.1038/nature09542
27. Groner AC, Cato L, de Tribolet-Hardy J, Bernasocchi T, Janouskova H, Melchers D, et al. TRIM24 Is an Oncogenic Transcriptional Activator in Prostate Cancer. *Cancer Cell* (2016) 29:846–58. doi: 10.1016/j.ccell.2016.04.012
28. Lv D, Jia F, Hou Y, Sang Y, Alvarez AA, Zhang W, et al. Histone Acetyltransferase KAT6A Upregulates PI3K/AKT Signaling through TRIM24 Binding. *Cancer Res* (2017) 77:6190–201. doi: 10.1158/0008-5472.CAN-17-1388
29. Dong Q, Lv C, Zhang G, Yu Z, Kong C, Fu C, et al. Impact of RNA-binding Motif 3 Expression on the Whole Transcriptome of Prostate Cancer Cells: An RNA Sequencing Study. *Oncol Rep* (2018) 40:2307–15. doi: 10.3892/or.2018.6618
30. Xia W, Su L, Jiao J. Cold-induced Protein RBM3 Orchestrates Neurogenesis via Modulating Yap mRNA Stability in Cold Stress. *J Cell Biol* (2018) 217:3464–79. doi: 10.1083/jcb.201801143
31. Yin D, Lu X, Su J, He X, De W, Yang J, et al. Long Noncoding RNA AFAP1-AS1 Predicts a Poor Prognosis and Regulates Non-Small Cell Lung Cancer cellular proliferation by Epigenetically Repressing p21 Expression. *Mol Cancer* (2018) 17:92. doi: 10.1186/s12943-018-0836-7
32. Zhao Y, Chu Y, Sun J, Song R, Li Y, Xu F, et al. LncRNA GAS8-AS Inhibits Colorectal Cancer (CRC) cellular proliferation by Downregulating lncRNA AFAP1-AS1. *Gene* (2019) 710:140–4. doi: 10.1016/j.gene.2019.05.040
33. Zhang K, Liu P, Tang H, Xie X, Kong Y, Song C, et al. AFAP1-AS1 Promotes Epithelial-Mesenchymal Transition and Tumorigenesis Through Wnt/β-Catenin Signaling Pathway in Triple-Negative Breast Cancer. *Front Pharmacol* (2018) 9:1248. doi: 10.3389/fphar.2018.01248
34. Luo H, Huang M, Guo J, Fan R, Xia X, He J, et al. AFAP1-AS1 Is Upregulated and Promotes Esophageal Squamous Cell Carcinoma cellular proliferation and Inhibits Cell Apoptosis. *Cancer Med* (2016) 5:2879–85. doi: 10.1002/cam4.848
35. Song L, Tang H, Liao W, Luo X, Li Y, Chen T, et al. FOXC2 Positively Regulates YAP Signaling and Promotes the Glycolysis of Nasopharyngeal Carcinoma. *Exp Cell Res* (2017) 357:17–24. doi: 10.1016/j.yexcr.2017.04.019
36. Gao L, Cheng X, Gao H. LncRNA THOR Attenuates Cisplatin Sensitivity of Nasopharyngeal Carcinoma Cells via Enhancing Cells Stemness. *Biochimie* (2018) 152:63–72. doi: 10.1016/j.biochi.2018.06.015
37. Park J, Kwon Y. Hippo-YAP/TAZ Signaling in Angiogenesis. *BMB Rep* (2018) 51:157–62. doi: 10.5483/BMBRep.2018.51.3.016
38. Li Z, Wang Y, Hu R, Xu R, Xu W. LncRNA B4GALT1-AS1 Recruits HuR to Promote Osteosarcoma Cells Stemness and Migration via Enhancing YAP Transcriptional Activity. *Cell Prolif* (2018) 51:e12504. doi: 10.1111/cpr.12504
39. Chen P, Yue X, Xiong H, Lu X, Ji Z. RBM3 upregulates ARPC2 by binding the 3'UTR and contributes to breast cancer progression. *Int J Oncol* (2019) 54:1387–97. doi: 10.3892/ijo.2019.4698
40. Siesing C, Sorbye H, Dragomir A, Pfeiffer P, Qvortrup C, Pontén F, et al. High RBM3 expression is associated with an improved survival and oxaliplatin response in patients with metastatic colorectal cancer. *PLoS One* (2017) 12:e0182512. doi: 10.1371/journal.pone.0182512

Conflict of Interest: The authors declare that the research was conducted in the absence of any commercial or financial relationships that could be construed as a potential conflict of interest.

Copyright © 2020 Fang, Zhang, Wang, Wei, Wu, Mou, Zhang, Liang and Tang. This is an open-access article distributed under the terms of the Creative Commons Attribution License (CC BY). The use, distribution or reproduction in other forums is permitted, provided the original author(s) and the copyright owner(s) are credited and that the original publication in this journal is cited, in accordance with accepted academic practice. No use, distribution or reproduction is permitted which does not comply with these terms.

frontiers in Oncology

ORIGINAL RESEARCH
published: 27 November 2020
doi: 10.3389/fonc.2020.533616

Expression Profile of Circular RNAs in Oral Squamous Cell Carcinoma

Yanxiong Shao[1,2,3†], *Yuhan Song*[1,2,3†], *Siming Xu*[1,2,3†], *Siyi Li*[2,3,4*] *and Haiwen Zhou*[1,2,3*]

[1] Department of Oral Mucosal Diseases, Shanghai Ninth People's Hospital, College of Stomatology, Shanghai Jiao Tong University School of Medicine, Shanghai, China, [2] National Clinical Research Center for Oral Diseases, Shanghai, China, [3] Shanghai Key Laboratory of Stomatology & Shanghai Research Institute of Stomatology, Shanghai, China, [4] Department of Oral Maxillofacial-Head and Neck Oncology, Shanghai Ninth People's Hospital, College of Stomatology, Shanghai Jiao Tong University School of Medicine, Shanghai, China

OPEN ACCESS

Edited by:
Ming Yann Lim,
Tan Tock Seng Hospital, Singapore

Reviewed by:
Valerie Heong,
Nanyang Technological University, Singapore
Yijin Jereme Gan,
Tan Tock Seng Hospital, Singapore
Yvonne Tay,
National University of Singapore, Singapore

***Correspondence:**
Siyi Li
dr.lisiyi@hotmail.com
Haiwen Zhou
haiwen39@126.com

[†]*These authors have contributed equally to this work*

Specialty section:
This article was submitted to Head and Neck Cancer, a section of the journal Frontiers in Oncology

Received: *09 February 2020*
Accepted: *27 October 2020*
Published: *27 November 2020*

Citation:
Shao Y, Song Y, Xu S, Li S and Zhou H (2020) Expression Profile of Circular RNAs in Oral Squamous Cell Carcinoma. Front. Oncol. 10:533616. doi: 10.3389/fonc.2020.533616

Background: Circular RNAs (circRNAs) are involved in the pathogenesis of several diseases. Among oral maxillofacial cancers, oral squamous cell carcinoma (OSCC) has the highest incidence. However, the role of circRNAs in OSCC is still not clear. The aim of our study was to evaluate the circRNA expression profile in OSCC and explore further the potential role of circRNAs in the pathogenesis of OSCC.

Methods: CircRNA sequencing was performed in 6 pairs of samples of OSCC and normal oral mucosal tissues. Expression of selected circRNAs was validated by qRT-PCR. GO and KEGG analyses were performed and binding relationships between circRNAs and miRNAs were predicted. The hsa_circ_0001766/miR-877-3p/VEGFA axis was selected to further elucidate its role in OSCC.

Results: We showed that there were 122 differentially expressed (DE) circRNAs. Eight out of 10 selected circRNAs were validated by qRT-PCR. GO and KEGG analyses indicated that the identified DE circRNAs might be involved in the progression of OSCC. Then, after identification by Sanger sequencing and RNase R assay, the upregulated hsa_circ_0001766 was selected to investigate its potential role in OSCC. Bioinformatics analysis showed that hsa_circ_0001766 might act as a competing endogenous RNA (ceRNA) that sponged miR-877-3p to upregulate VEGFA expression. We selected OSCC cell lines SCC9 and SCC25. PCR results showed that the expression of hsa_circ_0001766 and VEGFA was upregulated in SCC9 and SCC25. Subsequently, using western blot, PCR, CCK8, and colony formation assays, we found that knocking down circRNA0001766 inhibited the expression of VEGFA and the proliferation of OSCC cells. Following this, miR-877-3p inhibitor reversed the inhibitory effect of si-hsa_circ_0001766 on expression of VEGFA and proliferation of OSCC cells.

Conclusions: In conclusion, our study revealed the possible role of circRNAs in the pathogenesis of OSCC, and identified the potential role of the hsa_circ_0001766/miR-877-3p/VEGFA axis in OSCC progression.

Keywords: oral squamous cell carcinoma, circRNA, pathogenesis, non-coding RNA, sequencing

INTRODUCTION

Oral squamous cell carcinoma (OSCC) is the commonest cancer in the oral maxillofacial region, and is often accompanied by regional lymph node metastasis and even distant metastasis. However, the pathogenesis of OSCC is still unclear and there are no effective or satisfactory treatments available currently. According to reports, the 3-year overall survival rates for low-risk, intermediate-risk, and high-risk OSCC are 93, 70.8, and 46.2%, respectively, and the current 5-year survival rate for OSCC is 63% (1). Molecularly-targeted anti-tumor drugs have been widely used in various cancers clinically in recent years, since they have less side effects and better efficacy. Therefore, looking for key molecules in the pathogenesis of OSCC is of vital importance in the treatment for OSCC.

Circular RNAs (circRNAs) are a novel class of non-coding RNAs that are mainly distributed in eukaryotic cells and are over hundreds of nucleotides in length. CircRNAs are characterized by covalent closed loop structures with neither 5′ or 3′ polarities nor polyadenylated tails, which renders them resistant to degradation by RNA exonuclease and endows them with high conservatism and stability (2). The circRNAs discovered so far are mainly structured by head-to-tail splicing of exons (3). There are other types of circRNAs, such as intronic and sense overlapping ones.

Produced by back-splicing, most circRNAs distribute in the eukaryotic cells' cytoplasm and have tissue and disease specificity. CircRNAs play an important role in the development of various diseases through regulation of gene expression by processes, such as transcription, translation, and splicing. In addition, numerous microRNA (miRNA) binding sites are located on circRNAs, which makes circRNAs the competing endogenous RNA (ceRNA) of miRNAs (4). Functioning as a miRNA sponge, circRNA can ameliorate the inhibitory effect of miRNA on its host gene and promote gene expression.

Stomatology researchers have expressed concern about circRNAs' role in the pathogenesis of multiple diseases, such as oral squamous cell carcinoma (5–10), oral mucosal melanoma (11), and mucoepidermoid carcinoma of salivary glands (12). Regarding OSCC, Chen et al. (5) found that circRNA_100290 could regulate the function of cyclin-dependent kinase 6 (CDK6) by miR-26 sponging. Wang et al. (6) speculated that circDOCK1 is related to cellular apoptosis in OSCC. The knockdown of circDOCK1 expression and the upregulation of miR-196a-5p expression led to a decrease in BIRC3 formation and an increase in apoptosis in OSCC cells. Qiu et al. (7) detected 322 differentially expressed (DE) circRNAs between human tongue squamous cell carcinoma and corresponding adjacent tissues through high-throughput sequencing. Wang et al. (8) identified that circ_000334, circ_006740, and circ_006371 were significantly downregulated in OSCC and could act as ceRNA participating in the development of OSCC. Ouyang et al. (9) demonstrated that knockdown of has_circ_0109291 inhibited proliferation and migration of OSCC cell lines *in vitro*. Su et al. (10) verified that has_circ_0007059 was downregulated in OSCC and suppressed cell growth, migration, and invasion of SCC15 and CAL27 cells *via* AKT/mTOR signaling. Despite the putative role of circRNAs in OSCC reported in previous studies, the results of circRNA sequencing in OSCC varied in different studies, perhaps because of the limited amounts of samples (due to high costs), different control group selection, varied sites of sampling, and significant individual differences.

In this study, we aimed to evaluate the circRNA expression profile in OSCC and normal oral mucosa tissue samples and further explore the ceRNA networks and the potential role of circRNAs in the OSCC.

MATERIALS AND METHODS

Patients and Samples

Twelve patients were enrolled in this research at the Shanghai Ninth People's Hospital from August 2018 through December 2018. OSCC tissues were obtained from 4 males and 2 females (n = 6) with a histopathological diagnosis of OSCC and subjected to primary surgical treatment in the Department of Oral and Maxillofacial-Head and Neck Oncology. Normal oral mucosal tissues were obtained from 2 males and 4 females (n = 6) who underwent plastic surgery in the Department of Plastic and Reconstructive Surgery. All tissue samples were frozen in liquid nitrogen immediately after resection and stored at −80°C until RNA extraction. Patients with a previous history of chemo- or radiotherapy, and those suffering from severe diseases, including but not limited to cardiac dysfunction, hepatic and renal dysfunction, as well as pregnant women were excluded. Written informed consent was taken from all subjects prior to sample collection. The Ethics Committee of Shanghai Ninth People's Hospital approved this study.

RNA Extraction

Trizol reagent (Life Technologies, Carlsbad, CA, USA) was used to extract total RNA from tissue samples. The concentration and purity were detected by the NanoDrop ND1000 (Thermo Fisher Scientific, Waltham, MA, USA). All RNA samples passed the quality control according to the OD260/OD280 readings (1.8–2.1).

CircRNA Sequencing

CloudSeq Biotech (Shanghai, China) provided high-throughput sequencing service. CircRNA high-throughput sequencing and bioinformatics analysis were done by Cloud-Seq Biotech. After ribosomal RNAs (rRNAs) were removed from the total RNA using Ribo-Zero rRNA Removal Kits (Illumina, USA), RNA libraries were constructed by using rRNA-depleted RNAs with TruSeq Stranded Total RNA Library Prep Kit (Illumina). The quality of libraries was controlled by the BioAnalyzer 2100 system (Agilent Technologies, USA). Libraries of 10 pM were denatured as single-stranded DNA molecules and sequenced for 150 cycles on Illumina HiSeq 4000 Sequencer (Illumina, San Diego, CA, USA).

CircRNA Profiling Analysis

Paired-end reads were harvested by Illumina HiSeq 4000 sequencer, and the quality was controlled by Q30. After 3′ adaptor-trimming and removal of low-quality reads by cutadapt software (v1.9.3), the high-quality trimmed reads

were left for circRNA analysis. Then, the high-quality reads were aligned to the reference genome/transcriptome with STAR software (v2.5.1b). CircRNAs were detected and identified by DCC software (v0.4.4). edgeR software (v3.16.5) was used to normalize the data and analyze DE circRNAs. CircRNAs with a fold change (FC) in expression ≥ 2.0 ($P < 0.05$) between the OSCC and the control samples were considered statistically significant and selected for further analysis. GO and KEGG analyses were performed. Binding relationships between circRNAs and miRNAs were predicted by TargetScan 7.0 and miRanda v3.3a. The network of circRNAs, miRNAs, and mRNAs was constructed with Cytoscape 3.1 software.

Quantitative Real-Time Polymerase Chain Reaction (qRT-PCR) Validation

qRT-PCR was used to identify the selected circRNAs in the circRNA profile. Total RNA (2 μg), dNTPs Mix (HyTestLtd, Turku, Finland), SuperScript III Reverse Transcriptase (Thermo Fisher Scientific, Chino, CA, USA), and RNase Inhibitor (Enzymatics, GreenBay, Wisconsin, USA) were used for cDNA synthesis. GAPDH served as an endogenous control gene for circRNAs. qRT-PCR was performed by QuantStudio 5 Real-Time PCR System (Thermo Fisher Scientific). The experiment was duplicated in three times. Data analysis was performed by the 2-△△Ct method.

The primers were designed as follows: hsa_circ_0000857, 5'-CAGACGGACCCCACAGAC-3' (forward) and 5'-TGGCGT TGAAACTGGGAT-3' (reverse); hsa_circ_0006151, 5'-GGCAC CAGCATAGCCAGT-3' (forward) and 5'-CCAGGCGCTT TTCACAGT-3' (reverse); hsa_circ_0005050, 5'-CCCAGCTGC TAGAGAACCA-3' (forward) and 5'-TTGGTTGCCTGCT GGATT-3' (reverse); hsa_circ_0001766, 5'-CCCATTCCTGTT GCCAAG-3' (forward) and 5'-TCCTCCTCCTCCTCCTCTTC-3' (reverse); hsa_circ_0032822, 5'-AGAAAGGCAGGAGCAG CTT-3' (forward) and 5'-TCCAGCTGACCACGATGA-3' (reverse); hsa_circ_0001470, 5'-TGCTCCAACAGGGGATGT-3' (forward) and 5'-CGTCTCATTCCACAAGCCT-3' (reverse); hsa_circ_0004390, 5'-CGGAGGACACCCATGAAG-3' (forward) and 5'-GGCAGAAAAACGTCCCAA-3' (reverse); hsa_circ_0104368, 5'-ATGGCGAATGTGGCTGAT-3' (forward) and 5'-TAGTTGACCCGAGCTGCC-3' (reverse); hsa_circSENP2, 5'-CCTCAACAGCTGAATGGGA-3' (forward) and 5'-CCCACATCTCCCCCTTCT-3' (reverse); hsa_circ_0008603, 5'-TCAAAGGTGGATTGGGGA-3' (forward) and 5'-CATCCAGCATGGTGAGCA-3' (reverse); VEGFA, 5'- AGGGCAGAATCATCACGAAGT-3' (forward) and 5'- AGGGTCTCGATTGGATGGCA-3' (reverse). miR-877-3p, 5'- TCCTCTTCTCCCTCCTCCCAG-3'. GAPDH, 5'-GGCCTCCAAGGAGTAAGACC-3' (forward) and 5'-AGGGG AGATTCAGTGTGGTG-3' (reverse). U6, 5'- CTCGCTTCGG CAGCACA-3' (forward) and 5'- AACGCTTCACGAATTT GCGT-3' (reverse)

RNase R Assay and Sanger Sequencing

After total RNAs were extracted, RNA solutions were treated with RNase R (20U/μl, Epicentre) and the treated RNAs were detected by qRT-PCR. RNase R could digest linear RNA molecules, but not circRNAs. So, the change of results of PCR could determine the circular structure of RNAs. Additionally, Sanger sequencing was performed to verify the sequence and head-to-tail splicing structure of circRNAs.

RNA Interference

Small interfering RNA (si-RNA) targeting hsa_circ_0001766 (5'GATTCTTCTAACA3') and an inhibitor targeting miR-877-3p (5'GGGAGGAGGGAG3') were constructed (Shanghai Asia-Vector Biotechnology Co., Ltd). Non-targeting control siRNA and inhibitor negative control were used as controls. Cells were transfected using Lipofectamine 3000 transfection reagent (Invitrogen, USA).

Cell Culture

OSCC cell lines SCC9 and SCC25 were obtained from Cell Bank of China. Cells were cultured in DMEM/F12 culture medium supplemented with 10% fetal bovine serum (FBS). HOK cells were purchased from BeNa Culture Collection and were grown in RPMI 1640 medium with 10% FBS. All cells were incubated at 37°C in a humidified atmosphere of 5% CO_2.

Western Blotting

SCC9 and SCC25 cells were collected and total protein was collected using RIPA lysis buffer. The following antibodies and reagents were used: anti-VEGFA (Abcam, ab46154), anti-GAPDH (Cell Signaling Technology, #5174), and anti-rabbit IgG (Cell Signaling Technology, #7074). Then, samples were subjected to western blot.

Cell Viability and Colony Formation Assays

Cell viability was tested using Cell Counting Kit-8 (CCK-8, Dojindo) assay according to the manufacturer's guidance. SCC9 and SCC25 cells were incubated in an incubator at 37°C for 0, 24, 48, 72, and 96 h. The cell viability was determined by the absorbance at 450 nm using a microplate reader (Bioteck, Epoch2). About 1,000 cells/well were plated in six-well plates. Cells were incubated for 2 weeks to form colonies. Then, cells were fixed with 4% paraformaldehyde and stained with 0.1% crystal violet. Visible colonies with more 50 cells were manually counted. The experiments were duplicated in three times.

Statistical Analysis

All data were analyzed using SPSS 19.0 (SPSS, Chicago, IL, USA). Data were represented as mean ± SD. The grouped t-test was used to compare between-group differences. All statistical tests employed a level of significance of $\alpha = 0.05$ at 95% confidence level.

RESULTS

CircRNA Expression Profile

We analyzed the circRNA expression profile in 6 pairs of samples of OSCC and normal oral mucosal tissues. A total of 21,505 DE

circRNAs were detected, including 16,420 upregulated and 5,085 downregulated circRNAs. One hundred and twenty-two DE circRNAs, among which 109 ones were upregulated and 13 ones were downregulated, fitted the standard (FC ≥ 2 and $P \geq 0.05$) and were considered statistically significant. The statistically significantly DE circRNAs are shown in a cluster heatmap (**Figure 1A**) and volcano plots (**Figure 1B**).

Among the 122 DE circRNAs, 12 circRNAs were identified for the first time as novel circRNAs. The other 110 circRNAs can be searched in the existing circRNA database (**Figure 1C**). The lengths of most of the 122 DE circRNAs were less than 2,000 nucleotides (**Figure 1D**). The 122 DE circRNAs were localized in all human chromosomes (**Figure 1E**). The circRNAs, based on the sequences, were categorized into 3 types, including exonic circRNAs consisting of only exonic sequences, intronic circRNAs consisting of only intronic sequences, and sense overlapping circRNAs consisting of both exonic and intronic sequences. Among the 122 DE circRNAs, there were 108 exonic circRNAs, 7 intronic circRNAs, and 7 sense-overlapping circRNAs (**Figure 1F**).

Validation for Top 10 DE CircRNAs

According to the fold changes, *P* values, and cancer-association of the DE circRNAs between the 6 pairs of samples of OSCC and normal oral mucosa tissues, we selected the top 10 DE circRNAs (7 upregulated and 3 downregulated) for validation in the same samples from 6 pairs of patients by qRT-PCR. The results suggested that 8 out of 10 circRNAs showed the same trends of expression changes significantly as the circRNA sequencing (**Figure 2**). Then, Sanger sequencing and RNase R assay were done. Two out of 10 circRNAs (hsa_circ_0005050 and hsa_circ_0001766) were identified as DE circRNAs. The biological features of the 2 validated circRNAs are summarized in **Table 1**.

Bioinformatics Analysis

GO and KEGG analyses were used to predict the role of DE circRNAs. We predicted the function of host genes by GO enrichment analysis, based on biological process, cellular components, and molecular function. Top annotation cluster terms (collective biological process, cellular components and molecular function) of upregulated and downregulated circRNAs are shown in **Figure 3**. In addition, possible functions of validated circRNAs are shown in **Table 2**.

KEGG pathway analysis was performed to elucidate the role of host genes of circRNAs in different pathways. Thirty pathways that were related to the functions of 30 DE circRNAs were found in the KEGG analysis. In the validated DE circRNAs, hsa_circ_0001470 was involved in transcriptional misregulation in cancer (hsa05202), whereas hsa_circ_0004390 was involved in pathways in cancer (hsa05200) and Rap1 signaling pathway (hsa04015), which have been reported to contribute to the regulation of tumorigenesis and tumor progression (**Figure 4**) (13).

Hsa_circ_0001766 Could Potentially Act as a ceRNA in OSCC

Considering the *P* values in the qRT-PCR results, hsa_circ_0001766 was chosen to carry out further research. CircRNAs could regulate the activities of miRNAs by miRNA sponging, thereby regulating gene expression. The binding relationship between hsa_circ_0001766 and miR-877-3p was predicted by TargetScan 7.0 and miRanda v3.3a, which showed that hsa_circ_0001766 might be a ceRNA of miR-877-3p. It has been reported that miR-877-3p targets VEGFA and negatively regulates VEGFA (14). Moreover, multiple studies have demonstrated the role of VEFGA in OSCC (15–18). Hence, we hypothesized that hsa_circ_0001766 sponged miR-877-3p to upregulate VEGFA expression.

Subsequently, we investigated the possible role of hsa_circ_0001766/miR-877-3p/VEGFA in OSCC. Compared with HOK cells, in OSCC cell lines SCC9 and SCC25, expressions of hsa_circ_0001766 and VEGFA mRNA were significantly upregulated (**Figures 5A, B**). Using qRT-PCR and western blotting, we identified the role and effect of hsa_circ_0001766 and miR-877-3p on VEGFA. While knockdown of hsa_circ_0001766 inhibited the expression of VEGFA, miR-877-3p inhibitor reversed this inhibitory effect of si-hsa_circ_0001766 on expression of VEGFA (**Figures 5C–F**). To elucidate the role of hsa_circ_0001766 on OSCC cell proliferation, CCK8 and colony formation assays were done (**Figure 6**). In SCC9 and SCC25 cell lines, knockdown of hsa_circ_0001766 suppressed cell proliferation. However, when SCC9 and SCC25 cells were treated with si-hsa_circ_0001766 plus miR-877-3p, the inhibitory effect of si-circ001766 on cell proliferation was inversed by underexpression of miR-877-3p. These findings indicated that hsa_circ_0001766 might act as a ceRNA in OSCC and play an important role in OSCC cell proliferation through the hsa_circ_0001766/miR-877-3p/VEGFA axis.

DISCUSSION

CircRNA is a new class of RNA, which is widely expressed in many animals. Since the publications on circRNAs by Memczak and Hansen in 2013 (3, 4), an increasing number of studies have found that circRNAs are involved in the pathogenesis of various human diseases. The functions of circRNA include protein binding, miRNA sponging, and promoting host gene expression and protein translation. In recent years, circRNAs have been shown to play an important role in the pathogenesis of cancer and could be potential biomarkers for this disease.

In this study, we investigated the circRNA expression profiles in 6 pairs of samples of OSCC and normal oral mucosal tissues. One hundred and twenty-two DE circRNAs, among which 109 were upregulated and 13 were downregulated, were considered statistically significant. We validated 8 circRNAs by qRT-PCR, which showed the same directions and statistical significance as the expression changes of the circRNA sequencing. Then, hsa_circ_0005050 and hsa_circ_0001766 were identified as DE circRNAs using Sanger sequencing and RNase R assay. Hsa_circ_0005050 is spliced from XPO1, which could regulate the nuclear export of cellular proteins. Hsa_circ_0005050 has been reported to be differential expressed in many cells and tissues, including platelets, brain, epidermal keratinocytes, and liver cancer cells (19–21). Hsa_circ_0001766 is derived from

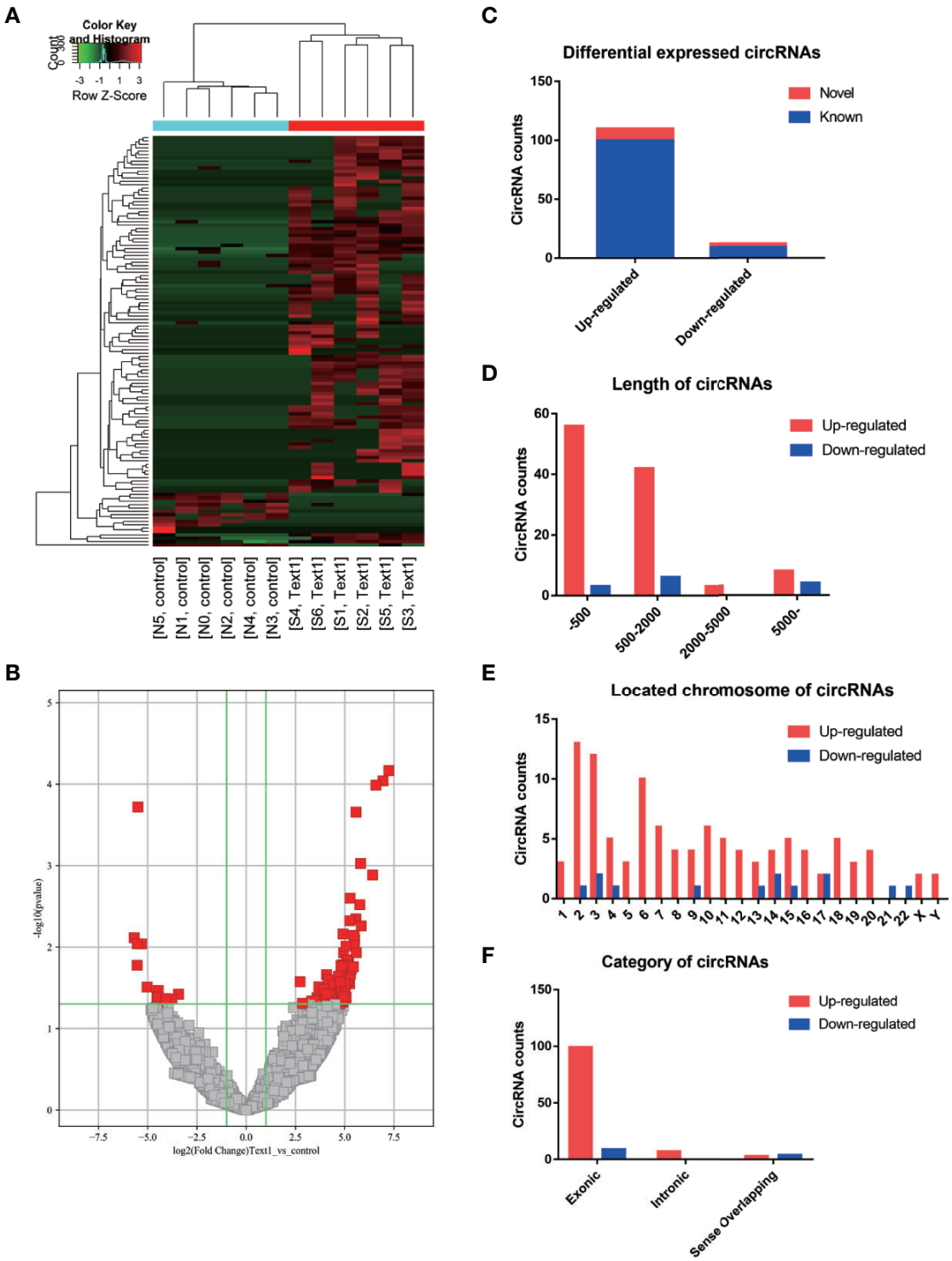

FIGURE 1 | Identification of DE circRNAs in OSCC. **(A)** The characteristics of statistically significantly DE circRNAs with heatmap. **(B)** The characteristics of statistically significantly DE circRNAs with volcano plots. **(C)** The number of statistically significantly DE circRNAs. **(D)** The length of statistically significantly DE circRNAs. **(E)** The chromosomal localization of statistically significantly DE circRNAs. **(F)** The category of statistically significantly DE circRNAs.

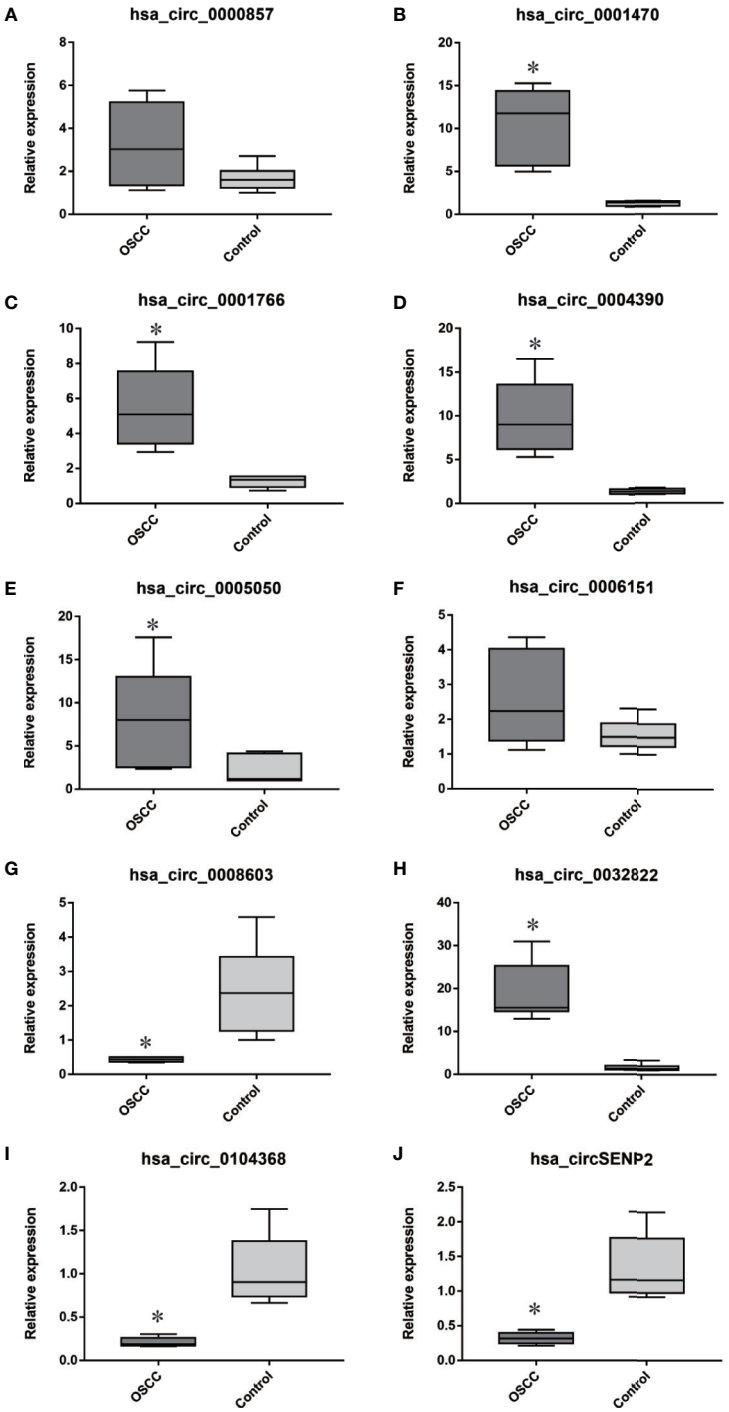

FIGURE 2 | Eight out of 10 circRNAs showed the same directions and statistical significance as the expression changes of the circRNA sequencing, using PCR (*$P < 0.05$). **(A–J)** Expression of hsa_circ_0000857, hsa_circ_0001470, hsa_circ_0001766, hsa_circ_0004390, hsa_circ_0005050, hsa_circ_0006151, hsa_circ_0008603, hsa_circ_0032822, hsa_circ_0104368, hsa_circSENP2 in OSCC tissues and normal oral mucosal tissues.

PDIA4, which encodes protein disulfide isomerase in the endoplasmic reticulum. To our knowledge, this is the first study to report that hsa_circ_0001766 is upregulated in OSCC. After taking the *P* values in the results of qRT-PCR into consideration, hsa_circ_0001766 was selected to explore further the role of circRNA in OSCC.

The results of GO enrichment analysis suggest that DE circRNAs participate in numerous biological processes. The

TABLE 1 | Biological features of validated circular RNAs (circRNAs).

CircRNA ID	GeneName	CircBase ID	Relative levels	P value	Category	Length
chr2:61712903-61717911-	XPO1	has_circ_0005050	3.921	0.031	Exonic	621
chr7:148716084-148718239-	PDI4	hashsa_circ_0001766	4.373	0.002	Exonic	387

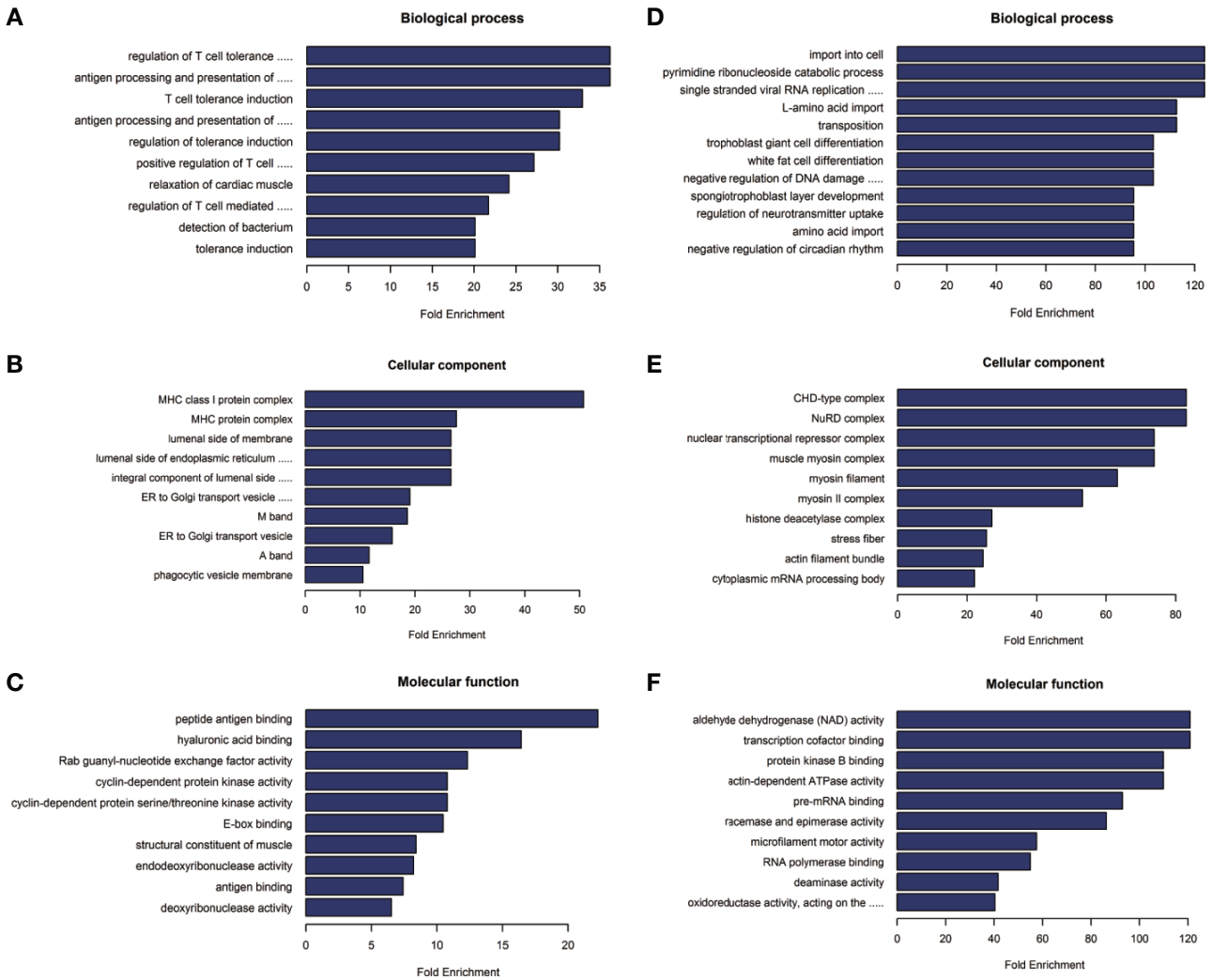

FIGURE 3 | **(A–C)** The top annotation cluster terms of upregulated circRNAs. **(D–F)** The top annotation cluster terms of downregulated circRNAs.

TABLE 2 | Biological processes of validated circRNAs.

circRNA ID	GO ID	GO terms
hsa_circ_0005050	GO:1901363;	Heterocyclic compound binding;
	GO:0097159;	Organic cyclic compound binding;
	GO:0005488;	Binding;
	GO:0003676;	Nucleic acid binding;
hsa_circ_0001766	GO:1901363;	Heterocyclic compound binding;
	GO:0097159;	Organic cyclic compound binding;
	GO:0005488;	Binding;
	GO:0003676;	Nucleic acid binding;

biological processes that upregulated circRNAs participate in include T cell tolerance induction, regulation of T cell tolerance induction, positive regulation of T cell-mediated cytotoxicity, and regulation of T cell-mediated immunity. Sun et al. (22) found that regulatory T cells are important components in the tumor microenvironment and play a role in local immune regulation. CD4+ T cells increased gradually with the progression of oral dysplasia in oral mucosa. This suggested that the local change to immunosuppressive cells had significant effects on progression of OSCC (22). Furthermore, it is reported that Gal3, that is highly expressed in OSCC, on one hand, is involved in negative selection of

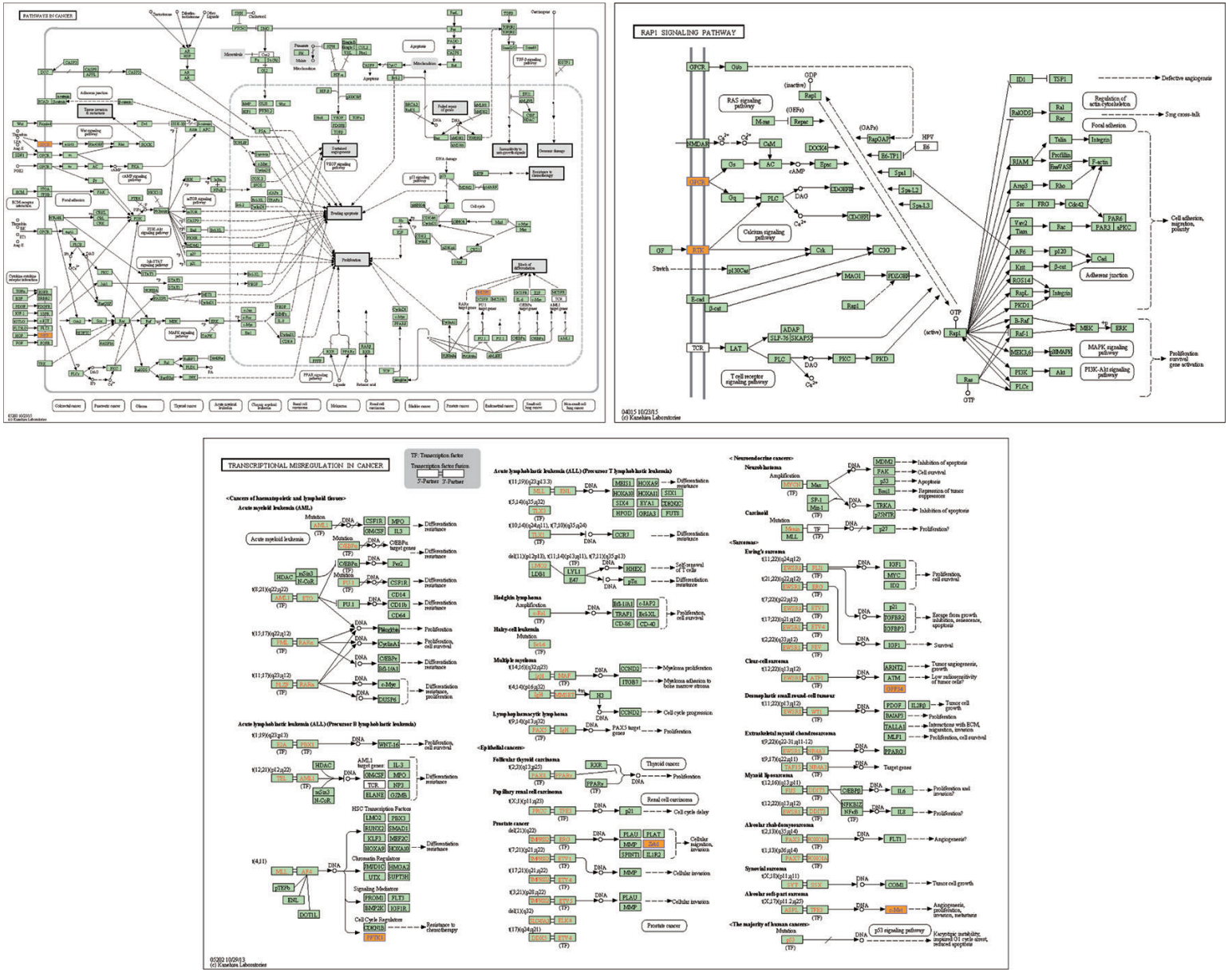

FIGURE 4 | Transcriptional misregulation in cancer (hsa05202), Rap1 signaling pathway (hsa04015), and pathways in cancer (hsa05200).

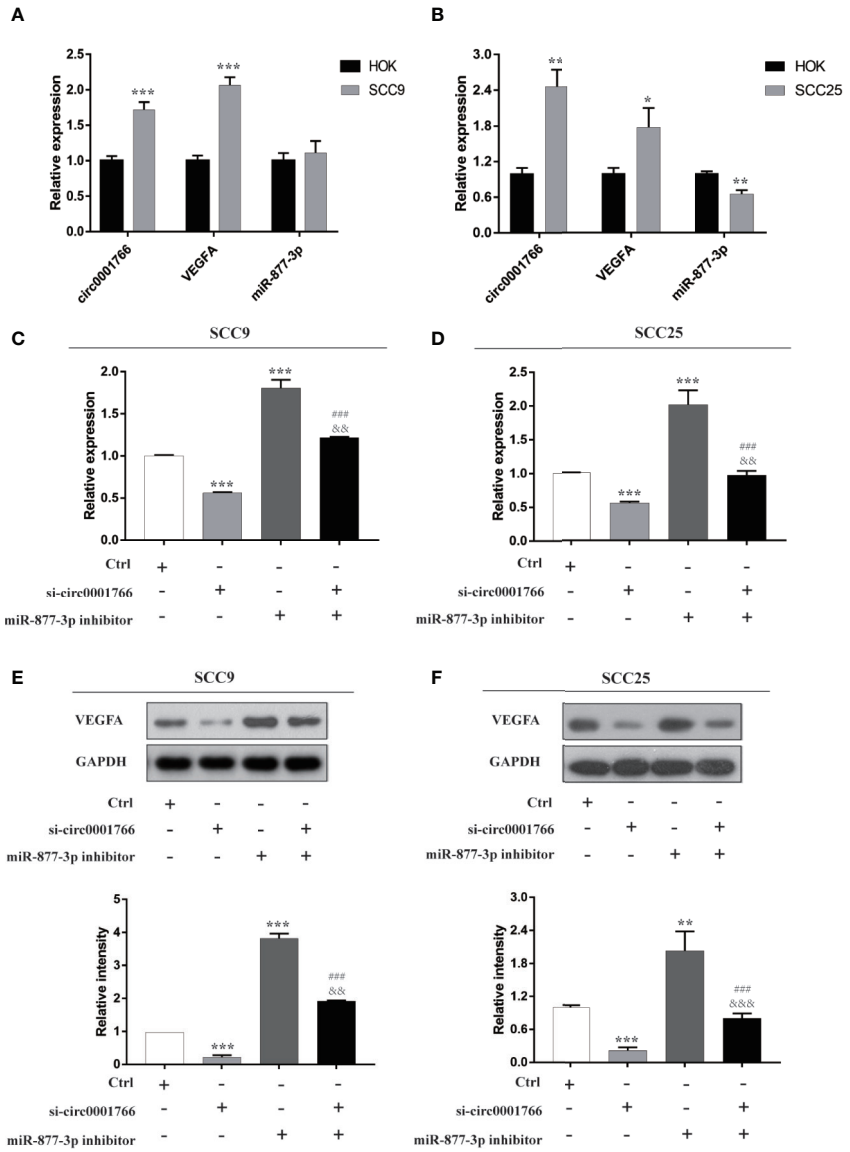

FIGURE 5 | miR-877-3p inhibitor reversed the inhibitory role of si-circ0001766 on expression of VEGFA in SCC9 and SCC25 cell lines. **(A, B)** circ0001766 and VEGFA were upregulated in SCC9 and SCC25. miR-877-3p was downregulated in SCC25. **(C–F)** Identification of the effects of si-circ0001766 and miR-877-3p on VEGFA in SCC9 and SCC25, using PCR and western blotting. * vs Ctrl $p < 0.05$; ** vs Ctrl $p < 0.01$; *** vs Ctrl $p < 0.001$; ### vs si-circ0001766 $p < 0.001$; && vs miR-877-3p inhibitor $p < 0.001$; &&& vs miR-877-3p inhibitor $p < 0.001$.

T cells during thymic T cell maturation and, thereby promotes central immune tolerance, and on the other hand, Gal3 can act as an immune checkpoint to inhibit T cell activation and thus promotes peripheral immune tolerance. Immune tolerance plays an important role in progression of OSCC (23). The biological processes that downregulated circRNAs participate in include regulation of neurotransmitter uptake and negative regulation of the circadian rhythm. The body clock has an effect on cells and tissues through endocrine and neurotransmitter regulation; the circadian rhythm plays an important role in the development of tumors, and in the therapeutic and side effects of anticancer drugs (24). These indicate that DE circRNAs may modulate the aforementioned biological processes to influence OSCC progression. The results of KEGG analysis suggested that hsa_circ_0001470 is involved in transcriptional deregulation in cancer, whereas hsa_circ_0004390 is involved in pathways in cancer and Rap1 signaling pathway, which have been reported to contribute to the regulation of tumorigenesis and tumor progression (13). This may perhaps explain the role of circRNAs in the pathogenesis of OSCC.

CircRNAs can regulate the activities of miRNAs by miRNA sponging and, thereby participate in the pathogenesis of cancer. In our study, binding relationships between circRNAs and miRNAs were predicted by TargetScan 7.0 and miRanda v3.3a. The results of

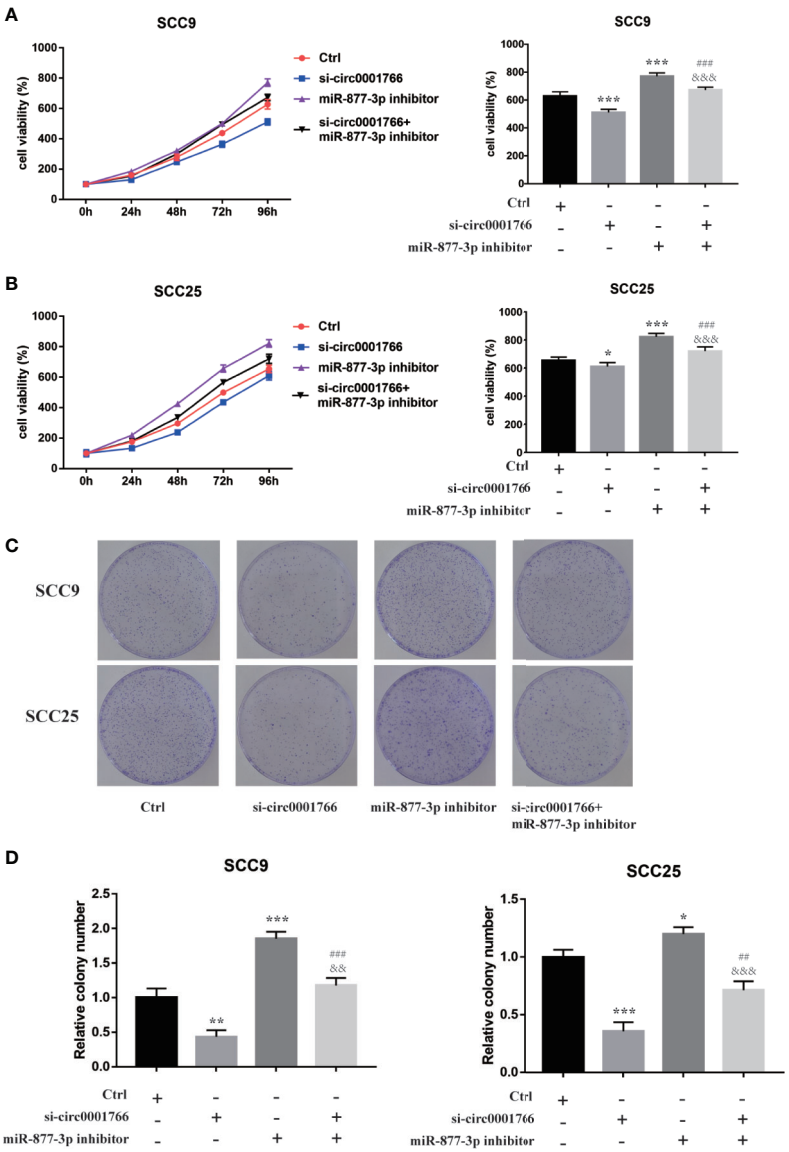

FIGURE 6 | miR-877-3p inhibitor reversed the inhibitory role of si-circ0001766 on expression of cell proliferation in SCC9 and SCC25 cell lines. **(A, B)** CCK assays revealed the effects of circ0001766 and miR-877-3p on cell proliferation in SCC25 and SCC25 cell lines. **(C, D)** Colony formation assay was used to evaluate cell viability after knocking down of circ0001766 and/or miR-877-3p. * vs Ctrl $p < 0.05$; ** vs Ctrl $p < 0.01$; *** vs Ctrl $p < 0.001$; $^{\#\#}$ vs si-circ0001766 $p < 0.01$; $^{\#\#\#}$ vs si-circ0001766 $p < 0.001$; $^{\&\&}$ vs miR-877-3p inhibitor $p < 0.001$; $^{\&\&\&}$ vs miR-877-3p inhibitor $p < 0.001$.

prediction showed that hsa_circ_0001766 might act as a ceRNA and targets miR-877-3p. It has been reported that miR-877-3p targets VEGFA and negatively regulates VEGFA (14). Positive expression of VEGFA was associated with significantly poor prognosis in OSCC (15, 16). VEGFA contributed to OSCC cell proliferation and tumor initiation (17, 18). In OSCC cell lines SSC9 and SCC25, hsa_circ_0001766 and VEGFA were upregulated. Subsequently, miR-877-3p inhibitor reversed the inhibitory effect of si-hsa_circ_0001766 on inhibition of VEGFA. We further investigated the role of hsa_circ_0001766 in OSCC cell proliferation. While knockdown of hsa_circ_0001766 suppressed cell proliferation, miR-877-3p inhibitor reversed the inhibitory effect of si-hsa_circ_0001766 on cell proliferation. These findings indicated hsa_circ_0001766 might act as a ceRNA in OSCC and played an important role in OSCC cell proliferation through the hsa_circ_0001766/miR-877-3p/VEGFA axis.

In conclusion, we have established that numerous circRNAs were dysregulated in OSCC and normal oral mucosal tissues in this study. Results of bioinformatics analysis implied that circRNAs were enriched in many cancer-related biological processes and might be involved in these pathways. However, this study has a few limits, such as limited numbers of patients and using normal tissues in the non-cancer patients as control. Then, we identified the potential role of the hsa_circ_0001766/miR-877-3p/VEGFA axis in OSCC cell

proliferation. Our study not only reveals the possible role of circRNAs in the progression of OSCC, but also provides a base for future research on elucidation of new biomarkers in OSCC.

DATA AVAILABILITY STATEMENT

The datasets generated for this study can be found in the GENE EXPRESSION OMNIBUS GSE131182.

ETHICS STATEMENT

The studies involving human participants were reviewed and approved by The Ethics Committee of Shanghai Ninth People's Hospital. The patients/participants provided their written informed consent to participate in this study.

AUTHOR CONTRIBUTIONS

HZ and SL conceived the study. YXS, YHS, and SX conducted the experiments, analyzed the data, and wrote the manuscript. All authors contributed to the article and approved the submitted version.

FUNDING

This research was supported by the National Key R&D Program of China (2017YFC0840100, 2017YFC0840110), National Construction Project of Clinical Key Specialized Department (2013) 544, Shanghai Science and Technology Commission (Grant No. 20151005), and Shanghai Health Development Planning Commission (Grant No. 201540257). We would like to appreciate all the staff of the Department of Oral Mucosal Diseases for supporting this study.

REFERENCES

1. Chi AC, Day TA, Neville BW. Oral cavity and oropharyngeal squamous cell carcinoma–an update. *CA Cancer J Clin* (2015) 65:401–21. doi: 10.3322/caac.21293
2. Guarnerio J, Bezzi M, Jeong JC, Paffenholz SV, Berry K, Naldini MM, et al. Oncogenic Role of Fusion-circRNAs Derived from Cancer-Associated Chromosomal Translocations. *Cell* (2016) 166:1055–6. doi: 10.1016/j.cell.2016.07.035
3. Memczak S, Jens M, Elefsinioti A, Torti F, Krueger J, Rybak A, et al. Circular RNAs are a large class of animal RNAs with regulatory potency. *Nature* (2013) 495:333–8. doi: 10.1038/nature11928
4. Hansen TB, Jensen TI, Clausen BH, Bramsen JB, Finsen B, Damgaard CK, et al. Natural RNA circles function as efficient microRNA sponges. *Nature* (2013) 495:384–8. doi: 10.1038/nature11993
5. Chen L, Zhang S, Wu J, Cui J, Zhong L, Zeng L, et al. circRNA_100290 plays a role in oral cancer by functioning as a sponge of the miR-29 family. *Oncogene* (2017) 36:4551–61. doi: 10.1038/onc.2017.89
6. Wang L, Wei Y, Yan Y, Wang Y, Yang J, Zheng Z, et al. CircDOCK1 suppresses cell apoptosis via inhibition of miR196a5p by targeting BIRC3 in OSCC. *Oncol Rep* (2018) 39:951–66. doi: 10.3892/or.2017.6174
7. Qiu X, Ke X, Ma H, Han L, Chen Q, Zhang S, et al. Profiling and bioinformatics analyses reveal differential expression of circular RNA in tongue cancer revealed by high-throughput sequencing. *J Cell Biochem* (2019) 120:4102–12. doi: 10.1002/jcb.27695
8. Wang Y, Li B, Sun S, Li X, Su W, Wang Z, et al. Circular RNA Expression in Oral Squamous Cell Carcinoma. *Front Oncol* (2018) 8:398:398. doi: 10.3389/fonc.2018.00398
9. Ouyang S, Wang J, Zhao S, Zhang X, Liao L. CircRNA_0109291 regulates cell growth and migration in oral squamous cell carcinoma and its clinical significance. *Iran J Basic Med Sci* (2018) 21:1186–91. doi: 10.22038/IJBMS.2018.30347.7313
10. Su W, Wang Y, Wang F, Zhang B, Zhang H, Shen Y, et al. Circular RNA hsa_circ_0007059 indicates prognosis and influences malignant behavior via AKT/mTOR in oral squamous cell carcinoma. *J Cell Physiol* (2019) 234:15156–66. doi: 10.1002/jcp.28156
11. Ju H, Zhang L, Mao L, Liu S, Xia W, Hu J, et al. Altered expression pattern of circular RNAs in metastatic oral mucosal melanoma. *Am J Cancer Res* (2018) 8:1788–1800. eCollection 2018.
12. Lu H, Han N, Xu W, Zhu Y, Liu L, Liu S, et al. Screening and bioinformatics analysis of mRNA, long non-coding RNA and circular RNA expression profiles in mucoepidermoid carcinoma of salivary gland. *Biochem Biophys Res Commun* (2019) 508:66–71. doi: 10.1016/j.bbrc.2018.11.102
13. Ishida D, Kometani K, Yang H, Kakugawa K, Masuda K, Iwai K, et al. Myeloproliferative stem cell disorders by deregulated Rap1 activation in SPA-1-deficient mice. *Cancer Cell* (2003) 4:55–65. doi: 10.1016/s1535-6108(03)00163-6
14. Lu J, Wang YH, Yoon C, Huang XY, Xu Y, Xie JW, et al. Circular RNA circ-RanGAP1 regulates VEGFA expression by targeting miR-877-3p to facilitate gastric cancer invasion and metastasis. *Cancer Lett* (2020) 471:38–48. doi: 10.1016/j.canlet.2019.11.038
15. Peterle GT, Maia LL, Trivilin LO, de Oliveira MM, Dos Santos JG, Mendes SO, et al. PAI-1, CAIX, and VEGFA expressions as prognosis markers in oral squamous cell carcinoma. *J Oral Pathol Med* (2018) 47:566–74. doi: 10.1111/jop.12721
16. Sales CB, Buim ME, de Souza RO, de Faro Valverde L, Mathias Machado MC, Reis MG, et al. Elevated VEGFA mRNA levels in oral squamous cell carcinomas and tumor margins: a preliminary study. *J Oral Pathol Med* (2016) 45:481–5. doi: 10.1111/jop.12398
17. Goel HL, Mercurio AM. VEGF targets the tumour cell. *Nat Rev Cancer* (2013) 13:871–82. doi: 10.1038/nrc3627
18. Gao P, Wang D, Liu M, Chen S, Yang Z, Zhang J, et al. DNA methylation-mediated repression of exosomal miR-652-5p expression promotes oesophageal squamous cell carcinoma aggressiveness by targeting PARG and VEGF pathways. *PloS Genet* (2020) 16:e1008592. doi: 10.1371/journal.pgen.1008592. Published 2020 Apr 28.
19. Salzman J, Chen RE, Olsen MN, Wang PL, Brown PO. Cell-type specific features of circular RNA expression. *PloS Genet* (2013) 9:e1003777. doi: 10.1371/journal.pgen.1003777
20. Rybak-Wolf A, Stottmeister C, Glažar P, Jens M, Pino N, Giusti S, et al. Circular RNAs in the Mammalian Brain Are Highly Abundant, Conserved, and Dynamically Expressed. *Mol Cell* (2015) 58:870–85. doi: 10.1016/j.molcel.2015.03.027
21. Maass PG, Glažar P, Memczak S, Dittmar G, Hollfinger I, Schreyer L, et al. A map of human circular RNAs in clinically relevant tissues. *J Mol Med (Berl)* (2017) 95:1179–89. doi: 10.1007/s00109-017-1582-9
22. Sun Y, Liu N, Guan X, Wu H, Sun Z, Zeng H. Immunosuppression Induced by Chronic Inflammation and the Progression to Oral Squamous Cell Carcinoma. *Mediators Inflamm* (2016) 2016:5715719. doi: 10.1155/2016/5715719
23. Wehrhan F, Büttner-Herold M, Distel L, Ries J, Moebius P, Preidl R, et al. Galectin 3 expression in regional lymph nodes and lymph node metastases of oral squamous cell carcinomas. *BMC Cancer* (2018) 18:823. doi: 10.1186/s12885-018-4726-6

24. Zhao N, Tang H, Yang K, Chen D. Circadian rhythm characteristics of oral squamous cell carcinoma growth in an orthotopic xenograft model. *Onco Targets Ther* (2013) 6:41–6. doi: 10.2147/OTT.S39955

Conflict of Interest: The authors declare that the research was conducted in the absence of any or financial relationships that could be construed as a potential conflict of interest.

Copyright © 2020 Shao, Song, Xu, Li and Zhou. This is an open-access article distributed under the terms of the Creative Commons Attribution License (CC BY). The use, distribution or reproduction in other forums is permitted, provided the original author(s) and the copyright owner(s) are credited and that the original publication in this journal is cited, in accordance with accepted academic practice. No use, distribution or reproduction is permitted which does not comply with these terms.

frontiers in Oncology

ORIGINAL RESEARCH
published: 27 November 2020
doi: 10.3389/fonc.2020.592415

Monocyte Chemoattractant Protein 1 Promotes VEGF-A Expression in OSCC by Activating ILK and MEK1/2 Signaling and Downregulating miR-29c

Ming-Yu Lien[1,2†], An-Chen Chang[3†], Hsiao-Chi Tsai[4†], Ming-Hsui Tsai[1,5], Chun-Hung Hua[5], Shih-Ping Cheng[4,6,7], Shih-Wei Wang[6,8] and Chih-Hsin Tang[1,9,10]*

[1] School of Medicine, China Medical University, Taichung, Taiwan, [2] Division of Hematology and Oncology, Department of Internal Medicine, China Medical University Hospital, Taichung, Taiwan, [3] Translational Medicine Center, Shin-Kong Wu Ho-Su Memorial Hospital, Taipei, Taiwan, [4] Department of Medical Research, MacKay Memorial Hospital, Taipei, Taiwan, [5] Department of Otolaryngology, China Medical University Hospital, Taichung, Taiwan, [6] Department of Medicine, Mackay Medical College, New Taipei, Taiwan, [7] Department of Surgery, MacKay Memorial Hospital, Taipei, Taiwan, [8] College of Pharmacy, Graduate Institute of Natural Products, Kaohsiung Medical University, Kaohsiung, Taiwan, [9] Department of Biotechnology, College of Health Science, Asia University, Taichung, Taiwan, [10] Chinese Medicine Research Center, China Medical University, Taichung, Taiwan

Oral squamous cell carcinoma (OSCC) is an aggressive tumor that has a poor prognosis, with high levels of local invasion and lymph node metastasis. Vascular endothelial growth factor A (VEGF-A) plays essential roles in OSCC tumor angiogenesis and metastasis. Monocyte chemoattractant protein-1 (MCP-1, CCL2) is implicated in various inflammatory conditions and pathological processes, including oral cancer. The existing evidence has failed to confirm any correlation between MCP-1 or VEGF-A expression and OSCC angiogenesis. In this study, high expression levels of MCP-1 and VEGF-A were positively correlated with disease stage in patients with OSCC. In oral cancer cells, MCP-1 increased VEGF-A expression and subsequently promoted angiogenesis; miR-29c mimic reversed MCP-1 activity. We also found that MCP-1 modulated VEGF-A expression and angiogenesis through CCR2/ILK/MEK1/2 signaling. *Ex vivo* results of the chick embryo chorioallantoic membrane (CAM) assay revealed the angiogenic qualities of MCP-1, with increased numbers of visible blood vessel branches. Our data suggest that MCP-1 is a new molecular therapeutic target for the inhibition of angiogenesis and metastasis in OSCC.

Keywords: monocyte chemoattractant protein-1, vascular endothelial growth factor A, miR-29c, oral squamous cell carcinoma, angiogenesis

OPEN ACCESS

Edited by:
Ming Yann Lim,
Tan Tock Seng Hospital, Singapore

Reviewed by:
Cheng-Chia Yu,
Chung Shan Medical University, Taiwan
Hong-Quan Duong,
Hanoi University of Public Health, Vietnam

***Correspondence:**
Chih-Hsin Tang
chtang@mail.cmu.edu.tw

†These authors have contributed equally to this work

Specialty section:
This article was submitted to Head and Neck Cancer, a section of the journal Frontiers in Oncology

Received: *07 August 2020*
Accepted: *21 October 2020*
Published: *27 November 2020*

Citation:
Lien M-Y, Chang A-C, Tsai H-C, Tsai M-H, Hua C-H, Cheng S-P, Wang S-W and Tang C-H (2020) Monocyte Chemoattractant Protein 1 Promotes VEGF-A Expression in OSCC by Activating ILK and MEK1/2 Signaling and Downregulating miR-29c. Front. Oncol. 10:592415. doi: 10.3389/fonc.2020.592415

INTRODUCTION

Oral squamous cell carcinoma (OSCC) is an aggressive oral epithelial neoplasm that has a low overall 5-year survival rate of 50–60% (1), largely because of the development of metastasis (2). Research has therefore tended to concentrate on therapeutic strategies that interrupt the metastatic process in advanced-stage OSCC (3). OSCC metastasis is a complex process that is largely driven by angiogenesis (4, 5). Few therapeutic options are available for OSCC patients with metastatic disease (4). The production of monocyte chemotactic protein-1 (MCP-1, also known as CCL2) in the tumor microenvironment is recognized as having a crucial role in the growth, dissemination, and metastasis of head and neck cancer (6). The importance of targeting MCP-1 in metastatic disease has been highlighted in experimental models (7). MCP-1 can accelerate breast cancer metastasis by promoting angiogenesis in a vascular endothelial growth factor (VEGF)-A-dependent manner (8). MCP-1 is also involved in the migration and invasion of a variety of different types of cancer cells, such as breast, prostate, glioblastoma, ovarian, bladder, and chondrosarcoma (7). Some evidence suggests that MCP-1 might be involved in the development of OSCC (4, 9), including inducing changes in epithelial-mesenchymal transition (EMT) markers *via* paracrine or autocrine signaling (3), but the exact mechanism remains unclear.

OSCC is characterized by genomic and epigenomic alterations (10), although the mechanisms of OSCC tumorigenesis remain unclear. MicroRNAs (miRNAs) are small, non-coding RNAs capable of regulating gene expression by binding to the 3′-untranslated region (UTR) of target genes (11, 12) and are implicated in the regulation of tumor metastasis due to their influence upon cancer cell proliferation, migration, and angiogenesis (13). Dysregulated miRNA expression has been considered to play a role in OSCC progression and metastasis (14), but it remains to be explained as to how miRNAs mediate MCP-1–mediated VEGF-A expression in OSCC.

In this study, we demonstrate that MCP-1 promotes VEGF-A expression in OSCC by activating integrin-linked kinase (ILK) and MEK1/2 signaling and downregulating miR-29c expression, all of which subsequently enhances VEGF-A-induced tumor angiogenesis.

MATERIALS AND METHODS

Materials

Human recombinant monocyte chemoattractant protein 1 (MCP-1) protein was purchased from PeproTech (Rocky Hill, NJ, USA). Anti-rabbit and anti-mouse IgG-conjugated horseradish peroxidase, rabbit polyclonal antibodies (specific for p-GSK3β (Santa Cruz sc-135653) and GSK3β (Santa Cruz sc-9166)), and mouse monoclonal antibodies (specific for VEGF-A (Santa Cruz sc-7269), β-actin (Santa sc-47778), MCP-1 (Santa Cruz sc-32771), ILK (Santa Cruz sc-20019), p-MEK1/2 (Santa Cruz sc-271914), MEK1/2 (Santa Cruz sc-6250), p-ERK1/2 (Santa Cruz sc-7383), and ERK1/2 (Santa Cruz sc-1647)) were purchased from Santa Cruz Biotechnology (Santa Cruz, CA, USA). The control miRNA and miR-29c mimic were purchased from Life Technologies (Carlsbad, CA, USA). Lipofectamine 2000 was purchased from Invitrogen (Carlsbad, CA, USA). All other chemicals were purchased from Sigma-Aldrich (St. Louis, MO, USA).

Cell Culture

The human OSCC cell line used in this study was SCC4, and was purchased from the Bioresource Collection and Research Center (BCRC) (Hsinchu, Taiwan). Cells were cultured in 10% DMEM+F-12 medium and maintained at 37°C in a humidified atmosphere of 5% CO_2. Human endothelial progenitor cells (EPCs) were provided by Dr. Wang Shih Wei. The EPCs were seeded onto 1% gelatin-coated plasticware and grown in endothelial cell growth medium MV2 with 20% FBS at 37°C in an atmosphere of 5% CO_2.

Immunohistochemical (IHC) Staining

Before proceeding with the staining protocol, the tissue array sections were deparaffinized and hydrated in xylene and graded ethanol solutions in distilled water. IHC analysis was performed according to the conditions of our previous protocol (15). Human MCP-1 or VEGF-A antibody was applied at 4°C overnight. The results were scored by accounting for the percentage of positive detection and intensity of the staining. Quantitative data were obtained using ImageJ software.

Western Blot Analysis

After washing the cell culture dish with PBS, we added ice-cold RIPA lysis buffer containing protease inhibitors to lysate the cells. SDS-PAGE gels were used to separate protein samples, which were transferred to PVDF membranes according to our previously described methodology (15).

ILK Kinase Activity Assay

ILK kinase activity was analyzed with Nonidet P-40 (NP-40) lysis buffer (16) and a GSK-3β phosphorylation assay was performed by Western blot analysis, as previously reported (17). Western blot visualized the phosphorylation of GSK-3β. Anti-ILK was used as a loading control.

Quantitative Real-Time PCR

Quantitative real-time PCR was performed using the StepOnePlus™ sequence detection system, under the established protocol (18–20). VEGF-A primer sequences used were forward 5'-GCAGAATCAT CACGAAGTGG-3' and reverse 5'-GCATGGTGATGTTG GACTCC-3'. The Mir-X™ miRNA First-Strand Synthesis and SYBR® qRT-PCR kits detected miRNA expression. The specific primer sequence for miR-29c was 5'-TAGCACCATTTGA AATCGGTTA-3'. GAPDH or U6 snRNA expression level was used as the endogenous control for normalization purposes.

ELISA

Cells were seeded in 6-well plates for 24 h and then the culture medium (CM) was changed to serum-free medium. Some cells were left untreated (controls), while others were treated only with MCP-1 for 24 h. Other cells were treated with pharmacological inhibitors or transfected with miRNA mimic for 30 min, then with MCP-1 for 24 h. The CM was then collected from all cells and

VEGF-A concentrations were detected using the human VEGF-A/VEGF Quantikine ELISA kit (R&D Systems, MN, USA), according to the manufacturer's protocol.

Tube Formation Assay

The 48-well plates were coated with Matrigel (100 µl/well) before use. EPC cells (1×10^4) were seeded into each well in 50% MV2 medium and 50% CM, then incubated for 16 h at 37°C. Quantitative data were obtained using ImageJ software.

Migration Assay

The migration assay was performed in a 24-well Transwell cell culture chamber with 8.0-µm pore size inserts. EPCs (2×10^4) were seeded onto the upper chamber and incubated in the lower chamber with 50% MV2 medium and 50% CM at 37°C in 5% CO_2 for 24 h. Migratory ability was assayed using the procedure described in our previous publication (15).

Luciferase Activity Assay

Cells were seeded onto 24-well plates and transiently transfected with wild-type- or mutant-type-VEGF-A 3'-UTR luciferase plasmids. Luciferase activity was assayed using our previously described procedure (21).

Chick Chorioallantoic Membrane (CAM) Assay

The CAM assay detected the influence of MCP-1 on angiogenesis. We used 10-day-old fertilized chick embryos, with minor modifications from the procedures described in our previous study (15). The eggs were incubated in a humidified atmosphere of 80–90% at 38°C for 7 days. An approximate 1-cm opening was created in the air sac of each egg, into which 50 µl of CM (suspended in 50 µl Matrigel) was added, before the shells were covered with adhesive tape and the eggs were incubated for a further 72 h. Chorioallantoic membranes were collected for microscopy and photographic documentation. We manually counted the numbers of blood vessel branches within the defined area of the membrane, to form the angiogenic index.

Statistical Analysis

Data are expressed as the mean ± SD. Between-group differences were analyzed using the Student's *t*-test of variance and one-way analysis of variance (ANOVA) was used to compare means between two or more groups. The difference was considered significant if the *p* value was less than 0.05. Each experimental procedure was independently repeated three times, with similar results.

RESULTS

Clinical Significance of MCP-1 Expression in Oral Squamous Cell Carcinoma

Previous research has demonstrated that VEGF-A and angiopoietin 2 (ANGPT2) are critical players in tumor angiogenesis, while VEGF-A has been considered the primary factor driving the expansion of the tumor angiogenesis (22, 23). To confirm the clinical significance of MCP-1 in OSCC angiogenesis, we obtained data from the Oncomine database, which contains 65 gene chip datasets, 4700 chips, and 480 million gene expression data (24, 25). We found higher levels of MCP-1, VEGF-A, and ANGPT2 expression in tissue from OSCC patients compared with normal healthy controls (**Figures 1A–C**). Furthermore, IHC staining demonstrated that higher MCP-1 and VEGF-A expression correlated with higher clinical disease stage (**Figures 1D–F**). These findings suggest that MCP-1 has an important role in OSCC progression.

MCP-1 Promotes Angiogenesis in Human OSCC Cells *via* VEGF-A-Dependent Signaling

We sought to determine whether MCP-1–induced angiogenesis of OSCC cells involves VEGF-A signaling. As shown in **Figures 2A-C**, incubation of SCC4 cells with human recombinant MCP-1 significantly increased VEGF-A mRNA expression and protein secretion. We found that incubation of EPCs with CM from MCP-1–treated OSCC cells promoted EPC tube formation and migration; these activities were abolished when 5 µg/ml of VEGF-A monoclonal antibody (mAb) was added (**Figures 2D, E**). These results confirmed that MCP-1 promotes angiogenesis through the VEGF-A-dependent pathway.

MCP-1 Promotes VEGF-A Expression and Angiogenesis *via* the CCR2 Receptor

Targeting MCP-1/CCR2 signaling may alter the tumor microenvironment and enhance angiogenesis in cancer (26, 27). We therefore used RS102895, a potent CCR2 antagonist, to evaluate whether MCP-1–induced stimulation of VEGF-A expression and angiogenesis is influenced by CCR2. RS102895 treatment significantly reduced protein and mRNA expression levels (**Figures 3A–C**). RS102895 also significantly inhibited EPC tube formation and migration (**Figures 3D, E**). The CCR2 receptor therefore plays an important role in MCP-1–induced stimulation of VEGF-A expression and angiogenesis.

The ILK/MEK1/2 Signaling Pathway Is Involved in MCP-1–Induced VEGF-A Expression and Angiogenesis

ILK is considered to be crucial for tumor angiogenesis (28). The GSK-3 crosstide peptide is a substrate of ILK, and phosphorylation of GSK-3β is regulated by ILK in many cells (29). Here, we found that MCP-1 promotes ILK kinase activity by promoting the phosphorylation of GSK-3β (**Figure 4A**) and mitogen-activated protein kinase kinase (MEK 1/2) in a time-dependent manner (**Figure 4B**). In addition, the phosphorylation of extracellular signal-regulated protein kinase (ERK1/2) was also promoted in a time-dependent manner (**Figure 4B**). Pretreatment with KP-392 (a potent and selective inhibitor of ILK) or PD98059 (a potent and selective inhibitor of MEK1/2) significantly reduced MCP-1–induced increases in VEGF-A expression (**Figures 4C, D**), as well as EPC tube formation and migration (**Figures 4E, F**). These results indicate that MCP-1 promotes VEGF-A expression and angiogenesis in OSCC cells through ILK and MEK1/2 signaling.

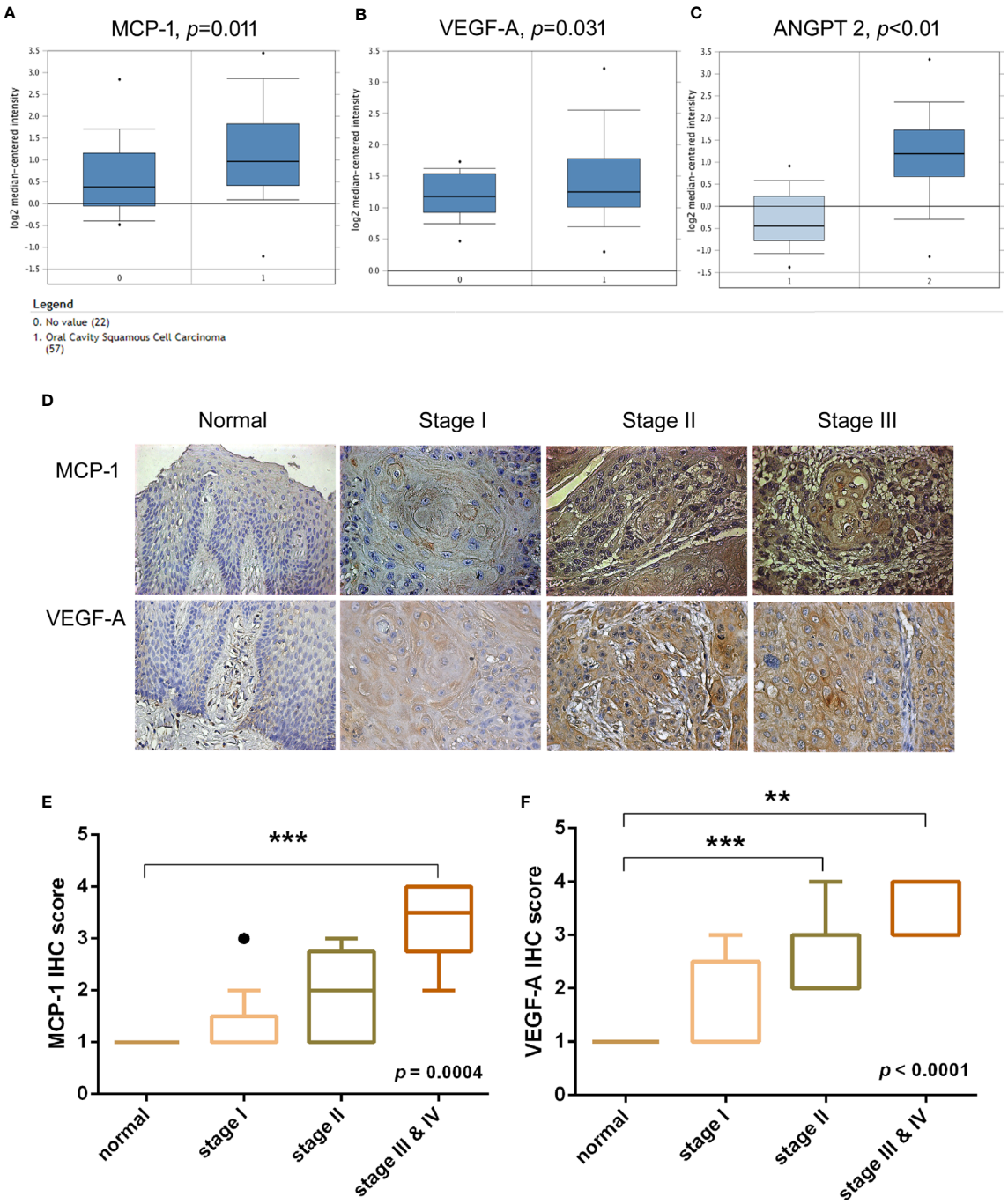

FIGURE 1 | Clinical significance of MCP-1 in angiogenesis of oral squamous cell carcinoma. **(A–C)** OSCC tissue and adjacent normal tissue data from the Oncomine database (https://www.oncomine.org) were analyzed for MCP-1, VEGF-A, and ANGPT2 expression. **(D)** IHC photographs of tissue array sections (OR601) immunostained with anti-MCP-1 or anti-VEGF-A antibody. **(E, F)** IHC results were scored on a scale of 1–5 for staining intensity. Levels of MCP-1 and VEGF-A expression correlated with OSCC clinical grade. $^{**}p < 0.005$, $^{***}p < 0.0005$ compared with controls. **(A–C, E)** are box-and-whisker plots that plot outliers as individual points (dots).

MiR-29c Is a Key miRNA in MCP-1–Promoted VEGF-A Expression and Angiogenesis

We used open-source miRNA prediction software (miRanda, DIANA Tools, TargetScan, and miRDB) to identify 13 candidate miRNAs that target VEGF-A mRNA (**Figure 5A**). Of all miRNAs, miR-29c was the most downregulated after MCP-1 treatment (**Figure 5B**). Exogenous MCP-1 dose-dependently and significantly inhibited miR-29c expression (**Figure 5C**). Transfection of cells with miR-29c mimic reduced the ability

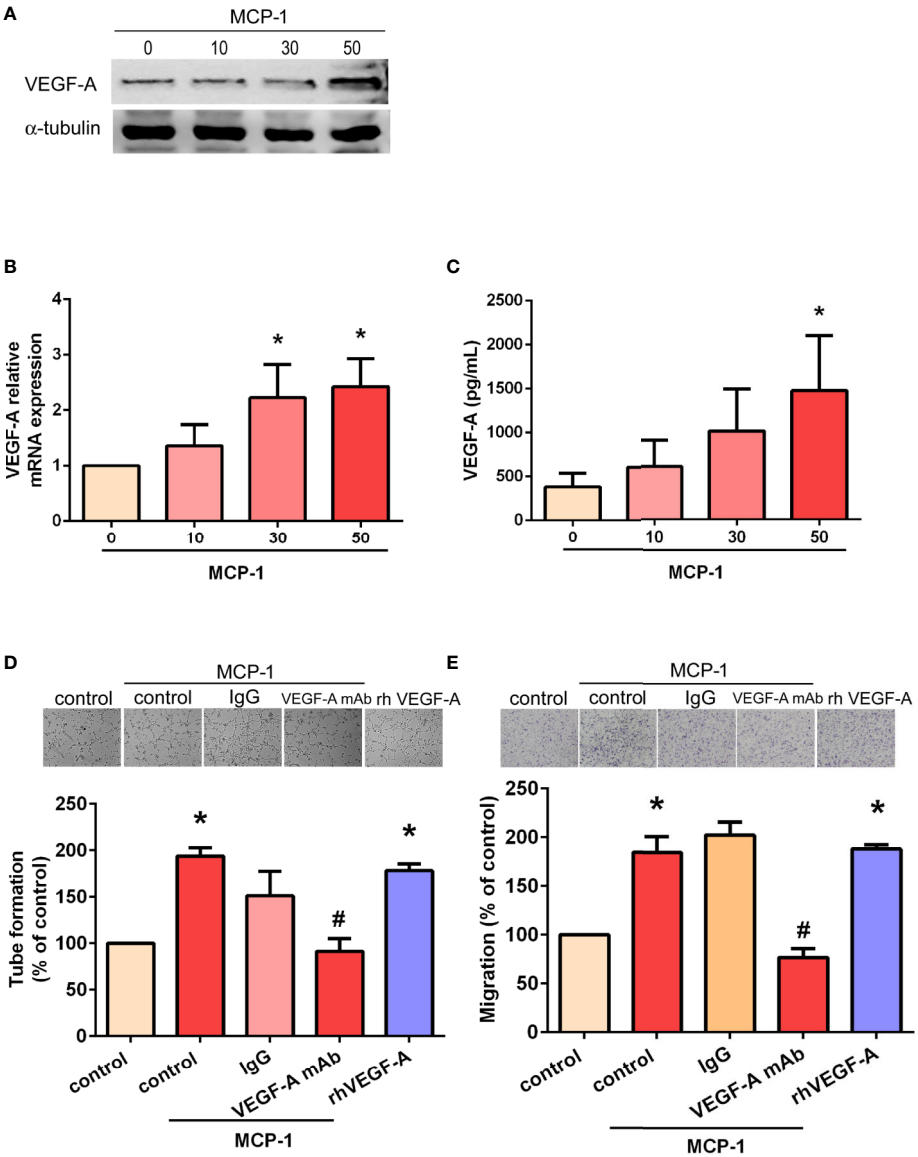

FIGURE 2 | MCP-1 promotes human OSCC cell angiogenesis through the VEGF-A-dependent pathway. Cells were incubated with MCP-1 (0–50 ng/ml) for 24 h and VEGF-A expression was determined by Western blot **(A)**, RT-qPCR **(B)**, and ELISA assays **(C)**. The CM was collected and used to treat the EPCs for 24 h. We used the tube formation assay to examine capillary-like structure formation **(D)** and the Transwell assay to examine cell migration **(E)**. $^{*}p < 0.05$ compared with controls; $^{\#}p < 0.05$ compared with MCP-1–treated controls. Each experimental procedure was independently repeated three times, with similar results.

of MCP-1 to enhance VEGF-A expression (**Figure 5D**), EPC tube formation (**Figure 5E**) and EPC migration (**Figure 5F**). CCR2/ILK/MEK1/2 signaling was involved in the effects of MCP-1 on miR-29c expression (**Figure 5G**). To confirm that miR-29c directly binds to the 3'-UTR of VEGF-A and inhibits VEGF-A mRNA translation, we constructed wild- and mutant-type luciferase reporter vectors harboring VEGF-A 3'-UTR (**Figure 5H**), then transfected these vectors into OSCC cells. We found that MCP-1 increased luciferase activity in the wild-type plasmid *via* CCR2, ILK, and MEK1/2 signaling, but no such effect was observed with the mutant-type plasmid (**Figure 5I**). When we examined tumor samples from the TCGA database, we found much lower levels of miR-29c expression in oral cancer tissue than in adjacent normal tissue (**Figure 5J**). These data indicate that miR-29c suppresses VEGF-A protein expression by binding to the 3′-UTR of the human *VEGF-A* gene *via* CCR2/ILK/MEK1/2 signaling.

Effects of MCP-1 on VEGF-A-Induced Angiogenesis in the CAM Model

We used the CAM assay to characterize the effect of MCP-1 on VEGF-A-induced angiogenesis. As illustrated in **Figures 6A, B**, we

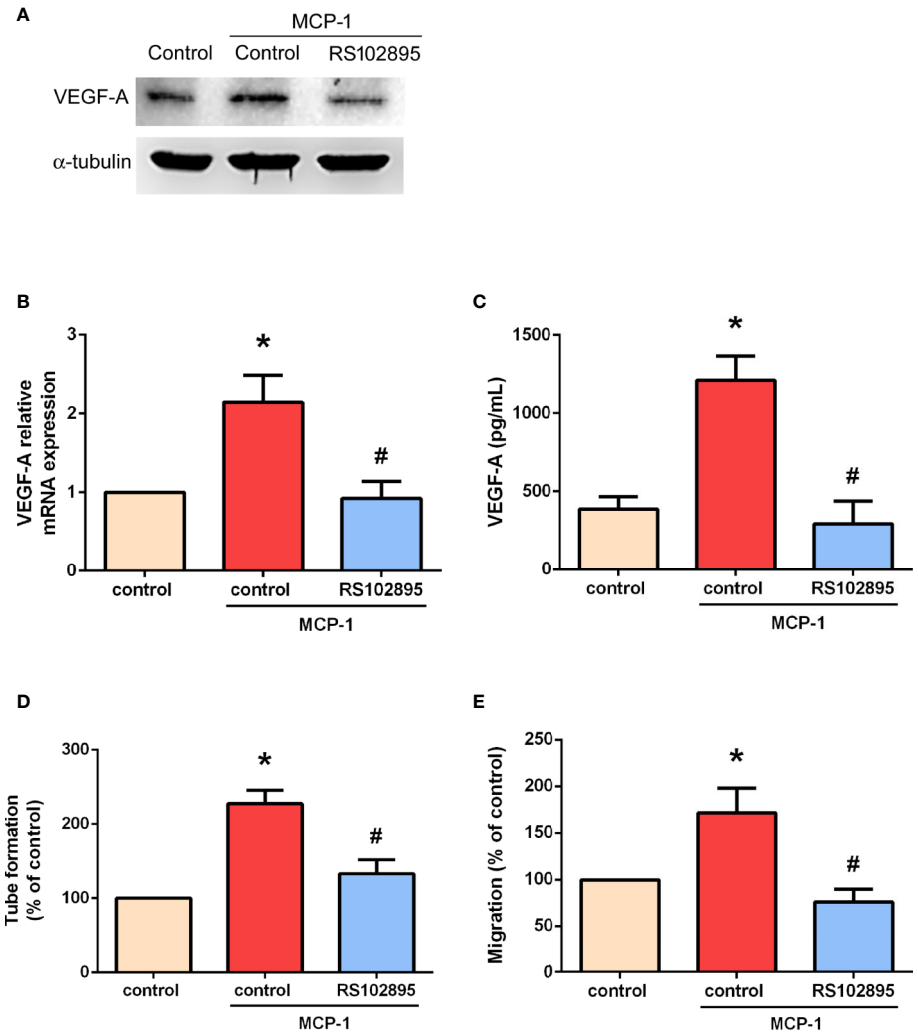

FIGURE 3 | MCP-1 promotes VEGF-A expression and angiogenesis *via* the CCR2 receptor. Cells were treated with a CCR2 antagonist (RS102895; 100 ng/ml) for 30 min and then stimulated with MCP-1 (50 ng/ml) for 24 h. VEGF-A expression was measured by Western blot **(A)**, RT-qPCR **(B)**, and ELISA assays **(C)**. Cells were treated with RS102895 (100 ng/ml) for 30 min and then stimulated with MCP-1 (50 ng/ml) for 24 h, then CM was collected. After treating the EPCs with CM for 24 h, capillary-like structure formation was examined using the tube formation assay **(D)** and cell migration was examined with the Transwell assay **(E)**. $^{*}p < 0.05$ compared with controls; $^{\#}p < 0.05$ compared with MCP-1–treated controls. Each experimental procedure was independently repeated three times, with similar results.

found that the CM collected from MCP-1–treated OSCC cells enhanced the number of blood vessel branches compared with untreated cells, whereas MCP-1–enhanced blood vessel growth was significantly reduced in cells pretreated with VEGF-A mAb. These results indicate that MCP-1 promotes angiogenesis *ex vivo*.

DISCUSSION

Angiogenesis is a critical feature of OSCC progression (30). Some evidence suggests the involvement of MCP-1 in the development of OSCC (4, 9), including the induction of epithelial-mesenchymal transition (3), although the exact mechanisms remain unclear. Our study evidence indicates that MCP-1 is an important player in OSCC angiogenesis, as we observed a correlation between higher levels of MCP-1 expression and OSCC disease status.

Dysregulation of chemokine or chemokine receptors has been linked to many diseases, especially those associated with cancer (31). In various human tissues, MCP-1 preferentially binds to the CCR2 receptor and has been implicated in the promotion of metastasis (27). Here, we found that inhibiting CCR2 functioning dramatically suppressed VEGF-A-induced angiogenesis. The ILK kinase is considered to be an important regulator in many key biological processes and is known to enhance OSCC tumorigenesis (32, 33). Knockdown of ILK reportedly inhibits OSCC proliferation, invasion and metastasis of xenograft tumors *in vivo* (34). In this study, we identified a new function of ILK in OSCC, namely, its regulation of MCP-1–mediated VEGF-A-associated angiogenesis.

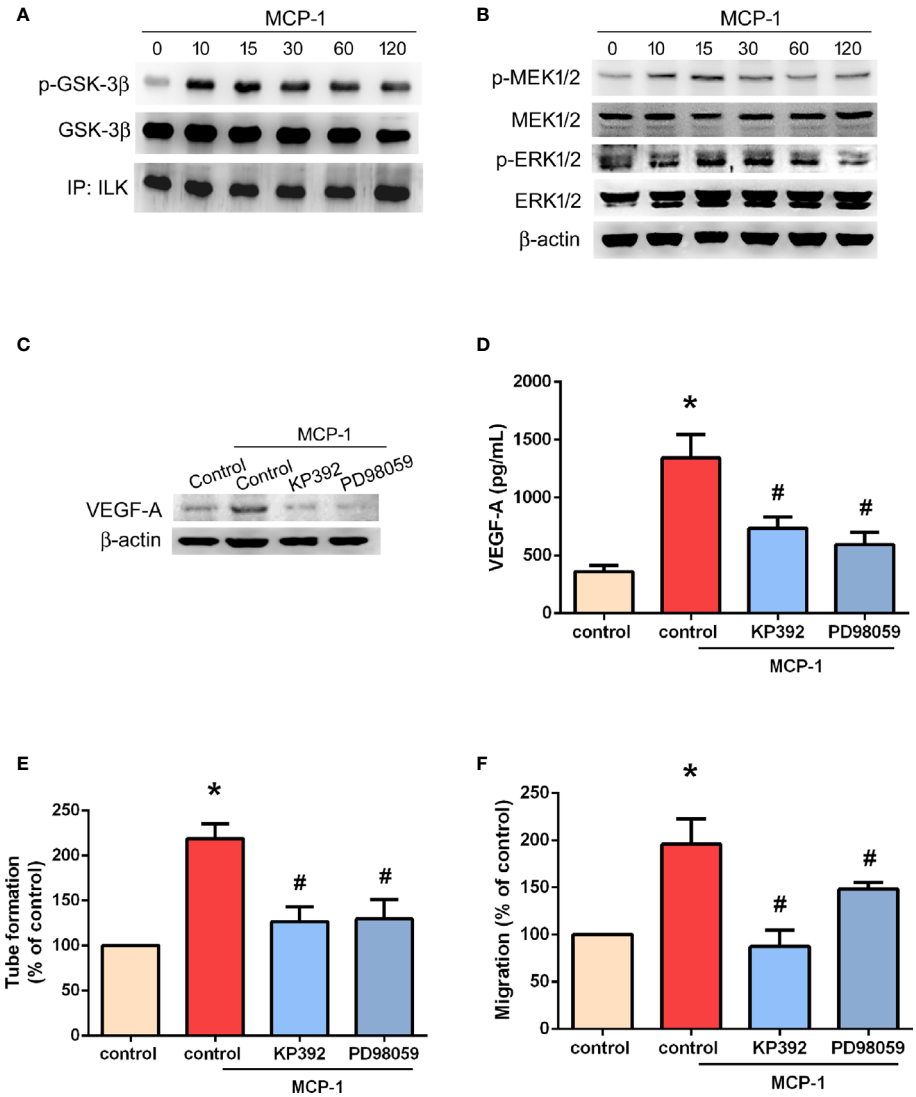

FIGURE 4 | ILK/MEK1/2 signaling is involved in MCP-1–induced VEGF-A expression and angiogenesis. Cells were incubated with MCP-1 (50 ng/ml) for the indicated time intervals; **(A)** Cell lysates were immunoprecipitated (IP) with ILK antibodies prior to Western blotting using p-GSK-3β, GSK-3β, and ILK antibodies. **(B)** MEK1/2, and ERK1/2 activation was examined by the Western blot assay. **(C, D)** Cells were treated with an ILK inhibitor (KP392; 10 μM) or MEK1/2 inhibitor (PD98059; 10 μM) for 30 min, then stimulated with MCP-1 (50 ng/ml) for 24 h. VEGF-A expression was measured by Western blot and ELISA assays. **(E, F)** Cells were treated with a KP392 (10 μM) or PD98059 (10 μM) for 30 min, then stimulated with MCP-1 (50 ng/ml) for 24 h. CM was applied to EPCs for 24 h, then capillary-like structure formation was examined by the tube formation assay **(E)** and cell migration by the Transwell assay **(F)**. $^{*}p < 0.05$ compared with controls; $^{\#}p < 0.05$ compared with MCP-1–treated controls. Each experimental procedure was independently repeated three times, with similar results.

MEK1/2 has been shown to regulate the development and progression of cancer-associated angiogenesis (35, 36). The function of MEK1/2 in OSCC mostly involves cancer proliferation, chemoresistance, and invasion/migration (37–39). Here, we report that MEK1/2 inhibitors antagonized MCP-1–induced VEGF-A expression. Incubation of OSCC cells with MCP-1 promoted, ILK and MEK1/2 phosphorylation, suggesting that their activation plays a crucial role in MCP-1–stimulated VEGF-A production and angiogenesis in OSCC cells.

Evidence of significant downregulation of miR-29c in many cancers suggests that miR-29c acts as a suppressor miRNA in these diseases (40, 41). In laryngeal squamous cell carcinoma, significant correlations have been observed between decreased miR-29c expression and the smoking index, tumor size, tumor site, tumor differentiation, T classification, TNM stage of laryngeal squamous cell carcinoma, and lymph node metastasis (42). Interestingly, miR-29c appears to contribute to a paracrine cross-talk mechanism between cancer-secreted insulin-like growth factor 2 (IGF2) and VEGF expression in cancer-associated fibroblasts (CAFs), with evidence indicating that higher IGF2 expression in cancer cells combined with increased VEGF expression in CAFs is associated with an unfavorable prognosis in esophageal squamous cell

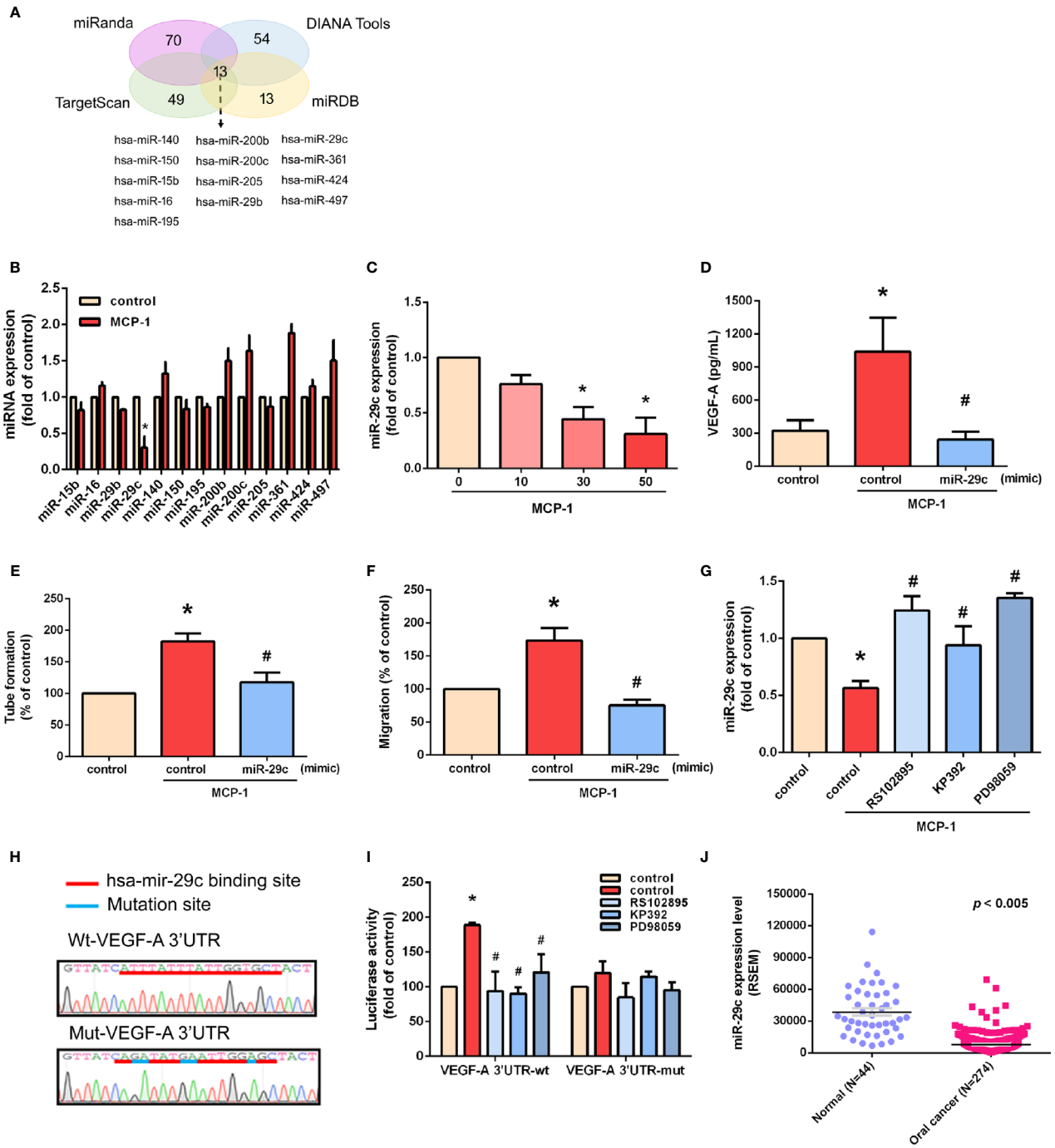

FIGURE 5 | miR-29c is a key miRNA in MCP-1–induced stimulation of VEGF-A expression and angiogenesis. **(A)** MiRNA target prediction program software was used to identify miRNAs that potentially bind to the VEGF-A 3'-UTR. **(B)** Cells were incubated with MCP-1 for 24 h and expression levels of the indicated miRNAs were subjected to qPCR analysis. **(C)** Cells were incubated with MCP-1 (0–50 ng/ml) for 24 h and miR-29c expression was determined by qPCR. **(D)** Cells were transfected with miR-29c mimic (10 nM) then incubated with MCP-1 for 24 h. VEGF-A expression was measured by ELISA. **(E, F)** CM was applied to EPCs for 24 h then capillary-like structure formation was examined by the tube formation assay and cell migration by the Transwell assay. **(G)** Cells were treated for 30 min with RS102895 (100 ng/ml), KP392 (10 μM), or PD98059 (10 μM) then incubated with MCP-1 for 24 h. miR-29c expression was examined by qPCR analysis. **(H)** The wild-type or mutant VEGF-A 3'-UTRs containing the miR-29c binding site was inserted into the pmirGLO vector. **(I)** Cells were transfected with wt-VEGF-A-3'-UTR or mut-VEGF-A-3'-UTR plasmid for 24 h, then stimulated for 30 min with RS102895 (100 ng/ml), KP392 (10 μM), or PD98059 (10 μM), followed by MCP-1 treatment for 24 h; luciferase activities were measured. **(J)** TCGA database records were analyzed for levels of miR-29c expression in tumor tissue and adjacent normal tissue. $^{*}p < 0.05$ compared with controls; $^{\#}p < 0.05$ compared with MCP-1–treated controls. Each experimental procedure was independently repeated three times, with similar results.

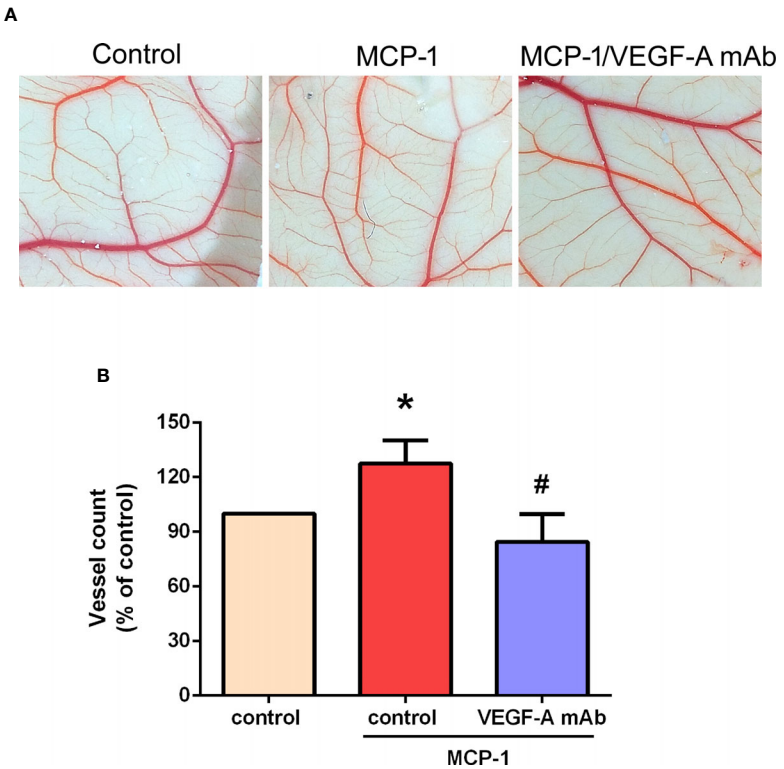

FIGURE 6 | Effects of MCP-1 on VEGF-A-induced angiogenesis in the CAM model. **(A)** Cells were incubated with or without MCP-1 (50 ng/ml) for 24 h, or treated for 30 min with VEGF-A antibody (5 μg/ml) followed by MCP-1 (50 ng/ml) for 24 h. CM was collected and suspended in Matrigel, then incubated with chick embryos (n=5 in each group) for another 72 h. Chorioallantoic membranes were collected for microscopy and photographic documentation. **(B)** Angiogenesis was quantified by manually counting the number of blood vessel branches. $^{*}p < 0.05$ compared with controls; $^{\#}p < 0.05$ compared with MCP-1–treated controls. Each experimental procedure was independently repeated three times, with similar results.

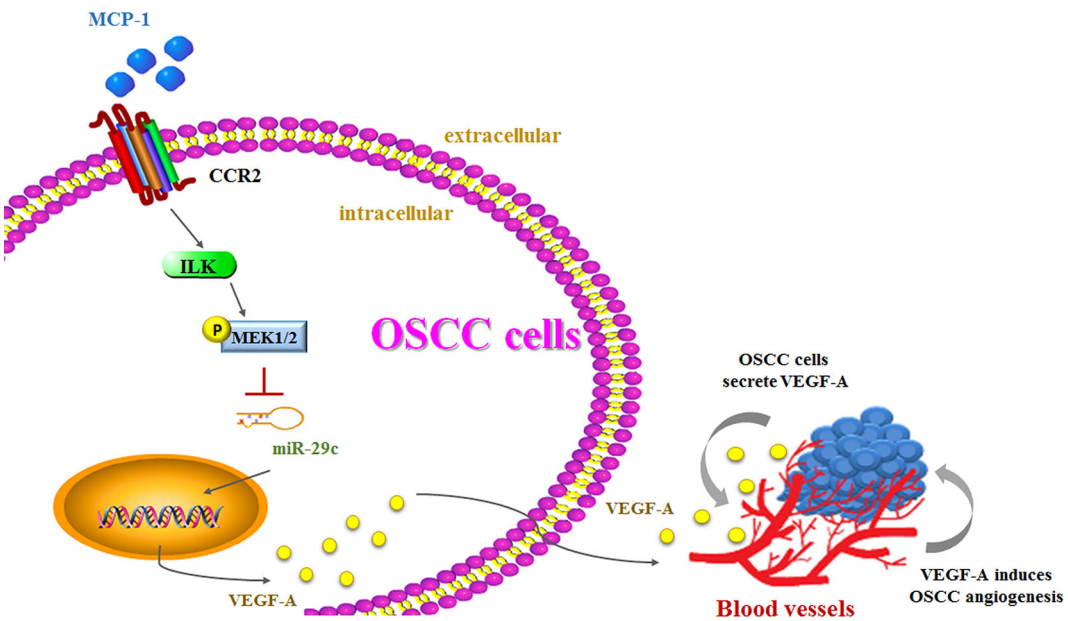

FIGURE 7 | The schema depicts the involvement of signaling pathways in MCP-1–induced stimulation of VEGF-A expression and angiogenesis.

carcinoma (43). In analyses of predictive algorithms, miR-29c has a high predictive score for *VEGF* 3′-UTR-binding sites and is one of the most significantly downregulated miRNAs in IGF2-treated CAFs (43). Moreover, miR-29c overexpression has been linked to a significant and consistent downregulation of VEGF in CAFs (43). It is well known that miR-29c acts as an anti-angiogenic agent by potently inhibiting VEGF-A (44). The expression of hsa-miR-29c is related to its DNA copy number and is differentially expressed in metastatic and nonmetastatic samples taken from patients with OSCC (45). In this study, we found that among all identified miRNAs, the level of miR-29c expression was reduced by the greatest extent after MCP-1 stimulation. Co-transfection with miR-29c mimic significantly reduced MCP-1–induced VEGF-A expression, EPC tube formation and migration. We also found that miR-29c directly represses VEGF-A protein expression by using ILK/MEK1/2 signaling to bind to the 3'-UTR of the human *VEGF-A* gene, and negatively regulating VEGF-A-mediated angiogenesis. Importantly, levels of miR-29c expression may serve as a biomarker of carcinogenesis in OSCC, as miR-29c has shown good discriminatory power for differentiating between OSCC and cancer-free tissue, as well as between tumor-adjacent and noncancerous tissue (46). Notably, the lack of a significant difference between miR-29c expression in tumor and tumor-adjacent tissues suggests a field cancerization effect in OSCC, whereby the dysregulation of miR-29c expression in tumor-adjacent tissue may promote oral carcinogenesis in that environment (46). In addition, miR-29c targets the phosphate and tensin homolog (*PTEN*) and *DICER1* genes, both of which contribute to oral carcinogenesis (46). In this respect, molecular analysis of miR-29c expression could be very important for OSCC prognosis. We suggest that combining miR-29c with other therapies that effectively target VEGF-A may improve the treatment of OSCC.

CONCLUSIONS

Higher MCP-1 expression levels in patients with OSCC are associated with more advanced disease. In cellular experiments, we found that MCP-1 promotes VEGF-A expression and angiogenesis by downregulating miR-29c expression *via* the ILK/MEK1/2 signaling pathways (**Figure 7**). Our evidence indicates that MCP-1 may be a new molecular therapeutic target for inhibition of angiogenesis and metastasis in OSCC.

DATA AVAILABILITY STATEMENT

The raw data supporting the conclusions of this article will be made available by the authors, without undue reservation.

AUTHOR CONTRIBUTIONS

M-YL and A-CC designed the experiments and performed data analysis. M-YL, A-CC, and H-CT performed cell culture and *ex vivo* experiments. A-CC and H-CT performed data analysis. M-HT, C-HH, S-PC, and S-WW contributed to and discussed the research strategy and data interpretation. The paper was written by H-CT and edited by C-HT. All authors contributed to the article and approved the submitted version.

FUNDING

This work was supported by grants from the Ministry of Science and Technology of Taiwan (MOST 108-2320-B-039-055; MOST 107-2320-B-039-019-MY3), China Medical University Hospital (DMR-109-205; CMU109-MF-44), and Shin Kong Wu Ho-Su Memorial Hospital (2020SKHBND001).

ACKNOWLEDGMENTS

We would like to thank Iona J. MacDonald from China Medical University for careful reading of the manuscript and for revision of the English grammar.

REFERENCES

1. Ong TK, Murphy C, Smith AB, Kanatas AN, Mitchell DA. Survival after surgery for oral cancer: a 30-year experience. *Br J Oral Maxillofac Surg* (2017) 55(9):911–6. doi: 10.1016/j.bjoms.2017.08.362
2. Ding D, Stokes W, Eguchi M, Hararah M, Sumner W, Amini A, et al. Association Between Lymph Node Ratio and Recurrence and Survival Outcomes in Patients With Oral Cavity Cancer. *JAMA Otolaryngol Head Neck Surg* (2019) 145(1):53–61. doi: 10.1001/jamaoto.2018.2974
3. Ling Z, Yang X, Chen X, Xia J, Cheng B, Tao X. CCL2 promotes cell migration by inducing epithelial-mesenchymal transition in oral squamous cell carcinoma. *J Oral Pathol Med* (2019) 48(6):477–82. doi: 10.1111/jop.12869
4. Ku WT, Tung JJ, Lee TJ, Lai KC. Long-Term Exposure to Oroxylin A Inhibits Metastasis by Suppressing CCL2 in Oral Squamous Cell Carcinoma Cells. *Cancers (Basel)* (2019) 11(3):353. doi: 10.3390/cancers11030353
5. Cui Z, Liu QL, Sun SQ, Jiao K, Liu DR, Zhou XC, et al. MiR-378a-5p inhibits angiogenesis of oral squamous cell carcinoma by targeting KLK4. *Neoplasma* (2020) 67(1):85–92. doi: 10.4149/neo_2019_190306N191
6. Lee CC, Ho HC, Su YC, Lee MS, Hung SK, Lin CH. MCP1-Induced Epithelial-Mesenchymal Transition in Head and Neck Cancer by AKT Activation. *Anticancer Res* (2015) 35(6):3299–306.
7. Lim SY, Yuzhalin AE, Gordon-Weeks AN, Muschel RJ. Targeting the CCL2-CCR2 signaling axis in cancer metastasis. *Oncotarget* (2016) 7(19):28697–710. doi: 10.18632/oncotarget.7376
8. Bonapace L, Coissieux MM, Wyckoff J, Mertz KD, Varga Z, Junt T, et al. Cessation of CCL2 inhibition accelerates breast cancer metastasis by promoting angiogenesis. *Nature* (2014) 515(7525):130–3. doi: 10.1038/nature13862
9. Gao L, Wang FQ, Li HM, Yang JG, Ren JG, He KF, et al. CCL2/EGF positive feedback loop between cancer cells and macrophages promotes cell migration and invasion in head and neck squamous cell carcinoma. *Oncotarget* (2016) 7 (52):87037–51. doi: 10.18632/oncotarget.13523
10. Momen-Heravi F, Bala S. Emerging role of non-coding RNA in oral cancer. *Cell Signal* (2018) 42:134–43. doi: 10.1016/j.cellsig.2017.10.009
11. Kulshreshtha R, Ferracin M, Negrini M, Calin GA, Davuluri RV, Ivan M. Regulation of microRNA expression: the hypoxic component. *Cell Cycle* (2007) 6(12):1426–31. doi: 10.4161/cc.6.12.4410

12. Esquela-Kerscher A, Slack FJ. Oncomirs - microRNAs with a role in cancer. *Nat Rev Cancer* (2006) 6(4):259–69. doi: 10.1038/nrc1840
13. Zhang Y, Yang P, Wang XF. Microenvironmental regulation of cancer metastasis by miRNAs. *Trends Cell Biol* (2014) 24(3):153–60. doi: 10.1016/j.tcb.2013.09.007
14. Sasahira T, Kurihara M, Bhawal UK, Ueda N, Shimomoto T, Yamamoto K, et al. Downregulation of miR-126 induces angiogenesis and lymphangiogenesis by activation of VEGF-A in oral cancer. *Br J Cancer* (2012) 107(4):700–6. doi: 10.1038/bjc.2012.330
15. Tsai HC, Cheng SP, Han CK, Huang YL, Wang SW, Lee JJ, et al. Resistin enhances angiogenesis in osteosarcoma via the MAPK signaling pathway. *Aging (Albany NY)* (2019) 11(21):9767–77. doi: 10.18632/aging.102423
16. Nho RS, Xia H, Kahm J, Kleidon J, Diebold D, Henke CA. Role of integrin-linked kinase in regulating phosphorylation of Akt and fibroblast survival in type I collagen matrices through a beta1 integrin viability signaling pathway. *J Biol Chem* (2005) 280(28):26630–9. doi: 10.1074/jbc.M411798200
17. Lin YM, Chang ZL, Liao YY, Chou MC, Tang CH. IL-6 promotes ICAM-1 expression and cell motility in human osteosarcoma. *Cancer Lett* (2013) 328 (1):135–43. doi: 10.1016/j.canlet.2012.08.029
18. Chen CY, Su CM, Hsu CJ, Huang CC, Wang SW, Liu SC, et al. CCN1 Promotes VEGF Production in Osteoblasts and Induces Endothelial Progenitor Cell Angiogenesis by Inhibiting miR-126 Expression in Rheumatoid Arthritis. *J Bone Miner Res* (2017) 32(1):34–45. doi: 10.1002/jbmr.2926
19. Lee HP, Wang SW, Wu YC, Lin LW, Tsai FJ, Yang JS, et al. Soya-cerebroside inhibits VEGF-facilitated angiogenesis in endothelial progenitor cells. *Food Agr Immunol* (2020) 31(1):193–204. doi: 10.1080/09540105.2020.1713055
20. Liu SC, Tsai CH, Wu TY, Tsai CH, Tsai FJ, Chung JG, et al. Soya-cerebroside reduces IL-1 beta-induced MMP-1 production in chondrocytes and inhibits cartilage degradation: implications for the treatment of osteoarthritis. *Food Agr Immunol* (2019) 30(1):620–32. doi: 10.1080/09540105.2019.1611745
21. Wang YH, Kuo SJ, Liu SC, Wang SW, Tsai CH, Fong YC, et al. Apelin Affects the Progression of Osteoarthritis by Regulating VEGF-Dependent Angiogenesis and miR-150-5p Expression in Human Synovial Fibroblasts. *Cells* (2020) 9(3). doi: 10.3390/cells9030594
22. Li C, Sun CJ, Fan JC, Geng N, Li CH, Liao J, et al. Angiopoietin-2 expression is correlated with angiogenesis and overall survival in oral squamous cell carcinoma. *Med Oncol* (2013) 30(2):571. doi: 10.1007/s12032-013-0571-2
23. Claesson-Welsh L, Welsh M. VEGFA and tumour angiogenesis. *J Intern Med* (2013) 273(2):114–27. doi: 10.1111/joim.12019
24. Hu L, Zhang P, Sun W, Zhou L, Chu Q, Chen Y. PDPN is a prognostic biomarker and correlated with immune infiltrating in gastric cancer. *Med (Baltimore)* (2020) 99(19):e19957. doi: 10.1097/MD.0000000000019957
25. Fei Y, Yu H, Huang S, Chen P, Pan L. Expression and prognostic analyses of early growth response proteins (EGRs) in human breast carcinoma based on database analysis. *PeerJ* (2019) 7:e8183. doi: 10.7717/peerj.8183
26. Brummer G, Fang W, Smart C, Zinda B, Alissa N, Berkland C, et al. CCR2 signaling in breast carcinoma cells promotes tumor growth and invasion by promoting CCL2 and suppressing CD154 effects on the angiogenic and immune microenvironments. *Oncogene* (2020) 39(11):2275–89. doi: 10.1038/s41388-019-1141-7
27. Chen CH, Su LJ, Tsai HT, Hwang CF. ELF-1 expression in nasopharyngeal carcinoma facilitates proliferation and metastasis of cancer cells via modulation of CCL2/CCR2 signaling. *Cancer Manag Res* (2019) 11:5243–54. doi: 10.2147/CMAR.S196355
28. Zhao W, Zhang X, Zang L, Zhao P, Chen Y, Wang X. ILK promotes angiogenic activity of mesenchymal stem cells in multiple myeloma. *Oncol Lett* (2018) 16(1):1101–6. doi: 10.3892/ol.2018.8711
29. Maydan M, McDonald PC, Sanghera J, Yan J, Rallis C, Pinchin S, et al. Integrin-linked kinase is a functional Mn2+-dependent protein kinase that regulates glycogen synthase kinase-3beta (GSK-3beta) phosphorylation. *PLoS One* (2010) 5(8):e12356. doi: 10.1371/journal.pone.0012356
30. Balakrishnan S, Nirmal M, Priyadharshini I, Ravi S. Role of Angiogenesis in Oral Squamous Cell Carcinoma – A Review. *J Adv Med Dental Sci Res* (2018) 6:127–30. doi: 10.4248/IJOS11077
31. Marcuzzi E, Angioni R, Molon B, Cali B. Chemokines and Chemokine Receptors: Orchestrating Tumor Metastasization. *Int J Mol Sci* (2018) 20 (1):96. doi: 10.3390/ijms20010096
32. Qiao B, Cai JH, King-Yin Lam A, He BX. MicroRNA-542-3p inhibits oral squamous cell carcinoma progression by inhibiting ILK/TGF-beta1/Smad2/3 signaling. *Oncotarget* (2017) 8(41):70761–76. doi: 10.18632/oncotarget.19986
33. Chang AC, Lien MY, Tsai MH, Hua CH, Tang CH. WISP-1 Promotes Epithelial-Mesenchymal Transition in Oral Squamous Cell Carcinoma Cells Via the miR-153-3p/Snail Axis. *Cancers (Basel)* (2019) 11(12):1903. doi: 10.3390/cancers11121903
34. Que L, Zhao D, Tang XF, Liu JY, Zhang XY, Zhan YH, et al. Effects of lentivirus-mediated shRNA targeting integrin-linked kinase on oral squamous cell carcinoma in vitro and in vivo. *Oncol Rep* (2016) 35(1):89–98. doi: 10.3892/or.2015.4374
35. Chen CY, Wu SM, Lin YH, Chi HC, Lin SL, Yeh CT, et al. Induction of nuclear protein-1 by thyroid hormone enhances platelet-derived growth factor A mediated angiogenesis in liver cancer. *Theranostics* (2019) 9 (8):2361–79. doi: 10.7150/thno.29628
36. Tong X, Wang Q, Wu D, Bao L, Yin T, Chen H. MEK inhibition by cobimetinib suppresses hepatocellular carcinoma and angiogenesis in vitro and in vivo. *Biochem Biophys Res Commun* (2020) 523(1):147–52. doi: 10.1016/j.bbrc.2019.12.032
37. Kashyap T, Pramanik KK, Nath N, Mishra P, Singh AK, Nagini S, et al. Crosstalk between Raf-MEK-ERK and PI3K-Akt-GSK3beta signaling networks promotes chemoresistance, invasion/migration and stemness via expression of CD44 variants (v4 and v6) in oral cancer. *Oral Oncol* (2018) 86:234–43. doi: 10.1016/j.oraloncology.2018.09.028
38. Yang WE, Ho YC, Tang CM, Hsieh YS, Chen PN, Lai CT, et al. Duchesnea indica extract attenuates oral cancer cells metastatic potential through the inhibition of the matrix metalloproteinase-2 activity by down-regulating the MEK/ERK pathway. *Phytomedicine* (2019) 63:152960. doi: 10.1016/j.phymed.2019.152960
39. Liu YS, Wei B. Over-expression of Bcl2-associated athanogene 2 in oral cancer promotes cellular proliferation and is associated with poor prognosis. *Arch Oral Biol* (2019) 102:164–70. doi: 10.1016/j.archoralbio.2019.04.015
40. Li W, Yi J, Zheng X, Liu S, Fu W, Ren L, et al. miR-29c plays a suppressive role in breast cancer by targeting the TIMP3/STAT1/FOXO1 pathway. *Clin Epigenet* (2018) 10:64. doi: 10.1186/s13148-018-0495-y
41. Hu Z, Cai M, Zhang Y, Tao L, Guo R. miR-29c-3p inhibits autophagy and cisplatin resistance in ovarian cancer by regulating FOXP1/ATG14 pathway. *Cell Cycle* (2020) 19(2):193–206. doi: 10.1080/15384101.2019.1704537
42. Fang R, Huang Y, Xie J, Zhang J, Ji X. Downregulation of miR-29c-3p is associated with a poor prognosis in patients with laryngeal squamous cell carcinoma. *Diagn Pathol* (2019) 14(1):109. doi: 10.1186/s13000-019-0893-2
43. Xu WW, Li B, Guan XY, Chung SK, Wang Y, Yip YL, et al. Cancer cell-secreted IGF2 instigates fibroblasts and bone marrow-derived vascular progenitor cells to promote cancer progression. *Nat Commun* (2017) 8:14399. doi: 10.1038/ncomms14399
44. Kwon JJ, Factora TD, Dey S, Kota J. A. Systematic Review of miR-29 in Cancer. *Mol Ther Oncolyt* (2019) 12:173–94. doi: 10.1016/j.omto.2018.12.011
45. Serrano NA, Xu C, Liu Y, Wang P, Fan W, Upton MP, et al. Integrative analysis in oral squamous cell carcinoma reveals DNA copy number-associated miRNAs dysregulating target genes. *Otolaryngol Head Neck Surg* (2012) 147(3):501–8. doi: 10.1177/0194599812442490
46. Lopes CB, Magalhaes LL, Teofilo CR, Alves A, Montenegro RC, Negrini M, et al. Differential expression of hsa-miR-221, hsa-miR-21, hsa-miR-135b, and hsa-miR-29c suggests a field effect in oral cancer. *BMC Cancer* (2018) 18 (1):721. doi: 10.1186/s12885-018-4631-z

Conflict of Interest: The authors declare that the research was conducted in the absence of any commercial or financial relationships that could be construed as a potential conflict of interest.

Copyright © 2020 Lien, Chang, Tsai, Tsai, Hua, Cheng, Wang and Tang. This is an open-access article distributed under the terms of the Creative Commons Attribution License (CC BY). The use, distribution or reproduction in other forums is permitted, provided the original author(s) and the copyright owner(s) are credited and that the original publication in this journal is cited, in accordance with accepted academic practice. No use, distribution or reproduction is permitted which does not comply with these terms.

frontiers in Oncology

REVIEW
published: 01 December 2020
doi: 10.3389/fonc.2020.596132

The Role of Exosomes in Thyroid Cancer and Their Potential Clinical Application

Kaixiang Feng[1,2,3], *Runsheng Ma*[1,2,3], *Lele Zhang*[1,2], *Hongqiang Li*[1,2], *Yifeng Tang*[1,2], *Gongbo Du*[1,2,3], *Dongpeng Niu*[1,2,3] *and Detao Yin*[1,2*]

[1] Department of Thyroid Surgery, The First Affiliated Hospital of Zhengzhou University, Zhengzhou, China, [2] Department of Thyroid Surgery, Key Discipline Laboratory of Clinical Medicine of Henan, Zhengzhou, China, [3] Academy of Medical Sciences, Zhengzhou University, Zhengzhou, China

The incidence of thyroid cancer (TC) is rapidly increasing worldwide. The diagnostic accuracy and dynamics of TC need to be improved, and traditional treatments are not effective enough for patients with poorly differentiated thyroid cancer. Exosomes are membrane vesicles secreted specifically by various cells and are involved in intercellular communication. Recent studies have shown that exosomes secreted by TC cells contribute to tumor progression, angiogenesis and metastasis. Exosomes in liquid biopsies can reflect the overall molecular information of tumors, and have natural advantages in diagnosing TC. Exosomes also play an important role in tumor therapy due to their special physicochemical properties. TC patients will benefit as more exosome patterns are discovered. In this review, we discuss the role of TC-derived exosomes in tumorigenesis and development, and describe the application of exosomes in the diagnosis and treatment of TC.

Keywords: extracellular vesicles, exosome, thyroid cancer, biomarker, oncology treatment

OPEN ACCESS

Edited by:
Qiang Shen,
Louisiana State University,
United States

Reviewed by:
Jafar Rezaie,
Urmia University of Medical Sciences,
Iran
Yu Wang,
Tianjin Medical University Cancer Institute and Hospital, China

***Correspondence:**
Detao Yin
detaoyin@zzu.edu.cn

Specialty section:
This article was submitted to Head and Neck Cancer, a section of the journal Frontiers in Oncology

Received: *18 August 2020*
Accepted: *30 October 2020*
Published: *01 December 2020*

Citation:
Feng K, Ma R, Zhang L, Li H, Tang Y, Du G, Niu D and Yin D (2020) The Role of Exosomes in Thyroid Cancer and Their Potential Clinical Application. Front. Oncol. 10:596132. doi: 10.3389/fonc.2020.596132

INTRODUCTION

Thyroid cancer (TC), one of the fastest-growing cancers in the world, has become the most common malignancy of the endocrine system in recent years (1–3). More than 90% of TCs diagnosed annually are differentiated thyroid cancer (DTC), which histologically includes papillary thyroid cancer (PTC) and follicular thyroid cancer (FTC), whereas the remaining subset of TC comprises medullary thyroid cancer (MTC) and anaplastic thyroid cancer (ATC); however, these two subtypes are associated with a poor prognosis (4, 5). Through common treatment methods, including surgery, radioactive iodine therapy, chemotherapy, external irradiation, and targeted therapy, most cases of TC have high cure rates and low tumor recurrence (6). However, there are still not adequate treatment options for advanced TC (7, 8). The median survival time of patients with ATC is less than 6 months regardless of stage. Although aggressive therapy has been used, it has not significantly changed in recent years (9). The exploration of new treatment strategies is mandatory to improve the survival of these patients and guarantee good quality of life (8, 10).

Extracellular vesicles (EVs) are heterogeneous groups of vesicles with membranous subcellular structures released by almost all cell types. They can be found in various physiological fluids including blood, urine, saliva, lymph, and seminal fluid (11, 12). Based on the origin and diameter of

vesicles, EVs can be divided into three major subclasses: exosomes, microvesicles, and apoptotic bodies. Exosomes are of endosomal origin and range in size from 30 to 120 nm and can be released by both eukaryotic and prokaryotic cells (13–15). Exosomes produced by tumor cells can create favorable conditions for tumor progression, such as induction of the angiogenic switch, increased vascular permeability, enhanced drug resistance and instigation of immune escape (16, 17). In addition, different types of cells, including mesenchymal stem cells (MSCs), adipocytes, fibroblasts, and immune cells in the tumor microenvironment (TME), can also induce the release of exosomes that promote tumor progression (18, 19). Understanding the role of exosomes in these cells will help unravel the mechanism underlying cancer. Furthermore, exosomes and their functions will provide more ways to diagnose, predict, and treat cancer (20). The utility of exosome detection in liquid biopsies is particularly promising for TC, and exploration of the use of exosomes as vehicles for the delivery of drug payloads is actively in progress. With the vast amount of information on exosomes emerging in the literature, these particles will likely be increasingly used in organisms. This review describes the function, separation methods, and biomedical applications of exosomes as well as current information on exosomes in TC.

THE BIOGENESIS AND ISOLATION OF EXOSOMES

The general understanding of EVs continued to improve for decades since they were first defined as "platelet dust" in the 1960s (21). There has been a paradigm shift from garbage carriers to new modes of intercellular communication and clinical applications (22–24). EVs are nanoparticles surrounded by lipid membranes that contain proteins, lipids, metabolites, and biologically active nucleic acids, which include DNA, mRNA, and noncoding RNA (ncRNA). These contents can be transported to recipient cells and interact with them to trigger biological responses (25, 26). In response to various internal and external conditions, the molecular properties and contents of EVs are often altered (11). Exosomes are an important class of EVs and an attractive tool for diagnosing and treating diseases, with special biological significance. Exosomes play critical roles in a variety of pathways, including cancer (27), cardiovascular disease (28), nervous system disorders (29), infectious diseases (30), and immunological diseases (31). However, normal bodily functions are also dependent on exosomes (32). For example, exosomes can protect host cells *in vitro* by acting as scavenging agents for a variety of toxins (33, 34). TSHR exosomes from patients with Graves' disease can reduce autoantibody-mediated activation of thyroid function (35). The dichotomous behavior and plasticity of exosomes have encouraged researchers to put more efforts into manipulating exosomes and determining how they can harm or benefit an organism.

Exosomes arise from either intraluminal vesicles (ILVs) released after multivesicular bodies (MVBs) fusion with the plasma membrane or other means (22, 27, 32) (**Figure 1**). The formation of exosomes begins with the emergence of the initial endosomes through the endocytosis of extracellular components and then their gradual maturation into late sorting endosomes before they finally become MVBs, which contain several ILVs (22, 36). Concomitant with this process, proteins, DNA and RNA can be selectively loaded into MVBs, after which the exosomes are released into the extracellular space by MVBs. Furthermore, MVBs can also be degraded by fusion with lysosomes or recovered by the plasma membrane through the back-fusion pathway (32, 37). The released exosomes can deliver cargo to target cells through endocytosis, receptor-ligand interactions, and fusion with the plasma membrane. Indeed, the biogenesis of exosomes and the sorting of exosome cargoes are complex and worthy of further investigation. Both lipids, such as lysophospholipids and ceramides, and proteins, such as CD81, CD9, Rab, Ral, Alix, and the endosomal sorting complexes required for transport (ESCRT), participate in these processes (20, 27, 37). It should be emphasized that protein classification in endosomes is crucial for protein stability, endosome maturation, etc., and the ESCRT mechanism is an important contributor to this activity (38). ESCRT located on the MVB membrane encompasses four complexes: 0, I, II, and III. ESCRT-0 combined with ESCRT-I recruits ESCRT-II and cargoes, and then ESCRT-II recruits ESCRT-III to assist with ILV budding. Other studies have shown that proteins containing Bro1 domains, such as ALIX, HD-PTP, and yeast Bro1, can bypass ESCRT-II and ESCRT-I and promote the assembly of ESCRT-III components (38–40). Interestingly, there are also ESCRT-independent mechanisms that can influence exosome occurrence. For example, RAB31 drives the formation of ILV independently of the ESCRT machinery and tetraspanin pathway (41). In general, multiple molecules and mechanisms are involved in the biological processes of exosomes, but their control pathways are still poorly understood. Due to their cellular origin, intrinsic biology, microenvironment and other factors, the size, content, inclusion, and function of exosomes may also differ (20). Basic research on exosomes is key for their clinical development; however, technical barriers to exosome extraction procedures limit the basic and applied research of exosomes to a certain extent (42).

Current exosome separation strategies include ultracentrifugation, ultrafiltration, size-exclusion chromatography, immunoaffinity capture, charge neutralization-based polymer precipitation, and microfluidic techniques, but none of them are sufficient for high-yield extractions (43, 44). Although ultracentrifugation is the most widely used primary isolation method for exosomes, it is also susceptible to contamination, and has low reproducibility, and low sample throughput (45, 46). Exosome heterogeneity also remains a research challenge. Because the current exosome separation technology is still limited and there is no particularly uniform standard, the term "exosome" used in this paper is not specifically distinguished from a mixture of EVs, as suggested in the guidelines of the International Society for Extracellular Vesicles (ISEV) (47). Appropriate separation techniques or combination applications will help researchers solve many of

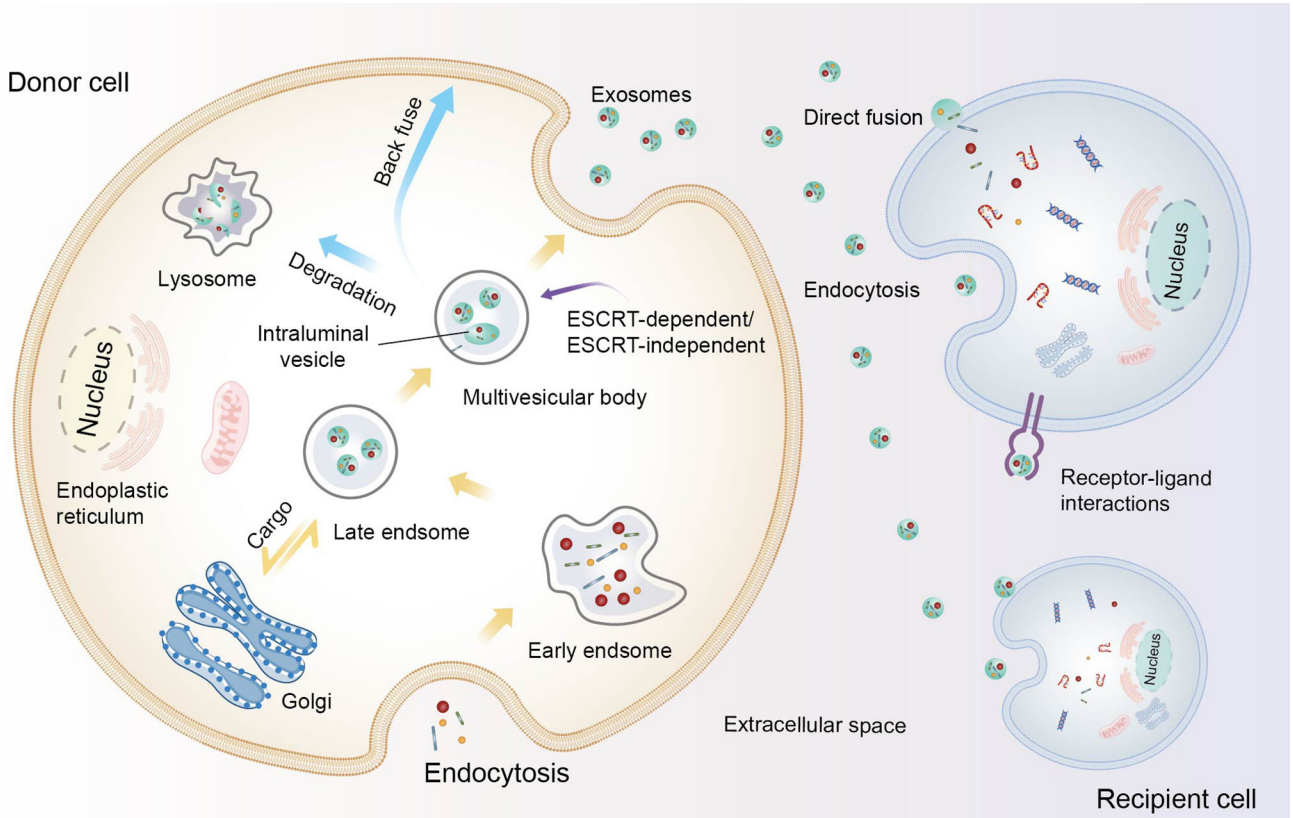

FIGURE 1 | The biogenesis of exosomes and their communication with recipient cells. Constituents from the extracellular space enter the cell by endocytosis, leading to the formation of early endosomes and gradually maturing into late endosomes. After the endosomes undergo inward budding and the cargo is further packaged, intraluminal vesicles (ILVs) form and constitute multivesicular bodies (MVBs). Subsequently, MVBs degrade in lysosomes, are transported back to the plasma membrane, or fuse with the plasma membrane to release ILVs as exosomes. These loaded exosomes release proteins, nucleic acids, and other contents to recipient cells though direct fusion, internalization, and ligand-receptor interactions.

the problems facing exosome research (43). Standardized exosome separation criteria will need to be developed in the future to meet the growing need for the specific screening of different sample types and for accurate exosome characterization.

EXOSOME BIOMARKERS FOR TC

The diagnosis of TC is a challenging issue. Multiple methods, including radionuclide scanning, high-resolution ultrasonography, and fine needle aspiration cytology (FNAC), are used to diagnose TC (48) (**Figure 2**). FNAC is a reliable application but not perfect, and a small ratio of indeterminate samples results in unnecessary surgeries or missed diagnoses (49). In oncology, liquid biopsy is an alternative, complementary diagnostic and prognostic tool that can overcome some weaknesses of tissue biopsy. It lacks the pitfalls of invasive and nonrepeatable sampling and may have more advantages in safety, early diagnosis, and dynamic monitoring (50, 51). In liquid biopsies, compared with circulating tumor cells (CTCs), circulating tumor DNA (ctDNA), cell-free DNA (cfDNA), and cell-free RNA (cfRNA), exosomes are more likely to have unique advantages in patients sometimes (52, 53). For example, KRAS mutations can be detected in tumor exosomes at a higher rate than in cfDNA for patients with pancreatic ductal adenocarcinoma (54).

Recent studies have shown that exosomal microRNAs (miRNAs) are an appropriate and promising marker for the clinical diagnosis of tumors. The advantage of miRNAs in diagnosis is that they are highly stable, protected by a bilayer membrane, and contain key information related to the biological response of the tumor (55, 56). Lee and his collaborator found that the levels of miR-146b and miR-222 in TPC-1 exosomes were higher than those in NTHY cells, indicating that these two miRNAs may be biomarkers for PTC recurrence (57). Interestingly, another study detected plasma exosomes in PTC patients with or without lymph node metastasis (LNM), confirming that circulating exosomal miR-146b-5p and miR-222-3p have high diagnostic value for predicting LNM in PTC patients (58). Although most PTC patients have a good prognosis, LNM often occurs in the early stage, and predicting and diagnosing LNM in advance can prevent patients from experiencing unnecessary pain. The discrimination of follicular

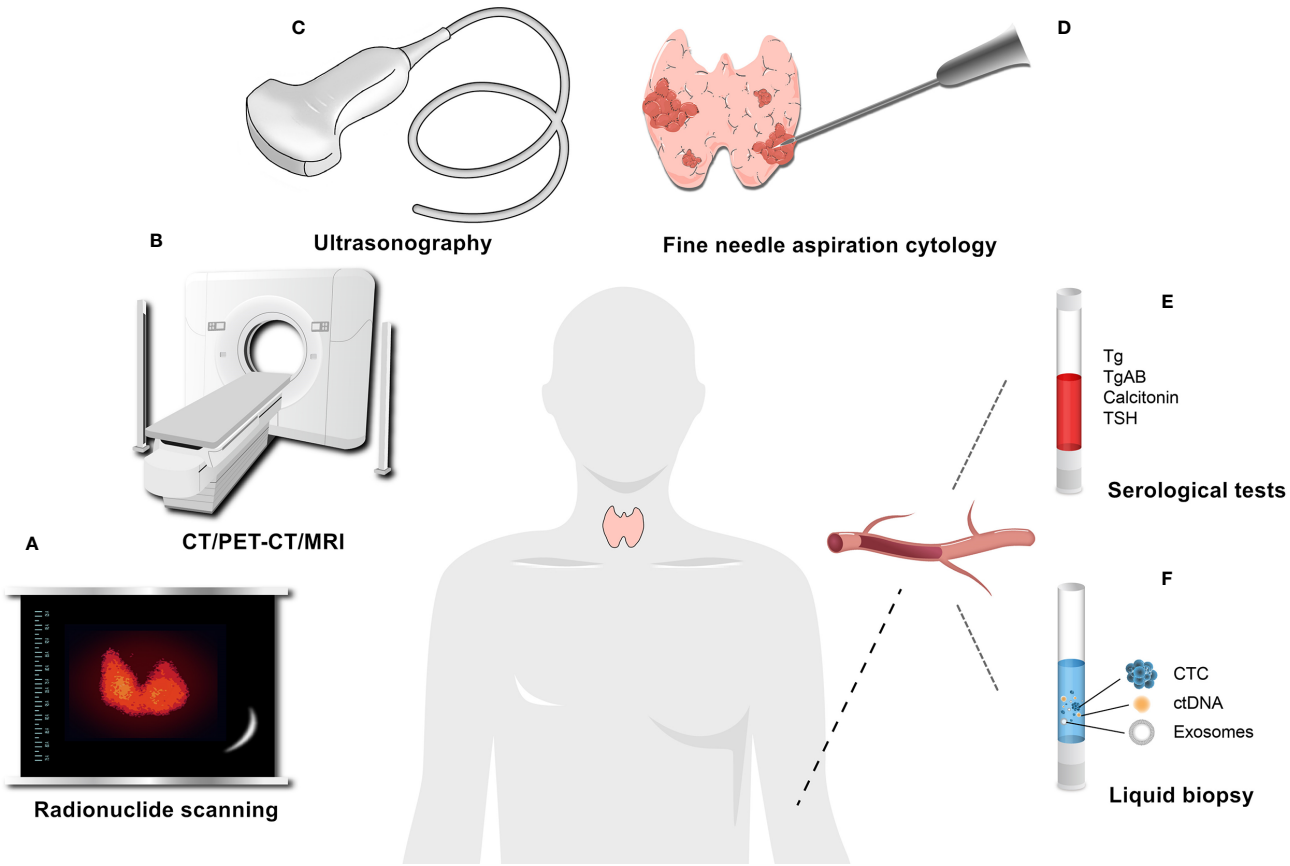

FIGURE 2 | Common auxiliary examinations for thyroid cancer. **(A)** Radionuclide scanning. **(B)** CT/PET-CT/MRI. **(C)** Ultrasonography. **(D)** Fine needle aspiration cytology (FNAC). **(E)** Serological tests, such as Tg and Calcitonin, which are commonly used serum markers, can be used for the postoperative assessment and monitoring of DTC and the diagnosis and follow-up of MTC, respectively. **(F)** Liquid biopsy.

lesions is another difficulty in TC, and the current traditional diagnostic methods are often inadequate (52, 59). Samsonov et al. compared patients with benign thyroid nodules, and found that miR-31 in the serum exosomes of PTC patients was significantly upregulated. Moreover, miR-21 in the serum exosomes of FTC patients also showed the same changes. In addition, compared with FTC patients, PTC patients have reduced miR-21 levels in serum exosomes but significantly upregulated miR-181a-5p content. Therefore, these miRNAs in exosomes can be used as diagnostic markers for PTC and FTC (60). With the continuous improvement in high-throughput assays, more miRNAs were subsequently discovered. Wang ZY et al. conducted a plasma miRNA profile analysis on PTC patients and healthy subjects and then verified the experimental results. Among the candidate miRNAs, miR-346, miR-34a-5p, and miR-10a-5p were found to be upregulated in PTC plasma exosomes (61). Pan Q et al. isolated exosomes from the plasma of patients with PTC and nodular goiters through small RNA sequencing and a comprehensive analysis and identified a group of miRNAs in plasma exosomes as candidate biomarkers for the diagnosis of thyroid nodules; among these, miR-5189-3p had the best effect on diagnosing PTC (55). Dai D et al. discovered that miR-485-3p and miR-4433a-5p might serve as biomarkers for PTC diagnosis. Plasma exosomal miR-485-3p could enable discrimination between high-risk and low-risk PTCs (62). Li MH et al. screened a panel of miRNAs in plasma exosomes by analyzing exosomes from different patients and found that the combination of these miRNAs is more effective in identifying PTC and thyroid nodules than any single marker (63). These results suggest that the comprehensive detection of multiple exosome contents may be more advantageous.

Exosomes contain a large amount of ncRNAs that are involved in every stage of cancer progression. Circular RNAs (circRNAs) are a class of covalently closed endogenous biomolecules of ncRNAs. Special structural features make them highly stable (64). Under the protection of exosomes, circRNAs have been proposed as novel predictive biomarkers with clinical promise (65). Wu G et al. investigated the expression of circRNAs in PTC tissues and normal tissues by microarray analysis and demonstrated that circRASSF2 was upregulated in serum exosomes from PTC patients, suggesting the importance

of circRASSF2 in tumor progression (66). Yang C et al. identified altered circRNA expression in serum exosomes from patients with PTC by high-throughput sequencing. circ_007293, circ_031752, and circ_020135 have been shown to be differentially expressed in the plasma of patients with PTC (67). In addition to serum exosomes, thyroglobulin in urine exosomes has also been found to be an emerging diagnostic marker for TC (68). These results suggest that the application of exosomes detected in TC could contribute to its diagnosis. However, due to the complex fluid composition of tumors, the dynamics of biomarkers, and the need for efficient enrichment and high sensitivity, the application of exosomes in cancer diagnosis remains challenging (26, 51). In recent years, the rapid development of nanotechnologies, including single-exosome analysis used for the rapid and readable detection and molecular analysis of exosomes, may provide a great opportunity for expanding the use of exosomes (23, 51, 69). The combined application of multiple diagnostic methods, including exosomes, will accelerate the arrival of an era of more precise and refined thyroid diagnoses.

TC-DERIVED EXOSOMES IN TUMOR PROGRESSION

The development of tumors is a complex process, and malignant cells constantly interact with their surroundings (70). During this process, exosomes act as connectors and regulators to help the tumor grow. We have come to realize that the biological changes that occur in exosomes reflect their cell state (including oncogenic transformation) (11). A large body of evidence suggests that tumor cells often secrete more exosomes than do healthy cells, and the onset of cancer may cause changes in the molecular cargo of exosomes (71, 72). The number of exosomes is significantly higher in TC patients than in healthy subjects (53, 73), suggesting that exosomes are an important mediator in the progression of TC (**Figure 3**).

The Role of Exosomes in TC Growth and Metastasis

An increasing number of studies have shown that exosomes can not only be used for clinical diagnosis and treatment, but also play an important role in the formation and metastasis of TC. Exosome-mediated intercellular communication plays a critical role in the development of cancer (74). Tumor cells actively produce, release, and utilize exosomes to promote tumor growth (72). As mentioned earlier, miR-146b and miR-222, which are relatively abundant in the exosomes of TPC-1 cells, caused a negative proliferative effect on both TPC-1 and NTHY cells (57). Jiang K et al. observed that exosomal miR-146b-5p and miR-222-3p were not only associated with LNM but also significantly enhanced the migration and invasion abilities of PTC cells (58). The exosome cargo continuously changes, and the quantity depends on the course of disease progression (75). For

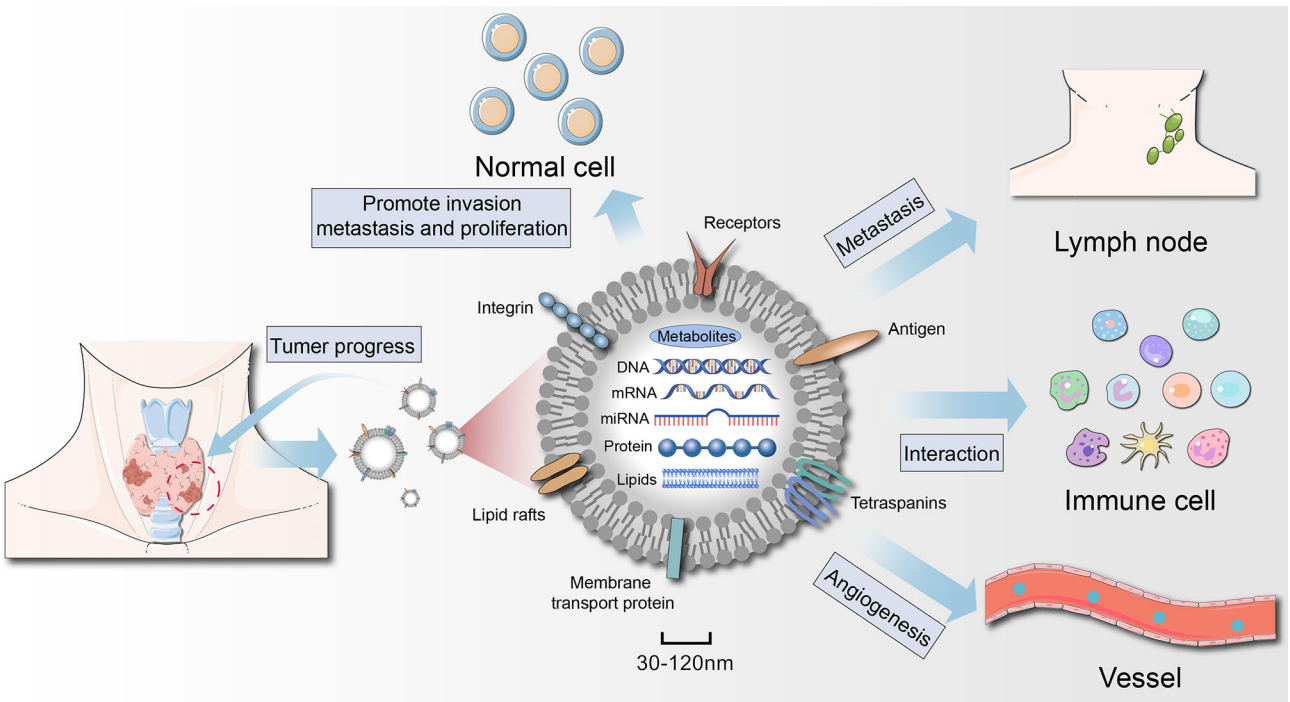

FIGURE 3 | Role of thyroid cancer-derived exosomes in cancer progression. Exosomes act on tumor cells themselves, regulate angiogenesis, induce immunosuppression, and then remodel the tumor microenvironment to achieve tumor growth and metastasis. Exosomes secreted by thyroid cancer (thyroid CSCs) can also promote the oncogenic transformation of normal cells.

instance, high expression of exosomal miR-485-3p correlates with tumor size, extrathyroidal extension, the BRAF mutation, LNM and an advanced clinical stage (62). Ye W et al. revealed that miR-423-5p may be involved in the carcinogenic activities of TC. Silencing miR-423-5p in TPC-1 cells inhibited PTC cell migration and invasion owing to reduced miR-423-5p in exosomes, providing a new approach for the treatment of PTC (76). The substances in exosomes play a significant role in the formation and metastasis of TC. Wu G et al. indicated the oncogenic property of circFNDC3B in PTC cells; circFNDC3B was upregulated in serum exosomes from PTC patients compared with healthy patients and could modulate PTC progression by activating the miR-1178/TLR4 pathway (77). In addition, Wu G confirmed that circRASSF2 can exert oncogenic activity in the tumorigenesis of PTC by sponging miR-1178 to upregulate TLR4 expression (66). The metastasis and survival of tumor cells depend on the TME in addition to intrinsic changes in cancer cells. Exosomes released by cancer cells can alter the behavior of localized or recruited stromal cells *via* external interactions that shift the phenotype of these stromal cells into a metastatic one. This leads to the formation of premetastatic niches that promote tumor growth (71, 78). Cancer-related fibroblasts (CAFs) are the primary stromal cells in the TME and play an essential role in several processes in cancer biology (79). Exosomes released from CAFs contribute to tumor progression and metastasis by transferring substances to cancer cells, and exosomes secreted by cancer cells can promote CAF transformation (20, 80). The crosstalk between TC cells and CAFs has been continuously revealed, and the role of exosomes in their interactions is worthy of further investigation (81). The ongoing revelation of the underlying mechanisms and pathogenesis of TC progression, as well as the influence of exosomes on these mechanisms, may provide more strategies for eventually curing TC.

Epithelial-Mesenchymal Transition (EMT) in TC

EMT is a cellular process during which epithelial cells acquire mesenchymal phenotypes and behaviors following the downregulation of proteins that indicate epithelial features (82). EMT arises early during tumor metastasis, playing a key role in mediating the development of an aggressive and invasive tumor phenotype. The main features of EMT include reduced adhesion and increased motility (83). EMT is triggered when a cell receives a signal from the microenvironment (82, 84). Studies have found a close link between EMT and cancer stem-like cells (CSCs), which are subsets of malignant tumor cells with the potential for self-renewal and differentiation and the ability to initiate tumors *in vivo* (85, 86). There are multiple ways by which EMT and CSCs interplay with each other (84, 87). Hardin et al. found that exosomes from thyroid CSCs transferred the long noncoding RNA (lncRNA) MALAT1, lncRNA ROR, and the EMT marker SLUG and induced EMT in normal thyroid cells (73). PTC-CSCs can also transmit the exosomal lncRNA DOCK9-AS2 to PTC, which can aggravate its malignant activities, including EMT, through the Wnt/β-catenin pathway (88). Critical components such as nucleotides, proteins, and organic intermediates in exosomes can serve as promising EMT regulators (89). Luo D et al. reported the differential expression of several proteins including the overexpression of proteins that are significantly related to cancer cell metastasis are associated with EMT (SRC, TLN1, ITGB2, and CAPNS1), in the exosomes of PTC patients with LNM (90). Some well-characterized miRNAs are important mediators involved in EMT-related signaling pathways induced by exosomes (91). Myriem et al. found that the overexpression of miR-145 in TPC-1 cells inhibited VEGF secretion and N-cadherin expression, which are closely related to the EMT process. Tumors actively excrete miR-145 into the blood *via* exosomes to reduce its expression in tumor tissue, thus inducing EMT and promoting the growth and metastasis of TC (92). Growing evidence has revealed that tumor cells are often in a different state along the EMT spectrum, as EMT is a continuous process with varying degrees of epithelial and mesenchymal characteristics and is often reversible (93, 94). We hypothesize that exosomes are involved in the dynamic changes between the epithelial and mesenchymal states. Future studies that show the inhibition of EMT-related changes and the reversal of EMT induction of tumors through exosomes will provide evidence of the use of exosomes to mitigate TC invasion and metastasis.

Effect of Exosomes on TC Angiogenesis

The growth and metastasis of malignant tumors depend on the formation and dilation of blood vessels (95). Exosomes from various tumors, such as breast cancer (15), colorectal cancer (96), gastric cancer (97), and lung cancer (80), have been shown to play an important role in promoting angiogenesis. It should be noted that the exact mechanism of exosome-driven angiogenesis is not clear, and the angiogenic characteristics of exosome cargoes from different tumor cells vary widely (98). The thyroid is an important endocrine organ with abundant vascularity (99). In addition, there are more blood vessels in thyroid tumor tissue than in normal thyroid tissue (100). In cancerous tissues, angiogenesis is implicated not only in primary tumors but also in the formation and further outgrowth of metastases (101). Some conditions, such as hypoxia or acidosis, enhance the secretion of exosomes into bodily fluids (102). Tumors are often hypoxic, and this hypoxic state results in advanced but dysfunctional vascularization and can alter different aspects of tumor metabolism (103). Feng W and colleagues revealed that exosomal miR-21-5p secreted by hypoxic PTC cells enhanced the angiogenic activities of human umbilical vein endothelial cells (HUVECs) both *in vitro* and *in vivo*. Exosomal miR-21-5p is a potent proangiogenic factor that increases angiogenesis by inhibiting the expression of TGFBI and COL4A1. In addition, it was also found to be elevated in the serum of PTC patients (104). This enhanced angiogenesis and increased vascular permeability in tumors support tumor growth and metastasis by continuously providing sufficient oxygen and nutrients to meet the nutritional needs of subsequent rapid metastatic growth, thereby increasing the proliferation of cancer cells and the formation of a premetastatic niche (105, 106). Currently, some drugs, such as docosahexaenoic acid and

curcumin, that can inhibit the angiogenic effects induced by exosomes have been reported (107, 108).

Exosomes Mediate the Immune Regulation of TC

Cancer immune surveillance is considered a significant host protection process to maintain cell homeostasis and inhibit carcinogenesis (109). Cancer cells secrete exosomes to regulate the function and abundance of components in the TME, including immune effector cells and antigen-presenting cells, to escape their surveillance (110). In the microenvironment, exosomes also interact with tumor-associated macrophages (TAMs), which contribute to tumor growth, invasion, angiogenesis, and overall metastasis (105). Cancer-derived exosomes can act as cellular messengers to modulate macrophage polarization to the M2 phenotype, thus providing an immunosuppressive microenvironment for cancer cell survival and invasion (111). Macrophage infiltration is frequently detected in human thyroid tumors (112), and an increase in TAM density is positively correlated with the progression of TC, with TAMs accounting for more than 50% of nucleated cells in cases of ATC (113, 114). We suspect that TC can also affect TAMs through exosomes, but this hypothesis requires further study. Natural killer (NK) cells are recognized as particularly effective immune cells involved in immune surveillance because they are not restricted by the expression of MHC molecules (115). Exosomes from different tumor cells can not only be taken up by NK cells, but also inhibit NK cell cytotoxicity in several cancer types (116, 117). Cancer-derived exosomes induce NK cell dysfunction, inhibit antigen-presenting cells, block T cell activation, and enhance T cell apoptosis to block adaptive immune responses and suppress the antitumor immune response (118, 119). Additionally, the stimulation of NK cells, for example, with cytokines, can improve their tumor-killing effects. Zhu et al. demonstrated that exposure of NK cells to IL-15 results in the increased production of EVs and enhances the immunotherapeutic effects of EVs against several human cancers, including TC (120). Heat shock proteins (HSPs) can mediate immunomodulatory effects and the immune response (121). Caruso et al. found that the levels of Hsp27, Hsp60, and Hsp90 were increased in TPC tissue compared with normal peritumoral tissue and benign goiters. The levels of HSPs in the exosomes of patients with TPC before surgery were significantly higher than those in the exosomes from the same patients after surgery and from patients with benign goiters (122). TC is considered one of the most immunogenic cancers (123); thus, the rapid development of immunotherapy and exosomes as a delivery system brings new opportunities for the treatment of TC.

The Potential of Exosomes in TC Treatment

The ability of exosomes to transport biomolecules to recipient cells has led to the increased exploration of exosomes as a tool in the field of cancer therapy (23). Elucidation of the role of exosomes in improving drug sensitivity, tumor radiosensitivity, and other responses to treatments will provide ideas for patients with advanced TC. Therapeutic applications of exosomes are promising because they have been shown to be well tolerated and have high bioavailability, low toxicity, and low immunogenicity (124). Notably, employing exosomes as a drug delivery system can easily avoid the first-pass metabolic effect and be effectively delivered to target sites. Compared to liposomes, exosomes can function better at a distance because of their superior systemic retention (125). Encapsulating anticancer drugs within exosomes has shown potential for targeted delivery to tumors in animal models. Gangadaran et al. isolated EVs containing Renilla luciferase in conditioned medium from cultured ATC cells (CAL62) to test the targeting ability of tumor-derived exosomes to their parental tumor in a mouse model. Exosomes injected into ATC model mice were directly internalized into CAL62 tumors and accumulated in the tumor region 30 min after injection (126). Previous studies have shown that cancer cells readily internalize EVs to a greater extent than normal cells. These results support the notion that cancer cell-derived exosomes harbor a specific tropism that can be exploited to deliver drugs into tumor cells. Despite the controversy, the ability of exosomes secreted by stem cells (such as MSCs) to inhibit tumorigenic properties has raised interest in research into their treatment of tumors (127). For instance, bone marrow MSCs can deliver exosomal miR-152 to repress the proliferation and migration of TC cells by targeting DPP4 (128). MSC-derived exosomes have many advantages over stem cells or synthetic nanoparticles, such as availability, ease of manipulation, and preferential access to tumors (24, 129). However, continuous efforts are still needed before exosomes can be applied clinically. Driven by chemical engineering and nanotechnology, *in silico* exosomes have been fully developed and are predicted to further promote the development of treatments.

The benefits of using exosomes to enhance antitumor immune responses in tumor microenvironment are also emerging. As mentioned above, the IL-15-mediated release of EVs by NK cells has an immunotherapeutic effect on TC (120). More experiments are underway; for instance, engineered macrophage-coated nanoparticles are a promising drug delivery strategy for treating triple-negative breast cancer (130). Exosomes derived from processed dendritic cells showed strong antitumor effects in inducing effective antigen-specific humoral and cellular immune responses (131). Clinical trials of exosomes as cancer vaccines are also underway with the help of immune cells (26). Another benefit of using exosomes therapeutically is that certain environmental niches may allow only exosomes to pass through (24). With the joint efforts of researchers from different disciplines, these nanoparticles will translate from the laboratory to the clinic faster and more efficiently (69).

CONCLUSIONS AND PERSPECTIVES

Exosomes promote the growth and development of TC *via* various strategies. The critical role of exosomes and their

TABLE 1 | Function of exosomal substances in thyroid cancer.

	Components	Histotype	Functions	Year	References
miRNA	miR-5189-3p	PTC	Biomarker	2020	(55)
	miR-16-2-3p, miR-34c-5p, miR-182-5p, miR-223-3p, miR-223-5p, miR-146b-5p	PTC	Biomarker	2020	(63)
	miR-485-3p, miR-4433a-5p	PTC	Biomarker, Progression	2020	(62)
	miR-146b-5p, miR-222-3p	PTC	Biomarker, Metastasis	2020	(58)
	miR-21-5p	PTC (hypoxic)	Promotes angiogenesis	2019	(104)
	miRNA423-5p	PTC	Biomarker, Migration, Invasion	2019	(76)
	miR-346, miR-34a-5p, miR-10a-5p	PTC	Biomarker	2019	(61)
	miR-21, miR-181a	PTC, FTC	Biomarker	2016	(60)
	miRNA-146b, miRNA-222	PTC	Biomarker, Proliferation	2015	(57)
	miR-145	PTC, FTC, ATC	Biomarker, Metastasis, Stemness	2014	(92)
lncRNA	lncRNA DOCK9-AS2	PTC CSCs	Proliferation, Migration, Stemness	2020	(88)
	lncRNA MALAT1, lncRNA ROR	Thyroid CSCs	Metastasis, Stemness	2018	(73)
circRNA	circFNDC3B	PTC	Biomarker, Metastasis, Proliferation	2020	(77)
	circRASSF2	PTC	Biomarker, Tumorigenesis	2020	(66)
	circ-007293, circ-031752, circ_020135	PTC	Biomarker	2019	(67)
proteins	Thyroglobulin	PTC, FTC	Biomarker	2020	(68)
	TSHR	PTC, FTC, ATC	Unknown	2019	(35)
	Hsp27, Hsp60, Hsp90	PTC	Biomarker	2019	(122)
	SRC, TLN1, ITGB2, CAPNS1	PTC	Invasion, Metastasis	2018	(90)

miRNA, microRNA; lncRNA, long noncoding RNA; circRNA, circular RNA; CSCs, cancer stem-like cells; TSHR, thyrotropin receptor; HSP, heat shock proteins.

cargoes in TC has led to many insightful studies (**Table 1**). As discussed, tumor-derived exosomes can be used as a potentially valuable noninvasive diagnostic tool for TC in the field of liquid biopsy because they provide a broad diagnostic window for TC detection and monitoring, and future studies will aim to clinically validate promising treatments that may benefit more TC patients. In addition, work aimed at the clinical validation of promising treatments is ongoing. Although the field of exosome research has been deepened and enriched in recent years, the mechanistic understanding and clinical application of exosomes in TC are still lacking. Tumor immunity, drug resistance, radiotherapy sensitivity, and other aspects of TC are the primary difficulties associated with treating advanced TC, however, studies on the involvement of exosomes in these processes are rare. In addition to research on the cancer-promoting mechanism of tumor exosomes, for most TC patients with a good prognosis, the role of exosomes in tumor inhibition may provide ideas for the treatment of other tumors. Further research on exosomes will contribute to a more comprehensive and multidimensional understanding of TC. We also recognize that there is still a long way to go before exosomes are ready for clinical use, as the underlying mechanisms relating to exosome biogenesis, selective cargo loading, transport and function need to be clarified, and the best practices for isolating and identifying large numbers of high-quality vesicles for clinical use remain problematic (26). Considering the complexity of exosomes, more research is needed to deepen the understanding of exosomes and develop new diagnostic and therapeutic strategies for TC.

AUTHOR CONTRIBUTIONS

DY conceived the idea and provided guidance. KF wrote the manuscript, GD and DN completed the figures, and RM and LZ carefully reviewed the manuscript. HL and YT made critical revisions to the manuscript. All authors contributed to the article and approved the submitted version.

FUNDING

This study was supported by the National Natural Science Foundation of China (81372863), the University Scientific and Technological Innovation Team Project of Henan Province (19IRTSTHN002), the Thousand Talents Science and Technology Innovation Leading Talents Subsidy Project of Central Plains (194200510011) and the Major Scientific Research Projects of Traditional Chinese Medicine in Henan Province (No.20-21ZYZD14).

REFERENCES

1. Cramer JD, Fu P, Harth KC, Margevicius S, Wilhelm SM. Analysis of the rising incidence of thyroid cancer using the Surveillance, Epidemiology and End Results national cancer data registry. *Surgery* (2010) 148(6):1147–52; discussion 52-3. doi: 10.1016/j.surg.2010.10.016
2. Carling T. Udelsman RJArom. *Thyroid Cancer* (2014) 65:125–37. doi: 10.1146/annurev-med-061512-105739
3. Miller K, Fidler-Benaoudia M, Keegan T, Hipp H, Jemal A, Siegel RJ. Cancer statistics for adolescents and young adults, 2020. *Cacjfc* (2020). doi: 10.3322/caac.21637
4. Xing M. Molecular pathogenesis and mechanisms of thyroid cancer. *Cancer Nr* (2013) 13(3):184–99. doi: 10.1038/nrc3431
5. Xu B, Ghossein R. Genomic Landscape of poorly Differentiated and Anaplastic Thyroid Carcinoma. *Endocr Pathol* (2016) 27(3):205–12. doi: 10.1007/s12022-016-9445-4

6. Luster M, Aktolun C, Amendoeira I, Barczynski M, Bible KC, Duntas LH, et al. European Perspective on 2015 American Thyroid Association Management Guidelines for Adult Patients with Thyroid Nodules and Differentiated Thyroid Cancer: Proceedings of an Interactive International Symposium. *Thyroid* (2019) 29(1):7–26. doi: 10.1089/thy.2017.0129
7. Naoum GE, Morkos M, Kim B, Arafat W. Novel targeted therapies and immunotherapy for advanced thyroid cancers. *Mol Cancer* (2018) 17(1):51. doi: 10.1186/s12943-018-0786-0
8. Kim WB, Jeon MJ, Kim WG, Kim TY, Shong YK. Unmet Clinical Needs in the Treatment of Patients with Thyroid Cancer. *Endocrinol Metab (Seoul)* (2020) 35(1):14–25. doi: 10.3803/EnM.2020.35.1.14
9. Qiu B, Li H, Chang Q, Yin D. Nomograms Predict Survival in Patients with Anaplastic Thyroid Carcinoma. *smimjoe Res c* (2019) 25:8447–56. doi: 10.12659/msm.918245
10. Salehian B, Liem SY, Mojazi Amiri H, Maghami E. Clinical Trials in Management of Anaplastic Thyroid Carcinoma; Progressions and Set Backs: A Systematic Review. *Int J Endocrinol Metab* (2019) 17(1):e67759. doi: 10.5812/ijem.67759
11. Möller A, Lobb RJ. The evolving translational potential of small extracellular vesicles in cancer. *NrC* (2020). doi: 10.1038/s41568-020-00299-w
12. Jabbari N, Karimipour M, Khaksar M, Akbariazar E, Heidarzadeh M, Mojarad B, et al. Tumor-derived extracellular vesicles: insights into bystander effects of exosomes after irradiation. *Lasers Med Sci* (2020) 35 (3):531–45. doi: 10.1007/s10103-019-02880-8
13. Thery C, Zitvogel L, Amigorena S. Exosomes: composition, biogenesis and function. *Nat Rev Immunol* (2002) 2(8):569–79. doi: 10.1038/nri855
14. Théry C, Witwer K, Aikawa E, Alcaraz M, Anderson J, Andriantsitohaina R, et al. Minimal information for studies of extracellular vesicles 2018 (MISEV2018): a position statement of the International Society for Extracellular Vesicles and update of the MISEV2014 guidelines. *J Extracell Vesicles* (2018) 7(1):1535750. doi: 10.1080/20013078.2018.1535750
15. Jabbari N, Akbariazar E, Feqhhi M, Rahbarghazi R, Rezaie JJ. Breast cancer-derived exosomes: Tumor progression and therapeutic agents. *Jocp* (2020) 235(10):6345–56. doi: 10.1002/jcp.29668
16. Han Q, Zhao H, Jiang Y, Yin C, Zhang J. HCC-Derived Exosomes: Critical Player and Target for Cancer Immune Escape. *Cells* (2019) 8(6). doi: 10.3390/cells8060558
17. Wu M, Wang G, Hu W, Yao Y, Yu XF. Emerging roles and therapeutic value of exosomes in cancer metastasis. *Mol Cancer* (2019) 18(1):53. doi: 10.1186/s12943-019-0964-8
18. de Araujo Farias V, O'Valle F, Serrano-Saenz S, Anderson P, Andres E, Lopez-Penalver J, et al. Exosomes derived from mesenchymal stem cells enhance radiotherapy-induced cell death in tumor and metastatic tumor foci. *Mol Cancer* (2018) 17(1):122. doi: 10.1186/s12943-018-0867-0
19. Munteanu R, Onaciu A, Moldovan C, Zimta AA, Gulei D, Paradiso AV, et al. Adipocyte-Based Cell Therapy in Oncology: The Role of Cancer-Associated Adipocytes and Their Reinterpretation as Delivery Platforms. *Pharmaceutics* (2020) 12(5). doi: 10.3390/pharmaceutics12050402
20. Kalluri R, LeBleu VS. The biology, function, and biomedical applications of exosomes. *Science* (2020) 367(6478). doi: 10.1126/science.aau6977
21. Wolf P. The nature and significance of platelet products in human plasma. *Br J Haematol* (1967) 13(3):269–88. doi: 10.1111/j.1365-2141.1967.tb08741.x
22. Pan BT, Teng K, Wu C, Adam M, Johnstone RM. Electron microscopic evidence for externalization of the transferrin receptor in vesicular form in sheep reticulocytes. *J Cell Biol* (1985) 101(3):942–8. doi: 10.1083/jcb.101.3.942
23. Srivastava A, Amreddy N, Pareek V, Chinnappan M, Ahmed R, Mehta M, et al. Progress in extracellular vesicle biology and their application in cancer medicine. *Wiley Interdiscip Rev Nanomed Nanobiotechnol* (2020) 12(4): e1621. doi: 10.1002/wnan.1621
24. Madhusoodanan J. The therapeutic potential of exosomes. *Nature* (2020) 581(7807):S10–S1. doi: 10.1038/d41586-020-01375-9
25. Pathan M, Fonseka P, Chitti SV, Kang T, Sanwlani R, Van Deun J, et al. Vesiclepedia 2019: a compendium of RNA, proteins, lipids and metabolites in extracellular vesicles. *Nucleic Acids Res* (2019) 47(D1):D516–D9. doi: 10.1093/nar/gky1029
26. O'Brien K, Breyne K, Ughetto S, Laurent LC, Breakefield XO. RNA delivery by extracellular vesicles in mammalian cells and its applications. *Nat Rev Mol Cell Biol* (2020) 22(10):586–606. doi: 10.1038/s41580-020-0251-y
27. Pegtel DM, Gould SJ. Exosomes. *Annu Rev Biochem* (2019) 88:487–514. doi: 10.1146/annurev-biochem-013118-111902
28. Zhang J, Cui X, Guo J, Cao C, Zhang Z, Wang B, et al. Small but significant: Insights and new perspectives of exosomes in cardiovascular disease. *J Cell Mol Med* (2020) 24(15):8291–303. doi: 10.1111/jcmm.15492
29. Peng C, Trojanowski JQ, Lee VM. Protein transmission in neurodegenerative disease. *Nat Rev Neurol* (2020) 16(4):199–212. doi: 10.1038/s41582-020-0333-7
30. Hassanpour M, Rezaie J, Nouri M, Panahi YJI. genetics, epidemiology ejom, diseases egii. The role of extracellular vesicles in COVID-19 virus infection. *Infect Genet Evol* (2020) 85:104422. doi: 10.1016/j.meegid.2020.104422
31. Ocansey DKW, Zhang L, Wang Y, Yan Y, Qian H, Zhang X, et al. Exosome-mediated effects and applications in inflammatory bowel disease. *Biol Rev Camb Philos Soc* (2020) 95(5):1287–307. doi: 10.1111/brv.12608
32. van Niel G, D'Angelo G, Raposo G. Shedding light on the cell biology of extracellular vesicles. *Nat Rev Mol Cell Biol* (2018) 19(4):213–28. doi: 10.1038/nrm.2017.125
33. Keller MD, Ching KL, Liang FX, Dhabaria A, Tam K, Ueberheide BM, et al. Decoy exosomes provide protection against bacterial toxins. *Nature* (2020) 579(7798):260–4. doi: 10.1038/s41586-020-2066-6
34. Du Toit A. Distracting your enemy with bubbles. *Nat Rev Microbiol* (2020) 18(5):263. doi: 10.1038/s41579-020-0355-6
35. Edo N, Kawakami K, Fujita Y, Morita K, Uno K, Tsukamoto K, et al. Exosomes Expressing Thyrotropin Receptor Attenuate Autoantibody-Mediated Stimulation of Cyclic Adenosine Monophosphate Production. *Thyroid* (2019) 29(7):1012–7. doi: 10.1089/thy.2018.0772
36. Ludwig A, BJTijob G. biology c. *Exosomes: small vesicles participating intercellular communication* (2012) 44(1):11–5. doi: 10.1016/j.biocel.2011.10.005
37. Mathieu M, Martin-Jaular L, Lavieu G, Thery C. Specificities of secretion and uptake of exosomes and other extracellular vesicles for cell-to-cell communication. *Nat Cell Biol* (2019) 21(1):9–17. doi: 10.1038/s41556-018-0250-9
38. Vietri M, Radulovic M, Stenmark H. The many functions of ESCRTs. *Nat Rev Mol Cell Biol* (2020) 21(1):25–42. doi: 10.1038/s41580-019-0177-4
39. Bissig C, Gruenberg J. ALIX and the multivesicular endosome: ALIX in Wonderland. *JTicb* (2014) 24(1):19–25. doi: 10.1016/j.tcb.2013.10.009
40. Tang S, Buchkovich N, Henne W, Banjade S, Kim Y, Emr SJE. ESCRT-III activation by parallel action of ESCRT-I/II and ESCRT-0/Bro1 during MVB biogenesis. *Elife* (2016). doi: 10.7554/eLife.15507
41. Wei D, Zhan W, Gao Y, Huang L, Gong R, Wang W, et al. RAB31 marks and controls an ESCRT-independent exosome pathway. *Cell Res* (2020). doi: 10.1038/s41422-020-00409-1
42. Fais S, O'Driscoll L, Borras FE, Buzas E, Camussi G, Cappello F, et al. Evidence-Based Clinical Use of Nanoscale Extracellular Vesicles in Nanomedicine. *ACS Nano* (2016) 10(4):3886–99. doi: 10.1021/acsnano.5b08015
43. Yang D, Zhang W, Zhang H, Zhang F, Chen L, Ma L, et al. Progress, opportunity, and perspective on exosome isolation - efforts for efficient exosome-based theranostics. *Theranostics* (2020) 10(8):3684–707. doi: 10.7150/thno.41580
44. Ludwig N, Whiteside TL, Reichert TE. Challenges in Exosome Isolation and Analysis in Health and Disease. *Int J Mol Sci* (2019) 20(19). doi: 10.3390/ijms20194684
45. Gardiner C, Di Vizio D, Sahoo S, Thery C, Witwer KW, Wauben M, et al. Techniques used for the isolation and characterization of extracellular vesicles: results of a worldwide survey. *J Extracell Vesicles* (2016) 5:32945. doi: 10.3402/jev.v5.32945
46. Konoshenko MY, Lekchnov EA, Vlassov AV, Laktionov PP. Isolation of Extracellular Vesicles: General Methodologies and Latest Trends. *BioMed Res Int* (2018) 2018:8545347. doi: 10.1155/2018/8545347
47. Théry C, Witwer KW, Aikawa E, Alcaraz MJ, Anderson JD, Andriantsitohaina R, et al. Minimal information for studies of extracellular vesicles 2018 (MISEV2018): a position statement of the International Society for Extracellular Vesicles and update of the MISEV2014 guidelines. *J Extracell Vesicles* (2018) 7(1):1535750. doi: 10.1080/20013078.2018.1535750
48. Duick DS, Klopper JP, Diggans JC, Friedman L, Kennedy GC, Lanman RB, et al. The impact of benign gene expression classifier test results on the endocrinologist-patient decision to operate on patients with thyroid nodules

with indeterminate fine-needle aspiration cytopathology. *Thyroid* (2012) 22 (10):996–1001. doi: 10.1089/thy.2012.0180
49. Wong CKH, Liu X, Lang BHH. Cost-effectiveness of fine-needle aspiration cytology (FNAC) and watchful observation for incidental thyroid nodules. *J Endocrinol Invest* (2020) 43(11):1645–54. doi: 10.1007/s40618-020-01254-0
50. Kulasinghe A, Kapeleris J, Kimberley R, Mattarollo S, Thompson E, Thiery J, et al. The prognostic significance of circulating tumor cells in head and neck and non-small-cell lung cancer. *Cancer Med* (2018) 7(12):5910–9. doi: 10.1002/cam4.1832
51. Li W, Wang H, Zhao Z, Gao H, Liu C, Zhu L, et al. Emerging Nanotechnologies for Liquid Biopsy: The Detection of Circulating Tumor Cells and Extracellular Vesicles. *Adv Mater* (2019) 31(45):e1805344. doi: 10.1002/adma.201805344
52. Khatami F, Tavangar SM. Liquid Biopsy in Thyroid Cancer: New Insight. *Int J Hematol Oncol Stem Cell Res* (2018) 12(3):235–48.
53. Rappa G, Puglisi C, Santos MF, Forte S, Memeo L, Lorico A. Extracellular Vesicles from Thyroid Carcinoma: The New Frontier of Liquid Biopsy. *Int J Mol Sci* (2019) 20(5). doi: 10.3390/ijms20051114
54. Allenson K, Castillo J, San Lucas F, Scelo G, Kim D, Bernard V, et al. High prevalence of mutant KRAS in circulating exosome-derived DNA from early-stage pancreatic cancer patients. *Ann Onco* (2017) 28(4):741–7. doi: 10.1093/annonc/mdx004
55. Pan Q, Zhao J, Li M, Liu X, Xu Y, Li W, et al. Exosomal miRNAs are potential diagnostic biomarkers between malignant and benign thyroid nodules based on next-generation sequencing. *Carcinogenesis* (2020) 41 (1):18–24. doi: 10.1093/carcin/bgz160
56. Hu C, Meiners S, Lukas C, Stathopoulos GT, Chen J. Role of exosomal microRNAs in lung cancer biology and clinical applications. *Cell Prolif* (2020) 53(6):e12828. doi: 10.1111/cpr.12828
57. Lee JC, Zhao JT, Gundara J, Serpell J, Bach LA, Sidhu S. Papillary thyroid cancer-derived exosomes contain miRNA-146b and miRNA-222. *J Surg Res* (2015) 196(1):39–48. doi: 10.1016/j.jss.2015.02.027
58. Jiang K, Li G, Chen W, Song L, Wei T, Li Z, et al. Plasma Exosomal miR-146b-5p and miR-222-3p are Potential Biomarkers for Lymph Node Metastasis in Papillary Thyroid Carcinomas. *Onco Targets Ther* (2020) 13:1311–9. doi: 10.2147/OTT.S231361
59. Jee HG, Kim BA, Kim M, Yu HW, Choi JY, Kim SJ, et al. Expression of SLC5A5 in Circulating Tumor Cells May Distinguish Follicular Thyroid Carcinomas from Adenomas: Implications for Blood-Based Preoperative Diagnosis. *J Clin Med* (2019) 8(2). doi: 10.3390/jcm8020257
60. Samsonov R, Burdakov V, Shtam T, Radzhabovsmall A CZ, Vasilyev D, Tsyrlina E, et al. Plasma exosomal miR-21 and miR-181a differentiates follicular from papillary thyroid cancer. *Tumour Biol* (2016) 37(9):12011–21. doi: 10.1007/s13277-016-5065-3
61. Wang Z, Lv J, Zou X, Huang Z, Zhang H, Liu Q, et al. A three plasma microRNA signature for papillary thyroid carcinoma diagnosis in Chinese patients. *Gene* (2019) 693:37–45. doi: 10.1016/j.gene.2019.01.016
62. Dai D, Tan Y, Guo L, Tang A, Zhao Y. Identification of exosomal miRNA biomarkers for diagnosis of papillary thyroid cancer by small RNA sequencing. *Eur J Endocrinol* (2020) 182(1):111–21. doi: 10.1530/EJE-19-0524
63. Liang M, Yu S, Tang S, Bai L, Cheng J, Gu Y, et al. A Panel of Plasma Exosomal miRNAs as Potential Biomarkers for Differential Diagnosis of Thyroid Nodules. *Front Genet* (2020) 11:449. doi: 10.3389/fgene.2020.00449
64. Zhang L, Hou C, Chen C, Guo Y, Yuan W, Yin D, et al. The role of N-methyladenosine (mA) modification in the regulation of circRNAs. *Mol Cancer* (2020) 19(1):105. doi: 10.1186/s12943-020-01224-3
65. Huang A, Zheng H, Wu Z, Chen M, Huang Y. Circular RNA-protein interactions: functions, mechanisms, and identification. *Theranostics* (2020) 10(8):3503–17. doi: 10.7150/thno.42174
66. Wu G, Zhou W, Lin X, Sun Y, Li J, Xu H, et al. circRASSF2 Acts as ceRNA and Promotes Papillary Thyroid Carcinoma Progression through miR-1178/TLR4 Signaling Pathway. *Mol Ther Nucleic Acids* (2020) 19:1153–63. doi: 10.1016/j.omtn.2019.11.037
67. Yang C, Wei Y, Yu L, Xiao Y. Identification of Altered Circular RNA Expression in Serum Exosomes from Patients with Papillary Thyroid Carcinoma by High-Throughput Sequencing. *Med Sci Monit* (2019) 25:2785–91. doi: 10.12659/MSM.915658
68. Huang T, Wang C, Chen K, Huang L. Urinary Exosomal Thyroglobulin in Thyroid Cancer Patients With Post-ablative Therapy: A New Biomarker in. *Thyroid Cancer* (2020) 11:382. doi: 10.3389/fendo.2020.00382
69. Tran PHL, Xiang D, Tran TTD, Yin W, Zhang Y, Kong L. Exosomes and Nanoengineering: A Match Made for Precision Therapeutics. *Adv Mater* (2020) 32(18):e1904040. doi: 10.1002/adma.201904040
70. Tan S, Xia L, Yi P, Han Y, Tang L, Pan Q, et al. Exosomal miRNAs in tumor microenvironment. *J Exp Clin Cancer Res* (2020) 39(1):67. doi: 10.1186/s13046-020-01570-6
71. Bebelman MP, Smit MJ, Pegtel DM, Baglio SR. Biogenesis and function of extracellular vesicles in cancer. *Pharmacol Ther* (2018) 188:1–11. doi: 10.1016/j.pharmthera.2018.02.013
72. Whiteside TL. Tumor-Derived Exosomes and Their Role in Cancer Progression. *Adv Clin Chem* (2016) 74:103–41. doi: 10.1016/bs.acc.2015.12.005
73. Hardin H, Helein H, Meyer K, Robertson S, Zhang R, Zhong W, et al. Thyroid cancer stem-like cell exosomes: regulation of EMT via transfer of lncRNAs. *Lab Invest* (2018) 98(9):1133–42. doi: 10.1038/s41374-018-0065-0
74. Tai YL, Chu PY, Lee BH, Chen KC, Yang CY, Kuo WH, et al. Basics and applications of tumor-derived extracellular vesicles. *J BioMed Sci* (2019) 26 (1):35. doi: 10.1186/s12929-019-0533-x
75. Wang Y, Xu F, Zhong JY, Lin X, Shan SK, Guo B, et al. Exosomes as Mediators of Cell-to-Cell Communication in Thyroid Disease. *Int J Endocrinol* (2020) 2020:4378345. doi: 10.1155/2020/4378345
76. Ye W, Deng X, Fan Y. Exosomal miRNA423-5p mediated oncogene activity in papillary thyroid carcinoma: a potential diagnostic and biological target for cancer therapy. *Neoplasma* (2019) 66(4):516–23. doi: 10.4149/neo_2018_180824N643
77. Wu G, Zhou W, Pan X, Sun Z, Sun Y, Xu H, et al. Circular RNA Profiling Reveals Exosomal circ_0006156 as a Novel Biomarker in Papillary Thyroid Cancer. *Mol Ther Nucleic Acids* (2020) 19:1134–44. doi: 10.1016/j.omtn.2019.12.025
78. Biswas AK, Acharyya S. Understanding cachexia in the context of metastatic progression. *Nat Rev Cancer* (2020) 20(5):274–84. doi: 10.1038/s41568-020-0251-4
79. Sun LP, Xu K, Cui J, Yuan DY, Zou B, Li J, et al. Cancerassociated fibroblastderived exosomal miR3825p promotes the migration and invasion of oral squamous cell carcinoma. *Oncol Rep* (2019) 42(4):1319–28. doi: 10.3892/or.2019.7255
80. Fan J, Xu G, Chang Z, Zhu L, Yao J. miR-210 transferred by lung cancer cell-derived exosomes may act as proangiogenic factor in cancer-associated fibroblasts by modulating JAK2/STAT3 pathway. *Clin Sci (Lond)* (2020) 134 (7):807–25. doi: 10.1042/CS20200039
81. Minna E, Brich S, Todoerti K, Pilotti S, Collini P, Bonaldi E, et al. Cancer Associated Fibroblasts and Senescent Thyroid Cells in the Invasive Front of Thyroid Carcinoma. *Cancers (Basel)* (2020) 12(1). doi: 10.3390/cancers12010112
82. Yang J, Antin P, Berx G, Blanpain C, Brabletz T, Bronner M, et al. Guidelines and definitions for research on epithelial-mesenchymal transition. *Nat Rev Mol Cell Biol* (2020) 21(6):341–52. doi: 10.1038/s41580-020-0237-9
83. Baum B, Settleman J, Quinlan MP. Transitions between epithelial and mesenchymal states in development and disease. *Semin Cell Dev Biol* (2008) 19(3):294–308. doi: 10.1016/j.semcdb.2008.02.001
84. Yu C, Liu Q, Chen C, Wang J. Quantification of the Underlying Mechanisms and Relationships Among Cancer, Metastasis, and Differentiation and Development. *Front Genet* (2019) 10:1388:1388. doi: 10.3389/fgene.2019.01388
85. Jimenez-Pascual A, Hale JS, Kordowski A, Pugh J, Silver DJ, Bayik D, et al. ADAMDEC1 Maintains a Growth Factor Signaling Loop in Cancer Stem Cells. *Cancer Discov* (2019) 9(11):1574–89. doi: 10.1158/2159-8290.CD-18-1308
86. Magee JA, Piskounova E, Morrison SJ. Cancer stem cells: impact, heterogeneity, and uncertainty. *Cancer Cell* (2012) 21(3):283–96. doi: 10.1016/j.ccr.2012.03.003
87. Kalluri R, Weinberg RA. The basics of epithelial-mesenchymal transition. *J Clin Invest* (2009) 119(6):1420–8. doi: 10.1172/JCI39104
88. Dai W, Jin X, Han L, Huang H, Ji Z, Xu X, et al. Exosomal lncRNA DOCK9-AS2 derived from cancer stem cell-like cells activated Wnt/β-catenin pathway to aggravate stemness, proliferation, migration, and invasion in

papillary thyroid carcinoma. *Cell Death Dis* (2020) 11(9):743. doi: 10.1038/s41419-020-02827-w
89. Kim H, Lee S, Shin E, Seong KM, Jin YW, Youn H, et al. The Emerging Roles of Exosomes as EMT Regulators in Cancer. *Cells* (2020) 9(4). doi: 10.3390/cells9040861
90. Luo D, Zhan S, Xia W, Huang L, Ge W, Wang T. Proteomics study of serum exosomes from papillary thyroid cancer patients. *Endocr Relat Cancer* (2018) 25(10):879–91. doi: 10.1530/ERC-17-0547
91. Mannavola F, Pezzicoli G, Tucci M. DLC-1 down-regulation via exosomal miR-106b-3p exchange promotes CRC metastasis by the epithelial-to-mesenchymal transition. *Clin Sci (Lond)* (2020) 134(8):955–9. doi: 10.1042/CS20200181
92. Boufraqech M, Zhang L, Jain M, Patel D, Ellis R, Xiong Y, et al. miR-145 suppresses thyroid cancer growth and metastasis and targets AKT3. *Endocr Relat Cancer* (2014) 21(4):517–31. doi: 10.1530/ERC-14-0077
93. Nieto MA, Huang RY, Jackson RA, Thiery JP. Emt: 2016. *Cell* (2016) 166 (1):21–45. doi: 10.1016/j.cell.2016.06.028
94. Liao TT, Yang MH. Hybrid Epithelial/Mesenchymal State in Cancer Metastasis: Clinical Significance and Regulatory Mechanisms. *Cells* (2020) 9(3). doi: 10.3390/cells9030623
95. Nishida N, Yano H, Nishida T, Kamura T, Kojiro M. Angiogenesis in cancer. *Vasc Health Risk Manag* (2006) 2(3):213–9. doi: 10.2147/vhrm.2006.2.3.213
96. Shang A, Wang X, Gu C, Liu W, Sun J, Zeng B, et al. Exosomal miR-183-5p promotes angiogenesis in colorectal cancer by regulation of FOXO1. *Aging (Albany NY)* (2020) 12(9):8352–71. doi: 10.18632/aging.103145
97. Du J, Liang Y, Li J, Zhao JM, Wang ZN, Lin XY. Gastric Cancer Cell-Derived Exosomal microRNA-23a Promotes Angiogenesis by Targeting PTEN. *Front Oncol* (2020) 10:326. doi: 10.3389/fonc.2020.00326
98. Ahmadi M, Rezaie J. Tumor cells derived-exosomes as angiogenenic agents: possible therapeutic implications. *J Trans Med* (2020) 18(1):249. doi: 10.1186/s12967-020-02426-5
99. Rajabi S, Dehghan MH, Dastmalchi R, Jalali Mashayekhi F, Salami S, Hedayati M. The roles and role-players in thyroid cancer angiogenesis. *Endocr J* (2019) 66(4):277–93. doi: 10.1507/endocrj.EJ18-0537
100. Akslen LA, Livolsi VA. Increased angiogenesis in papillary thyroid carcinoma but lack of prognostic importance. *Hum Pathol* (2000) 31 (4):439–42. doi: 10.1053/1-ip.2000.6548
101. Hanahan D, Weinberg RA. Hallmarks of cancer: the next generation. *Cell* (2011) 144(5):646–74. doi: 10.1016/j.cell.2011.02.013
102. Mashouri L, Yousefi H, Aref AR, Ahadi AM, Molaei F, Alahari SK. Exosomes: composition, biogenesis, and mechanisms in cancer metastasis and drug resistance. *Mol Cancer* (2019) 18(1):75. doi: 10.1186/s12943-019-0991-5
103. Muz B, de la Puente P, Azab F, Azab AK. The role of hypoxia in cancer progression, angiogenesis, metastasis, and resistance to therapy. *Hypoxia (Auckl)* (2015) 3:83–92. doi: 10.2147/HP.S93413
104. Wu F, Li F, Lin X, Xu F, Cui RR, Zhong JY, et al. Exosomes increased angiogenesis in papillary thyroid cancer microenvironment. *Endocr Relat Cancer* (2019) 26(5):525–38. doi: 10.1530/ERC-19-0008
105. Feng W, Dean DC, Hornicek FJ, Shi H, Duan Z. Exosomes promote pre-metastatic niche formation in ovarian cancer. *Mol Cancer* (2019) 18(1):124. doi: 10.1186/s12943-019-1049-4
106. Zhou W, Fong MY, Min Y, Somlo G, Liu L, Palomares MR, et al. Cancer-secreted miR-105 destroys vascular endothelial barriers to promote metastasis. *Cancer Cell* (2014) 25(4):501–15. doi: 10.1016/j.ccr.2014.03.007
107. Hannafon B, Carpenter K, Berry W, Janknecht R, Dooley W, Ding WJMC. Exosome-mediated microRNA signaling from breast cancer cells is altered by the anti-angiogenesis agent docosahexaenoic acid (DHA). *Mol Cancer* (2015) 14:133. doi: 10.1186/s12943-015-0400-7
108. Taverna S, Fontana S, Monteleone F, Pucci M, Saieva L, De Caro V, et al. Curcumin modulates chronic myelogenous leukemia exosomes composition and affects angiogenic phenotype via exosomal miR-21. *Oncotarget* (2016) 7 (21):30420–39. doi: 10.18632/oncotarget.8483
109. Kim R, Emi M, Tanabe K. Cancer immunoediting from immune surveillance to immune escape. *Immunology* (2007) 121(1):1–14. doi: 10.1111/j.1365-2567.2007.02587.x
110. Yi M, Xu L, Jiao Y, Luo S, Li A, Wu K. The role of cancer-derived microRNAs in cancer immune escape. *J Hematol Oncol* (2020) 13(1):25. doi: 10.1186/s13045-020-00848-8
111. Baig MS, Roy A, Rajpoot S, Liu D, Savai R, Banerjee S, et al. Tumor-derived exosomes in the regulation of macrophage polarization. *Inflamm Res* (2020) 69(5):435–51. doi: 10.1007/s00011-020-01318-0
112. Mazzoni M, Mauro G, Erreni M, Romeo P, Minna E, Vizioli MG, et al. Senescent thyrocytes and thyroid tumor cells induce M2-like macrophage polarization of human monocytes via a PGE2-dependent mechanism. *J Exp Clin Cancer Res* (2019) 38(1):208. doi: 10.1186/s13046-019-1198-8
113. Caillou B, Talbot M, Weyemi U, Pioche-Durieu C, Al Ghuzlan A, Bidart JM, et al. Tumor-associated macrophages (TAMs) form an interconnected cellular supportive network in anaplastic thyroid carcinoma. *PLoS One* (2011) 6(7):e22567. doi: 10.1371/journal.pone.0022567
114. Huang FJ, Zhou XY, Ye L, Fei XC, Wang S, Wang W, et al. Follicular thyroid carcinoma but not adenoma recruits tumor-associated macrophages by releasing CCL15. *BMC Cancer* (2016) 16:98. doi: 10.1186/s12885-016-2114-7
115. Caligiuri MA. Human natural killer cells. *Blood* (2008) 112(3):461–9. doi: 10.1182/blood-2007-09-077438
116. Huyan T, Du Y, Huang Q, Huang Q, Li Q. Uptake Characterization of Tumor Cell-derived Exosomes by Natural Killer Cells. *Iran J Public Health* (2018) 47(6):803–13.
117. Hedlund M, Nagaeva O, Kargl D, Baranov V, Mincheva-Nilsson L. Thermal- and oxidative stress causes enhanced release of NKG2D ligand-bearing immunosuppressive exosomes in leukemia/lymphoma T and B cells. *PLoS One* (2011) 6(2):e16899. doi: 10.1371/journal.pone.0016899
118. Czernek L, Duchler M. Functions of Cancer-Derived Extracellular Vesicles in Immunosuppression. *Arch Immunol Ther Exp (Warsz)* (2017) 65(4):311–23. doi: 10.1007/s00005-016-0453-3
119. Guo Y, Ji X, Liu J, Fan D, Zhou Q, Chen C, et al. Effects of exosomes on pre-metastatic niche formation in tumors. *Mol Cancer* (2019) 18(1):39. doi: 10.1186/s12943-019-0995-1
120. Zhu L, Gangadaran P, Kalimuthu S, Oh JM, Baek SH, Jeong SY, et al. Novel alternatives to extracellular vesicle-based immunotherapy - exosome mimetics derived from natural killer cells. *Artif Cells Nanomed Biotechnol* (2018) 46(sup3):S166–S79. doi: 10.1080/21691401.2018.1489824
121. Taha EA, Ono K, Eguchi T. Roles of Extracellular HSPs as Biomarkers in Immune Surveillance and Immune Evasion. *Int J Mol Sci* (2019) 20(18). doi: 10.3390/ijms20184588
122. Caruso Bavisotto C, Cipolla C, Graceffa G, Barone R, Bucchieri F, Bulone D, et al. Immunomorphological Pattern of Molecular Chaperones in Normal and Pathological Thyroid Tissues and Circulating Exosomes: Potential Use in Clinics. *Int J Mol Sci* (2019) 20(18). doi: 10.3390/ijms20184496
123. Chakladar J, Li WT, Bouvet M, Chang EY, Wang-Rodriguez J, Ongkeko WM. Papillary Thyroid Carcinoma Variants are Characterized by Co-dysregulation of Immune and Cancer Associated Genes. *Cancers (Basel)* (2019) 11(8). doi: 10.3390/cancers11081179
124. Kamerkar S, LeBleu VS, Sugimoto H, Yang S, Ruivo CF, Melo SA, et al. Exosomes facilitate therapeutic targeting of oncogenic KRAS in pancreatic cancer. *Nature* (2017) 546(7659):498–503. doi: 10.1038/nature22341
125. Lim W, Kim HS. Exosomes as Therapeutic Vehicles for Cancer. *Tissue Eng Regener Med* (2019) 16(3):213–23. doi: 10.1007/s13770-019-00190-2
126. Gangadaran P, Li XJ, Kalimuthu SK, Min OJ, Hong CM, Rajendran RL, et al. New Optical Imaging Reporter-labeled Anaplastic Thyroid Cancer-Derived Extracellular Vesicles as a Platform for In Vivo Tumor Targeting in a Mouse Model. *Sci Rep* (2018) 8(1):13509. doi: 10.1038/s41598-018-31998-y
127. Shojaei S, Hashemi SM, Ghanbarian H, Salehi M, Mohammadi-Yeganeh S. Effect of mesenchymal stem cells-derived exosomes on tumor microenvironment: Tumor progression versus tumor suppression. *J Cell Physiol* (2019) 234(4):3394–409. doi: 10.1002/jcp.27326
128. Tang M, Wang Q, Wang K, Wang F. Mesenchymal stem cells-originated exosomal microRNA-152 impairs proliferation, invasion and migration of thyroid carcinoma cells by interacting with DPP4. *J Endocrinol Invest* (2020) 43(12):1787–96. doi: 10.1007/s40618-020-01406-2
129. Galland S, Stamenkovic I. Mesenchymal stromal cells in cancer: a review of their immunomodulatory functions and dual effects on tumor progression. *J Pathol* (2020) 250(5):555–72. doi: 10.1002/path.5357
130. Li S, Wu Y, Ding F, Yang J, Li J, Gao X, et al. Engineering macrophage-derived exosomes for targeted chemotherapy of triple-negative breast cancer. *Nanoscale* (2020) 12(19):10854–62. doi: 10.1039/d0nr00523a
131. Matsumoto A, Asuka M, Takahashi Y, Takakura Y. Antitumor immunity by small extracellular vesicles collected from activated dendritic cells through

effective induction of cellular and humoral immune responses. *Biomaterials* (2020) 252:120112. doi: 10.1016/j.biomaterials.2020.120112

Conflict of Interest: The authors declare that the research was conducted in the absence of any commercial or financial relationships that could be construed as a potential conflict of interests.

Copyright © 2020 Feng, Ma, Zhang, Li, Tang, Du, Niu and Yin. This is an open-access article distributed under the terms of the Creative Commons Attribution License (CC BY). The use, distribution or reproduction in other forums is permitted, provided the original author(s) and the copyright owner(s) are credited and that the original publication in this journal is cited, in accordance with accepted academic practice. No use, distribution or reproduction is permitted which does not comply with these terms.

frontiers in Oncology

ORIGINAL RESEARCH
published: 11 December 2020
doi: 10.3389/fonc.2020.583682

CircRNA_ACAP2 Suppresses EMT in Head and Neck Squamous Cell Carcinoma by Targeting the miR-21-5p/STAT3 Signaling Axis

Chuan Ma[1,2], *Tingting Shi*[1,2], *Zhuli Qu*[3], *Aobo Zhang*[1,2], *Zuping Wu*[4], *Huaqiang Zhao*[1,2], *Haoming Zhao*[1,2*] *and Hongyu Chen*[2,5]

[1] Department of Oral and Maxillofacial Surgery, School and Hospital of Stomatology, Cheeloo College of Medicine, Shandong University, Jinan, China, [2] Shandong Key Laboratory of Oral Tissue Regeneration and Shandong Engineering Laboratory for Dental Materials and Oral Tissue Regeneration, Jinan, China, [3] Department of Stomatology, Shandong Medical College, Jinan, China, [4] State Key Laboratory of Oral Diseases, West China Hospital of Stomatology, Sichuan University, Chengdu, China, [5] Department of Emergency School and Hospital of Stomatology, Cheeloo College of Medicine, Shandong University, Jinan, China

OPEN ACCESS

Edited by:
Qiang Shen,
Louisiana State University,
United States

Reviewed by:
Xuan Zhou,
Tianjin Medical University Cancer Institute and Hospital, China
Yu Ren,
Tianjin Medical University, China

***Correspondence:**
Haoming Zhao
168277500@qq.com
Hongyu Chen
155171808@qq.com

Specialty section:
This article was submitted to Head and Neck Cancer, a section of the journal Frontiers in Oncology

Received: 15 July 2020
Accepted: 09 November 2020
Published: 11 December 2020

Citation:
Ma C, Shi T, Qu Z, Zhang A, Wu Z, Zhao H, Zhao H and Chen H (2020) CircRNA_ACAP2 Suppresses EMT in Head and Neck Squamous Cell Carcinoma by Targeting the miR-21-5p/STAT3 Signaling Axis. Front. Oncol. 10:583682. doi: 10.3389/fonc.2020.583682

Circular RNAs (circRNAs) contain microRNA (miRNA)-specific binding sites and can function as miRNA sponges to regulate gene expression by suppressing the inhibitory effect of miRNAs on their target genes. MiR-21-5p has been reported to be involved in the development of head and neck squamous cell carcinoma (HNSCC) and plays an important role in the activation of epithelial-mesenchymal transition (EMT). However, the upstream regulatory mechanism and downstream targets of miR-21-5p in tumor cells remain unknown. CircRNA_ACAP2 inhibits the function of miR-21-5p by binding to its specific binding sites in HNSCC cells. Overexpression of CircRNA_ACAP2 inhibits the proliferation and migration of HNSCC cells, while downregulation of CircRNA_ACAP2 has the opposite effect. STAT3 is a direct target gene of miR-21-5p and a transcription factor of ZEB1. We demonstrate that CircRNA_ACAP2 functions as a tumor suppressor gene in HNSCC and that its function is regulated *via* the miR-21-5p/STAT3 signaling axis.

Keywords: HNSCC, microRNA, circRNA, STAT3, Zeb1

INTRODUCTION

Head and neck squamous cell carcinoma (HNSCC) refers to an epithelial malignant tumor that originates in the head and neck, and over 600,000 new cases are reported every year (1, 2). The current treatment of head and neck cancer (HNC) patients is mainly based on the stage and anatomical location of the tumor, and therapies based on biological discoveries are rare. Although advances in technology and supportive treatment have improved the quality of life of HNC patients, the overall prognosis is still poor due to local recurrence and distant metastasis after surgery (3). Therefore, there is an urgent need to better understand the molecular mechanism of HNC progression to improve the prevention, diagnosis and personalized treatment of patients.

Circular RNAs (circRNAs) are an abundant and diverse class of noncoding RNA molecules that form a ring structure by covalent bonds and do not have a 5' end cap or a 3' end poly(A) tail (4, 5). The currently identified circRNAs are mainly derived from exons, but there are other types of circRNAs, such as intronic, intergenic, antisense, and sense overlapping (6, 7). MicroRNAs (miRNAs) are a group of evolutionarily conserved noncoding single-stranded RNAs consisting of 22–25 nucleotides that bind to the 3' untranslated region (3'UTR) of target mRNA to repress gene expression (8, 9). As regulatory factors, miRNAs regulate physiological and pathological processes by blocking protein translation or inducing mRNA degradation to inhibit target gene expression and are widely involved in many biological processes, such as cell metabolism, proliferation, differentiation and apoptosis (10, 11).

In a previous study, CircRNA_ACAP2 was identified as a therapeutic target for the treatment of colon cancer (10). However, the mechanism of action of CircRNA_ACAP2 in HNSCC progression remains unknown. We determined the expression levels of miR-21-5p and CircRNA_ACAP2. The linear isomers of CircRNA_ACAP2 in HNSCC tissues were used to determine its expression pattern. Moreover, we overexpressed CircRNA_ACAP2 in HNSCC cell lines and performed cell proliferation experiments to elucidate its function. We demonstrated that the CircRNA-ACAP2/miR-21-5p/STAT3 regulatory feedback loop could affect the epithelial-mesenchymal transition (EMT) of HNSCC cells. By exploring this hypothesis, we may gain insights into the pathogenicity of HNC and provide new therapeutic targets for the treatment of HNSCC.

MATERIALS AND METHODS

Patients

A total of 102 patients diagnosed with HNSCC were included in this study. All fresh tissues were collected between July 2011 and Dec 2015 during radical surgery at the Department of Oral and Maxillofacial Surgery, School and Hospital of Stomatology, Cheeloo College of Medicine, Shandong University. The samples were frozen in liquid nitrogen for 5 min and stored at −80°C. None of the enrolled patients received chemotherapy, radiotherapy, or targeted therapy before radical surgery. All patients were followed up for over 5 years or until Dec 2019. The study protocol was approved by the Institutional Review Board of School and Hospital of Stomatology, Cheeloo College of Medicine, Shandong University. Informed consent was obtained from all patients involved in this study. All methods were performed in accordance with the relevant guidelines and regulations.

Immunohistochemistry

Excised tumor and adjacent tissues were fixed in 4% paraformaldehyde, dehydrated, paraffin-embedded, and cut into sections. Consecutive 4-μm-thick sections were analyzed using primary antibodies against ZEB1 (human; ab181451; 1:200; Abcam), phospho-STAT3 (human; #9145; 1:100; Cell Signaling Technology), STAT3 (human; #4695; 1:100; Cell Signaling Technology), TWIST-1(human; PA5-49688; 1:100; Invitrogen)and a biotin-conjugated goat anti-rabbit polyclonal antibody (1:50; ZSGB-BIO, Beijing, China) as the secondary antibody. Images were obtained by light microscopy (Olympus, Japan) at 100× and 400× magnification and quantified using Image-Pro Plus. Five random fields were examined per animal.

Cell Culture

Human HNSCC cell lines, namely, HN-4, HN-9, HN-30, SCC-4, SCC-9, SCC-25, and CAL-27, were used in this study. HN-4, HN-9, HN-30, SCC-4, SCC-9, and SCC-25 cells were purchased from the Cell Bank of the Chinese Academy of Sciences (Shanghai, China), and CAL-27 cells were purchased from the American Type Culture Collection, Manassas, VA. These cells were cultured in Dulbecco's modified Eagle's medium (DMEM; Gibco-BRL, Grand Island, NY).

All cell lines were cultured in DMEM/F12 (1:1) medium (Gibco-BRL). The media were supplemented with 10% heat-inactivated fetal bovine serum (FBS) (Gibco-BRL), penicillin (100 units/ml), and streptomycin (100 μg/ml). The cells were cultured at 37°C in a humidified 5% CO_2 atmosphere.

miRNA-21-5p-Mimic Transfection

The miR-21-5p mimic and its negative control (NC) were synthesized by RiboBio (Guangzhou, China). Wild-type cells (5.0×10^5 cells/well) were grown in 6-well plates in 2 ml culture medium. When cell confluence reached 50%–60%, the miR-21-5p mimic and its negative control were treated with Lipofectamine 2000 reagent (Invitrogen, USA) according to the manufacturer's instructions. The cells were transfected in Opti-MEM (Gibco, USA) for 8 h, and then the medium was changed to normal culture medium. After 48 h, the cells were harvested for western blot and qRT-PCR. All groups were plated in 6-well culture plates at the same time and were harvested 48 h later.

Lentiviral Transduction and Screening of Stable Strains

The CircRNA-ACAP2 and miR-21-5p lentiviral expression vectors (wild-type and mutant) were constructed by GeneChem Biotechnology Co., Ltd. The CircRNA-ACAP2 lentiviral expression vector (CircRNA-ACAP2 vector) conferred puromycin resistance, while the miR-21-5p lentiviral expression vector (miR-21-5p vector) was C-terminally tagged with an HA epitope and conferred blasticidin resistance. Lentiviral transduction was performed following the manufacturer's instructions. After 72 h of transfection, the culture medium was mixed with puromycin/blasticidin at a final concentration of 3–10 μg/ml. After culturing with puromycin/blasticidin and passaging 2–3 times, stably transduced cells were screened.

Wound Healing Assay

Tumor cells were plated in 6-well plates, transfected or pre-treated as indicated, and cultured to confluency. Cells were serum-starved and scraped with a P200 tip (time 0), washed

with PBS, and incubated with serum-free DMEM. Pictures of five non-overlapping fields were taken at 24 h.

Cell Proliferation Assay

Cells transfected for 24 h with miRNA mimic or stably transduced cells were seeded into 96-well plates at a density of 1000 cells per well in triplicate. The cells were harvested, and 10 µl of CCK-8 reagent (Dojindo, Kumamoto, Japan) was added to 100 µl of culture medium. The cells were subsequently incubated for 2 h at 37°C, and the optical density was measured at 450 nm using a microplate reader (SpectraMax i3, Molecular Devices, USA).

Reverse Transcription-Quantitative Polymerase Chain Reaction Analysis

For RNA extraction, HNSCC tissues were harvested and cut into small pieces ($< 2 \times 2$ mm^2). The pieces were immediately frozen in liquid nitrogen and then ground into powder. Total RNA was extracted using TRIzol reagent (Invitrogen) according to the manufacturer's protocol. For RT-PCR, we used the SYBR Two Step Reverse Transcription-Quantitative Polymerase Chain Reaction (RT-qPCR) Kit (TaKaRa, USA, catalog number RR037A) following the manufacturer's instructions. The cycles were as follows: initial denaturation at 95°C for 30 s, followed by 40 amplification cycles of 95°C for 5 s and 60°C for 30 s. Values were quantified using the comparative cycle threshold method, and samples were normalized to GAPDH. Quantification of the relative expression levels was performed by the $2^{-\Delta\Delta CT}$ method.

Western Blotting

Cell and tissue lysates were prepared using modified RIPA buffer. Total protein concentrations were determined by a bicinchoninic acid (BCA) protein assay kit (Beyotime, catalog number P0012). Protein solution (approximately 15 µl) was resolved by 10% SDS-polyacrylamide gel electrophoresis and transferred to a polyvinylidene difluoride (PVDF) membrane (Millipore, catalog number IPVH00010). PVDF membranes containing the protein were blocked in 5% nonfat milk at room temperature for 2 h, and then the membranes were incubated with the following primary antibodies: anti-ZEB1 (human; ab181451; 1:1,000; Abcam), anti-phospho-STAT3 (human; #9145; 1:1,000; Cell Signaling Technology), and anti-STAT3 (human; #4695; 1:1,000; Cell Signaling Technology). All primary antibodies were diluted with 5% TBST buffer (with 0.1% Tween 20) and incubated overnight at 4°C. After washing with TBST buffer (with 0.1% Tween 20) three times, the membranes were incubated for 2 h with secondary horseradish peroxidase-conjugated anti-mouse (1:10,000, Servicebio, catalog number GB23301) and anti-rabbit (1:10,000, Servicebio, catalog number GB23303) antibodies. After the membranes were washed with TBST, the target proteins on the membrane were detected by an ECL detection system (Millipore, catalog MA01821). Protein band images were digitally captured, and the intensity of the bands (pixels/band) was determined using ImageJ densitometry analysis software in arbitrary optical density units.

Fluorescence *In Situ* Hybridization Assay

Fluorescence-labeled probes for CricRNA-ACAP2, miR-21-5p were designed and synthesized, and fluorescence *in situ* hybridization (FISH) experiments were performed using a Ribo™ Fluorescent *In Situ* Hybridization kit (RiboBio). Images were acquired on a TCS SP2 laser-scanning confocal microscope (Leica Microsystems, Germany).

Target Prediction

TargetScan and miRanda were used to predict potential CircRNA_ACAP2 targets. Only one target miRNA with expression in human tissues was studied further. The target genes of miR-21-5p were STAT3, GDF-5, STAT3, TIMP-3, and Smed2/3, and STAT3 was the most differentially expressed in cancer tissues and noncancerous tissues. The 3′UTR of STAT3 mRNA possesses a putative miR-21-5p binding site.

Luciferase Reporter Assay

A dual-luciferase reporter assay was performed to validate the target relationship. A CircRNA_ACAP2 segment (112 bp) with either a mutant or wild-type seed region was synthesized, cloned into the psiCHECK-2 vector (Applied Biosystems, USA), and inserted into the pmirGLO Dual-Luciferase Vector (Promega, catalog number E133A). All cell lines were transfected using Lipofectamine 2000 (Invitrogen, USA). The cells (1×10^5 cells/well) were transiently transfected with the CircRNA_ACAP2 segment vector. To knock down miR-21-5p expression, siRNAs against miR-21-5p and a negative control siRNA (NC-siRNA) were prepared (GeneChem, Shanghai, China). Cotransfection of 20 nmol/L miR-21-5p mimics or control was then performed. After 48 h, HN-9 and SCC-25 cells were harvested, and luciferase activity was assayed using the Dual-Luciferase Reporter Assay System (Promega, catalog number E1910).

Statistical Analysis

The statistical analyses were performed using GraphPad Prism software (GraphPad Software Inc.). For data with normal distribution and/or equal variances, significant differences between two and more than three groups were determined by two-tailed Student's t test and one-way ANOVA followed by Bonferroni's *post hoc* comparison test, respectively. P values lower than 0.05 were considered to be statistically significant. The results are presented as the mean ± SEM from at least three independent experiments.

RESULTS

CircRNA-ACAP2 Is Downregulated in HNSCC Tissues, and miR-21-5p, P-STAT3 Are Upregulated and Negatively Correlated

We investigated 102 pairs of human HNSCC specimens and adjacent noncancerous tissue samples *via* RT-qPCR to confirm CircRNA_ACAP2 expression in HNSCC. CircRNA_ACAP2

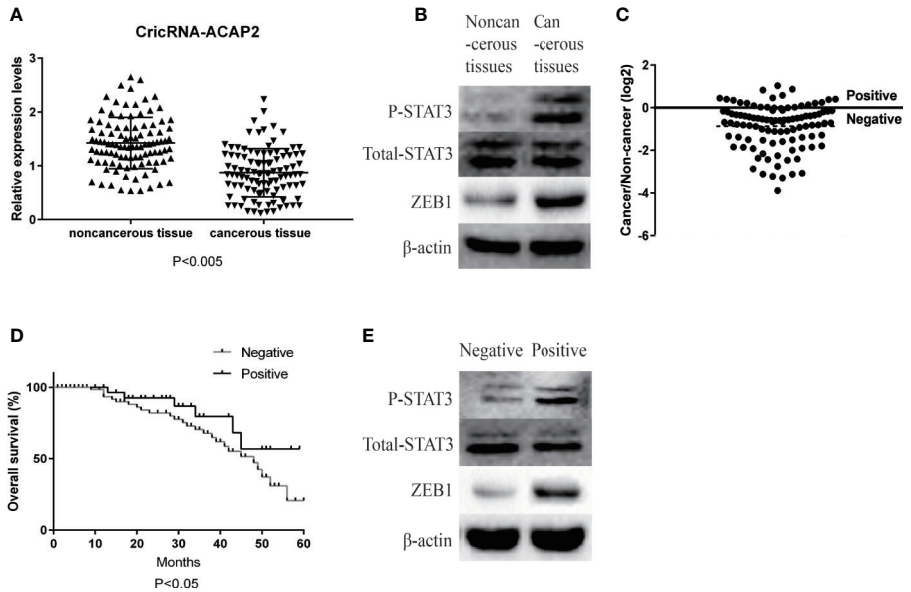

FIGURE 1 | Relative expression level of CricRNA-ACAP2. **(A)** Relative expression level of CricRNA-ACAP2 in 102 head and neck squamous cell carcinoma (HNSCC) tissues and in paired adjacent normal tissues. **(B)** Relative protein expression level of STAT3,P-STAT3,ZEB1 in HNSCC tissues and in paired adjacent normal tissues. **(C)** Cancer/non-cancer ratio of CricRNA-ACAP2 expression level in 102 HNSCC tissues and in paired adjacent normal tissues. **(D)** The Kaplan-Meier survival analysis indicated that negative group has a worse overall survival compared to the positive group. **(E)** Relative protein expression level of STAT3,P-STAT3, ZEB1 in negative HNSCC tissues and in positive HNSCC tissues. Error bars represent mean ± standard deviation (SD). P value was written in the figure.

expression was markedly downregulated in 89.2% (91/102) of HNSCC tissues (**Figure 1A**) and was significantly lower than that in the corresponding adjacent noncancerous tissues ($P < 0.005$). We examined the expression of P-STAT3 and ZEB1 in cancer tissues and noncancerous tissues and found that the expression of ZEB1 in HNSCC tissue was significantly upregulated, while STAT3 was significantly phosphorylated (**Figure 1B**). In addition, we divided all the cases into two groups according to the ratio of CircRNA_ACAP2 expression levels in cancer tissues and noncancerous tissues (**Figure 1C**). The results of Kaplan-Meier survival analysis indicated that the positive group had better overall survival than the negative group (**Figure 1D**). We compared the expression of P-STAT3 and ZEB1 at the protein level and found that the expression of ZEB1 at the protein level was significantly higher in the negative group than in the positive group, while the phosphorylation level of STAT3 was obviously higher in the negative group than in the positive group (**Figure 1E**).

We detected P-STAT3, ZEB1, and Twist1 in squamous cell carcinoma tissues and adjacent tissues by immunohistochemistry. These proteins are all related to the epithelial-mesenchymal transition effect of tumor cells, and these proteins are expressed in cancer tissues. Higher than adjacent tissues. We selected the STAT3 protein as a control, and found that the total STAT3 expression did not change significantly (**Figure 2**). The expression of CricRNA-ACAP2 in non-cancerous tissues is higher than that in cancerous tissues, while the expression trend of miR-21 is opposite (**Figure 3**). The amount of CricRNA-ACAP2 in the cytoplasm was higher than that observed in the nucleus, revealing that CricRNA-ACAP2 is predominantly located in the cytoplasm.

The Expression of CircRNA_ACAP2 and miR-21-5p in Various Head and Neck Squamous Cell Carcinoma Cell Lines

The potential targets of CircRNA_ACAP2 were searched in bioinformatics databases *via* TargetScan and miRanda to explore the underlying molecular mechanism. In addition, the potential binding sites of miR-21-5p in STAT3 were predicted (**Figure 4A**). We analyzed miR-21-5p expression in human HNSCC cell lines. The expression level of miR-21-5p in HNSCC tissues was significantly higher than that in adjacent tissues ($P<0.005$) (**Figure 4B**). To explore the relationship between CircRNA_ACAP2 and miR-21-5p in various HNSCC cells, we examined the expression levels of CircRNA-ACAP2 (**Figure 4C**) and miR-21-5p (**Figure 4D**) in different HNSCC cell lines, namely, HN-4, HN-9, HN-30, SCC-4, SCC-9, SCC-25, and CAL-27. A significant negative correlation was found between the expression levels of miR-21-5p and CircRNA-ACAP2 (**Figure 4E**).

MiR-21-5p Is a Direct Target of CircRNA-ACAP2, and STAT3 Is a Direct Target Gene of miR-21-5p

To determine whether miR-21-5p directly targets CircRNA_ ACAP2, we generated dual-luciferase reporter plasmids carrying a fragment of the mutant or wild-type CircRNA_ACAP2 sequence

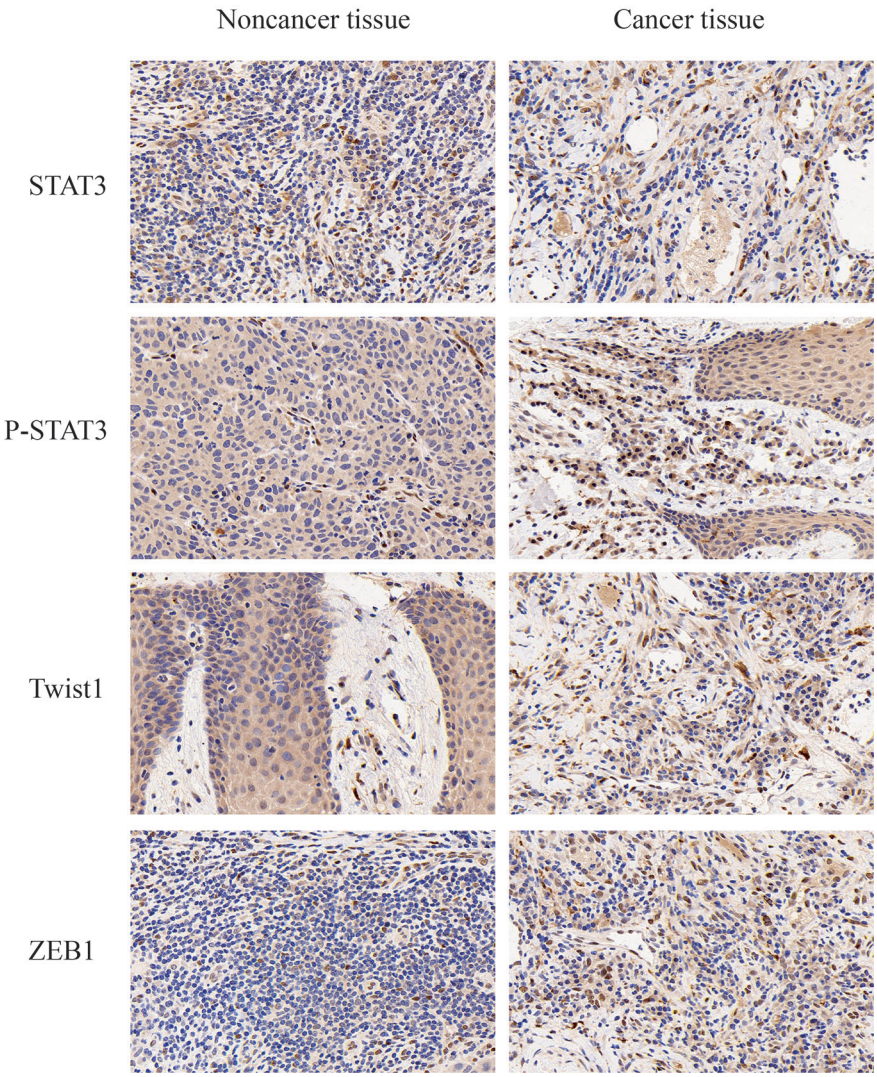

FIGURE 2 | Immunohistochemistry. P-STAT3, ZEB1, and Twist1 in squamous cell carcinoma tissues and adjacent tissues were detected by immunohistochemistry. P value was written in the figure.

and the predicted miR-21-5p binding site. A dual-luciferase reporter assay was then performed in randomly selected HN-9 and SCC-25 cells. The normalized fluorescence intensity of the wild-type CircRNA_ACAP2 reporter was considerably lower in cancer cells cotransfected with the miR-21-5p mimics than the control (**Figure 5A**). In contrast, no significant difference was found between the control cells and cells cotransfected with miR-21-5p mimics and the mutant CircRNA_ACAP2 reporter (**Figure 5B**).

A dual-luciferase reporter assay was conducted to investigate whether STAT3 mRNA is a target of miR-21-5p. HN-9 and SCC-25 cells were cotransfected with the miR-21-5p mimic and pmirGLO vectors, and a considerable reduction was observed in the STAT3 wild-type 3′UTR group relative to the negative control vector group, but no significant reduction was found in the STAT3 mutant 3′UTR group (**Figures 5C, D**). Collectively, the abovementioned results suggested that miR-21-5p could regulate STAT3 protein expression in chondrocytes by targeting the STAT3 mRNA 3′UTR.

Different Effects of CircRNA-ACAP2 and miR-21-5p on the Proliferation of Head and Neck Squamous Cell Carcinoma Cells

We performed a functional assay by transfecting pcDNA3.1-CircRNA_ACAP2/miR-21-5p mimics or negative control reagents into HN-9 and SCC-25 cells, and the results showed that CircRNA_ACAP2 had low expression in all cell lines tested. We evaluated the effect of CircRNA_ACAP2 on the proliferation of HNSCC cells through the CCK-8 assay. Overexpression of CircRNA_ACAP2 inhibited the proliferation of HN-9 and SCC-25 cells (**Figures 6A, C**). Therefore, our results showed that

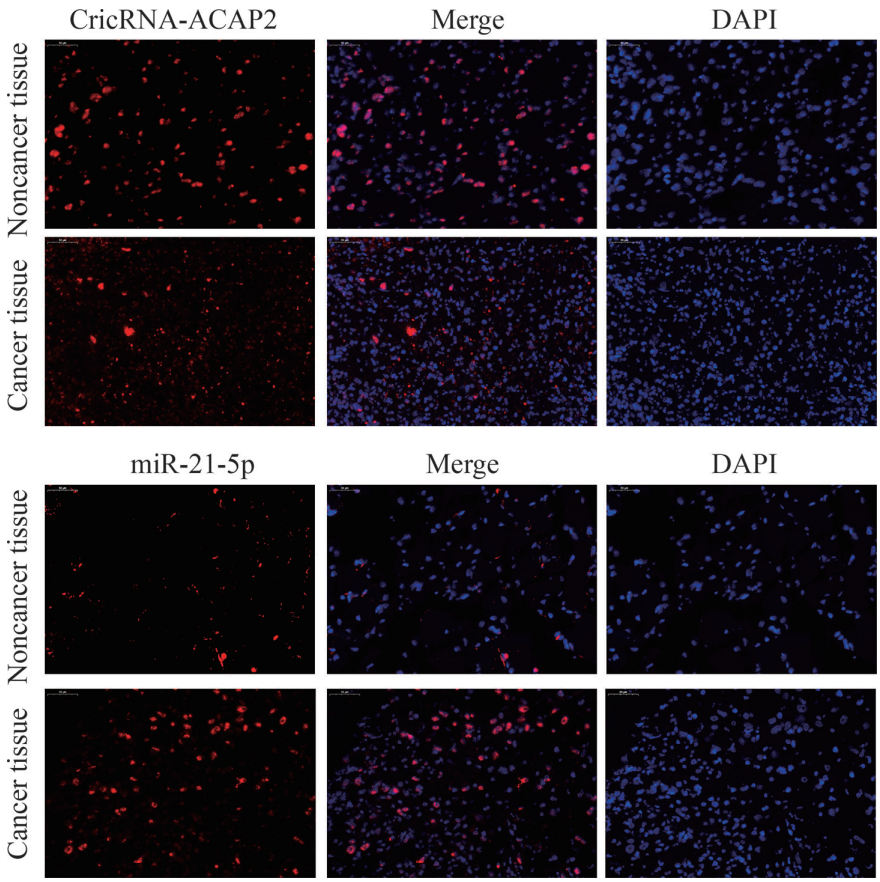

FIGURE 3 | Fluorescence *in situ* hybridization (FISH) assay. FISH analysis of CricRNA-ACAP2 and miR-21-5p in HNSCC tissue. (The nuclei were stained with DAPI).

CircRNA_ACAP2 inhibited the proliferation of HNSCC cells. If the effect of CircRNA_ACAP2 is specific, the effect of CircRNA_ACAP2 overexpression must be suppressed by coexpression of miR-21-5p. To test this hypothesis, miR-21-5p mimics (which increase miR-21-5p levels) were cotransfected with pcDNA3.1-CircRNA_ACAP2 into HN-9 and SCC-25 cells. Then, CCK-8 measurements were performed. In HN-9 and SCC-25 cells, cells coexpressing CircRNA_ACAP2 and miR-21-5p mimics had significantly increased growth rates compared to cells coexpressing CircRNA_ACAP2 and the control (**Figures 6B, D**). The results of Wound-healing assay demonstrated that CircRNA_ACAP2 overexpression suppressed cell migration and invasion in SCC-25 cells, while CircRNA_ACAP2 overexpression has no effect on cell migration and invasion in SCC-9 cells (**Figure 7**).

CircRNA-ACAP2 and miR-21-5p Regulate Epithelial–Mesenchymal Transition Through STAT3

When SCC-25 cells were transfected with pcDNA3.1-CircRNA-ACAP2, the expression of miR-21-5p was significantly suppressed (**Figure 8A**). Conversely, when miR-21-5p was knocked down by siRNA, the expression of CircRNA-ACAP2 was significantly upregulated (**Figure 8B**). Simultaneously, in the pcDNA3.1-CircRNA-ACAP2 group, we found that the expression of ZEB1 was significantly upregulated and that STAT3 was phosphorylated, with no significant change in the expression of total STAT3. When cells were transfected with the miR-21-5p mimic, the expression of ZEB1 was significantly increased, and the phosphorylation of STAT3 was significantly upregulated. However, after cotransfection of CircRNA_ACAP2 and miR-21-5p mimics, the expression of ZEB1 was inhibited (**Figure 8C**).

DISCUSSION

CircRNAs are an intriguing class of RNA molecules due to their covalently closed structure, high stability, and implicated roles in gene regulation (12). The downregulation of circRNAs in proliferative cells across different tumor types could indicate that some circRNAs may have tumor-suppressive roles (13). Although circRNAs were discovered 40 years ago, they have become a hot spot in related disease research in recent years due to the increased understanding of their biological characteristics,

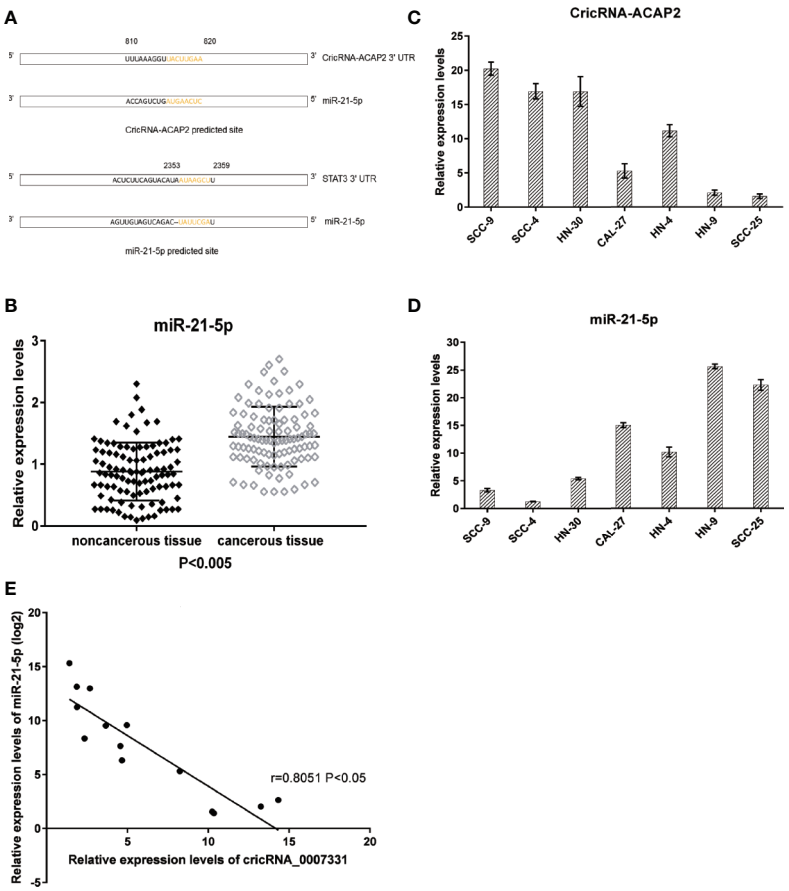

FIGURE 4 | Predicted downstream miRNA and target gene. **(A)** Predicted binding site of downstream miRNA and target gene. **(B)** Relative expression level of miR-21-5p in 102 HNSCC tissues and in paired adjacent normal tissues. **(C, D)** Endogenous CricRNA-ACAP2 and miR-21-5p expression in serial HNSCC cell lines. **(E)** Correlation of expression between miR-21-5p and CricRNA-ACAP2. Error bars represent mean ± standard deviation (SD). P value was written in the figure.

production mechanism and functional significance (14). Most circRNAs are endogenous noncoding RNAs that have a high degree of conservation among species (7). Compared to linear RNAs, circRNAs have high stability. Some circRNAs have miRNA-specific binding sites (12, 15). Consequently, by competitively binding with miRNAs to inhibit the degradation of the corresponding target gene mRNAs, circRNAs can function similar to lncRNAs, which act as miRNA sponges to adsorb miRNAs and regulate the expression of downstream target genes (16, 17).

Due to the development of microarray chips and sequencing technology, a large number of studies have detected the abnormal expression of circRNAs in cancer samples (15). In pancreatic ductal adenocarcinoma (PDAC), the abnormal expression of circRNAs has been confirmed as one of the characteristics of early PDAC (18). circRNA_100855 and circRNA_104912 are the most significantly deregulated circRNAs in laryngeal cancer, while circRNA_001059 and circRNA_000167 are significantly inactivated in radiation-resistant esophageal cancer (19, 20). Many circRNAs with miRNA response elements (MREs) are found in basal cell carcinoma (BBC) and cutaneous squamous cell carcinoma (CSCC) (21, 22). More recently, it was reported that 69 differentially expressed circRNAs might interact with certain miRNAs to influence mRNA expression in HNSCC (23).

Through bioinformatics analysis, we found that hsa_circ-ACAP2 is upregulated in many types of tumor tissues. Hsa_circ_ACAP2 is encoded by the ACAP2 gene, which is a homolog of *C. elegans* CNT-1, a gene that promotes apoptosis, and has the same inositol phosphate-binding pattern as CNT-1. We predicted that hsa-miR-21-5p is a specific target of circRNA-ACAP2 through the bioinformatics tools TargetScan and miRanda (10). Moreover, some studies have found that miRNA-21-5p is highly related to STAT3 transcription, and it is also one of the few miRNAs that can promote STAT3 expression. Through comparisons and screening of human gene libraries, we know that the target genes of miRNA-21-5p include IL-6 receptor (IL-6R), STAT3, TIMP3 and so on (24). The JAK/STAT3 signaling pathway activated by the IL6/IL-6R/IL-6Rβ (gp130) complex plays a key role in the growth and development of many human cancers. The IL-6/JAK/STAT3 pathway is overactivated in many cancer patients, and numerous studies involving preclinical *in vitro* and *in vivo* models have

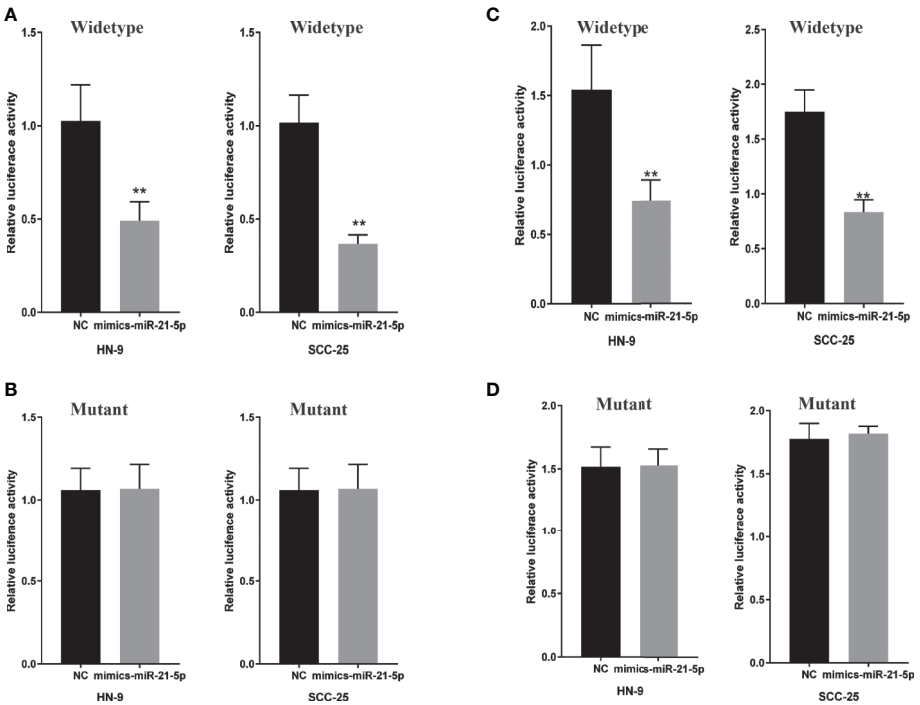

FIGURE 5 | MiR-21-5p is a direct target of CricRNA-ACAP2 and P-STAT3 is a direct target gene of miR-21-5p. **(A)** Fluorescence intensity of CricRNA-ACAP2 segment was significantly reduced in the miR-21-5p mimics and wild-type dual-luciferase reporter plasmid transfected group in the two HNSCC cell lines. **(B)** Fluorescence intensity of CricRNA-ACAP2 segment showed no significant change in the miR-21-5p mimics and mutant dual-luciferase reporter plasmid-transfected group in the two HNSCC cell lines. **(C, D)** Dual luciferase reporter assay to validate target relationship between Spry-1 and miR-21-5p. HN-9 and SCC-25 were transfected with mimic miR-21-5p. Error bars represent mean of three separate determinations ± standard deviation (SD). Asterisk indicates statistically significant changes: * ($P < 0.05$), ** ($P < 0.01$).

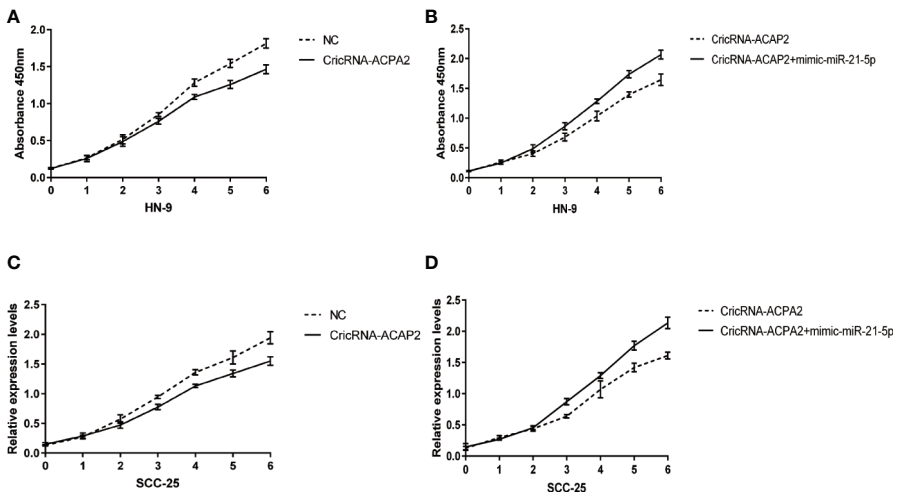

FIGURE 6 | CricRNA-ACAP2-miR-21-5p axis mediated proliferation of head and neck squamous cell carcinoma (HNSCC) cell lines. **(A, C)** CricRNA-ACAP2 overexpression inhibits cell growth in HN-9 and SCC-25. **(B, D)** miR-21-5p can interrupt the cell growth inhibition function of CricRNA-ACAP2.

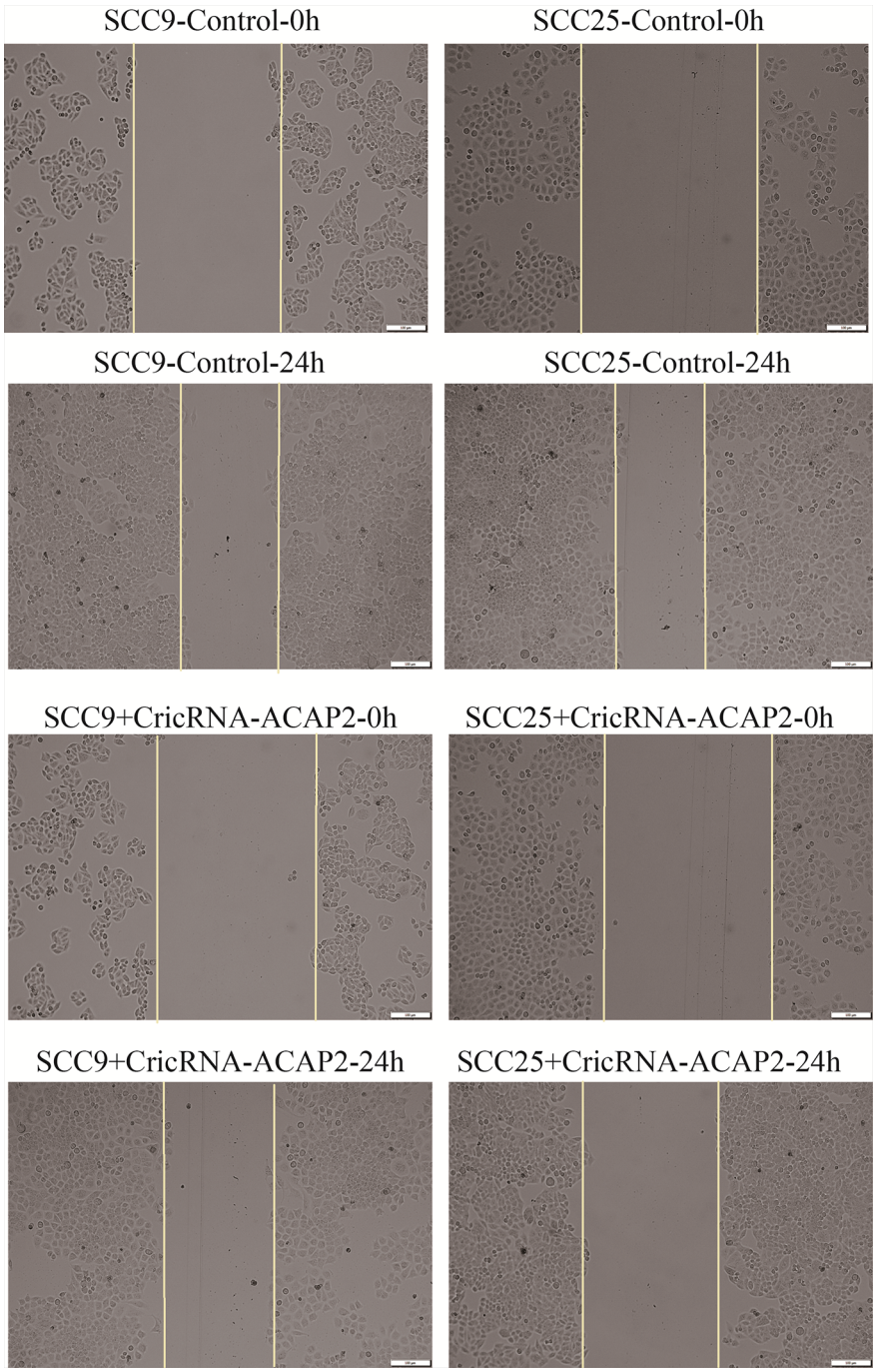

FIGURE 7 | Wound healing assay. The results of Wound healing assay demonstrated that CircRNA_ACAP2 overexpression suppressed cell migration and invasion in SCC-25 cells, while CircRNA_ACAP2 overexpression has no effect on cell migration and invasion in SCC-9 cells.

shown that targeting a single nodule in this pathway can have antitumor effects. Therefore, therapies targeting this pathway may benefit cancer patients by inhibiting tumor cell growth and stimulating antitumor immunity. IL-6 levels are elevated in a large number of patients with malignant solid tumors (25). Elevated IL-6 levels stimulate excessive activation of the JAK/STAT3 signaling pathway, often predicting poor patient prognosis. Increased IL-6 levels have been observed in the serum and tumor microenvironment, and all immune cells (such as NK cells, effector T cells, and DCs) in the tumor microenvironment express IL-6R. The activated STAT3 signaling pathway initiates the transcription process, including

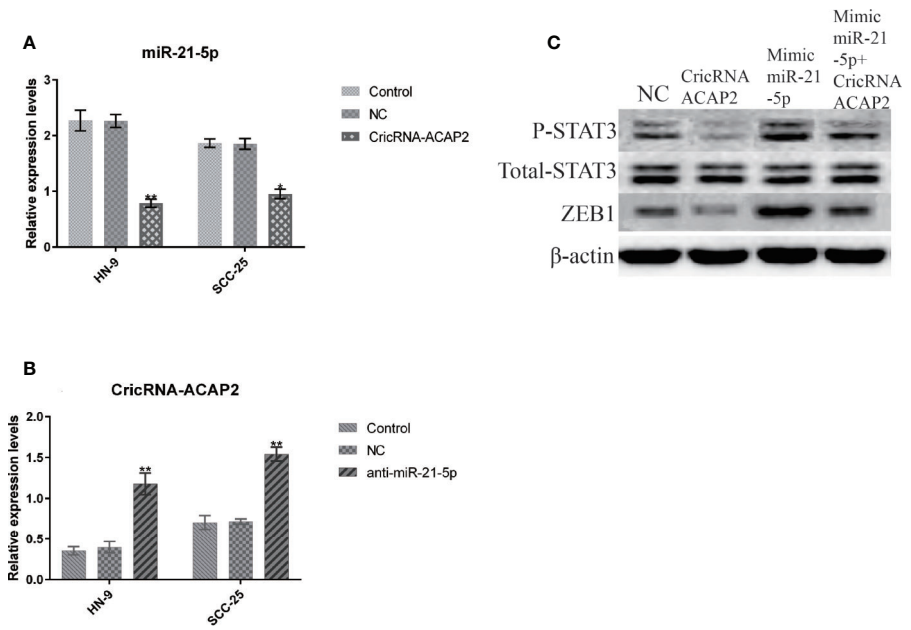

FIGURE 8 | CricRNA-ACAP2 and miR-21-5p regulate ERK phosphorylation through P-STAT3. **(A)** The expression of miR-21-5p in HN-9 and SCC-25 is significantly suppressed *via* transfecting pcDNA3.1-CricRNA-ACAP2. **(B)** When miR-21-5p was knocked down by siRNA, the expression of CricRNA-ACAP2 was significantly up-regulated. **(C)** CricRNA-ACAP2 and miR-21-5p regulate ERK phosphorylation throughP-STAT3.

the expression of PD-L1, which in turn enhances tumor immunosuppression. Therefore, the effects of inhibiting miR-21-5p will affect the tumor in two aspects in terms of inhibiting the expression of IL-6R and STAT3 (26, 27). Drugs targeting various lymph nodes, including IL-6, IL-6R, and JAK, have been approved by the FDA and can be used to treat inflammatory diseases or myeloproliferative tumors. At present, many such drugs are also under active research to treat other malignant tumors and solid tumors of the hematopoietic system (25).

EMT is a process in which polar epithelial cells transform into mesenchymal cells and acquire invasion and migration capabilities (28). Current studies have found that partial activation of EMT is the main driving force for tumors from initiation to metastasis (29). EMT is a multistep dynamic process, in which the connections between epithelial cells disappear, the tissue structure becomes loose, and cubic epithelial cells acquire a spindle-shaped fibrous cell morphology and exhibit aggressiveness (30). HNSCC cells with an EMT phenotype have strong motility, allowing them to infiltrate locally, invade blood vessels and lymphatic vessels, and migrate to target organs for secondary metastasis. After reaching the target organ, cancer cells can initiate mesenchymal epithelial transformation to rebuild intercellular connections and the cytoskeleton to form metastases. Epithelioid tumor cells have strong proliferation ability and help metastatic cancer cells complete metastatic colonization (31).

Our study showed that miR-21-5p is of great significance in the early diagnosis, treatment and prognosis of HNSCC. However, it is still difficult to use miR-21-5p as a therapeutic target. CircRNAs are more stable than miRNAs. We think that it can be used as a targeted drug for the treatment of HNSCC. In addition, IL-6R is one of the target genes of miR-21-5p, and secreted IL-6R (sIL-6R) is associated with metastasis and immunosuppression in most cancers. Furthermore, the JAK/STAT3 signaling pathway is regulated by the IL-6/IL-6R/gp130 complex. Epigenetic changes play an important role in the abnormal activation of the IL-6/IL-6R/JAK/STAT3 pathway in cancer, and changes in transcription factor expression and/or activation may be involved in cancer progression (25). MiR-21-5p can simultaneously target two signaling pathways mediated by IL-6 (32, 33). Circulating IL-6 levels have been verified to be a prognostic indicator of survival in several different types of cancers and a predictor of the response to treatment.

DATA AVAILABILITY STATEMENT

The raw data supporting the conclusions of this article will be made available by the authors, without undue reservation.

ETHICS STATEMENTS

The studies involving human participants were reviewed and approved by The Ethics Committee of Shandong University. The patients/participants provided their written informed consent to

participate in this study. No animal studies are presented in this manuscript. No potentially identifiable human images or data is presented in this study.

AUTHOR CONTRIBUTIONS

Conceived and designed the experiments: CM, TS, HAZ; Performed the experiments: HC, ZQ, CM; Analyzed the data: AZ, ZW; Contributed reagents/materials/analysis tools: CM, TS, HUZ, HAZ. All authors contributed to the article and approved the submitted version.

FUNDING

This work was supported by the Natural Science Foundation of Shandong Province (No. ZR2018PH022) and the China Postdoctoral Science Foundation (No. 2019M652408).

REFERENCES

1. Siegel RL, Miller KD, Jemal A. Cancer statistics, 2016. *CA Cancer J Clin* (2016) 66:7–30. doi: 10.3322/caac.21332
2. Hedberg ML, Goh G, Chiosea SI, Bauman JE, Freilino ML, Zeng Y, et al. Genetic landscape of metastatic and recurrent head and neck squamous cell carcinoma. *J Clin Invest* (2016) 126:1606. doi: 10.1172/JCI86862
3. Sacco AG, Cohen EE. Current Treatment Options for Recurrent or Metastatic Head and Neck Squamous Cell Carcinoma. *J Clin Oncol* (2015) 33:3305–13. doi: 10.1200/JCO.2015.62.0963
4. Li J, Yang J, Zhou P, Le Y, Zhou C, Wang S, et al. Circular RNAs in cancer: novel insights into origins, properties, functions and implications. *Am J Cancer Res* (2015) 5:472–80.
5. Jiang Y, Zhang Q, Hu Y, Li T, Yu J, Zhao L, et al. ImmunoScore Signature: A Prognostic and Predictive Tool in Gastric Cancer. *Ann Surg* (2018) 267:504–13. doi: 10.1097/SLA.0000000000002116
6. Memczak S, Papavasileiou P, Peters O, Rajewsky N. Identification and Characterization of Circular RNAs As a New Class of Putative Biomarkers in Human Blood. *PloS One* (2015) 10:e0141214–e0141214. doi: 10.1371/journal.pone.0141214
7. Memczak S, Jens M, Elefsinioti A, Torti F, Krueger J, Rybak A, et al. Circular RNAs sare a large class of animal RNAs with regulatory potency. *Nature* (2013) 495:333–8. doi: 10.1038/nature11928
8. Hansen TB, Jensen TI, Clausen BH, Bramsen JB, Finsen B, Damgaard CK, et al. Natural RNA circles function as efficient microRNA sponges. *Nature* (2013) 495:384–8. doi: 10.1038/nature11993
9. Jeck WR, Sharpless NE. Detecting and characterizing circular RNAs. *Nat Biotechnol* (2014) 32:453–61. doi: 10.1038/nbt.2890
10. He J-H, Li Y-G, Han Z-P, Zhou J-B, Chen W-M, Lv Y-B, et al. The CircRNA-ACAP2/Hsa-miR-21-5p/ Tiam1 Regulatory Feedback Circuit Affects the Proliferation, Migration, and Invasion of Colon Cancer SW480 Cells. *Cell Physiol Biochem: Int J Exp Cell Physiol Biochem Pharmacol* (2018) 49:1539–50. doi: 10.1159/000493457
11. Wang X, Zhang Y, Huang L, Zhang J, Pan F, Li B, et al. Decreased expression of hsa_circ_001988 in colorectal cancer and its clinical significances. *Int J Clin Exp Pathol* (2015) 8:16020–5.
12. Vo JN, Cieslik M, Zhang Y, Shukla S, Xiao L, Zhang Y, et al. The Landscape of Circular RNA in Cancer. *Cell* (2019) 176:869–881.e13. doi: 10.1016/j.cell.2018.12.021
13. Kristensen LS, Andersen MS, Stagsted LVW, Ebbesen KK, Hansen TB, Kjems J. The biogenesis, biology and characterization of circular RNAs. *Nat Rev Genet* (2019) 20:675–91. doi: 10.1038/s41576-019-0158-7
14. Chen L-L, Yang L. Regulation of circRNA biogenesis. *RNA Biol* (2015) 12:381–8. doi: 10.1080/15476286.2015.1020271
15. Qu S, Song W, Yang X, Wang J, Zhang R, Zhang Z, et al. Microarray expression profile of circular RNAs in human pancreatic ductal adenocarcinoma. *Genom Data* (2015) 5:385–7. doi: 10.1016/j.gdata.2015.07.017
16. Zhang Z, Xie Q, He D, Ling Y, Li Y, Li J, et al. Circular RNA: new star, new hope in cancer. *BMC Cancer* (2018) 18:834. doi: 10.1186/s12885-018-4689-7
17. Gao Y, Zhang C, Liu Y, Wang M. Circular RNA profiling reveals circRNA1656 as a novel biomarker in high grade serous ovarian cancer. *Biosci Trends* (2019) 13:204–11. doi: 10.5582/bst.2019.01021
18. Li H, Hao X, Wang H, Liu Z, He Y, Pu M, et al. Circular RNA Expression Profile of Pancreatic Ductal Adenocarcinoma Revealed by Microarray. *Cell Physiol Biochem Int J Exp Cell Physiol Biochem Pharmacol* (2016) 40:1334–44. doi: 10.1159/000453186
19. Xuan L, Qu L, Zhou H, Wang P, Yu H, Wu T, et al. Circular RNA: a novel biomarker for progressive laryngeal cancer. *Am J Trans Res* (2016) 8:932–9.
20. Su H, Lin F, Deng X, Shen L, Fang Y, Fei Z, et al. Profiling and bioinformatics analyses reveal differential circular RNA expression in radioresistant esophageal cancer cells. *J Transl Med* (2016) 14:225–5. doi: 10.1186/s12967-016-0977-7
21. Sand M, Bechara FG, Sand D, Gambichler T, Hahn SA, Bromba M, et al. Circular RNA expression in basal cell carcinoma. *Epigenomics* (2016) 8:619–32. doi: 10.2217/epi-2015-0019
22. Sand M, Bechara FG, Gambichler T, Sand D, Bromba M, Hahn SA, et al. Circular RNA expression in cutaneous squamous cell carcinoma. *J Dermatol Sci* (2016) 83:210–8. doi: 10.1016/j.jdermsci.2016.05.012
23. Chen X, Yu J, Tian H, Shan Z, Liu W, Pan Z, et al. Circle RNA hsa_circRNA_100290 serves as a ceRNA for miR-378a to regulate oral squamous cell carcinoma cells growth via Glucose transporter-1 (GLUT1) and glycolysis. *J Cell Physiol* (2019) 234:19130–40. doi: 10.1002/jcp.28692
24. Sheng B, Zhao L, Zang X, Zhen J, Chen W. miR-375 ameliorates sepsis by downregulating miR-21 level via inhibiting JAK2-STAT3 signaling. *Biomed Pharmacother Biomed Pharmacother* (2017) 86:254–61. doi: 10.1016/j.biopha.2016.11.147
25. Johnson DE, O'Keefe RA, Grandis JR. Targeting the IL-6/JAK/STAT3 signalling axis in cancer. *Nat Rev Clin Oncol* (2018) 15:234–48. doi: 10.1038/nrclinonc.2018.8
26. Calvier L, Chouvarine P, Legchenko E, Hoffmann N, Geldner J, Borchert P, et al. PPARγ Links BMP2 and TGFβ1 Pathways in Vascular Smooth Muscle Cells, Regulating Cell Proliferation and Glucose Metabolism. *Cell Metab* (2017) 25:1118–34.e7. doi: 10.1016/j.cmet.2017.03.011
27. Mishra A, La Perle K, Kwiatkowski S, Sullivan LA, Sams GH, Johns J, et al. Mechanism, Consequences, and Therapeutic Targeting of Abnormal IL15 Signaling in Cutaneous T-cell Lymphoma. *Cancer Discovery* (2016) 6:986–1005. doi: 10.1158/2159-8290.CD-15-1297
28. Iser IC, Pereira MB, Lenz G, Wink MR. The Epithelial-to-Mesenchymal Transition-Like Process in Glioblastoma: An Updated Systematic Review and In Silico Investigation. *Med Res Rev* (2017) 37:271–313. doi: 10.1002/med.21408
29. Dominguez C, David J, Palena C. Epithelial-mesenchymal transition and inflammation at the site of the primary tumor. *Semin Cancer Biol* (2017) 47:177–84. doi: 10.1016/j.semcancer.2017.08.002
30. Mittal V. Epithelial Mesenchymal Transition in Tumor Metastasis. *Annu Rev Pathol* (2018) 13:395–412. doi: 10.1146/annurev-pathol-020117-043854
31. Chen H, Liu H, Mao M, Tan Y, Mo X, Meng X, et al. Crosstalk between autophagy and epithelial-mesenchymal transition and its application in cancer therapy. *Mol Cancer* (2019) 18:101. doi: 10.1186/s12943-019-1030-2
32. Ma S, Zhang A, Li X, Zhang S, Liu S, Zhao H, et al. MiR-21-5p regulates extracellular matrix degradation and angiogenesis in TMJOA by targeting Spry1. *Arthritis Res Ther* (2020) 22:99. doi: 10.1186/s13075-020-2145-y
33. Liu Y, Luo F, Wang B, Li H, Xu Y, Liu X, et al. STAT3-regulated exosomal miR-21 promotes angiogenesis and is involved in neoplastic processes of

transformed human bronchial epithelial cells. *Cancer Lett* (2016) 370:125–35. doi: 10.1016/j.canlet.2015.10.011

Conflict of Interest: The authors declare that the research was conducted in the absence of any commercial or financial relationships that could be construed as a potential conflict of interest.

Copyright © 2020 Ma, Shi, Qu, Zhang, Wu, Zhao, Zhao and Chen. This is an open-access article distributed under the terms of the Creative Commons Attribution License (CC BY). The use, distribution or reproduction in other forums is permitted, provided the original author(s) and the copyright owner(s) are credited and that the original publication in this journal is cited, in accordance with accepted academic practice. No use, distribution or reproduction is permitted which does not comply with these terms.

frontiers in Oncology

ORIGINAL RESEARCH
published: 21 December 2020
doi: 10.3389/fonc.2020.544476

Down-Regulation of *MiR-181c-5p* Promotes Epithelial-to-Mesenchymal Transition in Laryngeal Squamous Cell Carcinoma *via* Targeting *SERPINE1*

Xin Li[1,2,3], *Ping Wu*[1,2,3]*, *Yaoyun Tang*[1,2,3], *Yuhua Fan*[1,2,3], *Yalan Liu*[1,2,3], *Xing Fang*[1,2,3], *Wei Wang*[1,2,3] *and Suping Zhao*[1,2,3]

[1] Department of Otorhinolaryngology Head and Neck Surgery, Xiangya Hospital of Central South University, Changsha, China, [2] Province Key Laboratory of Otolaryngology Critical Diseases, Xiangya Hospital of Central South University, Changsha, China, [3] National Clinical Research Center for Geriatric Disorders, Xiangya Hospital of Central South University, Changsha, China

OPEN ACCESS

Edited by:
Qiang Shen,
Louisiana State University,
United States

Reviewed by:
Jun Zhang,
University of California, Davis,
United States
Xuan Zhou,
Tianjin Medical University Cancer Institute and Hospital, China

***Correspondence:**
Ping Wu
wupingcsu@hotmail.com

Specialty section:
This article was submitted to Head and Neck Cancer, a section of the journal Frontiers in Oncology

Received: 20 March 2020
Accepted: 18 November 2020
Published: 21 December 2020

Citation:
Li X, Wu P, Tang Y, Fan Y, Liu Y, Fang X, Wang W and Zhao S (2020) Down-Regulation of MiR-181c-5p Promotes Epithelial-to-Mesenchymal Transition in Laryngeal Squamous Cell Carcinoma via Targeting SERPINE1. Front. Oncol. 10:544476. doi: 10.3389/fonc.2020.544476

Laryngeal squamous cell carcinoma (LSCC) arises from the squamous epithelium of the larynx and is associated with a high incidence of cervical lymph node metastasis. MicroRNAs (miRNAs) play a crucial role in the epigenetic regulation of cellular biological processes, including cancer metastasis. However, the molecular mechanisms of specific miRNAs responsible for LSCC metastasis and their clinical significance have yet to be fully elucidated. In this study, LSCC cohort datasets from the Gene Expression Omnibus (GEO) and The Cancer Genome Atlas (TCGA) were downloaded and examined by comprehensive bioinformatics analysis, which revealed that upregulation of mRNA *SERPINE1* and downregulation of *miR-181c-5p* were associated with unfavorable overall survival. Our analysis showed that *SERPINE1* expression negatively correlated with the expression level of *miR-181c-5p* in our LSCC patient samples. Silencing of *miR-181c-5p* expression promoted cell migration and invasion in cell lines, whereas the overexpression of *miR-181c-5p* suppressed cell migration and epithelial-to-mesenchymal transition (EMT) through the downregulation of *SERPINE1.* Further analysis showed that the enhancement effect on EMT and metastasis induced by silencing *miR-181c-5p* could be rescued through knockdown of *SERPINE1* expression *in vitro.* Collectively, our findings indicated that *miR-181c-5p* acted as an EMT suppressor miRNA by downregulation of *SERPINE1* in LSCC and offers novel strategies for the prevention of metastasis in LSCC.

Keywords: miRNA, mRNA, laryngeal squamous cell carcinoma, epithelial-to-mesenchymal transition, biomarker

INTRODUCTION

Laryngeal cancer (LC) is the most common malignant neoplasm in head and neck. The predominant histopathological characteristic of LC is squamous cell cancer; this can affect different regions of the larynx and is associated with different symptoms and various treatment approaches (1, 2). Epidemiologically, the incidence of laryngeal squamous cell cancer (LSCC) has increased over recent years and now represents a serious threat for human health. Each year, over 110,000 new cases are diagnosed and of these, approximately 40 percent progress to an advanced stage (3). Tobacco smoking and alcohol consumption are known to be significant risk factors for LSCC (4). Therapeutic interventions for patients with LSCC vary according to the stage of cancer, and can involve surgery, radiotherapy, adjuvant radiation, or chemoradiation, which can be applied as a single modality or as a multimodal strategy (2). However, due to loco-regional relapse and/or distant metastasis, the overall survival (OS) of advanced LSCC has improved only slightly over the past decades and appropriate treatment remains a major challenge. The identification of molecular biomarkers for LSCC metastasis could help to improve the prognosis of patients and may also facilitate the prediction of patient survival.

MicroRNAs (miRNAs) are a class of small non-coding single-stranded RNA molecules that are located on the endogenous chromosomes. These molecules are approximately 19–25 nucleotides in length and are known to play a role in post-transcriptional gene regulation (5). MiRNAs can regulate the expression of target genes involved in the development and progression of cancer by acting as oncogenes or tumor suppressor genes (6). Over recent years, evidence has grown to support the potential regulatory role of miRNAs in the pathological changes that occur in LSCC. For example, *mir-141*, *mir-203*, and *miR-1469* can influence the progression of LSCC cells *via* their involvement in epithelial-to-mesenchymal transition (EMT) (7), lymph node metastasis (8), and the p53-mediated pathway (9). Other studies have indicated that *miR-21*, *miR-155*, *miR-192*, and *miR-375* regulate activation of the NF-kB pathway in LSCC (10). Therefore, these specific miRNAs may have great potential as LSCC biomarkers to improve the early detection.

EMT is a complex process through which epithelial cells lose their characteristic features such as cell polarity and cell–cell adhesion, and gain a mesenchymal-like phenotype including the acquisition of migratory and invasive properties (11). Carcinoma cells in primary tumors are able to reactivate the EMT program to promote new invasive and metastatic properties (12). Genetic and epigenetic programs are involved in the regulation of EMT transcription factors (EMT-TF), including, but not limited to, SNAI1/2, TWIST1, and ZEB1/2, which can repress epithelial (*e.g.*, E-cadherin) or activate the transcription of mesenchymal markers (*e.g.*, vimentin, fibronectin, N-cadherin) (13). Thus, the activation status of EMT can be evaluated through the detection of the dynamic changes of these protein markers. Recent research has demonstrated that miRNAs play a critical role in metastasis and recurrence, that is, by regulating genes involved in EMT, migration, and invasion (14). For example, upregulation of miR-21 has been reported to be correlated with lymph node metastasis in head and neck squamous cell carcinoma (HNSCC) and actives the expression of cyclin-dependent kinase 5 through the STAT3/miRNA-21 pathway, which has also been shown to promote EMT (15). Conversely, miR-26a/b, miR-29a/b/c, and miR-218 by regulating LOXL2 expression have been reported to inhibit cancer cell migration and invasion in HNSCC (16). However, the role and mechanism of specific miRNAs involved in EMT and their influence on cell invasion and metastasis in LSCC, are still not well understood.

Herein, we designed an experimental strategy to identify crucial miRNAs, and their relative target genes, involved in metastasis and invasion of LSCC (**Figure 1**). First, the expression profiles of mRNAs and miRNAs in LSCC samples were downloaded from the Gene Expression Omnibus (GEO) (GSE51985, GSE59102) and The Cancer Genome Atlas (TCGA) databases. A comprehensive series of analyses subsequently identified *miR-181c-5p/SERPINE1* as being dysregulated in LSCC. In addition, functional experiments *in vitro* demonstrated that *miR-181c-5p* negatively regulated *SERPINE1*, a potential oncogene, and significantly repressed the invasion, metastasis, and EMT of LSCC. In conclusion, our findings indicated that *miR-181c-5p* could potentially be used as a novel biomarker and therapeutic target in LSCC patients.

MATERIALS AND METHODS

Raw Data Acquisition and Identification of Differentially Expressed mRNAs

Two expression profiling datasets (GSE51985, GSE59102) were downloaded from the GEO database at the NCBI using the following search terms: ((“gene” OR “mRNA” OR “miRNA” [all fields] AND (“laryngeal cancer” OR “laryngeal squamous cell carcinoma” [all fields]) AND “Homo sapiens” [porgn]). The GSE51985 and GSE59102 datasets, based on the Illumina HumanHT-12 V4.0 expression BeadChip platform, and the Agilent-014850 Whole Human Genome Microarray 4x44K G4112F platform, respectively contained a total of 62 tissue samples (39 LSCC tissues and 23 adjacent cancer tissues). In addition, the TCGA LSCC cohort was used to obtain differentially expressed (DE) miRNAs and contained 117 LSCC tissues and 12 normal tissues.

Original gene expression profiles were obtained from the two mRNA datasets. Differently expressed mRNAs (DE mRNAs)

Abbreviations: LSCC, laryngeal squamous cell carcinoma; miRNAs, microRNAs; GEO, Gene Expression Omnibus; TCGA, The Cancer Genome Atlas; EMT, epithelial-to-mesenchymal transition; LC, laryngeal cancer; OS, overall survival; EMT-TF, epithelial-to-mesenchymal transition transcription factors; HNSCC, head and neck squamous cell carcinoma; DE miRNAs, differentially expressed miRNAs; DE mRNAs, differentially expressed mRNAs; FC, fold-change; GO, Gene Ontology; MF, molecular function; BP, biological process; CC, cellular component; STRING, Search Tool for the Retrieval of Interacting Genes; PPI, protein–protein interaction; FBS, fetal bovine serum; WT, wild-type; Mut, mutant-type; U6, small RNA RNU6; CCK8, Cell Counting Kit-8; OD, optical density; HR, hazard ratio.

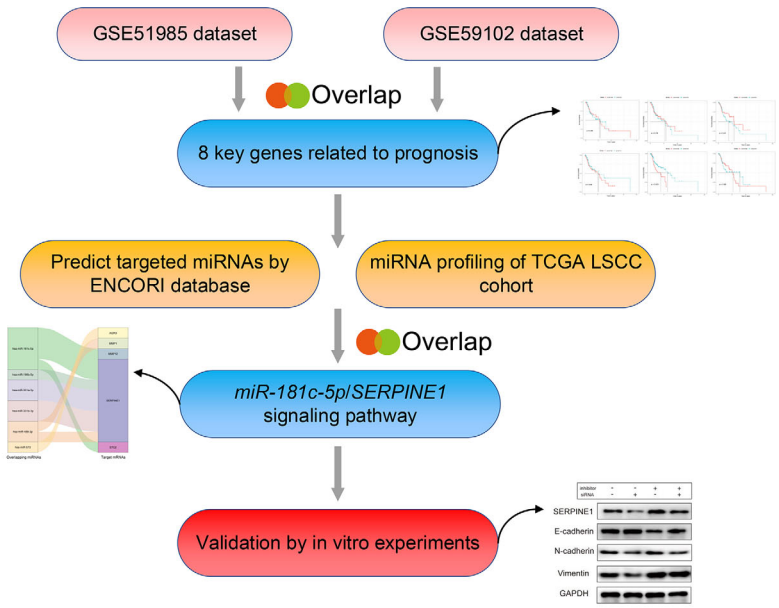

FIGURE 1 | The bioinformatics analysis strategy in this study.

were identified by GEO2R, using the "limma" package in R; therefore secondary normalization was unnecessary. Volcano plots of the mRNAs contained in the two GEO datasets were built using the ggplot2 package in Ra. The log2 fold change (FC) was set as the abscissa and the negative logarithm of the P-value as the ordinate. The threshold of the DE mRNAs in both datasets was set as log2 (FC) >2 or < −2 and P <0.05. Venn diagrams were used to identify overlapping genes and were created by the set of online tool: Venny 2.1 (17). We also used the "pheatmap" package in *R* to create a heatmap. DE miRNAs were identified from the above cohorts using a threshold of log2 (FC) >2 or <−2 and P<0.05.

Enrichment Analysis and PPI Network Construction

In order to demonstrate functional annotations, we used the "clusterProfiler" package in *R* to perform Gene Ontology (GO) functional annotation and the Kyoto Encyclopedia of Genes and Genomes (KEGG) pathway enrichment analysis (18). GO functional annotations were sorted into three broad categories: molecular function (MF), biological process (BP), and cellular components (CC). Using these three functional categories, gene function could be defined and described from multiple aspects. Ultimately, the significant terms or pathways were displayed using the "ggplot2" package in R. To analyze the connection between proteins and to score these relationships based on experimental data and forecast data, we used the Search Tool for the Retrieval of Interacting Genes (STRING) database to identify interactions between the identified DE mRNAs (19). The Protein–Protein Interaction (PPI) network was visualized by Cytoscape in which the degree attribute of the DE mRNAs was >8 (20).

Identification of Prognosis-Related Key mRNAs

The transcriptome sequencing data and corresponding clinical data of patients with LSCC were downloaded from TCGA database (up to April 07, 2020). The detailed TCGA IDs of LSCC patients including RNA-seq samples and miRNA-seq samples are shown in **Table S1**. Next, we performed univariate Cox proportional hazards analysis to obtain prognosis-related mRNAs based on TCGA LSCC cohort and a P-value <0.05 was considered statistically significant. Next, multivariate Cox regression analysis was performed using mRNAs with a P <0.05 and to remove potential confounding demographic factors including age and sex on the correlation between mRNAs and prognosis. We used the *R package 'vioplot'* to generate a violin plot of the expression levels of key genes in LSCC samples. These relative expression levels were normalized and log2 transformed. Comparisons between the two groups (cancer tissues and adjacent non-cancer tissues) were made using non-parametric tests (Mann–Whitney test) as appropriate.

Prediction of Key miRNA–mRNA Interactions

ENCORI was used to predict the targeted miRNAs for each of the eight key mRNAs; this is an open-source platform for studying mRNA–miRNA interactions and performing survival and differential expression analysis (21). The CLIP data filtering threshold was set to 'three' and the pan-cancer filtering threshold was set to 'five'; these settings ensured high stringency when predicting the target miRNAs. Next, the data predicted by ENCORI and DE miRNAs analyzed for the TCGA LSCC cohort were combined and the overlaps were computed. We identified

overlapping miRNAs as candidates for miRNA–mRNA interaction parings. Finally, the Kaplan-Meier survival analysis and correlation analysis conducted on these overlapping miRNAs with their target mRNAs identified prognostic related miRNA–mRNA pairing. The Kaplan–Meier method was used to generate survival curves for these patients with LSCC and to classify these patients into two groups according to gene expression (high or low). The median expression level was used as the cut-off point to classify patients into either the high expression group or the low expression group. Differences between the high and low expression groups were assessed using a log-rank test, and $P < 0.05$ was regarded as statistically significant.

Cell Culture and Transfection

HNSCC cell lines *Fadu*, *SCC-4*, *Cal-27,* and *Tu686* were purchased from the *Hunan Fenghui Biotechnology Co., Ltd. Fadu* and *Cal-27* cells were cultured in DMEM medium (BI, Israel) with 8% fetal bovine serum (FBS). *SCC-4* cells were cultured in RPMI-1640 medium (BI, Israel) with 8% FBS. *Tu686* cells were cultured in DMEM: F12 (1:1) medium (BI, Israel) with 8% FBS. All cells were cultured in medium supplemented with 1% PenStrep (100 U/ml penicillin and 100 μg/ml streptomycin) at 37°C in an atmosphere of 5% CO_2. *SERPINE1* siRNA, *miR-181c-5p* mimic, and inhibitor (RiboBio, Guangzhou, China) were transfected using *riboFECT* (RiboBio, Guangzhou, China).

Luciferase Reporter Assays

The 3′-UTR sequences of *SERPINE1* that including wild-type (WT) or mutant-type (Mut) *miR-181c-5p* binding sites were synthesized by Genecopoeia, Guangzhou, China. *Fadu* cells were co-transfected with *SERPINE1* 3′-UTR reporter plasmids [wild type (wt) or mutant (mut)] luciferase plasmids and *miR-181c-5p* mimic or mimic NC. After 48–72 h of transfection, luciferase activity was detected with a Cytation™ 5 system (BioTek, Winooski, VT, USA). *Renilla luciferase* activity was normalized to that of *Firefly luciferase* activity.

Quantitative Real-Time PCR Analysis

Total RNA was extracted from HNSCC cells and homogenized in TRizol reagent (Life Technologies, Shanghai, China) in accordance with the manufacturer's instructions. Reverse transcription was performed using a First Strand cDNA Synthesis Kit (Genecopeia, Guangzhou, China); qPCR assays were conducted using the All-in-One™ mRNA Detection kit (Genecopoeia, Guangzhou, China) based on SYBR-Green. MiRNA expression was measured using the All-in-One™ miRNA qRT-PCR detection kit (Genecopeia, Guangzhou, China). A QuantStudio7 Flex (Life Technologies, Carlsbad, CA) instrument was used to perform the qRT-PCR assay. Relative mRNA expression was normalized to *GAPDH* expression levels, and small RNA *RNU6* (*U6*) was used to normalize relative miRNA expression levels. The primers used in our analyses are shown in **Table 1**. Relative mRNA expression was measured using the $2^{-\Delta\Delta CT}$ method.

TABLE 1 | Primers of RNAs for qRT-PCR validation.

Symbol	Primer sequence 5′–3′
SERPINE1	F: AATGGAAGTGAAGGAAGG
	R: AAAGTGCTGGGATTATAGG
E-cadherin	F: ATTGCAAATTCCTGCCATTC
	R: GTTGTCCCGGGTGTCATC
N-cadherin	F: CAGTGGCGGAGATCCTACTG
	R: CCTTGGCTAATGGCACTTG
Vimentin	F: TACAGGAAGCTGCTGGAAGG
	R: ACCAGAGGGAGTGAATCCAG
GAPDH	F: CAGGGCTGCTTTTAACTCTGG
	R: TGGGTGGAATCATATTGGAACA

Cell Proliferation Assay

After transfection with *SERPINE1* siRNA, miRNA mimic, or miRNA inhibitor, cell proliferation rate was determined at 0, 24, 48, and 72 h using the Cell Counting Kit-8 (CCK8) (NCM Biotech, Suzhou, China); then the optical density (OD) value was measured at 450 nm on an enzyme-labeling instrument (BioTek, Winooski, VT, USA).

Colony Formation Assay

Transfected *Fadu* or *SCC-4* were seeded in 6-well plates at 300 cells per well, then cultured for 14 days. Colonies were fixed by anhydrous methanol for 15 min, then left to get dry for 5 min at room temperature and stained with 0.2% crystal violet for 30 min. Images were obtained by digital capture and positive colonies was defined as those with >50 cells.

Wound Healing and Cell Invasion Assay

Transfected *Fadu* or *SCC-4* cells were routinely cultured in 6-well plates until they reached monolayer confluence. Wounds were generated by scratching the monolayer of cells with a sterile 200-μl pipette tip; the cell debris was washed away with sterile 1× PBS. Images of the wound were captured at designated times (0, 48 h) to assess wound closure rates. The percent wound closure was calculated as: (1 − width at 48 h / width at 0 h) × 100%. Moreover, transwell assays were performed to explore cell invasion using a Matrigel invasion chamber (8 μm, BD Bioscience, USA). Briefly, cells (2×10^4) were seeded in the upper chamber without serum. The lower chamber was filled with DMEM or RPMI-1640 medium with 8% FBS. Then cells were cultured for 48 h, and the invaded cells were stained with 0.2% crystal violet. All experiments were carried out in triplicate.

Western Blot Assay

The total proteins were extracted from *Fadu* and *SCC-4* cells using RIPA lysis buffer (NCM Biotech, Suzhou, China), and the target proteins were detected by western blotting. Primary antibodies anti-PAI1 (A6211), anti-E-cadherin (A3044), anti-N-cadherin (A3055), and anti-Vimentin (A2584) were all purchased from Abclonal, Wuhan, China. Anti-GAPDH (AC001, Abclonal) was used to normalize the signals, and the second antibody, goat anti-rabbit IgG HRP-linked antibody, was purchased from Jackson Company (111-005-003, ImmunoResearch Laboratories, Inc. USA, 1:100,000).

Statistical Analyses

All statistical data were analyzed using R version 3.6 or GraphPad Prism 8 (GraphPad Software, La Jolla, CA). Analysis

of associations of gene expression levels in TCGA LSCC cohort were conducted using Student's t test, while the Mann–Whitney U test was used to evaluate data with unequal variance. The log-rank test, Cox regression analysis and Kaplan–Meier method were used to evaluate associations between mRNAs, miRNAs and OS. A P-value <0.05 was regarded as statistically significant.

RESULTS

Identification of DE mRNAs

Using the GEO2R algorithm, we identified a total of 1051 and 827 DE mRNAs from the GSE51985 and GSE59102 datasets, respectively (**Table S2**). A volcano plot was constructed by plotting the P-values of DE mRNAs *versus* the absolute log fold change (**Figures 2A, B**). Venn diagrams were constructed to identify a total of 283 overlapping genes (**Figure 2C**, **Table S2**). Two heatmaps for the mRNAs derived from the two datasets are shown in **Figures 3A, B**.

GO Enrichment, KEGG Analysis, and PPI Network of DE mRNAs

Based on results derived from the "clusterProfiler" package, we were able to gain a better understanding of the function of the DE mRNAs (**Figure 3C**). With regard to BP, the top ten enriched processes were extracellular structure organization, retina homeostasis, extracellular matrix organization, cornification, positive regulation of monocyte chemotaxis, tissue homeostasis,

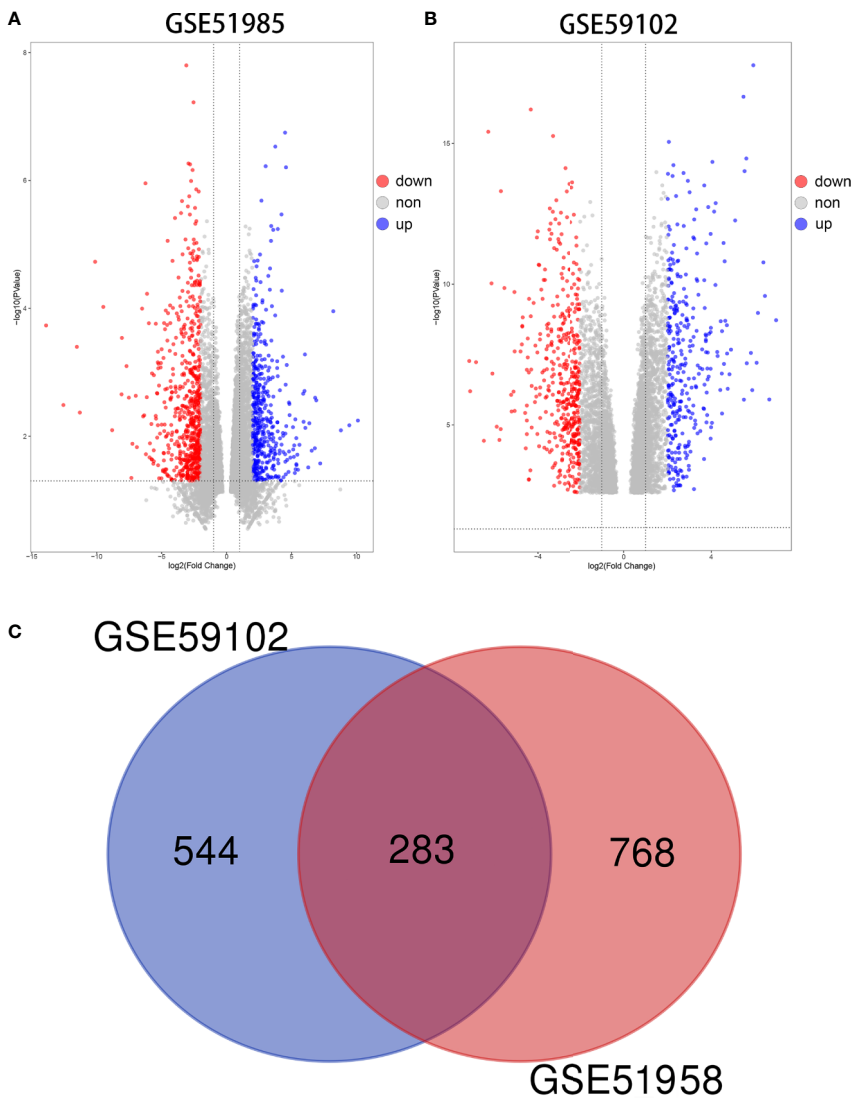

FIGURE 2 | Differentially expressed mRNAs (DE mRNAs). **(A)** Volcano plot of DE mRNAs in GSE51985. **(B)** Volcano plot of DE mRNAs in GSE59102. **(C)** Venn diagram of 283 overlapping DE mRNAs.

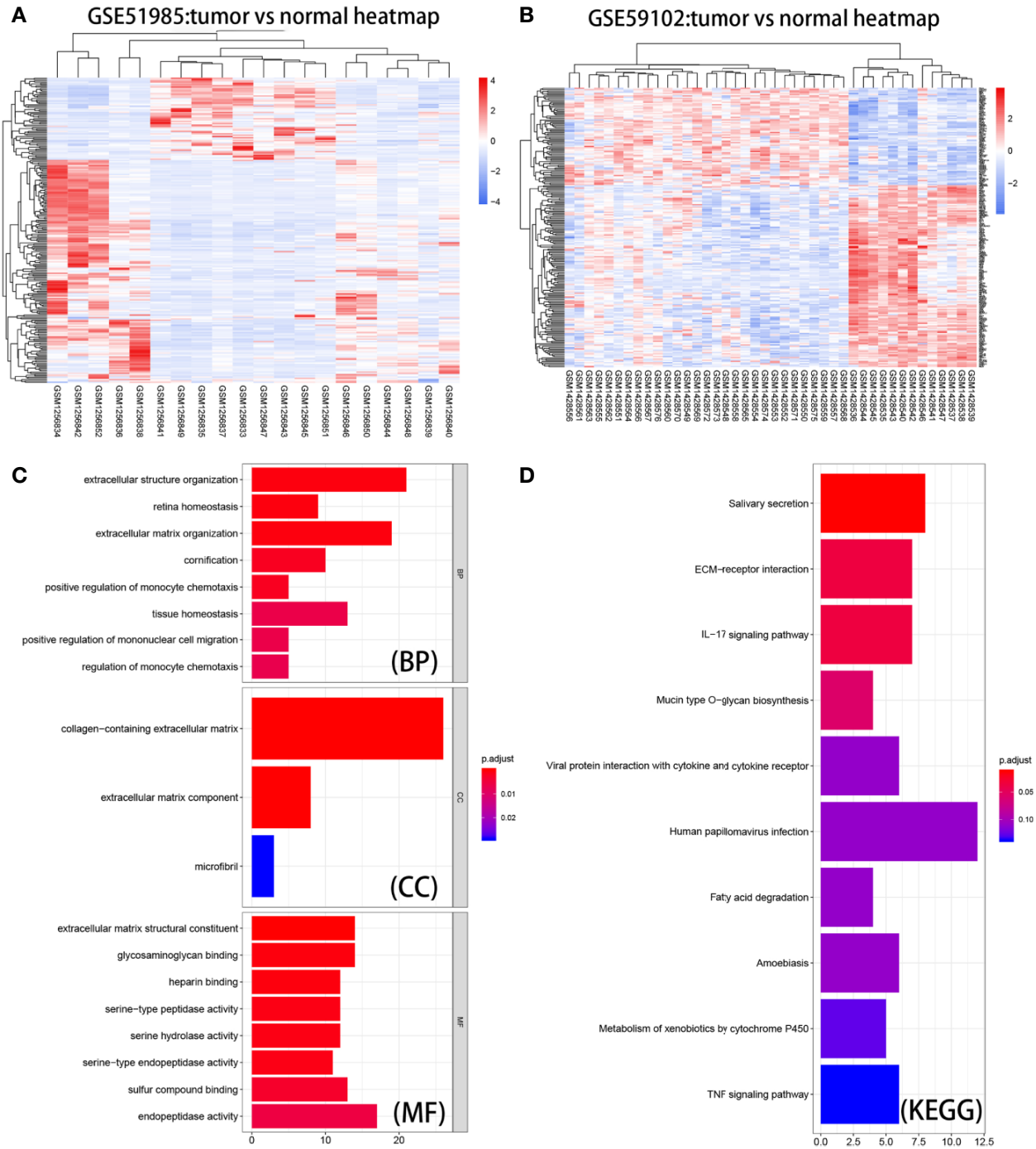

FIGURE 3 | Heatmaps, GO enrichment, and KEGG pathway analysis of DE mRNAs. **(A)** Heat map of the overlapping DE mRNAs in GSE51985. **(B)** Heatmap of the overlapping DE mRNAs in GSE59102. **(C)** Biological process (BP), cellular component (CC), and molecular function (MF) of DE mRNAs. **(D)** KEGG pathway analysis of DE mRNAs.

mononuclear cell migration, and regulation of monocyte chemotaxis. With regard to CC, the DE mRNAs showed enrichment in collagen-containing extracellular matrix, extracellular matrix component, and microfibrils. With regard to MF, the DE mRNAs were significantly enriched in extracellular matrix structural constituent, glycosaminoglycan binding, serine-type peptidase activity, serine hydrolase activity, serine-type endopeptidase activity, sulfur compound binding, and

endopeptidase activity. As shown in **Figure 3D**, KEGG pathway enrichment analysis showed that the top three significantly enriched KEGG pathways were pathways associated with salivary secretion, ECM–receptor interaction, and the IL-17 signaling pathway. The information gained from these analyses could be used to explore the function of vital molecules during the development of LSCC. STRING analysis allowed us to build a PPI network for 283 DE mRNAs (**Figure S1**). We set 'degree' to above 8 as the cut-off criterion and subsequently visualized the interaction among 84 mRNAs (**Figure 4A**) using Cytoscape software.

Selection and Expression Level of Key mRNAs

The LSCC RNA-Seq data of 123 samples (111 tumor, 12 normal), and their corresponding clinical information were retrieved and downloaded from TCGA database. The miRNA-Seq data of LSCC patients were obtained from 117 tumor samples and 12 normal samples. The potential effects of the 283 genes on the OS of TCGA LSCC patients were analyzed by univariate Cox regression analysis. A total of 21 mRNAs were significantly related to clinical outcome of LSCC patients ($P < 0.05$) (**Figure 4C**. Multivariate Cox regression analysis further indicated that eight mRNAs showed a significant prognostic value: *AGR3* [Hazard ratio (HR): 1.115 (1.009–1.231), P = 0.032], *ADGRG2* [HR: 0.001 (0.000–0.250), P = 0.013], *MMP12* [HR: 1.005 (1.000–1.010), P = 0.042], *ERVMER34-1* [HR: 1.113 (1.009–1.227), P = 0.032], *AURKB* [HR: 0.943 (0.894–0.995), P < 0.001], *SERPINE1* [HR: 1.499 (1.105–2.035), P = 0.009], *MMP1* [HR: 1.002 (1.000–1.003), P<0.011] and *STC2* [HR 1.047(1.011–1.085), P = 0.010] (**Figure 4D**). Moreover, the Mann–Whitney test revealed that the expression

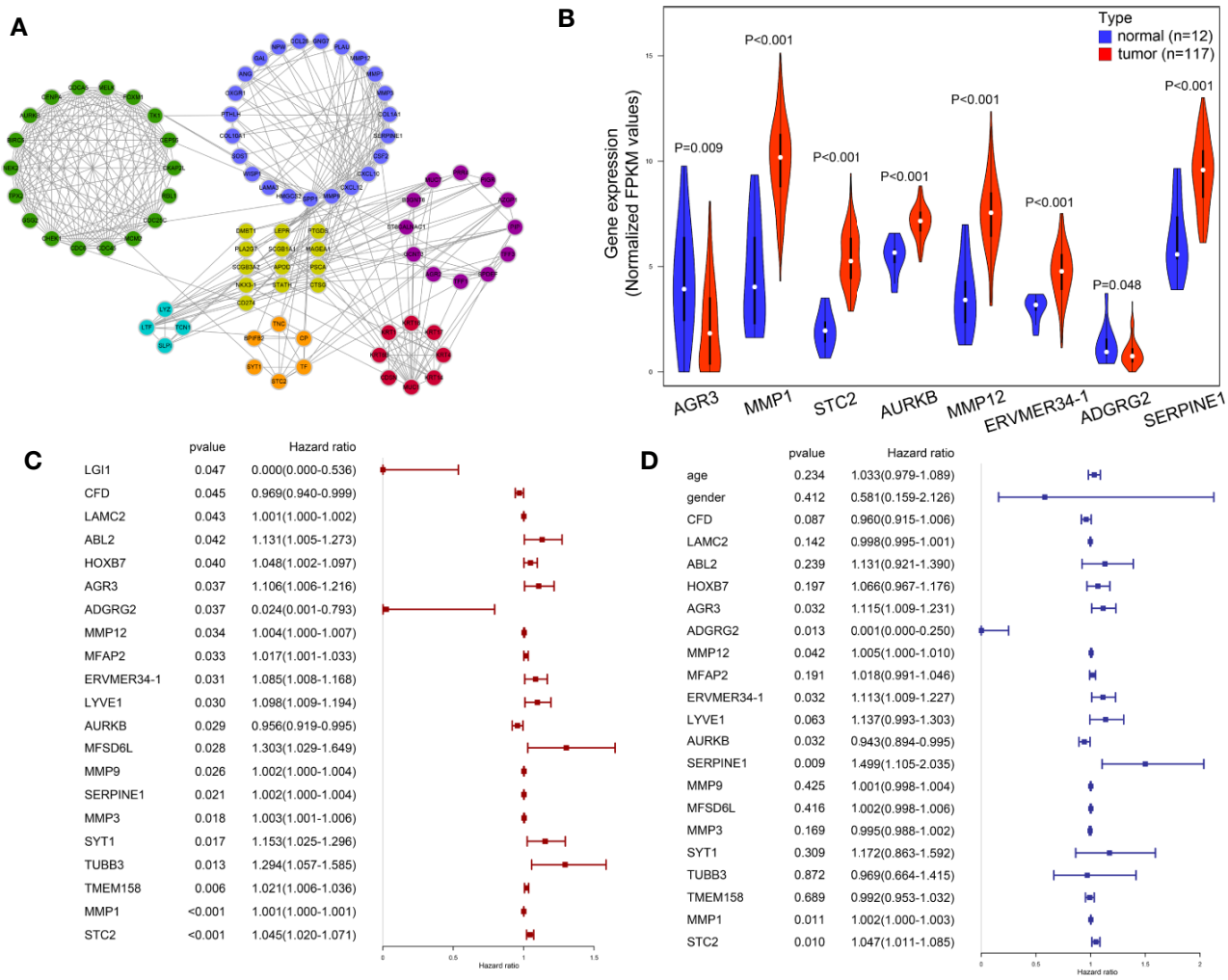

FIGURE 4 | Visualization and identification of key mRNAs. **(A)** 84 candidate mRNAs' PPI network. **(B)** Expression level of key mRNAs in cancer tissues and para-cancer normal tissues was compared in a violin plot. **(C)** Univariate Cox regression results of 21 candidate mRNAs in TCGA LSCC patients. **(D)** Multivariate Cox regression of eight key mRNAs in TCGA LSCC patients.

levels of six key mRNAs in LSCC were significantly higher than that of tissues adjacent to the tumors, whereas *AGR3* and *ADGRG2* were significantly expressed in lower levels in LSCC tissues compared to adjacent non-cancerous tissues (**Figure 4B**) ($P < 0.05$).

Identification of *miR-181c-5p/SERPINE1* Signaling Pathway

It is known that miRNAs can suppress the expression levels of their target genes by acting as oncogenes or tumor suppressors, and thus play important roles in the regulation of cancer pathogenesis and metastasis (22). Therefore, we identified a total of 93 miRNAs strongly predicted to be associated with *AGR3*, *ADGRG2*, *MMP12*, *ERVMER34-1*, *AURKB*, *SERPINE1*, *MMP1* and *STC2* expression (**Figure 5A**). Of these, 78 DE miRNAs were filtered out from the TCGA LSCC cohort (**Table S3**). Six overlapping miRNAs, including *miR-181c-5p*, *miR-301a*, *miR-196b*, *miR-488*, *miR-301b*, and *miR-573* were identified as crucial target miRNAs of key mRNAs (**Figure 5B**). Among these six miRNAs, Kaplan–Meier survival analysis showed that only the low *miR-181c-5p* expression LSCC patient group exhibited poorer prognosis than the higher *miR-181c-5p* group ($P = 0.021$) (**Figures 5C–H**). Based on Spearman's correlation analysis, a further inverse expression relationship between *miR-181c-5p* and *SERPINE1* was identified (correlation coefficient: −0.218; $P = 8.88e\text{-}07$) (**Figures 5I–K**).

Overexpression of *miR-181c-5p* Inhibits Metastasis and EMT *In Vitro*

miRNAs have been proven to play important roles in HNSCC suppression or progression (23, 24). Initially, we tested whether *miR-181c-5p* mediated cell proliferation, migration, invasion, or EMT *in vitro*. Because laryngeal carcinoma cell line Hep2 has been largely contaminated by HeLa cell line, we used HNSCC cell lines for cell experiments. First, the expression of *miR-181c-5p* was quantified in four HNSCC cell lines (**Figure 6A**). We found that *miR-181c-5p* was expressed relatively higher in *SCC-4* cells but was expressed in lower levels in *Fadu* cells. Thus, *Fadu* and *SCC-4* cells were chosen to investigate the influence of *miR-181c-5p* on biological function. Next, we transfected the *miR-181c-5p* mimic and inhibitor into *Fadu* and *SCC-4* cells, respectively (**Figure 6B**) to determine their effects on biological function.

The cell viability assay and colony formation assay showed that *miR-181c-5p* had no effects on *Fadu* and *SCC-4* cell proliferation (**Figures 6C, D**). The transwell assay revealed a clear decrease in the invasive capacity of *Fadu* cells transfected with *miR-181c-5p* mimic (**Figure 6E**). In contrast, *SCC-4* cells transfected with inhibitor markedly promoted cell invasion when compared with the negative control transfection (**Figure 6E**). In addition, the wound healing assay indicated that overexpression of *miR-181c-5p* attenuated cell migratory capacity in *Fadu* cells, whereas this function was enhanced by silencing *miR-181c-5p* in *SCC-4* cells (**Figure 6F**). To further analyze the effects of *miR-181c-5p* on EMT in LSCC, the expression of E-cadherin, N-cadherin and vimentin were determined by qPCR (**Figure 6G**) and western blotting (**Figure 6H**). We found that overexpression of *miR-181c-5p* resulted in the up-regulation of E-cadherin and down-regulation of N-cadherin and vimentin in *Fadu* cells, while silencing *miR-181c-5p* induced repression of E-cadherin and enhancement of N-cadherin and vimentin in *SCC-4* cells. Consistent with these results, we revealed that *miR-181c-5p* inhibits cancer cells metastasis and EMT, indicating that the epithelial cells eliminated mesenchymal properties.

MiR-181c-5p Restrains Migration and EMT Through the Regulation of *SERPINE1*

SERPINE1 is considered an oncogene in various types of cancers and can enable cancer cells to gain new properties such as migration, EMT, and apoptosis resistance (25–26).The expression of *SERPINE1* was quantified in four HNSCC cell lines (**Figure 7A**). Then, in order to measure the potential effects of *SERPINE1* on LSCC, we transfected *SERPINE1* siRNAs to knockdown its expression in *Fadu* cells. Silencing of *SERPINE1* was confirmed by qPCR and western blotting (**Figure 7B**). The cell viability assay showed that silencing *SERPINE1* significantly inhibited *Fadu* cell proliferation at 72 h (**Figure 7C**). Furthermore, the colony formation ability of *Fadu* cells transfected siRNA was suppressed compared with that of the control group (**Figure 7D**). In addition, transwell assays (**Figure 7E**) and wound healing (**Figure 7F**) results demonstrated that *SERPINE1* knockdown slowed down migration and mitigated the invasion of *Fadu* cells. Altogether, these data suggest that the silencing of *SERPINE1*expression attenuates tumorigenicity and metastasis in HNSCC cells.

Next, we examined whether *miR-181c-5p* could target the regulation of *SERPINE1* expression. Two separate binding sites were predicted for the *miR-181c-5p* and *SERPINE1* mRNA sequence (**Figure 7G**). Luciferase reporter assays showed that transfection of *miR-181c-5p* mimic remarkably inhibited the luciferase activities of *SERPINE1*-3′UTR-WT compared with the negative control, whereas the mimic did not alter the luciferase activities of the *SERPINE1* 3′UTR-Mut (**Figure 7G**). *miR-181c-5p* mimic also significantly suppressed the expression of *SERPINE1* at both the mRNA and protein levels (**Figure 7H**), these findings were consistent with the results of the luciferase reporter assay. Next, we explored whether *miR-181c-5p* inhibited metastasis and EMT in function of *SERPINE1 expression.* Wound healing and transwell assays demonstrated that the repression of *miR-181c-5p* promoted migration and invasion in *SCC-4* cells, which was reversed by silencing of *SERPINE1* (**Figures 7I, J**). In addition, western blotting assays revealed that inhibition of *miR-181c-5p* decreased the protein expression of the epithelial marker E-cadherin, but increased mesenchymal markers N-cadherin and vimentin in *SCC-4* cells. Importantly, the effects of *miR-181c-5p* silencing were effectively reversed by *SERPINE1* siRNA co-transfection (**Figure 7K**). These results indicated that *miR-181c-5p* restrained cell migration and EMT through downregulation of *SERPINE1*.

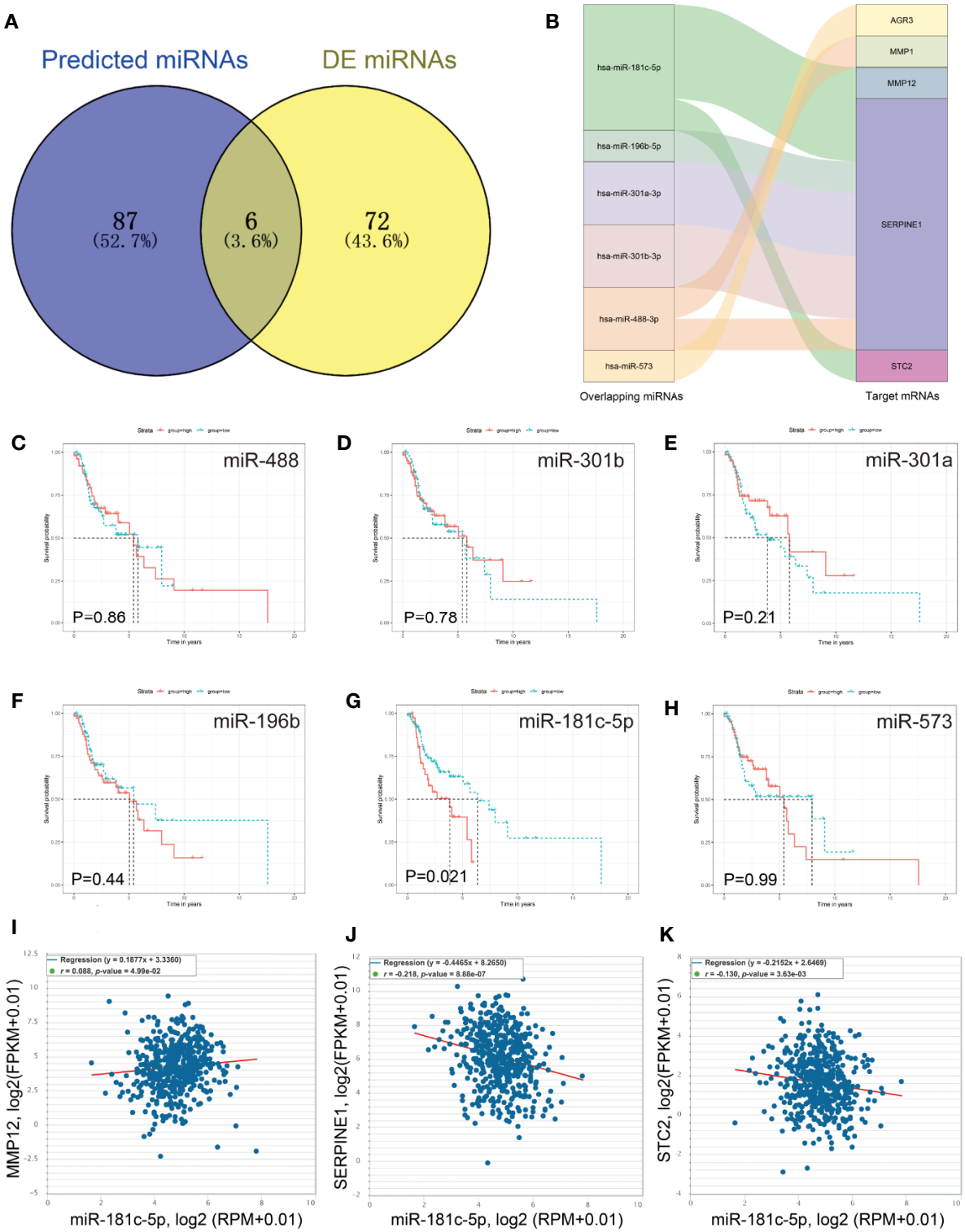

FIGURE 5 | Identification of *miR-181c-5p* and *SERPINE1* interaction. **(A)** Predicted target miRNAs by overlapping two databases. **(B)** The key miRNA/mRNA interactions shown as a Sankey diagram. **(C–H)** Kaplan–Meier overall survival curve for patients according to miRNA expression. **(I–K)** The expression correlation of *miR-181c-5p* and *MMP12, SERPINE1 and STC2*.

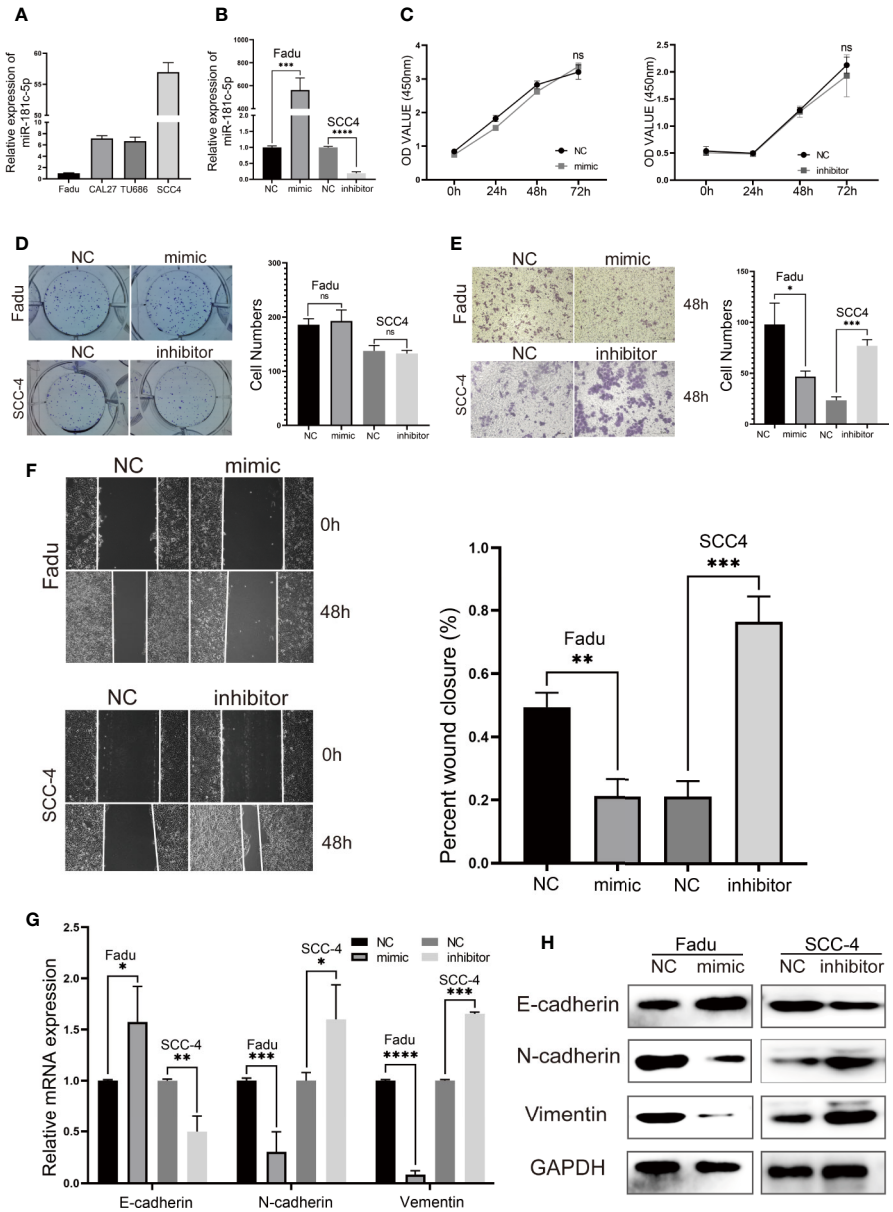

FIGURE 6 | *miR-181c-5p* inhibits epithelial–mesenchymal transition (EMT) and metastasis in head and neck squamous cell carcinoma (HNSCC) cell lines. **(A)** qPCR results of 4 HNSCC cell lines showed the expression level of *miR-181c-5p*. **(B)** The expression of *miR-181c-5p* was successfully overexpressed or knocked down by *miR-181c-5p* mimic or inhibitor in *Fadu* and *SCC-4* cell lines. **(C)** The results of cell viability assay after cancer cells transfected *miR-181c-5p* mimic and inhibitor. **(D)** Colony formation assay were conducted in *Fadu* and *SCC-4* cells at the indicated time points. **(E)** Invasion of tumor cells through Matrigel in the transwell assay (magnification, ×100). **(F)** Wound healing assay revealed there was a different healing ratio between the group of negative control and mimic/inhibitor in *Fadu* and *SCC-4* cells following by transient transfected for 48 **(h) (G, H)** Expression of EMT markers including E-cadherin, N-cadherin, and vimentin in *Fadu* and *SCC-4* cells were detected by qRT-PCR and western blotting. ns, no significance; *P < 0.05; **P < 0.01; ***P < 0.001; ****P < 0.0001.

DISCUSSION

The dysregulation of miRNAs has been reported to be involved in the tumorigenesis and progression of HNSCC, and to mediate cellular biological processes such as cell cycle regulation, differentiation, apoptosis, and migration in the epigenetic level (27–28). Several studies have reported expression profiles of miRNAs show remarkable diversity when comparing normal and malignant tissues, tumor types, as well as in different cancer stages, or prognosis (29, 30). In fact, specific miRNAs have found application as potential clinical diagnostic, prognostic, and therapeutic biomarkers in HNSCC (31). Studies have also revealed that miRNAs were dysregulated and associated with cellular proliferation, apoptosis and metastasis in LSCC cell lines,

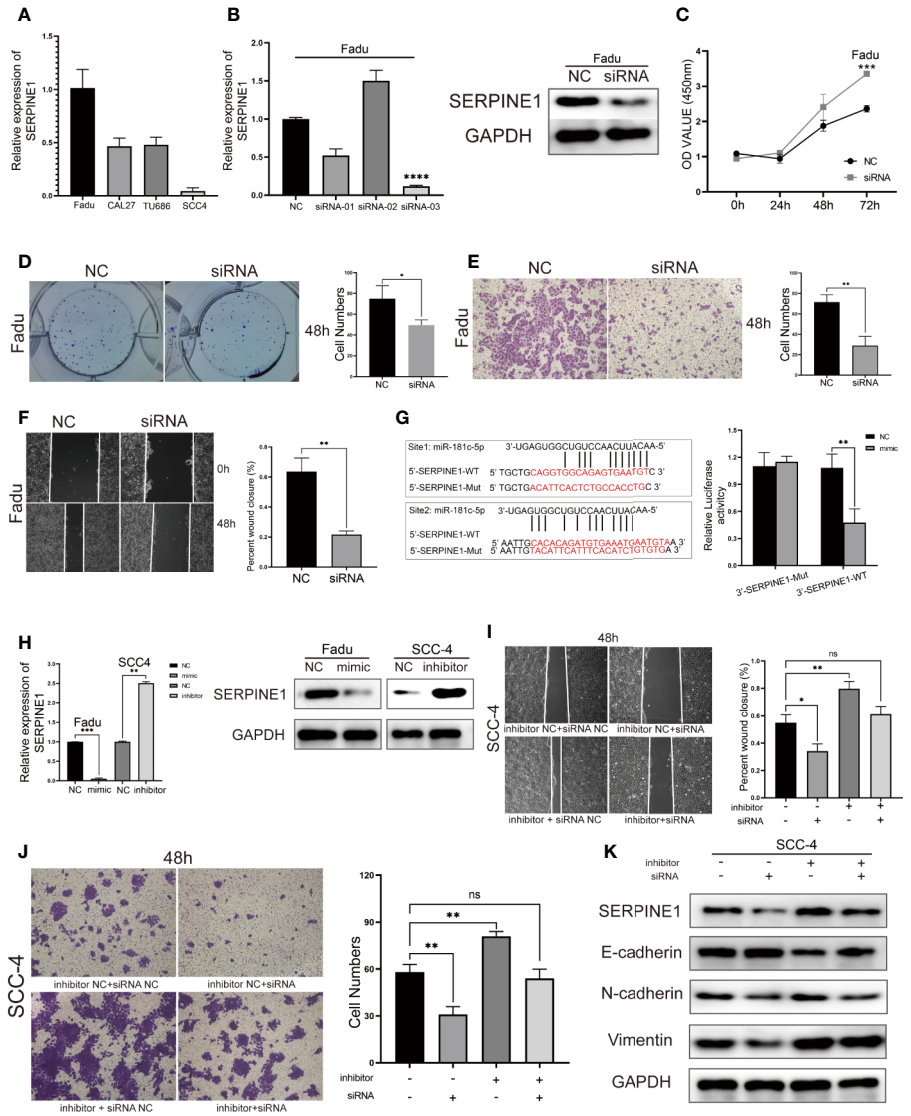

FIGURE 7 | *SERPINE1* is a direct target of *miR-181c-5p* and rescues its inhibition in HNSCC cell lines. **(A)** qPCR results of four HNSCC cell lines showed the expression level of *SERPINE1*. **(B)** Expression level of SERPINE1 was significantly down-regulated after *SERPINE1* siRNA-03 transfection proved by qRT-PCR and western blotting. Effects of silencing *SERPINE1* on proliferation, migration, and metastasis in *Fadu* cells determined by CCK8 cell viability **(C)**, colony formation **(D)**, transwell migration **(E)** and wound-healing assay **(F)**. **(G)** Two binding sites of *miR-181c-5p* in *SERPINE1* 3′-UTR; mutations were designed as indicated, and luciferase reporter assays showed *SERPINE1* was a direct binding target of *miR-181c-5p*. Relative luciferase activity was expressed as firefly/Renilla luciferase activity. **(H)** Relative expression of *SERPINE1* mRNA and protein in *Fadu* cells that transfected with *miR-181c-5p* mimic, and in *SCC-4* cells transfected with *miR-181c-5p* inhibitor. Effects of restoration of *SERPINE1* on migration and metastasis in *SCC-4* cells determined by wound-healing **(I)**, transwell migration **(J)** and western blotting assay **(K)**. *P < 0.05; **P < 0.01; ***P < 0.001; ****P < 0.0001.

whereas most of these findings were based on *in vitro* experiments and have found limited application as biomarkers in the clinical setting (8, 32). In this study, using bioinformatics and RNA sequencing datasets from clinical tumor samples, we identified and validated the role of a miRNA which may potentially serve as a valuable candidate for diagnosis and therapeutics in LSCC.

We identified *eight* key mRNAs that associated with poor prognosis in patients with LSCC, as predicted by Cox regression and expression analysis. Among these, *MMP12*, *AURKB*, *SERPINE1*, and *MMP1* have been confirmed to play important roles in squamous cell carcinoma including LSCC (33–34). Currently, the influence of the other genes on LSCC has not been reported; however, they have been confirmed to be involved in several important signaling pathways in other human cancers. For example, *AGR3* has been shown to facilitate the stemness of colorectal cancer by regulating Wnt/β-catenin signaling (35); *STC2* has been shown to be involved in resistance to treatment with EGFR tyrosine kinase inhibitors and to promote the progression of lung cancer by regulating *JUN/AXL* signaling (36).

Based on our expression and survival analysis results, we believe that the eight key mRNAs that we identified play a central part in the progression of LSCC.

The interplay between miRNA and target mRNA has achieved great interest in the field of tumor epigenetics. It has been extensively demonstrated that miRNAs act by inhibiting the expression of their targeted mRNAs (37). Our objective was to identify miRNAs having the potential ability to regulate the expression of key mRNA in LSCC. *MiR-181c-5p* was validated as the only candidate miRNA that not only was dysregulated in LSCC but its repressed expression was associated with poor clinical prognosis. *miR-181b-5p*, is a member of the miR-181 family, and has been reported to act as a tumor suppressor in a variety of tumors. miR-181b-5p targets the KPNA4 gene to inhibit EMT progression, and impede invasion and proliferation capacity of glioblastoma cells (38). In addition, Li et al. recently found that *miR-181c-5p* overexpression, through targeting of the *GSKIP* gene promotes E-cadherin expression in SiHa human cervical cancer cells, and repressed the expression of N-cadherin and vimentin (39) during EMT progression. Therefore, we boldly speculated that the dysregulation of this specific miRNA could result in abnormal biological functionality, including migration and invasion of LSCC cells.

Our *in vitro* experiments showed that miR-181b-5p is a key regulator of EMT and inhibits the cell invasion-metastasis cascade but not proliferation. Bioinformatics analysis demonstrated there was a negative correlation between miR-181b-5p and *SERPINE1* expression in LSCC, and the knockdown of *SERPINE1* attenuated tumor growth, EMT, and metastasis of cells, supporting its activity as an oncogene. Moreover, the downregulation of miR-181b-5p led to an elevated expression of *SERPINE1*, while up-regulation of miR-181b-5p resulted in the opposite tendency. These results revealed that miR-181b-5p repressed the mesenchymal phenotype in LSCC, at least in part, via directly targeting *SERPINE1*.

SERPINE1, a member of the urokinase plasminogen activating system (uPAS), was initially defined as a primary inhibitor of endogenous plasminogen activators and is synthesized in the liver and by fat tissue (40, 41). *SERPINE1* and its family members have been shown to promote different aspects of cancer development ranging from local proliferation to the migration and invasion of malignant cells (42, 43). Recent studies have also suggested that *SERPINE1* plays an important role in breast and pancreatic cancer (44, 45), and that the overexpression of *SERPINE1* could induce activation of the EGFR signaling pathway in breast cancer cells (44). Previous studies have shown that *SERPINE1* is abnormally expressed in HNSCC, whereas these studies did not attempt to identify the molecular mechanisms involved (40, 46). Herein, we demonstrated that the expression of *SERPINE1* was elevated in LSCC as a result of the down-regulation of miR-181b-5p and acts as one of the direct targets of miR-181b-5p. Further *SERPINE1* mediates the effects of miR-181b-5p on EMT and migration of LSCC cells.

Our findings revealed that *miR-181c-5p/SERPINE1* regulatory signaling was strongly associated with migration and invasion of LSCC, and *miR-181b-5p* acts as suppressor during the regulation of EMT progression. However, we acknowledge there are some limitations in this study. Further investigations focusing on clinical samples and the upstream signaling pathway and those of downstream of *miR-181c-5p/SERPINE1* in the development of LSCC are required.

CONCLUSION

We used a series of integrated bioinformatics analyses to identify a new miRNA–mRNA signaling pathway for responsible in the pathogenetic mechanisms underlying LSCC. Based on our *in vitro* evidence we propose that *miR-181c-5p* might negatively regulate the expression of oncogene *SERPINE1*, and impede the invasion and metastasis by decreasing EMT. The components of the *miR-181c-5p/SERPINE1* signaling pathway may therefore be utilized as promising therapeutic targets and prognostic biomarkers in the future.

DATA AVAILABILITY STATEMENT

The original contributions presented in the study are included in the article/**Supplementary Materials**. Further inquiries can be directed to the corresponding author.

ETHICS STATEMENT

The studies involving human participants were reviewed and approved by the Ethics Committee of Xiangya Hospital. The patients provided their written informed consent to participate in this study.

AUTHOR CONTRIBUTIONS

XL, WW, YL, XF, and YF performed the experiments, analyzed the data, and drafted the manuscript. PW, and YT designed the study and critically revised the manuscript. SZ polished the language. All authors contributed to the article and approved the submitted version.

FUNDING

This research was supported by The National Natural Science Foundation of China (81302355).

SUPPLEMENTARY MATERIAL

The Supplementary Material for this article can be found online at: https://www.frontiersin.org/articles/10.3389/fonc.2020.544476/full#supplementary-material

REFERENCES

1. Steuer CE, El-Deiry M, Parks JR, Higgins KA, Saba NF. An update on larynx cancer. *CA Cancer J Clin* (2017) 67:31–50. doi: 10.3322/caac.21386
2. Marur S, Forastiere AA. Head and neck squamous cell carcinoma: Update on epidemiology, diagnosis, and treatment. *Mayo Clin Proc* (2016) 91:386–96. doi: 10.1016/j.mayocp.2015.12.017
3. Siegel R, Ward E, Brawley O, Jemal A. Cancer statistics, 2011: The impact of eliminating socioeconomic and racial disparities on premature cancer deaths. *CA Cancer J Clin* (2011) 61:212–36. doi: 10.3322/caac.20121
4. Secretan B, Straif K, Baan R, Grosse Y, El Ghissassi F, Bouvard V, et al. A review of human carcinogens–part e: Tobacco, areca nut, alcohol, coal smoke, and salted fish. *Lancet Oncol* (2009) 10:1033–4. doi: 10.1016/s1470-2045(09)70326-2
5. He L, Hannon GJ. Micrornas: Small rnas with a big role in gene regulation. *Nat Rev Genet* (2004) 5:522–31. doi: 10.1038/nrg1379
6. Barbato S, Solaini G, Fabbri M. Micrornas in oncogenesis and tumor suppression. *Int Rev Cell Mol Biol* (2017) 333:229–68. doi: 10.1016/bs.ircmb.2017.05.001
7. de Jong MC, Ten Hoeve JJ, Grenman R, Wessels LF, Kerkhoven R, Te Riele H, et al. Pretreatment microrna expression impacting on epithelial-to-mesenchymal transition predicts intrinsic radiosensitivity in head and neck cancer cell lines and patients. *Clin Cancer Res* (2015) 21:5630–8. doi: 10.1158/1078-0432.CCR-15-0454
8. Chen L, Sun DZ, Fu YG, Yang PZ, Lv HQ, Gao Y, et al. Upregulation of microrna-141 suppresses epithelial-mesenchymal transition and lymph node metastasis in laryngeal cancer through hoxc6-dependent tgf-beta signaling pathway. *Cell Signal* (2020) 66:109444. doi: 10.1016/j.cellsig.2019.109444
9. Ma CH, Zhang YX, Tang LH, Yang XJ, Cui WM, Han CC, et al. Microrna-1469, a p53-responsive microrna promotes genistein induced apoptosis by targeting mcl1 in human laryngeal cancer cells. *BioMed Pharmacother* (2018) 106:665–71. doi: 10.1016/j.biopha.2018.07.005
10. Sasaki CT, Vageli DP. Mir-21, mir-155, mir-192, and mir-375 deregulations related to nf-kappab activation in gastroduodenal fluid-induced early preneoplastic lesions of laryngeal mucosa in vivo. *Neoplasia* (2016) 18:329–38. doi: 10.1016/j.neo.2016.04.007
11. Lamouille S, Xu J, Derynck R. Molecular mechanisms of epithelial-mesenchymal transition. *Nat Rev Mol Cell Biol* (2014) 15:178–96. doi: 10.1038/nrm3758
12. Nieto MA, Huang RY, Jackson RA, Thiery JP. Emt: 2016. *Cell* (2016) 166:21–45. doi: 10.1016/j.cell.2016.06.028
13. Gonzalez DM, Medici D. Signaling mechanisms of the epithelial-mesenchymal transition. *Sci Signal* (2014) 7:re8. doi: 10.1126/scisignal.2005189
14. Lages E, Ipas H, Guttin A, Nesr H, Berger F, Issartel JP. Microrna: Molecular features and role in cancer. *Front Biosci (Landmark Ed)* (2012) 17:2508–40. doi: 10.2741/4068
15. Sun SS, Zhou X, Huang YY, Kong LP, Mei M, Guo WY, et al. Targeting stat3/mir-21 axis inhibits epithelial-mesenchymal transition via regulating cdk5 in head and neck squamous cell carcinoma. *Mol Cancer* (2015) 14:213. doi: 10.1186/s12943-015-0487-x
16. Fukumoto I, Kikkawa N, Matsushita R, Kato M, Kurozumi A, Nishikawa R, et al. Tumor-suppressive microrna (mir-26a/b, mir-29a/b/c and mir-218) concertedly suppressed metastasis-promoting loxl2 in head and neck squamous cell carcinoma. *J Hum Genet* (2016) 61:109–18. doi: 10.1038/jhg.2015.120
17. Oliveros JC. *Venny. An interactive tool for comparing lists with Venn's diagrams* (2007-2015). Available at: https://bioinfogp.cnb.csic.es/tools/venny/index.html.
18. Yu G, Wang LG, Han Y, He QY. Clusterprofiler: An r package for comparing biological themes among gene clusters. *OMICS* (2012) 16:284–7. doi: 10.1089/omi.2011.0118
19. Szklarczyk D, Gable AL, Lyon D, Junge A, Wyder S, Huerta-Cepas J, et al. String v11: Protein-protein association networks with increased coverage, supporting functional discovery in genome-wide experimental datasets. *Nucleic Acids Res* (2019) 47:D607–D13. doi: 10.1093/nar/gky1131
20. Shannon P, Markiel A, Ozier O, Baliga NS, Wang JT, Ramage D, et al. Cytoscape: A software environment for integrated models of biomolecular interaction networks. *Genome Res* (2003) 13:2498–504. doi: 10.1101/gr.1239303
21. Li JH, Liu S, Zhou H, Qu LH, Yang JH. Starbase v2.0: Decoding mirna-cerna, mirna-ncrna and protein-rna interaction networks from large-scale clip-seq data. *Nucleic Acids Res* (2014) 42:D92–7. doi: 10.1093/nar/gkt1248
22. Lou W, Liu J, Gao Y, Zhong G, Chen D, Shen J, et al. Micrornas in cancer metastasis and angiogenesis. *Oncotarget* (2017) 8:115787–802. doi: 10.18632/oncotarget.23115
23. Zhang S, Li G, Liu C, Lu S, Jing Q, Chen X, et al. Mir-30e-5p represses angiogenesis and metastasis by directly targeting aeg-1 in squamous cell carcinoma of the head and neck. *Cancer Sci* (2020) 111:356–68. doi: 10.1111/cas.14259
24. Sun Q, Chen S, Zhao X, Yan M, Fang Z, Wang H, et al. Dysregulated mir-645 affects the proliferation and invasion of head and neck cancer cell. *Cancer Cell Int* (2015) 15:87. doi: 10.1186/s12935-015-0238-5
25. Klein RM, Bernstein D, Higgins SP, Higgins CE, Higgins PJ. Serpine1 expression discriminates site-specific metastasis in human melanoma. *Exp Dermatol* (2012) 21:551–4. doi: 10.1111/j.1600-0625.2012.01523.x
26. Arroyo-Solera I, Pavon MA, Leon X, Lopez M, Gallardo A, Cespedes MV, et al. Effect of serpine1 overexpression on the primary tumor and lymph node, and lung metastases in head and neck squamous cell carcinoma. *Head Neck* (2019) 41:429–39. doi: 10.1002/hed.25437
27. Shiah SG, Hsiao JR, Chang WM, Chen YW, Jin YT, Wong TY, et al. Downregulated mir329 and mir410 promote the proliferation and invasion of oral squamous cell carcinoma by targeting wnt-7b. *Cancer Res* (2014) 74:7560–72. doi: 10.1158/0008-5472.CAN-14-0978
28. Tan H, Zhu G, She L, Wei M, Wang Y, Pi L, et al. Mir-98 inhibits malignant progression via targeting mtdh in squamous cell carcinoma of the head and neck. *Am J Cancer Res* (2017) 7:2554–65.
29. Lu J, Getz G, Miska EA, Alvarez-Saavedra E, Lamb J, Peck D, et al. Microrna expression profiles classify human cancers. *Nature* (2005) 435:834–8. doi: 10.1038/nature03702
30. Calin GA, Croce CM. Microrna signatures in human cancers. *Nat Rev Cancer* (2006) 6:857–66. doi: 10.1038/nrc1997
31. Rapado-Gonzalez O, Lopez-Lopez R, Lopez-Cedrun JL, Triana-Martinez G, Muinelo-Romay L, Suarez-Cunqueiro MM. Cell-free micrornas as potential oral cancer biomarkers: From diagnosis to therapy. *Cells* (2019) 8:1653. doi: 10.3390/cells8121653
32. Karatas OF. Antiproliferative potential of mir-33a in laryngeal cancer hep-2 cells via targeting pim1. *Head Neck* (2018) 40:2455–61. doi: 10.1002/hed.25361
33. Impola U, Uitto VJ, Hietanen J, Hakkinen L, Zhang L, Larjava H, et al. Differential expression of matrilysin-1 (mmp-7), 92 kd gelatinase (mmp-9), and metalloelastase (mmp-12) in oral verrucous and squamous cell cancer. *J Pathol* (2004) 202:14–22. doi: 10.1002/path.1479
34. Osei-Sarfo K, Gudas LJ. Retinoids induce antagonism between foxo3a and foxm1 transcription factors in human oral squamous cell carcinoma (oscc) cells. *PloS One* (2019) 14:e0215234. doi: 10.1371/journal.pone.0215234
35. Chi J, Zhang H, Hu J, Song Y, Li J, Wang L, et al. Agr3 promotes the stemness of colorectal cancer via modulating wnt/beta-catenin signalling. *Cell Signal* (2020) 65:109419. doi: 10.1016/j.cellsig.2019.109419
36. Liu YN, Tsai MF, Wu SG, Chang TH, Tsai TH, Gow CH, et al. Acquired resistance to egfr tyrosine kinase inhibitors is mediated by the reactivation of stc2/jun/axl signaling in lung cancer. *Int J Cancer* (2019) 145:1609–24. doi: 10.1002/ijc.32487
37. Esquela-Kerscher A, Slack FJ. Oncomirs - micrornas with a role in cancer. *Nat Rev Cancer* (2006) 6:259–69. doi: 10.1038/nrc1840
38. Wang H, Tao T, Yan W, Feng Y, Wang Y, Cai J, et al. Upregulation of mir-181s reverses mesenchymal transition by targeting kpna4 in glioblastoma. *Sci Rep* (2015) 5:13072. doi: 10.1038/srep13072
39. Li N, Cheng C, Wang T. Mir-181c-5p mitigates tumorigenesis in cervical squamous cell carcinoma via targeting glycogen synthase kinase 3beta interaction protein (gskip). *Onco Targets Ther* (2020) 13:4495–505. doi: 10.2147/OTT.S245254
40. Saleh AD, Cheng H, Martin SE, Si H, Ormanoglu P, Carlson S, et al. Integrated genomic and functional microrna analysis identifies mir-30-5p as a tumor suppressor and potential therapeutic nanomedicine in head and neck cancer. *Clin Cancer Res* (2019) 25:2860–73. doi: 10.1158/1078-0432.CCR-18-0716
41. Yu XM, Jaskula-Sztul R, Georgen MR, Aburjania Z, Somnay YR, Leverson G, et al. Notch1 signaling regulates the aggressiveness of differentiated thyroid

cancer and inhibits serpine1 expression. *Clin Cancer Res* (2016) 22:3582–92. doi: 10.1158/1078-0432.CCR-15-1749
42. Blasi F, Carmeliet P. Upar: A versatile signalling orchestrator. *Nat Rev Mol Cell Biol* (2002) 3:932–43. doi: 10.1038/nrm977
43. Ulisse S, Baldini E, Sorrenti S, D'Armiento M. The urokinase plasminogen activator system: A target for anti-cancer therapy. *Curr Cancer Drug Targets* (2009) 9:32–71. doi: 10.2174/156800909787314002
44. Azimi I, Petersen RM, Thompson EW, Roberts-Thomson SJ, Monteith GR. Hypoxia-induced reactive oxygen species mediate n-cadherin and serpine1 expression, egfr signalling and motility in mda-mb-468 breast cancer cells. *Sci Rep* (2017) 7:15140. doi: 10.1038/s41598-017-15474-7
45. Akula SM, Ruvolo PP, McCubrey JA. Tp53/mir-34a-associated signaling targets serpine1 expression in human pancreatic cancer. *Aging (Albany N Y)* (2020) 12:2777–97. doi: 10.18632/aging.102776
46. Xu X, Li M, Hu J, Chen Z, Yu J, Dong Y, et al. Expression profile analysis identifies a two-gene signature for prediction of head and neck squamous cell carcinoma patient survival. *J Cancer Res Ther* (2018) 14:1525–34. doi: 10.4103/jcrt.JCRT_557_18

Conflict of Interest: The authors declare that the research was conducted in the absence of any commercial or financial relationships that could be construed as a potential conflict of interest.

Copyright © 2020 Li, Wu, Tang, Fan, Liu, Fang, Wang and Zhao. This is an open-access article distributed under the terms of the Creative Commons Attribution License (CC BY). The use, distribution or reproduction in other forums is permitted, provided the original author(s) and the copyright owner(s) are credited and that the original publication in this journal is cited, in accordance with accepted academic practice. No use, distribution or reproduction is permitted which does not comply with these terms.

frontiers in Oncology

ORIGINAL RESEARCH
published: 07 January 2021
doi: 10.3389/fonc.2020.600927

Long Non-Coding RNA MAPK8IP1P2 Inhibits Lymphatic Metastasis of Thyroid Cancer by Activating Hippo Signaling *via* Sponging miR-146b-3p

*Xiaoli Liu[1], Qingfeng Fu[1], Xuehai Bian[1], Yantao Fu[1], Jingwei Xin[1], Nan Liang[1], Shijie Li[1], Yishen Zhao[1], Li Fang[1], Changlin Li[1], Jiao Zhang[1], Gianlorenzo Dionigi[2] and Hui Sun[1]**

[1] Division of Thyroid Surgery, China–Japan Union Hospital of Jilin University, Jilin Provincial Key Laboratory of Surgical Translational Medicine, Changchun, China, [2] Division for Endocrine and Minimally Invasive Surgery, Department of Human Pathology in Adulthood and Childhood "G. Barresi", University Hospital "G. Martino", University of Messina, Messina, Italy

The principal issue derived from thyroid cancer is its high propensity to metastasize to the lymph node. Aberrant exprssion of long non-coding RNAs have been extensively reported to be significantly correlated with lymphatic metastasis of thyroid cancer. However, the clinical significance and functional role of lncRNA-MAPK8IP1P2 in lymphatic metastasis of thyroid cancer remain unclear. Here, we reported that MAPK8IP1P2 was downregulated in thyroid cancer tissues with lymphatic metastasis. Upregulating MAPK8IP1P2 inhibited, while silencing MAPK8IP1P2 enhanced anoikis resistance *in vitro* and lymphatic metastasis of thyroid cancer cells *in vivo*. Mechanistically, MAPK8IP1P2 activated Hippo signaling by sponging miR-146b-3p to disrupt the inhibitory effect of miR-146b-3p on NF2, RASSF1, and RASSF5 expression, which further inhibited anoikis resistance and lymphatic metastasis in thyroid cancer. Importantly, miR-146b-3p mimics reversed the inhibitory effect of MAPK8IP1P2 overexpression on anoikis resistance of thyroid cancer cells. In conclusion, our findings suggest that MAPK8IP1P2 may serve as a potential biomarker to predict lymphatic metastasis in thyroid cancer, or a potential therapeutic target in lymphatic metastatic thyroid cancer.

Keywords: thyroid cancer, lymph node metastasis, anoikis resistance, MAPK8IP1P2, Hippo signaling

OPEN ACCESS

Edited by:
Wei Cao,
Shanghai Jiao Tong University, China

Reviewed by:
Xin Zhang,
Jiangmen Central Hospital, China
Yanjie Zhang,
Shanghai Jiao Tong University, China

***Correspondence:**
Hui Sun
s_h@jlu.edu.cn

Specialty section:
This article was submitted to Head and Neck Cancer, a section of the journal Frontiers in Oncology

Received: *31 August 2020*
Accepted: *09 November 2020*
Published: *07 January 2021*

Citation:
Liu X, Fu Q, Bian X, Fu Y, Xin J, Liang N, Li S, Zhao Y, Fang L, Li C, Zhang J, Dionigi G and Sun H (2021) Long Non-Coding RNA MAPK8IP1P2 Inhibits Lymphatic Metastasis of Thyroid Cancer by Activating Hippo Signaling via Sponging miR-146b-3p. Front. Oncol. 10:600927. doi: 10.3389/fonc.2020.600927

INTRODUCTION

Thyroid cancer is one of the most prevalent endocrine malignancies with an increasing incidence in recent years worldwide (1, 2). According to histological classification, thyroid carcinoma can be divided into papillary thyroid cancer (PTC), follicular thyroid cancer (FTC), anaplastic thyroid cancer (ATC), and medullary thyroid cancer (MTC), where PTC is the most common histological type, accounting for 85–90% of all cases (3). Most PTCs are effectively treated by surgical removal, followed by adjuvant radioactive iodine therapy, and has a favorable 5-year survival rate exceeding 95% (4). However, the principal issue derived from PTC is its high propensity to metastasize to lymph node, which significantly affects the prognosis of thyroid cancer patients (5). Therefore,

identification of lymph node metastasis-relevant factor will facilitate early detection of lymph node metastasis and development of anti-lymph node metastasis therapeutic strategy in thyroid cancer patients.

With recent technological advances enabling us to detect rare circulating tumor cells that are anoikis resistant, anoikis resistance becomes a hot topic in cancer research. Anoikis resistance that is a kind of capacity of cancer cells to survive under suspension conditions has been extensively reported to be a hallmark of metastatic cancer cells, which significantly contributes to distant metastasis in various cancer types, including bone metastasis of prostate cancer (6) and multiple organs metastasis in non-small cell lung cancer (7). Furthermore, anoikis resistance has also been demonstrated to play an important role in metastatic thyroid cancer. Kittirat Saharat and colleagues have reported that tumor susceptibility gene 101 protein (TSG101) was identified to be upregulated in anoikis resistant thyroid cancer cells, which was accompanied with decreased expression of an apoptotic marker (cleaved poly-ADP ribose polymerase) and a pro-apoptotic protein (BCL-2 like protein 4) (8). Our previous study revealed that anoikis resistance induced by miR-424-5p promoted lung metastasis of thyroid cancer by inactivating Hippo signaling *via* simultaneously targeting WWC1, SAV1, and LAST2 (9). Recently, the critical role of anoikis resistance in lymphatic metastasis of cancer seizes great attention (10, 11). In several cancer scenario, anoikis resistance correlated significantly with positive lymph node metastasis status, including esophageal carcinoma (12, 13), melanoma (14), tongue cancer (15), breast cancer (16), and colorectal cancer (17). Importantly, development of anoikis resistance has been reported to significantly contribute to lymphatic metastasis of thyroid cancer (18–20). Therefore, investigating the underlying mechanism of anoikis resistance in lymphatic metastasis of thyroid cancer is of great necessity.

The long non-coding RNAs (lncRNAs) are a kind of newly discovered class of non-coding RNA with the length longer than 200 nucleotides (21, 22). They implicate several biological processes through various mechanisms, including transcriptional regulation as enhancers to modulate transcription of their target genes, post-transcription as decoys to bind proteins or scaffolds to regulate interactions between proteins and genes, and epigenetic modification as competing endogenous RNAs (ceRNA) to sponge target miRNAs so as to disrupt the miRNAs-mediated degradation of target genes (21, 22). A great deal of attention has focused on the role of lncRNAs in miRNA-mediated lncRNA/mRNA crosstalk (23), and dysregulation of miRNAs is inherently linked to the progression and metastasis of various types of cancer (9, 24–26). Recently, there is a great body of evidence reporting the role of lncRNAs in the development, progression, and metastasis in a number of cancers (27–29), including lymph node metastasis (30, 31). Notably, numerous studies have shown that aberrant expression of lncRNAs is significantly correlated with lymph node metastasis in thyroid cancer patients (32–34). Although these findings indicated that lncRNAs may hold clinical applicable value as the potential predictive markers for early detection of lymph node metastasis in thyroid cancer, whether lncRNAs affects lymph node metastasis of thyroid cancer *in vivo* is not determined in these studies. Therefore, further investigation of the functional role of lncRNA in lymph node metastasis of thyroid cancer *in vivo* will provide experimental evidence to support the applicable potential of lncRNAs to predict lymph node metastasis in thyroid cancer patients.

In the current study, we found that MAPK8IP1P2 was downregulated in thyroid cancer tissues, and particularly in thyroid cancer tissues with lymphatic metastasis, which was correlated with poor progression-free survival in thyroid cancer patients. Gain and loss of function assays showed that upregulating MAPK8IP1P2 inhibited, while silencing MAPK8IP1P2 enhanced anoikis resistance *in vitro* and lymphatic metastasis of thyroid cancer cells *in vivo*. Mechanistic investigations revealed that MAPK8IP1P2 activated Hippo signaling by sponging miR-146b-3p to disrupt the inhibitory effect of miR-146b-3p on NF2, RASSF1, and RASSF5 expression, which further inhibited anoikis resistance and lymphatic metastasis in thyroid cancer. Taken together, our findings provide the experimental evidence regarding the clinical significance and biological role of MAPK8IP1P2 in lymphatic metastasis of thyroid cancer, suggesting that MAPK8IP1P2 may be used as a potential biomarker to predict lymphatic metastasis in thyroid cancer patients.

MATERIALS AND METHODS

Cell Lines and Cell Culture

Normal primary thyroid follicular epithelial cells (PTFE) were purchased from Procell (Procell Life Science & Technology Co., Ltd., Wuhan, China). Thyroid cancer cell lines, including PTC cell lines (B-CPAP and KTC-1) and anaplastic thyroid cancer (ATC) cell lines (BHT-101, CAL-62, KMH-2, and 8305C), were obtained from Cell Bank of Shanghai Institute of Cell Biology, Chinese Academy of Sciences (Shanghai, China). PTFE were cultured in CM-H023 medium (Procell, China), and thyroid cancer cell lines were cultured in RPMI-1640 medium (Life Technologies, Carlsbad, CA, USA) supplemented with penicillin G (100 U/ml), streptomycin (100 mg/ml), and 10% fetal bovine serum (FBS, Life Technologies). All cell lines were cultured at 37°C in a humidified atmosphere with 5% CO_2.

Patients and Tumor Tissues

The total of 48 fresh thyroid cancer tissues and 24 adjacent normal tissues were obtained during surgery at the China-Japan Union Hospital of Jilin University (Changchun, China) between January 2018 and December 2018 (**Table 1**). Patients were diagnosed based on clinical and pathological evidence, and the specimens were immediately snap-frozen and stored in liquid nitrogen tanks. For the use of these clinical materials for research purposes, prior patients' consents and approval from the Institutional Research Ethics Committee were obtained (approval number #: 2019-NSFC-026).

TABLE 1 | The basic information of 48 thyroid carcinoma patients for MAPK8IP1P2 RNA expression analysis.

		Cases (n)	Percentage (%)
Histologic	PTC	48	100.0
	Other	0	0.0
Gender	Male	1	2.1
	Female	47	97.9
Age	<50	41	85.4
	≥50	7	14.6
T classification	T1	22	45.8
	T2	15	31.2
	T3	9	18.8
	T4	2	4.2
N classification	N0	10	20.8
	N1	38	79.2
M classification	M0	48	100.0
	M1	0	0.0

PTC, papillary thyroid carcinoma.

Plasmid and Transfection

Human MAPK8IP1P2 cDNA (Vigene Biosciences, Shandong, China) was cloned into the pcDNA3.1(+) plasmid. Knockdown of endogenous MAPK8IP1P2 was performed by cloning two short hairpin RNA (shRNA) oligonucleotides into the GV493 vector (GenChem, Shanghai, China). The sequences of the two separate shRNA fragments are listed in **Table 2**. The 3′UTR regions of NF2, RASSF1, RASSF5, and the region including MAPK8IP1P2 sequence targeted by miR-146b-3p were PCR-amplified from genomic DNA and cloned into pmirGLO vectors (Promega, USA), and the list of primers used in cloning reactions was provided in **Table 2**. miR-146b-3p mimics were synthesized and purified by RiboBio. Transfection of plasmids was performed as previously described (35).

RNA Extraction, Reverse Transcription, and Real-Time PCR

RNA from tissues and cells was extracted (TRIzol, Life Technologies) according to the manufacturer's instructions. Messenger RNA (mRNA), lncRNA, and miRNA were reverse transcribed from the total RNA using the Revert Aid First Strand cDNA Synthesis Kit (Thermo, USA) according to the manufacturer's protocol. Complementary DNA (cDNA) was amplified and quantified on ABI 7500HT system (Applied Biosystems, Foster City, CA, USA) using SYBR Green I (Applied Biosystems). The primers used in the reactions are listed in **Table 3**. Primers for U6 and miR-146b-3p were synthesized and purified by RiboBio (Guangzhou, China). Real-time PCR was performed as described previously (36). Glyceraldehyde-3-phosphate dehydrogenase (GAPDH) was used as the endogenous controls for mRNA and lncRNA, and U6 was used as the endogenous control for miRNA. Relative fold expressions were calculated with the comparative threshold cycle (37).

TABLE 2 | A list of primers used in the reactions for clone PCR.

Gene	Sequence (5` – 3`)
shMAPK8IP1P2-1#-up	CCGGGCAGTTTCACAAGCAGTTTCTCGA GAAACTGCTTGTGAAACTGCTTTTTTG
shMAPK8IP1P2-1#-dn	AATTCAAAAAGCAGTTTCACAAGCAGTTT CTCGAGAAACTGCTTGTGAAACTGCT
shMAPK8IP1P2-2#-up	CCGGCCGGACCATATTCAGGTTTCTCG AGAAACCTGAATATGGTCCGGTTTTTTG
shMAPK8IP1P2-2#-dn	AATTCAAAAACCGGACCATATTCAGGTTT CTCGAGAAACCTGAATATGGTCCGGT
MAPK8IP1P2-up	ATAGGTGTCAAGGCCGATGACTC
MAPK8IP1P2-dn	CGCAGATGACAGAGCTGAGAAC
NF2-3`UTR-up	CTCTCATGGCGTTCTAGTTCTCTG
NF2-3`UTR-dn	AAAGTGAGGCCTGGGTACAAC
RASSF1-3`UTR-up	TTGTACCCCCAGGTGGAAGG
RASSF1-3`UTR-dn	GATGATGACTGTCACCCCAACC
RASSF5-3`UTR-up	CCTGGAAAAAGAGGAGCAGGAC
RASSF5-3`UTR-dn	TCTGAGCCAGCCTCAGCTTTG

Western Blotting Analysis

Western blot was performed according to a standard method, as described previously (38). Antibodies against BAX (#5023), BAD (#9239), BCL2L1 (#2764), BCL2 (#2872), p-MST1 (Thr183)/2 (Thr180) (#3681), MST1 (#14946), p-LATS1(Thr1079) (#8654), LATS1 (#9153), p-YAP(Ser127) (#13008), YAP (#14074), NF2 (#6995), and RASSF1 (#86026) were purchased from Cell Signaling Technology, and TAZ from Abcam (ab224239), RASSF5 from Sigma (N5912). The membranes were stripped and reprobed with an anti–α-tubulin antibody (Cell Signaling Technology) as the loading control.

Anchorage-Independent Growth Assay

Five hundred cells were trypsinized and resuspended in complete medium containing 0.3% agar (Sigma). This experiment was performed as previously described (39) and carried out three times independently for each cell line.

TABLE 3 | A list of primers used in the reactions for real-time RT-PCR.

Gene	Sequence (5`– 3`)
MAPK8IP1P2-up	GGGAGAGCATTCCAGCAGTTTC
MAPK8IP1P2-dn	TCCTCAAGCAGTGCCACATC
GAPDH-up	TCCTCTGACTTCAACAGCGACAC
GAPDH-dn	CACCCTGTTGCTGTAGCCAAATTC
CTGF-up	TGGAGATTTTGGGAGTACGG
CTGF-dn	CAGGCTAGAGAAGCAGAGCC
CYR61-up	GGTCAAAGTTACCGGGCAGT
CYR61-dn	GGAGGCATCGAATCCCAGC
HOXA1-up	TCCTGGAATACCCCATACTTAGC
HOXA1-dn	GCACGACTGGAAAGTTGTAATCC
SOX9-up	AGCGAACGCACATCAAGAC
SOX9-dn	CTGTAGGCGATCTGTTGGGG
RPL13A-up	GCCATCGTGGCTAAACAGGTA
RPL13A-dn	GTTGGTGTTCATCCGCTTGC
PPIA-up	GGCAAATGCTGGACCCAACACA
PPIA-dn	TGCTGGTCTTGCCATTCCTGGA
NF2-up	AGTGGCCTGGCTCAAAATGG
NF2-dn	TGTTGTGTGATCTCCTGAACCA
RASSF1-up	AGGACGGTTCTTACACAGGCT
RASSF1-dn	TGGGCAGGTAAAAGGAAGTGC
RASSF5-up	GGGCATGAAACTGAGTGAAGA
RASSF5-dn	TGGCATCATAGATGGACTGGG

Cell Counting Kit-8 Analysis

Next, 2×10^3 cells were seeded into 96 well plates and the specific staining process and methods were performed according to the previous study (40).

Colony Formation Assay

The cells were trypsinized as single cell and suspended in the media with 10% FBS. The indicated cells (300 cells per well) were seeded into of 6-well plate for ~10–14 days. Colonies were stained with 1% crystal violet for 10 min after fixation with 10% formaldehyde for 5 min. Plating efficiency was calculated as previously described (41). Different colony morphologies were captured under a light microscope (Olympus).

Cell Cycle Analysis

Pretreatment and staining was performed using Cell Cycle Detection Kit (KeyGEN, China) as previously described (42). Briefly, cells (5×10^5) were harvested by trypsinization, washed in ice-cold phosphate-buffered saline (PBS), and fixed in 75% ice-cold ethanol in PBS. Before staining, cells were gently resuspended in cold PBS, and ribonuclease was added into cells' suspension tube incubated at 37°C for 30 min, followed by incubation with propidium iodide (PI) for 20 min at room temperature. Cell samples (2×10^4) were then analyzed by FACSCanto II flow cytometer (Becton, Dickinson and Company, Franklin Lakes, NJ, USA) and the data were analyzed using FlowJo 7.6 software (TreeStar Inc., Ashland, OR, USA).

Anoikis Induction Assay

Cell culture plates were coated with poly-HEMA (P3932; Sigma-Aldrich, St. Louis, USA), a non-adhesive substratum, and allowed to evaporate to dryness at room temperature. Cells were kept in suspension by using poly-HEMA coated plates to prevent adhesion. After 48 h of suspension, cells were harvested for cell viability analysis by 3-(4,5-dimethyl-2-thiazolyl)-2,5-diphenyl-2-H-tetrazolium bromide (MTT) assay and cell apoptosis analysis by flow cytometry.

Annexin V Apoptosis Detection

Flow cytometric analyzed of apoptosis were using the FITC Annexin V Apoptosis Detection Kit I (BD, USA), and performed as previously described (43). The cell's inner mitochondrial membrane potential ($\Delta\psi m$) was detected by flow cytometric using MitoScreen JC-1 staining kit (BD) (44). Briefly, cells were dissociated with trypsin and resuspended at 1×10^6 cells/ml in Assay Buffer, and then incubated at 37°C for 15 minutes with 10 μl/ml JC-1. Before analyzed by flow cytometer, cells were washed twice by Assay Buffer. Flow cytometry data were analyzed using FlowJo 7.6 software (TreeStar Inc., USA) as previously described (45).

Caspase-9 or Caspase-3 Activity Assays

Activity of caspase-9 or caspase-3 was analysis by spectrophotometry using Caspase-9 Colorimetric Assay Kit or Caspase-3 Colorimetric Assay Kit (Keygen, China), and was presented as protocol described. Briefly, 5×10^6 cells or 100 mg fresh tumor tissues were washed with cold PBS and resuspended in Lysis Buffer and incubated on ice for 30 min, then mixed the 50 μl cell suspension, 50 μl Reaction Buffer, and 5 μl Caspase-3/-9 substrate, and then incubated at 37°C for 4 hours. The absorbance was measured at 405 nm, and BCA protein quantitative analysis was used as the reference to normal each experiment groups.

Animal Study

Eight-week-old BALB/c-nu mice were purchased from the Experimental Animal Center of the Guangzhou University of Chinese Medicine and housed as previously described (46). The mice were randomly divided into three groups (n = 6 per group) and the indicated K1 cells (1×10^6) were injected into footpad of mice. The primary tumors were allowed to form, then the mice were euthanized on the end-points, and the inguinal lymph nodes were excised and paraffin embedded. Sections of the lymph nodes were subjected to H & E staining for histological examination, and the tumor cell number was counted as previously described (7). Animal study was approved from the Institutional Research Ethics Committee of Jilin University, and approval number was KT201902051.

Luciferase Assay

Cells (4×10^4) were seeded in triplicate in 24-well plates and cultured for 24 h, and the luciferase reporter assay was performed as previously described (47). Cells were transfected with 100 ng HOP-Flash (Catalog # 83467, Addgene) or HIP-Flash luciferase reporter plasmid (Catalog # 83466, Addgene), plus 5 ng pRL-TK Renilla plasmid (Promega) using Lipofectamine 3000 (Invitrogen) according to the manufacturer's recommendation. Luciferase and Renilla signals were measured 36 h after transfection using a Dual Luciferase Reporter Assay Kit (Promega) according to the manufacturer's protocol.

Statistical Analysis

All values are presented as means ± standard deviation (SD). Significant differences were determined using GraphPad 5.0 software (USA). Student's t-test was used to determine statistical differences between two groups. One-way ANOVA was used to determine statistical differences between multiple testing. Survival curves were plotted using the Kaplan Meier method and compared by log-rank test. $P < 0.05$ was considered significant. All the experiments were repeated three times.

RESULTS

MAPK8IP1P2 Is Downregulated in Thyroid Cancer With Lymph Node Metastasis

By analyzing RNA sequencing dataset of thyroid cancer from The Cancer Genome Atlas (TCGA), we found that MAPK8IP1P2 was marked downregulated in thyroid cancer tissues compared with that in the adjacent normal tissues (ANT) (**Figure 1A**). Consistently, MAPK8IP1P2 expression was reduced in our 24 paired thyroid cancer tissues compared with the matched ANT (**Figure 1B**). Interestingly, we found that downexpression of MAPK8IP1P2 occurred in 4/9 (44.4%) thyroid cancer tissues without lymph node metastasis, and was 10/15 (66.7%) in thyroid cancer tissues with lymph node metastasis (**Figure 1B**). Our results further

indicated that MAPK8IP1P2 expression in thyroid cancer tissues without lymph node metastasis had no significant difference compared with that in ANT (**Figures 1C, D**), but was dramatically and significantly downregulated in thyroid cancer tissues with lymph node metastasis (**Figure 1C**), even in lymph node metastatic thyroid cancer tissues with T1-T2 (**Figure 1D**). However, there was no significant difference of MAPK8IP1P2 expression between in T1-2 thyroid cancer tissues and in T3-4 thyroid cancer tissues, although MAPK8IP1P2 was downregulated in both compared with that in ANT (**Figure 1E**). These findings suggested that downexpression of MAPK8IP1P2 may play an important role in lymphatic metastasis of thyroid cancer. TCGA analysis further supported this finding that MAPK8IP1P2 expression was reduced in thyroid cancer tissues compared with that in ANT, especially in thyroid cancer tissues with lymph node metastasis (**Figures 1F–H**). Therefore, our results combined with TCGA analysis suggest that downexpression of MAPK8IP1P2 may be implicated in lymphatic metastasis of thyroid cancer.

Upregulating MAPK8IP1P2 Inhibits Lymphatic Metastasis *In Vivo*

Then, the effect of MAPK8IP1P2 on lymphatic metastasis of thyroid cancer cells *in vivo* was further investigated using the inguinal lymph node metastasis model. First, the expression levels of MAPK8IP1P2 in 7 thyroid cancer cell lines and a normal thyroid follicular epithelial cell line PTFE were measured. As shown in **Figure 2A**, MAPK8IP1P2 was differentially downregulated in thyroid cancer cells compared

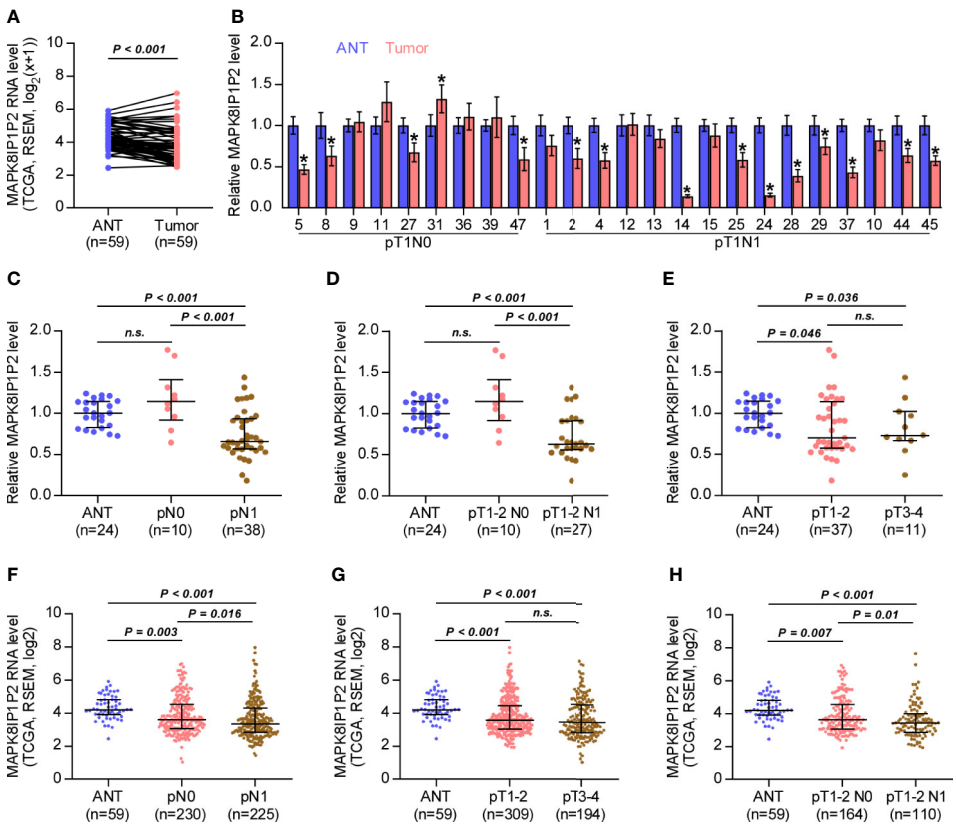

FIGURE 1 | MAPK8IP1P2 is downregulated in thyroid cancer with lymphatic metastasis. **(A)** MAPK8IP1P2 expression in 59 paired thyroid cancer tissues and the matched adjacent normal tissues in the thyroid cancer dataset from TCGA. **(B)** Real-time PCR analysis of MAPK8IP1P2 expression in our 24 paired thyroid cancer tissues and their matched adjacent normal tissues, including 9 thyroid cancer tissues without lymphatic metastasis and 15 thyroid cancer tissues with lymphatic metastasis. The number on the abscissa indicated the patient number according to our record when collecting patient information. GAPDH was used as endogenous controls. *P < 0.05. **(C)** Real-time PCR analysis of MAPK8IP1P2 expression in ANT (n = 24), thyroid cancer tissues without lymphatic metastasis (n = 10), and thyroid cancer tissues with lymphatic metastasis (n = 38). GAPDH was used as endogenous controls. n.s. indicates no significance. **(D)** Real-time PCR analysis of MAPK8IP1P2 expression in ANT (n = 24), thyroid cancer tissues of T1-T2 grade without lymphatic metastasis (n = 10), and thyroid cancer tissues of T1-T2 grade with lymphatic metastasis (n = 27). GAPDH was used as endogenous controls. n.s. indicates no significance. **(E)** Real-time PCR analysis of MAPK8IP1P2 expression in ANT (n = 24), thyroid cancer tissues with T1-T2 grade (n = 37), and thyroid cancer tissues with T3-T4 grade (n = 11). GAPDH was used as endogenous controls. n.s. indicates no significance. **(F)** MAPK8IP1P2 expression in ANT (n = 59), thyroid cancer tissues without lymphatic metastasis (n = 230), and thyroid cancer tissues with lymphatic metastasis (n = 225) in the thyroid cancer dataset from TCGA. **(G)** MAPK8IP1P2 expression in ANT (n = 59), thyroid cancer tissues with T1-T2 grade (n = 309), and thyroid cancer tissues with T3-T4 grade (n = 194) in the thyroid cancer dataset from TCGA. **(H)** MAPK8IP1P2 expression in ANT (n = 59), thyroid cancer tissues of T1-T2 grade without lymphatic metastasis (n = 164), and thyroid cancer tissues of T1-T2 grade with lymphatic metastasis (n = 110) in the thyroid cancer dataset from TCGA.

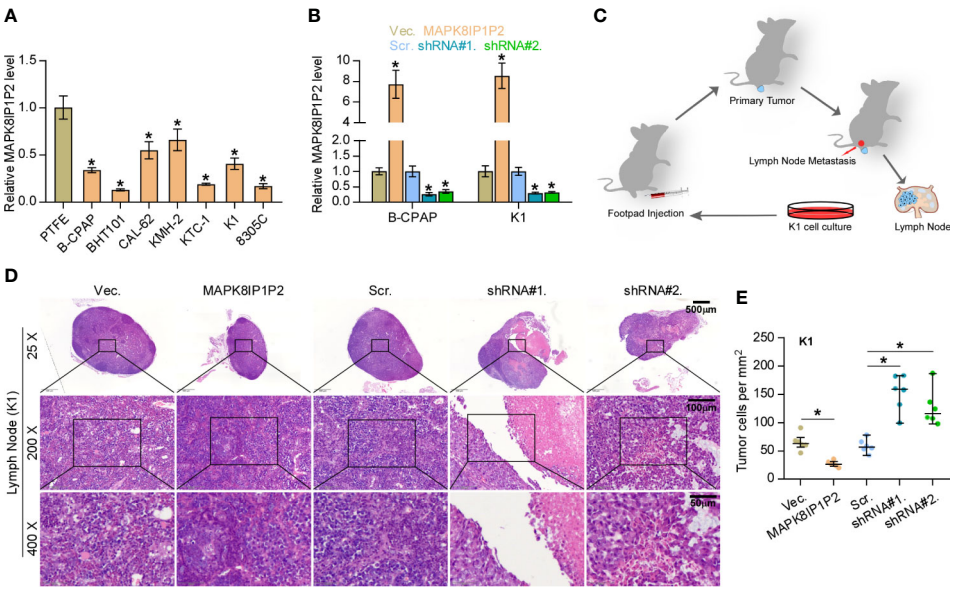

FIGURE 2 | Upregulating MAPK8IP1P2 inhibits cancer stem cell characteristics in thyroid cancer cells. **(A)** Real-time PCR analysis of MAPK8IP1P2 expression in 7 thyroid cancer cells, including 4 PTC cell lines, B-CPAP, BHT101, KTC-1, and K1, and 2 ATC cell lines, CAL-62 and 8305C, and 1 thyroid duct cell carcinoma cells, TT, and a normal thyroid follicular epithelial cell line PTFE. GAPDH was used as endogenous controls. *$P < 0.05$. **(B)** MAPK8IP1P2 expression in the vector, MAPK8IP1P2 overexpression scramble, MAPK8IP1P2 shRNA#1, and MAPK8IP1P2 shRNA#2 thyroid cancer cells using real-time PCR. Transcript levels were normalized by GAPDH expression. *$P < 0.05$. **(C)** Schematic model of lymphatic metastasis model *in vivo*. **(D)** H & E staining analysis of tumors in lymph node from the indicated mice group. **(E)** The count of tumor cells in the tumor areas of lymph node from the indicated mice group. *$P < 0.05$.

with that in PTFE cells. We further constructed MAPK8IP1P2-stably overexpressing B-CPAP and K1 cells and endogenously knocked down MAPK8IP1P2 expression in B-CPAP and K1 cells, both of which expressed moderate levels of MAPK8IP1P2 compared with that in other thyroid cancer cell lines (**Figure 2B**). Then, Vector-, MAPK8IP1P2-overexpressing, scramble and MAPK8IP1P2-downexpressing K1 cells were injected into the surrounding tissues in the foot pads of the mice (n = 6/group) using the inguinal lymph node metastasis model (**Figure 2C**). The metastatic inguinal lymph nodes were excised after 4 weeks and analyzed by H & E staining. As show in **Figures 2D, E**, histological examination of the lymph node metastatic tumors revealed that the tumors in lymph nodes formed from MAPK8IP1P2-overexpressing cells exhibited reduce tumor burden and the decreased number of tumor cells compared with those injected with the vector-control cells. Conversely, the tumors in lymph nodes formed from MAPK8IP1P2-downexpressing cells had larger tumor burden and more number of tumor cells than those inoculated with the scramble cells (**Figures 2D, E**). These findings indicate that upregulating MAPK8IP1P2 inhibits lymphatic metastasis *in vivo*.

Upregulating MAPK8IP1P2 Improves Anoikis Resistance in Thyroid Cancer Cells

The biological function of MAPK8IP1P2 in lymphatic metastasis of thyroid cancer was further CCK-8 assay showed that either upregulating or downregulating MAPK8IP1P2 had no significant effect on the cell growth of B-CPAP and K1 cells (**Figures 3A–D**). Similarly, neither colony-formation ability nor cell cycle progression was impeded by the changed expression of MAPK8IP1P2 in thyroid cancer cells (**Figures 3E, F**). However, upregulating MAPK8IP1P2 inhibited, while silencing MAPK8IP1P2 increased anchorage-independent growth capability of thyroid cancer cells (**Figure 3G**). These results indicate that the proliferation ability of thyroid cancer cells was not impeded by MAPK8IP1P2 *in vitro*.

Notably, upregulating MAPK8IP1P2 represses anchorage-independent growth capability of thyroid cancer cells as demonstrated above. Accumulating studies have shown that the capacity of cancer cells to survive under suspension conditions, namely anoikis resistance, is an important characteristic contributing to tumor progression and metastasis (6, 48, 49), including thyroid cancer (9, 28). Therefore, the effect of MAPK8IP1P2 on anoikis resistance in thyroid cancer cells was further evaluated. As shown in **Figure 4A**, upregulating MAPK8IP1P2 enhanced, while silencing MAPK8IP1P2 reduced the apoptosis rate of thyroid cancer cells. Mitochondrial potential assay showed that upregulating MAPK8IP1P2 attenuated, while silencing MAPK8IP1P2 elevated the mitochondrial potential of thyroid cancer cells (**Figure 4B**). The results of caspase activity assay and western blot analysis revealed that upregulating MAPK8IP1P2 increased the activity of caspase-3 or -9 and expression of pro-apoptotic proteins BAD and BAX, but reduced expression of anti-apoptotic proteins BCL2 and BCL2L1 (**Figures 4C–E**); conversely,

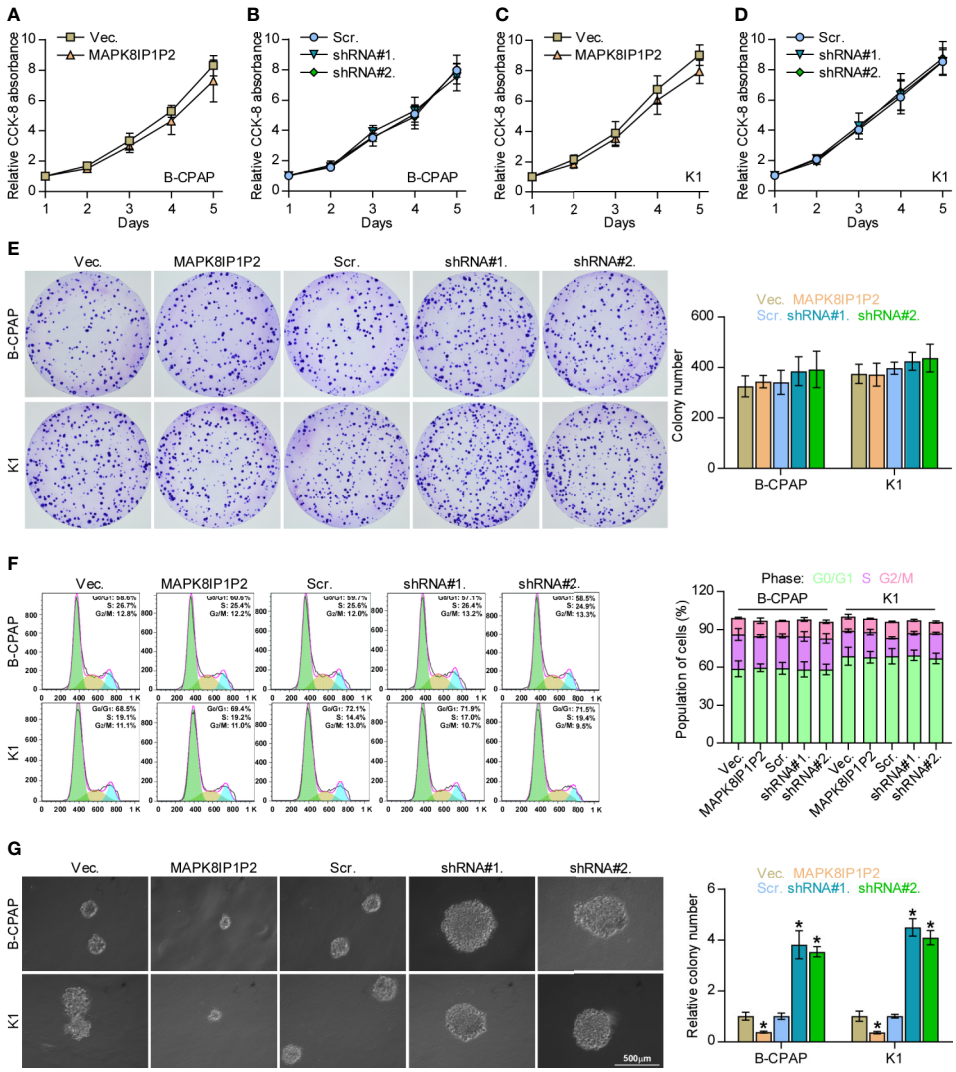

FIGURE 3 | Upregulating MAPK8IP1P2 does not affect proliferation of thyroid cancer cells. **(A–D)** The effect of overexpression or silencing MAPK8IP1P2 on the cell growth in the indicated thyroid cancer cells by CCK-8 assay. **(E)** The effect of overexpression or silencing MAPK8IP1P2 on colony-formation ability of the indicated thyroid cancer cells by colony-formation assay. **(F)** The effect of overexpression or silencing MAPK8IP1P2 on cell cycle progression of the indicated thyroid cancer cells by flow cytometry. **(G)** The effect of overexpression or silencing MAPK8IP1P2 on survival ability in the indicated thyroid cancer cells by anchorage-independent growth assay. *$P < 0.05$.

silencing MAPK8IP1P2 yielded the opposite effect in thyroid cancer cells (**Figures 4C–E**). Taken together, our results indicate that upregulating MAPK8IP1P2 abrogates anoikis resistance in thyroid cancer cells.

MAPK8IP1P2 Activates Hippo Signaling Pathway in Thyroid Cancer Cells

To determine the underlying mechanism implicated in anti-lymphatic metastatic role of MAPK8IP1P2 in thyroid cancer, Gene Set Enrichment Analysis (GSEA) was performed based on MAPK8IP1P2 expression in the thyroid cancer dataset from TCGA. As shown in **Figure 5A**, MAPK8IP1P2 overexpression was positively correlated with activity of Hippo signaling pathway, but negatively associated with the transcriptional activity of downstream co-activators YAP1/TAZ of Hippo signaling. Inactivation of Hippo signaling has been widely reported to be implicated in anoikis resistance and metastatic thyroid cancer (9, 50, 51), as well as in lymphatic metastasis process of cancers (52, 53), suggesting that Hippo signaling may mediate the functional role of MAPK8IP1P2 in lymphatic metastasis of thyroid cancer. Luciferase reporter assay showed that upregulating MAPK8IP1P2 reduced, while silencing MAPK8IP1P2 increased the luciferase reporter activity of HOP-Flash, but not the HIP-Flash (**Figure 5B**), suggesting that upregulating MAPK8IP1P2 inhibits the TEAD-dependent luciferase activity in thyroid cancer cells. Furthermore, upregulating MAPK8IP1P2 enhanced the expression of phophorylated MST1/2 (p-MST1/2), phophorylated LATS1

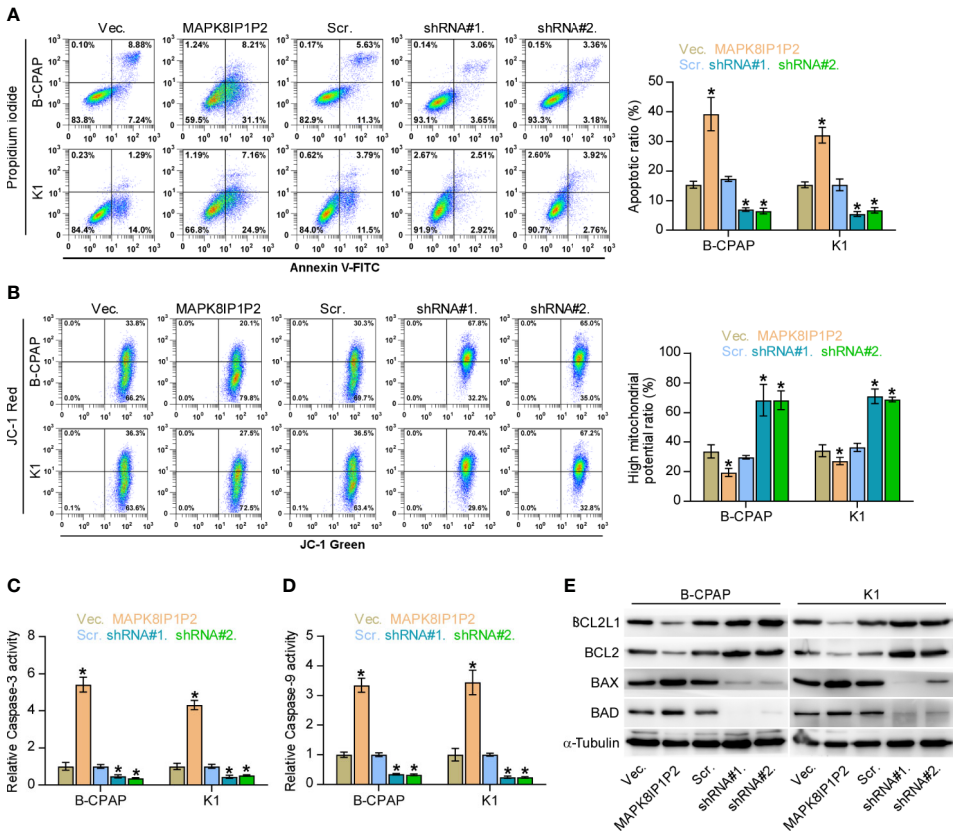

FIGURE 4 | Upregulating MAPK8IP1P2 inhibits anoikis resistance in thyroid cancer cells. **(A)** The effect of overexpression or silencing MAPK8IP1P2 on the apoptotic ratio in the indicated thyroid cancer cells by Annexin V-FITC/PI staining. *$P < 0.05$. **(B)** The effect of overexpression or silencing MAPK8IP1P2 on mitochondrial potential in the indicated thyroid cancer cells by JC-1 staining. *$P < 0.05$. **(C, D)** The effect of overexpression or silencing MAPK8IP1P2 on the activities of caspase-3 **(C)** and caspase-9 **(D)** in the indicated thyroid cancer cells. *$P < 0.05$. **(E)** Western blotting analysis of the effect of overexpression or silencing MAPK8IP1P2 on anti-apoptotic proteins, BCL2 and BCL2L1, and pro-apoptotic proteins, BAD and BAX, in the indicated thyroid cancer cells. α-Tubulin served as the loading control.

(p-LATS1) and phophorylated YAP1 (p-YAP1), reduced the nuclear translocation of YAP1 and TAZ, but had no effect on total level of MST1 and LATS1 in thyroid cancer cells (**Figure 5C**). In contrast, silencing MAPK8IP1P2 reduced p-MST1/2, p-LATS1, and p-YAP1 expression, and increased the nuclear expression of YAP1 and TAZ (**Figure 5C**). Real-time PCR analysis showed that upregulating MAPK8IP1P2 decreased, while silencing MAPK8IP1P2 increased the expression levels of multiple downstream genes of Hippo pathway, including CTGF, CYR61, HOXA1, PPIA, RPL13A, and SOX9 (54, 55), in thyroid cancer cells (**Figure 5D**). Therefore, these findings indicate that MAPK8IP1P2 activates Hippo signaling in thyroid cancer cells.

MAPK8IP1P2 Activates Hippo Signaling by Sponging miR-146b-3p

Accumulating studies have reported that lncRNAs can serve as competitive endogenous RNAs (ceRNAs) to de-repress miRNA-targeted mRNA expression (56, 57). Therefore, we further explored the potential binding miRNAs of MAPK8IP1P2 by analyzing the correlation of MAPK8IP1P2 with all reported miRNAs in the thyroid cancer dataset from TCGA. As shown in **Figure 6A**, the only miR-146b-3p expression level was negatively correlated with MAPK8IP1P2 expression, and was upregulated in thyroid cancer tissues compared with that in ANT. Using several publicly available algorithms, including miRanda and targetscan, we found that miR-146b-3p had the potential recognition sequences on MAPK8IP1P2, and NF2, RASSF1, and RASSF5 were the potential targets of miR-146b-3p (**Figure 6B**). NF2, RASSF1, and RASSF5 have been reported to promote activity of Hippo signaling by varying mechanism (58–60). Luciferase assay demonstrated that miR-146b-3p mimics suppressed the 3'UTR reporter activity of MAPK8IP1P2, NF2, RASSF1, and RASSF5, but not of the mutant 3'UTR of MAPK8IP1P2 (**Figures 6C, D**). RT-PCR and Western blot analysis revealed that upregulating MAPK8IP1P2 increased, while silencing MAPK8IP1P2 decreased the mRNA and protein levels of NF2, RASSF1, and RASSF5 (**Figures 6E–G**). Importantly, miR-146b-3p mimics not only reversed the NF2, RASSF1, and RASSF5 level enhanced by MAPK8IP1P2 overexpression (**Figures 6H, I**), but also inactivated Hippo signaling in MAPK8IP1P2-overexpressing thyroid cancer cells as indicated by elevated the luciferase reporter activity of

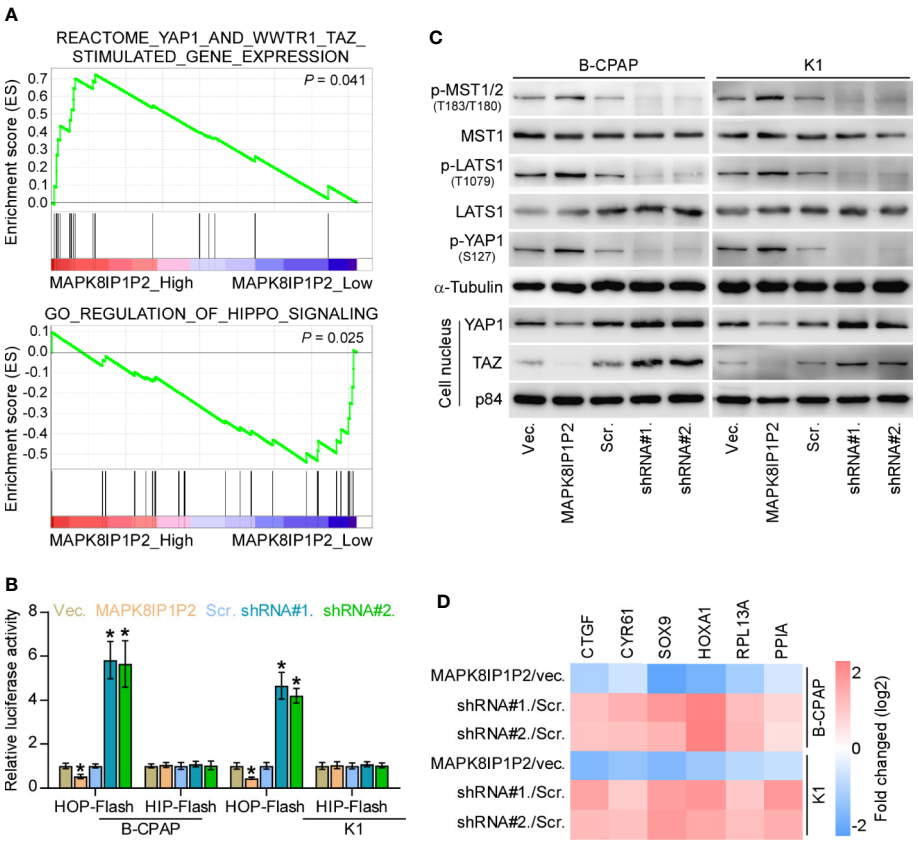

FIGURE 5 | MAPK8IP1P2 activates Hippo signaling pathway in thyroid cancer cells. **(A)** Gene set enrichment analysis (GSEA) revealed that MAPK8IP1P2 expression positively correlated with Hippo signaling. **(B)** The effect of overexpression or silencing MAPK8IP1P2 on TEAD transcriptional activity was assessed by HOP-Flash luciferase reporter in the indicated cells. Error bars represent the mean ± S.D. of three independent experiments. *$P < 0.05$. **(C)** Western blotting analysis of the effect of overexpression or silencing MAPK8IP1P2 on phophorylated MST1/2 (p-MST1/2), phophorylated LATS1 (p-LATS1), phophorylated YAP1 (p-YAP1), total levels of MST1 and LATS1 and nuclear translocation of YAP1 and TAZ in the indicated thyroid cancer cells. α-Tubulin and p84 were served as the cytoplasmic and nuclear loading control respectively. **(D)** Real-time PCR analysis of the effect of overexpression or silencing MAPK8IP1P2 on CTGF, CYR61, HOXA1, PPIA, RPL13A, and SOX9 in the indicated cells. Transcript levels were normalized by GAPDH expression. Error bars represent the mean ± S.D. of three independent experiments. *$P < 0.05$.

HOP-Flash (**Figure 6J**). Thus, these results indicate that MAPK8IP1P2 activates Hippo signaling by sponging miR-146b-3p to disrupt the inhibitory effect of miR-146b-3p on NF2, RASSF1, and RASSF5 expression in thyroid cancer.

Upregulating MAPK8IP1P2 Inhibits Anoikis Resistance by Sponging miR-146b-3p

We further investigated whether miR-146b-3p mediates the effect of MAPK8IP1P2 on anoikis resistance in thyroid cancer cells. As shown in **Figures 7A, B**, miR-146b-3p mimics enhanced the anchorage-independent growth capability and mitochondrial potential in MAPK8IP1P2-overexpressing thyroid cancer cells. In contrast, our results further revealed that miR-146b-3p mimics attenuated the stimulatory effects of MAPK8IP1P2 overexpression on the apoptotic ratio and activity of caspase-3 or -9 in thyroid cancer cells (**Figures 7C–E**). Collectively, our results demonstrate that MAPK8IP1P2 inhibits anoikis resistance by sponging miR-146b-3p in thyroid cancer cells (**Figure 7F**).

DISCUSSION

The critical findings of the current study present novel insights into the pivotal role of MAPK8IP1P2 in lymphatic metastasis of thyroid cancer by the miR-146b-3p/Hippo signaling axis. Here, we reported that MAPK8IP1P2 was dramatically downregulated in thyroid cancer tissues, especially in those with lymph node metastasis. Gain and loss of function assays demonstrated that upregulating MAPK8IP1P2 inhibited, while silencing MAPK8IP1P2 promoted anoikis resistance *in vitro* and lymphatic metastasis of thyroid cancer cells *in vivo*. Our results further revealed that upregulating MAPK8IP1P2 activated Hippo signaling by disrupting the repressive effect of miR-146b-3p on NF2, RASSF1, and RASSF5 expression by

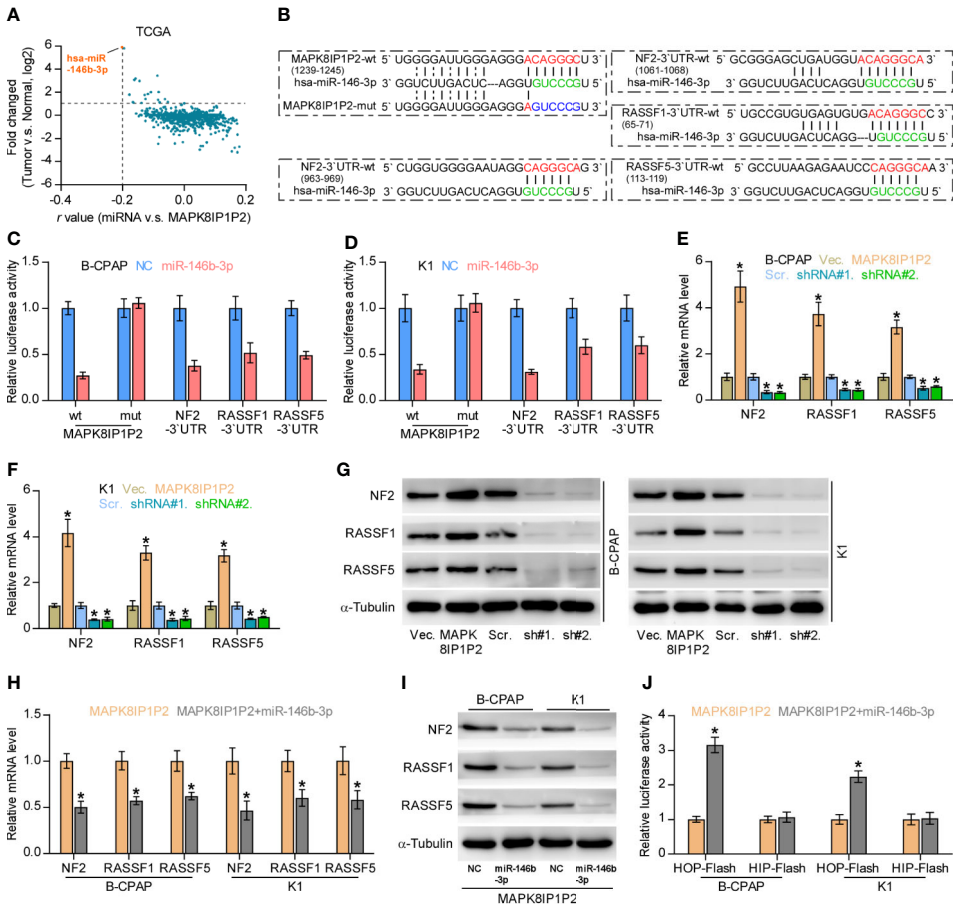

FIGURE 6 | MAPK8IP1P2 activates Hippo signaling by sponging miR-146b-3p. **(A)** Volcano plot analyzed the clinical correlation of MAPK8IP1P2 with all reported miRNAs in thyroid cancer dataset from TCGA. The orange colors represent significantly and negatively correlated miRNAs with fold change > 2 and r value < -0.2. **(B)** Predicted recognition sites of miR-146b-3p on MAPK8IP1P2, and predicted miR-146b-3p targeting sequence and mutant sequences in 3'UTR s of NF2, RASSF1, and RASSF5. **(C, D)** The effect of miR-146b-3p on the luciferase activity of wild-type or mutant MAPK8IP1P2, NF2, RASSF1 and RASSF5 in the indicated cells. Error bars represent the mean ± S.D. of three independent experiments. *$P < 0.05$. **(E, F)** Real-time PCR analysis of the effect of overexpression or silencing MAPK8IP1P2 on NF2, RASSF1, and RASSF5 expression in the indicated cells. Transcript levels were normalized by GAPDH expression. Error bars represent the mean ± S.D. of three independent experiments. *$P < 0.05$. **(G)** Western blot analysis of the effect of overexpression or silencing MAPK8IP1P2 on NF2, RASSF1 and RASSF5 expression in the indicated cells. α-Tubulin served as the loading control. **(H, I)** Real-time PCR **(H)** and Western blot **(I)** analysis of the effect of miR-146b-3p mimics on NF2, RASSF1, and RASSF5 expression in MAPK8IP1P2-overexpressing thyroid cancer cells. Transcript levels were normalized by GAPDH expression. α-Tubulin served as the loading control. Error bars represent the mean ± S.D. of three independent experiments. *$P < 0.05$. **(J)** The effect of miR-146b-3p mimics on TEAD transcriptional activity was assessed by HOP-Flash luciferase reporter in MAPK8IP1P2-overexpressing thyroid cancer cells. Error bars represent the mean ± S.D. of three independent experiments. *$P < 0.05$.

sponging miR-146b-3p as ceRNA, which further suppressed anoikis resistance in thryoid cancer cells. Therefore, our results unravel a novel mechanism by which MAPK8IP1P2 inhibits the anoikis resistance and lymphatic metastasis of thyroid cancer cells, determining the tumor-suppressive role of MAPK8IP1P2 in lymphatic metastasis of thyroid cancer.

As a kind of versatile non-coding RNA, lncRNAs have been extensively validated to function their biological role *via* varying mechanisms (21, 22), in which functioning as ceRNA to sponge target miRNAs to disrupt the miRNAs-mediated degradation of target genes seizes great momentum (56, 57) to be implicated in tumor progression and metastasis (27, 61). Importantly, miRNA-mediated lncRNA/mRNA crosstalk plays an important role in the development and metastasis of thyroid cancer (28, 62, 63), including lymphatic metastasis (32–34). In this study, our results revealed that MAPK8IP1P2 functioned as ceRNA to sponge miR-146b-3p, which further disrupted the inhibitory effect of miR-146b-3p on NF2, RASSF1, and RASSF5 expression. MAPK8IP1P2-mediated this lncRNA/mRNA crosstalk activated Hippo signaling, which further inhibited anoikis resistance and lymphatic metastasis in thyroid cancer. Therefore, our findings uncover a novel mechanism by which MAPK8IP1P2 inhibits the anoikis resistance and lymphatic metastasis of thyroid cancer cells.

Loss or downregulation of core components of Hippo signaling contributes to inactivation of Hippo signaling, which

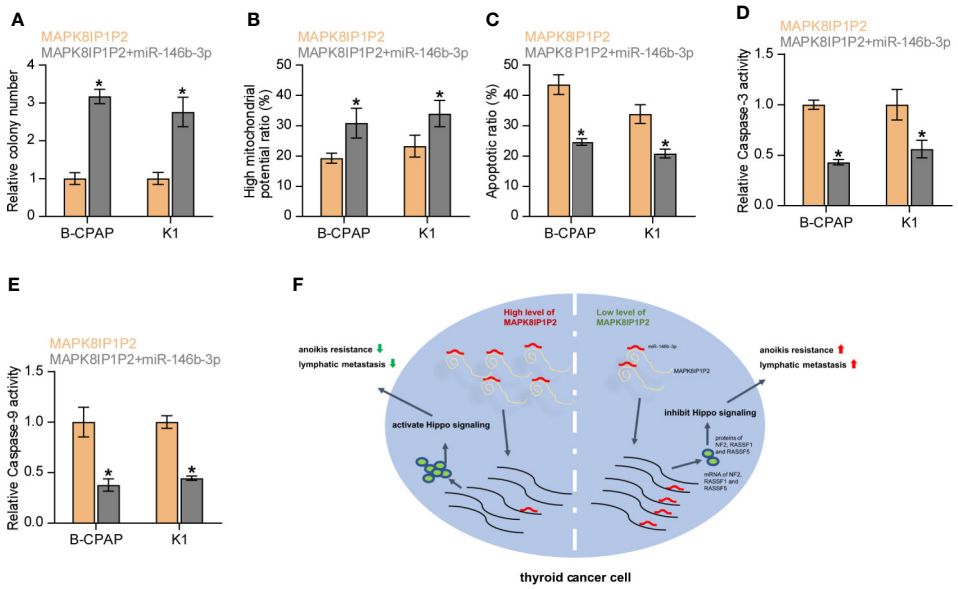

FIGURE 7 | Upregulating MAPK8IP1P2 inhibits anoikis resistance by sponging miR-146b-3p. **(A)** The effect of miR-146b-3p mimics on colony-formation ability in MAPK8IP1P2-overexpressing thyroid cancer cells. Error bars represent the mean ± S.D. of three independent experiments. *$P < 0.05$. **(B)** The effect of miR-146b-3p mimics on mitochondrial potential in MAPK8IP1P2-overexpressing thyroid cancer cells. Error bars represent the mean ± S.D. of three independent experiments. *$P < 0.05$. **(C)** The effect of miR-146b-3p mimics on apoptotic ratio in MAPK8IP1P2-overexpressing thyroid cancer cells. Error bars represent the mean ± S.D. of three independent experiments. *$P < 0.05$. **(D, E)** The effect of miR-146b-3p mimics on caspase-3 **(D)** and caspase-9 **(E)** in MAPK8IP1P2-overexpressing thyroid cancer cells. Error bars represent the mean ± S.D. of three independent experiments. *$P < 0.05$. **(F)** Hypothetical model illustrates the role and underlying mechanism of MAPK8IP1P2 in lymphatic metastasis of thyroid cancer by miR-146b-3p/Hippo signaling axis.

contributes to tumor progression and metastasis. For example, deficiency or inactivation of NF2, which functions to initiate and orchestrate the Hippo pathway (58), has been reported to be a frequent tumorigenic event in several cancer types (64–66). Furthermore, the upstream regulator of the Hippo pathway, ras association domain family (RASSF), suppresses cancer tumorigenesis (67, 68) by regulating MST1/2 activity (59, 60). However, how these regulators of the Hippo signaling are simultaneously disrupted in cancers, leading to constitutively inactivation of Hippo signaling, remains unclear. In this study, our results revealed that the relieved function of MAPK8IP1P2 as a ceRNA to sponge miR-146b-3p upregulated miR-146b-3p. Overexpression of miR-146b-3p directly targeted NF2, RASSF1, and RASSF5 in thyroid cancer cells and inactivated Hippo signaling, which further promoted anoikis resistance and lymphatic metastasis of thyroid cancer. Collectively, our findings clarify that MAPK8IP1P2 activates Hippo signaling by sponging miR-146b-3p to disrupt the inhibitory effect of miR-146b-3p on NF2, RASSF1, and RASSF5 expression in thyroid cancer.

Several lines of evidence have reported the pivotal role of anoikis resistance in lymphatic metastasis of cancer (10, 11), even in lymphatic metastasis of thyroid cancer (18–20). Furthermore, anoikis resistance was reported to be significantly correlated with positive lymph node metastasis in various cancers (12–17). In this scenario, multiple signaling pathways have been demonstrate to promote anoikis resistance, including TGF-β, PI3K/AKT, and Hippo signaling, where the role of Hippo signaling in inducing anoikis resistance gains more attention (9, 50, 51). Importantly, inactivation of Hippo signaling has also been reported to promote lymphatic metastasis of cancers (52, 53). However, the effect of Hippo signaling on lymphatic metastasis of thyroid cancer remains unclear. In the current study, our results showed that MAPK8IP1P2 activated Hippo signaling by sponging miR-146b-3p to disrupt targeting effect of miR-146b-3p on NF2, RASSF1, and RASSF5, which inhibited anoikis resistance and lymphatic metastasis of thyroid cancer. Collectively, our findings provide experimental evidence to support the critical role of Hippo signaling lymphatic metastasis of thyroid cancer.

In summary, our results demonstrate that MAPK8IP1P2 activates Hippo signaling by sponging miR-146b-3p as a ceRNA to disrupt the inhibitory effect of miR-146b-3p on NF2, RASSF1, and RASSF5 expression, which further suppresses lymphatic metastasis of thyroid cancer. Therefore, our results provide novel insights into the underlying mechanism by which MAPK8IP1P2 inhibits lymphatic metastasis in thyroid cancer, supporting the notion that MAPK8IP1P2 can be used as a lymph node metastatic marker in thyroid cancer.

DATA AVAILABILITY STATEMENT

The original contributions presented in the study are included in the article/supplementary materials. Further inquiries can be directed to the corresponding author.

ETHICS STATEMENT

The studies involving human participants were reviewed and approved by The Institutional Research Human Ethics Committee. The patients/participants provided their written informed consent to participate in this study. The animal study was reviewed and approved by The Institutional Research Animal Ethics Committee.

AUTHOR CONTRIBUTIONS

XL and HS conceived the project and drafted the manuscript. QF, JZ, and XL conducted the experiments and contributed to the analysis of data. CL, SL, and YZ performed the animal experiments. NL, LF, and YZ analyzed the informatics data. SL, JX, YF, and XL performed IHC and the analysis of data. XB and JZ conducted the patient information's organizing. SL and NL contributed to the cell biology and molecular biology experiments. XL and GD edited and revised the manuscript. All authors contributed to the article and approved the submitted version.

FUNDING

This study was granted by the National Natural Science Foundation of China (grant number 81702652, 81972499) and the Department of Science and Technology of Jilin Province, China (grant number 20200201181JC).

REFERENCES

1. Albores-Saavedra J, Henson DE, Glazer E, Schwartz AM. Changing patterns in the incidence and survival of thyroid cancer with follicular phenotype–papillary, follicular, and anaplastic: a morphological and epidemiological study. *Endocr Pathol* (2007) 18:1–7. doi: 10.1007/s12022-007-0002-z
2. Blomberg M, Feldt-Rasmussen U, Andersen KK, Kjaer SK. Thyroid cancer in Denmark 1943-2008, before and after iodine supplementation. *Int J Cancer* (2012) 131:2360–6. doi: 10.1002/ijc.27497
3. Mao Y, Xing M. Recent incidences and differential trends of thyroid cancer in the USA. *Endocr Relat Cancer* (2016) 23:313–22. doi: 10.1530/ERC-15-0445
4. Hay ID, Thompson GB, Grant CS, Bergstralh EJ, Dvorak CE, Gorman CA, et al. Papillary thyroid carcinoma managed at the Mayo Clinic during six decades (1940-1999): temporal trends in initial therapy and long-term outcome in 2444 consecutively treated patients. *World J Surg* (2002) 26:879–85. doi: 10.1007/s00268-002-6612-1
5. Zhang X, Shen YP, Li JG, Chen G. Clinical feasibility of imaging with indocyanine green combined with carbon nanoparticles for sentinel lymph node identification in papillary thyroid microcarcinoma. *Medicine* (2019) 98: e16935. doi: 10.1097/MD.0000000000016935
6. Tang Y, Pan J, Huang S, Peng X, Zou X, Luo Y, et al. Downregulation of miR-133a-3p promotes prostate cancer bone metastasis via activating PI3K/AKT signaling. *J Exp Clin Cancer Res CR* (2018) 37:160. doi: 10.1186/s13046-018-0813-4
7. Chen J, Liu A, Lin Z, Wang B, Chai X, Chen S, et al. Downregulation of the circadian rhythm regulator HLF promotes multiple-organ distant metastases in non-small cell lung cancer through PPAR/NF-kappab signaling. *Cancer Lett* (2020) 482:56–71. doi: 10.1016/j.canlet.2020.04.007
8. Saharat K, Lirdprapamongkol K, Chokchaichamnankit D, Srisomsap C, Svasti J, Paricharttanakul NM. Tumor Susceptibility Gene 101 Mediates Anoikis Resistance of Metastatic Thyroid Cancer Cells. *Cancer Genomics Proteomics* (2018) 15:473–83. doi: 10.21873/cgp.20106
9. Liu X, Fu Y, Zhang G, Zhang D, Liang N, Li F, et al. miR-424-5p Promotes Anoikis Resistance and Lung Metastasis by Inactivating Hippo Signaling in Thyroid Cancer. *Mol Ther Oncolytics* (2019) 15:248–60. doi: 10.1016/j.omto.2019.10.008
10. Simpson CD, Anyiwe K, Schimmer AD. Anoikis resistance and tumor metastasis. *Cancer Lett* (2008) 272:177–85. doi: 10.1016/j.canlet.2008.05.029
11. Kim YN, Koo KH, Sung JY, Yun UJ, Kim H. Anoikis resistance: an essential prerequisite for tumor metastasis. *Int J Cell Biol* (2012) 2012:306879. doi: 10.1155/2012/306879
12. Wang XC, Wu YP, Ye B, Lin DC, Feng YB, Zhang ZQ, et al. Suppression of anoikis by SKP2 amplification and overexpression promotes metastasis of esophageal squamous cell carcinoma. *Mol Cancer Res MCR* (2009) 7:12–22. doi: 10.1158/1541-7786.MCR-08-0092
13. Yin C, Toiyama Y, Okugawa Y, Shigemori T, Yamamoto A, Ide S, et al. Rac GTPase-Activating Protein 1 (RACGAP1) as an Oncogenic Enhancer in Esophageal Carcinoma. *Oncology* (2019) 97:155–63. doi: 10.1159/000500592
14. Lee Y, Yao W, Yang C, Li Y, Ni H, Wang L, et al. MIST1 regulates SNAI1 and acts through the PTEN/AKT signaling axis to promote anoikisresistance in human melanoma cells. *Exp Ther Med* (2018) 16:695–703. doi: 10.3892/etm.2018.6225
15. Jiang H, Liu L, Ye J, Liu H, Xing S, Wu Y. Focal adhesion kinase serves as a marker of cervical lymph node metastasis and is a potential therapeutic target in tongue cancer. *J Cancer Res Clin Oncol* (2010) 136:1295–302. doi: 10.1007/s00432-010-0780-4
16. Workman HC, Miller JK, Ingalla EQ, Kaur RP, Yamamoto DI, Beckett LA, et al. The membrane mucin MUC4 is elevated in breast tumor lymph node metastases relative to matched primary tumors and confers aggressive properties to breast cancer cells. *Breast Cancer Res BCR* (2009) 11:R70. doi: 10.1186/bcr2364
17. Lin Y, Buckhaults PJ, Lee JR, Xiong H, Farrell C, Podolsky RH, et al. Association of the actin-binding protein transgelin with lymph node metastasis in human colorectal cancer. *Neoplasia* (2009) 11:864–73. doi: 10.1593/neo.09542
18. Pan Y, Zhu X, Wang K, Chen Y. MicroRNA-363-3p suppresses anoikis resistance in human papillary thyroid carcinoma via targeting integrin alpha 6. *Acta Biochim Biophys Sin* (2019) 51:807–13. doi: 10.1093/abbs/gmz066
19. Li J, Luo M, Ou H, Liu X, Kang X, Yin W. Integrin beta4 promotes invasion and anoikis resistance of papillary thyroid carcinoma and is consistently overexpressed in lymphovascular tumor thrombus. *J Cancer* (2019) 10:6635–48. doi: 10.7150/jca.36125
20. Cheng SP, Lee JJ, Chang YC, Lin CH, Li YS, Liu CL. Overexpression of chitinase-3-like protein 1 is associated with structural recurrence in patients with differentiated thyroid cancer. *J Pathol* (2020) 252:114–24. doi: 10.1002/path.5503
21. Ponting CP, Oliver PL, Reik W. Evolution and functions of long noncoding RNAs. *Cell* (2009) 136:629–41. doi: 10.1016/j.cell.2009.02.006
22. Salehi S, Taheri MN, Azarpira N, Zare A, Behzad-Behbahani A. State of the art technologies to explore long non-coding RNAs in cancer. *J Cell Mol Med* (2017) 21:3120–40. doi: 10.1111/jcmm.13238
23. Li W, Li N, Shi K, Chen Q. Systematic review and meta-analysis of the utility of long non-coding RNA GAS5 as a diagnostic and prognostic cancer biomarker. *Oncotarget* (2017) 8:66414–25. doi: 10.18632/oncotarget.19040
24. Ren D, Yang Q, Dai Y, Guo W, Du H, Song L, et al. Oncogenic miR-210-3p promotes prostate cancer cell EMT and bone metastasis via NF-kappaB signaling pathway. *Mol Cancer* (2017) 16:117. doi: 10.1186/s12943-017-0688-6
25. Dai Y, Wu Z, Lang C, Zhang X, He S, Yang Q, et al. Copy number gain of ZEB1 mediates a double-negative feedback loop with miR-33a-5p that

regulates EMT and bone metastasis of prostate cancer dependent on TGF-beta signaling. *Theranostics* (2019) 9:6063–79. doi: 10.7150/thno.36735
26. Zhang X, Liu J, Zang D, Wu S, Liu A, Zhu J, et al. Upregulation of miR-572 transcriptionally suppresses SOCS1 and p21 and contributes to human ovarian cancer progression. *Oncotarget* (2015) 6:15180–93. doi: 10.18632/oncotarget.3737
27. Lang C, Dai Y, Wu Z, Yang Q, He S, Zhang X, et al. SMAD3/SP1 complex-mediated constitutive active loop between lncRNA PCAT7 and TGF-beta signaling promotes prostate cancer bone metastasis. *Mol Oncol* (2020) 14 (4):808–28. doi: 10.1002/1878-0261.12634
28. Liu X, Fu Q, Li S, Liang N, Li F, Li C, et al. LncRNA FOXD2-AS1 Functions as a Competing Endogenous RNA to Regulate TERT Expression by Sponging miR-7-5p in Thyroid Cancer. *Front Endocrinol* (2019) 10:207. doi: 10.3389/fendo.2019.00207
29. Chen J, Liu A, Wang Z, Wang B, Chai X, Lu W, et al. LINC00173.v1 promotes angiogenesis and progression of lung squamous cell carcinoma by sponging miR-511-5p to regulate VEGFA expression. *Mol Cancer* (2020) 19:98. doi: 10.1186/s12943-020-01217-2
30. Chen C, He W, Huang J, Wang B, Li H, Cai Q, et al. LNMAT1 promotes lymphatic metastasis of bladder cancer via CCL2 dependent macrophage recruitment. *Nat Commun* (2018) 9:3826. doi: 10.1038/s41467-018-06152-x
31. Chen C, Luo Y, He W, Zhao Y, Kong Y, Liu H, et al. Exosomal long noncoding RNA LNMAT2 promotes lymphatic metastasis in bladder cancer. *J Clin Invest* (2020) 130:404–21. doi: 10.1172/JCI130892
32. Li D, Chai L, Yu X, Song Y, Zhu X, Fan S, et al. The HOTAIRM1/miR-107/TDG axis regulates papillary thyroid cancer cell proliferation and invasion. *Cell Death Dis* (2020) 11:227. doi: 10.1038/s41419-020-2416-1
33. Zhuang X, Tong H, Ding Y, Wu L, Cai J, Si Y, et al. Long noncoding RNA ABHD11-AS1 functions as a competing endogenous RNA to regulate papillary thyroid cancer progression by miR-199a-5p/SLC1A5 axis. *Cell Death Dis* (2019) 10:620. doi: 10.1038/s41419-019-1850-4
34. Feng J, Zhou Q, Yi H, Ma S, Li D, Xu Y, et al. A novel lncRNA n384546 promotes thyroid papillary cancer progression and metastasis by acting as a competing endogenous RNA of miR-145-5p to regulate AKT3. *Cell Death Dis* (2019) 10:433. doi: 10.1038/s41419-019-1637-7
35. Wu N, Ren D, Li S, Ma W, Hu S, Jin Y, et al. RCC2 over-expression in tumor cells alters apoptosis and drug sensitivity by regulating Rac1 activation. *BMC Cancer* (2018) 18:67. doi: 10.1186/s12885-017-3908-y
36. Miller N, Feng Z, Edens BM, Yang B, Shi H, Sze CC, et al. Non-aggregating tau phosphorylation by cyclin-dependent kinase 5 contributes to motor neuron degeneration in spinal muscular atrophy. *J Neurosci* (2015) 35:6038–50. doi: 10.1523/JNEUROSCI.3716-14.2015
37. Dai Y, Ren D, Yang Q, Cui Y, Guo W, Lai Y, et al. The TGF-beta signalling negative regulator PICK1 represses prostate cancer metastasis to bone. *Br J Cancer* (2017) 117(5):685–94. doi: 10.1038/bjc.2017.212
38. Shi H, Deng HX, Gius D, Schumacker PT, Surmeier DJ, Ma YC. Sirt3 protects dopaminergic neurons from mitochondrial oxidative stress. *Hum Mol Genet* (2017) 26:1915–26. doi: 10.1093/hmg/ddx100
39. Zhang X, Zhang L, Lin B, Chai X, Li R, Liao Y, et al. Phospholipid Phosphatase 4 promotes proliferation and tumorigenesis, and activates Ca2+-permeable Cationic Channel in lung carcinoma cells. *Mol Cancer* (2017) 16:147. doi: 10.1186/s12943-017-0717-5
40. Zhang X, Ren D, Guo L, Wang L, Wu S, Lin C, et al. Thymosin beta 10 is a key regulator of tumorigenesis and metastasis and a novel serum marker in breast cancer. *Breast Cancer Res BCR* (2017) 19:15. doi: 10.1186/s13058-016-0785-2
41. Wang M, Ren D, Guo W, Huang S, Wang Z, Li Q, et al. N-cadherin promotes epithelial-mesenchymal transition and cancer stem cell-like traits via ErbB signaling in prostate cancer cells. *Int J Oncol* (2016) 48:595–606. doi: 10.3892/ijo.2015.3270
42. Li X, Liu F, Lin B, Luo H, Liu M, Wu J, et al. miR150 inhibits proliferation and tumorigenicity via retarding G1/S phase transition in nasopharyngeal carcinoma. *Int J Oncol* (2017) 50(4):1097–108. doi: 10.3892/ijo.2017.3909
43. Ren D, Lin B, Zhang X, Peng Y, Ye Z, Ma Y, et al. Maintenance of cancer stemness by miR-196b-5p contributes to chemoresistance of colorectal cancer cells via activating STAT3 signaling pathway. *Oncotarget* (2017) 8(30):49807–23. doi: 10.18632/oncotarget.17971
44. Miller N, Shi H, Zelikovich AS, Ma YC. Motor neuron mitochondrial dysfunction in spinal muscular atrophy. *Hum Mol Genet* (2016) 25:3395–406. doi: 10.1093/hmg/ddw262
45. Edens BM, Vissers C, Su J, Arumugam S, Xu Z, Shi H, et al. FMRP Modulates Neural Differentiation through m(6)A-Dependent mRNA Nuclear Export. *Cell Rep* (2019) 28:845–54.e5. doi: 10.1016/j.celrep.2019.06.072
46. Ma Y, Huang H, Jiang J, Wu L, Lin C, Tang A, et al. AVE 0991 attenuates cardiac hypertrophy through reducing oxidative stress. *Biochem Biophys Res Commun* (2016) 474:621–5. doi: 10.1016/j.bbrc.2015.09.050
47. Ren D, Dai Y, Yang Q, Zhang X, Guo W, Ye L, et al. Wnt5a induces and maintains prostate cancer cells dormancy in bone. *J Exp Med* (2018) 216 (2):428–49. doi: 10.1084/jem.20180661
48. Buchheit CL, Weigel KJ, Schafer ZT. Cancer cell survival during detachment from the ECM: multiple barriers to tumour progression. *Nat Rev Cancer* (2014) 14:632–41. doi: 10.1038/nrc3789
49. Haemmerle M, Taylor ML, Gutschner T, Pradeep S, Cho MS, Sheng J, et al. Platelets reduce anoikis and promote metastasis by activating YAP1 signaling. *Nat Commun* (2017) 8:310. doi: 10.1038/s41467-017-00411-z
50. Li SY, Wang H, Mai HF, Li GF, Chen SJ, Li GS, et al. Down-regulated long non-coding RNA RNAZFHX4-AS1 suppresses invasion and migration of breast cancer cells via FAT4-dependent Hippo signaling pathway. *Cancer Gene Ther* (2019) 26:374–87. doi: 10.1038/s41417-018-0066-6
51. Lin BY, Wen JL, Zheng C, Lin LZ, Chen CZ, Qu JM. Eva-1 homolog A promotes papillary thyroid cancer progression and epithelial-mesenchymal transition via the Hippo signalling pathway. *J Cell Mol Med* (2020) 24 (22):13070–80. doi: 10.1111/jcmm.15909
52. Xu J, Li N, Deng W, Luo S. Long noncoding RNA FER1L4 suppresses proliferation, invasion, migration and lymphatic metastasis of gastric cancer cells through inhibiting the Hippo-YAP signaling pathway. *Am J Trans Res* (2020) 12:5481–95.
53. Zhou GX, Li XY, Zhang Q, Zhao K, Zhang CP, Xue CH, et al. Effects of the hippo signaling pathway in human gastric cancer. *Asian Pac J Cancer Prev APJCP* (2013) 14:5199–205. doi: 10.7314/APJCP.2013.14.9.5199
54. Wang X, Sun D, Tai J, Chen S, Yu M, Ren D, et al. TFAP2C promotes stemness and chemotherapeutic resistance in colorectal cancer via inactivating hippo signaling pathway. *J Exp Clin Cancer Res CR* (2018) 37:27. doi: 10.1186/s13046-018-0683-9
55. Wu X, Zhang X, Yu L, Zhang C, Ye L, Ren D, et al. Zinc finger protein 367 promotes metastasis by inhibiting the Hippo pathway in breast cancer. *Oncogene* (2020) 39(12):2568–82. doi: 10.1038/s41388-020-1166-y
56. Karreth FA, Tay Y, Perna D, Ala U, Tan SM, Rust AG, et al. In vivo identification of tumor- suppressive PTEN ceRNAs in an oncogenic BRAF-induced mouse model of melanoma. *Cell* (2011) 147:382–95. doi: 10.1016/j.cell.2011.09.032
57. Tay Y, Kats L, Salmena L, Weiss D, Tan SM, Ala U, et al. Coding-independent regulation of the tumor suppressor PTEN by competing endogenous mRNAs. *Cell* (2011) 147:344–57. doi: 10.1016/j.cell.2011.09.029
58. Han H, Qi R, Zhou JJ, Ta AP, Yang B, Nakaoka HJ, et al. Regulation of the Hippo Pathway by Phosphatidic Acid-Mediated Lipid-Protein Interaction. *Mol Cell* (2018) 72:328–40.e8. doi: 10.1016/j.molcel.2018.08.038
59. Matallanas D, Romano D, Yee K, Meissl K, Kucerova L, Piazzolla D, et al. RASSF1A elicits apoptosis through an MST2 pathway directing proapoptotic transcription by the p73 tumor suppressor protein. *Mol Cell* (2007) 27:962–75. doi: 10.1016/j.molcel.2007.08.008
60. Praskova M, Khoklatchev A, Ortiz-Vega S, Avruch J. Regulation of the MST1 kinase by autophosphorylation, by the growth inhibitory proteins, RASSF1 and NORE1, and by Ras. *Biochem J* (2004) 381:453–62. doi: 10.1042/BJ20040025
61. Xu J, Meng Q, Li X, Yang H, Xu J, Gao N, et al. Long Noncoding RNA MIR17HG Promotes Colorectal Cancer Progression via miR-17-5p. *Cancer Res* (2019) 79:4882–95. doi: 10.1158/0008-5472.CAN-18-3880
62. Credendino SC, Bellone ML, Lewin N, Amendola E, Sanges R, Basu S, et al. A ceRNA Circuitry Involving the Long Noncoding RNA Klhl14-AS, Pax8, and Bcl2 Drives Thyroid Carcinogenesis. *Cancer Res* (2019) 79:5746–57. doi: 10.1158/0008-5472.CAN-19-0039
63. Yao N, Fu Y, Chen L, Liu Z, He J, Zhu Y, et al. Long non-coding RNA NONHSAT101069 promotes epirubicin resistance, migration, and invasion of breast cancer cells through NONHSAT101069/miR-129-5p/Twist1 axis. *Oncogene* (2019) 38:7216–33. doi: 10.1038/s41388-019-0904-5

64. Wu J, Minikes AM, Gao M, Bian H, Li Y, Stockwell BR, et al. Intercellular interaction dictates cancer cell ferroptosis via NF2-YAP signalling. *Nature* (2019) 572:402–6. doi: 10.1038/s41586-019-1426-6
65. Garcia-Rendueles ME, Ricarte-Filho JC, Untch BR, Landa I, Knauf JA, Voza F, et al. NF2 Loss Promotes Oncogenic RAS-Induced Thyroid Cancers via YAP-Dependent Transactivation of RAS Proteins and Sensitizes Them to MEK Inhibition. *Cancer Discov* (2015) 5:1178–93. doi: 10.1158/2159-8290.CD-15-0330
66. Hmeljak J, Sanchez-Vega F, Hoadley KA, Shih J, Stewart C, Heiman D, et al. Integrative Molecular Characterization of Malignant Pleural Mesothelioma. *Cancer Discov* (2018) 8:1548–65. doi: 10.1158/2159-8290.CD-18-0804
67. Kim SH, Jin H, Meng RY, Kim DY, Liu YC, Chai OH, et al. Activating Hippo Pathway via Rassf1 by Ursolic Acid Suppresses the Tumorigenesis of Gastric Cancer. *Int J Mol Sci* (2019) 20(19):4709. doi: 10.3390/ijms20194709
68. Zhu Y, He D, Bo H, Liu Z, Xiao M, Xiang L, et al. The MRVI1-AS1/ATF3 signaling loop sensitizes nasopharyngeal cancer cells to paclitaxel by regulating the Hippo-TAZ pathway. *Oncogene* (2019) 38:6065–81. doi: 10.1038/s41388-019-0858-7

Conflict of Interest: The authors declare that the research was conducted in the absence of any commercial or financial relationships that could be construed as a potential conflict of interest.

Copyright © 2021 Liu, Fu, Bian, Fu, Xin, Liang, Li, Zhao, Fang, Li, Zhang, Dionigi and Sun. This is an open-access article distributed under the terms of the Creative Commons Attribution License (CC BY). The use, distribution or reproduction in other forums is permitted, provided the original author(s) and the copyright owner(s) are credited and that the original publication in this journal is cited, in accordance with accepted academic practice. No use, distribution or reproduction is permitted which does not comply with these terms.

frontiers in Oncology

ORIGINAL RESEARCH
published: 08 January 2021
doi: 10.3389/fonc.2020.566365

Downregulation of miR-146b-3p Inhibits Proliferation and Migration and Modulates the Expression and Location of Sodium/Iodide Symporter in Dedifferentiated Thyroid Cancer by Potentially Targeting MUC20

Shasha Hou[1], Xiaorui Xie[2], Jing Zhao[3], Cailan Wu[4], Ning Li[1], Zhaowei Meng[1], Chunquan Cai[5] and Jian Tan[1]**

[1] Department of Nuclear Medicine, Tianjin Medical University General Hospital, Tianjin, China, [2] Department of Pediatrics, Tianjin Medical University General Hospital, Tianjin, China, [3] Department of Ultrasound, Tianjin Medical University Cancer Institute and Hospital, Tianjin, China, [4] Department of Nuclear Medicine, Tianjin Fourth Central Hospital, Tianjin, China, [5] Department of Pediatrics, Tianjin Children's Hospital, Tianjin, China

The dedifferentiation of differentiated thyroid cancer (DTC) is a challenging problem for radioactive iodine (^{131}I) treatment, also known as radioiodine refractory differentiated thyroid cancer (RAIR-DTC). The purpose of this study was to further explore the mechanism of the redifferentiation of dedifferentiated thyroid cancer. Ineffective and effective groups of ^{131}I therapy were analyzed and compared in both our clinical and TCGA samples. Whole-exome sequencing, mutation analysis, transcriptome analysis, and *in vitro* functional experiments were conducted. *FLG*, *FRG1*, *MUC6*, *MUC20*, and *PRUNE2* were overlapping mutation genes between our clinical cases, and the TCGA cases only appeared in the ineffective group. The expression of *miR-146b-3p* target *MUC20* was explored. The expression levels of *miR-146b-3p* and *MUC20* were significantly increased, and the inhibition of *miR-146b-3p* expression significantly inhibited proliferation and migration, promoted apoptosis, regulated the expression and location of thyroid differentiation-related genes, and sodium/iodide symporter (NIS) in dedifferentiated thyroid cancer cells (WRO). Thus, *miR-146b-3p* potentially targets *MUC20* participation in the formation of DTC dedifferentiation, resulting in resistance to ^{131}I and the loss of the iodine uptake ability of DTC cancer foci, promoting refractory differentiated thyroid cancer. *miR-146b-3p* may be a potentially therapeutic target for the reapplication of ^{131}I therapy in dedifferentiated thyroid cancer patients.

Keywords: miR-146b-3p, radioiodide therapy, sodium/iodide symporter, dedifferentiated thyroid cancer, *MUC20*

OPEN ACCESS

Edited by:
Qiang Shen,
Louisiana State University,
United States

Reviewed by:
Dengfeng Li,
Tongji University, China
Guojun Li,
University of Texas MD Anderson Cancer Center, United States

****Correspondence:***
Jian Tan
tanpost@163.com
Chunquan Cai
tj837547870@163.com

Specialty section:
This article was submitted to Head and Neck Cancer, a section of the journal Frontiers in Oncology

Received: *27 May 2020*
Accepted: *17 November 2020*
Published: *08 January 2021*

Citation:
Hou S, Xie X, Zhao J, Wu C, Li N, Meng Z, Cai C and Tan J (2021) Downregulation of miR-146b-3p Inhibits Proliferation and Migration and Modulates the Expression and Location of Sodium/Iodide Symporter in Dedifferentiated Thyroid Cancer by Potentially Targeting MUC20. Front. Oncol. 10:566365. doi: 10.3389/fonc.2020.566365

INTRODUCTION

Thyroid cancer is the most common malignant tumor in the endocrine system. According to the most recent statistics, the incidence of thyroid cancer in the United States ranks sixth among female malignant tumors in 2019 (1). Differentiated thyroid cancer (DTC) is the most frequent subtype of thyroid cancer. Radioiodine (^{131}I) is a classic radiotheragnostic agent used for the treatment of DTC following a thyroidectomy based on sodium-iodine symporter expression in normal and neoplastic thyroid tissue (2). Non-iodine uptake is an independent predictor of poor prognosis in DTC patients, and our previous study found that 30% of DTC patients with lung metastases did not take iodine (3). Surgery followed by radioactive iodine (^{131}I) is effective in most DTC patients (4); however, some DTC dedifferentiate during treatment, and subsequently develop into radioiodine refractory differentiated thyroid cancer (RAIR-DTC). RAIR-DTC is a difficult problem associated with clinical treatment with rapid disease progression and poor prognosis.

Researches into relevant mechanisms are extremely important for the effective treatment of RAIR-DTC and some progress had been achieved. It has been reported that some DTC patients with metastases underwent degenerative changes in the morphology and function of tumor cells during ^{131}I therapy. In addition, impaired expression of iodine key protein and a loss of iodine uptake eventually developed into dedifferentiated thyroid cancer (5). At this point, the DTC is RAIR-DTC, which cannot benefit from ^{131}I therapy, and the survival time is much shorter than that of those with favorable iodine intake. For the RAIR-DTC therapy, restoring the ability of dedifferentiated thyroid cancer to uptake ^{131}I may represent a potential solution. It is currently believed that the main mechanisms of ^{131}I treatment of thyroid cancer are closely related to mutations in RAS, BRAFV600E, and TERT, activate the MAPK pathway, PI3KCA mutation activates the PI3K/Akt pathway, and β-catenin mutation activate the wnt/β-catenin pathway. They may cause cellular proliferation and dedifferentiation, which leads to an abnormal silence or decreased expression of key iodine uptake proteins (NIS, TSHR, TPO, and Tg) and thyroid transcription factors (e.g., TTF1 and TTF2) (6–9).

At present, several methods have been reported to improve the radioiodine uptake ability of dedifferentiated cancer cells, including prolonging the effective half-life of ^{131}I, inducing cell redifferentiation, and transgene therapy (10). However, these methods are all associated with some shortcomings, including unstable iodine uptake, rapid iodine outflow, inadequate radiation efficiency, toxic side effects of molecular targeted drugs, and acquired drug resistance. Additionally, it is extremely important for radionuclide therapy of thyroid cancer to redifferentiate undifferentiated lesions or metastatic lesions and improve their uptake of ^{131}I. Therefore, in order to identify a more effective strategy for the treatment of redifferentiation, it is necessary to further explore the mechanisms associated with the occurrence and development of RAIR-DTC.

MATERIALS AND METHODS

Human Tissues and DNA Extraction

Six DTC patients accepted ^{131}I therapy following total thyroidectomy which is a complete removal of the thyroid tumor and tissue, performed at Tianjin Medical University General Hospital from October 2016 to August 2018.

The iodine uptake capacity of tumor tissue was mainly evaluated using ^{131}I whole-body scan (^{131}I-WBS) after radioiodine therapy, A combination of ^{131}I-WBS, serum Tg and TgAb levels, and imaging examinations were performed to assess RAIR-DTC.

Among these patients, three were RAIR-DTC patients without iodine uptake of lung metastases after 131I remnant ablation successful, all of which exhibited post-operative lung metastases (test group, **Figures 1A, B**). The other three cases possessed good iodine uptake capacity of lung metastases and were sensitive to radioiodine therapy (control group, **Figures 1C, D**). The primary surgical excision tissues were collected from

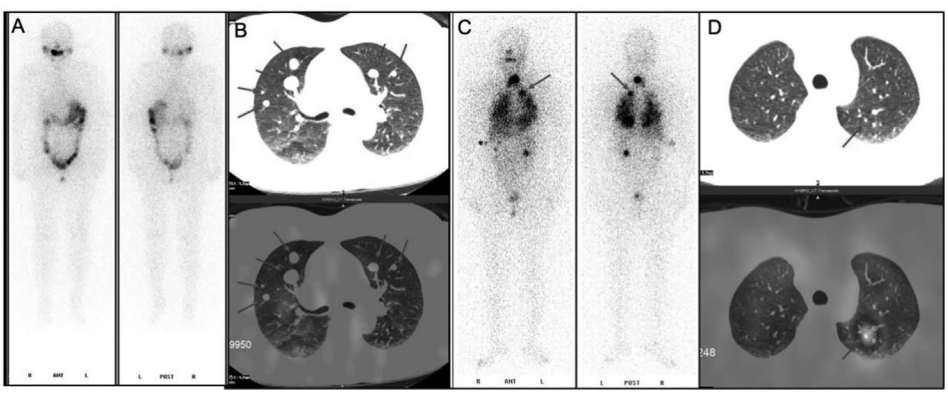

FIGURE 1 | ^{131}I whole-body scan (^{131}I-WBS) after radioiodine therapy. **(A, B)** ^{131}I-WBS and CT image of a patient without iodine uptake of lung metastases after 131I remnant ablation successful. **(C, D)** ^{131}I-WBS and CT image of a patient with iodine uptake of lung metastases.

these patients. All patients provided voluntary informed consent, and the study was approved by the ethics committee at our hospital. Genomic DNA was extracted and the concentration with a QIAamp® DNA Micro kit (Qiagen, Heidelberg, Germany) in accordance with the manufacturer's protocol. A Qubit system was used to quantify genomic DNA before library preparation.

Cell Culture

According to our previous experiments and reported studies (5, 11, 12), the dedifferentiated thyroid cancer cell line WRO was selected for subsequent experiments. The WRO cell line was purchased from Sigma-Aldrich (Munich, Gemany) and the cells were cultured in DMEM medium (Gibco, USA) containing 10% fetal bovine serum (FBS, Gibco, USA), 1% penicillin (100 U/mL)/ streptomycin (100 μg/mL; Gibco, USA), and were maintained in a 37°C incubator in a humidified, 5% CO_2 atmosphere.

TCGA Data Screening and Download of Mutation Information

A total of 491 thyroid cancer cases were selected from The Cancer Genome Atlas (TCGA) database based on the following screening criteria: 1) postoperative radioiodine therapy; 2) clear effect of iodine therapy; 3) complete information of gene mutation; and 4) complete information regarding microRNA (miRNA) expression data. Disease stabilization and progression were considered to be ineffective treatment (test group), and both a partial or complete responses were effective (control group). Thus, 167 ineffective and 324 effective patients were included. Subsequently, the single nucleotide variant (SNV) and insertion/ deletion (Indel) mutations were downloaded and analyzed between the test and control groups. In addition, the mutation genes occurred only in the test group but not in control group were screened out, and recorded as a test-specific mutation gene set.

Whole-Exome Sequencing and Mutation Analysis for Clinical Patients

After sheering and repairing the ends, the DNA samples were purified using AMPure XP beads (Beckman-Coulter, Indianapolis, USA). Subsequently, the paired-end adaptor was ligated, the samples were purified, the adaptor-ligated library was amplified, the amplified library was purified, and the quality and quantity were assessed using a Qubit Fluorometer (Invitrogen, Carlsbad, USA). A library hybridization kit, SeqCap EZ MedExome Enrichment kit (Roche NimbleGen, Madison, USA), was used to capture the target sequences. A whole-exon probe system was customized from Roche NimbleGen to capture target sequences, capture magnetic beads, and the elution of hybridization libraries. After amplifying the captured library by PCR, the constructed library was sequenced with an Illumina HiSeq Xten sequencer. The average sequencing depth of the tissue samples was 500X, which could detect mutations in tumor genes with very low frequency of 0.1%.

The sequencing data were filtered by SOAPnuke to remove the Adapter-containing sequences and low quality data. The quality of the raw data after filtering met the Q30 requirement of > 85%. BWA was used to compare the data to the human reference genome (hg19.fa). GATK was used to re-align the reads in the interval, calibrate and rearrange the alkali matrix quality values, and count the sequencing depth and coverage. An indel detection was conducted with GATK and VarScant, SNV was detected with MuTect and VarScan, and CNV was detected with CONTRA. The test-specific mutation gene set was also sifted out. Finally, they were annotated to a catalogue of somatic mutations in cancer (COSMIC, https://cancer.sanger.ac.uk/ cosmic), the single nucleotide polymorphism database (dbSNP, https://www.ncbi.nlm.nih.gov/snp/), and the important genes related to the occurrence, development, treatment and prognosis of thyroid cancer, were selected out. A Venn diagram was drawn based on these genes and the TCGA data. Accordingly, the overlapping test-specific mutation genes were selected between TCGA cases and our clinical cases, and studied in in-depth.

Identification of Participating Pathways Associated With Overlapping Mutation Genes

Using the Rectome database (https://www.reactome.org/), a free, open-source, curated and peer reviewed pathway database, we analyzed the pathways of the above overlapping genes.

Transcriptome Analysis and Regulation Network Construction

The mRNA and miRNA expression data were obtained from TCGA data. After standardization with preprocessCore function package V3.5 (http://www.bioconductor.org/packages/release/ bioc/html/preprocessCore.html), the differentially expressed genes (DEGs) and differentially expressed microRNAs (DEGs) were identified with the limma V3.18.13 software package (http://www.bioconductor.org/packages/2.13/bioc/html/limma.html) in the test group compared with control group. $P < 0.05$ and $|\log (\text{fold-change})| > 2$ were used as the threshold criteria. Using mirwall 3.0 (http://mirwalk.umm.uni-heidelberg.de/), we obtained the targeting relationship (gene-miRNA pairs) between the DEMs and overlapping genes. The protein-protein interactions (PPI) were analyzed *via* the STRING V10.0 database (http://string-db.org), and the PPI pairs of the overlapping mutation genes were screened out using more than 500 scores. Based on the above pairs, the regulation network was ultimately constructed and visualized using Cytoscape V3.5.1 software (http://www.cytoscape.org/ download.php).

miR-146b-3p Inhibitors/nc Oligonucleotides and Cellular Transfection

The expression of *miR-146b-3p* and likely target *MUC20* were explored between our clinical cases and TCGA cases, and only appeared in the ineffective group. Then *miR-146b-3p* inhibitors and individual nc oligonucleotide products (GenePharma, China) were synthesized. WRO cells were transfected with 100 nM of the indicated oligonucleotides separately using Lipofectamine 3000 (Invitrogen) according to the manufacturer's protocol. At 24 to 48 h post-transfection, the resultant cells were used for functional assays. The remaining cells were

harvested for quantitative polymerase chain reaction (qRT-PCR) analysis.

RNA Extraction and RT-PCR Analysis

The expressions of the overlapping mutation genes *(FLG*, *FRG1*, *MUC6*, *MUC20*, and *PRUNE2)* were detected in the above clinical surgical excision tissues. The primer sequences of the genes are listed in **Table 1**. The total RNA was extracted using TRIzol (Invitrogen; Thermo Fisher Scientific, Inc., Waltham, USA). All of the specific primers were designed and synthesized by Takara Biotechnology Co., Ltd (Dalian, China), and are listed in **Table 1**. A PrimeScript® 1st Stand cDNA Synthesis kit (Takara Biotechnology Co., Ltd., Dalian, China) and SYBR® Premix Ex Taq™ kit (Takara Biotechnology Co., Ltd., Dalian, China) were used to conduct reverse transcription PCR (RT-PCR) in accordance with the manufacturer's protocols. The reaction conditions for reverse transcription were as follows: 30°C for 10 min, 42°C for 60 min, and 95°C for 5 min. Finally, the relative expression value of the optical density was calculated for the target gene.

Cell Proliferation Assay

A WRO Cell Counting Kit-8 (CCK-8; Dojindo, Japan) assay was used to assess the level of cell proliferation/viability according to the manufacturer's instructions. After an incubation with miR-146b-3p inhibitors (100 nmol/μl) or the same volume of 0.1% DMSO (as control) for 24, 48, and 72 h, CCK8 reagent was added into each well, and the cells were incubated at 37°C for 2 h. Cell viability was measured by the level of absorbance (optical density) at a wavelength of 450 nm using a microplate reader.

Cell Apoptosis Assay

WRO cells were seeded into six-well plates and treated with 100 nmol/μl *miR-146b-3p* inhibitors or the same volume of 0.1% DMSO (as control) for 72 h, then harvested and stained with Annexin V/propidium iodide (PI) staining kit (Beyotime, China) according to the manufacturer's instructions. Finally, the apoptotic rates were obtained by flow cytometry.

Colony Formation Assay

Different groups of WRO cells were cultured in six-well plates. The cells were cultured in a 37°C incubator under humidified, 5% CO_2 conditions for 7 to 10 days. The cells were then fixed and stained with a crystal violet solution for 30 min and images were obtained.

TABLE 1 | Primer sequences of qRT-PCR of genes.

The name of the primer		Primer sequences(5′-3′)
FLG	Forward	GCTGAAGGAACTTCTGGAAA
	Reverse	CATCAGAAGAAACTCAGTGAA
FRG1	Forward	GCTCCACACAAAGAAGTTGA
	Reverse	CTCTTGGTCCAATTGCATCT
MUC20	Forward	GATCACAACCTCAGCGAAGA
	Reverse	GAGCTGCTGCATCAGCCTTT
MUC6	Forward	CTCAACAAGGTGTGTGCAGA
	Reverse	GGAAAGGTCTCCTCGTAGTT
PRUNE2	Forward	CAGTTCAGTGCTCAGGGTTT
	Reverse	CCAAACTTGTCTGTAAATGCTT
ACTING	Forward	CTGGACTTCGAGCAAGAGAT
	Reverse	GATGTCCACGTCACACTTCA

Transwell Assay

Different groups of WRO cells were cultured, and a total of 1×10^5 cells in 100 μl serum-free DMEM were seeded into the upper chamber of the transwell plates precoated with Matrigel (Millipore). Complete DMEM medium was added to the lower chamber. After 24 h, cells that invaded the membrane were fixed, stained with a crystal violet solution for 2 min and counted.

Wound-Healing Assay

Different groups of WRO cells were transfected with miR-146b-3p inhibitors or negative control and cultured until the cells reached 90% confluence. The wound was created using a 200 μl tip and the cells were continued to be cultured in DMEM medium for another 24 h or 48 h. Cellular migration was recorded by an inverted microscope and images were obtained.

Immunofluorescence

WRO cells were transfected with miR-146b-3p inhibitors or negative control and were fixed in 4% paraformaldehyde in phosphate-buffered saline. The cells were subsequently incubated with an anti-NIS antibody (Bioss, China) overnight at 4°C and subsequently incubated with a fluorescein-conjugated secondary antibody (CST, USA) for 2 h. The nuclei were treated with RNase- and stained with 20 mg/ml propidium iodide (PI; Beyotime, China). Fluorescence was observed using a fluorescence microscope (Nikon Instruments Inc., Melville, NY, USA).

Western Blot

Different groups of WRO cells were seeded into 24-well plates with a cover glass over each well and cultured for 24 h. Total, membranous and cytoplasmic NIS and MUC20 proteins were extracted according to the standard steps of the protein extraction kits.

Lysates were quantified spectrophotometrically using the bicinchoninic-acid-based (BCA) method. Twenty-five micrograms of each sample was separated on gradient polyacrylamide gels and transferred onto polyvinyldifluoride membranes. Membranes were incubated with a primary antibody (anti-NIS, Bioss, China; MUC 20, Abnova, USA; MET, abcam, UK; MET pY1234/5, CST, USA; β-actin, CST, USA) overnight at 4°C in TTBS/milk. The samples were subsequently incubated with horseradish peroxidase-conjugated secondary anti-mouse antibodies (CST, USA). The protein was visualized using an enhanced chemiluminescence Western blot detection system (Thermo Fisher Scientific). Multiplication of the intensity and area of protein bands indicated the relative levels of protein expression.

Radioiodide Uptake Assay (RAIU)

WRO cells were transfected with miR-146b-3p inhibitors or negative control and were seeded into 24-well plates, the cells were washed with ice-cold modified Hanks' balanced salt

solution (HBSS) three times and then incubated at 37°C with 500 µl buffered HBSS containing 2 µCi $Na^{125}I$ for 30 min. Then, radioactive medium was aspirated and cells were washed (×3) with 1ml of ice-cold HBSS for 1min. Cells were harvested using trypsin and counted with a hemacytometer. The radioactivity was measured with a gamma counter. The radioactivity was normalized to the number of cells present at the time of the assay as cpm every 10^6 cells.

Statistical Analysis

SPSS V23.0 software (SPSS Inc., Chicago, USA) was used for all statistical analyses, and the data were expressed as the mean ± SD. A t-test was used to compare the differences between two groups, and $P < 0.05$ was considered to be statistically significant.

RESULTS

The Expression of miR-146b-3p Target MUC20 Were Explored by Bioinformatics Analysis

From the TCGA cases, a total of 7,335 mutation genes were identified in 491 thyroid cancer samples. It was further found that there were 1,915 specific mutation genes in test group compared with the control group. In our clinical cases, there were 55 test-specific variation sites in the test that occurred in 41 genes. After annotating to COSMIC and dbSNP, 10 genes were directly related to thyroid cancer, and 9 genes may have been related to thyroid cancer (associated with other cancers and radiation therapy). The 19 genes were listed in **Figures 2A, B**, as well as a Venn diagram and the above 1915 test-specific mutation genes are shown in **Figure 2C**. Five test-specific mutation genes were overlapped in TCGA and our clinical cases (i.e., *FLG*, *FRG1*, *MUC6*, *MUC20*, and *PRUNE2*).

The gene-miRNA regulation network was further analyzed. Among the TCGA cases, the results of the differential expression analysis of the above overlapping mutation genes were compared between the test group and control group, and *MUC20* and *FRG1* were found to be differentially expressed (**Figure 2D**). Simultaneously, 10 DEMs were identified in the test group compared with control group, including *miR-204*, *miR-7-2*, and *miR-551b* (**Table 2**). Furthermore, the gene-miRNA pairs were obtained by miRwall 3.0 and exhibited in **Table 3** (e.g., *miR-146b-3p-MUC20* and *hsa-miR-146b-3p-PRUNE2*). After screening with STRING V10.0, 196 PPI pairs were obtained. Eventually, the regulated network was constructed and presented in **Figure 3A**. The network contained four functional groups, which were recorded as the: 1) *MUC6-MUC20* group; 2) *PRUNE2* group; 3) *FLG* group; and 4) *FRG1* group. Interestingly, *hsa-miR-146b-3p* connected the *MUC6-MUC20* group and *PRUNE2* group. Similarly, *hsa-miR-551b-5p* linked the *PRUNE2* group and *FRG1* group together.

After analysis of the above overlapping mutation genes, only *MUC20* was found to be participating in the pathways, "negative regulation of MET activity" and "MET activates RAS signaling" (**Figure 4**). *FLG*, *FRG1*, *MUC6*, and *PRUNE2* were not found to participate in any pathways.

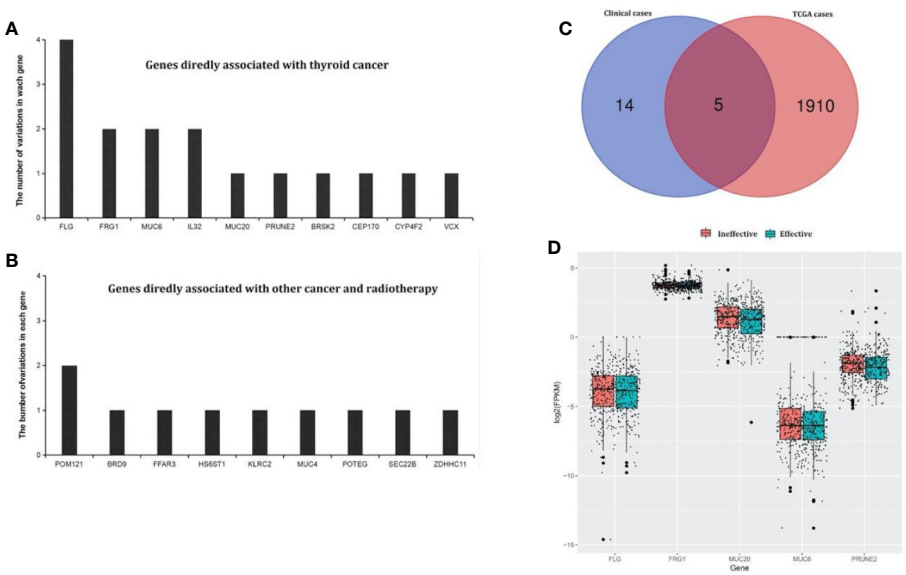

FIGURE 2 | Test-specific mutation genes directly and indirectly associated with thyroid cancer identified in our clinical samples. **(A)** Genes in the annotated database that showed clear evidence of being associated with thyroid cancer. There were 10 genes that were directly related to thyroid cancer. **(B)** Genes in the annotated database that showed clear evidence of being associated with other cancers and radiotherapy. There were nine genes that may be related to thyroid cancer (associated with other cancers and radiation therapy). **(C)** The Venn diagram of test-specific mutation genes between our clinical and TCGA cases. There were five overlapping test-specific mutation genes in TCGA and our clinical cases (*FLG*, *FRG1*, *MUC6*, *MUC20*, and *PRUNE2*). **(D)** Differential expression analysis of the overlapping genes in the TCGA cases between the test an control groups. *MUC20* and *FRG1* were differentially expressed.

TABLE 2 | The DEMs identified in test group compared with control group among TCGA cases.

MiRNA	LogFC	AveExpr	T Value	P Value
hsa-mir-204	0.863062063	6.400199623	3.88062297	0.000120147
hsa-mir-7-2	0.862249179	3.948694306	3.800144007	0.000164985
hsa-mir-551b	-0.831391274	6.423744887	-3.54704631	0.000431436
hsa-mir-7-3	0.718090127	2.127805746	3.40904965	0.000711975
hsa-mir-676	0.527504431	3.443443543	3.378238087	0.000794446
hsa-mir-6715a	0.803311975	2.771116168	3.299026227	0.001049064
hsa-mir-146b	-0.780099202	16.03598508	-3.161258887	0.001679494
hsa-mir-31	-0.746292503	7.960612802	-3.151052959	0.00173794
hsa-mir-1179	0.65710791	3.225364061	3.096506992	0.002083391
hsa-mir-375	-0.662702182	14.03006948	-2.844438491	0.004656558

DEMs, differential expression microRNAs; LogFC, Log (fold-change); AveExpr, average expression.

TABLE 3 | The gene-miRNA pairs between DEMs and overlapped mutation genes.

MiRNA	Gene	LogFC_miRNA	LogFC_gene	Position
hsa-miR-146b-3p	MUC20	-0.780099202	-0.519617606	CDS
hsa-miR-146b-3p	PRUNE2	-0.780099202		CDS
hsa-miR-204-3p	PRUNE2	0.863062063		CDS
hsa-miR-204-5p	PRUNE2	0.863062063		CDS
hsa-miR-31-3p	PRUNE2	-0.746292503		CDS
hsa-miR-375	MUC6	-0.662702182		CDS
hsa-miR-551b-3p	PRUNE2	-0.831391274		3'UTR
hsa-miR-551b-5p	PRUNE2	-0.831391274		3'UTR
hsa-miR-551b-5p	FRG1	-0.831391274	-0.70594252	CDS
hsa-miR-6715a-3p	PRUNE2	0.803311975		CDS
hsa-miR-676-5p	PRUNE2	0.527504431		3'UTR

DEMs, differential expression microRNAs; LogFC, Log (fold-change); LogFC_miRNA, the logFC of miRNA; LogFC_gene, the logFC of gene; CDS, coding sequence; 3'UTR, 3' untranslated region.

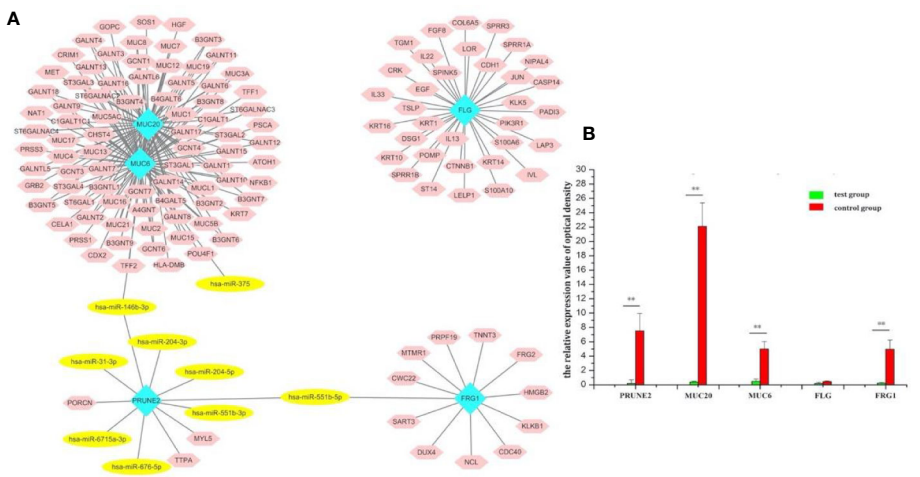

FIGURE 3 | Screening of the target genes and exploration of the miR-146b-3p target MUC20. **(A)** The regulated network of the overlapping mutation genes. The network contained four functional groups, recorded as: *MUC6-MUC20* group, *PRUNE2* group, *FLG* group, and *FRG1* group. Interestingly, *miR-146b-3p* was connected to the *MUC6-MUC20* group and *PRUNE2* group, and *miR-551b-5p* linked the *PRUNE2* and *FRG1* groups together. **(B)** RT-PCR results regarding the expression of the overlapping mutation genes. *MUC20* was significantly highly expressed. (**p < 0.01).

Furthermore, the expression overlapping mutation genes in thyroid cancer was validated by qRT-PCR. After verification by RT-PCR, *FRG1*, *MUC6*, *MUC20*, and *PRUNE2* were significantly different between the FTC-133 and WRO groups (**Figure 3B**). In particular, *MUC20* was the most remarkable ($p < 0.01$). Through the above bioinformatics analysis, the expression of miR-146b-3p target MUC20 were explored.

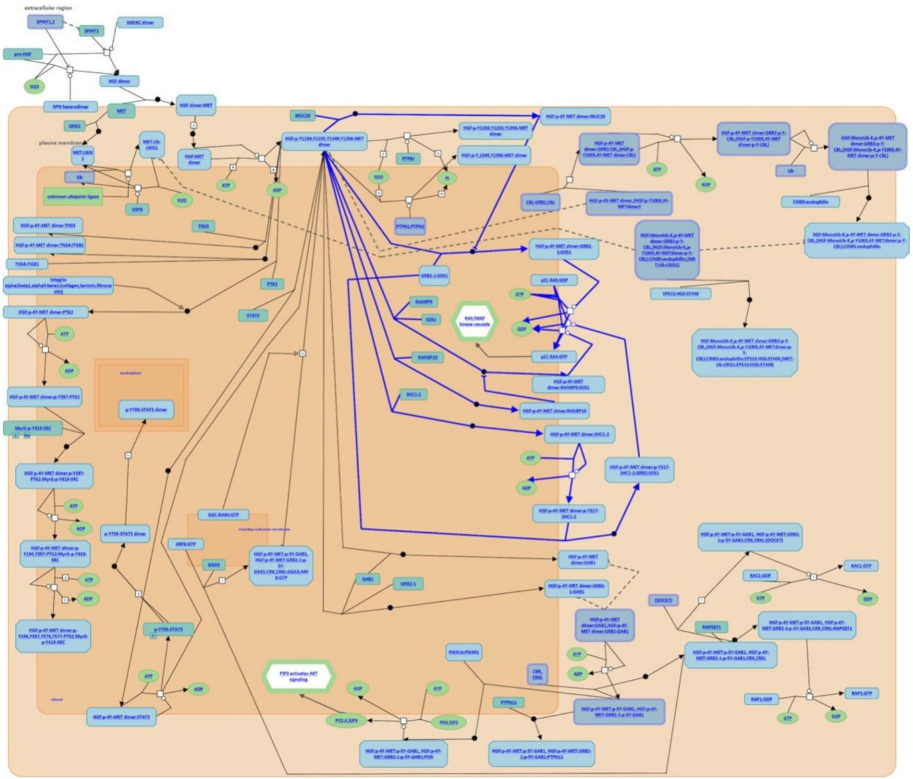

FIGURE 4 | Participating pathways analysis. Only MUC20 was found to participate in the pathways, "negative regulation of MET activity" and "MET activates RAS signaling".

The Overexpression of *miR-146b-3p* in Dedifferentiated Thyroid Cancer Cells

To investigate the possible function of *miR-146b-3p* in the regulation of dedifferentiated thyroid cancer, we first examined the level of *miR-146b-3p* mRNA expression in differentiated and dedifferentiated thyroid cancer cell lines (TPC-1 and WRO) by qRT-PCR. Interestingly, *miR-146b-3p* expression was significantly increased in dedifferentiated thyroid cancer WRO cell lines (**Figure 5A**). Presumably, it is possible to associate *miR-146b-3p* expression with the dedifferentiation of differentiated thyroid cancer.

To confirm our hypothesis, we established *miR-146b-3p* knockdown models. As a result, the transfected cells carrying *miR-146b-3p* inhibitors (*anti-miR-146b-3p*)/nc are considered ideal tools for *miR-146b-3p* research.

Figure 5B shows that *miR-146b-3p* expression is apparently lower than the nc control upon the transfection of inhibitors.

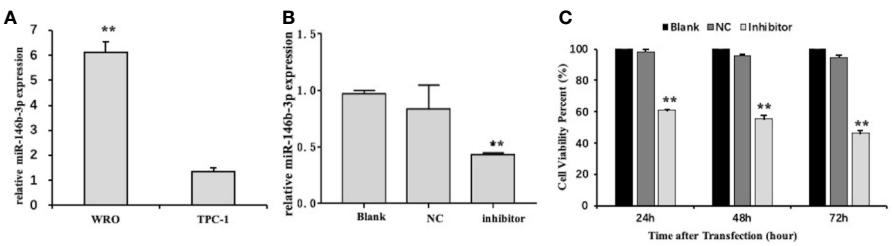

FIGURE 5 | The level of miR-146b-3p overexpression in dedifferentiated thyroid cancer cells. **(A)** Expression of miR-146b-3p in thyroid cancer cells with different degrees of differentiation. The level of miR-146b-3p expression was significantly increased in the dedifferentiated thyroid cancer WRO cell lines. **(B)** Expression of miR-146b-3p following transfection with an inhibitor. The miR-146b-3p expression was substantially lower than that of the control groups following transfection with inhibitors (**p < 0.01). **(C)** Effects of anti-miR-146b-3p on thyroid cancer cell proliferation was determined by CCK-8 cell proliferation assays. Data were represented as the means ± SD.

This finding indicates that *miR-146b-3p* inhibitors have a remarkable effect on a *miR-146b-3p* knockdown.

Anti-miR-146b-3p Inhibited Cell Proliferation, Invasion, and Migration, as Well as Induced Apoptosis in Dedifferentiated Thyroid Cancer Cells

To analyze the role of *miR-146b-3p* in regulating the proliferation of WRO cells, a CCK-8 assay was used. As indicated in **Figure 5C** *miR-146b-3p* inhibitors significantly suppressed the proliferation of WRO cells in a time-dependent manner. Following transfection with *miR-146b-3p* inhibitors for 24 h, 48 h, and 72 h, the viability rates of WRO cells were 60.79% ± 0.34%, 55.44% ± 2.17%, and 46.38% ± 1.64%, respectively ($P < 0.01$). These findings revealed that *miR-146b-3p* overexpression could significantly increase the proliferation of dedifferentiated thyroid cancer cells.

Cell apoptosis was measured by flow cytometry. The results showed that the level of apoptosis was significantly higher in the *miR-146b-3p* inhibitors transfection group compared to that of the control groups (**Figure 6A**). In the three groups of WRO cells, apoptosis rates of 15.73% ± 1.2%, 5.89% ± 0.35%, 5.86% ± 1.4%, and were observed in the *miR-146b-3p* inhibitors transfection group and control groups, respectively ($P < 0.01$). The results revealed that *anti-miR-146b-3p* could significantly increase apoptosis in dedifferentiated thyroid cancer cells.

We studied the effects of *miR-146b-3p* on cell growth and colony formation by a colony-formation assay. The results revealed that the number of *miR-146b-3p* inhibitor-transfected cells was significantly lower than that of the control groups (**Figure 6B**). This indicated that *miR-146b-3p* overexpression could significantly increase growth in dedifferentiated thyroid cancer cells.

Cell migration and invasion are critical for tumor growth. To explore the effect of *miR-146b-3p* on WRO cell migration and invasion, we performed both wound-healing and transwell assays. The results showed that inhibition miR-146b-3p expression obviously suppressed the migratory and invasive ability of WRO cells compared to that of the control groups. This revealed that *miR-146b-3p* overexpression could significantly promote WRO cell migration and invasion (**Figures 6C, D**).

Together, these findings suggest that the upregulation of miR-146b-3p may contribute to dedifferentiated thyroid cancer progression by promoting cell proliferation and metastasis.

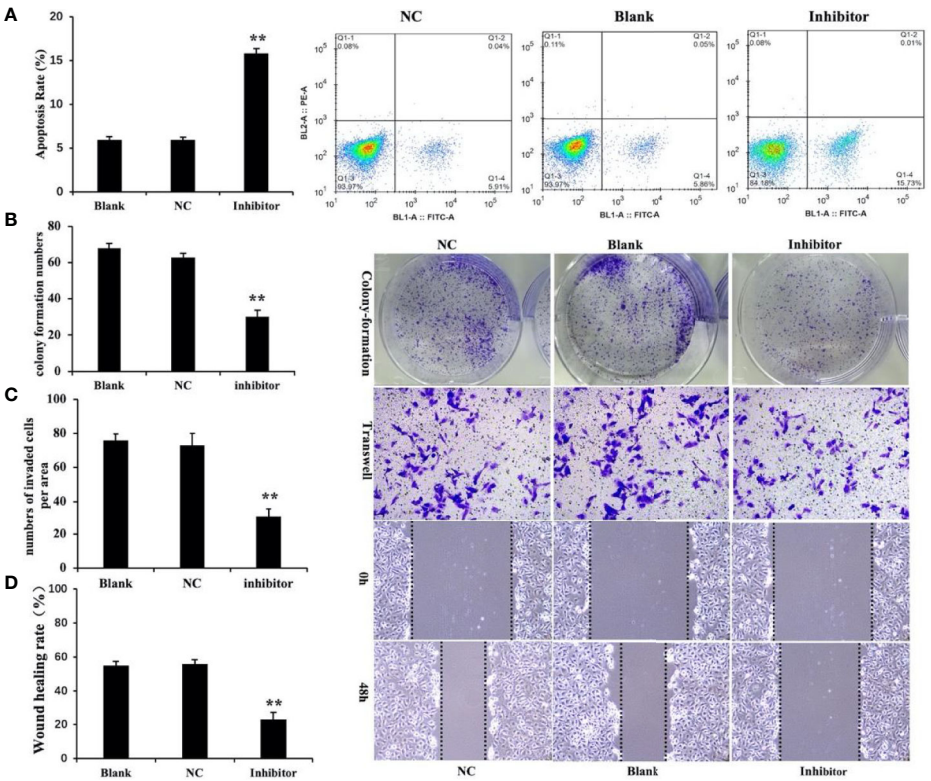

FIGURE 6 | Anti-miR-146b-3p inhibited dedifferentiated thyroid cancer cell proliferation, invasion, migration, and induction of apoptosis. **(A)** The effects of anti-miR-146b-3p on thyroid cancer cell apoptosis was measured by flow cytometry. Data were represented as the means ± SD. **(B–D)** The effects of anti-miR-146b-3p on thyroid cancer cell proliferation, invasion, and migration were determined by colony formation, transwell, and wound healing assays. The results showed that treatment with miR-146b-3p inhibitors significantly suppressed the proliferation and invasion of WRO cells (**p < 0.01).

Anti-miR-146b-3p Upregulated NIS Expression in Dedifferentiated Thyroid Cancer Cells

We previously found that *anti-miR-146b-3p* caused significant inhibition of WRO cell proliferation, growth, migration, as well as the induction of apoptosis. We subsequently detected the level of NIS protein expression by Western blot. The results showed that the level of NIS protein (total and membranous/cytoplasmic) expression in *miR-146b-3p* inhibitor-transfected cells were obviously increased compared to that of the control groups (**Figures 7A, B**). We further investigated the effect of *anti-miR-146b-3p* on NIS protein translocation by immunofluorescence. The results showed that *anti-miR-146b-3p* increased both cytoplasmic and cytomembrane-located NIS expression, the latter of which was more significant (**Figure 8A**).

*miR-146b-3*p/*MUC20*/*MET* Signaling Pathway Modulates the NIS-Mediated Radioiodide Uptake in Dedifferentiated Thyroid Cancer Cells

We further explore and study the mechanism of *miR-146b-3p* involving in dedifferentiation of thyroid cancer. The results suggested that MUC*20*, MET, and phosphorylation of MET (p-MET) significantly inhibited after inhibiting the *miR-146b-3p* (**Figure 7C**). Moreover, we found that inhibition of *miR-146b-3p* expression improve NIS-mediated radioiodide uptake ability compared to the control groups (**Figure 8B**).

The above results indicated that *miR-146b-3p*/*MUC20*/*MET* signal pathways may play vital roles in NIS expression and radioiodide uptake by inhibition of *mi*R-146b-3p expression to induce redifferentiation of dedifferentiated thyroid cancer cells.

DISCUSSION

Radioiodine refractoriness is primarily related to the NIS expression of the thyroid cancer cells. For RAIR-DTC, it is mainly due to a decrease in the level of NIS expression or the appearance of heterotopic expression outside the basement membrane of the thyroid cancer cells. This makes the treatment of ^{131}I ineffective, which causes disease progression. The NIS is a membrane glycoprotein that can transport two sodium ions and one iodide ion into the cytosol *via* extracellular fluid (8, 13). Since radioiodine also can be taken up by the NIS, radioiodine can be used to visualize or selectively kill DTC cells. To upregulate the expression of NIS, restoration or improvement of the treatment of ^{131}I is an important measure for clinical RAIR-DTC patients.

Recently, an in-depth study of miRNAs showed that miRNAs can function as tumor suppressor genes or oncogenes, which are closely related to the formation and development of thyroid cancer and has become a topic of research interest in the field of cancer (14–16). Some miRNAs have been found to participate in the regulation of tumor radiosensitivity by regulating the expression of target genes and vital signaling pathways (17, 18). In our study, we sequenced and analyzed the pathological specimens of RAIR-DTC patients, pathogenic *miR-146b-3p* was selected as the key research objective. And through the bioinformatics analysis, the expression of miR-146b-3p target MUC20 were explored. Whether it is involved in dedifferentiation of DTC is largely unknown.

Recent studies have shown that miR-146b is related to the occurrence, development, proliferation, invasion, and metastasis of thyroid cancer (19–21). Several reports have confirmed *miR-146b* to be highly expressed in patients with a

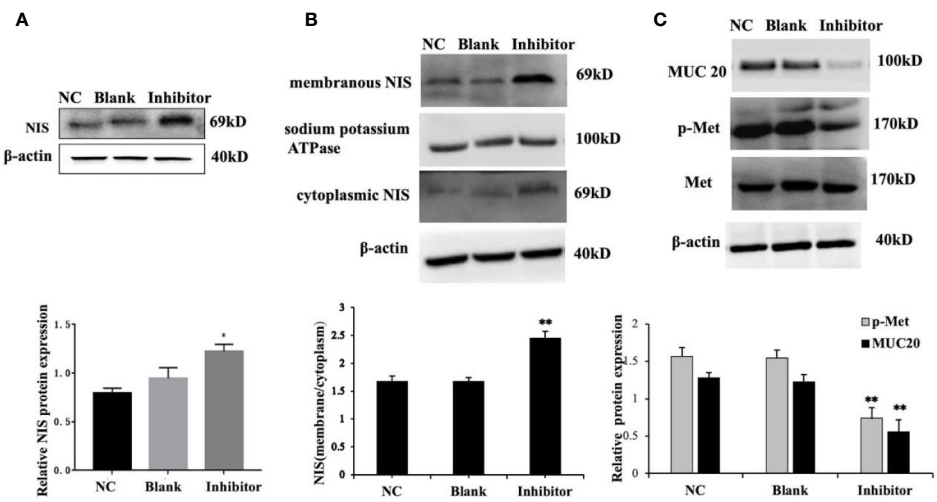

FIGURE 7 | *miR-146b-3p*/*MUC20*/*MET* signaling pathway modulates the sodium/iodide symporter (NIS)-mediated radioiodide uptake in dedifferentiated thyroid cancer cells. **(A, B)** The expressions of NIS protein in total, cytomembrane and cytoplasm in WRO cells with *Anti-miR-146b-3*p in time course experiments were determined by western blot analysis with quantification. The results showed that the level of NIS protein expression in the miR-146b-3p inhibitor-transfected cells were notably increased compared to that of the control groups (*p < 0.05; **p < 0.01). **(C)** The expression of MUC20, MET, p-MET were inhibited by *Anti-miR-146b-3*p and was related to MET Signaling pathways.

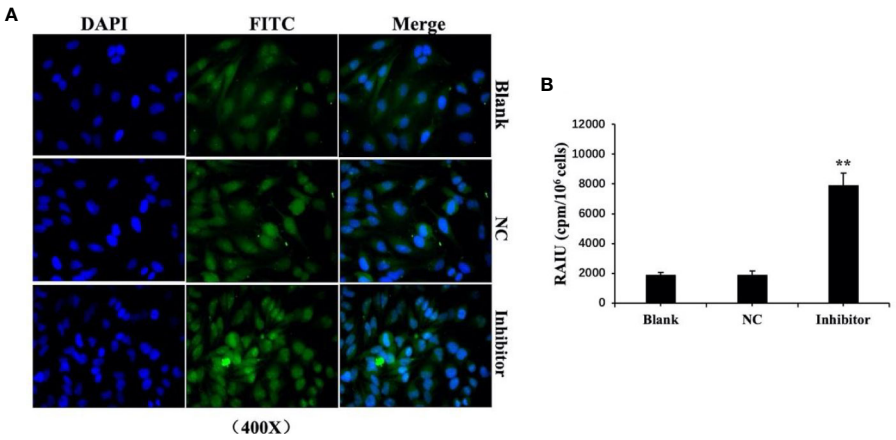

FIGURE 8 | Anti-miR-146b-3p upregulated the expression and translocation of sodium/iodide symporter (NIS)-mediated radioiodide uptake in dedifferentiated thyroid cancer cells. **(A)** Effect of anti-miR-146b-3p on NIS protein translocation by immunofluorescence. The results showed that anti-miR-146b-3p increased both cytoplasmic and cytomembrane-located NIS expression, the latter of which being more significant. **(B)** Radioactive iodine (RAIU) uptake in WRO cells was determined. The results showed that anti-miR-146b-3p increased the radioactive iodine uptake (**p < 0.01).

high risk of BRAF V600E mutations and advanced PTC (P = 0.001), suggesting that miR-146b is a marker of recurrence or metastasis in PTC patients (20). Riesco-Eizaguirre et al (22). reported that miR-146b-3p could directly bind to the 3'-UTR of the iodine metabolism-related proteins, PAX8, and NIS, resulting in decreased NIS expression and iodine uptake. In our study, we first confirmed that *miR-146b-3p* was highly expressed in WRO cells and positively correlated with the degree of DTC malignancy, which could lead to decrease NIS protein expression. We further investigated the biological function of *miR-146b-3p* in a WRO model for tumor progression and metastasis. Combined with the results of MTS, flow cytometry, colony-forming, wound-healing and transwell assays, we inferred that *anti-miR-146b-3p* had a significant inhibitory effect on tumor growth, invasion, migration, and induction of apoptosis in dedifferentiated thyroid cancer cells. Furthermore, the western blot results combined with immunofluorescence and Radioactive iodine uptake, inferred that *anti-miR-146b-3p* could increase NIS-induced iodide uptake by upregulating the expression and trafficking of NIS to the cell surface of WRO cells. Similar results were observed in previous studies (19, 22, 23). Therefore, *miR-146b-3p* may play an important role in the process of DTC dedifferentiation and represent a potential target for the treatment of RAIR-DTC.

MUC is primarily encoded by its polypeptide gene (*MUC* gene), a high molecular weight glycoprotein produced by epithelial cells, which lubricates and protects the mucosa (24). At present, more than 20 kinds of MUC have been reported, mainly including the MUC1-20 subtype. Recent studies have shown that different subtypes of MUC play an important role in the occurrence and development of various cancers (25). MUC20 is over-expressed in many cancers, and has been shown to regulate cell growth, differentiation, metastasis, adhesion, and invasive immune surveillance. MUC20 is also an independent prognostic factor for the poor survival rate of malignant tumors (26, 27). In thyroid cancer, studies have found that MUC1, MUC4, and MU15 are overexpressed in PTC. MUC1 overexpression has been studied as a key molecular event in the pathogenesis of invasive PTC. For PTC patients with a BRAF V600E mutation, MUC1 is an important oncogene that could be used as a prognostic indicator (28). The study by Nam et al. found that elderly, multifocal PTC patients with distant metastasis were often accompanied by the overexpression of MUC15 (29). MUC15 could be used as a prognostic marker and represent a potential new therapeutic target for PTC and marker for evaluating prognosis. At present, there have been no reports regarding MUC20 in dedifferentiated thyroid cancer. Our findings reveal that *MUC20* is prone to mutation in the group for which radioiodine therapy was ineffective. Moreover, *MUC20* exhibited significantly high expression in dedifferentiated thyroid cancer cells. Therefore, MUC20 may be related to the formation of DTC dedifferentiation.

To further explore and study the mechanism of resistance to treatment with ^{131}I and DTC dedifferentiation, we performed a pathway analysis and found that miR-146b-3p/*MUC20* participated in the pathways, "negative regulation of MET activity", and "MET activates RAS signaling". The MET pathway is insensitive to targeted drugs (e.g., BRAF or MEK inhibitors) in refractory thyroid cancer, which can cause a BRAFV600E mutation by activating the downstream PI3K/Akt pathway (30, 31). Other studies have shown that combined treatment with MET and MAPK pathway inhibitors can effectively inhibit the proliferation and differentiation of thyroid cancer cells (32). Our results suggested that MUC*20*, MET, and phosphorylation of MET (p-MET) significantly inhibited after inhibiting the *miR-146b-3p* (**Figure 7C**). Moreover, inhibition of *miR-146b-3p*

expression could improve NIS-mediated radioiodide uptake ability compared to the control groups (**Figure 8B**). Therefore, it indicated that *miR-146b-3p/MUC20/MET* pathways may play important role in NIS expression and radioiodide uptake by inhibition of *mi*R-146b-3p expression to induce redifferentiation of dedifferentiated thyroid cancer cells. These studies indicate that the *miR-146b-3p/MUC20/MET pat*hway may be related to the occurrence and development of dedifferentiation of thyroid cancer. Thus, inhibiting MET pathway may become a new strategy for the treatment of dedifferentiation of thyroid cancer. Consequently, we suspect that the *miR-146b-3p*/*MUC20*/MET signaling pathway the targeting relationship of might play a role in the redifferentiation of iodine-refractory thyroid cancer.

In our study, we assessed the therapeutic potential of *miR-146b-3p* small-molecule inhibitor (*anti-miR-146b-3p*) for RAIR-DTC using WRO cell lines. WRO is the same as WRO82-1, and some websites stated that WRO and WRO82-1 are the same line (https://www.wikidata.org/wiki/Q54994417, https://web.expasy.org/cellosaurus/CVCL_0582). therefore, WRO cell line were selected based on Shang and Ashley N Reeb studies (11, 12), which showed that the expression of NIS and the radioiodine uptake capacity of thyroid cancer cells in WRO were reduced.

Overall, our study synthesized relevant findings, and demonstrated that *miR-146b-3p* was related to the formation of DTC dedifferentiation, resulting in decreased NIS expression and iodine uptake. Combined with a bioinformatics analysis, we put forth the following reasonable hypothesis: the regulation of the MET pathway by *miR-146b-3p* likely targets *MUC20*, which participates in the formation of DTC dedifferentiation. This results in resistance to ^{131}I and loss of the ability for DTC cancer foci to uptake iodine, becoming refractory differentiated thyroid cancer.

The following factors make the results of this study significant: 1) due to the difficulties associated with AIR-DTC, we analyzed and screened the pathological tissue samples of RAIR-DTC patients, verified the biological function of the target gene *in vitro*, and predicted related pathways that might represent potential biomarkers of refractory thyroid cancer; 2) the *miR-146b-3p*/*MUC20*/MET signaling pathway provided a novel targets for the clinical treatment of RAIR-DTC, and the possibility of its further application in radioactive therapy of dedifferentiated thyroid-derived tumors was explored; 3) we demonstrated the possibility that *miR-146b-3p* and *MUC20* were likely oncogenes of refractory thyroid cancer, two novel biological markers for screening refractory thyroid cancer, and potential drug targets for gene therapy. Therefore, these results have important clinical significance and provide possible avenues for clinical transformation.

However, there are also some limitations associated with the present study, including the small clinical sample size. Clinical samples were difficult to obtain as a result of the long interval between the determination of clinical effectiveness of radioiodine therapy and surgical excision. The associated timing can take at least six months or even longer than one year, and there is a relatively small number of ineffective patients. We collected samples throughout the past three years, excluding those with severe nucleic acid degradation, unclear therapeutic effects, lost to follow-up, and exhibiting non-lung metastasis. Only three suitable samples were screened out in the experimental group. To further clarify and verify the associated mechanism, the targeting relationship of *miR-146b-3p*/*MUC20*/MET signaling pathway should be further validated. In addition, the role and mechanism of the targets in this pathway should be studied in-depth in the context of redifferentiation of iodine-refractory thyroid cancer.

CONCLUSION

In conclusion, our present findings show that *anti-miR-146b-3p* could restore radioiodine uptake in dedifferentiated thyroid cancer by up-regulating NIS expression and translocation to the cell membrane *in vitro* by targeting MUC20 through MET Signaling pathways. This provides valuable evidence that *anti-miR-146b-3p* may represent a promising anticancer drug for the treatment of dedifferentiated thyroid cancers.

DATA AVAILABILITY STATEMENT

The original contributions presented in the study are publicly available. This data can be found here: https://www.ncbi.nlm.nih.gov/Traces/study/?acc=PRJNA683915.

ETHIC STATEMENT

The studies involving human participants were reviewed and approved by The Ethical Committee of Tianjin Medical University General Hospital. The patients/participants provided their written informed consent to participate in this study.

AUTHOR CONTRIBUTIONS

JT, CC, and SH designed the project. SH, XX, and JZ consulted literature, collected human tissues, and performed the cell experiments. SH wrote the main manuscripts.SH and CW analyzed data. NL conducted bioinformatics analysis. ZM supervised experiments. All authors contributed to the article and approved the submitted version.

FUNDING

This investigation was supported by the Program of Tianjin Science and Technology Plan 18ZXDBSY00170 (awarded to CC).

REFERENCES

1. Siegel R, Miller K, Jemal A. Cancer Statistics. 2019. *CA Cancer J Clin* (2019) 69 (1):7–34. doi: 10.3322/caac.21551
2. Clerc J, Verburg FA, Avram AM, Giovanella L, Hindié E, Taïeb D, et al. Radioiodine treatment after surgery for differentiated thyroid cancer: a reasonable option. *Eur J Nuclear Med Mol Imaging* (2017) 44(6):918–25. doi: 10.1007/s00259-017-3654-z
3. Wang R, Zhang Y, Tan J, Zhang G, Zhang R, Zheng W, et al. Analysis of radioiodine therapy and prognostic factors of differentiated thyroid cancer patients with pulmonary metastasis: An 8-year retrospective study. *Medicine* (2017) 96(19):e6809. doi: 10.1097/MD.0000000000006809
4. Cabanillas ME, McFadden DG, Durante C. Thyroid cancer. *Lancet* (2016) 388 (10061):2783–95. doi: 10.1016/S0140-6736(16)30172-6
5. Feng F, Wang H, Hou S, Fu H. Re-induction of cell differentiation and (131)I uptake in dedifferentiated FTC-133 cell line by TSHR gene transfection. *Nuclear Med Biol* (2012) 39(8):1261–5. doi: 10.1016/j.nucmedbio.2012.07.004
6. Mendes CS, De CDP, Vaisman M. New perspectives on the treatment of differentiated thyroid cancer. *Arquivos Brasileiros Endocrinol Metabol* (2007) 51(4):612–24. doi: 10.1590/S0004-27302007000400017
7. Cheng L, Jin Y, Liu M, Ruan M, Chen L. HER inhibitor promotes BRAF/MEK inhibitor-induced redifferentiation in papillary thyroid cancer harboring BRAFV600E. *Oncotarget* (2017) 8(12):19843–54. doi: 10.18632/oncotarget.15773
8. Moon HC, Byeong-Cheol A. Redifferentiation of Radioiodine Refractory Differentiated Thyroid Cancer for Reapplication of I-131 Therapy. *Front Endocrinol* (2017) 8:260. doi: 10.3389/fendo.2017.00260
9. Larson SM, Osborne JR, Grewal RK, Tuttle RM. Redifferentiating Thyroid Cancer: Selumetinib-enhanced Radioiodine Uptake in Thyroid Cancer. *Mol Imaging Radionuclide Ther* (2017) 26(Suppl 1):80–6. doi: 10.4274/2017.26.suppl.09
10. Tesselaar MH, Smit JW, Nagarajah J, Netea-Maier RT, Plantinga TS. Pathological processes and therapeutic advances in radioiodide refractory thyroid cancer. *J Mol Endocrinol* (2017) 59(4):R141–54. doi: 10.1530/JME-17-0134
11. Shang HX, Zhao JY, Yao JM, Wang HJ, Domg JJ, Liao L. Nevirapine Increases Sodium/Iodide Symporter-Mediated Radioiodide Uptake by Activation of TSHR/cAMP/CREB/PAX8 Signaling Pathway in Dedifferentiated Thyroid Cancer. *Front Oncol* (2020) 10:404. doi: 10.3389/fonc.2020.00404
12. Reeb AN, Ziegler A, Lin R-Y. Characterization of human follicular thyroid cancer cell lines in preclinical mouse models. *Endocrine Connections* (2016) 5:41–54. doi: 10.1530/EC-15-0114
13. Ahn BC. Sodium iodide symporter for nuclear molecular imaging and gene therapy: from bedside to bench and back. *Theranostics* (2012) 2(4):392–402. doi: 10.7150/thno.3722
14. Shen CT, Qiu ZL, Song HJ, Wei WJ, Luo QY. miRNA-106a directly targeting RARB associates with the expression of Na(+)/I(-) symporter in thyroid cancer by regulating MAPK signaling pathway. *J Exp Clin Cancer Res* (2016) 35(1):101. doi: 10.1186/s13046-016-0377-0
15. Ortiz IMDP, Barros-Filho MC, Dos Reis MB, Beltrami CM, Marchi FA, Kuasne H, et al. Loss of DNA methylation is related to increased expression of miR-21 and miR-146b in papillary thyroid carcinoma. *Clin Epigenet* (2018) 10 (1):144. doi: 10.1186/s13148-018-0579-8
16. Chou CK, Liu RT, Kang HY. MicroRNA-146b: A Novel Biomarker and Therapeutic Target for Human Papillary Thyroid Cancer. *Int J Mol Sci* (2017) 18:636. doi: 10.3390/ijms18030636
17. Nikiforova MN, Gandhi M, Gandi M, Kelly L, Nikiforov YE. MicroRNA dysregulation in human thyroid cells following exposure to ionizing radiation. *Thyroid* (2011) 21(3):261–6. doi: 10.1089/thy.2010.0376
18. Penha RCC, Pellecchia S, Pacelli R, Pinto LFR, Fusco A. Ionizing Radiation Deregulates the MicroRNA Expression Profile in Differentiated Thyroid Cells. *Thyroid* (2018) 28(3):407–21. doi: 10.1089/thy.2017.0458
19. Yu C, Zhang L, Luo D, Yan F, Liu J, Shao S, et al. MicroRNA-146b-3p promotes cell metastasis by directly targeting NF2 in human papillary thyroid cancer. *Thyroid* (2018) 28(12):1627–41. doi: 10.1089/thy.2017.0626
20. Chou C, Chen R, Chou F, Chang H, Chen Y, Lee Y, et al. miR-146b is Highly Expressed in Adult Papillary Thyroid Carcinomas with High Risk Features Including Extrathyroidal Invasion and the BRAF V600E Mutation. *Thyroid* (2010) 20(5):489–94. doi: 10.1089/thy.2009.0027
21. Pan Y, Yun W, Shi B, Cui R, Liu C, Ding Z, et al. Downregulation of miR-146b-5p via iodine involvement repressed papillary thyroid carcinoma cell proliferation. *J Mol Endocrinol* (2020) 65(2):1–10. doi: 10.1530/JME-19-0198
22. Riesco-Eizaguirre G, Wert-Lamas L, Perales-Patón J, Sastre-Perona A, Fernández LP, Santisteban P. The miR-146b-3p/PAX8/NIS regulatory circuit modulates the differentiation phenotype and function of thyroid cells during carcinogenesis. *Cancer Res* (2015) 75(19):4119–30. doi: 10.1158/0008-5472.CAN-14-3547
23. Wächter S, Wunderlich A, Greene BH, Roth S, Elxnat M, Fellinger SA, et al. Selumetinib Activity in Thyroid Cancer Cells: Modulation of Sodium Iodide Symporter and Associated miRNAs. *Int J Mol Sci* (2018) 19(7):pii: E2077. doi: 10.3390/ijms19072077
24. Corfield AP. Mucins: a biologically relevant glycan barrier in mucosal protection. *Biochim Biophys Acta (BBA)-General Subj* (2015) 1850(1):236–52. doi: 10.1016/j.bbagen.2014.05.003
25. Bhatia R, Gautam S, Cannon A, Thompson C, Hall B, Aithal A, et al. Cancer-associated mucins: role in immune modulation and metastasis. *Cancer Metastasis Rev* (2019) 38(1–2):223–36. doi: 10.1007/s10555-018-09775-0
26. Chen ST, Kuo TC, Liao YY, Lin MC, Tien YW, Huang MC. Silencing of MUC20 suppresses the malignant character of pancreatic ductal adenocarcinoma cells through inhibition of the HGF/MET pathway. *Oncogene* (2018) 37(46):6041–53. doi: 10.1038/s41388-018-0403-0
27. Chen C, Wang S, Chen C, Huang M, Hung J, Huang H, et al. MUC20 overexpression predicts poor prognosis and enhances EGF-induced malignant phenotypes via activation of the EGFR–STAT3 pathway in endometrial cancer. *Gynecol Oncol* (2013) 128(3):560–7. doi: 10.1016/j.ygyno.2012.12.012
28. Li Q, Jin W, Jin Y, Zheng Z, Zhou X, Wang Q, et al. Clinical effect of MUC1 and its relevance to BRAF V600E mutation in papillary thyroid carcinoma: a case–control study. *Cancer Manage Res* (2018) 10:1351–8. doi: 10.2147/CMAR.S161501
29. Nam KH, Noh TW, Chung SH, Lee SH, Lee MK, Hong SW, et al. Expression of the membrane mucins MUC4 and MUC15, potential markers of malignancy and prognosis, in papillary thyroid carcinoma. *Thyroid* (2011) 21(7):745–50. doi: 10.1089/thy.2010.0339
30. Byeon HK, Na HJ, Yang YJ, Kwon HJ, Chang JW, Ban MJ, et al. c-Met-mediated reactivation of PI3K/AKT signaling contributes to insensitivity of BRAF(V600E) mutant thyroid cancer to BRAF inhibition. *Mol Carcinog* (2016) 55(11):1678–87. doi: 10.1002/mc.22418
31. Hayes DN, Lucas AS, Tanvetyanon T, Krzyzanowska MK, Chung CH, Murphy BA, et al. Phase II efficacy and pharmacogenomic study of Selumetinib (AZD6244; ARRY-142886) in iodine-131 refractory papillary thyroid carcinoma with or without follicular elements. *Clin Cancer Res* (2012) 18(7):2056–65. doi: 10.1158/1078-0432.CCR-11-0563
32. Barollo S, Bertazza L, Baldini E, Ulisse S, Cavedon E, Boscaro M, et al. The combination of RAF265, SB590885, ZSTK474 on thyroid cancer cell Lines deeply impact on proliferation and MET and PI3K/Akt signaling pathways. *Invest New Drugs* (2014) 32(4):626–35. doi: 10.1007/s10637-014-0108-3

Conflict of Interest: The authors declare that the research was conducted in the absence of any commercial or financial relationships that could be construed as a potential conflict of interest.

Copyright © 2021 Hou, Xie, Zhao, Wu, Li, Meng, Cai and Tan. This is an open-access article distributed under the terms of the Creative Commons Attribution License (CC BY). The use, distribution or reproduction in other forums is permitted, provided the original author(s) and the copyright owner(s) are credited and that the original publication in this journal is cited, in accordance with accepted academic practice. No use, distribution or reproduction is permitted which does not comply with these terms.

frontiers in Oncology

REVIEW
published: 15 January 2021
doi: 10.3389/fonc.2020.616717

Long Noncoding RNAs in the Metastasis of Oral Squamous Cell Carcinoma

Yuming Xu, Erhui Jiang, Zhe Shao and Zhengjun Shang**

The State Key Laboratory Breeding Base of Basic Science of Stomatology (Hubei-MOST) & Key Laboratory of Oral Biomedicine Ministry of Education, School & Hospital of Stomatology, Wuhan University, Wuhan, China

Oral squamous cell carcinoma (OSCC) is a common malignant tumor worldwide. Metastasis is the main cause of the death of OSCC patients. Long noncoding RNAs (lncRNAs), one of the key factors affecting OSCC metastasis, are a subtype of RNA with a length of more than 200 nucleotides that has little or no coding potential. In recent years, the important role played by lncRNAs in biological processes, such as chromatin modification, transcription regulation, RNA stability regulation, and mRNA translation, has been gradually revealed. More and more studies have shown that lncRNAs can regulate the metastasis of various tumors including OSCC at epigenetic, transcriptional, and post-transcriptional levels. In this review, we mainly discussed the role and possible mechanisms of lncRNAs in OSCC metastasis. Most lncRNAs act as oncogenes and only a few lncRNAs have been shown to inhibit OSCC metastasis. Besides, we briefly introduced the research status of cancer-associated fibroblasts-related lncRNAs in OSCC metastasis. Finally, we discussed the research prospects of lncRNAs-mediated crosstalk between OSCC cells and the tumor microenvironment in OSCC metastasis, especially the potential research value of exosomes and lymphangiogenesis. In general, lncRNAs are expected to be used for screening, treatment, and prognosis monitoring of OSCC metastasis, but more work is still required to better understand the biological function of lncRNAs.

Keywords: lncRNAs, cancer-associated fibroblasts, exosomes, oral squamous cell carcinoma, tumor microenvironment, metastasis

OPEN ACCESS

Edited by:
Wei Cao,
Shanghai Jiao Tong University, China

Reviewed by:
Yanjie Zhang,
Shanghai Jiao Tong University, China
Xuan Zhou,
Tianjin Medical University Cancer Institute and Hospital, China

****Correspondence:***
Zhe Shao
shaozhe@whu.edu.cn
Zhengjun Shang
shangzhengjun@whu.edu.cn

Specialty section:
This article was submitted to Head and Neck Cancer, a section of the journal Frontiers in Oncology

Received: *13 October 2020*
Accepted: *26 November 2020*
Published: *15 January 2021*

Citation:
Xu Y, Jiang E, Shao Z and Shang Z (2021) Long Noncoding RNAs in the Metastasis of Oral Squamous Cell Carcinoma. Front. Oncol. 10:616717. doi: 10.3389/fonc.2020.616717

INTRODUCTION

Oral squamous cell carcinoma (OSCC) is the most common type of head and neck squamous cell carcinoma (HNSCC) which ranks sixth among cancers worldwide (1). The initiation and progression of OSCC are the results of the combined action of various factors, and tobacco, alcohol, and human papillomavirus (HPV) infection are considered as the main causes of OSCC (2). Surgical resection is an effective method to treat OSCC, and the surgical cure rate of patients with early-stage OSCC can reach more than 80% (3). However, the overall prognosis of patients with OSCC is poor, with a 5-year survival rate of only about 60% (4, 5). Metastasis is the major factor leading to the low survival rate of OSCC patients, and the 5-year survival rate of OSCC patients with metastasis is only about 40% (5). Notably,

about 40% of OSCC patients may have metastasis (5). In addition, for non-metastatic patients, local resection of the primary tumor can achieve an ideal therapeutic effect, while metastatic patients generally need neck lymph node dissection, which not only increases the risk of surgery but also often causes postoperative dysfunction and maxillofacial deformities (6, 7). Whereas, it is still difficult to accurately determine whether OSCC patients have metastasis before surgery, which may lead to over-medical treatment (performing neck dissection for patients without lymph node metastasis) or insufficient treatment (patients with lymph node metastasis did not undergo neck dissection). Therefore, finding effective methods to screen, block, and treat OSCC metastasis is a top priority in OSCC research.

The metastasis of OSCC has two characteristics (5, 8): on the one hand, the metastasis rate of OSCC occurring in diverse anatomical parts is different, which is about 40% in the buccal and soft palate, but less than 30% in the tongue and floor of mouth; on the other hand, OSCC metastasis mainly manifests as regional cervical lymph node metastasis, distant metastasis is rare. Although the mechanisms behind this phenomenon are still unclear, current research indicated that enhanced migration and invasion ability of tumor cells (9) and lymphangiogenesis (10) may be critical factors that promote OSCC metastasis. Todorović et al. found that the expression levels of plakoglobin and desmoglein 2 (both are involved in maintaining intercellular adhesion) in squamous carcinoma cells derived from the top of the oral cavity are significantly lower than those in squamous carcinoma cells derived from the tongue, which is helpful for the migration and invasion of cells, and may be used to explain why the metastasis rate of OSCC in the soft palate is higher than that in the tongue (9). By analyzing the lymphatic vessel density in paraffin-embedded OSCC tissues, Sasahira et al. discovered that high lymphatic vessel density is closely related to lymph node metastasis and poor prognosis, which suggests that lymphangiogenesis may play a key role in the metastasis of OSCC (10). Unfortunately, scholars still have a limited understanding of the mechanisms of OSCC migration, invasion, and lymphangiogenesis, and have yet to find effective biomarkers.

Long noncoding RNAs (lncRNAs) are a subtype of RNA with a length of more than 200 nucleotides that has little or no coding potential (11). There are large amounts of lncRNAs in human cells that 68% of the human genome transcripts can be classified as lncRNAs (12). The expression of lncRNAs has certain tissue specificity (13), which suggests that they may play an important role in the biological processes of cells. Studies have confirmed that lncRNAs can interact with biological macromolecules including chromatin, protein, and RNA (14). In addition, many lncRNAs have been found to be abnormally expressed in various cancers, such as liver cancer (15), breast cancer (16), bladder cancer (17), and colorectal cancer (18), and regulate tumor cell metastasis through different mechanisms. In studies related to OSCC, lncRNAs were elucidated to be involved in tumor initiation (19) and prognosis (20). Furthermore, lncRNAs, such as MALAT1 (metastasis associated lung adenocarcinoma transcript 1) (21), UCA1 (urothelial cancer-associated 1) (22), AFAP1-AS1 (actin filament associated protein 1 antisense RNA 1) (23) and MEG3 (maternally expressed gene 3) (24) have been shown to participate in the regulation of OSCC migration, invasion, and metastasis. These studies have demonstrated the potential of lncRNAs for screening, treatment, and prognostic monitoring of OSCC metastasis. Therefore, in this paper, we review the role and possible mechanisms of lncRNAs in OSCC metastasis. In particular, we introduced the research status of cancer-associated fibroblasts-related lncRNAs in OSCC metastasis and discussed the research prospects of lncRNAs-mediated crosstalk between OSCC cells and the tumor microenvironment in OSCC metastasis, especially the potential research value of exosomes and lymphangiogenesis, aiming to provide innovative ideas for research related to OSCC metastasis.

THE ROLE OF LncRNAs IN CANCER METASTASIS

Studies have shown that lncRNAs can affect tumor metastasis by regulating a variety of biological processes, such as chromatin modification (18), transcription activation (18, 25), transcription interference (26), RNA stability regulation (15), and mRNA translation (16), etc. Xu et al. found that lncRNA SATB2-AS1 (antisense transcript of special AT-rich binding protein 2) is lowly expressed in colorectal cancer (CRC) tissues. Further research showed that SATB2-AS1 could directly bind to WDR5 (WD repeat domain 5) and GADD45A (growth arrest and DNA damage-inducible alpha), and then activate SATB2 transcription by mediating the tri-methylation of lysine 4 on histone 3 (H3K4me3) and the DNA demethylation of the promoter region of SATB2, thus inhibiting the migration, invasion, and metastasis of CRC (18). In contrast, lncRNA CF129 (CF129145.1) was confirmed to inhibit the invasion and metastasis of pancreatic cancer cells by interfering with the transcription of FOXC2 (forkhead box protein C2) (26). Intriguingly, lncRNA BLACAT2 (bladder cancer-associated transcript 2) is also able to bind directly to WDR5, but it promotes lymphangiogenesis and lymphatic metastasis of bladder cancer by enhancing the expression of VEGF-C (vascular endothelial growth factor C) (17). Additionally, He et al. reported the inhibitory effect of long intergenic noncoding RNA 1093 (LINC01093) on the migration, invasion, and metastasis of liver cancer cells. Mechanistically, by directly binding to IGF2BP1 (insulin-like growth factor 2 mRNA-binding protein 1), LINC01093 could interfere with the interaction between IGF2BP1 and GLI1 (glioma-associated oncogene homolog 1) mRNA, thus leading to the degradation of GLI1 mRNA, which further affects the expression of GLI1 downstream genes involved in the development of liver cancer (15). In addition, in breast cancer, lncRNA RP1 (RP1-5O6.5) was demonstrated to promote the invasion and metastasis of tumor cells through inhibiting the translation of p27kip1 mRNA (16).

Notably, lncRNAs can function as competitive endogenous RNAs (ceRNAs) to sponge miRNAs, blocking their regulation on the expression of their downstream genes, and then inducing various biological effects (27). Moreover, functioning as ceRNAs is also an important mechanism by which lncRNAs regulate

tumor metastasis. For example, *via* competitively binding to miR-16-5p, lncRNA AGAP2-AS1 (AGAP2 antisense RNA 1) could weaken the inhibitory effect of miR-16-5p on annexin A11, thereby promoting the migration and invasion of liver cancer cells by enhancing the activation of AKT (protein kinase B) signal pathway (28). Similarly, lncRNA JPX (just proximal to Xist) was indicated to directly target miR-33a-5p, thus upregulating the expression of its downstream gene Twist1, which in turn promotes the metastasis of lung cancer cells through activating the Wnt/β-catenin signaling pathway (29).

In general, metastasis is a common feature in the development of many tumors, and the mechanisms of metastasis in different tumors are similar to some extent (30). Therefore, lncRNAs may also regulate the migration, invasion, and lymphangiogenesis of OSCC *via* (but not limited to) the above mechanisms, thereby inhibiting or promoting the metastasis of OSCC (**Table 1**).

OVERVIEW OF LncRNAs INVOLVED IN OSCC METASTASIS

LncRNAs Regulate Metastasis by Inducing EMT

Epithelial-mesenchymal transition (EMT) is a process of epithelial phenotype cells differentiating into mesenchymal phenotype cells. In this process, epithelial cells lose polarity and intercellular adhesion and instead acquire the characteristics of migration and invasion (75). Furthermore, the expression levels of some EMT markers will also change significantly during this process, mainly manifested by the decreased expression of E-cadherin (76) and Claudin1 (77), as well as the increased expression of β-catenin (78), Snail (79) and Vimentin (76), etc. Studies have shown that some lncRNAs regulate the metastasis of OSCC by inducing or inhibiting the EMT process. HOX transcript antisense intergenic RNA (HOTAIR) is a typical example of carcinogenic lncRNAs, which has been found to play a key role in the metastasis of various tumors. For example, in gastric cancer, HOTAIR, functioning as a connecting scaffold, could facilitate the ubiquitination and degradation of Runx3 (runt-related transcription factor 3) by enhancing the interaction between E3 ubiquitin ligase Mex3b (mex-3 RNA binding family member B) and Runx3, thus inhibiting the expression of E-cadherin and Claudin1, and ultimately promoting the migration and invasion of gastric cancer (80). Specifically, HOTAIR has also been shown to be involved in the regulation of OSCC metastasis. Lu et al. revealed that HOTAIR is highly expressed in OSCC tissues, especially in tissues with metastasis. Subsequent studies showed that overexpression of HOTAIR could enhance the metastatic potential of OSCC cells and the expression of EMT markers such as Vimentin, Snail, and Twist. It is worth noting that in clinical samples, HOTAIR is positively correlated with the expression of mesenchymal markers (Snail, Vimentin) and negatively correlated with the expression of epithelial marker (E-cadherin) (41). Additionally, Wu et al.'s research also yielded similar results. Their data indicated that HOTAIR overexpression is closely related to OSCC metastasis. Moreover, the overexpression of HOTAIR points to lower overall survival and disease-free survival. Mechanistically, HOTAIR is able to recruit histone lysine methyltransferase EZH2 (enhancer of zeste homolog 2) to the promoter region of E-cadherin and then promote H3K27me3 (tri-methylation of lysine 27 on histone 3), thus downregulating the expression of E-cadherin. These data suggest that HOTAIR may regulate the metastasis of OSCC cells by promoting their EMT (42).

In addition to HOTAIR, lncRNA SNHG16 (small nucleolar RNA host gene 16) is also overexpressed in OSCC tissues and can promote the migration and invasion of OSCC cells. Mechanism studies showed that silencing SNHG16 will increase the expression of E-cadherin, and also downregulate the expression of N-cadherin and Snail (58). Interestingly, another lncRNA of the SNHG family, SNHG6 (small nucleolar RNA host gene 6), has also been confirmed to be highly expressed in OSCC tissues, and the expression level of SNHG6 is closely related to lymph node metastasis. Meanwhile, the knockdown of SNHG6 could induce the expression of E-cadherin and inhibit the expression of N-cadherin and Vimentin (59). HNF1A-AS1 (HNF1A antisense RNA 1) is another lncRNA that is highly expressed in OSCC tissues and can promote tumor cell migration and EMT. Mechanistically, HNF1A-AS1 exerts its pro-metastatic effect by activating the Notch signaling pathway (63). In highly metastatic OSCC cells, Li et al. found that the expression of lncRNA AC132217.4 is significantly upregulated. Not only that, but AC132217.4 could also promote the migration and EMT of OSCC cells and accelerate its metastasis. The mechanism is that AC132217.4 interacts with the 3'UTR (3'untranslated region) of IGF2 (insulin-like growth factor 2) mRNA and enhances its stability, thereby enhancing the expression level of IGF2 (61). In another experiment, LINC00460 (long intergenic noncoding RNA 460) was also observed to be highly expressed in OSCC tissues and cells, and its expression level is positively correlated with lymph node metastasis. Further research exhibited the promotion of LINC00460 on the migration, invasion, EMT, and metastasis of OSCC cells. Mechanism research confirmed that there is a direct interaction between LINC00460 and PRDX1 (peroxiredoxin 1) protein, which could facilitate PRDX1 to enter the nucleus. Subsequently, PRDX1 will be enriched in the promoter regions of EMT-related genes, such as ZEB1 (zinc finger E box binding homeobox 1), ZEB2 (zinc finger E box binding homeobox 2), and Vimentin, and plays a role in promoting transcription (62). In a nutshell, EMT is a key driving factor for OSCC metastasis, and lncRNAs also play an important role in the EMT of OSCC cells. However, more research is still needed to better understand the mechanisms by which lncRNAs regulate the EMT of OSCC cells.

LncRNAs Regulate Metastasis Through the Wnt/β-Catenin Signaling Pathway

Wnt/β-catenin signaling pathway is one of the key pathways regulating tumor development. To date, activation of the Wnt/β-catenin signaling pathway has been proved to contribute to the

TABLE 1 | Regulatory roles of long noncoding RNAs (lncRNAs) in the metastasis-related biological processes of oral squamous cell carcinoma (OSCC).

LncRNA	Expression in OSCC	Correlation with tumor metastasis	Functions in OSCC	Potential mechanism	Refs
H19	Overexpressed	Positive	↑Migration, invasion, EMT	CeRNA (let-7a/HMGA2 axis; miR-138/EZH2 axis)	(31, 32)
LINC00152	Overexpressed	Positive	↑Migration, invasion, EMT	CeRNA (miR-139-5p; miRNA-193b-3p/PI3K/AKT axis)	(33, 34)
HOXA11-AS	Overexpressed	–	↑Migration, invasion, EMT	CeRNA (miR-98-5p/YBX2 axis)	(35)
GAS5	Downregulated	–	↓Migration, invasion, EMT	CeRNA (miR-21/PTEN/PI3K/AKT axis)	(36)
MALAT1	Overexpressed	Positive	↑Migration, invasion, EMT	CeRNA (miR-140-5p/PAK1 axis; miR-124/JAG1 axis);	(21, 37)
				AKT pathway;	(38)
				Wnt/β-catenin pathway;	(39)
				NF-κB pathway	(40)
HOTAIR	Overexpressed	Positive	↑Migration, invasion, EMT	CeRNA (miR-326/MTA2 axis);	(41, 42)
				Chromatin modification;	(43)
				SNPs	(44)
MEG3	Downregulated	Negative	↓Migration, invasion	CeRNA (miR-548d-3p/SOCS5-SOCS6/JAK/STAT axis; miR-21);	(45)
				Wnt/β-catenin pathway	(24, 46)
AFAP1-AS1	Overexpressed	–	↑Migration, invasion, EMT	Wnt/β-catenin pathway	(23)
UCA1	Overexpressed	Positive	↑Migration, invasion, EMT	CeRNA (miR-124/TGF-β1/JAG1/Notch axis; miR-143-3p/MYO6 axis);	(47)
				Wnt/β-catenin pathway	(22, 48)
TUG1	Overexpressed	Positive	↑Migration, invasion	CeRNA (miR-524-5p/DLX1 axis; miR-219/FMNL2 axis);	(49)
				Wnt/β-catenin pathway	(50, 51)
CASC15	Overexpressed	–	↑Migration, invasion	CeRNA (miR-33a-5p/ZEB1 axis)	(52)
Lnc-p23154	Overexpressed	Positive	↑Migration, invasion, EMT	CeRNA (miR-378a-3p/Glut1 axis)	(53)
CCAT1	Overexpressed	–	↑Migration, invasion	CeRNA (miR-181a/Wnt/β-catenin axis);	(54)
				AKT pathway	(55)
LINC01116	Overexpressed	Positive	↑Migration, invasion, EMT	CeRNA (miR-136/FN1 axis)	(56)
SNHG17	Overexpressed	Positive	↑Migration, invasion	CeRNA (miR-876/SP1 axis)	(57)
SNHG16	Overexpressed	–	↑Migration, invasion, EMT	–	(58)
SNHG6	Overexpressed	Positive	↑EMT	–	(59)
SNHG3	Overexpressed	–	↑Migration	By recruiting ELAVL1 to stabilize NFYC mRNA	(60)
AC132217.4	Overexpressed	Positive	↑Migration, EMT	By upregulating IGF2	(61)
LINC00460	Overexpressed	Positive	↑Migration, invasion, EMT	By promoting PRDX1 to enter the nucleus	(62)
HNF1A-AS1	Overexpressed	Positive	↑Migration, EMT	Notch pathway	(63)
FTH1P3	Overexpressed	–	↑Migration, invasion	AKT pathway	(64)
MIR31HG	Overexpressed	Positive	↑Migration, invasion	By facilitating the formation of HIF-1 complex	(65)
HAS2-AS1	Overexpressed	Positive	↑Invasion, EMT	By enhancing the expression and stability of HAS2	(66)
HOTTIP	Overexpressed	Positive	↑Migration, invasion, EMT	CeRNA (miR-124-3p/HMGA2/Wnt/β-catenin axis)	(67, 68)
LEF1-AS1	Overexpressed	–	↑Migration	Hippo pathway	(69)
CCAT2	Overexpressed	Positive	↑Migration, invasion	–	(70)
PANDAR	Overexpressed	Positive	↑Migration, invasion	–	(71)
NKILA	Downregulated	–	↓Migration, invasion	NF-κB pathway	(72)
RC3H2	Overexpressed	Positive	↑Migration, invasion	CeRNA (miR-101-3p/EZH2 axis)	(73)
TIRY	Overexpressed	–	↑Migration, invasion, EMT	CeRNA (miR-14/Wnt/β-catenin axis) based on exosomes	(74)

metastasis of lung cancer (81), CRC (82), breast cancer (83), and OSCC (39, 45). Studies have shown that lncRNAs are important factors in regulating the Wnt/β-catenin signaling pathway of OSCC cells. Liu et al. reported that MEG3 is able to inhibit the migration of OSCC cells by weakening the activation of the Wnt/β-catenin pathway (45). On the contrary, MALAT1 induces the migration, invasion, and EMT of tongue squamous cell carcinoma (TSCC) cells by activating the Wnt/β-catenin pathway (39). As another lncRNA that is highly expressed in OSCC tissue, the expression level of AFAP1-AS1 is negatively correlated with overall survival. Further research confirmed that AFAP1-AS1 is capable of promoting the migration and invasion of OSCC by enhancing the activation of the Wnt/β-catenin pathway and the expression of EMT-related genes (23). Yang et al. validated the association between high expression of UCA1 and lymph node metastasis of OSCC. Mechanism research verified that UCA1 could boost the activation of the Wnt/β-catenin pathway, thereby promoting the metastasis of OSCC (47). Similarly, the study by Liang et al. showed that high expression of lncRNA TUG1 (taurine upregulated gene 1) is also significantly associated with lymph node metastasis of OSCC. Furthermore, knocking down TUG1 inhibits the expression of β-catenin and the invasion ability of tumor cells. However, the use of LiCl (lithium chloride), a catalyst of the Wnt/β-catenin pathway, will weaken the inhibitory effect of TUG1 knockdown on the invasion of OSCC. These data suggest that TUG1 may regulate the migration of OSCC through the Wnt/β-catenin pathway (49). Nowadays, specific mechanisms by which lncRNAs regulate the Wnt//β-catenin signaling pathway remains to be explored.

LncRNAs Regulate Metastasis Through the AKT Signaling Pathway

AKT signaling pathway is another pathway that has been widely studied and plays an important role in the metastasis of pancreatic cancer (84), gastric cancer (85), lung cancer (86),

and OSCC (38, 55). In OSCC cells, the AKT signaling pathway is also regulated by various lncRNAs. FTH1P3 (ferritin heavy chain 1 pseudogene 3) is a lncRNA that is significantly overexpressed in OSCC tissues. Knocking down FTH1P3 will inhibit the migration and invasion of OSCC cells. Further investigation showed that silencing FTH1P3 contributes to the inhibition of AKT phosphorylation, which may be the mechanism by which FTH1P3 regulates the progression of OSCC (64). Based on the analysis of the expression level of MALAT1 in tissue samples, Yuan et al. reported that the overall survival of TSCC patients with high expression of MALAT1 is significantly lower than that of patients with low expression of MALAT1. Moreover, knocking down MALAT1 will cause the phosphorylation of AKT in TSCC cells to decrease, and also significantly suppress the migration and invasion of TSCC cells, while the application of PI3K (phosphatidylinositol 3-kinase) activator could reverse the inhibitory effect of MALAT1 knockdown on the migration and invasion of TSCC cells, suggesting that MALAT1 may promote the metastasis of TSCC by activating the PI3K/AKT pathway (38). In another experiment, lncRNA CCAT1 (colon cancer-associated transcript 1) was demonstrated to be overexpressed in OSCC cells and be able to promote their migration and invasion. Further mechanistic studies identified that CCAT1 is capable of improving the expression of DDR2 (discoidin domain receptor 2) and directly interacting with it. Subsequently, DDR2 could activate the ERK (extracellular signal-regulated kinase 1)/AKT signaling pathway, thus promoting the invasion and migration of OSCC cells (55). At present, the regulatory role of lncRNAs on the AKT signaling pathway remains to be further explored.

LncRNAs Regulate Metastasis Through the NF-κB Signaling Pathway

The key role of the NF-κB signaling pathway in tumor metastasis has been proved by several studies (87, 88). Besides, lncRNAs play an important role in the regulation of the NF-κB signaling pathway. For example, Zheng et al. found that the decreased expression of lncRNA KRT19P3 (Keratin 19 Pseudogene 3) is associated with lymph node metastasis of gastric cancer. Mechanistically, KRT19P3 can directly bind COPS7A and then enhance the stability of COPS7A protein, which subsequently promotes the deubiquitinylation of IκBα and then inactivates the NF-κB signaling pathway, thus suppressing tumor metastasis (89). Previous studies have shown that lncRNAs can also regulate the metastasis of OSCC through the NF-κB signaling pathway. Hu et al. showed that lncRNA NKILA (NF-κB interacting lncRNA) is lowly expressed in OSCC tissues and cells, and the overexpression of NKILA could reduce the invasion and migration of tumor cells, as well as the levels of IκBα and cytoplasm-p65, which indicates that NKILA may regulate the metastasis of OSCC through inhibiting the NF-κB signaling pathway (72). In contrast, in another study, MALAT1 knockdown was revealed to significantly suppress the levels of NF-κB and the migration and invasion of OSCC cells (40). However, the mechanism of how lncRNAs regulate OSCC metastasis through the NF-κB signaling pathway is still unclear.

LncRNAs Regulate Metastasis Through the IL-6/STAT3 Signaling Pathway

IL-6/STAT3 is an important signaling pathway related to lncRNAs-caused tumor metastasis. Su et al. reported that lncRNA UICC (upregulated in cervical cancer) is highly expressed in cervical cancer tissues, and its high expression is also related to lymph node metastasis. *In vitro* and *in vivo* experiments showed that UICC could facilitate the expression of IL-6 by combining with its promoter and directly interact with the phospho-STAT3 to improve its protein stability, thus promoting tumor growth and metastasis (90). There have been some studies showing that the IL-6/STAT3 signaling pathway plays an important role in the metastasis of OSCC (91, 92), but there is no research involving the role of lncRNAs in this process.

LncRNAs Regulate Metastasis by Functioning as ceRNAs

MALAT1

MALAT1 is an evolutionarily highly conserved lncRNA, and its mature transcripts are mainly located in the nucleus, which suggests that MALAT1 may play an important role in the biological processes of cells (93). Recent studies have shown that by regulating chromatin modification (94), gene transcription (95), or acting as ceRNAs (96), MALAT1 is involved in the migration, invasion, and metastasis of tumors. Taking transcription regulation as an example, MALAT1 can recruit EZH2 to the promoter region of ABI3BP (ABI family member 3 binding protein) and then promote H3K27me3, thereby inhibiting the transcription of ABI3BP and ultimately promoting the metastasis of gallbladder cancer (95). In addition, *via* directly binding to miR-1914-3p, MALAT1 is capable of enhancing the stability of YAP (Yes-associated protein) mRNA, thus promoting the invasion and metastasis of non-small cell lung cancer (96). Recently, some studies have illustrated that MALAT1 also plays the role of ceRNAs in the regulation of OSCC metastasis. Zhu et al. observed that the expression of MALAT1 in TSCC tissues is significantly increased compared to adjacent non-cancerous tissues. Moreover, high expression of MALAT1 is also closely related to lymph node metastasis. Further experiments showed that after knocking down MALAT1 in TSCC cells, the expression of miR-140-5p is enhanced while the expression of PAK1(p21-activated kinase 1) is downregulated. Mechanism studies confirmed the promoting effects of MALAT1 on the expression of PAK1 and the migration and invasion of TSCC by targeting miR-140-5p (21). Apart from that, Zhang et al.'s research also support MALAT1's role of ceRNAs in the regulation of OSCC metastasis. Their data revealed that MALAT1 knockdown could repress the metastasis of TSCC cells *in vivo* and *in vitro* by enhancing the expression of JAG1 (jagged 1) through the miR-124/JAG1 axis (37).

H19

H19 is abnormally expressed in various human cancers, such as pancreatic cancer (97), nasopharyngeal cancer (98), and lung cancer (99), and is usually associated with cancer progression, metastasis, and poor prognosis. Additionally, by acting as

ceRNAs, H19 has been confirmed to regulate the migration, invasion, and metastasis of various tumors, including nasopharyngeal carcinoma (98), bladder cancer (100), and breast cancer (101). For example, in nasopharyngeal carcinoma, H19 overexpression is closely related to the poor prognosis of patients. Moreover, knocking down H19 could suppress the migration and invasion of tumor cells and delay the progression of transplanted tumor and lung metastasis in nude mice. Mechanistically, H19 upregulates the expression of its downstream proto-oncogene HRAS (HRas proto-oncogene, GTPase) by sponging miRNA let-7, thus promoting the carcinogenic activity of HRAS in nasopharyngeal carcinoma (98). Similarly, the interaction between H19 and various miRNAs is also an important mechanism for its regulation of OSCC metastasis. Kou et al. found that the expression of H19 in metastatic TSCC tissues is higher than that of non-metastatic TSCC tissues, and H19 knockdown could attenuate the migration and invasion of TSCC cells. The speculated mechanism of which is that H19 potentiates the expression of HMGA2 (high mobility group AT-hook 2), a key regulator of tumor metastasis, by targeting let-7. Conversely, inhibition of let-7a will dampen the inhibitory effect of H19 knockdown on the migration and invasion of TSCC cells (31). Another study revealed that the expression of H19 is positively correlated with the TNM stage and negatively related to overall survival. Further data implied that H19 can enhance the expression of its target gene EZH2 by sponging miR-138, thereby promoting the migration, invasion, and EMT of OSCC cells (32).

MEG3

Unlike MALAT1 and H19, MEG3 usually plays the role of a tumor suppressor. Numerous studies have confirmed that MEG3 is lowly expressed in various tumors, such as CRC (102), bladder cancer (103), and renal cell cancer (104), and inhibits their migration, invasion, and metastasis. Zhu et al. reported that MEG3 is downregulated in CRC tissues. In addition, overexpression of MEG3 could suppress the migration, invasion, and metastasis of tumor cells by inhibiting the expression of clusterin (102). A study on bladder cancer validated that by competing with PHLPP2 (PH domain and leucine-rich repeat protein phosphatase 2) mRNA to bind miR-27a, thereby promoting the expression of PHLPP2, MEG3 can restrain the invasion and metastasis of bladder cancer cells (103). Similarly, MEG3 can also suppress the migration and invasion of OSCC by exerting the function of ceRNAs. Tan et al. proved the low expression of MEG3 in OSCC tissues. Moreover, overexpression of MEG3 contributes to the downregulation of miR-548d-3p as well as the migration and invasion of OSCC cells. Mechanistically, the inhibitory effect of MEG3 on miR-548d-3p enhances the expression of miR-548d-3p downstream targets SOCS5 (suppressor of cytokine signaling 5) and SOCS6 (suppressor of cytokine signaling 6). Next, SOCS5/SOCS6 could repress the migration and invasion of OSCC by weakening the activation of the JAK/STAT (janus kinase/signal transducer and activator of transcription) pathway (24). Another study reported that MEG3 in OSCC tissue is negatively correlated with miR-21. Subsequent dual luciferase assay identified the direct interaction between MEG3 and miR-21. Furthermore, inhibiting the expression of miR-21 will reduce the migration ability of OSCC cells, and knocking down MEG3 could partially reverse the inhibitory effect of miR-21 downregulation on the migration of OSCC cells (46), which implies that MEG3 may dampen the migration of OSCC by targeting miR-21, but its downstream molecular mechanisms need further investigation. At the same time, more *in vivo* experiments are desired to clarify the role of MEG3 in OSCC metastasis.

LINC00152

LINC00152 (long intergenic noncoding RNA 152), transcribed from the region between protein-coding genes PLGLB2 (plasminogen like B2) and PLGLB1 (plasminogen like B1), is also known as CYTOR (cytoskeleton regulator RNA). Through interfering with cell signaling pathways such as PI3K/AKT (105), FSCN1 (fascin actin-bundling protein 1) (106), and Wnt/β-catenin (107, 108), LINC00152 was demonstrated to promote the invasion and metastasis of diverse tumors. At present, research on the function of LINC00152 in OSCC metastasis is also mainly focused on its role of ceRNAs. By analyzing two sets of TSCC gene expression profile data (GSE30784 and GSE9844), Yu et al. found that LINC00152 is significantly upregulated in TSCC tissues, and this result was also confirmed in fresh specimens and paraffin-embedded specimens. Further analysis showed that high expression of LINC00152 is closely related to lymph node metastasis of TSCC (109). Similarly, Li et al. validated that LINC00152 is highly expressed in OSCC tissues and cells. Moreover, knocking down LINC00152 could restrain the migration, invasion, and EMT of OSCC cells *in vitro*. Mechanistically, LINC00152 might play a role in promoting cancer by competitively binding miR-139-5p (33). Beyond that, miRNA-193b-3p is also a target of LINC00152. Further data implied that the inhibitory effect of LINC00152 on miRNA-193b-3p is responsible for the activation of the PI3K/AKT signaling pathway, which contributes to the migration and invasion of TSCC *in vitro* (34). However, more *in vivo* experiments are still needed to further illustrate the impact of LINC00152 on OSCC metastasis.

UCA1

UCA1 was first discovered in bladder cancer (110) and has been proved to promote the migration and invasion of bladder cancer cells (111). Not only that, but UCA1 can also regulate the metastasis of gastric cancer (112), osteosarcoma (113), and breast cancer (114), etc. Taking gastric cancer as an example, Gong et al. confirmed that UCA1 expression is abnormally increased in gastric cancer tissues, and high expression of UCA1 is significantly associated with lymph node metastasis. Additionally, overexpression of UCA1 was demonstrated to promote the migration, invasion, and metastasis of gastric cancer cells. The mechanism is that the direct interaction between UCA1 and miR-203 enhances the expression of miR-203 target ZEB2 (112). Recently, abnormal expression of UCA1 has also been found to be associated with OSCC metastasis. Fang et al. observed that UCA1 is highly expressed in TSCC tissues, and its expression level is positively correlated with lymph node

metastasis (115). Similarly, Zhang et al. also identified the correlation between UCA1 overexpression and the poor prognosis (lymph node metastasis and shorter survival time) in patients with TSCC. Interestingly, in TSCC cells, UCA1 can sponge miR-124 and negatively regulate each other. Further research showed that by targeting miR-124 to increase the expression of TGF-β1 (transforming growth factor β1), UCA1 can activate the JAG1/Notch pathway, which in turn promotes invasion and EMT of TSCC cells (22). Moreover, in another experiment, UCA1 was found to competitively bind miR-143-3p with MYO6 (myosin VI), thus promoting the migration, invasion, and EMT of TSCC cells (48).

TUG1

TUG1 is another lncRNA that has been extensively explored. One study proved that TUG1 plays a role in promoting the metastasis of CRC *via* upregulating the expression of Twist1 (116). Apart from that, by competitively binding miR-143-5p, TUG1 could enhance the expression of HIF-1α (hypoxia inducible factor 1 subunit alpha), thereby facilitating the metastasis of osteosarcoma cells (117). Similarly, the chain reaction caused by the direct binding of TUG1 to miR-455-3p also contributes to liver cancer metastasis (118). In particular, TUG1 was unveiled to promote the metastasis of OSCC by weakening the inhibitory effect of miRNAs on their downstream targets. Liu et al. confirmed that TUG1 is highly expressed in OSCC cells, and can enhance the migration potential of OSCC cells. The mechanism may be that TUG1 competitively binds miR-524-5p with DLX1(distal-less homeobox 1) and thus improves the expression of DLX1 (50). Apart from that, Yan et al. discovered that TUG1 knockdown could suppress the migration and invasion of OSCC cells, while overexpression of TUG1 will boost the metastasis of OSCC *in vivo*. Further experiments verified that there is mutual inhibition between TUG1 and miR-219, and repression of miR-219 could reverse the inhibitory effect of TUG1 knockdown on OSCC cells. Mechanistically, by acting as a ceRNA to sponge miR-219, TUG1 can enhance the expression of miR-219 target FMNL2 (formin-like protein 2) and thereby exerting its pro-metastasis effect (51).

Other LncRNAs Functioning as ceRNAs in OSCC Metastasis

LncRNA HOXA11-AS (homeobox A11 antisense RNA) was found to be highly expressed in OSCC tissues and cells. Moreover, HOXA11-AS was demonstrated to trigger the expression of YBX2 (Y box binding protein 2) by targeting miR-98-5p, thus promoting the migration, invasion, and EMT of OSCC cells (35). In contrast, lncRNA GAS5 (growth-arrest-specific transcript 5) is lowly expressed in OSCC. Furthermore, upregulating the expression of GAS5 could inhibit the migration, invasion, and EMT of OSCC cells, and the mechanism is also to play the role of ceRNA. Specifically, GAS5 enhances the expression of PTEN (phosphatase and tensin homolog) by combining with miR-21, and then dampened the activation of the PI3K/AKT signaling pathway. Beyond that, the inhibition of miR-21 by GAS5 also increased the expression of E-cadherin, while decreased the expression of N-cadherin, Vimentin, and Snail, suggesting that the EMT of OSCC cells was repressed as well (36). The results of another study showed that HOTAIR can improve the expression of MTA2 (metastasis-associated gene 2) *via* the miR-326/MTA2 axis, thereby facilitating the migration, invasion, and EMT of OSCC cells (43). Similarly, lncRNA CASC15 (cancer susceptibility candidate 15) has also played a role in promoting metastasis in the development of OSCC. The mechanism may be that the combination of CASC15 and miR-33a-5p elevates the expression level of the downstream target ZEB1 of miR-33a-5p (52). Wang et al. found that lncRNA lnc-p23154 is highly expressed in OSCC tissues and cells. Mechanism studies confirmed that by directly binding to miR-378a-3p, lnc-p23154 is capable of upregulating the expression of Glut1 (glucose transporter 1), thereby reinforcing the glycolysis of OSCC cells, and ultimately inducing the migration, invasion, EMT, and metastasis of OSCC cells (53). Additionally, lncRNAs CCAT1 (54), LINC01116 (long intergenic noncoding RNA 1162) (56), SNHG17 (small nucleolar RNA host gene 17) (57), and RC3H2 (73) have been proved to facilitate the metastasis-related biological behaviors of OSCC cells *via* regulating miR-181a/Wnt/β-catenin, miR-136/FN1 (fibronectin1), miR-876/SP1 (specificity protein 1), and miR-101-3p/EZH2 signaling pathways respectively (**Figure 1**). In a word, lncRNAs play a key role in the metastasis of OSCC by acting as ceRNAs.

LncRNAs Involved in the Distant Metastasis of OSCC

The probability of distant metastasis occurring in patients with OSCC is relatively low, only about 10% (119, 120). However, once a distant metastasis occurs, the patient's hope of being cured is very slim. Studies have unveiled that lncRNAs participate in regulating the distant metastasis of various tumors including OSCC. Wang et al. found that lncRNA APC1 (adenomatous polyposis coli 1) is lowly expressed in CRC tissues, and its expression level is negatively correlated with distant metastasis. In addition, in a nude mouse model, the overexpression of APC1 could attenuate lung metastasis of CRC cells. The mechanism may be that APC1 directly binds to Rab5b mRNA and reduces its stability, thereby inhibiting the production of exosomes derived from tumor cells (121). In contrast, lncRNA BX11 (BX111887) is overexpressed in pancreatic cancer, and its expression level is positively related to distant metastasis. Further research confirmed that by recruiting the transcription factor YB1 (Y-box binding protein 1) to the promoter region of ZEB1, BX11 is able to activate the transcription of ZEB1, thus promoting the distant metastasis of tumor cells (122).

Currently, there are few studies on the role of lncRNAs in the distant metastasis of OSCC. LncRNA HOTTIP (HOXA transcript at the distal tip) was reported to be overexpressed in TSCC tissues, and its high expression is associated with distant metastasis (120). Mu et al. observed that knocking down HOTTIP could restrain the migration, invasion, and EMT of TSCC cells (67). Moreover, the results of another study identified

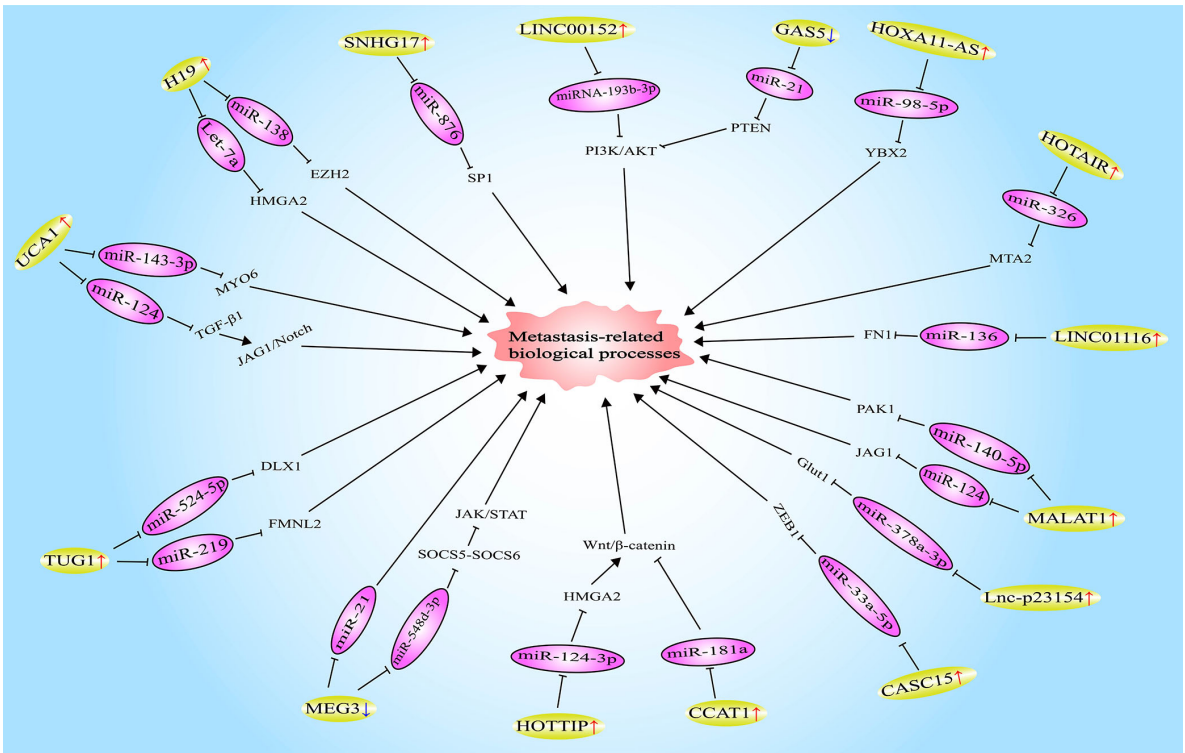

FIGURE 1 | Long noncoding RNAs (LncRNAs) involved in oral squamous cell carcinoma (OSCC) metastasis by functioning as competitive endogenous RNAs (ceRNAs).

that HOTTIP is upregulated in TSCC tissues with lymph node metastasis compared to those without lymph node metastasis. Mechanism research showed that by targeting miR-124-3p, HOTTIP is capable of enhancing the expression of HMGA2 (high mobility group AT-hook 2), which will further activate the Wnt/β-catenin pathway and promote the migration and invasion of TSCC cells (68). However, potential mechanisms of HOTTIP to regulate the distant metastasis of OSCC remain to be studied. In addition to HOTTIP, the high expression of lncRNA CCAT2 (colon cancer-associated transcript 2) (70) and lncRNA PANDAR (promoter of CDKN1A antisense DNA damage activated RNA) (71) are all associated with the distant metastasis of OSCC. Furthermore, both knockdowns of CCAT2 and PANDAR could inhibit the migration and invasion of OSCC cells. Whereas, the mechanisms by which CCAT2 and PANDAR regulate the distant metastasis of OSCC are still unclear.

Other Potential Mechanisms of LncRNAs Regulating the Metastasis of OSCC

To evaluate the influence of HOTAIR gene polymorphism and environmental factors on the susceptibility of OSCC, Su et al. detected four single-nucleotide polymorphisms (SNPs) of HOTAIR, namely rs920778, rs1899663, rs4759314, and rs12427129, in 1200 control participants and 907 OSCC patients. They found that rs920778 is associated with a high rate of lymph node metastasis. In addition, a motif search on the HOTAIR enhancer region showed that rs920778 is located in the putative binding motif of PRDM14 (PRDI-BF1 and RIZ domain containing 14). In particular, PRDM14 is a transcription factor that plays an anti-cancer role in HPV-positive OSCC cells (123). Moreover, data from the GTEx (gnotype-tissue expression) database shows that HOTAIR is differentially expressed in muscle skeletal tissues of individuals carrying the polymorphic allele of rs920778. These results suggest that the alteration in HOTAIR expression caused by SNPs might affect the development of OSCC, and this change may come from abnormal regulation of HOTAIR expression caused by SNPs, the mechanisms of which needs to be further explored (44).

Studies have validated that in a hypoxic environment, some lncRNAs could accelerate the metastasis of OSCC. Shih et al. reported that the expression of lncRNA MIR31HG (miR-31 host gene) in OSCC tissues is increased and can be induced by hypoxia. In addition, MIR31HG overexpression is also closely related to lymph node metastasis. Furthermore, MIR31HG in the hypoxic environment has a more obvious promotion effect on the migration, invasion, and metastasis of OSCC cells, compared with that in the normoxic environment. Mechanism studies confirmed that MIR31HG is capable of promoting the transcription of HIF-1α and bind to it, thereby assisting its binding to HIF-1β (hypoxia inducible factor 1 subunit beta) and histone acetylase p300, thus forming the HIF-1 complex.

Apart from that, MIR31HG is also able to recruit the HIF-1 complex to the promoter region of the metastasis-promoting genes, such as VEGF (vascular endothelial growth factor), LICAM(L1 cell adhesion molecule), and LOXL2 (lysyloxidase homologe2), to activate their transcription (65). Similarly, lncRNA HAS2-AS1 (hyaluronan synthase 2 antisense 1) is highly expressed in OSCC tissues and cells under hypoxic conditions, and HAS2-AS1 overexpression is also closely associated with lymph node metastasis. Subsequent studies exhibited that hypoxia-induced overexpression of HAS2-AS1 depends on HIF-1α, which can directly bind to the promoter region of HAS2-AS1 and activate its transcription. Additionally, HAS2-AS1 was proved to promote the hypoxia-induced invasion and EMT of OSCC cells. The potential mechanism is that HAS2-AS1 increases the level of hyaluronic acid in OSCC cells by enhancing the expression and stability of HAS2 (hyaluronan synthase 2) (66).

LncRNA SNHG3 (small nucleolar RNA host gene 3) was found to be overexpressed in OSCC cells. Silencing SNHG3 will inhibit the migration ability of OSCC cells. Further research showed that by recruiting ELAVL1 (ELAV like RNA-binding protein 1) to bind with NFYC (nuclear transcription factor Y subunit gamma) mRNA and then enhance its stability, SNHG3 could increase the expression of NFYC and thereby induce the migration of OSCC cells (60). As another lncRNA highly expressed in OSCC tissues and cells, LEF1-AS1 (lymphoid enhancer-binding factor 1 antisense RNA 1) has been validated to inhibit the activation of the Hippo pathway by direct interaction with LATS1 (large tumor suppressor 1), thus promoting the migration of OSCC cells (69). In general, mechanisms by which lncRNAs regulate OSCC metastasis are complex. One lncRNA could regulate OSCC metastasis through multiple mechanisms, while diverse lncRNAs acting on the same signaling pathway may produce opposite effects. To fully understand the biological function of lncRNAs, especially its role in OSCC metastasis, there are still many studies to be carried out.

THE REGULATION OF CAFs-RELATED LNCRNAS ON THE METASTASIS OF OSCC

In recent years, the tumor microenvironment composed of cells (such as fibroblasts, endothelial cells, and immune cells) and extracellular components (such as growth factors, hormones, and extracellular matrix) has become a hot spot in tumor research (124). Studies have confirmed that the heterogeneity of the tumor microenvironment contributes to the occurrence and metastasis of tumors (125, 126). Cancer-associated fibroblasts (CAFs) are an important component of the tumor microenvironment. The interaction of CAFs with tumor cells not only plays an important part in mediating the formation of CAFs (127) but also affects the process of tumor metastasis (128). It interests to note that lncRNAs participates in the regulation of CAFs on the metastasis of tumors (**Figure 2**). Ren et al. reported that high expression of HOTAIR is associated with breast cancer metastasis. In addition, the conditioned medium of CAFs-derived from breast cancer could significantly enhance the expression of HOTAIR and promote the metastasis of breast cancer cells. Subsequently, mechanism research validated the promoting effect of TGF-β1 secreted by CAFs on the transcription of HOTAIR in breast cancer cells, which will enhance the expression of CDK5 (cyclin dependent kinase 5), thereby facilitating the metastasis of breast cancer cells (129). In another experiment, lncRNA LINC00092 (long intergenic noncoding RNA 92) was found to be highly expressed in ovarian cancer tissues, and its overexpression is associated with tumor metastasis. Further investigation showed that CXCL14 (C-X-C motif chemokine ligand 14) derived from CAFs could increase the expression of LINC00092 in ovarian cancer cells. Moreover, LINC00092 was demonstrated to promote the glycolysis of tumor cells and induce the metastasis of ovarian cancer cells by enhancing the expression of glycolytic enzyme PFKFB2 (6-phosphofructo-2-kinase/fructose-2,6-bisphosphatase 2) and combining with it (130). In addition to regulating the expression of lncRNAs in tumor cells, CAFs may also regulate tumor metastasis by delivering lncRNAs to tumor cells. Ren et al. confirmed that CAFs derived from CRC are capable of transferring H19 to CRC cells through exosomes, thereby increasing the level of H19 in tumor cells and promoting the proliferation of tumor cells. The mechanism is that the direct binding of H19 to miR-141 activates the Wnt/β-catenin signaling pathway in tumor cells (131). As mentioned earlier, the activation of the Wnt/β-catenin signaling pathway has been shown to promote the metastasis of CRC (82). Besides, H19 overexpression is also an important factor inducing CRC metastasis (132). However, further research is needed to confirm whether CAFs-derived H19 can promote the metastasis of CRC.

Currently, only one study has explored the role of lncRNAs in the regulation of CAFs on the metastasis of OSCC. Jin et al. observed that lncRNA TIRY is highly expressed in CAFs derived from OSCC tissues. Furthermore, after co-cultivation of OSCC cells with conditioned medium of CAFs treated with TIRY overexpression plasmids, the capabilities of migration and invasion of OSCC cells were significantly improved. Moreover, knocking down TIRY caused increased expression of miR-14 in CAFs and their exosomes, whose mechanism is the direct binding of TIRY to miR-14. Further research showed that the overexpression of TIRY inhibits the transmission of miR-14 from CAFs to tumor cells through the transport of exosomes, thus enhancing the activation of the Wnt/β-catenin signaling pathway in tumor cells and promoting EMT. This may be the mechanism by which TIRY in CAFs regulates the migration and invasion of OSCC cells. Interestingly, the expression of miR-14 in OSCC cells was substantially increased after treatment with conditioned medium of TIRY-silenced CAFs (74). However, it is still unknown whether TIRY can be directly transported into OSCC cells through CAFs-derived exosomes and then affect the metastasis of OSCC. At present, research on the role of CAFs-related lncRNAs in OSCC metastasis has just begun, and there is still much work to be done.

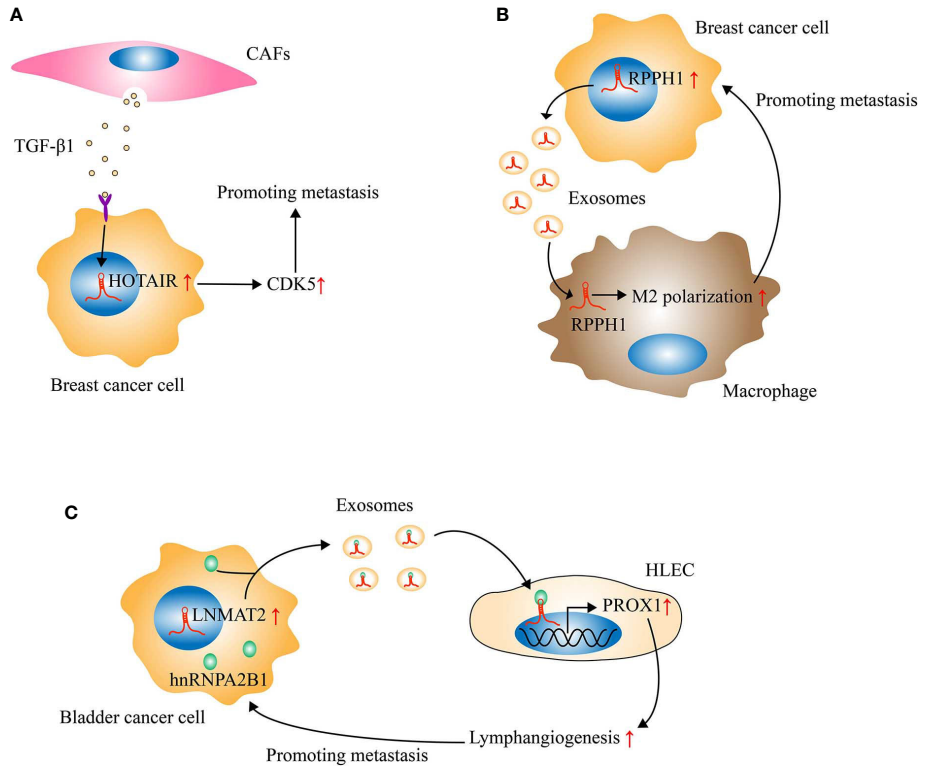

FIGURE 2 | Long noncoding RNAs (LncRNAs) regulate tumor metastasis by mediating the crosstalk between tumor cells and tumor microenvironment. **(A)** Cancer-associated fibroblasts (CAFs) derived from breast cancer could secrete TGF-β1 to activate the transcription of HOX transcript antisense intergenic RNA (HOTAIR) in breast cancer cells, thereby enhancing the expression of CDK5 and then inducing metastasis. **(B)** Through exosomes, RPPH1 derived from breast cancer cells could be transported into macrophages and then induce M2 polarization of macrophages, which will further accelerate the metastasis of breast cancer. **(C)** LNMAT2 could be encapsulated into the exosomes secreted by bladder cancer cells through direct interaction with hnRNPA2B1. Subsequently, the exosomal LNMAT2 internalized by human lymphatic endothelial cell (HLEC) could promote the expression of PROX1 in HLEC, thus leading to lymphangiogenesis and lymph node metastasis.

CONCLUSION

Research in the past decade has partially revealed the key role played by lncRNAs in the development of OSCC. In particular, abnormally expressed lncRNAs are also important factors affecting OSCC metastasis. LncRNAs can regulate the metastasis of OSCC through different mechanisms at epigenetic (18), transcription (26), and post-transcriptional (16) levels, and play the role of oncogene or tumor suppressor. Nonetheless, the current focus of scholars is mainly on the effect of abnormal expression of autologous lncRNAs in OSCC cells on tumor metastasis. The role of lncRNAs-mediated crosstalk between OSCC cells and the tumor microenvironment in tumor metastasis is still seldom studied. However, the stromal cells (such as CAFs (129), endothelial cells (133) and immune cells (134)), exosomes (135), and lymphangiogenesis (133) involved in this crosstalk have been shown to be involved in the metastasis of other tumors (**Figure 2**).

As mentioned previously, based on the crosstalk between CAFs and tumor cells, CAFs-related lncRNAs play an important role in tumor metastasis. It is worth noting that exosomes can act as messengers between tumor cells and CAFs. Moreover, exosomes are also the key link between tumor cells and other stromal cells, which contribute to the metastasis of various tumors as well (133, 134). The regulation of exosomes on tumor metastasis depends on their special structure (membranous microcapsules with diameters ranging from 50 to 150nm) and contents (RNA, DNA, proteins, etc.) (136). Previous studies have identified that exosomes could transfer lncRNAs to target cells and induce a series of chain reactions, thereby regulating tumor metastasis (134, 135). For example, Liang et al. found that the expression of lncRNA RPPH1 (ribonuclease P RNA component H1) in breast cancer tissues is significantly upregulated. Moreover, RPPH1 overexpression is associated with metastasis and poor prognosis. In addition, the *in vivo* study demonstrated that RPPH1 is able to promote the metastasis of breast cancer. Mechanistically, through exosomes transport into macrophages, RPPH1 derived from breast cancer cells could induce M2 polarization of macrophages. In turn, M2-polarized macrophages will further accelerate breast cancer metastasis (134). However, there is currently no study on the effect of exosomal lncRNAs on OSCC metastasis. Therefore, further exploration of the role of exosomal lncRNAs in OSCC metastasis will provide more valuable information on the metastasis of OSCC.

The high rate of lymph node metastasis is the main cause of death in patients with OSCC (5). Not only OSCC, but many other tumors can also have lymph node metastasis (112, 133, 134). As an important channel for lymph node metastasis of tumor cells, lymphatic vessels and the mechanisms of their generation naturally attract the attention of scholars. Studies have confirmed that lncRNAs are involved in inducing lymphangiogenesis of tumors (133, 137). Taking lncRNA LNMAT2 (lymph node metastasis-associated transcript 2) as an example (133), Chen et al. found that bladder cancer-derived exosomal LNMAT2 can enhance the ability of tube formation and migration of human lymphatic endothelial cells (HLEC) *in vitro*, and facilitate tumor lymphangiogenesis and lymph node metastasis *in vivo*. Further mechanistic studies uncovered that LNMAT2 could be encapsulated into exosomes secreted by bladder cancer cells through direct interaction with hnRNPA2B1 (heterogeneous nuclear ribonucleoprotein A2B1). Subsequently, the exosomal LNMAT2 will be internalized by HLEC, and then promote the expression of PROX1 (prospero homeobox 1) at the epigenetic level, thus leading to lymphangiogenesis and lymph node metastasis of the tumor. Therefore, LNMAT2 has the potential to serve as a therapeutic target for lymph node metastasis of bladder cancer. However, to date, there has been no research on the regulation of lncRNAs on OSCC lymphangiogenesis. Subsequent research should pay more attention to this direction.

In addition to the crosstalk between tumor cells and stromal cells, the crosstalk between tumor cells and the extracellular matrix (ECM) also plays a critical role in the metastasis of tumors. Huang et al. reported that integrin alpha 2 (ITGA2), upregulated in omental metastases of patients with ovarian cancer, can trigger tumor cell adhesion to collagen, and then facilitates the migration and peritoneal metastasis of tumor cells. The speculated mechanism of which is that ITGA2 activates the phosphorylation of focal adhesion kinase and the mitogen-activated protein kinase pathway (138). In another study, lncRNA CASC9 (cancer susceptibility 9) was revealed to be associated with the prognosis and metastasis of esophageal squamous cell carcinoma (ESCC). Besides, CASC9 knockdown could significantly inhibit the migration, invasion, and metastasis of ESCC cells. Mechanistically, CASC9 can enhance the enrichment of the transcriptional coactivator CREB-binding protein and H3K27 acetylation in the promoter of LAMC2, an upstream inducer of the integrin pathway, thus promoting its expression. Nevertheless, the impact of the crosstalk between tumor cells and ECM regulated by lncRNAs on OSCC metastasis has not been studied.

In summary, lncRNAs are expected to serve as indicators for screening, treatment, and prognostic monitoring of OSCC metastasis. However, the current understanding of the role of lncRNAs in OSCC metastasis is still in its infancy. Therefore, further research on the role of lncRNAs in the crosstalk between OSCC cells and tumor microenvironment will help enrich the blueprint of the mechanisms of OSCC metastasis.

AUTHOR CONTRIBUTIONS

YX and EJ discussed and designed the study. YX performed the research and analyzed the data. ZS and ZJS revised the article. All authors contributed to the article and approved the submitted version.

FUNDING

This study was supported by grants from the National Natural Science Foundation of China 81772897, 81672666.

REFERENCES

1. Ketabat F, Pundir M, Mohabatpour F, Lobanova L, Koutsopoulos S, Hadjiiski L, et al. Controlled Drug Delivery Systems for Oral Cancer Treatment-Current Status and Future Perspectives. *Pharmaceutics* (2019) 11(7):302. doi: 10.3390/pharmaceutics11070302
2. Torre LA, Bray F, Siegel RL, Ferlay J, Lortet-Tieulent J, Jemal A. Global cancer statistics, 2012. *CA Cancer J Clin* (2015) 65(2):87–108. doi: 10.3322/caac.21262
3. Ganly I, Patel S, Shah J. Early stage squamous cell cancer of the oral tongue–clinicopathologic features affecting outcome. *Cancer* (2012) 118(1):101–11. doi: 10.1002/cncr.26229
4. Alves AM, Diel LF, Lamers ML. Macrophages and prognosis of oral squamous cell carcinoma: A systematic review. *J Oral Pathol Med* (2018) 47(5):460–7. doi: 10.1111/jop.12643
5. Zanoni DK, Montero PH, Migliacci JC, Shah JP, Wong RJ, Ganly I, et al. Survival outcomes after treatment of cancer of the oral cavity (1985-2015). *Oral Oncol* (2019) 90:115–21. doi: 10.1016/j.oraloncology.2019.02.001
6. Romer CAE, Broglie Daeppen MA, Mueller M, Huber GF, Guesewell S, Stoeckli SJ. Long-term speech and swallowing function after primary resection and sentinel node biopsy for early oral squamous cell carcinoma. *Oral Oncol* (2019) 89:127–32. doi: 10.1016/j.oraloncology.2018.12.027
7. Guo CB, Feng Z, Zhang JG, Peng X, Cai ZG, Mao C, et al. Supraomohyoid neck dissection and modified radical neck dissection for clinically node-negative oral squamous cell carcinoma: a prospective study of prognosis, complications and quality of life. *J Craniomaxillofac Surg* (2014) 42 (8):1885–90. doi: 10.1016/j.jcms.2014.07.007
8. Moratin J, Metzger K, Kansy K, Ristow O, Engel M, Hoffmann J, et al. The prognostic significance of the lymph node ratio in oral cancer differs for anatomical subsites. *Int J Oral Maxillofac Surg* (2020) 49(5):558–63. doi: 10.1016/j.ijom.2019.10.015
9. Todorović V, Desai BV, Eigenheer RA, Yin T, Amargo EV, Mrksich M, et al. Detection of differentially expressed basal cell proteins by mass spectrometry. *Mol Cell Proteomics* (2010) 9(2):351–61. doi: 10.1074/mcp.M900358-MCP200
10. Sasahira T, Kirita T, Kurihara M, Yamamoto K, Bhawal UK, Bosserhoff AK, et al. MIA-dependent angiogenesis and lymphangiogenesis are closely associated with progression, nodal metastasis and poor prognosis in tongue squamous cell carcinoma. *Eur J Cancer* (2010) 46(12):2285–94. doi: 10.1016/j.ejca.2010.04.027
11. Slavoff SA, Mitchell AJ, Schwaid AG, Cabili MN, Ma J, Levin JZ, et al. Peptidomic discovery of short open reading frame-encoded peptides in human cells. *Nat Chem Biol* (2013) 9(1):59–64. doi: 10.1038/nchembio.1120

12. Iyer MK, Niknafs YS, Malik R, Singhal U, Sahu A, Hosono Y, et al. The landscape of long noncoding RNAs in the human transcriptome. *Nat Genet* (2015) 47(3):199–208. doi: 10.1038/ng.3192
13. Yan X, Hu Z, Feng Y, Hu X, Yuan J, Zhao SD, et al. Comprehensive Genomic Characterization of Long Non-coding RNAs across Human Cancers. *Cancer Cell* (2015) 28(4):529–40. doi: 10.1016/j.ccell.2015.09.006
14. Begolli R, Sideris N, Giakountis A. LncRNAs as Chromatin Regulators in Cancer: From Molecular Function to Clinical Potential. *Cancers (Basel)* (2019) 11(10)):1524. doi: 10.3390/cancers11101524
15. He J, Zuo Q, Hu B, Jin H, Wang C, Cheng Z, et al. A novel, liver-specific long noncoding RNA LINC01093 suppresses HCC progression by interaction with IGF2BP1 to facilitate decay of GLI1 mRNA. *Cancer Lett* (2019) 450:98–109. doi: 10.1016/j.canlet.2019.02.033
16. Jia X, Shi L, Wang X, Luo L, Ling L, Yin J, et al. KLF5 regulated lncRNA RP1 promotes the growth and metastasis of breast cancer via repressing p27kip1 translation. *Cell Death Dis* (2019) 10(5):373. doi: 10.1038/s41419-019-1566-5
17. He W, Zhong G, Jiang N, Wang B, Fan X, Chen C, et al. Long noncoding RNA BLACAT2 promotes bladder cancer-associated lymphangiogenesis and lymphatic metastasis. *J Clin Invest* (2018) 128(2):861–75. doi: 10.1172/jci96218
18. Xu M, Xu X, Pan B, Chen X, Lin K, Zeng K, et al. LncRNA SATB2-AS1 inhibits tumor metastasis and affects the tumor immune cell microenvironment in colorectal cancer by regulating SATB2. *Mol Cancer* (2019) 18(1):135. doi: 10.1186/s12943-019-1063-6
19. Zhou S, Zhu Y, He Z, Zhang D, Guo F, Jian X, et al. Long Non-Coding RNA Expression Profile Associated with Malignant Progression of Oral Submucous Fibrosis. *J Oncol* (2019) 2019:6835176. doi: 10.1155/2019/6835176
20. Cao W, Liu JN, Liu Z, Wang X, Han ZG, Ji T, et al. A three-lncRNA signature derived from the Atlas of ncRNA in cancer (TANRIC) database predicts the survival of patients with head and neck squamous cell carcinoma. *Oral Oncol* (2017) 65:94–101. doi: 10.1016/j.oraloncology.2016.12.017
21. Zhu MH, Zhang CY, Chen DH, Chen SC, Zheng HL. lncRNA MALAT1 potentiates the progression of tongue squamous cell carcinoma through regulating miR-140-5p-PAK1 pathway. *Onco Targets Ther* (2019) 12:1365–77. doi: 10.2147/ott.S192069
22. Zhang TH, Liang LZ, Liu XL, Wu JN, Su K, Chen JY, et al. LncRNA UCA1/miR-124 axis modulates TGF1-induced epithelial-mesenchymal transition and invasion of tongue cancer cells through JAG1/Notch signaling. *J Cell Biochem* (2019) 120(6):10495–504. doi: 10.1002/jcb.28334
23. Wang ZY, Hu M, Dai MH, Xiong J, Zhang S, Wu HJ, et al. Upregulation of the long non-coding RNA AFAP1-AS1 affects the proliferation, invasion and survival of tongue squamous cell carcinoma via the Wnt/beta-catenin signaling pathway. *Mol Cancer* (2018) 17(1):3. doi: 10.1186/s12943-017-0752-2
24. Tan JW, Xiang LX, Xu GC. LncRNA MEG3 suppresses migration and promotes apoptosis by sponging miR-548d-3p to modulate JAK-STAT pathway in oral squamous cell carcinoma. *IUBMB Life* (2019) 71(7):882–90. doi: 10.1002/iub.2012
25. Zhang H, Zhang N, Liu Y, Su P, Liang Y, Li Y, et al. Epigenetic Regulation of NAMPT by NAMPT-AS Drives Metastatic Progression in Triple-Negative Breast Cancer. *Cancer Res* (2019) 79(13):3347–59. doi: 10.1158/0008-5472.Can-18-3418
26. Liu M, Zhong J, Zeng Z, Huang K, Ye Z, Deng S, et al. Hypoxia-induced feedback of HIF-1α and lncRNA-CF129 contributes to pancreatic cancer progression through stabilization of p53 protein. *Theranostics* (2019) 9(16):4795–810. doi: 10.7150/thno.30988
27. Yamamura S, Imai-Sumida M, Tanaka Y, Dahiya R. Interaction and cross-talk between non-coding RNAs. *Cell Mol Life Sci* (2018) 75(3):467–84. doi: 10.1007/s00018-017-2626-6
28. Liu Z, Wang Y, Wang L, Yao B, Sun L, Liu R, et al. Long non-coding RNA AGAP2-AS1, functioning as a competitive endogenous RNA, upregulates ANXA11 expression by sponging miR-16-5p and promotes proliferation and metastasis in hepatocellular carcinoma. *J Exp Clin Cancer Res* (2019) 38(1):194. doi: 10.1186/s13046-019-1188-x
29. Pan J, Fang S, Tian H, Zhou C, Zhao X, Tian H, et al. lncRNA JPX/miR-33a-5p/Twist1 axis regulates tumorigenesis and metastasis of lung cancer by activating Wnt/β-catenin signaling. *Mol Cancer* (2020) 19(1):9. doi: 10.1186/s12943-020-1133-9
30. Welch DR, Hurst DR. Defining the Hallmarks of Metastasis. *Cancer Res* (2019) 79(12):3011–27. doi: 10.1158/0008-5472.Can-19-0458
31. Kou N, Liu S, Li XJ, Li WW, Zhong WJ, Gui L, et al. H19 Facilitates Tongue Squamous Cell Carcinoma Migration and Invasion via Sponging miR-let-7. *Oncol Res* (2019) 27(2):173–82. doi: 10.3727/096504018x15202945197589
32. Hong Y, He H, Sui W, Zhang J, Zhang S, Yang D. [Corrigendum] Long non−coding RNA H19 promotes cell proliferation and invasion by acting as a ceRNA of miR−138 and releasing EZH2 in oral squamous cell carcinoma. *Int J Oncol* (2018) 53(2):915. doi: 10.3892/ijo.2018.4428
33. Li MH, Ning J, Li ZH, Wang J, Zhao CO, Wang LE. LINC00152 promotes the growth and invasion of oral squamous cell carcinoma by regulating miR-139-5p. *Onco Targets Ther* (2018) 11:6295–304. doi: 10.2147/ott.S168807
34. Li XH, Rui B, Cao YB, Gong XJ, Li HJ. Long non-coding RNA LINC00152 acts as a sponge of miRNA-193b-3p to promote tongue squamous cell carcinoma progression. *Oncol Lett* (2020) 19(3):2035–42. doi: 10.3892/ol.2020.11293
35. Niu XY, Yang B, Liu F, Fang QG. LncRNA HOXA11-AS promotes OSCC progression by sponging miR-98-5p to upregulate YBX2 expression. *BioMed Pharmacother* (2020) 121:10. doi: 10.1016/j.biopha.2019.109623
36. Zeng BH, Li Y, Jiang FF, Wei CB, Chen GH, Zhang WL, et al. LncRNA GAS5 suppresses proliferation, migration, invasion, and epithelial-mesenchymal transition in oral squamous cell carcinoma by regulating the miR-21/PTEN axis. *Exp Cell Res* (2019) 374(2):365–73. doi: 10.1016/j.yexcr.2018.12.014
37. Zhang T-H, Liang L-Z, Liu X-L, Wu J-N, Su K, Chen J-Y, et al. Long non-coding RNA MALAT1 interacts with miR-124 and modulates tongue cancer growth by targeting JAG1. *Oncol Rep* (2017) 37(4):2087–94. doi: 10.3892/or.2017.5445
38. Yuan J, Xu XJ, Lin Y, Chen QY, Sun WJ, Tang L, et al. LncRNA MALAT1 expression inhibition suppresses tongue squamous cell carcinoma proliferation, migration and invasion by inactivating PI3K/Akt pathway and downregulating MMP-9 expression. *Eur Rev Med Pharmacol Sci* (2019) 23(1):198–206. doi: 10.26355/eurrev_201901_16765
39. Liang J, Liang LZ, Ouyang KX, Li ZQ, Yi XP. MALATI induces tongue cancer cells' EMT and inhibits apoptosis through Wnt/beta-catenin signaling pathway. *J Oral Pathol Med* (2017) 46(2):98–105. doi: 10.1111/jop.12466
40. Zhou X, Liu S, Cai G, Kong L, Zhang T, Ren Y, et al. Long Non Coding RNA MALAT1 Promotes Tumor Growth and Metastasis by inducing Epithelial-Mesenchymal Transition in Oral Squamous Cell Carcinoma. *Sci Rep* (2015) 5:15972. doi: 10.1038/srep15972
41. Lu MY, Liao YW, Chen PY, Hsieh PL, Fang CY, Wu CY, et al. Targeting LncRNA HOTAIR suppresses cancer stemness and metastasis in oral carcinomas stem cells through modulation of EMT. *Oncotarget* (2017) 8(58):98542–52. doi: 10.18632/oncotarget.21614
42. Wu YS, Zhang L, Zhang L, Wang Y, Li H, Ren XB, et al. Long non-coding RNA HOTAIR promotes tumor cell invasion and metastasis by recruiting EZH2 and repressing E-cadherin in oral squamous cell carcinoma. *Int J Oncol* (2015) 46(6):2586–94. doi: 10.3892/ijo.2015.2976
43. Tao DT, Zhang ZX, Liu X, Zhang ZW, Fu Y, Zhang P, et al. LncRNA HOTAIR promotes the invasion and metastasis of oral squamous cell carcinoma through metastasis-associated gene 2. *Mol Carcinog* (2020) 59(4):353–64. doi: 10.1002/mc.23159
44. Su SC, Hsieh MJ, Lin CW, Chuang CY, Liu YF, Yeh CM, et al. Impact of HOTAIR Gene Polymorphism and Environmental Risk on Oral Cancer. *J Dental Res* (2018) 97(6):717–24. doi: 10.1177/0022034517749451
45. Liu Z, Wu C, Xie N, Wang P. Long non-coding RNA MEG3 inhibits the proliferation and metastasis of oral squamous cell carcinoma by regulating the WNT/beta-catenin signaling pathway. *Oncol Lett* (2017) 14(4):4053–8. doi: 10.3892/ol.2017.6682
46. Zhang LL, Hu D, Zou LH. Low expression of lncRNA MEG3 promotes the progression of oral squamous cell carcinoma by targeting miR-21. *Eur Rev Med Pharmacol Sci* (2018) 22(23):8315–23. doi: 10.26355/eurrev_201812_16529
47. Yang YT, Wang YF, Lai JY, Shen SY, Wang F, Kong J, et al. Long non-coding RNA UCA1 contributes to the progression of oral squamous cell carcinoma by regulating the WNT/beta-catenin signaling pathway. *Cancer Sci* (2016) 107(11):1581–9. doi: 10.1111/cas.13058

48. Duan Q, Xu M, Wu M, Zhang X, Gan M, Jiang H. Long noncoding RNA UCA1 promotes cell growth, migration, and invasion by targeting miR-143-3p in oral squamous cell carcinoma. *Cancer Med* (2020) 9(9):3115–29. doi: 10.1002/cam4.2808
49. Liang S, Zhang S, Wang P, Yang C, Shang C, Yang J, et al. LncRNA, TUG1 regulates the oral squamous cell carcinoma progression possibly via interacting with Wnt/beta-catenin signaling. *Gene* (2017) 608:49–57. doi: 10.1016/j.gene.2017.01.024
50. Liu SY, Liu LH, Hu WW, Wang M. Long noncoding RNA TUG1 regulates the development of oral squamous cell carcinoma through sponging miR-524-5p to mediate DLX1 expression as a competitive endogenous RNA. *J Cell Physiol* (2019) 234(11):20206–16. doi: 10.1002/jcp.28620
51. Yan G, Wang X, Yang M, Lu L, Zhou Q. Long non-coding RNA TUG1 promotes progression of oral squamous cell carcinoma through upregulating FMNL2 by sponging miR-219. *Am J Cancer Res* (2017) 7(9):1899–912.
52. Zuo ZB, Ma L, Gong ZD, Xue LD, Wang QB. Long non-coding RNA CASC15 promotes tongue squamous carcinoma progression through targeting miR-33a-5p. *Environ Sci Pollut Res* (2018) 25(22):22205–12. doi: 10.1007/s11356-018-2300-z
53. Wang Y, Zhang XJ, Wang Z, Hu QC, Wu J, Li YY, et al. LncRNA-p23154 promotes the invasion-metastasis potential of oral squamous cell carcinoma by regulating Glut1-mediated glycolysis. *Cancer Lett* (2018) 434:172–83. doi: 10.1016/j.canlet.2018.07.016
54. Li GH, Ma ZH, Wang X. Long non-coding RNA CCAT1 is a prognostic biomarker for the progression of oral squamous cell carcinoma via miR-181a-mediated Wnt/beta-catenin signaling pathway. *Cell Cycle* (2019) 18 (21):2902–13. doi: 10.1080/15384101.2019.1662257
55. Sun MY, Shen ZY. Knockdown of Long Non-Coding RNA (lncRNA) Colon Cancer-Associated Transcript-1 (CCAT1) Suppresses Oral Squamous Cell Carcinoma Proliferation, Invasion, and Migration by Inhibiting the Discoidin Domain Receptor 2 (DDR2)/ERK/AKT Axis. *Med Sci Monit* (2020) 26:10. doi: 10.12659/msm.920020
56. Chen ZF, Tao Q, Qiao B, Zhang LT. Silencing of LINC01116 suppresses the development of oral squamous cell carcinoma by up-regulating microRNA-136 to inhibit FN1. *Cancer Manage Res* (2019) 11:6043–59. doi: 10.2147/cmar.S197583
57. Liu X, Zhang B, Jia Y, Fu M. SNHG17 enhances the malignant characteristics of tongue squamous cell carcinoma by acting as a competing endogenous RNA on microRNA-876 and thereby increasing specificity protein 1 expression. *Cell Cycle* (2020) 19(6):711–25. doi: 10.1080/15384101.2020.1727399
58. Li S, Zhang S, Chen J. c-Myc induced upregulation of long non-coding RNA SNHG16 enhances progression and carcinogenesis in oral squamous cell carcinoma. *Cancer Gene Ther* (2019) 26(11-12):400–10. doi: 10.1038/s41417-018-0072-8
59. Zhao Y, Wang J, Ma K. [Knockdown of lncRNA SNHG6 inhibites the proliferation and epithelial mesenchymal transition in tongue cancer cells]. *Xi Bao Yu Fen Zi Mian Yi Xue Za Zhi* (2018) 34(9):806–11. doi: 10.13423/j.cnki.cjcmi.008671
60. Liu Z, Tao H. Small nucleolar RNA host gene 3 facilitates cell proliferation and migration in oral squamous cell carcinoma via targeting nuclear transcription factor Y subunit gamma. *J Cell Biochem* (2020) 121(3):2150–8. doi: 10.1002/jcb.29421
61. Li X, Ma C, Zhang L, Li N, Zhang X, He J, et al. LncRNAAC132217.4, a KLF8-regulated long non-coding RNA, facilitates oral squamous cell carcinoma metastasis by upregulating IGF2 expression. *Cancer Lett* (2017) 407:45–56. doi: 10.1016/j.canlet.2017.08.007
62. Jiang YY, Cao W, Wu K, Qin X, Wang XN, Li Y, et al. LncRNA LINC00460 promotes EMT in head and neck squamous cell carcinoma by facilitating peroxiredoxin-1 into the nucleus. *J Exp Clin Cancer Res* (2019) 38(1):19. doi: 10.1186/s13046-019-1364-z
63. Liu Z, Li H, Fan SM, Lin H, Lian WW. STAT3-induced upregulation of long noncoding RNA HNF1A-AS1 promotes the progression of oral squamous cell carcinoma via activating Notch signaling pathway. *Cancer Biol Ther* (2019) 20(4):444–53. doi: 10.1080/15384047.2018.1529119
64. Liu M, Gao X, Liu CL. Increased expression of lncRNA FTH1P3 promotes oral squamous cell carcinoma cells migration and invasion by enhancing PI3K/Akt/GSK3b/Wnt/beta-catenin signaling. *Eur Rev Med Pharmacol Sci* (2018) 22(23):8306–14. doi: 10.26355/eurrev_201812_16528
65. Shih JW, Chiang WF, Wu ATH, Wu MH, Wang LY, Yu YL, et al. Long noncoding RNA LncHIFCAR/MIR31HG is a HIF-1alpha co-activator driving oral cancer progression. *Nat Commun* (2017) 8:15874. doi: 10.1038/ncomms15874
66. Zhu G, Wang S, Chen J, Wang Z, Liang X, Wang X, et al. Long noncoding RNA HAS2-AS1 mediates hypoxia-induced invasiveness of oral squamous cell carcinoma. *Mol Carcinog* (2017) 56(10):2210–22. doi: 10.1002/mc.22674
67. Mu MK, Li Y, Zhan YB, Li X, Zhang B. Knockdown of HOXA transcript at the distal tip suppresses the growth and invasion and induces apoptosis of oral tongue squamous carcinoma cells. *Onco Targets Ther* (2018) 11:8033–44. doi: 10.2147/ott.S174637
68. Xiong L, Tang Y, Tang J, Liu Z, Wang X. Downregulation of lncRNA HOTTIP Suppresses the Proliferation, Migration, and Invasion of Oral Tongue Squamous Cell Carcinoma by Regulation of HMGA2-Mediated Wnt/β-Catenin Pathway. *Cancer Biother Radiopharm* (2020) 35(9):720–30. doi: 10.1089/cbr.2019.3017
69. Zhang CQ, Bao CC, Zhang XX, Lin XS, Pan D, Chen YZ. Knockdown of lncRNA LEF1-AS1 inhibited the progression of oral squamous cell carcinoma (OSCC) via Hippo signaling pathway. *Cancer Biol Ther* (2019) 20(9):1213–22. doi: 10.1080/15384047.2019.1599671
70. Zhou NG, Liao W, Huang ZK, Hu ZW, Huang WZ, Wang QT. Overexpression of long non-coding RNA CCAT2 predicts a poor prognosis in patients with oral squamous cell carcinoma. *Int J Clin Exp Pathol* (2016) 9(1):110–7.
71. Huang Z, Sang T, Zheng Y, Wu J. Long non-coding RNA PANDAR overexpression serves as a poor prognostic biomarker in oral squamous cell carcinoma. *Int J Clin Exp Pathol* (2018) 11(5):2728–34.
72. Hu D, Zhong T, Dai Q. Long Non-Coding RNA NKILA Reduces Oral Squamous Cell Carcinoma Development Through the NF-KappaB Signaling Pathway. *Technol Cancer Res Treat* (2020) 19:1533033820960747. doi: 10.1177/1533033820960747
73. Wu K, Jiang Y, Zhou W, Zhang B, Li Y, Xie F, et al. Long Noncoding RNA RC3H2 Facilitates Cell Proliferation and Invasion by Targeting MicroRNA-101-3p/EZH2 Axis in OSCC. *Mol Ther Nucleic Acids* (2020) 20:97–110. doi: 10.1016/j.omtn.2020.02.006
74. Jin N, Jin NQ, Bu WH, Li X, Liu LL, Wang ZL, et al. Long non-coding RNA TIRY promotes tumor metastasis by enhancing epithelial-to-mesenchymal transition in oral cancer. *Exp Biol Med* (2020) 245(7):585–96. doi: 10.1177/1535370220903673
75. Lee JM, Dedhar S, Kalluri R, Thompson EW. The epithelial-mesenchymal transition: new insights in signaling, development, and disease. *J Cell Biol* (2006) 172(7):973–81. doi: 10.1083/jcb.200601018
76. Xia E, Shen Y, Bhandari A, Zhou X, Wang Y, Yang F, et al. Long non-coding RNA LINC00673 promotes breast cancer proliferation and metastasis through regulating B7-H6 and epithelial-mesenchymal transition. *Am J Cancer Res* (2018) 8(7):1273–87.
77. Velmurugan BK, Yeh KT, Hsieh MJ, Yeh CM, Lin CC, Kao CY, et al. UNC13C Suppress Tumor Progression via Inhibiting EMT Pathway and Improves Survival in Oral Squamous Cell Carcinoma. *Front Oncol* (2019) 9:728:728. doi: 10.3389/fonc.2019.00728
78. Zhang Q, Li Y, Zhao R, Wang X, Fan C, Xu Y, et al. The gain-of-function mutation E76K in SHP2 promotes CAC tumorigenesis and induces EMT via the Wnt/beta-catenin signaling pathway. *Mol Carcinog* (2018) 57(5):619–28. doi: 10.1002/mc.22785
79. Yi Y, Wang Z, Sun Y, Chen J, Zhang B, Wu M, et al. The EMT-related transcription factor snail up-regulates FAPalpha in malignant melanoma cells. *Exp Cell Res* (2018) 364(2):160–7. doi: 10.1016/j.yexcr.2018.01.039
80. Xue M, Chen LY, Wang WJ, Su TT, Shi LH, Wang L, et al. HOTAIR induces the ubiquitination of Runx3 by interacting with Mex3b and enhances the invasion of gastric cancer cells. *Gastric Cancer* (2018) 21(5):756–64. doi: 10.1007/s10120-018-0801-6
81. Li Y, Chen F, Shen W, Li B, Xiang R, Qu L, et al. WDR74 induces nuclear β-catenin accumulation and activates Wnt-responsive genes to promote lung cancer growth and metastasis. *Cancer Lett* (2020) 471:103–15. doi: 10.1016/j.canlet.2019.12.011
82. He Y, Davies CM, Harrington BS, Hellmers L, Sheng Y, Broomfield A, et al. CDCP1 enhances Wnt signaling in colorectal cancer promoting nuclear

localization of β-catenin and E-cadherin. *Oncogene* (2020) 39(1):219–33. doi: 10.1038/s41388-019-0983-3
83. Eyre R, Alférez DG, Santiago-Gómez A, Spence K, McConnell JC, Hart C, et al. Microenvironmental IL1β promotes breast cancer metastatic colonisation in the bone via activation of Wnt signalling. *Nat Commun* (2019) 10(1):5016. doi: 10.1038/s41467-019-12807-0
84. Li BQ, Liang ZY, Seery S, Liu QF, You L, Zhang TP, et al. WT1 associated protein promotes metastasis and chemo-resistance to gemcitabine by stabilizing Fak mRNA in pancreatic cancer. *Cancer Lett* (2019) 451:48–57. doi: 10.1016/j.canlet.2019.02.043
85. Zhang X, Wang S, Wang H, Cao J, Huang X, Chen Z, et al. Circular RNA circNRIP1 acts as a microRNA-149-5p sponge to promote gastric cancer progression via the AKT1/mTOR pathway. *Mol Cancer* (2019) 18(1):20. doi: 10.1186/s12943-018-0935-5
86. Huang K, Liang Q, Zhou Y, Jiang LL, Gu WM, Luo MY, et al. A Novel Allosteric Inhibitor of Phosphoglycerate Mutase 1 Suppresses Growth and Metastasis of Non-Small-Cell Lung Cancer. *Cell Metab* (2019) 30(6):1107–19.e8. doi: 10.1016/j.cmet.2019.09.014
87. Dimitrakopoulos FD, Kottorou AE, Kalofonou M, Kalofonos HP. The Fire Within: NF-κB Involvement in Non-Small Cell Lung Cancer. *Cancer Res* (2020) 80(19):4025–36. doi: 10.1158/0008-5472.Can-19-3578
88. Khan H, Ullah H, Castilho P, Gomila AS, D'Onofrio G, Filosa R, et al. Targeting NF-κB signaling pathway in cancer by dietary polyphenols. *Crit Rev Food Sci Nutr* (2020) 60(16):2790–800. doi: 10.1080/10408398.2019.1661827
89. Zheng J, Zhang H, Ma R, Liu H, Gao P. Long non-coding RNA KRT19P3 suppresses proliferation and metastasis through COPS7A-mediated NF-κB pathway in gastric cancer. *Oncogene* (2019) 38(45):7073–88. doi: 10.1038/s41388-019-0934-z
90. Su K, Zhao Q, Bian A, Wang C, Cai Y, Zhang Y. A novel positive feedback regulation between long noncoding RNA UICC and IL-6/STAT3 signaling promotes cervical cancer progression. *Am J Cancer Res* (2018) 8(7):1176–89.
91. Alves A, Diel L, Ramos G, Pinto A, Bernardi L, Yates J, et al. Tumor microenvironment and Oral Squamous Cell Carcinoma: A crosstalk between the inflammatory state and tumor cell migration. *Oral Oncol* (2020) 112:105038. doi: 10.1016/j.oraloncology.2020.105038
92. Qu Y, He Y, Yang Y, Li S, An W, Li Z, et al. ALDH3A1 acts as a prognostic biomarker and inhibits the epithelial mesenchymal transition of oral squamous cell carcinoma through IL-6/STAT3 signaling pathway. *J Cancer* (2020) 11(9):2621–31. doi: 10.7150/jca.40171
93. Tripathi V, Ellis JD, Shen Z, Song DY, Pan Q, Watt AT, et al. The nuclear-retained noncoding RNA MALAT1 regulates alternative splicing by modulating SR splicing factor phosphorylation. *Mol Cell* (2010) 39 (6):925–38. doi: 10.1016/j.molcel.2010.08.011
94. Li GQ, Fang YX, Liu Y, Meng FR, Wu X, Zhang CW, et al. MALAT1-Driven Inhibition of Wnt Signal Impedes Proliferation and Inflammation in Fibroblast-Like Synoviocytes Through CTNNB1 Promoter Methylation in Rheumatoid Arthritis. *Hum Gene Ther* (2019) 30(8):1008–22. doi: 10.1089/hum.2018.212
95. Lin N, Yao Z, Xu M, Chen J, Lu Y, Yuan L, et al. Long noncoding RNA MALAT1 potentiates growth and inhibits senescence by antagonizing ABI3BP in gallbladder cancer cells. *J Exp Clin Cancer Res CR* (2019) 38 (1):244. doi: 10.1186/s13046-019-1237-5
96. Jin D, Guo J, Wu Y, Du J, Yang L, Wang X, et al. m(6)A mRNA methylation initiated by METTL3 directly promotes YAP translation and increases YAP activity by regulating the MALAT1-miR-1914-3p-YAP axis to induce NSCLC drug resistance and metastasis. *J Hematol Oncol* (2019) 12(1):135. doi: 10.1186/s13045-019-0830-6
97. Yoshimura H, Matsuda Y, Yamamoto M, Michishita M, Takahashi K, Sasaki N, et al. Reduced expression of the H19 long non-coding RNA inhibits pancreatic cancer metastasis. *Lab Invest J Tech Methods Pathol* (2018) 98(6):814–24. doi: 10.1038/s41374-018-0048-1
98. Zhang Y, Zhu R, Wang J, Cui Z, Wang Y, Zhao Y. Upregulation of lncRNA H19 promotes nasopharyngeal carcinoma proliferation and metastasis in let-7 dependent manner. *Artif Cells Nanomed Biotechnol* (2019) 47(1):3854–61. doi: 10.1080/21691401.2019.1669618
99. Zhou Y, Zhang Y. Inhibition of LncRNAH19 has the effect of anti-tumour and enhancing sensitivity to Gefitinib and Chemotherapy in Non-small-cell lung cancer in vivo. *J Cell Mol Med* (2020) 24(10):5811–6. doi: 10.1111/jcmm.15245
100. Lv M, Zhong Z, Huang M, Tian Q, Jiang R, Chen J. lncRNA H19 regulates epithelial-mesenchymal transition and metastasis of bladder cancer by miR-29b-3p as competing endogenous RNA. *Biochim Biophys Acta Mol Cell Res* (2017) 1864(10):1887–99. doi: 10.1016/j.bbamcr.2017.08.001
101. Zhou W, Ye XL, Xu J, Cao MG, Fang ZY, Li LY, et al. The lncRNA H19 mediates breast cancer cell plasticity during EMT and MET plasticity by differentially sponging miR-200b/c and let-7b. *Sci Signal* (2017) 10(483): eaak9557. doi: 10.1126/scisignal.aak9557
102. Zhu Y, Chen P, Gao Y, Ta N, Zhang Y, Cai J, et al. MEG3 Activated by Vitamin D Inhibits Colorectal Cancer Cells Proliferation and Migration via Regulating Clusterin. *EBioMedicine* (2018) 30:148–57. doi: 10.1016/j.ebiom.2018.03.032
103. Huang C, Liao X, Jin H, Xie F, Zheng F, Li J, et al. MEG3, as a Competing Endogenous RNA, Binds with miR-27a to Promote PHLPP2 Protein Translation and Impairs Bladder Cancer Invasion. *Mol Ther Nucleic Acids* (2019) 16:51–62. doi: 10.1016/j.omtn.2019.01.014
104. Zhou H, Tang K, Liu H, Zeng J, Li H, Yan L, et al. Regulatory Network of Two Tumor-Suppressive Noncoding RNAs Interferes with the Growth and Metastasis of Renal Cell Carcinoma. *Mol Ther Nucleic Acids* (2019) 16:554–65. doi: 10.1016/j.omtn.2019.04.005
105. Cai Q, Wang ZQ, Wang SH, Li C, Zhu ZG, Quan ZW, et al. Upregulation of long non-coding RNA LINC00152 by SP1 contributes to gallbladder cancer cell growth and tumor metastasis via PI3K/AKT pathway. *Am J Trans Res* (2016) 8(10):4068–81.
106. Ou C, Sun Z, He X, Li X, Fan S, Zheng X, et al. Targeting YAP1/LINC00152/FSCN1 Signaling Axis Prevents the Progression of Colorectal Cancer. *Adv Sci (Weinh)* (2020) 7(3):1901380. doi: 10.1002/advs.201901380
107. Yue B, Liu C, Sun H, Liu M, Song C, Cui R, et al. A Positive Feed-Forward Loop between LncRNA-CYTOR and Wnt/β-Catenin Signaling Promotes Metastasis of Colon Cancer. *Mol Ther* (2018) 26(5):1287–98. doi: 10.1016/j.ymthe.2018.02.024
108. Shi Y, Sun H. Down-regulation of lncRNA LINC00152 Suppresses Gastric Cancer Cell Migration and Invasion Through Inhibition of the ERK/MAPK Signaling Pathway. *Onco Targets Ther* (2020) 13:2115–24. doi: 10.2147/ott.S217452
109. Yu JJ, Liu Y, Guo C, Zhang SS, Gong ZJ, Tang YY, et al. Upregulated long non-coding RNA LINC00152 expression is associated with progression and poor prognosis of tongue squamous cell carcinoma. *J Cancer* (2017) 8 (4):523–30. doi: 10.7150/jca.17510
110. Wang XS, Zhang Z, Wang HC, Cai JL, Xu QW, Li MQ, et al. Rapid identification of UCA1 as a very sensitive and specific unique marker for human bladder carcinoma. *Clin Cancer Res* (2006) 12(16):4851–8. doi: 10.1158/1078-0432.Ccr-06-0134
111. Xue M, Chen W, Xiang A, Wang R, Chen H, Pan J, et al. Hypoxic exosomes facilitate bladder tumor growth and development through transferring long non-coding RNA-UCA1. *Mol Cancer* (2017) 16(1):143. doi: 10.1186/s12943-017-0714-8
112. Gong P, Qiao F, Wu H, Cui H, Li Y, Zheng Y, et al. LncRNA UCA1 promotes tumor metastasis by inducing miR-203/ZEB2 axis in gastric cancer. *Cell Death Dis* (2018) 9(12):1158. doi: 10.1038/s41419-018-1170-0
113. Su Y, Zhou Y, Sun YJ, Wang YL, Yin JY, Huang YJ, et al. Macrophage-derived CCL18 promotes osteosarcoma proliferation and migration by upregulating the expression of UCA1. *J Mol Med (Berlin Germany)* (2019) 97(1):49–61. doi: 10.1007/s00109-018-1711-0
114. Li GY, Wang W, Sun JY, Xin B, Zhang X, Wang T, et al. Long non-coding RNAs AC026904.1 and UCA1: a "one-two punch" for TGF-β-induced SNAI2 activation and epithelial-mesenchymal transition in breast cancer. *Theranostics* (2018) 8(10):2846–61. doi: 10.7150/thno.23463
115. Fang Z, Wu L, Wang L, Yang Y, Meng Y, Yang H. Increased expression of the long non-coding RNA UCA1 in tongue squamous cell carcinomas: a possible correlation with cancer metastasis. *Oral Surg Oral Med Oral Pathol Oral Radiol* (2014) 117(1):89–95. doi: 10.1016/j.oooo.2013.09.007
116. Shen X, Hu X, Mao J, Wu Y, Liu H, Shen J, et al. The long noncoding RNA TUG1 is required for TGF-β/TWIST1/EMT-mediated metastasis in colorectal cancer cells. *Cell Death Dis* (2020) 11(1):65. doi: 10.1038/s41419-020-2254-1

117. Yu X, Hu L, Li S, Shen J, Wang D, Xu R, et al. Long non-coding RNA Taurine upregulated gene 1 promotes osteosarcoma cell metastasis by mediating HIF-1α via miR-143-5p. *Cell Death Dis* (2019) 10(4):280. doi: 10.1038/s41419-019-1509-1
118. Lin YH, Wu MH, Huang YH, Yeh CT, Cheng ML, Chi HC, et al. Taurine up-regulated gene 1 functions as a master regulator to coordinate glycolysis and metastasis in hepatocellular carcinoma. *Hepatology* (2018) 67(1):188–203. doi: 10.1002/hep.29462
119. Yang CZ, Ma J, Zhu DW, Liu Y, Montgomery B, Wang LZ, et al. GDF15 is a potential predictive biomarker for TPF induction chemotherapy and promotes tumorigenesis and progression in oral squamous cell carcinoma. *Ann Oncol* (2014) 25(6):1215–22. doi: 10.1093/annonc/mdu120
120. Zhang H, Zhao L, Wang YX, Xi M, Liu SL, Luo LL. Long non-coding RNA HOTTIP is correlated with progression and prognosis in tongue squamous cell carcinoma. *Tumour Biol* (2015) 36(11):8805–9. doi: 10.1007/s13277-015-3645-2
121. Wang FW, Cao CH, Han K, Zhao YX, Cai MY, Xiang ZC, et al. APC-activated long noncoding RNA inhibits colorectal carcinoma pathogenesis through reduction of exosome production. *J Clin Invest* (2019) 129(2):727–43. doi: 10.1172/jci122478
122. Deng SJ, Chen HY, Ye Z, Deng SC, Zhu S, Zeng Z, et al. Hypoxia-induced LncRNA-BX111 promotes metastasis and progression of pancreatic cancer through regulating ZEB1 transcription. *Oncogene* (2018) 37(44):5811–28. doi: 10.1038/s41388-018-0382-1
123. Snellenberg S, Cillessen SA, Van Criekinge W, Bosch L, Meijer CJ, Snijders PJ, et al. Methylation-mediated repression of PRDM14 contributes to apoptosis evasion in HPV-positive cancers. *Carcinogenesis* (2014) 35 (11):2611–8. doi: 10.1093/carcin/bgu197
124. Wu T, Dai Y. Tumor microenvironment and therapeutic response. *Cancer Lett* (2017) 387:61–8. doi: 10.1016/j.canlet.2016.01.043
125. Jackstadt R, van Hooff SR, Leach JD, Cortes-Lavaud X, Lohuis JO, Ridgway RA, et al. Epithelial NOTCH Signaling Rewires the Tumor Microenvironment of Colorectal Cancer to Drive Poor-Prognosis Subtypes and Metastasis. *Cancer Cell* (2019) 36(3):319–36. doi: 10.1016/j.ccell.2019.08.003
126. Zanconato F, Cordenonsi M, Piccolo S. YAP and TAZ: a signalling hub of the tumour microenvironment. *Nat Rev Cancer* (2019) 19(8):454–64. doi: 10.1038/s41568-019-0168-y
127. Jiang E, Xu Z, Wang M, Yan T, Huang C, Zhou X, et al. Tumoral microvesicle-activated glycometabolic reprogramming in fibroblasts promotes the progression of oral squamous cell carcinoma. *FASEB J* (2019) 33(4):5690–703. doi: 10.1096/fj.201802226R
128. Kong J, Tian H, Zhang F, Zhang Z, Li J, Liu X, et al. Extracellular vesicles of carcinoma-associated fibroblasts creates a pre-metastatic niche in the lung through activating fibroblasts. *Mol Cancer* (2019) 18(1):175. doi: 10.1186/s12943-019-1101-4
129. Ren Y, Jia HH, Xu YQ, Zhou X, Zhao XH, Wang YF, et al. Paracrine and epigenetic control of CAF-induced metastasis: the role of HOTAIR stimulated by TGF-ß1 secretion. *Mol Cancer* (2018) 17(1):5. doi: 10.1186/s12943-018-0758-4
130. Zhao L, Ji G, Le X, Wang C, Xu L, Feng M, et al. Long Noncoding RNA LINC00092 Acts in Cancer-Associated Fibroblasts to Drive Glycolysis and Progression of Ovarian Cancer. *Cancer Res* (2017) 77(6):1369–82. doi: 10.1158/0008-5472.Can-16-1615
131. Ren J, Ding L, Zhang D, Shi G, Xu Q, Shen S, et al. Carcinoma-associated fibroblasts promote the stemness and chemoresistance of colorectal cancer by transferring exosomal lncRNA H19. *Theranostics* (2018) 8(14):3932–48. doi: 10.7150/thno.25541
132. Cen B, Lang JD, Du Y, Wei J, Xiong Y, Bradley N, et al. Prostaglandin E(2) Induces miR675-5p to Promote Colorectal Tumor Metastasis via Modulation of p53 Expression. *Gastroenterology* (2020) 158(4):971–84. doi: 10.1053/j.gastro.2019.11.013
133. Chen C, Luo Y, He W, Zhao Y, Kong Y, Liu H, et al. Exosomal long noncoding RNA LNMAT2 promotes lymphatic metastasis in bladder cancer. *J Clin Invest* (2020) 130(1):404–21. doi: 10.1172/jci130892
134. Liang ZX, Liu HS, Wang FW, Xiong L, Zhou C, Hu T, et al. LncRNA RPPH1 promotes colorectal cancer metastasis by interacting with TUBB3 and by promoting exosomes-mediated macrophage M2 polarization. *Cell Death Dis* (2019) 10(11):829. doi: 10.1038/s41419-019-2077-0
135. Chen CW, Fu M, Du ZH, Zhao F, Yang WW, Xu LH, et al. Long Noncoding RNA MRPL23-AS1 Promoteoid Cystic Carcinoma Lung Metastasis. *Cancer Res* (2020) 88(11):2273–85. doi: 10.1158/0008-5472.Can-19-0819
136. O'Brien K, Breyne K, Ughetto S, Laurent LC, Breakefield XO. RNA delivery by extracellular vesicles in mammalian cells and its applications. *Nat Rev Mol Cell Biol* (2020) 22(10):585–606. doi: 10.1038/s41580-020-0251-y
137. Li X, Lv X, Li Z, Li C, Li X, Xiao J, et al. Long Noncoding RNA ASLNC07322 Functions in VEGF-C Expression Regulated by Smad4 during Colon Cancer Metastasis. *Mol Ther Nucleic Acids* (2019) 18:851–62. doi: 10.1016/j.omtn.2019.10.012
138. Huang YL, Liang CY, Ritz D, Coelho R, Septiadi D, Estermann M, et al. Collagen-rich omentum is a premetastatic niche for integrin α2-mediated peritoneal metastasis. *Elife* (2020) 9:e59442. doi: 10.7554/eLife.59442

Conflict of Interest: The authors declare that the research was conducted in the absence of any commercial or financial relationships that could be construed as a potential conflict of interest.

Copyright © 2021 Xu, Jiang, Shao and Shang. This is an open-access article distributed under the terms of the Creative Commons Attribution License (CC BY). The use, distribution or reproduction in other forums is permitted, provided the original author(s) and the copyright owner(s) are credited and that the original publication in this journal is cited, in accordance with accepted academic practice. No use, distribution or reproduction is permitted which does not comply with these terms.

frontiers in Oncology

ORIGINAL RESEARCH
published: 26 January 2021
doi: 10.3389/fonc.2020.603864

Identification of Three Autophagy-Related Long Non-Coding RNAs as a Novel Head and Neck Squamous Cell Carcinoma Prognostic Signature

Ya Guo[*†], *Peng Tao Yang*[†], *Zhong Wei Wang*, *Kun Xu*, *Wei Hua Kou* and *Heng Luo*

Department of Radiation Oncology, Second Affiliated Hospital, Xi'an Jiaotong University, Xi'an, China

Head and neck squamous cell carcinoma (HNSCC) has a poor prognosis. Considerable evidence indicates that autophagy and non-coding RNA play essential roles in the biological processes involved in cancers, but associations between autophagy-related long non-coding RNAs (lncRNAs) and HNSCC remain unclear. In the present study, HNSCC RNA sequences and autophagy-related gene data were extracted from The Cancer Genome Atlas database and the Human Autophagy Database. A total of 1,153 autophagy-related lncRNAs were selected *via* calculating Pearson's correlation coefficient. Three prognosis-related autophagy lncRNAs were identified *via* univariate Cox regression, least absolute shrinkage and selection operator analysis, and multivariate Cox regression analysis. We also constructed a prognostic model based on these autophagy-related lncRNAs and evaluated its ability to accurately and independently predict the prognosis of HNSCC patients. The area under the curve (AUC) was 0.864 (3-year) and 0.836 (5-year), and our model can independently predict the prognosis of HNSCC. The prognostic value of the three autophagy lncRNAs was confirmed *via* analysis of samples from five databases. To further identify the functions of the three lncRNAs, a co-expression network was constructed and pathway analysis was performed. In that analysis the lncRNAs were correlated with 189 related genes and 20 autophagy-related genes, and these lncRNAs mainly involved homologous recombination, the Fanconi anemia pathway, the autophagy-related pathway, and immune-related pathways. In addition, we validated the expression levels of three lncRNAs and autophagy markers (ATG12, BECN1, and MAP1LC3B) based on TIMER, Oncomine, and HPA database analysis. Our results indicated that TTTY15 was increased in HPV positive and HPV negative HNSCC patients, and three autophagy markers were up-regulated in all HNSCCC patients. Lastly, association between three lncRNAs and autophagy markers was performed, and our results showed that TTTY15 and MIF-AS1 were associated with autophagy markers. Collectively, these results suggested that three autophagy-related lncRNAs have prognostic value in HNSCC patients.

Keywords: head and neck squamous cell carcinoma, autophagy, long non-coding RNA, prognosis, The Cancer Genome Atlas

OPEN ACCESS

Edited by:
Wei Cao,
Shanghai Jiao Tong University, China

Reviewed by:
Zheqi Liu,
Shanghai Jiao Tong University, China
Xin Zou,
Shanghai Jiaotong University, China

***Correspondence:**
Ya Guo
gy8569851@163.com

[†]*These authors share first authorship*

Specialty section:
This article was submitted to Head and Neck Cancer, a section of the journal Frontiers in Oncology

Received: *08 September 2020*
Accepted: *09 November 2020*
Published: *26 January 2021*

Citation:
Guo Y, Yang PT, Wang ZW, Xu K, Kou WH and Luo H (2021) Identification of Three Autophagy-Related Long Non-Coding RNAs as a Novel Head and Neck Squamous Cell Carcinoma Prognostic Signature. Front. Oncol. 10:603864. doi: 10.3389/fonc.2020.603864

INTRODUCTION

Head and neck squamous cell carcinoma (HNSCC) is the sixth most common cancer in the world and accounts for more than 90% of head and neck cancers (1). Advances in surgical treatment combined with radiotherapy, chemotherapy, or biotherapy have resulted in improved HNSCC prognoses, but advanced-stage HNSCC is still associated with an unfavorable prognosis and a high mortality rate (2, 3). Prognoses are mainly based on the TNM classification system, but that system currently does not incorporate enough information from which to derive accurate prognosis (4). Therefore, the identification of effective biomarkers for early diagnosis, assessment, and prognosis of HNSCC is essential.

Autophagy is a self-degradative process that maintains cellular homeostasis. It plays complex roles at different stages of tumorigenesis, and it may promote oncogenesis in some contexts but participate in tumor suppression in others (5). Clarifying the mechanisms involved in autophagy may contribute to the development of new cancer treatment strategies. Several studies suggest that inhibiting autophagy in patients with advanced cancers may enhance the treatment of malignancy, and that the promotion of autophagy in HNSCC can protect cells (6). Therefore, further attention to elucidate the roles and clarify the mechanisms of autophagy in HNSCC is needed.

Long non-coding RNAs (lncRNAs) are defined as non-coding RNAs that are ≥ 200 nucleotides in length, and they are reportedly associated with HNSCC prognosis (5, 7). Previous studies suggest that lncRNAs have an important role in the regulation of autophagy *via* the mediation of autophagy-related gene (ATG) expression (8, 9). Increasing evidence indicates that autophagy and lncRNAs play a key role in tumorigenesis and cancer cell survival, but whether lncRNAs modulate autophagy in HNSCC remains unknown, and the molecular mechanisms involved in autophagy-related lncRNA in HNSCC have not been elucidated (10).

The aim of the present study was to identify autophagy-related lncRNAs, and evaluate their prognostic value with respect to HNSCC. HNSCC RNA sequencing and ATG data from The Cancer Genome Atlas (TCGA) database and the Human Autophagy Database were extracted and analyzed to identify autophagy-related lncRNAs (11, 12). Univariate Cox regression analysis and least absolute shrinkage and selection operator analysis were performed to identify key autophagy related lncRNAs, which were then used to construct a prognostic model using multivariate Cox regression analysis. Receiver operating characteristic (ROC) curves and Kaplan-Meier survival curves were plotted, and concordance indexes were calculated to evaluate the prognostic accuracy of the models. The prognostic value of three lncRNAs was then investigated *via* analyses incorporating five databases. To putatively predict the function of these three lncRNAs, a co-expression network was constructed and pathway analysis was performed. Moreover, the mRNA and protein expression of three lncRNAs and autophagy markers ATG12, BECN1, and MAP1LC3B were measured through analysis in Tumor Immune Estimation Resource (TIMER), Oncomine, and Human Protein Atlas (HPA) database. Lastly, we analyzed the correlation between three lncRNAs and autophagy makers.

MATERIALS AND METHODS

Data Collection and Preparation

Raw RNA sequencing data and corresponding clinical data from HNSCC patients were obtained from the TCGA database (https://portal.gdc.cancer.gov/) (11). These HNSCC samples were mainly derived from patients with laryngeal cancer, nasopharyngeal cancer, tonsil cancer, and lip cancer. As well as 155 HNSCC samples, the gene expression profiles of 12 normal control samples were included in the study. Data post-processing and clinical information extraction were performed using a programming language (strawberry-perl-5.32.0.1-64bit.msi, http://www.perl.org) (13). Protein-coding genes and lncRNAs were annotated and classified using Ensembl human genome browser GRCh38.p13 (http://asia.ensembl.org/index.html) (14). Prior to assessing the prognostic value of the autophagy-related lncRNAs, survival time and survival status data were merged with autophagy-related lncRNA expression data. The study excluded repeated samples and survival times of patients more than 30 days. Because the study data were obtained from the TCGA database, no ethics committee approval or patient consent was required.

Identification of Autophagy-Related lncRNAs

Autophagy-related genes (ATGs) were downloaded from the Human Autophagy Database (http://www.autophagy.lu/) (12). Pearson's correlational coefficients were calculated to assess associations between lncRNA expression and ATGs. lncRNAs with correlational coefficients > 0.3 and p values < 0.001 were deemed to be putatively autophagy-related lncRNAs.

Autophagy-Related lncRNA Prognostic Model Construction

Univariate Cox regression was used to assess associations between autophagy-related lncRNA expression and overall survival using the "survival" software package in R (cran.r-project.org/web/packages/survival/index.html). A significant difference was defined as $p < 0.05$. LASSO regression was performed based on the results of univariate Cox regression analysis using the survival software and the "glmnet" software package (https://cran.rproject.org/web/packages/glmnet/index.html). After the identification of prognosis-related lncRNAs *via* LASSO regression analysis, multivariate Cox regression analysis with stepwise selection to identify optimal prognostic autophagy related lncRNAs according to Akaike information criterion (AIC) value (15). We then calculated a risk score for each patient (16). HNSCC patients were divided into high-risk ($n = 77$) and low-risk ($n = 77$) groups based on the median risk score. To investigate relationships between prognosis and expression levels of the autophagy-related lncRNAs identified,

Kaplan-Meier survival curves were then plotted for three key lncRNAs. Based on average expression levels of candidate lncRNAs, HNSCC patients were divided into high and low expression groups.

Evaluation of Accuracy of Our Model

Kaplan-Meier survival curves were plotted to compare the difference in overall survival between the low-risk and high-risk groups using the survival package (17). Using the survival and time ROC (cran.r-project.org/web/packages/timeROC/index.html) software packages, 3-year and 5-year ROC curves were generated, and areas under the curves (AUCs) and concordance indexes were calculated to investigate the predictive capacity of the prognostic model (18). AUC values range from 0.5 to 1.0. AUC: 0.5 means without any predictive power; AUC: 0.5–0.7 represents low accuracy; AUC: 0.7–0.9 means medium accuracy; AUC > 0.9 represents high accuracy. Concordance index values range from 0.5 to 1.0. Univariate and multivariate Cox regression analyses were used to determine whether risk score was independent of other clinical characteristics (age, sex, grade, stage) for the prediction of HNSCC prognosis. HR>1 and p-value<0.05 represent poor prognostic factors. HR<1 and p-value<0.05 represent favorable prognostic factors.

Validation of the Prognostic Value of Three Autophagy-Related lncRNAs

The Gene Expression Profiling Interactive Analysis database (GEPIA; http://gepia.cancerpku.cn/detail.php) is a web server tool based on TCGA and GTEx data that can be used to conduct patient survival analysis, differential expression analysis, and correlational analysis, among other things (19). The Head and Neck Cancer database (http://hncdb.canceromics.org/) is a comprehensive source that includes head and neck cancer-related genes and an expression analysis platform. Lnc2Cancer (http://www.bio-bigdata.net/lnc2cancer/) is a database that provides comprehensive experimentally supported associations between lncRNA and human cancer (20). The Online Consensus Survival for Head and Neck Squamous Cell Carcinoma database (OShnscc, http://bioinfo.henu.edu.cn/HNSC/HNSCList.jsp) is an online prognostic biomarker analysis tool for head and neck squamous cell carcinoma (21). UALCAN (http://ualcan.path.uab.edu/) is a user-friendly web resource for analyzing cancer OMICS data that allows the user to analyze associations between gene expression and patient survival (22). In the present study the GEPIA, Head and Neck Cancer database, Lnc2cancer, OShnscc, and UALCAN resources were used to investigate the prognostic value of the lncRNAs identified. $P < 0.05$ was considered statistically significant.

Co-expression and Function Enrichment Analysis

To investigate the function of three autophagy-related lncRNAs and the potential mechanisms involved in the effects of these lncRNAs on HNSCC prognosis, associations between the expression levels of the lncRNAs and protein coding genes (PCGs) were assessed using R software. Pearson's correlational coefficient > 0.4 and $p < 0.001$ were considered to indicate significant correlations. A visual co-expression network reflecting the three autophagy-related lncRNAs and PCG co-expression was generated *via* Cytoscape software (version 3.7.2) (18). To assess associations between the three lncRNAs, PCGs, and risk status the "ggalluvial" component of the R package was used to visualize interaction modules between them (23). Lastly, gene ontology and Kyoto Encyclopedia of Genes and Genomes (KEGG) enrichment analyses were performed on three lncRNA-related PCGs using Metascape and the R package (24). $P < 0.05$ was considered significant in gene ontology and KEGG pathway analyses. Enriched gene ontology terms and KEGG pathways were defined as the potential functional terms of the three lncRNAs.

Associations Between Three lncRNAs and Autophagy-Related Pathway

Associations between three lncRNAs and ATGs were investigated by calculating Pearson's correlational coefficients. Sankey plots were then constructed to visualize association networks between the three lncRNAs, ATGs, and risk status. Gene ontology and KEGG pathway analyses of the three lncRNA-related ATGs were conducted using Metascape (http://metascape.org/gp/index.html) (24). $P < 0.05$ was considered statistically significant.

Confirmation of the Expression of Three lncRNAs and Autophagy Makers and Evaluation of Their Correlation

The mRNA expression level of three lncRNAs and autophagy markers ATG12, BECN1, and MAP1LC3B were examined through analysis DiffExp module of TIMER database (https://cistrome.shinyapps.io/timer/) and Oncomine database (http://www.oncomine.org) (25, 26). The protein expression level of these makers were compared between HNSCC and normal tissues using HPA database (https://www.proteinatlas.org/) (27). Association analyses between three lncRNAs and autophagy related genes was also performed by GEPIA database and correlation module of TIMER database (19, 25).

Statistical Analysis

Data were processed using the PERL language (strawberry-perl-5.32.0.1-64bit.msi, http://www.perl.org). All statistical analyses were conducted using R software (version 3.6.3, https://www.r-project.org/). $P < 0.05$ was considered statistically significant.

RESULTS

Identification of Autophagy-Related lncRNAs

The analysis procedure of the current study is shown in **Supplementary Material 1**. A total of 14,142 lncRNAs were identified by analyzing RNA sequence data from HNSCC patient tissue samples in the TCGA database, and 232 ATGs were extracted

from the Human Autophagy Database (**Supplementary Material 2**). From the initial dataset, 1,153 autophagy-related lncRNAs were selected by calculating Pearson's correlational coefficients between the lncRNAs and the ATGs (**Supplementary Material 3**).

Establishment of a Three-Autophagy-Related lncRNA Prognostic Signature

In univariate Cox regression analysis of 1,153 autophagy-related lncRNAs, 19 autophagy-related lncRNAs were significantly associated with HNSCC prognosis ($p < 0.05$, **Table 1**). LASSO regression analysis was conducted to assess the correlations between these 19 lncRNAs and survival. That analysis indicated that 13 lncRNAs had prognostic value (**Figures 1A, B**). In multivariate Cox regression analysis three autophagy-related lncRNAs were significantly correlated with HNSCC prognosis; AL121899.1, TTTY15, and MIF-AS1 (**Figure 1C**). AL121899.1 was considered a risk factor with a hazard ratio (HR) > 1, and TTTY15 and MIF-AS1 were considered protective factors with hazard ratios < 1. In Kaplan-Meier survival curve analysis of the three autophagy-related lncRNAs AL121899.1 overexpression was correlated with a poor prognosis, and high expressions of TTTY15 and MIF-AS were associated with a good prognosis (**Figures 1D–F**).

Evaluation of the Prognostic Model

Risk scores were calculated for each HNSCC patient, and the patients were divided into high-risk ($n = 77$) and low-risk ($n = 77$) groups based on the median risk score. HNSCC patients were ranked based on risk scores, and survival rate was significantly associated with risk score (**Figure 2A**). The survival time of patients with higher risk scores was lower than that of patients with low risk scores (**Figure 2B**). Heat mapping indicated that three autophagy-related lncRNAs were significantly differentially expressed in the high-risk group and the low-risk group (**Figure 2C**). AL121899.1 expression was higher in high-risk patients than in low-risk patients, and TTTY15 and MIF-AS expression were lower in high-risk patients than in low-risk patients. In Kaplan-Meier survival analysis patients with low risk scores survived significantly longer than those with high risk scores (**Figure 2D**). To assess the predictive value of the prognostic model, 3-year and 5-year ROC curves were plotted and the concordance index was calculated. The AUC values were 0.864 (3-year ROC) and 0.836 (5-year ROC), and the concordance index was 0.743 (**Figure 2E**). This result suggested that our model had a medium accuracy to evaluate the prognosis of head and neck squamous cell carcinoma patients. Univariate and multivariate Cox regression analyses demonstrated that risk score was an independent predictor of a poor prognosis in HNSCC patients (**Figures 3A, B**).

Three Autophagy-Related lncRNAs Have Prognostic Value in HNSCC

Multiple databases were used to confirm the prognostic value of the aforementioned three autophagy-related lncRNAs. TTTY15 overexpression had a protective effect on overall survival in different databases, including the GEPIA, Lnc2cancer3.0, Head and Neck Cancer database, UALCAN, and OShnscc (**Figures 4A–E**, **Table 2**). These observations are fully consistent with the results of the current study. In GSE27020 analysis, high MIF-AS1 expression was associated with progression-free survival in HNSCC patients, but there were no significant correlations between MIF-AS1 overexpression and progression-free survival or overall survival in analyses of the GES31056, GSE41613, and Lnc2cancer3.0 databases (**Figures 4F–I**, **Table 2**). AL121899.1 was not found in the five aforementioned databases.

Potential Functions of the Three Autophagy-Related lncRNAs

A co-expression network including the three autophagy-related lncRNAs and PCGs was constructed to predict the function of

TABLE 1 | Prognosis-related autophagy lncRNAs by univariate Cox regression analysis.

lncRNA	KM	B	SE	HR	Low	Upper	p-value
AC073611.1	0.0032	0.5092	0.1812	1.6639	1.1664	2.3736	0.005
MIR4435-2HG	0.0008	0.3496	0.1049	1.4185	1.1548	1.7423	0.0009
AL121899.1	0.0088	0.3302	0.0776	1.3912	1.195	1.6196	0
CYTOR	0.0082	0.1949	0.052	1.2151	1.0974	1.3455	0.0002
MYOSLID	0.0082	0.0626	0.0192	1.0646	1.0253	1.1055	0.0011
LINC01139	0.0071	-0.1196	0.045	0.8872	0.8123	0.9691	0.0079
EBLN3P	0.0026	-0.1721	0.048	0.8419	0.7663	0.925	0.0003
MIR9-3HG	0.0041	-0.1789	0.062	0.8362	0.7405	0.9442	0.0039
TTTY15	0.0076	-0.4966	0.1909	0.6086	0.4187	0.8848	0.0093
LINC00324	0.0004	-0.4996	0.1848	0.6068	0.4224	0.8717	0.0069
AL035587.1	0.0001	-0.535	0.2034	0.5857	0.3931	0.8725	0.0085
AC108010.1	0.0088	-0.5403	0.2008	0.5826	0.393	0.8635	0.0071
AC091057.1	0.0009	-0.7382	0.261	0.478	0.2866	0.7972	0.0047
DTX2P1-UPK3BP1-PMS2P11	0.0002	-0.7479	0.2691	0.4733	0.2794	0.8021	0.0054
AC008763.1	0.0008	-0.8182	0.3163	0.4412	0.2374	0.8201	0.0097
MIF-AS1	0.0003	-0.8733	0.3209	0.4176	0.2226	0.7832	0.0065
ZNF436-AS1	0.0033	-0.879	0.324	0.4152	0.22	0.7836	0.0067
AC093627.4	0.0081	-0.8912	0.3316	0.4101	0.2141	0.7856	0.0072
AC098484.1	0.0048	-0.9006	0.2977	0.4063	0.2267	0.7282	0.0025

HR, Hazard ratio; lncRNA, long noncoding RNA.

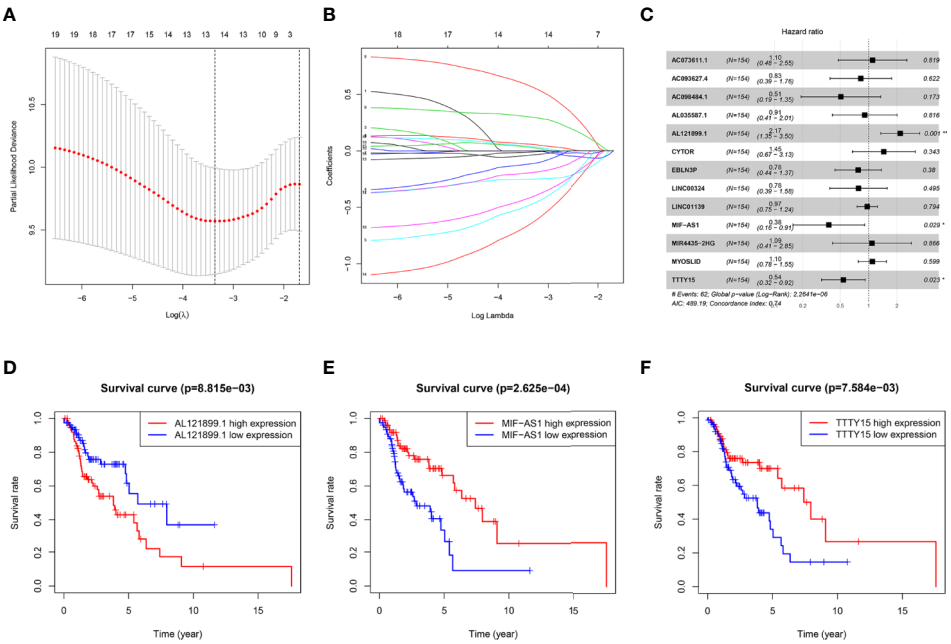

FIGURE 1 | Identification of a three-autophagy-related lncRNA prognostic signature. **(A)** Partial likelihood deviance was plotted versus log(λ). The vertical dotted line indicates the lambda value with the minimum error and the largest lambda value, where the deviance is within one standard error of the minimum. **(B)** LASSO coefficient profiles of genes associated with overall survival of head and neck squamous cell carcinoma. **(C)** Forest plot depicting associations between lncRNAs and risk value determined *via* multivariate Cox regression analysis. $^{*}p < 0.05$, $^{**}p < 0.01$. **(D–F)** Kaplan–Meier survival curves derived from three autophagy-related lncRNAs and HNSCC patients. These lncRNAs were considered to constitute a prognostic signature for HNSCC. AL121899.1 was identified as a negative prognostic factor, and TTTY15 and MIF-AS1 were identified as positive prognostic factors. **(D)** AL121899, **(E)** MIF-AS, **(F)** TTTY15.

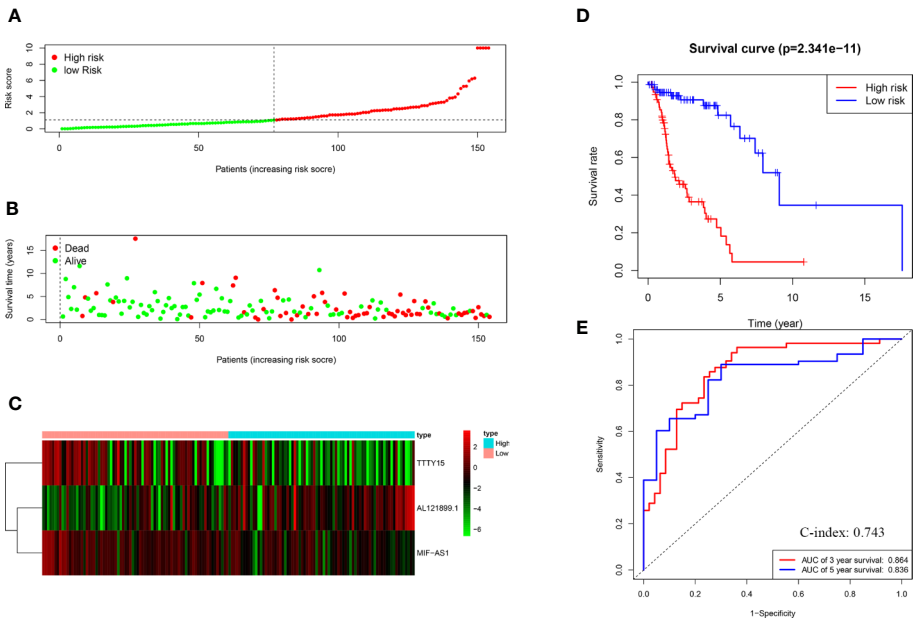

FIGURE 2 | Construction and evaluation of the risk score model. **(A)** Survival rate was significantly associated with risk score. **(B)** Scatterplot of patient survival. **(C)** Expression heatmap of three autophagy-related lncRNAs. **(D)** Kaplan-Meier survival curves of the high-risk group and the low-risk group. **(E)** ROC curve based on the risk score model. AUC: 0.5 means without any predictive power; AUC: 0.5–0.7 represents low accuracy; AUC: 0.7–0.9 means medium accuracy; AUC > 0.9 represents high accuracy.

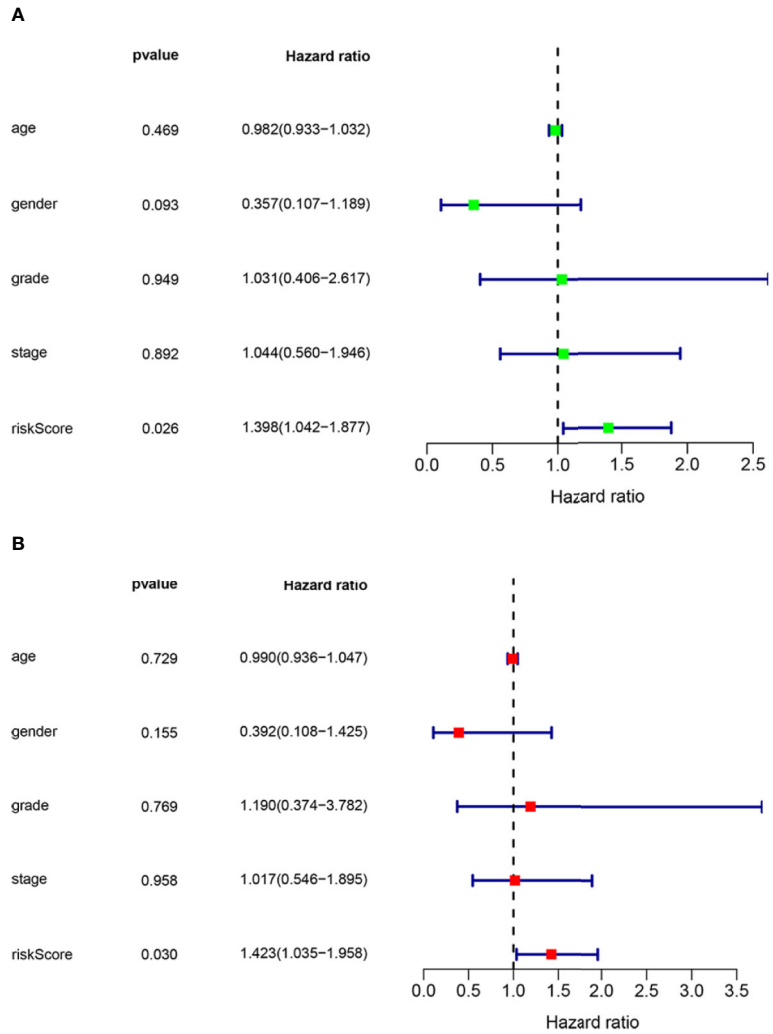

FIGURE 3 | Assessment of the independence of the HNSCC prognostic model. **(A)** Univariate analysis and **(B)** multivariate Cox regression analysis confirmed the independence of the prognostic model. HNSCC, head and neck squamous cell carcinoma. HR>1 and p-value<0.05 represent poor prognostic factors. HR<1 and p-value <0.05 represent favorable prognostic factors.

the three lncRNAs and investigate the potential mechanisms that they were involved in that affected HNSCC prognosis. The three lncRNAs interacted with 189 PCGs (**Figure 5A**). Associations between the three lncRNAs, the PCGs, and different risk types were then evaluated. TTTY15 and MIF-AS1 and their related PCGs were putative protective factors. AL121899.1 and its related PCGs were putative risk factors (**Figure 5B**). To predict the functions of the three lncRNAs, 189 PCGs were assessed *via* gene enrichment and KEGG pathway analysis. The enriched gene ontology terms were mainly involved in DNA replication, the cell cycle, DNA-dependent DNA replication, activation of ATRs in response to replication stress, cell division, the PID HNF3A pathway, and so on (**Figure 5C**). In KEGG pathway analysis 189 PCGs were mainly involved in homologous recombination and the Fanconi anemia pathway (**Figures 5D, E**). These identified gene ontology terms or KEGG pathways were considered indicative of the potential functions of the three lncRNAs.

The lncRNAs Were Associated With the Autophagy-Related Pathway

Three lncRNAs were significantly associated with 20 autophagy-related genes (**Figure 6A**). Sankey plots indicated that AL121899.1 and related ATGs were associated with an unfavorable prognosis, whereas TTTY15 and MIF-AS1 and their related ATGs were associated with a favorable prognosis (**Figure 6B**). Gene ontology and KEGG pathway analysis indicated that the ATGs were mainly involved in measles, autophagy, the P53 pathway, the PID MTOR pathway, the nuclear factor kappa B signaling pathway, regulation of mitogen-activated protein kinase activity, and the immune related pathway (**Figure 6C**).

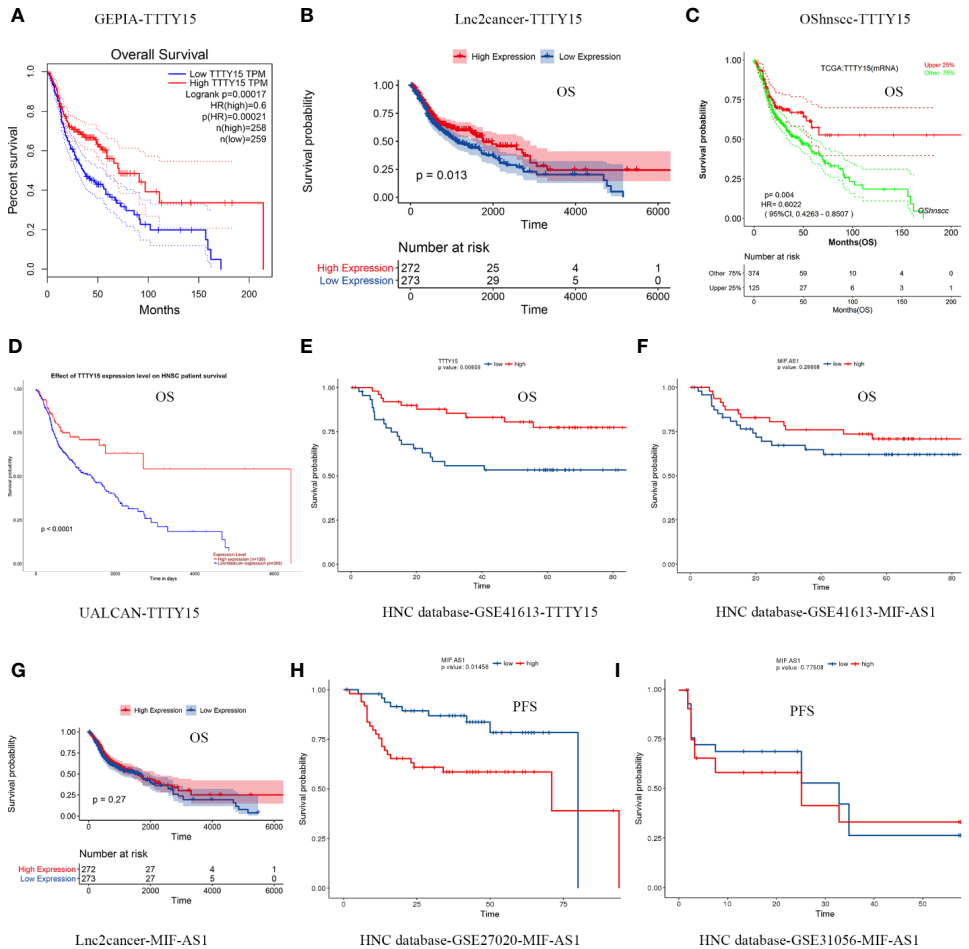

FIGURE 4 | Confirmation of the prognostic value of the three autophagy-related lncRNAs. **(A–E)** Five databases were used to examine the prognostic value of TTTY15. **(A)** GEPIA database, **(B)** Lnc2cancer 3.0 online database, **(C)** OShnscc database, **(D)** UALCAN database, **(E)** HNC database. **(F–I)** Analyses of associations between MIF-AS1 and overall survival and progression-free survival based on different databases. **(F)** Association between MIF-AS1 and overall survival based on the GSE41613 database. **(G)** Association between MIF-AS1 and overall survival based on the lnc2cancer 3.0 online database. **(H)** Association between MIF-AS1 and progression-free survival based on the GSE27020 database. **(I)** Association between MIF-AS1 and progression-free survival based on the GSE31056 database. PFS, progression-free survival; OS, overall survival.

TABLE 2 | Confirmation of prognostic value of three autophagy related lncRNAs.

lncRNA	Database	Datasets	Endpoint	p	HR	Prognostic
MIF-AS1	HNC database	GSE41613	OS	0.28668		
MIF-AS1	HNC database	GSE27020	PFS	0.01456		Poor
MIF-AS1	HNC database	GSE31056	PFS	0.77508		
MIF-AS1	Lnc2cancer3.0		OS	0.27		
TTTY15	GEPIA	TCGA and GTEx	OS	0.00021	0.6	Good
TTTY15	HNC database	GSE41613	OS	0.00858		Good
TTTY15	HNC database	GSE27020	PFS	0.0802		
TTTY15	HNC database	GSE31056	PFS	0.99911		
TTTY15	Lnc2cancer3.0		OS	0.013		Good
TTTY15	OShnscc	TCGA	OS	0.0004	0.6022	Good
TTTY15	UALCAN	TCGA	OS	<0.0001		Good

Five databases were used to validate the correlation between the three autophagy related lncRNAs and prognosis in HNSCC. HR, Hazara Ratio, PFS, Progression Free Survival; OS, Overall Survival.

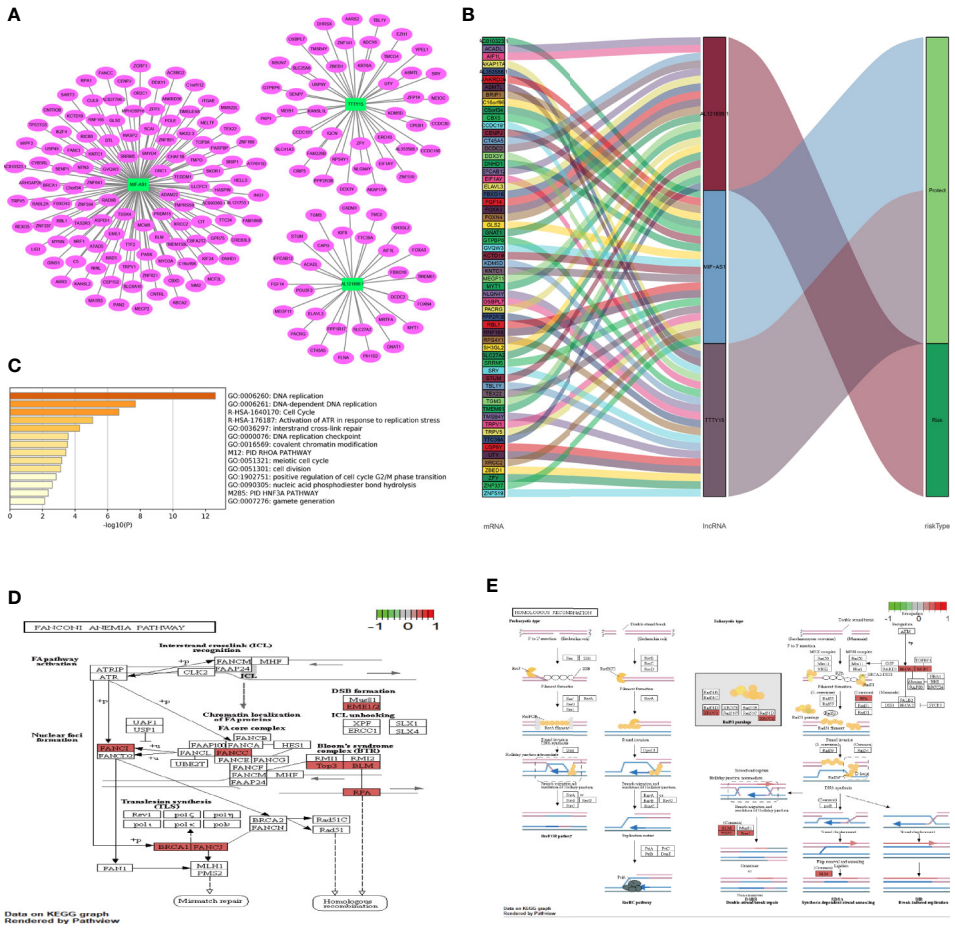

FIGURE 5 | Co-expression network and function enrichment analysis. **(A)** Construction of a co-expression network between three prognosis-related autophagy lncRNAs and PCGs. The green rectangles represent three prognosis-related lncRNAs, and the red ovals represent PCGs. **(B)** Sankey plots were generated to visualize association networks between the three lncRNAs, PCGs, and risk status. Due to the size of the image, the module on the left only shows the first 20 PCGs of each lncRNA. **(C)** Gene enrichment analysis of 189 PCGs. **(D, E)** KEGG pathway analysis of 189 PCGs. The red highlighted part represents the PCGs in the current study. **(D)** Eight PCGs involved in the Fanconi anemia pathway. **(E)** Seven PCGs associated with homologous recombination. PCG, protein coding gene; lncRNA, long non-coding RNA.

Three lncRNAs Are Correlated With Autophagy Markers

We verified the expression levels of the three lncRNAs and autophagy markers ATG12, BECN1, and MAP1LC3B through analysis TIMER, Oncomine, and HPA database. As shown in **Figure 7A**, TTTY15 was highly expressed in HPV (+) and HPV (-) patients, while TTTY15 expression had no difference in HNSCC patients compared with normal tissues. ATG12, BECN1, and MAP1LC3B were increased in HNSCC tissue, HPV (+), and HPV (-) patients compared with normal tissues. ATG12 and BECN1 were upregulated in HNSCC tissue compared with normal tissues based on Oncomine database. There was no significant difference discovered in HNSCC patients with an expression level of TTTY15 and MAP1LC3B (**Figure 7B**). The protein level of three autophagy makers were highly expressed in HNSCC tissues (**Figures 7C–E**). The results of GEPIA analysis showed that MIF-AS1 was positively correlated with ATG12 and LC3, and TTTY15 was positively related to three autophagy markers (ATG12, Bclin1, LC3) (**Figures 8A–F**). TTTY15 was positively correlated with ATG12 and BECN1 in different HNSCC patients, including HNSCC patients, HPV (+) HNSCC patients, and HPV (-) HNSCC patients (**Figures 8G–L**). The positive association between TTTY15 and MAP1LC3B was detected in HNSCC samples and HPV (-) HNSCC samples based on correlation module of TIMER analysis (**Figures 8M–O**). MIF-AS1 was not found in TIMER database.

DISCUSSION

More than 500,000 new cases of head and neck cancer are diagnosed every year. HNSCC is the most common pathological type of head and neck cancer, and it is typically highly aggressive and has a poor prognosis (28). TNM staging is

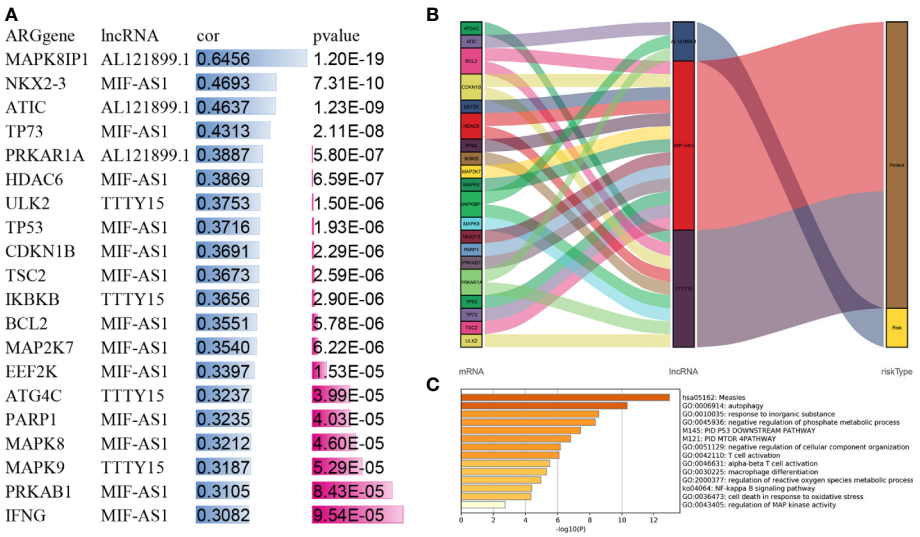

FIGURE 6 | Associations between the three lncRNAs and the autophagy-related pathway. **(A)** Three lncRNAs interacted with 20 ATGs. **(B)** Sankey plot depicting degrees of connection between 20 ATGs and 3 autophagy-related lncRNAs (risk/protective). **(C)** Metascape analysis of the gene ontology terms and pathways of three lncRNA-related ATGs. ATG, autophagy-related gene.

not sensitive enough to accurately predict HNSCC prognosis, thus a new method for formulating HNSCC prognosis is required (29). Due to the increased amount of gene expression profile data that has become available in recent years in conjunction with developments in bioinformatics, increased attention has been given to investigating associations between the alteration of RNA, non-coding RNA, and HNSCC prognosis (30, 31). Autophagy plays complex roles in HNSCC. Further investigation to elucidate the roles and clarify the mechanisms of autophagy in HNSCC is imperative (32–34). The analyses conducted in the current study suggest that autophagy-related lncRNAs may provide novel insights into the prediction of HNSCC prognoses. Little is known about the prognostic value of autophagy-related lncRNAs in HNSCC.

AL121899.1 has previously been identified as a tumor suppressor gene in esophageal squamous cell carcinoma *via* differential co-expression analysis (35). MIF-AS1 is reportedly significantly upregulated in ovarian cancer, and that upregulation can promote the proliferative, migratory, and invasive capacities of ovarian cancer cells. Higher levels of MIF-AS1 predicted poorer prognoses in ovarian cancer patients (36). In breast cancer and gastric cancer, lncRNA MIF-AS1 evidently promotes cell proliferation (37, 38). In a previous study, TTTY15 expression was downregulated in patients with non-small cell lung cancer, and low expression of TTTY15 was associated with tumor stage and poorer prognosis (39). TTTY15 was also reportedly upregulated in most prostate cancer patients and could promote prostate cancer progression by sponging let-7 (40). However, there are no reports on associations between HNSCC prognosis and AL121899.1, MIF-AS1, or TTTY15. In the present study MIF-AS1 and TTTY15 were identified as favorable prognostic biomarkers, and AL121899.1 was identified as an unfavorable prognostic biomarker. These findings were consistent with our understanding that the three lncRNAs were associated with the prognosis of cancer. Moreover, previous study suggested that TTTY15 was associated with HPV infection, and which was upregulated in HPV-positive patients (41). Previous studies reported that Beclin 1 (BECN1) and LC3 are unique autophagy-related protein (42). ATG12, ATG5, and MAP1LC3/LC3 have been reported to mediate the formation of the autophagosome (43). The prognosis for HPV positive patients is significantly longer than those with HPV negative carcinomas in cases of similar treatment (44). We discovered that TTTY15 had upregulation both in HPV (+) and HPV (-) patients, and which was positively correlated with autophagy makers in different HPV status. Positive correlation between MIF-AS1 and autophagy makers (ATG12 and LC3) was examined in HNSCC patients. Taken together, three autophagy-related lncRNAs may regulate the prognosis of HNSCC patients with different HPV status, which provides new insights for evaluating the prognosis of HNSCC.

In previous studies, moderate autophagy reportedly promoted homologous recombination (45, 46). Autophagy can regulate proteins in the homologous recombination repair pathway. DNA damage occurs, the activation of ATG promotes autophagy and activates the downstream STAT3-BRCA1 pathway, allowing BRCA1 protein to participate in chain scission during homologous recombination repair (46). Inhibition of the classic PI3K/Akt/mTOR autophagy pathway can significantly reduce the level of autophagy in prostate cancer cells, and suppress homologous recombination repair (47). Fanconi anemia pathway genes play an important role in tumor suppression and repair of damage to nuclear DNA. Defects in

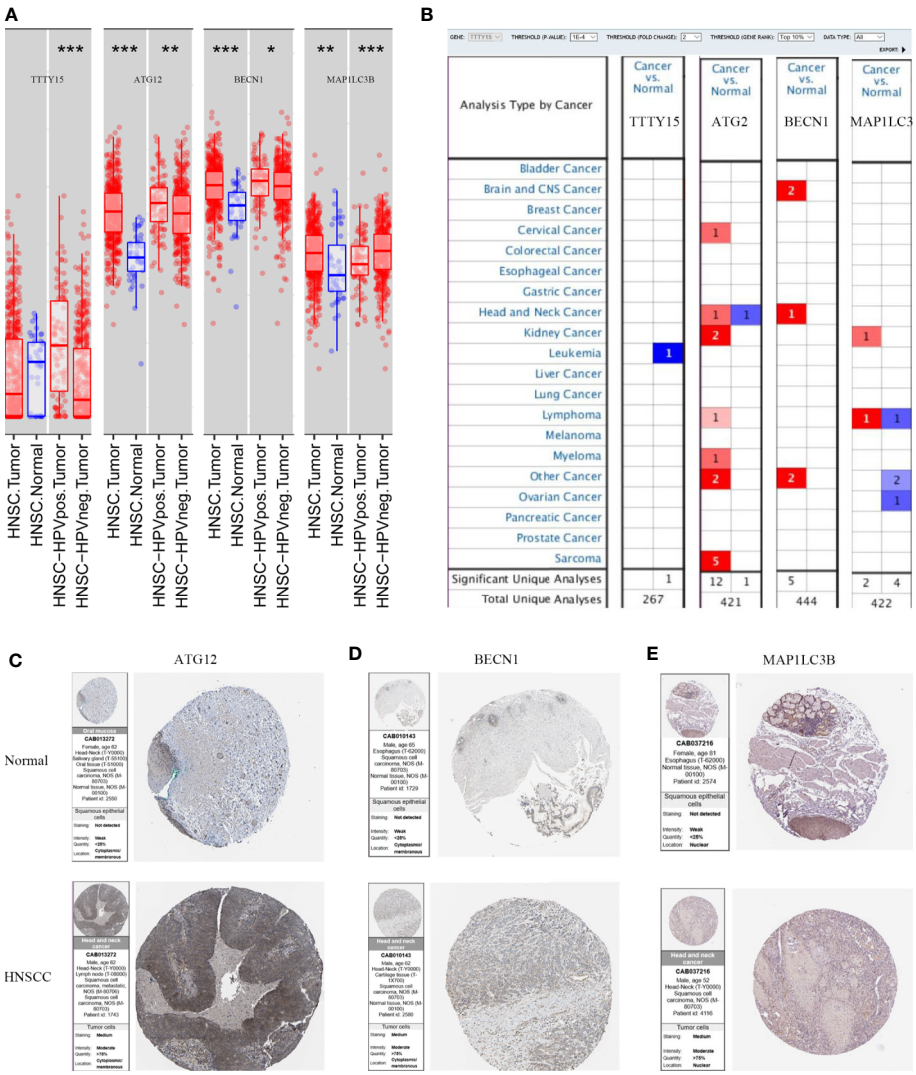

FIGURE 7 | The expression of three lncRNAs and autophagy related genes at mRNA and protein level. **(A)**TIMER analyze the expression of three lncRNAs and ATGs at the RNA level. **(B)** Different expression of three lncRNAs and ATGs in HNSCC and normal sample from Oncomine database. Red indicates up-regulated, blue represents down-regulated. **(C–E)** The protein expression levels of ATG12, BECN1, and MAP1LC3B for HNSCC tissues and normal tissues from HPA database. **(C)** ATG12, **(D)** BECN1, **(E)** MAP1LC3B. Autophagy Related Genes=ATGs. BECN1=Beclin1. Statistical significance was defined by a p value:*** means 0 ≤p-value < 0.001, ** represents 0.001≤p-value < 0.01, * represents 0.01≤p-value < 0.05,. means 0.05 ≤p-value <0.1.

selective autophagy have profound effects on mutations in Fanconi anemia pathway genes (48). Fanconi anemia genes have also been implicated in breast, ovarian, and pancreatic cancer (49). The three Fanconi anemia genes FANCC, FANCF, and FANCL were identified as candidate autophagy factors *via* whole genome screening (50). It has been reported that autophagy can be regulated by different pathways, such as those involving AKT, MTOR, mitogen-activated protein kinase, AMP-activated protein kinase, PIK3C3, and the proteins encoded by ATG genes (51). Nuclear factor kappa B contributes to repression of tumor necrosis factor alpha-induced autophagy (52). In a previous study a prognostic model was constructed based on autophagy-related lncRNA, and bladder urothelial carcinoma (BLCA) patients were divided into high-risk and low-risk groups. The PPAR signaling pathway, mitogen-activated protein kinase signaling pathway, P53 signaling pathway, and mTOR signaling pathway were associated with high risk in BLCA patients, whereas immune-related pathways were significantly enriched in a low-risk group (14). Co-expression network and pathway analysis in the current study indicated that functionally the three lncRNAs identified were mainly involved in homologous recombination, the Fanconi anemia pathway, the autophagy-related pathway, and the immune-related pathway. These results are consistent with previous studies indicating that autophagy is regulated by the aforementioned pathways, which may play critical roles in regulating HNSCC prognosis.

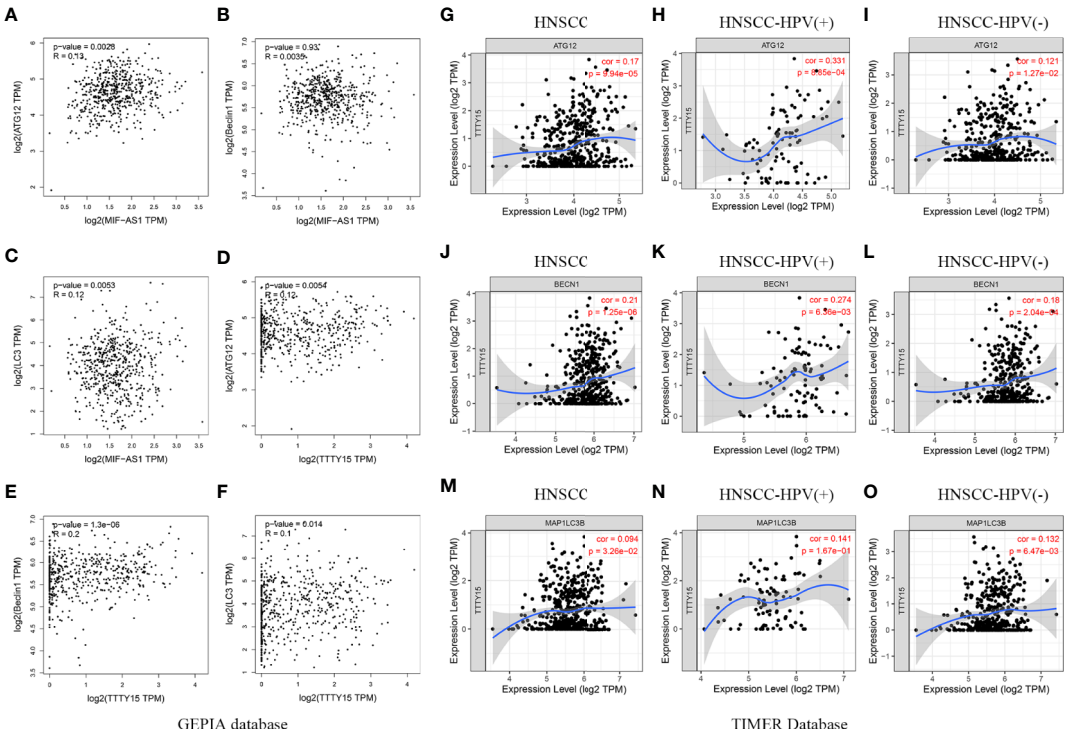

FIGURE 8 | Correlation between three lncRNAs and autophagy makers. **(A–C)** The association between MIF-AS1 and three autophagy makers was evaluated using GEPIA database. **(A)** ATG12, **(B)** Beclin1, **(C)** LC3. **(D–F)** Association between TTTY15 and three autophagy makers was assessed by GEPIA analysis. **(D)** ATG12, **(E)** Beclin1, **(F)** LC3. **(G–I)** The correlation between TTTY15 and ATG12 in different HNSCC patients was analyzed using TIMER database. **(G)** HNSCC patients, **(H)** HPV (+) HNSCC patients, **(I)** HPV (-) HNSCC patients. **(J–L)** The association between TTTY15 and BECN1 was detected in different HNSCC patients. **(J)** HNSCC patients, **(K)** HPV (+) HNSCC patients, **(L)** HPV (-) HNSCC patients. **(M–O)** Evaluation the correlation between TTTY15 and MAP1LC3B based on TIMER database. **(M)** HNSCC patients, **(N)** HPV (+) HNSCC patients, **(O)** HPV (-) HNSCC patients.

CONCLUSION

Three autophagy-related lncRNAs have prognostic value with respect to HNSCC, and their related pathways may be involved in regulating HNSCC prognosis. Further investigations and experiments such as quantitative real-time PCR, western blotting, and clinical data analyses are required to validate the results of the present study. We will perform further experiments to investigate the molecular mechanisms involved in the effects of autophagy-related lncRNAs on HNSCC prognosis, and their effects on clinical transformation in HNSCC patients.

DATA AVAILABILITY STATEMENT

Publicly available datasets were analyzed in this study. RNA-seq and corresponding clinical data were available from the TCGA database (https://portal.gdc.cancer.gov/).

AUTHOR CONTRIBUTIONS

YG conceived and designed the study and wrote the manuscript. PY participated in data analysis. ZW reviewed the manuscript. KX performed language editing. WK and HL prepared the figures and tables. All authors contributed to the article and approved the submitted version.

FUNDING

This work was supported by the Shaanxi Provincial Natural Science Foundation (2017JQ8057).

ACKNOWLEDGMENTS

We thank Zhong Guo Liang for his bioinformatics-related technical support.

SUPPLEMENTARY MATERIAL

The Supplementary Material for this article can be found online at: https://www.frontiersin.org/articles/10.3389/fonc.2020.603864/full#supplementary-material

REFERENCES

1. Ge D, Han L, Huang S, Peng N, Wang P, Jiang Z, et al. Identification of a novel MTOR activator and discovery of a competing endogenous RNA regulating autophagy in vascular endothelial cells. *Autophagy* (2014) 10:957–71.
2. Luan F, Chen W, Chen M, Yan J, Chen H, Yu H, et al. An autophagy-related long non-coding RNA signature for glioma. *FEBS Open Bio* (2019) 9:653–67.
3. Butera G, Mullappilly N, Masetto F, Palmieri M, Scupoli MT, Pacchiana R, et al. Regulation of Autophagy by Nuclear GAPDH and Its Aggregates in Cancer and Neurodegenerative Disorders. *Int J Mol Sci* (2019) 20:2062–89.
4. Huang Z, Liu J, Luo L, Sheng P, Wang B, Zhang J, et al. Genome-Wide Identification of a Novel Autophagy-Related Signature for Colorectal Cancer. *Dose-response* (2019) 17:1559325819894179.
5. Xing L, Zhang X, Chen A. Prognostic 4-lncRNA-based risk model predicts survival time of patients with head and neck squamous cell carcinoma. *Oncol Lett* (2019) 18:3304–16.
6. Lin P, He Y, Wen D-Y, Li X-J, Zeng J-J, Mo W-J, et al. Comprehensive analysis of the clinical significance and prospective molecular mechanisms of differentially expressed autophagy-related genes in thyroid cancer. *Int J Oncol* (2018) 53:603–19.
7. Cao W, J-n L, Liu Z, Wang X, Han Z-G, Ji T, et al. A three-lncRNA signature derived from the Atlas of ncRNA in cancer (TANRIC) database predicts the survival of patients with head and neck squamous cell carcinoma. *Oral Oncol* (2017) 65:94–101.
8. Masui T, Ota I, Kanno M, Yane K, Hosoi H. Low-intensity ultrasound enhances the anticancer activity of cetuximab in human head and neck cancer cells. *Exp Ther Med* (2013) 5:11–6.
9. Sun T. Long noncoding RNAs act as regulators of autophagy in cancer. *Pharmacol Res* (2018) 129:151–5.
10. Meng W, Ou W, Chandwani S, Chen X, Black W, Cai Z. Temporal phenotyping by mining healthcare data to derive lines of therapy for cancer. *J Biomed Inf* (2019) 100:103335.
11. Yang C, Han C, Wang X, Liao X, Liu X, Qin W, et al. Clinical Implication and the Hereditary Factors of NM23 in Hepatocellular Carcinoma Based on Bioinformatics Analysis and Genome-Wide Association Study. *J Oncol* (2018) 2018:6594169.
12. An Y, Bi F, You Y, Liu X, Yang Q. Development of a Novel Autophagy-related Prognostic Signature for Serous Ovarian Cancer. *J Cancer* (2018) 9:4058–71.
13. Su VY-F, Hu L-Y, Yeh C-M, Chiang H-L, Shen C-C, Chou K-T, et al. Chronic obstructive pulmonary disease associated with increased risk of bipolar disorder. *Chronic Respir Dis* (2017) 14:151–60.
14. Sun Z, Jing C, Xiao C, Li T. An autophagy-related long non-coding RNA prognostic signature accurately predicts survival outcomes in bladder urothelial carcinoma patients. *Aging* (2020) 12:15624–37.
15. Vrieze S. Model selection and psychological theory: a discussion of the differences between the Akaike information criterion (AIC) and the Bayesian information criterion (BIC). *Psychol Methods* (2012) 17:228–43.
16. Jiang H-Y, Ning G, Wang Y-S, Lv W-B. 14-CpG-Based Signature Improves the Prognosis Prediction of Hepatocellular Carcinoma Patients. *BioMed Res Int* (2020) 9762067:2020.
17. Yang F, Song Y, Ge L, Zhao G, Liu C, Ma L. Long non-coding RNAs as prognostic biomarkers in papillary renal cell carcinoma. *Oncol Lett* (2019) 18:3691–7.
18. Marburger S, Monnahan P, Seear PJ, Martin SH, Koch J, Paajanen P, et al. Interspecific introgression mediates adaptation to whole genome duplication. *Nat Commun* (2019) 10:5218.
19. Tang Z, Li C, Kang B, Gao G, Li C, Zhang Z. GEPIA: a web server for cancer and normal gene expression profiling and interactive analyses. *Nucleic Acids Res* (2017) 45:W98–W102.
20. Gao Y, Wang P, Wang Y, Ma X, Zhi H, Zhou D, et al. Lnc2Cancer v2.0: updated database of experimentally supported long non-coding RNAs in human cancers. *Nucleic Acids Res* (2019) 47:D1028–33.
21. Zheng H, Zhang G, Zhang L, Wang Q, Li H, Han Y, et al. Comprehensive Review of Web Servers and Bioinformatics Tools for Cancer Prognosis Analysis. *Front Oncol* (2020) 10:68.
22. Chandrashekar DS, Bashel B, Balasubramanya SAH, Chad J, Creighton‡ IP-R, Chakravarthi BVSK, et al. UALCAN: A Portal for Facilitating Tumor Subgroup Gene Expression and Survival Analyses. *Neoplasia (New York NY)* (2017) 19:649–58.
23. Hu Y, Wang X, Hu B, Mao Y, Chen Y, Yan L, et al. Dissecting the transcriptome landscape of the human fetal neural retina and retinal pigment epithelium by single-cell RNA-seq analysis. *PLoS Biol* (2019) 17: e3000365.
24. Zhou Y, Zhou B, Pache L, Chang M, Khodabakhshi AH, Tanaseichuk O, et al. Metascape provides a biologist-oriented resource for the analysis of systems-level datasets. *Nat Commun* (2019) 10:1523.
25. Li T, Fan J, Wang B, Traugh N, Chen Q, Liu J, et al. TIMER: A Web Server for Comprehensive Analysis of Tumor-Infiltrating Immune Cells. *Cancer Res* (2017) 77:e108–10.
26. Zhu T, Shi L, Yu C, Dong Y, Qiu F, Shen L, et al. Ferroptosis Promotes Photodynamic Therapy: Supramolecular Photosensitizer-Inducer Nanodrug for Enhanced Cancer Treatment. *Theranostics* (2019) 9:3293–307.
27. Uhlén M, Fagerberg L, Hallström B, Lindskog C, Oksvold P, Mardinoglu A, et al. Proteomics. Tissue-based map of the human proteome. *Science (New York NY)* (2015) 347:1260419.
28. Markwell SM, Weed SA. Tumor and stromal-based contributions to head and neck squamous cell carcinoma invasion. *Cancers* (2015) 7:382–406.
29. Lydiatt WM, Patel SG, O'Sullivan B, Brandwein MS, Ridge JA, Migliacci JC, et al. Head and Neck cancers-major changes in the American Joint Committee on cancer eighth edition cancer staging manual. *CA: Cancer J Clin* (2017) 67:122–37.
30. Vossen DM, Verhagen CVM, Heijden MVD, Essers PBM, Bartelink H, Verheij M, et al. Genetic Factors Associated with a Poor Outcome in Head and Neck Cancer Patients Receiving Definitive Chemoradiotherapy. *Cancers* (2019) 11:445–59.
31. Xie X, Xiong G, Wang Q, Ge Y, Cui X. Long non-coding RNA LINC00460 promotes head and neck squamous cell carcinoma cell progression by sponging miR-612 to up-regulate AKT2. *Am J Trans Res* (2019) 11:6326–40.
32. Simonet S, Rodriguez-Lafrasse C, Beal D, Gerbaud S, Malesys C, Tillement O, et al. Gadolinium-Based Nanoparticles Can Overcome the Radioresistance of Head and Neck Squamous Cell Carcinoma Through the Induction of Autophagy. *J Biomed Nanotechnol* (2020) 16:111–24.
33. Panzarini E, Inguscio V, Tenuzzo BA, Carata E, Dini L. Nanomaterials and autophagy: new insights in cancer treatment. *Cancers* (2013) 5:296–319.
34. Ji Y, Wang Q, Zhao Q, Zhao S, Li L, Sun G, et al. Autophagy suppression enhances DNA damage and cell death upon treatment with PARP inhibitor Niraparib in laryngeal squamous cell carcinoma. *Appl Microbiol Biotechnol* (2019) 103:9557–68.
35. Liu W, Gan C-Y, Wang W, Liao L-D, Li C-Q, Xu L-Y, et al. Identification of lncRNA-associated differential subnetworks in oesophageal squamous cell carcinoma by differential co-expression analysis. *J Cell Mol Med* (2020) 24:4804–18.
36. Fan LW Y, Han X-C, Ma H-Y, Zhang N, Zhe L. LncRNA MIF-AS1 aggravates the progression of ovarian cancer by sponging miRNA-31-5p. *Eur Rev Med Pharmacol Sci* (2020) 24:2248–55.
37. Ding J, Wu W, Yang J, Wu M. Long non-coding RNA MIF-AS1 promotes breast cancer cell proliferation, migration and EMT process through regulating miR-1249-3p/HOXB8 axis. *Pathol Res Pract* (2019) 215:152376.
38. Li L, Li Y, Huang Y, Ouyang Y, Zhu Y, Wang Y, et al. Long non-coding RNA MIF-AS1 promotes gastric cancer cell proliferation and reduces apoptosis to upregulate NDUFA4. *Cancer Sci* (2018) 109:3714–25.
39. Lai I-L, Chang Y-S, Chan W-L, Lee Y-T, Yen J-C, Yang C-A, et al. TTTY15Male-Specific Long Noncoding RNA Inhibits Non-Small Cell Lung Cancer Proliferation and Metastasis via TBX4. *Int J Mol Sci* (2019) 20:3473–90.
40. Xiao G, Yaoa J, Kong D, Ye C, Chen R, Li L, et al. The Long Noncoding RNA TTTY15, Which Is Located on the Y Chromosome, Promotes Prostate Cancer Progression by Sponging let-7. *Eur Urol* (2019) 76:315–26.
41. Kopczyńska MK, Kolenda T, Guglas K, Sobocińska JS, Teresiak A, Bliźniak RB, et al. PRINS lncRNA Is a New Biomarker Candidate for HPV Infection and Prognosis of Head and Neck Squamous Cell Carcinomas. *Diagn (Basel Switzerland)* (2020) 10:762–79.

42. Zhang XJ, Tang X, Liu HQ, Li LX, Hou Q, Gao JM. Autophagy induced by baicalin involves downregulation of CD147 in SMMC-7721 cells in vitro. *Oncol Rep* (2012) 27:1128–34.
43. Liu J, Wang H, Gu J, Deng T, Yuan Z, Hu B, et al. BECN1-dependent CASP2 incomplete autophagy induction by binding to rabies virus phosphoprotein. *Autophagy* (2017) 13:739–53.
44. Fakhry C, Westra W, Li S, Cmelak A, Ridge J, Pinto H, et al. Improved survival of patients with human papillomavirus-positive head and neck squamous cell carcinoma in a prospective clinical trial. *J Natl Cancer Inst* (2008) 100:261–9.
45. Zimmerlin L, Zambidis E. Pleiotropic roles of tankyrase/PARP proteins in the establishment and maintenance of human naïve pluripotency. *Exp Cell Res* (2020) 390:111935.
46. Hewitt G, Korolchuk VI. Repair, Reuse, Recycle: The Expanding Role of Autophagy in Genome Maintenance. *Trends Cell Biol* (2017) 27:340–51.
47. Chang L, Graham P, Hao J, Ni J, Bucci J, Cozzi P, et al. PI3K/Akt/mTOR pathway inhibitors enhance radiosensitivity in radioresistant prostate cancer cells through inducing apoptosis, reducing autophagy, suppressing NHEJ and HR repair pathways. *Cell Death Dis* (2014) 5:e1437.
48. Rhea Sumpter J, Sirasanagandla S, Fernández ÁF, Wei Y, Dong X, Franco L, et al. Fanconi Anemia Proteins Function in Mitophagy and Immunity. *Cell* (2016) 165:867–81.
49. Kupfer GM. Fanconi anemia: a signal transduction and DNA repair pathway. *Yale J Biol Med* (2013) 86:491–7.
50. Orvedahl A, Rhea Sumpter J, Xia G, Ng A, Zou Z, Tang Y, et al. Image-based genome-wide siRNA screen identifies selective autophagy factors. *Nature* (2011) 480:113–7.
51. Yang Y, Liang Z, Gu Z, Qin Z. Molecular mechanism and regulation of autophagy. *Acta Pharmacol Sin* (2005) 26:1421–34.
52. Djavaheri-Mergny M, Amelotti M, Mathieu J, Besançon F, Bauvy C, Souquère S, et al. NF-kappaB activation represses tumor necrosis factor-alpha-induced autophagy. *J Biol Chem* (2006) 281:30373–82.

Conflict of Interest: The authors declare that the research was conducted in the absence of any commercial or financial relationships that could be construed as a potential conflict of interest.

Copyright © 2021 Guo, Yang, Wang, Xu, Kou and Luo. This is an open-access article distributed under the terms of the Creative Commons Attribution License (CC BY). The use, distribution or reproduction in other forums is permitted, provided the original author(s) and the copyright owner(s) are credited and that the original publication in this journal is cited, in accordance with accepted academic practice. No use, distribution or reproduction is permitted which does not comply with these terms.

frontiers in Oncology

ORIGINAL RESEARCH
published: 10 February 2021
doi: 10.3389/fonc.2020.614487

Distinguishable Prognostic miRNA Signatures of Head and Neck Squamous Cell Cancer With or Without HPV Infection

Xiao-jie Luo[1†], Min Zheng[2†], Ming-xin Cao[1], Wei-long Zhang[1], Mei-chang Huang[1], Li Dai[1], Ya-ling Tang[1] and Xin-hua Liang[1*]*

[1] State Key Laboratory of Oral Diseases and National Clinical Research Center for Oral Diseases, West China Hospital of Stomatology, Sichuan University, Chengdu, China, [2] Department of Stomatology, Zhoushan Hospital, Wenzhou Medical University, Zhoushan, China

OPEN ACCESS

Edited by:
Qiang Shen,
Louisiana State University,
United States,

Reviewed by:
Jun Zhang,
University of California, Davis,
United States
Dengfeng Li,
Tongji University, China

***Correspondence:**
Ya-ling Tang
tangyaling@scu.edu.cn
Xin-hua Liang
lxh88866@scu.edu.cn

[†]These authors have contributed equally to this work

Specialty section:
This article was submitted to Head and Neck Cancer, a section of the journal Frontiers in Oncology

Received: 06 October 2020
Accepted: 08 December 2020
Published: 10 February 2021

Citation:
Luo X-j, Zheng M, Cao M-x, Zhang W-l, Huang M-c, Dai L, Tang Y-l and Liang X-h (2021) Distinguishable Prognostic miRNA Signatures of Head and Neck Squamous Cell Cancer With or Without HPV Infection. Front. Oncol. 10:614487. doi: 10.3389/fonc.2020.614487

Since their discovery in the 1990's, microRNAs (miRNA) have opened up new vistas in the field of cancer biology and are found to have fundamental roles in tumorigenesis and progression. As head and neck squamous cell carcinoma (HNSCC) with positive human papillomavirus (HPV+) is significantly distinct from its HPV negative (HPV–) counterpart in terms of both molecular mechanisms and clinical prognosis, the current study aimed to separately develop miRNA signatures for HPV+ and HPV– HNSCC as well as to explore the potential functions. Both signatures were reliable for the prediction of prognosis in their respective groups. Then Enrichment analysis was performed to predict the potential biological functions of the signatures. Importantly, combining previous studies and our results, we speculated that HPV+ HNSCC patients with low signature score had better immunity against the tumors and enhanced the sensitivity of therapies leading to improved prognosis, while HPV– HNSCC patients with high signature score acquired resistance to therapeutic approaches as well as dysregulation of cell metabolism leading to poor prognosis. Hence, we believe that the identified signatures respectively for HPV+ and HPV– HNSCC, are of great significance in accessing patient outcomes as well as uncovering new biomarkers and therapeutic targets, which are worth further investigation through molecular biology experiments.

Keywords: HPV – human papillomavirus, HNSCC (head and neck squamous cell carcinoma), miRNA - microRNA, prognostic model, immune

INTRODUCTION

Based on the latest GLOBOCAN data (September 2018), head and neck squamous cell carcinomas (HNSCC), further classified as oral cavity, oropharynx, nasopharynx, larynx, and hypopharynx according to their primary site of origin, had the top eight combined incidence rate and was the 5th leading cancer by combined 5-year prevalence worldwide (1, 2). Despite the application of multimodal therapy and the marked improvement in overall survival (OS) for other tumors, the 5-year OS rate of HNSCC patients with locally advanced disease remains poor (25–40%) (3).

Apart from excessive alcohol drinking and cigarette smoking, human papillomavirus (HPV) infection with increasing attention is also considered to be an important risk factor in HNSCC, particularly oropharyngeal tumors (4). In western world, alcohol and tobacco induced HNSCC is decreasing, while the incidence of HPV associated HNSCC, especially oropharyngeal, is significantly increasing in younger population (5). Accumulating evidence has showed that HPV positive (HPV+) HNSCC is significantly dissimilar to its HPV negative (HPV−) counterpart at the molecular level, with the respects of genetic, epigenetic, and protein expression profile (6–8). Furthermore, HPV+ is closely related with favorable overall survival (OS) in oropharyngeal squamous cell carcinoma (OPSCC), clinically. And as for non-OPSCC in HNSCC, the effect of HPV status on OS is controversial (9). However, the treatments for HPV+ and HPV− HNSCC patients remain almost the same, in spite of the vital differences between these two groups (10). Therefore, it is crucial to identify more specific and sensitive signatures for HPV+ and HPV− HNSCC respectively so as to develop better prognostic markers and therapeutic targets. It is indicated that HNSCC is more likely to be an epigenetic disease, rather than genetic (11), suggesting that miRNAs involved in epigenetic changes may be promising biomarkers in cancers (12–14).

MicroRNAs (miRNAs) are non-coding RNA molecules with about 22 nucleotides in length, which mainly act as negative regulators of target genes and have been shown to play an essential role in a range of biological functions, including cell proliferation, apoptosis, tumor growth, and metastasis (15). Nevertheless, to our knowledge, limited studies have been performed to identify the cancer specific miRNAs and tap the hidden value of their prognostic and therapeutic potentials, especially in HNSCC with division of HPV status.

In the current study, we integrated miRNA-Seq data and corresponding clinical follow-up information of HNSCC patients from The Cancer Genome Atlas (TCGA) database and Genome Data Analysis Centers (GDAC) server to identify features of miRNAs associated with prognosis. As it has been required to accurately discriminate between HPV-related and HPV-unrelated HNSCC, we then developed distinct miRNA signatures by dividing samples into HPV+ group and HPV− group. Enrichment analysis was further performed to investigate the potential functions, of which the results were truly distinguishable compared the two groups. The exploration procedure of the current study was illustrated in **Figure 1**.

MATERIALS AND METHODS

Expression Data and Clinic Information Processing

The level three miRNA isoform expression quantification data and level three RNA-sequencing data (RNA-Seq-HTSeq-FPKM) of HNSCC patients was download from The Cancer Genome Atlas (TCGA; http://cancergenome.nih.gov/) on March 9, 2020. The matched patients' clinical information was downloaded from the Broad Genome Data Analysis Centers Firehose server (https://gdac.broadinstitute.org/). The annotation of mRNAs was performed based on GENCODE (Release 33) and all miRNAs were renamed according to miRBase database v22 (www.mirbase.org) (16). The expression is taken as the median for the same gene or miRNA. All miRNAs with a row mean read less than or equal to one were ruled out. Then the raw counts of miRNA expression data were normalized by R (version 3.6.3)/Bioconductor (version 3.10) package "DESeq2" (17). The "DESeq2" and "apeglm" (18) was further used to detect the differentially expressed miRNAs between HPV+, HPV− and normal-adjacent control samples. The thresholds were set at the values of |log2 (fold change [FC])| >1 and p. adjust <0. 05. Deregulated miRNAs were compared with R package "VennDiagram".

Development of the miRNA-Based Prognostic Models

Cases with follow-up less than 90 days were excluded in advance and the prognostic value of each miRNA was calculated in the univariate Cox regression analysis using R package "survival" (p<0. 01). After primary filtration, Cox Least Absolute Shrinkage and Selection Operator (LASSO) regression with 10-fold cross-validation was built to pick out candidate miRNAs. Multivariate Cox regression was further performed using R package "survival" based on miRNAs disclosed in the above steps and constructed a prognostic risk score model. Risk score = *Expression (miRNAi)* × *Coefficient (miRNAi)*. Patients were divided into high risk and low risk groups according to the median risk score. Kaplan-Meier analysis was conducted using R package "survminer" and "survival." The receiver operating characteristic (ROC) curve was obtained by R package "survivalROC." Univariate and multiple Cox regression analysis were used to identify independent prognostic factors ($p < 0.05$).

Enrichment Analysis

Target genes of prognosis-related miRNAs were predicted by three databases (TargetScan, miRTarBase, miRDB) simultaneously. Kyoto Encyclopedia of Genes and Genomes (KEGG) pathway enrichment analysis for the target genes was conducted by R packages "org.Hs.eg.db" and "clusterProfiler" (19) ($p < 0.05$, $q < 0.05$). The matched mRNA expression data (FPKM) was divided into high-risk group and low-risk group by the mean risk score and was analyzed using GSEA version 4.0.3 ($p < 0.05$, FDR < 0.25).

RESULTS

Patient Characteristics

A total of 515 HNSCC samples and 44 normal-adjacent control tissues with corresponding clinic data were included in this study. The cases were further grouped by HPV status and the basic characteristics of the patients were summarized in **Table S1** (in **Supplementary Materials**). The majority patients were male (73%), had no clinical metastasis (94.0%), with advanced stage

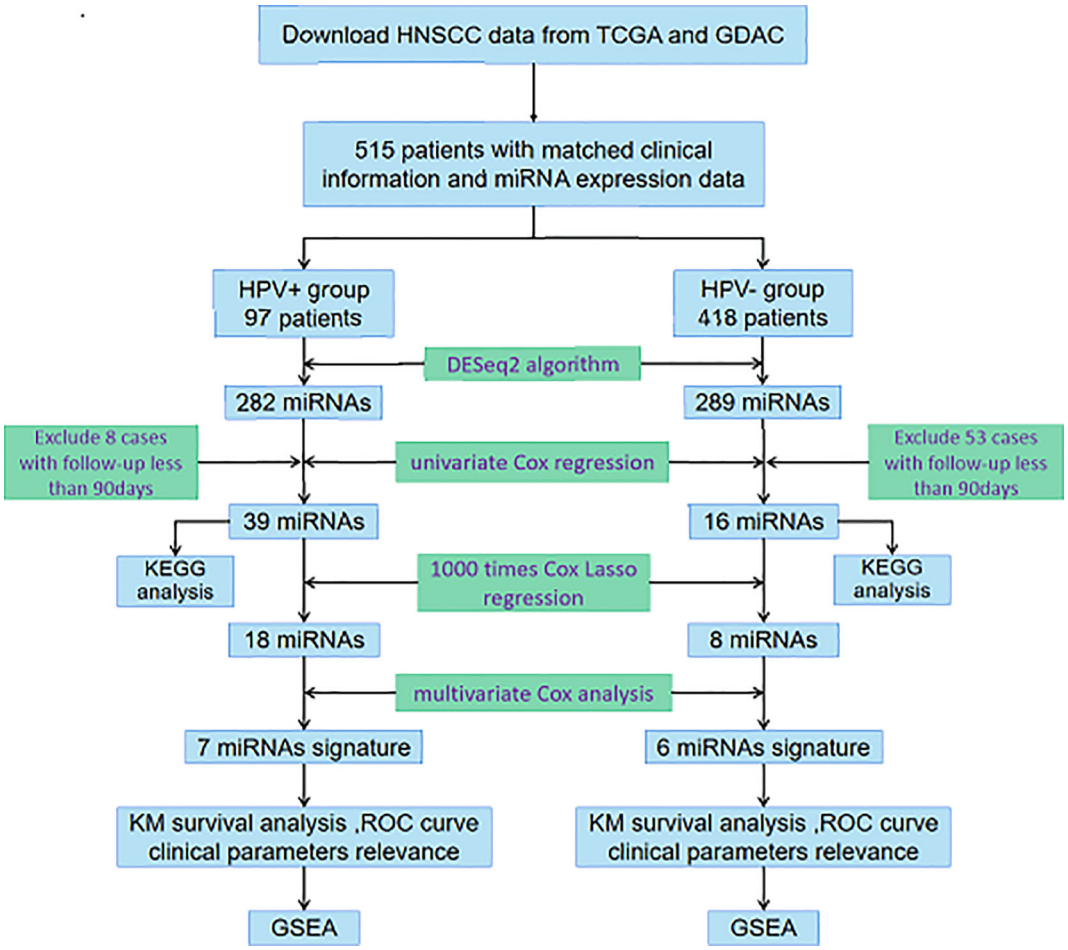

FIGURE 1 | Flowchart illustrates the exploration procedure for the HNSCC prognostic miRNAs with division of HPV status.

disease (stage III or worse, 75.0%). Average age was 60.9 years (range 19–90) with a median of 61 years. Ninety-seven (18.8%) samples harbored HPV transcripts, among which 74 (76.3%) were HPV-16, and 23 (23.7%) were HPV-Other (16 HPV-33, 3 HPV-35, 3 HPV-18, and 1 HPV-56). Oropharyngeal tumors accounted for approximately 55.7% in the HPV positive samples compared with the oral cavity (33.0%), the larynx (6.2%), and the hypopharynx (5.2%). HPV+ patients were younger than HPV− patients (average of 57.8 *vs* 61.7 years); and the difference was statistically significant.

Identification of Differentially Expressed miRNAs and Prognostic Signatures for HPV+ and HPV− Groups Respectively

The DESeq2 algorithm identified differentially expressed miRNAs ($p < 0.05$) for three groups (HPV+ *vs* normal, HPV− *vs* normal, HPV+ *vs* HPV−), respectively. The lists of significantly deregulated miRNAs in each group were compared with Venn Diagram (**Figure 2A**). Given the significant distinctness between HPV+ and HPV− HNSCC at molecular level, we made our efforts to separately discover molecular biomarkers which could serve as available prognostic factors. Among the differentially expressed miRNAs, we further identified survival-related miRNAs ($p < 0.01$) for the two groups, accompanied by Venn Diagram (**Figure 2B**). Then the survival-related miRNAs were applied to 1,000 times Cox Lasso regression with 10-fold CV (**Figure 3**). Based on the screened-out miRNAs, multivariate Cox analysis developed distinct signatures for each group, respectively. No miRNAs were common between the two signatures. Risk score of each patient was calculated based on the expression and coefficient of miRNAs in the signatures. The formula of HPV+ group was as follows: Risk Score = (−0.00039788 × hsa-miR-378a-3p) + (−0.069642608 × hsa-miR-16-1-3p) + (−0.050112958 × hsa-miR-493-3p) + (0.238905909 × hsa-miR-380-5p) + (0.04184412 × hsa-miR-376c-3p) + (0.06043184 × hsa-miR-338-5p). The formula of HPV− group was as follows: Risk Score = (−0.035373051 × hsa-miR-135b-3p) + (0.144736959 × hsa-miR-605-5p) + (0.051610835 × hsa-miR-383-5p) +

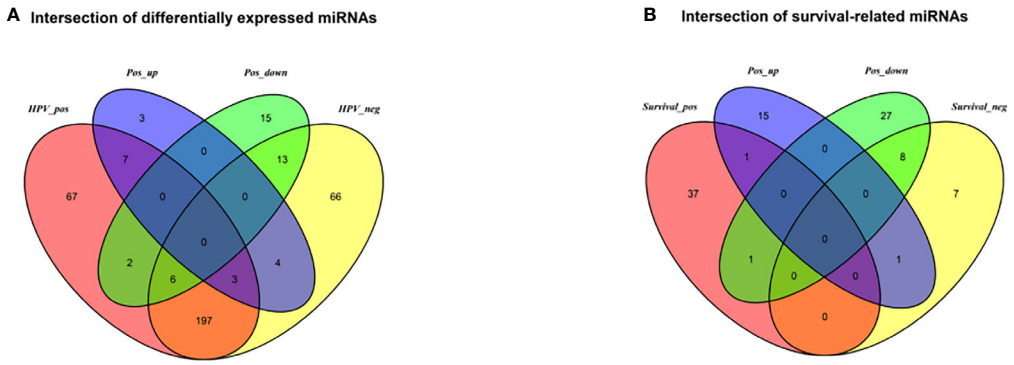

FIGURE 2 | **(A)** Venn diagram of differentially deregulated miRNA sequences across groups; **(B)** Venn diagram of survival-related miRNAs. HPV_pos = differentially expressed miRNAs between HPV+ and normal-adjacent tissues; HPV_neg = differentially expressed miRNAs between HPV- and normal-adjacent tissues; Pos_up = up-regulated miRNAs compared HPV+ with HPV- tissues; Pos_down = down-regulated miRNAs compared HPV+ with HPV- tissues; Survival_pos = survival-related miRNAs in HPV_pos; Survival_neg = survival-related miRNAs in HPV_neg.

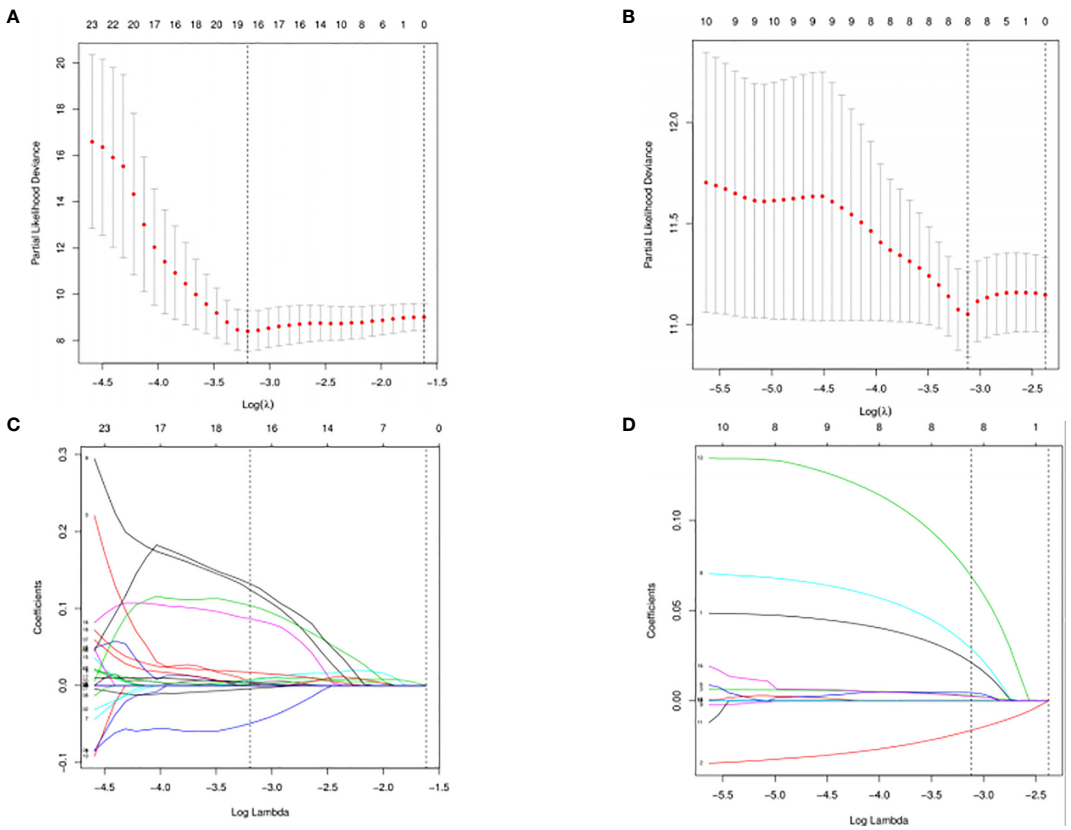

FIGURE 3 | Cross-validated and lassopath of LASSO COX. HPV+ group: **(A)** and **(C)**; HPV- group: **(B)** and **(D)**. 18 variables were selected according to the lmin; log(lmin) = −3:20; **(C)** and **(D)** HPV- group, 8 variables were selected according to the lmin; log(lmin) = −3:12.

(0.011764307 × hsa-miR-518a-5p) + (0.006540076 × hsa-miR-1911-5p) + (0.074201442 × hsa-miR-548k). Negative values are bad for the occurrence of HNSCC, while positive values are favorable for it. The higher the risk score is, the worse the patient prognosis is.

Evaluation of Clinical Outcomes for HPV+ and HPV– HNSCC Patients

The median risk score was selected as a cutoff to further separate HPV+ and HPV– patients into high-risk and low-risk groups, respectively. As was shown in **Figures 4A, B**, both HPV+ and

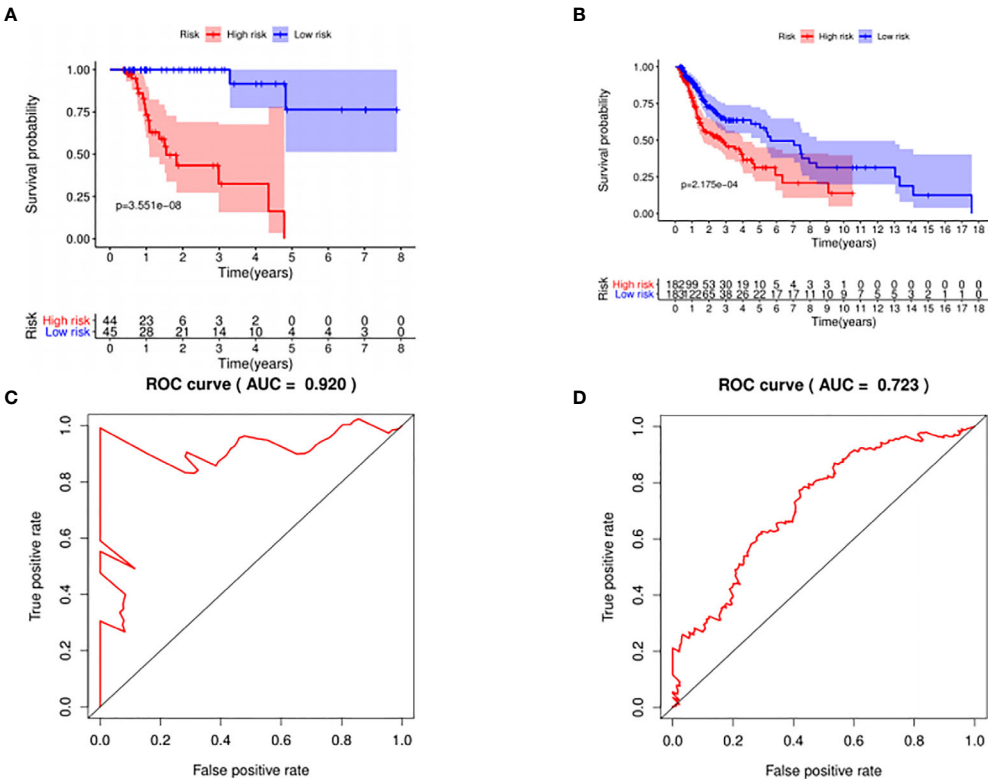

FIGURE 4 | The prognostic value of the signature. HPV+ group: **(A)** and **(C)**; HPV- group: **(B)** and **(D)**. **(A, B)**: The overall survival curve of high risk score group and low risk score group. **(C, D)**: Receiver operating characteristic curve of the 5-year survival estimated via risk score.

HPV− HNSCC patients in the low-risk group had longer OS ($p < 0.001$) than those of the high-risk group. And according to the 5-year survival receiving operating characteristic (ROC) curve, the area under curve (AUC) of risk score reached 0.920 in HPV+ group (**Figure 4C**) and 0.723 in HPV− group (**Figure 4D**). The detailed relationships between risk score, miRNAs expression, and survival information was shown in **Figure 5**.

Univariate and multiple regression analysis indicated both signatures for HPV+ and HPV− could serve as an independent predictor after other parameters were adjusted, including Tumor site, Age, Alcohol, Gender, Smoking, Grade, Clinical stage, Clinical T, Clinical N [**Table S2** (in **Supplementary Materials**)]. Relationships were also analyzed between the signatures and clinical characteristics [**Table S3** (in **Supplementary Materials**)]. Risk score of HPV+ was significantly lower ($p < 0.001$) in oropharynx than other sub-sites while there was no significant relationships between risk score of HPV− and clinical parameters.

Functional Enrichment of the Survival-Related miRNAs

Kyoto Encyclopedia of Genes (KEGG) pathway analysis was performed to assess the functional involvement of the survival-related miRNAs (**Figure 6**). Only the ones predicted by three databases (TargetScan, miRTarBase, miRDB) simultaneously were recognized as target genes for a given miRNA. As was shown in **Figure 6**, HPV+ group shared 11 common pathways with HPV− group, among which the gene ratio of HPV− group was generally higher than that of HPV+ group. And the selected different pathways in each group were also displayed at the lower area divided by the gray line. Furthermore, gene set enrichment analysis (GSEA) was implemented to investigate whether alternations of risk scores were linked to specific functional categories (**Figure 7**). GSEA of the signature score indicated that HPV+ samples with low risk score were mainly enriched in immune-related pathways, suggesting that HPV+ HNSCC patients with favorable prognosis might have better immune systems against the tumors (**Figure 7A**). As for HPV− group, high risk score appeared to be associated with metabolism and other vital oncogenic pathways showed in **Figure 7B**.

Immune Cells Associated With Survival-Related miRNAs Signature for HPV+ and HPV− HNSCC Patients

Then, we further calculated the fractions of immune-related cells in the tumor micro-environment (TME) through CIBERSORTx and uncovered the relationships between the signature and these cells (**Table 1**). The results in HPV+ group showed that miRNAs associated with poor prognosis was negatively correlated with CD8 + T lymphocyte. Similarly, miRNAs associated with good prognosis was positively correlated with activated NK cells and T regulatory cells (Tregs). And the signature score was negatively correlated with T follicular helper cells (T_{FH}) and T regulatory cells (Tregs).

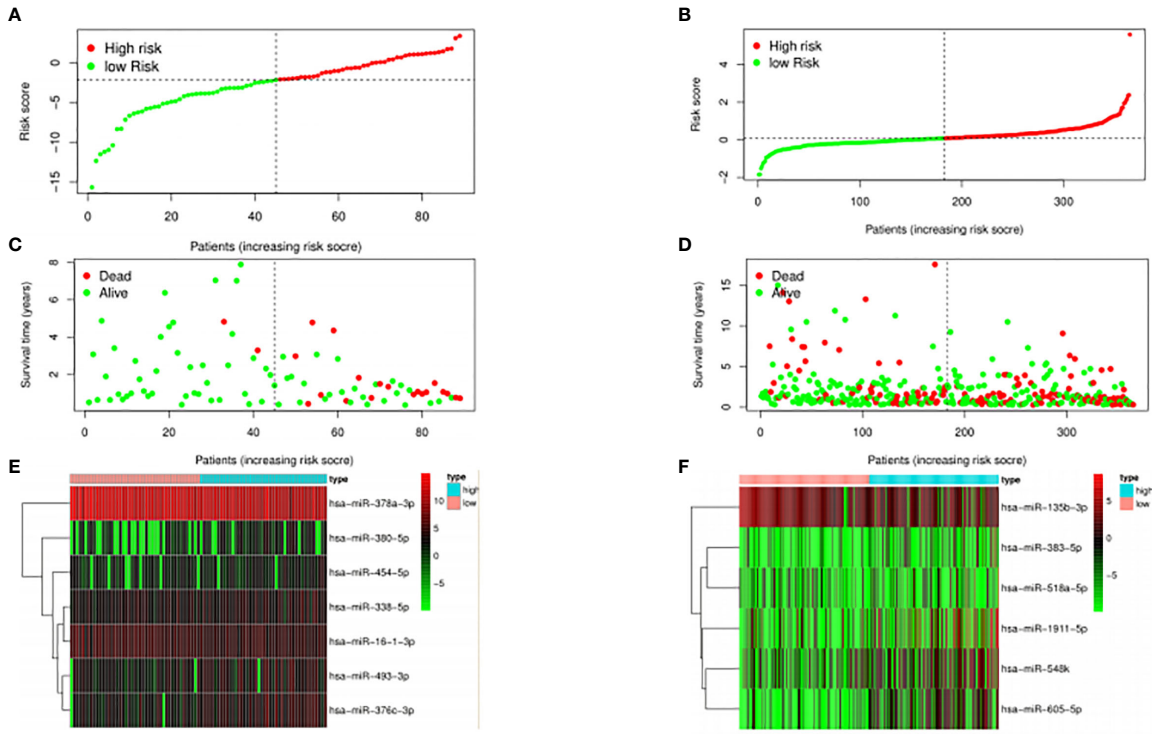

FIGURE 5 | Expression profiles of the signature.

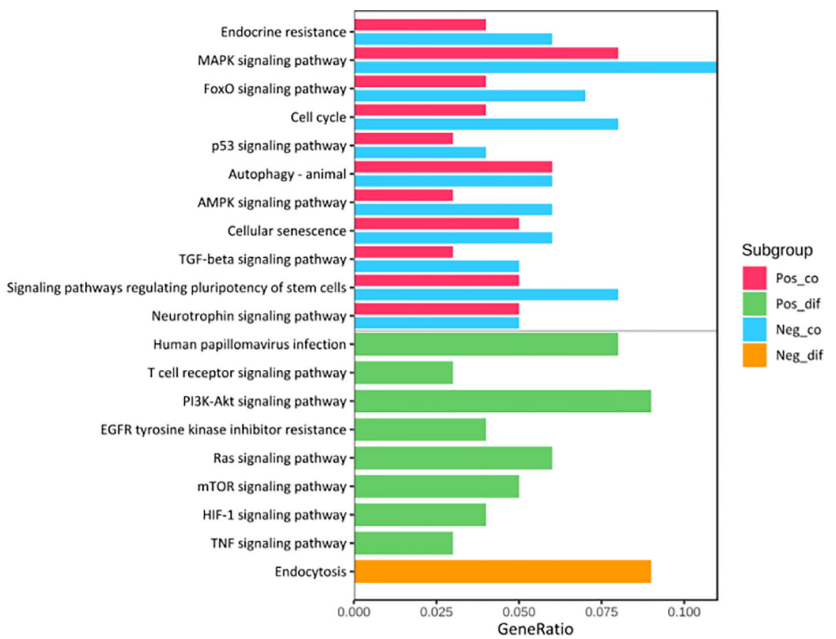

FIGURE 6 | KEGG Pathway Enrichment Analysis. The pathways at the upper area divided by a grey line were the common ones between HPV+ and HPV- groups while those at the lower area were the distinct ones. Pos_co colored red stood for the enrichment outcomes of common pathways in HPV+ group and Neg_co colored blue stood for those in HPV- group. Pos_dif colored green were the enrichment outcomes of different pathways in HPV+ group and Neg_dif colored green were those in HPV- group.

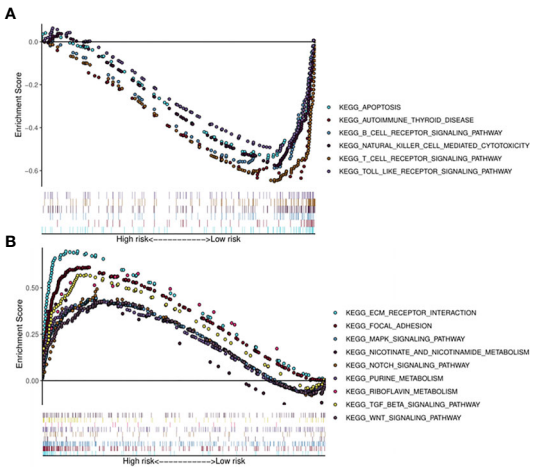

FIGURE 7 | Risk score correlated enrichment gene analysis with multi- GSEA. HPV+ group: **(A)**; HPV- group: **(B)**.

For the signature of HPV− group, miR-605-5p related to unfavorable prognosis was found negatively associated with CD8+ T cells, macrophages M1, and activated memory CD4+ T cells, which acted as tumor suppressors. miR-135b-3p related to good prognosis was found negatively correlated with macrophages M2 which could promote tumor progression. And the signature score was negatively correlated with T_{FH} and activated memory CD4+ T cells. These findings implied that these miRNAs in the signature had potential for serving as biomarkers and therapy targets in HNSCC and deserved further investigation.

Targeted mRNA of the Survival-Related miRNAs for HPV+ and HPV− HNSCC Patients

We have further found targeted mRNAs of survival-related miRNAs for HPV+ and HPV− HNSCC patients by TargetScan, miRTarBase, and miRDB. TCGA has been used to choose them and the negative correlation of miRNA and mRNA was applied to validate them. Then 1 mRNA in HPV− miRNA group and 10 mRNAs in HPV+ miRNA group were obtained and shown in **Table 2**.

DISCUSSION

Over the past decade, the role of HPV has attracted increasing attention in HNSCC, and the significant differences of HPV+ HNSCC in prognosis and etiologic mechanisms from its HPV− counterpart have made it critical to describe and discuss the two subgroups separately whenever possible. Although this vital distinction mainly referred to oropharyngeal tumors within HNSCC, as this was the best-studied entity, HPV was also involved in 23.5% of oral cancer and 24% of laryngeal cancer cases (20). However, most of the identified prognostic signatures so far were still performed using total HNSCC samples regardless of HPV status (21–25). When HPV status was considered, most publications mainly focused on identifying differences in miRNA expression levels between HPV+ and HPV−, and HPV-associated oncogenic miRNA panel has potential utility in diagnosis and disease stratification of HNSCC (26–29). Therefore, to add the current knowledge, it is urgently required to discover robust prognostic factors for HPV+ and HPV−

TABLE 1 | Relationships between signatures and immune cells.

HPV+ group				HPV− group			
miRNA	**Immune cell**	**Cor**	**P**	**miRNA**	**Immune cell**	**Cor**	**P**
hsa-miR-380-5p	T cells CD8	−0.489	0.002	hsa-miR-135b-3p	Macrophages M2	−0.224	0.001
hsa-miR-338-5p	T cells CD8	−0.454	0.004	hsa-miR-605-5p	T cells CD8	−0.189	0.007
hsa-miR-16-1-3p	NK cells activated	0.438	0.006	hsa-miR-605-5p	T cells CD4 memory activated	−0.277	<0.001
hsa-miR-378a-3p	T cells regulatory (Tregs)	0.662	<0.001	hsa-miR-605-5p	Macrophages M1	−0.182	0.009
Risk Score	T cells follicular helper	−0.51	0.001	Risk Score	T cells CD4 memory activated	−0.24	<0.001
Risk Score	T cells regulatory (Tregs)	−0.625	<0.001	Risk Score	T cells follicular helper	−0.187	0.007

TABLE 2 | Targeted mRNA of the survival-related miRNAs for HPV+ and HPV− HNSCC patients.

	miRNA	**mRNA**	**miRNALog_2FC**	**mRNALog_2FC**
HPV+	miR-16-1-3p	CPS1	1.050639269	-1.010646906
	miR-16-1-3p	USP25	1.050639269	-0.718755746
	miR-16-1-3p	ITSN2	1.050639269	-0.684864346
	miR-16-1-3p	SLITRK4	1.050639269	-1.760387923
	miR-16-1-3p	DUSP5	1.050639269	-1.757895916
	miR-16-1-3p	WDR26	1.050639269	-0.781833209
	miR-338-5p	CSMD1	-2.24647131	1.859003192
	miR-338-5p	HOXA10	-2.24647131	3.622947307
	miR-376c-3p	BCL11A	-2.609241735	0.556674985
	miR-493-3p	XPR1	-1.197011744	0.620381708
HPV-	miR-605-5p	SLC16A1	-1.013638579	1.376851067

HNSCC which can provide new insights into finding potential prognosis biomarkers and therapeutic targets, respectively.

In the present study, we separately developed distinct miRNA signatures associated with OS of patients for the two groups. Both signatures were reliable for the prediction of prognosis in their respective groups according to the ROC curve. The lists of significantly deregulated miRNAs and survival-related miRNAs in each group were compared with Venn Diagram. Noteworthy were no survival-related miRNA in common compared HPV+ to HPV− groups, reinforcing their differences at the molecular level. Further, KEGG pathways analysis displayed that there were 11 common pathways between HPV+ group and HPV− group, and the gene ratio of HPV− group was generally higher than that of HPV+ group. In addition, GSEA of the signature score showed that HPV+ samples with low risk score were mainly enriched in immune-related pathways and HPV− group with high risk score appeared to be associated with metabolism and other vital oncogenic pathways. Previous studies have shown pronounced advances achieved in cancer immunotherapy. Despite the success, a relative lower overall clinical response of HNSCC was observed compared to other types of tumor treated with similar approaches, highlighting the need to gain better understanding of the complex immune landscape within TME of HNSCC (30, 31).

As our analysis implied that the identified signature of HPV+ group was highly correlated with immune-related pathways, we further calculated the fractions of immune-related cells in the TME and uncovered that survival-related miRNAs was correlated with CD8+ T lymphocyte, activated NK cells and Tregs and T_{FH}. As components of the immune system, CD8+ T cells and NK cells have important roles in suppressing tumors by killing tumor cells with cytotoxic molecules, and the presence of tumor dense CD8+ T cells infiltration possibly represents pre-existing anti-tumor immune responses (32). T_{FH}, a distinct subset of CD4+ cells, whose functions in cancers are rarely reported, seems to act as a protector in non-lymphoid tumors and hazardous factor in lymphoid tumors (33). Remarkably, the increased levels of Tregs, known to be capable of suppressing anti-tumor immunity, was observed in HPV+ HNSCC patients with better prognosis, opposite from the general findings in other tumor types. This was supported by previous publications. Lukesova et al. (34) found that higher infiltration of Tregs and lower ratio of CD8/Tregs associated with the better prognosis of HPV+ HNSCC. The reason of the different roles of Tregs were that Tregs may impair Th17-cell-dependent proinflammatory and also maintain HPV-positive status in HNSCC. Wansom et al. (35) showed that increased FoxP3+ Tregs infiltration closely associated with lower T stage and better survival in both HPV+ and HPV− HNSCC. The possible explanation is that pre-existing immunosurveillance against the HPV proteins actives the negative feedback of repressive mechanism, resulting in elevation of Tregs (3). We further identified a MEred module related with risk scores by WGCNA and performed GO and KEGG enrichment analysis for the module [**Figure S** (in **Supplementary Materials**)], whose results confirmed our findings that the miRNA signature of HPV+ was highly associated with immune systems. These provide a basis for the functional analysis in the immune-related pathways, indicating these miRNAs have crucial roles in immune infiltration within TME of HPV+ HNSCC, and the underlying mechanisms remain to be uncovered in the future.

Some identified miRNAs in HPV+ signature have been previously reported to be involved in progressions of several cancer types. A research showed that miR-378a-3p was related with favorable prognosis in ovarian cancer, which could suppress cell proliferation, promote cell apoptosis, and enhance the sensitivity to cisplatin by sponging MAPK1 and GRB2 (36). Wang et al. implied that miR-16-1-3p played an important role in gastric cancer by directly targeting Twist1 and suppressing Twist1-EMT pathways, and might also serve as available therapeutic targets for EMT process in other tumor types (37). miR-493-3p was found to induce apoptosis of ovarian cancer cells through targeting multiple genes, including AKT2, STK38L, HMGA2, ETS1, and E2F5 (38). It was reported that the inhibition of miR-380-5p could increase p53 expression and induce extensive cell apoptosis in human neuroblastoma cell lines (39). A study suggested that miR-376c-3p exerted an oncogenic role in hepatocellular carcinoma progression *via* repressing ARID2 (40). miR-338-5p appeared to induce invasion and metastasis of colorectal cancer partly through PIK3C3-related autophagy pathway and improved the proliferation and metastasis of malignant melanoma through targeting CD82 (41, 42). Herein, we hypothesized that the miRNAs might serve similar functions in HPV+ HNSCC, which deserved further investigation by molecular biology experiments.

Importantly, combining the outcomes of GSEA analysis for HPV− group and previous studies, it could be speculated that HPV − HNSCC patients with high risk score acquired resistance to therapies as well as dysregulation of cell metabolism responsible for poor prognosis. In order to satisfy the energy demands for malignant cell proliferation, tumors reprogram pathways of metabolism, which are recognized as hallmarks of cancers (43). Besides, it has been shown that cell adhesion to extracellular matrix (ECM) essentially linked to tumor cell resistance to radiation therapy, chemotherapy, as well as targeted drugs (44). Other vital oncogenic pathways were also enriched in those with high risk score, such as "MAPK SIGNALING PATHWAY," "NOTCH SIGNALING PATHWAY," "TGF BETA SIGNALING PATHWAY." MAPK pathways essentially regulate malignant cell behavior in respect of cancer-related proliferation, invasion, migration, and survival, which are considered as viable targets for cancer therapy (45). Studies have revealed NOTCH pathway have a key role in HNSCC related to epithelial-mesenchymal transition (EMT) as well as immune system and its inhibition can decrease cell proliferation and migration, which are recognized as an attractive cancer therapeutic target (46). Apart from the ability of TGF-β pathway to impact diverse cellular processes including cell proliferation, invasion, and ECM remodeling, a research has shown TGF-β-mediated effects on squamous cell carcinoma are linked to metabolic reprogramming, which in particular play a vital role in the responses to anti-tumor therapeutic approaches (47). Thus, it can be inferred that HPV− HNSCC patients with high signature score may acquire more benefits from targeted medicine against the above pathways. The relationships between the

signature of HPV− group and immune cells were also explored (**Table 1**). miR-605-5p and miR-135b-3p related to prognosis associated with CD8+ T cells, macrophages M1, and activated memory CD4+ T cells and macrophages M2. And the signature score was negatively correlated with T_{FH} and activated memory CD4+ T cells. These indicated that these miRNAs in the signature had potential to serve as therapy targets in HPV− HNSCC. However, as far as we know, there are limited studies towards the identified miRNAs in HPV-signature. A research implied that miR-605-5p promoted proliferation and invasion of non-small-cell lung cancer cell carcinoma *via* sponging TNFAIP3 (48). It was reported miR-135b-3p could inhibit cell clonogenicity and metastasis in triple-negative breast cancer by targeting RGMA (49). Nevertheless, in contrast to our findings, researches suggested that miR-383-5p acted as an inhibitor of cell proliferation and related with poor prognosis in several tumor types, such as ovarian, gastric, and breast cancer (50–52). Similarly, miR-518a-5p was reported to suppress proliferation and promote apoptosis of gastrointestinal stromal tumor while our results showed miR-518a-5p was correlated with poor prognosis of HPV− HNSCC patients (53).

Personalized treatment on the basis of HPV status with better efficacy and minimal side effects is on the horizon. Compared with previously established signatures irrespective of HPV status (21–25), the current study might be more accurate in predicting prognosis of HNSCC patients and, more importantly, better describe the potential molecular mechanisms by dividing samples into HPV+ group and HPV− group. According to the results, we speculated that HPV+ HNSCC patients with low signature score might have better immunity against the tumors and enhance the sensitivity of therapeutic interventions leading to improved prognosis, while HPV− HNSCC patients with high signature score acquired resistance to therapeutic approaches as well as dysregulation of cell metabolism responsible for poor prognosis. Thus, immunotherapy may be useful for HPV+ HNSCC patients with low signature score. We believe the identified signatures respectively for HPV+ and HPV− HNSCC, are of great significance in accessing patient prognosis as well as uncovering new biomarkers and therapeutic targets. However, specific limitations of our study should be mentioned. First, the present signatures based only on single public database, were not validated with an additional data set and the sample size of HPV+ group was relatively small. Second, despite the marked heterogeneity exists between HNSCC subtypes derived from different primary site, we did not separately construct type-specific signatures on account of limited sample size for a specific subtype. Finally, clinical specimen validation along with molecular biology experiments was not performed to uncover the potential mechanisms regulated by hub miRNAs which need to further investigate in the future.

DATA AVAILABILITY STATEMENT

The original contributions presented in the study are included in the article/**Supplementary Material**. Further inquiries can be directed to the corresponding authors.

AUTHOR CONTRIBUTIONS

X-JL, Y-LT, and X-HL conceived and designed the study. X-JL drafted the manuscript. X-JL analyzed and interpreted all the data. X-JL prepared the figures and tables. X-JL, M-XC, W-lZ, M-CH, LD, Y-LT, and X-HL reviewed and revised the manuscript. All authors contributed to the article and approved the submitted version.

FUNDING

This work was supported by National Natural Science Foundation of China grants (Nos. 82073000 and 81972542), National Science Foundation of Sichuan Province (No. 2020JDRC0018 and 2020YFS0171), Clinical Project of West China College of Stomatoloy, Sichuan University (LCYJ2019-8), and Exploration and research projects of West China College of Stomatoloy, Sichuan University (LCYJ2020-YJ-1).

SUPPLEMENTARY MATERIAL

The Supplementary Material for this article can be found online at: https://www.frontiersin.org/articles/10.3389/fonc.2020.614487/full#supplementary-material

REFERENCES

1. Bray F, Ferlay J, Soerjomataram I, Siegel RL, Torre LA, Jemal A. Global cancer statistics 2018: GLOBOCAN estimates of incidence and mortality worldwide for 36 cancers in 185 countries. *CA Cancer J Clin* (2018) 68(6):394–424. doi: 10.3322/caac.21492
2. Ferlay J, Colombet M, Soerjomataram I, Mathers C, Parkin DM, Pineros M, et al. Estimating the global cancer incidence and mortality in 2018: GLOBOCAN sources and methods. *Int J Cancer* (2019) 144(8):1941–53. doi: 10.1002/ijc.31937
3. Canning M, Guo G, Yu M, Myint C, Groves MW, Byrd JK, et al. Heterogeneity of the Head and Neck Squamous Cell Carcinoma Immune Landscape and Its Impact on Immunotherapy. *Front Cell Dev Biol* (2019) 7:52. doi: 10.3389/fcell.2019.00052
4. Leemans CR, Snijders PJF, Brakenhoff RH. The molecular landscape of head and neck cancer. *Nat Rev Cancer* (2018) 18(5):269–82. doi: 10.1038/nrc.2018.11
5. Kobayashi K, Hisamatsu K, Suzui N, Hara A, Tomita H, Miyazaki T. A Review of HPV-Related Head and Neck Cancer. *J Clin Med* (2018) 7(9):241. doi: 10.3390/jcm7090241
6. Seiwert TY, Zuo Z, Keck MK, Khattri A, Pedamallu CS, Stricker T, et al. Integrative and comparative genomic analysis of HPV-positive and HPV-negative head and neck squamous cell carcinomas. *Clin Cancer Res* (2015) 21 (3):632–41. doi: 10.1158/1078-0432.CCR-13-3310
7. Worsham MJ, Chen KM, Ghanem T, Stephen JK, Divine G. Epigenetic modulation of signal transduction pathways in HPV-associated HNSCC. *Otolaryngol Head Neck Surg* (2013) 149(3):409–16. doi: 10.1177/0194599813490895
8. Gameiro SF, Ghasemi F, Barrett JW, Koropatnick J, Nichols AC, Mymryk JS, et al. Treatment-naive HPV+ head and neck cancers display a T-cell-inflamed

phenotype distinct from their HPV- counterparts that has implications for immunotherapy. *Oncoimmunology* (2018) 7(10):e1498439. doi: 10.1080/2162402X.2018.1498439
9. Wookey VB, Appiah AK, Kallam A, Ernani V, Smith LM, Ganti AK. HPV Status and Survival in Non-Oropharyngeal Squamous Cell Carcinoma of the Head and Neck. *Anticancer Res* (2019) 39(4):1907–14. doi: 10.21873/anticanres.13299
10. Keck MK, Zuo Z, Khattri A, Stricker TP, Brown CD, Imanguli M, et al. Integrative analysis of head and neck cancer identifies two biologically distinct HPV and three non-HPV subtypes. *Clin Cancer Res* (2015) 21(4):870–81. doi: 10.1158/1078-0432.CCR-14-2481
11. Masuda M, Wakasaki T, Toh S. Stress-triggered atavistic reprogramming (STAR) addiction: driving force behind head and neck cancer? *Am J Cancer Res* (2016) 6(6):1149–66.
12. Kasinski AL, Slack FJ. Epigenetics and genetics. MicroRNAs en route to the clinic: progress in validating and targeting microRNAs for cancer therapy. *Nat Rev Cancer* (2011) 11(12):849–64. doi: 10.1038/nrc3166
13. Domingues C, Serambeque BP, Laranjo Candido MS, Marto CMM, Veiga FJB, Sarmento Antunes Cruz Ribeiro AB, et al. Epithelial-mesenchymal transition and microRNAs: Challenges and future perspectives in oral cancer. *Head Neck* (2018) 40(10):2304–13. doi: 10.1002/hed.25381
14. Koshizuka K, Hanazawa T, Arai T, Okato A, Kikkawa N, Seki N. Involvement of aberrantly expressed microRNAs in the pathogenesis of head and neck squamous cell carcinoma. *Cancer Metastasis Rev* (2017) 36(3):525–45. doi: 10.1007/s10555-017-9692-y
15. Ganju A, Khan S, Hafeez BB, Behrman SW, Yallapu MM, Chauhan SC, et al. miRNA nanotherapeutics for cancer. *Drug Discov Today* (2017) 22(2):424–32. doi: 10.1016/j.drudis.2016.10.014
16. Kozomara A, Birgaoanu M, Griffiths-Jones S. miRBase: from microRNA sequences to function. *Nucleic Acids Res* (2019) 47(D1):D155–62. doi: 10.1093/nar/gky1141
17. Love MI, Huber W, Anders S. Moderated estimation of fold change and dispersion for RNA-seq data with DESeq2. *Genome Biol* (2014) 15(12):550. doi: 10.1186/s13059-014-0550-8
18. Zhu A, Ibrahim JG, Love MI. Heavy-tailed prior distributions for sequence count data: removing the noise and preserving large differences. *Bioinformatics* (2019) 35(12):2084–92. doi: 10.1093/bioinformatics/bty895
19. Yu G, Wang LG, Han Y, He QY. clusterProfiler: an R package for comparing biological themes among gene clusters. *OMICS* (2012) 16(5):284–7. doi: 10.1089/omi.2011.0118
20. Fakhry C, Westra WH, Li S, Cmelak A, Ridge JA, Pinto H, et al. Improved survival of patients with human papillomavirus-positive head and neck squamous cell carcinoma in a prospective clinical trial. *J Natl Cancer Inst* (2008) 100(4):261–9. doi: 10.1093/jnci/djn011
21. Zhang ZL, Zhao LJ, Chai L, Zhou SH, Wang F, Wei Y, et al. Seven LncRNA-mRNA based risk score predicts the survival of head and neck squamous cell carcinoma. *Sci Rep* (2017) 7(1):309. doi: 10.1038/s41598-017-00252-2
22. Xing L, Zhang X, Chen A. Prognostic 4-lncRNA-based risk model predicts survival time of patients with head and neck squamous cell carcinoma. *Oncol Lett* (2019) 18(3):3304–16. doi: 10.3892/ol.2019.10670
23. Pan Y, Liu G, Wang D, Li Y. Analysis of lncRNA-Mediated ceRNA Crosstalk and Identification of Prognostic Signature in Head and Neck Squamous Cell Carcinoma. *Front Pharmacol* (2019) 10:150. doi: 10.3389/fphar.2019.00150
24. Yang B, Shen J, Xu L, Chen Y, Che X, Qu X, et al. Genome-Wide Identification of a Novel Eight-lncRNA Signature to Improve Prognostic Prediction in Head and Neck Squamous Cell Carcinoma. *Front Oncol* (2019) 9:898. doi: 10.3389/fonc.2019.00898
25. Cui J, Wen Q, Tan X, Piao J, Zhang Q, Wang Q, et al. An integrated nomogram combining lncRNAs classifier and clinicopathologic factors to predict the recurrence of head and neck squamous cell carcinoma. *Sci Rep* (2019) 9(1):17460. doi: 10.1038/s41598-019-53811-0
26. Lajer CB, Garnaes E, Friis-Hansen L, Norrild B, Therkildsen MH, Glud M, et al. The role of miRNAs in human papilloma virus (HPV)-associated cancers: bridging between HPV-related head and neck cancer and cervical cancer. *Br J Cancer* (2012) 106(9):1526–34. doi: 10.1038/bjc.2012.109
27. Lajer CB, Nielsen FC, Friis-Hansen L, Norrild B, Borup R, Garnaes E, et al. Different miRNA signatures of oral and pharyngeal squamous cell carcinomas: a prospective translational study. *Br J Cancer* (2011) 104 (5):830–40. doi: 10.1038/bjc.2011.29
28. Bozinovic K, Sabol I, Dediol E, Milutin Gasperov N, Manojlovic S, Vojtechova Z, et al. Genome-wide miRNA profiling reinforces the importance of miR-9 in human papillomavirus associated oral and oropharyngeal head and neck cancer. *Sci Rep* (2019) 9(1):2306. doi: 10.1038/s41598-019-38797-z
29. Miller DL, Davis JW, Taylor KH, Johnson J, Shi Z, Williams R, et al. Identification of a human papillomavirus-associated oncogenic miRNA panel in human oropharyngeal squamous cell carcinoma validated by bioinformatics analysis of the Cancer Genome Atlas. *Am J Pathol* (2015) 185(3):679–92. doi: 10.1016/j.ajpath.2014.11.018
30. Cillo AR, Kurten CHL, Tabib T, Qi Z, Onkar S, Wang T, et al. Immune Landscape of Viral- and Carcinogen-Driven Head and Neck Cancer. *Immunity* (2020) 52(1):183–99 e9. doi: 10.1016/j.immuni.2019.11.014
31. Hanna GJ, Liu H, Jones RE, Bacay AF, Lizotte PH, Ivanova EV, et al. Defining an inflamed tumor immunophenotype in recurrent, metastatic squamous cell carcinoma of the head and neck. *Oral Oncol* (2017) 67:61–9. doi: 10.1016/j.oraloncology.2017.02.005
32. Hegde PS, Karanikas V, Evers S. The Where, the When, and the How of Immune Monitoring for Cancer Immunotherapies in the Era of Checkpoint Inhibition. *Clin Cancer Res* (2016) 22(8):1865–74. doi: 10.1158/1078-0432.CCR-15-1507
33. Vinuesa CG, Linterman MA, Yu D, MacLennan IC. Follicular Helper T Cells. *Annu Rev Immunol* (2016) 34:335–68. doi: 10.1146/annurev-immunol-041015-055605
34. Lukesova E, Boucek J, Rotnaglova E, Salakova M, Koslabova E, Grega M, et al. High level of Tregs is a positive prognostic marker in patients with HPV-positive oral and oropharyngeal squamous cell carcinomas. *BioMed Res Int* (2014) 2014:303929. doi: 10.1155/2014/303929
35. Wansom D, Light E, Thomas D, Worden F, Prince M, Urba S, et al. Infiltrating lymphocytes and human papillomavirus-16–associated oropharyngeal cancer. *Laryngoscope* (2012) 122(1):121–7. doi: 10.1002/lary.22133
36. Xu ZH, Yao TZ, Liu W. miR-378a-3p sensitizes ovarian cancer cells to cisplatin through targeting MAPK1/GRB2. *BioMed Pharmacother* (2018) 107:1410–7. doi: 10.1016/j.biopha.2018.08.132
37. Wang T, Hou J, Li Z, Zheng Z, Wei J, Song D, et al. miR-15a-3p and miR-16-1-3p Negatively Regulate Twist1 to Repress Gastric Cancer Cell Invasion and Metastasis. *Int J Biol Sci* (2017) 13(1):122–34. doi: 10.7150/ijbs.14770
38. Kleemann M, Schneider H, Unger K, Bereuther J, Fischer S, Sander P, et al. Induction of apoptosis in ovarian cancer cells by miR-493-3p directly targeting AKT2, STK38L, HMGA2, ETS1 and E2F5. *Cell Mol Life Sci* (2019) 76(3):539–59. doi: 10.1007/s00018-018-2958-x
39. Swarbrick A, Woods SL, Shaw A, Balakrishnan A, Phua Y, Nguyen A, et al. miR-380-5p represses p53 to control cellular survival and is associated with poor outcome in MYCN-amplified neuroblastoma. *Nat Med* (2010) 16 (10):1134–40. doi: 10.1038/nm.2227
40. Wang Y, Chang W, Chang W, Chang X, Zhai S, Pan G, et al. MicroRNA-376c-3p Facilitates Human Hepatocellular Carcinoma Progression via Repressing AT-Rich Interaction Domain 2. *J Cancer* (2018) 9(22):4187–96. doi: 10.7150/jca.27939
41. Chu CA, Lee CT, Lee JC, Wang YW, Huang CT, Lan SH, et al. MiR-338-5p promotes metastasis of colorectal cancer by inhibition of phosphatidylinositol 3-kinase, catalytic subunit type 3-mediated autophagy pathway. *EBioMedicine* (2019) 43:270–81. doi: 10.1016/j.ebiom.2019.04.010
42. Long J, Luo J, Yin X. MiR-338-5p promotes the growth and metastasis of malignant melanoma cells via targeting CD82. *BioMed Pharmacother* (2018) 102:1195–202. doi: 10.1016/j.biopha.2018.03.075
43. Vander Heiden MG, DeBerardinis RJ. Understanding the Intersections between Metabolism and Cancer Biology. *Cell* (2017) 168(4):657–69. doi: 10.1016/j.cell.2016.12.039
44. Eke I, Cordes N. Focal adhesion signaling and therapy resistance in cancer. *Semin Cancer Biol* (2015) 31:65–75. doi: 10.1016/j.semcancer.2014.07.009
45. Lee S, Rauch J, Kolch W. Targeting MAPK Signaling in Cancer: Mechanisms of Drug Resistance and Sensitivity. *Int J Mol Sci* (2020) 21(3):1102. doi: 10.3390/ijms21031102
46. Mao L, Zhao ZL, Yu GT, Wu L, Deng WW, Li YC, et al. gamma-Secretase inhibitor reduces immunosuppressive cells and enhances tumour immunity in

head and neck squamous cell carcinoma. *Int J Cancer* (2018) 142(5):999–1009. doi: 10.1002/ijc.31115
47. Oshimori N, Oristian D, Fuchs E. TGF-beta promotes heterogeneity and drug resistance in squamous cell carcinoma. *Cell* (2015) 160(5):963–76. doi: 10.1016/j.cell.2015.01.043
48. Liao Y, Cao L, Wang F, Pang R. miR-605-5p promotes invasion and proliferation by targeting TNFAIP3 in non-small-cell lung cancer. *J Cell Biochem* (2020) 121(1):779–87. doi: 10.1002/jcb.29323
49. Bao C, Lu Y, Chen J, Chen D, Lou W, Ding B, et al. Exploring specific prognostic biomarkers in triple-negative breast cancer. *Cell Death Dis* (2019) 10(11):807. doi: 10.1038/s41419-019-2043-x
50. Jiang J, Xie C, Liu Y, Shi Q, Chen Y. Up-regulation of miR-383-5p suppresses proliferation and enhances chemosensitivity in ovarian cancer cells by targeting TRIM27. *BioMed Pharmacother* (2019) 109:595–601. doi: 10.1016/j.biopha.2018.10.148
51. Wei C, Gao JJ. Downregulated miR-383-5p contributes to the proliferation and migration of gastric cancer cells and is associated with poor prognosis. *PeerJ* (2019) 7:e7882. doi: 10.7717/peerj.7882
52. Zhang J, Kong X, Shi Q, Zhao B. MicroRNA-383-5p acts as a potential prognostic biomarker and an inhibitor of tumor cell proliferation, migration, and invasion in breast cancer. *Cancer Biomark* (2020) 27(4):423–32. doi: 10.3233/CBM-190704
53. Shi Y, Gao X, Hu Q, Li X, Xu J, Lu S, et al. PIK3C2A is a gene-specific target of microRNA-518a-5p in imatinib mesylate-resistant gastrointestinal stromal tumor. *Lab Invest* (2016) 96(6):652–60. doi: 10.1038/labinvest.2015.157

Conflict of Interest: The authors declare that the research was conducted in the absence of any commercial or financial relationships that could be construed as a potential conflict of interest.

Copyright © 2021 Luo, Zheng, Cao, Zhang, Huang, Dai, Tang and Liang. This is an open-access article distributed under the terms of the Creative Commons Attribution License (CC BY). The use, distribution or reproduction in other forums is permitted, provided the original author(s) and the copyright owner(s) are credited and that the original publication in this journal is cited, in accordance with accepted academic practice. No use, distribution or reproduction is permitted which does not comply with these terms.

frontiers in Oncology

ORIGINAL RESEARCH
published: 25 February 2021
doi: 10.3389/fonc.2020.624752

Down-Regulation of Long Non-Coding RNA TINCR Induces Cell Dedifferentiation and Predicts Progression in Oral Squamous Cell Carcinoma

Zehang Zhuang[1,2†], Jing Huang[1,2†], Weiwang Wang[1,2,3†], Cheng Wang[1,2], Pei Yu[4,5], Jing Hu[1,2], Haichao Liu[1,2], Hanqi Yin[6,7], Jinsong Hou[1,2] and Xiqiang Liu[8*]*

[1] Department of Oral and Maxillofacial Surgery, Guanghua School of Stomatology, Hospital of Stomatology, Sun Yat-sen University, Guangzhou, China, [2] Guangdong Provincial Key Laboratory of Stomatology, Sun Yat-sen University, Guangzhou, China, [3] Department of Oral and Maxillofacial Surgery, Xiangya Hospital, Central South University, Changsha, China, [4] Department of Prothodontics, Affiliated Stomatology Hospital of Guangzhou Medical University, Guangzhou, China, [5] Guangzhou Key Laboratory of Basic and Applied Research of Oral Regenerative Medicine, Guangzhou, China, [6] State Key Laboratory of Biocontrol, School of Life Sciences, Sun Yat-Sen University, Guangzhou, China, [7] South China Institute of Biomedine, Guangzhou, China, [8] Department of Oral and Maxillofacial Surgery, NanFang Hospital, Southern Medical University, Guangzhou, China

OPEN ACCESS

Edited by:
Wei Cao,
Shanghai Jiao Tong University, China

Reviewed by:
Yanjie Zhang,
Shanghai Jiao Tong University, China
Gaurisankar Sa,
Bose Institute, India
Chengzhong Lin,
Shanghai Ninth People's Hospital, China

***Correspondence:**
Xiqiang Liu
xiqiangliu@aliyun.com
Jinsong Hou
houjs@mail.sysu.edu.cn

†These authors have contributed equally to this work

Specialty section:
This article was submitted to Head and Neck Cancer, a section of the journal Frontiers in Oncology

Received: *01 November 2020*
Accepted: *30 December 2020*
Published: *25 February 2021*

Citation:
Zhuang Z, Huang J, Wang W, Wang C, Yu P, Hu J, Liu H, Yin H, Hou J and Liu X (2021) Down-Regulation of Long Non-Coding RNA TINCR Induces Cell Dedifferentiation and Predicts Progression in Oral Squamous Cell Carcinoma. Front. Oncol. 10:624752. doi: 10.3389/fonc.2020.624752

Objectives: Recently long non-coding RNAs (lncRNAs) have emerged as novel gene regulators involved in tumorigenic processes, including oral squamous cell carcinoma (OSCC). Here, we identified a differentiation-related lncRNA, terminal differentiation-induced non-coding RNA (TINCR). However, its biological function and clinicopathological significance in OSCC still remain unclear.

Methods: The lncRNA expression profiles in OSCC tissues and paired adjacent non-tumor tissues (NATs) from 10 patients were detected by lncRNA microarrays. Weighted gene co-expression network analysis (WGCNA) and gene ontology (GO) enrichment were performed to identify the most significant module and module functional annotation, respectively. Potential differentiation-related lncRNAs were screened by differential expression analysis. TINCR was further confirmed in OSCC cell lines and tissues of another patient cohort by using qRT-PCR. The correlation between the TINCR expression level and clinicopathological characteristics was analyzed. The effects of TINCR on cell differentiation, migration and invasion were assessed by knockdown or knock-in *in vitro* and *in vivo*.

Results: WGCNA and GO enrichment analysis showed that one co-expression network was significantly enriched for epithelial cell differentiation, among which, TINCR was significantly downregulated. qRT-PCR analyses validated down-regulation of TINCR in tumor tissues compared with paired NATs, and its expression was closely correlated with pathological differentiation and lymph node metastasis in patients with OSCC. Patients with lower TINCR expression levels had worse survival. Cell function experiments showed

that TINCR played a crucial role in epithelial differentiation. Both TINCR and epithelial differentiation-associated genes, including IVL and KRT4, were significantly upregulated during OSCC cell calcium-induced differentiation but were reduced when cell dedifferentiation occurred in tumor spheres. Overexpression of TINCR dramatically suppressed cell dedifferentiation, migration and invasion *in vitro*, while knockdown of TINCR had the opposite effects. Upregulation of TINCR significantly elevated the expression of terminal differentiation genes and repressed tumor growth *in vivo*. Moreover, TINCR significantly suppressed the activation of JAK2/STAT3 signaling in OSCC cells.

Conclusion: Our study suggests that TINCR functions as a tumor suppressor by inducing cell differentiation through modulating JAK2/STAT3 signaling in OSCC. TINCR may serve as a prognostic biomarker and therapeutic target for OSCC.

Keywords: lncRNAs (long non-coding RNAs), TINCR (tissue differentiation-inducing non-protein coding RNA), OSCC (oral squamous cell carcinoma), cell differentiation, metastasis, progression

INTRODUCTION

Head and neck cancer is the sixth most common malignancy and is a major cause of cancer morbidity and mortality worldwide (1). Oral squamous cell carcinoma (OSCC), comprising a major portion of head and neck cancers, accounts for approximately 90% of all oral malignancies (2). Based on the statistics from the American Cancer Society (http://seer.cancer.gov/statfacts/html/oralcav.html), an estimated 48,000 new OSCC cases occurred in 2016, composing 3% of all new malignancies (3). Despite aggressive treatment methods, including radiation therapy, chemotherapy and surgery, the 5-year survival rate remains at 50–55%, with little improvement due to rapid metastasis and a high regional relapse rate (4). Thus, there is an urgent need for a deeper understanding of OSCC pathogenesis to develop effective therapeutic approaches.

Long non-coding RNAs (lncRNAs) were first described during the large-scale sequencing of full-length cDNA libraries in the mouse (5) and refer to RNAs with no protein coding potential that are transcribed to RNA molecules longer than 200 nucleotides (6). Although lncRNAs have been extensively studied over the past several decades, very little is known about the specific role of lncRNAs. However, the recent explosion of knowledge highlighting the importance of lncRNAs in the regulation of diverse major biological processes, including but not limited to development, differentiation, and metabolism, has brought these ignored molecular players to the forefront (6).

Terminal differentiation-induced non-coding RNA (TINCR) is an important regulatory molecule for epithelial differentiation. Studies have shown that TINCR regulates the differentiation-related gene KRT80 by forming a TINCR-STAU1 complex (7). Accumulating evidence suggests that TINCR is involved in malignant progression, including tumor growth, metastasis, and chemoradiation resistance (8–12). However, the relationship between TINCR and tumor differentiation and the potential mechanism remain unclear.

In this study, we aimed to explore the role of TINCR in OSCC, especially the relationship between TINCR and tumor cell differentiation. We hoped to find a potential biomarker for predicting the prognosis of OSCC patients that is beneficial for OSCC treatment.

MATERIALS AND METHODS

Patient Tissue Samples

A total of 42 human OSCC specimens were enrolled in this study that were pathologically diagnosed at the Hospital of Stomatology, Sun Yat-Sen University between 2013 and 2015. All patients received radical surgery without receiving any form of pre-surgical adjuvant therapy. All patients were given written informed consent for the purposes of the study. The study was approved by the Ethical Committee of Hospital of Stomatology, Sun Yat-sen University. All studies of patient specimens were conducted in accordance with the Declaration of Helsinki.

Cell Lines

The human OSCC cell lines SCC9, SCC15, and CAL27 were obtained from ATCC (Rockville, MD, USA). UM1, UM2 and SCC1 were provided by Dr. Xiaofeng Zhou (University of Illinois at Chicago, IL, USA). HSC3, HSC6, HN6, CAL33 and normal oral keratinocytes (NOK) were kindly provided by J. Silvio Gutkind (NIH, Bethesda, MD, USA). UM1, UM2, SCC9, SCC15 and SCC25 cell lines were cultured in Dulbecco's modified Eagle's medium/Ham's F12 (Gibco, Rockville, MD, USA) supplemented with 10% fetal bovine serum (FBS, Gibco). SCC1, HSC3, HSC6, HN6, CAL27 and CAL33 cells were cultivated in Dulbecco's modified Eagle's medium (DMEM, Gibco) supplemented with 10% FBS (Gibco). NOK cells were grown in keratinocyte serum-free medium containing human recombinant epidermal growth factor and bovine pituitary extract (Life Technologies). All cells were incubated at 37°C in a humidified atmosphere with 5% CO_2. All cell lines were routinely tested for Mycoplasma with PlasmoTest^{TM} Mycoplasma contamination detection kit (InvivoGen).

mRNA and lncRNA Microarray

Total RNA was amplified and labeled with a Low Input Quick Amp Labeling Kit, One-Color (Agilent Technologies, Santa Clara, CA, USA) following the manufacturer's instructions. Labeled cRNA was purified with an RNeasy mini kit (QIAGEN, Duesseldorf, Germany). Each slide was hybridized with 1.65 μg Cy3-labeled cRNA using a Gene Expression Hybridization Kit (Agilent Technologies) in a hybridization oven (Agilent Technologies) according to the manufacturer's instructions. After 17 h of hybridization, slides were washed in staining dishes (Thermo Shandon, Waltham, MA, USA) with a Gene Expression Wash Buffer Kit (Agilent Technologies). Slides were then scanned by an Agilent Microarray Scanner (Agilent Technologies) with default settings (dye channel: green, scan resolution = 3 μm, 20 bit). Data were extracted with Feature Extraction software 10.7 (Agilent Technologies). Raw data were normalized by the quantile algorithm, Gene Spring Software 11.0 (Agilent Technologies).

Subcellular Fractionation Location

Nuclear and cytoplasmic components were isolated by using the PARIS Kit (Life Technologies, USA) according to the manufacturer's instructions.

Quantitative Real-Time PCR (qRT-PCR)

Briefly, TRIzol reagent (Invitrogen, CA, USA) was used to isolate total RNA according to the manufacturer's instructions. PrimeScript™ RT Master Mix (TaKaRa, Japan) was used to perform reverse transcription. qRT-PCR was performed using SYBR GREEN I Master Mix (Roche, Basel, Switzerland) on a Light Cycler 480 system (Roche) according to the manufacturer's instructions. After normalization to the GAPDH expression levels, the relative expression levels were calculated using the $2^{-\Delta\Delta T}$ method. The forward and reverse primer sequences used for qRT-PCR are shown in **Supplementary Table 1**.

Western Blotting

Western blotting was performed as described previously (13). Specifically, antibodies against KRT4 (Abcam, Cambridge, UK) and IVL (Sigma-Aldrich, St Louis, MO, USA) were used as primary antibodies at a dilution of 1:1000. GAPDH (1:1000, Cell Signaling Technology, Danvers, MA, USA) was used as an internal reference. The target proteins were detected with an ECL kit (Millipore, Billerica, MA, USA) and quantified with ImageJ software analysis.

RNAScope Assay

The RNAScope targeting probe of TINCR was designed and synthesized by Advanced Cell Diagnostics, and the analysis of TINCR expression was performed with the RNAscope® 2.5 High Definition (HD) Detection Reagent-BROWN (Advanced Cell Diagnostics, USA) according to the manufacturer's instructions. The images were acquired by an Aperio ImageScope (Leica Biosystems, Germany).

Cell Transfection

Transient transfection was performed using Lipofectamine RNA iMAX Transfection Reagent (Invitrogen) according to the manufacturer's instructions. TINCR siRNA was designed and synthesized by GenePharma (Shanghai, China). The sequences were designed as follows: sense, 5'-GGUACUGGCUGA AGGAAUATT-3'; antisense, 5'-UAUUCCUUCAGCCAGU ACCTT-3'. The TINCR lentiviral vector (pEZ-TINCR) and control vector were constructed by GeneCopoeia (Rockville, MD, USA).

Transwell Assay

Cell migration and invasion were measured with a BD BioCoat™ system (BD Biosciences, San Jose, CA, USA). The assays were performed as previously described (14). Briefly, for migration assays, cells were seeded into the upper chambers without Matrigel-coated membranes and cultured with serum-free medium, while the lower chambers were filled with complete medium. For invasion assays, cells were seeded into the upper chambers with Matrigel-coated membranes. The cells were incubated at 37°C for 24 h. The cells on the top surface of the chamber were removed with a cotton swab, and then the cells on the lower surface of the membrane were fixed in 4% paraformaldehyde for 25 min. Cells were stained with 0.1% crystal violet (Sigma-Aldrich), and the cells were counted under a Zeiss microscope (Germany).

Wound Healing Assay

Cells were plated into 6-well plates and incubated at 37°C for 24 h. A 200-μL pipette tip was used to make a straight scratch, and the cells was washed with PBS. Then, medium without FBS was added. Images were taken under an inverted microscope (Carl Zeiss).

Cell Counting Kit-8 Assay

Cell proliferation was analyzed using the Cell Counting Kit-8 (CCK-8, Sigma-Aldrich). Briefly, 2×10^3 cells were seeded in triplicate into a 96-well plate. Cell viability was assessed at 0, 24, 48, 72, and 96 h. The absorbance was measured at 450 nm using a microplate reader (Genios TECAN, Männedorf, Schweiz).

Tumor Sphere-forming Assay

Tumor sphere-forming assays were performed as previously described (14). In brief, cells were plated into ultra-low attachment 6-well plates with serum-free medium supplemented with 2% B27 (Invitrogen), 10 ng/mL epidermal growth factor (EGF, Invitrogen), and 10 ng/mL basic fibroblast growth factor (bFGF, Invitrogen). The medium was changed every three days until the diameters of spheres exceeded 40 μm.

In Vivo Experiments

All animal studies were conducted with the approval of the Sun Yat-sen University Institutional Animal Care and Use Committee and were performed in accordance with established guidelines. Female BALB/c nude mice aged 4–6 weeks were purchased from the Animal Care Unit of Guangdong and maintained in specific pathogen-free (SPF) conditions. After being suspended in 100 μL sterilized PBS, 1×10^6 HSC3 cells were subcutaneously injected into the armpit of the forelimb. Tumor growth was observed on a regular basis, and the volume

was measured with a Vernier caliper. Tumor volume was calculated with the following formula: tumor volume = (length × width × width/2). At 18 days after injection, the mice were sacrificed, and the tumor xenografts were weighed and collected.

Weighted Gene Co-Expression Network Construction

The expression profile of the microarray was used to construct a gene co-expression network by using the R package "WGCNA". Pearson's correlation analysis of all pairs of genes was used to construct an adjacency matrix, which was used to construct a scale-free co-expression network based on the soft-thresholding parameter β. Then, the adjacency matrix was turned into a topological overlap matrix (TOM), which represented the overlap in the shared neighbors to further identify functional modules in the co-expression network.

Identification of Clinical Significant Modules

The correlation between modules and clinical features was evaluated by Pearson's correlation coefficient (PCC) analysis. Clinical information included tissue (cancerous or not) and lymph node status (metastatic or not). The correlation between the module eigengenes (MEs) and the clinical features was assessed to identify clinical significant modules.

Gene Ontology (GO) Enrichment Analysis

GO enrichment analysis was performed on key modules using the R package clusterProfiler. $P<0.01$ was defined as a significant enrichment analysis result.

Statistical Analysis

All statistical analyses were performed using SPSS 20.0 software (SPSS Inc., Chicago, IL, USA) or GraphPad Prism 8 (La Jolla, CA, USA). Student's *t*-test, the Wilcoxon test or the χ^2 test was used to analyze two-group comparisons. The Kaplan–Meier method and log-rank test were performed to evaluate survival outcomes. Differences were considered statistically significant at $P < 0.05$.

RESULTS

WGCNA Construction and Gene Module Recognition

To screen lncRNAs that are deregulated in OSCC, we comparatively analyzed mRNA and lncRNA profiles of 10 OSCC patient samples and their paired non-cancerous adjacent counterparts. The microarray data were subjected to differential expression analysis. According to the microarray data, we identified 1603 transcripts that were upregulated with a more than 2-fold change (FC) in OSCC samples compared to non-cancerous adjacent tissues (NATs), while 989 transcripts were downregulated by more than 2-fold (**Supplementary Figure 1**).

To further explore the co-expression patterns of the lncRNAs and mRNAs in OSCC, weighed gene co-expression network analysis (WGCNA) was performed. A total of 16130 genes, consisting of 4549 lncRNAs and 11581 mRNAs, were used for cluster analysis with the WGCNA package. In this study, a power of $\beta = 20$ (scale-free $R^2 = 0.80$) was selected for the soft-thresholding to ensure the network was scale-free, and 23 modules were obtained for subsequent analysis (**Figure 1A**). Each of the modules was marked by a color, while the gray module was a gene that was not co-expressed (**Figure 1B**).

We constructed a topological overlap matrix (TOM) plot to analyze the interaction among the 23 modules, which demonstrated the relative independence of the modules. We also found the strong co-expression relationships among the genes in the blue module (**Figure 1C**). To determine whether any of the identified expression modules were associated with the progression of OSCC, we explored the relationships between the modules and tissue (cancerous or not), and lymph node status (metastatic or not). As shown in **Figure 1D**, compared with other modules, the blue module, as well as the dark turquoise and turquoise modules, were strongly correlated with the tissue and lymph node status, respectively. Among them, the blue and dark turquoise modules were both positively correlated with the tissue ($r = 0.88$, $p = 4e\text{-}07$ for blue, $r = 0.77$, $p = 6e\text{-}05$ for dark turquoise) and lymph node status ($r = 0.77$, $p = 7e\text{-}05$ for blue, $r = 0.77$, $p = 8e\text{-}05$ for dark turquoise), whereas the turquoise module had the highest negative correlation with the tissue ($r = -0.93$, $p = 2e\text{-}09$) and lymph node status ($r = -0.82$, $p = 9e\text{-}06$) in OSCC. In addition, the heatmap based on adjacencies showed that the blue module was most closely related to the tissue status (**Figure 1E**). The scatter plot also illustrated the associations between the blue modules and the genetic significance (**Figure 1F**). All the results suggest that the blue module is the module that is the most relevant to OSCC progression. Therefore, the blue module was chosen for further analysis.

Module Functional Annotation and Screening Cell Differentiation Related LncRNAs in OSCC

To elucidate the biological functions of the module genes, GO enrichment analysis of the blue module was performed by using the "clusterProfiler" R package (**Figure 2A**). The results showed that the principal biological functions of the blue module were closely related to epithelial development and epithelial cell differentiation, which demonstrated that the genes of the blue module were mainly involved in the regulation of epithelial cell differentiation (**Figure 2A**).

Of the 2052 mapped genes in the blue module, 1005 genes with high fluorescence intensity on the Agilent Microarray Platform were identified based on the threshold of spot flag≥9 in 10 OSCC samples or in 10 non-cancerous adjacent counterparts. Then, the 1005 genes were subjected to differential expression analysis (**Figure 2B**). A total of 375 differentially expressed genes (DEGs) were screened under the threshold of false discovery rate (FDR) <0.05 and $\log_2$FC ≥1 or ≤-1, of which 2 lncRNAs were identified, TINCR and C5orf66-AS1 (**Figure 2B**). Recent studies have revealed that TINCR plays a pivotal role in normal epidermal differentiation. In addition, emerging evidence has

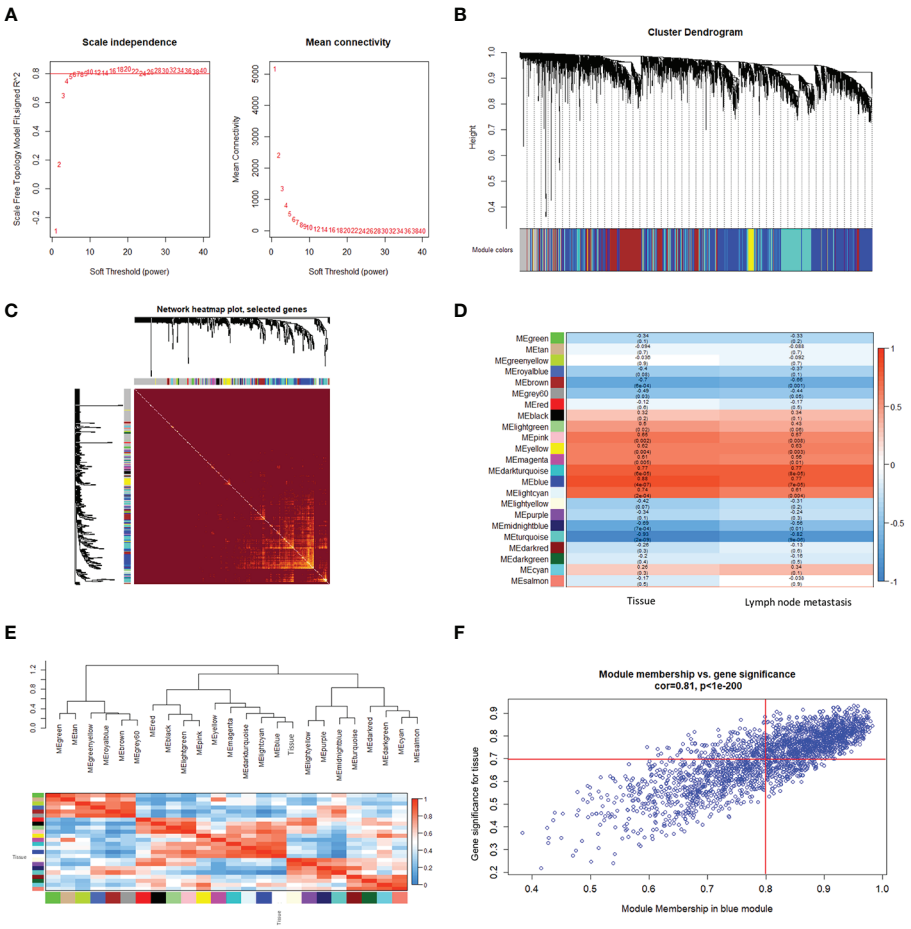

FIGURE 1 | Construction of a weighted gene co-expression network. **(A)** Analysis of the scale-free fitting index for soft threshold powers (β) and the mean connectivity for soft threshold powers. **(B)** Hierarchical clustering dendrograms of identified co-expressed genes in modules in OSCC. Each colored row represents a color-coded module that contains a group of highly connected genes. The gray module indicates none co-expression between the genes. **(C)** Twenty-three significant co-expression gene modules were identified with a topological overlap matrix (TOM) plot. The different colors of the horizontal and vertical axes represent different modules. The yellow brightness in the middle indicates the degree of connection between the different modules. **(D)** Heatmap of the Pearson correlation coefficient (PCC) between module eigengenes (MEs) and clinical information of OSCC. Each cell contains the correlation coefficient and *P*-value. The color of the cell reflects the size of the correlation coefficient, as shown in the legend on the right. **(E)** Correlated heatmap plot of the adjacency modules in the WGCNA. The rectangle of each row and column represents an ME. In the correlated heatmap plot, light blue represents low adjacency, while red represents high adjacency. **(F)** Scatter plot of module eigengenes related to the tissue in the blue module.

suggested that the aberrant expression of TINCR is associated with cell growth, metastasis, and drug resistance in human cancers. However, the specific role of TINCR in the cell differentiation of OSCC is still not fully understood. Therefore, TINCR was selected for further investigation.

TINCR Was Downregulated in OSCC Tissues and Associated With a Poor Prognosis

To explore the expression of TINCR in OSCC tissues, 42 OSCC samples and their paired non-cancerous adjacent counterparts were employed to detect the expression of TINCR by qRT-PCR. Our results showed that TINCR was dramatically downregulated in OSCC tissues compared to NATs (**Figure 2C**). To further clarify the association of TINCR expression with clinicopathological characteristics in OSCC patients, the 42 patients were divided into a low-expression group (n = 24, 57.1%) and a high-expression group (n = 18, 42.9%) based on the median expression level of TINCR. As presented in **Table 1**, the expression level of TINCR was negatively associated with lymph node metastasis (**Figure 2D**) and positively correlated with pathological differentiation (**Figure 2E**) in OSCC patients. However, no significant association between TINCR expression level and patient sex, age, tumor size, T classification or clinical stage was observed (**Table 1**). To further confirm these findings, we downloaded the RNA sequencing dataset of 481 head and neck squamous cell carcinoma (HNSCC) tissues from the TCGA database. As expected, the expression level of TINCR was significantly lower in poorly differentiated tissues than in well-differentiated tissues (**Figure 2F**). Furthermore, Kaplan-Meier

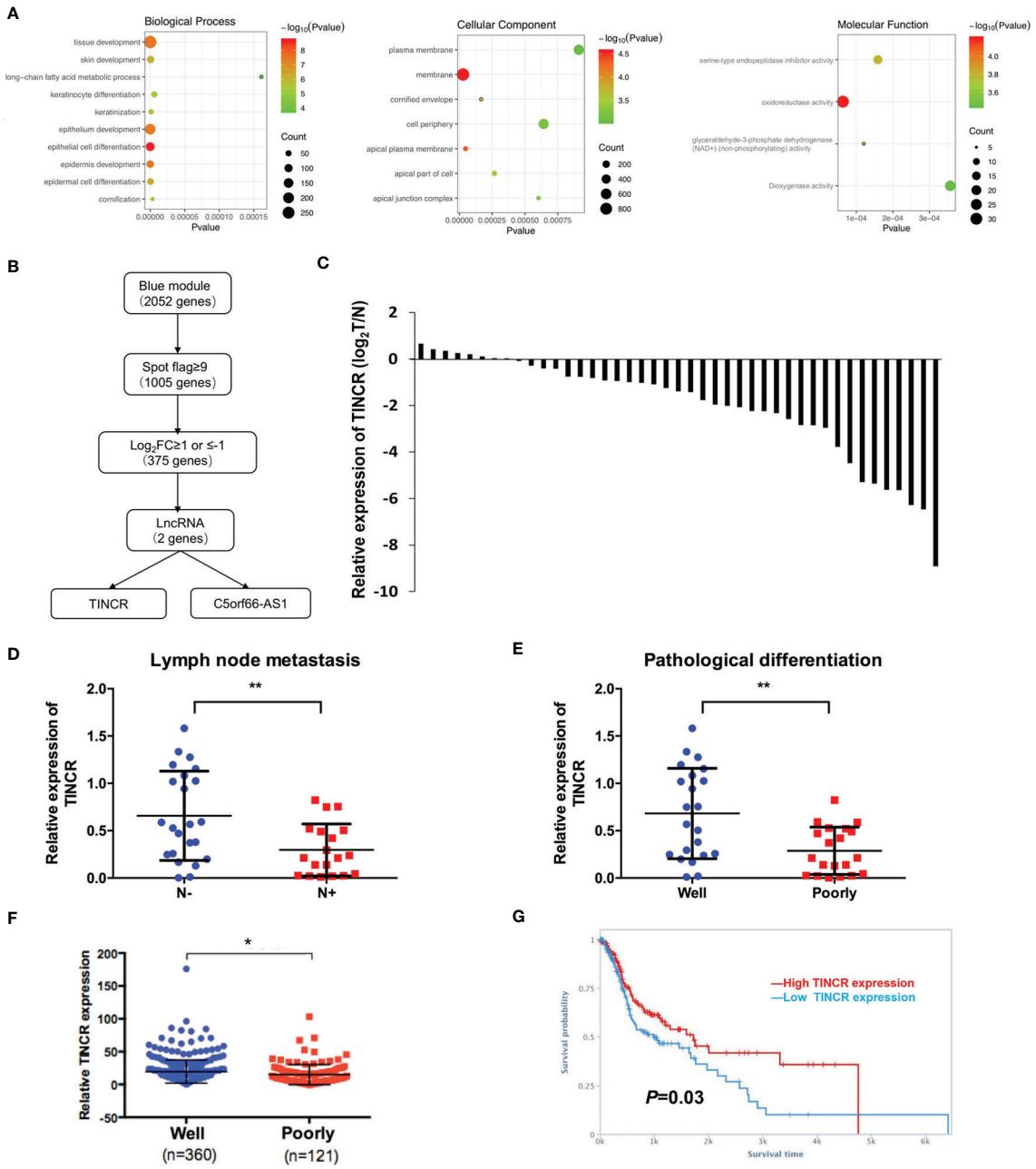

FIGURE 2 | TINCR was downregulated in OSCC tissues. **(A)** Enrichment of the gene ontology (GO) terms of mRNAs in the blue module. **(B)** A workflow of lncRNA screening. **(C)** The expression of TINCR in OSCC tissues and non-cancerous adjacent tissues (NATs) was shown by qRT-PCR. qRT-qPCR analysis of TINCR expression in OSCC samples grouped by the lymph node metastasis **(D)** and the pathological differentiation **(E)**. **(F)** Analysis of TINCR expression in HNSCC samples from the TCGA database, and the HNSCC samples were grouped by the pathological differentiation. **(G)** Kaplan-Meier analysis from TANRIC database based on the HNSCC patient cohort of TCGA showed that the high TINCR expression group had a higher survival rate than the low TINCR expression group. *P < 0.05, **P < 0.01.

analysis showed that overall survival was significantly worse in the TINCR low-expression group than that in the TINCR high group (**Figure 2G**). These results indicate that down-regulation of TINCR is associated with tumor progression and worse prognosis in patients with OSCC.

TINCR Was Involved in the Cell Differentiation of OSCC

To choose appropriate cell lines to manipulate the expression of TINCR and examine its potential biological function, the expression of TINCR in several OSCC cell lines and normal

TABLE 1 | Correlation of TINCR expression with clinicopathological features of OSCC patients (n = 42).

Characteristics	Number	TINCR Expression		*P*
		Low	High	
Gender				
Male	26	16	10	0.463
Female	16	8	8	
Age				
≤55y	25	15	10	0.650
>55y	17	9	8	
Tumor size				
≤4cm	22	12	10	0.721
>4cm	20	12	8	
LN metastasis				
Negative	23	10	13	**0.049**
Positive	19	14	5	
Pathological differentiation				
Well	22	9	13	**0.026**
Moderately/Poorly	20	15	5	
T classification				
T1-T1	22	12	10	0.721
T3-T4	20	12	8	
Clinical stage				
I-II	15	8	7	0.710
III-IV	27	16	11	

Bold values means P < 0.05.

oral keratinocytes (NOKs) was detected by using qRT-PCR. The results in **Figure 3A** showed that TINCR expression was markedly lower in a panel of 11 OSCC cell lines than that in NOK cells, which was consistent with the findings in the OSCC tissues. Notably, the expression of TINCR in UM1 and HSC6 cell lines was higher than that in CAL33 and HSC6 cells, which were then subjected to further experiments *in vitro*. To determine the subcellular localization of TINCR, we detected the expression level of TINCR in the cytoplasmic and nuclear fractions of HSC3 and HSC6 cells. As shown in **Supplementary Figures 2A, B**, qRT-PCR analysis revealed that 86.65 and 73.61% of the TINCR transcripts were detected in the nuclear fraction, respectively, while 13.35 and 26.39% were found in the cytoplasmic fraction. To examine alterations in TINCR expression during OSCC cell differentiation, we treated the OSCC cell lines HSC3 and CAL33 with $CaCl_2$ (2.4 mmol/liter) for 2 days, and then total RNA and proteins were extracted. We found that the expression of TINCR was increased during OSCC cells calcium-induced differentiation. Meanwhile, both involucrin (IVL) and keratin 4 (KRT4), two commonly recognized differentiation-associated genes (15), were upregulated as well (**Figures 3B, C**). A Western blotting assay confirmed the increased levels of IVL and KRT4 proteins (**Figures 3D, E**). To further validate these findings, we treated the HSC3 cell line with all-trans retinoic acid (ATRA, 10 mmol/liter), another well-accepted differentiation inducer. As expected, ATRA increased expression levels of TINCR, IVL and KRT4 over time (**Supplementary Figures 3A, B**). Tumor sphere-forming assays were also performed to confirm our findings. Two OSCC cell lines, UM1 and HSC6, were cultured in non-adherent serum-free conditions, and total RNA and protein were collected for further analysis. As illustrated in **Figures 3F, G**, the mRNA levels of IVL and KRT4 were suppressed, accompanied by the down-regulation of TINCR when cell dedifferentiation occurred in tumor spheres. Similar results were also observed in the results of a Western blotting assay (**Figures 3H, I**). Correlation analysis showed that the expression of endogenous TINCR was positively correlated with expression levels of KRT4 and IVL (**Supplementary Figures 4A, B**). Moreover, a positive correlation between the basic expression level of TINCR and IVL or KRT4 was also observed in HNSCC patients from TCGA database using GEPIA (**Supplementary Figures 4C, D**). Taken together, our data suggested that TINCR may play a pivotal role in OSCC cell differentiation.

TINCR Induced Cell Differentiation and Suppressed Migration, Invasion and Proliferation in OSCC Cells

To investigate the effect of TINCR on OSCC cell differentiation, functional analyses were performed by using the lentivirus-mediated stable overexpression of TINCR (pEZ-TINCR) in OSCC cell lines, including HSC3 and CAL33, both of which have low TINCR expression levels. The TINCR transfection efficiency was determined by qRT-PCR (**Figures 4A, B**). According to the qRT-PCR results, the elevated expression of TINCR led to the increased expression of differentiation-associated genes, including IVL and KRT4 (**Figures 4A, B**). The results of a Western blotting assay also demonstrated that protein levels of IVL and KRT4 were upregulated by TINCR overexpression (**Figures 4C, D**). In addition, overexpression of TINCR induced a dramatic change in cell-cell contact. Distinct spaces between cells became much less apparent (**Supplementary Figure 5**). Then, siRNA method was adopted to knock down TINCR in UM1 and HSC6 cell lines, in which TINCR was relatively highly expressed. As expected, TINCR depletion significantly reduced the expression of IVL and KRT4 at both the mRNA and protein levels relative to the negative control (**Figures 4E–H**). To study the effect of TINCR on cell migration and invasion, a Transwell assay was performed with TINCR-overexpressing cells. As shown in **Figure 5A**, overexpression of TINCR decreased the migration of CAL33 cells. Similar results were also observed in the HSC3 cell line (**Figure 5B**). Wound healing assays further confirmed that the exogenous upregulation of TINCR contributed to the repression of cell motility in CAL33 and HSC cells (**Figures 5C, D**). Moreover, to explore the effect of TINCR on tumor growth in *vitro*, a CCK-8 assay was performed. As shown in **Figure 5E, F**, overexpression of TINCR decreased the proliferation of HSC3 cells, while deletion of TINCR promoted cell growth in UM1 cells. These results were consistent with our findings in OSCC patients described above and supported the hypothesis that TINCR induces cell differentiation and functions as a tumor suppressor in OSCC.

Overexpression of TINCR Inhibited the Tumorigenesis of OSCC *In Vivo*

To further validate the suppressive effects of TINCR on OSCC tumorigenesis *in vivo*, a xenograft model was established. The TINCR-overexpressing cells (pEZ-TINCR) and corresponding

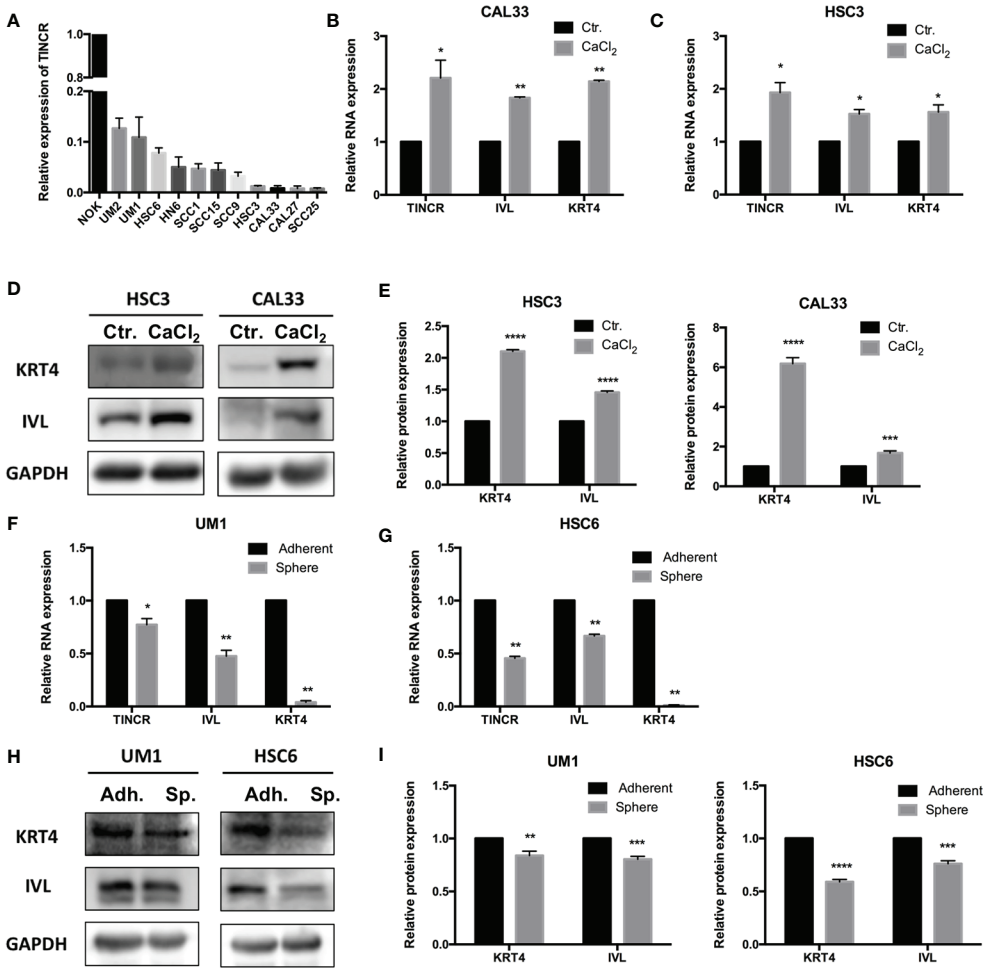

FIGURE 3 | TINCR was involved in the cell differentiation of OSCC. **(A)** The expression of TINCR in OSCC cell lines and NOK cells was examined with qRT-PCR. The expression of TINCR in 11 OSCC cell lines was lower than that in NOK cells. **(B, C)** The expression of TINCR, IVL and KRT4 in OSCC cell lines was examined by qRT-PCR after cells were treated with $CaCl_2$ (2.4 mmol/liter). **(D, E)** Western blot analysis showed that the protein expression of both IVL and KRT4 was upregulated after treatment with $CaCl_2$. Quantification of the relative protein expression levels is shown. **(F, G)** qRT-PCR analysis revealed that the expression of TINCR, IVL and KRT4 was reduced in tumor spheres compared to adherent cells. **(H, I)** Western blot analysis showed that the protein expression of IVL and KRT4 was decreased in tumor spheres. Quantification of the relative protein expression levels is shown. $^{*}P < 0.05$, $^{**}P < 0.01$, $^{***}P < 0.001$, and $^{****}P < 0.0001$.

control cells (NC) were subcutaneously injected into BALB/c nude mice. As shown in **Figures 6A–C**, mice bearing cells overexpressing TINCR had smaller tumors with a lower tumor volume and weight than mice in the control group. Meanwhile, the tumor growth rate in the TINCR overexpression group was slower than that in the control group (**Figure 6B**). Furthermore, the expression level of TINCR in xenograft tumors was also confirmed by qRT-PCR and in situ hybridization assays (**Figures 6D, E**). Xenograft sections stained with IHC showed that the expression of IVL and KRT4 was increased in the TINCR overexpression group compared to the control group, supporting that TINCR may suppress tumor progression by inducing cell differentiation. Collectively, these data suggested that TINCR inhibits OSCC tumorigenesis *in vivo*.

JAK2/STAT3 Signaling Pathway Was Involved in TINCR-Mediated Cell Differentiation

A couple of studies have proven that JAK2/STAT3 signaling plays a key role in modulating keratinocyte differentiation and epithelial carcinogenesis (16–19). Our previous data also suggested that JAK2/STAT3 signaling was involved in the tumorigenesis of HNSCC (20). To investigate the role of JAK2/STAT3 signaling in the TINCR-mediated cell differentiation of OSCC, the expression of key factors in JAK2/STAT3 signaling was detected after TINCR overexpression. Our results showed that TINCR overexpression significantly reduced the expression of JAK2, p-JAK2, STAT3, and p-STAT3 in HSC3 cells (**Figure 6F**). In contrast, all of these proteins were increased after TINCR

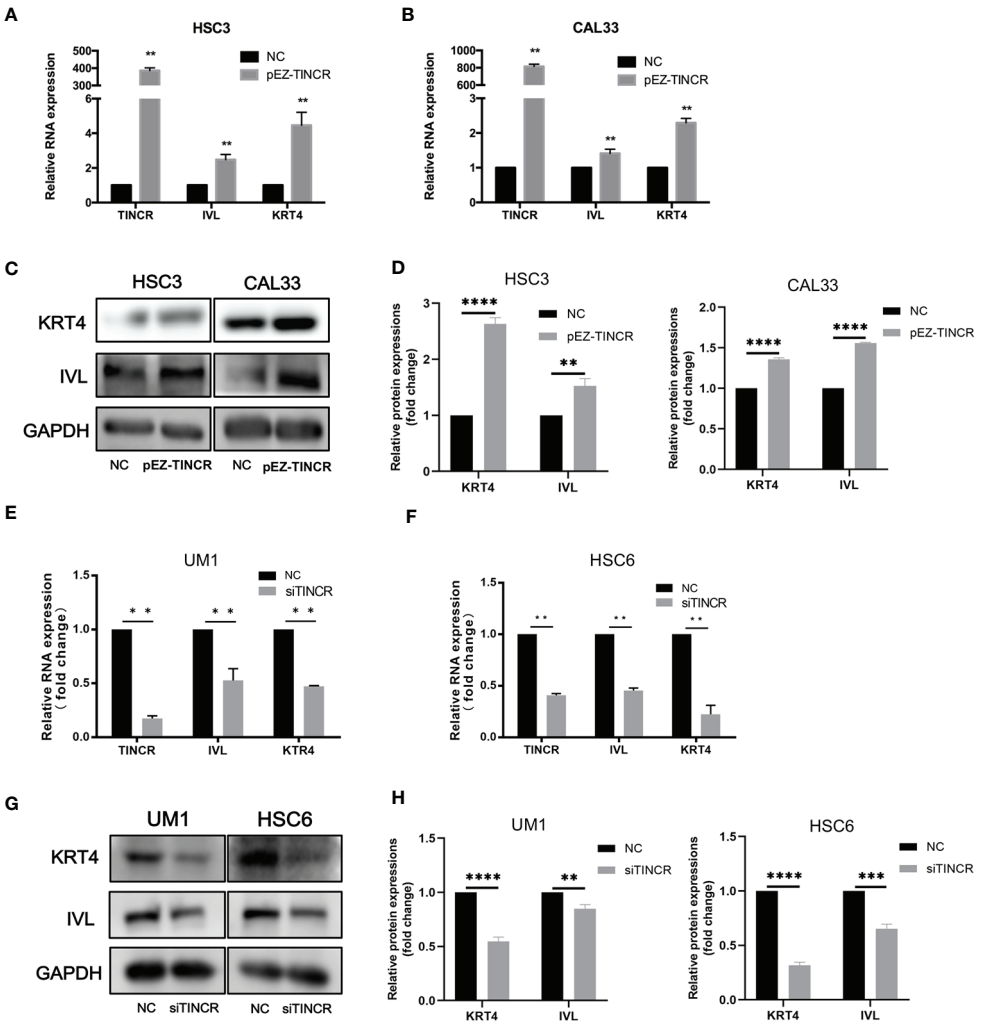

FIGURE 4 | TINCR induced cell differentiation in OSCC cells. **(A, B)** The expression of TINCR, IVL and KRT4 in OSCC cell lines was measured by qRT-PCR after cells were transfected with the TINCR overexpression plasmid. **(C, D)** The protein expression of KRT4 and IVL was detected by Western blotting. Quantification of the relative protein expression levels is shown. **(E, F)** The expression of TINCR, IVL and KRT4 in OSCC cell lines was measured by qRT-PCR after cells were transfected with TINCR siRNA. **(G, H)** Western blot results showing the protein expression of IVL and KRT4. Quantification of the relative protein expression levels is shown. $^{**}P < 0.01$, $^{***}P < 0.001$, and $^{****}P < 0.0001$.

deletion (**Figure 6G**). Taken together, our results suggested that JAK2/STAT3 signaling might be involved in TINCR-mediated cell differentiation.

DISCUSSION

Increasing evidence suggests that some lncRNAs act as oncogenes or tumor suppressors in tumorigenesis and progression. However, the molecular mechanisms have yet to be fully elucidated. In the present study, WGCNA was performed to explore the specific lncRNAs correlated with the pathogenesis of OSCC. A total of 23 gene modules were identified based on the microarray data, of which the blue module was significantly associated with OSCC and the lymph node status. A differentiation-related lncRNA, TINCR, was finally screened from the blue module by using GO enrichment and gene differential expression analysis. We verified that TINCR was dramatically downregulated in OSCC tissues, and was associated with pathological differentiation, lymph node metastasis, and poor survival in OSCC patients. We further showed that the expression of TINCR increased during cell differentiation and reduced during cell dedifferentiation. Functional analyses demonstrated that overexpression of TINCR mediated cell differentiation and suppressed the migration of OSCC cells. Furthermore, we also found that overexpression of TINCR decreased xenograft tumor volume and weight and promoted cell differentiation *in vivo*. Interestingly, down-regulation of TINCR led to the activation of JAK2/STAT3

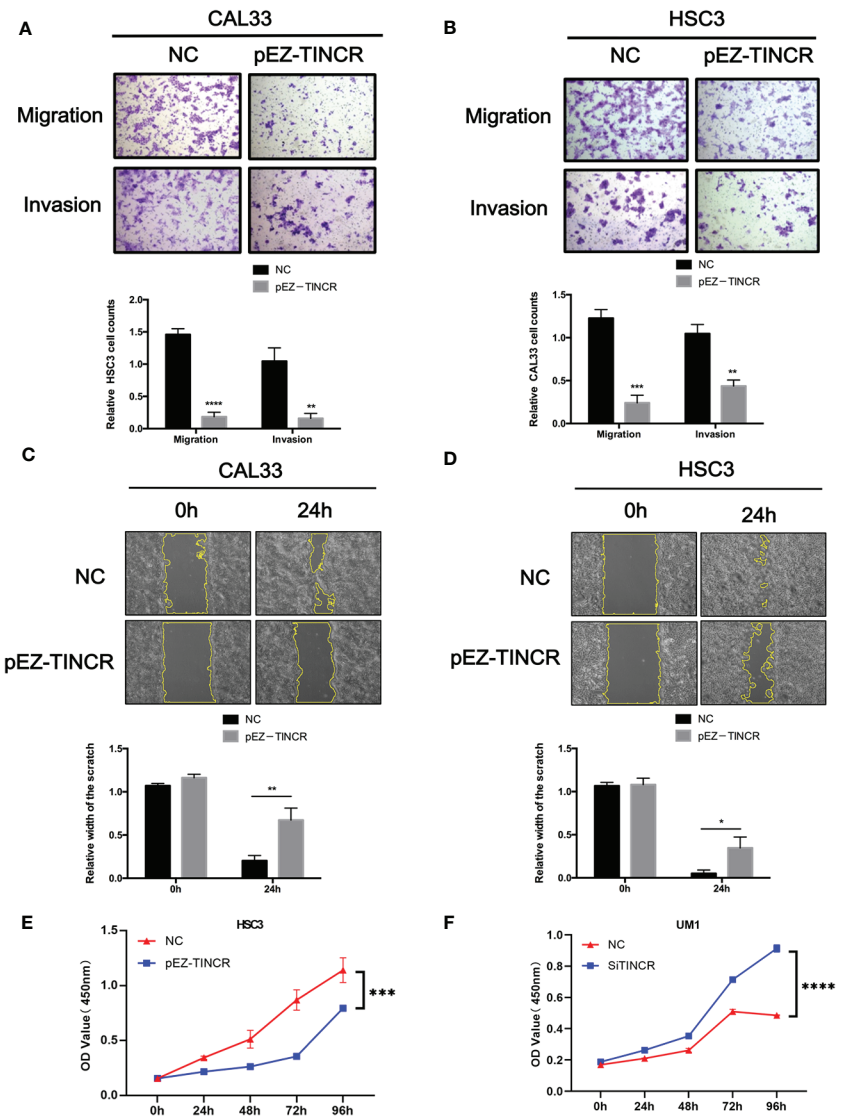

FIGURE 5 | TINCR suppressed the migration, invasion, and proliferation of OSCC cells. **(A, B)** Transwell assays were used to evaluate the effect of TINCR overexpression on cell migration or invasion (upper panel). The relative numbers of cells that migrated or invaded are shown (lower panel). **(C, D)** Cell motility was evaluated by a wound healing assay in OSCC cells treated with the TINCR overexpression vector and control vector (upper panel). The relative width of the scratch in 0 h and 24 h is shown (lower panel). **(E)** Cell growth was evaluated by a CCK-8 assay in OSCC cells treated with the TINCR overexpression vector and control vector. **(F)** Cell growth was evaluated by a CCK-8 assay in OSCC cells treated with the TINCR siRNA and negative control. $^{*}P < 0.05$, $^{**}P < 0.01$, $^{***}P < 0.001$, and $^{****}P < 0.0001$.

signaling. These findings suggested that TINCR may serve as a tumor suppressor and induce cell differentiation by modulating JAK2/STAT3 signaling in OSCC.

LncRNAs have been widely reported to be involved in the proliferation, differentiation, apoptosis, invasion and metastasis of various human cancers (21–23). For example, the lncRNA LOWEG is remarkably downregulated in gastric cancer and suppresses migration and invasion in gastric cancer by acting as a tumor suppressor (24). In melanoma, ILF3-AS1 promotes cell proliferation, invasion and migration by negatively regulating miR-200b/a/429 (25). In colorectal cancer, GAPLINC is significantly upregulated and promotes cell migration and invasion by regulating miR-34a/c-MET (26). In addition, increased levels of H19 promote the invasion, angiogenesis, and stemness of glioblastoma cells. Upregulation of H19 in $CD133^{+}$ glioblastoma cells is significantly related to the increased neurosphere formation of glioblastoma cells (27). All of these studies demonstrated that dysregulated lncRNAs are critical contributors to tumorigenesis and cancer progression. Moreover, accumulating evidence has revealed that lncRNAs exert crucial influences on the development of HNSCC, including the OSCC (28–30). H19, which is upregulated in OSCC, promotes cell

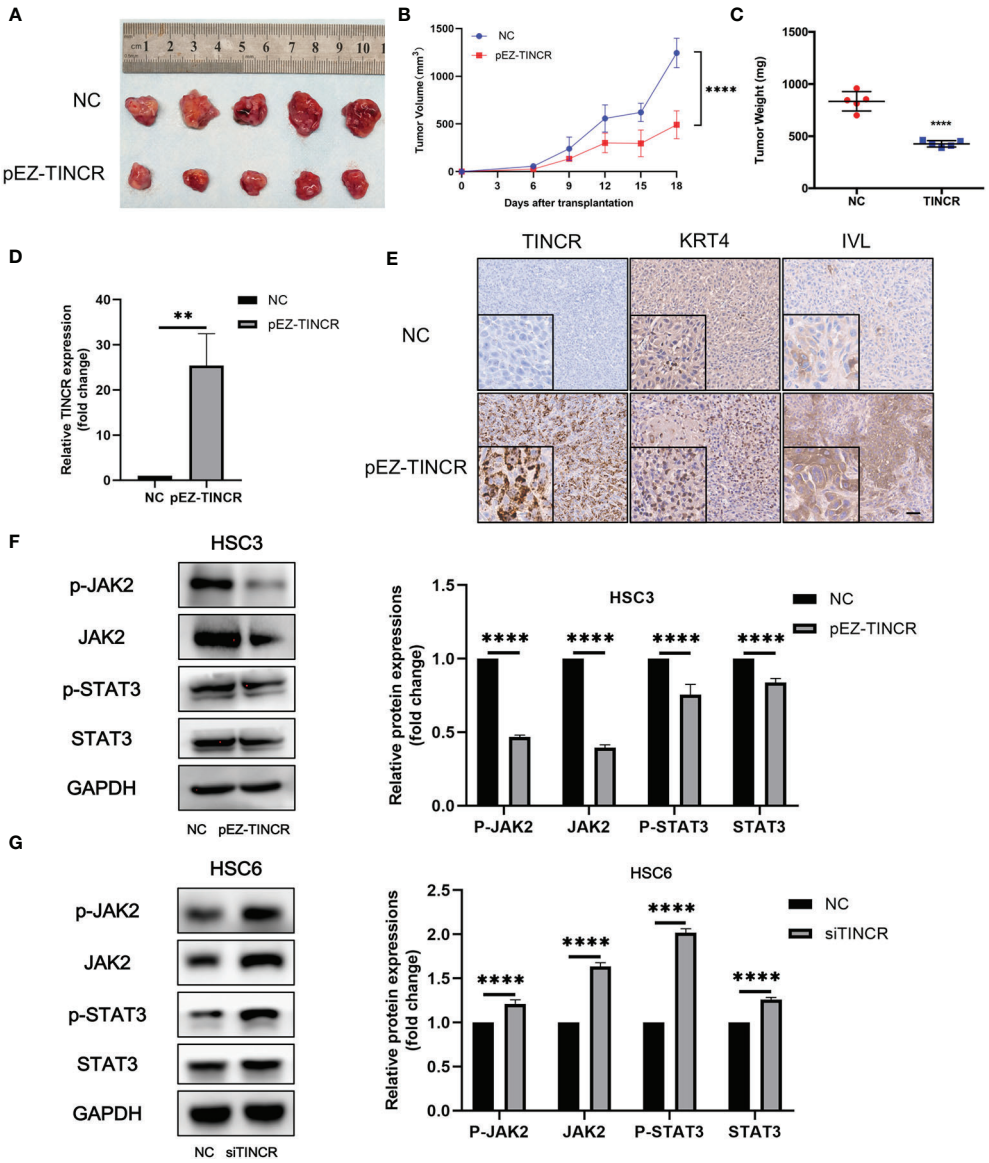

FIGURE 6 | TINCR overexpression inhibited OSCC xenograft tumor growth. **(A)** Representative image of tumor xenografts after the subcutaneous injection of OSCC cells overexpressing TINCR or control cells. **(B)** Growth curves of the tumor volumes in the TINCR overexpression group and control group are shown. The tumor volumes were recorded every 3 days post-injection. **(C)** The tumor weight of the TINCR overexpression group was significantly lower than that of the control group. **(D)** qRT-PCR analysis verified that the expression of TINCR in the TINCR overexpression group was much higher than that in the control group. **(E)** RNAScope and IHC assays were used to detect the expression of TINCR, KRT4 and IVL in tumor xenografts, respectively. **(F)** Western blot analysis showed that the protein expression of p-JAK2, JAK2, p-STAT3 and STAT3 was remarkably inhibited in HSC3 cells after transfection with the TINCR overexpression plasmid (left panel). Quantitative analysis of p-JAK2, JAK2, p-STAT3 and STAT3 is shown (right panel). **(G)** Western blot analysis showed that the protein expression of p-JAK2, JAK2, p-STAT3 and STAT3 was significantly increased in HSC6 cells after transfection with TINCR siRNA (left panel). Quantitative analysis of p-JAK2, JAK2, p-STAT3 and STAT3 is shown (right panel). $^{**}P < 0.01$, $^{****}P < 0.0001$.

proliferation and invasion (31). Huang et al. found that the down-regulation of NEAT1 represses cell proliferation and invasion in OSCC (32). Unfortunately, it remains a major challenge to effectively screen the specific lncRNAs from numerous lncRNA transcripts in high-throughput data. Few studies have focused on the clinical characteristics specific lncRNAs. WGCNA can transform gene expression data into co-expression modules and build correlation with clinical characteristics (33), which makes it a powerful tool for identifying modules of highly associated genes that can be widely applied to identify candidate biomarkers or therapeutic targets. In this study, a total of 23 gene modules were identified based on the WGCNA, of which the blue module was significantly related to the tissue and lymph node status. TINCR was then screened by both GO enrichment and gene differential

expression analysis. We further validated that TINCR expression was strongly decreased in OSCC tissues compared with the NATs.

TINCR is aberrantly expressed in many human malignancies and closely associated with cancer occurrence, progression, invasion and metastasis, and prognosis (8, 34, 35). TINCR is downregulated in prostate cancer, and the low expression of TINCR is associated with advanced clinical T stage, lymph node metastasis, distant metastasis and poor prognosis (36). Yu et al. reported that upregulation of TINCR is negatively correlated with the overall survival of patients with colorectal cancer (37). TINCR is overexpressed in hepatocellular carcinoma and is related to tumor size, pathological differentiation, TNM classification, hematogenous metastasis and poor prognosis (34). However, its role in OSCC is still largely unknown. Here, the clinicopathological analysis was performed that revealed a close relationship between TINCR expression and pathological differentiation and lymph node metastasis in patients with OSCC. Lower TINCR expression is significantly associated with short survival. All of these results suggested that TINCR may serve as a tumor suppressor in OSCC progression.

TINCR plays a key regulatory role during human epidermal differentiation by interacting with a series of differentiation-related genes. A series of functional assays had confirmed that TINCR is necessary for epithelial cell differentiation and that its aberrant expression contributes to tumor occurrence and progression. An increasing number of studies have verified that TINCR serves as a regulatory factor in human squamous cell carcinoma, including breast cancer (38, 39), gastric cancer (10, 40), prostate cancer (36), lung cancer (41), hepatocellular carcinoma (34), bladder cancer (8), colorectal cancer (35), etc. In our study, we demonstrated that the expression of TINCR in OSCC cells was significantly upregulated, accompanied by an increase in IVL and KRT4 during cell differentiation induced by $CaCl_2$. In contrast, the expression level of TINCR was dramatically suppressed, accompanied by IVL and KRT4 down-regulation, when OSCC cells were dedifferentiated in tumor spheres.

IVL is an important keratinocyte differentiation marker (42), and barrier protein (43). Chen et al. found that S100A has a prominent effect on IVL and therefore regulates esophageal cancer cell differentiation (44). KRT4 is a member of the keratin family, whose aberrant expression usually causes many diseases, and even cancer (45). According to sequence homology, keratins are classified into type I and type II clusters (46). Zhang et al. found that KRT4 is aberrantly expressed in human white sponge nevus (WSN) (47). Ohkura et al. observed the down-regulation of KRT4 in OSCC cells, but its upregulation in leukoplakia, suggesting that the expression level of KRT4 is closely related to malignancy in OSCC (48). Here, we explored the association among TINCR, KRT4, and IVL. Correlation analysis showed that the expression of endogenous TINCR was positively correlated with the expression levels of KRT4 and IVL. Moreover, the expression levels of IVL and KRT4 were remarkably decreased when TINCR was deleted. Conversely, the expression of IVL and KRT4 was distinctly increased in cells overexpressing TINCR. These results suggested that TINCR plays an important role in the process of epithelial differentiation and carcinogenesis of OSCC.

The Janus kinase (JAK)/signal transducer and activator of transcription (STAT) signaling pathway is an evolutionarily conserved pathway (49). It is activated in response to many protein ligands, such as cytokines and growth factors, which regulate various cellular processes, including cell proliferation, differentiation, and apoptosis (50, 51). JAK/STAT3 has been observed in numerous tumors and underpins a majority of features of cancer (52), including cell proliferation (53), antiapoptosis (54), angiogenesis (55), metastasis (56), and cancer stem cell maintenance (57). In addition, increasing evidence has proven that JAK/STAT3 signaling plays a key role in modulating keratinocyte differentiation and epithelial carcinogenesis (16–19). Amano et al. demonstrated that suppressing STAT3 activation by JAK inhibitors increases the levels of terminal differentiation and improves skin barrier function (17). Chan et al. also found that abrogation of STAT3 function leads to the significant repression of the growth of initiated keratinocytes and papilloma cells (18). In the present study, TINCR overexpression significantly suppressed the activation of JAK2/STAT3 signaling in OSCC cells, while the deletion of TINCR enhanced the JAK2/STAT3 signaling. Our findings indicated that JAK2/STAT3 signaling might be involved in the TINCR-mediated cell differentiation of OSCC. However, the underlying mechanism still needs further exploration.

In summary, our data suggest that TINCR functions as a tumor suppressor by inducing cell differentiation by modulating JAK2/STAT3 signaling in OSCC. TINCR may act as a prognostic biomarker and therapeutic target for OSCC.

DATA AVAILABILITY STATEMENT

The microarray data discussed in this study have been deposited in the NCBI Gene Expression Omnibus with the accession number GSE160042. The publicly available datasets analyzed in this study can be found in The Cancer Genome Atlas (TCGA) database (https://portal.gdc.cancer.gov)

ETHICS STATEMENT

The studies involving human participants were reviewed and approved by Ethical Committee of Hospital of Stomatology, Sun Yat-sen University. The patients/participants provided their written informed consent to participate in this study. The animal study was reviewed and approved by Sun Yat-sen University Institutional Animal Care and Use Committee.

AUTHOR CONTRIBUTIONS

XL and JSH conceived the study and designed the experiments. ZZ, JH, CW, WW, and PY performed the *in vitro* and *in vivo* experiments and analyzed the data. JH and HL collected the patient samples and performed the clinical data analysis. HY and ZZ performed the bioinformatics analysis. ZZ, JH, and XL wrote the manuscript. All authors contributed to the article and approved the submitted version.

FUNDING

This work was supported by the National Natural Science Foundation of China (81802704, 81772889, 81874128, 81702699, and 81572661).

SUPPLEMENTARY MATERIAL

The Supplementary Material for this article can be found online at: https://www.frontiersin.org/articles/10.3389/fonc.2020.624752/full#supplementary-material

REFERENCES

1. Gadewal NS, Zingde SM. Database and interaction network of genes involved in oral cancer:Version II. *Bioinformation* (2011) 6:169–70. doi: 10.6026/97320630006169
2. Warnakulasuriya S. Global epidemiology of oral and oropharyngeal cancer. *Oral Oncol* (2009) 45:309–16. doi: 10.1016/j.oraloncology.2008.06.002
3. Siegel RL, Miller KD, Jemal A. Cancer statistics, 2016. *CA Cancer J Clin* (2016) 66:7–30. doi: 10.3322/caac.21332
4. Joseph JP, Harishankar MK, Pillai AA, Devi A. Hypoxia induced EMT: A review on the mechanism of tumor progression and metastasis in OSCC. *Oral Oncol* (2018) 80:23–32. doi: 10.1016/j.oraloncology.2018.03.004
5. Carninci P, Kasukawa T, Katayama S, Gough J, Frith MC. The Transcriptional Landscape of the Mammalian Genome. *science* (2005) 309:1559–63. doi: 10.1126/science.1112014
6. Wang KC, Chang HY. Molecular mechanisms of long noncoding RNAs. *Mol Cell* (2011) 43(6):904–14. doi: 10.1016/j.molcel.2011.08.018
7. Kretz M, Siprashvili Z, Chu C, Webster DE, Zehnder A, Qu K, et al. Control of somatic tissue differentiation by the long non-coding RNA TINCR. *Nature* (2013) 493:231–5. doi: 10.1038/nature11661
8. Chen Z, Liu Y, He A, Li J, Chen M, Zhan Y, et al. Theophylline controllable RNAi-based genetic switches regulate expression of lncRNA TINCR and malignant phenotypes in bladder cancer cells. *Sci Rep* (2016) 6:30798. doi: 10.1038/srep30798
9. Hazawa M, Lin DC, Handral H, Xu L, Chen Y, Jiang YY, et al. ZNF750 is a lineage-specific tumour suppressor in squamous cell carcinoma. *Oncogene* (2017) 36:2243–54. doi: 10.1038/onc.2016.377
10. Xu TP, Liu XX, Xia R, Yin L, Kong R, Chen WM, et al. SP1-induced upregulation of the long noncoding RNA TINCR regulates cell proliferation and apoptosis by affecting KLF2 mRNA stability in gastric cancer. *Oncogene* (2015) 34:5648–61. doi: 10.1038/onc.2015.18
11. Martens-Uzunova ES, Bottcher R, Croce CM, Jenster G, Visakorpi T, Calin GA. Long noncoding RNA in prostate, bladder, and kidney cancer. *Eur Urol* (2014) 65:1140–51. doi: 10.1016/j.eururo.2013.12.003
12. Ma X, Huang C, Luo D, Wang Y, Tang R. Tag SNPs of long non-coding RNA TINCR affect the genetic susceptibility to gastric cancer in a Chinese population. *oncotarget* (2016) 7:87114–23. doi: 10.18632/oncotarget.13513
13. Liu X, Wang C, Chen Z, Jin Y, Wang Y, Kolokythas A, et al. MicroRNA-138 suppresses epithelial-mesenchymal transition in squamous cell carcinoma cell lines. *Biochem J* (2011) 440:23–31. doi: 10.1042/BJ20111006
14. Zhuang Z, Xie N, Hu J, Yu P, Wang C, Hu X, et al. Interplay between ΔNp63 and miR-138-5p regulates growth,metastasis and stemness of oral squamous cell carcinoma. *oncotarget* (2017) 8:21954–73. doi: 10.18632/oncotarget.15752
15. Sakamoto K, Aragaki T, Morita K, Kawachi H, Kayamori K, Nakanishi S, et al. Down-regulation of keratin 4 and keratin 13 expression in oral squamous cell carcinoma and epithelial dysplasia: a clue for histopathogenesis. *Histopathology* (2011) 58:531–42. doi: 10.1111/j.1365-2559.2011.03759.x
16. Somuncu S, Somuncu ÖS, Ballıca B, Tabandeh B. Deficiency of epithelial-mesenchymal transition causes child indirect inguinal hernia. *J Pediatr Surg* (2020) 55:665–71. doi: 10.1016/j.jpedsurg.2019.06.020
17. Amano W, Nakajima S, Kunugi H, Numata Y, Kitoh A, Egawa G, et al. The Janus kinase inhibitor JTE-052 improves skin barrier function through suppressing signal transducer and activator of transcription 3 signaling. *J Allergy Clin Immunol* (2015) 136:667–77.e7. doi: 10.1016/j.jaci.2015.03.051
18. Chan KS, Sano S, Kiguchi K, Anders J, Komazawa N, Takeda J, et al. Disruption of Stat3 reveals a critical role in both the initiation and the promotion stages of epithelial carcinogenesis. *J Clin Invest* (2004) 114:720–8. doi: 10.1172/jci21032
19. Kim DJ, Chan KS, Sano S, Digiovanni J. Signal transducer and activator of transcription 3 (Stat3) in epithelial carcinogenesis. *Mol Carcinog* (2007) 46:725–31. doi: 10.1002/mc.20342
20. Zhuang Z, Yu P, Xie N, Wu Y, Liu H, Zhang M, et al. MicroRNA-204-5p is a tumor suppressor and potential therapeutic target in head and neck squamous cell carcinoma. *Theranostics* (2020) 10:1433–53. doi: 10.7150/thno.38507
21. Gupta RA, Shah N, Wang KC, Kim J, Horlings HM, Wong DJ, et al. Long non-coding RNA HOTAIR reprograms chromatin state to promote cancer metastasis. *Nature* (2010) 464:1071–6. doi: 10.1038/nature08975
22. Guttman M, Donaghey J, Carey BW, Garber M, Grenier JK, Munson G, et al. lincRNAs act in the circuitry controlling pluripotency and differentiation. *Nature* (2011) 477:295–300. doi: 10.1038/nature10398
23. Wang L, Zhao Z, Feng W, Ye Z, Dai W, Zhang C, et al. Long non-coding RNA TUG1 promotes colorectal cancer metastasis via EMT pathway. *Oncotarget* (2016) 7:51713–9. doi: 10.18632/oncotarget.10563
24. Zhao JH, Sun JX, Song YX, Chen XW, Yang YC, Ma B, et al. A novel long noncoding RNA-LOWEG is low expressed in gastric cancer and acts as a tumor suppressor by inhibiting cell invasion. *J Cancer Res Clin Oncol* (2016) 142:601–9. doi: 10.1007/s00432-015-2071-6
25. Chen X, Liu S, Zhao X, Ma X, Gao G, Yu L, et al. Long noncoding RNA ILF3-AS1 promotes cell proliferation, migration, and invasion via negatively regulating miR-200b/a/429 in melanoma. *Biosci Rep* (2017) 37: BSR20171031. doi: 10.1042/BSR20171031.
26. Luo Y, Ouyang J, Zhou D, Zhong S, Wen M, Ou W, et al. Long Noncoding RNA GAPLINC Promotes Cells Migration and Invasion in Colorectal Cancer Cell by Regulating miR-34a/c-MET Signal Pathway. *Dig Dis Sci* (2018) 63:890–9. doi: 10.1007/s10620-018-4915-9
27. Jiang X, Yan Y, Hu M, Chen X, Wang Y, Dai Y, et al. Increased level of H19 long noncoding RNA promotes invasion, angiogenesis, and stemness of glioblastoma cells. *J Neurosurg* (2016) 124:129–36. doi: 10.3171/2014.12.JNS1426
28. Cao W, Liu JN, Liu Z, Wang X, Han ZG, Ji T, et al. A three-lncRNA signature derived from the Atlas of ncRNA in cancer (TANRIC) database predicts the survival of patients with head and neck squamous cell carcinoma. *Oral Oncol* (2017) 65:94–101. doi: 10.1016/j.oraloncology.2016.12.017
29. Ghafouri-Fard S, Mohammad-Rahimi H, Jazaeri M, Taheri M. Expression and function of long non-coding RNAs in head and neck squamous cell carcinoma. *Exp Mol Pathol* (2020) 112:104353. doi: 10.1016/j.yexmp.2019.104353 104353.
30. Wang Y, Wang S, Ren Y, Zhou X. The Role of lncRNA Crosstalk in Leading Cancer Metastasis of Head and Neck Squamous Cell Carcinoma. *Front Oncol* (2020) 10:561833. doi: 10.3389/fonc.2020.561833
31. Hong Y, He H, Sui W, Zhang J, Zhang S, Yang D. Long non-coding RNA H1 promotes cell proliferation and invasion by acting as a ceRNA of miR138 and releasing EZH2 in oral squamous cell carcinoma. *Int J Oncol* (2018) 52:901–12. doi: 10.3892/ijo.2018.4247
32. Huang G, He X, Wei XL. lncRNA NEAT1 promotes cell proliferation and invasion by regulating miR365/RGS20 in oral squamous cell carcinoma. *Oncol Rep* (2018) 39:1948–56. doi: 10.3892/or.2018.6283
33. Miller JA, Cai C, Langfelder P, Geschwind DH, Kurian SM, Salomon DR, et al. Strategies for aggregating gene expression data: the collapseRows R function. *BMC Bioinf* (2011) 12:322. doi: 10.1186/1471-2105-12-322
34. Tian F, Xu J, Xue F, Guan E, Xu X. TINCR expression is associated with unfavorable prognosis in patients with hepatocellular carcinoma. *Biosci Rep* (2017) 37:BSR20170301. doi: 10.1042/BSR20170301
35. Zhang Z, Lu Y, Zhang Z, Chang Y, Zheng L, Yuan L, et al. Loss of TINCR expression promotes proliferation, metastasis through activating EpCAM cleavage in colorectal cancer. *Oncotarget* (2016) 7:22639–49. doi: 10.18632/oncotarget.8141

36. Dong L, Ding H, Li Y, Xue D, Liu Y. LncRNA TINCR is associated with clinical progression and serves as tumor suppressive role in prostate cancer. *Cancer Manag Res* (2018) 10:2799–807. doi: 10.2147/CMAR.S170526
37. Yu S, Wang D, Shao Y, Zhang T, Xie H, Jiang X, et al. SP1-induced lncRNA TINCR overexpression contributes to colorectal cancer progression by sponging miR-7-5p. *Aging* (2019) 11:1389–403. doi: 10.18632/aging.101839
38. Dong H, Hu J, Zou K, Ye M, Chen Y, Wu C, et al. Activation of LncRNA TINCR by H3K27 acetylation promotes Trastuzumab resistance and epithelial-mesenchymal transition by targeting MicroRNA-125b in breast Cancer. *Mol Cancer* (2019) 18:3. doi: 10.1186/s12943-018-0931-9
39. Liu Y, Du Y, Hu X, Zhao L, Xia W. Up-regulation of ceRNA TINCR by SP1 contributes to tumorigenesis in breast cancer. *BMC Cancer* (2018) 18:367. doi: 10.1186/s12885-018-4255-3
40. Chen Z, Liu H, Yang H, Gao Y, Zhang G, Hu J. The long noncoding RNA, TINCR, functions as a competing endogenous RNA to regulate PDK1 expression by sponging miR-375 in gastric cancer. *Oncol Targets Ther* (2017) 10:3353–62. doi: 10.2147/OTT.S137726
41. Liu X, Ma J, Xu F, Li L. TINCR suppresses proliferation and invasion through regulating miR-544a/FBXW7 axis in lung cancer. *BioMed Pharmacother* (2018) 99:9–17. doi: 10.1016/j.biopha.2018.01.049
42. Dugu L, Nakahara T, Wu Z, Uchi H, Liu M, Hirano K, et al. Neuronatin is related to keratinocyte differentiation by up-regulating involucrin. *J Dermatol Sci* (2014) 73:225–31. doi: 10.1016/j.jdermsci.2013.10.008
43. Bao L, Alexander JB, Zhang H, Shen K, Chan LS. Interleukin-4 Downregulation of Involucrin Expression in Human Epidermal Keratinocytes Involves Stat6 Sequestration of the Coactivator CREB-Binding Protein. *J Interferon Cytokine Res* (2016) 36:374–81. doi: 10.1089/jir.2015.0056
44. Chen H, Ma J, Sunkel B, Luo A, Ding F, Li Y, et al. S100A14: novel modulator of terminal differentiation in esophageal cancer. *Mol Cancer Res* (2013) 11:1542–53. doi: 10.1158/1541-7786.MCR-13-0317
45. Paller AS. The Molecular Bases for the Palmoplantar Keratodermas. *Pediatr Dermatol* (1999) 16:483–6. doi: 10.1046/j.1525-1470.1999.00126.x
46. Chao SC, Tsai YM, Yang MH, Lee JY. A novel mutation in the keratin 4 gene causing white sponge naevus. *Br J Dermatol* (2003) 148:1125–8. doi: 10.1046/j.1365-2133.2003.05337.x
47. Zhang J, Quan J, Ren Y, Chen M, Yang J, Zhang X. Keratin 4 regulates the development of human white sponge nevus. *J Oral Pathol Med* (2018) 47:598–605. doi: 10.1111/jop.12728
48. Ohkura S, Kondoh N, Hada A, Arai M, Yamazaki Y, Sindoh M, et al. Differential expression of the keratin-4, -13, -14, -17 and transglutaminase 3 genes during the development of oral squamous cell carcinoma from leukoplakia. *Oral Oncol* (2005) 41:607–13. doi: 10.1016/j.oraloncology.2005.01.011
49. Hou SX, Zheng Z, Chen X, Perrimon N. The Jak/STAT pathway in model organisms: emerging roles in cell movement. *Dev Cell* (2002) 3:765–78. doi: 10.1016/s1534-5807(02)00376-3
50. Rawlings JS, Rosler KM, Harrison DA. The JAK/STAT signaling pathway. *J Cell Sci* (2004) 117:1281–3. doi: 10.1242/jcs.00963
51. O'Shea JJ, Holland SM, Staudt LM. JAKs and STATs in immunity, immunodeficiency, and cancer. *New Engl J Med* (2013) 368:161–70. doi: 10.1056/NEJMra1202117
52. Yuan J, Zhang F, Niu R. Multiple regulation pathways and pivotal biological functions of STAT3 in cancer. *Sci Rep* (2015) 5:17663. doi: 10.1038/srep17663
53. Banerjee K, Resat H. Constitutive activation of STAT3 in breast cancer cells: A review. *Int J Cancer* (2016) 138:2570–8. doi: 10.1002/ijc.29923
54. Gritsko T, Williams A, Turkson J, Kaneko S, Bowman T, Huang M, et al. Persistent activation of stat3 signaling induces survivin gene expression and confers resistance to apoptosis in human breast cancer cells. *Clin Cancer Res* (2006) 12:11–9. doi: 10.1158/1078-0432.Ccr-04-1752
55. Doucette TA, Kong LY, Yang Y, Ferguson SD, Yang J, Wei J, et al. Signal transducer and activator of transcription 3 promotes angiogenesis and drives malignant progression in glioma. *Neuro-oncology* (2012) 14:1136–45. doi: 10.1093/neuonc/nos139
56. Xiong H, Hong J, Du W, Lin YW, Ren LL, Wang YC, et al. Roles of STAT3 and ZEB1 proteins in E-cadherin down-regulation and human colorectal cancer epithelial-mesenchymal transition. *J Biol Chem* (2012) 287:5819–32. doi: 10.1074/jbc.M111.295964
57. Sherry MM, Reeves A, Wu JK, Cochran BH. STAT3 is required for proliferation and maintenance of multipotency in glioblastoma stem cells. *Stem Cells (Dayton Ohio)* (2009) 27:2383–92. doi: 10.1002/stem.185

Conflict of Interest: The authors declare that the research was conducted in the absence of any commercial or financial relationships that could be construed as a potential conflict of interest.

Copyright © 2021 Zhuang, Huang, Wang, Wang, Yu, Hu, Liu, Yin, Hou and Liu. This is an open-access article distributed under the terms of the Creative Commons Attribution License (CC BY). The use, distribution or reproduction in other forums is permitted, provided the original author(s) and the copyright owner(s) are credited and that the original publication in this journal is cited, in accordance with accepted academic practice. No use, distribution or reproduction is permitted which does not comply with these terms.

frontiers in Oncology

ORIGINAL RESEARCH
published: 16 April 2021
doi: 10.3389/fonc.2021.656628

A Super-Enhancer Driven by FOSL1 Controls miR-21-5p Expression in Head and Neck Squamous Cell Carcinoma

Yuehan Wan[1,2†], Rosalie G. Hoyle[3†], Nan Xie[2,4], Wenjin Wang[1,2], Hongshi Cai[1,2], Ming Zhang[1,2], Zhikun Ma[3], Gan Xiong[1,2], Xiuyun Xu[1,2], Zhengxian Huang[1,2], Xiqiang Liu[5], Jiong Li[3,6] and Cheng Wang[1,2*]*

[1] Department of Oral and Maxillofacial Surgery, Hospital of Stomatology, Guanghua School of Stomatology, Sun Yat-Sen University, Guangzhou, China, [2] Guangdong Provincial Key Laboratory of Stomatology, Sun Yat-Sen University, Guangzhou, China, [3] Department of Medicinal Chemistry, Institute for Structural Biology, Drug Discovery and Development, School of Pharmacy and the Massey Cancer Center, Virginia Commonwealth University, Richmond, VA, United States, [4] Department of Oral Pathology, Guanghua School of Stomatology, Hospital of Stomatology, Sun Yat-Sen University, Guangzhou, China, [5] Department of Oral and Maxillofacial Surgery, Nanfang Hospital, Southern Medical University, Guangzhou, China, [6] Department of Oral and Craniofacial Molecular Biology, Philips Institute for Oral Health Research, School of Dentistry, Virginia Commonwealth University, Richmond, VA, United States

OPEN ACCESS

Edited by:
Wei Cao,
Shanghai Jiao Tong University, China

Reviewed by:
Zheqi Liu,
Shanghai Jiao Tong University, China
Yanjie Zhang,
Shanghai Jiao Tong University, China

***Correspondence:**
Cheng Wang
wangch75@mail.sysu.edu.cn
Jiong Li
jli29@vcu.edu

†These authors have contributed equally to this work

Specialty section:
This article was submitted to Head and Neck Cancer, a section of the journal Frontiers in Oncology

Received: *21 January 2021*
Accepted: *25 March 2021*
Published: *16 April 2021*

Citation:
Wan Y, Hoyle RG, Xie N, Wang W, Cai H, Zhang M, Ma Z, Xiong G, Xu X, Huang Z, Liu X, Li J and Wang C (2021) A Super-Enhancer Driven by FOSL1 Controls miR-21-5p Expression in Head and Neck Squamous Cell Carcinoma. Front. Oncol. 11:656628. doi: 10.3389/fonc.2021.656628

MiR-21-5p is one of the most common oncogenic miRNAs that is upregulated in many solid cancers by inhibiting its target genes at the posttranscriptional level. However, the upstream regulatory mechanisms of miR-21-5p are still not well documented in cancers. Here, we identify a super-enhancer associated with the *MIR21* gene (MIR21-SE) by analyzing the *MIR21* genomic regulatory landscape in head and neck squamous cell carcinoma (HNSCC). We show that the MIR21-SE regulates miR-21-5p expression in different HNSCC cell lines and disruption of MIR21-SE inhibits miR-21-5p expression. We also identified that a key transcription factor, FOSL1 directly controls miR-21-5p expression by interacting with the MIR21-SE in HNSCC. Moreover, functional studies indicate that restoration of miR-21-5p partially abrogates FOSL1 depletion-mediated inhibition of cell proliferation and invasion. Clinical studies confirmed that miR-21-5p expression is positively correlated with FOSL1 expression. These findings suggest that FOSL1-SE drives miR-21-5p expression to promote malignant progression of HNSCC

Keywords: super enhancer, FOSL1, miR-21-5p, head and neck squamous cell carcinoma, metastasis

INTRODUCTION

Head and neck squamous cell carcinoma (HNSCC) is one of the most common malignant tumors worldwide, with a 5-year survival rate of only about 50% (1, 2). HNSCC easily invades surrounding tissues and spreads to cervical lymph nodes (LN), ultimately leading to relapse and death (3). Although a significant progress on the pathogenesis of HNSCC has been made in the past decades, the exact molecular mechanisms are still not well understood. Increasing evidences implicates that dysregulation of miRNAs has a critical role in the development and progression of HNSCC (4–10).

In our previous studies, we also confirmed that miRNAs are involved in the tumor growth, stemness and metastasis of HNSCC by targeting a cohort of key oncogenes or tumor suppressors, including miR-21, miR-204-5p, miR320a, miR-138 (11–13). Interestingly, the alterations of miRNA landscape showed that most of deregulated miRNA are downregulated in HNSCC as compared to normal tissue (14–17). Contrarily, only several upregulated miRNAs were identified, including miR-21-5p, miR-7 and miR-31 (18–22). Notably, miR-21-5p is one of the most common oncogenic miRNAs that is robustly upregulated and function as an oncogene in many solid cancers by inhibiting its target genes at the posttranscriptional level, including HNSCC (23, 24). However, the upstream regulatory mechanisms of miR-21 are still not well documented in cancers.

Herein, we aimed to investigate the upstream regulatory mechanisms of miR-21-5p in HNSCC. Strikingly, a MIR21-associated super enhancer (MIR21-SE) was identified in HNSCC and disruption of this super enhancer inhibits miR-21-5p expression. Interestingly, a key transcription factor, FOSL1, was confirmed to directly promote miR-21-5p expression by interacting with the MIR21-SE in HNSCC. Taken together, these findings showed that the miR-21-5p expression was controlled by a FOSL1-driving-SE in HNSCC.

MATERIALS AND METHODS

Samples

95 OSCC tissues samples, 16 matched adjacent non-cancerous normal tissues (ANCT) were collected at the Department of Oral and Maxillofacial Surgery, Hospital of Stomatology, Sun Yat-sen University between January 2013 and July 2018. Tissue samples applied in this study were conducted in accordance with the Declaration of Helsinki's guidelines. All patients did not receive any form of preoperative treatment. The study was approved by the Ethical Committee of the hospital. Tumor grade was determined according to the 8th American Joint Committee on Cancer Staging System. Immunohistochemical and *in situ* hybridization analysis were used to assess the gene expression.

Immunohistochemistry and *In Situ* Hybridization

Formalin-fixed, paraffin-embedded tissue samples were cut into 4-μm sections for immunohistochemistry analysis. The tissue sections were incubated at 4°C with primary antibodies against FRA1/FOSL1(1:100, ab232745, Abcam) overnight. Diamino benzidine (DAB, GK600510, Gene Tech, China) was used to visualize and hematoxylin (D006, Nanjing Jiancheng Biotech, China) was applied to counterstain. Two pathologists who were blinded to the clinical data evaluated the immunohistochemical stain independently. The intensity of FOSL1 staining was evaluated as 0: no staining; 1: weak; 2: moderate; and 3: strong. The proportion was evaluated as 0–100% positive cells. Staining index(SI: 0–300)=staining intensity × the proportion of positive cells. Samples with SI>100 were defined as "high expression" and those with SI ≤ 100 were defined as "low expression".

miR-21-5p expression was examined by *in situ* hybridization according to the manufacturer's instructions (microRNA ISH Optimization Kit for FFPE, Exiqon, Vedbaek, Denmark). miR-21-5p was hybridized with Double-DIG-labeled LNA™ microRNA probes (1:1250, Exiqon) overnight after demasking. The sections were blocked and incubated with goat anti-digoxigenin-AP (1:1000, Roche) and then counterstained with nitro blue tetrazolium/5-bromo-4-chloro-3-indolylphosphate (NBT/BCIP). The staining intensity of the cells was recorded as follows: The intensity staining was evaluated as 0: no staining; 1: weak, light blue; 2: moderate, blue; and 3: strong, dark blue. The proportion was evaluated as 0: negative; 1:<10%; 2: 11–50%; 3: 51–80% or 4: >80% positive cells. The staining index (SI) =staining intensity × the proportion of positive cells. SI (miR-21-5p)>4 was defined as "high expression" and SI ≤ 4 was defined as "low expression".

Chromatin Immunoprecipitation Assay (ChIP)

For ChIP assay, 10^6 cells were treated with 1% formaldehyde at 37°C for 10 min to crosslink their DNA. Agarose gel electrophoresis was used to assess the DNA fragments between 500 bp and 800 bp the cells were lysed. The chromatin crosslink was incubated at 4°C overnight. Then purify the immunoprecipitated DNA after reversing the DNA–protein crosslink. Quantitative real-time PCR (qPCR) was used to quantify the final precipitated DNA. The PCR result was expressed with the percentage of input DNA. The primer sequences of ChIP-qPCR were listed as below. MIR21 super enhancer (MIR21-SE) 5'-AAACCACACTCTGTCG TATCTGTG-3' and 5'-TACAGAACGGCAAGAAAACTGGG-3' and negative control primer (MIR21-NEG) 5'- CCACCAT GCCCAGCCTTGAAGTTA-3' and 5'-TGGAGAGGGCT GACCTTAACCAA-3'.

Luciferase Reporter Assay

MIR21-SE and MIR21-NEG fragments were inserted into pLG4.23 luciferase reporter through Kpn1 and Xho1 restriction sites using standard PCR-cloning method. The primer sequences for cloning MIR21-SE were 5'- GGGTACCGTTCTAGAAAAGAAGTGAA GGCCAGTCG-3' and 5'- CCTCGAGTTAGACATGCTT GCAGGCGTTT-3'. The primer sequences for cloning MIR21-NEG were 5'- GGGTACCACCATGCCCAGCCTTGAAGTTAA-3' and 5'- CCTCGAGACTGAGTGGGGAGAATTGCCTA -3'. For luciferase assay, SCC1 and 293T cells were plated in 24-well plates at 40-50% confluence. For luciferase assay in SCC1 cells, 12h after seeding, the cells were transfected with FOSL1 siRNA or control siRNA. Then, after 24h, the cells were transfected with 50 ng of luciferase reporters and 20 ng of CMV-galactosidase constructs. For luciferase assay in 293T cells, 12h after seeding, the cells were transfected with 50 ng of luciferase reporters, 20 ng of CMV-galactosidase, and expression constructs of FOSL1 and JUN. The reporter activities were determined 24h after DNA transfection. The luciferase and β-galactosidase activity of total cell lysates were determined by Bright-Glo Luciferase Assay System (Promega; cat#E2620) and GalactoStar Reporter Gene Assay System (Applied Biosystems, cat#T1012), respectively. The luciferase

reporter activity was normalized against the β-galactosidase activity of each cell lysate sample.

RNA Isolation and Quantitative Real-Time PCR (RT-qPCR)

RNAzol® RT (RN190, Molecular Research Center, USA) was used to extracted RNA from the cells per the manufacturer's protocol. 1 μg of total RNA was applied to reverse transcription with the ribo SCRIPT Reverse Transcription kit (C11027, RIBOBIO, China). All miR-21-5p (RT primter: ssD809230239; qPCR primer: ssD809230931 and ssD089261711) and U6 (RT primter: ssD0904071008; qPCR primer: ssD0904071006 and ssD0904071007) RT-qPCR primers were ordered from RIBOBIO. The 3-step RT-qPCR reactions were carried out with a SYBR Green Master Mix (11201ES08, Yeasen, China) in the LightCycler 96 System (Roche, Germany). The thermal cycling parameters were as follows: preincubation at 95°C for 5 min, followed by 40 cycles of amplification as: 95°C for 10 s, 60°C for 20 s, and 72°C for 20 s, with a final cycle of 95°C for 15 s, 60°C for 60 s, and 95°C for 15 s as the melting curve. The relative expression level of miR-21-5p was calculated by $2-\Delta\Delta Ct$. Human U6 was served as an internal reference.

Cell Lines, Cell Culture, and Treatments

SCC1 cells were obtained from University of Michigan and HN6 cells were obtained from Wayne State University. UM1 and UM2 cells were provided by Dr. Xiaofeng Zhou (University of Illinois at Chicago, IL, USA). SCC9, SCC15, SCC25 and CAL27 were obtained from the American Type Culture Collection (ATCC; Manassas, VA, USA). The SCC1, HN6 and CAL27 cell lines were cultivated in Dulbecco's modified Eagle's medium (DMEM, Gibco, USA) supplemented with 10% fetal bovine serum (FBS, Gibco, USA). The SCC9, SCC15, SCC25, UM1 and UM2 cell lines were grown in DMEM/F12 medium (DMEM/F12, Gibco, USA) supplemented with 10% FBS. Cells were kept at 37°C under a humidified atmosphere with 5% CO2. Lipofectamine (Lipofectamine RNAiMAX Transfection Reagent, Thermo Fisher) was used to transfect miR-21-5p mimics (50nM, RIBOBIO), FOSL1 siRNA (100nM, RIBOBIO) and their respective negative controls. For the BET bromodomain Inhibitor treatment groups, cells were treated with 1μmol/mL (+)-JQ1 (HY-13030, MCE, USA) or iBET-151 (HY-13235, MCE, USA).

Cell Proliferation

HN6 and SCC1 cells were seeded in 96-well plates at a density of 1000 or 1500 cells per well. The cell confluence of untreated cells and treated cells were detected and analyzed using the Incucyte® S3 Live-Cell Analysis System (Essen BioScience, USA) at the indicated time points.

Wound-Healing, Migration, and Invasion Assays

Wound-healing assay was carried out with a sterile pipette tip to make scratches when cells reached 90% fusion degree in 6-well plates. FBS-free media was then used to cultivate cells for 48h. 2×10^5 HN6 cells or 4×10^5 SCC1 cells with 200μl FBS-free media were seeded into the upper chambers (pore size: 8-μm, Corning, China) with or without Matrigel (354234, Corning, China) to verify the invasion or migration assays. 600μl of 10% fetal bovine serum (FBS) was added into the lower chambers. Cells stranded in the upper chambers after 24h were removed, and the fixed cells on the lower surface of the membrane were stained with hematoxylin. Five random views were selected and photographed under a microscope (ZEISS, German). Image J was used to calculate the cell numbers and wound healing area.

Statistical Analysis

GraphPad prism 8.0. (GraphPad Software Inc.) was used for statistical analysis with the mean ± standard deviation (SD). All statistical tests were two-tailed. P-values of <0.05 were considered statistically significant.

RESULTS

miR-21-5p Is Upregulated and Correlated With Malignant Progression of HNSCC

To investigate the potential role of miR-21-5p in HNSCC, we firstly evaluated miR-21-5p expression based on The Cancer Genome Atlas (TCGA) HNSCC datasets. As shown in **Figure 1A**, the expression of miR-21-5p was significantly increased in HNSCC as compared to normal tissue. To further validate these findings, we performed *in situ* hybridization to detect the expression of miR-21-5p in 95 HNSCC tissues. As expected, we found that miR-21-5p expression was mainly located in cytoplasm and significantly increased in HNSCC when compared to normal epithelium (**Figures 1B, C**). Moreover, the expression of miR-21-5p was also upregulated in HNSCC patient with T3,4 stage as compared to patients with T1,2 stage. Similar results were observed in HNSCC patient with lymph node metastasis as compared to patient without lymph node metastasis (**Figures 1D, E**). An increase of miR-21-5p was also observed in an 8 HNSCC cell lines panel as compared to NOK cells (**Figure 1F**).

To further investigate the functional role miR-21-5p in HNSCC, HNSCC cells, HN6 and SCC1 were transfected with miR-21-5p mimics and we found that cell proliferation and invasion were increased in cells treated with miR-21-5p mimics (**Figures 1G–J**). Taken together, these findings confirmed that miR-21-5p is upregulated in HNSCC and promotes malignant phenotypes in HNSCC.

Targeting FOSL1 Suppresses miR-21-5p Expression by Interacting With the MIR21-SE

To dissect the upstream regulatory machinery of miR-21-5p, we tried to analyze its promoter and enhancer region of the *MIR21*

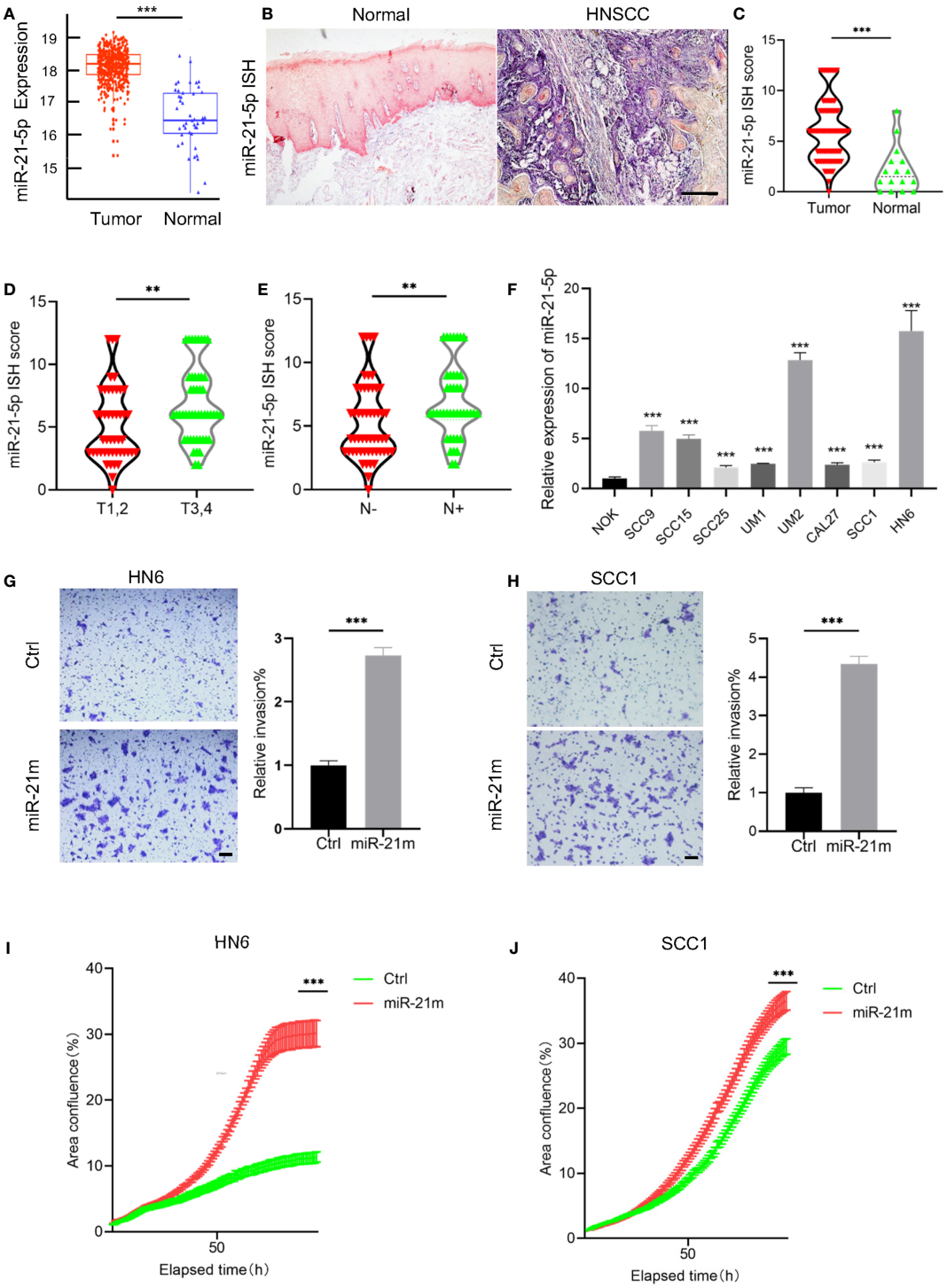

FIGURE 1 | The expression of miR-21-5p was upregulated and correlated with malignant progression in HNSCC. **(A)** The expression of miR-21-5p was upregulated in HNSCC as compared to the normal tissue. Data was from TCGA HNSCC datasets downloaded using the UCSC Xena browser (https://xenabrowser.net). ***P < 0.001. **(B)** The representative images of miR-21-5p ISH staining. Scale bar, 300μm **(C)** The quantitative analysis of miR-21-5p ISH staining in HNSCC patient samples. ***P< 0.001 by Student's t-test **(D)** The expression of miR-21-5p was increased in T3,4 stage HNSCC patient as comparted to those with T1,2 stage. **P < 0.01 by Student's t-test **(E)** The expression of miR-21-5p was increased in HNSCC patient with lymph node metastasis as comparted to those without lymph node metastasis. **P < 0.01 by Student's t-test **(F)** The relative of miR-21-5p was upregulated in 8 HNSCC cell lines as compared to NOK cells. ***P < 0.001 by Student t-test. **(G, H)** Overexpression of miR-21-5p promotes cell invasion of SCC1 and HN6 cells. ***P < 0.001 by Student's t-test. Scale bar, 200μm **(I, J)** Overexpression of miR-21-5p promotes proliferation of SCC1 and HN6 cells. ***P < 0.001 by two-way ANOVA

gene based on our MED1 ChIP-seq results of human SCC cells from a different study (**Figure 2A**). Unexpectedly, we discovered that SEs were associated with *MIR21*. In agreement with ChIP-seq findings, RT-qPCR showed that the expression of miR-21-5p was decreased in SCC1 and HN6 cells upon JQ1 and iBET-151 treatment (**Figures 2B, C**), two well-known BET inhibitors which can disrupt SE. Consistently, ChIP-PCR showed that the enrichments of MED1 and BRD4 on miR-21-SE region were also significantly suppressed in cells treated with JQ1 and iBET-151 (**Figures 2D, E**). Interestingly, the enrichment of FOSL1 in promoter region of MIR21 was also decreased upon JQ1 and iBET-151 treatment (**Figure 2F**).

To further investigate the role of FOSL1 in establishment of the MIR21-SE, we analyzed the promoter and enhancer region of *MIR21* based on our FOSL1 ChIP-seq results of human SCC cells. Surprisingly, we found that FOSL1 was also significantly enriched in MIR21-SE region and MED1 occupancies on SEs in MIR21 were inhibited in cells treated with FOSL1 siRNAs (**Figure 2A**). ChIP-PCR results confirmed that the enrichments of MED1, BRD4 and FOSL1 on MIR21-SE region were significantly eliminated in cells treated with FOSL1 siRNA (**Figures 2G–I**). To further validate that FOSL1 can interact with the MIR21-SE, we cloned a fragment of MIR21-SE regions as well as a similar length negative control region into the pLG4.23 luciferase reporter. As shown in **Figure 2J**, knockdown of FOSL1 significantly suppressed the MIR21-SE luciferase activity. Consistently, the MIR21-SE fragment was also capable of elevating the luciferase reporter activity as compared to the negative control (**Figure 2K**). As expected, the expression of miR-21-5p was significantly inhibited in cells transfected with FOSL1 siRNA (**Figures 2L, M**). These findings support a notion that FOSL1 promotes miR-21-5p expression by interacting with MIR21-SE.

Restoration of miR-21 Attenuates FOSL1 Depletion-Mediated Inhibition of Cell Proliferation and Invasion in HNSCC Cells

To clarify the functional role of miR-21-5p in FOSL1-mediation cell proliferation and invasion, simultaneous knockdown of FOSL1 and restoration of miR-21-5p were performed in HNSCC cells. As shown in **Figures 3A–F**, FOSL1 depletion-mediated inhibition of cell invasion and migration were attenuated by overexpressing miR-21-5p. Similar results were also observed in cell proliferation assay (**Figures 3G, H**). These findings indicate that miR-21-5p is involved in FOSL1-mediated invasion and proliferation in HNSCC *in vitro*.

The Expression of miR-21-5p Is Positively Correlated With FOSL1 and Indicates Poor Prognosis in HNSCC

Next, we analyzed the correlation of FOSL1 and miR-21-5p and then assessed their prognostic value in HNSCC. As shown in **Figures 4A, B**, FOSL1 expression was positively correlated with miR-21-5p expression in HNSCC, supporting the notion that FOSL1 promotes expression of miR-21-5p at the transcriptional level. As expected, the expression of FOSL1 was upregulated in HNSCC as compared to the normal tissue (**Figure 4C**). The increased expression of FOSL1 was also observed in T3,4 stage HNSCC when comparing to T1,2 stage HNSCC (**Figure 4D**). Similar results were also observed in HNSCC patients with lymph node metastasis as compared to those without lymph node metastasis (**Figure 4E**). The survival analysis revealed that high expression of miR-21-5p and FOSL1 indicated a poor prognosis in HNSCC (**Figures 4F, G**). Moreover, HNSCC patients with high expression of miR-21-5p and FOSL1 showed the worst overall survival as compared to the other groups (**Figure 4H**).

DISCUSSION

MiR-21-5p has been extensively studied in variety of cancers and can function as an oncomiR to promote malignant progression of cancer, including HNSCC (25). As a result, miR-21-5p has been proposed as a promising diagnostic and prognostic biomarker, as well as an attractive therapeutic target for cancer treatment (25). However, the regulation of miR-21 is not well understood in HNSCC. Increasing evidences imply that miR-21 expression is maintained by transcriptional and post-transcriptional regulation (26, 27). Notably, it has been reported that AP-1, Ets/PU.1, C/EBPα, NFI, SRF, p53, STAT3 and AR binding sites were observed in the promoter region of the MIR21 gene, indicating that miR-21 expression is controlled by a transcriptional activator or suppressor (26, 28, 29). In agreement with these findings, our data shows that FOSL1, a member of the AP-1 family, occupied the promoter region of the MIR21 gene and regulated miR-21 expression. Moreover, FOSL1 is frequently dysregulated in HNSCC and has a critical role in the invasive growth, metastasis and stemness of HNSCC (30, 31). These results indicate that dysregulation of FOSL1 might exert its function by upregulation of miR-21-5p expression.

Recently, several studies implicating SEs have an important role in the regulation of ncRNAs, including miRNAs, circRNA and lincRNAs (32–34). As a new type of gene regulatory center, SEs are is often found to be positively correlated with oncogenes in cancer (35, 36). Strikingly, we found that a SE was formed around the MIR21 gene, which is enriched with FOSL1, indicating that miR-21 was controlled by FOSL1-associated SE in HNSCC. SEs are considered to be a large cluster of regulatory elements, which have a high binding capacity with transcriptional coactivators (such as BRD4, Mediator, CDK7 or EP300) as compared to typical enhancer binding, and SEs have high potential to activate their target gene transcription to control cell identity (37–40). To investigate the functional role of SEs in the regulation of miR-21-5p, JQ1 and iBET-151, two well-known BET inhibitors, were used to disrupt the SE (41). As expected, the expression of miR-21-5p was significantly suppressed in HNSCC cells upon treatment with JQ1 and iBET-151. Importantly, ChIP-qPCR data showed that the enrichments of MED1, BRD4 and FOSL1 were decreased in SE

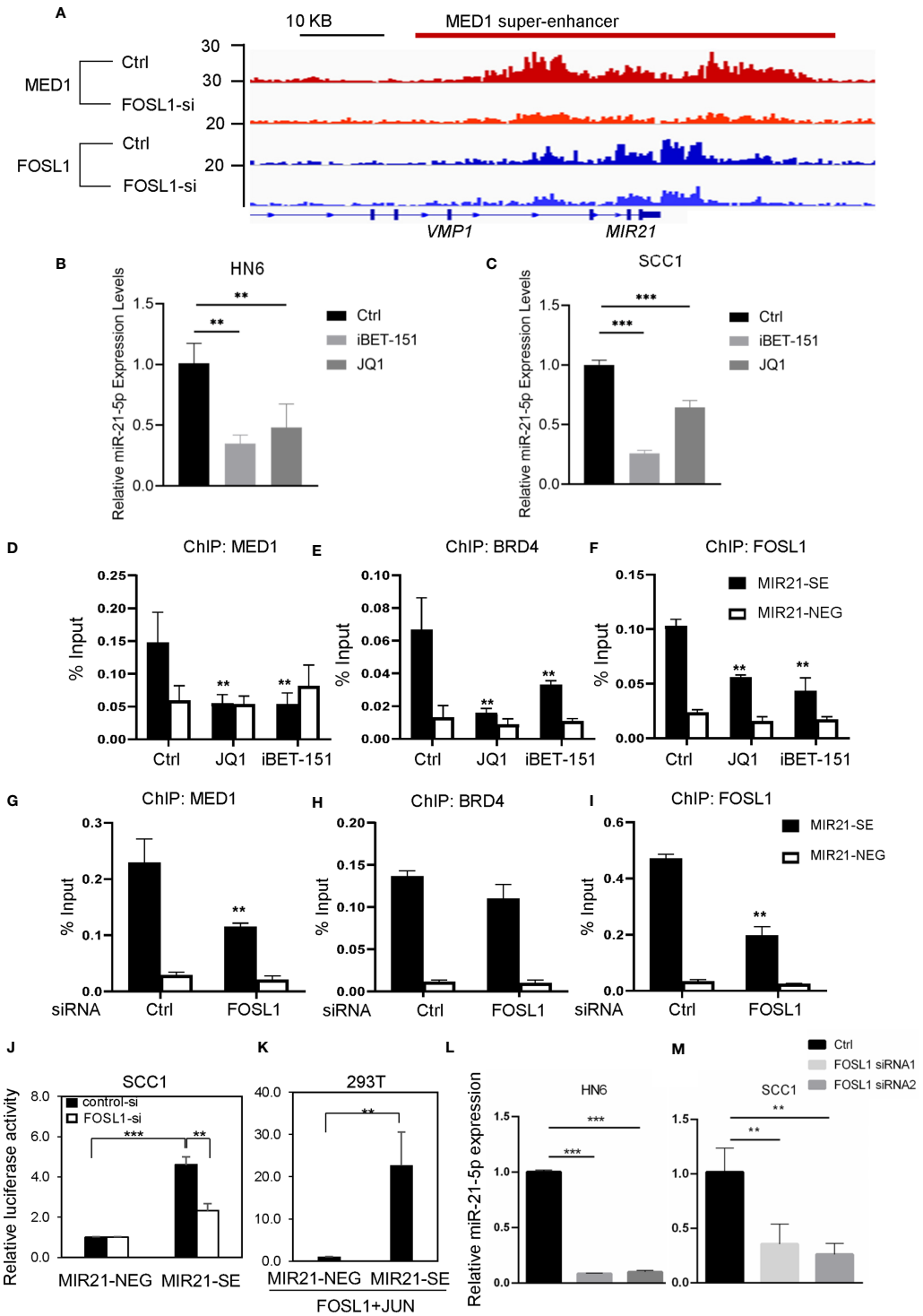

FIGURE 2 | Targeting FOSL1 suppresses miR-21-5p expression by interacting with the MIR21-SE. **(A)** ChIP-seq data revealed SE was formed around the MIR21 gene region and knockdown of FOSL1 suppressed the enrichment of MED1 and FOSL1 in the MIR21-SE. **(B, C)** Disruption of SE by JQ1 and iBET-151 inhibited the expression of miR-21-5p. **P< 0.01, ***P < 0.001 by one-way ANOVA. **(D–F)** The enrichments of MED1, BRD4 and FOSL1 in the MIR21-SE were eliminated in HNSCC cells upon JQ1 and iBET-151 treatment. **P < 0.01 by one-way ANOVA. **(G–I)** The enrichments of MED1 and FOSL1 in the MIR21-SE were eliminated in HNSCC cells treated with FOSL1 siRNA. **P < 0.01 by one-way ANOVA. **(J)** Knockdown of FOSL1 significantly suppressed the MIR21-SE luciferase activity. ***P < 0.001, **P<0.01 by one-way ANOVA. **(K)** MIR21-SE fragment was capable of elevating the luciferase reporter activity as compared to the negative control. **P < 0.01 by Student's t-test **(L, M)** Knockdown of FOSL1 inhibited the expression of miR-21-5p. **P < 0.01, ***P < 0.001 by one-way ANOVA.

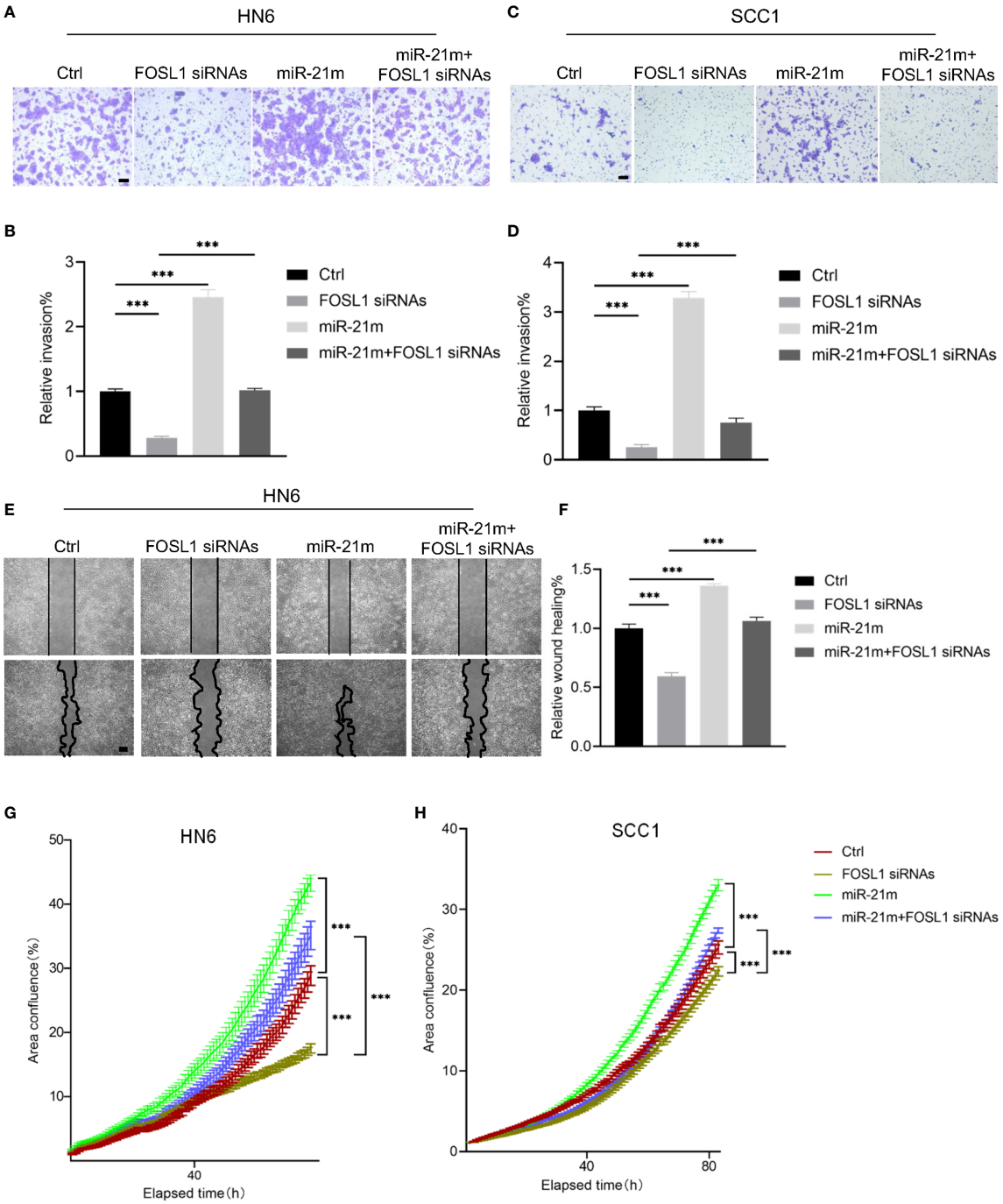

FIGURE 3 | miR-21-5p was required for FOSL1-medaited malignant progression in HNSCC. **(A-D)** FOSL1 depletion-mediated inhibition of cell invasion was attenuated by overexpressing miR-21-5p in SCC1 and HN6 cells. ***P < 0.001 by one-way ANOVA. Scale bar, 200μm **(E, F)** FOSL1 depletion-mediated inhibition of cell migration was rescued by overexpressing miR-21-5p in HN6 cells. ***P < 0.001 by one-way ANOVA. Scale bar, 200μm **(G, H)** FOSL1 depletion-mediated inhibition of cell proliferation was impaired by overexpressing miR-21-5p in SCC1 and HN6 cells. ***P < 0.001 by two-way ANOVA.

region of MIR21. To further demonstrate the role of FOSL1 in SE, we knocked-down the endogenous expression of FOSL1 in HNSCC cells, the ChIP-seq and ChIP-qPCR results revealed that MED1 and BRD4 enrichment on the MIR21-SE were also decreased. In agreement with these findings, the expression of miR-21-5p was significantly decreased in HNSCC cells treated with FOSL1 siRNA, supporting the notion that miR-21-5p was controlled by FOSL1 driven SE in HNSCC.

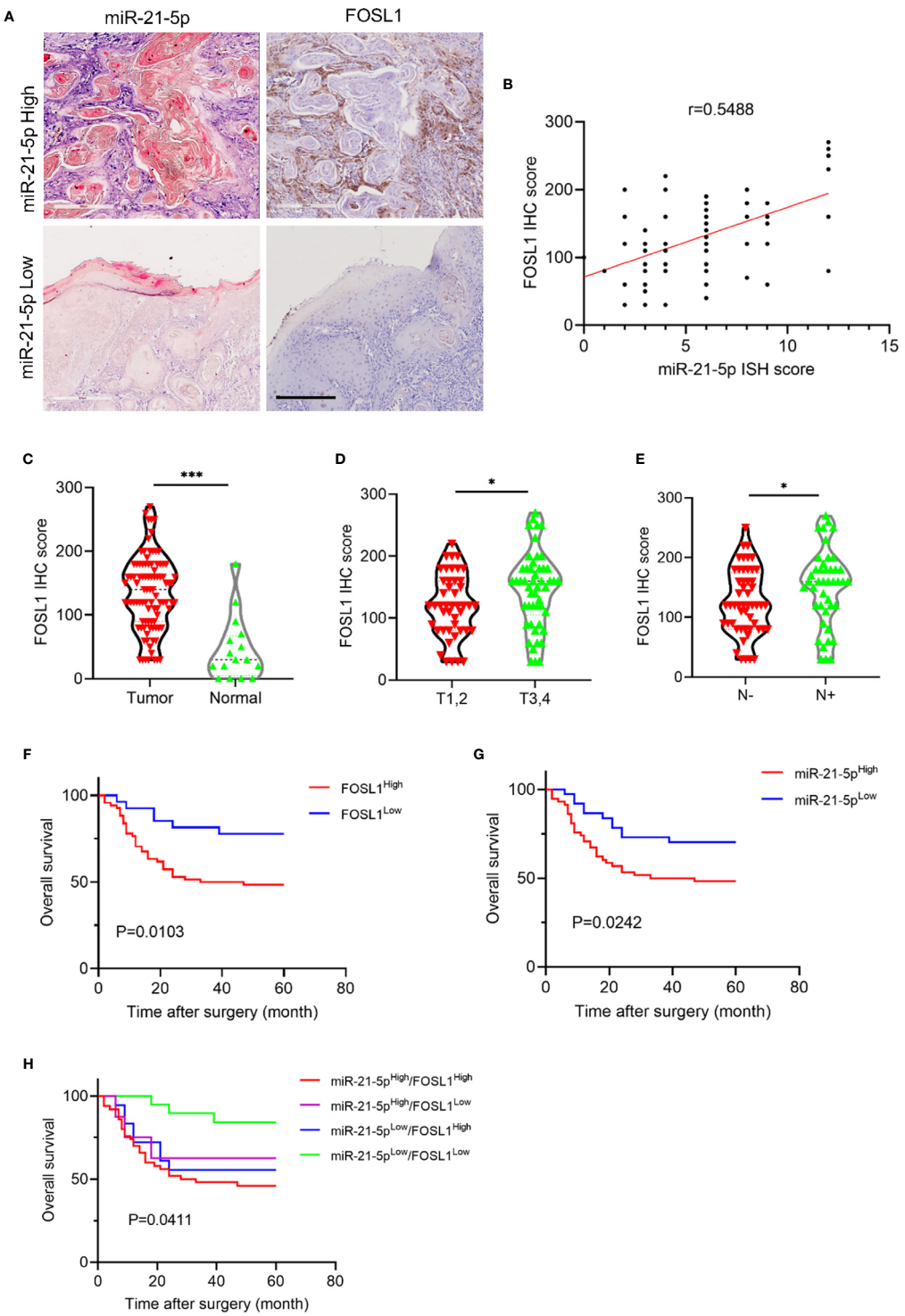

FIGURE 4 | miR-21-5p expression was positively correlated with FOSL1 in HNSCC. **(A)** The representative images of miR-21-5p ISH staining and FOSL1 IHC staining. Scale bar, 300μm **(B)** FOSL1 expression was positively correlated with miR-21-5p expression. **(C)** The expression of FOSL1 was increased in HNSCC as comparted to the normal tissue. ***P < 0.001 by Student's t-test **(D)** The expression of FOSL1 was increased in T3,4 stage HNSCC patient as comparted to those with T1,2 stage. *P < 0.05 by Student's t-test **(E)** The expression of FOSL1 was increased in HNSCC patient with lymph node metastasis as comparted to those without lymph node metastasis. *P < 0.05 by Student's t-test. **(F)** HNSCC patient with high FOSL1 expression levels indicated a poor overall survival. **(G)** HNSCC patient with high miR-21-5p expression levels indicated a poor overall survival. **(H)** HNSCC patient with high FOSL1 and miR-21-5p expression levels indicated a poorest overall survival.

Taken together, we identified a SE associated with the MIR21 gene driven by FOSL1 in HNSCC, which uncovers a novel mechanism underlying miR-21-5p regulation in cancer.

DATA AVAILABILITY STATEMENT

The datasets presented in this study can be found in online repositories. The names of the repository/repositories and accession number(s) can be found below: https://www.ncbi.nlm.nih.gov/, GSM4567094 and GSM4567097.

ETHICS STATEMENT

The studies involving human participants were reviewed and approved by Medical Ethics Committee of Hospital of Stomatology, Sun Yat-Sen University. The patients/participants provided their written informed consent to participate in this study.

AUTHOR CONTRIBUTIONS

CW and JL conceived the study and designed experiments. YW, RH, NX, WW, HC, MZ, GX, ZM, XX, XL, and ZH performed the *in vitro* experiment, immunohistochemical staining and clinical analysis. CW, JL, YW, and RH analyzed data, wrote, and edited the manuscript. All authors have discussed the results and provided comments on the manuscript for improving the manuscript. All authors contributed to the article and approved the submitted version.

FUNDING

This work was supported by the National Natural Science Foundation of China (82073265, 81572661, 81772889), Guangdong Financial Fund for High-Caliber Hospital Construction (174-2018-XMZC-0001-03-0125/D-14), and Natural Science Foundation of Guangdong Province (2017A030313515, 2017A030313558).

REFERENCES

1. Pignon JP, le Maître A, Maillard E, Bourhis J. Meta-analysis of chemotherapy in head and neck cancer (MACH-NC): an update on 93 randomised trials and 17,346 patients. *Radiother Oncol J Eur Soc Ther Radiol Oncol* (2009) 92(1):4–14. doi: 10.1016/j.radonc.2009.04.014
2. Rêgo DF, Elias ST, Amato AA, Canto GL, Guerra EN. Anti-tumor effects of metformin on head and neck carcinoma cell lines: A systematic review. *Oncol Lett* (2017) 13(2):554–66. doi: 10.3892/ol.2016.5526
3. Amit M, Liu C, Gleber-Netto FO, Kini S, Tam S, Benov A, et al. Inclusion of extranodal extension in the lymph node classification of cutaneous squamous cell carcinoma of the head and neck. *Cancer* (2020). doi: 10.1002/cncr.33373
4. Wu ZH, Zhong Y, Zhou T, Xiao HJ. miRNA biomarkers for predicting overall survival outcomes for head and neck squamous cell carcinoma. *Genomics* (2020) 113(1 Pt 1):135–41. doi: 10.1016/j.ygeno.2020.12.002
5. Zhao X, Cui L. A robust six-miRNA prognostic signature for head and neck squamous cell carcinoma. *J Cell Physiol* (2020) 235(11):8799–811. doi: 10.1002/jcp.29723
6. Holt J, Walter V, Yin X, Marron D, Wilkerson MD, Choi HY, et al. Integrative Analysis of miRNAs Identifies Clinically Relevant Epithelial and Stromal Subtypes of Head and Neck Squamous Cell Carcinoma. *Clin Cancer Res an Off J Am Assoc Cancer Res* (2020) 27(3):831–42. doi: 10.1158/1078-0432.Ccr-20-0557
7. Koshizuka K, Hanazawa T, Arai T, Okato A, Kikkawa N, Seki N. Involvement of aberrantly expressed microRNAs in the pathogenesis of head and neck squamous cell carcinoma. *Cancer Metastasis Rev* (2017) 36(3):525–45. doi: 10.1007/s10555-017-9692-y
8. Diez-Fraile A, Ceulaer J, Derpoorter C, Spaas C, Backer T, Lamoral P, et al. Circulating Non-Coding RNAs in Head and Neck Cancer: Roles in Diagnosis, Prognosis, and Therapy Monitoring. *Cells* (2020) 10(1):48. doi: 10.3390/cells10010048
9. Ren ZH, Wu K, Yang R, Liu ZQ, Cao W. Differential expression of matrix metalloproteinases and miRNAs in the metastasis of oral squamous cell carcinoma. *BMC Oral Health* (2020) 20(1):24. doi: 10.1186/s12903-020-1013-0
10. Zhang C, Cao W, Wang J, Liu J, Liu J, Wu H, et al. A prognostic long non-coding RNA-associated competing endogenous RNA network in head and neck squamous cell carcinoma. *PeerJ* (2020) 8:e9701. doi: 10.7717/peerj.9701
11. Zhuang Z, Yu P, Xie N, Wu Y, Liu H, Zhang M, et al. MicroRNA-204-5p is a tumor suppressor and potential therapeutic target in head and neck squamous cell carcinoma. *Theranostics* (2020) 10(3):1433–53. doi: 10.7150/thno.38507
12. Xie N, Wang C, Zhuang Z, Hou J, Liu X, Wu Y, et al. Decreased miR-320a promotes invasion and metastasis of tumor budding cells in tongue squamous cell carcinoma. *Oncotarget* (2016) 7(40):65744–57. doi: 10.18632/oncotarget.11612
13. Zhuang Z, Xie N, Hu J, Yu P, Wang C, Hu X, et al. Interplay between ΔNp63 and miR-138-5p regulates growth, metastasis and stemness of oral squamous cell carcinoma. *Oncotarget* (2017) 8(13):21954–73. doi: 10.18632/oncotarget.15752
14. Saleh AD, Cheng H, Martin SE, Si H, Ormanoglu P, Carlson S, et al. Integrated Genomic and Functional microRNA Analysis Identifies miR-30-5p as a Tumor Suppressor and Potential Therapeutic Nanomedicine in Head and Neck Cancer. *Clin Cancer Res an Off J Am Assoc Cancer Res* (2019) 25(9):2860–73. doi: 10.1158/1078-0432.Ccr-18-0716
15. Manikandan M, Deva Magendhra Rao AK, Rajkumar KS, Rajaraman R, Munirajan AK. Altered levels of miR-21, miR-125b-2*, miR-138, miR-155, miR-184, and miR-205 in oral squamous cell carcinoma and association with clinicopathological characteristics. *J Oral Pathol Med Off Publ Int Assoc Oral Pathol Am Acad Oral Pathol* (2015) 44(10):792–800. doi: 10.1111/jop.12300
16. Chen Z, Jin Y, Yu D, Wang A, Mahjabeen I, Wang C, et al. Down-regulation of the microRNA-99 family members in head and neck squamous cell carcinoma. *Oral Oncol* (2012) 48(8):686–91. doi: 10.1016/j.oraloncology.2012.02.020
17. Garo Kyurkchiyan S, Miroslavov Popov T, Stancheva G, Rangachev J, Ivanov Mitev V, Petrova Popova D, et al. Novel insights into laryngeal squamous cell carcinoma from association study of aberrantly expressed miRNAs, lncRNAs and clinical features in Bulgarian patients. *J BUON Off J Balkan Union Oncol* (2020) 25(1):357–66.
18. Sun Z, Li S, Kaufmann AM, Albers AE. miR-21 increases the programmed cell death 4 gene-regulated cell proliferation in head and neck squamous carcinoma cell lines. *Oncol Rep* (2014) 32(5):2283–9. doi: 10.3892/or.2014.3456
19. Kan X, Sun Y, Lu J, Li M, Wang Y, Li Q, et al. Co–inhibition of miRNA–21 and miRNA–221 induces apoptosis by enhancing the p53–mediated expression of pro–apoptotic miRNAs in laryngeal squamous cell carcinoma. *Mol Med Rep* (2016) 13(5):4315–20. doi: 10.3892/mmr.2016.5048
20. Zhang J, Hu H, Zhao Y, Zhao Y. CDR1as is overexpressed in laryngeal squamous cell carcinoma to promote the tumour's progression via miR-7 signals. *Cell Proliferation* (2018) 51(6):e12521. doi: 10.1111/cpr.12521
21. Kao YY, Chou CH, Yeh LY, Chen YF, Chang KW, Liu CJ, et al. MicroRNA miR-31 targets SIRT3 to disrupt mitochondrial activity and increase oxidative stress in oral carcinoma. *Cancer Lett* (2019) 456:40–8. doi: 10.1016/j.canlet.2019.04.028
22. Qiang H, Zhan X, Wang W, Cheng Z, Ma S, Jiang C. A Study on the Correlations of the miR-31 Expression with the Pathogenesis and Prognosis of Head and Neck Squamous Cell Carcinoma. *Cancer Biotherapy Radiopharmaceuticals* (2019) 34(3):189–95. doi: 10.1089/cbr.2018.2621
23. Lu J, Tan T, Zhu L, Dong H, Xian R. Hypomethylation Causes MIR21 Overexpression in Tumors. *Mol Ther Oncolytics* (2020) 18:47–57. doi: 10.1016/j.omto.2020.05.011

24. Pfeffer SR, Yang CH, Pfeffer LM. The Role of miR-21 in Cancer. *Drug Dev Res* (2015) 76(6):270–7. doi: 10.1002/ddr.21257
25. Bautista-Sanchez D, Arriaga-Canon C, Pedroza-Torres A, De La Rosa-Velazquez IA, Gonzalez-Barrios R, Contreras-Espinosa L, et al. The Promising Role of miR-21 as a Cancer Biomarker and Its Importance in RNA-Based Therapeutics. *Mol Ther Nucleic Acids* (2020) 20:409–20. doi: 10.1016/j.omtn.2020.03.003
26. Kumarswamy R, Volkmann I, Thum T. Regulation and function of miRNA-21 in health and disease. *RNA Biol* (2011) 8(5):706–13. doi: 10.4161/rna.8.5.16154
27. Wang C, Peng R, Zeng M, Zhang Z, Liu S, Jiang D, et al. An autoregulatory feedback loop of miR-21/VMP1 is responsible for the abnormal expression of miR-21 in colorectal cancer cells. *Cell Death Dis* (2020) 11(12):1067. doi: 10.1038/s41419-020-03265-4
28. Fujita S, Ito T, Mizutani T, Minoguchi S, Yamamichi N, Sakurai K, et al. miR-21 Gene expression triggered by AP-1 is sustained through a double-negative feedback mechanism. *J Mol Biol* (2008) 378(3):492–504. doi: 10.1016/j.jmb.2008.03.015
29. Ribas J, Lupold SE. The transcriptional regulation of miR-21, its multiple transcripts, and their implication in prostate cancer. *Cell Cycle* (2010) 9 (5):923–9. doi: 10.4161/cc.9.5.10930
30. Chen D, Wu M, Li Y, Chang I, Yuan Q, Ekimyan-Salvo M, et al. Targeting BMI1(+) Cancer Stem Cells Overcomes Chemoresistance and Inhibits Metastases in Squamous Cell Carcinoma. *Cell Stem Cell* (2017) 20(5):621–34 e6. doi: 10.1016/j.stem.2017.02.003
31. Ding X, Pan H, Li J, Zhong Q, Chen X, Dry SM, et al. Epigenetic activation of AP1 promotes squamous cell carcinoma metastasis. *Sci Signaling* (2013) 6 (273):ra28.1–13, S0-5. doi: 10.1126/scisignal.2003884
32. Suzuki HI, Young RA, Sharp PA. Super-Enhancer-Mediated RNA Processing Revealed by Integrative MicroRNA Network Analysis. *Cell* (2017) 168 (6):1000–14 e15. doi: 10.1016/j.cell.2017.02.015
33. Huang S, Li X, Zheng H, Si X, Li B, Wei G, et al. Loss of Super-Enhancer-Regulated circRNA Nfix Induces Cardiac Regeneration After Myocardial Infarction in Adult Mice. *Circulation* (2019) 139(25):2857–76. doi: 10.1161/CIRCULATIONAHA.118.038361
34. Xie JJ, Jiang YY, Jiang Y, Li CQ, Lim MC, An O, et al. Super-Enhancer-Driven Long Non-Coding RNA LINC01503, Regulated by TP63, Is Over-Expressed and Oncogenic in Squamous Cell Carcinoma. *Gastroenterology* (2018) 154 (8):2137–51 e1. doi: 10.1053/j.gastro.2018.02.018
35. Kim TM, Huang W, Park R, Park PJ, Johnson MD. A developmental taxonomy of glioblastoma defined and maintained by MicroRNAs. *Cancer Res* (2011) 71(9):3387–99. doi: 10.1158/0008-5472.Can-10-4117
36. Wang D, Gu J, Wang T, Ding Z. OncomiRDB: a database for the experimentally verified oncogenic and tumor-suppressive microRNAs. *Bioinf (Oxford England)* (2014) 30(15):2237–8. doi: 10.1093/bioinformatics/btu155
37. Tsang FH, Law CT, Tang TC, Cheng CL, Chin DW, Tam WV, et al. Aberrant Super-Enhancer Landscape in Human Hepatocellular Carcinoma. *Hepatol (Baltimore Md)* (2019) 69(6):2502–17. doi: 10.1002/hep.30544
38. Di Micco R, Fontanals-Cirera B, Low V, Ntziachristos P, Yuen SK, Lovell CD, et al. Control of embryonic stem cell identity by BRD4-dependent transcriptional elongation of super-enhancer-associated pluripotency genes. *Cell Rep* (2014) 9(1):234–47. doi: 10.1016/j.celrep.2014.08.055
39. Sur I, Taipale J. The role of enhancers in cancer. *Nat Rev Cancer* (2016) 16 (8):483–93. doi: 10.1038/nrc.2016.62
40. Heinz S, Romanoski CE, Benner C, Glass CK. The selection and function of cell type-specific enhancers. *Nat Rev Mol Cell Biol* (2015) 16(3):144–54. doi: 10.1038/nrm3949
41. Di Costanzo A, Del Gaudio N, Migliaccio A, Altucci L. Epigenetic drugs against cancer: an evolving landscape. *Arch Toxicol* (2014) 88(9):1651–68. doi: 10.1007/s00204-014-1315-6

Conflict of Interest: The authors declare that the research was conducted in the absence of any commercial or financial relationships that could be construed as a potential conflict of interest.

Copyright © 2021 Wan, Hoyle, Xie, Wang, Cai, Zhang, Ma, Xiong, Xu, Huang, Liu, Li and Wang. This is an open-access article distributed under the terms of the Creative Commons Attribution License (CC BY). The use, distribution or reproduction in other forums is permitted, provided the original author(s) and the copyright owner(s) are credited and that the original publication in this journal is cited, in accordance with accepted academic practice. No use, distribution or reproduction is permitted which does not comply with these terms.

frontiers in Oncology

ORIGINAL RESEARCH
published: 21 April 2021
doi: 10.3389/fonc.2021.657876

Long Non-Coding RNA LINC01929 Accelerates Progression of Oral Squamous Cell Carcinoma by Targeting the miR-137-3p/FOXC1 Axis

Hongze Che[1], *Yanhai Che*[2], *Zhimin Zhang*[1]* *and Qing Lu*[3]*

[1] Department of Endodontics, Hospital of Stomatology, Jilin University, Changchun, China, [2] Department of Science and Education, Hospital of Stomatology, Jilin University, Changchun, China, [3] Department of General Dentistry, Hospital of Stomatology, Jilin University, Changchun, China

Recently, additional long noncoding RNAs (lncRNAs) have been identified and their possible roles were investigated in a variety of human tumors. One of these lncRNAs, LINC01929, promoted the progression of some cancers, whereas its expression and biological function in human oral squamous cell carcinoma (OSCC) remains still mostly uncertain. The LINC01929 expression in OSCC tissues or cell lines was identified *via* quantitative real-time polymerase chain reaction. The cell counting kit-8, transwell migration, wound-healing, and flow cytometry assays were utilized to characterize the functions of LINC01929 in OSCC cells. The interactive relationships between LINC01929 and miR-137-3p, miR-137-3p and Forkhead box C1 (FOXC1) were investigated by the dual-luciferase activity assay. Our findings demonstrated that LINC01929 was highly expressed in OSCC tissue samples and cell lines, whereas miR-137-3p expression was downregulated. LINC01929 acted as a carcinogenic lncRNA with accelerated OSCC cell proliferation, migration and invasion, and suppression of apoptosis. We further indicated that LINC01929 facilitated tumor growth in xenograft mouse models. Mechanistically, LINC01929 acted as a sponge for miR-137-3p to elevate FOXC1 expression, which is the target of miR-137-3p. In addition, downregulated miR-137-3p expression rescued the suppressive behaviors of LINC01929 knockdown on the biological behaviors of OSCC cells. Taken together, LINC01929 functioned as a tumor-promoting lncRNA *via* the miR-137-3p/FOXC1 axis in OSCC, suggesting novel targets for OSCC therapy.

Keywords: FOXC1, oral squamous cell carcinoma, LINC01929, ceRNA, miR-137-3p

OPEN ACCESS

Edited by:
Wei Cao,
Shanghai Jiao Tong University, China

Reviewed by:
Marco Mascitti,
Marche Polytechnic University, Italy
Zheqi Liu,
Shanghai Jiao Tong University, China

***Correspondence:**
Zhimin Zhang
zhangzhim@jlu.edu.cn
Qing Lu
lu123qing@jlu.edu.cn

Specialty section:
This article was submitted to Head and Neck Cancer, a section of the journal Frontiers in Oncology

Received: *24 January 2021*
Accepted: *22 March 2021*
Published: *21 April 2021*

Citation:
Che H, Che Y, Zhang Z and Lu Q (2021) Long Non-Coding RNA LINC01929 Accelerates Progression of Oral Squamous Cell Carcinoma by Targeting the miR-137-3p/FOXC1 Axis. Front. Oncol. 11:657876. doi: 10.3389/fonc.2021.657876

INTRODUCTION

Oral squamous cell carcinoma (OSCC) accounts for a remarkable cases of human malignant tumors that occur in the head and neck region. It has the sixth highest incidence rate and a high mortality rate (1, 2). There have been remarkable advances in recent years in OSCC treatment, including surgery, radiotherapy, and chemotherapy. However, OSCC is accompanied with a low five-year survival rate

(3, 4). The literature indicates that the progression of OSCC is accompanied with coding and non-coding gene disorders (5).

Scholars have defined long noncoding RNAs (lncRNAs) as non-coding RNAs that cannot encode genes and are less than 200 nucleotides in length (6–8). Numerous reports have suggested substantial role of lncRNAs in controlling gene expression at the transcriptional, post-transcriptional, and chromosomal levels, and also participated in the biological progression of proliferation, invasion, and apoptosis of tumor cells (9–11). Increasingly, additional lncRNAs have been shown to regulate mRNA expression at the post-transcriptional level by sponging miRNA with competitive endogenous RNA (ceRNA) mechanisms (12–15). Several researches pointed out that lncRNAs were involved in the development of OSCC (16–18). LncRNA BLACAT1 knockdown could inhibit invasion and migration of OSCC cells by sponging miR-142-5p (19). LncRNA ANRIL advanced the proliferation of OSCC cells and inhibited apoptosis by regulating the TGF-/Smad signaling pathway (20).

LINC01929 could promote tumor progression as a carcinogenic lncRNA in hepatocellular carcinoma and non-small cell lung carcinoma (21, 22). However, the role of LINC01929 in OSCC remains unclear.

We, in the present research, measured LINC01929 expression in OSCC tissues and OSCC cells and characterized its function *via in vitro* and *in vivo* experiments. We also attempted to evaluate the molecular mechanism by which LINC01929 plays a role in OSCC.

MATERIALS AND METHODS

Tissue Collection

OSCC tissues and paired adjacent tissues of 27 confirmed patients were collected from the Stomatological Hospital of Jilin University. Prior to surgical removal, none of the patients received anticancer treatment. All patients signed informed consent. The confirmation of the present research could be achieved from the Ethics Committee of Stomatological Hospital of Jilin University.

Cell Cultivation

Human oral keratinocytes (HOK) and OSCC cells (CAL-27, CAL-33, SCC-9, SCC-25, and HSC-3) were acquired from the Chinese Academy of Sciences. These were cultivated with DMEM with 10% FBS and maintained at 37°C in a humidified 5% CO_2 incubator.

Cell Transfection

ShRNA against LINC01929 (sh-LINC01929), control shRNA (sh-NC), pcDNA3.1-LINC01929 (pLINC01929), control pcDNA3.1 (pcDNA3.1), as well as pcDNA3.1-FOXC1 (pcDNA-FOXC1), and the empty control vector (pcDNA-NC) were utilized (GenePharma, Shanghai, China). To silence miR-137-3p, miR-137-3p inhibitor (miR-137-3p in) and negative control (miR-NC) were provided by GenePharma. Lipofectamine 2000 was applied to transfect the constructs separately into CAL-27 or SCC-9 cells.

Quantitative Real-Time Polymerase Chain Reaction (qRT-PCR)

Total RNA of OSCC tissues and OSCC cells was extracted by TRIZOL reagent. Reverse transcription into cDNA was accomplished with the PrimerScript RT Reagent Kit. The reaction was performed on the ABI7500 system with SYBR Premix Ex Taq. Primers used in experiments are summarized in **Table 1**. GAPDH and U6 were used as internal controls for the cytoplasm and nucleus, respectively.

Nucleus-Cytoplasm Separation

PARIS™ Kit was used to detect the cytoplasmic and nuclear distribution of LINC01929 in CAL-27 and SCC-9 cells. The expression levels of LINC01929, GAPDH, and U6 in cytoplasm and nucleus were detected by qRT-PCR.

Cell Counting Kit-8 (CCK-8)

CAL-27 and SCC-9 cells ($5x10^3$ cells/well) were used to coat onto 96-well plates for 24, 48, 72, and 96 h. Afterwards, CCK-8 reagent was mixed with the cells for 1 h incubation at 37 °C. Finally, the absorption value at 450 nm was measured with a microporous plate.

Wound-Healing Assay

Transfected cells were coated onto 6-well plates and allowed to multiply until 100% confluence was reached. A scratch was then created with a 200 μL pipette tip, and the scratch distance was recorded through a microscope (Olympus) after 0 and 48 h in serum-free medium.

Transwell Assay

The transwell assay was employed to measure invasion with Transwell chambers. Transfected cells in serum-free medium were added to the upper compartment, followed by adding DMEM with 10% FBS to the lower compartment. Once 24 h was passed after cultivation, the upper layer cells were gently removed, and the invaded cells in the lower layer were immobilized by 4% paraformaldehyde and crystal violet. Five fields were randomly selected and photographed with a microscope.

TABLE 1 | The primer of referred genes.

Primers		Sequence (5'→3')
LINC01929	Forward	5'-TGCCTTTGGTGTGGTCCTGTTTC -3'
	Reverse	5'-AAGATGCCCATACCAGACCTCCAG-3'
FOXC1	Forward	5'-GGCGAGCAGAGCTACTACC-3'
	Reverse	5'-TGCGAGTACACGCTCATGG-3'
GAPDH	Forward	5'-GGTCTCCTCTGACTTCAACA -3'
	Reverse	5'-GTGAGGGTCTCTCTCTTCCT-3'
miR-137-3p	Forward	5' -CCATTCATTCGTTATTGCTTAAGA -3'
	Reverse	5'- TATGCTTGTTCTCGTCTCTGTGTC-3'
U6	Forward	5'- CTCGCTTCGGCAGCACA -3'
	Reverse	5'- AACGCTTCACGAATTTGCGT -3'

Flow Cytometry Assay

The annexin V-fluorescein isothiocyanate (FITC)-apoptosis detection kit was used. Concisely, we attempted to wash transfected cells with PBS for two times, followed by staining with Annexin V-FitC in darkness at room temperature for 5 min and then with 10 μL of PI for 15 min. Finally, flow cytometry was employed for detecting apoptosis.

Luciferase Reporter Assay

Mutant plasmids (FOXC1-MUT, LINC01929-MUT) and wild-type plasmids (FOXC1-WT, LINC01929-WT) were constructed using the pmirGLO double-luciferase vector. Once we co-transfected the plasmids with miR-137-3p mimics or NC mimics, Renilla luciferase activity was detected.

Tumor Xenograft Assay

Immunodeficient female BALB/c nude mice (4-6 weeks old) were provided by Shanghai Laboratory Animal Company and maintained at the Animal Laboratory Center of Jilin University. The animal experiment ethics committee of Jilin University approved the animal experiments. The knockdown transfected cells (5×10^6/mL, 100 μL) were then injected subcutaneously into nude mice (n = 3/group). We attempted to quantify tumor volumes once a week. The mice were killed four weeks after the mold was made. The OSCC tissues of mice were removed, weighed, photographed, and stored for subsequent qRT-PCR and Western blotting.

Western Blotting

According to the kit instructions, radioimmunoprecipitation assay (RIPA) protein lysis buffer was applied to extract protein lysates from OSCC tissues or OSCC cells, and 10% SDS-PAGE was applied for separation, followed by transferring the protein to PVDF membrane, and blocking with skim milk. The blot was incubated at 4°C with primary and secondary antibodies, separately. The band signal was visualized through BeyoECL.

Statistical Analysis

Data analyses were undertaken with GraphPad PRISM 6 and SPSS 17.0 software. The findings were summarized as mean ± standard deviation (SD), from three independent experiments and analyzed *via* the Student's *t*-test. $P < 0.05$ was served to show statistical significance.

RESULTS

LINC01929 Was Highly Expressed in OSCC Tissues and OSCC Cells

In our study, LINC01929 expression was detected for the first time in 27 OSCC tissues. The findings unveiled that LINC01929 expression was remarkably elevated in OSCC tissues (**Figure 1A**). To explore the markedly upregulated LINC01929 expression in OSCC, we attempted to divide patients into groups of high LINC01929 expression and low LINC01929 expression. This revealed that elevated LINC01929 expression was linked with advanced lymph node metastasis (**Table 2**). We also measured the LINC01929 expression in HOKs and OSCC cells, including CAL-27, CAL-33, SCC-9, SCC-25, and HSC-3. LINC01929 expression was upregulated in OSCC cells, while CAL-27 and SCC-9 cells showed the highest expression (**Figure 1B**). Thus, CAL-27 and SCC-9 cells were selected for subsequent experiments. Kaplan-Meier assays suggested that patients with higher LINC01929 expression had poorer overall survival rates than those with lower LINC01929 expression (**Figure 1C**). In general, the level of LINC01929 was higher in OSCC tissues and OSCC cells and correlated with poorer OSCC clinical outcomes.

LINC01929 Regulated Proliferation, Migration, Invasion, and Apoptosis of OSCC *In Vitro*

To detect the biological function of LINC01929 in OSCC cells, we firstly used sh-LINC01929 to knockdown LINC01929 in CAL-27 cells, while pLINC01929 to overexpress LINC01929 in SCC-9 cells. qRT-PCR highlighted the successfully transfection of sh-LINC01929 and pLINC01929 (**Figure 2A**). CCK-8 assay indicated that downregulation of LINC01929 dramatically reduced, whereas LINC01929 overexpression promoted proliferation (**Figure 2B**).

As illustrated in **Figures 2C, D**, migration and invasion in the sh-LINC01929 group were limited and the pLINC01929 group were increased compared with the control group. Then, flow cytometry was used to examine apoptosis, and the data showed that apoptosis of OSCC cells was notably elevated after LINC01929 knockdown, while inhibited after LINC01929 upregulation (**Figure 2E**). In summary, the above-mentioned findings indicated that LINC01929 regulated cell proliferation, migration, invasion, and apoptosis of OSCC cells.

LINC01929 Sponged miR-137-3p in OSCC Cells

The subcellular distribution of lncRNAs determines their biological actions. Through the nuclear-cytoplasmic fractionation assay, LINC01929 was mainly found in the cytoplasm (**Figure 3A**). Therefore, we speculated that LINC01929 regulated the function of OSCC through a ceRNA mechanism. The miRDB prediction revealed a sequence that suggested that binding of miR-137-3p to LINC01929 was possible (**Figure 3B**). As depicted in **Figure 3C**, dual-luciferase activity assay verified that miR-137-3p mimics downregulated the luciferase activity of LINC01929-WT. However, the effect of miR-137-3p expression on LINC01929-MUT was not noticeable. Through qRT-PCR, we discovered that miR-137-3p expression was attenuated in OSCC tissues compared with paracancer tissues (**Figure 3D**), and was downregulated in OSCC cells (**Figure 3E**). In addition, after LINC01929 expression

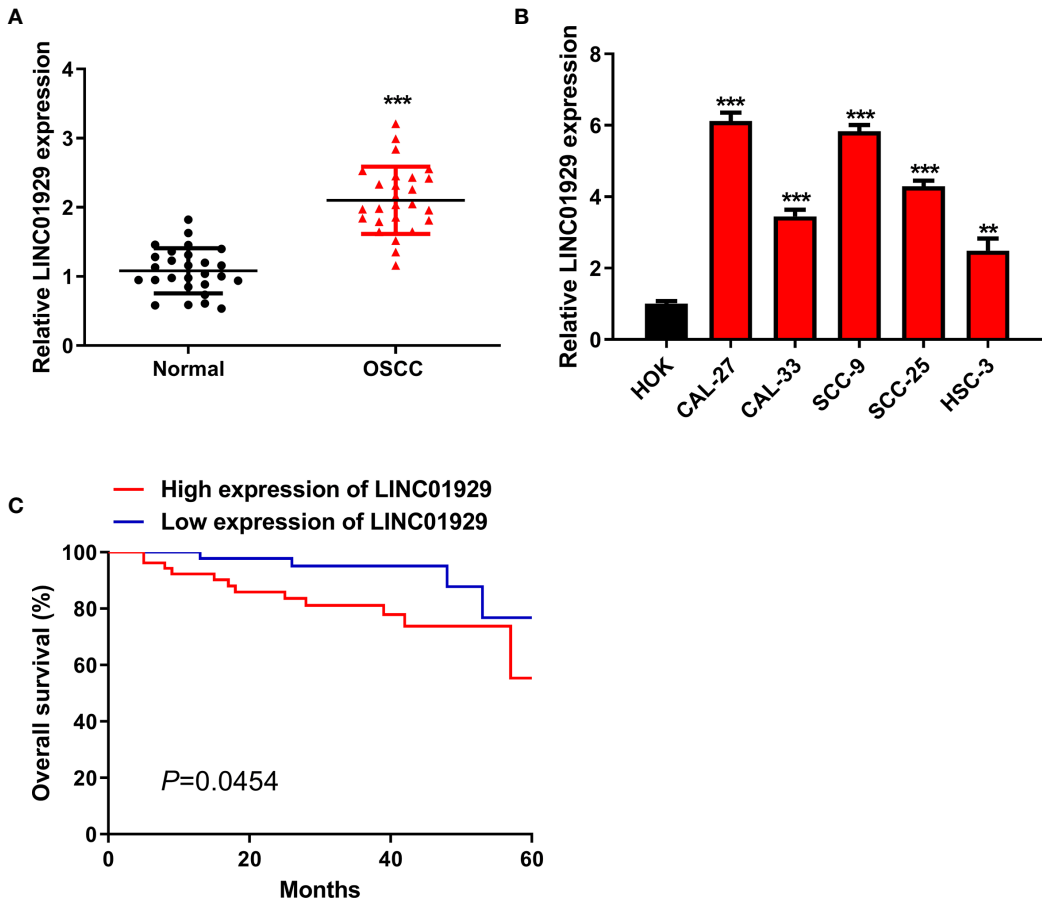

FIGURE 1 | High LINC01929 expression in OSCC tissues and OSCC cells. **(A)** LINC01929 expression was measured by qRT-PCR in OSCC tissues and paired non-tumor tissues (n = 27). **(B)** The LINC01929 expression was identified by qRT-PCR in HOKs and OSCC cells. **(C)** Survival curves were generated with Kaplan-Meier to measure the correlation between LINC01929 expression and overall survival of OSCC patients. **p < 0.01, ***p < 0.001.

TABLE 2 | Correlation between LINC01929 expression and clinicopathological factors in patients of OSCC.

Factors	LINC01929 expression		*P*-value
	Low	High	
Age (years)			0.4743
<60	5	8	
≥60	7	7	
Gender			0.6471
Male	4	6	
Female	8	9	
Tumor size (cm)			0.3928
<5	8	10	
≥5	4	5	
TNM stage			0.0885
I-II	6	7	
III-IV	6	8	
Lymph node metastasis			0.0183*
Yes	2	13	
No	10	2	

**P < 0.05 was considered statistically significant.*

was knocked down in OSCC cells, miR-137-3p expression was markedly elevated (**Figure 3F**). When miR-137-3p was upregulated, this was associated with a remarkable inhibition in LINC01929 expression (**Figure 3G**). **Figure 3H** depicts that the lower miR-137-3p expression in OSCC tissues was negatively correlated with that of LINC01929. In conclusion, LINC01929 could target miR-137-3p in OSCC cells.

We conducted *in vitro* experiments to explore whether the binding between miR-137-3p and LINC01929 affects OSCC progression. Sh-LINC01929 and miR-137-3p inhibitor were co-transfected into CAL-27 cells. The cell proliferation of sh-LINC01929 cells was rescued by the introduction of miR-137-3p inhibitor (**Figure 4A**). Wound healing and transwell assays demonstrated that miR-137-3p inhibitor significantly reversed sh-LINC01929-attenuated migration and invasion activity of CAL-27 cells (**Figure 4B, C**). Furthermore, flow cytometry assay indicated co-introduction of miR-137-3p remarkedly decreased cell apoptosis compared with sh-LINC01929 group (**Figure 4D**).

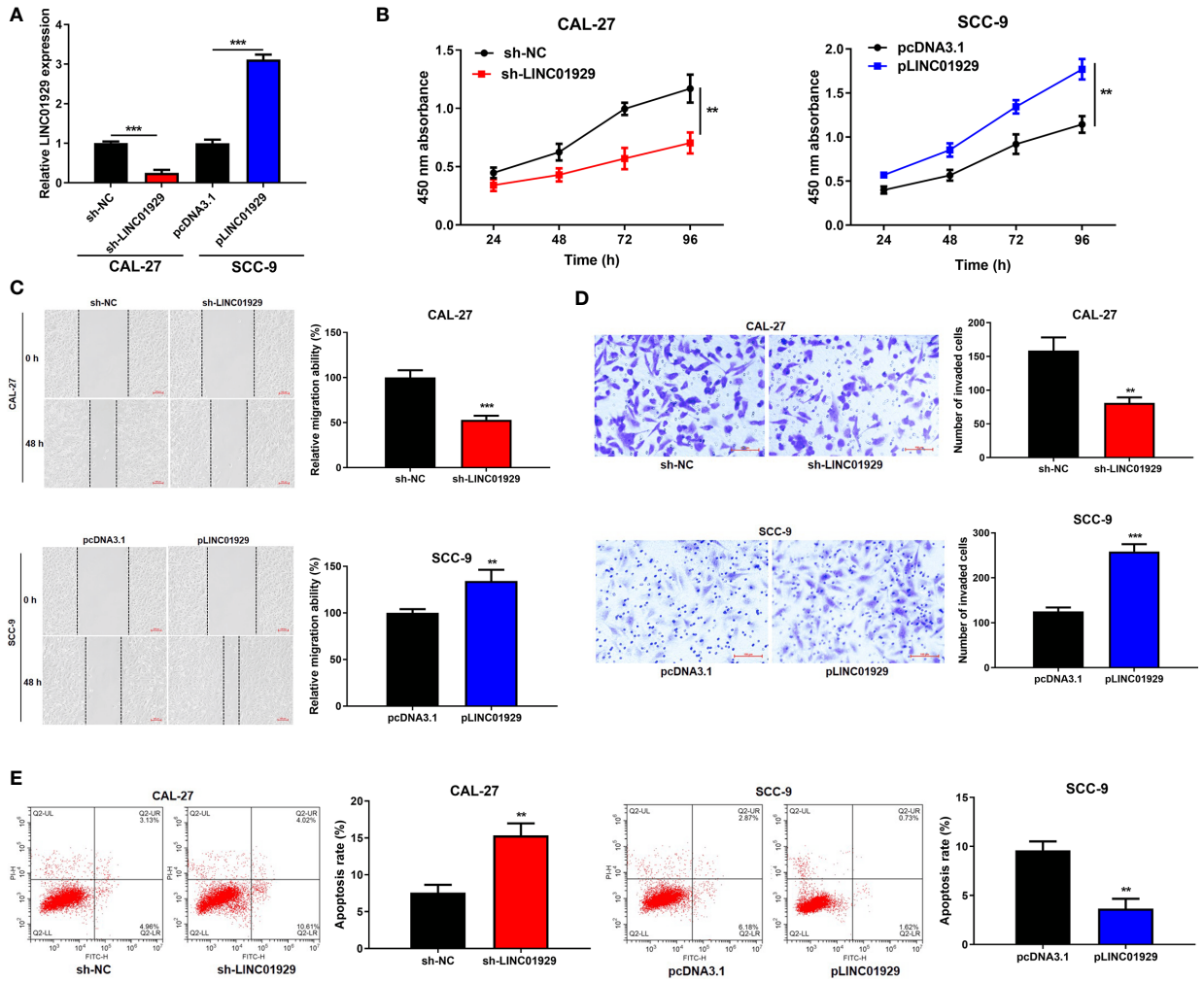

FIGURE 2 | LINC01929 regulated proliferation, migration, invasion, and apoptosis of OSCC *in vitro*. **(A)** qRT-PCR analysis was used to examine the efficiency of sh-LINC01929 and pLINC01929. **(B)** Proliferation was monitored by CCK-8 assay after transfecting sh-LINC01929 or pLINC01929 into selected OSCC cells. **(C, D)** Wound-healing assay and transwell assay were employed to assess migration and invasion after LINC01929 knockdown or overexpression. **(E)** The effects of sh-LINC01929 or pLINC01929 on apoptosis was detected by flow cytometry. $^{**}p < 0.01$, $^{***}p < 0.001$.

MiR-137-3p Directly Interacted With FOXC1

We sought to identify the target of miR-137-3p and found that FOXC1 contained a putative binding site for miR-137-3p (**Figure 5A**). We found that luciferase activity of cells transfected with FOXC1-WT was notably inhibited by miR-137-3p mimics (**Figure 5B**). Moreover, we found that FOXC1 expression was notably upregulated in OSCC tissues compared with neighbor non-tumor tissues (**Figure 5C**). Furthermore, FOXC1 was upregulated in OSCC cells (**Figure 5D**). Finally, outcomes of Spearman's correlation analysis suggested that FOXC1 was negatively correlated with miR-137-3p, and LINC01929 expression and FOXC1 expression showed a notable positive correlation (**Figures 5E, F**). The above-mentioned findings highlighted that LINC01929 sponged miR-137-3p, acted as a ceRNA, and released FOXC1 from the inhibitory effect of miR-137-3p.

The LINC01929/miR-137-3p/FOXC1 Axis Regulated the Behavior of OSCC Cells

We speculated that LINC01929/miR-137-3p may influence OSCC progression *via* FOXC1. The findings highlighted that transfection of pcDNA-FOXC1 remarkably elevated its expression level (**Figure 6A**). qRT-PCR and Western blotting indicated that miR-137-3p expression downregulation or FOXC1 expression upregulation could reverse the LINC01929 knockdown-mediated inhibition on FOXC1 expression (**Figures 6B, C**). CCK-8 assay revealed that FOXC1 overexpression could restore the LINC01929 knockdown-mediated inhibition on proliferation (**Figure 6D**). Furthermore, FOXC1

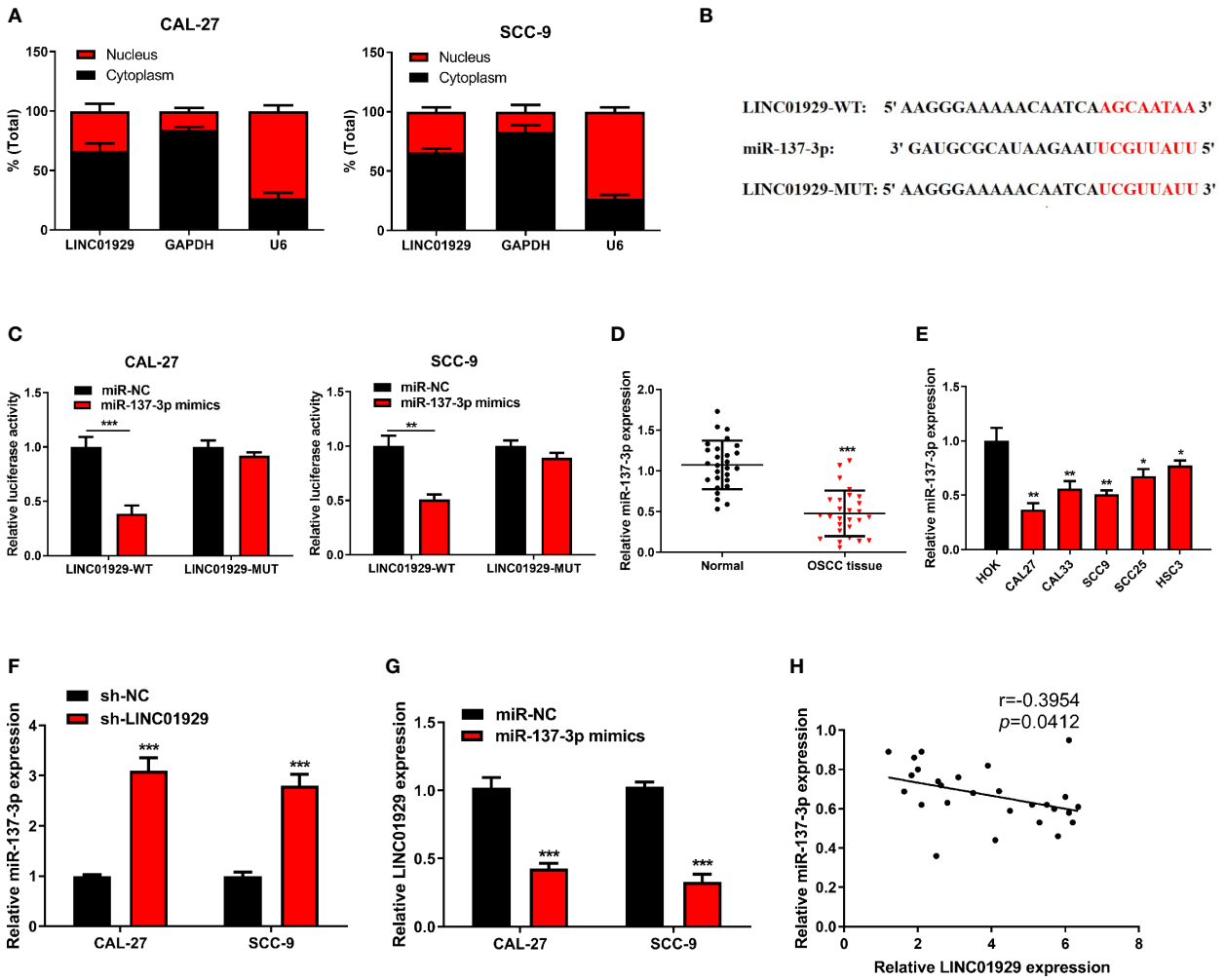

FIGURE 3 | LINC01929 sponged miR-137-3p in OSCC cells. **(A)** Identification of LINC01929 expression by nuclear and cytoplasmic fractionation to analyze its subcellular location. **(B)** The binding site between LINC01929-MUT and miR-137-3p was predicted with bioinformatics analysis. **(C)** The luciferase gene reporter assay was applied to test the binding relationship between LINC01929 and miR-137-3p mimics. **(D, E)** The miR-137-3p expression was detected by qRT-PCR in OSCC tissues and OSCC cells. **(F)** The miR-137-3p expression was identified in LINC01929 knockdown OSCC cells. **(G)** The LINC01929 expression was tested after transfecting with miR-137-3p mimics into OSCC cells. **(H)** Spearman's correlation analysis was used to analyze the relevance between LINC01929 and miR-137-3p. *p < 0.05, **p < 0.01, ***p < 0.001.

overexpression had a partial reversal effect on the migration and invasion changes in CAL-27 cells caused by LINC01929 knockdown (**Figures 6E, F**). Flow cytometry assay confirmed that the enhanced apoptosis of OSCC cells caused by sh-LINC01929 could be reversed by FOXC1 upregulation (**Figure 6G**). In general, LINC01929 promoted proliferation, migration, and invasion of OSCC cells *via* the miR-137-3p/FOXC1 axis.

Downregulation of LINC01929 Inhibited Tumor Growth *In Vivo*

Immuno-deficient nude mice were used in a xenograft model to detect the influence of LINC01929 on OSCC progression. LINC01929 knockdown markedly attenuated tumor growth as well as tumor weight (**Figures 7A–C**). qRT-PCR assay confirmed enhanced miR-137-3p and reduced FOXC1 expression in sh-LINC01929 tumors (**Figure 7D**). The above-mentioned consequences demonstrated that downregulation of LINC01929 expression noticeably limited tumor growth *in vivo*.

DISCUSSION

Several recently conducted researches have pointed out that lncRNA expression disorders actively participate in the development of tumors (23–27). In OSCC, more and more

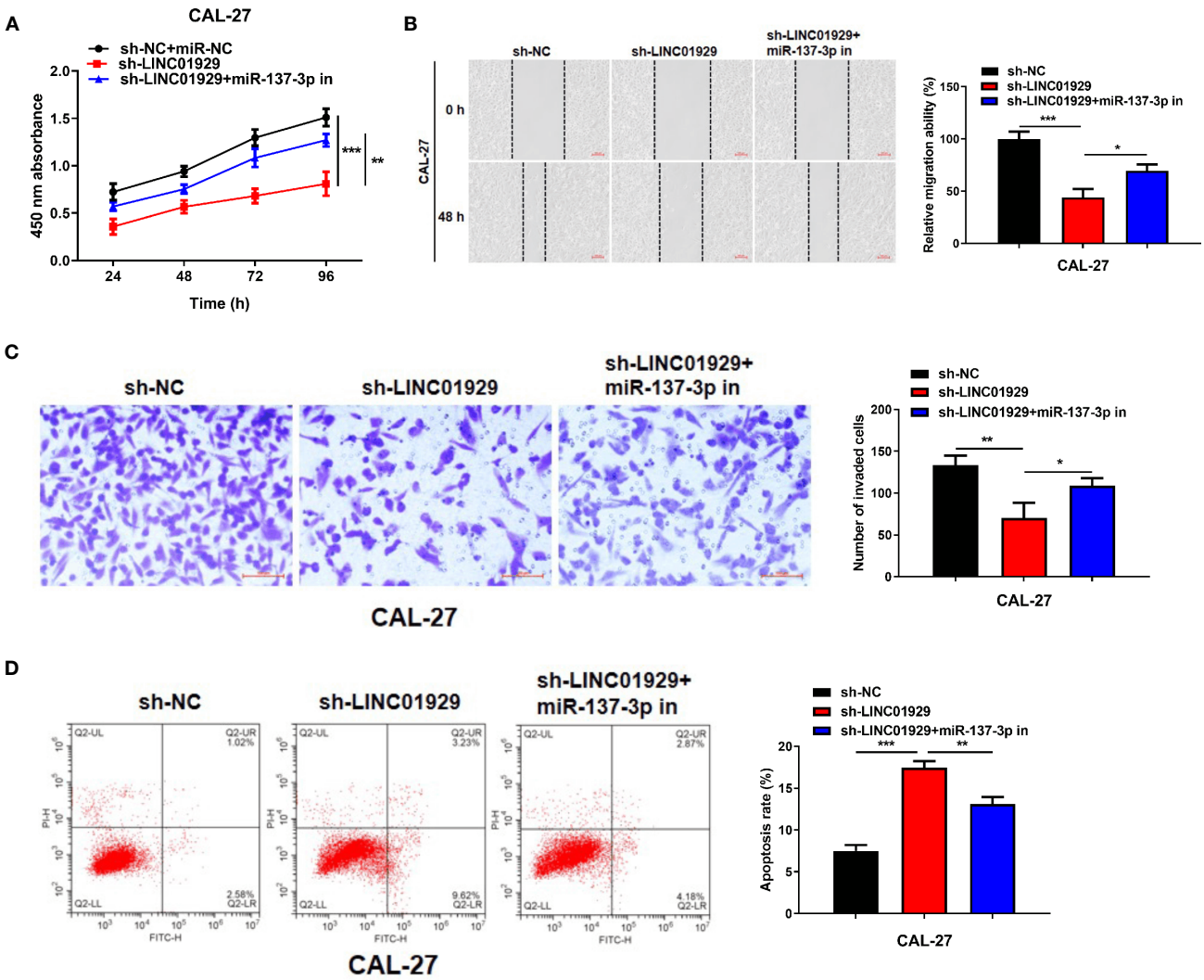

FIGURE 4 | MiR-137-3p inhibitor restored the effect of LINC01929 knockdown on OSCC cells. **(A)** CCK-8 assay showed CAL-27 cells proliferation after transfection of sh-NC, sh-LINC01929 and sh-LINC01929+miR-137-3p inhibitor. **(B, C)** Wound healing assay and transwell assay showed CAL-27 cells migration and invasion after transfection of sh-NC, sh-LINC01929 and sh-LINC01929+miR-137-3p inhibitor. **(D)** The flow cytometry was applied to measure apoptosis in each group.

lncRNAs have been shown to be involved in changing the biological functions of tumor cells (28–30). For instance, Shao et al. stated that LncRNA AC007271.3 accelerates proliferation, invasion, and migration of OSCC cells, and suppresses apoptosis of OSCC through the Wnt/β-catenin signaling pathway (31). Xu et al. pointed out that lncRNA FezF1-AS1 accelerates the occurrence and development of OSCC by directly binding to miR-196 (32). Scholars pointed out that LINC01929 has carcinogenic effects in several types of cancer (21, 22). In the present research, we sought to understand the functions and molecular mechanisms of LINC01929 in OSCC. We revealed that LINC01929 was highly expressed in OSCC tissues and OSCC cells. Functional experiments indicated that LINC01929 promoted proliferation, migration, and invasion of OSCC cells *in vitro*, as well as regulated tumor growth *in vivo*. This demonstrates that LINC01929 also has an oncogenic role in OSCC.

The function of lncRNA depends on its downstream binding molecules, such as ceRNA, which can competitively bind miRNA and thus regulate the changes of targeted mRNA expression. In gastric cancer, lncRNA MT1JP as ceRNA sponges miR-92a-3p to regulate the expression of FBXW7 and then influence the progression of gastric cancer (33). LINC01087 is enhanced in breast cancer, and LINC01087 affects the expression of ROCK1 by sponging miR-335-5p, thus affecting the migration and invasion of breast cells (34). Using bioinformatics and dual-luciferase activity

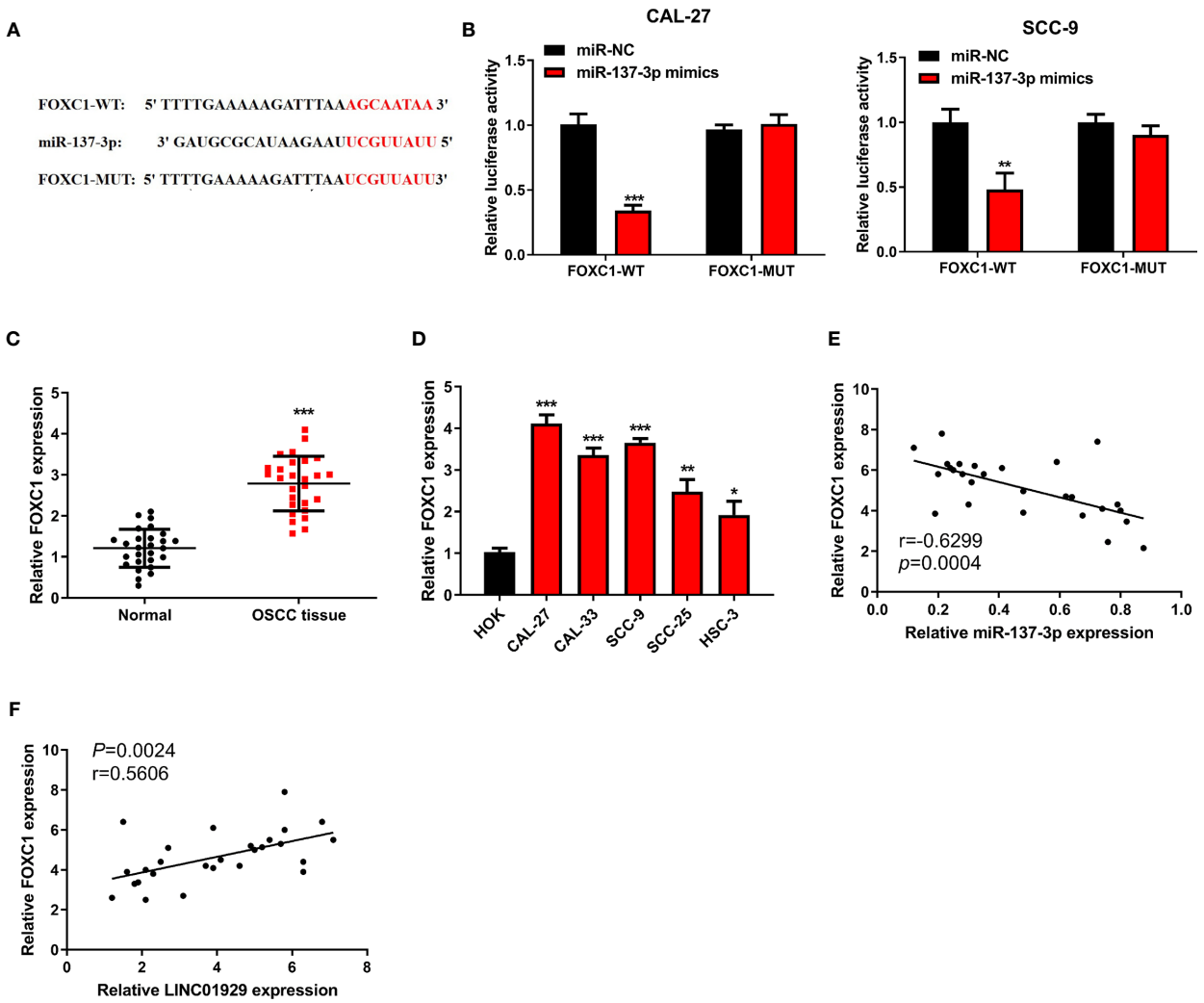

FIGURE 5 | MiR-137-3p directly interacted with FOXC1. **(A)** Potential binding and mutant sequences were constructed. **(B)** The putative site of miR-137-3p in the FOXC1 3'UTR was detected by the dual-luciferase reporter assay. **(C)** FOXC1 expression was monitored by qRT-PCR in OSCC tissues and paired adjacent normal tissues. **(D)** The FOXC1 expression was measured by qRT-PCR in OSCC cells and the HOKs. **(E)** Correlation analysis of miR-137-3p expression with FOXC1 expression. **(F)** Correlation analysis of LINC01929 expression with FOXC1 expression.

assays, we verified that LINC01929 and miR-137-3p could fully bind to each other. The miR-137-3p expression was downregulated in OSCC tissues and OSCC cells compared with normal materials. Some reports suggest that miR-137-3p acts as a tumor suppressor gene in cancer. In colorectal cancer, miR-137-3p is low expressed and suppresses migration of colorectal cancer cells *via* regulating a KDM1A-dependent EMT process (35). Overexpression of miR-137-3p inhibits the tumor growth of prostate cancer by regulating the JNK3/EZH2 signal pathway (36). In the present research, suppressing miR-137-3p expression partially abolished the inhibition of proliferation, migration, and invasion of OSCC cells upon LINC01929 knockdown. Overall, the outcomes highlight that LINC01929 knockdown suppresses the growth of OSCC cells by regulating miR-137-3p expression.

FOXC1, which is also known as FREAC3, Fkh-1, or Mf1, is a single exon gene which encodes a 533 amino acid protein located at 6p25 in the nucleus, where it can bind to DNA and regulate gene expression (37–40). In recent years, FOXC1 has been found to play a key role in tumorigenesis. FOXC1 expression is upregulated in some types of cancer and participates in tumor formation as an oncogene. Knockdown of FOXC1 expression by siRNA dramatically inhibits proliferation, migration, and invasion of basal-like breast cancer cell lines (41). FOXC1 upregulates the expression levels of CCL2 and CXCR1 by directly binding to their

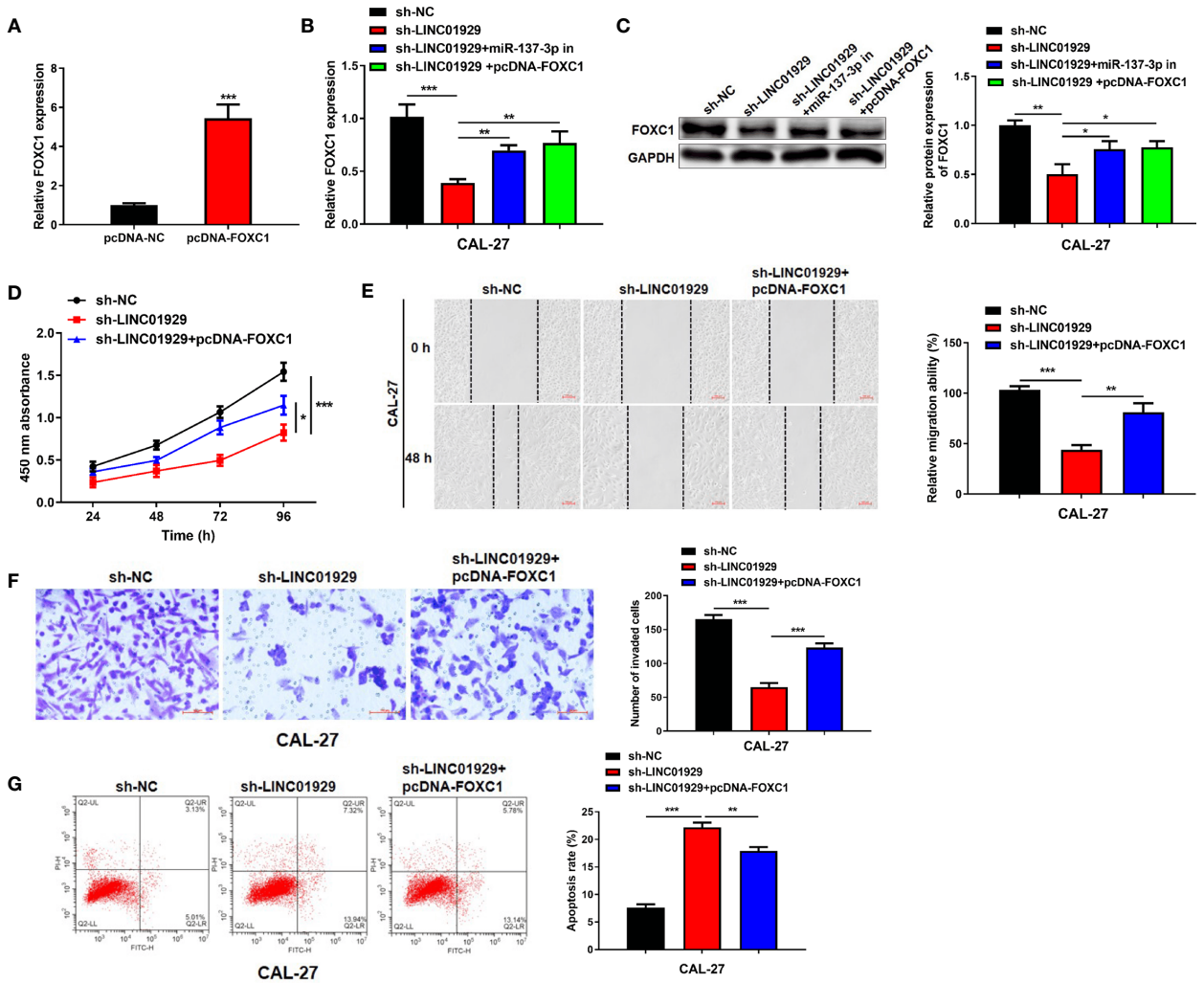

FIGURE 6 | The LINC01929/miR-137-3p/FOXC1 axis regulated the behavior of OSCC cells. **(A)** The efficiency of FOXC1 overexpression was measured by qRT-PCR. **(B)**The mRNA and **(C)** protein expressions of FOXC1 were identified by qRT-PCR and Western blotting in OSCC cells transfected with sh-NC, sh-LINC01929, sh-LINC01929+miR-137-3p in and sh-LINC01929+pcDNA-FOXC1. **(D)** The CCK-8 assay was applied to identify the proliferation in each group. The migration **(E)** and invasion **(F)** in each group were identified by wound-healing assay and transwell assay. **(G)** The flow cytometry was applied to measure apoptosis in each group.

promoters in hepatocellular carcinoma cells. The elevated expression of CXCR1 accelerates invasion and metastasis of hepatocellular carcinoma cells (42). FOXC1 functions as an oncogene in OSCC cells. LncRNA-FOXCUT and FOXC1 are overexpressed in OSCC patients and knockdown of either FOXCUT or FOXC1 inhibits the proliferation and migration of OSCC cell Tca8113 and SCC-9 (43). FOXC1-silenced OSCC cells exhibits decreased growth and migration, accompanied by a downregulation of MMP-2 and MMP-9 (44). Employing the dual-luciferase activity assay, we confirmed that FOXC1 is a direct target gene of miR-137-3p. It could be elevated in OSCC tissues and OSCC cells. It accelerated the proliferation, invasion, and migration of OSCC cells. FOXC1 partially reversed the changes in biological behaviors induced by sh-LINC01929.

In summary, the present research elucidated that LINC01929 targets FOXC1 *via* miR-137-3p to enhance the OSCC (**Figure 8**). As far as we know, this is the first research aimed to characterize the function and mechanism of the LINC01929 in OSCC. The outcomes may provide new targets for the diagnosis and treatment of OSCC.

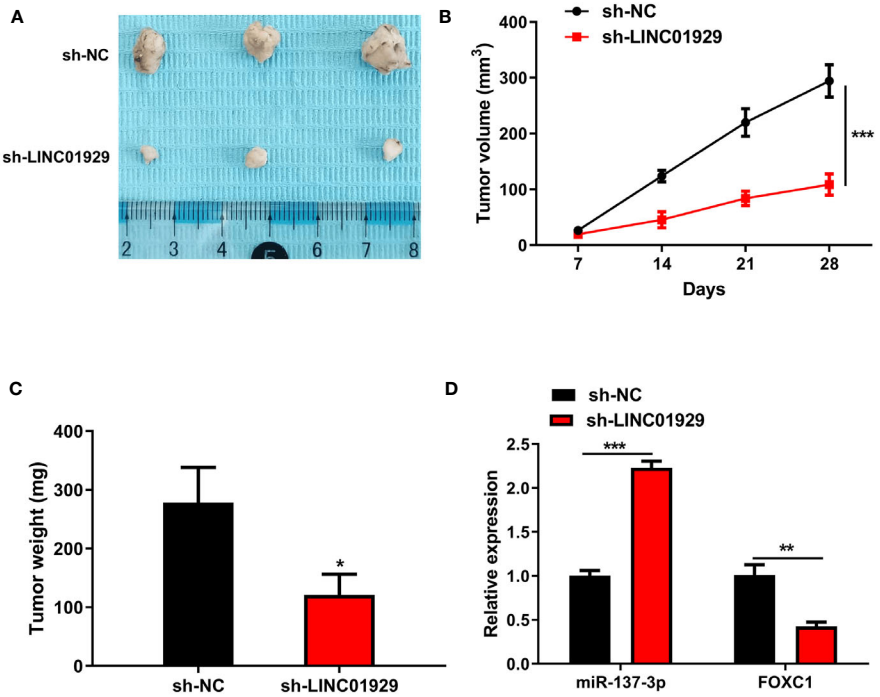

FIGURE 7 | Downregulation of LINC01929 inhibited tumor growth *in vivo*. **(A)** Tumor images at 28 days post-xenotransplantation from the sh-LINC01929 groups and sh-NC groups. **(B)** Quantification of tumor volume was undertaken every seven days after the xenotransplantation. **(C)** Tumor weight was monitored after the experiment. **(D)** qRT-PCR was employed to identify miR-137-3p expression and FOXC1 expression in xenograft tumors. *p < 0.05, **p < 0.01, ***p < 0.001.

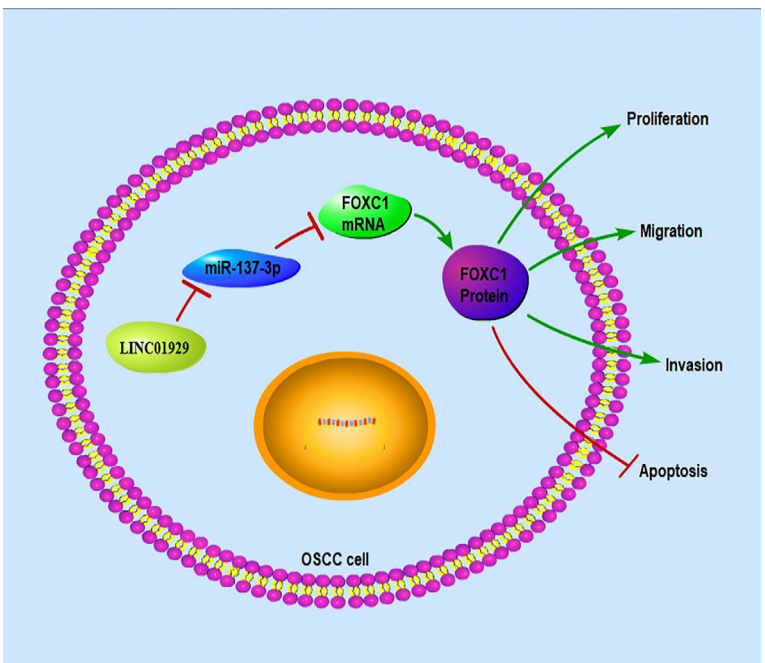

FIGURE 8 | Schematic of the LINC01929/miR-137-3p/FOXC1 axis in OSCC cells.

DATA AVAILABILITY STATEMENT

The original contributions presented in the study are included in the article. Further inquiries can be directed to the corresponding authors.

ETHICS STATEMENT

The studies involving human participants were reviewed and approved by Stomatological Hospital of Jilin University. The patients/participants provided their written informed consent to participate in this study. The animal study was reviewed and approved by The First Hospital of Jilin University.

AUTHOR CONTRIBUTIONS

HC and QL designed experiments and wrote the manuscript. HC and YC performed the experiments and data analysis. All authors critically discussed the results and the manuscript. ZZ and QL supervised the project and gave final approval. All authors contributed to the article and approved the submitted version.

FUNDING

This work was supported by the China Postdoctoral Science Foundation funded project (2020M670865).

ACKNOWLEDGMENTS

The authors would like to thank TopEdit (www.topeditsci.com) for its linguistic assistance during the preparation of this manuscript.

REFERENCES

1. Pan L, Chen H, Bai Y, Wang Q, Chen L. Long non-coding RNA CASC2 serves as a ceRNA of microRNA-21 to promote PDCD4 expression in oral squamous cell carcinoma. *Onco Targets Ther* (2019) 12:3377–85. doi: 10.2147/OTT.S198970
2. Sun CC, Zhang L, Li G, Li SJ, Chen ZL, Fu YF, et al. Wu QM *et al*: The lncRNA PDIA3P Interacts with miR-185-5p to Modulate Oral Squamous Cell Carcinoma Progression by Targeting Cyclin D2. *Mol Ther Nucleic Acids* (2017) 9:100–10. doi: 10.1016/j.omtn.2017.08.015
3. Jiang X, Liu J, Li S, Jia B, Huang Z, Shen J, et al. CCL18-induced LINC00319 promotes proliferation and metastasis in oral squamous cell carcinoma via the miR-199a-5p/FZD4 axis. *Cell Death Dis* (2020) 11(9):777. doi: 10.1038/s41419-020-02978-w
4. Santarelli A, Mascitti M, Lo Russo L, Sartini D, Troiano G, Emanuelli M, et al. Survivin-Based Treatment Strategies for Squamous Cell Carcinoma. *Int J Mol Sci* (2018) 19(4):971–95. doi: 10.3390/ijms19040971
5. Duan Q, Xu M, Wu M, Zhang X, Gan M, Jiang H. Long noncoding RNA UCA1 promotes cell growth, migration, and invasion by targeting miR-143-3p in oral squamous cell carcinoma. *Cancer Med* (2020) 9(9):3115–29. doi: 10.1002/cam4.2808
6. Ferre F, Colantoni A, Helmer-Citterich M. Revealing protein-lncRNA interaction. *Brief Bioinform* (2016) 17(1):106–16. doi: 10.1093/bib/bbv031
7. Qian X, Zhao J, Yeung PY, Zhang QC, Kwok CK. Revealing lncRNA Structures and Interactions by Sequencing-Based Approaches. *Trends Biochem Sci* (2019) 44(1):33–52. doi: 10.1016/j.tibs.2018.09.012
8. Xu J, Bai J, Zhang X, Lv Y, Gong Y, Liu L, et al. Zhang G *et al*: A comprehensive overview of lncRNA annotation resources. *Brief Bioinform* (2017) 18(2):236–49. doi: 10.1093/bib/bbw015
9. Ma Y, Zhang J, Wen L, Lin A. Membrane-lipid associated lncRNA: A new regulator in cancer signaling. *Cancer Lett* (2018) 419:27–9. doi: 10.1016/j.canlet.2018.01.008
10. Bhan A, Soleimani M, Mandal SS, Long Noncoding RNA. and Cancer: A New Paradigm. *Cancer Res* (2017) 77(15):3965–81. doi: 10.1158/0008-5472.CAN-16-2634
11. Chen LL: Linking Long Noncoding RNA Localization and Function. *Trends Biochem Sci* (2016) 41(9):761–72. doi: 10.1016/j.tibs.2016.07.003
12. Yang XZ, Cheng TT, He QJ, Lei ZY, Chi J, Tang Z, et al. LINC01133 as ceRNA inhibits gastric cancer progression by sponging miR-106a-3p to regulate APC expression and the Wnt/beta-catenin pathway. *Mol Cancer* (2018) 17(1):126. doi: 10.1186/s12943-018-0874-1
13. Fan CN, Ma L, Liu N. Systematic analysis of lncRNA-miRNA-mRNA competing endogenous RNA network identifies four-lncRNA signature as a prognostic biomarker for breast cancer. *J Transl Med* (2018) 16(1):264. doi: 10.1186/s12967-018-1640-2
14. Wang W, Lou W, Ding B, Yang B, Lu H, Kong Q, et al. A novel mRNA-miRNA-lncRNA competing endogenous RNA triple sub-network associated with prognosis of pancreatic cancer. *Aging (Albany NY)* (2019) 11(9):2610–27. doi: 10.18632/aging.101933
15. Gao H, Gong N, Ma Z, Miao X, Chen J, Cao Y, et al. LncRNA ZEB2-AS1 promotes pancreatic cancer cell growth and invasion through regulating the miR-204/HMGB1 axis. *Int J Biol Macromol* (2018) 116:545–51. doi: 10.1016/j.ijbiomac.2018.05.044
16. Wu K, Jiang Y, Zhou W, Zhang B, Li Y, Xie F, et al. Long Noncoding RNA RC3H2 Facilitates Cell Proliferation and Invasion by Targeting MicroRNA-101-3p/EZH2 Axis in OSCC. *Mol Ther Nucleic Acids* (2020) 20:97–110. doi: 10.1016/j.omtn.2020.02.006
17. Cao W, Liu JN, Liu Z, Wang X, Han ZG, Ji T, et al. A three-lncRNA signature derived from the Atlas of ncRNA in cancer (TANRIC) database predicts the survival of patients with head and neck squamous cell carcinoma. *Oral Oncol* (2017) 65:94–101. doi: 10.1016/j.oraloncology.2016.12.017
18. Liu Z, Zhou W, Lin C, Wang X, Zhang X, Zhang Y, et al. Dysregulation of FOXD2-AS1 promotes cell proliferation and migration and predicts poor prognosis in oral squamous cell carcinoma: a study based on TCGA data. *Aging (Albany NY)* (2020) 13(2):2379–96. doi: 10.18632/aging.202268
19. Dai D, Feng XD, Zhu WQ, Bao YN. LncRNA BLACAT1 regulates the viability, migration and invasion of oral squamous cell carcinoma cells by targeting miR-142-5p. *Eur Rev Med Pharmacol Sci* (2019) 23(23):10313–23. doi: 10.26355/eurrev_201912_19669
20. Liu L, Ning SB, Fu S, Mao Y, Xiao M, Guo B. Effects of lncRNA ANRIL on proliferation and apoptosis of oral squamous cell carcinoma cells by regulating TGF-beta/Smad pathway. *Eur Rev Med Pharmacol Sci* (2019) 23(14):6194–201. doi: 10.26355/eurrev_201907_18435
21. Ye J, Wu S, Pan S, Huang J, Ge L. Risk scoring based on expression of long noncoding RNAs can effectively predict survival in hepatocellular carcinoma patients with or without fibrosis. *Oncol Rep* (2020) 43(5):1451–66. doi: 10.3892/or.2020.7528
22. Acha-Sagredo A, Uko B, Pantazi P, Bediaga NG, Moschandrea C, Rainbow L, et al. Long non-coding RNA dysregulation is a frequent event in non-small cell lung carcinoma pathogenesis. *Br J Cancer* (2020) 122(7):1050–8. doi: 10.1038/s41416-020-0742-9
23. Goodall GJ, Wickramasinghe VO. RNA in cancer. *Nat Rev Cancer* (2020) 21(1):22–36. doi: 10.1038/s41568-020-00306-0
24. Xu G, Xu WY, Xiao Y, Jin B, Du SD, Mao YL, et al. The emerging roles of non-coding competing endogenous RNA in hepatocellular carcinoma. *Cancer Cell Int* (2020) 20:496. doi: 10.1186/s12935-020-01581-5

25. Bande M, Fernandez-Diaz D, Fernandez-Marta B, Rodriguez-Vidal C, Lago-Baameiro N, Silva-Rodriguez P, et al. The Role of Non-Coding RNAs in Uveal Melanoma. *Cancers (Basel)* (2020) 12(10):2944–66. doi: 10.3390/cancers12102944
26. Ahn YH, Kim JS. Long Non-Coding RNAs as Regulators of Interactions between Cancer-Associated Fibroblasts and Cancer Cells in the Tumor Microenvironment. *Int J Mol Sci* (2020) 21(20):7484–500. doi: 10.3390/ijms21207484
27. Wang Y, Zhou L, Lu J, Jiang B, Liu C, Guo J, et al. Research progress on long non-coding RNAs and their roles as potential biomarkers for diagnosis and prognosis in pancreatic cancer. *Cancer Cell Int* (2020) 20:457. doi: 10.1186/s12935-020-01550-y
28. Chan JJ, Tay Y. Noncoding RNA:RNA Regulatory Networks in Cancer. *Int J Mol Sci* (2018) 19(5):1310–36. doi: 10.3390/ijms19051310
29. Huang G, He X, Wei XL. lncRNA NEAT1 promotes cell proliferation and invasion by regulating miR365/RGS20 in oral squamous cell carcinoma. *Oncol Rep* (2018) 39(4):1948–56. doi: 10.3892/or.2018.6283
30. Zhang C, Bao C, Zhang X, Lin X, Pan D, Chen Y. Knockdown of lncRNA LEF1-AS1 inhibited the progression of oral squamous cell carcinoma (OSCC) via Hippo signaling pathway. *Cancer Biol Ther* (2019) 20(9):1213–22. doi: 10.1080/15384047.2019.1599671
31. Shao TR, Zheng ZN, Chen YC, Wu QQ, Huang GZ, Li F, et al. LncRNA AC007271.3 promotes cell proliferation, invasion, migration and inhibits cell apoptosis of OSCC via the Wnt/beta-catenin signaling pathway. *Life Sci* (2019) 239:117087. doi: 10.1016/j.lfs.2019.117087
32. Xu L, Hou TJ, Yang P. Mechanism of lncRNA FEZF1-AS1 in promoting the occurrence and development of oral squamous cell carcinoma through targeting miR-196a. *Eur Rev Med Pharmacol Sci* (2019) 23(15):6505–15. doi: 10.26355/eurrev_201908_18534
33. Zhang G, Li S, Lu J, Ge Y, Wang Q, Ma G, et al. LncRNA MT1JP functions as a ceRNA in regulating FBXW7 through competitively binding to miR-92a-3p in gastric cancer. *Mol Cancer* (2018) 17(1):87. doi: 10.1186/s12943-018-0829-6
34. She JK, Fu DN, Zhen D, Gong GH, Zhang B. LINC01087 is Highly Expressed in Breast Cancer and Regulates the Malignant Behavior of Cancer Cells Through miR-335-5p/Rock1. *Onco Targets Ther* (2020) 13:9771–83. doi: 10.2147/OTT.S255994
35. Ding X, Zhang J, Feng Z, Tang Q, Zhou X. MiR-137-3p Inhibits Colorectal Cancer Cell Migration by Regulating a KDM1A-Dependent Epithelial-Mesenchymal Transition. *Dig Dis Sci* (2020). doi: 10.1007/s10620-020-06518-6
36. Zang Y, Zhu J, Li Q, Tu J, Li X, Hu R, et al. miR-137-3p Modulates the Progression of Prostate Cancer by Regulating the JNK3/EZH2 Axis. *Onco Targets Ther* (2020) 13:7921–32. doi: 10.2147/OTT.S256161
37. Berry FB, Saleem RA, Walter MA. FOXC1 transcriptional regulation is mediated by N- and C-terminal activation domains and contains a phosphorylated transcriptional inhibitory domain. *J Biol Chem* (2002) 277 (12):10292–7. doi: 10.1074/jbc.M110266200
38. Sabapathi N, Sabarimurugan S, Madurantakam Royam M, Kumarasamy C, Xu X, Xu G, et al. Prognostic Significance of FOXC1 in Various Cancers: A Systematic Review and Meta-Analysis. *Mol Diagn Ther* (2019) 23(6):695–706. doi: 10.1007/s40291-019-00416-y
39. Yang Z, Jiang S, Cheng Y, Li T, Hu W, Ma Z, et al. FOXC1 in cancer development and therapy: deciphering its emerging and divergent roles. *Ther Adv Med Oncol* (2017) 9(12):797–816. doi: 10.1177/1758834017742576
40. Han B, Bhowmick N, Qu Y, Chung S, Giuliano AE, Cui X. FOXC1: an emerging marker and therapeutic target for cancer. *Oncogene* (2017) 36 (28):3957–63. doi: 10.1038/onc.2017.48
41. Ray PS, Wang J, Qu Y, Sim MS, Shamonki J, Bagaria SP, et al. FOXC1 is a potential prognostic biomarker with functional significance in basal-like breast cancer. *Cancer Res* (2010) 70(10):3870–6. doi: 10.1158/0008-5472.CAN-09-4120
42. Huang W, Chen Z, Zhang L, Tian D, Wang D, Fan D, et al. Interleukin-8 Induces Expression of FOXC1 to Promote Transactivation of CXCR1 and CCL2 in Hepatocellular Carcinoma Cell Lines and Formation of Metastases in Mice. *Gastroenterology* (2015) 149(4):1053–67.e1014. doi: 10.1053/j.gastro.2015.05.058
43. Kong XP, Yao J, Luo W, Feng FK, Ma JT, Ren YP, et al. The expression and functional role of a FOXC1 related mRNA-lncRNA pair in oral squamous cell carcinoma. *Mol Cell Biochem* (2014) 394(1-2):177–86. doi: 10.1007/s11010-014-2093-4
44. Liu Z, Xu S, Chu H, Lu Y, Yuan P, Zeng X. Silencing FOXC1 inhibits growth and migration of human oral squamous cell carcinoma cells. *Exp Ther Med* (2018) 16(4):3369–76. doi: 10.3892/etm.2018.6627

Conflict of Interest: The authors declare that the research was conducted in the absence of any commercial or financial relationships that could be construed as a potential conflict of interest.

Copyright © 2021 Che, Che, Zhang and Lu. This is an open-access article distributed under the terms of the Creative Commons Attribution License (CC BY). The use, distribution or reproduction in other forums is permitted, provided the original author(s) and the copyright owner(s) are credited and that the original publication in this journal is cited, in accordance with accepted academic practice. No use, distribution or reproduction is permitted which does not comply with these terms.

frontiers in Oncology

REVIEW
published: 29 April 2021
doi: 10.3389/fonc.2021.616202

Research Progress of circRNAs in Head and Neck Cancers

*Panchun Li[1], Kunjie Zhu[2], Yongzhen Mo[3], Xiangying Deng[3], Xianjie Jiang[3], Lei Shi[4], Can Guo[3], Wenling Zhang[3], Zhaoyang Zeng[3], Guiyuan Li[3], Wei Xiong[3], Shanshan Zhang[5] and Zhaojian Gong[1]**

[1] Department of Oral and Maxillofacial Surgery, The Second Xiangya Hospital, Central South University, Changsha, China, [2] Department of Head and Neck Surgery, The Affiliated Cancer Hospital of Xiangya School of Medicine, Central South University, Changsha, China, [3] NHC Key Laboratory of Carcinogenesis, Cancer Research Institute and School of Basic Medical Sciences, Central South University, Changsha, China, [4] Department of Pathology, The Second Xiangya Hospital, Central South University, Changsha, China, [5] Department of Stomatology, The Key Laboratory of Carcinogenesis and Cancer Invasion of the Chinese Ministry of Education, Xiangya Hospital, Central South University, Changsha, China

Circular RNAs (circRNAs) are a novel type of non-coding RNAs. Because of their characteristics of a closed loop structure, disease- and tissue-specificity, and high conservation and stability, circRNAs have the potential to be biomarkers for disease diagnosis. Head and neck cancers are one of the most common malignant tumors with high incidence rates globally. Affected patients are often diagnosed at the advanced stage with poor prognosis, owing to the concealment of anatomic sites. The characteristics, functions, and specific mechanisms of circRNAs in head and neck cancers are increasingly being discovered, and they have important clinical significance for the early diagnosis, treatment, and prognosis evaluation of patients with cancer. In this study, the generation, characteristics, and functions of circRNAs, along with their regulatory mechanisms in head and neck cancers have been summarized. We report that circRNAs interact with molecules such as transcription and growth factors to influence specific pathways involved in tumorigenesis. We conclude that circRNAs have an important role to play in the proliferation, invasion, metastasis, energy and substance metabolism, and treatment resistance in cancers.

Keywords: circRNA, non-coding RNA, biomarker, head and neck cancer, miRNA sponge

OPEN ACCESS

Edited by:
Ming Yann Lim,
Tan Tock Seng Hospital, Singapore

Reviewed by:
Yumin Wang,
Central South University, China
Ming Yu Lien,
China Medical University Hospital, Taiwan

***Correspondence:**
Zhaojian Gong
gongzhaojian4458@csu.edu.cn

Specialty section:
This article was submitted to Head and Neck Cancer, a section of the journal Frontiers in Oncology

Received: *11 October 2020*
Accepted: *07 April 2021*
Published: *29 April 2021*

Citation:
Li P, Zhu K, Mo Y, Deng X, Jiang X, Shi L, Guo C, Zhang W, Zeng Z, Li G, Xiong W, Zhang S and Gong Z (2021) Research Progress of circRNAs in Head and Neck Cancers. Front. Oncol. 11:616202. doi: 10.3389/fonc.2021.616202

INTRODUCTION

Head and neck cancers (HNC) are malignant tumors occurring in the oral cavity, hypopharynx, nasopharynx, and larynx. Depending on the location, HNC can be divided into hypopharyngeal squamous cell carcinoma (HSCC), oral squamous cell carcinoma (OSCC), laryngeal squamous cell carcinoma (LSCC), and nasopharyngeal carcinoma (NPC). With about 600,000 new patients per year, HNC ranks seventh in the incidence rate of malignant tumors worldwide (1). There are many ways to treat HNC, such as surgical treatment, radiotherapy, and chemotherapy. However, due to the lack of early diagnosis methods, patients with HNC are often diagnosed in the late stage. The 5-year overall survival rate of patients is 54.7%–65.9% and has not significantly improved over the years (2, 3). Therefore, it is necessary to elucidate the potential molecular regulation mechanism of HNC and to find possible molecular markers and targets. Circular RNAs (circRNAs) have the

potential to be HNC biomarkers (4). This review summarizes the research progress of circRNAs in HNC and seeks to understand the occurrence, development, and metastasis of HNC, and the possible molecular markers and therapeutic targets.

CLASSIFICATION AND FORMATION OF CIRCRNA

According to the composition of the source, circRNA can be divided into 4 categories: exonic circRNAs (ecircRNA), intronic circRNAs (ciRNAs), exon-intron circRNAs (EIciRNA), and tRNA intronic circRNA(tricRNA) (5). Although the formation mechanism of circRNAs is not completely clear, the current research results reveal two different formation modes (4).

Lariat-driven circularization: Lasso-driven cyclization is also known as the exon-skipping model (4), whereby non-adjacent exons of pre-mRNA are close to each other during transcription, causing part of exons to be skipped and eventually not appear on mature mRNA. By exon skipping, the exons and introns that are skipped form a lasso structure, and after the introns are removed, the ecircRNA is formed.

Intron-pairing-driven circularization model: There are reverse complementary sequences in flanking introns of pre-mRNA, which can assist pre-mRNA to form lasso structures through complementary base pairing. For example, inverted repeated Alu sequences can make introns move close to each other in space and form a hairpin structure, and finally form a lasso structure containing exons and introns. After the introns are removed, ecircRNA containing only the exons is formed (6). During this process, introns are sometimes retained in the circRNA resulting in formation of EIciRNA (7). However, the specific mechanisms of EIciRNA formation are not clear. In addition, when the two ends of an intron have complementary sequences, the cyclization of a single intron can occur and form ciRNA (8). The formation of ciRNA (mainly occurring in the nucleus) depends on a consensus motif containing a seven-nucleotide (nt) GU-rich element near the 5′ splice site and an 11 nt C-rich element close to the branchpoint site (8).

RNA-binding proteins (RBP) are also involved in the circRNA cyclization; they can bind to introns, assist the interaction of upstream and downstream introns, and promote circRNA cyclization (8). Quaking is an RBP, which can form dimers and bind to the binding site of flanking introns, and promote the production of circRNA (9).

CHARACTERISTICS OF CIRCRNA

Up to now, more than one million circRNAs have been found in human tissues by high-throughput sequencing technology. Because of their characteristics of a closed loop structure, disease- and tissue-specificity, and high conservation and stability, circRNAs have the potential to be biomarkers for disease diagnosis.

The highly stable structure of circRNAs is a closed loop, without 3′ and 5′ ends and a poly (A) tail. Therefore, compared with linear RNAs, circRNAs are not easily hydrolyzed by RNase. It is reported that the half-life of circRNAs can reach more than 48 h, while that of linear RNAs is only 10 h (10).

Types and expression abundance: circRNAs are numerous and widely available in human cells (11). Over 1,000,000 circRNAs have been found in human tissues using high-throughput sequencing technology (4). The expression abundance of different circRNAs varies greatly. The expression of some circRNAs is much higher than that of linear mRNAs, and even more than 10 times that of their linear isomers (4). However, most circRNAs have low expression abundance.

Conservation: Because of the stability of circRNAs, most of them are conserved in the evolution process of different species (12, 13). For example, 5¬–30% of circRNAs from human and mouse homologous genes are completely conserved (14). The conservation of circRNAs proves that they are not by-products of transcription but play an important role in life activities.

Expression specificity: The expression of circRNAs is tissue- and disease-specific (12). The expression of circRNAs in embryo, brain, heart, stomach, lung, liver, and other organs is very different. For example, in the brain, the amount of circRNAs is higher than that of other tissues (15, 16). Expression specificity indicates that circRNAs may play a specific function in disease development and may serve as a biomarker for disease diagnosis.

THE FUNCTIONS OF CIRCRNAs

miRNA sponging: CircRNAs are rich in miRNA binding sites, which can act as competitive endogenous RNA (ceRNA) to adsorb miRNA, thereby regulating the activity of downstream target genes of miRNA (11). For example, CDR1as contains more than 70 miR-7 binding sites, which act as ceRNA regulatory target genes in many biological processes (16–19).

Combination with protein: CircRNAs can directly bind to proteins and affect the function of downstream proteins. For example, circ-CCND1 can inhibit the binding of HuR to CCND1 mRNA by binding to HUR (20). In addition, circRNAs can act as a scaffold to make multiple proteins form complex and accelerate the reaction.

Translation of proteins: CircRNAs without 5'cap and 3'poly (A) tail lack internal ribosome entry site, so circRNAs are defined as non-coding RNA. However, studies have shown that circRNAs with open reading frames can translate functional proteins through internal ribosome entry site (IRES) or m6A-mediated translation initiation mechanisms (21). IRES can fold into a tRNA-like structure and mediate the binding of ribosomes to RNA. For example, circAKT3 in brain tumors can encode functional protein AKT3-174aa through IRES, and regulate PI3K/AKT signaling pathway (22). In addition, m6A modified circRNAs can directly bind to eukaryotic initiation factor 3, realizing a cap-independent translation initiation mode (23).

CIRCRNAs ARE WIDELY EXPRESSED AND SERVE AS MARKERS AND TARGETS IN HNC

With the development of high-throughput sequencing, microarray technology, and bioinformatics, it has been increasingly found that circRNAs have abnormal expression and potential functions in HNC (24–27). For example, in HSCC, Feng et al. analyzed the expression profiles of four paired HSCC tissues and found 173 differentially expressed circRNAs. The authors performed enrichment analysis on 40 circRNAs with the most significant differences and found that these circRNAs are most likely to play a role in the ErbB and Hippo signaling pathways (28). In addition, Cheng et al. constructed a circRNA expression profile of LSCC by performing second generation sequencing on five paired LSCC tissues. They detected 21,444 circRNAs, and further analysis using the Kyoto Encyclopedia of Genes and Genomes showed that peroxisome proliferator-activated receptor-, axon guidance, and Wnt signaling pathways are the key pathways of circRNAs in the occurrence of LSCC (26).

CircRNAs are not only widely expressed in HNC but are also correlated to the prognosis of patients. They have the potential as biomarkers for tumor diagnosis and prognosis (29–37). For example, the expression of hsa_circ_0092125 is related to the tumor size, tumor node metastasis stage, and lymph node metastasis in OSCC patients. Survival analysis shows that patients with a higher expression of hsa_circ_0092125 survive longer (29).

The receiver operating characteristic (ROC) curve and the area under curve (AUC) can be used as indices to evaluate the accuracy of biomarkers. The AUC values of hsa_circ_0072387, hsa_circ_001242, hsa_circ_009755, hsa_circ_0004491, hsa_circ_0036722, hsa_circ_0008309 and hsa_circ_0086414 are 0.746, 0.784, 0.782, 0.751, 0.838, 0.764 and 0.749, indicating the reliability of these molecules as biomarkers (30–37). Body fluids also contain a large amount of circRNAs. For example, Zhao et al. reported that the expression of hsa_circ_0001874 and hsa_circ_0001971 was upregulated in OSCC saliva, and the AUC value of the combination of these two molecules was 0.922 (33). Serum exosomes can reflect the pathological conditions of the body and are considered as a potential auxiliary diagnostic marker. CircRASSF2 is upregulated in the serum exosomes of patients with LSCC and can affect the progression of LSCC (38). Those circRNAs in body fluids can be easily detected and have a great clinical value and significance.

In addition, circRNAs have the potential to be therapeutic targets. Fucoidan is a component of the seaweed cell wall, which can inhibit OSCC growth, migration, and invasion. Zhang et al. reported that circFLNA is a fucoidan target. They found that fucoidan increased the expression of circFLNA in OSCC cell lines and affected the expression of key proteins related to growth, apoptosis, migration, and invasion (39).

CIRCRNAs ARE ASSOCIATED WITH PROLIFERATION IN HNC

The uncontrolled proliferation of tumor cells is the basis of tumorigenesis. Multiple circRNAs have been demonstrated to be involved in HNC development through the regulation of the proliferation process (**Figure 1**). CircATRNL1 (40), hsa_circ_0007059 (41), circRNA_002178 (42), hsa_circ_0046263 (43), hsa_circ_0005379 (44), circUHRF1 (45), circPVT1 (46, 47), circHIPK3 (48, 49), circRNA_0000140 (50), circRNA_100290 (51), circDOCK1 (52), hsa_circ_0055538 (53), circITCH (54), hsa_circRNA_101036 (55), circCCND1 (20), circMYLK (56), CDR1as (17, 57, 58), circPKD2 (59), circLARP4 (60), hsa_circ_0042666 (61), hsa_circRNA_100533 (62), circMDM2 (63), circ_0067934 (64), circRPMS1 (65), circ-ZNF609 (66, 67), hsa_circ_0072387 (68), circRASSF2 (38), hsa_circ_0023028 (69), circCTDP1 (70), circ_0008450 (71), circMATR3 (72), hsa_circ_0057481 (73), circ_0001742 (74), circ_0000218 (75), circ_0001971 (76), circCORO1C (77), hsa_circ_0109291 (78), hsa_circ_0036722 (34), hsa_circ_0002203 (79) and hsa_circ_0066755 (80) are associated with tumor proliferation (**Table 1**).

Tumor proliferation is regulated by multiple cellular pathways, such as the PI3K/Akt/mTOR signaling pathway, and some circRNAs are involved in the regulation of tumor proliferation through these pathways. In OSCC, circATRNL1 can induce apoptosis and cell cycle arrest through the PI3K/Akt/mTOR signaling pathway (40). CircATRNL1 is downregulated in OSCC and can target miR-23a-3p to eliminate the inhibition of phosphatase and tensin homolog (PTEN) by miR-23a-3p. PTEN is one of the most common tumor suppressor genes, which regulates cell apoptosis and cell cycle through PI3K/Akt/mTOR signaling pathway (82). PTEN can enhance BAD activity, inhibit caspase-3 activation, and induce apoptosis by antagonizing the PI3K/Akt/mTOR signaling pathway (83, 84). In addition, PTEN induces the expression of the cell cycle inhibitor p21, resulting in cell G0/G1 arrest (85). Therefore, circATRNL1 affects the progression of OSCC through the PTEN/PI3K/Akt/mTOR signaling pathway (40). Similarly, hsa_circ_0007059 and circRNA_002178 also affect OSCC growth through AKT signaling pathway (41, 42). The transforming growth factor β (TGF-β) signaling pathway can also regulate cell proliferation (86). Zhao et al. reported that circUHRF1 positively regulates the c-Myc oncogene by competitively binding miR-526b-5. In addition to activating the TGF-β1 pathway, c-Myc can also promote the expression of ESRP1. ESRP1 promotes the generation of circUHRF1 by combining with the flanking introns of circUHRF1, and finally forms a positive feedback regulation loop. CircUHRF1 eventually activates the TGF-β pathway to promote tumor growth (45).

Various growth factors such as insulin-like growth factors (IGFs) and their receptors are also involved in the growth of HNC (87, 88). When IGF-1R is combined with its ligand, it can

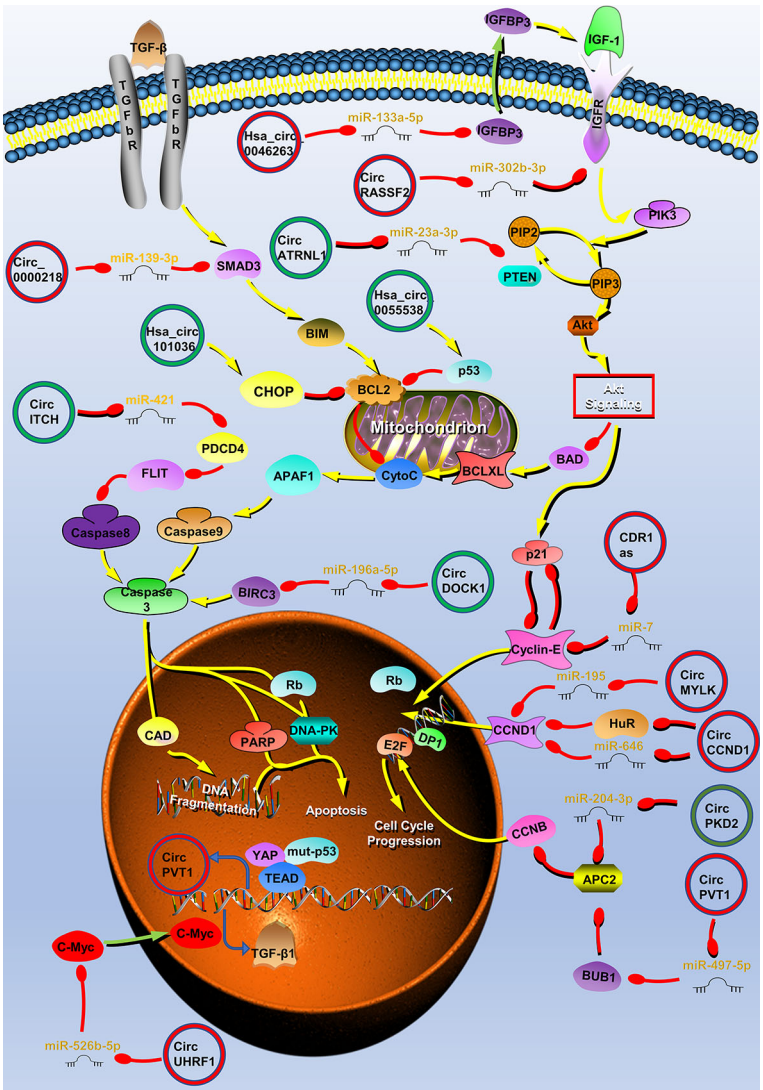

FIGURE 1 | Circular RNAs (circRNAs) associated with proliferation in head and neck cancers (HNC). CircRNAs that are known to regulate proliferation processes and their validated targets in HNC. CircRNAs regulate the growth of HNC by regulating PI3K/Akt/mTOR, insulin-like growth factor (IGFR), transforming growth factor (TGF) β, p53 signaling pathways, apoptosis, and cell cycle-related molecules. Red circle, upregulated circRNAs in HNC; green circle, downregulated circRNAs in HNC; yellow arrow, positive regulation; red arrow, negative regulation.

activate the PI3K/Akt/mTOR signaling pathway, and play an important role in the proliferation and apoptosis of tumor cells (88, 89). CircRASSF2 can adsorb miR-302b-3p as a competitive endogenous RNA (ceRNA), increase the expression of IGF-1R, and promote the progression of LSCC (38). IGFBP3 is the transporter of IGF-1, and it can extend the half-life of IGF-1 and promote the binding of IGF-1 and IGF-1R. IGFBP3 is the downstream target of miR-133a-5p and hsa_circ_0046263 acts as a sponge of miR-133a-5p in NPC and promotes IGFBP3 expression. Therefore, hsa_circ_0046263 can also activate the IGFR signaling pathway to promote LSCC (43).

P53 is the most commonly mutated gene in HNC; the mutation and deletion of this gene leads to the disorder of intracellular signal pathways and the uncontrolled growth of tumor cells (90). The expression of circPVT1 is upregulated in patients with HNC with a p53 mutation. Further research found that the complex formed by mutant p53, yes-associated protein, and TEA domain combined with the circPVT1 promoter to regulate circPVT1 expression at the transcriptional level. CircPVT1 acts as an oncogene and can regulate the expression of miR-497-5p and its downstream genes, which are involved in cell proliferation (46). In addition to the above mechanisms, circRNAs can regulate the proliferation of HNC through different mechanisms such as affecting apoptosis and cell cycle.

Resistance to cell death is one of the ten characteristics of tumors. Apoptosis is the main way to clear cells that are potentially harmful to the body, and almost all cancer cells have anti-apoptotic mechanisms (91). CircRNAs can directly

TABLE 1 | The proliferation-related circular RNAs in head and neck cancers.

CircRNAs	Primary sites of cancer	Expression change	Mechanism	Functions	References
CircPVT1	HNC	Up	mut-p53-YAP-TEAD complex/ CircPVT1/miR-497-5p/bub1	Promote proliferation	(46)
CircPVT1	OSCC	Up	miR–125b/STAT3	Promote proliferation	(47)
CDR1as	NPC	Up	miR-7-5p/E2F3	Promote proliferation	(57)
CDR1as	LSCC	Up	miR-7/CCNE1 and PIK3CD	Promote proliferation	(17)
CDR1as	OSCC	Up	miR-671-5p and AKT/ERK/mTOR	Promote proliferation	(58)
Circ-ZNF609	NPC	Up	microRNA-150-5p/Sp1	Promote proliferation	(66)
Circ-ZNF609	NPC	Up	miR-188/ELF2	Promote proliferation	(67)
CircHIPK3	NPC	Up	miR-4288/ELF3	Promote proliferation	(48)
CircHIPK3	OSCC	Up	miR-124	Promote proliferation	(49)
CircMDM2	OSCC	Up	miR-532-3p/HK2	Promote proliferation	(63)
Circ_0001971	OSCC	Up	miR-194 and miR-204	Promote proliferation	(33)
Circ_0001742	OSCC	Up	miR-431-5p/ATF3、miR-634/RAB1A	Promote proliferation	(74)
Circ_0000218	LSCC	Up	miR-139-3p/Smad3	Promote proliferation	(75)
CircUHRF1	OSCC	Up	miR-526b-5p/c-Myc/TGF-β1/ESRP1feedback loop	Promote proliferation	(45)
Hsa_circ_0072387	OSCC	Up	–	Promote proliferation	(68)
Hsa_circ_0109291	OSCC	Up	–	Promote proliferation	(78)
CircRPMS1	NPC	Up	miR-203, miR-31 and miR-451	Promote proliferation	(65)
CircCTDP1	NPC	Up	microRNA-320b/HOXA10/TGFβ2	Promote proliferation	(70)
Circ_0008450	NPC	Up	miR-577/CXCL9	Promote proliferation	(71)
Hsa_circ_0046263	NPC	Up	miR-133a-5p/IGFBP3	Promote proliferation	(43)
Circ_0067934	LSCC	Up	miR-1324	Promote proliferation	(64)
Circ-CCND1	LSCC	Up	HuR and miR-646/CCND1	Promote proliferation	(20)
CircMYLK	LSCC	Up	miR-195/CCND1	Promote proliferation	(56)
CircRASSF2	LSCC	Up	miR-302b-3p/IGF-1R	Promote proliferation	(38)
Hsa_circ_0023028	LSCC	Up	miR-194-5p	Promote proliferation	(69)
CircRNA_100290	LSCC	Up	miR-136-5p/RAP2C	Promote proliferation	(51)
Hsa_circRNA_101036	OSCC	Up	CHOP and Bcl-2	Promote proliferation	(55)
Hsa_circ_0057481	LSCC	Up	miR-200c/ZEB1	Promote proliferation	(73)
CircCORO1C	LSCC	Up	let-7c-5p/PBX3	Promote proliferation	(77)
CircMATR3	HSCC	Up	–	Promote proliferation	(72)
CircRNA_002178	OSCC	Up	Akt/mTOR	Promote proliferation	(42)
Hsa_circ_0066755	NPC	Up	miR-651	Promote proliferation	(80)
Hsa_circ_0005379	OSCC	Down	EGFR	Inhibit proliferation	(44)
CircATRNL1	OSCC	Down	miR-23a-3p/PTEN/PI3K/Akt	Inhibit proliferation	(40)
Hsa_CircRNA_100533	OSCC	Down	miR-933/GNAS	Inhibit proliferation	(62)
Hsa_circ_0007059	OSCC	Down	AKT/mTOR	Inhibit proliferation	(41)
Hsa_circ_0055538	OSCC	Down	p53/Bcl-2/caspase	Inhibit proliferation	(53)
Circ-PKD2	OSCC	Down	miR-204-3p/APC2	Inhibit proliferation	(81)
Circ-ITCH	OSCC	Down	miR-421/PDCD4	Inhibit proliferation	(54)
Hsa_circ_0002203	OSCC	Down	–	Inhibit proliferation	(79)
CircLARP4	NPC	Down	ROCK1	Inhibit proliferation	(60)
CircRNA_0000140	OSCC	Down	miR-31/LATS2	Inhibit proliferation	(50)
Hsa_circ_0042666	LSCC	Down	miR-223/TGFBR3	Inhibit proliferation	(61)
Hsa_circ_0036722	LSCC	Down	miR-1248/RHCG	Inhibit proliferation	(34)
circDOCK1	OSCC	Down	miR–196a–5p/BIRC3	Inhibit proliferation	(52)

regulate molecules related to the apoptosis pathway. For example, Wang et al. found that circDOCK1 can act as the ceRNA of miR–196a–5p to regulate the expression of Baculoviral IAP repeat-containing protein 3 (BIRC3). BIRC3 is an endogenous inhibitor of a cysteine proteolytic enzyme (caspase), which can prevent the conversion of the p19 subunit of caspase-3 to the p17 subunit and inhibit the activity of caspase 3 (92, 93). Wang et al. used tumor necrosis factor α to stimulate the OSCC cell line CAL-27 to establish an OSCC apoptosis model, establish an apoptosis-related circRNA profile through microarray sequencing, and screen the apoptosis-related molecule circDOCK1 (52). Finally, the authors found that circDOCK1 regulates the expression of BIRC3 by acting as a ceRNA and participates in the process of OSCC cell apoptosis (52). The p53 molecule is the central mediating switch of apoptosis and can downregulate the expression of Bcl-2 to promote cell apoptosis (94). Su et al. found that the overexpression of hsa_circ_0055538 in OSCC increased the expression levels of p53, Bax, and caspase 3, and decreased the expression of Bcl-2. These indicate that hsa_circ_0055538 may affect OSCC apoptosis through the p53/Bcl-2/caspase signaling pathway (53). Programmed cell death 4 (PDCD4) is a tumor suppressor gene related to apoptosis. Studies have found that PDCD4 inhibits FLIP-mediated tumor cell apoptosis. In addition, circ-ITCH can directly bind to miR-421 and block its inhibition of PDCD4 in OSCC and induce cell apoptosis (54). Endoplasmic reticulum stress is another way to induce apoptosis. The main signs of endoplasmic reticulum stress are the

upregulation of related proteins CHOP and Bcl-2 (95). After the overexpression of hsa_circRNA_101036 in OSCC, the levels of these proteins levels of CHOP and Bcl-2 can be found to increase, and hsa_circRNA_101036 may exert a tumor suppressor effect by regulating the endoplasmic reticulum stress in cancer cells (55). Autophagy is also a way of cell death, but under severe conditions, tumor cells can promote cell survival through autophagy. According to reports, CDR1as can promote autophagy and growth of OSCC by adsorbing miR-671-5p and promoting the AKT/ERK/mTOR signaling pathway (58).

The cell cycle is closely related to the growth of tumors (96). Abnormal expression of cyclin will result in abnormal cell growth. Cyclin D (CCND1) plays an important positive regulatory role in G1/S phase transition. Its high expression can shorten the G1 phase and accelerate the cell cycle. CircCCND1 is a circRNA derived from the CCND1 gene (97). CircCCND1 can block the inhibition of CCND1 by adsorbing miR-646. In addition, circ-CCND1 also inhibits the binding of the human antigen R to CCND1 mRNA by binding to HUR, thereby enhancing the stability of CCND1 mRNA (20). Briefly, circ-CCND1 regulates CCND1 in these two ways and regulates the transformation of cells from G1 to S phase. circMYLK also promotes CCND1 expression in LSCC by binding to miR-195 (56). Cyclin E1 also plays an important role in the G1/S phase transition (98). As the first reported circRNA molecule, CDR1as can inhibit miR-7, upregulate the expression of cyclin E1, and promote LSCC progression (17). Gao et al. found that the expression of circPKD2 was downregulated in the OSCC circRNA expression profile and experimentally proved that circPKD2 can induce cell cycle arrest. CircPKD2 also acts as a sponge for miR-204-3p, inhibiting miR-204-3p from acting on APC2 (59). APC2 can work with DNA-PKcs to inhibit the stability of CCND1 (81). Therefore, circ-PKD2 plays a tumor suppressor effect by promoting APC2.

CIRCRNAs ARE ASSOCIATED WITH INVASION AND METASTASIS IN HNC

Invasion and metastasis are the most essential biological features of malignant tumors and are also the direct cause of treatment failure in tumor patients. CircRNAs in HNC have important roles in HNC metastasis and invasion (**Figure 2**). Hsa_circ_0007059 (41), circUHRF1 (45), circHIPK3 (48), circRNA_0000140 (50), circRNA_100290 (51), hsa_circ_0055538 (53), CDR1as (17, 57), circPKD2 (59), circLARP4 (60), hsa_circ_0042666 (61), hsa_circRNA_100533 (62), circ_0067934 (64), circRPMS1 (65), circ-ZNF609 (66), hsa_circ_0072387 (68), circRASSF2 (38), hsa_circ_0023028 (69), circCTDP1 (70), circ_0008450 (71), circMATR3 (72), hsa_circ_0057481 (73), circ_0001742 (74), circCORO1C (77), hsa_circ_0004491 (37), circ_0001971 (33), circFLNA (99), hsa_circ_0001162 (100), circARHGAP12 (101), circCRIM1 (102), circEPSTI1 (103), hsa_circ_0109291 (78), circRNA_002178 (42), hsa_circ_0002203 (79) and hsa_circ_0066755 (80) are involved in the regulation of HNC invasion and metastasis (**Table 2**).

The PI3K/Akt/mTOR, IGF-1/IGF-1R, Hippo, P53, and TGFβ signaling pathways mentioned above also play a role in the regulation of HNC invasion and metastasis by circRNA (38, 40–42, 45, 50, 75, 104). For example, TGF-β can act on the transcription factors Snail, Twist, etc., and is a key factor in inducing epithelial mesenchymal transition (EMT) (105). EMT is an important biological process for malignant tumor cells derived from epithelial cells to acquire the ability of migration and invasion (105). As mentioned above, circUHRF1 competitively binds miR-526b-5 and positively regulates c-Myc, which activates the TGF-β1 pathway (45). Therefore, circUHRF1 can promote the EMT and invasion and metastasis of HNC by activating the TGF-β1 pathway.

ZEB1 is also an important factor which promotes tumor EMT (106). It can work with snail and slug to inhibit downstream adhesion molecules and promoter molecules, and ultimately induce EMT. Hsa_circ_0057481 can directly capture miR-200c, promote the expression of the ZEB1, and promote the invasion and metastasis of LSCC (73).

Matrix metalloproteinases (MMPs) can promote tumor invasion and metastasis by promoting the degradation of the extracellular matrix (107). Hsa_circ_0001162 is a circRNA derived from MMP9, which blocks the inhibitory effect of miR-149 on the 3′ end of MMP9 by adsorbing miR-149, and promotes the migration and invasion of OSCC (100). In addition, there is also an AU-rich element RBP 1 binding motif on MMP9 mRNA 3′-UTR, which does not overlap with the binding site of miR-149 on MMP9 3′-UTR. Therefore, hsa_circ_0001162 can also enhance the stability of MMP9 mRNA by antagonizing the attenuation of MMP9 mRNA induced by the AU-rich element RBP 1 in OSCC (100). Rap2c is a member of the RAS oncogene family and it is reported that it can increase the activity of MMP2. Highly-expressed circRNA_100290 promotes the migration of LSCC by blocking miR-136-5p inhibiting this protein (51).

The realization of tumor migration and invasion requires the rearrangement of intracellular cytoskeletal proteins. The protein encoded by the EZR gene is a component of the microvilli, acting as an intermediate product between the plasma membrane and the actin cytoskeleton, and can regulate cell adhesion and skeletal reorganization (108). Studies have found that circARHGAP12 can bind to the 3′-UTR of EZR mRNA and promote its stability (101). EZR can interact with TPM3 and RhoA to regulate cytoskeleton remodeling and promote NPC invasion and metastasis (101). Rock1 protein plays a key role in cell surface structure adhesion and cytoskeleton recombination (109). Pan et al. proved that ROCK1 is the direct target of circLARP4, which inhibits cell migration and invasion of NPC by regulating the kinase (60). FLNA can limit tumor migration by regulating the activation of integrins and the morphology and degradation of focal adhesions (110). CircFLNA can act as a miRNA sponge for miR-486-3p, thereby protecting FLNA from miR-486-3p-mediated silencing, and inhibiting the migration of LSCC cells (99).

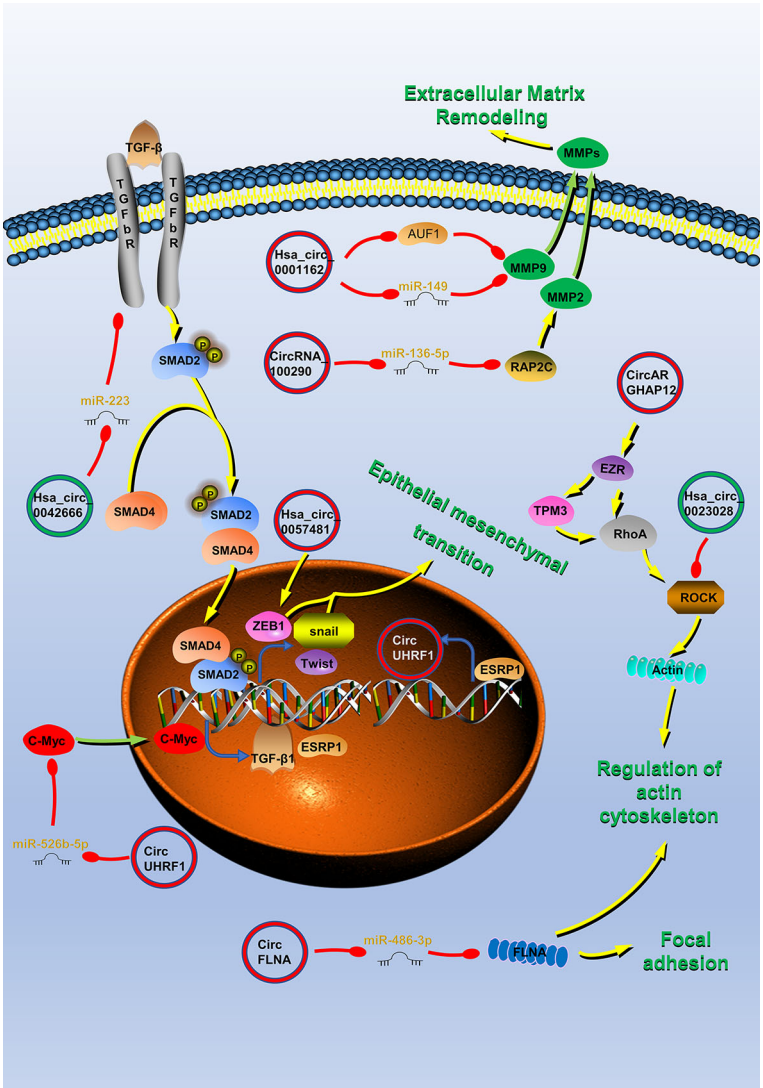

FIGURE 2 | Circular RNAs (circRNAs) associated with invasion and metastasis in head and neck cancers (HNC). CircRNAs that are known to regulate invasion and metastasis processes and their validated targets in HNC. CircRNAs regulate the cytoskeleton remodeling, local adhesion, extracellular matrix remodeling, and the epithelial–mesenchymal transition (EMT) of HNC by regulating invasion and metastasis-related molecules to promote tumor invasion and metastasis. Red circle, upregulated circRNAs in HNC; green circle, downregulated circRNAs in HNC; yellow arrow, positive regulation; red arrow, negative regulation.

CIRCRNAs ARE RELATED TO THE REGULATION OF TUMOR GLUCOSE METABOLISM IN HNC

The various biological characteristics of tumors are closely related to the metabolism of substances and energy. Tumor metabolism provides energy for the biological behavior of tumors, promotes tumor growth, metastasis, and other activities (111). CircRNAs such as circPVT1 (112), circ_0000140 (113), circRNA_100290 (114), CDR1as (57), circMDM2 (63), hsa_circ_0072387 (68) and circGDI2 (115) (**Table 3**) can also affect tumor growth through glucose metabolism (**Figure 3**).

Glucose transporter 1 (GLUT1) plays an important role in the glycolysis process by regulating glucose uptake (116). CircRNA_100290 can alleviate the inhibitory effect of miR-378a on GLUT1. Therefore, overexpression of circRNA_100290 can increase the glucose uptake rate of tumor cells and meet their high metabolic need (114). Hexokinase 2 (HK2) is also a key enzyme in the glycolysis pathway, and its expression in HNC cells is significantly increased (117). Studies have shown that circRNAs can regulate the HK2 gene, thereby affecting the glycolysis of HNC cells. For example, in OSCC, circPVT1 and circMDM2 upregulate HK2 expression by inhibiting miR-497-5p and miR-532-3p, respectively, thereby promoting glycolysis (63, 112).

TABLE 2 | The migration and invasion-related circular RNAs in head and neck cancers.

CircRNAs	Primary sites of cancer	Expression change	Mechanism	Functions	References
Circ_0001971	OSCC	Up	miR-194 and miR-204	Promote invasion and metastasis	(33)
Hsa_circ_0001162	OSCC	Up	AUF1 and miR-149/MMP9	Promote invasion and metastasis	(100)
CircUHRF1	OSCC	Up	miR-526b-5p/c-Myc/TGF-β1/ ESRP1feedback loop	Promote invasion and metastasis	(45)
CircEPSTI1	OSCC	Up	mir-942-5p/LTBP2	Promote invasion and metastasis	(103)
Circ_0001742	OSCC	Up	miR-431-5p/ATF3、miR-634/RAB1A	Promote invasion and metastasis	(74)
Hsa_circ_0072387	OSCC	Up	–	Promote invasion and metastasis	(68)
Hsa_circ_0109291	OSCC	Up	–	Promote invasion and metastasis	(78)
CircRPMS1	NPC	Up	miR-203, miR-31和miR-451	Promote invasion and metastasis	(65)
CircCRIM1	NPC	Up	miR-422a/FOXQ1	Promote invasion and metastasis	(102)
CircCORO1C	LSCC	Up	let-7c-5p/PBX3	Promote invasion and metastasis	(77)
CircHIPK3	NPC	Up	miR-4288/ELF3	Promote invasion and metastasis	(48)
Circ-ZNF609	NPC	Up	microRNA-150-5p/Sp1	Promote invasion and metastasis	(66)
CircCTDP1	NPC	Up	microRNA-320b/HOXA10/TGFβ2	Promote invasion and metastasis	(70)
Circ_0008450	NPC	Up	miR-577/CXCL9	Promote invasion and metastasis	(71)
CircARHGAP12	NPC	Up	EZR	Promote invasion and metastasis	(101)
Circ_0067934	LSCC	Up	miR-1324	Promote invasion and metastasis	(64)
CircFLNA	LSCC	Up	miR-486-3p/FLNA	Promote invasion and metastasis	(99)
CircRASSF2	LSCC	Up	miR-302b-3p/IGF-1R	Promote invasion and metastasis	(38)
CDR1as	LSCC	Up	miR-7/CCNE1 and PIK3CD	Promote invasion and metastasis	(17)
Hsa_circ_0023028	LSCC	Up	miR-194-5p	Promote invasion and metastasis	(69)
CircRNA_100290	LSCC	Up	miR-136-5p/RAP2C	Promote invasion and metastasis	(51)
Hsa_circ_0057481	LSCC	Up	miR-200c/ZEB1	Promote invasion and metastasis	(73)
CircMATR3	HSCC	Up	–	Promote invasion and metastasis	(72)
CircRNA_002178	OSCC	Up	Akt/mTOR	Promote invasion and metastasis	(42)
Hsa_circ_0066755	NPC	Up	miR-651	Promote invasion and metastasis	(80)
Hsa_circ_0004491	OSCC	Down	EMT related protein	Inhibit invasion and metastasis	(37)
circRNA_0000140	OSCC	Down	miR-31/LATS2	Inhibit proliferation	(50)
Hsa_circRNA_100533	OSCC	Down	miR-933/GNAS	Inhibit invasion and metastasis	(62)
Hsa_circ_0007059	OSCC	Down	AKT/mTOR	Inhibit invasion and metastasis	(41)
Hsa_circ_0055538	OSCC	Down	p53/Bcl-2/caspase	Inhibit invasion and metastasis	(53)
Circ-PKD2	OSCC	Down	miR-204-3p/APC2	Inhibit invasion and metastasis	(81)
Hsa_circ_0002203	OSCC	Down	–	Inhibit invasion and metastasis	(79)
CircLARP4	NPC	Down	ROCK1	Inhibit invasion and metastasis	(60)
Hsa_circ_0042666	LSCC	Down	miR-223/TGFBR3	Inhibit invasion and metastasis	(61)

CIRCRNAs ARE ASSOCIATED WITH RADIOCHEMOTHERAPY RESISTANCE IN HNC

Surgery combined with radiotherapy and chemotherapy is the main treatment for HNC, but many patients develop radiochemotherapy resistance. Therefore, exploring the molecular mechanisms of HNC radiochemotherapy resistance has important practical significance for further improving the therapeutic effect. Recently, several lines of evidence have suggested that circRNAs, such as circRNA_000543 (118), circRNA_0000285 (119), hsa_circRNA_001387 (120), circATRNL1 (40) circ_0001971 (33), hsa_circ_0109291 (78), circCRIM1 (102), hsa_circ_0028007 (121), hg_circ_0005033 (122) and hsa_circ_0005379 (44) (**Table 4**) are likely to play vital roles in radiochemotherapy resistance in HNC (**Figure 4**).

To find radiotherapy resistance-related circRNAs, Chen et al. performed high-throughput sequencing on radiotherapy-sensitive and -insensitive NPC tissues and found that the expression of circRNA_000543 was upregulated in radiotherapy-insensitive NPC, which may be a carcinogenic circRNA involved in radiotherapy resistance. Further studies have shown that miR-9 can bind to circRNA_000543, and a bioinformatics software predicts that miR-9 can bind to the 3′ UTR of the PDFGRB. Therefore, the author finally proved that circRNA_000543 is involved in radiation resistance of NPC by blocking inhibition of miR-9 to PDFGRB (77).

Radiotherapy is also one of the main treatment methods of OSCC. The resistance to radiation often leads to poor prognosis and tumor recurrence in patients with OSCC. As mentioned above, circATRNL1 in OSCC induces tumor apoptosis and cell cycle arrest through PTEN/PI3K/AKT. Therefore, circATRNL1

TABLE 3 | The glycolysis-related circular RNAs in head and neck cancers.

CircRNAs	Primary sites of cancer	Expression change	Mechanism	Functions	References
CircMDM2	OSCC	Up	miR-532-3p/HK2	Promote glycolysis	(63)
CircRNA_100290	OSCC	Up	miR-378a/GLUT1	Promote glycolysis	(114)
CircPVT1	OSCC	Up	miR-106a-5p/HK2	Promote glycolysis	(112)
hsa_circ_0072387	OSCC	Up	–	Promote glycolysis	(68)
CDR1as	NPC	Up	miR-7-5p/E2F3	Promote glucose metabolism	(57)
Circ_0000140	OSCC	Down	miR-182-3p/CDC73	Inhibit glycolysis	(113)
CircGDI2	OSCC	Down	miR-424-5p/SCAI	Inhibit glycolysis	(115)

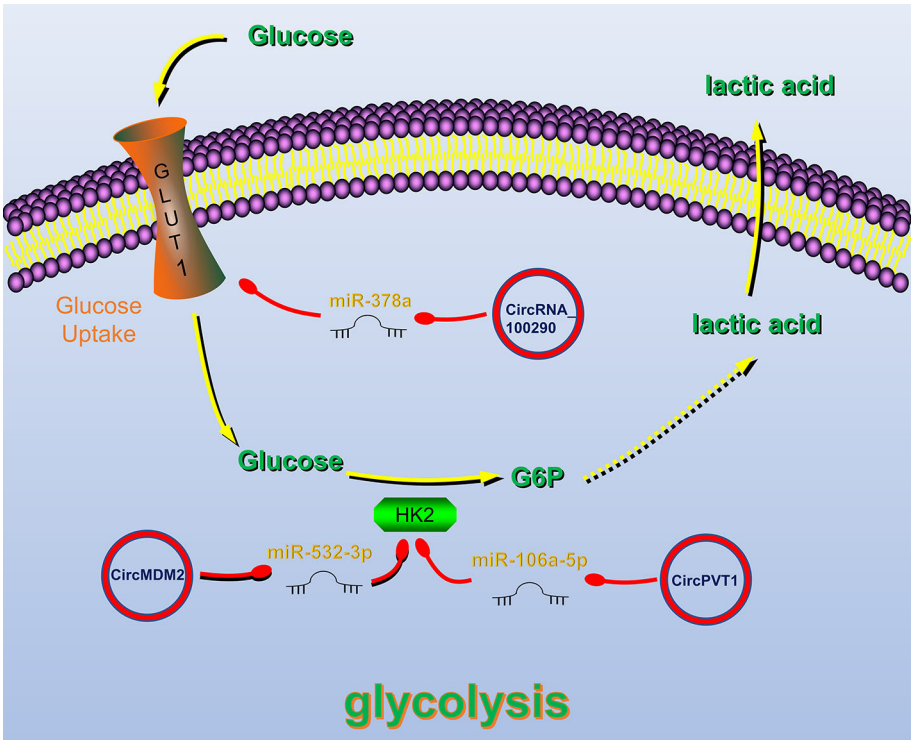

FIGURE 3 | Circular RNAs (circRNAs) related to regulation of tumor glucose metabolism in head and neck cancers (HNC). CircRNAs that are known to regulate glucose metabolism processes and their validated targets in HNC. CircRNAs regulate HNC glucose metabolism by regulating Glucose transporter 1 (GLUT1) and Hexokinase 2, key enzymes of glycolysis. Red circle, upregulated circRNAs in HNC; green circle, downregulated circRNAs in HNC; yellow arrow, positive regulation; red arrow, negative regulation.

also improves the radiosensitivity of OSCC cells through this mechanism (40).

Systemic induction chemotherapy is also an important auxiliary method. Recent studies reported that circCRIM1 can promote NPC metastasis and docetaxel chemoresistance. CircRNA sequencing was performed on high- and low-metastatic ability cell lines and obtained metastasis-related circRNA expression profiles, among which circCRIM1 was the most upregulated molecule. Further studies have shown that circCRIM1 upregulates FOXQ1 expression by acting as a miR-422a sponge, thereby promoting the process of NPC. The author performs enrichment analysis on the expression profile of NPC with high and low expression of FOXQ1 and found that chemoresistance was significantly rich. Furthermore, *in vitro* and *in vivo* experiments both showed that circCRIM1 promotes chemoresistance of NPC docetaxel (102). Cetuximab is an IgG1 monoclonal antibody with high affinity for the epidermal growth factor receptor (EGFR) (44). It can inhibit cell cycle progression and induce tumor cell apoptosis by specifically binding to the extracellular EGFR domain. Su et al. found that hsa_circ_0005379 can act on EGFR to significantly enhance the sensitivity of OSCC to cetuximab drugs (123). Functional experiments show that hsa_circ_0005379 can inhibit the growth and metastasis of OSCC, and increase the sensitivity to cetuximab drugs (123).

TABLE 4 | The radiochemotherapy resistance related circular RNAs in head and neck cancers.

CircRNAs	Primary sites of cancer	Expression change	Mechanism	Functions	References
Circ_0001971	OSCC	Up	miR-194 and miR-204	Inhibit chemotherapy sensitivity	(33)
Hsa_circ_0109291	OSCC	Up	–	Inhibit cisplatin sensitivity	(78)
CircRNA_000543	NPC	Up	miR-9/PDGFRB	Inhibit radiosensitivity	(118)
CircCRIM1	NPC	Up	miR-422a/FOXQ1	Inhibit docetaxel sensitivity	(102)
CircRNA_0000285	NPC	Up	–	Inhibit radiosensitivity	(119)
Hsa_circ_0028007	NPC	UP	–	Inhibit chemotherapy sensitivity	(121)
Hsa_circRNA_001387	NPC	UP	–	Inhibit radiosensitivity	(120)
Hg_circ_0005033	LSCC	Up	miR-4521	Inhibit chemotherapy sensitivity	(122)
Hsa_circ_0005379	OSCC	Down	EGFR	Promote cetuximab sensitivity	(44)
CircATRNL1	OSCC	Down	miR-23a3p/PTEN/PI3K/Akt	Promote radiosensitivity	(40)

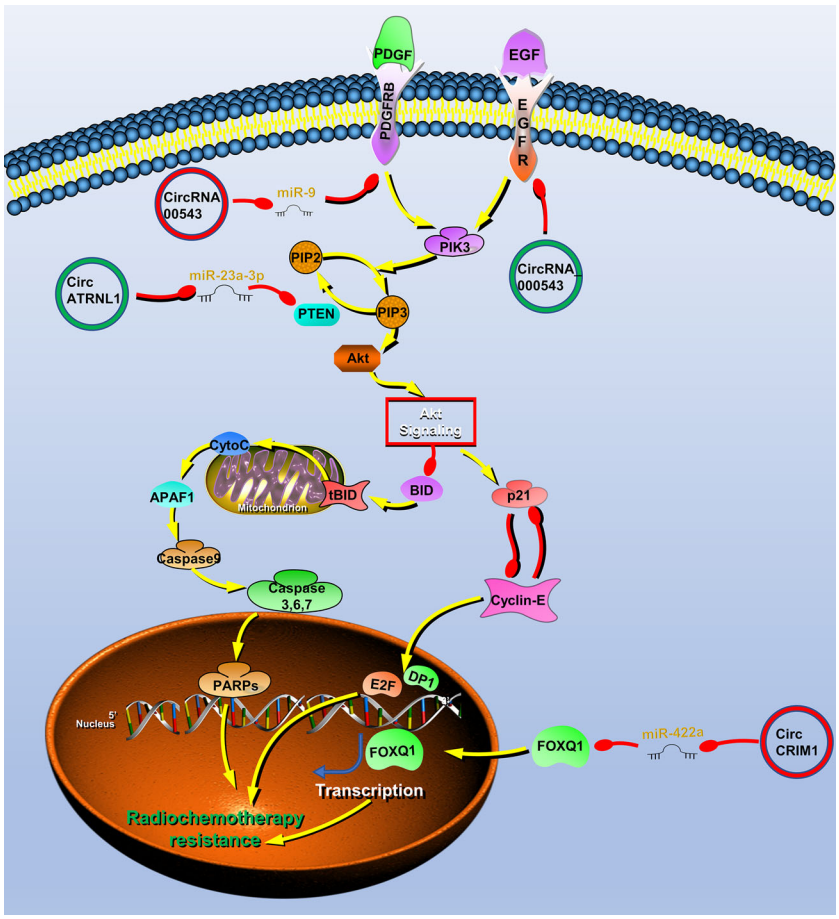

FIGURE 4 | Circular RNAs (circRNAs) associated with radiochemotherapy resistance in head and neck cancers (HNC). CircRNAs that are known to regulate radiochemotherapy resistance processes and their validated targets in HNC. CircRNAs regulate the radiochemotherapy resistance of HNC through phosphatase and tensin homolog (PTEN)/PI3K/Akt/mTOR, epidermal growth factor receptor (EGFR), platelet-derived growth factor receptor A (PDGFR) signaling pathway and transcription factor forkhead box Q1 (FOXQ1). Red circle, upregulated circRNAs in HNC; green circle, downregulated circRNAs in HNC; yellow arrow, positive regulation; red arrow, negative regulation.

CIRCRNAs PRODUCED BY VIRUSES IN HNC

EBV and HPV are closely related to the pathogenesis of HNC. It is reported that about 98% of NPC patients are EBV positive (124), and about 70% of oral and pharyngeal squamous cell carcinoma are associated with HPV infection (125). Therefore, it is very important to understand the carcinogenic mechanism of the virus. Studies have shown that DNA viruses can produce circRNA in host cells, and these circRNAs may also be a potential mechanism of virus carcinogenesis (126, 127).

EBV is the first virus reported to produce circRNAs in the host genome. Toptan et al. used circRNA Seq to sequence the EBV genome and found that the BART, LMP2, and BHLF1 genes in the EBV genome can produce circRNA (126). In another study, the authors developed a tool called circleVis and found more than 30 circRNAs produced by EBV (127). Among them, circRPMS1 encoded by BART has been verified by other studies, and it has been found that circRPMS1 can promote the proliferation and metastasis of NPC by acting as a miRNA sponge (65, 128). circLMP2A was also verified to exist in gastric cancer, but there is no research of circLMP2A in HNC (129). Similarly, HPV can also produce circRNAs. Wang et al. found that the E7 gene in HPV16 virus can produce circular RNA-CircE7 in cervical cancer, and CircE7 can be translated into protein and promote tumor growth (130). However, the study of circRNAs produced by HPV in HNC has not been reported yet. Whether the circRNA produced by these tumor viruses also functions in HNC is worthy of further investigation.

CONCLUSION AND FUTURE PROSPECTS

CircRNAs have a closed-loop structure, lack free ends, and are not easily hydrolyzed by RNase. In addition, because of their high conservation, stability, expression abundance, and tissue and disease expression-specificity, circRNAs have the potential to become diagnostic or predictive biomarkers for disease. Notably, circRNAs can be detected in body fluids including peripheral blood, saliva, and urine. For example, there are a large number of circRNAs in human saliva (131), and hsa_circ_0001874 and hsa_circ_0001971 in saliva may be used as biomarkers for OSCC (33). In addition, circRNAs are enriched in exosomes (132). CircRASSF2 has been reported to be upregulated in serum exosomes in patients with LSCC and affects the progression of LSCC (38). These characteristics make the detection of circRNAs in body fluids of patients with HNC possible and have great clinical value and significance.

In HNC, circRNAs can affect tumor development through various mechanisms such as cell cycle, apoptosis, EMT, metabolism, and radiochemotherapy resistance. However, circRNAs also affect tumor development in other ways, such as immune escape, cancer stem cells. Immune checkpoint refers to a group of factors involved in negative regulation in the immune system and is closely related to the immune escape mechanism (133). Recently, inhibitors of immune checkpoint PD1 or PDL1 have been approved for the treatment of advanced HNC (134), and have become a new trend in the clinical treatment of HNC. Studies have shown that circRNA can also play a regulatory role in immune checkpoints, and may be used as a target for immune checkpoint therapy. For example, Circ-CPA4 acts as miRNA sponge for let-7 to down-regulate the expression of PD-L1, thereby promoting lung cancer cell death (135), while circFGFR1 can induce lung cancer cell resistance to PD-1 drugs by inhibiting miR-381-3p (136). However, the study of circRNA related to PD1 or PD-L1 in HNC has not been reported yet, and further research is needed. In addition, anti-tumor research for innate immunity is also very necessary. It has recently been reported that exogenous circRNA can activate innate immunity and is an effective adjuvant for inducing anti-tumor immunity *in vivo* (137). Exogenous viruses associated with HNC can also produce circRNA, such as EBV and HPV (65, 138–140). Therefore, the role of exogenous circRNA encoded by EBV or HPV genome in innate immunity deserves further study. In short, more efforts are needed to promote the research on the immune regulation of circRNA in HNC.

Cancer stem cells have the ability to induce tumor self-renewal and high chemoradiotherapy resistance in tumors, so cancer stem cells are one of the main reasons for drug resistance and high recurrence in tumor treatment (141). In HNC, circRNA participates in chemoradiotherapy resistance by regulating cancer stem cells. For example, curcumin mediates the regulation of cancer stem cell-like cells through the circRNA network and enhances the radiosensitization effect of NPC (142). In addition, Hg19_circ_0005033 affects LSCC stem cells, promotes tumor occurrence and chemotherapy resistance (122). However, the research on cancer stem cells in HNC just emerges, and there may be other regulatory mechanisms for circRNA. The main pathways involved in cancer stem cells are Hedgehog, Wnt, PI3K/PTEN, Notch, and Hippo signaling pathways (143), and many circRNAs in HNC are related to some of these signaling pathways (28, 82). Therefore, circRNAs may also participate in the regulation of cancer stem cells through these signaling pathways. Studying the role of circRNA in cancer stem cells will contribute to the improvement of tumor diagnosis and treatment methods, and further research is needed.

As with some studies, this manuscript has also limitations. In HNC, circRNAs affect tumor progression mainly by acting as miRNA sponges or binding proteins. But a few circRNAs with open reading frames can translate functional proteins under the mediation of IRES or m6A. Since there is no report on circRNA encoded protein in HNC, this article does not cover it. However, it cannot be ruled out that the circRNA in HNC can also play a role through the mechanism of encoding protein. In addition, the current research on circRNA has just emerged, and more clinical research is needed before clinical application. However, with the development of research, circRNAs will play a more important role. The emergence of circRNAs has greatly enriched the regulatory network of non-coding RNAs in human diseases and which may be used as new disease biomarkers and therapeutic targets with great potential.

AUTHOR CONTRIBUTIONS

PL, KZ, YM, XD, XJ, LS, CG, WZ, ZZ, GL WX, SZ, and ZG conceived and wrote the manuscript. PL and ZG did the figure. All authors contributed to the article and approved the submitted version.

FUNDING

The present study was supported by the National Natural Science Foundation of China (grant nos. 81803025 and 81772901).

REFERENCES

1. Bray F, Ferlay J, Soerjomataram I, Siegel RL, Torre LA, Jemal A. Global Cancer Statistics 2018: GLOBOCAN Estimates of Incidence and Mortality Worldwide for 36 Cancers in 185 Countries. *CA Cancer J Clin* (2018) 68 (6):394–424. doi: 10.3322/caac.21492
2. Siegel R, Ward E, Brawley O, Jemal A. Cancer Statistics, 2011: The Impact of Eliminating Socioeconomic and Racial Disparities on Premature Cancer Deaths. *CA Cancer J Clin* (2011) 61(4):212–36. doi: 10.3322/caac.20121
3. Pulte D, Brenner H. Changes in Survival in Head and Neck Cancers in the Late 20th and Early 21st Century: A Period Analysis. *Oncolog* (2010) 15 (9):994–1001. doi: 10.1634/theoncologist.2009-0289
4. Jeck WR, Sorrentino JA, Wang K, Slevin MK, Burd CE, Liu J, et al. Circular RNAs are Abundant, Conserved, and Associated With ALU Repeats. *RNA (New York NY)* (2013) 19(2):141–57. doi: 10.1261/rna.035667.112
5. Qu S, Yang X, Li X, Wang J, Gao Y, Shang R, et al. Circular RNA: A New Star of Noncoding Rnas. *Cancer Lett* (2015) 365(2):141–8. doi: 10.1016/j.canlet.2015.06.003
6. Jeck WR, Sharpless NE. Detecting and Characterizing Circular Rnas. *Nat Biotechnol* (2014) 32(5):453–61. doi: 10.1038/nbt.2890
7. Li Z, Huang C, Bao C, Chen L, Lin M, Wang X, et al. Exon-Intron Circular RNAs Regulate Transcription in the Nucleus. *Nat Struct Mol Biol* (2015) 22 (3):256–64. doi: 10.1038/nsmb.2959
8. Zhang Y, Zhang XO, Chen T, Xiang JF, Yin QF, Xing YH, et al. Circular Intronic Long Noncoding Rnas. *Mol Cell* (2013) 51(6):792–806. doi: 10.1016/j.molcel.2013.08.017
9. Conn SJ, Pillman KA, Toubia J, Conn VM, Salmanidis M, Phillips CA, et al. The RNA Binding Protein Quaking Regulates Formation of Circrnas. *Cell* (2015) 160(6):1125–34. doi: 10.1016/j.cell.2015.02.014
10. Suzuki H, Zuo Y, Wang J, Zhang MQ, Malhotra A, Mayeda A. Characterization of RNase R-Digested Cellular RNA Source That Consists of Lariat and Circular RNAs From pre-mRNA Splicing. *Nucleic Acids Res* (2006) 34(8):e63. doi: 10.1093/nar/gkl151
11. Memczak S, Jens M, Elefsinioti A, Torti F, Krueger J, Rybak A, et al. Circular RNAs are a Large Class of Animal RNAs With Regulatory Potency. *Nature* (2013) 495(7441):333–8. doi: 10.1038/nature11928
12. Salzman J, Chen RE, Olsen MN, Wang PL, Brown PO. Cell-Type Specific Features of Circular RNA Expression. *PloS Genet* (2013) 9(9):e1003777. doi: 10.1371/journal.pgen.1003777
13. Wang PL, Bao Y, Yee MC, Barrett SP, Hogan GJ, Olsen MN, et al. Circular RNA is Expressed Across the Eukaryotic Tree of Life. *PloS One* (2014) 9(6): e90859. doi: 10.1371/journal.pone.0090859
14. Guo JU, Agarwal V, Guo H, Bartel DP. Expanded Identification and Characterization of Mammalian Circular Rnas. *Genome Biol* (2014) 15 (7):409. doi: 10.1186/s13059-014-0409-z
15. Xia S, Feng J, Lei L, Hu J, Xia L, Wang J, et al. Comprehensive Characterization of Tissue-Specific Circular RNAs in the Human and Mouse Genomes. *Brief Bioinform* (2017) 18(6):984–92. doi: 10.1093/bib/bbw081
16. Hansen TB, Jensen TI, Clausen BH, Bramsen JB, Finsen B, Damgaard CK, et al. Natural RNA Circles Function as Efficient microRNA Sponges. *Nature* (2013) 495(7441):384–8. doi: 10.1038/nature11993
17. Zhang J, Hu H, Zhao Y, Zhao Y. CDR1as is Overexpressed in Laryngeal Squamous Cell Carcinoma to Promote the Tumour's Progression Via miR-7 Signals. *Cell Prolif* (2018) 51(6):e12521. doi: 10.1111/cpr.12521
18. Huang H, Wei L, Qin T, Yang N, Li Z, Xu Z, et al. Circular RNA ciRS-7 Triggers the Migration and Invasion of Esophageal Squamous Cell Carcinoma Via miR-7/KLF4 and NF-κb Signals. *Cancer Biol Ther* (2019) 20(1):73–80. doi: 10.1080/15384047.2018.1507254
19. Liu L, Liu F-B, Huang M, Xie K, Xie Q-S, Liu C-H, et al. Circular RNA ciRS-7 Promotes the Proliferation and Metastasis of Pancreatic Cancer by Regulating Mir-7-Mediated EGFR/STAT3 Signaling Pathway. *Hepatobil Pancreat Dis Int* (2019) 18(6):580–6. doi: 10.1016/j.hbpd.2019.03.003
20. Zang Y, Li J, Wan B, Tai Y. circRNA circ-CCND1 Promotes the Proliferation of Laryngeal Squamous Cell Carcinoma Through Elevating CCND1 Expression Via Interacting With HuR and Mir-646. *J Cell Mol Med* (2020) 24(4):2423–33. doi: 10.1111/jcmm.14925
21. Wu P, Mo Y, Peng M, Tang T, Zhong Y, Deng X, et al. Emerging Role of Tumor-Related Functional Peptides Encoded by lncRNA and Circrna. *Mol Cancer* (2020) 19(1):22. doi: 10.1186/s12943-020-1147-3
22. Xia X, Li X, Li F, Wu X, Zhang M, Zhou H, et al. A Novel Tumor Suppressor Protein Encoded by Circular AKT3 RNA Inhibits Glioblastoma Tumorigenicity by Competing With Active Phosphoinositide-Dependent Kinase-1. *Mol Cancer* (2019) 18(1):131. doi: 10.1186/s12943-019-1056-5
23. Yang Y, Fan X, Mao M, Song X, Wu P, Zhang Y, et al. Extensive Translation of Circular RNAs Driven by N-Methyladenosine. *Cell Res* (2017) 27(5):626–41. doi: 10.1038/cr.2017.31
24. Qiu X, Ke X, Ma H, Han L, Chen Q, Zhang S, et al. Profiling and Bioinformatics Analyses Reveal Differential Expression of Circular RNA in Tongue Cancer Revealed by High-Throughput Sequencing. *J Cell Biochem* (2019) 120(3):4102–12. doi: 10.1002/jcb.27695
25. Yang J, Gong Y, Jiang Q, Liu L, Li S, Zhou Q, et al. Circular RNA Expression Profiles in Nasopharyngeal Carcinoma by Sequence Analysis. *Front Oncol* (2020) 10:601. doi: 10.3389/fonc.2020.00601
26. Lu C, Shi X, Wang AY, Tao Y, Wang Z, Huang C, et al. Rna-Seq Profiling of Circular RNAs in Human Laryngeal Squamous Cell Carcinomas. *Mol Cancer* (2018) 17(1):86. doi: 10.1186/s12943-018-0833-x
27. Cao S, Wei D, Li X, Zhou J, Li W, Qian Y, et al. Novel Circular RNA Expression Profiles Reflect Progression of Patients With Hypopharyngeal Squamous Cell Carcinoma. *Oncotarget* (2017) 8(28):45367–79. doi: 10.18632/oncotarget.17488
28. Feng C, Li Y, Lin Y, Cao X, Li D, Zhang H, et al. CircRNA-associated ceRNA Network Reveals ErbB and Hippo Signaling Pathways in Hypopharyngeal Cancer. *Int J Mol Med* (2019) 43(1):127–42. doi: 10.3892/ijmm.2018.3942
29. Gao L, Wang QB, Zhi Y, Ren WH, Li SM, Zhao CY, et al. Down-Regulation of Hsa_Circ_0092125 is Related to the Occurrence and Development of Oral Squamous Cell Carcinoma. *Int J Oral Maxillofac Surg* (2020) 49(3):292–7. doi: 10.1016/j.ijom.2019.07.014
30. Dou Z, Li S, Ren W, Wang Q, Liu J, Kong X, et al. Decreased Expression of Hsa_Circ_0072387 as a Valuable Predictor for Oral Squamous Cell Carcinoma. *Oral Dis* (2019) 25(5):1302–8. doi: 10.1111/odi.13094
31. Sun S, Li B, Wang Y, Li X, Wang P, Wang F, et al. Clinical Significance of the Decreased Expression of Hsa_Circ_001242 in Oral Squamous Cell Carcinoma. *Dis Markers* (2018) 2018:6514795. doi: 10.1155/2018/6514795
32. Wang Z, Tang J, Wang Y, Sun S, Chen Y, Shen Y, et al. Circular RNA Hsa_Circ_009755 Downregulation Correlates With Clinicopathology in Oral Squamous Cell Carcinoma. *OncoTargets Ther* (2019) 12:4025–31. doi: 10.2147/ott.S196618
33. Zhao SY, Wang J, Ouyang SB, Huang ZK, Liao L. Salivary Circular Rnas Hsa_Circ_0001874 and Hsa_Circ_0001971 as Novel Biomarkers for the Diagnosis of Oral Squamous Cell Carcinoma. *Cell Physiol Biochem* (2018) 47 (6):2511–21. doi: 10.1159/000491624
34. Guo Y, Huang Q, Zheng J, Hsueh CY, Yuan X, Heng Y, et al. Diagnostic Role of Dysregulated Circular RNA Hsa_Circ_0036722 in Laryngeal Squamous Cell Carcinoma. *Onco Targets Ther* (2020) 13:5709–19. doi: 10.2147/ott.S231076
35. Li B, Wang F, Li X, Sun S, Shen Y, Yang H. Hsa_Circ_0008309 May be a Potential Biomarker for Oral Squamous Cell Carcinoma. *Dis Markers* (2018) 2018:7496890. doi: 10.1155/2018/7496890
36. Li L, Zhang ZT. Hsa_Circ_0086414 Might be a Diagnostic Biomarker of Oral Squamous Cell Carcinoma. *Med Sci Monit* (2020) 26:e919383. doi: 10.12659/msm.919383
37. Li X, Zhang H, Wang Y, Sun S, Shen Y, Yang H. Silencing Circular RNA Hsa_Circ_0004491 Promotes Metastasis of Oral Squamous Cell Carcinoma. *Life Sci* (2019) 239:116883. doi: 10.1016/j.lfs.2019.116883
38. Tian L, Cao J, Jiao H, Zhang J, Ren X, Liu X, et al. CircRASSF2 Promotes Laryngeal Squamous Cell Carcinoma Progression by Regulating the miR-302b-3p/IGF-1R Axis. *Clin Sci (Lond)* (2019) 133(9):1053–66. doi: 10.1042/cs20190110
39. Zhang N, Gao L, Ren W, Li S, Zhang D, Song X, et al. Fucoidan Affects Oral Squamous Cell Carcinoma Cell Functions In Vitro by Regulating FLNA-derived Circular RNA. *Ann New York Acad Sci* (2020) 1462(1):65–78. doi: 10.1111/nyas.14190
40. Chen G, Li Y, He Y, Zeng B, Yi C, Wang C, et al. Upregulation of Circular Rna circATRNL1 to Sensitize Oral Squamous Cell Carcinoma to Irradiation. *Mol Ther Nucleic Acids* (2020) 19:961–73. doi: 10.1016/j.omtn.2019.12.031

41. Su W, Wang Y, Wang F, Zhang B, Zhang H, Shen Y, et al. Circular RNA Hsa_Circ_0007059 Indicates Prognosis and Influences Malignant Behavior Via AKT/mTOR in Oral Squamous Cell Carcinoma. *J Cell Physiol* (2019) 234(9):15156–66. doi: 10.1002/jcp.28156
42. Yang Y, Ci HS, Mao YL, Li JW, Zuo JH. CircRNA_002178 Promotes the Proliferation and Migration of Oral Squamous Cell Carcinoma Cells by Activating the Akt/mTOR Pathway. *Eur Rev Med Pharmacol Sci* (2020) 24 (11):6122–30. doi: 10.26355/eurrev_202006_21507
43. Yin L, Chen J, Ma C, Pei S, Du M, Zhang Y, et al. Hsa_Circ_0046263 Functions as a ceRNA to Promote Nasopharyngeal Carcinoma Progression by Upregulating IGFBP3. *Cell Death Dis* (2020) 11(7):562–. doi: 10.1038/s41419-020-02785-3
44. London M, Gallo E. Epidermal Growth Factor Receptor (EGFR) Involvement in Epithelial-Derived Cancers and its Current Antibody-Based Immunotherapies. *Cell Biol Int* (2020) 44:1267–82. doi: 10.1002/cbin.11340
45. Zhao W, Cui Y, Liu L, Qi X, Liu J, Ma S, et al. Splicing Factor Derived Circular RNA circUHRF1 Accelerates Oral Squamous Cell Carcinoma Tumorigenesis Via Feedback Loop. *Cell Death Differ* (2020) 27(3):919–33. doi: 10.1038/s41418-019-0423-5
46. Verduci L, Ferraiuolo M, Sacconi A, Ganci F, Vitale J, Colombo T, et al. The Oncogenic Role of circPVT1 in Head and Neck Squamous Cell Carcinoma is Mediated Through the Mutant p53/YAP/TEAD Transcription-Competent Complex. *Genome Biol* (2017) 18(1):237. doi: 10.1186/s13059-017-1368-y
47. He T, Li X, Xie D, Tian L. Overexpressed circPVT1 in Oral Squamous Cell Carcinoma Promotes Proliferation by Serving as a miRNA Sponge. *Mol Med Rep* (2019) 20(4):3509–18. doi: 10.3892/mmr.2019.10615
48. Ke Z, Xie F, Zheng C, Chen D. CircHIPK3 Promotes Proliferation and Invasion in Nasopharyngeal Carcinoma by Abrogating Mir-4288-Induced ELF3 Inhibition. *J Cell Physiol* (2019) 234(2):1699–706. doi: 10.1002/jcp.27041
49. Wang J, Zhao SY, Ouyang SS, Huang ZK, Luo Q, Liao L. [Circular RNA circHIPK3 Acts as the Sponge of microRNA-124 to Promote Human Oral Squamous Cell Carcinoma Cells Proliferation]. *Zhonghua Kou Qiang Yi Xue Za Zhi* (2018) 53(8):546–51. doi: 10.3760/cma.j.issn.1002-0098.2018.08.009
50. Peng Q-S, Cheng Y-N, Zhang W-B, Fan H, Mao Q-H, Xu P. circRNA_0000140 Suppresses Oral Squamous Cell Carcinoma Growth and Metastasis by Targeting miR-31 to Inhibit Hippo Signaling Pathway. *Cell Death Dis* (2020) 11(2):112. doi: 10.1038/s41419-020-2273-y
51. Wang Z, Huang C, Zhang A, Lu C, Liu L. Overexpression of circRNA_100290 Promotes the Progression of Laryngeal Squamous Cell Carcinoma Through the miR-136-5p/RAP2C Axis. *Biomed Pharmacother Biomed Pharmacother* (2020) 125:109874. doi: 10.1016/j.biopha.2020.109874
52. Wang L, Wei Y, Yan Y, Wang H, Yang J, Zheng Z, et al. CircDOCK1 Suppresses Cell Apoptosis Via Inhibition of miR−196a−5p by Targeting BIRC3 in OSCC. *Oncol Rep* (2018) 39(3):951–66. doi: 10.3892/or.2017.6174
53. Su W, Sun S, Wang F, Shen Y, Yang H. Circular RNA Hsa_Circ_0055538 Regulates the Malignant Biological Behavior of Oral Squamous Cell Carcinoma Through the p53/Bcl-2/caspase Signaling Pathway. *J Trans Med* (2019) 17(1):76. doi: 10.1186/s12967-019-1830-6
54. Hao C, Wangzhou K, Liang Z, Liu C, Wang L, Gong L, et al. Circular RNA Itch Suppresses Cell Proliferation But Induces Apoptosis in Oral Squamous Cell Carcinoma by Regulating miR-421/PDCD4 Axis. *Cancer Manag Res* (2020) 12:5651–8. doi: 10.2147/cmar.S258887
55. Deng W, Fu J, Wang T, Chen JX, Fu LB, Peng W. Hsa_circRNA_101036 Acts as Tumor-Suppressor in Oral Squamous Cell Carcinoma Cells Via Inducing Endoplasmic Reticulum Stress. *Eur Rev Med Pharmacol Sci* (2020) 24(11):6111–21. doi: 10.26355/eurrev_202006_21506
56. Duan X, Shen N, Chen J, Wang J, Zhu Q, Zhai Z. Circular RNA MYLK Serves as an Oncogene to Promote Cancer Progression Via Microrna-195/Cyclin D1 Axis in Laryngeal Squamous Cell Carcinoma. *Biosci Rep* (2019) 39 (9):BSR20190227 doi: 10.1042/bsr20190227
57. Zhong Q, Huang J, Wei J, Wu R. Circular RNA CDR1as Sponges miR-7-5p to Enhance E2F3 Stability and Promote the Growth of Nasopharyngeal Carcinoma. *Cancer Cell Int* (2019) 19:252. doi: 10.1186/s12935-019-0959-y
58. Gao L, Dou Z-C, Ren W-H, Li S-M, Liang X, Zhi K-Q. CircCDR1as Upregulates Autophagy Under Hypoxia to Promote Tumor Cell Survival Via AKT/ERK (½)/mTOR Signaling Pathways in Oral Squamous Cell Carcinomas. *Cell Death Dis* (2019) 10(10):745–. doi: 10.1038/s41419-019-1971-9
59. Gao L, Zhao C, Li S, Dou Z, Wang Q, Liu J, et al. circ-PKD2 Inhibits Carcinogenesis Via the miR-204-3p/APC2 Axis in Oral Squamous Cell Carcinoma. *Mol Carcinogenesis* (2019) 58(10):1783–94. doi: 10.1002/mc.23065
60. Pan JY, Bao XL, Zhu K. Circular RNA_LARP4 Inhibits Cell Proliferation and Invasion of Nasopharyngeal Carcinoma by Repressing ROCK1. *Eur Rev Med Pharmacol Sci* (2019) 23(22):9915–22. doi: 10.26355/eurrev_201911_19557
61. Wei Z, Chang K, Fan C. Hsa_Circ_0042666 Inhibits Proliferation and Invasion Via Regulating miR-223/TGFBR3 Axis in Laryngeal Squamous Cell Carcinoma. *Biomed Pharmacother* (2019) 119:109365. doi: 10.1016/j.biopha.2019.109365
62. Zhu X, Shao P, Tang Y, Shu M, Hu WW, Zhang Y. Hsa_circRNA_100533 Regulates GNAS by Sponging Hsa_miR_933 to Prevent Oral Squamous Cell Carcinoma. *J Cell Biochem* (2019) 120(11):19159–71. doi: 10.1002/jcb.29245
63. Zheng Z, Ma X, Li H. Circular RNA circMDM2 Accelerates the Glycolysis of Oral Squamous Cell Carcinoma by Targeting Mir-532-3p/HK2. *J Cell Mol Med* (2020) 24(13):7531–7. doi: 10.1111/jcmm.15380
64. Chu YL. Circ_0067934 Correlates With Poor Prognosis and Promotes Laryngeal Squamous Cell Cancer Progression by Sponging Mir-1324. *Eur Rev Med Pharmacol Sci* (2020) 24(8):4320–7. doi: 10.26355/eurrev_202004_21013
65. Liu Q, Shuai M, Xia Y. Knockdown of EBV-encoded circRNA circRPMS1 Suppresses Nasopharyngeal Carcinoma Cell Proliferation and Metastasis Through Sponging Multiple Mirnas. *Cancer Manag Res* (2019) 11:8023–31. doi: 10.2147/CMAR.S218967
66. Zhu L, Liu Y, Yang Y, Mao XM, Yin ZD. Circrna ZNF609 Promotes Growth and Metastasis of Nasopharyngeal Carcinoma by Competing With Microrna-150-5p. *Eur Rev Med Pharmacol Sci* (2019) 23(7):2817–26. doi: 10.26355/eurrev_201904_17558
67. Li M, Li Y, Yu M. Circrna ZNF609 Knockdown Suppresses Cell Growth Via Modulating Mir-188/ELF2 Axis in Nasopharyngeal Carcinoma. *Onco Targets Ther* (2020) 13:2399–409. doi: 10.2147/ott.S234230
68. Han L, Cheng J, Li A. Hsa_Circ_0072387 Suppresses Proliferation, Metastasis, and Glycolysis of Oral Squamous Cell Carcinoma Cells by Downregulating Mir-503-5p. *Cancer Biother Radiopharmaceut* (2020) 36 (1):84–94. doi: 10.1089/cbr.2019.3371
69. Chen X, Su X, Zhu C, Zhou J. Knockdown of Hsa_Circ_0023028 Inhibits Cell Proliferation, Migration, and Invasion in Laryngeal Cancer by Sponging Mir-194-5p. *Biosci Rep* (2019) 39(6):BSR20190177. doi: 10.1042/bsr20190177
70. Li H, You J, Xue H, Tan X, Chao C. CircCTDP1 Promotes Nasopharyngeal Carcinoma Progression Via a Microrna−320b/HOXA10/Tgfβ2 Pathway. *Int J Mol Med* (2020) 45(3):836–46. doi: 10.3892/ijmm.2020.4467
71. Wei H, Liu D, Sun J, Mao Y, Zhao L, Zhu W, et al. Circular RNA Circ_0008450 Upregulates CXCL9 Expression by Targeting miR-577 to Regulate Cell Proliferation and Invasion in Nasopharyngeal Carcinoma. *Exp Mol Pathol* (2019) 110:104288. doi: 10.1016/j.yexmp.2019.104288
72. Wang Z, Wei P, Wei D, Cao S, Liu H, Chen L, et al. Effect of Up-Regulation of circMATR3 on the Proliferation, Metastasis, Progression and Survival of Hypopharyngeal Carcinoma. *J Cell Mol Med* (2020) 24(8):4687–97. doi: 10.1111/jcmm.15134
73. Fu D, Huang Y, Gao M. Hsa_Circ_0057481 Promotes Laryngeal Cancer Proliferation and Migration by Modulating the miR-200c/ZEB1 Axis. *Int J Clin Exp Pathol* (2019) 12(11):4066–76.
74. Hu YT, Li XX, Zeng LW. Circ_0001742 Promotes Tongue Squamous Cell Carcinoma Progression Via miR-431-5p/ATF3 Axis. *Eur Rev Med Pharmacol Sci* (2019) 23(23):10300–12. doi: 10.26355/eurrev_201912_19668
75. Bai Y, Hou J, Wang X, Geng L, Jia X, Xiang L, et al. Circ_0000218 Plays a Carcinogenic Role in Laryngeal Cancer Through Regulating microRNA-139-3p/Smad3 Axis. *Pathol Res Pract* (2020) 216(9):153103. doi: 10.1016/j.prp.2020.153103
76. Tan X, Zhou C, Liang Y, Lai YF, Liang Y. Circ_0001971 Regulates Oral Squamous Cell Carcinoma Progression and Chemosensitivity by Targeting miR-194/miR-204 In Vitro and In Vivo. *Eur Rev Med Pharmacol Sci* (2020) 24(5):2470–81. doi: 10.26355/eurrev_202003_20515
77. Wu Y, Zhang Y, Zheng X, Dai F, Lu Y, Dai L, et al. Circular RNA circCORO1C Promotes Laryngeal Squamous Cell Carcinoma Progression by Modulating the let-7c-5p/PBX3 Axis. *Mol Cancer* (2020) 19(1):99. doi: 10.1186/s12943-020-01215-4

78. Ouyang SB, Wang J, Zhao SY, Zhang XH, Liao L. CircRNA_0109291 Regulates Cell Growth and Migration in Oral Squamous Cell Carcinoma and its Clinical Significance. *Iran J Basic Med Sci* (2018) 21(11):1186–91. doi: 10.22038/ijbms.2018.30347.7313
79. Su W, Wang YF, Wang F, Yang HJ, Yang HY. [Effect of Circular RNA Hsa_Circ_0002203 on the Proliferation, Migration, Invasion, and Apoptosis of Oral Squamous Cell Carcinoma Cells]. *Hua Xi Kou Qiang Yi Xue Za Zhi* (2019) 37(5):509–15. doi: 10.7518/hxkq.2019.05.011
80. Wang J, Kong J, Nie Z, Chen D, Qiang J, Gao W, et al. Circular RNA Hsa_Circ_0066755 as an Oncogene Via Sponging miR-651 and as a Promising Diagnostic Biomarker for Nasopharyngeal Carcinoma. *Int J Med Sci* (2020) 17(11):1499–507. doi: 10.7150/ijms.47024
81. Shang ZF, Tan W, Liu XD, Yu L, Li B, Li M, et al. DNA-Pkcs Negatively Regulates Cyclin B1 Protein Stability Through Facilitating its Ubiquitination Mediated by Cdh1-APC/C Pathway. *Int J Biol Sci* (2015) 11(9):1026–35. doi: 10.7150/ijbs.12443
82. Haddadi N, Lin Y, Travis G, Simpson AM, Nassif NT, McGowan EM. Pten/Ptenp1: 'Regulating the Regulator of RTK-dependent PI3K/Akt Signalling', New Targets for Cancer Therapy. *Mol Cancer* (2018) 17(1):37. doi: 10.1186/s12943-018-0803-3
83. Zhu Y, Tang H, Zhang L, Gong L, Wu G, Ni J, et al. Suppression of miR-21-3p Enhances TRAIL-mediated Apoptosis in Liver Cancer Stem Cells by Suppressing the PI3K/Akt/Bad Cascade Via Regulating PTEN. *Cancer Manag Res* (2019) 11:955–68. doi: 10.2147/cmar.S183328
84. She Q-B, Solit DB, Ye Q, O'Reilly KE, Lobo J, Rosen N. The BAD Protein Integrates Survival Signaling by EGFR/MAPK and PI3K/Akt Kinase Pathways in PTEN-deficient Tumor Cells. *Cancer Cell* (2005) 8(4):287–97. doi: 10.1016/j.ccr.2005.09.006
85. Choi HJ, Chung TW, Kang SK, Lee YC, Ko JH, Kim JG, et al. Ganglioside GM3 Modulates Tumor Suppressor PTEN-mediated Cell Cycle Progression–Transcriptional Induction of p21(WAF1) and p27(kip1) by Inhibition of PI-3K/AKT Pathway. *Glycobiology* (2006) 16(7):573–83. doi: 10.1093/glycob/cwj105
86. Zhang L, Zhou F, ten Dijke P. Signaling Interplay Between Transforming Growth Factor-β Receptor and PI3K/AKT Pathways in Cancer. *Trends Biochem Sci* (2013) 38(12):612–20. doi: 10.1016/j.tibs.2013.10.001
87. Vlasova-St Louis I, Bohjanen PR. Post-Transcriptional Regulation of Cytokine and Growth Factor Signaling in Cancer. *Cytokine Growth Factor Rev* (2017) 33:83–93. doi: 10.1016/j.cytogfr.2016.11.004
88. Kasprzak A, Kwasniewski W, Adamek A, Gozdzicka-Jozefiak A. Insulin-Like Growth Factor (IGF) Axis in Cancerogenesis. *Mutat Res Rev Mutat Res* (2017) 772:78–104. doi: 10.1016/j.mrrev.2016.08.007
89. Galvan V, Logvinova A, Sperandio S, Ichijo H, Bredesen DE. Type 1 Insulin-Like Growth Factor Receptor (IGF-IR) Signaling Inhibits Apoptosis Signal-Regulating Kinase 1 (ASK1). *J Biol Chem* (2003) 278(15):13325–32. doi: 10.1074/jbc.M211398200
90. Sarig R, Rivlin N, Brosh R, Bornstein C, Kamer I, Ezra O, et al. Mutant p53 Facilitates Somatic Cell Reprogramming and Augments the Malignant Potential of Reprogrammed Cells. *J Exp Med* (2010) 207(10):2127–40. doi: 10.1084/jem.20100797
91. Gudipaty SA, Conner CM, Rosenblatt J, Montell DJ. Unconventional Ways to Live and Die: Cell Death and Survival in Development, Homeostasis, and Disease. *Annu Rev Cell Dev Biol* (2018) 34:311–32. doi: 10.1146/annurev-cellbio-100616-060748
92. Pocsfalvi G, Stanly C, Fiume I, Vékey K. Chromatography and its Hyphenation to Mass Spectrometry for Extracellular Vesicle Analysis. *J Chromatogr A* (2016) 1439:26–41. doi: 10.1016/j.chroma.2016.01.017
93. Kavanagh E, Rodhe J, Burguillos MA, Venero JL, Joseph B. Regulation of Caspase-3 Processing by cIAP2 Controls the Switch Between Pro-Inflammatory Activation and Cell Death in Microglia. *Cell Death Dis* (2014) 5(12):e1565. doi: 10.1038/cddis.2014.514
94. Aubrey BJ, Kelly GL, Janic A, Herold MJ, Strasser A. How Does p53 Induce Apoptosis and How Does This Relate to p53-mediated Tumour Suppression? *Cell Death Differ* (2018) 25(1):104–13. doi: 10.1038/cdd.2017.169
95. Iurlaro R, Muñoz-Pinedo C. Cell Death Induced by Endoplasmic Reticulum Stress. *FEBS J* (2016) 283(14):2640–52. doi: 10.1111/febs.13598
96. Diaz-Moralli S, Tarrado-Castellarnau M, Miranda A, Cascante M. Targeting Cell Cycle Regulation in Cancer Therapy. *Pharmacol Ther* (2013) 138(2):255–71. doi: 10.1016/j.pharmthera.2013.01.011
97. Gao X, Leone GW, Wang H. Cyclin D-CDK4/6 Functions in Cancer. *Adv Cancer Res* (2020) 148:147–69. doi: 10.1016/bs.acr.2020.02.002
98. Caruso JA, Duong MT, Carey JPW, Hunt KK, Keyomarsi K. Low-Molecular-Weight Cyclin E in Human Cancer: Cellular Consequences and Opportunities for Targeted Therapies. *Cancer Res* (2018) 78(19):5481–91. doi: 10.1158/0008-5472.Can-18-1235
99. Wang JX, Liu Y, Jia XJ, Liu SX, Dong JH, Ren XM, et al. Upregulation of circFLNA Contributes to Laryngeal Squamous Cell Carcinoma Migration by circFLNA-miR-486-3p-FLNA Axis. *Cancer Cell Int* (2019) 19:196. doi: 10.1186/s12935-019-0924-9
100. Xia B, Hong T, He X, Hu X, Gao Y. A Circular RNA Derived From MMP9 Facilitates Oral Squamous Cell Carcinoma Metastasis Through Regulation of MMP9 mRNA Stability. *Cell Transplant* (2019) 28(12):1614–23. doi: 10.1177/0963689719875409
101. Fan C, Qu H, Xiong F, Tang Y, Tang T, Zhang L, et al. CircARHGAP12 Promotes Nasopharyngeal Carcinoma Migration and Invasion Via Ezrin-Mediated Cytoskeletal Remodeling. *Cancer Lett* (2021) 496:41–56. doi: 10.1016/j.canlet.2020.09.006
102. Hong X, Liu N, Liang Y, He Q, Yang X, Lei Y, et al. Circular RNA CRIM1 Functions as a ceRNA to Promote Nasopharyngeal Carcinoma Metastasis and Docetaxel Chemoresistance Through Upregulating FOXQ1. *Mol Cancer* (2020) 19(1):33. doi: 10.1186/s12943-020-01149-x
103. Wang J, Jiang C, Li N, Wang F, Xu Y, Shen Z, et al. The circEPSTI1/mir-942-5p/LTBP2 Axis Regulates the Progression of OSCC in the Background of OSF Via EMT and the PI3K/Akt/mTOR Pathway. *Cell Death Dis* (2020) 11(8):682. doi: 10.1038/s41419-020-02851-w
104. Qin JB, Chang W, Yuan GH, Huang L, Qiu ZF. Circular RNA Hsa_Circ_0000285 Acts as an Oncogene in Laryngocarcinoma by Inducing Wnt/β-Catenin Signaling Pathway. *Eur Rev Med Pharmacol Sci* (2019) 23(24):10803–9. doi: 10.26355/eurrev_201912_19783
105. Inan S, Hayran M. Cell Signaling Pathways Related to Epithelial Mesenchymal Transition in Cancer Metastasis. *Crit Rev Oncog* (2019) 24(1):47–54. doi: 10.1615/CritRevOncog.2018029509
106. Wu HT, Zhong HT, Li GW, Shen JX, Ye QQ, Zhang ML, et al. Oncogenic Functions of the EMT-related Transcription Factor ZEB1 in Breast Cancer. *J Transl Med* (2020) 18(1):51. doi: 10.1186/s12967-020-02240-z
107. Conlon GA, Murray GI. Recent Advances in Understanding the Roles of Matrix Metalloproteinases in Tumour Invasion and Metastasis. *J Pathol* (2019) 247(5):629–40. doi: 10.1002/path.5225
108. Zhan XH, Jiao JW, Zhang HF, Xu XE, He JZ, Li RL, et al. Loxl2 Upregulates Phosphorylation of Ezrin to Promote Cytoskeletal Reorganization and Tumor Cell Invasion. *Cancer Res* (2019) 79(19):4951–64. doi: 10.1158/0008-5472.Can-19-0860
109. Yuan J, Chen L, Xiao J, Qi XK, Zhang J, Li X, et al. SHROOM2 Inhibits Tumor Metastasis Through RhoA-ROCK Pathway-Dependent and -Independent Mechanisms in Nasopharyngeal Carcinoma. *Cell Death Dis* (2019) 10(2):58. doi: 10.1038/s41419-019-1325-7
110. Xu Y, Bismar TA, Su J, Xu B, Kristiansen G, Varga Z, et al. Filamin A Regulates Focal Adhesion Disassembly and Suppresses Breast Cancer Cell Migration and Invasion. *J Exp Med* (2010) 207(11):2421–37. doi: 10.1084/jem.20100433
111. Boroughs LK, DeBerardinis RJ. Metabolic Pathways Promoting Cancer Cell Survival and Growth. *Nat Cell Biol* (2015) 17(4):351–9. doi: 10.1038/ncb3124
112. Zhu X, Du J, Gu Z. Circ-PVT1/miR-106a-5p/HK2 Axis Regulates Cell Growth, Metastasis and Glycolytic Metabolism of Oral Squamous Cell Carcinoma. *Mol Cell Biochem* (2020) 474(1–2):147–58. doi: 10.1007/s11010-020-03840-5
113. Guo J, Su Y, Zhang M. Circ_0000140 Restrains the Proliferation, Metastasis and Glycolysis Metabolism of Oral Squamous Cell Carcinoma Through Upregulating CDC73 Via Sponging Mir-182-5p. *Cancer Cell Int* (2020) 20:407. doi: 10.1186/s12935-020-01501-7
114. Chen X, Yu J, Tian H, Shan Z, Liu W, Pan Z, et al. Circle RNA Hsa_circRNA_100290 Serves as a ceRNA for miR-378a to Regulate Oral Squamous Cell Carcinoma Cells Growth Via Glucose Transporter-1 (GLUT1) and Glycolysis. *J Cell Physiol* (2019) 234(11):19130–40. doi: 10.1002/jcp.28692

115. Zhang Y, Tang K, Chen L, Du M, Qu Z. Exosomal CircGDI2 Suppresses Oral Squamous Cell Carcinoma Progression Through the Regulation of MiR-424-5p/SCAI Axis. *Cancer Manag Res* (2020) 12:7501–14. doi: 10.2147/cmar.S255687
116. Ma L, Zong X. Metabolic Symbiosis in Chemoresistance: Refocusing the Role of Aerobic Glycolysis. *Front Oncol* (2020) 10:5. doi: 10.3389/fonc.2020.00005
117. Li WC, Huang CH, Hsieh YT, Chen TY, Cheng LH, Chen CY, et al. Regulatory Role of Hexokinase 2 in Modulating Head and Neck Tumorigenesis. *Front Oncol* (2020) 10:176. doi: 10.3389/fonc.2020.00176
118. Chen L, Zhou H, Guan Z. CircRNA_000543 Knockdown Sensitizes Nasopharyngeal Carcinoma to Irradiation by Targeting miR-9/platelet-derived Growth Factor Receptor B Axis. *Biochem Biophys Res Commun* (2019) 512(4):786–92. doi: 10.1016/j.bbrc.2019.03.126
119. Shuai M, Hong J, Huang D, Zhang X, Tian Y. Upregulation of circRNA_0000285 Serves as a Prognostic Biomarker for Nasopharyngeal Carcinoma and is Involved in Radiosensitivity. *Oncol Lett* (2018) 16 (5):6495–501. doi: 10.3892/ol.2018.9471
120. Shuai M, Huang L. High Expression of Hsa_circRNA_001387 in Nasopharyngeal Carcinoma and the Effect on Efficacy of Radiotherapy. *Onco Targets Ther* (2020) 13:3965–73. doi: 10.2147/ott.S249202
121. Qiongna D, Jiafeng Z, Yalin H, Ping H, Chuan Z, Xiaojie J, et al. Implication of Hsa_Circ_0028007 in Reinforcing Migration, Invasion, and Chemo-Tolerance of Nasopharyngeal Carcinoma Cells. *J Clin Lab Anal* (2020) 34 (9):e23409. doi: 10.1002/jcla.23409
122. Wu Y, Zhang Y, Niu M, Shi Y, Liu H, Yang D, et al. Whole-Transcriptome Analysis of CD133+CD144+ Cancer Stem Cells Derived From Human Laryngeal Squamous Cell Carcinoma Cells. *Cell Physiol Biochem* (2018) 47 (4):1696–710. doi: 10.1159/000490992
123. Su W, Wang Y, Wang F, Sun S, Li M, Shen Y, et al. Hsa_Circ_0005379 Regulates Malignant Behavior of Oral Squamous Cell Carcinoma Through the EGFR Pathway. *BMC Cancer* (2019) 19(1):400. doi: 10.1186/s12885-019-5593-5
124. Tsao SW, Tsang CM, To KF, Lo KW. The Role of Epstein-Barr Virus in Epithelial Malignancies. *J Pathol* (2015) 235(2):323–33. doi: 10.1002/path.4448
125. Westra WH. The Changing Face of Head and Neck Cancer in the 21st Century: The Impact of HPV on the Epidemiology and Pathology of Oral Cancer. *Head Neck Pathol* (2009) 3(1):78–81. doi: 10.1007/s12105-009-0100-y
126. Toptan T, Abere B, Nalesnik MA, Swerdlow SH, Ranganathan S, Lee N, et al. Circular DNA Tumor Viruses Make Circular Rnas. *Proc Natl Acad Sci U S A* (2018) 115(37):E8737–45. doi: 10.1073/pnas.1811728115
127. Ungerleider N, Concha M, Lin Z, Roberts C, Wang X, Cao S, et al. The Epstein Barr Virus Circrnaome. *PloS Pathog* (2018) 14(8):e1007206. doi: 10.1371/journal.ppat.1007206
128. Huang JT, Chen JN, Gong LP, Bi YH, Liang J, Zhou L, et al. Identification of Virus-Encoded Circular RNA. *Virology* (2019) 529:144–51. doi: 10.1016/j.virol.2019.01.014
129. Gong LP, Chen JN, Dong M, Xiao ZD, Feng ZY, Pan YH, et al. Epstein-Barr Virus-Derived Circular RNA LMP2A Induces Stemness in EBV-associated Gastric Cancer. *EMBO Rep* (2020) 21(10):e49689. doi: 10.15252/embr.201949689
130. Zhao J, Lee EE, Kim J, Yang R, Chamseddin B, Ni C, et al. Transforming Activity of an Oncoprotein-Encoding Circular RNA From Human Papillomavirus. *Nat Commun* (2019) 10(1):2300. doi: 10.1038/s41467-019-10246-5
131. Bahn JH, Zhang Q, Li F, Chan TM, Lin X, Kim Y, et al. And Circular RNA in Human Saliva. *Clin Chem* (2015) 61(1):221–30. doi: 10.1373/clinchem.2014.230433
132. Li Y, Zheng Q, Bao C, Li S, Guo W, Zhao J, et al. Circular RNA is Enriched and Stable in Exosomes: A Promising Biomarker for Cancer Diagnosis. *Cell Res* (2015) 25(8):981–4. doi: 10.1038/cr.2015.82
133. Goleva E, Lyubchenko T, Kraehenbuehl L, LaCouture ME, Leung DYM, Kern JA. Our Current Understanding of Checkpoint Inhibitor Therapy in Cancer Immunotherapy. *Ann Allergy Asthma Immunol* (2021). doi: 10.1016/j.anai.2021.03.003
134. Ye J, Ji X, Dennis PA, Abdullah H, Mukhopadhyay P. Relationship Between Progression-Free Survival, Objective Response Rate, and Overall Survival in Clinical Trials of PD-1/PD-L1 Immune Checkpoint Blockade: A Meta-Analysis. *Clin Pharmacol Ther* (2020) 108(6):1274–88. doi: 10.1002/cpt.1956
135. Hong W, Xue M, Jiang J, Zhang Y, Gao X. Circular RNA circ-CPA4/ Let-7 miRNA/PD-L1 Axis Regulates Cell Growth, Stemness, Drug Resistance and Immune Evasion in non-Small Cell Lung Cancer (NSCLC). *J Exp Clin Cancer Res* (2020) 39(1):149. doi: 10.1186/s13046-020-01648-1
136. Zhang PF, Pei X, Li KS, Jin LN, Wang F, Wu J, et al. Circular RNA circFGFR1 Promotes Progression and anti-PD-1 Resistance by Sponging miR-381-3p in non-Small Cell Lung Cancer Cells. *Mol Cancer* (2019) 18(1):179. doi: 10.1186/s12943-019-1111-2
137. Chen YG, Chen R, Ahmad S, Verma R, Kasturi SP, Amaya L, et al. N6-Methyladenosine Modification Controls Circular Rna Immunity. *Mol Cell* (2019) 76(1):96–109.e9. doi: 10.1016/j.molcel.2019.07.016
138. Shannon-Lowe C, Rickinson A. The Global Landscape of EBV-Associated Tumors. *Front Oncol* (2019) 9:713. doi: 10.3389/fonc.2019.00713
139. Sun Y, Zhang Y, Liu L, Song X, Li G. Genetic Polymorphisms and HPV Infection in Oral Squamous Cell Carcinomas. *Curr Opin Virol* (2015) 14:1–6. doi: 10.1016/j.coviro.2015.05.004
140. Tsang CM, Lui VWY, Bruce JP, Pugh TJ, Lo KW. Translational Genomics of Nasopharyngeal Cancer. *Semin Cancer Biol* (2020) 61:84–100. doi: 10.1016/j.semcancer.2019.09.006
141. Peiris-Pages M, Martinez-Outschoorn UE, Pestell RG, Sotgia F, Lisanti MP. Cancer Stem Cell Metabolism. *Breast Cancer Res* (2016) 18(1):55. doi: 10.1186/s13058-016-0712-6
142. Zhu D, Shao M, Yang J, Fang M, Liu S, Lou D, et al. Curcumin Enhances Radiosensitization of Nasopharyngeal Carcinoma Via Mediating Regulation of Tumor Stem-Like Cells by a CircRNA Network. *J Cancer* (2020) 11 (8):2360–70. doi: 10.7150/jca.39511
143. Matsui WH. Cancer Stem Cell Signaling Pathways. *Med (Baltimore)* (2016) 95(1 Suppl 1):S8–S19. doi: 10.1097/MD.0000000000004765

Conflict of Interest: The authors declare that the research was conducted in the absence of any commercial or financial relationships that could be construed as a potential conflict of interest.

The reviewer YW declared a shared affiliation, with no collaboration, with the authors to the handling editor at the time of the review.

Copyright © 2021 Li, Zhu, Mo, Deng, Jiang, Shi, Guo, Zhang, Zeng, Li, Xiong, Zhang and Gong. This is an open-access article distributed under the terms of the Creative Commons Attribution License (CC BY). The use, distribution or reproduction in other forums is permitted, provided the original author(s) and the copyright owner(s) are credited and that the original publication in this journal is cited, in accordance with accepted academic practice. No use, distribution or reproduction is permitted which does not comply with these terms.

frontiers in Oncology

ORIGINAL RESEARCH
published: 14 June 2021
doi: 10.3389/fonc.2021.685026

A Novel Prognostic Signature Based on Metabolism-Related Genes to Predict Survival and Guide Personalized Treatment for Head and Neck Squamous Carcinoma

Ying Li[†], *Youliang Weng*[†], *Yuhui Pan*, *Zongwei Huang*, *Xiaochuan Chen*, *Wenquan Hong*, *Ting Lin*, *Lihua Wang*, *Wei Liu and Sufang Qiu*[*]

Department of Radiation Oncology, Fujian Medical University Cancer Hospital, Fujian Cancer Hospital, Fuzhou, China

OPEN ACCESS

Edited by:
Wei Cao,
Shanghai Jiao Tong University, China

Reviewed by:
Yizhen Jia,
The University of Hong Kong-Shenzhen Hospital, China
Yanjie Zhang,
Shanghai Jiao Tong University, China

***Correspondence:**
Sufang Qiu
sufangqiu@fjmu.edu.cn

[†]*These authors have contributed equally to this work*

Specialty section:
This article was submitted to Head and Neck Cancer, a section of the journal Frontiers in Oncology

Received: *24 March 2021*
Accepted: *27 May 2021*
Published: *14 June 2021*

Citation:
Li Y, Weng Y, Pan Y, Huang Z, Chen X, Hong W, Lin T, Wang L, Liu W and Qiu S (2021) A Novel Prognostic Signature Based on Metabolism-Related Genes to Predict Survival and Guide Personalized Treatment for Head and Neck Squamous Carcinoma. Front. Oncol. 11:685026. doi: 10.3389/fonc.2021.685026

Metabolic reprogramming contributes to patient prognosis. Here, we aimed to reveal the comprehensive landscape in metabolism of head and neck squamous carcinoma (HNSCC), and establish a novel metabolism-related prognostic model to explore the clinical potential and predictive value on therapeutic response. We screened 4752 metabolism-related genes (MRGs) and then identified differentially expressed MRGs in HNSCC. A novel 10-MRGs risk model for prognosis was established by the univariate Cox regression analysis and the least absolute shrinkage and selection operator (Lasso) regression analysis, and then verified in both internal and external validation cohort. Kaplan-Meier analysis was employed to explore its prognostic power on the response of conventional therapy. The immune cell infiltration was also evaluated and we used tumor immune dysfunction and exclusion (TIDE) algorithm to estimate potential response of immunotherapy in different risk groups. Nomogram model was constructed to further predict patients' prognoses. We found the MRGs-related prognostic model showed good prediction performance. Survival analysis indicated that patients suffered obviously poorer survival outcomes in high-risk group ($p < 0.001$). The metabolism-related signature was further confirmed to be the independent prognostic value of HNSCC (HR = 6.387, 95% CI = 3.281-12.432, $p < 0.001$), the efficacy of predictive model was also verified by internal and external validation cohorts. We observed that HNSCC patients would benefit from the application of chemotherapy in the low-risk group ($p = 0.029$). Immunotherapy may be effective for HNSCC patients with high risk score ($p < 0.01$). Furthermore, we established a predictive nomogram model for clinical application with high performance. Our study constructed and validated a promising 10-MRGs signature for monitoring outcome, which may provide potential indicators for metabolic therapy and therapeutic response prediction in HNSCC.

Keywords: metabolism, prognostic signature, head and neck squamous carcinoma, survival, therapeutic response prediction

INTRODUCTION

Head and neck squamous carcinoma (HNSCC) is a heterogeneous epithelial tumor, accounting for more than 830,000 newly diagnosed cases, and no more than half a million individuals' deaths annually in the world (1). Although advances in various treatment regimens, patient's prognosis is still poor (2). The 5-year survival time is only nearly 50% and there is strong tendency of distant metastasis and local recurrence in HNSCC (3). There are limited effective indicators that can predict prognosis in HNSCC patients (4). It is hence significant to identify novel predictors for clinical outcomes and predicting therapeutic response to provide new insights for optimizing individual treatment in HNSCC.

The oncogenesis and development of HNSCC are closely associated with viral infection, genetic changes, environmental factors and imbalanced metabolism (5). Metabolic reprogramming is regarded as a hallmark of cancers, which defined as the remarkably changes of metabolic patterns in the occurrence and evolution of cancer (6). It includes several metabolic pathways, involving in the glycolysis, amino acid metabolism, the tricarboxylic acid (TCA) cycle, nucleic acid metabolism, etc. (7). It's significative to reveal the neoplastic metabolic patterns, thereby which may benefit for personalized treatment management and disease monitoring.

Previous findings have shown that the unique metabolic pattern of tumor cells is a positive alteration of heredity expression to regulate the neoplasm oncogenesis and invasiveness (8, 9). Regulation of metabolism-related genes (MRGs) was suggested to be an important mechanism by which the specific metabolic mode exerts its functions in cancers (10). Given the targeting tumor metabolism as a potential and promising novel treatment strategy, exploring MRGs-related signature which can serve as a predictor for the evaluation of diagnosis, treatment, and prognosis, has received increasing attention and demonstrated in several cancers (11–13). Some recent studies also revealed the imbalance metabolic patterns of HNSCC in a single metabolic pathway or metabolite, based on glycolysis (14), lipid metabolism (15, 16), and pyruvate catabolism (17). However, the overall landscape of MRGs in HNSCC has not been fully revealed and the predictive role on therapy response remains unclear.

In present study, we use the public dataset, The Cancer Genome Atlas (TCGA) databases, to develop a MRGs-related risk model in HNSCC. We evaluated and verified the specificity and sensitivity of this model to determine prognostic significance and make an evaluation into its prognostic value on both conventional therapy and immunotherapy in HNSCC.

Abbreviations: HNSCC, head and neck squamous carcinoma; MRGs, metabolism-related genes; TCGA, The Cancer Genome Atlas; TMB, tumor mutation burden; GEO, Gene Expression Omnibus; DEGs, differentially expressed genes; DEMRGs, differentially expressed metabolism-related genes; PPI, protein-protein interaction; STRING, Search Tool for Recurring Instances of Neighbouring Genes; GO, Gene Ontology; KEGG, Kyoto Encyclopedia of Genes and Genomes; Lasso, least absolute shrinkage and selection operator; ROC, Receiver operating characteristic curve; AUC, area under the curve; TME, tumour microenvironment; ssGSEA, single sample Gene Set Enrichment Analysis; ICB, immune checkpoint blockade; TIDE, Tumor Immune Dysfunction and Exclusion; Tfh, T cell follicular helpers; Tregs, regulatory T cells; CTL, cytotoxic T lymphocytes.

MATERIALS AND METHODS

Samples and Data Acquisition

The whole-genome RNA-seq data (normalized RPKM) with corresponding somatic mutation data and clinical information was obtained from the TCGA database (https://portal.gdc.cancer.gov/). The somatic mutation data of tumor samples was utilized to calculate tumor mutation burden (TMB), which refers to the frequency of somatic alterations per megabase of the genome (18). Moreover, patients' clinical follow-up information was collected, including age, gender, grade, TNM stage, survival time (days), survival status, and application of radiotherapy or chemotherapy. An independent HNSCC cohort (GSE41613 from GPL570 platform) with complete overall survival (OS) information was extracted from the Gene Expression Omnibus (GEO) available database (https://www.ncbi.nlm.nih.gov/gds/) for validation (19). We used R package "sva" to remove data batch effects. These data were obtained from the online public sources, so all informed consents were available and we conducted this study as requested on using these databases.

Identification of MRGs Set

A list of 2752 MRGs was extracted from previously published report, which was associated with metabolism process and encoded the known human metabolic enzymes and transporters (20). Additionally, differentially expressed genes (DEGs) between HNSCC and compared normal samples were derived from the GEPIA v2.0 database (http://gepia2.cancer-pku.cn/), with the criteria of the threshold value of adj. $p < 0.01$ and $|\log2 \text{ fold change (FC)}| > 1.0$. Venn was used to identify differentially expressed metabolism-related genes (DEMRGs) by the two groups drawn using "VennDiagram" R packages. We presented a protein-protein interaction (PPI) network *via* the Search Tool for Recurring Instances of Neighbouring Genes (STRING) database (https://string-db.org/cgi/input.pl) for the overlapping DEMRGs to retrieve interaction.

Gene-Enrichment and Functional Annotation Analysis

Gene functional enrichment analysis were carried out to illustrate various functions and differential disturbing pathways of DEMRGs, including the Gene Ontology (GO) and Kyoto Encyclopedia of Genes and Genomes (KEGG) enrichment analysis, conducted by "clusterProfiler" R package. GO analysis, consisting of biological processes (BPs), molecular functions (MFs), and cellular components (CCs), offers integrative annotation to identify characteristic biological meaning in MRGs. We applied the "GOplot" R package to visualize the enrichment terms. Additionally, the KEGG analysis revealed potential signaling pathways which the candidate MRGs participate in. The results accurately were visualized by the R packages "enrichplot" and "ggplot2".

Construction and Validation of the Risk Model Based on MRGs

Totally 499 HNSCC patients were randomly divided at a 7:3 ratio, served as the training and internal validation cohorts with the "caret" R package. The prognostic value of DEMRGs on HNSCC patients was evaluated by the univariate Cox regression model using the data from the training cohort. Initially, the potential prognostic DEMRGs were selected (p-value < 0.01 was chosen). Then the least absolute shrinkage and selection operator (Lasso) regression analysis was screened to construct the MRGs-derived risk signature with the "glmnet" R package. We used CBioPortal (http://www.cbioportal.org/) to show the related genetic changes of particular genes. The formula of risk score was generated as following: risk score = $\sum$ (expression level of each particular gene × individual regression coefficient). According to the median of risk score as the cutoff, we classified subjects into low- and high-risk groups. PCA was performed to explore the distribution of different groups with the "stats" R package, based on the expression of genes in the signature. Besides, survival differences were assessed by Kaplan-Meier curve using the "survival" R packages. Receiver operating characteristic (ROC) curves were conducted to investigate the prediction accuracy of the model for 3/5-year OS using area under the ROC curve (AUC) estimation with the "survival ROC" R package. An AUC value of 0.70 or greater was considered as a significant predictive value. The internal validation cohort and GSE41613 cohort were also subject to the same analysis to verify the predictive power of the risk signature.

Correlation Analysis of Clinicopathologic Characteristics

Univariate and multivariate Cox regression analysis were carried out to examine the prognostic significance of the risk score and clinicopathologic characteristics for OS. We further evaluated differences of prognostic MRGs and risk score in clinical features. Subsequently, we employed the "survival" R packages to estimate the clinical utility of risk model for patients subjected to chemotherapy or radiotherapy.

Tumor-Infiltrating Immune Cell Analysis

In order to characterize immune cell infiltration in tumour microenvironment (TME) in different risk groups, two algorithms, the single sample Gene Set Enrichment Analysis (ssGSEA) algorithm and the CIBERSORT were performed based on the gene expression in TCGA training cohort. The former calculated HNSCC tissue purity, immune and stromal scores using the "ESTIMATE" R package. The relative fractions of 22 types of immune cell in TME in each sample of HNSCC were determined by "CIBERSORT" R package with all proportions normalized to 1 in each sample. This algorithm used Monte Carlo sampling to calculate a p-value for each case, and cases with p-value > 0.05 were excluded for subsequent analysis. We illustrated the results as a stacked bar plot, with the various immune cells. The box plots were exhibited for better visualization to show the difference abundance of infiltrating immune cells with "ggplot2" R package. Subsequently, we evaluate the correlations of immune cell infiltration and risk score.

Prediction of Immune Checkpoint Blockade (ICB) Therapy Response

Potential tumor therapeutic response with ICB was predicted by Tumor Immune Dysfunction and Exclusion (TIDE) score, a computational algorithm based on gene expression profile (http://tide.dfci.harvard.edu). It demonstrated that patients exhibit lower sensitivity with ICB agents, who had high TIDE score, thus indicating high possibility of antitumor immune escape (21). The details of the algorithm are described elsewhere (21). Meanwhile, the TMB, also as a useful marker for ICB selection, was performed to validate the predictive effectiveness of immunotherapy response.

Construction and Validation of the Nomogram Model

We established a nomogram model using prognosis factors from univariate Cox regression analysis to visualize the score for each variable on the point scale by the "rms" R package. Then we evaluated the predictive probabilities for 3- and 5-year clinical outcomes by depicted calibration curves. The ROC curves were also employed to determine the exactitude of the model.

Statistical Analysis

R software v3.6.2 (https://www.r-project.org/) together with SPSS Statistics v25.0 assisted in performing all statistical analysis. We also used R software, GraphPad Prism 7.0 and Cytoscape software for diagram drawing. Unpaired Student's t-test and Whitney U-test were employed for comparing differences between two sets containing parameters with normally and non-normally distributions, respectively. A Chi-square test was used for categorical variables. A Wilcoxon rank-sum test was applied to compare non-parametric parameters for two sets, while the Kruskal-Wallis test was used for multiple sets. Pearson's chi-square test was made to analyze the correlation between qualitative parameters. If not specified above, it represented statistical significance with p-value < 0.05.

RESULTS

Initial Screening of DEMRGs in HNSCC From the TCGA Database

The HNSCC transcriptome data comprised 546 samples, which involved 502 tumor samples and 44 normal samples from TCGA database. Among 2752 genes involved in metabolism, 2751 MRGs were finally selected after filtering repeated genes. Afterward, we analyzed the DEGs between cancer and compared normal samples from online database and 2751 MRGs, and then identified 306 DEMRGs shown in **Figure 1A**. We identified PPI network of DEMRGs with high confidence levels (> 0.7) in **Figure 1B**. After excluding the samples without complete survival information, 499 HNSCC patients were finally enrolled for further analysis.

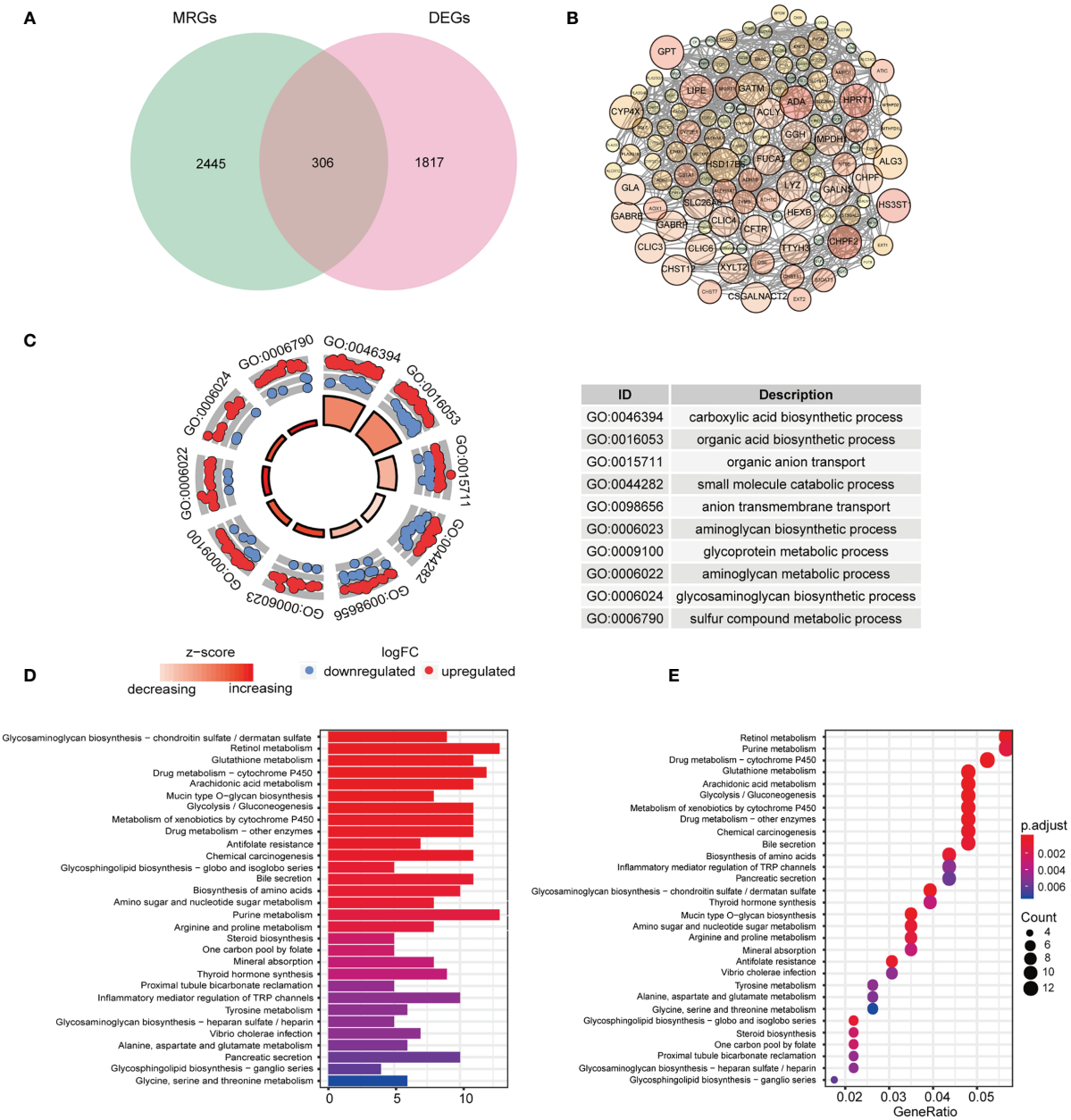

FIGURE 1 | Identification and functional analysis of candidate DEMRGs. **(A)** Venn diagram depicting overlap to identify DEMRGs between HNSCC tumor and normal tissue. **(B)** The interactions among MRGs showing in PPI network. **(C)** The GO circle plot of biological process (BP) differentially enriched in patients. **(D, E)** Enriched KEGG pathways of differentially expressed MRGs.

Gene-Enrichment and Functional Annotation for DEMRGs in HNSCC

According to the functional enrichment analysis of the 306 DEMRGs, we obtained GO and KEGG annotations of these genes in HNSCC. Not surprisingly, it showed that these genes were significantly related to metabolism process, including organic compounds biosynthesis, transport and metabolic process in the biological processes (**Figure 1C**). In the CC term of GO analysis, membrane-transport-related components, such as "intrinsic component of Golgi membrane", "transporter complex", and "integrin complex" were significantly enriched by DEMRGs (**Figure S1**). In terms of MF analysis, "transmembrane transporter activity", "transferase activity" and "oxidoreductase activity" were mainly categories for these genes to play important roles (**Figure S1**). For KEGG analysis, these DEGs were also shown to mainly enrich in several tumor metabolic pathways,

like amino acids, purine and drug metabolism. Interestingly, it indicated that these genes were also related to chemical carcinogenesis as general oncogenes (**Figures 1D, E**).

Construction and Internal Validation of the MRGs-Related Prognostic Risk Signature

499 HNSCC patients were divided into two cohorts, namely, a training set with 350 patients and an internal validation set with 149 patients. **Table 1** presented the baseline clinical characteristics, which showing the compared characteristics of the two cohorts were matched. Next, the univariate Cox regression analysis was performed to identify prognosis-related genes using 306 DEMRGs in the training group. A total of 14 DEARGs were obviously associated with the OS (**Figure 2A**, *ps*< 0.05). To construct an optimal risk model for predicting prognosis of HNSCC patients, 10 MRGs identified by Lasso regression analysis were used for further research on their prognostic value (**Figures 2B, C**). Among these 10 genes, ADA, ALG3, CHPF2, HPRT1, and HSD17B6 showed higher expressions than adjacent non-cancerous tissues, while CYP4X1, GATM, GPT, HS3ST1, and LIPE were low expressions in tumors (**Figure 2D**). The mutational landscape of 10 MRGs revealed ALG3 was the most frequently mutated gene (20%), followed by GPT with an alteration frequency of 10% (**Figure 2E**). The detailed interactions of these 10 genes in MRGs were presented in **Figure S2**. The coefficients to calculate risk scores based on expression level of genes obtained by the LASSO algorithm were listed in **Table S1**.

To detect the robustness of the model established by training set, we utilized the same coefficients to calculate the risk scores in validation cohort. Based on the median value of risk score (0.63) as a cut-off point, subjects were classified into high- and low-risk groups in training and validation sets, respectively. **Figures 3A, B** exhibited the ranked risk scores' distribution, survival status of individual patients, and the heatmap of 10 MRGs expression in two cohorts. The distribution map of survival status showed patients suffered more mortal risks with increasing risk score. The heatmap results suggested that therisky MGRs, including ADA, ALG3, CHPF2, HPRT1, and HS3ST1, were highly expressed in the high-risk group, while the expression of CYP4X1, GATM, GPT, HSD17B6, and LIPE were upregulated as protective MRGs in the low-risk group. PCA analysis depicted by scatter plots revealed the patterns of risk-genes expression in different risk groups (**Figures 3C, D**). The Kaplan-Meier curves showed remarkably worse OS with high risk (**Figures 3E, F**, $p < 0.001$) in training and validation cohort. To evaluate the predictive power of the risk score, the time-dependent ROC curves were utilized and the AUC for 3-, and 5-year OS reached 0.69, and 0.73, respectively (**Figure 3G**). Consistently, as shown in **Figure 3H**, the AUC values for 10 risk signatures were 0.66 at 3 year, and 0.72 at 5 years in validation cohorts.

TABLE 1 | Demographic characteristics of the training cohort and the test cohort in HNSCC.

		Training cohort (N = 350)	Validation cohort (N = 149)	*P* Value
Age	≤65	227 (64.9%)	97 (65.1%)	0.958
	>65	123 (35.1%)	52 (34.9%)	
Gender	Male	250 (71.4%)	116 (77.9%)	0.137
	Female	100 (28.6%)	33 (22.1%)	
Grade	G1-2	258 (73.7%)	101 (67.8%)	0.124
	G3-4	78 (22.3%)	43 (28.9%)	
	NA	14 (4.0%)	5 (3.4%)	
Stage	Stage I-II	69 (19.7%)	36 (24.1%)	0.265
	Stage III-IV	281 (80.3%)	113 (75.9%)	
T	T1-2	123 (35.1%)	53 (35.5%)	0.768
	T3-4	222 (63.4%)	90 (60.4%)	
	NA	5 (1.4%)	6 (4.0%)	
N	N0	177 (50.6%)	63 (42.3%)	0.110
	N1-3	161 (46.0%)	79 (53.0%)	
	NA	12 (3.4%)	7 (4.7%)	
M	M0	332 (94.9%)	142 (94.0%)	0.145
	M1	5 (1.4%)	0 (0.0%)	
	NA	13 (3.7%)	7 (4.7%)	

NA, not applicable; Ambiguous variables (NA) were excluded from Chi-square test.

Validation of the MRGs-Related Prognostic Risk Model *via* External Cohort

We used an independent cohort with 97 patients from GEO dataset GSE41613 to verify the model accuracy externally. The risk scores and grouping did with the same ways mentioned previously (the median value of risk score = 0.63). **Figure 4A** showed the survival status together with the 10 MRGs expression, based on patients with increasing risk scores. PCA analysis showed a segregated tendency of gene expression patterns in two risk groups based on MRGs-related signature (**Figure 4B**). As demonstrated by TCGA cohorts, patients with high risk exhibited worse OS (**Figure 4C**, $p = 0.011$). Correspondingly, the 3- and 5-year AUC value in predicting prognosis were 0.67 and 0.70, respectively (**Figure 4D**). It was further revealed the predictive performance of the 10-MRGs prognosis signature of HNSCC patients by these results.

Assessment of Relevance Between the Prognostic Signature and Clinical Characteristics

Univariate and multivariate Cox regression analysis were utilized to explore prognostic factors for OS in TCGA cohorts, as shown in **Table 2**. Among the available variables, age, gender, stage and risk score (HR = 6.945, 95% CI = 3.538-13.632, $p < 0.001$) were prognosis factors of HNSCC in the training cohort. However, it was validated that only the risk score was significantly correlative with OS *via* validation cohort (HR= 3.217, 95% CI = 1.691-6.118, $p < 0.001$). The results of multivariate Cox regression analysis indicated the role of risk score working as an independent predictor for HNSCC prognosis (training cohort: HR =6.387, 95% CI = 3.281-12.432, $p < 0.001$; validation cohort: HR=2.812, 95% CI = 1.439-5.495, $p = 0.002$). Then we further evaluated the associations between clinical features and risk signature. We found that the risk score was correlated with survival state, as mentioned above (**Figure 5A**). And the T3-4 stage had higher risk scores than T1-2 stage ($p < 0.05$), indicting poor prognosis, as shown in **Figure 5B**. In addition, some signature-related genes were differentially expressed among clinical parameters. Patients with stage III-IV had higher ALG3 expression than early stage

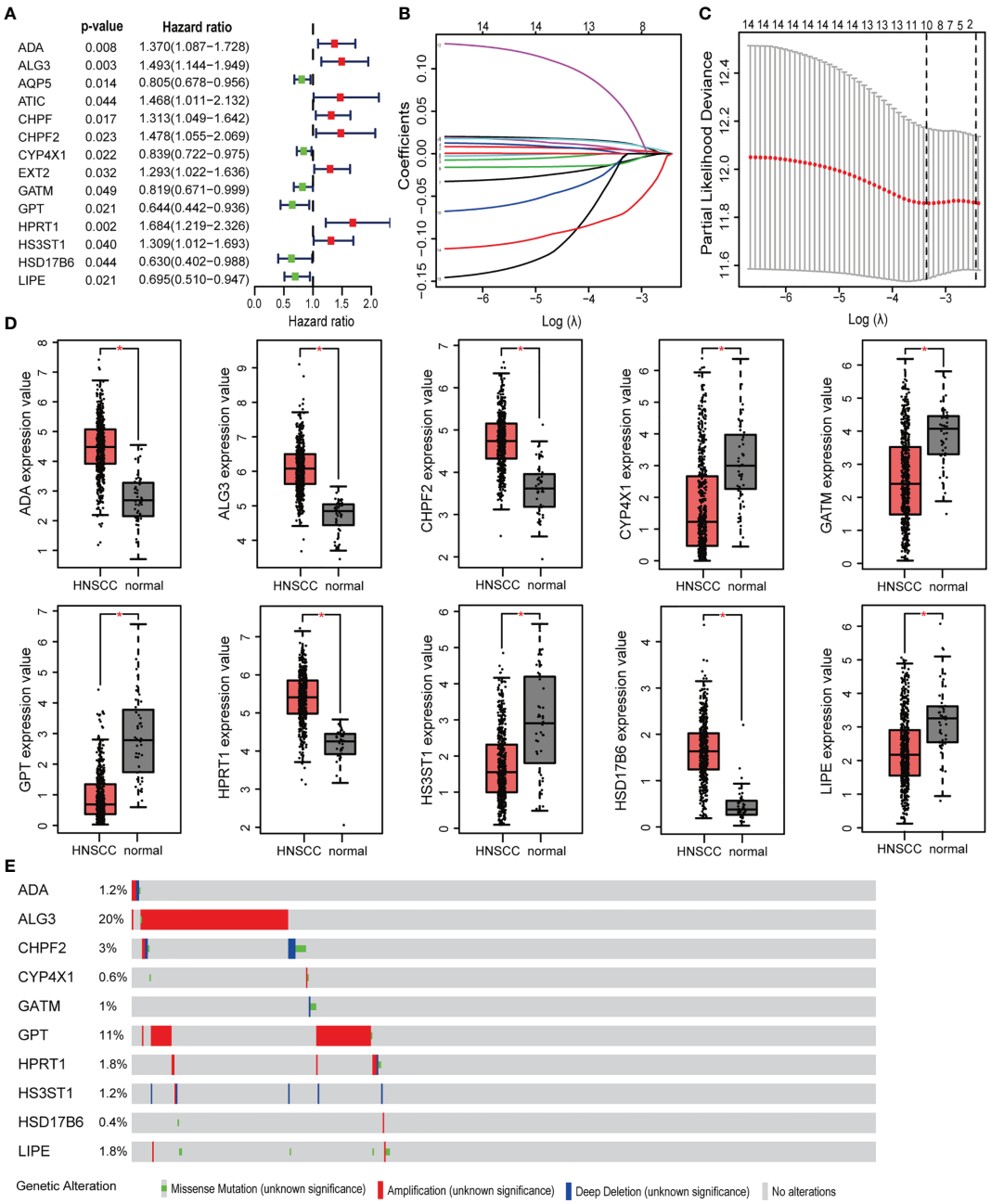

FIGURE 2 | Prognosis MRGs-related signature identified by Lasso regression analysis. **(A)** Forest plots showing the prognostic metabolic genes determined by the univariate Cox regression analysis (green represents protective factors, and red represents risk factors). **(B)** Lasso coefficient profiles of selected 14 MRGs and **(C)** the optimal values of the penalty parameter λ for OS. **(D)** The expression of 10 MRGs based on TCGA databases from GEPIA. **(E)** The mutation patterns of 10 differentially expressed MRGs. (*$p < 0.05$).

(**Figure 5C**). And the expression of CYP4X1, GATM, GPT, and LIPE were related to grade (**Figures 5D–G**).

We further evaluated the clinical utility of risk model for patients subjected to radiotherapy or chemotherapy in HNSCC. We observed that HNSCC patients would benefit from the application of chemotherapy, patients with chemotherapy (n = 59) had a higher probability of survival than those without chemotherapy (n = 116) in the low-risk group (**Figure 5H**, $p = 0.029$). The survival benefit with chemotherapy was not significant in the high-risk group (n = 64, with chemotherapy; n = 111, without chemotherapy; $p = 0.59$, **Figure 5I**). We didn't observe the same results in the application of radiotherapy (**Figures S3A, B**). Moreover, patients with low risk score significantly suffered more beneficial prognosis from

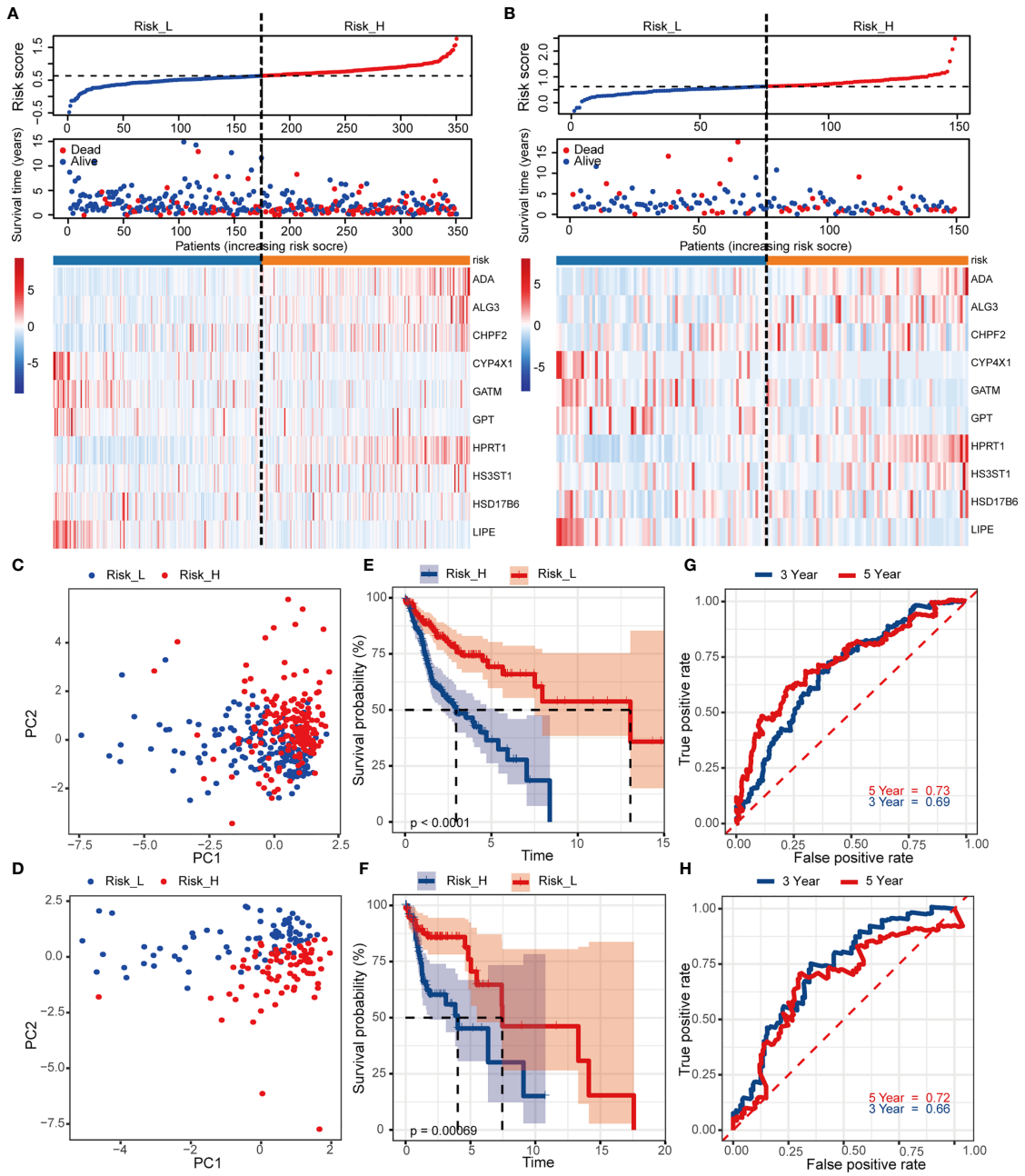

FIGURE 3 | Construction and internal validation of the prognosis-related risk model based on MRGs in TCGA cohort. The risk scores distribution, vital status of patients, and heatmap of identified 10 MRGs expression level in **(A)** training and **(B)** validation cohorts. **(C, D)** PCA plot of prognostic metabolism signature. **(E, F)** Kaplan-Meier curves of OS and **(G, H)** time-dependent ROC analysis for 3/5-year survival to predict OS.

chemotherapy (**Figure S3C**, $p < 0.001$) or radiotherapy (**Figure S3D**, $p = 0.012$).

Comprehensive Analysis of Immune Characteristics and ICB Therapy in Different Risk Subtypes

To elucidate the difference of immune microenvironment of HNSCC, we analyzed the immune scores and immune cell infiltrating density between high- and low-risk groups. It revealed significant differences in purity of tumor (p =0.021, **Figure 6A**) and immune scores (p = 0.007, **Figure 6B**), but not in stromal scores (**Figure 6C**) between the two groups. The high-risk group showing lower immune scores presented lower immune infiltration in TME. It also indicated poor prognosis which was consistent with worse survival outcomes of patients in the high-risk group. Subsequently, we analyzed the fraction of 22 types of immune cell *via*

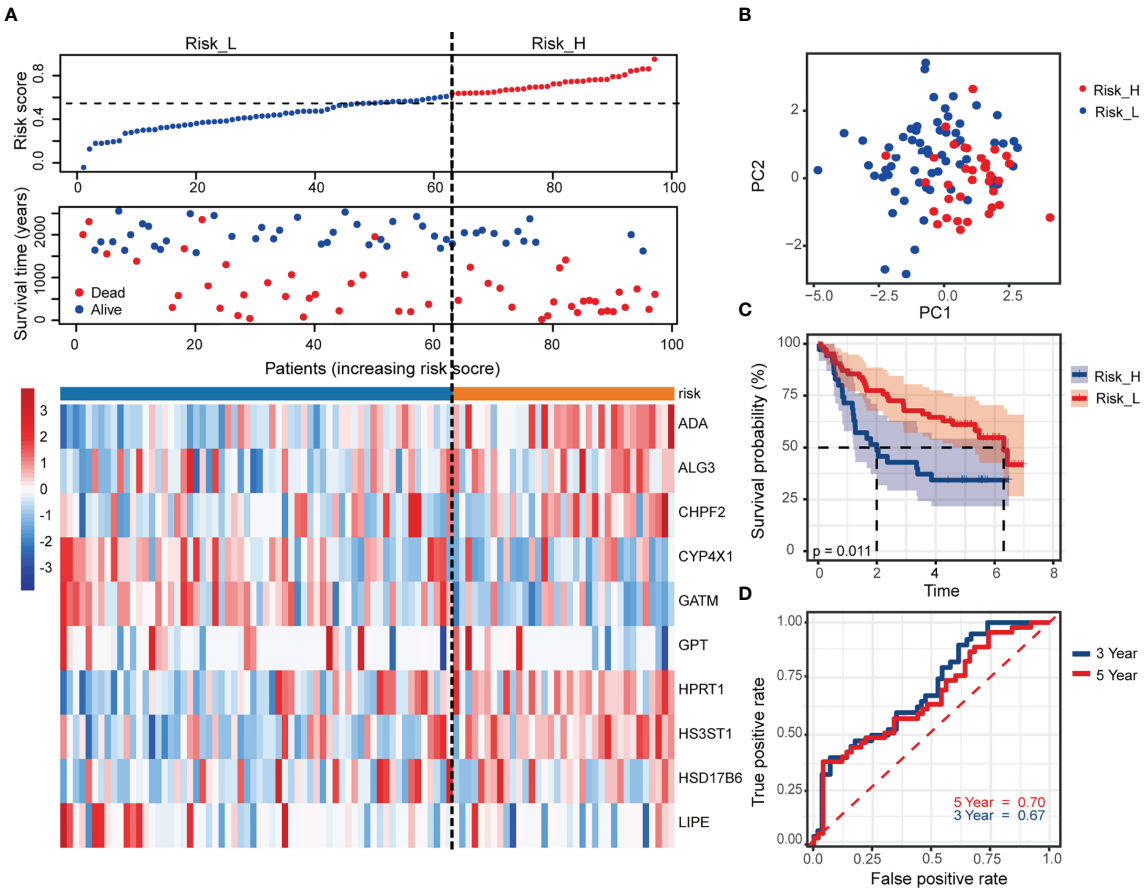

FIGURE 4 | Validation of the risk signature in external GSE41613 cohort. **(A)** The distribution of risk score, survival status of patients and heatmap of 10 MRGs. **(B)** PCA plot of prognostic metabolism signature. **(C)** Kaplan-Meier curves of OS and **(D)** time-dependent ROC curve of 3- and 5-year survival rate.

TABLE 2 | Univariate and multivariate Cox regression analyses of OS in the TCGA training and internal validation cohorts of HNSCC.

Variables	Univariate analysis		Multivariate analysis	
	HR (95% CI)	*p*-value	HR (95% CI)	*p*-value
TCGA training cohort				
Age	1.033 (1.015–1.051)	**<0.001**	1.031 (1.012–1.051)	**0.002**
Gender	0.622 (0.423–0.914)	**0.016**	0.833 (0.548–1.266)	0.393
Grade	0.985 (0.731–1.328)	0.923	1.081 (0.797–1.467)	0.617
Stage	1.326 (1.050–1.674)	**0.018**	1.681 (1.237–2.283)	**<0.001**
T	1.025 (0.843–1.247)	0.803	0.801 (0.635–1.009)	0.06
N	1.055 (0.851–1.306)	0.626	1.052 (0.830–1.334)	0.674
Risk score	6.945 (3.538–13.632)	**<0.001**	6.387 (3.281–12.432)	**<0.001**
TCGA validation cohort				
Age	1.007 (0.980–1.034)	0.622	1.004 (0.975–1.035)	0.785
Gender	1.855 (0.823–4.181)	0.136	1.589 (0.684–3.690)	0.281
Grade	1.353 (0.877–2.090)	0.172	1.151 (0.725–1.826)	0.551
Stage	1.198 (0.850–1.690)	0.302	1.170 (0.684–2.002)	0.566
T	1.123 (0.811–1.555)	0.484	0.999 (0.628–1.591)	0.997
N	1.066 (0.774–1.470)	0.694	0.964 (0.647–1.436)	0.856
Risk score	3.217 (1.691–6.118)	**<0.001**	2.812 (1.439–5.495)	**0.002**

HR, Hazard ratio. Bold value showed significance.

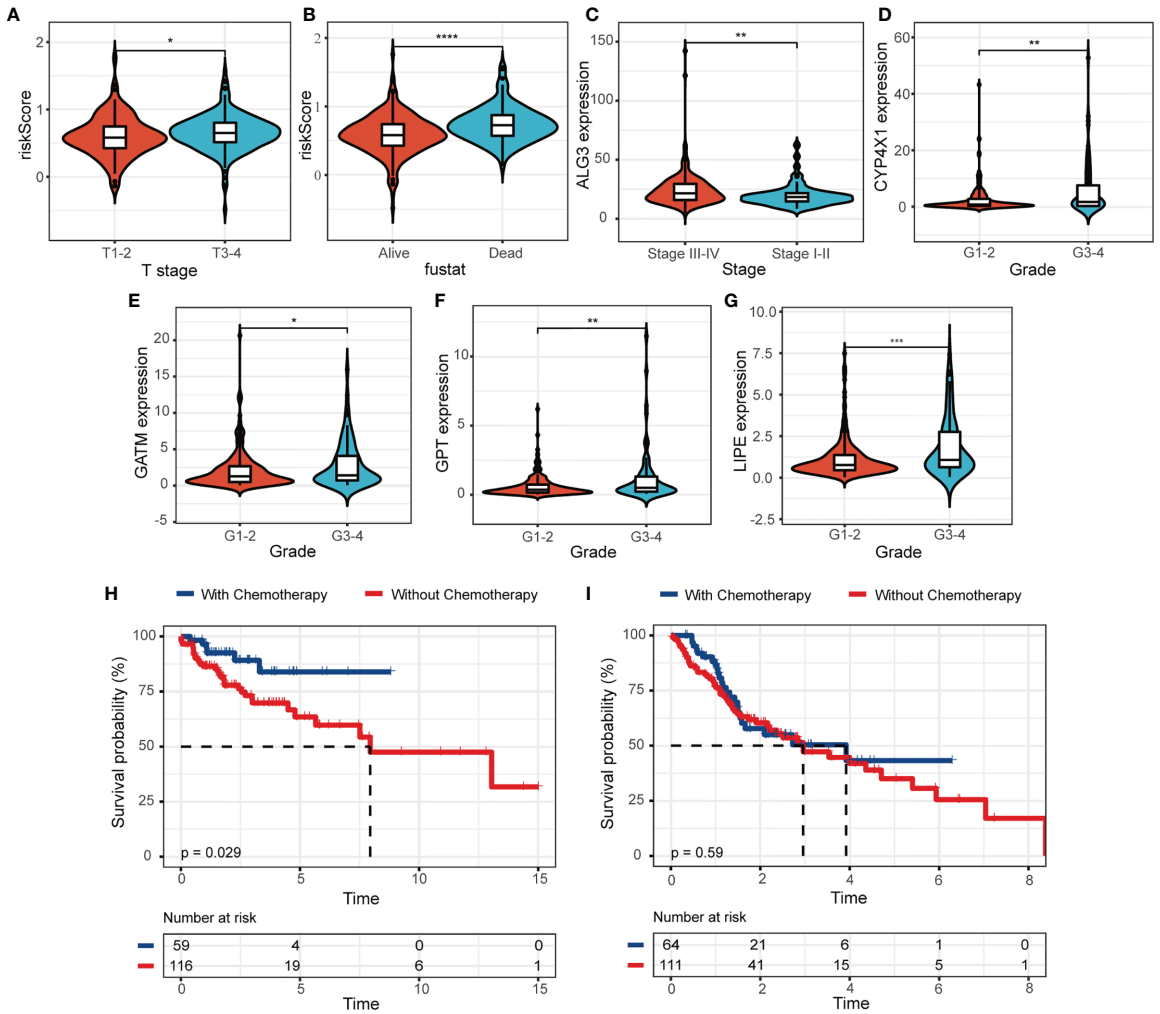

FIGURE 5 | The relevance between the risk model and clinicopathologic features. **(A, B)** The correlations between risk score and clinical characteristics. **(C–G)** The associations between MRGs expression level and clinical features. Kaplan-Meier survival analysis for patients in **(H)** low- and **(I)** high-risk groups with the application of chemotherapy. (*$p < 0.05$; **$p < 0.01$; ***$p < 0.001$; ****$p < 0.0001$).

CIBERSORTx algorithms. The stacked bar plot illustrated the infiltrating difference of immune cells in each case (**Figure 6D**). Additionally, **Figure 6E** showed the differential distributions of infiltrating immune cells in the two risk groups. Among them, the infiltration levels of naive B cells ($p < 0.001$), plasma cells ($p < 0.05$), T cell follicular helpers (Tfh) ($p < 0.05$), and regulatory T cells (Tregs) ($p < 0.01$) were significantly higher in low-risk group. While the resting NK cells ($p < 0.05$), monocytes ($p < 0.05$), and activated mast cells infiltration ($p < 0.01$) were higher in high-risk group. Moreover, we evaluated the relationships between different immune infiltrates and risk score. The infiltration of naive B cells, plasma cells, CT8+ T cells, Tfh, Tregs, and resting mast cells was found to be negatively associated with prognostic risk, while M2 macrophages and resting NK cells were positively associated (**Figure 6F**).

To investigate the association between risk subtyping of HNSCC and its response of immune checkpoint inhibitor, we estimated the potential clinical response of ICB therapy with TIDE algorithm. The low-risk group was featured by higher TIDE score ($p < 0.01$, **Figure 6G**), composed of higher TIDE dysfunction signatures ($p < 0.01$, **Figure 6H**) and lower TIDE exclusion scores ($p < 0.05$, **Figure 6I**), compared to the high-risk group. It indicated the mechanism of tumor immune evasion was mainly associated with the infiltration of dysfunctional tumor cytotoxic T lymphocytes (CTL) in low-risk group. What's more, the patients with high risk score were featured by higher TMB shown in **Figure 6J** ($p < 0.05$). Our findings suggested that ICB therapy may be effective for HNSCC patients with high-risk subtype.

Construction and Validation of the Nomogram Model

To further predict patients' prognoses, we constructed a nomogram that enrolled all prognosis factors, including age,

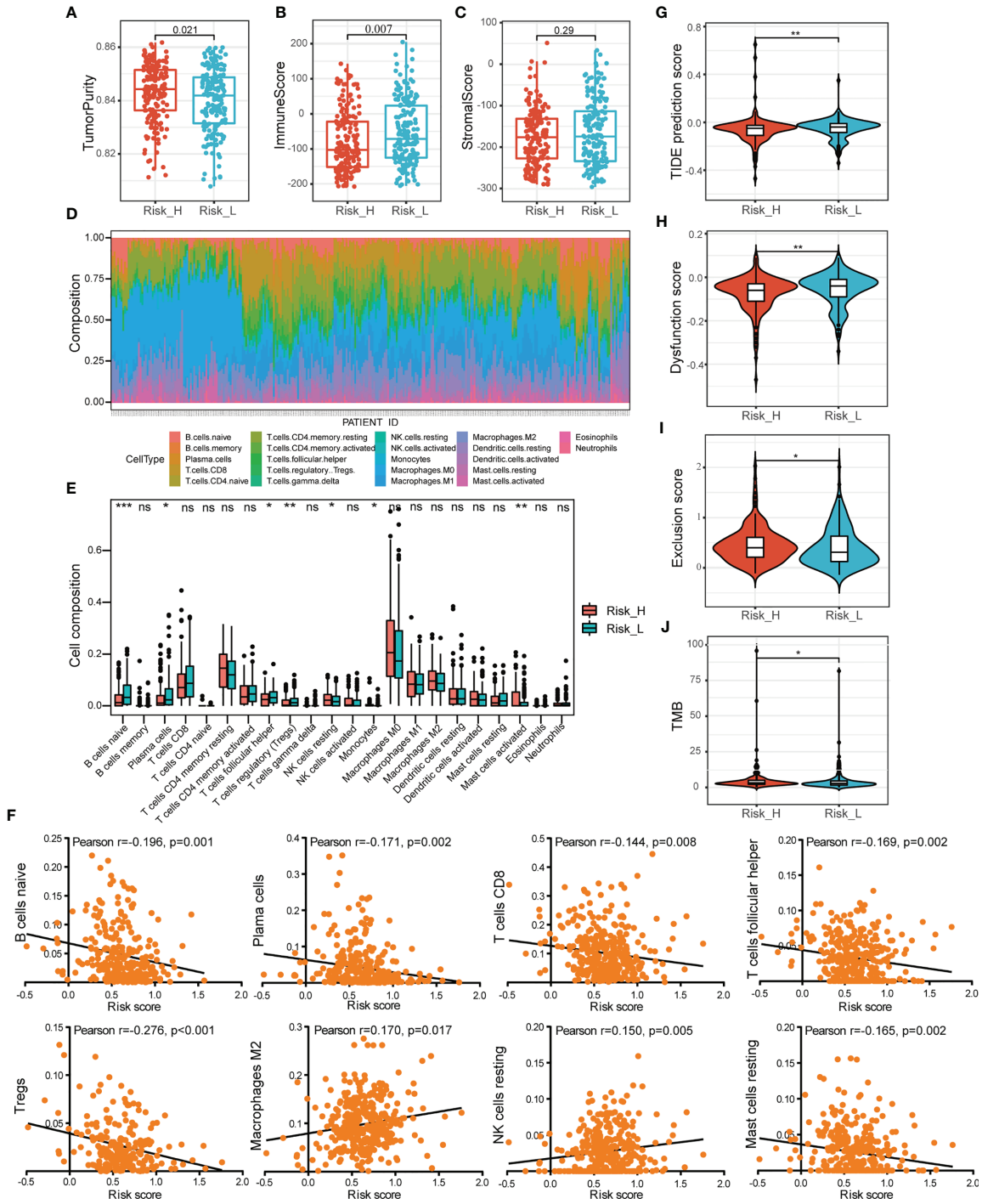

FIGURE 6 | Comprehensive analysis of immune characteristics. **(A–C)** Comparison of the ssGSEA scores (tumor purity, immune and stromal scores) between different risk groups. **(D)** A stacked bar plot presenting the fractions of 22 types of infiltrating immune cell estimated using CIBERSORT algorithm in HNSCC from TCGA training cohort. **(E)** The differences of immune cells infiltration between high- and low-risk groups in boxplots. **(F)** The correlations between immune cells infiltration and risk scores. **(G–I)** The violin plot of different prediction score of TIDE, together with dysfunction score and exclusion score in two groups analyzed by the t-test. **(J)** The difference of TMB in two groups. (ns, $p > 0.05$, $^{*}p < 0.05$; $^{**}p < 0.01$; $^{***}p < 0.001$).

gender, TNM stage, and risk score to quantitatively predict HNSCC prognosis in the TCGA training cohort (**Figure 7A**). It was an assessment that is tailored to an individual HNSCC patient, the estimate probability of 3- and 5-year OS was easy to ascertain by calculating each score for prognosis variables and then gaining the total score on the point scale. Compared to the other prognosis factors, risk score based on MRGs-related signature had the most score points. Calibration curves were developed to validate the nomogram's performance. It showed that the curves were close to the 45° line which was regarded the best prediction (**Figure 7B**). Meanwhile, the AUC for the nomogram model was 0.74 and 0.81, respectively (3-, 5-year OS prediction), which significantly improved the predictive performance, compared to the AUC of risk signature (**Figure 7C**).

DISCUSSION

In this study, we used mRNA expression data together with 4751 MRGs to analyze the overall landscape of imbalance metabolism in HNSCC. Functional analysis confirmed differentially expressed MRGs primarily involved in amino acids, purine and drug metabolism process. We constructed a prognosis-related 10-MRGs signature (ADA, ALG3, CHPF2, CYP4X1, GATM, GPT, HPRT1, HS3ST1, HSD17B6, and LIPE) for establishing risk stratification and predicting clinical outcomes. We found lower risk score suggested better survival outcome, which was also effectively validated by internal and external validation cohorts. The metabolism-related risk score was verified to be an independent prognostic factor of HNSCC. The risk signature was associated with survival status and tumor size. Furthermore, we evaluated the clinical role of risk model for predicting responses to various therapies. We observed that patients in low-risk group were more likely to benefit from the application of chemotherapy. ICB therapy may be efficacious for HNSCC patients in high-risk group. Moreover, we constructed a valuable predictive nomogram model with MRGs-related signature and other prognosis factors, which could work as a better predictive model for survival in clinically application.

The role of most of the 10 identified MRGs in oncogenesis and progression of tumors has been reported. ADA, encoding an enzyme involving the crucial purine metabolism, mainly exerted its function on T lymphocytes proliferation and differentiation (22). Besides, some studies also shown the functionality of HPRT in purine regulation (23). It has been revealed that ADA was served as a potential therapeutic target for breast cancer and a biomarker in oral cancer (24, 25). Increased expression of ALG3 was observed in HNSCC cell line (26). Moreover, ALG3 as a class of glycosyltransferases promotes the proliferation and radiosensitivity of cancer cells and is related with poor prognosis and lymph node metastasis (27, 28). CHPF2 acts as an oncogene that is up-regulated in cancers to exert its positive role in cell proliferation and metastasis, including breast cancer, hepatocellular carcinoma, lung adenocarcinoma, *etc.* (29–31). CYP4X1, a member of the cytochromes P450 family, oxidatively metabolizes a wide range of physiological substrates and plays a potential role in the body in response to cancer chemotherapy (32). Additionally, GATM enhances creatine synthesis in relation to the metabolism of human thermogenic fat (33). GPT is thought to be involved amino acid metabolism and be a novel target for cancer therapy (34). HS3ST1

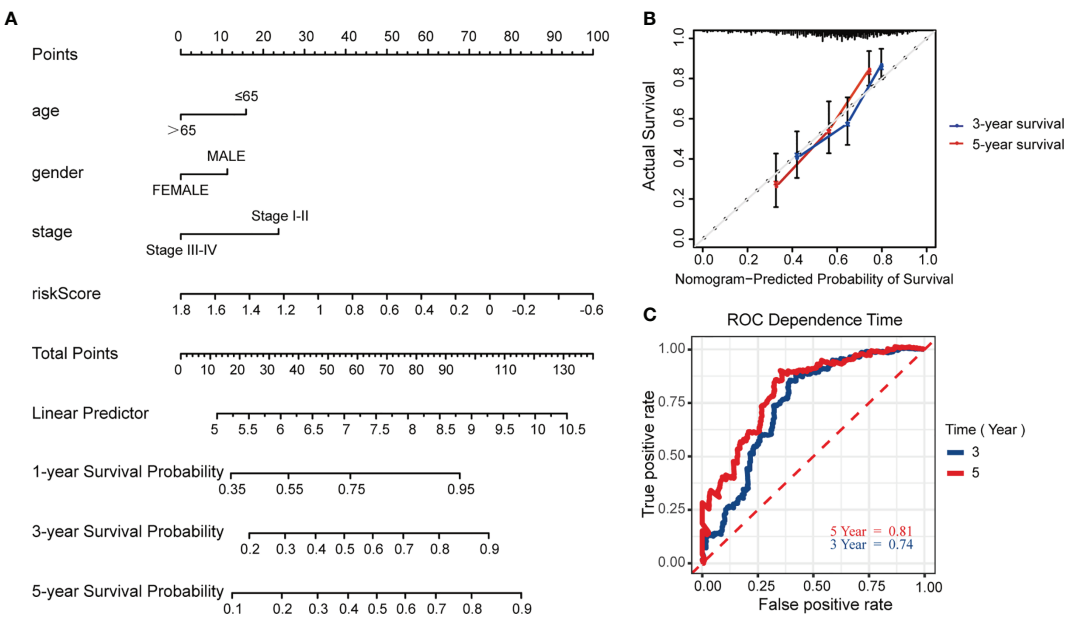

FIGURE 7 | Construction and validation of the predictive nomogram model. **(A)** Nomogram model established by prognosis factors to estimate the survival possibility for 3 and 5 years in HNSCC patients. **(B)** The calibration curves for validation of the nomogram. **(C)** The time-dependent ROC curves of the nomogram of 3-year and 5-year survival rate.

might acts as a molecular biomarker for tumor diagnosis and prognosis (35). HSD17B6 has important functionality in androgen catabolism and was remarkably downregulated in hepatocellular carcinoma, which predicted poor prognosis and high tumor immune infiltrates (36). It was identified that LIPE is up-regulated in cervical cancer and promotes cell proliferation, invasion, and epithelial-mesenchymal transformation (37).

Metabolic reprogramming contributes to patient prognosis, as previous studies demonstrated (9, 38). Recent findings have shown that gene mutations and epigenetic regulation could be triggered by dysfunction metabolism during HNSCC progression (11, 39). Several metabolism-related prognostic biomarkers have been proposed based on gene expression profiles in HNSCC using RNA-Seq technology. Liu and his team developed a new risk model with identified glycolysis-related genes to predict prognosis of HNSCC patients (14). Xiong et al. found lipid metabolism was correlated with worse prognosis and may reflect the immune status of HNSCC patients (15). It was determined that pyruvate catabolism key genes made great progress in HNSCC neoplastic progression (17). Wu et al. provided support for dysregulated metabolism underlying OSCC tumorigenesis (10). Nevertheless, most studies mainly focused on an individual metabolic pathway, which may not sufficiently characterize integrative hallmarks of cancer-related metabolism. In previous study, a metabolism-related signature was identified by several dysregulated metabolic pathways in HNSCC rather than using the common methods based on gene sets, giving the chance to know the impact of abnormal cancer metabolic profiles on survival outcome (40). A comprehensive signature based on multiple MRGs can be better to capture tumorous metabolic changes and have favorable advantage in prognostic prediction (10). Our results also suggested that the risk stratification based on integrative MRGs sets played an important part in HNSCC prognosis and we established a nomogram model with satisfactory predictive value in HNSCC.

HNSCC is a highly heterogeneous malignant tumor with surgery, radiotherapy, chemotherapy, or targeted therapy as single or combinational therapeutic regimens generally (41). In addition, immunotherapy as research hotspot has gained much interest for cancer treatment in recent years. However, only about 20% of patients can benefit from it (42). Accordingly, identification of effective markers contributing to predicting therapeutic response among patients could allow individualization of therapy for HNSCC patients (43, 44). In present study, we found MRGs-related signature could be regarded as an indicator for the efficiency of chemotherapy. However, the survival benefit of HNSCC patients with radiotherapy was to no avail, with probably reason for too much missing clinical information. Compared with conventional therapies, ICB therapy, such as anti-programmed death 1 (PD1) therapy, has been confirmed to obtained indications for treating recurrent or metastatic HNSCC patients in 2016 (42). However, the low response rate becomes the major limitation for survival benefit in patients (41). Deeper characterization of the TME of HNSCC was needed to evaluate the potential predictive role of MRGs signature in tumor immunotherapy.

The immune cell infiltration in the TME plays important roles in the biological behaviors of HNSCC (45). We found patients with superior prognosis and low risk score had higher immune score by ssGSEA algorithm, as demonstrated in several previous studies (46, 47). Additionally, we characterized 22 immune cells infiltration in HNSCC by CIBERSORT algorithm. The infiltration of naive B cells accounted for the most obvious difference in two risk groups, emphasizing their roles in HNSCC. We found the abundance of Tfh, Tregs, and plasma cells were higher in the low-risk group, consisting with the results of Jiang (48). The negative correlation has been recognized between an increasing infiltration of these three cells and a decreased risk score in present study. However, the low-risk group exhibited a higher Tregs infiltration level, which contradicts several previous studies (46, 49, 50). Interestingly, it was found that the monocytes was highly infiltrated in high-risk group, suggesting the HNSCC promoting effect of monocytes in TME (51). What's more, our results further confirmed the speculation from Jin et al. that resting mast cells may inhibit HNSCC malignant progression (49). As a subgroup of T cells, it was demonstrated that CD8+ T cell infiltration indicated better survival outcomes in HNSCC patients (52). Although we didn't observe the difference of CD8+ T cells, the correlation analysis revealed the potential tendency of high infiltration in low-risk group. These findings suggested that infiltrated immune cells may occur complicated communications in different metabolism pattern of HNSCC.

We further explored the predictive performance of MRGs-related risk model in the response of immunotherapy. The potential clinical utility of ICB therapy was reflected by TIDE algorithm, which integrates two mechanisms modeling tumor immune evasion, including the CTL dysfunction and exclusion based on gene expression signatures (21). Our study revealed the low-risk group had higher TIDE suggesting poor responsive to ICB therapy with the mechanism of tumor immune escape contributing to high level infiltration of dysfunctional CTL. The dysfunction signatures of TIDE represent the dysfunctional profiles of late-stage T cell (53). Anti-PD1 therapy can recover the function of the early-stage T cells dysfunction, while the dysfunctional T cells at the late stage are resistant to ICB reprogramming (53). Tumour-infiltrating Tregs were reported to exert their immunosuppressive function which contributing to the failure of anti-PD1 immunotherapy (54), which may explain patients with low risk score had poor response to ICB with high Tregs infiltration. Additionally, investigations have revealed that TMB can trigger T-cell responses and neoantigen-rich tumors may be responding to immunotherapy (55, 56). Compared to overexpressed PD-L1, as a prognostic biomarker in tumor cells, high TMB is regarded as a predictive indicator implicated a greater potential of immunotherapy response (57). The high-risk group in this study had significantly higher TMB, which result in exposing neoantigens continuously and subsequent activating the immune response (56). It further supported our result that patients with high risk score may exhibit a better therapeutic response to ICB.

Despite we constructed a prognostic signature and provide innovative insights for improving HNSCC management, there still exist several limitations in present study. On one hand, the missing data may affect the results to a certain degree, which resulting in the lack of prognostic values of radiotherapy. And our external validation

cohort only consisted of OS, which cannot further validate our signature effectively. The findings need to be validated by more independent cohorts to prove the clinical utility of risk model. Furthermore, further functional experiments require to explore the underlying mechanisms of 10 MRGs in HNSCC. Finally, the links between the immune activity and risk score have not yet been experimentally confirmed. A prospective clinical trial is encouraged to further validate the clinical value of risk model in ICB decision.

CONCLUSION

In conclusion, we constructed a novel 10-metabolic-genes signature and confirmed their prognostic value in HNSCC. Our study also provides potential promising indicators for predicting therapeutic response, which contributing to HNSCC individualized treatment in clinical practice.

DATA AVAILABILITY STATEMENT

Publicly available datasets were analyzed in this study. This data can be found here: https://portal.gdc.cancer.gov/ https://www.ncbi.nlm.nih.gov/gds/.

AUTHOR CONTRIBUTIONS

Conceptualization and writing: YL. Methodology: YW and YP. Software: ZH and XC. Validation: WH. Investigation: TL. Data curation: LW, Formal analysis: WL. Project administration and funding acquisition: SQ. All authors contributed to the article and approved the submitted version.

FUNDING

The project was funded by the grants of Joint Funds for the innovation of science and Technology, Fujian province (2018Y9105); United Fujian Provincial Health and Education Project for Tackling the Key Research, China (2019-WJ-03); Science and Technology Program of Fujian Province, China (2018Y2003); National Natural Science Foundation of China (11974077); and National Natural Science Foundation of China (82072986).

SUPPLEMENTARY MATERIAL

The Supplementary Material for this article can be found online at: https://www.frontiersin.org/articles/10.3389/fonc.2021.685026/full#supplementary-material

REFERENCES

1. Ferlay J, Colombet M, Soerjomataram I, Mathers C, Parkin DM, Piñeros M, et al. Estimating the Global Cancer Incidence and Mortality in 2018: GLOBOCAN Sources and Methods. *Int J Cancer* (2019) 144:1941–53. doi: 10.1002/ijc.31937
2. Chow LQM. Head and Neck Cancer. *N Engl J Med* (2020) 382:60–72. doi: 10.1056/NEJMra1715715
3. Zhang XM, Song LJ, Shen J, Yue H, Han YQ, Yang CL, et al. Prognostic and Predictive Values of Immune Infiltrate in Patients With Head and Neck Squamous Cell Carcinoma. *Hum Pathol* (2018) 82:104–12. doi: 10.1016/j.humpath.2018.07.012
4. Alsahafi E, Begg K, Amelio I, Raulf N, Lucarelli P, Sauter T, et al. Clinical Update on Head and Neck Cancer: Molecular Biology and Ongoing Challenges. *Cell Death Dis* (2019) 10:540. doi: 10.1038/s41419-019-1769-9
5. Lee YA, Li S, Chen Y, Li Q, Chen CJ, Hsu WL, et al. Tobacco Smoking, Alcohol Drinking, Betel Quid Chewing, and the Risk of Head and Neck Cancer in an East Asian Population. *Head Neck* (2019) 41:92–102. doi: 10.1002/hed.25383
6. Satriano L, Lewinska M, Rodrigues PM, Banales JM, Andersen JB. Metabolic Rearrangements in Primary Liver Cancers: Cause and Consequences. *Nat Rev Gastroenterol Hepatol* (2019) 16:748–66. doi: 10.1038/s41575-019-0217-8
7. Kato Y, Maeda T, Suzuki A, Baba Y. Cancer Metabolism: New Insights Into Classic Characteristics. *Jpn Dent Sci Rev* (2018) 54:8–21. doi: 10.1016/j.jdsr.2017.08.003
8. Leemans CR, Snijders PJF, Brakenhoff RH. The Molecular Landscape of Head and Neck Cancer. *Nat Rev Cancer* (2018) 18:269–82. doi: 10.1038/nrc.2018.11
9. Cairns RA, Harris IS, Mak TW. Regulation of Cancer Cell Metabolism. *Nat Rev Cancer* (2011) 11:85–95. doi: 10.1038/nrc2981
10. Wu X, Yao Y, Li Z, Ge H, Wang D, Wang Y. Identification of a Transcriptional Prognostic Signature From Five Metabolic Pathways in Oral Squamous Cell Carcinoma. *Front Oncol* (2020) 10:572919. doi: 10.3389/fonc.2020.572919
11. Yang J, Guo Y, Seo W, Zhang R, Lu C, Wang Y, et al. Targeting Cellular Metabolism to Reduce Head and Neck Cancer Growth. *Sci Rep* (2019) 9:4995. doi: 10.1038/s41598-019-41523-4
12. Huo J, Wu L, Zang Y, Dong H, Liu X, He F, et al. Eight-Gene Metabolic Signature Related With Tumor-Associated Macrophages Predicting Overall Survival for Hepatocellular Carcinoma. *BMC Cancer* (2021) 21:31. doi: 10.1186/s12885-020-07734-z
13. Wang L, Li X. Identification of an Energy Metabolism–Related Gene Signature in Ovarian 558 Cancer Prognosis. *Oncol Rep* (2020) 43:1755–70. doi: 10.3892/or.2020.7548
14. Liu Y, Yin S. A Novel Prognostic Index Based on the Analysis of Glycolysis-Related Genes in Head and Neck Squamous Cell Carcinomas. *J Oncol* (2020) 2020:7353874. doi: 10.1155/2020/7353874
15. Xiong Y, Si Y, Feng Y, Zhuo S, Cui B, Zhang Z. Prognostic Value of Lipid Metabolism-Related Genes in Head and Neck Squamous Cell Carcinoma. *Immun Inflamm Dis* (2021) 9:196–209. doi: 10.1002/iid3.379
16. Hu Q, Peng J, Chen X, Li H, Song M, Cheng B, et al. Obesity and Genes Related to Lipid Metabolism Predict Poor Survival in Oral Squamous Cell Carcinoma. *Oral Oncol* (2019) 89:14–22. doi: 10.1016/j.oraloncology.2018.12.006
17. Chen TY, Hsieh YT, Huang JM, Liu CJ, Chuang LT, Huang PC, et al. Determination of Pyruvate Metabolic Fates Modulates Head and Neck Tumorigenesis. *Neoplasia* (2019) 21:641–52. doi: 10.1016/j.neo.2019.04.007
18. Yarchoan M, Hopkins A, Jaffee EM. Tumor Mutational Burden and Response Rate to PD-1 Inhibition. *N Engl J Med* (2017) 377:2500–1. doi: 10.1056/NEJMc1713444
19. Lohavanichbutr P, Méndez E, Holsinger FC, Rue TC, Zhang Y, Houck J, et al. A 13-Gene Signature Prognostic of HPV-Negative OSCC: Discovery and External Validation. *Clin Cancer Res* (2013) 19:1197–203. doi: 10.1158/1078-0432.CCR-12-2647
20. Possemato R, Marks KM, Shaul YD, Pacold ME, Kim D, Birsoy K, et al. Functional Genomics Reveal That the Serine Synthesispathway Is Essential in Breast Cancer. *Nature* (2011) 476:346–50. doi: 10.1038/nature10350

21. Fu J, Li K, Zhang W, Wan C, Zhang J, Jiang P, et al. Large-Scale Public Data Reuse to Model Immunotherapy Response and Resistance. *Genome Med* (2020) 12:21. doi: 10.1186/s13073-020-0721-z
22. Pacheco R, Martinez-Navio JM, Lejeune M, Climent N, Oliva H, Gatell JM, et al. CD26, Adenosine Deaminase, and Adenosine Receptors Mediate Costimulatory Signals in the Immunological Synapse. *Proc Natl Acad Sci U S A* (2005) 102:9583–8. doi: 10.1073/pnas.0501050102
23. Townsend MH, Robison RA, O'Neill KL. A Review of HPRT and its Emerging Role in Cancer. *Med Oncol* (2018) 35:89. doi: 10.1007/s12032-018-1144-1
24. Kutryb-Zajac B, Koszalka P, Mierzejewska P, Bulinska A, Zabielska MA, Brodzik K, et al. Adenosine Deaminase Inhibition Suppresses Progression of 4T1 Murine Breast Cancer by Adenosine Receptor-Dependent Mechanisms. *J Cell Mol Med* (2018) 22:5939–54. doi: 10.1111/jcmm.13864
25. Kelgandre DC, Pathak J, Patel S, Ingale P, Swain N. Adenosine Deaminase - A Novel Diagnostic and Prognostic Biomarker for Oral Squamous Cell Carcinoma. *Asian Pac J Cancer Prev* (2016) 17:1865–8. doi: 10.7314/apjcp.2016.17.4.1865
26. Zhou H, Cao T, Li WP, Wu G. Combined Expression and Prognostic Significance of PPFIA1 and ALG3 in Head and Neck Squamous Cell Carcinoma. *Mol Biol Rep* (2019) 46:2693–701. doi: 10.1007/s11033-019-04712-y
27. Sun X, He Z, Guo L, Wang C, Lin C, Ye L, et al. ALG3 Contributes to Stemness and Radioresistance Through Regulating Glycosylation of TGF-β Receptor II in Breast Cancer. *J Exp Clin Cancer Res* (2021) 40:149. doi: 10.1186/s13046-021-01932-8
28. Ke SB, Qiu H, Chen JM, Shi W, Han C, Gong Y, et al. ALG3 Contributes to the Malignancy of Non-Small Cell Lung Cancer and Is Negatively Regulated by MiR-98-5p. *Pathol Res Pract* (2020) 216:152761. doi: 10.1016/j.prp.2019.152761
29. Li Y, Gong H, Feng L, Mao D, Xiao Y, Wang Y, et al. Chondroitin Polymerizing Factor Promotes Breast Carcinoma Cell Proliferation, Invasion and Migration and Affects Expression of Epithelial-Mesenchymal Transition-Related Markers. *FEBS Open Bio* (2021) 11:423–34. doi: 10.1002/2211-5463.13062
30. Xu Q, Lin W, Tao C, Huang X, Li J. Chondroitin Polymerizing Factor (CHPF) Contributes to Malignant Proliferation and Migration of Hepatocellular Carcinoma Cells. *Biochem Cell Biol* (2020) 98:362–9. doi: 10.1139/bcb-2019-0227
31. Hou XM, Zhang T, Da Z, Wu XA. CHPF Promotes Lung Adenocarcinoma Proliferation and Anti-Apoptosis Via the MAPK Pathway. *Pathol Res Pract* (2019) 215:988–94. doi: 10.1016/j.prp.2019.02.005
32. Hlaváč V, Václavíková R, Brynychová V, Ostašov P, Koževnikovová R, Kopečková K, et al. Role of Genetic Variation in Cytochromes P450 in Breast Cancer Prognosis and Therapy Response. *Int J Mol Sci* (2021) 22:2826. doi: 10.3390/ijms22062826
33. Kazak L, Chouchani ET, Lu GZ, Jedrychowski MP, Bare CJ, Mina AI, et al. Genetic Depletion of Adipocyte Creatine Metabolism Inhibits Diet-Induced Thermogenesis and Drives Obesity. *Cell Metab* (2017) 26:660–71.e3. doi: 10.1016/j.cmet.2017.08.009
34. Cao Y, Lin SH, Wang Y, Chin YE, Kang L, Mi J. Glutamic Pyruvate Transaminase GPT2 Promotes Tumorigenesis of Breast Cancer Cells by Activating Sonic Hedgehog Signaling. *Theranostics* (2017) 7:3021–33. doi: 10.7150/thno.18992
35. Zhang G, Wang H, Zhu K, Yang Y, Li J, Jiang H, et al. Investigation of Candidate Molecular Biomarkers for Expression Profile Analysis of the Gene Expression Omnibus (GEO) in Acute Lymphocytic Leukemia (ALL). *BioMed Pharmacother* (2019) 120:109530. doi: 10.1016/j.biopha.2019.109530
36. Lv L, Zhao Y, Wei Q, Zhao Y, Yi Q. Downexpression of HSD17B6 Correlates With Clinical Prognosis and Tumor Immune Infiltrates in Hepatocellular Carcinoma. *Cancer Cell Int* (2020) 20:210. doi: 10.1186/s12935-020-01298-5
37. Zhang J, Jiang P, Wang S, Cheng W, Fu S. LncRNA LIPE-AS1 Predicts Poor Survival of Cervical Cancer and Promotes its Proliferation and Migration Via Modulating miR-195-5p/MAPK Pathway. *Front Oncol* (2021) 11:639980. doi: 10.3389/fonc.2021.639980
38. Pavlova NN, Thompson CB. The Emerging Hallmarks of Cancer Metabolism. *Cell Metab* (2016) 23:27–47. doi: 10.1016/j.cmet.2015.12.006
39. Hsieh YT, Chen YF, Lin SC, Chang KW, Li WC. Targeting Cellular Metabolism Modulates Head and Neck Oncogenesis. *Int J Mol Sci* (2019) 20:3960. doi: 10.3390/ijms20163960
40. Xing L, Guo M, Zhang X, Zhang X, Liu F. A Transcriptional Metabolic Gene-Set Based Prognostic Signature Is Associated With Clinical and Mutational Features in Head and Neck Squamous Cell Carcinoma. *J Cancer Res Clin Oncol* (2020) 146:621–30. doi: 10.1007/s00432-020-03155-4
41. Sacco AG, Cohen EE. Current Treatment Options for Recurrent or Metastatic Head and Neck Squamous Cell Carcinoma. *J Clin Oncol* (2015) 33:3305–13. doi: 10.1200/JCO.2015.62.0963
42. Seiwert TY, Burtness B, Mehra R, Weiss J, Berger R, Eder JP, et al. Safety and Clinical Activity of Pembrolizumab for Treatment of Recurrent or Metastatic Squamous Cell Carcinoma of the Head and Neck (KEYNOTE-012): An Open-Label, Multicentre, Phase 1b Trial. *Lancet Oncol* (2016) 17:956–65. doi: 10.1016/S1470-2045(16)30066-3
43. Cao W, Liu JN, Liu Z, Wang X, Han ZG, Ji T, et al. A Three-lncRNA Signature Derived From the Atlas of ncRNA in Cancer (TANRIC) Database Predicts the Survival of Patients With Head and Neck Squamous Cell Carcinoma. *Oral Oncol* (2017) 65:94–101. doi: 10.1016/j.oraloncology.2016.12.017
44. Wu K, Jiang Y, Zhou W, Zhang B, Li Y, Xie F, et al. Long Noncoding RNA RC3H2 Facilitates Cell Proliferation and Invasion by Targeting microRNA-101-3p/EZH2 Axis in OSCC. *Mol Ther Nucleic Acids* (2020) 20:97–110. doi: 10.1016/j.omtn.2020.02.006
45. Chen Y, Li ZY, Zhou GQ, Sun Y. An Immune-Related Gene Prognostic Index for Head and Neck Squamous Cell Carcinoma. *Clin Cancer Res* (2021) 27:330–41. doi: 10.1158/1078-0432.CCR-20-2166
46. Liang JY, Wang DS, Lin HC, Chen XX, Yang H, Zheng Y, et al. A Novel Ferroptosis-Related Gene Signature for Overall Survival Prediction in Patients With Hepatocellular Carcinoma. *Int J Biol Sci* (2020) 16:2430–41. doi: 10.7150/ijbs.45050
47. Zhou YJ, Zhu GQ, Lu XF, Zheng KI, Wang QW, Chen JN, et al. Identification and Validation of Tumour Microenvironment-Based Immune Molecular Subgroups for Gastric Cancer: Immunotherapeutic Implications. *Cancer Immunol Immunother* (2020) 69:1057–69. doi: 10.1007/s00262-020-02525-8
48. Jiang X, Gao Y, Zhang N, Yuan C, Luo Y, Sun W, et al. Establishment of Immune-Related Gene Pair Signature to Predict Lung Adenocarcinoma Prognosis. *Cell Transplant* (2020) 29:963689720977131. doi: 10.1177/0963689720977131
49. Liang B, Tao Y, Wang T. Profiles of Immune Cell Infiltration in Head and Neck Squamous Carcinoma. *Biosci Rep* (2020) 40:BSR20192724. doi: 10.1042/BSR20192724
50. Zhang M, Wang X, Chen X, Zhang Q, Hong J. Novel Immune-Related Gene Signature for Risk Stratification and Prognosis of Survival in Lower-Grade Glioma. *Front Genet* (2020) 11:363. doi: 10.3389/fgene.2020.00363
51. Liu YZ, Saito S, Morris GF, Miller CA3rd, Li J, Lefante JJ. Proportions of Resting Memory T Cells and Monocytes in Blood Have Prognostic Significance in Idiopathic Pulmonary Fibrosis. *Genomics* (2019) 111:1343–50. doi: 10.1016/j.ygeno.2018.09.006
52. She Y, Kong X, Ge Y, Yin P, Liu Z, Chen J, et al. Immune-Related Gene Signature for Predicting the Prognosis of Head and Neck Squamous Cell Carcinoma. *Cancer Cell Int* (2020) 20:22. doi: 10.1186/s12935-020-1104-7
53. Jiang P, Gu S, Pan D, Fu J, Sahu A, Hu X, et al. Signatures of T Cell Dysfunction and Exclusion Predict Cancer Immunotherapy Response. *Nat Med* (2018) 24:1550–8. doi: 10.1038/s41591-018-0136-1
54. Soundararajan R, Fradette JJ, Konen JM, Moulder S, Zhang X, Gibbons DL, et al. Targeting the Interplay Between Epithelial-to-Mesenchymal-Transition and the Immune System for Effective Immunotherapy. *Cancers (Basel)* (2019) 11:714. doi: 10.3390/cancers11050714
55. Godec J, Tan Y, Liberzon A, Tamayo P, Bhattacharya S, Butte AJ, et al. Compendium of Immune Signatures Identifies Conserved and Species-Specific Biology in Response to Inflammation. *Immunity* (2016) 44:194–206. doi: 10.1016/j.immuni.2015.12.006
56. Gavrielatou N, Doumas S, Economopoulou P, Foukas PG, Psyrri A. Biomarkers for Immunotherapy Response in Head and Neck Cancer. *Cancer Treat Rev* (2020) 84:101977. doi: 10.1016/j.ctrv.2020.101977

57. George AP, Kuzel TM, Zhang Y, Zhang B. The Discovery of Biomarkers in Cancer Immunotherapy. *Comput Struct Biotechnol J* (2019) 17:484–97. doi: 10.1016/j.csbj.2019.03.015

Conflict of Interest: The authors declare that the research was conducted in the absence of any commercial or financial relationships that could be construed as a potential conflict of interest.

Copyright © 2021 Li, Weng, Pan, Huang, Chen, Hong, Lin, Wang, Liu and Qiu. This is an open-access article distributed under the terms of the Creative Commons Attribution License (CC BY). The use, distribution or reproduction in other forums is permitted, provided the original author(s) and the copyright owner(s) are credited and that the original publication in this journal is cited, in accordance with accepted academic practice. No use, distribution or reproduction is permitted which does not comply with these terms.

frontiers in Oncology

ORIGINAL RESEARCH
published: 13 July 2021
doi: 10.3389/fonc.2021.616576

LncRNA FENDRR in Carcinoma-Associated Fibroblasts Regulates the Angiogenesis of Oral Squamous Cell Carcinoma Through the PI3K/AKT Pathway

Yuming Xu[1†], *Erhui Jiang*[1†], *Zhe Shao*[1,2*] *and Zhengjun Shang*[1,2*]

[1] *The State Key Laboratory Breeding Base of Basic Science of Stomatology (Hubei-MOST) & Key Laboratory of Oral Biomedicine Ministry of Education, School & Hospital of Stomatology, Wuhan University, Wuhan, China,* [2] *Department of Oral and Maxillofacial Head Neck Surgery, School & Hospital of Stomatology, Wuhan University, Wuhan, China*

OPEN ACCESS

Edited by:
Wei Cao,
Shanghai Jiao Tong University, China

Reviewed by:
Yanjie Zhang,
Shanghai Jiao Tong University, China
Zheqi Liu,
Shanghai Jiao Tong University, China

***Correspondence:**
Zhe Shao
shaozhe@whu.edu.cn
Zhengjun Shang
shangzhengjun@whu.edu.cn

[†]*These authors have contributed equally to this work*

Specialty section:
This article was submitted to Head and Neck Cancer, a section of the journal Frontiers in Oncology

Received: *12 October 2020*
Accepted: *13 April 2021*
Published: *13 July 2021*

Citation:
Xu Y, Jiang E, Shao Z and Shang Z (2021) LncRNA FENDRR in Carcinoma-Associated Fibroblasts Regulates the Angiogenesis of Oral Squamous Cell Carcinoma Through the PI3K/AKT Pathway. Front. Oncol. 11:616576. doi: 10.3389/fonc.2021.616576

Angiogenesis is essential for the development of tumors. Studies have shown that carcinoma-associated fibroblasts (CAFs) are involved in regulating tumor angiogenesis, but the mechanism remains unclear. Recently, long noncoding RNAs (lncRNAs) have been proved to play an important role in the angiogenesis of various tumors. However, there is currently no research involving the regulation of CAFs on the angiogenesis of oral squamous cell carcinoma (OSCC) mediated by lncRNAs. By analyzing microarray data, we identified that the expression of lncRNA FOXF1 adjacent noncoding developmental regulatory RNA (FENDRR) in OSCC patients is downregulated, compared to that in normal tissues. Quantitative polymerase chain reaction (qPCR) results demonstrated that FENDRR expression is lower in CAFs compared to normal fibroblasts (NFs) of OSCC patients. KEGG pathway analysis revealed that some genes differentially expressed between CAFs and NFs of HNSCC patients are enriched to the PI3K/AKT pathway. Further experiments confirmed that the downregulation of FENDRR can activate the PI3K/AKT pathway in NFs and enhances the expression of matrix metalloproteinase 9 (MMP9). The overexpression of FENDRR had the opposite effect. Besides, we co-cultured human umbilical vein endothelial cells (HUVECs) with CAFs, and the tube-forming ability of HUVECs co-cultured with CAFs overexpressing FENDRR decreased significantly. However, activation of the AKT pathway of CAFs overexpressing FENDRR can weaken the inhibitory effect of FENDRR on angiogenesis. In summary, our experiments are focused on the influence of lncRNAs in CAFs on OSCC angiogenesis for the first time and prove that FENDRR mediates CAFs' regulation of OSCC angiogenesis through the PI3K/AKT pathway.

Keywords: LncRNA, angiogenesis, OSCC, PI3K - AKT pathway, CAFs, FENDRR

INTRODUCTION

Oral squamous cell carcinoma (OSCC) is the most common type of head and neck squamous cell carcinoma (HNSCC) which ranks sixth among cancers worldwide (1). The prognosis of patients with OSCC is poor, especially for metastatic patients, whose 5-year survival rate is only about 40% (2). Angiogenesis is a critical factor leading to the low survival rate of OSCC patients, which has been illustrated to be closely related to the metastasis of OSCC (3, 4). The formation of new blood vessels around the tumor facilitates the tumor's access to oxygen and nutrients. Besides, the increased permeability of newly formed blood vessels is conducive to the metastasis of tumor cells (5, 6). Therefore, controlling angiogenesis plays an important role in the fight against cancer.

Carcinoma-associated fibroblasts (CAFs), often known as activated fibroblasts, are generally derived from the tissue-resident normal fibroblasts (NFs) and can promote tumor angiogenesis by secreting higher levels of proteolytic enzymes, such as matrix metalloproteinase 9 (MMP9) (7). Recently, The proangiogenic effect of CAFs has been demonstrated in various cancers, such as breast cancer (8), melanoma (9), and colorectal cancer (10). However, few studies have addressed the role of CAFs in OSCC angiogenesis.

Long noncoding RNAs (lncRNAs) are a subtype of RNA with a length of more than 200 nucleotides that have little or no coding potential (11). To date, lncRNAs have been found to be abnormally expressed in various cancers, such as colon cancer (12), gastric cancer (13), and cervical cancer (14), and regulate tumor angiogenesis through different mechanisms. In addition, some lncRNAs were demonstrated to be differentially expressed in OSCC (15), regulate OSCC development (16), and can be used as prognostic biomarkers for OSCC (17). Moreover, studies have confirmed that the abnormal expression of lncRNAs has a non-negligible effect on the biological function of CAFs (18, 19). However, there has been no research involving the role of lncRNAs in the proangiogenic effect of CAFs derived from OSCC.

Herein, for the first time, we explored the regulation of lncRNAs on the proangiogenic effect of CAFs derived from OSCC. Our experiments show that lncRNA FENDRR, downregulated in CAFs derived from OSCC, can inhibit the proangiogenic effect of CAFs through the PI3K/AKT pathway, which makes FENDRR a potential therapeutic target for anti-angiogenic therapy of OSCC treatment.

MATERIALS AND METHODS

GEO Data Download and Annotation

An OSCC microarray profiling dataset (GSE9844) and a fibroblasts RNA-seq dataset (GSE83314) were downloaded from the GEO database (https://www.ncbi.nlm.nih.gov/geo/query/acc.cgi?acc=GSE9844 and https://www.ncbi.nlm.nih.gov/geo/query/acc.cgi?acc=GSE83314). The "hgu133plus2.db" package was used to perform probe reannotation for the GSE9844 profiling dataset. The "FactoMineR" and "factoextra" packages were used to perform the principal component analysis (PCA). GSE9844 profiling data was used to verify the differential expression of FENDRR in OSCC tissues compared with normal tissues. The "ggpubr" package was used to draw statistical charts. The RNA-seq dataset GSE83314 was used to identify differentially expressed genes in CAFs compared with NFs using the "edgeR" package in R software. $|\text{Fold Change}| > 1$ and $P < 0.05$ were set as the statistical threshold of differentially expressed genes.

KEGG Pathways Enrichment Analysis and Survival Analysis

The "clusterProfiler" package was used to perform the Kyoto Encyclopedia of Genes and Genomes (KEGG) pathways enrichment analysis. Differentially expressed genes in CAFs compared with NFs were used for enrichment analysis. The statistical threshold of enriched pathways was set to $P < 0.05$. The survival analysis was performed using the GEPIA database (http://gepia.cancer-pku.cn/) (20). Quartile was used as the Group Cutoff. $P < 0.05$ was considered to be significant.

Antibodies and Reagents

MMP9 antibody was obtained from Proteintech (Wuhan, China). β-actin antibody, anti-rabbit IgG, and anti-mouse IgG were acquired from Abbkine (CA, USA). AKT1, phospho-AKT1 (P-AKT1), phosphatidylinositol-3-kinase (PI3K), phospho-PI3K (P-PI3K), and vimentin antibodies were purchased from Cell Signaling Technology (MA, USA). FAP antibody was obtained from Abcam (Cambridge, England). Matrigel used for tube formation assay was acquired from Corning (NY, USA). Bicinchoninic acid protein assay kit used to measure the protein concentration was purchased from Thermo Fisher. Trizol reagent for RNA extraction was obtained from Takara (Kyoto, Japan). SC79 was acquired from TOPSCIENCE (Shanghai, China).

Cell Culture

The CAFs and NFs were isolated from 7 OSCC patients according to a previous study (21). To put it simply, the OSCC tissues and normal tissues were cut into 1-2 mm size tissue blocks, and then put into a 15 ml centrifuge tube and washed with PBS (phosphate buffered saline) containing 5% double antibiotics (Penicillin and Streptomycin) for 8 times. Subsequently, the tissue blocks were inoculated to the bottom of the culture bottle and put into a constant temperature cell incubator. After 4-6 hours, 1 ml of complete medium containing 20% FBS was added. When it was observed that the cells crawling out between different tissue blocks come into contact, cell passage can be carried out. All procedures conformed with the Ethics Committee of School and Hospital of Stomatology at Wuhan University. The OSCC cell lines SCC25 and CAL27 were purchased from the China Center for Type Culture Collection (Shanghai, China). The OSCC cell lines SCC4, SCC9, and HN4

were kindly provided by Doctor Xinmiao-Wang. The fibroblasts, HN4 and CAL27 were cultured in high-glucose Dulbecco's modified Eagle's medium (DMEM) (HyClone, UT, USA) containing 10% fetal bovine serum (FBS) (Natocor, Córdoba, Argentina). The SCC4, SCC9, and SCC25 were cultivated in DMEM:F12 (1:1) containing 10% FBS. The HUVECs were purchased from ScienCell (CA, USA) and cultured in endothelial cell medium (ECM) (ScienCell, CA, USA) containing 5% FBS (ScienCell, CA, USA). The human immortalized oral epithelial cells (HIOECs) were kindly provided by Professor Cheng-zhang Li and Doctor Zhen-Zhang and were cultured in KGM gold (Lonza, MD, USA) containing 5% FBS (Lonza, MD, USA). All cells were cultivated in a 5% CO_2 environment at 37°C.

Cell Immunofluorescence

On the first day, we seeded CAFs and NFs cells in 24-well plates. When the cell confluence reached 70%-90%, the cells were fixed with paraformaldehyde, washed 3 times with PBS solution, and then blocked with BSA for 1 hour. Finally, the cells were incubated with the primary antibody overnight at 4°C. The next day, the cells were incubated with the second fluorescent antibody for 1 hour. Nuclear staining was performed using DAPI and the images of stained cells were obtained using a Fluorescence microscope (Carl Zeiss, Germany).

Cell Migration Assay

The co-culture model of CAFs and HUVECs was established using Transwell membrane chambers (24-well plate, 8-μm pore size, 6.5-mm insert) acquired from Corning (NY, USA). The CAFs transfected with FENDRR lentiviral vectors (Lent-FENDRR) or negative control vectors (Lent-NC) were seeded into the lower chambers at a density of $3x10^5$ cells per well, cultured for 24 hours. Subsequently, $2.5x10^5$ HUVECs were seeded in serum-free medium in the upper chambers. After 48 hours of incubation, the cells on the chambers were fixed and stained with crystal violet. Finally, five random fields were selected to count the number of cells traversing to the reverse face.

In Situ Hybridization

In situ hybridization (ISH) was performed with digoxigenin-labeled FENDRR probe: 5′-DIG-CAGTGGTTGCTGGGGT TGAAGAGAGGGATGAATA-DIG-3′, following the instructions of the ISH kit purchased from Boster (CA, USA). The slices of 4 pairs of OSCC and normal oral mucosa tissues were treated with conventional dewaxing, rehydration, and then 3% hydrogen peroxide at room temperature for 20 minutes. Then, the slices were digested with pepsin diluted with 3% citric acid at room temperature for 20 minutes to expose RNA fragments. Next, the slices were pre-hybridized for 4 hours and hybridized with FENDRR probe (1.5 ug/ml) overnight. Then the slices were blocked with blocking fluid, followed by incubation with biotinylated mouse anti-digoxigenin and avidin-biotin peroxidase. Finally, a DAB kit (Mxb Bio, China) and hematoxylin were used for visualization. The score used for statistical analyses were calculated as: 1.0*(%Weak positive) + 2.0*(%Positive) + 3.0*(%Strong positive), using Aperio ImageScope (Leica, Germany) (22).

RNA Isolation and Real-Time PCR

Total RNA was extracted from cells using Trizol reagent, which was subsequently reversely transcribed into cDNA using the PrimeScript RT Reagent Kit (Takara, Kyoto, Japan). Real-time quantitative PCR, conducted on a QuantStudio™ 6 Flex (Life Technologies, USA), was performed by using the SYBR® Premix Ex Taq™ II Kit (Takara Bio). The primers synthesized by Sangon Biotech (Shanghai, China) were as follows: FENDRR (forward 5'-GTGATGCAGTTGCTGGCAAA-3' and reverse 5'-CAGTTG ACTGCAAAGCACCC-3') and glyceraldehyde-3-phosphate dehydrogenase (GAPDH) (forward 5'-GGAGCGAGATCC CTCCAAAAT-3' and reverse 5'-GGCTGTTGTCATACTTCT CATGG-3'). RNA expression levels, normalized to that of GAPDH, were calculated using the $2^{-\triangle\triangle Ct}$ method.

Western Blotting Analysis

The total protein of cells was extracted on ice using a mammalian protein extraction reagent (MPER) (Thermo Fisher Scientific) containing protease and phosphatase inhibitors (MilliporeSigma), whose concentration was then measured with a bicinchoninic acid protein assay kit. Next, loading buffer (5x) purchased from Beyotime (Shanghai, China) was added into the protein solutions and heated for 10 minutes at 95°C. 10 ug of protein samples were subjected into 10% SDS-PAGE (60 V, 30 minutes; 120 V, 65 minutes), and then transferred to polyvinylidene fluoride membrane (MilliporeSigma) in the electroblotting buffer (100 V, 53 minutes). Subsequently, at room temperature, the membranes were blocked with 5% nonfat milk in Tris-buffered saline for 1.5 hours and then inoculated with antibodies overnight at 4°C. Finally, the bound antibodies were detected using horseradish peroxidase-conjugated anti-rabbit IgG or anti-mouse IgG.

Lentivirus Vectors and Short Interfering RNAs

FENDRR lentiviral vectors and negative control vectors were purchased from Hanbio (Shanghai, China). The siRNAs targeting FENDRR (si-FENDRR) and negative control siRNAs (si-NC) were purchased from RiboBio (Guangzhou, China). Before transfection, CAFs or NFs were seeded into 6-well plates and cultured to achieve cell confluency of about 50%. For lentiviral vectors transfection, CAFs were treated with vectors for 24 hours. The mixture in the plates was then replaced with fresh medium. For siRNAs transfection, NFs were treated with siRNAs and transfection reagents for 48 hours. The efficiency of transfection was confirmed by using Real-Time PCR after 48 hours. The target sequences of siRNAs were as follows: si-FENDRR1 (CCAGCCATGTGATTCCAAA), si-FENDRR2 (CCACAGAGCTTCATAGAAT).

Tube Formation Assay

The co-culture model of CAFs and HUVECs was established using Transwell membrane chambers (24-well plate, 0.4-μm pore size, 6.5-mm insert) acquired from Corning (NY, USA). The CAFs transfected with Lent-FENDRR or Lent-NC were seeded into the upper chambers at a density of $3x10^5$ cells per well, cultured for 24 hours. Subsequently, the HUVECs were seeded into the lower chambers precoated with Matrigel (BD Biosciences, San Jose, CA, USA) at a density of $2.5x10^4$ cells per well. Then, the upper and lower chambers were placed together to co-culture CAFs and HUVECs. After 8 hours of incubation, the images of the capillary-like structure were taken using a microscope (Carl Zeiss, Germany).

Tumor Xenografts in Nude Mice

The experiment was approved by the Review Board of the Ethics Committee of the Hospital of Stomatology at Wuhan University. A mixture of CAL27 (2×10^6) cells and CAFs (5×10^5) in 50 ul PBS with 50 ul Matrigel was inoculated subcutaneously into the flanks of the female BALB/c nude mice (18–20 g; Beijing Vital River Laboratory Animal Technology Co., Ltd., Beijing, China). After 23 days, the mice were euthanized, and the tumor tissues were excised and analyzed. The tumor volumes were calculated according to the formula (width^2 × length)/2 (23).

Statistical Analysis

GraphPad Prism 7.0 was used for statistical analysis, and the statistical significance of the differences between groups was determined by Student's t-test or Wilcoxon test. The results are expressed as means ± SD. When P <0.05, the results were considered to be statistically significant.

RESULTS

CAFs and NFs Were Extracted From the Tissues of 7 OSCC Patients

Through the optical microscope, we observed that NFs are mostly slender spindle-shaped and relatively uniform in shape, while CAFs are diverse in shape, mainly short spindle-shaped and polygonal, which accords with the functional diversity of CAFs (**Figure 1A**). Besides, the results of cellular immunofluorescence and western blotting showed that the expression of α-SMA (smooth muscle alpha-actin), vimentin, and FAP (fibroblast activation protein), three markers of CAFs, in CAFs were significantly stronger than that in NFs, which indicated that the primary cells we extracted conformed to the characteristics of CAFs (**Figures 1B, C**).

FENDRR Is Low Expressed in OSCC Tissues and CAFs Derived From OSCC

Through PCA (**Figure 2A**), 12 groups of data from GSE9844 dataset were used for differential expression analysis (GSM248652, GSM248655, GSM248658, GSM248660, GSM248687, GSM248780, GSM248665, GSM248668, GSM248677, GSM248678, GSM248682, GSM248685). The results showed that FENDRR is low expressed in OSCC tissues (**Figure 2B**). To further explore the expression

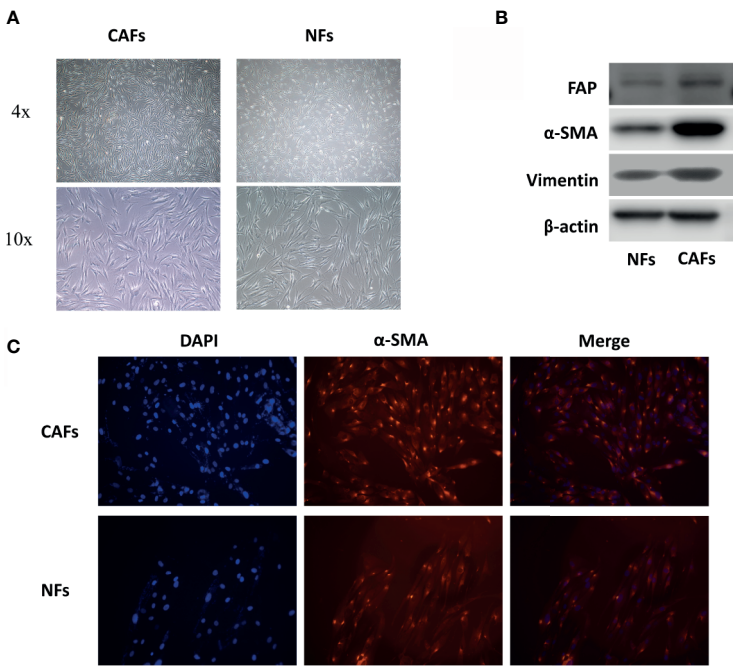

FIGURE 1 | CAFs and NFs were extracted from the tissues of 7 OSCC patients. **(A)** The morphology of CAFs and NFs. **(B)** The results of western blotting of α-SMA, FAP, and vimentin in CAFs and NFs. **(C)** The results of cellular immunofluorescence experiments of α-SMA in CAFs and NFs.

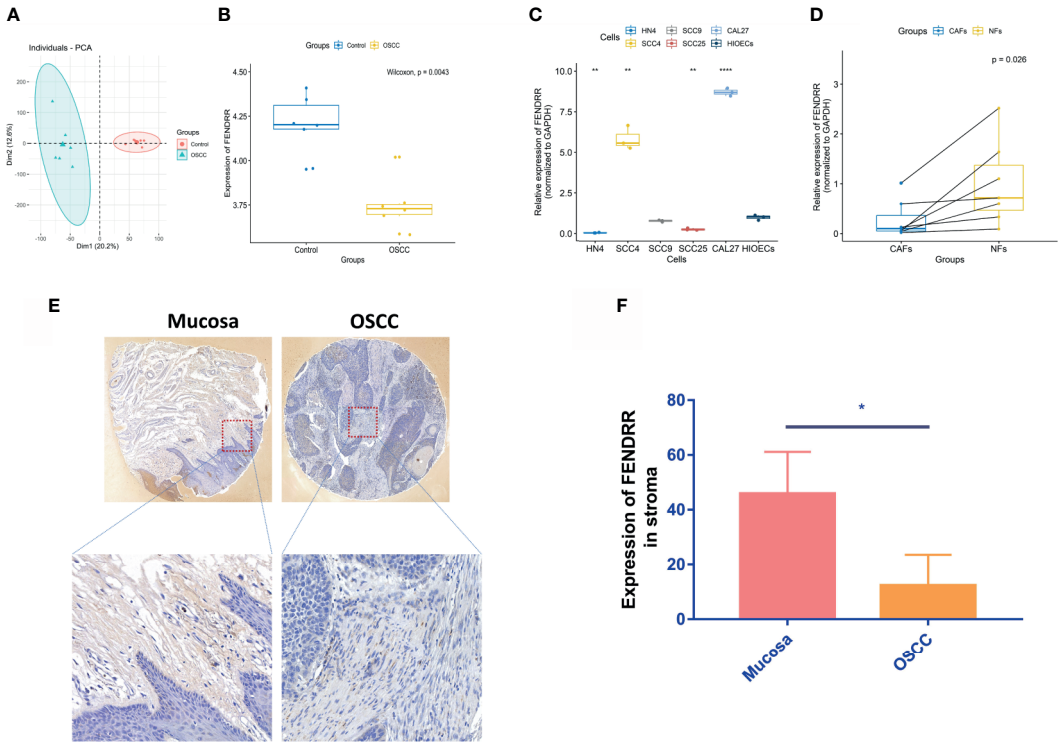

FIGURE 2 | Gene expression analyses of FENDRR. **(A)** 12 groups of data from the GSE9844 dataset were selected through PCA. **(B)** Selected 12 groups were used for differential expression analysis of FENDRR in OSCC and negative control. **(C)** Real-time PCR was used to detect the expression of FENDRR in SCC4, SCC9, SCC25, CAL27, HN4, and HIOECs. **(D)** Real-time PCR was used to detect the expression of FENDRR in 7 pairs of CAFs and NFs derived from OSCC tissues. **(E, F)** The expression of FENDRR in 4 pairs of OSCC and mucosal tissues was detected using ISH. $^{*}P < 0.05$, $^{**}P < 0.01$, $^{****}P < 0.0001$.

of FENDRR in OSCC, we extracted the RNA of HIOECs, SCC4, SCC9, SCC25, CAL27, HN4, and 7 pairs of CAFs and NFs isolated from 7 OSCC patients. Interestingly, FENDRR is low expressed in HN4 and SCC25 compared to that in HIOECs, but highly expressed in SCC4 and CAL27 (**Figure 2C**). However, FENDRR is stably low expressed in CAFs compared to that in NFs (**Figure 2D**). Furthermore, the results of ISH indicated that FENDRR is mainly expressed in the stroma, and the expression level of FENDRR in the normal oral mucosal stroma is significantly higher than that in OSCC stroma (**Figures 2E, F**). Taking the lower expression level of FENDRR in OSCC tissues into account, we speculated that FENDRR may have a more significant effect on fibroblasts.

FENDRR Inhibits the Proangiogenic Effect of CAFs

Our previous studies confirmed that CAFs can promote the angiogenesis of melanoma (9). To explore the effect of FENDRR on the proangiogenic ability of OSCC-derived CAFs, we used lentiviral vectors to overexpress FENDRR in CAFs derived from OSCC. Real-time PCR was used to confirm the transfection effect. The results showed that FENDRR was significantly overexpressed in CAFs transfected with lent-FENDRR (**Figure 3A**). Subsequently, the CAFs transfected with Lent-FENDRR or Lent-NC were utilized to perform the migration and tube formation experiments. As shown in **Figures 3B–E**, the migration and tube-forming ability of HUVECs co-cultured with CAFs transfected with FENDRR was significantly suppressed, indicating that FENDRR can inhibit the proangiogenic ability of OSCC-derived CAFs.

Survival Analysis and KEGG Analysis

Angiogenesis is an essential factor leading to the low survival rate of OSCC patients (3, 4). Considering that FENDRR can weaken the angiogenesis of OSCC, we next performed the survival analysis of FENDRR using the GEPIA database. The results exhibited that HNSCC patients with high expression of FENDRR have a better prognosis (**Figure 4A**), which can further indicate that FENDRR may influence the progress of OSCC mainly by regulating fibroblasts. To further explore the possible effects of FENDRR on CAFs, we used the HNSCC dataset GSE83314, which contains two pairs of OSCC-derived CAFs and NFs, for differential expression analysis, and the differentially expressed genes were subsequently utilized for KEGG analysis. The results showed that genes differentially expressed between CAFs and NFs of HNSCC patients are mainly enriched to the PI3K/AKT pathway (**Figures 4B, C**).

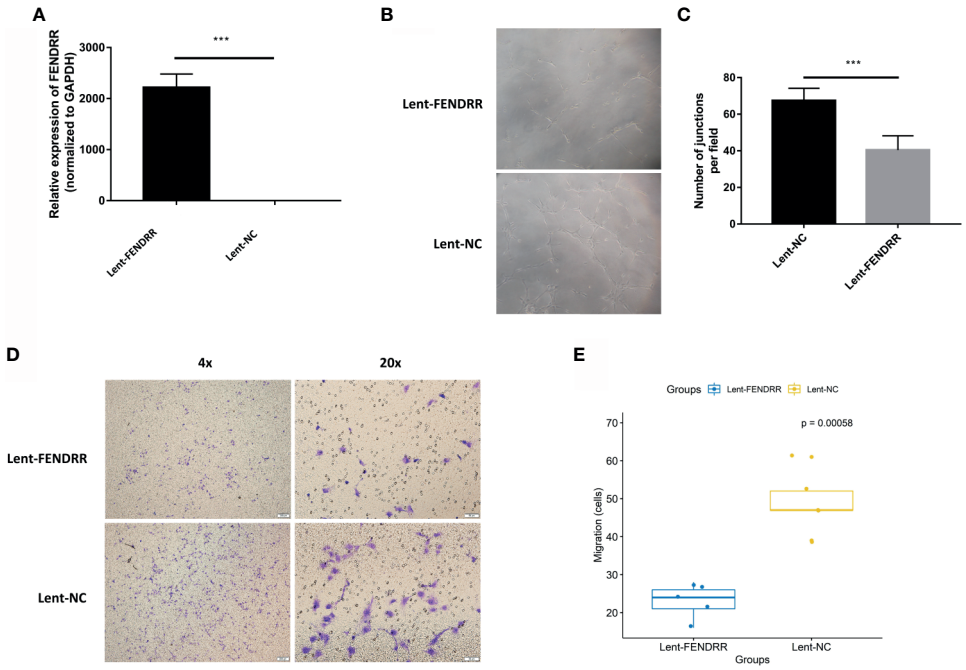

FIGURE 3 | FENDRR inhibits the proangiogenic effect of CAFs. **(A)** FENDRR was significantly overexpressed in CAFs transfected with lent-FENDRR. **(B, C)** The number of the capillary-like structure formed by HUVECs co-cultured with CAFs transfected with Lent-FENDRR was significantly reduced. **(D, E)** The migration assay showed that CAFs transfected with Lent-FENDRR could inhibit the migration ability of HUVECs. ***$P < 0.001$.

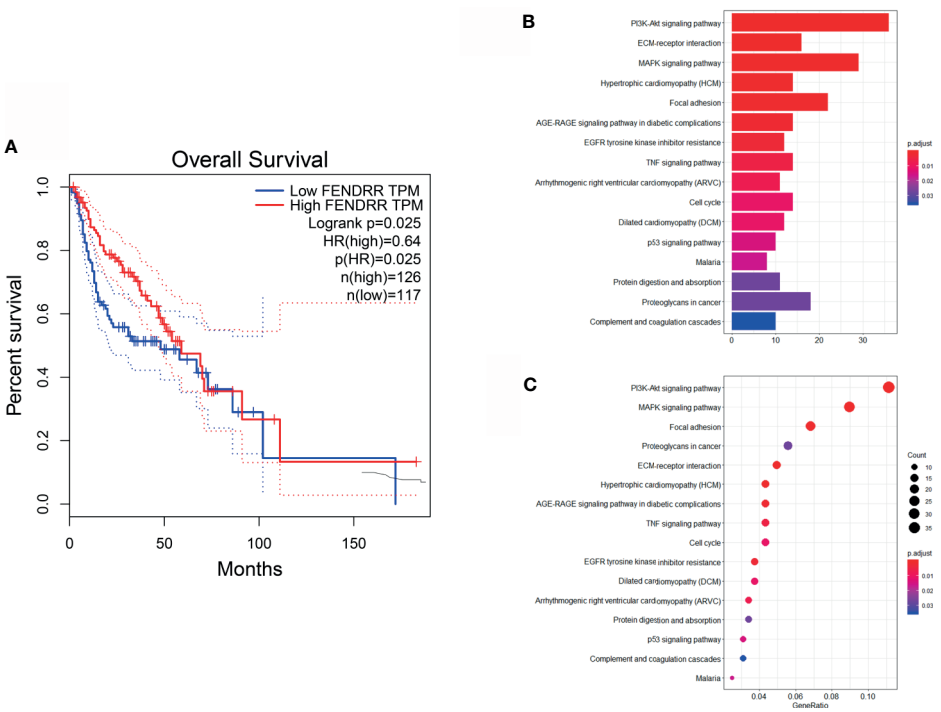

FIGURE 4 | Survival analysis and KEGG analysis. **(A)** Survival analysis showed that HNSCC patients with high expression of FENDRR have a better prognosis. **(B, C)** KEGG analysis showed that genes differentially expressed between CAFs and NFs derived from HNSCC patients are mainly enriched to the PI3K/AKT pathway.

FENDRR Inhibits the Activation of the PI3K/AKT Pathway

Our previous study had demonstrated that the activation of the PI3K/AKT can promote the angiogenesis of OSCC (24). Herein, we continue to explore the influence of FENDRR on the PI3K/AKT pathway in CAFs. On the one hand, we used siRNAs to reduce the expression of FENDRR in NFs. On the other hand, lent-FENDRR and its negative control were used to overexpress FENDRR in CAFs. As shown in **Figure 5A**, the si-FENDRR2 has a better silencing effect than si-FENDRR1, so we chose si-FENDRR2 for subsequent knockdown experiments. Our results showed that the downregulation of FENDRR can activate the PI3K/AKT pathway in NFs and enhance the expression of MMP9. Consistently, the overexpression of FENDRR had opposite effects in CAFs (**Figure 5B**).

FENDRR Inhibits the Proangiogenic Effect of CAFs Through the PI3K/AKT Pathway

To further explore whether FENDRR regulates the proangiogenic ability of CAFs through the PI3K/AKT pathway, we used SC79, a selective AKT activator (25), to activate the PI3K/AKT pathway in CAFs overexpressing FENDRR derived from OSCC, which then were used to perform the tube formation experiments. As shown in **Figures 5C, D**, the tube-forming ability of HUVECs co-cultured with SC79-treated CAFs transfected with FENDRR was significantly enhanced, indicating that FENDRR may inhibit the proangiogenic ability of OSCC-derived CAFs through the PI3K/AKT pathway.

CAFs Overexpressing FENDRR Inhibit OSCC Progression *In Vivo*

To investigate the impact of FENDRR in CAFs on the progression of OSCC, the nude mice were divided into Lent-NC and Lent-FENDRR groups. CAL27 cells were mixed with CAFs transfected with Lent-NC and Lent-FENDRR respectively, and subcutaneously injected into nude mice. On the 23rd day, the tumors were excised and analyzed. The volume and weight of tumors in the Lent-FENDRR group significantly decreased compared with those in the Lent-NC group (**Figures 6A–D**). *In vivo* results showed that the high expression of FENDRR in CAFs can inhibit the progression of OSCC.

DISCUSSION

LncRNAs have been illustrated to play an important role in regulating the angiogenesis of various cancers (12–14). For example, Wang et al. reported that lncRNA HITT (HIF-1α

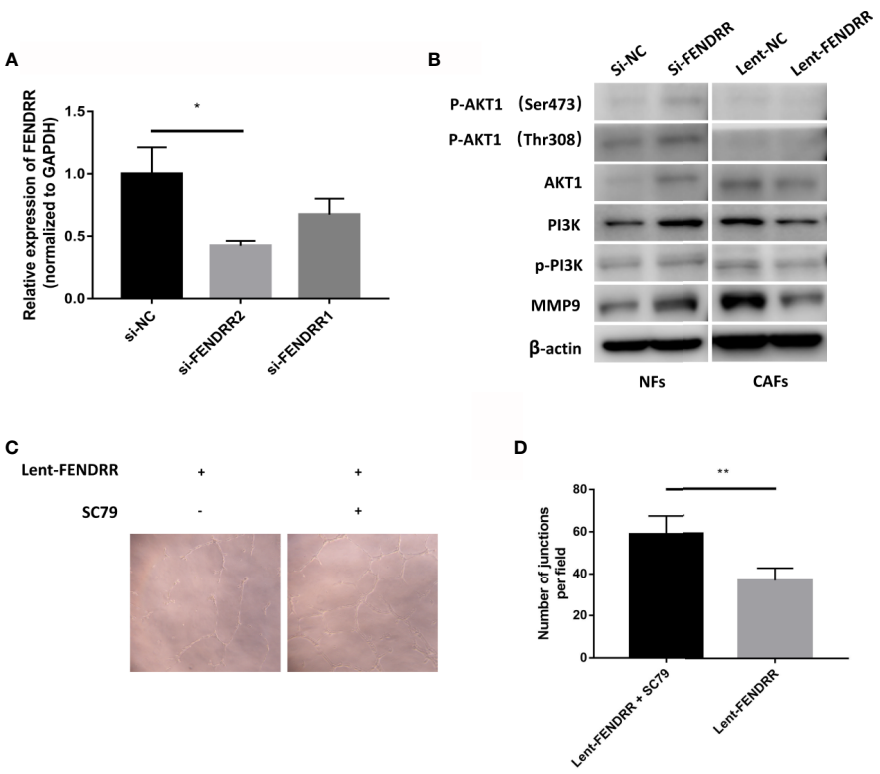

FIGURE 5 | FENDRR inhibits the activation of the PI3K/AKT pathway. **(A)** The silencing effect of siRNAs. **(B)** Western blotting analyses of PI3K/AKT pathway-related genes showed that the knockdown of FENDRR activated the PI3K/AKT pathway in NFs, while the overexpression of FENDRR weakened the activation of the PI3K/AKT pathway in CAFs. **(C, D)** The number of the capillary-like structure formed by HUVECs co-cultured with SC79-treated CAFs transfected with Lent-FENDRR increased significantly. $^{*}P < 0.05$, $^{**}P < 0.01$.

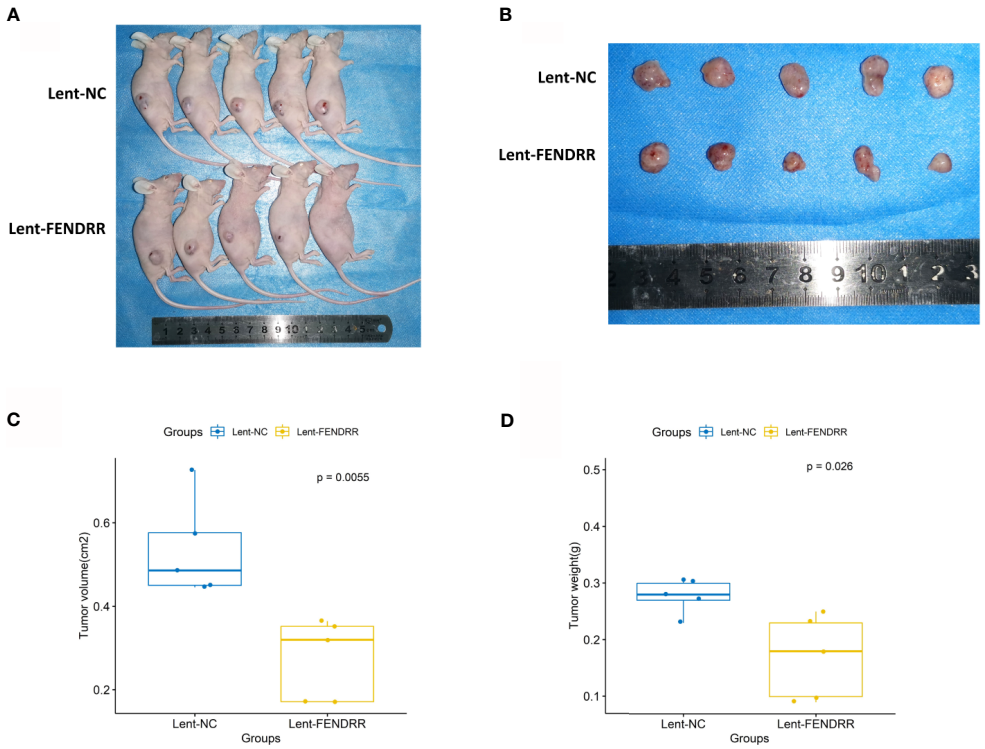

FIGURE 6 | Overexpression of FENDRR in CAFs inhibits the progression of OSCC *in vivo*. **(A)** Images of nude mice from the Lent-NC and Lent-FENDRR groups. **(B)** Xenograft tumors excised from nude mice. **(C)** Volumes of the xenograft tumors excised from nude mice. **(D)** Weights of the xenograft tumors excised from nude mice.

inhibitor at translation level) can inhibit the angiogenesis of colon cancer by reducing the translation of HIF-1α in cancer cells (12). Besides, the proangiogenic effect of CAFs has also been confirmed by a large number of experiments (9, 10). However, there is currently no research involving the regulation of CAFs on the angiogenesis of OSCC mediated by lncRNAs. Therefore, in this research, we studied the role of FENDRR in the proangiogenic effect of CAFs derived from OSCC.

FENDRR is a long noncoding RNA located on chr3q13.31. Studies have shown that FENDRR is low expressed in a variety of tumor tissues and can inhibit tumor progression (26, 27). However, the role of FENDRR in the development of OSCC is still unknown. By analyzing high-throughput data, we found that FENDRR is low expressed in OSCC tissues compared with normal tissues. Furthermore, survival analysis showed that the low expression of FENDRR is related to the poor prognosis of HNSCC patients. Given that OSCC is the most common type of HNSCC (1), we speculated that FENDRR may also affect the progress of OSCC. Thus, we used Real-Time PCR to detect the expression of FENDRR in CAL27 and HIOECs, as well as 7 pairs of CAFs and NFs isolated from tissue samples of 7 OSCC patients. Interestingly, our results showed that FENDRR is low expressed in HN4 and SCC25 compared to that in HIOECs, but highly expressed in SCC4 and CAL27. However, FENDRR is stably low expressed in CAFs compared to that in NFs. Furthermore, the results of ISH indicated that FENDRR was mainly expressed in the stroma, and the expression level of FENDRR in the normal oral mucosal stroma was significantly higher than that in the OSCC stroma. Considering that the overall expression level of FENDRR in HNSCC tissues is decreased and patients with high FENDRR expression have a better prognosis, we speculated that FENDRR may influence the progress of OSCC mainly by regulating fibroblasts.

In our previous study, it had been shown that CAFs can facilitate melanoma angiogenesis, and the expression of the angiogenic factor MMP9 in CAFs is upregulated compared with that in NFs (9). Research by Li et al. confirmed that CAFs derived from OSCC can also promote the tube-forming ability of HUVECs (28). However, the role of lncRNAs in the proangiogenic effect of OSCC-derived CAFs is still unclear. In our study, the proangiogenic ability of CAFs overexpressing FENDRR was significantly reduced, and whether it was knockdown or overexpression of FENDRR, the expression level of MMP9 was opposite to that of FENDRR, which indicated that FENDRR may play an important role in the angiogenesis of OSCC regulated by CAFs.

MMP9 is an important angiogenic factor that has been proved to be regulated by multiple signaling pathways, such as PI3K/AKT pathway (29), ERK pathway (30), and JAK/STAT pathway (31). On the one hand, the activation of the PI3K/AKT pathway can enhance the mRNA and protein expression of MMP9 (29). On the other hand, our previous study demonstrated that the activation of the PI3K/AKT can promote the angiogenesis of OSCC (24).

Herein, our results showed that the overexpression of FENDRR inhibited the PI3K/AKT signaling pathway in CAFs and decreased the expression level of MMP9. In addition, activation of the AKT pathway of CAFs overexpressing FENDRR can weaken the inhibitory effect of FENDRR on angiogenesis, which suggested that FENDRR may regulate the proangiogenic effect of CAFs derived from OSCC through the PI3K/AKT pathway.

At present, the specific mechanism by which FENDRR regulates the PI3K/AKT pathway is still unclear, and how CAFs overexpressing FENDRR affect the angiogenic ability of HUVECs still needs to be further explored.

CONCLUSIONS

In general, our research has initially verified that lncRNA FENDRR regulates the proangiogenic ability of CAFs derived from OSCC through the PI3K/AKT pathway, which provides a theoretical basis for subsequent research.

DATA AVAILABILITY STATEMENT

The raw data supporting the conclusions of this article will be made available by the authors, without undue reservation.

ETHICS STATEMENT

The animal study was reviewed and approved by the Review Board of the Ethics Committee of the Hospital of Stomatology at Wuhan University.

AUTHOR CONTRIBUTIONS

YX and EJ: conceived and designed the experiments, and contributed equally to this work. YX: analyzed the data and drafted the manuscript. ZJS and ZS: contributed to experimental studies and revised the manuscript. All authors contributed to the article and approved the submitted version.

FUNDING

This study was supported by grants from the National Natural Science Foundation of China 81772897, 81672666, and the Natural Science Foundation of Hubei Province 2019CFB503.

REFERENCES

1. Ketabat F, Pundir M, Mohabatpour F, Lobanova L, Koutsopoulos S, Hadjiiski L, et al. Controlled Drug Delivery Systems for Oral Cancer Treatment-Current Status and Future Perspectives. *Pharmaceutics* (2019) 11(7):302. doi: 10.3390/pharmaceutics11070302
2. Zanoni DK, Montero PH, Migliacci JC, Shah JP, Wong RJ, Ganly I, et al. Survival Outcomes After Treatment of Cancer of the Oral Cavity (1985-2015). *Oral Oncol* (2019) 90:115–21. doi: 10.1016/j.oraloncology.2019.02.001
3. Sakata J, Hirosue A, Yoshida R, Kawahara K, Matsuoka Y, Yamamoto T, et al. HMGA2 Contributes to Distant Metastasis and Poor Prognosis by Promoting Angiogenesis in Oral Squamous Cell Carcinoma. *Int J Mol Sci* (2019) 20 (10):2473. doi: 10.3390/ijms20102473
4. Sasahira T, Kirita T, Kurihara M, Yamamoto K, Bhawal UK, Bosserhoff AK, et al. MIA-Dependent Angiogenesis and Lymphangiogenesis are Closely Associated With Progression, Nodal Metastasis and Poor Prognosis in Tongue Squamous Cell Carcinoma. *Eur J Cancer* (2010) 46(12):2285–94. doi: 10.1016/j.ejca.2010.04.027
5. Fang JH, Zhang ZJ, Shang LR, Luo YW, Lin YF, Yuan Y, et al. Hepatoma Cell-Secreted Exosomal microRNA-103 Increases Vascular Permeability and Promotes Metastasis by Targeting Junction Proteins. *Hepatology* (2018) 68 (4):1459–75. doi: 10.1002/hep.29920
6. Zeng Z, Li Y, Pan Y, Lan X, Song F, Sun J, et al. Cancer-Derived Exosomal miR-25-3p Promotes Pre-Metastatic Niche Formation by Inducing Vascular Permeability and Angiogenesis. *Nat Commun* (2018) 9(1):5395. doi: 10.1038/s41467-018-07810-w
7. Zhou Y, Ren H, Dai B, Li J, Shang L, Huang J, et al. Hepatocellular Carcinoma-Derived Exosomal miRNA-21 Contributes to Tumor Progression by Converting Hepatocyte Stellate Cells to Cancer-Associated Fibroblasts. *J Exp Clin Cancer Res* (2018) 37(1):324. doi: 10.1186/s13046-018-0965-2
8. Calvo F, Ege N, Grande-Garcia A, Hooper S, Jenkins RP, Chaudhry SI, et al. Mechanotransduction and YAP-Dependent Matrix Remodelling Is Required for the Generation and Maintenance of Cancer-Associated Fibroblasts. *Nat Cell Biol* (2013) 15(6):637–46. doi: 10.1038/ncb2756
9. Zhou X, Yan T, Huang C, Xu Z, Wang L, Jiang E, et al. Melanoma Cell-Secreted Exosomal miR-155-5p Induce Proangiogenic Switch of Cancer-Associated Fibroblasts *via* SOCS1/JAK2/STAT3 Signaling Pathway. *J Exp Clin Cancer Res* (2018) 37(1):242. doi: 10.1186/s13046-018-0911-3
10. Pape J, Magdeldin T, Stamati K, Nyga A, Loizidou M, Emberton M, et al. Cancer-Associated Fibroblasts Mediate Cancer Progression and Remodel the Tumouroid Stroma. *Br J Cancer* (2020) 123(7):1178–90. doi: 10.1038/s41416-020-0973-9
11. Slavoff SA, Mitchell AJ, Schwaid AG, Cabili MN, Ma J, Levin JZ, et al. Peptidomic Discovery of Short Open Reading Frame-Encoded Peptides in Human Cells. *Nat Chem Biol* (2013) 9(1):59–64. doi: 10.1038/nchembio.1120
12. Wang X, Li L, Zhao K, Lin Q, Li H, Xue X, et al. A Novel LncRNA HITT Forms a Regulatory Loop With HIF-1α to Modulate Angiogenesis and Tumor Growth. *Cell Death Differ* (2020) 27(4):1431–46. doi: 10.1038/s41418-019-0449-8
13. Zhao J, Du P, Cui P, Qin Y, Hu C, Wu J, et al. LncRNA PVT1 Promotes Angiogenesis *Via* Activating the STAT3/VEGFA Axis in Gastric Cancer. *Oncogene* (2018) 37(30):4094–109. doi: 10.1038/s41388-018-0250-z
14. Ding X, Jia X, Wang C, Xu J, Gao SJ, Lu C. A DHX9-lncRNA-MDM2 Interaction Regulates Cell Invasion and Angiogenesis of Cervical Cancer. *Cell Death Differ* (2019) 26(9):1750–65. doi: 10.1038/s41418-018-0242-0
15. Liu Z, Zhou W, Lin C, Wang X, Zhang X, Zhang Y, et al. Dysregulation of FOXD2-AS1 Promotes Cell Proliferation and Migration and Predicts Poor Prognosis in Oral Squamous Cell Carcinoma: A Study Based on TCGA Data. *Aging (Albany NY)* (2020) 13(2):2379–96. doi: 10.18632/aging.202268
16. Wu K, Jiang Y, Zhou W, Zhang B, Li Y, Xie F, et al. Long Noncoding RNA RC3H2 Facilitates Cell Proliferation and Invasion by Targeting MicroRNA-101-3p/EZH2 Axis in OSCC. *Mol Ther Nucleic Acids* (2020) 20:97–110. doi: 10.1016/j.omtn.2020.02.006
17. Cao W, Liu JN, Liu Z, Wang X, Han ZG, Ji T, et al. A Three-lncRNA Signature Derived From the Atlas of ncRNA in Cancer (TANRIC) Database Predicts the Survival of Patients With Head and Neck Squamous Cell Carcinoma. *Oral Oncol* (2017) 65:94–101. doi: 10.1016/j.oraloncology.2016.12.017
18. Ren J, Ding L, Zhang D, Shi G, Xu Q, Shen S, et al. Carcinoma-Associated Fibroblasts Promote the Stemness and Chemoresistance of Colorectal Cancer by Transferring Exosomal lncRNA H19. *Theranostics* (2018) 8(14):3932–48. doi: 10.7150/thno.25541
19. Zhao L, Ji G, Le X, Wang C, Xu L, Feng M, et al. Long Noncoding RNA LINC00092 Acts in Cancer-Associated Fibroblasts to Drive Glycolysis and

Progression of Ovarian Cancer. *Cancer Res* (2017) 77(6):1369–82. doi: 10.1158/0008-5472.Can-16-1615
20. Tang Z, Li C, Kang B, Gao G, Li C, Zhang Z. GEPIA: A Web Server for Cancer and Normal Gene Expression Profiling and Interactive Analyses. *Nucleic Acids Res* (2017) 45(W1):W98–w102. doi: 10.1093/nar/gkx247
21. Wang X, Lu T, Wen J, Xu L, Zeng D, Wu Q, et al. Selective Responses of Human Gingival Fibroblasts and Bacteria on Carbon Fiber Reinforced Polyetheretherketone With Multilevel Nanostructured TiO2. *Biomaterials* (2016) 83:207–18. doi: 10.1016/j.biomaterials.2016.01.001
22. Riaz SM, Bjune GA, Wiker HG, Sviland L, Mustafa T. Mycobacterial Antigens Accumulation in Foamy Macrophages in Murine Pulmonary Tuberculosis Lesions: Association With Necrosis and Making of Cavities. *Scand J Immunol* (2020) 91(4):e12866. doi: 10.1111/sji.12866
23. Naito S, von Eschenbach AC, Giavazzi R, Fidler IJ. Growth and Metastasis of Tumor Cells Isolated From a Human Renal Cell Carcinoma Implanted Into Different Organs of Nude Mice. *Cancer Res* (1986) 46(8):4109–15.
24. Wang H, Wang L, Zhou X, Luo X, Liu K, Jiang E, et al. OSCC Exosomes Regulate miR-210-3p Targeting EFNA3 to Promote Oral Cancer Angiogenesis Through the PI3K/AKT Pathway. *BioMed Res Int* (2020) 2020:2125656. doi: 10.1155/2020/2125656
25. So EY, Ouchi T. BRAT1 Deficiency Causes Increased Glucose Metabolism and Mitochondrial Malfunction. *BMC Cancer* (2014) 14:548. doi: 10.1186/1471-2407-14-548
26. Yu Z, Zhao H, Feng X, Li H, Qiu C, Yi X, et al. Long Non-Coding RNA FENDRR Acts as a miR-423-5p Sponge to Suppress the Treg-Mediated Immune Escape of Hepatocellular Carcinoma Cells. *Mol Ther Nucleic Acids* (2019) 17:516–29. doi: 10.1016/j.omtn.2019.05.027
27. Chen XE, Chen P, Chen S, Lu J, Ma T, Shi G, et al. Long Non-Coding RNA FENDRR Inhibits Migration and Invasion of Cutaneous Malignant Melanoma Cells. *Biosci Rep* (2020) 40(3):BSR20191194. doi: 10.1042/bsr20191194
28. Li J, Liu X, Zang S, Zhou J, Zhang F, Sun B, et al. Small Extracellular Vesicle-Bound Vascular Endothelial Growth Factor Secreted by Carcinoma-Associated Fibroblasts Promotes Angiogenesis in a Bevacizumab-Resistant Manner. *Cancer Lett* (2020) 492:71–83. doi: 10.1016/j.canlet.2020.08.030
29. Yue Y, Hui K, Wu S, Zhang M, Que T, Gu Y, et al. MUC15 Inhibits Cancer Metastasis *Via* PI3K/AKT Signaling in Renal Cell Carcinoma. *Cell Death Dis* (2020) 11(5):336. doi: 10.1038/s41419-020-2518-9
30. Siu MKY, Jiang YX, Wang JJ, Leung THY, Han CY, Tsang BK, et al. Hexokinase 2 Regulates Ovarian Cancer Cell Migration, Invasion and Stemness *Via* FAK/ERK1/2/MMP9/NANOG/SOX9 Signaling Cascades. *Cancers (Basel)* (2019) 11(6):813. doi: 10.3390/cancers11060813
31. Boukhedouni N, Martins C, Darrigade AS, Drullion C, Rambert J, Barrault C, et al. Type-1 Cytokines Regulate MMP-9 Production and E-Cadherin Disruption to Promote Melanocyte Loss in Vitiligo. *JCI Insight* (2020) 5 (11):e133772. doi: 10.1172/jci.insight.133772

Conflict of Interest: The authors declare that the research was conducted in the absence of any commercial or financial relationships that could be construed as a potential conflict of interest.

Copyright © 2021 Xu, Jiang, Shao and Shang. This is an open-access article distributed under the terms of the Creative Commons Attribution License (CC BY). The use, distribution or reproduction in other forums is permitted, provided the original author(s) and the copyright owner(s) are credited and that the original publication in this journal is cited, in accordance with accepted academic practice. No use, distribution or reproduction is permitted which does not comply with these terms.

frontiers in Oncology

ORIGINAL RESEARCH
published: 13 July 2021
doi: 10.3389/fonc.2021.616372

Identification and Confirmation of the miR-30 Family as a Potential Central Player in Tobacco-Related Head and Neck Squamous Cell Carcinoma

Tingting Zhang[1,2,3†], Xueqin Zhu[1,2†], Qiang Sun[1,2,4], Xing Qin[1,2], Zhen Zhang[1,2], Yuanyong Feng[5], Ming Yan[1,2] and Wantao Chen[1,2,4*]*

[1] Department of Oral Maxillofacial Head and Neck Oncology, Shanghai Ninth People's Hospital, Shanghai Jiao Tong University School of Medicine, College of Stomatology, Shanghai Jiao Tong University, Shanghai, China, [2] National Center for Stomatology, National Clinical Research Center for Oral Diseases, Shanghai Key Laboratory of Stomatology, Shanghai, China, [3] Department of Oral and Maxillofacial Surgery, Stomatological Hospital, Tianjin Medical University, Tianjin, China, [4] Department of Oral and Maxillofacial Surgery, The First Affiliated Hospital of Zhengzhou University, Zhengzhou, China, [5] Department of Oral and Maxillofacial Surgery, the Affiliated Hospital of Qingdao University, Qingdao, China

OPEN ACCESS

Edited by:
Qiang Shen, Louisiana State University, United States

Reviewed by:
Dengfeng Li, Tongji University, China
Lin Fang, Tongji University, China

***Correspondence:**
Wantao Chen
chenwantao2002@hotmaill.com
Ming Yan
yanming8012@126.com

†These authors have contributed equally to this work

Specialty section:
This article was submitted to Head and Neck Cancer, a section of the journal Frontiers in Oncology

Received: *12 October 2020*
Accepted: *26 March 2021*
Published: *13 July 2021*

Citation:
Zhang T, Zhu X, Sun Q, Qin X, Zhang Z, Feng Y, Yan M and Chen W (2021) Identification and Confirmation of the miR-30 Family as a Potential Central Player in Tobacco-Related Head and Neck Squamous Cell Carcinoma. Front. Oncol. 11:616372. doi: 10.3389/fonc.2021.616372

Constituents of tobacco that can cause DNA adduct formation and oxidative stress are implicated in the development of head and neck squamous cell carcinoma (HNSCC). However, there are few studies on the mechanism(s) that underlie tobacco-associated HNSCC. Here, we used a model in which tumors were induced in rats using 4-nitroquinoline 1-oxide (4NQO), which mimicked tobacco-related HNSCC, and analyzed the expression profiles of microRNAs and mRNAs. Our results indicated that 57 miRNAs and 474 mRNA/EST transcripts exhibited differential expression profiles between tumor and normal tongue tissues. In tumor tissue, the expression levels of rno-miR-30 family members (rno-miR-30a, rno-miR-30a-3p, rno-miR-30b-5p, rno-miR-30c, rno-miR-30d, rno-miR-30e and rno-miR-30e-3p) were only 8% to 37% of those in the control group. The GO terms enrichment analysis of the differentially expressed miRNAs indicated that oxidation reduction was the most enriched process. Low expression of miR-30 family members in human HNSCC cell lines and tissues was validated by qPCR. The results revealed that the expression of miR-30b-5p and miR-30e-5p was significantly decreased in the TCGA HNSCC dataset and validation datasets, and this decrease in expression further distinguishes HNSCC associated with tobacco use from other subtypes of HNSCC. CCK8, colony formation, transwell migration and HNSCC xenograft tumor assays indicated that miR-30b-5p or miR-30e-5p inhibited proliferation, migration and invasion *in vitro*, and miR-30b-5p suppressed tumor growth *in vivo*. Moreover, we uncovered that KRAS might be the potential target gene of miR-30e-5p or miR-30b-5p. Thus, our data clearly showed that decreased expression of miR-30e-5p or miR-30b-5p may play a crucial role in cancer development, especially that of tobacco-induced HNSCC, and may be a novel candidate biomarker and target for this HNSCC subtype.

Keywords: head and neck squamous cell carcinoma, miR-30, 4-nitroquinoline 1-oxide, tobacco smoke, KRAS

INTRODUCTION

Head and neck squamous cell carcinoma (HNSCC) is one of the most common malignant tumors worldwide, accounting for approximately 3.8% of all malignant cancers (1, 2). The consumption of tobacco is an established major etiological factor in the development of HNSCC (3). In the Indian subcontinent, HNSCC is the single most common malignancy, and it is mainly caused by the use of chewing tobacco and related products (4). It was reported that smoking is responsible for most deaths from HNSCC in high-income countries (5). Over the past few decades, the HNSCC incidence rate has increased among both males and females in several countries in Eastern and Northern Europe and among females in Southern and Western Europe, which largely reflects the ongoing tobacco epidemic (6, 7). In many other more developed countries, as tobacco use has decreased, the HNSCC incidence rate has begun to decline in both males and females (7).

Over 60 chemicals found in tobacco products, such as dibenz [a,h]anthracene, benzo-(a)-pyrene, 4-aminobiphenyl, acetaldehyde, N-nitrosamines, catechol and benzene, have been shown to be carcinogenic (8, 9). Carcinogens can be metabolized by cytochrome P450 enzymes into water-soluble forms, generating DNA adducts (10). These adducts usually cause sequence variations in DNA. If not repaired correctly, these lesions lead to tumor formation (11). Despite treatment advances, the 5-year relative survival rate still has not improved significantly (12), which can be attributed primarily to diagnosis at an advanced stage characterized by invasion and metastasis to the lymph nodes and remote organs (13). Identification of predictive biomarkers for diagnosing HNSCC at earlier stages would be beneficial for patient survival. MicroRNAs (miRNAs) are a class of small noncoding RNAs that play an important role in regulating gene function through targeting mRNAs for translational repression or degradation (14). Deregulation of miRNA expression contributes to aberrant expression of mRNAs that mediate the complex malignant phenotypes of cancers. Changes in a number of miRNAs and genes that are required for the occurrence of HNSCC have already been identified, including increased expression of miR-21-5p and miR-31-5p and reduced expression of miR-375 and miR-100 family members. However, a large gap in our understanding of how the different miRNAs and mRNAs expressed during HNSCC development relate to exposure to tobacco remains.

4NQO is a synthetic, water-soluble carcinogen that can result in histological and molecular alterations very similar to those found in human tobacco-related oral carcinogenesis by promoting DNA adduct formation, A-G nucleotide substitution and intracellular oxidative stress (15, 16). The murine model of 4-nitroquinoline 1-oxide (4NQO)-induced oral carcinogenesis has been used extensively to identify how chronic tobacco abuse contributes to human HNSCC and how therapeutic treatments can alleviate or prevent these malignancies (16–18).

Determining the relationships among the expression levels of the various microRNAs and mRNAs could be useful for identifying diagnostic markers or therapeutic interventions. Most microRNAome and transcriptome data were derived from separate studies on oral cancer that did not address risk factors. In this study, we used the 4NQO-induced carcinogenesis model to mimic human tobacco abuse to identify the network of miRNAs and their predicted target mRNAs involved in HNSCC. Remarkably, we revealed downregulated expression rno-miR-30 family members which targeted several classical oncogenes, such as KRAS, centering on cell growth, proliferation and invasion, may be important in initiating the development of HNSCC, especially tobacco-related tumors.

MATERIAL AND METHODS

Tumor Induction

The animal model was established as previously described (19). Briefly, 40 male Sprague-Dawley (SD) rats, aged 6-7 weeks, were randomly divided into two groups. In the experimental group (n=20), the rats were fed daily with dissolved 4NQO (Sigma, USA) at a concentration of 0.02 g/L, whereas the control group (n=20) were fed distilled water only. At the end of the 36th week, all rats were sacrificed (**Figure 1A**). Tumors and normal tongue tissues were collected from the experimental and control groups, respectively; and separated into two parts: one was set aside for histopathological examination, and the other was instantly placed into liquid nitrogen and then stored at -80°C for RNA extraction.

Total RNA Isolation and miRNA/mRNA Microarray

Total RNA was extracted from 7 tongue SCC tumors and 7 normal tissues using mirVana RNA Isolation Kit (Applied Biosystem p/n AM1556) following homogenization. 7 rats per group were pooled for miRNA microarray, and 5 normal tongue tissue and 6 tongue SCC tumors were carried in mRNA microarrays. RNA labeling, hybridization and scanning were performed by ShanghaiBio Corporation using a Rat miRNA microarray (Agilent, G4473A). The GeneSpring GX software (Agilent Technologies) was used to analyze the microarray data. Preparation of antisense RNA, hybridization, staining, and scanning of the Rat Genome U34 Array (Affymetrix Inc.) was performed according to the Affymetrix standard protocol. Data normalization and analysis were performed with Microarray Suite version 5.0. Differential miRNA/mRNA expression was determined as at least a 2-fold difference between the experimental and control groups.

miRNA/mRNA qRT-PCR for Validation

MiR-30c, miR-30d and miR-30e-3p were chosen as the candidate miRNAs for microarray data validation. U6 RNA was chosen as an internal control. The 20 μL reverse transcriptase reactions contained 1 μg of RNA and were completed using Mircute enhanced miRNA cDNA first strand synthesis Kit (TIANGEN, China). Real-time PCR was performed using Mircute enhanced miRNA fluorescence quantitative detection kit (TIANGEN,

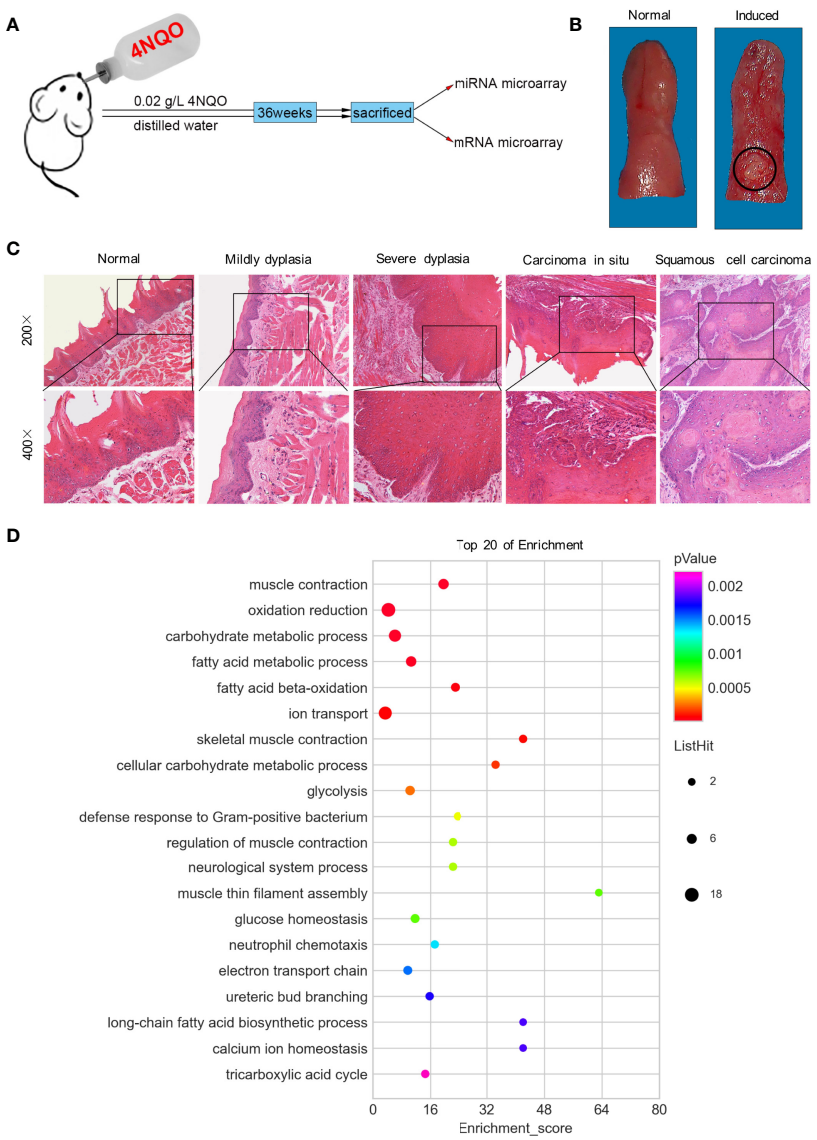

FIGURE 1 | Both macroscopic and microscopic changes in SD rats' tongue mucosa. **(A)** Experimental scheme of SD rats induced by 4NQO for 36 weeks. **(B)** Photograph of normal tongue (left) and exophytic neoplasm on tongue induced by 4NQO water for 36 weeks (right). **(C)** H&E staining showed the pathological changes of rat tongues base at different stages. **(D)** GO analysis of top 20 of functional enrichment based on mRNA microarray.

China). The genes of Ubadc1, Ldhb, and Cabc1 were selected to validate the microarray results by Quant one step qRT-PCR Kit (SYBR Green) (TIANGEN, China). β-actin was chosen as an internal control. The sequences of the PCR primers (synthesized by Sangon Biotech Co, China) were shown in **Table S1**.

Gene Ontology (GO) Analysis of rno-microRNA Target Genes

GO analysis was applied to analyze the main function of the differentially expressed microRNA targets according to the Gene Ontology database (http://www.geneontology.org/) (20). Fisher's exact test and $\chi 2$ test were used to classify the GO categories, and the false discovery rate (FDR) was calculated to correct the p-value. GOs that had a p-value of <0.05 and a FDR of < 0.05 were chosen for further study.

MiRNA-Gene-Network

The miRNA-gene-network was built according to the interactions of miRNA and genes in the Sanger miRNA database. The adjacency matrix of miRNAs and genes, A=[ai,j], is made by the attribute relationships among the genes and miRNAs, and ai,j represents the relative weight of gene i and miRNA j. Degree indicates the contribution of one miRNA to the nearby genes or the contribution of one gene to the nearby miRNAs.

MiRNA-GO-Network

A miRNA-go-network was built according to the relationship between significant GOs and genes as well as the relationships among miRNAs and genes. The adjacency matrix of microRNA and genes, A=[ai,j], was made by the attribute relationships among GOs and miRNA, and ai,j represented the relative weight of GO i and miRNA j. Degree indicated the contribution of one miRNA to the nearby GOs or the contribution of one GO to the nearby miRNAs.

SD Rat Cell Culture

The SD rat SCC cell lines Rca-T (21) and Rca-B (22) were cultured in DMEM (Gibco, USA) supplemented with 10% FBS, 100 units/mL penicillin and 100 mg/mL streptomycin at 37°C in a humidified atmosphere of 5% CO_2. The primary culture came from buccal mucosa of male Sprague-Dawley (SD) rats, aged 4-5 weeks. The tissue was cut to 0.2 cm×0.2 cm pieces, then they were incubated in 5 mL 0.8% dispase II (Roche, Switzerland) solution at 4°C overnight. Epithelium was isolated from basal lamina, and put into 3 mL 0.25% trypsin for 5 minutes. The suspension was centrifuged in low speed and supernatant was decanted. The deposition was resuspended and incubated with Defined Keratinocyte SFM (Gibco, USA) in a 6 cm dish.

Cell Culture

Human HNSCC cell lines HN4, HN6, HN30 and SCC9 were obtained from University of Maryland Baltimore School of Dentistry and ATCC, respectively. HN4, HN6, and HN30 cells were maintained in DMEM (Gibco, USA) supplemented with 10% FBS (Gibco, USA), 50 U/mL penicillin, and 50 μg/mL streptomycin. SCC9 cells were maintained in DMEM/F12 (proportion: DMEM with F12 was 1:1, Gibco, USA) supplemented with 10% FBS, 50 U/mL penicillin, and 50 μg/mL streptomycin. HEK-293 cells were incubated in DMEM supplemented with 10% FBS, 50 U/mL penicillin, and 50 μg/mL streptomycin. All the cells were incubated at 37°C in a humidified atmosphere with 5% CO_2. Human normal oral mucosa came from the local normal mucosal tissue removed during the extraction of impacted teeth, and the mucosal tissue was in a healthy state without inflammation. The procedure for the culture of primary cells of human oral mucosa is basically the same as that of primary cells of oral mucosa of SD rats.

Patients and Clinical Specimens

Paired HNSCC and adjacent noncancerous tissues were obtained from 32 primary HNSCC patients at the Department of Oral Surgery, Ninth People's Hospital, Shanghai Jiao Tong University School of Medicine, Shanghai, P. R. China. The experiment has been approved by the Ethics Committee of Ninth People's Hospital Affiliated to Shanghai Jiao Tong University School of Medicine. These tissues were flash-frozen in liquid nitrogen immediately after resection and stored at -80°C. None of the patients had received neoadjuvant chemo- or radio-therapy before surgery.

Real Time PCR

Total RNA was isolated from Rca-B, Rca-T, HN4, HN6, HN30, SCC9, human oral mucosal epithelial cells using the TRIZOL Reagent (Invitrogen, USA). Total RNA was isolated from 32 paired HNSCC and adjacent noncancerous tissues using the TRIZOL Reagent (Invitrogen, USA). MiR-30 family was detected by qRT-PCR. The procedure was the same as above. The sequences of the PCR primers (synthesized by Sangon Biotech Co, China) were shown in **Table S1**.

Cell Transfection

SCC9 or HN4 cells at a density of 1×10^5 per well were seeded into a 6-well plate and incubated overnight respectively, then transfected with mature miR-30b-5p mimic, miR-30e-5p mimic, miR-30b-5p inhibitor, miR-30e-5p inhibitor or negative control (Riobo Bio, China) using Lipofectamine 2000 (Invitrogen, USA) according to the manufacturer's instructions. Total cell RNA was extracted by addition of 1 mL TRIZOL reagent (Invitrogen, USA) to the cells in each well according to the manufacturer's protocol and used for qRT-PCR to detect the expression of miR-30b-5p and miR-30e-5p. The procedure is the same as above.

Cell Proliferation Assay

The transfected SCC9 or HN4 cells were plated in 96-well plates at 1000 cells per well and incubated at 37°C. CCK8 assay was performed at 0, 1, 2, 3, 4, 5, 6 day, respectively. A 10 μL of CCK8 solution (DOJINDO, Japan) was added and incubated for 2 h at 37°C, then optical density (OD) was measured at 450 nm in a microplate spectrophotometer.

Colony Formation Assay

The transfected SCC9 or HN4 cells at 500 cells per well were seeded into 6-well plate and incubated at 37°C for 10 days, colonies were fixed and stained with 0.1% crystal violet for 1 h. Then the clones were counted and normalized to the control group under a microscope.

Transwell Migration Assay

The transwell migration was performed using 24-well transwell chambers (8 μm, Millipore, USA). After transfection, 2×10^4 SCC9 or HN4 cells were resuspended in serum-free medium and seeded into the upper chambers. We added 0.6 mL medium containing 20% FBS to the bottom chambers. Following a 30 h incubation, cells on the upper surface of the membrane were removed using cotton swabs, and the invaded cells were fixed with 4% paraformaldehyde for 15 min, stained with 0.1% crystal violet for 1 h, and imaged using microscope. The areas of crystal violet were calculated by Image J 1.53 c (National Institutes of Health, USA).

Wound Healing Assay

About 1.5×10^6 transfected SCC9 or HN4 cells were seeded into 6-well plate and incubated at 37°C and grew until 100% confluence. Sterilized one-milliliter pipette tip was used to generate wounding across the cell monolayer, and the debris

was washed with PBS. Migration of cells into the wound was then observed under inverted microscope at 0 and 12 hours.

Luciferase Reporter Assays

Vectors encoding the wild-type or mutant 3'UTR of KRAS, cloned behind Renilla luciferase, were constructed by Genomeditech (China). HEK-293 cells were seeded 24-well plates, the miRNA mimics and vector were transfected with HG transgene reagent (Genomeditech, China) when the cell density up to 70%. The cells were lysed with cell lysing buffer and luciferase activity was detected using the Renilla-Glo® Luciferase Assay System (Promega, USA) following the manufacturer's instructions. All measurements represent the mean of 3 replicates in each experimental condition.

Western Blot

HN4 cells were transfected with miRNAs described above and then lysed by RIPA lysis buffer (Roche, Switzerland). The concentration of protein was determined using a BCA Protein Assay (Thermo Scientific, USA). Total protein at 30 μg was subjected to SDS-PAGE on a 4-12% gradient Bis-Tris gel (Invitrogen, USA). Protein was transferred to a 0.22 μm PVDF membrane which blocked with 5% skim milk. Primary antibodies used for probing are listed below. Secondary antibodies labelled with HRP (Beyotime, China) were used for detection at a dilution of 1:1000 and detected using Chemiluminescent HRP Substrate (Merck Millipore, USA), and signals were captured and observed using an Amersham Imager 600 (GE, USA). Primary antibodies: KRAS (1:5000, rabbit, Proteintech, China), GAPDH (1:10000, mouse, Proteintech, China).

Nude Mouse Tumorigenicity Assay

The nude mouse tumorigenicity model was constructed with 5-week-old male BALB/c nude mice. The mice were purchased from the Shanghai Sippr-BK laboratory animal Co. Ltd. and were housed in pathogen-free cages (n = 3/cage) with a controlled light/dark cycle (12/12 h) at a temperature of 21°C. The animal use protocol was approved by the Institutional Animal Care Committee and all procedures conformed to Animal Studies Committee-approved protocols. A total of 1×10^6 HN4 cells in 100 μL serum-free DMEM were injected into bilateral hip. A week later, the nude mice developed tumors in their buttocks. The mice were divided into 6 groups according to the miRNA injected: NC agomir, miR-30b-5p agomir, miR-30e-5p agomir, NC antagomir, miR-30b-5p antagomir, miR-30e-5p antagomir (Riobo Bio, China) (**Figure 6A**). Then miR-30b-5p or miR-30e-5p agomir were injected around the tumor at a dose of 5 nmol/tumor, twice a week for 4 times. MiR-30b-5p or miR-30e-5p antagomir was injected around the tumor at a dose of 10 nmol/tumor, twice a week for 4 times. The body weight and tumor size were measured regularly during the experiment. The mice were sacrificed at 12^{th} day and tumors were dissected, then the tumor fixed with formalin for further hematoxylin and eosin (H&E) staining and immunohistochemistry (IHC) analysis.

IHC

Excised tumor tissues were fixed in 4% paraformaldehyde, dehydrated, paraffin-embedded, and cut into 5 μm sections. The sections were analyzed using primary antibodies against KRAS (1:800, rabbit, Proteintech, China), Ki67 (1:2000, rabbit, Proteintech, China) and a biotin-conjugated goat anti-rabbit polyclonal antibody (1:50; ZSGB-BIO, China) as the secondary antibody. Images were obtained by light microscopy (Olympus, Japan) at 400× magnification.

Analysis of TCGA Data

The HNSCC miRNA expression profile from TCGA was download through GDC API, the expression matrix was tidied by TCGA biolinks (23, 24). The putative biological role of the targets genes was performed by clusterProfiler that described by Yu et al. (25).

Functional Enrichment Analysis

The target genes of selected miRNA were predicted with the ENCORI (The Encyclopedia of RNA Interactomes) method. Potential target genes of miR-30b-5p or miR-30e-5p were predicted by ENCORI (http://starbase.sysu.edu.cn/) (26). An intersection analysis of predicted target genes of miR-30b-5p or miR-30e-5p and differential genes in mRNA array was carried out using the Venn diagrams web tool (http://bioinformatics.psb.ugent.be/webtools/Venn/). Moreover, top 20 of functional enrichment analysis was conducted through the Database for Annotation, Visualization and Integrated Discovery (DAVID) v6.8 (https://david.ncifcrf.gov/). The data were further developed by using the cluster Profiler package in R (version 3.6.1).

Statistical Analysis

Data are expressed as mean ± SD, and analyzed using SPSS 19.0. The differences between groups were analyzed using one-way ANOVA or non-paired *t*-test. All statistical analyses were performed using GraphPad Prism 8 (GraphPad Software, Inc.), and $p < 0.05$ was considered as statistically significant.

RESULTS

Macroscopic and Microscopic Appearance of Rat Tumors

After 36 weeks, 17 rats with tongue tumors survived, and 3 rats died of pneumonia or gastroenteritis in the 4NQO induced group. In the control group, all 20 rats survived, and none exhibited tongue tumor formation. Based on macroscopic appearance, the tumors, which were consistently found on the dorsum of the tongue base, presented an exophytic neoplasm, while the normal mucosa was ruddy and smooth (**Figure 1B**). Histopathologically, the tumors spread into the submucosa and underlying muscle layer, forming small nests of atypical keratinizing epithelial cells that surrounded centrally located keratin pearls. No histopathological changes in epithelial cells were observed in the control group (**Figure 1C**).

miRNA and mRNA Expression Profiles in SD Rats With HNSCC

The expression levels of miR-30 family members (miR-30a-5p, miR-30a-3p, miR-30b-5p, miR-30c-3p, miR-30d-3p, miR-30e-5p and miR-30e-3p) were depressed in tongue SCC tissues (**Table S2**). The expression of the miRNAs miR-30c-5p, miR-30d-5p, and miR-30e-3p was verified to be decreased in tongue SCC tissues, which was in agreement with the results of miRNA microarray analysis (**Figure S1B**). Among the 8799 genes/ESTs analyzed, 372 genes were found to be differentially expressed in tongue SCC tumors (**Table S3**). The genes Ubadc1 (UBA domain containing 1), Ldhb (lactate dehydrogenase B), and Cabc1 (chaperone, ABC1 activity of bc1 complex homolog) were chosen for validation, and the results were consistent with the results of mRNA microarray analysis (**Figure S1A**).

The miRNA-mRNA interaction networks and top 20 enriched pathways suggested that oxidation-reduction might play a vital role in tongue SCC in SD rats (**Figure 1D** and **S1C**). There were 38 miRNAs related to oxidation reduction, including all members of the miR-30 family (**Table S4**). In addition, ion transport and carbohydrate metabolism might have been related to the development of tongue SCC in SD rats (**Figure 1D**).

The Expression of miR-30 Family Members Was Downregulated in HNSCC

The expression levels of miR-30 family members were measured in the SD rat oral squamous cell carcinoma cell lines Rca-T and Rca-B and primary oral mucosal epithelial cells from normal SD rats. As shown in **Figure 2A**, the expression levels of all the miR-30 family members were decreased significantly in Rca-T and Rca-B cells compared with normal SD rat oral mucosal epithelial cells. Similarly, the expression of miR-30 family members was shown to be downregulated in human HNSCC cell lines (HN4, HN6, HN30 and SCC9) (**Figure 2B**). Furthermore, miR-30b-5p and miR-30e-5p expression was significantly downregulated in human HNSCC tissues (**Figures 2C, D**). We found that the expression of miR-30b-5p and miR-30e-5p was lower in samples from the smoking group compared to those from the control group (**Figures 2E, F**).

The Proliferation and Migration of HNSCC Cells Were Decreased by miR-30b-5p or miR-30e-5p

First, the expression of miR-30b-5p and miR-30e-5p in SCC9 and HN4 cells was increased after mimic transfection and decreased following inhibitor transfection (**Figures 3A, B, E, F**). After transfection of miR-30b-5p or miR-30e-5p mimic, the proliferation of SCC9 and HN4 cells was decreased (**Figures 3C, G**), while the proliferation of SCC9 and HN4 cells transfected with miR-30b-5p or miR-30e-5p inhibitor was increased (**Figures 3D, H**). The results showed that the colony-forming ability of SCC9 and HN4 cells treated with miR-30e-5p mimic was significantly worse than that of nontreated cells. In contrast, the colony-forming ability of SCC9 and HN4 cells treated with miR-30e-5p inhibitor was significantly better than that of non-treated cells. However, the colony-forming ability of HN4 cells treated with miR-30b-5p or miR-30e-5p inhibitor was not significantly different from that of nontreated cells (**Figures 3I–N**). The results of the transwell migration and wound healing assays suggested that the migration of SCC9 and HN4 cells was decreased by miR-30b-5p or miR-30e-5p (**Figure 4**).

The Possible Target Genes of miR-30b-5p and miR-30e-5p

A total of 791 genes were predicted to be targets of miR-30b-5p by more than four websites (PITA, RNA22, miRmap microT, miRanda, PicTar, TargetScan), and 822 genes were predicted to be targets of miR-30e-5p by more than four websites (**Tables S5** and **S6**). Intersection of the differentially expressed genes identified by mRNA microarray analysis and the target genes of miR-30b-5p predicted by ENCORI led to the identification of 8 genes (**Figure 5A**). A total of 9 genes were identified by intersection of these data for miR-30e-5p (**Figure 5B**). Among these genes, the expression of CECAM, KRAS, LYN, MYO5A, RTN4R, SLC4A7 and STC1 was downregulated in the mRNA microarray analysis. The differential expression of these genes was validated by real-time PCR in SCC9 and HN4 cells. The expression of KRAS, MYO5A and SLC4A7 was downregulated in both SCC9 and HN4 cells after transfection with miR-30b-5p mimic. Furthermore, the expression of KRAS, MYO5A and SLC4A7 was downregulated by miR-30b-5p mimic (**Figures 5C, D** and **Figures S2A, B**). Base pairing of miR-30b-5p or miR-30e-5p with the 3' UTR of target mRNAs (KRAS, MYO5A and SLC4A7) was predicted by TargetScan (**Figures 5E, F**). In TCGA HNSCC samples, miR-30b expression was negatively correlated with KARS, MYO5A and SLC4A7 expression. MiR-30e expression had a negative correlation with MYO5A expression but a weak correlation with KRAS and SLC4A7 expression (**Figures S2C–H**). The results of the luciferase assay and western blot analysis revealed that the expression of KRAS could be inhibited by miR-30b-5p or miR-30e-5p, which indicates that KRAS might be the target gene of miR-30b-5p or miR-30e-5p (**Figures 5G, H**).

Tumor Growth Might Be Suppressed by miR-30b-5p or miR-30e-5p

Subcutaneous tumors were suppressed by miR-30b-5p agomir but promoted by the miR-30e-5p antagomir. The miR-30b-5p antagomir or miR-30e-5p agomir had little influence on tumor growth. Furthermore, no significant weight loss was observed in mice after miRNA injection, indicating that the miRNA had no toxic effects on mice (**Figures 6B–F**). H&E staining of tumors revealed obvious tumor features: large and hyperchromatic nuclei and mitosis were visible, but there was no obvious difference in these features between the six groups (**Figure 6G**). The expression of KRAS and Ki67 in tumors treated with miRNA agomir was weaker than that in tumor treated with the NC, indicating that KRAS expression might be decreased by miR-30b-5p or miR-30e-5p (**Figures 6H, I**).

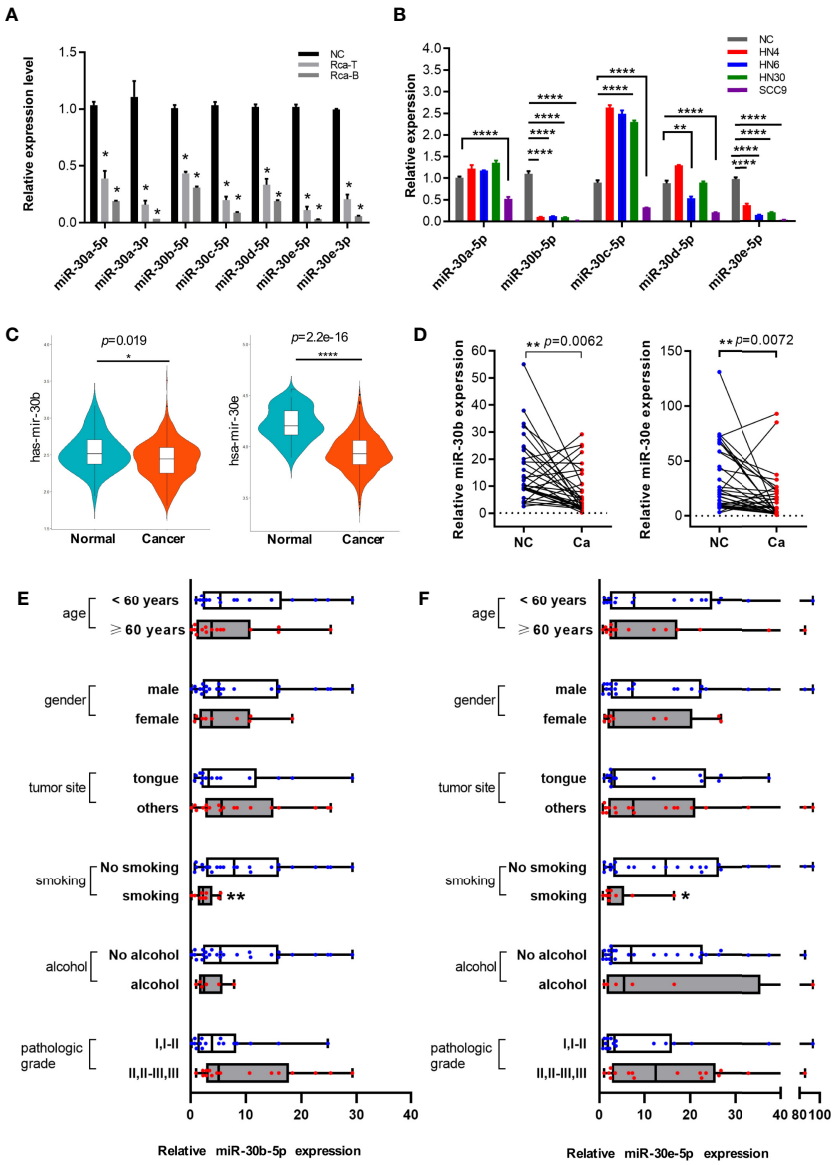

FIGURE 2 | The expression of miR-30 family was downregulated in HNSCC. **(A)** The relative expression level of miR-30 family in rat oral squamous cell lines. **(B)** The expression level of miR-30 family in HNSCC cell lines. **(C)** The expression tendency of miR-30b-5p and miR-30e-5p in HNSCC samples base on TCGA database. **(D)** The expression level of miR-30e-5p and miR-30b-5p in paired HNSCC tissues. **(E, F)** The relative expression level of miR-30b-5p or miR-30e-5p in oral tissues classified according to clinical data (age, gender, tumor site, smoking, alcohol, pathological grade). (*p<0.05, **p<0.01, ****p<0.0001).

DISCUSSION

The development of tobacco-induced head and neck carcinogenesis is a complicated process that is still not completely understood at the molecular level. In the present study, we used a rat model of 4NQO-induced carcinogenesis to identify miRNAs and their targets that are involved in regulating the onset of HNSCC caused by tobacco and to initially identify the key miRNAs contributing to gene regulation during this developmental period.

4NQO exerts potent intracellular oxidative stress effects, and its metabolic product binds to DNA predominantly at guanine residues, which appear to be similar to the damage imposed by the carcinogens present in tobacco (27). Furthermore, this model is similar to human oral carcinogenesis at both the histological and molecular levels (15, 16). In this study, no tumors were observed in the digestive tracts, lungs, or livers of the 4NQO-treated rats, which further confirmed that this rat model simulates aspects of human oral cavity carcinogenesis.

In this study, microarray analysis revealed a set of differentially expressed miRNAs and mRNAs between tumor and normal tissues. These results agree with those of previous studies. For example, miR-21 was found to be oncogenic in

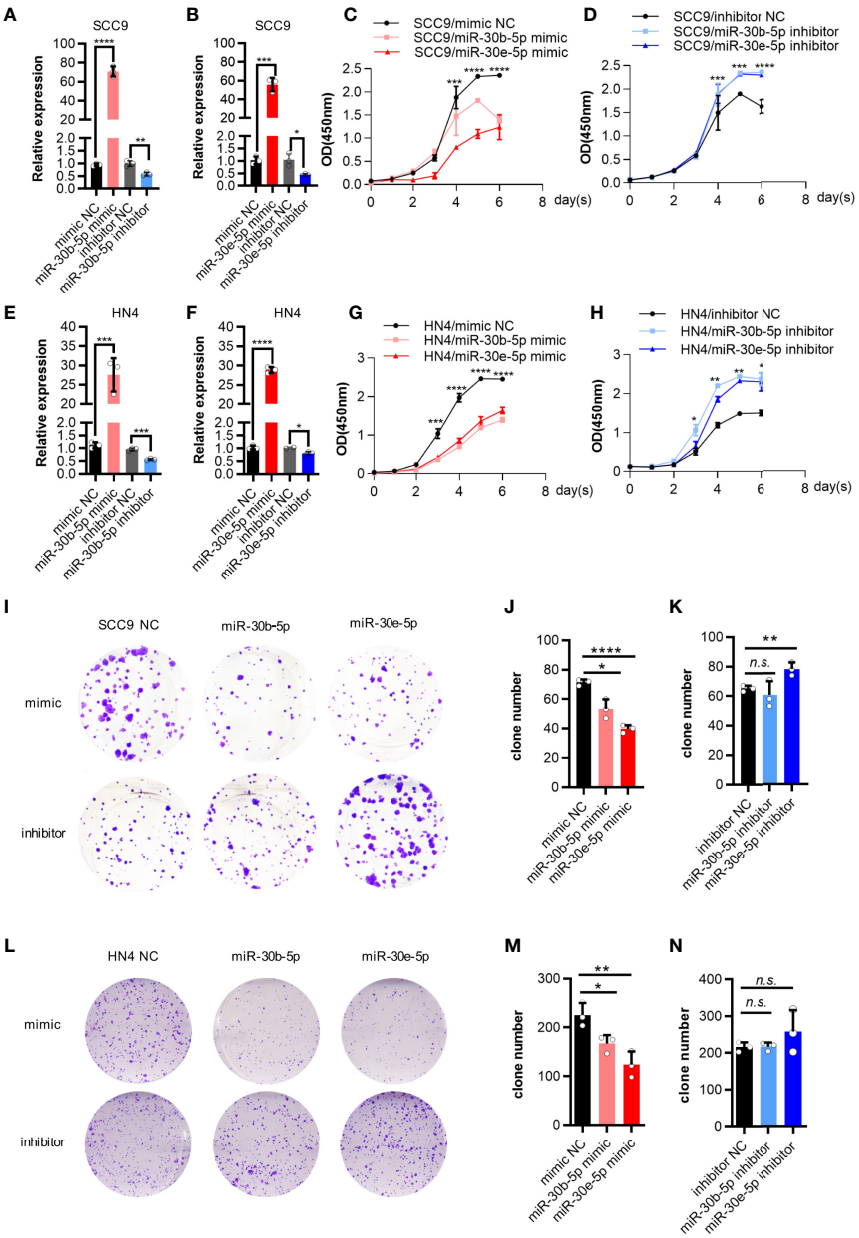

FIGURE 3 | The proliferation of SCC9 and HN4 cells was depressed by miR-30b-5p or miR-30e-5p. **(A)** The expression level of miR-30b-5p in SCC9 cells after transfection with miR-30b-5p mimic or inhibitor. **(B)** The expression level of miR-30e-5p in SCC9 cells after transfection with miR-30e-5p mimic or inhibitor. **(C)** The proliferation of SCC9 cells after transfection with miR-30b-5p or miR-30e-5p mimic. **(D)** The proliferation of SCC9 cells after transfection with miR-30b-5p or miR-30e-5p inhibitor. **(E)** The expression level of miR-30b-5p in HN4 cells after transfection with miR-30b-5p mimic or inhibitor. **(F)** The expression level of miR-30e-5p in HN4 cells after transfection with miR-30e-5p mimic or inhibitor. **(G)** The proliferation of HN4 cells after transfection with miR-30b-5p or miR-30e-5p mimic. **(H)** The proliferation of HN4 cells after transfection with miR-30b-5p or miR-30e-5p inhibitor. **(I–K)** The colony formation of SCC9 cells depressed by miR-30b-5p or miR-30e-5p. **(L–N)** The colony formation of HN4 cells depressed by miR-30b-5p or miR-30e-5p. (*p<0.05, **p<0.01, ***p<0.001, ****p<0.0001, n.s., no significance).

HNSCC (28); miR-100 expression is decreased in oral cancer (29); and CDK6 is highly expressed in HNSCC (30), while S100 calcium binding protein B (S100B) expression is downregulated during carcinogenesis (31). These results indicate that the regulatory mechanisms mediated by common miRNAs may play a fundamental role in carcinogenesis. However, more aberrantly expressed miRNAs and mRNAs were found in this study due to the different platforms and methods used as well as the different miRNA and mRNA probe sources. The functions of most of the miRNAs and mRNAs identified in this study were not clear. The functions of these miRNAs and mRNAs will be studied in the future.

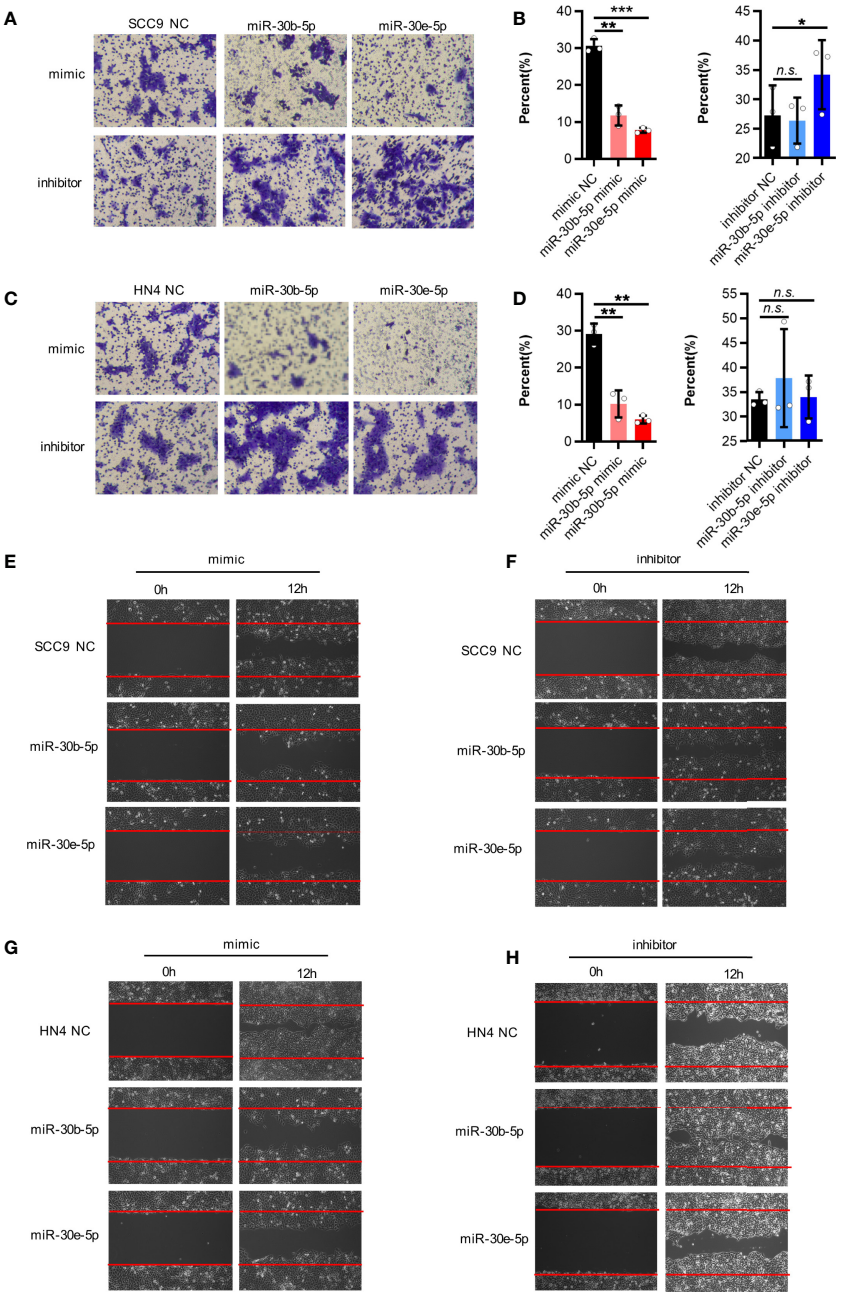

FIGURE 4 | The migration of SCC9 and HN4 cells were depressed by miR-30b-5p or miR-30e-5p. **(A, B)** MiR-30b-5p or miR-30e-5p influenced SCC9 cell migration. **(C, D)** MiR-30b-5p or miR-30e-5p influenced HN4 cell migration. **(E, F)** MiR-30b-5p or miR-30e-5p influenced the rate of SCC9 cell wound closure. **(G, H)** MiR-30b-5p or miR-30e-5p influenced the rate of HN4 cell wound closure. (*p<0.05, **p<0.01, ***p<0.001, n.s., no significance).

Furthermore, the miRNA-gene interaction networks based on the differential miRNA and mRNA expression data revealed some critical members during carcinogenesis. Targets of the downregulated miRNAs (i.e., rno-miR-30a and rno-miR-133a) and targets of the upregulated miRNAs (i.e., rno-miR-21, rno-miR-31, and rno-miR-188) share several target proteins, which indicates that the regulation of these proteins may be complex *in vivo*. This could explain why the expression levels of several targets did not always correlate with the modulation of miRNA levels. In addition, the five key miRNAs belonging to the miR-30 family, namely, rno-miR-30a, rno-miR-30b-5p, rno-miR-30c, rno-miR-30d and rno-miR-30e, were mainly enriched in the oxidation-reduction process. This result is not surprising because 4NQO has been shown to have similar effects as tobacco use, which potently induces intracellular oxidative stress (16). Moreover, miR-30 family members (miR-30b-5p, miR-30e-5p,

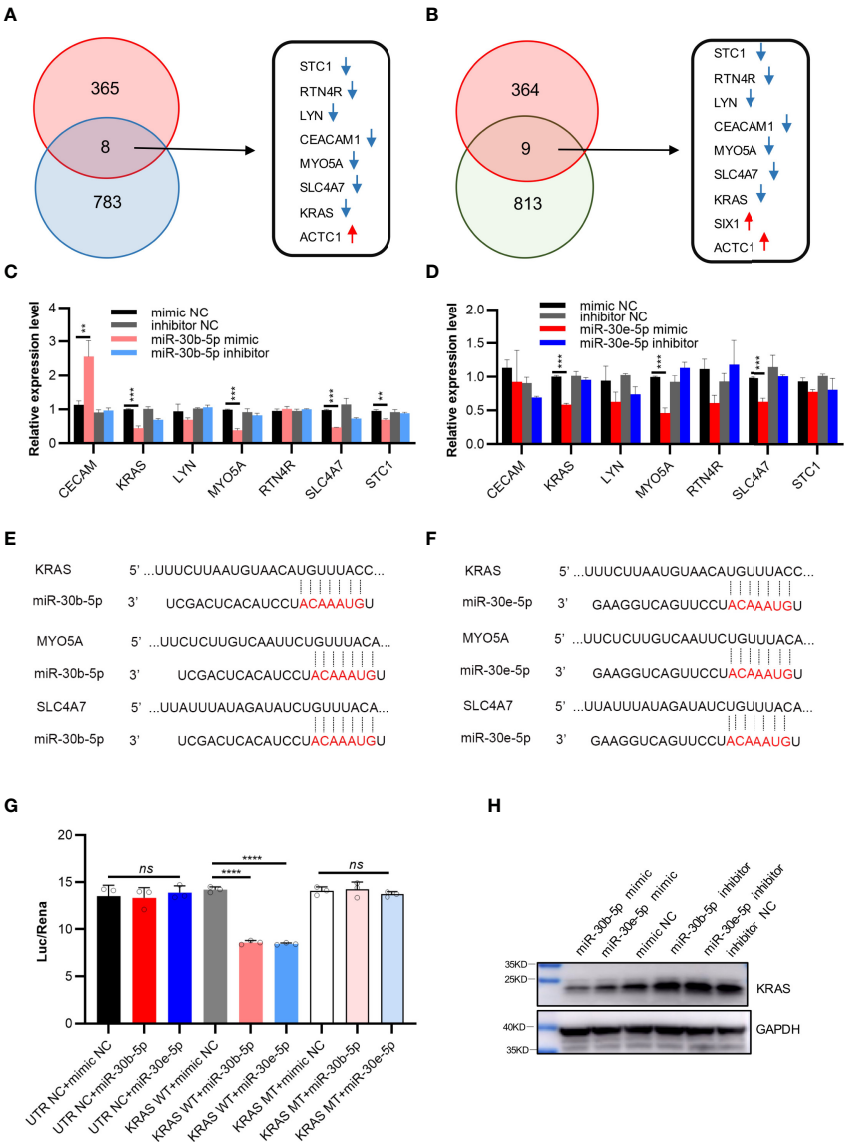

FIGURE 5 | Possible target genes of miR-30b-5p or miR-30e-5p in HNSCC. **(A)** The intersection of differential genes in mRNA microarray (373) and predicted targeted genes of miR-30b-5p by ENCORI (791). There were 8 genes in the intersection, the red arrows representing up-regulated genes and the blue arrows representing down-regulated genes. **(B)** The intersection of differential genes in mRNA microarray (373) and predicted potential targeted genes of miR-30e-5p by ENCORI (822). There were 9 genes in the intersection, the red arrows representing up-regulated genes and the blue arrows representing down-regulated genes. **(C)** The relative expression level of possible target genes in transfected SCC9 with miR-30b-5p mimic or inhibitor. **(D)** The relative expression level of target genes in transfected SCC9 with miR-30e-5p mimic or inhibitor. **(E, F)** Base pairing of miR-30b-5p or miR-30e-5p with 3' UTR of target mRNAs was predicted by TargetScan (http://www.targetscan.org/vert_72/). **(G)** Relative luciferase activity after cotransfection of 293T cells with miR-30b-5p or miR-30e-5p and vectors containing wilt-type KRAS 3' -UTR or 3'-mutant KRAS UTR cloned behind a Renilla luciferase reportor gene. **(H)** The expression of KRAS protein after transfection with miR-30b-5p or miR-30e-5p mimic or inhibitor. (**p<0.01, ***p<0.001, ****p<0.0001, n.s., no significance).

miR-30d-5p, and miR-30c-5p) were noted to have the highest ratio and enrichment in the miRNA-GO network, and microRNA-GO network analysis revealed that the miR-30 family likely has a critical role in tobacco-related HNSCC.

The miR-30 family includes miR-30a, miR-30b, miR-30c, miR-30d and miR-30e. They all contain the same "seed sequence" in their 5' termini and are abundantly expressed in the heart under physiological conditions (32). The modulation of miR-30, as a "hub" for the miRNA oncogenesis signal network in solid tumors, has profound impacts on tumorigenesis (33). Volinia et al. studied miRNA profiles in 4419 human samples (3312 neoplastic, 1107 nonmalignant), corresponding to 50 normal tissues and 51 cancer tissues, including epidermal SCC tissues (34). They found that miR-30 expression was downregulated and that this miRNA was

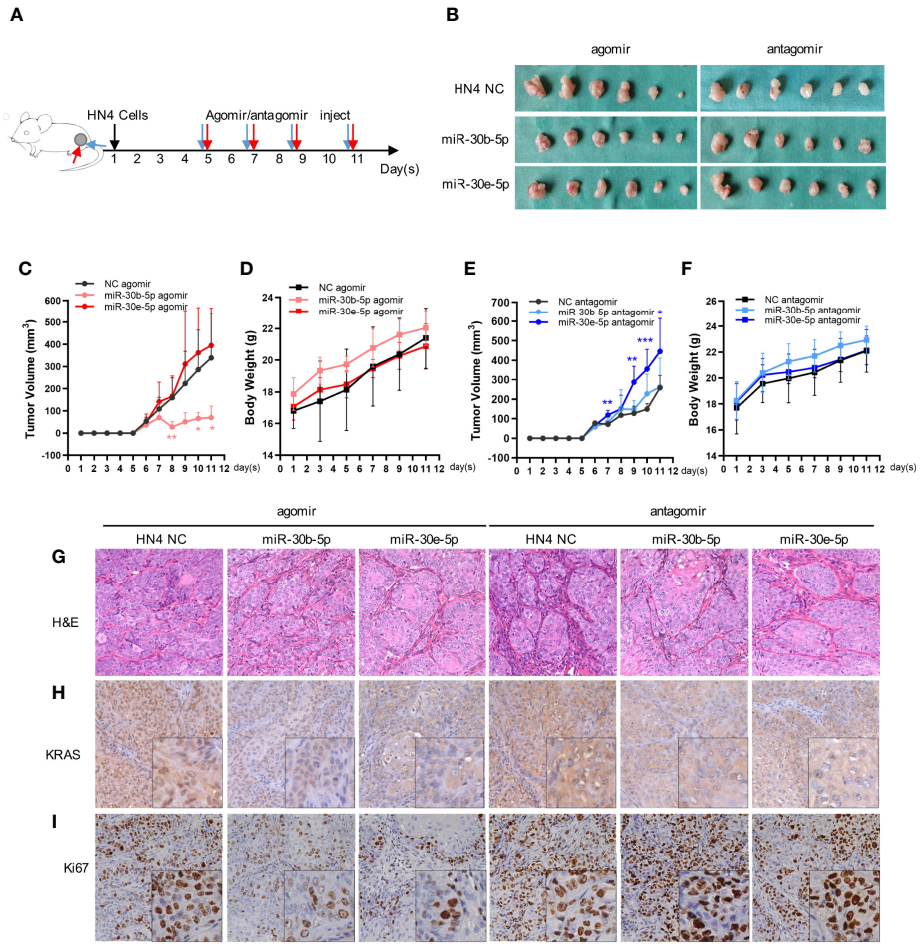

FIGURE 6 | The tumor growth might be suppressed by miR-30b-5p or miR-30e-5p. **(A)** Injection protocols of the miR-30b-5p or miR-30e-5p for subcutaneous tumorigenesis in nude mice. **(B)** Macro images of subcutaneous tumors. **(C, E)** The volume of subcutaneous tumors in nude mice. **(D, F)** The body weight of tumorigenesis nude mice. **(G)** Representative images of H&E staining of subcutaneous tumors injected with different miRNAs (400×). **(H, I)** The expression of KRAS or Ki67 in subcutaneous injected with different miRNAs (400×). (**p<0.01, ***p<0.001).

physically altered at the DNA copy number level in cancer tissues. MiR-30 family members were also identified as tumor suppressors in a subset of patients with head and neck squamous cell carcinoma (35). Braun et al. discovered that downregulation of miR-30 expression directs the mesenchymal-epithelial transition and invasive potential of anaplastic thyroid carcinomas (36). Downmodulation of miR-30 expression is also found in a variety of tumors. Low expression of miR-30 family members contributes to the development of non-small-cell lung cancer (37), colorectal cancer (38), bladder cancer (39), and so on. In addition, the expression levels of miR-30 members are lower in the lungs of rats exposed to cigarette smoke than those of rats not exposed to cigarette smoke, which indicates that a change in miR-30 family member expression is an early event following exposure to cigarette smoke (40). In this study, we found that miR-30e-5p and miR-30b-5p can inhibit the proliferation, adhesion and migration of HNSCC cells lines. We also observed that miR-30b-5p and miR-30e-5p displayed significantly decreased expression in TCGA HNSCC specimens and that miR-30b-5p and miR-30e-5p expression was associated with tobacco abuse, indicating that miR30-miR-30b-5p and miR-30e-5p may play an important role in HNSCC development caused by tobacco. Moreover, it has been reported that miR-30e-5p suppresses cell proliferation and migration in nasopharyngeal carcinoma (41) and bladder cancer (42). In human hepatocellular carcinoma tissues and cell lines, miR-30b-5p expression is significantly downregulated, and this miRNA mediates DNMT3A to repress proliferation (43). It can also regulate renal cell carcinoma cell proliferation and metastasis through downregulation of GNA13 expression (44). These data were consistent with our studies showing that lower expression of miR-30e-5p and miR-30b-5p inhibited cell proliferation and migration in tumor tissues.

However, miR-30 reported as a "dual" miRNA, with opposite functions in many tumors, including non–small cell lung cancer and pancreatic cancer. MiR-30 family members also act as oncogenic miRNAs in the tumorigenesis of some cancers,

indicating that their biological functions are complex. For example, MiR-30e expression is significantly upregulated in plasma samples from the malignant salivary gland tumor group compared to those from the benign group (45). Wang et al. revealed that upregulation of miR-30a expression contributed to tumor formation by inhibiting the expression of forkhead box protein L2 (FOXL2) in human granulosa COV43 cells (46). Moreover, miR-30a was overexpressed in the urine of ovarian serous adenocarcinoma patients (47). Gaziel-Sovran A et al. discovered that ectopic expression of miR-30b/30d promoted the metastatic behavior of melanoma cells by directly targeting the GalNAc transferase GALNT7 (48). Recent studies reported that the "dual" role of miR-30e within the same tumor type highlighting opposite effects based on different molecular backgrounds and in particular to *TP53* status (49). Tobacco-associated cancers are generally characterized by high mutation frequencies and definitely have different molecular genetic background from other oral cancers, while 4NQO as a DNA adduct-forming agent can sufficiently mimic the tobacco carcinogenic signature and act as a tobacco-mimetic promoting *TP53* mutation. It might explain why miR-30e-5p significantly downregulated in HNSCC samples but seemed have no effect in xenograft tumor models, which may due to the different genetic background of cell lines. Moreover, miR-30e may have other mechanisms in different tumor types. To the best of our knowledge, the expression of miR-30 in squamous cell carcinoma of epithelial origin is decreased, while in malignant tumors of nonepithelial origin is increased. The target genes of miR-30 in these two kinds of tumors may be different.

To identify which mRNAs are targeted by miR-30b-5p and miR-30e-5p in HNSCC, we predicted the target genes with ENCORI (The Encyclopedia of RNA Interactomes). Candidate targets were further identified from data on upregulated mRNAs in 4NQO-induced tumor specimens. Among these predicted miR-30b-5p and miR-30e-5p targets, *KRAS, MYO5A* and *SLC4A7* were also validated to be altered in different HNSCC cell lines, in which *KRAS* was further validated as the target genes. Remarkably, the *KRAS* gene is the most frequently mutated oncogene in human cancer. Mutant KRAS proteins are insensitive to GAP-induced GTP hydrolysis, which is linked to many aspects of tumor initiation and progression, including deregulation of key signal transduction pathways, altered metabolism, metastasis and drug resistance (50). KRAS mainly activates the PI3K/AKT/mTOR and BRAF/MEK/ERK pathways and activates inflammatory pathways such as the NFκB signaling pathway, which is required for tumor maintenance and malignant transformation (50). Furthermore, studies of KRAS-driven metabolism, including glycolysis, mitochondrial respiration, glutamine metabolism, and pyrimidine metabolism, have identified numerous potential lethal synthetic vulnerabilities that may be associated with a variety of tobacco-induced oncogenic stresses, such as DNA damage and oxidative stress (51). On the other hand, MYO5A and SLC4A7 were also reported to promote proliferation, invasion, metastasis and apoptosis resistance in many cancers (52, 53). Together, our data suggested that decreased miR-30b-5p and miR-30e-5p expression which may target the *KRAS* gene, are implicated in regulating the onset of HNSCC caused by tobacco and promoting the malignant phenotype.

In summary, our studies revealed that lower expression of miR-30 family members, which are part of miRNA-gene regulatory networks and miRNA-GO networks, is probably essential for the development of tobacco-related HNSCC. Targeting of KRAS by miR-30b-5p or miR-30e-5p inhibits cell growth, proliferation and migration in the context of HNSCC, which suggests the potential of miRNA-based therapeutics or the combination of simultaneous targeting of multiple mRNAs with tumor-targeted therapies or resistance mitigation strategies. Taken together, these findings support the role of miR-30b-5p and miR-30e-5p as potential biomarkers and therapeutic agents for tobacco-related HNSCC.

DATA AVAILABILITY STATEMENT

The original contributions presented in the study are included in the article/**Supplementary Materials**, further inquiries can be directed to the corresponding authors.

ETHICS STATEMENT

The studies involving human participants were reviewed and approved by The Research Ethics Committee of Ninth People's Hospital, Shanghai Jiao Tong University School of Medicine. The patients/participants provided their written informed consent to participate in this study. The animal study was reviewed and approved by The Experimental Animal Administrative Committee of Shanghai.

AUTHOR CONTRIBUTIONS

WC and MY designed the study. TZ and XZ drafted the manuscript. ZZ analyzed microarray data. TZ and QS participated in tissue collection and tissue sample analysis. XZ, XQ, QS and YF did in-vitro and *in vivo* experimental process. ZZ and XZ performed statistical analyses. WC and MY revised and finalized the manuscript. All authors contributed to the article and approved the submitted version.

FUNDING

This research was supported by National Natural Science Foundation of China (81874126, 81672829), the National Key Research and Development Program of China (2016YFC0902700), Science and Technology Commission of Shanghai Municipality (16431903300 and 18DZ2291500).

ACKNOWLEDGMENTS

The authors are very grateful to Dr. Shengfang Ge and Dr. Jianjun Zhang for assistance with microRNA expression data

analyses and the members of the Shanghai Key Laboratory of Stomatology for scientific input. We would also like to thank the surgeries of Ninth People's Hospital affiliated to Shanghai Jiao Tong University School of Medicine who provided surgical instruments and helped specimen preparation.

SUPPLEMENTARY MATERIAL

The Supplementary Material for this article can be found online at: https://www.frontiersin.org/articles/10.3389/fonc.2021.616372/full#supplementary-material

Supplementary Figure 1 | Bioinformatic analysis of miRNA and mRNA microarray. **(A)** The relative expression level of Ubadc1, Ldhb, Cabc1 in SD rat tongue SCC. **(B)** The relative expression level of miR-30c-5p, miR-30d-5p, miR-30e-3p in SD rat tongue SCC. **(C)** MicroRNA-gene-network. Red box nodes represent microRNA, and grey cycle nodes represent mRNA. Edges describe the inhibitive effect of microRNA on mRNA. **(D)** MicroRNA-GO-network. Red box nodes represent microRNA, and grey cycle nodes represent GO. Edges describe the effect of microRNA on GO. (**p<0.01, ***p<0.001, ****p<0.0001).

Supplementary Figure 2 | Possible target genes of miR-30b-5p or miR-30e-5p in HNSCC. **(A)** The relative expression level of possible target genes in HN4 after transfection with miR-30b-5p mimic or inhibitor. **(B)** The relative expression level of target genes in HN4 after transfection with miR-30e-5p mimic or inhibitor. **(C–E)** Correlation between miR-30b-5p and predicted possible genes in HNSCC samples of TCGA. **(F–H)** Correlation between miR-30e-5p and predicted possible genes in HNSCC samples of TCGA. (**p<0.01, ***p<0.001).

REFERENCES

1. Leemans CR, Snijders PJF, Brakenhoff RH. The molecular landscape of head and neck cancer. *Nat Rev Cancer* (2018) 18:269–82. doi: 10.1038/nrc.2018.11
2. Shield KD, Ferlay J, Jemal A, Sankaranarayanan R, Chaturvedi AK, Bray F, et al. The global incidence of lip, oral cavity, and pharyngeal cancers by subsite in 2012. *CA: Cancer J Clin* (2017) 67:51–64. doi: 10.3322/caac.21384
3. Lafuente Ibáñez de Mendoza I, Maritxalar Mendia X, García de la Fuente AM, Quindós Andrés G, Aguirre Urizar JM. Role of Porphyromonas gingivalis in oral squamous cell carcinoma development: A systematic review. *J Periodontal Res* (2020) 55:13–22. doi: 10.1111/jre.12691
4. Sharma U, Singhal P, Bandil K, Patle R, Kumar A, Neyaz K, et al. Genetic variations of TLRs and their association with HPV/EBV, co-infection along with nicotine exposure in the development of premalignant/malignant lesions of the oral cavity in Indian population. *Cancer Epidemiol* (2019) 61:38–49. doi: 10.1016/j.canep.2019.05.003
5. Danaei G, Vander Hoorn S, Lopez AD, Murray CJL, Ezzati M. Causes of cancer in the world: comparative risk assessment of nine behavioural and environmental risk factors. *Lancet (London England)* (2005) 366:1784–93. doi: 10.1016/S0140-6736(05)67725-2
6. Simard EP, Torre LA, Jemal A. International trends in head and neck cancer incidence rates: differences by country, sex and anatomic site. *Oral Oncol* (2014) 50:387–403. doi: 10.1016/j.oraloncology.2014.01.016
7. Torre LA, Bray F, Siegel RL, Ferlay J, Lortet-Tieulent J, Jemal A. Global cancer statistics, 2012. *CA: Cancer J Clin* (2015) 65:87–108. doi: 10.3322/caac.21262
8. Hecht SS. Tobacco carcinogens, their biomarkers and tobacco-induced cancer. *Nat Rev Cancer* (2003) 3:733–44. doi: 10.1038/nrc1190
9. Torre LA, Bray F, Siegel RL, Ferlay J, Lortet-Tieulent J, Jemal A. Preferential formation of benzo[a]pyrene adducts at lung cancer mutational hotspots in P53. *Sci (New York NY)* (1996) 274:430–2. doi: 10.1126/science.274.5286.430
10. Jalas JR, Hecht SS, Murphy SE. Cytochrome P450 enzymes as catalysts of metabolism of 4-(methylnitrosamino)-1-(3-pyridyl)-1-butanone, a tobacco specific carcinogen. *Chem Res Toxicol* (2005) 18:95–110. doi: 10.1021/tx049847p
11. Fan T, Sun G, Zhao L, Cui X, Zhong R. Metabolic Activation and Carcinogenesis of Tobacco-Specific Nitrosamine N'-Nitrosonornicotine (NNN): A Density Function Theory and Molecular Docking Study. *Int J Environ Res Public Health* (2019) 16:178. doi: 10.3390/ijerph16020178
12. Suzuki R, Matsushima Y, Okudaira N, Sakagami H, Shirataki Y. Cytotoxic Components Against Human Oral Squamous Cell Carcinoma Isolated from Andrographis paniculata. *Anticancer Res* (2016) 36:5931–5. doi: 10.21873/anticanres.11180
13. Lai Y-H, He R-Y, Chou J-L, Chan MWY, Li Y-F, Tai C-K. Promoter hypermethylation and silencing of tissue factor pathway inhibitor-2 in oral squamous cell carcinoma. *J Trans Med* (2014) 12:237. doi: 10.1186/s12967-014-0237-7
14. Shao Y, Qu Y, Dang S, Yao B, Ji M. MiR-145 inhibits oral squamous cell carcinoma (OSCC) cell growth by targeting c-Myc and Cdk6. *Cancer Cell Int* (2013) 13:51. doi: 10.1186/1475-2867-13-51
15. Urvalek AM, Osei-Sarfo K, Tang X-H, Zhang T, Scognamiglio T, Gudas LJ. Identification of Ethanol and 4-Nitroquinoline-1-Oxide Induced Epigenetic and Oxidative Stress Markers During Oral Cavity Carcinogenesis. *Alcohol Clin Exp Res* (2015) 39:1360–72. doi: 10.1111/acer.12772
16. Osei-Sarfo K, Tang X-H, Urvalek AM, Scognamiglio T, Gudas LJ. The molecular features of tongue epithelium treated with the carcinogen 4-nitroquinoline-1-oxide and alcohol as a model for HNSCC. *Carcinogenesis* (2013) 34:2673–81. doi: 10.1093/carcin/bgt223
17. Walk EL, McLaughlin S, Coad J, Weed SA. Use of high frequency ultrasound to monitor cervical lymph node alterations in mice. *PloS One* (2014) 9:e100185. doi: 10.1371/journal.pone.0100185
18. Paparella ML, Abrigo M, Bal de Kier Joffe E, Raimondi AR. Oral-specific ablation of Klf4 disrupts epithelial terminal differentiation and increases premalignant lesions and carcinomas upon chemical carcinogenesis. *J Oral Pathol Med Off Publ Int Assoc Oral Pathol Am Acad Oral Pathol* (2015) 44:801–9. doi: 10.1111/jop.12307
19. Jiang C, Ye D, Qiu W, Zhang X, Zhang Z, He D, et al. Response of lymphocyte subsets and cytokines to Shenyang prescription in Sprague-Dawley rats with tongue squamous cell carcinomas induced by 4NQO. *BMC Cancer* (2007) 7:40. doi: 10.1186/1471-2407-7-40
20. Ashburner M, Ball CA, Blake JA, Botstein D, Butler H, Cherry JM, et al. Gene ontology: tool for the unification of biology. The Gene Ontology Consortium. *Nat Genet* (2000) 25:25–9. doi: 10.1038/75556
21. Qin X, Yan M, Li R, Ye D, Zhang J, Xu Q, et al. Identification and characterization of a highly metastatic epithelial cancer cell line from rat tongue cancer. *Arch Oral Biol* (2018) 95:58–67. doi: 10.1016/j.archoralbio.2018.07.010
22. Qin X, Yan M, Zhang J, Xu Q, Lv Z, Chen W. Establishment of a highly metastatic buccal squamous cell carcinoma cell line from a Sprague-Dawley Rat. *Arch Oral Biol* (2016) 62:1–9. doi: 10.1016/j.archoralbio.2015.11.003
23. Colaprico A, Silva TC, Olsen C, Garofano L, Cava C, Garolini D, et al. TCGAbiolinks: an R/Bioconductor package for integrative analysis of TCGA data. *Nucleic Acids Res* (2016) 44:e71. doi: 10.1093/nar/gkv1507
24. Mounir M, Lucchetta M, Silva TC, Olsen C, Bontempi G, Chen X, et al. New functionalities in the TCGAbiolinks package for the study and integration of cancer data from GDC and GTEx. *PloS Comput Biol* (2019) 15:e1006701. doi: 10.1371/journal.pcbi.1006701
25. Yu G, Wang L-G, Han Y, He Q-Y. clusterProfiler: an R package for comparing biological themes among gene clusters. *Omics J Integr Biol* (2012) 16:284–7. doi: 10.1089/omi.2011.0118
26. Li J-H, Liu S, Zhou H, Qu L-H, Yang J-H. starBase v2.0: decoding miRNA-ceRNA, miRNA-ncRNA and protein-RNA interaction networks from large-scale CLIP-Seq data. *Nucleic Acids Res* (2014) 42:D92–D7. doi: 10.1093/nar/gkt1248
27. Kanojia D, Vaidya MM. 4-nitroquinoline-1-oxide induced experimental oral carcinogenesis. *Oral Oncol* (2006) 42:655–67. doi: 10.1016/j.oraloncology.2005.10.013
28. Tseng H-H, Tseng Y-K, You J-J, Kang B-H, Wang T-H, Yang C-M, et al. Next-generation Sequencing for microRNA Profiling: MicroRNA-21-3p Promotes Oral Cancer Metastasis. *Anticancer Res* (2017) 37:1059–66. doi: 10.21873/anticanres.11417

29. Henson BJ, Bhattacharjee S, O'Dee DM, Feingold E, Gollin SM. Decreased expression of miR-125b and miR-100 in oral cancer cells contributes to malignancy. *Genes Chromosomes Cancer* (2009) 48:569–82. doi: 10.1002/gcc.20666
30. Deng Z, Wang Y, Fang X, Yan F, Pan H, Gu L, et al. Research on miRNA-195 and target gene CDK6 in oral verrucous carcinoma. *Cancer Gene Ther* (2017) 24:282–8. doi: 10.1038/cgt.2017.18
31. Salama I, Malone PS, Mihaimeed F, Jones JL. A review of the S100 proteins in cancer. *Eur J Surg Oncol J Eur Soc Surg Oncol Br Assoc Surg Oncol* (2008) 34:357–64. doi: 10.1016/j.ejso.2007.04.009
32. Li J, Donath S, Li Y, Qin D, Prabhakar BS, Li P. miR-30 regulates mitochondrial fission through targeting p53 and the dynamin-related protein-1 pathway. *PloS Genet* (2010) 6:e1000795. doi: 10.1371/journal.pgen.1000795
33. Mao L, Liu S, Hu L, Jia L, Wang H, Guo M, et al. miR-30 Family: A Promising Regulator in Development and Disease. *BioMed Res Int* (2018) 2018:9623412. doi: 10.1155/2018/9623412
34. Volinia S, Galasso M, Costinean S, Tagliavini L, Gamberoni G, Drusco A, et al. Reprogramming of miRNA networks in cancer and leukemia. *Genome Res* (2010) 20:589–99. doi: 10.1101/gr.098046.109
35. Saleh AD, Cheng H, Martin SE, Si H, Ormanoglu P, Carlson S, et al. Integrated Genomic and Functional microRNA Analysis Identifies miR-30-5p as a Tumor Suppressor and Potential Therapeutic Nanomedicine in Head and Neck Cancer. *Clin Cancer Res Off J Am Assoc Cancer Res* (2019) 25:2860–73. doi: 10.1158/1538-7445.AM2018-4401
36. Braun J, Hoang-Vu C, Dralle H, Hüttelmaier S. Downregulation of microRNAs directs the EMT and invasive potential of anaplastic thyroid carcinomas. *Oncogene* (2010) 29:4237–44. doi: 10.1038/onc.2010.169
37. Ma Y-S, Yu F, Zhong X-M, Lu G-X, Cong X-L, Xue S-B, et al. miR-30 Family Reduction Maintains Self-Renewal and Promotes Tumorigenesis in NSCLC-Initiating Cells by Targeting Oncogene TM4SF1. *Mol Ther J Am Soc Gene Ther* (2018) 26:2751–65. doi: 10.1016/j.ymthe.2018.09.006
38. Jiang S, Miao D, Wang M, Lv J, Wang Y, Tong J. MiR-30-5p suppresses cell chemoresistance and stemness in colorectal cancer through USP22/Wnt/β-catenin signaling axis. *J Cell Mol Med* (2019) 23:630–40. doi: 10.1111/jcmm.13968
39. Ichimi T, Enokida H, Okuno Y, Kunimoto R, Chiyomaru T, Kawamoto K, et al. Identification of novel microRNA targets based on microRNA signatures in bladder cancer. *Int J Cancer* (2009) 125:345–52. doi: 10.1002/ijc.24390
40. Izzotti A, Calin GA, Arrigo P, Steele VE, Croce CM, De Flora S. Downregulation of microRNA expression in the lungs of rats exposed to cigarette smoke. *FASEB J Off Publ Fed Am Soc Exp Biol* (2009) 23:806–12. doi: 10.1096/fj.08-121384
41. Ma YX, Zhang H, Li XH, Liu YH. MiR-30e-5p inhibits proliferation and metastasis of nasopharyngeal carcinoma cells by target-ing USP22. *Eur Rev Med Pharmacol Sci* (2018) 22:6342–9. doi: 10.26355/eurrev_201810_16045
42. Zhang Z, Qin H, Jiang B, Chen W, Cao W, Zhao X, et al. miR-30e-5p suppresses cell proliferation and migration in bladder cancer through regulating metadherin. *J Cell Biochem* (2019) 120:15924–32. doi: 10.1002/jcb.28866
43. Qin X, Chen J, Wu L, Liu Z. MiR-30b-5p acts as a tumor suppressor, repressing cell proliferation and cell cycle in human hepatocellular carcinoma. *Biomed Pharmacother Biomed Pharmacother* (2017) 89:742–50. doi: 10.1016/j.biopha.2017.02.062
44. Liu W, Li H, Wang Y, Zhao X, Guo Y, Jin J, et al. MiR-30b-5p functions as a tumor suppressor in cell proliferation, metastasis and epithelial-to-mesenchymal transition by targeting G-protein subunit α-13 in renal cell carcinoma. *Gene* (2017) 626:275–81. doi: 10.1016/j.gene.2017.05.040
45. Cinpolat O, Unal ZN, Ismi O, Gorur A, Unal M. Comparison of microRNA profiles between benign and malignant salivary gland tumors in tissue, blood and saliva samples: a prospective, case-control study. *Braz J Otorhinolaryngol* (2017) 83:276–84. doi: 10.1016/j.bjorl.2016.03.013
46. Wang T, Li F, Tang S. MiR-30a upregulates BCL2A1, IER3 and cyclin D2 expression by targeting FOXL2. *Oncol Lett* (2015) 9:967–71. doi: 10.3892/ol.2014.2723
47. Zhou J, Gong G, Tan H, Dai F, Zhu X, Chen Y, et al. Urinary microRNA-30a-5p is a potential biomarker for ovarian serous adenocarcinoma. *Oncol Rep* (2015) 33:2915–23. doi: 10.3892/or.2015.3937
48. Gaziel-Sovran A, Segura MF, Di Micco R, Collins MK, Hanniford D, Vega-Saenz de Miera E, et al. miR-30b/30d regulation of GalNAc transferases enhances invasion and immunosuppression during metastasis. *Cancer Cell* (2011) 20:104–18. doi: 10.1016/j.ccr.2011.05.027
49. Gramantieri L, Pollutri D, Gagliardi M, Giovannini C, Quarta S, Ferracin M, et al. MiR-30e-3p Influences Tumor Phenotype through / Axis and Predicts Sorafenib Resistance in Hepatocellular Carcinoma. *Cancer Res* (2020) 80:1720–34. doi: 10.1158/0008-5472.CAN-19-0472
50. Weidhaas JB, Harris J, Schaue D, Chen AM, Chin R, Axelrod R, et al. The KRAS-Variant and Cetuximab Response in Head and Neck Squamous Cell Cancer: A Secondary Analysis of a Randomized Clinical Trial. *JAMA Oncol* (2017) 3:483–91. doi: 10.1001/jamaoncol.2016.5478
51. Davidson SM, Papagiannakopoulos T, Olenchock BA, Heyman JE, Keibler MA, Luengo A, et al. Environment Impacts the Metabolic Dependencies of Ras-Driven Non-Small Cell Lung Cancer. *Cell Metab* (2016) 23:517–28. doi: 10.1016/j.cmet.2016.01.007
52. Fernández-Pérez MP, Montenegro MF, Sáez-Ayala M, Sánchez-del-Campo L, Piñero-Madrona A, Cabezas-Herrera J, et al. Suppression of antifolate resistance by targeting the myosin Va trafficking pathway in melanoma. *Neoplasia (New York NY)* (2013) 15:826–39. doi: 10.1593/neo.13320
53. Lee S, Axelsen TV, Jessen N, Pedersen SF, Vahl P, Boedtkjer E. Na,HCO-cotransporter NBCn1 (Slc4a7) accelerates ErbB2-induced breast cancer development and tumor growth in mice. *Oncogene* (2018) 37:5569–84. doi: 10.1038/s41388-018-0353-6

Conflict of Interest: The authors declare that the research was conducted in the absence of any commercial or financial relationships that could be construed as a potential conflict of interest.

Copyright © 2021 Zhang, Zhu, Sun, Qin, Zhang, Feng, Yan and Chen. This is an open-access article distributed under the terms of the Creative Commons Attribution License (CC BY). The use, distribution or reproduction in other forums is permitted, provided the original author(s) and the copyright owner(s) are credited and that the original publication in this journal is cited, in accordance with accepted academic practice. No use, distribution or reproduction is permitted which does not comply with these terms.

Advantages of publishing in Frontiers

OPEN ACCESS
Articles are free to read for greatest visibility and readership

FAST PUBLICATION
Around 90 days from submission to decision

HIGH QUALITY PEER-REVIEW
Rigorous, collaborative, and constructive peer-review

TRANSPARENT PEER-REVIEW
Editors and reviewers acknowledged by name on published articles

Frontiers
Avenue du Tribunal-Fédéral 34
1005 Lausanne | Switzerland

Visit us: www.frontiersin.org
Contact us: frontiersin.org/about/contact

REPRODUCIBILITY OF RESEARCH
Support open data and methods to enhance research reproducibility

DIGITAL PUBLISHING
Articles designed for optimal readership across devices

FOLLOW US
@frontiersin

IMPACT METRICS
Advanced article metrics track visibility across digital media

EXTENSIVE PROMOTION
Marketing and promotion of impactful research

LOOP RESEARCH NETWORK
Our network increases your article's readership